CP-57037
Revision 1

Model Package Report: Plateau to River Groundwater Model

Version 8.2

Prepared for the U.S. Department of Energy
Assistant Secretary for Environmental Management

Contractor for the U.S. Department of Energy
under Contract DE-AC06-08RL14788

CH2MHILL
Plateau Remediation Company

P.O. Box 1600
Richland, Washington 99352

Approved for Public Release;
Further Dissemination Unlimited

CP-57037
Revision 1

Model Package Report: Plateau to River Groundwater Model

Version 8.2

Document Type: RPT Program/Project: EPS

T. J. Budge
CH2M HILL Plateau Remediation Company

Date Published
May 2019

Prepared for the U.S. Department of Energy
Assistant Secretary for Environmental Management

Contractor for the U.S. Department of Energy
under Contract DE-AC06-08RL14788

CH2MHILL
Plateau Remediation Company
P.O. Box 1600
Richland, Washington 99352

APPROVED
By Janis D. Aardal at 7:44 am, May 22, 2019

Release Approval Date

Approved for Public Release;
Further Dissemination Unlimited

TRADEMARK DISCLAIMER

Reference herein to any specific commercial product, process, or service by tradename, trademark, manufacturer, or otherwise, does not necessarily constitute or imply its endorsement, recommendation, or favoring by the United States Government or any agency thereof or its contractors or subcontractors.

This report has been reproduced from the best available copy.

Printed in the United States of America

Signature Page

Title: CP-57037, Rev. 1, *Model Package Report: Plateau to River Groundwater Model, Version 8.2*

Model Preparer: _____ 1-25-2019

T.J. Budge, Senior Modeler
CHPRC

Date

Model Checker: _____ 1/27/2019

Tingting Yan, Hydrogeologist
INTERA

Date

Model Senior Reviewer: _____ 1/25/2019

Bob Andrews, Principal Hydrogeologist
INTERA

Date

Responsible Manager: _____ 5/2/19

A.H. Aly, Risk Assessment and Model Integration Manager
CHPRC

Date

This page intentionally left blank.

Executive Summary

This model package report documents the groundwater flow component of the Plateau to River Groundwater Model (P2R Model), a groundwater flow and contaminant fate and transport (F&T) simulation model used to support remedial activities conducted by CH2M HILL Plateau Remediation Company at the Hanford Site in Washington State. The objective of this model package report is to describe the modeling objectives; conceptualization; model implementation; calibration, sensitivity, and uncertainty; configuration control; limitations; and future model enhancements of the groundwater flow component of the P2R Model.

This report documents the principal elements regarding development of the flow component of the numerical model itself, not a specific calculation made using the model. The report focuses on the spatial discretization of the model, parameterization, and the time discretization during the calibration period, with the goal of providing a technical basis for using the model to (1) assist with understanding and/or reconstructing past conditions at the site, and (2) make predictions of possible future conditions. Using the P2R Model to perform specific calculations (including application-specific boundary conditions), characterization of current contamination conditions and contaminant transport predictions will be described for each use of the model in separate environmental calculation files.

The P2R Model provides a computational framework to simulate the F&T of contaminants in groundwater associated with the 200-PO-1, 200-UP-1, 200-BP-5, and 200-ZP-1 Groundwater Operable Units (OUs) in the Central Plateau of the Hanford Site. In addition, the model covers adjacent areas and facilities (e.g., the State-Approved Land Disposal Site). Intended and anticipated uses of the model include the following:

- Calculating water levels, hydraulic gradients, and groundwater flows throughout the model domain (encompassing the 200-West and 200-East Areas) for use in subsequent F&T calculations for contaminants of concern (COCs)
- Developing scale-appropriate, telescopic-mesh refinement models for detailed evaluation of areas within the model domain where required

The overall objective of the modeling effort is to provide a basis for making informed remedial action decisions based on descriptions of current and expected future

contaminant concentrations in groundwater at decision points within the OU boundaries. The objective for the model development phase of the effort is to create a common modeling platform that can be used for investigations of the groundwater OUs in the Central Plateau and downgradient toward the Columbia River.

The model domain, representing the suprabasalt aquifers of and downgradient to the Central Plateau, has been divided into six hydrostratigraphic units (HSUs), with properties based on field observed information and established through model calibration. The boundaries between units are established from the Hanford South Geoframework model. A large number of historical water level measurements dating back to 1944 have been used in calibrating the HSU properties and other important model parameters.

The P2R Model calibration emphasized matching water-level data from the 1940s to 2010s to establish current flow conditions that become initial conditions for predictive simulations using the model. The model reproduces measured water levels satisfactorily throughout this period; however, there is room for improvement in several areas. Fate and transport of tritium was used to aid the calibration process. The calibration results indicated that the version of the latest calibration of the P2R Model, Version 8.2 (described in this document), provides adequate correspondence between modeled outputs and historical measurements in order to meet the objectives of the model.

Sources of uncertainty arise from heterogeneity of the HSUs, uncertainty in the boundaries between HSUs, and uncertainty in the elevation in the basalt surface. The calibration results and uncertainty analysis also suggest that improved correspondence between simulated water levels and hydraulic gradients, and those measured at the Hanford Site, could be achieved with further development of the P2R Model.

This page intentionally left blank.

Contents

1 Introduction 1-1

1.1 Modeling Need 1-3
1.2 Background 1-3
1.3 Document Organization 1-4

2 Model Objectives 2-1

3 Model Conceptualization 3-1

3.1 Geologic Overview 3-1
3.1.1 Ringold Units 3-1
3.1.2 Cold Creek Unit 3-3
3.1.3 Hanford Formation 3-4
3.1.4 Hanford South Geoframework 3-5
3.1.5 Hydraulic Parameter Characterization 3-6
3.2 Modeling-Related Features, Events, and Processes 3-11
3.2.1 Anthropogenic Recharge 3-14
3.2.2 Perching of Anthropogenic Recharge 3-16
3.2.3 Natural Recharge 3-18
3.2.4 Basalt Surface Fluxes 3-19
3.2.5 Basalt Ridge Flow Barrier 3-23
3.2.6 Flow Direction in the 200-East Area 3-28

4 Model Implementation 4-1

4.1 Software 4-1
4.1.1 MODFLOW Controlled Calculation Software 4-2
4.1.2 MODFLOW Support Software 4-3
4.1.3 Software Installation and Checkout 4-3
4.1.4 Statement of Valid Software Application 4-3
4.2 Model Domain and Discretization 4-3
4.2.1 Model Extent 4-3
4.2.2 Lateral Discretization 4-4
4.2.3 Vertical Discretization 4-5
4.3 Simulation Period 4-8
4.4 Parameterization 4-8
4.4.1 Specified Heads 4-16
4.4.2 Hydraulic Properties 4-19
4.4.3 Columbia River Boundary 4-20
4.4.4 Recharge 4-22

4.4.5 Extraction/Injection of Groundwater 4-23
4.4.6 Transport Parameters 4-31
4.5 Calibration 4-31
4.5.1 Calibration Data Set 4-31
4.5.2 Goodness-of-Fit Metrics 4-35
4.5.3 Hydraulic Gradients 4-36
4.5.4 Calibration Process 4-37

5 Model Sensitivity and Uncertainty Analyses 5-1

5.1 Sensitivity Analysis 5-1
5.1.1 Vertical Placement 5-4
5.1.2 Lateral Placement 5-4
5.2 Model Uncertainty 5-4
5.2.1 Conceptual Model Uncertainty — Scale of Heterogeneity Represented by Hydrologic Stratigraphic Units 5-5
5.2.2 Flow Estimates near Gable Gap 5-5
5.2.3 CRBG Intercommunication 5-6

6 Model Limitations 6-1

7 Model Configuration Management 7-1

7.1 Model Version History 7-1
7.1.1 Version 7.1 7-2
7.1.2 Version 8.2 7-2
7.2 Model Application History 7-2

8 Model Enhancement Recommendations 8-1

8.1 Channel Delineation 8-1
8.2 Grid Structure Alterations 8-1
8.2.1 Western Boundary 8-1
8.2.2 Model Layering 8-2
8.3 Null Space Monte Carlo 8-2
8.4 Recharge 8-3
8.4.1 Recharge Rates 8-3
8.4.2 Recharge Footprint 8-3
8.5 Cold Creek Irrigation 8-3

9 References 9-1

Appendices

A Software Installation and Checkout Forms for Approved Software Installations A-1

B List of Observation Wells Used in the Calibration Process B-1

C Hydraulic Gradient Plots for Observed Data and Simulated Results C-1

D Hydrographs for Observed Data and Simulated Results at Observation Wells D-1

E Copy of EMDT-BC-0002 Rev. 1 ..... E-1

F Copy of EMDT-DE-0006 Rev. 1 ..... F-1

G Copy of EMDT-HP-0010 Rev. 0 ..... G-1

H Copy of EMDT-ST-0004 Rev. 0 ..... H-1

Figures

Figure 1-1. Location of Central Plateau on the Hanford Site 1-2

Figure 1-2. P2R Model Domain 1-5

Figure 3-1. Generic Stratigraphic Column for the Central Plateau 3-2

Figure 3-2. Distribution of CCU Facies across the Central Plateau 3-4

Figure 3-3. Inferred Flood Routes and Associated Hanford Formation Deposit Facies 3-5

Figure 3-4. Extent of the HSGF Domain 3-8

Figure 3-5. Map Indicating the Spatial Variability of Hydraulic Conductivity Values at the Hanford Site 3-9

Figure 3-6. Hydraulic Conductivity Distribution Ringold Unit E 3-10

Figure 3-7. Historical Anthropogenic Recharge (1944 to 2016) 3-15

Figure 3-8. Liquid Disposals at Surface and Vadose Zone Simulated Artificial Recharge for the Sum of All Hanford Site Liquid Discharges (1944 to 2000) 3-16

Figure 3-9. Top of Carbonate Facies of the CCU 3-17

Figure 3-10. Area Upgradient of The Western Portion of the Model Domain that will Simulate Mountain Front Recharge for Rattlesnake Mountain 3-19

Figure 3-11. Map of Upper Confined Basalt Aquifer (Pink) Contact with Unconfined Aquifer of the CPGW Model 3-21

Figure 3-12. Location of Thrust and Normal Faults on the Hanford Site 3-22

Figure 3-13. Estimated Flux across Upper Basalt Surface for 1996 3-24

Figure 3-14. Temporally Varying Estimated Flux across the Upper Basalt Surface 3-25

Figure 3-15. Relative Contribution of Each Basalt Leakage Feature to Net Leakage 3-25

Figure 3-16. Basalt Surface Expression in Gable Gap and the 200-East Area 3-26

Figure 3-17. Example of Highly Irregular Topography Eroded by Ice Age Floods, Lower Grand Coulee, and Channeled Scabland 3-27

Figure 3-18. Historical Water-Level Measurements near the Basalt Ridge Saddle 3-29

Figure 3-19. Locations of Wells Referred to in Figure 3-18 3-30
Figure 3-20. Water Table Map for the Paleochannel North of the 200-East Area, April 2016 3-31
Figure 3-21. 200-East Area Average Water Table Map, CY 2015 3-32
Figure 4-1. CPGW Model Extent and Boundary Conditions 4-5
Figure 4-2. Comparison Cross-Section View of (a) Hanford South Geoframework HSU Estimates and (b) Initial MODFLOW Grid HSU Assignments 4-9
Figure 4-3. Comparison Cross-Section View of (a) Hanford South Geoframework HSU Estimates and (b) Initial MODFLOW Grid HSU Assignments 4-10
Figure 4-4. Comparison Cross-Section View of (a) Hanford South Geoframework HSU Estimates and (b) Initial MODFLOW Grid HSU Assignments 4-11
Figure 4-5. Comparison Cross-Section View of (a) Hanford South Geoframework HSU Estimates and (b) Initial MODFLOW Grid HSU Assignments 4-12
Figure 4-6. Comparison Cross-Section View of (a) Hanford South Geoframework HSU Estimates and (b) Initial MODFLOW Grid HSU Assignments 4-13
Figure 4-7. HSUs of Model Layers 1 through 4 Based Solely on HSGF 4-14
Figure 4-8. HSUs of Model Layers 5 through 7 Based Solely on HSGF 4-15
Figure 4-9. Historical Water Levels for Well 699-60-60 4-17
Figure 4-10. Historical Water Levels for Well 699-10-54A 4-17
Figure 4-11. Simulated and Observed Head Values at the Northeastern Boundary of the P2R Model Version 8.2 for the Historic Calibration Simulation 4-18
Figure 4-12. Location of the Horizontal Flow Barrier Cells used to Simulate the May Junction Fault .. 4-19
Figure 4-13. Rating Curve for the Priest Rapids Dam Gage on the Columbia River Including a Forecast above 11 m 4-20
Figure 4-14. Comparison of the Mean Yearly Stage for the Columbia River at the Priest Rapids Dam Gage for the P2R Model, v.8.2 Simulation Period to the Reference Stage at the Same Gage Location 4-21
Figure 4-15. Comparison between River Stage Simulated as part of the P2R Model based on the Yearly Average Flow and Rating Curve at the Priest Rapids Dam Gage Upstream of the Hanford Site for Three Distinct Stress Periods 4-21
Figure 4-16. Natural Recharge Fluxes used in the P2R Model Version 8.2 4-23
Figure 4-17. Model Grid Cell Locations Affected by Anthropogenic Recharge in the P2R Model 4-24
Figure 4-18. Total Cumulative Anthropogenic Recharge for Calendar Years 1944 to 2016 for Waste Sites Located on the Central Plateau 4-25
Figure 4-19. Example of the Distribution of Recharge at Waste Sites Overlapping Multiple Cells 4-26
Figure 4-20. Wells Selected for Calibration Targets (labeled locations were selected for display in this report) 4-33
Figure 4-21. Historical Tritium Plume Estimates Archived as Part of DOE/RL-2016-09 4-35
Figure 4-22. Locations of Gradient Calculations 4-38
Figure 4-23. Gradient for Well Triplet 1 (699-28-40, 699-31-31, and 699-24-33) 4-41
Figure 4-24. Locations of Pilot Points used to Interpolate Hydraulic Conductivity Values for the Far-Field Calibration of the P2R Model Version 8.2 4-42

Figure 4-25. Locations of Pilot Points used to Interpolate Scaling Factors for the Hydraulic Conductivity Field near 200-West Area 4-43

Figure 4-26. Alteration of the Pilot Point Locations used to Calibrate the Cold Creek Unit in both the Far-Field and 200-West Area 4-44

Figure 4-27. Adjustments of Recharge Extent made to Waste Sites 216-S-16P and 216-U-10 as part of the Calibration of P2R Model Version 8.2 4-45

Figure 4-28. Hydrograph of Simulated and Observed Hydraulic Head Data for Well 699-35-78A Showing Results with and without the use of Adjusted Extents for the Recharge Footprint 4-46

Figure 4-29. Extent of the HSU Zone Representing the High Conductivity Sediments within the P2R Model Domain 4-47

Figure 4-30. F-F' Cross-Section View of a) the Original Grid HSU Assignment and b) the Alteration Made to Simulate High Conductivity Zone with the P2R Model 4-48

Figure 4-31. Locations of Pilot Points used to Interpolate Hydraulic Conductivity Values for the Channel HSU Zone of the P2R Model Version 8.2 4-49

Figure 4-32. Comparison of Historic Contours Based on Field Data and Simulated Contours of Tritium Concentration from 1970 4-50

Figure 4-33. Comparison of Historic Contours Based on Field Data and Simulated Contours of Tritium Concentration from 1980 4-51

Figure 4-34. Comparison of Historic Contours based on Field Data and Simulated Contours of Tritium Concentration from 1990 4-51

Figure 4-35. Comparison of Historic Contours based on Field Data and Simulated Contours of Tritium Concentration from 2000 4-52

Figure 4-36. Comparison of Historic Contours based on Field Data and Simulated Contours of Tritium Concentration from 2010 4-52

Figure 4-37. Simulated Hydraulic Conductivity Distribution for the Hanford Formation in the Calibrated P2R Model Version 8.2 4-54

Figure 4-38. Simulated Hydraulic Conductivity Distribution for the Cold Creek Formation in the Calibrated P2R Model Version 8.2 4-55

Figure 4-39. Simulated Hydraulic Conductivity Distribution for the Taylor Flat Unit of the Ringold Formation in the Calibrated P2R Model Version 8.2 4-56

Figure 4-40. Simulated Hydraulic Conductivity Distribution for the Unit E of the Ringold Formation in the Calibrated P2R Model Version 8.2 4-57

Figure 4-41. Simulated Hydraulic Conductivity Distribution for the Lower Mud Unit of the Ringold Formation in the Calibrated P2R Model Version 8.2 4-58

Figure 4-42. Simulated Hydraulic Conductivity Distribution for the Unit A of the Ringold Formation in the Calibrated P2R Model Version 8.2 4-59

Figure 4-43. Simulated Hydraulic Conductivity Distribution for the Channel HSU in the Calibrated P2R Model Version 8.2 4-60

Figure 4-44. Simulated Total Transmissivity Distribution for Calendar Year 1965 in the Calibrated P2R Model Version 8.2 4-61

Figure 4-45. Simulated Total Transmissivity Distribution for Calendar Year 2016 in the Calibrated P2R Model Version 8.2 4-62

Figure 4-46. Comparison of Observed and Simulated Water Level for CPGW Model at Well 699-50-85 4-66

Figure 4-47. Comparison of Observed and Simulated Water Level for CPGW Model at Well 699-48-71 4-66
Figure 4-48. Comparison of Observed and Simulated Water Level for CPGW Model at Well 699-38-70 4-67
Figure 4-49. Comparison of Observed and Simulated Water Level for CPGW Model at Well 699-29-78 4-67
Figure 4-50. Comparison of Observed and Simulated Water Level for CPGW Model at Well 699-53-55A 4-68
Figure 4-51. Comparison of Observed and Simulated Water Level for CPGW Model at Well 299-E28-28 4-68
Figure 4-52. Comparison of Observed and Simulated Water Level for CPGW Model at Well 299-E18-2 4-69
Figure 4-53. Comparison of Observed and Simulated Water Level for CPGW Model at Well 699-33-56 4-69
Figure 4-54. Comparison of Observed and Simulated Water Level for CPGW Model at Well 699-25-55 4-70
Figure 4-55. Comparison of Observed and Simulated Water Level for CPGW Model at Well 699-11-45A 4-70
Figure 4-56. Comparison of Observed and Simulated Water Level for CPGW Model at Well 699-24-33 4-71
Figure 4-57. Comparison of Observed and Simulated Water Level for CPGW Model at Well 699-31-31 4-71
Figure 4-58. Comparison of Observed and Simulated Water Level for CPGW Model at Well 699-41-23 4-72
Figure 4-59. Comparison of Observed and Simulated Water Level for CPGW Model at Well 699-50-30 4-72
Figure 4-60. Comparison of Observed and Simulated Water Level for CPGW Model at Well 699-49-13E 4-73
Figure 4-61. Comparison of Observed and Simulated Water Level for CPGW Model at Well 699-42-2 4-73
Figure 4-62. Comparison of Observed and Simulated Water Level for CPGW Model at Well 699-35-9 4-74
Figure 4-63. Comparison of Observed and Simulated Water Level for CPGW Model at Well 699-21-17 4-74
Figure 4-64. Comparison of Observed and Simulated Water Level for CPGW Model at Well 699-8-32 4-75
Figure 4-65. Comparison of Observed and Simulated Water Level for CPGW Model at Well 699-8-17 4-75
Figure 4-66. Comparison of Observed and Simulated Water Level for CPGW Model at Well 699-12-14D 4-76
Figure 4-67. Comparison of Observed and Simulated Water Level for CPGW Model at Well 699-20-E12 4-76
Figure 4-68. Comparison of Observed and Simulated Water Level for CPGW Model at Well 699-2-7 4-77

Figure 4-69. Comparison of Observed and Simulated Water Level for CPGW Model at Well 699-1-18 4-77
Figure 4-70. Comparison of Observed and Simulated Water Level for CPGW Model at Well 699-S8-19 4-78
Figure 4-71. Comparison of Observed and Simulated Water Level for CPGW Model at Well 699-S6-45K 4-78
Figure 4-72. Comparison of Observed and Simulated Water Level for CPGW Model at Well 399-1-18A 4-79
Figure 4-73. Comparison of Observed and Simulated Hydraulic Gradient Azimuth and Magnitude for Well Triplet 6 4-80
Figure 4-74. Comparison of Observed and Simulated Hydraulic Gradient Azimuth and Magnitude for Well Triplet 15 4-81
Figure 4-75. Comparison of Observed and Simulated Hydraulic Gradient Azimuth and Magnitude for Well Triplet 23 4-82
Figure 4-76. Comparison of Observed and Simulated Hydraulic Gradient Azimuth and Magnitude for Well Triplet 40 4-83
Figure 4-77. Comparison of Observed and Simulated Hydraulic Gradient Azimuth and Magnitude for Well Triplet 52 4-84
Figure 4-78. Comparison of Observed and Simulated Hydraulic Gradient Azimuth and Magnitude for Well Triplet 67 4-85
Figure 4-79. Average Residual for Final Calibrated P2R Model Version 8.2 for Model Years 1944 to 2016 4-86
Figure 4-80. Average Residual for Final Calibrated P2R Model Version 8.2 for Model Years 2008 to 2016 4-87
Figure 4-81. Average Residual for Wells near 200-West Area for Final Calibrated P2R Model Version 8.2 for Model Years 1944 to 2016 4-88
Figure 4-82. Average Residual for Wells near 200-East Area for Final Calibrated P2R Model Version 8.2 for Model Years 1944 to 2016 4-89
Figure 4-83. Plot of Simulated Heads vs Observed Heads for P2R Model Version 8.2 for Model Years 1944 to 2016 4-90
Figure 4-84. Plot of Simulated Heads vs Observed Heads for P2R Model Version 8.2 for Model Years 2008 to 2016 4-91
Figure 4-85. Comparison of Simulated and Observed Water Table Contours for Calendar Year 1965..4-92
Figure 4-86. Comparison of Simulated and Observed Water Table Contours for Calendar Year 2016..4-93
Figure 4-87. Vertical Difference between Simulated Hydraulic Head in the P2R Model Version 8.2 for Calendar Year 1965 4-94
Figure 4-88. Vertical Difference between Simulated Hydraulic Head in the P2R Model Version 8.2 for Calendar Year 2016 4-95
Figure 4-89. Volumetric Budget Time-Series Plot for the Calibrated P2R Model Version 8.2 4-96
Figure 4-90. Volumetric Budget Time-Series Plot for Budget Components Less than 10,000 M^3/Day within the Calibrated P2R Model Version 8.2 4-97
Figure 5-1. Cumulative Distribution Function showing a Summary of Values Produced in the Correlation Coefficient Matrix Produced by PEST for the Calibrated P2R Model Version 8.2 5-3

Figure 5-2. Estimate of the Thickness of the Elephant Mountain Basalt.....5-8
Figure 5-3. Volumetric Water Budget of the P2R Model CRBG Sensitivity Simulation Including the Volumes Over Time that Enter and Exit the CRBG.....5-10
Figure 5-4. Volumetric Water Budget for Components Smaller than 10,000 m^3/day of the P2R Model CRBG Sensitivity Simulation Including the Volumes over Time that Enter and Exit the CRBG 5-10
Figure 5-5. Volumetric Water Budget for Components Related to Basalt Intercommunication of the P2R Model CRBG Sensitivity Simulation 5-11
Figure 5-6. Location of Wells used to compare Calibration Statistics near the CRBG Erosional Window in the Gable Gap Region of the P2R Model 5-12
Figure 5-7. Peak Simulated Tritium Concentration in the P2R Model that Exits the Specified Head Model Boundaries 5-14
Figure 7-1. Timeline Illustrating the Development and Version History of the P2R Model.....7-2
Figure 8-1. Current Lateral Extent of the P2R and CPGW models and the Proposed Extended Extent of an Update to the P2R Model.....8-2
Figure 8-2. Annual Maximum NDVI for CY 1985 at Cold Creek (Hanford Site West Boundary) 8-4

Tables

Table 3-1. Review of HSU Horizontal Hydraulic Conductivity 3-7
Table 3-2. Review of HSU Specific Yield 3-11
Table 3-3. Hanford Features, Events, and Processes 3-12
Table 4-1. HSUs in the P2R Model 4-6
Table 4-2. Model Layer Assignments by HSU for the Finite Difference Grid 4-7
Table 4-3. Temporal Discretization of Historical Calibration of the P2R Model 4-16
Table 4-4. Simulated Pumping Rates (gpm) for Extraction and Injections Wells used in the P2R Model Calibration 4-27
Table 4-5. Contaminant Transport Properties Assumed for F&T Analyses Using the P2R Model 4-32
Table 4-6. Well Triplets Used to Define Gradients 4-39
Table 4-7. Calibrated Model Input Parameter Summary for the P2R Model Version 8.2 4-63
Table 4-8. Summary Statistics for Calibration of P2R Model Version 8.2 4-64
Table 5-1. Summary Parameter Sensitivities Calculated by PEST 5-2
Table 5-2. Statistical Summary of Correlation Coefficient Cumulative Distribution Function 5-3
Table 5-3. Correlation Coefficients for Parameter Pairs with values Exceeding the 0.9 Threshold 5-3
Table 5-4. Percent Change Comparison of Volumetric Budget Elements between the Calibrated P2R Model and the CRBG Sensitivity Simulation 5-11
Table 5-5. Comparison of Summary Statistics between the Calibrated P2R Model and the CRBG Sensitivity Simulation 5-12
Table 5-6. Comparison of Tritium Activity for Model Boundaries for the Calibrated Model and the CRBG Sensitivity Simulation 5-13
Table 7-1. Applications of the P2R Model 7-3

Terms

CCU	Cold Creek unit
CHPRC	CH2M HILL Plateau Remediation Company
COC	contaminant of concern
CPGW Model	Central Plateau Groundwater Model
CRBG	Columbia River Basalt Group
CY	Calendar year
DOE	U.S. Department of Energy
EMMA	Environmental Model Management Archive
F&T	fate and transport
FEP	feature, event, and process
FS	feasibility study
FY	fiscal year
GHB	general head boundary
HEIS	Hanford Environmental Information System
HISI	Hanford Information System Inventory
HSGF	Hanford South Geoframework
HSU	hydrostratigraphic unit
K_d	distribution coefficient
K_h	horizontal hydraulic conductivity
MODFLOW	MODular groundwater FLOW code
MT3DMS	Modular Three-Dimensional Multiple Species transport code
NRDWL	Nonradioactive Dangerous Waste Landfill
OU	operable unit
P&T	pump and treat
PNNL	Pacific Northwest National Laboratory
RD/RAWP	remedial design/remedial action work plan
RMSE	root mean square error
ROD	Record of Decision
SALDS	State-Approved Land Disposal Site

STOMP	Subsurface Transport Over Multiple Phases
TEDF	Treated Effluent Disposal Facility

1 Introduction

A groundwater model, the Plateau to River Groundwater Model (P2R Model), has been developed for a region of the U.S. Department of Energy (DOE) Hanford Site covering the Central Plateau and extending eastward to the Columbia River. The Central Plateau is an informal geographic designation given to the broad central portion of the Hanford Site that encompasses the 200-West and 200-East Areas (Figure 1-1). The P2R Model primarily provides the computational basis for simulating the fate and transport (F&T) of contaminants in groundwater within the near and far-field portion of the affected aquifer associated with the 200-PO-1, 200-UP-1, 200-BP-5, and 200-ZP-1 Groundwater Operable Units (OU) in the Central Plateau. In addition, the model includes adjacent areas and facilities (e.g., the State-Approved Land Disposal Site [SALDS]) within the model domain.

The overall objective of the modeling effort is to provide a basis for making informed remedial action decisions based on descriptions of current and expected future contaminant concentrations in groundwater at decision points within the OU boundaries. The objective for the model development phase of the effort is to create a common modeling platform that can be used for investigations in each of the groundwater OUs in the Central Plateau.

This model package report is limited to development of the groundwater flow component of the model for the Central Plateau. Measurements made during the recent past, since 1944, are used to guide model development. Simulations of the F&T of tritium since 1944 were also used to evaluate groundwater flow directions as part of model development. The period encompassed by these past measurements is the simulation period for the model development described in this report. The model has been and will be used to provide the basis for predictions, with appropriate changes to represent future boundary conditions, of hydrologic conditions within the model domain. Problem-specific boundary conditions and characterization of current contamination conditions needed for contaminant transport predictions will be described for each use of the model in separate environmental calculation files.

Modeling is an iterative process; therefore, modifications to the P2R Model will occur periodically in response to new knowledge and information, and in response to new needs, possibly with each use of the model. A version number will identify the evolution of the P2R Model to delineate the changes made to the model over time. This model package report covers P2R Model Version 8.2. Revisions of this model package report will be made as the P2R Model is updated and will align with versions of that model. The evolution of the flow model is provided in this report by separating the P2R Model descriptions (as contained in this document) from descriptions of specific applications of the model that are documented separately in environmental calculation files. Detailed descriptions of simulation results from previous versions of the P2R Model are provided in respective model package reports. Section 7 summarizes the evolution of the model as it has been updated and provides details as to products that have utilized the model for calculations.

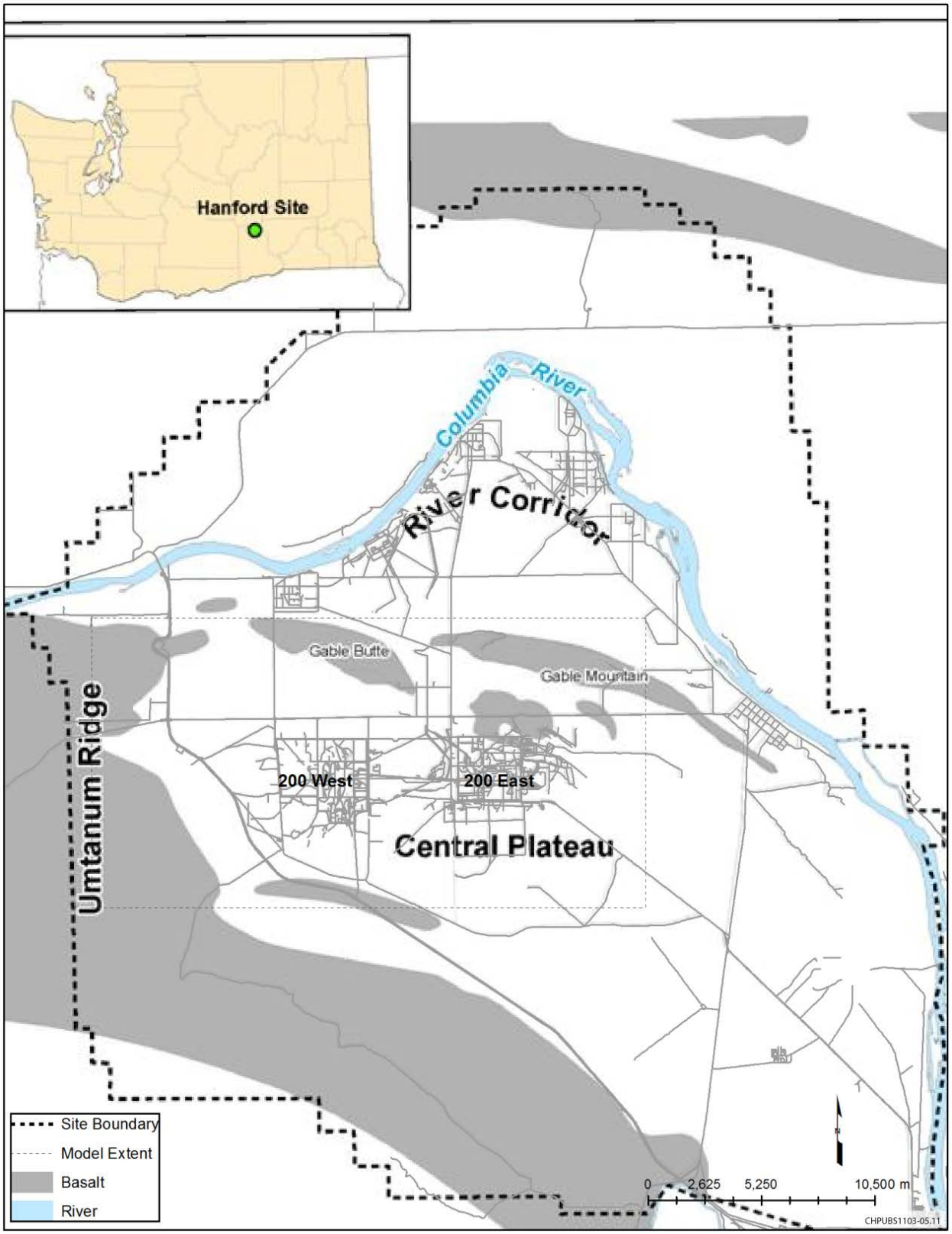

Figure 1-1. Location of Central Plateau on the Hanford Site

1.1 Modeling Need

Anticipated and intended uses of the P2R Model are to meet the following needs:

- Calculating water levels, hydraulic gradients, and groundwater flows throughout the model domain for use in subsequent F&T calculations for contaminants of concern (COCs)
- Estimating future groundwater concentrations of COCs to support risk screening within and possibly downgradient of each OU
- Estimating future groundwater concentrations of COCs to support evaluation of remedial alternatives
- Estimating the efficacy of selected remedial alternatives and optimizing final remedial design
- Calculating likely influent concentrations to remedies that extract contaminated water for treatment above ground
- Enabling the design and costing of treatment systems
- Developing scale-appropriate, telescopic-mesh refinement models for detailed evaluation of areas within the model domain where required

1.2 Background

A groundwater flow and advective/dispersive transport model was originally developed to perform contaminant F&T simulations in support of the 200-ZP-1 Groundwater OU feasibility study (FS) (DOE/RL-2007-28, *Feasibility Study for the 200-ZP-1 Operable Unit*), proposed plan, and final Record of Decision (ROD). This study used analytical and superposition techniques rather than a numerical model. In anticipation of the need for more rigorous analyses of groundwater flow and contaminant transport, this superposition model was replaced during fiscal year (FY) 2008 with a numerical groundwater flow and contaminant transport model. The model was developed to provide calculations in support of the post-ROD remedy design, focusing on the remedial design/remedial action work plan (RD/RAWP) for the 200-ZP-1 OU (DOE/RL-2008-56, *200-West Area Pre-Conceptual Design for Final Extraction/Injection Well Network: Modeling Analyses*; DOE/RL-2009-38, *Description of Modeling Analyses in Support of the 200-ZP-1 Remedial Design/Remedial Action Work Plan*; DOE/RL-2008-78, *200-West Area 200-ZP-1 Pump-and-Treat Remedial Design/Remedial Action Work Plan*).

The model developed in support of post-ROD activities at the 200-ZP-1 OU was constructed with a geographic extent (or domain) that covers most of the Central Plateau, which encompasses four groundwater OUs: 200-PO-1, 200-BP-5, 200-UP-1, and 200-ZP-1. This model was constructed using the software MODular groundwater FLOW code (MODFLOW) (USGS, 2000, *MODFLOW-2000, the U.S. Geological Survey Modular Ground-water Model – User Guide to Modularization Concepts and the Ground-Water Flow Process*) to simulate flow and Modular Three-Dimensional Multiple Species transport code (MT3DMS) (Zheng and Wang, 1999, *MT3DMS: A Modular Three-Dimensional Multispecies Transport Model for Simulation of Advection, Dispersion, and Chemical Reactions of Contaminants in Groundwater Systems; Documentation and User's Guide*) to simulate contaminant transport. For clarity in this report, the model developed for the 200-ZP-1 OU analyses is referred to as the 200-ZP-1 Model.

During FY 2009, the general premise (i.e., conceptual basis, computational grid, and discretization) of the 200-ZP-1 Model was accepted as a basis for modeling to be used throughout the Central Plateau in support of decision-making purposes at the encompassed OUs. Because 200-ZP-1 Model development focused on features, events, and processes (FEPs) associated with the 200-ZP-1 OU, additional model development was required so the model would be suitable for use at the other OUs. To distinguish the current version of this model from the precursor 200-ZP-1 Model, the model is referred to as the Central Plateau Groundwater Model (CPGW Model). The CPGW Model replaced the 200-ZP-1 Model in all groundwater simulations for the four groundwater OUs encompassed by the CPGW Model, including any calculations made for the 200-ZP-1 OU.

The 200-PO-1 Groundwater OU RI (DOE/RL-2009-85) utilized the CPGW Model (CP-47631, *Model Package Report: Central Plateau Groundwater Model Version 3.4*) for groundwater modeling of baseline future conditions within the spatial extent covered by that model's domain (Figure 1-2). This was sufficient for most COCs evaluated, but the 200-PO-1 Groundwater OU includes two notable mobile COCs that are dispersed in groundwater well downgradient (east and southeast) of the CPGW Model: tritium and iodine. For the purpose of this report, this portion of the model domain will be referred to as the "far-field" of the model. This includes the area south and east of the 200-East Area all the way to the Columbia River.

To address these relatively mobile COCs in the distal portions of the 200-PO-1 Groundwater OU, streamtube transport models (ECF-200PO1-09-2007, *200-PO-1 Operable Unit Remedial Investigation Report – Contaminant Fate & Transport Modeling in the Distal Portion of OU*) were developed. The adequacy of this modeling approach to meet RI objectives was evaluated in ECF-200PO1-10-0393, *Evaluating Adequacy of One-Dimensional Transport Calculation in the Saturated Zone of the Far-Field Portion of the 200-PO-1 Operable Unit*.

When the DOE/RL-2009-85 was reviewed by the Washington State Department of Ecology, it was noted that the modeling approach, using streamtube calculations, for the distal portion of the OU would be inadequate to the needs of the FS, and it was expected that the entire OU be evaluated in a three-dimensional groundwater model. Therefore, the P2R Model was developed to meet the needs of simulating both the near-field Central Plateau OUs and the distal plume toward the Columbia River. Version 7.1 of the P2R Model was the original of the model and was released in 2015. Section 7 of this report provides the version history and the uses of this model in all of its version. It also provides more discussion on the reason this model was created. This model package report (MPR) provides the documentation of an update to the original model that is titled the P2R Model version 8.2.

1.3 Document Organization

The organization of this model package report follows guidance set forth in Appendix G of CHPRC-00189, *CH2M Hill Plateau Remediation Company Quality Assurance Program Plan*. Chapter 2 of this report presents the objectives that the P2R Model is constructed to meet. Chapter 3 describes the conceptualization of the system to be simulated with a numerical model and identifies the relevant FEPs. Chapter 4 describes the implementation of the conceptual model as a numerical computer simulation model. Chapter 5 provides an overview of the sensitivity and describes sources of uncertainty for the predictions made with this model. Some intentional redundancy occurs in Chapters 3 to 5 to allow this report to be used as a reference document as well as a descriptive document. Chapter 6 lists the limitations of this model that result from the conceptualization, selection, and exclusion of relevant FEPs, assumptions, and numerical implementation. Chapter 7 describes how this model is uniquely identified, tracked, and preserved as a configuration management item. Chapter 8 lists recommended improvements to the model that could be made for future versions. Chapter 9 provides the references cited in this report.

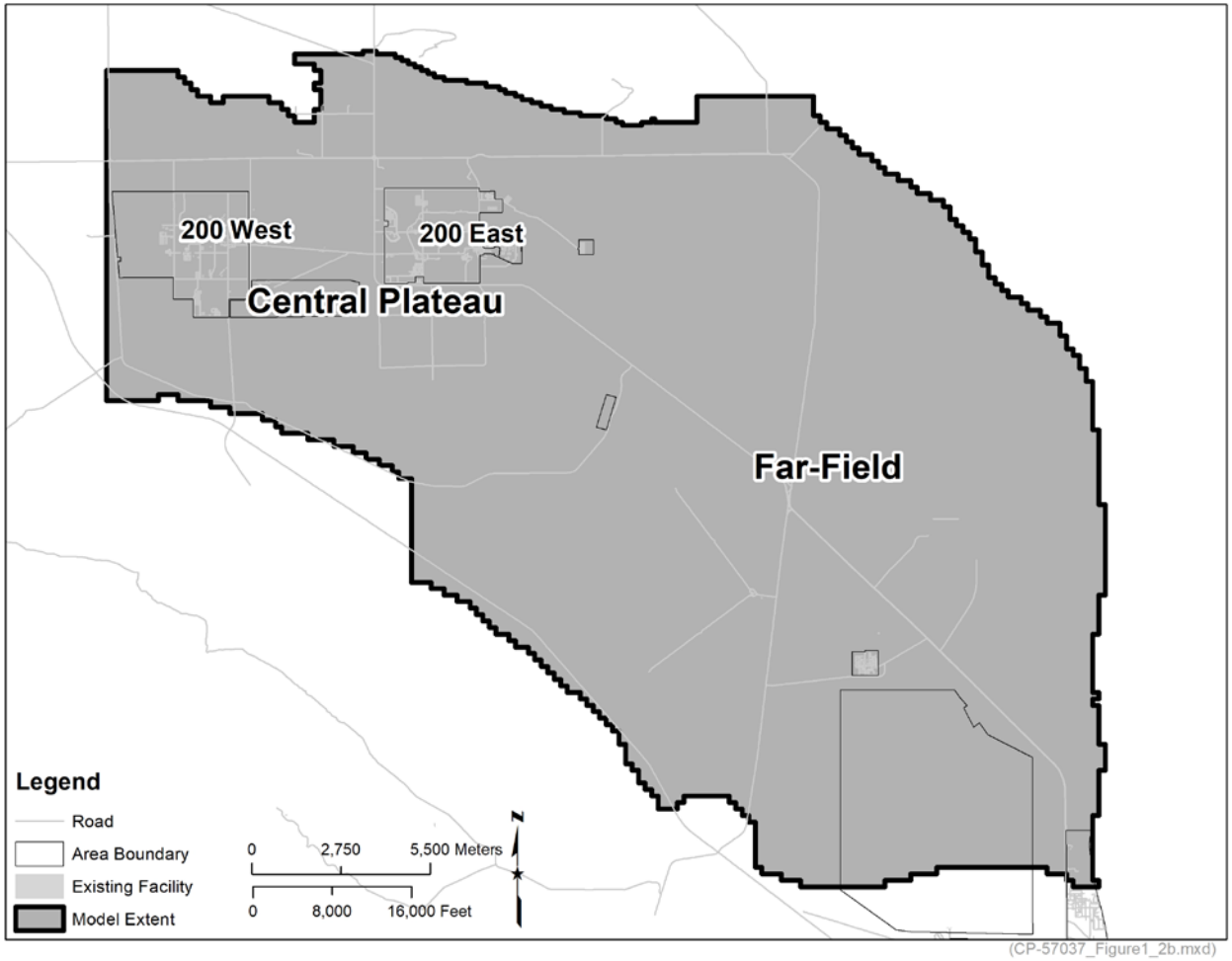

Figure 1-2. P2R Model Domain

This page intentionally left blank.

2 Model Objectives

The overall objectives of the modeling effort are to provide a basis for making informed remedial action decisions based on descriptions of current and expected future groundwater contaminant concentrations at decision points within the OU boundaries. The objective for the model development phase is to create a common modeling platform that can be used for investigations in each of the groundwater OUs in the Central Plateau.

This report is limited to development of the flow model for the Central Plateau and the far-field toward the Columbia River. Problem-specific boundary conditions, characterization of current contamination conditions, and transport predictions of contamination will be described for each use of the model in separate environmental calculation files.

Section 1.1 specifies the anticipated uses of the model. Although the model is developed for the primary purposes listed herein, other applications throughout the Central Plateau may use this model to support decisions and analyses. In these cases, each application is responsible to determine the applicability of the P2R Model version 8.2 to their specific objectives and scope. The P2R Model version 8.2 does not replace or supersede the CPGW Model version 8.4.5. Individual applications of either model must determine which model is appropriate for their respective applications.

This page intentionally left blank.

3 Model Conceptualization

The conceptualization for the P2R Model considers saturated porous media flow through the unconfined flow system. The unconfined aquifer occurs within fluvial, lacustrine, and glaciofluvial sediments overlying the Columbia River Basalts within the Pasco Basin (Figure 3-1). This uppermost, saturated zone is known as the unconfined aquifer system, although locally confined conditions may exist in certain areas. The local unconfined aquifer system provides a pathway for transport of contaminants released from past, present, and future site activities. Water enters the system through vertical recharge and recharge from upland areas to the west and southwest of the domain. The flow directions and rates are controlled by hydraulic pressures influenced by the geology of the subsurface, anthropogenic forces including injection or extraction of water, and hydraulic head at discharge points. Groundwater then exits through the western boundary of the model, Gable Gap, and the Columbia River. The following sections discusses the key features of geology and the features, events, and processes included in the conceptual framework for the P2R Model.

3.1 Geologic Overview

The overview of the geology and hydrogeology of the P2R Model domain presented in this section is a synopsis of the regional geology discussed in PNNL-17913, *Hydrogeology of the Hanford Site Central Plateau – A Status Report for the 200-West Area*. More detailed descriptions of the hydrogeology of the Central Plateau is also provided in PNNL-12261, *Revised Hydrogeology for the Suprabasalt Aquifer System, 200-East Area and Vicinity, Hanford Site, Washington*; PNNL-13858, *Revised Hydrogeology for the Suprabasalt Aquifer System, 200-West Area and Vicinity, Hanford Site, Washington*; and references therein.

The P2R Model simulates flow in the saturated portion of sedimentary deposits that have formed locally over the Columbia River Basalt Group (CRBG), a series of flood basalts that formed over a period of 17 to 6 million years ago in northcentral and northwest Oregon, eastern Washington, and western Idaho. Regional subsidence and uplift of the Pasco Basin has led to depositional and erosive periods, with depositional features also influenced by local deformation of the basalt. Major flooding events (most dramatically the Missoula floods) caused deep erosion and deposition during the last ice age.

3.1.1 Ringold Units

The oldest depositional sequence is the Ringold Formation deposited between 10.5 and 3.4 million years ago. BHI-00184, *Miocene- to Pliocene-Aged Suprabasalt Sediments of the Hanford Site, South-Central Washington*, divided the Ringold Formation into three informal members: Wooded Island, Taylor Flat, and Savage Island members (Figure 3-1). BHI-00184 subdivided the Wooded Island member into five subunits: A through E. The Ringold Formation underlying the Central Plateau mostly belongs to the Wooded Island member, along with remnants of the of the Taylor Flat member. For the P2R Model, these units have been grouped into the following:

- Ringold unit A (unit 9 in PNNL-12261)
- Ringold mud unit (also referred to as the Ringold lower mud), which is composed of units B, C, and D (units 8, 7, and 6 in PNNL-12261)
- Ringold unit E (unit 5 PNNL-12261)
- Ringold Taylor Flat member (unit 4 in PNNL-12261)

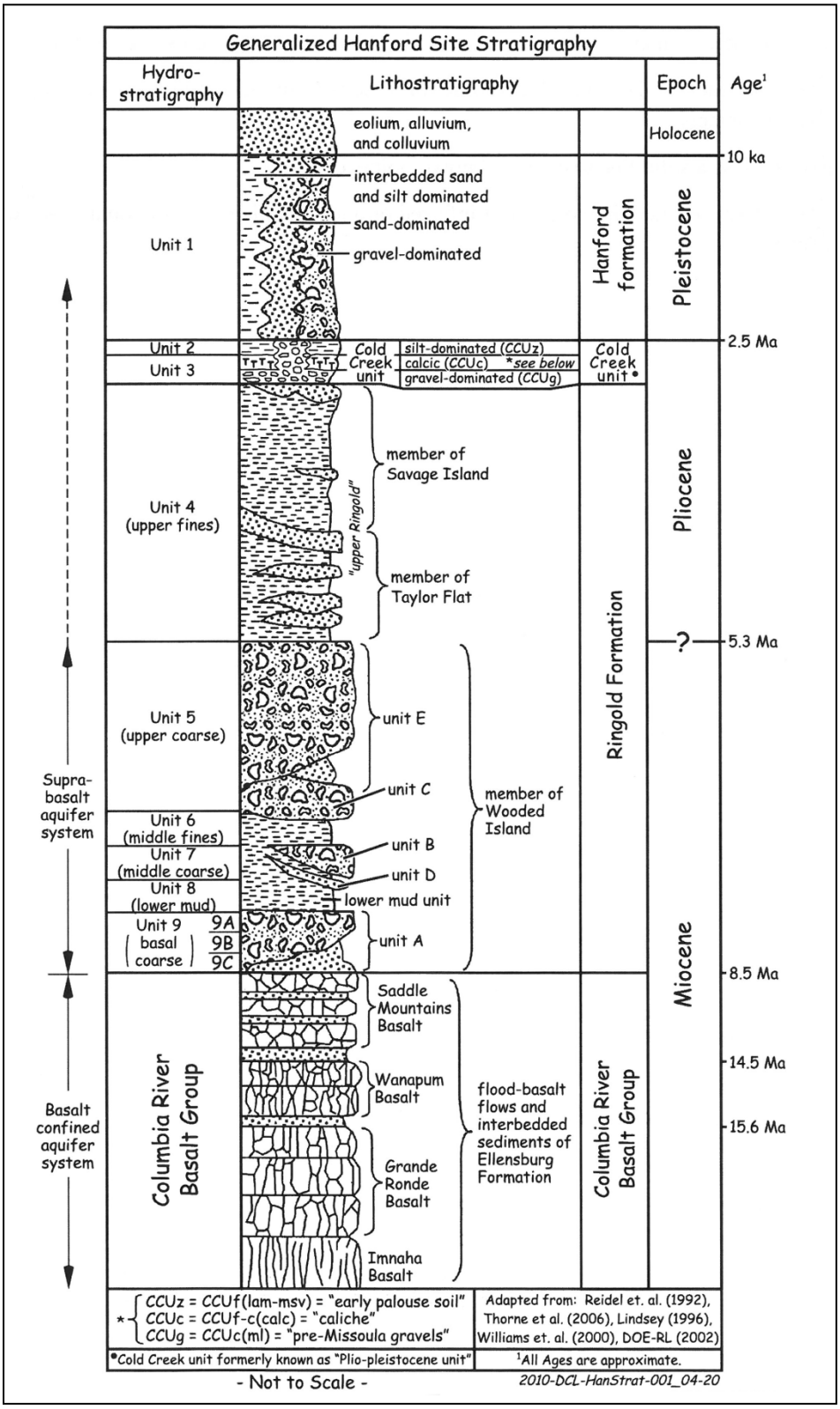

Source: PNNL-14898, *Results of Groundwater Modeling for Tritium Tracking at the Hanford Site 200 Area State-Approved Land Disposal Site – 2004*.

Figure 3-1. Generic Stratigraphic Column for the Central Plateau

Ringold unit A is composed of extensive gravel with interbedded sand. It was deposited in a braided plain of a meandering Columbia River that exited the Pasco Basin through the present Yakima River gap along the southeast end of the Rattlesnake Mountain anticline (Fecht et al., 1987, "Paleodrainage of the Columbia River on the Columbia Plateau of Washington State – A Summary"). About 6.7 million years ago, the river outlet was captured through the present Wallula Gap. The main river channel was still through the Central Plateau, but the depositional environment became a much lower energy sandy alluvial system with a period of lacustrine and overbank deposits of the Ringold mud unit.

The Ringold mud unit was subsequently covered by the extensive sequence of mostly alluvial gravels and sand of Ringold unit E. Locally, the Ringold unit E also contains fine-grained lenses that may have low permeability. About 5 million years ago, the depositional environment produced more than 90 m (295.3 ft) of sandy Taylor Flat deposits, followed by lacustrine deposits of the Savage Island member from 4.8 to 3.4 million years ago.

Regional uplift starting 3.4 million years ago led to extensive erosion, removing an estimated 100 m (328.1 ft) of deposits from the Hanford Site. The Savage Island member has been completely removed from the Central Plateau, and the Taylor Flat member has been removed over much of it as well. The erosion was deeper in the eastern portion of the Central Plateau, where the main river channel passed through the gap between Gable Mountain and Gable Butte.

3.1.2 Cold Creek Unit

A relatively dormant period followed the erosional period. Alluvial gravel, sand, and silt deposits developed along the main stream channel south of the Gable Gap, often referred to as the pre-Missoula gravels mainstream alluvium (Figure 3-2). Along Cold Creek and Dry Creek, deep drainage channel cuts were filled with alluvium. To the north of the Cold Creek paleochannel (Figure 3-2), overbank deposits form a soil that was calcified by the development of caliche within the soil. Later, less calcified overbank deposits continued to form top of this calcariferous layer. To the south of the Cold Creek paleochannel, coarser grained colluvium from Rattlesnake Mountain accumulated.

Only the pre-Missoula mainstream alluvium facies of the Cold Creek unit (CCU) are represented explicitly in the P2R Model. Except for very small segments of the Cold Creek channel fill, the western portion of the CCU lies above the historically high water level. Despite being located within the vadose zone (and, thus, not explicitly simulated in the P2R Model), the CCU near 200-West influenced aquifer recharge and groundwater dynamics during the operational period of the Hanford Site (PNNL-14070). Perching of water disposed near the surface delayed and laterally offset the arrival of this water at the aquifer. Section 3.2.2 discusses perching as a possible cause for variability in the extent that discharge ponds may have impacted groundwater.

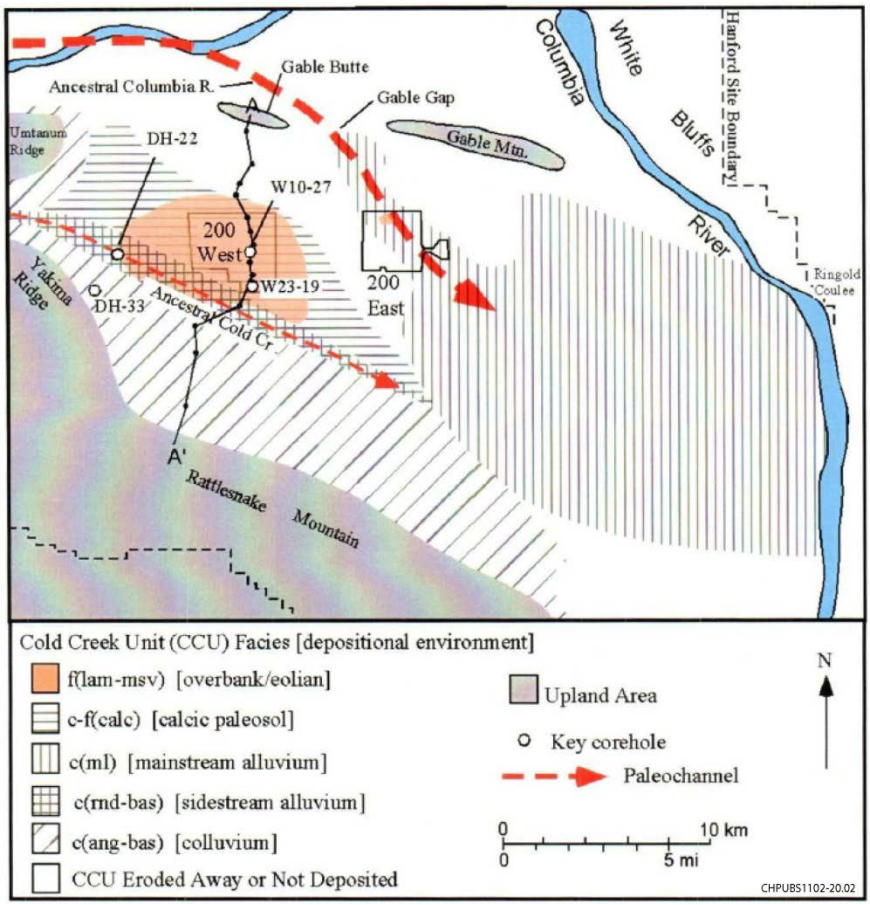

Source: DOE-RL-2002-39, *Standardized Stratigraphic Nomenclature for Post-Ringold Formation Sediments within the Central Pasco Basin*.

Figure 3-2. Distribution of CCU Facies across the Central Plateau

3.1.3 Hanford Formation

The cataclysmic outburst Missoula floods caused repeated large erosional and depositional events, which significantly shaped current Central Plateau geology. Some of the floods may have been the largest ever identified in the history of the world (O'Conner and Costa, 2004, *The World's Largest Floods, Past and Present – Their Causes and Magnitudes*). The many large floods left a series of overprinted features, including scour channels in the basalt, deep erosion of the CCU and Ringold Formation, highly conductive channel fill deposits extending from the Gable Gap southeast to the Columbia River, and relatively lower energy deposits across the western portion of the Central Plateau. Figure 3-3 depicts the inferred pathways of these floods and shows the distributions of the major facies groups. The majority of the regions of sand-dominated and interbedded sand and silt facies shown in the figure lie above the historical high water level and, hence, only a portion of these deposits are represented in the P2R Model. As would be expected of deposits formed from multiple erosive/depositional flood events, large vertical and horizontal variations occur within the gravel-dominated facies, ranging from fine sand to open framework deposits described as boulders in some drillers' logs.

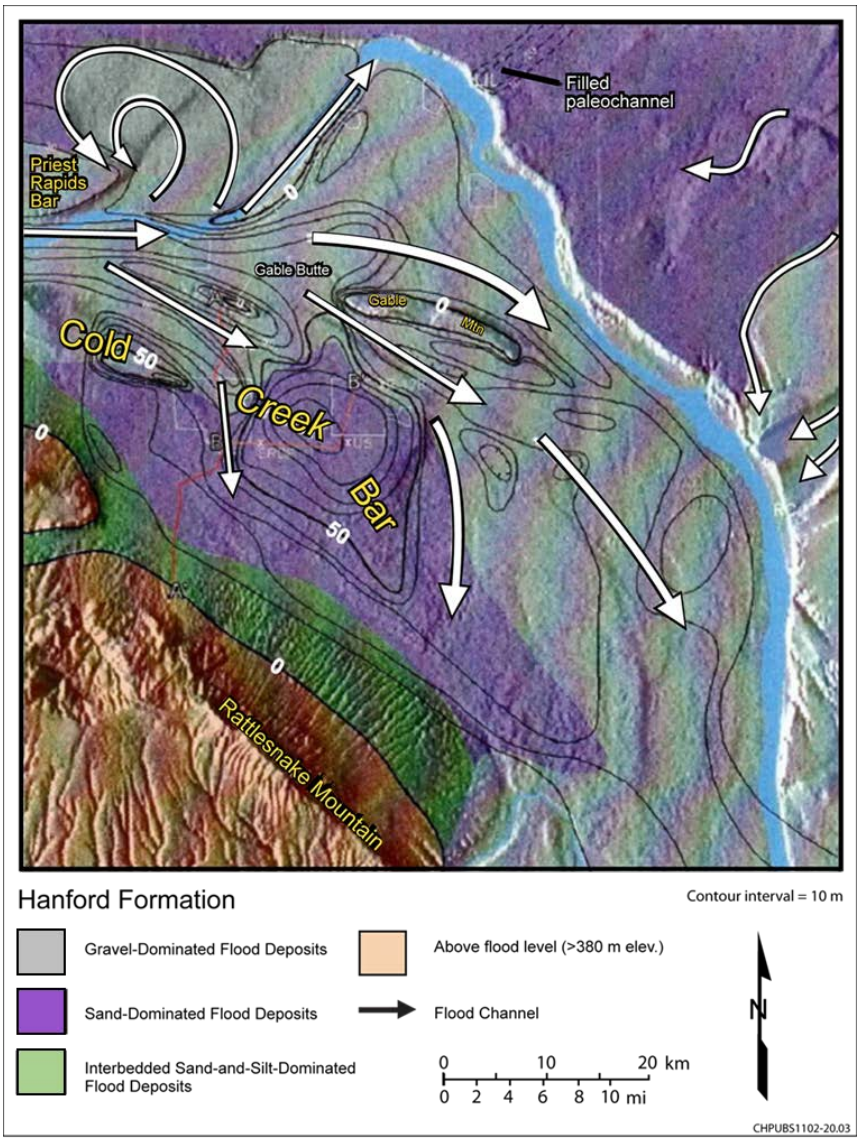

Source: DOE/RL-2002-39, *Standard Stratigraphic Nomenclature for Post-Ringold Formation Sediments within the Central Pasco Basin*.

Figure 3-3. Inferred Flood Routes and Associated Hanford Formation Deposit Facies

3.1.4 Hanford South Geoframework

The three-dimensional extent and thickness six hydrostratigraphic units (HSU) are estimated and documented in ECF-HANFORD-13-0029, *Development of the Hanford South Geologic Framework Model, Hanford Site, Washington*. These HSUs are:

- Ringold unit A
- Ringold mud unit
- Ringold unit E
- Ringold Taylor Flat
- CCU
- Hanford formation

The Hanford South Geoframework (HSGF) is a collection of polygonal meshes that represent the presence of a given HSU within the southern portion of the Hanford Site. Figure 3-4 shows a plan view of the extent of the HSGF. Vertically, the geoframework provides an estimate of the thickness of sediments from ground surface to the top of basalt. The HSGF is updated periodically to reflect the most recent well data collected at the site. The geoframework will be used to constrain the development of the numerical model grid and the assignment of hydraulic properties to the model. Chapter 4 discusses the application of the HSGF as it pertains to the P2R Model.

3.1.5 Hydraulic Parameter Characterization

This section presents a review of hydraulic property estimates by HSU. These estimates are drawn from compilations of aquifer testing interpretations and on parameter estimates used in previous modeling exercises. They include hydraulic conductivity, specific yield, and specific storage. Hydraulic property values presented in this section were used to constrain the values used as input parameters to the P2R Model version 8.2. Aquifer test results provide estimates of hydraulic properties on the scale of meters to hundreds of meters. When comparing the estimates presented in this section to the P2R model, it is useful to remember that a single model cell in the P2R Model is as small as 100 by 100 m (328.1 by 328.1 ft). Even the largest scale hydraulic tests of the aquifer are small compared to the scale of the entire model. Thus, parameter distributions in the model should reflect the ranges of hydraulic property data at the site but may not match values produced from aquifer test data. Thus, model calibration results are presented in this section to provide context to the ranges of input hydraulic parameter values that might be expected as a result of model calibration.

Aquifer test data are available for the Hanford Site through reports summarizing these field activities. EMDT-HP-0010, *Hydraulic and Transport Properties for Site-Wide Models*, and PNNL-14058, *Prototype Database and User's Guide of the Saturated Zone Hydraulic Properties for the Hanford Site*, (Appendix G) describe the available information. These tools are collections of hydraulic testing information that can be utilized to constrain hydraulic properties in numerical models at the Hanford Site.

A large portion of the data in these two data sources of hydraulic properties originates from PNL-10886, *Development of a Three-Dimensional Groundwater Model of the Hanford Site Unconfined Aquifer System: FY 1995 Status Report* and PNNL-13641, *Uncertainty Analysis Framework – Hanford Site-Wide Groundwater Flow and Transport Model*. Among other objectives these two reports provide synthesized interpretations of data from hydraulic testing of the suprabasalt aquifer at the Hanford Site. Table 3-1 presents ranges of hydraulic conductivity interpretations from these two reports.

Figure 3-5 shows the locations of many hydraulic tests compiled as part of PNNL-13641. This figure illustrates the variable nature of hydraulic conductivity over the Hanford Site both by location and sediment type. The figure portrays that the conductivity values for the Hanford and Cold Creek (referred to as "Pre-Missoula Gravels" in the figure) formations vary locally but tend to be higher in magnitude than the hydraulic conductivity values estimated from hydraulic testing of the Ringold Formation. Hanford and Cold Creek sediment hydraulic test results ranged from values of 10 to 10,000 m/d (33 to 32,808 ft/d) based on PNNL-13641 and PNNL-10886. Hydraulic conductivity values Ringold Formation sediments generally range in from 1 to 50 m/d (3.2 to 164 ft/d) (PNNL-13641). The limits of the results of aquifer testing were slightly higher, with maximum and minimum of 244 and 0.1 m/d (800 and 0.3 ft/d), respectively. In PNL-10886, Ringold unit A, Ringold unit 7, and Ringold unit E are discussed together.

Previous model calibrations provide an additional source of hydraulic parameter information. Pacific Northwest National Laboratory (PNNL) has developed a series of groundwater flow models. Table 3-1 presents results from two previous model calibrations PNNL-14398, *Transient Inverse Calibration of the Site-Wide Groundwater Flow Model (ACM-2): FY 2003 Progress Report*; and PNNL-14753,

Groundwater Data Package for Hanford Assessments. DOE/EIS-0391, *Final Tank Closure and Waste Management Environmental Impact Statement for the Hanford Site, Richland, Washington (TC & WM EIS)*, also based the hydraulic parameter characterization for their respective model calibrations on these reports. The model calibrations provide useful information with the respect of what parameter values were used to simulate hydraulic response on the model scale.

Both PNL-10886 and PNNL-13641 acknowledge that some Hanford formation deposits are essentially too permeable to test and could have hydraulic conductivity as large as 1,000,000 m/d (3,280,840 ft/d). The high energy deposits that correspond to the high conductivity values are mapped as paleo-channels in *Hydrogeologic Model for the Gable Gap Area, Hanford Site*, PNNL-19702, that are the result of ice-age flooding at the Hanford Site. DOE/EIS-0391, PNNL-14753, and the CPGW Model version 8.4.5 treated this area of the model as a separate HSU and refer to the location as either the high conductivity zone, coarse-gravel flood deposits, or channel deposits. The high conductivity zone described by PNNL-19702 is the presumed to cause of the generally flat water table at central region of the Hanford Site where wells exhibit minimal drawdown while being pumped. This area covers a large portion of 200-East Area north to the Gable Gap and southeast past the Nonradioactive Dangerous Waste Landfill (NRDWL) (DOE/EIS-0391). In 2015, a pumping test was performed in the 200-East Area (DOE/RL-2015-75, *Aquifer Treatability Test Report for the 200-BP-5 Groundwater Operable Unit*). The pumping test was conducted at well 299-E33-268 to estimate a transmissivity and hydraulic conductivity within the zone where previous attempts had not provided a reliable estimate. Test results estimated an average hydraulic conductivity at this well of 18,200 m/d (59,711.3 ft/d).

Recent evaluation of historic dye-tracer tests conducted in deposits near NRDWL indicate relatively high values of values of hydraulic conductivity in that region of the model domain. *Central Plateau Groundwater Tracer Study Phase I Report*, SGW-62323, indicate hydraulic conductivity values could be as high as 30,000 m/d (98,425 ft/day) to replicate observed breakthrough of dye in the historic experiments.

Table 3-1. Review of HSU Horizontal Hydraulic Conductivity

Unit	PNL-10886 Hydraulic Test Data (m/d)	PNNL-13641 Hydraulic Test Data (m/d)	PNNL-14753 Calibration (m/d)	DOE/EIS-0391 Calibration (m/d)
Hanford	1 – 10,000	10 – >3,500	6 – 20,195	0.171 – 3,982
Cold Creek			1.8 – 5,717	5.81 – 99.13
Ringold unit E	0.1 – 200	0.1 – 244	0.24 – 2,562	1.51 – 19.2
Ringold mud unit	0.03 – <0.06 (unit 6)	0.002 – 0.03 (unit 6)	0.00001 – 101	1.51
Ringold unit A	0.1 – 200	8	0.0005 – 4.2	1.51 – 19.2

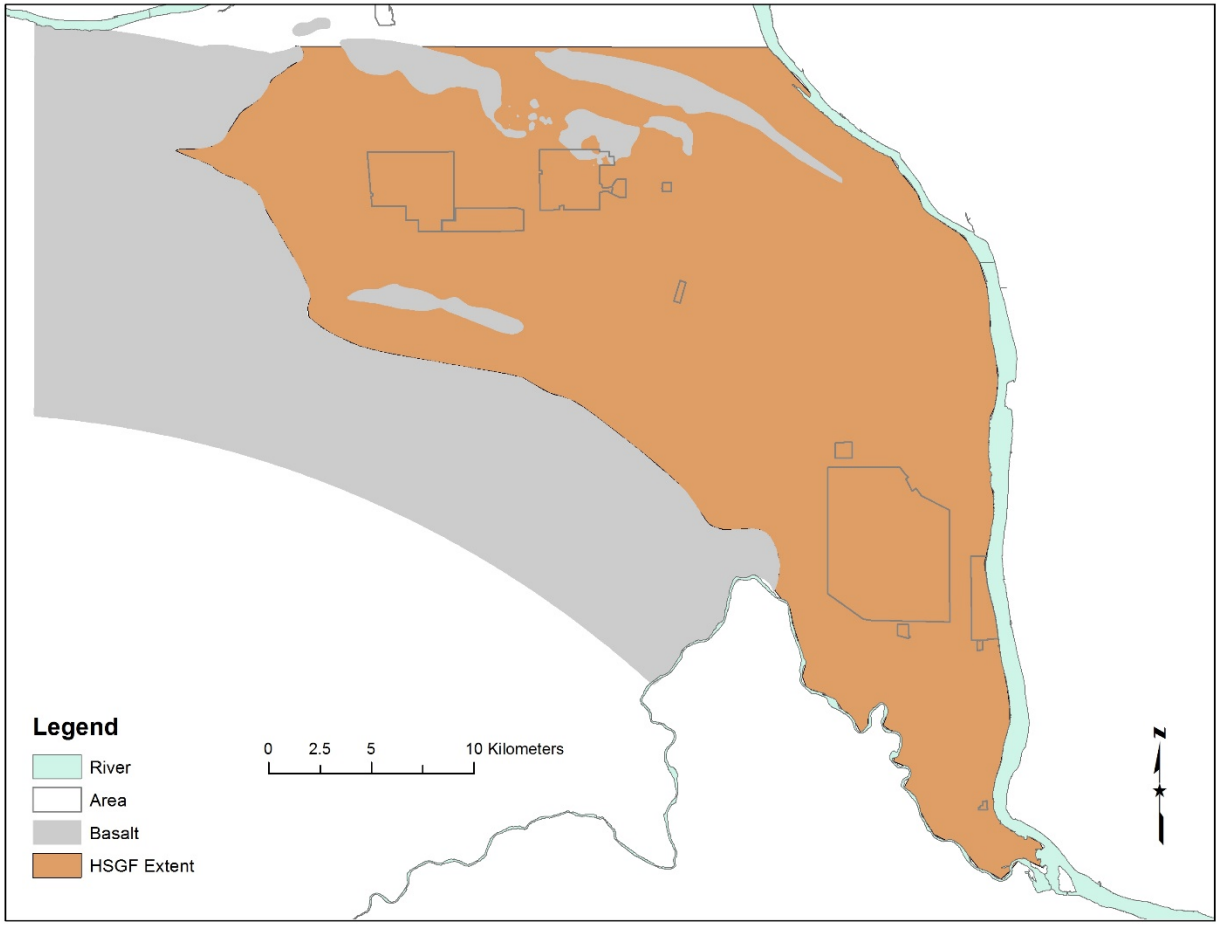

(Figure_3-4_GeoframeworkDomain)

Figure 3-4. Extent of the HSGF Domain

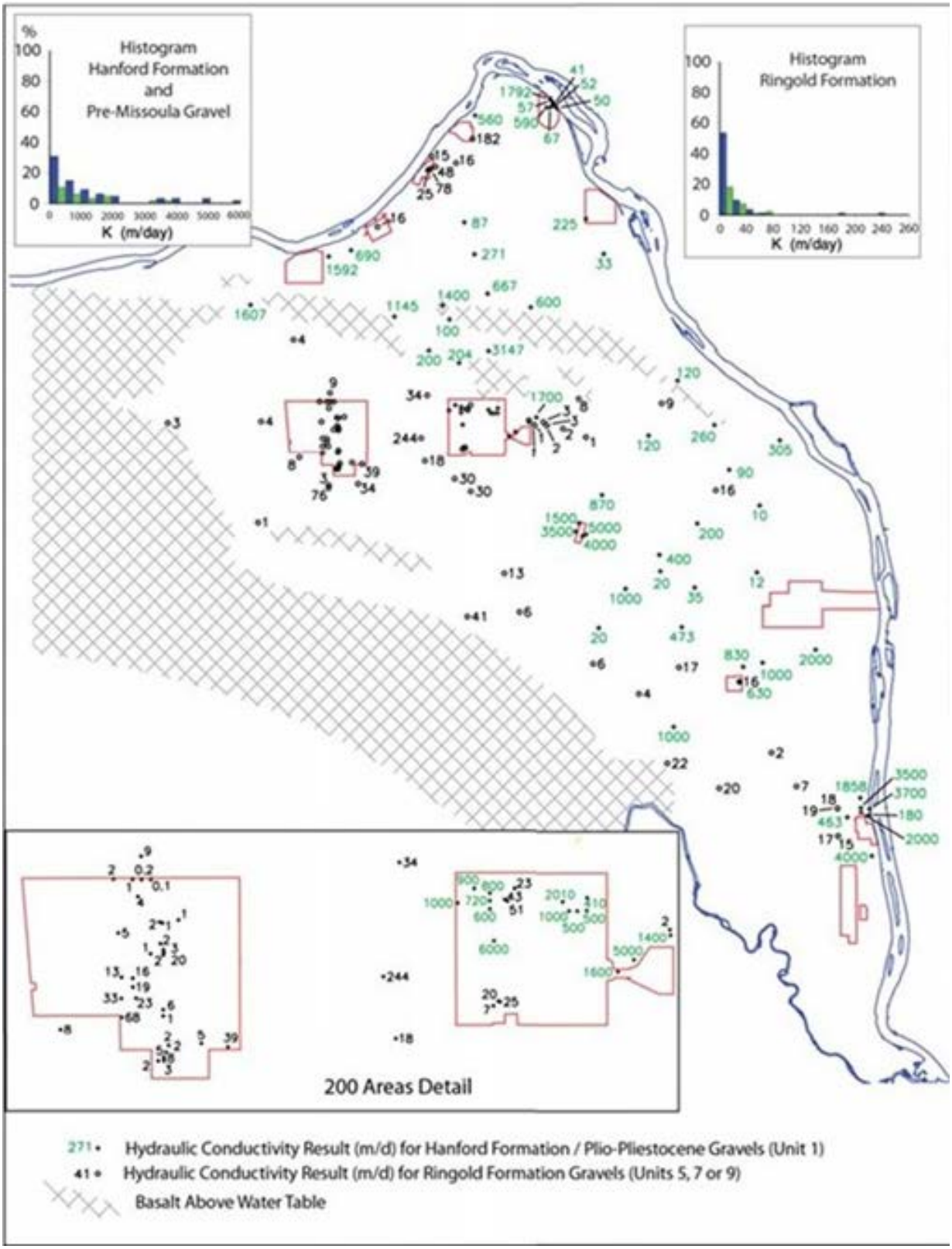

Source: PNNL-13641, *Uncertainty Analysis Framework – Hanford Site-Wide Groundwater Flow and Transport Model*.

Figure 3-5. Map Indicating the Spatial Variability of Hydraulic Conductivity Values at the Hanford Site

An updated review of Ringold unit E properties was conducted to develop the 200-ZP-1 Model (DOE/RL-2007-28). Figure 3-6 presents a distribution of hydraulic conductivity estimates derived from hydraulic testing. The figure contains data summarized from slug tests and sediment sample analysis, whereas the data summarized in Table 3-1 are limited to pumping test analysis.

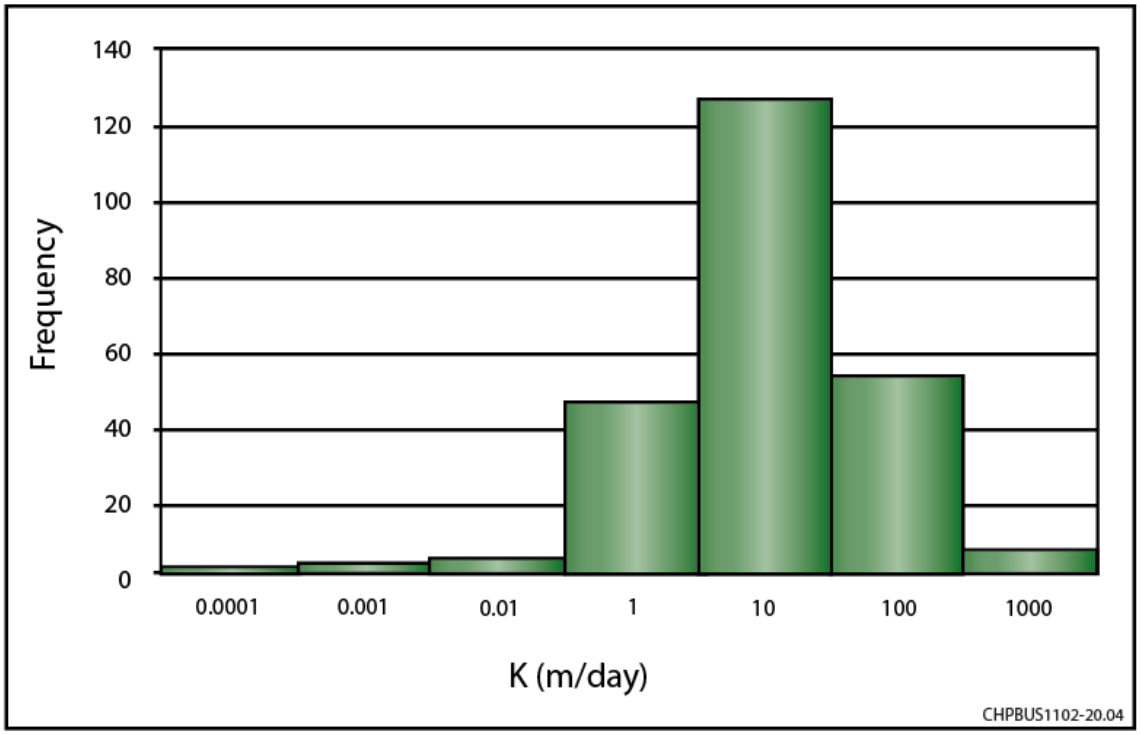

Source: DOE/RL-2007-28, *Feasibility Study Report for the 200-ZP-1 Groundwater Operable Unit.*

Figure 3-6. Hydraulic Conductivity Distribution Ringold Unit E

Vertical anisotropy has been estimated for pumping tests in Ringold unit E and for at least one test in the Hanford formation. Ringold unit E values range from 0.01 to 0.1 (PNL-10886) and 0.015 to 0.5 (DOE/RL-2007-28) for post-2000 testing. A Hanford formation estimate is 0.1 (Hanford Environmental Information System [HEIS] hydraulic properties database). Previous calibrations (prior to development of the P2R Model) found the calibration to be relatively insensitive to vertical anisotropy. This is largely because of the large horizontal scale of most modeling analyses (and lateral extent of the simulated HSUs) versus the relatively small vertical extent of the modeling analyses, and of the simulated HSUs. In addition, most wells are screened across the water table. There are few instances of multiple zones of measurement with depth. Therefore, anisotropy ratios obtained from (1) large-scale, site-specific pumping tests such as those recently conducted in the 200-ZP-1 OU; and (2) literature values for equivalent or similar aquifer materials are considered the most reliable source for this value. A value of 0.1 was assumed for all layers in the prior three-dimensional models (PNNL-14398; PNNL-14753, DOE/EIS-0391).

Specific yield has been estimated from tests of the Hanford formation and Ringold Formation. as presented in Table 3-2. Ringold units A and E are jointly described in PNL-10886. These models encompass a larger domain than the P2R Model. The models had the same water-level measurements over a larger domain that is available and showed limited sensitivity to specific yield. Only the specific yield of the Ringold unit E was modified in the calibration described in PNNL-14753. Specific yield was not estimated for the model described in PNNL-14398.

Table 3-2. Review of HSU Specific Yield

Unit	PNL-10886 Hydraulic Test Data (dimensionless)	PNNL-13641 Hydraulic Test Data (dimensionless)	PNNL-14753 Assumed (dimensionless)	DOE/EIS-0391 (dimensionless)
Hanford	0.1 - 0.3	0.2 - 0.37	0.1	0.15-0.3
Cold Creek			0.1	
Ringold E	0.05 - 0.2	0.05 - 0.37	0.11	
Ringold mud			0.1	
Ringold A	0.05 - 0.2	0.15	0.1	

Aquifer storage parameter estimates are available as part of EMDT-HP-0010 (Appendix G). There are 43 estimates of storativity that are accompanied by an estimate for saturated thickness. The geometric mean of the specific storage values calculated from the storativity data is 1.9 x 10^{-5} 1/m. *Field Test Report: Preliminary Aquifer Test Characterization Results for Well 299-W15-225: Supporting Phase I of the 200-ZP-1 Groundwater Operable Unit Remedial Design*, PNNL-18732, provides a recent analysis of storage coefficients within 200-ZP-1 OU located in the 200-West area. The results of the analysis of 3-day constant rate pumping test were a storativity value of 9.7 x 10^{-4} (dimensionless). The reported saturated thickness of 55.4 m produces a specific storage of 1.7 x 10^{-5} 1/m. DOE/RL-2015-75 provides results of 3-day constant rate testing in 200-East are conducted in October 2015. The geometric mean of specific storage data from the aquifer testing analysis estimate a value of 2.6 x 10^{-5} 1/m.

3.2 Modeling-Related Features, Events, and Processes

This section summarizes the relevant FEPs to be included and excluded from the P2R Model. The list of exclusions is not exhaustive; it is intended to be extensive enough to support the identification of model limitations addressed in Chapter 6.

The most comprehensive application of the FEPs methodology at the Hanford Site to date is presented in BHI-01573, *The Groundwater/Vadose Zone Integration Project: The Application of Feature, Event, and Process Methodology at the Hanford Site*, and discussed in Last et al., 2004, "A Comprehensive and Systematic Approach to Developing and Documenting Conceptual Models of Contaminant Release and Migration at the Hanford Site." The Hanford FEPs identified in BHI-01573 are identified in this report as either included or excluded. Additional FEPs not listed as Hanford FEPs that are considered have been added to the list. Table 3-3 lists the Hanford FEPs (if identified in BHI-01573), including the Hanford FEP number and the name of the FEP. A column labeled "Included" indicates whether the FEP is included in the historical period flow model (described in this report); used for predictive model flow and transport; or has not yet been not included in either phase, using the indicator terms "Flow," "F&T," and "No," respectively. In the final column labeled "Relevant to P2R Model," "Yes" identifies FEPs that are relevant to flow and transport in the P2R Model domain, and "No" indicates no relevancy. Many Hanford FEPs that could affect flow in the Central Plateau are listed as not relevant based on the assumption of geologic stability for the period to be simulated with this model or because they were rated low or moderate priority in the Hanford FEP evaluation for the groundwater technical element in BHI-01573.

Table 3-3. Hanford Features, Events, and Processes

Hanford FEP Number	Name	Included	Relevant to P2R Model
2.2.07.30	Groundwater flow (in geosphere).	Flow	Yes
3.2.07.35	Groundwater discharge to surface. Groundwater and associated contaminants (either solutes for suspended particulates) may eventually discharge to the Columbia River, to seeps near the river, to springs, or to wells.	Flow	Yes
2.2.07.51	Far-field transport; hydrodynamic dispersion.	F&T	Yes
2.2.04.01	Faulting (large scale, in geosphere). Hydraulic influence of May Junction Fault.	Flow	Yes
1.4.04.00.04	Future liquid waste disposal.	F&T	Yes
1.4.04.00.17	Water resource exploration.	No	Yes
1.1.11.00.02	Post closure monitoring.	No	Yes
2.3.11.13	Groundwater discharge. The Columbia River is the principal discharge area for the unconfined aquifer system. In this model, the discharge to the Columbia River is not directly modeled because the model domain does not extend to the river, but it is implicitly included with mixed type boundary conditions that represent the discharge to the river.	F&T	Yes
2.3.11.14	Groundwater recharge. Recharge issues related to groundwater flow and contaminant transport within the context of a conceptual model of the natural system on a large scale. Recharge refers to input of water to the groundwater flow system. Recharge of the uppermost unconfined aquifer takes place from infiltration of precipitation, particularly in elevated regions along the western boundary of the Hanford Site, from infiltration of imported water disposed to waste sites, leaked from distribution systems, and applied for irrigation, and from upward leakage from the deeper confined aquifer system. These are all included except for upward leakage from the deeper confined aquifer system, which is excluded from the model at present.	Flow	Yes
	Basalt surface. Section 3.2.4 discusses the assumption that the basalt surface is an impermeable lower boundary.	Flow	Yes
	Groundwater remedial actions (pump-and-treat systems).	Flow	Yes
	Spatial variability. Hydraulic property variation by HSU with differential vertical and horizontal hydraulic conductivity.	Flow	Yes
1.2.02.01.00	Fractures in basalt. The CRBG basalt is not explicitly simulated as part of this model as discussed in Section 3.2.4.	No	Yes
1.2.02.02.00	Faulting (movement along existing faults).	No	No
1.2.03.01.00	Seismic activity.	No	No
1.2.04.01.00	Magmatic activity affects hydrothermal conditions.	No	No
1.2.04.02.00	Magmatic activity affects hydrothermal conditions.	No	No
1.4.04.02.00	Abandoned and undetected boreholes.	No	No

Table 3-3. Hanford Features, Events, and Processes

Hanford FEP Number	Name	Included	Relevant to P2R Model
3.2.07.01.00	Isotopic dilution.	No	No
1.2.10.01.00	Hydrological response to seismic activity.	No	No
1.2.01.01.01	Folding, uplift, or subsidence lowers facility with respect to the current water table.	No	No
1.2.02.01.01	Changes in hydraulic properties of sediments (due to compaction).	No	No
1.2.04.01.01	Volcanism.	No	No
1.4.04.02.01	Exploratory borehole creates flow pathway.	No	No
1.2.10.01.01	Fault movement pumps fluid from saturated to unsaturated zone (seismic pumping).	No	No
1.2.01.01.02	Tectonic changes to local geothermal flux causes convective flow in saturated zone and elevates water table.	No	No
3.2.07.01.02	Natural radionuclides/elements (in host rock disturbed zone).	No	No
1.2.10.01.02	Fault creep causes short term fluctuations of the water table.	No	No
1.4.04.02.03	Waste-induced borehole flow (in waste and engineered barrier system).	No	No
1.2.10.01.03	New faulting breaches flow barrier controlling large hydraulic gradient to the north.	No	No
1.2.01.01.04	Uplift or subsidence changes drainage at site, increasing infiltration.	No	No
1.2.02.02.04	Movements along small-scale faults.	No	No
1.2.04.02.04	Igneous activity causes extreme changes in rock geochemical properties.	No	No
1.4.04.01.05	Drilling fluid flow.	No	No
1.4.04.02.05	Natural borehole fluid flow.	No	No
1.2.01.01.06	Effect of plate movements.	No	No
1.2.01.01.09	Regional vertical movements.	No	No
1.4.04.00.01	Geothermal (drilling associated with exploitation of geothermal sources).	No	No
1.4.04.00.02	Other resources (drilling to explore for other resources).	No	No
1.4.04.00.03	Enhanced oil and gas recovery.	No	No
1.4.04.00.05	Hydrocarbon storage.	No	No
1.4.04.00.06	Exploratory drilling for hydrocarbons.	No	No
1.4.04.00.07	Blowouts.	No	No
1.4.04.00.24	Oil and gas extraction.	No	No
1.4.04.00.25	Liquid waste disposal from oil and gas production.	No	No

Table 3-3. Hanford Features, Events, and Processes

Hanford FEP Number	Name	Included	Relevant to P2R Model
1.4.04.00.26	Enhanced oil and gas production.	No	No
1.1.11.00.01	Monitoring. Boreholes used to monitor performance could provide pathways for contaminant transport between different hydrogeological formations.	No	No
1.2.10.01.10	Fault establishes pathway through the saturated zone.	No	No
1.2.01.01.12	Regional horizontal movements.	No	No
	Vadose zone flow. This model is restricted to the fully saturated unconfined aquifer; therefore, vadose zone flow and transport is not included directly. However, the inclusion of the attenuating impact of the presence of the vadose zone is indirectly incorporated through the use of vadose zone simulated artificial recharge.	No	Yes
	Perching of artificial recharge, discussed in Section 3.2.2.	No	Yes
	Climate change. This model is restricted to recharge conditions that reflect current climate and does not incorporate climate change effects.	No	Yes
	Dam failure. Potential contaminant transport due to flooding of the site caused by upstream dam failure is not considered in the analysis.	No	Yes

CPGW Model = Central Plateau Groundwater Model
F&T = fate and transport
FEP = features, events, and processes
HSU = hydrostratigraphic unit

3.2.1 Anthropogenic Recharge

Wastewater discharges associated with activities at the Hanford Site were significant sources of water to the subsurface, at times exceeding tens of millions of cubic meters per year (Figure 3-7). Some of the largest sources of process-related water to the subsurface included T Swamp, U Pond (216-U-10), 216-U-14 Trench, B Pond (216-B-3), 200 Area Treated Effluent Disposal Facility (TEDF), and Gable Mountain Pond. These large releases exerted significant control on the rates and directions of groundwater flow and contaminant migration. The effects of the releases continue to exert some influence as the water table recovers to pre-development conditions. Detailed descriptions of various sources of recharge are provided in several publications, including PNL-6403, *Recharge at the Hanford Site: Status Report*; and PNL-10285, *Estimated Recharge Rates at the Hanford Site*. Both anthropogenic and natural sources of water must traverse a thick, unsaturated (vadose) zone to reach (and ultimately recharge) the unconfined aquifer beneath.

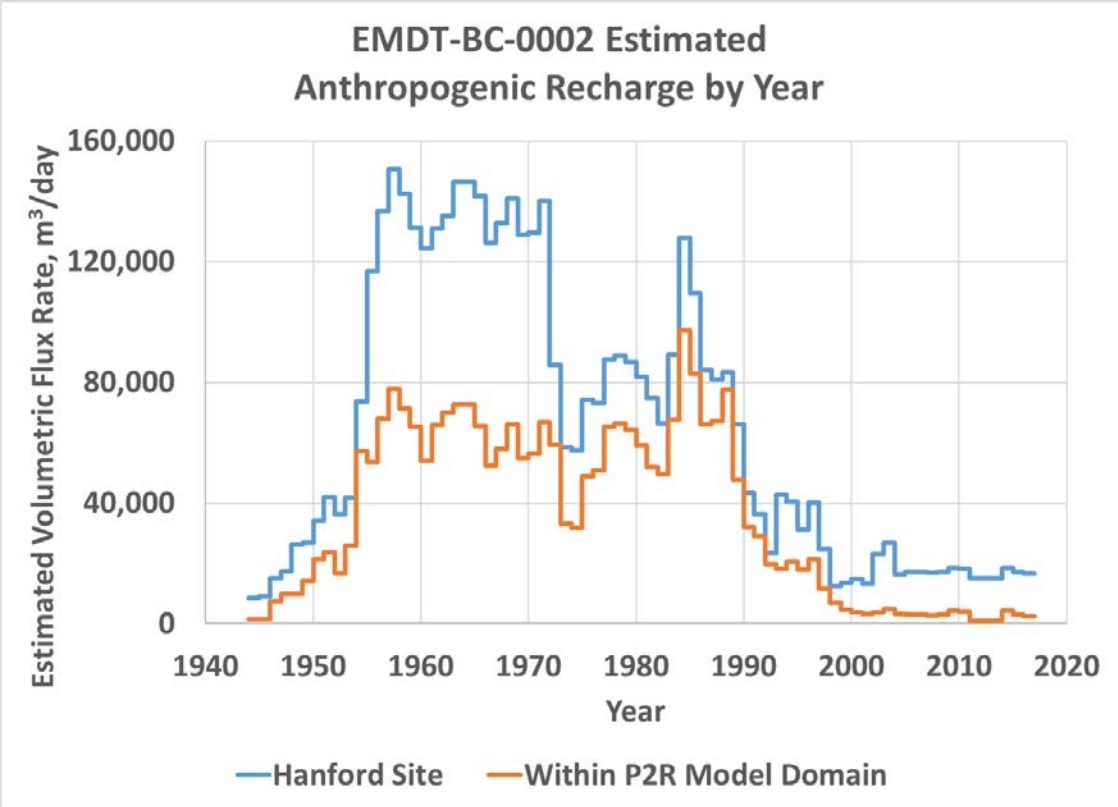

Figure 3-7. Historical Anthropogenic Recharge (1944 to 2016)

Arrival of surface discharges at the water table, where they provide recharge to the aquifer, is attenuated and delayed by the unsaturated zone. A vadose zone transmission of liquid discharges was simulated for each discharge site as a part of the EMDT-BC-0002, *Vadose Zone Attenuated Artificial Recharge for Input to a Ground Water Model* (Appendix E). Figure 3-8 presents the effects of simulated vadose zone attenuation and delay for the sum of all liquid discharge sites at the Hanford Site. The gray line in this figure is the discharge rate to the surface; the green line is the arrival of water flux at the water table. The discharge rates are plotted as "m^3/yr" over the length year for surface discharges and length of each calculation time step for the water table arrival. The results of these calculations were used to specify artificial recharge for the P2R Model in the historical period with the water table arrival averaged over each year. Because PNNL-14573 does not include the observed discharges from 2009, surface discharges occurring after 2009 have been applied directly to the water table rather than through the vadose zone simulation.

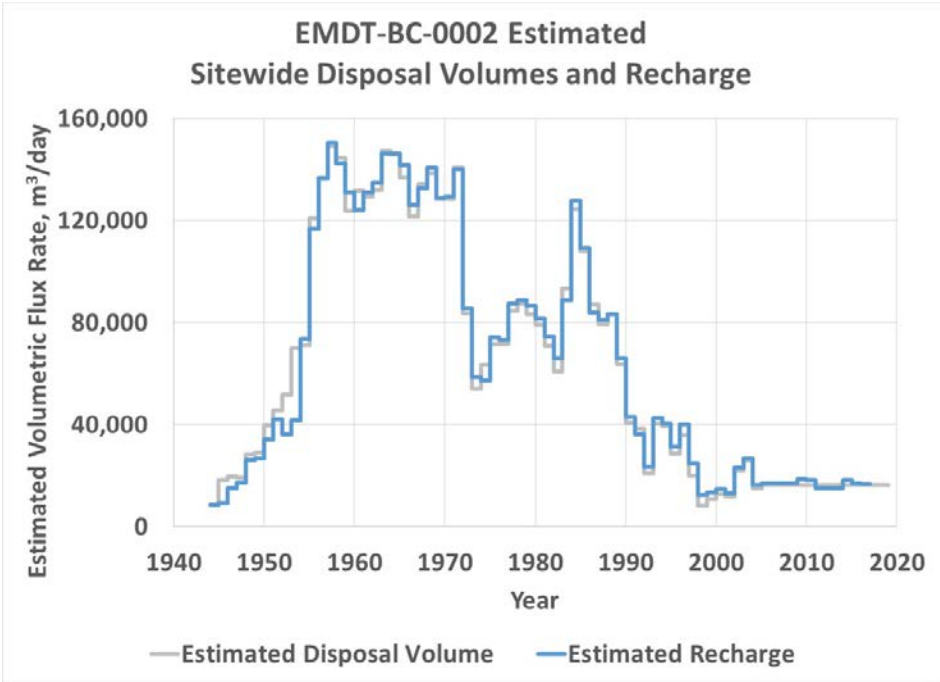

Figure 3-8. Liquid Disposals at Surface and Vadose Zone Simulated Artificial Recharge for the Sum of All Hanford Site Liquid Discharges (1944 to 2000)

3.2.2 Perching of Anthropogenic Recharge

There is evidence indicating that perching has occurred, influencing flow in the saturated aquifer. Perching is not included in the P2R Model as a simulated process. Some investigations have revealed large perched water bodies in the 200-West Area. Figure 3-9 illustrates locations and features that are mentioned in the summaries of the evidence of perching discussed below.

- In 1948, the Office of the Atomic Energy Commission discovered perched conditions in two of the 25 wells drilled during the investigation. In one well (identified today as well 699-45-69A), 1.6 to 3 m (5.2 to 9.8 ft) of water was found at an elevation of approximately 169 m (554.5 ft), which was approximately 43.6 m (143 ft) above the water table. The 169 m (554.5 ft) measurement is very close to the top of the CCU in this area (Figure 3-9), but the driller's log does not indicate a change in geologic unit at this elevation. This well is more than 2 km (1.2 mi) west of T Swamp, the largest known wastewater discharge location at that time. Perched water was also found in well 699-35-70, located 2 km (1.2 mi) or more south of T Swamp. The perched zone was thinner and lower (137 m [449.5 ft] elevation) than found in well 699-45-69A. The perched zone is well below the top of Ringold unit E.

- Well 699-35-78A was drilled in 1950. The following description is based on the driller's log available in the HEIS database. A saturated layer of water at an elevation of 128 m (419.9 ft) was found. Below an elevation of 127 m (416.7 ft), the well was dry again. It was cased and remained dry over a weekend until an elevation of 121.5 m (398.6 ft) was reached. The well then filled overnight to 128 m (419.9 ft). The rapid rise suggests that once the 121.5 m (398.6 ft) elevation was reached, the well was in hydraulic contact with the same body of water found at 128 m (419.9 ft). A 128 m (419.9 ft) water table elevation is consistent with other wells in the area. It is inferred that near the well, water was perched on a low-conductivity lens of Ringold unit E at 128 m (419.9 ft), but away from the well it was part of the saturated aquifer at nearly the same elevation. Alternately, the lens is

saturated but has so little conductivity that only a non-measurable amount of water entered the well over the weekend.

- A 1994 investigation of perching below the 216-U-14 Ditch identified perched conditions in wells 299-W19-91, 299-W19-92, 299-W19-93, 299-W18-250, 299-W18-251, and 299-W23-27, but not in well 299-W23-22 (WHC-EP-0698-FP, *Groundwater Impact Assessment Report for the 216-U-14 Ditch*). Perching was considered to be of limited extent beyond the ditch. The top of the perched zone in wells 299-W19-91, 299-W19-92, and 299-W19-93 varied between 190 and 169 m (623.4 and 554.5 ft) elevation from 1990 through 1994. The perched zone was presumed to extend downward to the top of the CCU, which is at an elevation of approximately 165 m (541.3 ft) at this location.

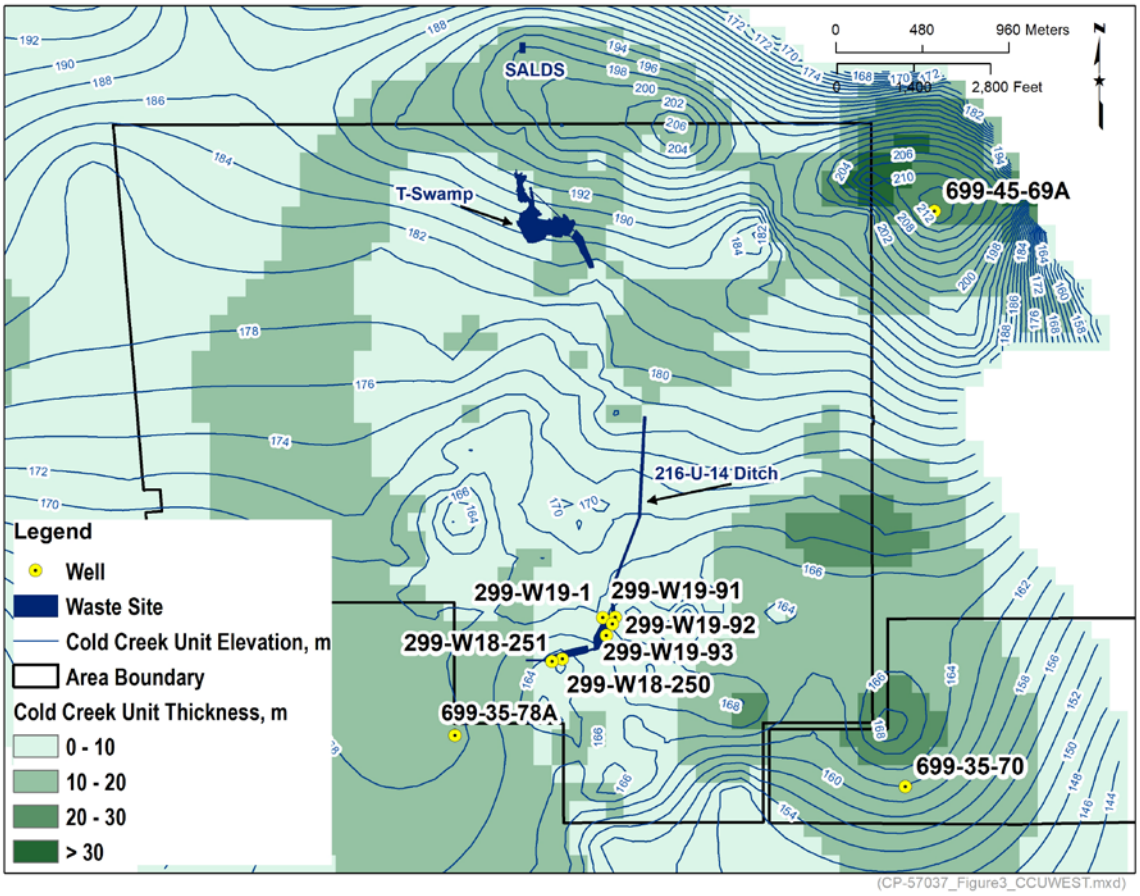

Figure 3-9. Top of Carbonate Facies of the CCU

- In two-dimensional simulations of a perched water table under a generic 200-West Area waste site incorporating the dip of the CCU, it was calculated that 99% of the water would exit the down-dip side of the simulation rather than directly below the discharge location (WHC-SA-0699-FP, *Effects of Varying Recharge on Radionuclide Flux Rates to the Water Table at the Low-Level Solid Waste Burial Site*).

- Mounding evaluations in the unconfined aquifer (in response to discharges at the SALDS) (Figure 3-9) suggest that the mounding is centered on an area laterally displaced from the SALDS effluent infiltration gallery. This lateral displacement arises from the movement of the discharge

water along the CCU (SGW-42604, *Results of Tritium Tracking and Groundwater Monitoring at the Hanford Site 200 Area State-Approved Land Disposal Site, Fiscal Year 2009*).

These five investigations suggest that perched water has occurred during the Hanford Site operational period and these areas of perching may have stored substantial volumes of water. In addition, there may have been lateral migration of water infiltrating through the vadose zone en route to the water table of the unconfined aquifer. The perching appears to have developed above the calcified CCU, and on low-conductivity lenses of Ringold unit E.

3.2.3 Natural Recharge

Natural recharge from precipitation at the Hanford Site is highly variable both spatially and temporally, ranging from near zero to more than 100 mm/yr depending on climate, vegetation, and soil texture (Gee et al., 1992, "Variations in Recharge at the Hanford Site"; PNL-10285). Vegetative areas and fine-texture, soil-like silt loams tend to have lower recharge rates, while areas with little vegetation and coarse-texture soil (e.g., dune sands) tend to have higher recharge rates. PNL-10285 developed estimates of natural recharge for 1992 conditions using a step-by-step procedure. First, distributions of soil and vegetation types were mapped. Then a recharge rate was assigned to each combination of soil/vegetation type based on data from lysimeters, tracer studies, neutron probe measurements, and computer modeling. The data used for these estimates were derived from a number of sources, such as distribution of recharge estimated using the 1992 climate, a 1966 soil map (BNWL-243, *Soil Survey Hanford Project in Benton County Washington*), and 1979 vegetation/land-use patterns. Estimated recharge rates for 1992 ranged from 2.6 to 127 mm/yr, and the total volume of natural recharge from precipitation over the Hanford Site was estimated to be 2.35×10^4 m^3/d. This value is of the same order of magnitude as the artificial recharge to the 200 Areas waste disposal facilities during 1992 and approximately one-sixth of peak discharges to these facilities during the 1960s (PNNL-14753). The 1992 estimates were used in the calibration of the 2005 model (PNNL-14753).Natural recharge includes both percolation of net precipitation to the water table and mountain-front recharge arising from infiltration of snowmelt, agricultural return-flows from irrigation, and runoff from elevated areas. The same pattern of natural recharge used in PNNL-14753 was adopted in the construction of the P2R Model version 8.2.

The major source of mountain-front recharge to the P2R Model is Rattlesnake mountain. Rates of net recharge from aerial precipitation were attained from PNNL-14753. Recharge associated with stream flows is a significant contributor to groundwater recharge upgradient of the Central Plateau (PNNL-17841, *Compendium of Data for the Hanford Site (Fiscal Years 2004 to 2008) Applicable to Estimation of Recharge Rates*). Since the amount of recharge occurring through the mountain front recharge at Rattlesnake Mountain is uncertain, the value has been included in the model and varied as calibration parameter. Previous estimates from model calibration ranged from 3,104 to 5,825 m^3/day. Figure 3-10 shows the area on the Hanford side of Rattlesnake Mountain above the active model domain. Multiply this area by the calibrated recharge values from the CPGW Model version 8.4.5 for silty sand and sand produce recharge volumes from this portion of the site ranging from 454 to 2,400 m^3/day, respectively. The small amounts of recharge from runoff of Gable Mountain, Gable Butte, and the basalt subcrop along the boundary of the model south of 200-West Area will not be included in the modeling.

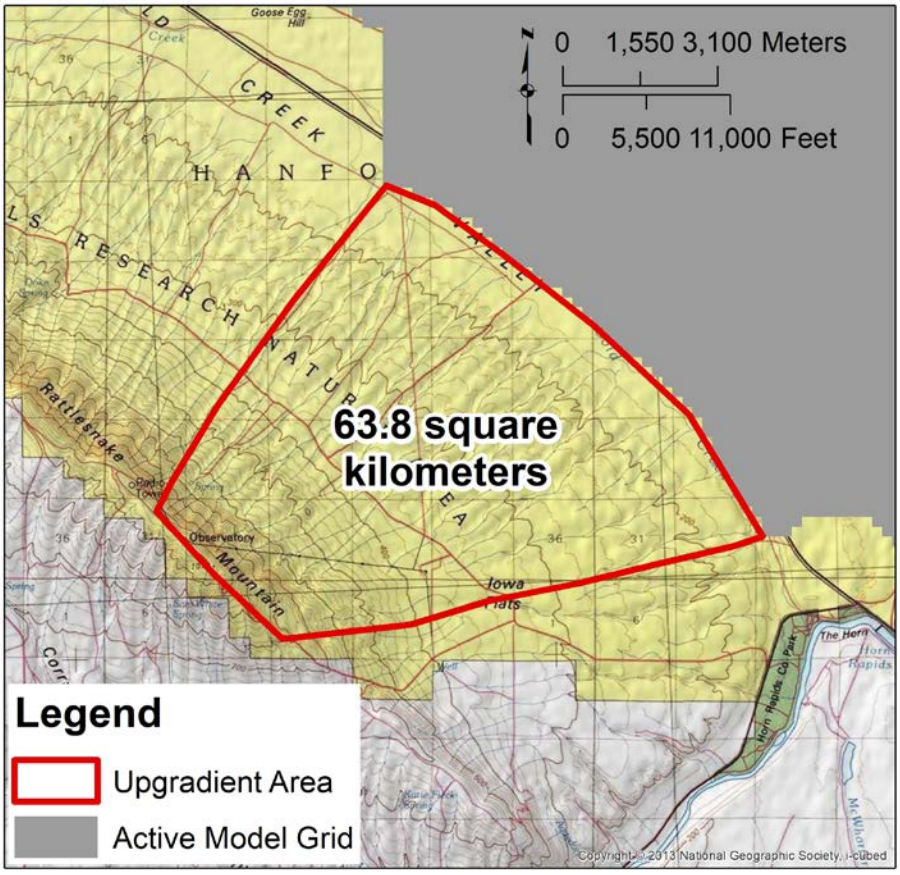

Figure 3-10. Area Upgradient of The Western Portion of the Model Domain that will Simulate Mountain Front Recharge for Rattlesnake Mountain

3.2.4 Basalt Surface Fluxes

The Hanford Site is located within the CRBG area, which comprises hundreds of stacked basalt flows throughout southern/eastern Washington, northeastern Oregon, and western Idaho. Results of studies completed at the Hanford Site specifically, and throughout the CRBG area, generally indicate that the basalt flows can be categorized broadly as a sequence of dense, low-permeability flow interiors. These are separated by more permeable interflow zones, which comprise the base of an overlying flow and the top

of the underlying flow, with occasional intermediate clastic sediments. In some locations throughout the CRBG area, these interflow zones are substantial enough to comprise aquifers.

The P2R Model is constructed based on the assumption that basalt forms an impermeable base to the unconfined aquifer. However, evidence exists showing the unconfined aquifer overlies and is connected with interflow zones. Upward and/or downward flow may occur between the unconfined clastic sediments and the basalt interflow. This process is not included in the current version of the P2R Model.

The process was investigated as a part of an alternate conceptual model investigation (PNNL-13623, *Transient Inverse Calibration of Site-Wide Groundwater Model to Hanford Operational Impacts from 1943 to 1996—Alternative Conceptual Model Considering Interaction with Uppermost Basalt Confined Aquifer*; PNNL-13641). The distributed flux through basalt was estimated using a three-dimensional inverse calibration (PNNL-13623) and considering the following types of leakage:

- Head-dependent spatially distributed leakage through the basalt-confining layer
- Increased leakage at an erosional window near Gable Mountain/Gable Butte
- Increased leakage at a smaller erosional feature near B Pond
- Increased leakage along two fault zones

PNNL-13623 and PNNL-13641 used older interpretations of the basalt surfaces, so the elevation contours illustrating the topography of the basalt surface are not based on the most current estimate of basalt elevation. The basalt elevation contours have been updated in SGW-48478, *Interpretation and Integration of Seismic Data in the Gable Gap*. However, presenting the previous older interpretations provides the basis used to determine that the P2R Model should treat the basalt as a no-flow boundary in the model.

Figure 3-11 shows the distribution of basalt surfaces for members of the Ellensburg Formation (Figure 3-1) that have been exposed due to upper basalt erosion. The erosion also exposed the Rattlesnake interbed, a permeable sedimentary confined aquifer below the topmost Elephant Mountain Member that forms the basalt surface below most of the Central Plateau. Basalt flow tops between members can also host permeable aquifers. The model described in PNNL-13623 included the roughly circular central core of the erosional window as a special surface flux feature. Thinning of the Elephant Mountain Member was simulated near B Pond. The larger contact with the Rattlesnake interbed north of B Pond was apparently not recognized at the time.

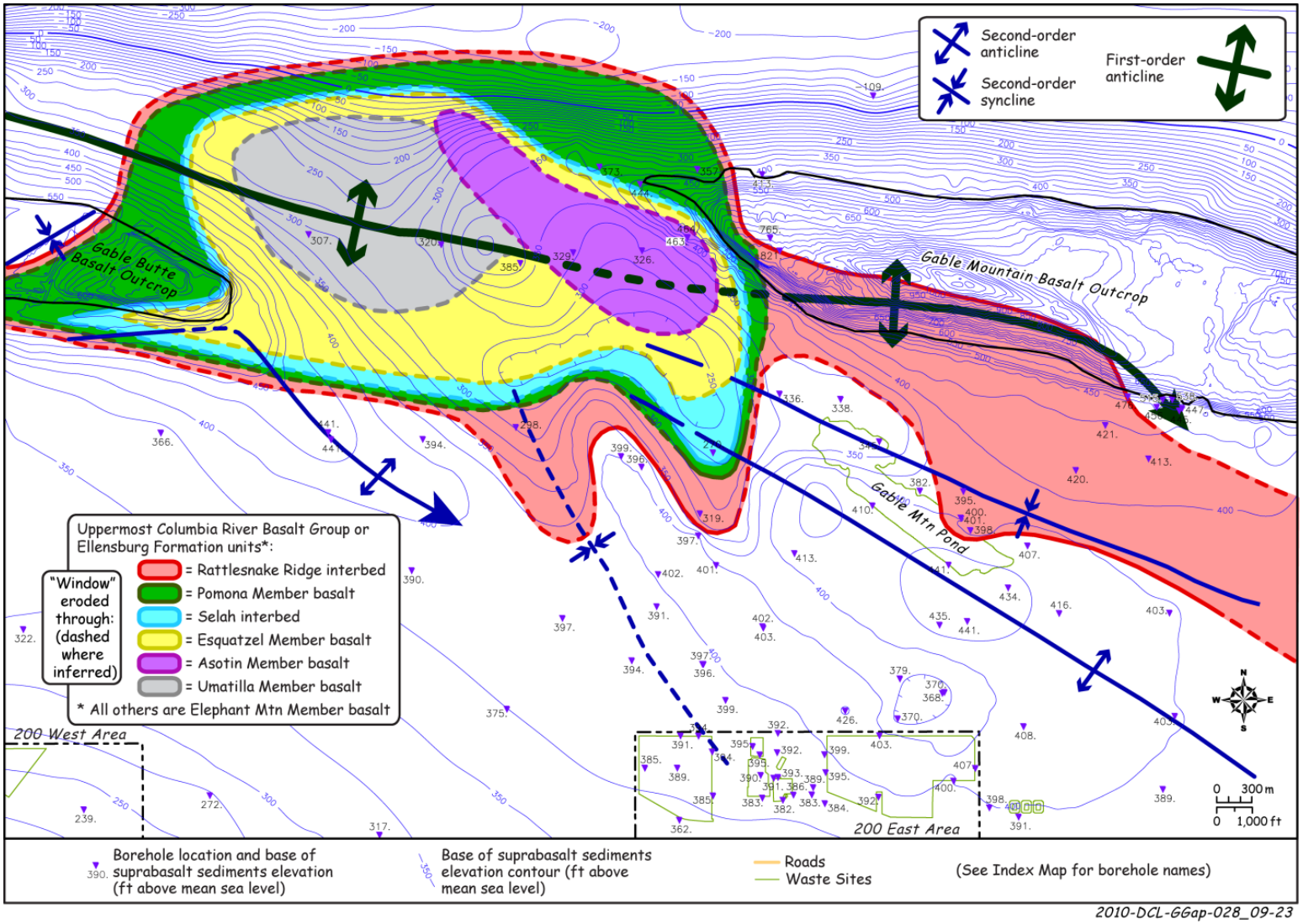

Source: PNNL-19702, *Hydrogeologic Model for the Gable Gap Area, Hanford Site*.

Figure 3-11. Map of Upper Confined Basalt Aquifer (Pink) Contact with Unconfined Aquifer of the CPGW Model

Figure 3-12 displays the location of four fault zones on the Hanford Site. The simulation described in PNNL-13623 included the two thrust fault zones. These faults are locations of discontinuity in the basalt, and hydraulically they may be locations of concentrated flux through the basalt/sedimentary aquifer interface. The two normal faults were not expected to be major contributors of flux. Limited portions of the Gable Mountain and Yakima Ridge faults cross the domain of the P2R Model. These locations are near the boundaries of the model.

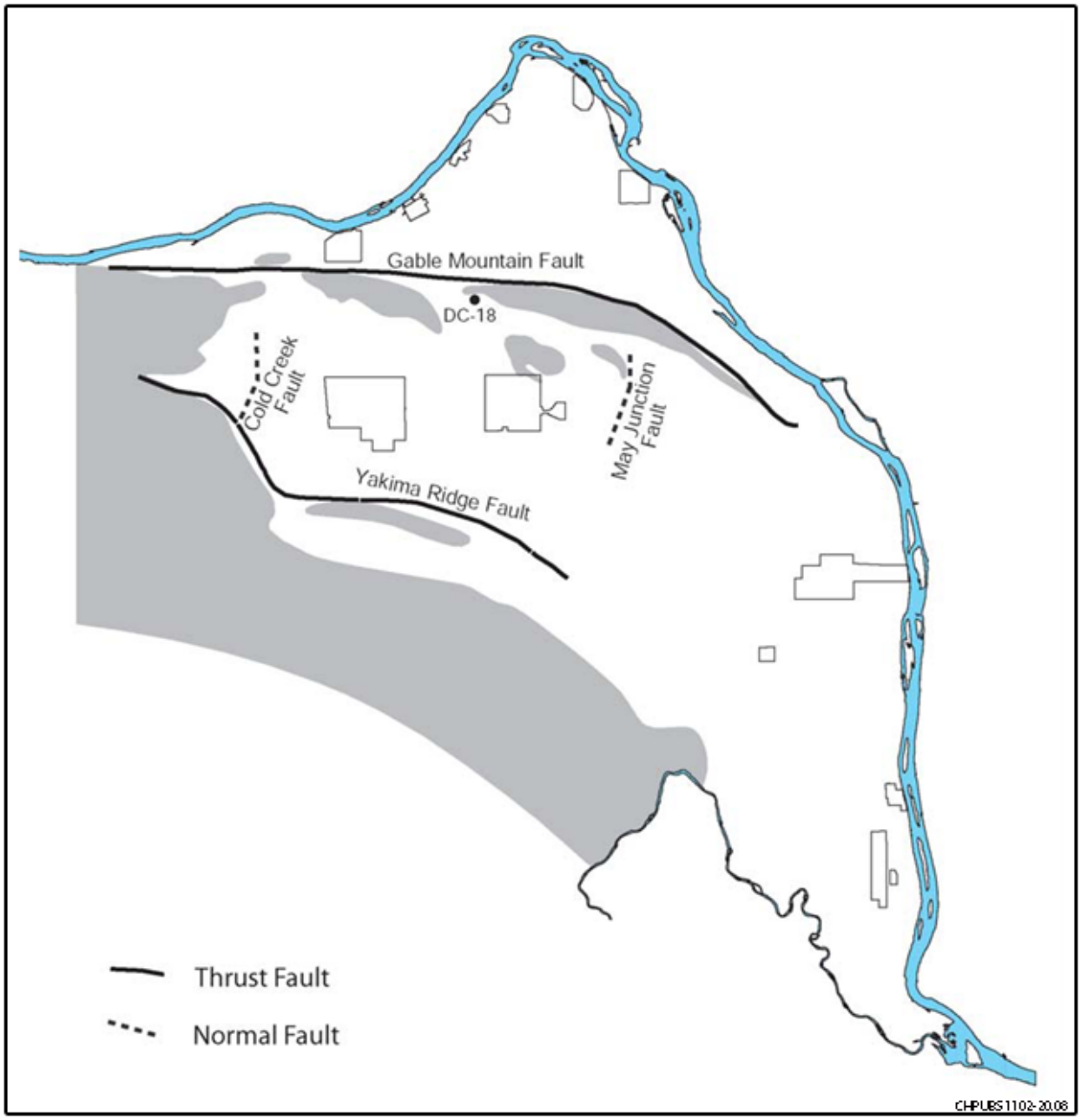

Source: PNNL-13623, *Transient Inverse Calibration of Site-Wide Groundwater Model to Hanford Operational Impacts from 1943 to 1996—Alternative Conceptual Model Considering Interaction with Uppermost Basalt Confined Aquifer*.

Figure 3-12. Location of Thrust and Normal Faults on the Hanford Site

Figure 3-13 depicts the estimated distributed flux across the basalt surface and erosional window for 1996. Closer inspection reveals much larger fluxes adjacent to the Columbia River as well as both upward and downward flux in the Central Plateau area in the figure. Figure 3-14 presents the estimates for cumulative upward, downward, and net distributed flux as a function of time. Figure 3-15 allows for comparison of the significance of each feature investigated, revealing that the distributed fluxes dominate the net fluxes. The erosional window and Yakima Ridge fault are also relatively minor contributors. Estimated flux of the Gable Mountain fault is relatively larger to other fluxes. Within the Central Plateau, the estimated basalt surface fluxes are small relative to an average 180,000 m^3/d anthropogenic recharge for 1980 (Figure 3-6). Fluxes through the basalt surfaces were not included in subsequent versions of the PNNL site-wide groundwater model. Because of the thinness of the aquifer, fluxes to and from the basalt surface have similar impact on simulated water levels as changes in natural recharge rates. It was concluded that neglecting basalt surface flux in these later models was compensated by the increased estimated precipitation recharge of 26,000 m^3/d (in the calibration described in PNNL-14753) over cumulative reported recharge determined by PNL-10285 (PNNL-14753, p. 5.8). A similar approach was used in the TC & WM EIS groundwater flow model (DOE/EIS-0391) where the groundwater model base is defined as the top of the CRBG basalts with no simulated interaction between the two aquifers.

3.2.5 Basalt Ridge Flow Barrier

Figure 3-16 presents an estimate of the top of the CRBG throughout the Gable Gap area of the Hanford Site, as developed in SGW-48478. The estimate was based on well data, seismic surveys, and previous work indicated by the locations shown in the figure. Even though SGW-48478 provides the most current, up-to-date estimate for basalt elevation, uncertainty exists on the configuration of any paleochannels and low elevations that may influence groundwater flow as a preferential pathway. However, the top-of-basalt estimate does provide likely low points that could provide for groundwater flow through Gable Gap as the water level slowly decreases.

Grand Coulee channeled scabland is an example of features that may exist in and south of Gable Gap. The scabland is about 150 km (93.2 mi) north of the Hanford Site. Figure 3-17 depicts the Lower Grand Coulee channeled scabland carved out by the Missoula floods. The figure shows multiple variations in surface elevation over distances that are small compared to the well spacing used to control the surface of the basalt in the Gable Gap area of the P2R Model. Being upstream of the Hanford Site, the erosional forces were larger at Grand Coulee, so the scale of erosional features is larger but similar to what would be expected in the 200-BP-5 OU. Figure 3-17 conveys the concept regarding the similarity of 200-BP-5 OU basalt to the Grand Coulee scablands, as it is impossible to estimate with high confidence the basalt surface elevations at the scale of the model cells within a meter (based on limited borehole contact information).

Water levels have dropped an average rate of about 0.14 m/yr (0.46 ft/yr) in the northern portion of the 200-East Area since the cessation of most surface water disposal (PNNL-15837, *Data Package for Past and Current Groundwater Flow and Contamination Beneath Single-Shell Tank Waste Management Areas*). If the water table drops far enough , the high ridge of basalt northeast of the 200-East Area will form a flow barrier between the 200-East Area and Gable Gap, effectively stopping the current flow direction northward from the Central Plateau. The timing of closure will affect contaminant transport.

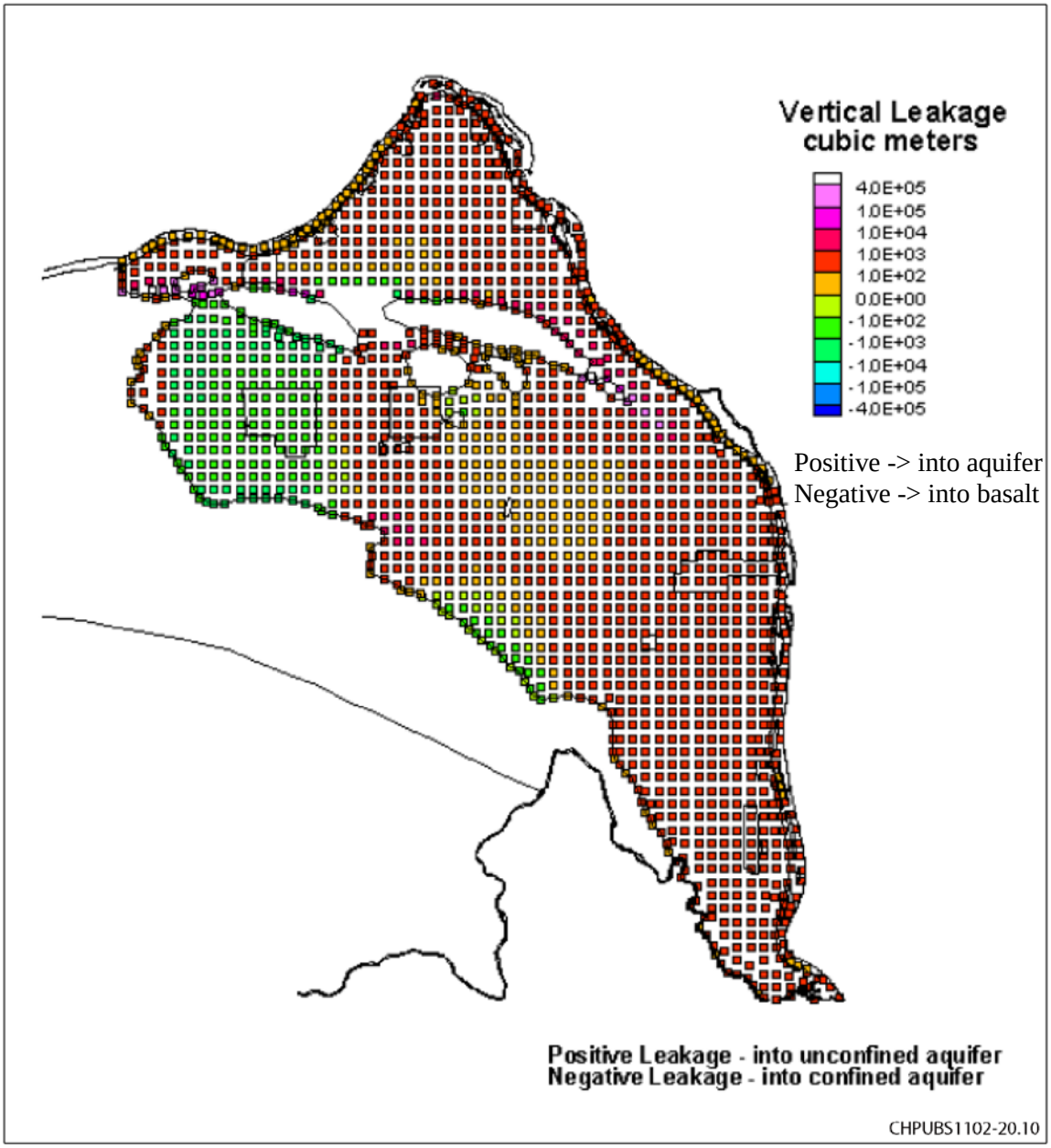

Source: PNNL-13623, *Transient Inverse Calibration of Site-Wide Groundwater Model to Hanford Operational Impacts from 1943 to 1996—Alternative Conceptual Model Considering Interaction with Uppermost Basalt Confined Aquifer.*

Figure 3-13. Estimated Flux across Upper Basalt Surface for 1996

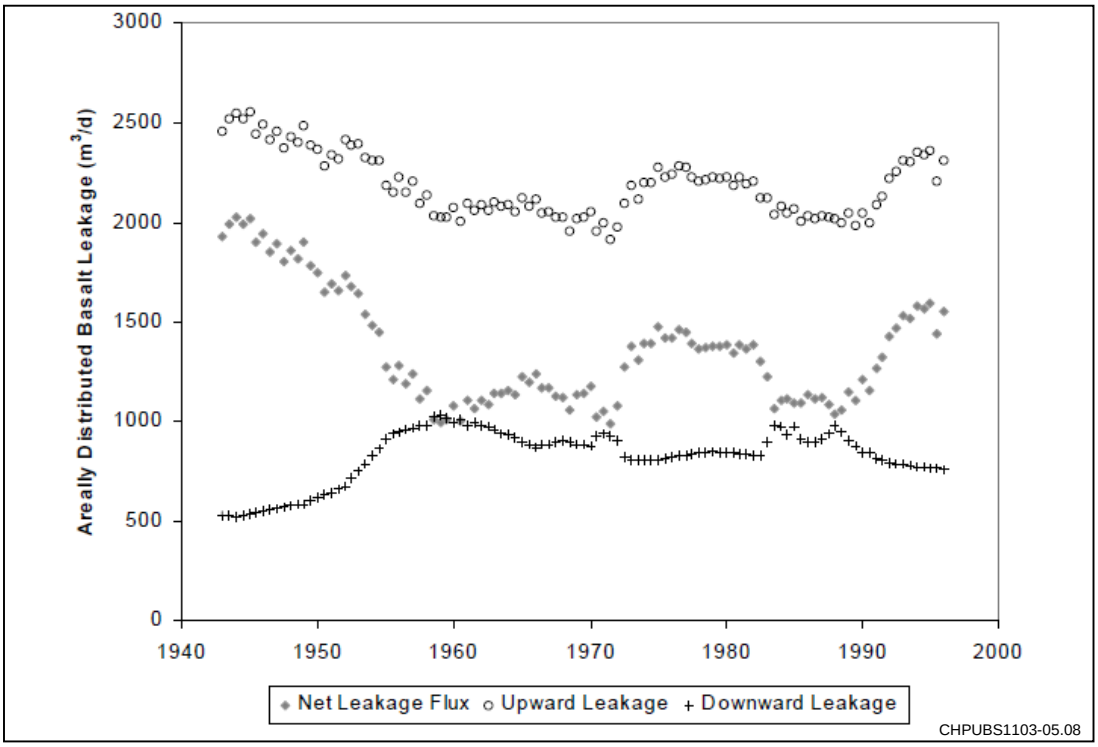

Source: PNNL-13623, *Transient Inverse Calibration of Site-Wide Groundwater Model to Hanford Operational Impacts from 1943 to 1996—Alternative Conceptual Model Considering Interaction with Uppermost Basalt Confined Aquifer*.

Figure 3-14. Temporally Varying Estimated Flux across the Upper Basalt Surface

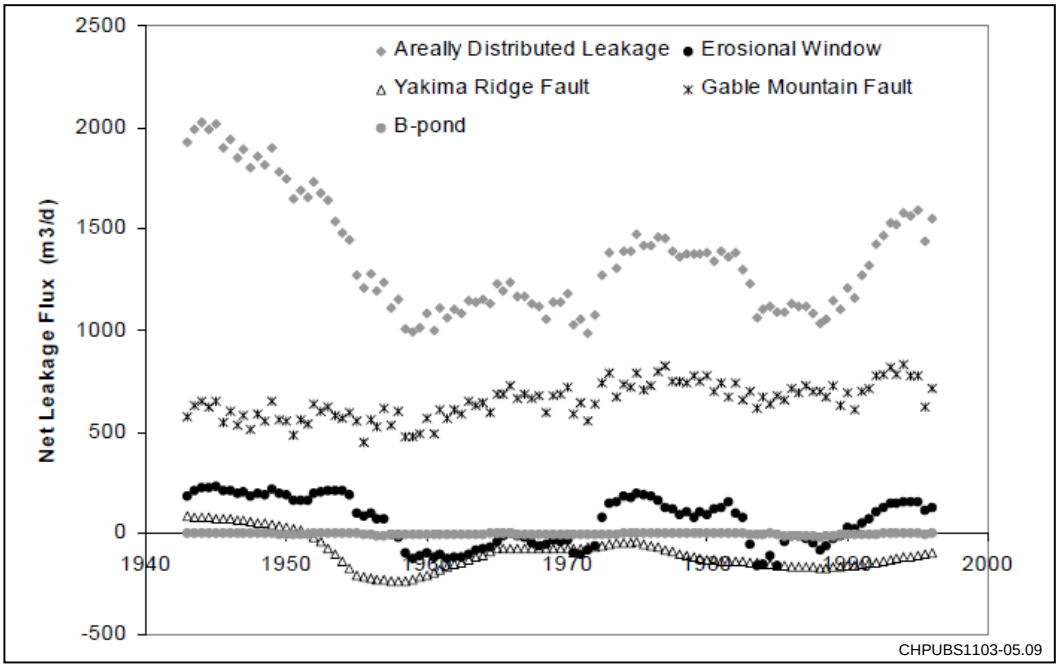

Source: PNNL-13623, *Transient Inverse Calibration of Site-Wide Groundwater Model to Hanford Operational Impacts from 1943 to 1996—Alternative Conceptual Model Considering Interaction with Uppermost Basalt Confined Aquifer*.

Figure 3-15. Relative Contribution of Each Basalt Leakage Feature to Net Leakage

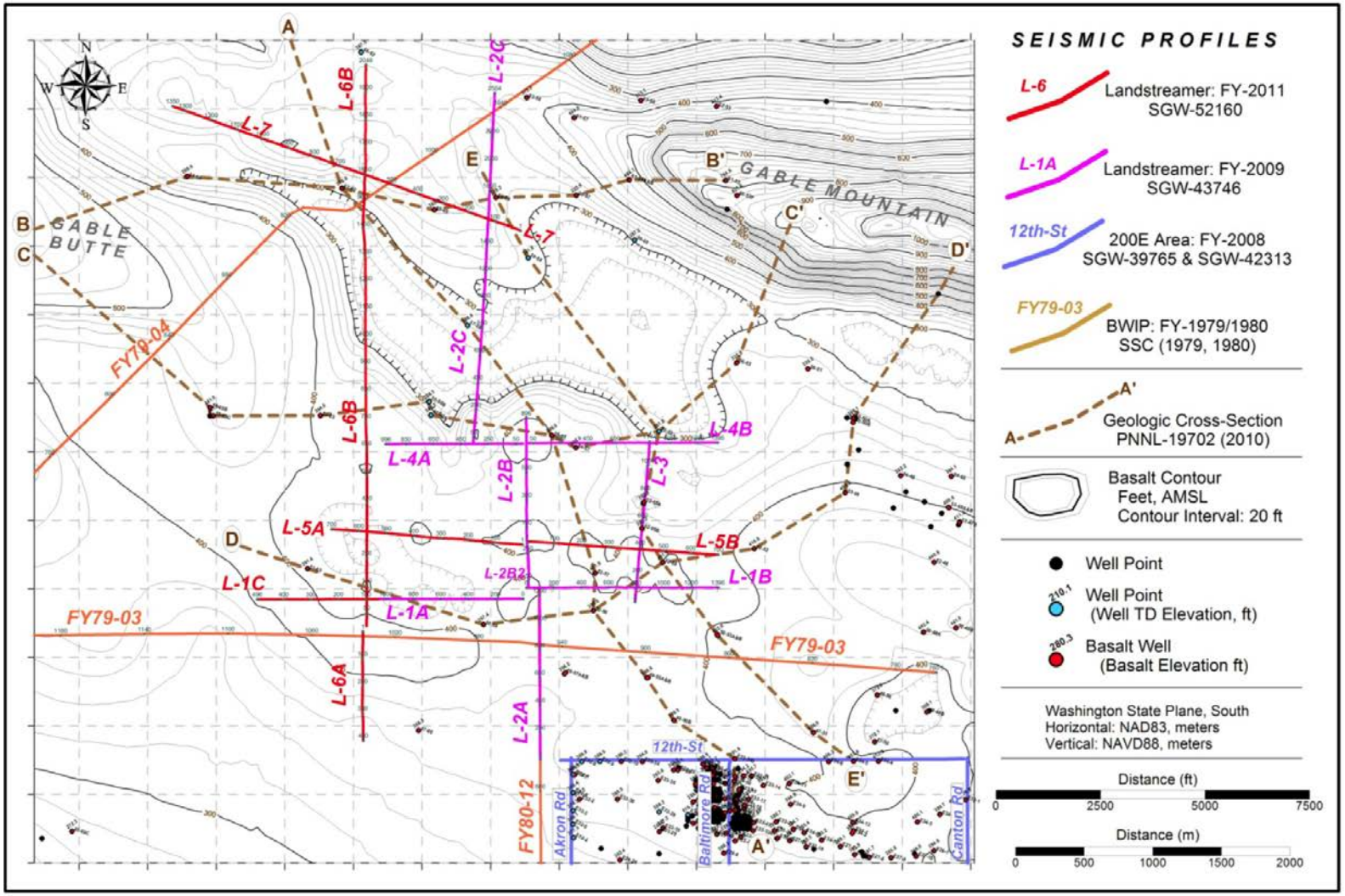

Source: SGW-48478, *Interpretation and Integration of Seismic Data in the Gable Gap*.

Figure 3-16. Basalt Surface Expression in Gable Gap and the 200-East Area

Source: PNNL-19702, *Hydrogeologic Model for the Gable Gap Area, Hanford Site*.
Note: View looking north; blue block arrows show general movement of floodwaters, which scoured and overtopped the crest of the basalt ridge along left side of image.

Figure 3-17. Example of Highly Irregular Topography Eroded by Ice Age Floods, Lower Grand Coulee, and Channeled Scabland

The basalt saddle to the northwest of the 200-East Area has a minimum elevation of 121.6 m (399 ft) in the model. Historical water-level measurements may indicate that this level is too high in the model compared to the actual geography. Figure 3-18 presents water-level measurements from 1948 to 1960 for five wells that straddle the basalt ridge saddle; the figure also shows Columbia River discharge measurements over the period. Figure 3-19 shows the locations of these wells. Wells 699-60-60 and 699-55-50A are north of the saddle. The plots indicate that these wells have an annual cycle that lags roughly 4 to 6 months behind the river. Starting in 1950, these wells indicate a steady rise in water level, possibly from discharges at B Pond or possibly due to discharges near the B, C, and/or K Reactors. Well 699-47-60, south of the saddle, indicates a hydraulic connection with the wells north of the saddle, below elevation 121.6 m (399 ft). The well was not installed in time to provide earlier water-level measurements.

In recent years, a set of monitoring wells was developed to evaluate the movement of water through Gable Gap. The wells were selected along a presumed flow path, from the Columbia River along the north side of Gable Butte, through Gable Gap, and just to the south of the basalt ridge indicated by the most current top-of-basalt maps. Water-level monitoring occurred monthly from 2014 through 2016. Figure 3-20 provides an example of one of the plots created from inverse distance-weighted interpolation of the head data collected and stored in HEIS for April 2016. The interpolation of these data indicate that the basalt ridge may be acting as a groundwater divide between the 200-East Area and Gable Gap.

3.2.6 Flow Direction in the 200-East Area

Measurement of flow direction within 200-East Area has been problematic due to the high hydraulic conductivity, low hydraulic gradient, and the depth to the water table. To overcome these problems, a special well network was developed as part of ECF-200E-16-0093, *Preparation of 200-East Area Water Table Maps for Calendar Year 2015*. The wells in this network were resurveyed for elevation of the casing and surveyed using a gyroscope to determine the borehole path. The data were analyzed using an inverse-distance weighting interpolation scheme, which produced an estimate for the water table across the 200-East Area. Figure 3-21 provides an example of the water table produced for calendar year (CY) 2015. The average water table condition indicates flow to the southeast through the 200-East Area.

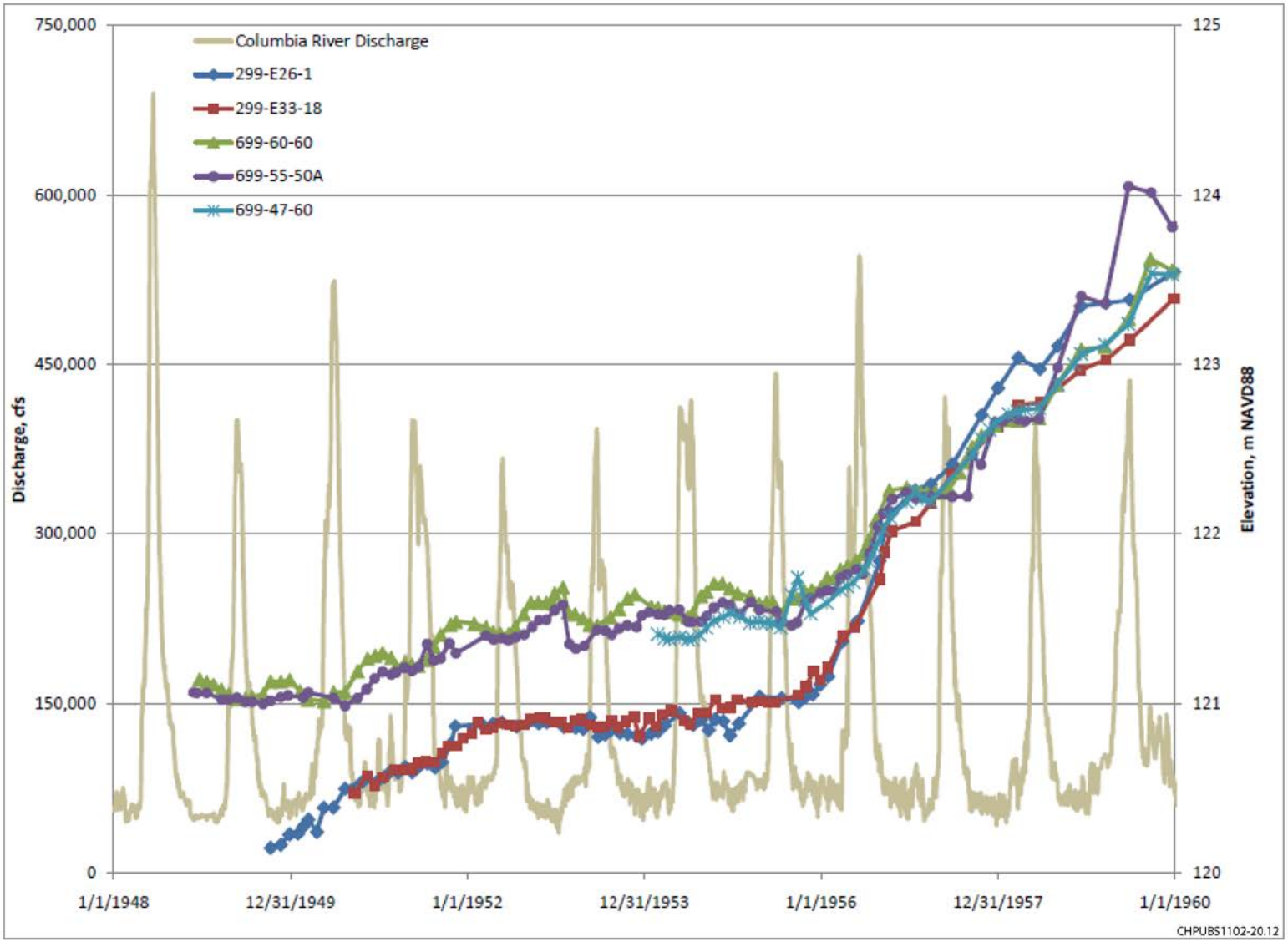

Figure 3-18. Historical Water-Level Measurements near the Basalt Ridge Saddle

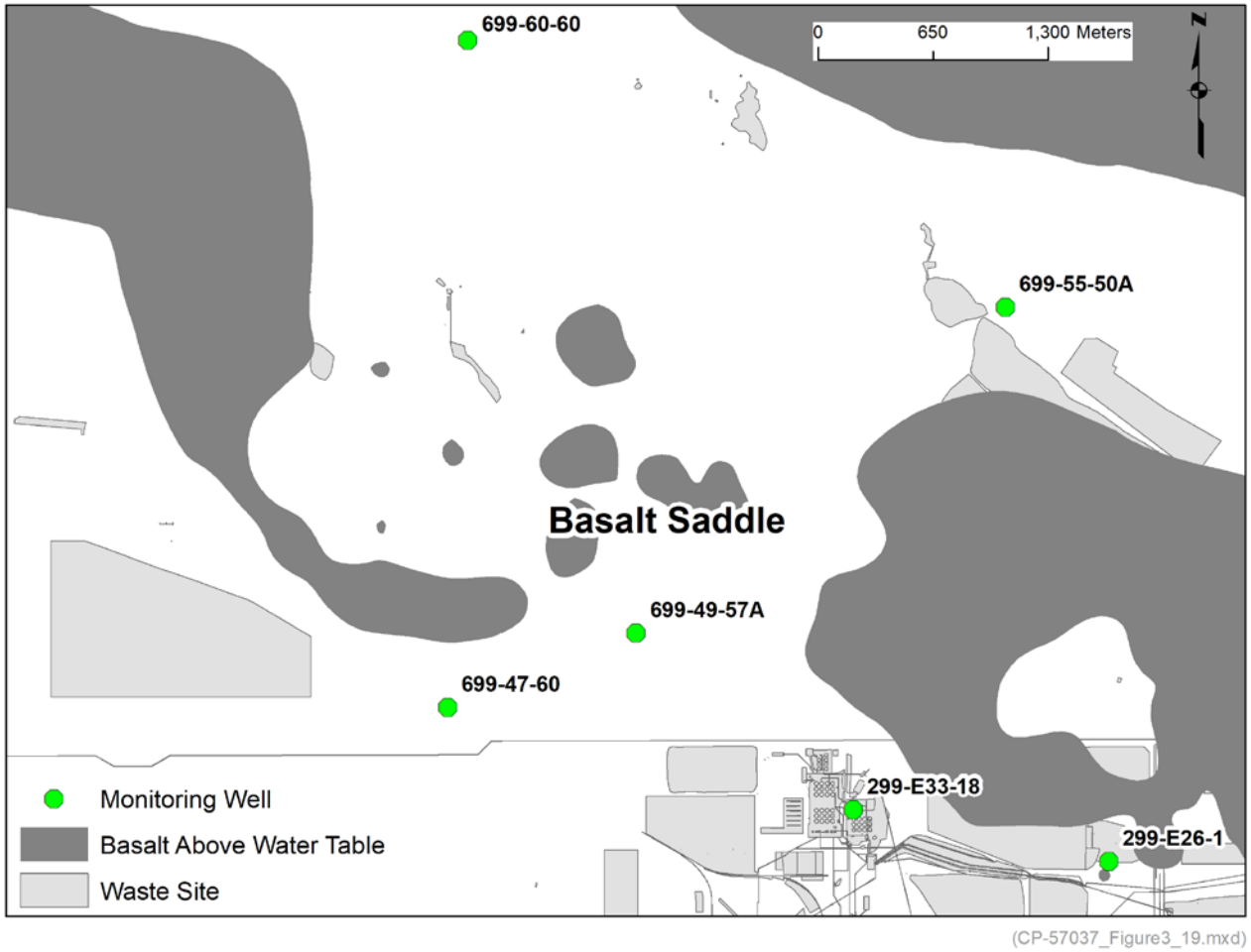

Figure 3-19. Locations of Wells Referred to in Figure 3-18

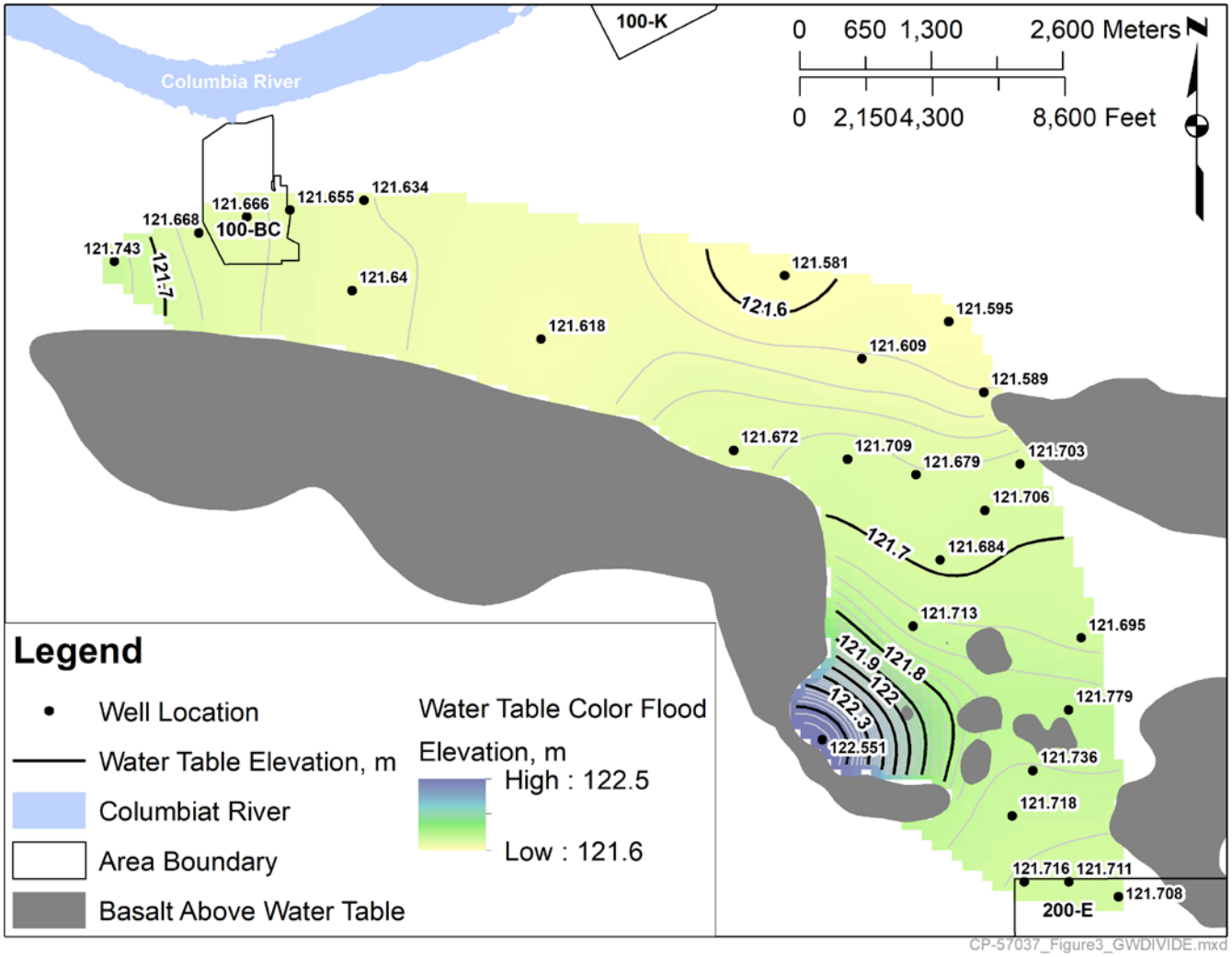

Figure 3-20. Water Table Map for the Paleochannel North of the 200-East Area, April 2016

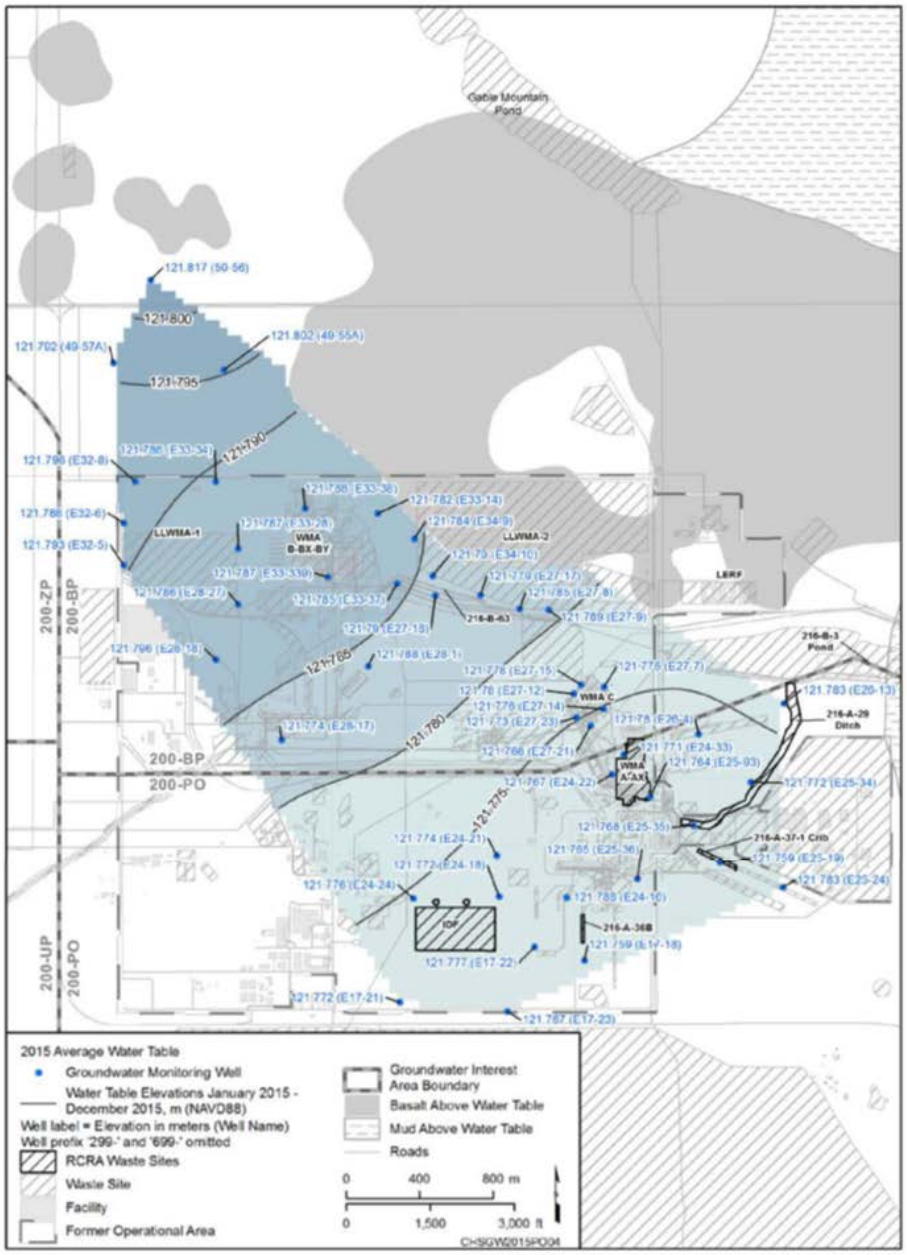

Figure 3-21. 200-East Area Average Water Table Map, CY 2015

4 Model Implementation

The approach to the groundwater flow and contaminant F&T modeling uses a mathematical hydrogeological construct to represent the physical conditions within the aquifer. This construct is developed using modified versions of the acquired computer software MODFLOW and MT3DMS (Section 4.1). This report specifies the data files that were used to develop the model. These data files are accessible through the Environmental Model Management Archive (EMMA), as required by the CH2M HILL Plateau Remediation Company (CHPRC) quality assurance project plan for modeling (Appendix K of CHPRC-00189).

Figure 4-1 depicts the domain of P2R Model. Basalt subcrops above the water table of the aquifer constrict the domain for portions of the north and south. These subcrops are assumed impermeable barriers to flow. A gap exists in the basalt subcrops along the northern boundary; in this region of the domain, the water table is above the basalt surface. This region is referred to as the Gable Gap. Along the eastern boundary and the easternmost part of the southern boundary, the water table is also above the basalt surface. In general, water has flowed out of all of these boundaries during the operational period of the Hanford Site. Cold Creek (located in the slot along the western boundary) and Dry Creek (the gap in the basalt subcrops in the southwest corner of the domain) are sources of inflow to the Central Plateau. Recharge from precipitation provides an additional source of inflow. Artificial recharge from the disposal of facility effluents to surface ponds, cribs, and shallow wells represented a very large source of inflow to the domain during the Hanford Site operational period.

The basic methodology for the development of the CPGW Model is as follows:

- Develop an understanding of the simulation/calculation needs across the Central Plateau.
- Define lateral and vertical extents (i.e., the domain) over which calculations of groundwater flow and subsequent contaminant transport are needed.
- Construct a representative flow model of the Central Plateau using the MODFLOW code, using site-specific descriptions of the local physical and hydrogeologic conditions.
- Verify the representativeness of the model by comparing the construct to available geologic descriptions, well logs, cross sections, and other appropriate sources of information.
- Define appropriate boundary conditions. Uncertain boundary conditions may be estimated through model calibration.
- Calibrate the hydraulic performance of the model by comparing the simulated groundwater head at selected locations to actual measurements at wells, and by comparing the simulated resulting groundwater gradient to the observed gradient in nearby wells. This calibration was implemented for the period from 1944 to 2016.
- Complete F&T simulation of historical tritium discharge to assess simulated flow directions.

4.1 Software

MODFLOW (USGS, 2000, *MODFLOW-2000, the U.S. Geological Survey Modular Ground-water Model — User Guide to Modularization Concepts and the Ground-Water Flow Process*) and MT3D were selected for implementing the P2R Model because they fulfill the following specifications:

- They are widely used software packages for models of this type.

- They are available and distributed with the source code.
- They are documented and have been verified in applications similar to those at the Hanford Site.
- They are capable of directly simulating the principal FEPs that are relevant to the Central Plateau simulation requirements.
- For those FEPs that they may not directly simulate, the needs can be met through links to other codes, such as linking to Subsurface Transport Over Multiple Phases (STOMP[1]) (PNNL-11216, *STOMP Subsurface Transport Over Multiple Phases: Application Guide*) for vadose calculations. as described in Section 3.2.3 for FEP recharge.

Use of MODFLOW and MT3D keeps with DOE direction for simulation of groundwater at the Hanford Site (Klein, 2006, "MEMO: Contract No. DE-AC06-96RL13200 – Hanford Groundwater Modeling Integration"). The software used to implement this model and to perform calculations was approved under the requirements of:

- CHPRC-00257, *MODFLOW and Related Codes Functional Requirements Document*
- CHPRC-00258, *MODFLOW and Related Codes Software Management Plan*
- CHPRC-00259, *MODFLOW and Related Codes Software Test Plan*
- CHPRC-00260, *MODFLOW and Related Codes Requirements Traceability Matrix*
- CHPRC-00261, *MODFLOW and Related Codes Acceptance Test Report*

CHPRC-00259 distinguishes between safety software and support software based on whether the software managed calculates reportable results or provides run support, visualization, or other similar functions.

4.1.1 MODFLOW Controlled Calculation Software

The following describes the MODFLOW controlled calculation software.

- **Software title:** MODFLOW-2000; solves transient groundwater flow equations using the finite difference discretization technique.
- **Software version:** MODFLOW-2000, modified by S.S. Papadopulos and Associates for minimum saturated thickness and to use the ORTHOMIN Solver. Approved as CHPRC Build 8 using executable file mf2k-mst-0008dpl.x (for Linux[2]) or mf2k-mst-0008dpl.exe (for Microsoft[3] Windows), both compiled to default double precision for real variables.
- **Hanford Information System Inventory (HISI) identification number:** 2517 (Safety Software S3, graded Level C).
- **Software title:** MT3DMS; solves transient advective/dispersive F&T equations using the finite difference discretization technique.

---

[1] Battelle Memorial Institute (Battelle) retains copyright on all versions, revisions, and operational modes of the Subsurface Transport Over Multiple Phases (STOMP) software simulator, as permitted by the U.S. Department of Energy. STOMP is used here under a limited government use license.

[2] Linux® is a registered trademark of the Linux Foundation, San Francisco, California.

[3] Microsoft® Windows, Excel, and other Microsoft products are registered trademarks or trademarks of Microsoft Corporation in the United States and/or in other countries.

- **Software version:** MT3DMS, modified by S.S. Papadopulos and Associates for minimum saturated thickness and to use the ORTHOMIN Solver. Approved as CHPRC Build 8 using executable file mt3d-mst-0008dpl.x (for Linux) or mt3d-mst-0008dpl.exe (for Microsoft Windows), both compiled to default double precision for real variables.
- **HISI identification number:** 2518 (Safety Software S3, graded Level C).

4.1.2 MODFLOW Support Software

Support software is used that has been identified in CHPRC-00258. Support software is used to develop inputs and process outputs from MODFLOW and MT3DMS. Specific applications that were used in the development of the model include MODPATH, PEST,[4] ArcGIS,[5] and Microsoft Excel.[3]

4.1.3 Software Installation and Checkout

Safety software (CHPRC Build 8 of MODFLOW-2000/MT3DMS) is checked out in accordance with procedures specified in CHPRC-00258. Executable files are obtained from the CHPRC software owner, who maintains the configuration-managed copies in MKS Integrity.[6] Installation tests identified in CHPRC-00259 are performed and successful installation confirmed. Software installation and checkout forms are required and must be approved for installations used to perform model runs. Approved users are registered in HISI for safety software. Appendix A provides the requisite software installation and checkout forms for this application of MODFLOW-2000 and MT3DMS.

4.1.4 Statement of Valid Software Application

Use of the software previously identified must be consistent with intended use for CHPRC (as identified in CHPRC-00257) and must be a valid use of this software for the problem addressed in this application. The software must be used within its limitations, as identified in CHPRC-00257.

4.2 Model Domain and Discretization

Discretization is the process of breaking up a continuous phenomenon into discrete pieces. This process can be completed for a volume, length, and/or time. For a numerical model such as the P2R Model Version 8.2, this process includes dividing the model domain into volumes called finite difference cells. These cell volumes are then used to make calculations of groundwater volume, elevation, and movement in the subsurface. This section discusses the extent and discretization of the model domain, spatially and temporally.

4.2.1 Model Extent

Figure 1-1 shows the location of the Hanford Site. The Central Plateau is south of Gable Butte and Gable Mountain and includes the 200-West and 200-East Areas. Figure 4-1 shows these features and the lateral extent of the model domain. To the north and south the domain is constricted by basalt subcrops (depicted as a gray-color in the figure). These subcrops are assumed to constitute impermeable boundaries to flow. There are several gaps in the basalt subcrops along the boundary of the model. These gaps occur in the

---

[4] PEST is and industry standard software package for parameter estimation and uncertainty analysis of complex environmental and other computer models.

[5] ArcGIS® is a registered trademark of ESRI, Redlands, California.

[6] PTC, The Product Development Company, MKS Integrity, Integrity and all other PTC product names and logos are trademarks or registered trademarks of Parametric Technology Corporation or its subsidiaries in the United States and in other countries.

north between Gable Butte and Gable Mountain known as the Gable Gap, to the east of Gable Mountain, along the Columbia River, along the western edge of the model near the Central Plateau, and where the Dry Creek Basin intersects the model domain. In these regions, the water table is above the basalt surface. As depicted in Figure 4-1, these locations are defined by specified head boundary conditions and are discussed in Sections 4.4.1 and 4.4.3. The southernmost boundary of the model is also a location where the water table is above the basalt surface. This boundary matches the extent of the P2R Model version 7.1 and was selected to run perpendicular to groundwater contours that are observed in this region of the model domain.

The model domain includes four groundwater OUs in the Central Plateau: 200-PO-1, 200-BP-5, 200-UP-1, and 200-ZP-1. Figure 4-1 identifies the boundaries of these four groundwater OUs with black lines. The model domain has the following lateral extent and boundaries: extent north to south is 26.1 km (16.2 mi), and extent east to west is 31.0 km (19.3 mi). The lower left corner of the model domain is located at easting 564,000 m and at northing 116,000 m in the Washington State Coordinate System (NAD_1983_StatePlane_Washington_South_FIPS_4602).

The vertical extent of the model comprises the subsurface sediments from ground surface to the uppermost unit of the CRBG. The basalt that is assumed to constitute an impermeable lower boundary defines the base of the domain. Since the P2R Model only simulates saturated groundwater flow, geologic differentiation was implemented only below the highest water table estimate based on the previous version of the model (Version 7.1). The water table is not static and was higher during the Hanford Site operational period than it is now. To permit simulation of historical water flow, the geologic media represented in the model includes sediments that are currently above the water table.

4.2.2 Lateral Discretization

The model domain is discretized into a finite difference grid. The grid in the lateral directions is broken up into variably sized cells of 100 m by 100 m (328.1 ft by 328.1 ft), 100 m by 200 m (328.1 ft by 656.2 ft), and 200 m by 200 m (656.2 ft by 656.2 ft). Compared to the previous version of the P2R Model, the discretization is more refined in the portion of the model domain representing the Central Plateau and equivalent to the discretization used toward the Columbia River. A total of 241 columns and 196 rows constitute a total of 47,236 cells within the model domain. Based on the boundaries of the model shown in Figure 4-1, only a maximum 31,047 of those cells are active in the model within each model layer.

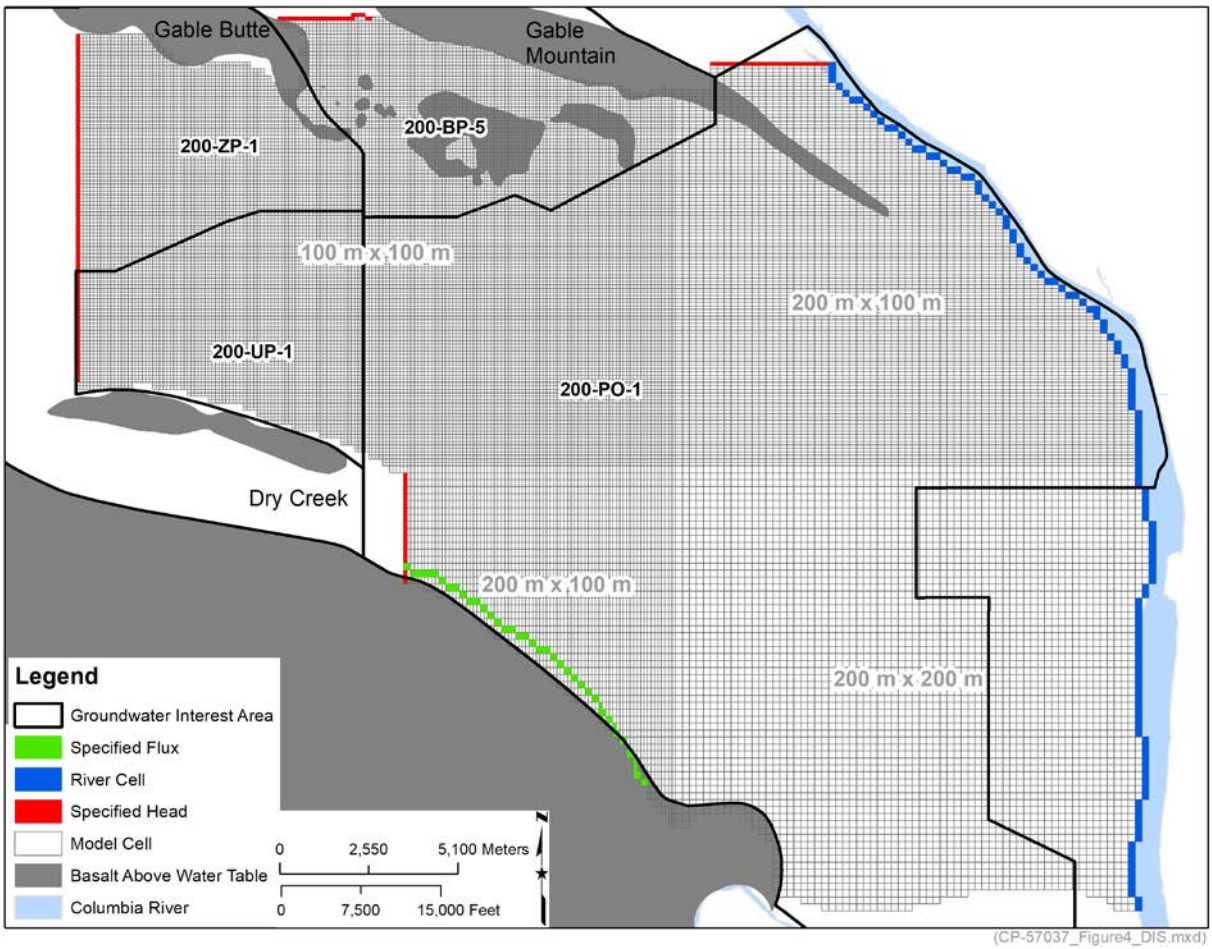

Figure 4-1. CPGW Model Extent and Boundary Conditions

4.2.3 Vertical Discretization

The P2R Model is vertically divided into seven model layers between the ground surface elevation and the top of the basalt surface. The seven vertical layers vary in thickness so any one model cell may not match the thickness of the adjacent cells. The discretization of the vertical layers varies in order to represent the thickness of geologic formations found within the model domain.

The representation of geology within the model is based on ECF-HANFORD-13-0029, which documents the development of the HSGF. The HSGF was created to provide a continuous estimate of geologic formation thickness across the southern portion of the site and to integrate the interpretation into a consistent format that can be used across other Hanford Site projects. The HSGF is a collection of meshes that describe the boundaries between the six major HSU classifications within the southern portion of the Hanford Site. Table 4-1 lists and describes the HSUs as they are presented in the HSGF.

Table 4-1. HSUs in the P2R Model

P2R Model HSU Number	Description	PNNL-14753 Unit Number	Notes
1	Hanford formation coarse-grained unit	Unit 1	Dominated by gravel and sand within the aquifer
2	Cold Creek unit	Unit 3	Dominated by gravelly sand, also called the pre-Missoula gravel
3	Ringold Formation Taylor Flat unit	Ringold unit 4	Uppermost Ringold Formation unit with dominated by sands and silts (BHI-00184)
4	Ringold Formation unit E	Ringold unit 5	Composed primarily of fluvial gravel that grades upward into interbedded fluvial sand (BHI-00184)
5	Ringold Formation lower mud unit	Combination of Ringold units 6, 7, and 8 (B, C, and D units)	Composed of a thick sequence of fluvial overbank, paleosol, and lacustrine silts and clay with minor sand and gravel (PNNL-13858)
6	Ringold Formation unit A	Unit 9	Composed primarily of fluvial gravel (PNNL-13858)

Note: An HSU is not equivalent to a model layer; rather, each HSU defined in this table may occur in one or more model layers, and each model layer contains multiple HSUs.

Sources:

BHI-00184, *Miocene- to Pliocene Aged Suprabasalt Sediments of the Hanford Site, South Central Washington*.

PNNL-13858, *Revised Hydrogeology for the Suprabasalt Aquifer System, 200-West Area and Vicinity, Hanford Site, Washington*.

PNNL-14753, *Groundwater Data Package for Hanford Assessments*.

CPGW Model = Central Platea Groundwater Model

HSU = hydrostratigraphic unit

The entirety of the model domain for the P2R Model lies within the boundaries of the HSGF. Thus, the estimates for thickness of the geologic formations are provided by this tool and are consistent with other modeling projects at the Hanford Site based on the HSGF. The following subsections describe the process of transferring the information from the HSGF to the seven model layers within the P2R Model. The process includes extracting elevation and thickness values from HSGF and assigning thicknesses to model layers of the grid.

4.2.3.1 Extract Hydrostratigraphic Unit Geometry

The HSGF is built in a software package called Leapfrog[7] Geo. In Leapfrog Geo, each HSU is represented by a "boundary representation solid." This is a mesh of points that define the boundary between an HSU and any surrounding HSU. Leapfrog Geo develops the solids using field-observed well data and some expert input; it also ensures that the boundary representation solids do not overlap in space. The software, the data used, and the estimate the HSU geometry are detailed in ECF-HANFORD-13-0029. The software also includes the ability to export the elevation and thickness of the HSUs represented in the HSGF in a raster format that is usable by ArcGIS. The elevations of the top and the bottom of the model, ground surface, and top of the CRBG, respectively, were assigned to a polygon feature class representing each cell in the model. The thickness of each of the six HSUs was also assigned to the polygon feature class representing the model grid.

4.2.3.2 Assign Thicknesses to Model Layers

An algorithm for transferring information from the HSGF to the P2R Model grid is presented in Jones et al., 2002, "Generating MODFLOW Grids from Boundary Representation Solid Models." This algorithm was applied to the HSGF for assigning elevations to the P2R Model layers. The algorithm relies on user input to specify the expected layer assignments for each HSU within the model domain. The algorithm accounts for situations where the particular HSUs may be absent, which occurs frequently throughout the model domain. Also, a minimum thickness is applied below when the algorithm assumes the HSU is not present. Therefore, the algorithm assigns model elevations and applies a smoothing algorithm to minimize the difference in adjacent cell sizes while preserving the thickness and presence of the HSUs defined by the solid model.

Table 4-2 shows the expected model layers that were assigned to the six HSUs in the HSGF. Where overlap exists, the algorithm determines the appropriate layer assignments on a cell-by-cell basis and to preserve the stratigraphic consistency of the deposition of the HSU. The minimum thickness of 2 m (6.6 ft) was used to determine if a HSU would be considered present. The model grid with layer and HSU assignments was read into Groundwater Vistas[8] for visual inspection if the algorithm produced reasonable results.

Table 4-2. Model Layer Assignments by HSU for the Finite Difference Grid

HSU Number	Description	Starting Layer	Ending Layer
1	Hanford	1	6
2	Cold Creek	2	3
3	Ringold Taylor Flat	2	3
4	Ringold unit E	3	5
5	Ringold lower mud	6	6
6	Ringold unit A	7	7

[7] Leapfrog® is a registered trademark of ARANZ Geo Limited, Christchurch, New Zealand.

[8] Groundwater Vistas is a sophisticated Microsoft Windows graphical user interface for three-dimensional groundwater flow and transport modeling.

Figures 4-2 through 4-6 show comparisons of the model layers assigned to HSUs and the boundary representation solid models developed as part of the HSGF. These are presented as a set of cross-sections taken of the HSGF and the respective MODFLOW grid. Overall, there is good agreement between the MODFLOW grid and the HSGF boundary representation solids. The figures show a variance between the HSGF solids and the P2R cells with respect to the top of the HSU in several locations near the top of the MODFLOW model grid. This variance is due to MODFLOW simulating only the saturated portion of the subsurface. The vadose zone is ignored as part of the MODFLOW simulation. However, in showing the model grid, the top uppermost layer is extended to ground surface elevation. Thus, if an HSU is present near the high water table (representing the bottom of model layer 1) and is assigned to the uppermost layer, the figure gives the appearance that the HSU is present all the way to ground surface. Only those units present near or below high water table will be considered in the MODFLOW model calculations. Figures 4-7 and 4-8 show the HSU assignments for each layer of the MODFLOW model grid.

4.3 Simulation Period

The time unit used for the P2R Model is days. Depending on the purpose of the simulation, a different temporal discretization scheme is used. Simulating the historical period for calibration was performed by simulating yearly stress periods from 1943 through 2016. The previous version of the P2R Model, Version 7.1, utilized a calibration period of 2006 to 2012. Table 4-3 summarizes the temporal discretization of Version 8.2 historical calibration model.

4.4 Parameterization

The purpose of this section is to discuss how the numerical model was constructed from the conceptual model. The conceptual model (discussed in Chapter 3) is represented in the numerical model as input parameters. The input parameters are used by the MODFLOW and MT3DMS code to make calculations of groundwater flow and transport. The following subsections describe the input parameters that represent (1) the specified head boundary within the Gable Gap, at Dry Creek, the western boundary, and the north eastern boundary, (2) the hydraulic properties assigned to the HSUs, (3) the Columbia River boundary at the eastern edge of the model, (4) the method for including recharge estimates in the model, (5) historical pumping rates, and (6) F&T properties.

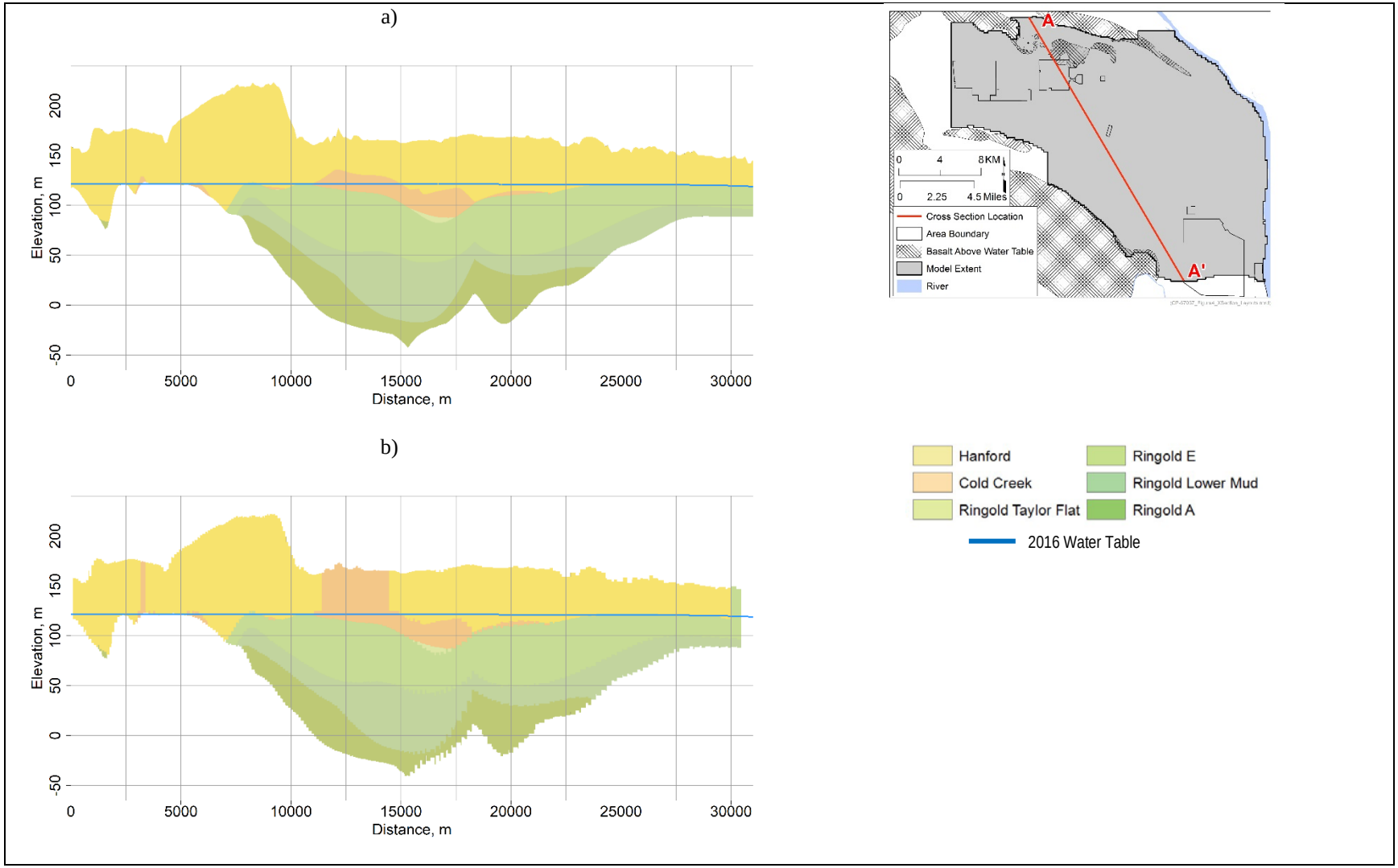

Figure 4-2. Comparison Cross-Section View of (a) Hanford South Geoframework HSU Estimates and (b) Initial MODFLOW Grid HSU Assignments

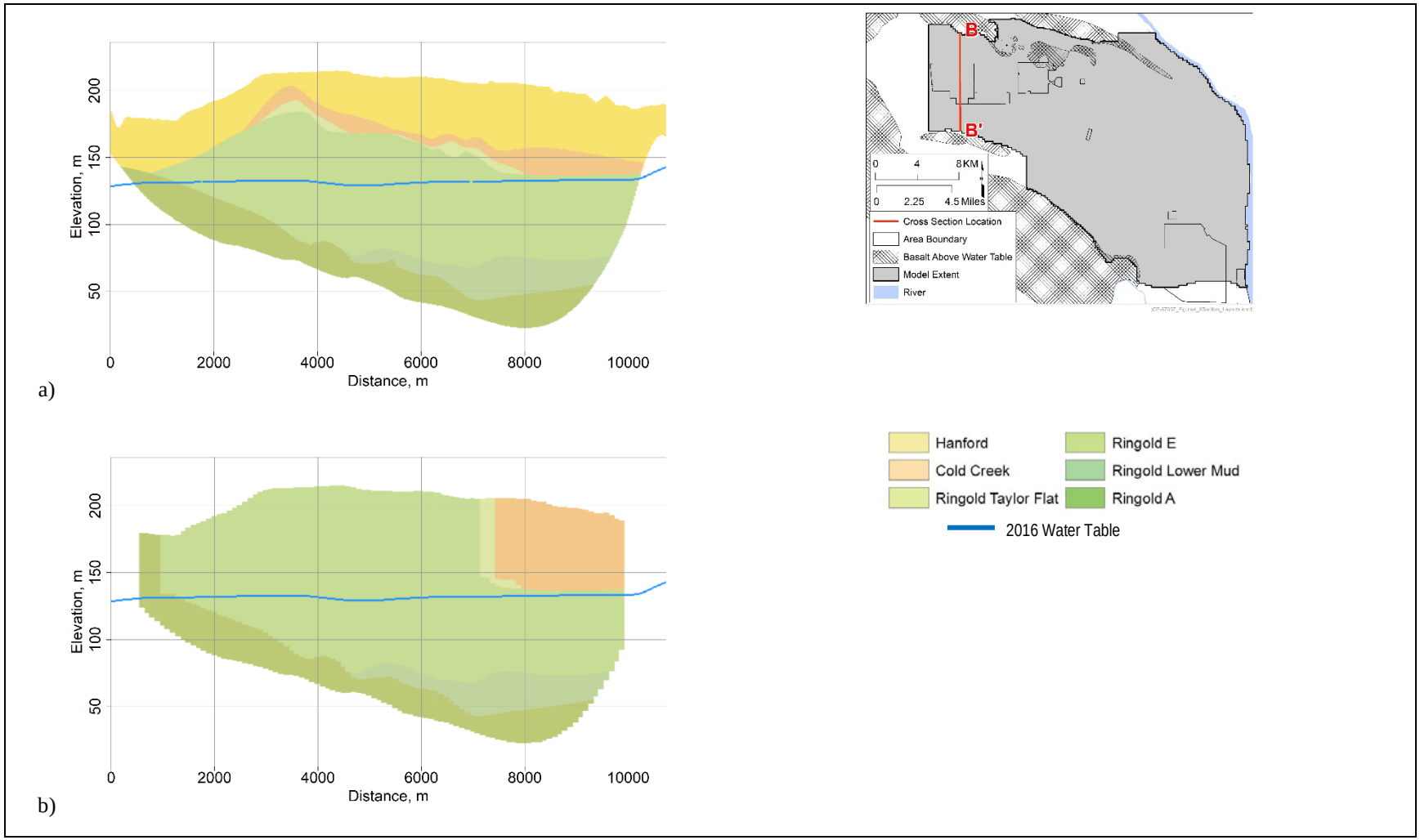

Figure 4-3. Comparison Cross-Section View of (a) Hanford South Geoframework HSU Estimates and (b) Initial MODFLOW Grid HSU Assignments

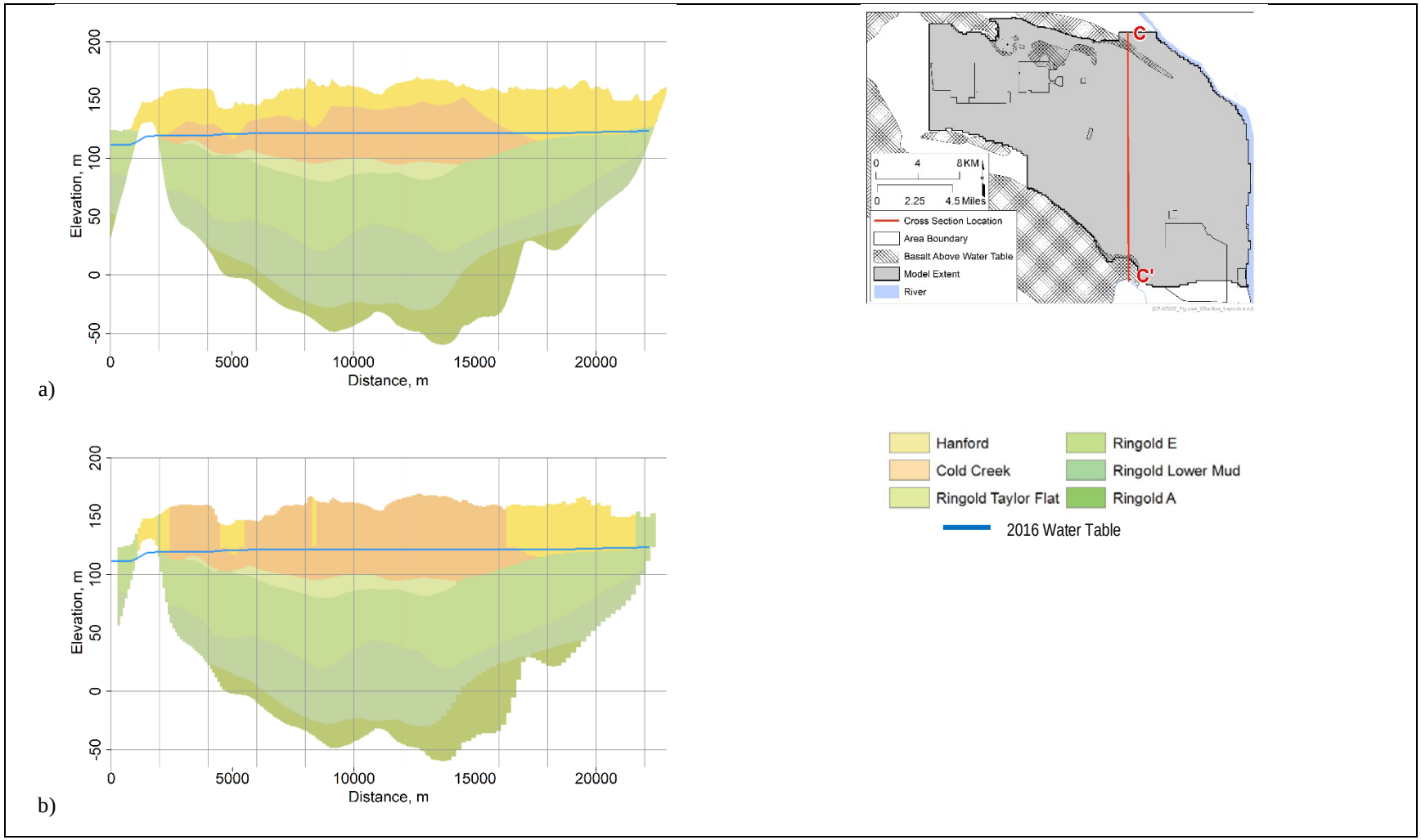

Figure 4-4. Comparison Cross-Section View of (a) Hanford South Geoframework HSU Estimates and (b) Initial MODFLOW Grid HSU Assignments

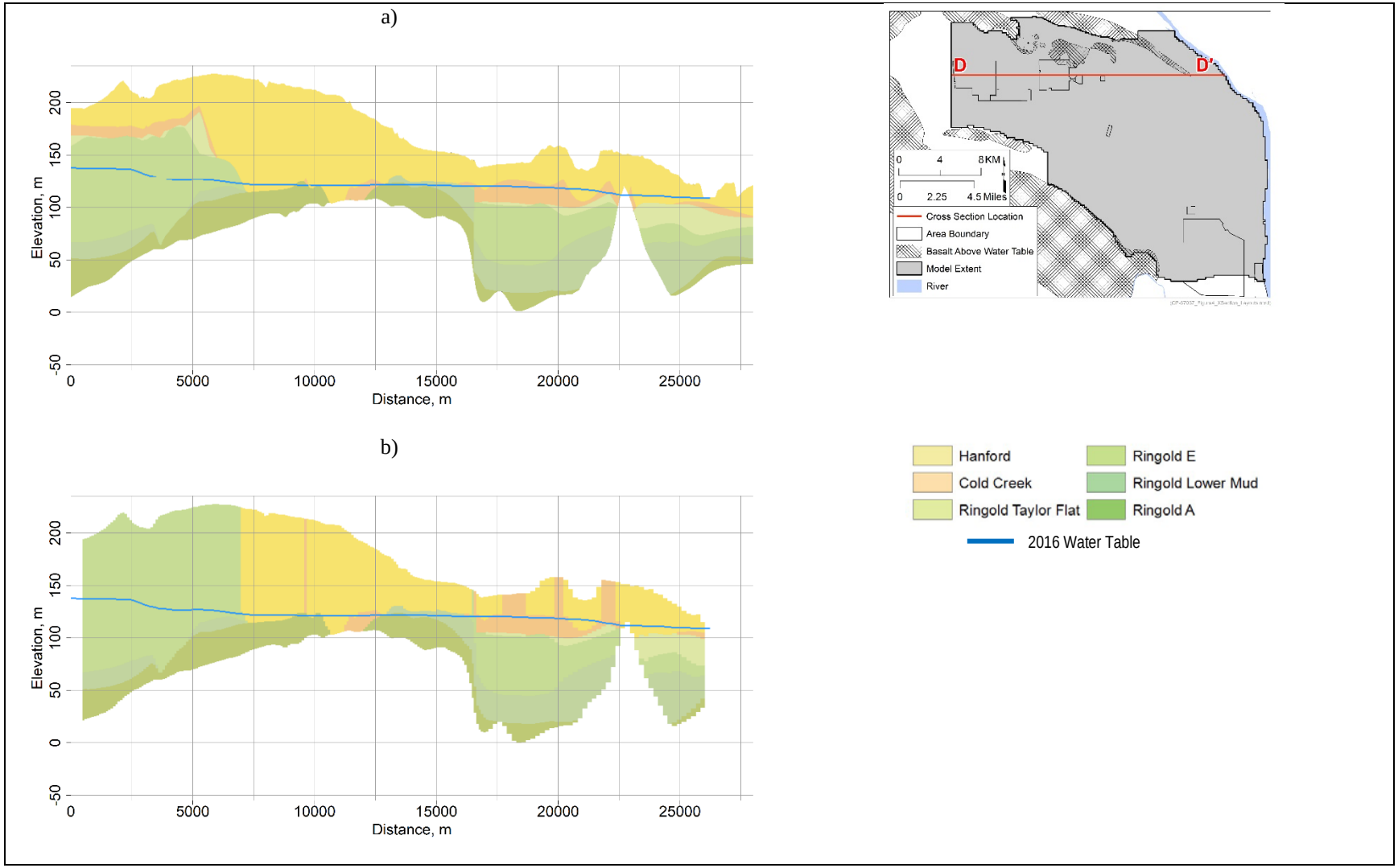

Figure 4-5. Comparison Cross-Section View of (a) Hanford South Geoframework HSU Estimates and (b) Initial MODFLOW Grid HSU Assignments

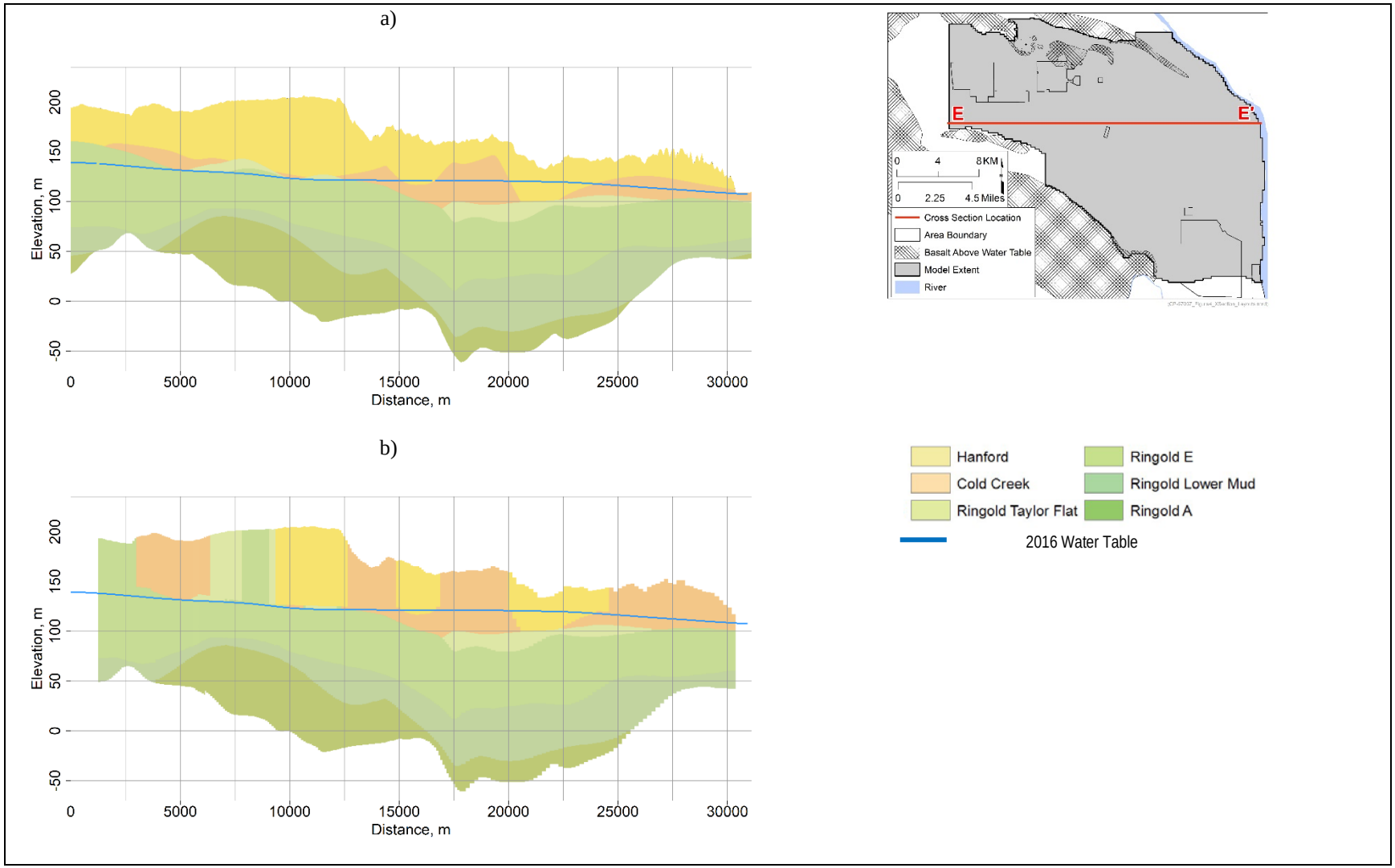

Figure 4-6. Comparison Cross-Section View of (a) Hanford South Geoframework HSU Estimates and (b) Initial MODFLOW Grid HSU Assignments

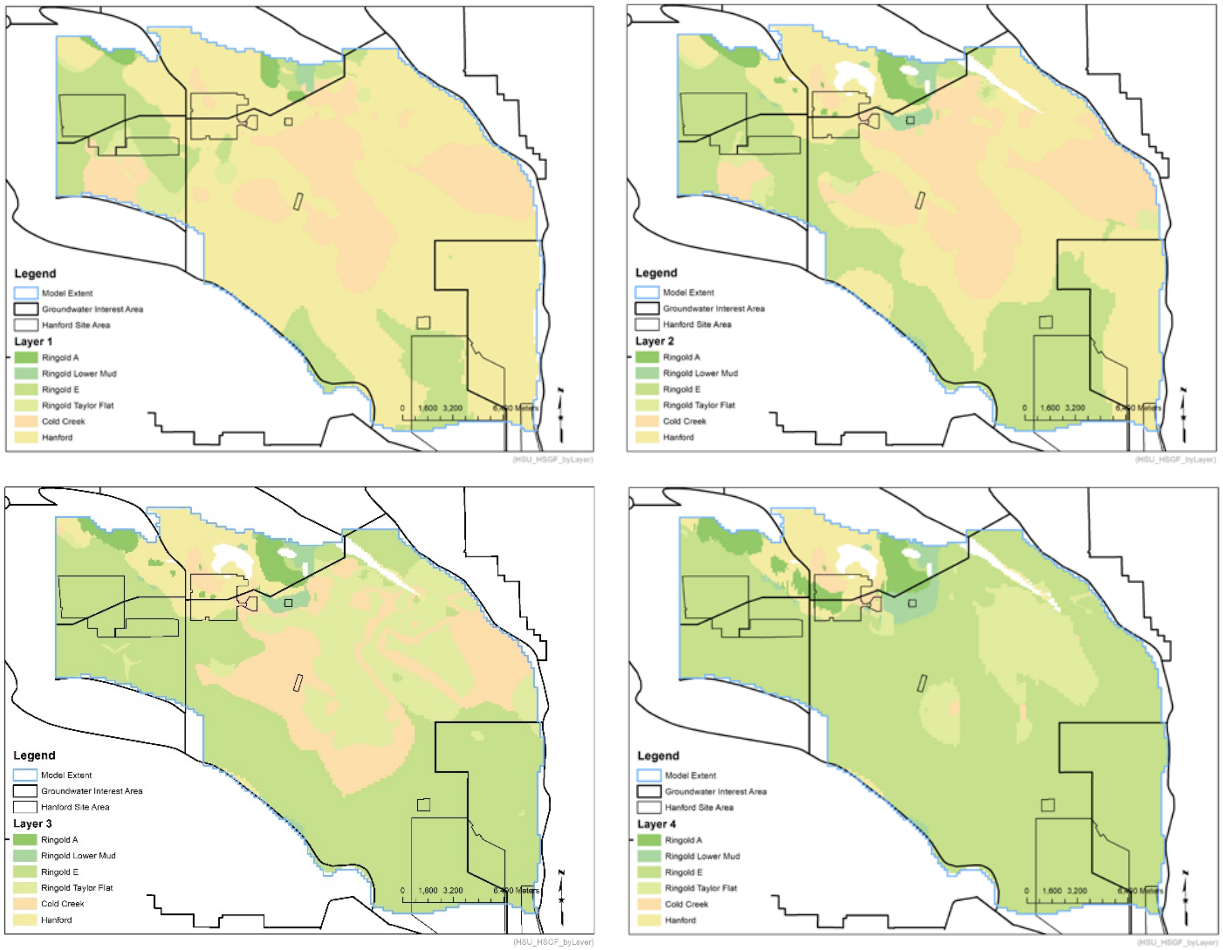

Figure 4-7. HSUs of Model Layers 1 through 4 Based Solely on HSGF

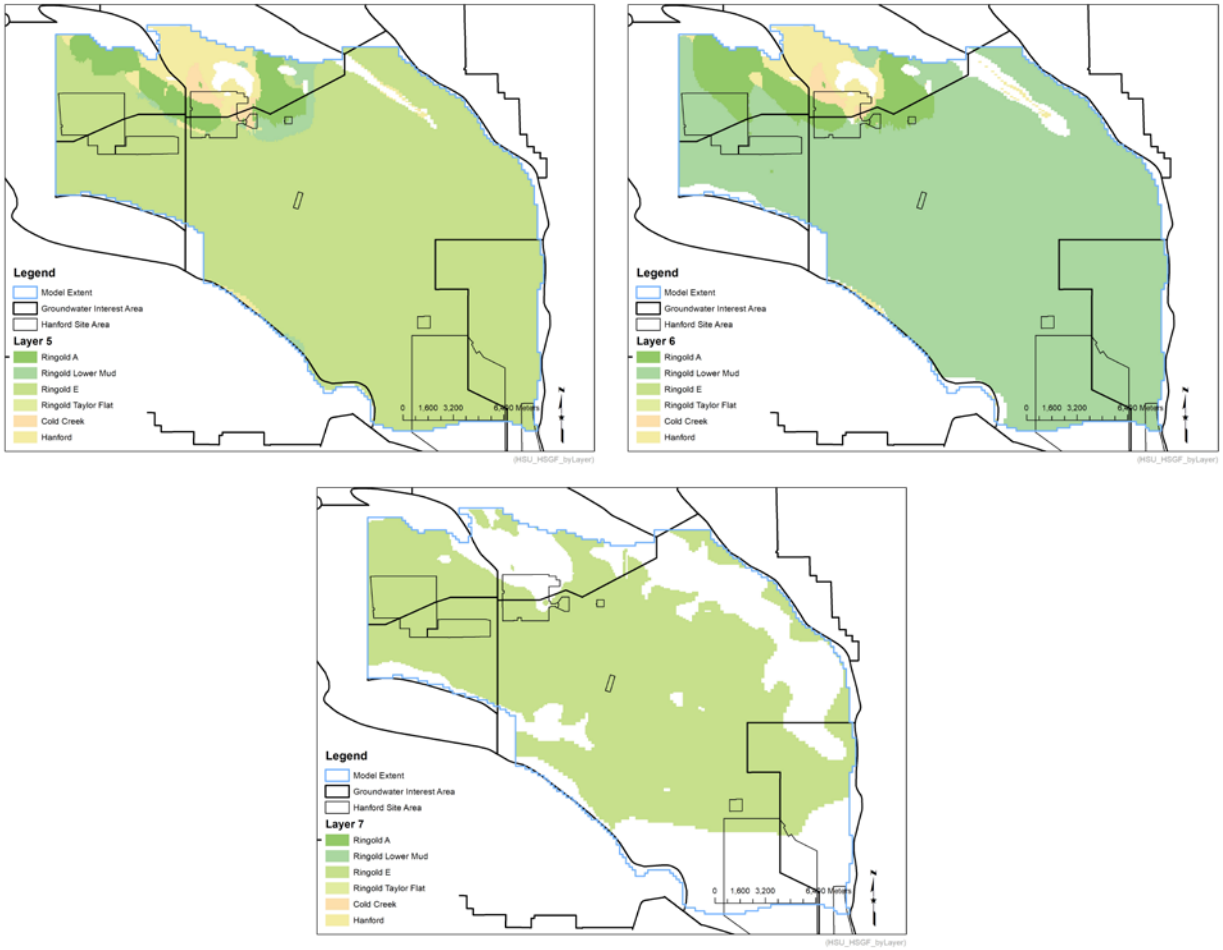

Figure 4-8. HSUs of Model Layers 5 through 7 Based Solely on HSGF

Table 4-3. Temporal Discretization of Historical Calibration of the P2R Model

Model	Stress Period(s)	Duration	Description
Historical calibration simulations	1 to 74	74 years	The 74 transient annual stress periods span the calibration period from 1943 through 2016.

4.4.1 Specified Heads

The basalt top elevation defines the bottom and most of the lateral boundaries of the model domain, depicted as gray-colored, cross-hatched regions in Figure 4-1. Four locations where the water table is above the top of the basalt are defined by specified head boundaries, as shown as red shading in Figure 4-1. The parameterization of lateral boundaries is as follows:

- The western boundary of the model is defined by the CPGW Model output for the historical calibration simulations documented in *Model Package Report: Central Plateau Groundwater Model, Version 8.4.5,* CP-47361. Simulated hydraulic head values from the historical calibration were interpolated to the cell centers of the P2R Model grid for the entire temporal domain of the P2R Model historical calibration.
- Water-level data from well 699-60-60 (from the HEIS database) were used to set the head for the Gable Gap boundary. Figure 4-9 presents the well 699-60-60 water-level measurement data used to define this boundary.
- In the southwestern boundary near Dry Creek, the boundary was defined by historic head data from well 699-10-54A shown in Figure 4-10. For time periods prior to the start of data collection at 699-10-54A (pre-1951) the water table elevation was based on the hindcast estimate of hydraulic head prior to operations at the Hanford Site developed as part of *Selected Water Table Contour Maps and Well Hydrographs for the Hanford Reservation 1944-1973,* BNWL-B-360.
- In the northeastern corner of the model, specified heads were developed from a set of wells (699-54-18B, 699-54-19, and 699-58-24) near the boundary that together provide an historic record of hydraulic head from 1956 through 2016. Figure 4-11 shows the observed levels from each of the wells at this site along with the curve representing the trend used to develop the yearly simulated values assigned as specified heads to the nodes along that boundary. The yellow crosses indicate the annual values sampled along that line. Prior to the availability of historical data, the initial head was estimated from the hindcast map presented in BNWL-B-360.

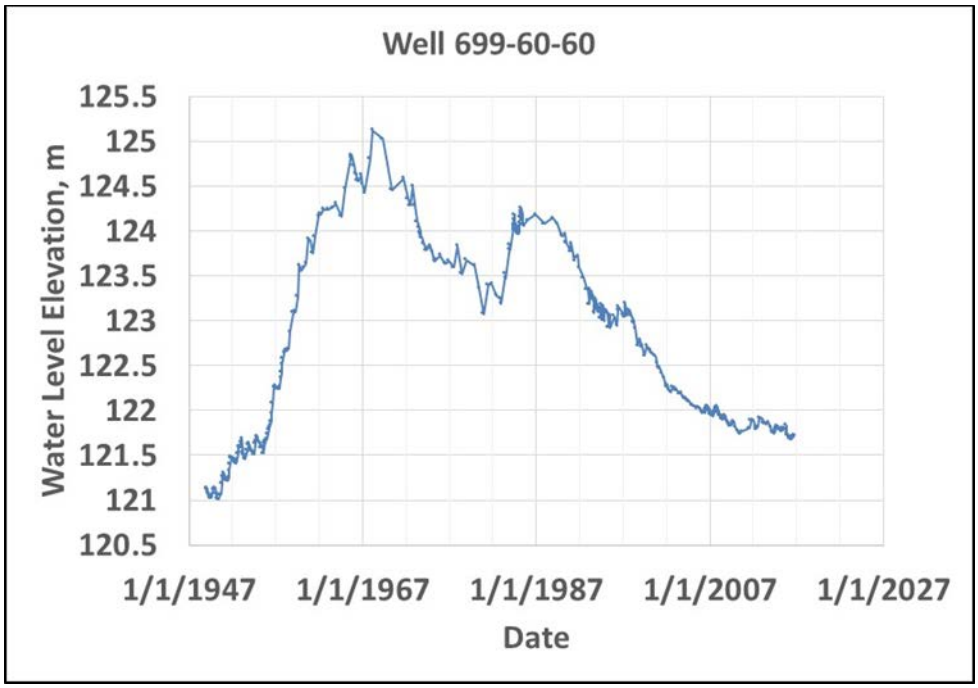

Note: Period prior to 1948 was estimated through calibration.

Figure 4-9. Historical Water Levels for Well 699-60-60

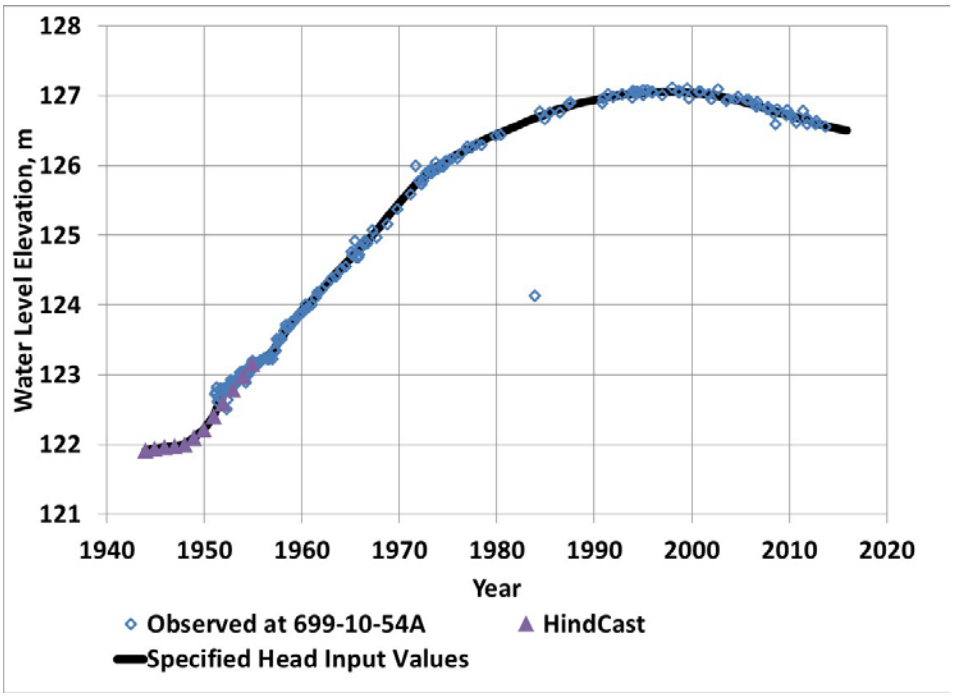

Figure 4-10. Historical Water Levels for Well 699-10-54A

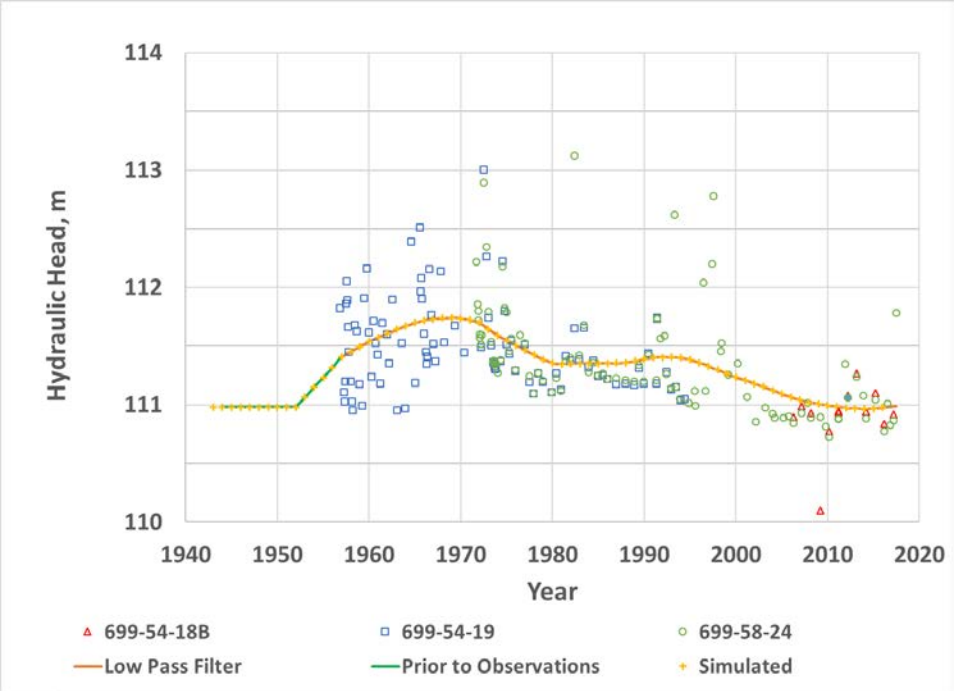

Figure 4-11. Simulated and Observed Head Values at the Northeastern Boundary of the P2R Model Version 8.2 for the Historic Calibration Simulation

4.4.2 Hydraulic Properties

The hydraulic properties used as input parameters to the P2R Model include hydraulic conductivity, specific yield, specific storage, and the hydraulic characteristic used to define the horizontal flow barrier representing the May Junction Fault. In previous version of the P2R Model, hydraulic properties were assigned as constant parameters across each of the HSUs defined in the model. The initial parameterization for the hydraulic parameters in the P2R Model were extracted from the CPGW version 8.4.5 where the models overlap and version 7.1 of the P2R Model. As part of the calibration process, pilot point calibration was used to introduce spatial variability into the hydraulic conductivity field to improve the match between simulated and observed hydraulic head values. The process of altering the hydraulic conductivity field is discussed in Section 4.5.

The hydraulic effects of the May Junction Fault are included as a feature in this model. First, the offset of HSUs caused by the fault is included in the HSGF that was used to develop the grid structure of the MODFLOW model. Hydraulic property assignment based on HSU will honor the contrasting hydraulic properties where HSUs are offset. Second, a horizontal flow barrier was assigned to layers 5 through 7 along the plane of the fault. Figure 4-12 shows the location of the fault and the simulated flow barrier. The hydraulic characteristic assigned to the flow barrier, 6.92E-03 day^{-1}, was calibrated in version 7.1 of the P2R model and was not altered for this version.

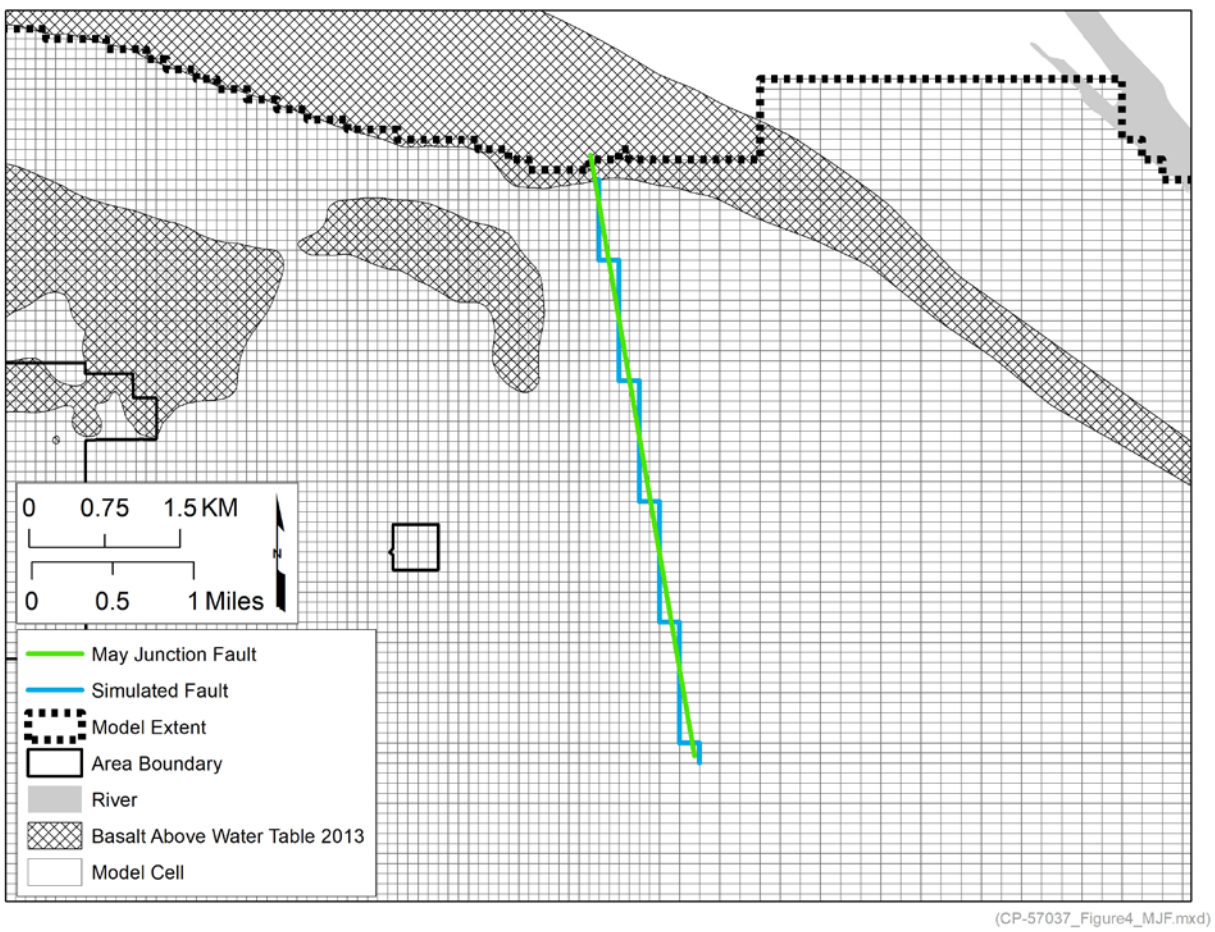

Figure 4-12. Location of the Horizontal Flow Barrier Cells used to Simulate the May Junction Fault

4.4.3 Columbia River Boundary

An important feature of the P2R model is the simulation of the interaction between the Columbia River and the aquifer. River stage for the Columbia River was determined based on observed data collected at a river gage just below the Priest Rapids Dam. This data is recorded by the USGS and available using the National Water Information System (U.S. Geological Survey, 2017). An estimated river gradient was developed as part of *Groundwater Data Package for Hanford Assessments*, PNNL-14753. This report provides the river gradient based on numerical simulations of the Columbia River throughout the Hanford Site. The observed flow from Priest Rapids Dam is used to estimate the river stage at the gage location using the rating curve developed for that location where both gage height and discharge were recorded at Priest Rapids Dam. The constructed rating curve for Priest Rapids Dam is shown in Figure 4-13. The historic flow was used to develop relative stage at the Priest Rapids gage for each month in the simulation time period of 1943 through 2016. These values are shown Figure 4-14.

The relative stage at the Priest Rapids dam can be estimated for each year in the simulation time frame of 1943 through 2016. Figure 4-14 shows the difference between the average stage for each year to the baseline stage at the Priest Rapids Dam. This relative stage was used to calculate the river stage for the simulation period in the model. Figure 4-15 shows a comparison average annual Columbia River stage at the boundary of the P2R Model for the years 1957, 1977, and 1997. The simulated stage in the model for these three years is a variation of stage for the baseline river gradient provided by PNNL-14753. The river stage along the entire reach of the Columbia River boundary condition is shifted up or down by the magnitude of the difference between the river stage at the Priest Rapids gage for the baseline year and each year of the simulation. This process was completed for each year of the simulation and formatted for input into the model using the MODFLOW River package. These river stages were applied to the river cells shown in Figure 4-1.

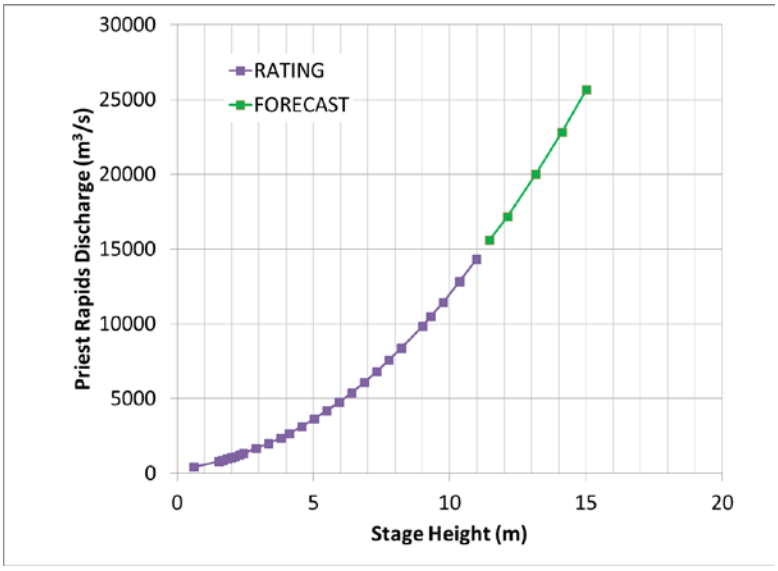

Figure 4-13. Rating Curve for the Priest Rapids Dam Gage on the Columbia River Including a Forecast above 11 m

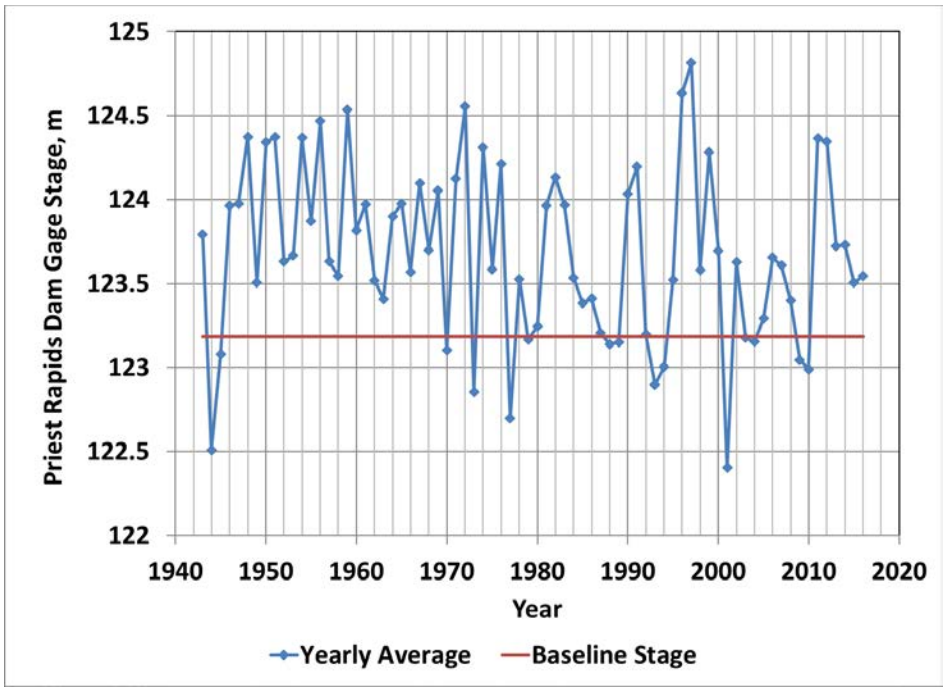

Figure 4-14. Comparison of the Mean Yearly Stage for the Columbia River at the Priest Rapids Dam Gage for the P2R Model, v.8.2 Simulation Period to the Reference Stage at the Same Gage Location

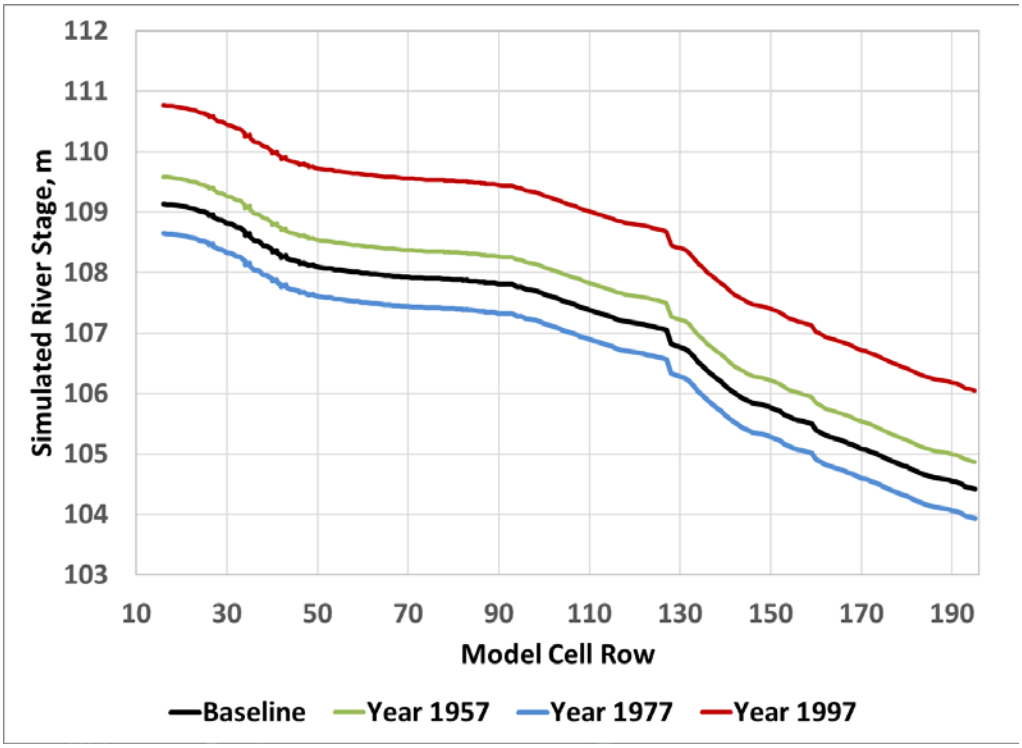

Figure 4-15. Comparison between River Stage Simulated as part of the P2R Model based on the Yearly Average Flow and Rating Curve at the Priest Rapids Dam Gage Upstream of the Hanford Site for Three Distinct Stress Periods

4.4.4 Recharge

Recharge at the water table in the historical model comprises the following contributions:

- Natural recharge - deep percolation of precipitation that is not evaporated/transpired and is not retained in storage in the vadose zone
- Mountain front recharge - infiltration of snowmelt and runoff from Rattlesnake Mountain
- Anthropogenic recharge - historical wastewater discharges at the Hanford Site

As discussed in Section 3.2.3 the parameterization for natural recharge is similar to the approach taken in PNNL-14753 and by the CPGW Model version 8.4.5. Recharge zones, based on surficial soil type, were delineated for each cell in the model domain based on surface soil maps. A recharge flux specific to the designated soil types was applied to each cell based on their particular soil type assignment. Initial net recharge from aerial precipitation rates were acquired from CPGW Model Version 8.4.5. Figure 4-16 displays natural recharge associated with precipitation and mountain-front recharge used in the model. The “pond” designation reflects the location of two major ponds, Gable Mountain and B-pond. These rates reflect the disturbance of the soil and increased recharge in these locations. Discharge amounts for these ponds are handled as part of anthropogenic recharge discussed later. The light green strip of polygons on the western side of the model are where the Rattlesnake Mountain fluxes are applied. These areas are offset from the edge of the model to prevent recharge from being directly applied to the low-conductivity Ringold mud unit. The total volumetric flux for the Rattlesnake Mountain front recharge is 809 m^3/day in the model inputs. This is within the estimated range provided in section 3.2.3. The final calibrated values for recharge from natural recharge and mountain front recharge are presented in Section 4.5.4.7.

Fluxes from surface water discharge due to operations at the Hanford Site are summarized in EMDT-BC-0002 (Appendix E). The data include the magnitudes and locations of operational discharges for the simulated time periods in the model on a yearly time step. Locations of discharge include waste sites, ponds, sewer discharge, french drains, and documented unplanned releases for the entire operational period and projections of future discharges. Figure 4-17 shows the locations of discharges listed in EMDT-BC-0002 that exist within the model domain. Figure 4-18 depicts the differences in magnitude of total anthropogenic recharge for the entire period of record between different waste sites.

For large waste sites, the footprint overlaps more than one model cell. In cases where this occurs, the total discharge is distributed in an area-weighted basis to all cells that intersect the footprint of the discharge location. Figure 4-19 shows an example waste site, 216-S-16P, that intersects a total of 18 model cells. The total discharge is applied to the 18 cells based on the percentage of the surface area that falls within the footprint of each cell. The more surface area that covers the cell, the greater the percentage of the total recharge that will enter the model at that location. The anthropogenic flux is added to the natural recharge component in order to establish the final total recharge flux used in the simulations. Discharges included in EMDT-BC-0002 have been attenuated to account for travel through the vadose zone. The changes vary with time according to the values provided in EMDT-BC-0002. Anthropogenic recharge values are not included in the first stress period included at the beginning of the simulation that represents pre-operational activities. Alterations to the footprint for two waste sites was altered during the calibration process. The alteration made for these waste sites is discussed in Section 4.5.4.4.

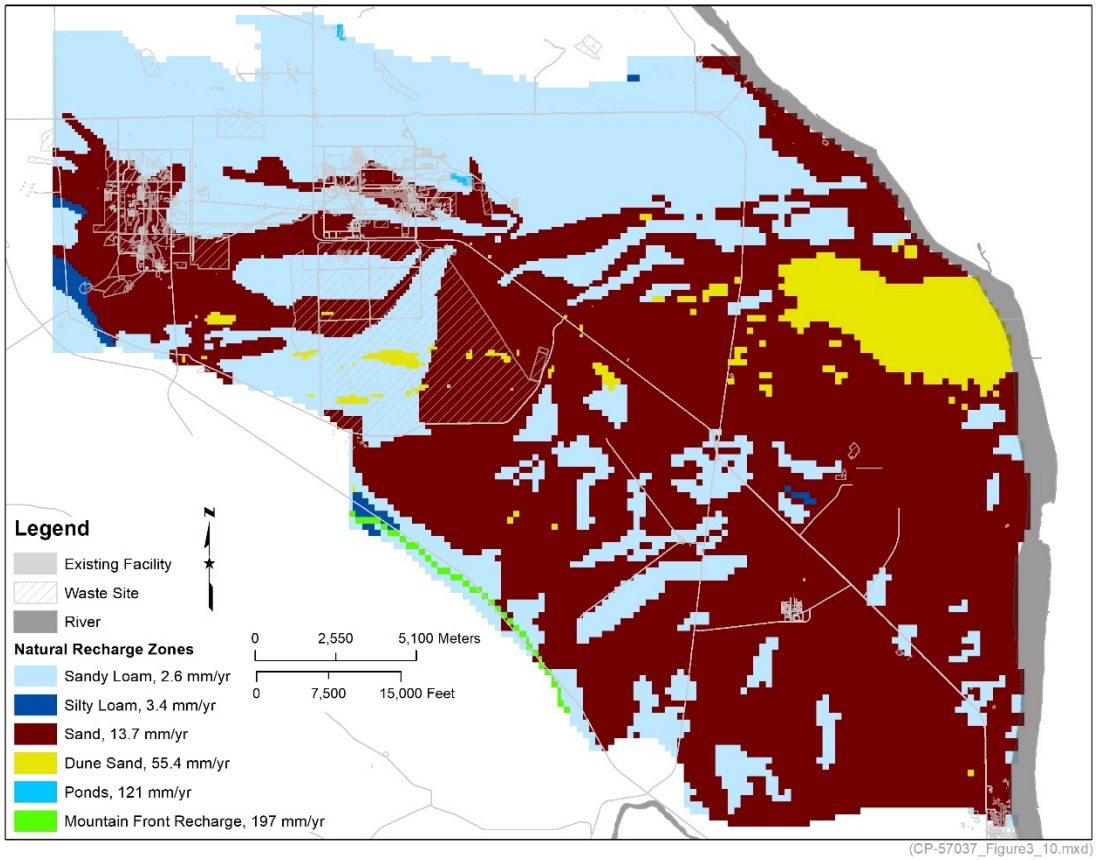

Figure 4-16. Natural Recharge Fluxes used in the P2R Model Version 8.2

4.4.5 Extraction/Injection of Groundwater

P2R Model Version 8.2 includes historical pumping rates obtained from annual summary reports for the 200-ZP-1 and 200-UP-1 OUs, as documented in EMDT-ST-0004, *Historical Pumping Rates 200-West Area* (Appendix H). The physical specifications for the relevant wells are available in the HEIS database and are the same as presented in ECF-200ZP1-16-0076, *Description of Groundwater Calculations and Assessments for the Calendar Year 2015 (CY 2015) 200 Areas Pump and Treat Report*. Extraction and injection were simulated using the multi-node well package for MODFLOW and the contaminant treatment system package for MT3DMS. The multi-node well package simulated the injection and extraction of groundwater from the aquifer. Table 4-4 provides the well names and rates that were simulated for the calibration period of the P2R Model version 8.2. All extraction/injection rates prior to the record provided in EMDT-ST-0004 are assumed to be zero.

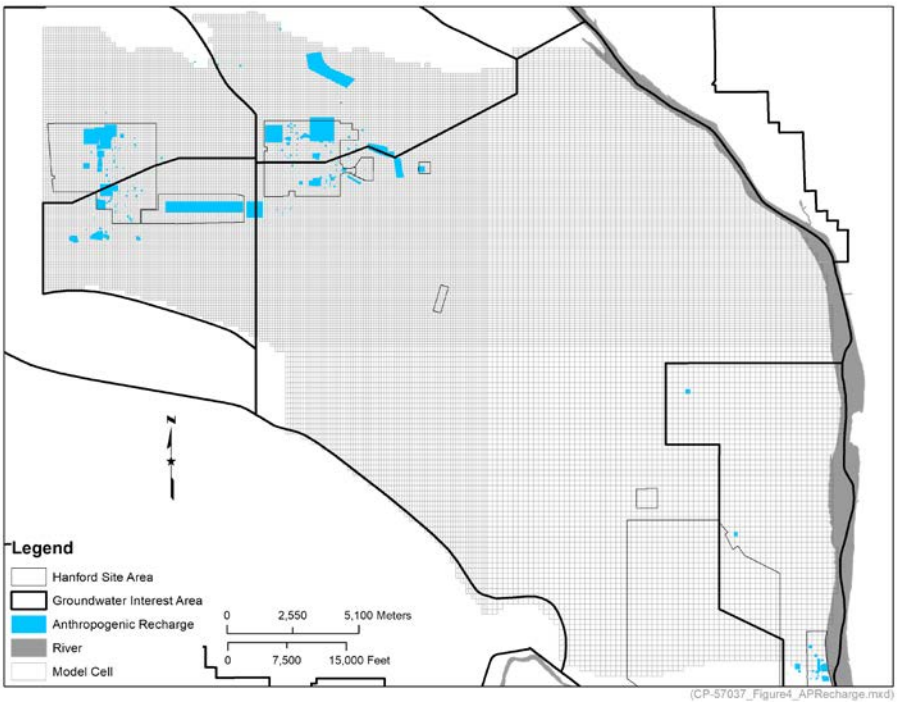

Figure 4-17. Model Grid Cell Locations Affected by Anthropogenic Recharge in the P2R Model

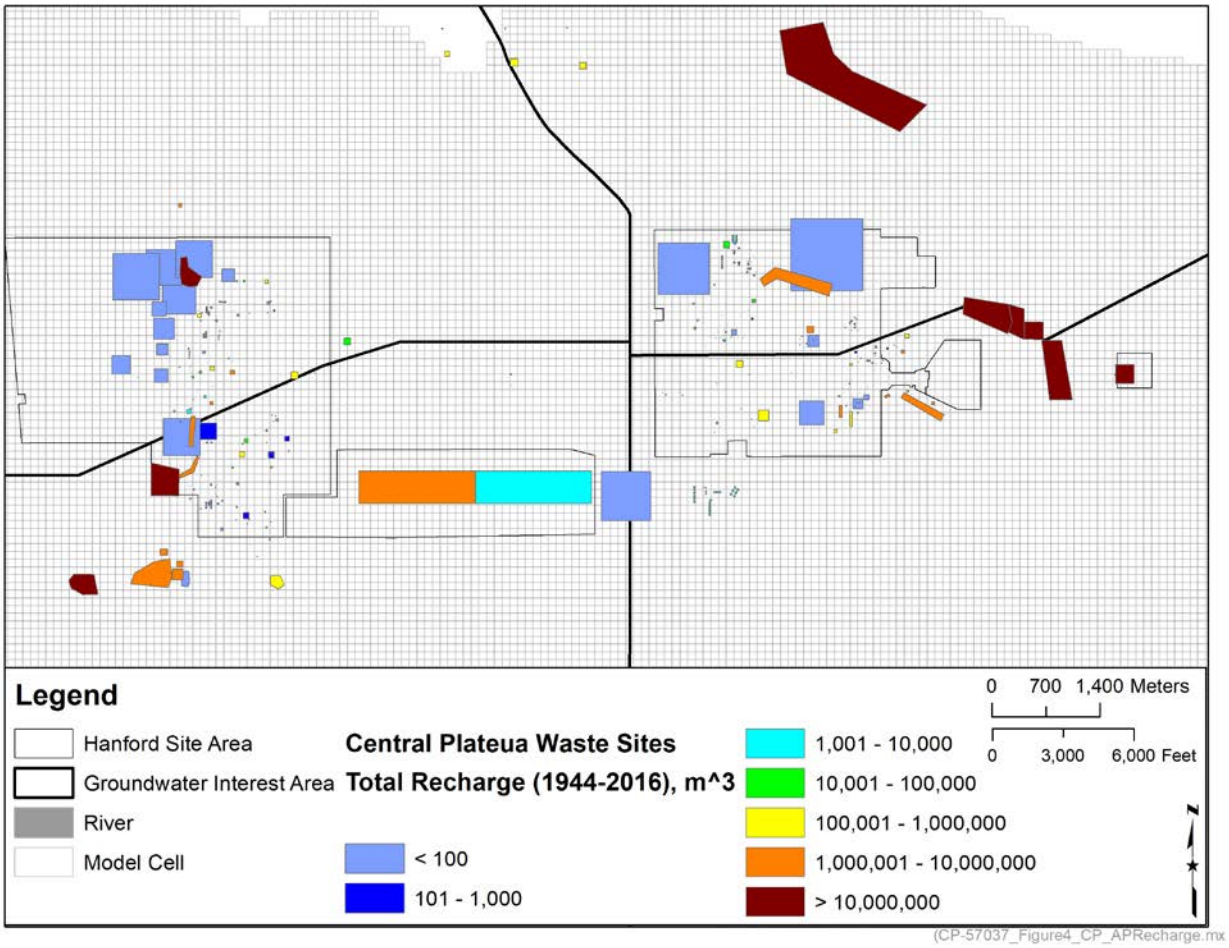

Figure 4-18. Total Cumulative Anthropogenic Recharge for Calendar Years 1944 to 2016 for Waste Sites Located on the Central Plateau

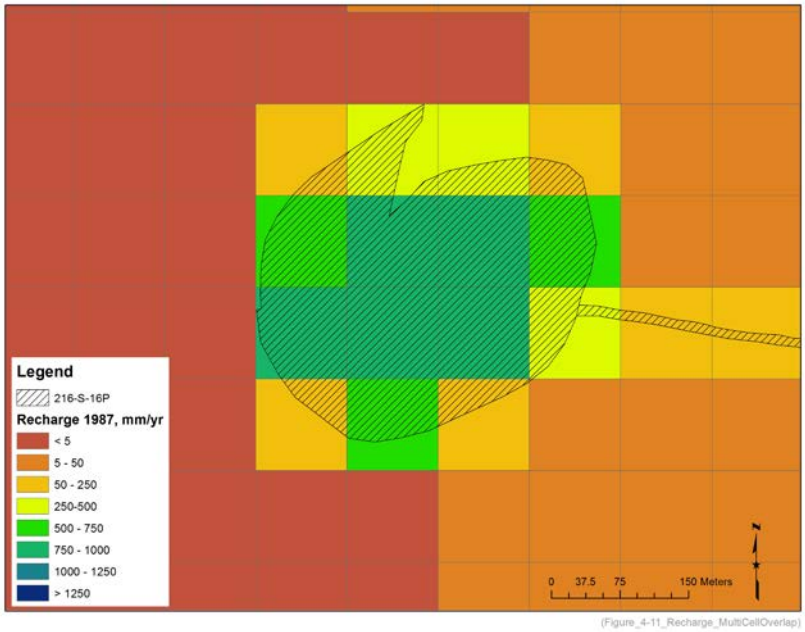

Figure 4-19. Example of the Distribution of Recharge at Waste Sites Overlapping Multiple Cells

Table 4-4. Simulated Pumping Rates (gpm) for Extraction and Injections Wells used in the P2R Model Calibration

Year/Stress Period	1994	1995	1996	1997	1998	1999	2000	2001	2002	2003	2004	2005	2006	2007	2008	2009	2010	2011	2012	2013	2014	2015	2016
Well Name	**52**	**53**	**54**	**55**	**56**	**57**	**58**	**59**	**60**	**61**	**62**	**63**	**64**	**65**	**66**	**67**	**68**	**69**	**70**	**71**	**72**	**73**	**74**
299-W19-23	-1	-2	0	0	0	0	0	0	0	0	0	0	0	0	0	0	0	0	0	0	0	0	0
299-W19-24	-1	-2	0	0	0	0	0	0	0	0	0	0	0	0	0	0	0	0	0	0	0	0	0
299-W19-25	3	4	0	0	0	0	0	0	0	0	0	0	0	0	0	0	0	0	0	0	0	0	0
299-W19-36E	0	0	0	0	0	0	0	0	-7	-4	-7	0	0	-4	-3	-3	-1	0	0	0	0	0	0
299-W19-36I	0	13	44	1	0	0	0	0	0	0	0	0	0	0	0	0	0	0	0	0	0	0	0
299-W19-39	0	-13	-44	-35	-47	-46	-45	-46	-32	-34	-36	-2	0	0	0	0	0	0	0	0	0	0	0
299-W19-43	0	0	0	0	0	0	0	0	0	-6	-9	0	0	-4	-2	-3	-1	-1	0	0	0	0	0
299-W18-1	-2	-7	-4	0	0	0	0	0	0	0	0	0	0	0	0	0	0	0	0	0	0	0	0
299-W18-4	2	7	4	0	0	0	0	0	0	0	0	0	0	0	0	0	0	0	0	0	0	0	0
299-W15-1	0	0	0	0	0	0	0	0	0	0	0	0	0	0	-3	-7	-8	-10	-3	0	0	0	0
299-W15-6	0	0	0	0	0	0	0	0	0	0	0	0	-2	-6	-4	-3	-3	-1	0	0	0	0	0
299-W15-7	0	0	0	0	0	0	0	0	0	0	0	0	0	0	-3	-7	-6	-5	-1	0	0	0	0
299-W15-11	0	0	0	0	0	0	0	0	0	0	0	0	0	0	-7	-10	-12	-11	-3	0	0	0	0
299-W15-32	0	0	0	-6	-18	-5	-15	-10	-8	-7	-1	0	0	0	0	0	0	0	0	0	0	0	0
299-W15-33	0	0	-8	-20	-15	-15	-11	-13	-5	-11	-3	0	0	0	0	0	0	0	0	0	0	0	0
299-W15-34	0	0	-10	-29	-24	-22	-25	-24	-17	-20	-18	-15	-17	-17	-11	-5	-9	-12	-3	0	0	0	0
299-W15-35	0	0	-21	-61	-81	-79	-80	-90	-72	-70	-58	-40	-45	-44	-28	-29	-25	-17	-1	0	0	0	0
299-W15-36	0	0	0	-7	-29	-27	-29	-35	-23	-18	-18	-11	-11	-16	-10	-5	0	0	0	0	0	0	0
299-W15-37	0	0	0	-6	-14	-16	-17	-1	0	0	0	0	0	0	0	0	0	0	0	0	0	0	0
299-W15-40	0	0	0	0	0	0	0	0	0	0	0	-3	-6	-6	-4	-3	-3	0	0	0	0	0	0
299-W15-43	0	0	0	0	0	0	0	0	0	0	0	-21	-46	-43	-25	-22	-20	-14	-3	0	0	0	0
299-W15-44	0	0	0	0	0	0	0	0	0	0	0	-4	-8	-5	-3	-3	0	0	0	0	0	0	0
299-W15-45	0	0	0	0	0	0	0	0	0	0	-28	-35	-32	-28	-15	-9	-21	-17	-4	0	0	0	0
299-W15-46	0	0	0	0	0	0	0	0	0	0	0	0	0	0	-11	-32	-44	-46	-9	0	0	0	0
299-W15-47	0	0	0	0	0	0	0	0	0	0	-22	-37	-34	-55	-31	-27	-9	-2	0	0	0	0	0
299-W15-765	0	0	0	0	0	0	0	0	0	0	0	-11	-25	-19	-13	-12	-6	-1	0	0	0	0	0
299-W11-45	0	0	0	0	0	0	0	0	0	0	0	0	0	-3	-3	-8	-8	-10	-1	0	0	0	0
299-W11-46	0	0	0	0	0	0	0	0	0	0	0	0	0	-8	-22	-27	-18	-20	-6	0	0	0	0
299-W15-225	0	0	0	0	0	0	0	0	0	0	0	0	0	0	0	0	-114	-246	-96	-81	-90	-96	-62
299-W14-20	0	0	0	0	0	0	0	0	0	0	0	0	0	0	0	0	0	0	-21	-93	-78	-109	-104
299-W14-73	0	0	0	0	0	0	0	0	0	0	0	0	0	0	0	0	0	0	-17	-82	-98	-125	-79
299-W14-74	0	0	0	0	0	0	0	0	0	0	0	0	0	0	0	0	0	0	-12	-99	-105	-127	-60
299-W12-2	0	0	0	0	0	0	0	0	0	0	0	0	0	0	0	0	0	0	-19	-86	-93	-104	-53
299-W11-50	0	0	0	0	0	0	0	0	0	0	0	0	0	0	0	0	0	0	-20	-91	-111	-108	-75
299-W11-90	0	0	0	0	0	0	0	0	0	0	0	0	0	0	0	0	0	0	-22	-103	-114	-109	-101
299-W11-96	0	0	0	0	0	0	0	0	0	0	0	0	0	0	0	0	0	0	-16	-88	-78	-95	-43
299-W17-3	0	0	0	0	0	0	0	0	0	0	0	0	0	0	0	0	0	0	-19	-88	-94	-122	-60
299-W17-2	0	0	0	0	0	0	0	0	0	0	0	0	0	0	0	0	0	0	-16	-73	-88	-87	-65
299-W19-111	0	0	0	0	0	0	0	0	0	0	0	0	0	0	0	0	0	0	0	0	0	0	0

Table 4-4. Simulated Pumping Rates (gpm) for Extraction and Injections Wells used in the P2R Model Calibration

Year/Stress Period	1994	1995	1996	1997	1998	1999	2000	2001	2002	2003	2004	2005	2006	2007	2008	2009	2010	2011	2012	2013	2014	2015	2016
Well Name	**52**	**53**	**54**	**55**	**56**	**57**	**58**	**59**	**60**	**61**	**62**	**63**	**64**	**65**	**66**	**67**	**68**	**69**	**70**	**71**	**72**	**73**	**74**
299-W11-49	0	0	0	0	0	0	0	0	0	0	0	0	0	0	0	0	0	0	-19	-92	-101	-125	-67
299-W11-97	0	0	0	0	0	0	0	0	0	0	0	0	0	0	0	0	0	0	0	0	0	-4	-28
299-W6-15	0	0	0	0	0	0	0	0	0	0	0	0	0	0	0	0	0	0	0	0	0	-49	-32
299-W14-21	0	0	0	0	0	0	0	0	0	0	0	0	0	0	0	0	0	0	-17	-86	-100	-77	-2
299-W11-92	0	0	0	0	0	0	0	0	0	0	0	0	0	0	0	0	0	0	-20	-98	-115	-111	-78
299-W5-1	0	0	0	0	0	0	0	0	0	0	0	0	0	0	0	0	0	0	0	0	-8	-66	-40
299-W12-3	0	0	0	0	0	0	0	0	0	0	0	0	0	0	0	0	0	0	-19	-96	-86	-66	-34
299-W12-4	0	0	0	0	0	0	0	0	0	0	0	0	0	0	0	0	0	0	-21	-98	-115	-117	-53
299-W14-22	0	0	0	0	0	0	0	0	0	0	0	0	0	0	0	0	0	0	0	0	-8	-80	-38
299-W22-90	0	0	0	0	0	0	0	0	0	0	0	0	0	0	0	0	0	0	-4	-20	-19	-24	-19
299-W22-91	0	0	0	0	0	0	0	0	0	0	0	0	0	0	0	0	0	0	-5	-27	-35	-34	-33
299-W22-92	0	0	0	0	0	0	0	0	0	0	0	0	0	0	0	0	0	0	-4	-21	-29	-34	-33
299-W19-113	0	0	0	0	0	0	0	0	0	0	0	0	0	0	0	0	0	0	0	0	0	-10	-52
299-W19-114	0	0	0	0	0	0	0	0	0	0	0	0	0	0	0	0	0	0	0	0	0	-23	-95
299-E33-268	0	0	0	0	0	0	0	0	0	0	0	0	0	0	0	0	0	0	0	0	0	-20	-62
299-W6-13	0	0	0	0	0	0	0	0	0	0	0	0	0	0	0	0	0	0	30	139	78	56	37
299-W6-14	0	0	0	0	0	0	0	0	0	0	0	0	0	0	0	0	0	0	22	133	222	196	121
299-W10-36	0	0	0	0	0	0	0	0	0	0	0	0	0	0	0	0	0	0	20	113	120	92	63
299-W10-35	0	0	0	0	0	0	0	0	0	0	0	0	0	0	0	0	0	0	22	135	149	106	65
299-W15-226	0	0	0	0	0	0	0	0	0	0	0	0	0	0	0	0	0	0	26	162	199	226	151
299-W15-227	0	0	0	0	0	0	0	0	0	0	0	0	0	0	0	0	0	0	20	136	161	103	86
299-W15-228	0	0	0	0	0	0	0	0	0	0	0	0	0	0	0	0	0	0	0	0	0	139	87
299-W18-41	0	0	0	0	0	0	0	0	0	0	0	0	0	0	0	0	0	0	0	0	0	55	48
699-49-69	0	0	0	0	0	0	0	0	0	0	0	0	0	0	0	0	0	0	0	0	24	56	31
699-45-67B	0	0	0	0	0	0	0	0	0	0	0	0	0	0	0	0	0	0	0	1	17	1	1
699-45-67	0	0	0	0	0	0	0	0	0	0	0	0	0	0	0	0	0	0	0	12	96	76	31
699-44-67	0	0	0	0	0	0	0	0	0	0	0	0	0	0	0	0	0	0	27	95	47	28	6
699-43-67	0	0	0	0	0	0	0	0	0	0	0	0	0	0	0	0	0	0	0	0	0	68	24
699-42-67	0	0	0	0	0	0	0	0	0	0	0	0	0	0	0	0	0	0	27	101	93	104	78
699-40-67	0	0	0	0	0	0	0	0	0	0	0	0	0	0	0	0	0	0	0	0	31	94	38
699-38-64	0	0	0	0	0	0	0	0	0	0	0	0	0	0	0	0	0	0	0	0	0	51	40
699-43-67B	0	0	0	0	0	0	0	0	0	0	0	0	0	0	0	0	0	0	29	80	39	46	27
299-W15-29	0	0	39	132	137	78	82	70	63	49	71	103	88	74	54	38	70	139	52	92	47	36	34
299-W18-36	0	0	0	0	37	45	47	46	42	47	47	47	87	94	48	39	62	86	39	80	88	64	54
299-W18-37	0	0	0	0	14	30	42	40	33	31	28	20	34	64	39	32	48	6	13	63	17	0	0
299-W18-38	0	0	0	0	2	0	0	0	0	1	9	7	25	12	10	25	50	70	32	49	74	48	41
299-W18-39	0	0	0	0	7	6	0	0	0	2	1	0	0	1	14	36	51	70	32	51	60	25	13
699-46-68	0	0	0	0	0	0	0	0	0	0	0	0	0	0	0	0	0	0	0	0	32	93	49
299-W15-229	0	0	0	0	0	0	0	0	0	0	0	0	0	0	0	0	0	0	0	0	10	145	72
299-W7-14	0	0	0	0	0	0	0	0	0	0	0	0	0	0	0	0	0	0	0	0	0	0	11
299-E20-1	0	0	0	0	0	0	0	0	0	0	0	0	0	0	0	0	0	0	0	0	0	12	59

Table 4-4. Simulated Pumping Rates (gpm) for Extraction and Injections Wells used in the P2R Model Calibration

Year/Stress Period	1994	1995	1996	1997	1998	1999	2000	2001	2002	2003	2004	2005	2006	2007	2008	2009	2010	2011	2012	2013	2014	2015	2016
Well Name	**52**	**53**	**54**	**55**	**56**	**57**	**58**	**59**	**60**	**61**	**62**	**63**	**64**	**65**	**66**	**67**	**68**	**69**	**70**	**71**	**72**	**73**	**74**
299-E20-2	0	0	0	0	0	0	0	0	0	0	0	0	0	0	0	0	0	0	0	0	0	10	31
299-E11-1	0	0	0	0	0	0	0	0	0	0	0	0	0	0	0	0	0	0	0	0	0	14	53

This page intentionally left blank.

4.4.6 Transport Parameters

P2R Model Version 8.2 used transport simulations for tritium to aid in the calibration process. The transport parameters are the same used in the most recent transport applications of the CPGW Model version 8.4.5, which are documented in ECF-200ZP1-16-0076 and listed in Table 4-5.

4.5 Calibration

Measured water-level data from 1944 to 2016 were used as the quantitative measure of model accuracy. During the calibration process, model input parameters were altered in a systematic and iterative fashion to improve the models fit to the observed data. Both manual and automated calibration to the set of historical water-level data using PEST parameter estimation software (Doherty, 2016, *PEST Model-Independent Parameter Estimation User Manual: 6th Edition*) was used to develop the estimate of the model parameter values. Automated calibration provides valuable information on the response of the model outputs to parameter changes and can help to identify structural weaknesses in a model. This section discusses the calibration process, including (1) development of the calibration data set, (2) metrics used to assess goodness-of-fit between calibration data and the model, (3) development of hydraulic gradient dataset, and (4) results of the calibration process. Information regarding the calibration of previous versions of the P2R model and CPGW Model is presented in their respective reports; this section discusses only the calibration process used for P2R Model Version 8.2.

4.5.1 Calibration Data Set

The assessment of the goodness-of-fit of a model calibration depends on the field observations used to assess the level to which the model mimics reality. The data must be gathered and assessed to determine if the information will provide a reasonable assessment that the model is simulating the FEPs that are identified within the model domain. For P2R Model Version 8.2, three types of data were developed for assessing the model calibration: hydraulic head data, contaminant concentration data for wells, and maps of plume estimates across the site.

4.5.1.1 Hydraulic Head Data

The selection criteria for wells chosen for the calibration data set of P2R Model Version 8.2 is the same as the data set used for assessing the calibration of the CPGW Model Version 8.4.5. Where the model domains overlap, the same wells and measurements were used for both datasets. These well locations and measurements were augmented with wells outside the shared model domain based on selection criteria below.

- Well location within the model domain
- Horizontal coordinate system and coordinates known
- Vertical datum known
- Screened interval known (data were supplemented from HEIS database for this purpose)
- Greater than or equal to 5-year period of record
- Well ground surface or brass plate elevation known or able to be calculated within tolerances

The locations of all 479 wells available for calibration and meeting the criteria are shown in Figure 4-20. Attachment B contains a table that lists every well used as part of this dataset. Not all wells are labeled in the figure to preserve legibility of the figure. The period of record for water-level measurements in these wells varies from 1948 to 2016. All individual measurements were weighted equally when calculating

summary statistics as part of the calibration process discussed in section 4.5.2.. Attachment D includes hydrographs from all wells shown in Figure 4-20.

Table 4-5. Contaminant Transport Properties Assumed for F&T Analyses Using the P2R Model

Chemical Dependent Transport Parameter Values for the Plateau to River Model Version 8.2						
COC	**K_d (mL/g)**	**Half-Life (yr)**	**Half-Life (day)**	**Degradation Rate (one/day)**	**Reference for K_d**	**Reference for Degradation Rate**
Tritium	0	12.3	4,500.0	0.000154	PNNL-18564, Table 6.9	EPA 402-R-99-001, Table 2.2a

Aquifer Dependent Transport Parameter Values for the Plateau to River Model		
Property	**Value**	**Comments**
Effective porosity	0.15	Approximate central value (Table D-2 of DOE/RL-2007-28)
Longitudinal dispersivity	3.5 – 6.2 m	Based on grid cell size according to Schulze-Makuch (2005)
Transverse dispersivity	0.7 – 1.24 m	20% of longitudinal (consistent with the ratio specified in DOE/RL-2008-56)
Vertical dispersivity	0.0 m	DOE/RL-2008-56
Molecular diffusion constant	0.0 m^2/day	Negligible term
Bulk density, Hanford, Cold Creek	1.93 g/cm^3	PNNL-18564, Table 6.2
Bulk density, Ringold Taylor Flat, unit E, lower mud, unit A	1.90 g/cm^3	PNNL-18564, Table 6.2

COC = contaminant of concern CY = calendar year K_d = distribution coefficient

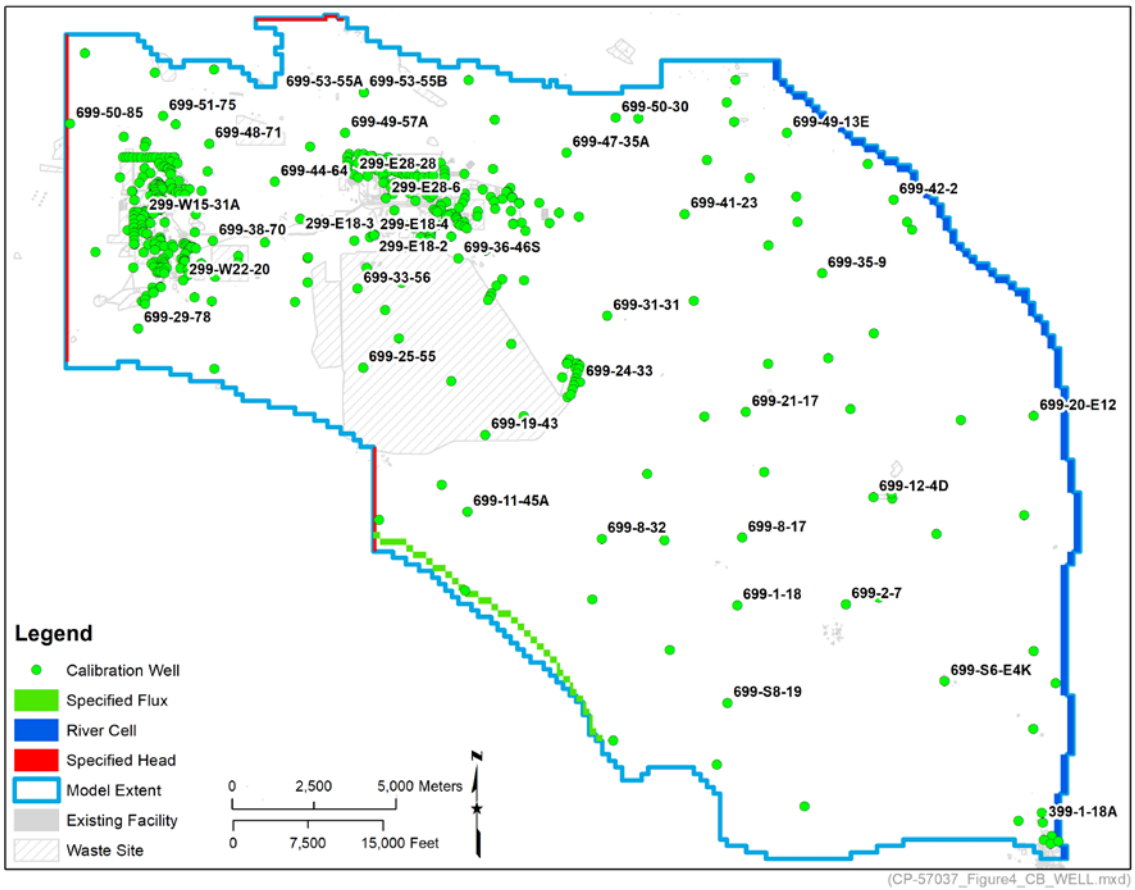

Figure 4-20. Wells Selected for Calibration Targets (labeled locations were selected for display in this report)

Well Screen Data

Screened interval information for the wells was not part of the original water-level data set. The following steps were taken to compile a sufficient tabulation of well screen data:

1. The available screen information was supplemented by the data set from the HEIS database. The query that retrieved these data was the same used to retrieve the original 969 wells from the 2008 groundwater monitoring report (DOE/RL-2008-66).

2. This table was joined to the water-level data set that had been refined to the wells only in the model area.

3. Well screen information compiled in support of the precursor 200-ZP-1 Model was added to this database. This screen information was sourced from the Integrated Document Management System database well construction and completion summary reports.

4. Screen bottom elevations were updated with the elevations of the bottom of the well where that elevation was greater than the original screen bottom elevation. This update resulted from some screens extending below a “cement plug.”

5. Some of the wells that were updated to match the bottom of the wells were reverted to the original well depth reflective of the period that the wells were functioning as water-level monitoring wells. These wells had experienced a collapse, and the current depth to bottom was not reflective of the depth when the well was actually used for monitoring. The information for making this change was obtained from Hanford Well Information System database.

4.5.1.2 Historical Plume Maps

Estimates of contaminant concentration are developed annually as part of DOE/RL-2016-09, *Hanford Site Groundwater Monitoring Report for 2015*, and its predecessor annual monitoring reports. The plumes represent an estimate of groundwater concentration near the top of the water table for major COCs across the site. The interactive report also archives the historical plume maps created in previous versions of the annual monitoring report. Using these archives, the historical plume maps were used to compare flow direction over the historical calibration period. These plume maps were used in a qualitative manner to assess the calibration process. Simulated plumes should generally move in the same direction and magnitude as the plumes prepared in the historical plume maps in order for the model to be considered calibrated. This process was used for a historical tritium simulation described in Section 4.5.4. Figure 4-21 shows the tritium plume over several years.

Reference: DOE/RL-2016-09, *Hanford Site Groundwater Monitoring Report for 2015*.

Figure 4-21. Historical Tritium Plume Estimates Archived as Part of DOE/RL-2016-09

4.5.2 Goodness-of-Fit Metrics

Four goodness-of-fit statistical measures were used to evaluate the comparison of observed and simulated hydraulic head values throughout the model domain: (1) root mean squared error (RMSE), (2) mean absolute error, (3) mean error, and (4) the Pearson correlation coefficient. Equations 4-1 through 4-4 provide the formulas for calculating each of these measures, respectively. In each case, the goal of calibration is to reduce the magnitude of the first three goodness-of-fit statistics and obtain a value approaching 1 for the correlation coefficient. However, care must be taken to ensure that improvements in the goodness-of-fit statistics are not achieved by using input parameter values or producing simulated results that violate the conceptual site model.

$$RMSE = \sqrt{\frac{1}{n}\sum_{i=1}^{n}(y_i - x_i)^2} \qquad \text{(Equation 4-1)}$$

$$MAE = \frac{1}{n}\sum_{i=1}^{n} abs(y_i - x_i) \qquad \text{(Equation 4-2)}$$

$$ME = \frac{1}{n}\sum_{i=1}^{n}(y_i - x_i) \qquad \text{(Equation 4-3)}$$

$$COR = \frac{\sum_{i=1}^{n}(x_i - \bar{x})(y_i - \bar{y})}{\sqrt{\sum_{i=1}^{n}(x_i - \bar{x})^2}\sqrt{\sum_{i=1}^{n}(y_i - \bar{y})^2}} \quad \text{(Equation 4-4)}$$

where:

RMSE	=	root mean squared error
MAE	=	mean absolute error
ME	=	mean error
COR	=	correlation coefficient
n	=	number of measurements
y_i	=	observed hydraulic head
x_i	=	simulated hydraulic head
$\bar{x}$	=	average simulated hydraulic head
$\bar{y}$	=	average observed hydraulic head

Each statistical measure provides a slightly different perspective on the comparison of simulated results. The mean error statistic is used to represent the overall bias (high or low) in the model. A positive value signifies that the model tends to under-predict hydraulic head. However, a mean error statistic is near zero may be the result of high and low values that cancel each other out of the calculation. Both the RMSE and the mean absolute error help with this issue by using the squared and absolute residual value (which are always positive) rather than the residual value (which can be positive or negative). The RMSE uses squared residual values to accentuate the effect of values away from the mean residual value. When the residual is large, raising it to the second power will weight that measurement more than those closer to one.

4.5.3 Hydraulic Gradients

Calculation of hydraulic gradients between monitoring wells has been introduced to the P2R Model Version 8.2 development and calibration. Gradients were introduced in areas over a large portion of the model domain to evaluate flow direction changes over time. It is possible to achieve visually (and statistically) good correspondence between model outputs and measured water levels although the simulated gradients may be inconsistent; therefore, flow directions can differ markedly from actual gradients and flow directions as reflected in the measured water-level data. The method used for this determination is a gradient calculated using water levels obtained at three wells that form a triangle. Using this method, if the simulated water level at only one well differs from the measured water level at that same location, then the gradient calculated using the model outputs can be of a different magnitude and, perhaps more importantly, a different direction than the measured gradient. This is important, as one of the intended uses of this model is to predict the F&T of contaminants in groundwater.

Gradients are constructed from measuring data at three wells (a triplet) that are used to define a hydraulic gradient plane. Figure 4-22 presents the locations of the gradients used for calibration. Table 4-6 lists the well triplets used to define the gradients. Figure 4-23 presents the direction and magnitude of the gradient for triplet set 1. Figure 4-23 introduces the concept of gradient calculations. The direction is plotted in terms of azimuth (degrees clockwise from north); an azimuth of 90 degrees is due east. A measured gradient can only be calculated when all three wells have measurements available during a given year. As illustrated in the figure, the triangulation of points around a given well provides calculation of gradients of several triangles affected by the results at one well. The wells were selected in an attempt to provide a long period of record with wells that had measurements in many years. The calibrated gradient for the previous version of the model and the CPGW Model Version 8.4.5 (where model domains overlap) are included on the plots for reference purposes. All gradient plots are included in attachment C of this document.

4.5.4 Calibration Process

Calibration of the P2R Model is an evolving process that involves more than manipulating parameter values. Modifications to the interpreted HSU geometry and the method of assigning the GHB conditions are also part of the calibration process. As model development has progressed, features introduced in earlier calibrations have been subsequently retained. This section discusses only the calibration process for P2R Model Version 8.2. Details regarding the calibration process for previous model versions are provided in previous revisions of this report. However, in order to assess the process of calibration, quantitative and qualitative comparisons will be made to the previous version, Version 7.1, and to the CPGW Model Version 8.4.5. Comparisons to the CPGW Model Version 8.4.5 are made because of the overlap in the model domain of the two models.

The following subsections present the complete evolution of the model development. The major milestones and changes made to the model are also discussed as part of the calibration process. These include (1) the implementation of CPGW Model Version 8.4.5 parameters in the shared model domain, (2) calibration of hydraulic properties in the far-field portion of the model domain, (3) calibration of hydraulic properties in 200-West Area, (4) calibration of recharge parameters in 200-West, (5) high conductivity channel development, and (6) historical transport comparison of tritium transport.

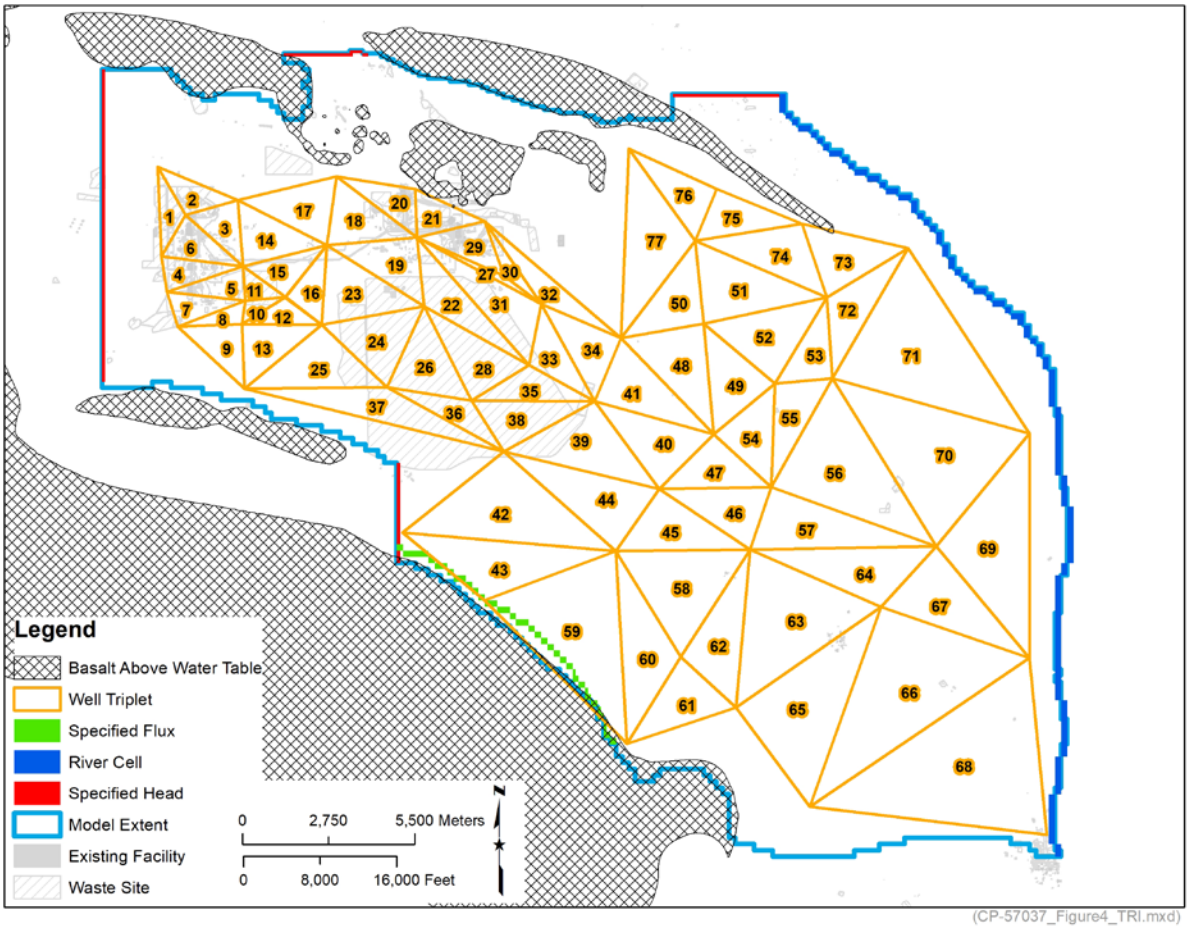

Note: Triangle 78 is not pictured because it intersects triangles 29, 30, 27, 31, and 33. The wells that make this triplet are in Table 4-6.

Figure 4-22. Locations of Gradient Calculations

Table 4-6. Well Triplets Used to Define Gradients

Triangle ID	Well 1	Well 2	Well 3	Triangle ID	Well 1	Well 2	Well 3
1	699-49-79	299-W10-1	699-39-79	40	699-24-33	699-15-26	699-20-20
2	699-49-79	299-W10-1	299-W12-1	41	699-20-20	699-24-33	699-31-31
3	299-W12-1	299-W10-1	699-38-70	42	699-10-54A	699-8-32	699-19-43
4	699-35-78A	699-38-70	699-39-79	43	699-8-32	699-10-54A	699-3-45
5	699-35-78A	699-38-70	699-35-70	44	699-15-26	699-19-43	699-8-32
6	699-38-70	299-W10-1	699-39-79	45	699-8-32	699-8-17	699-15-26
7	699-32-77	699-35-78A	699-35-70	46	699-15-15A	699-8-17	699-15-26
8	699-32-77	699-35-70	699-32-70B	47	699-15-15A	699-15-26	699-20-20
9	699-32-77	699-25-70	699-32-70B	48	699-20-20	699-32-22A	699-31-31
10	699-35-66A	699-35-70	699-32-70B	49	699-32-22A	699-26-15A	699-20-20
11	699-35-66A	699-35-70	699-38-70	50	699-32-22A	699-31-31	699-41-23
12	699-32-62	699-35-66A	699-32-70B	51	699-32-22A	699-35-9	699-41-23
13	699-32-62	699-25-70	699-32-70B	52	699-26-15A	699-35-9	699-32-22A
14	699-40-62	699-38-70	299-W12-1	53	699-26-15A	699-35-9	699-27-8
15	699-35-66A	699-38-70	699-40-62	54	699-15-15A	699-20-20	699-26-15A
16	699-32-62	699-40-62	699-35-66A	55	699-15-15A	699-27-8	699-26-15A
17	699-47-60	699-40-62	299-W12-1	56	699-27-8	699-9-E2	699-15-15A
18	699-47-60	299-E23-1	699-40-62	57	699-8-17	699-9-E2	699-15-15A
19	699-34-51	299-E23-1	699-40-62	58	699-S3-25	699-8-32	699-8-17
20	299-E33-14	699-47-60	299-E23-1	59	699-8-32	699-S12-29	699-3-45
21	299-E33-14	299-E26-13	299-E23-1	60	699-8-32	699-S3-25	699-S12-29
22	699-34-51	699-28-40	299-E23-1	61	699-S12-29	699-S8-19	699-S3-25
23	699-34-51	699-32-62	699-40-62	62	699-S8-19	699-S3-25	699-8-17
24	699-34-51	699-32-62	699-25-55	63	699-S8-19	699-2-3	699-8-17
25	699-25-55	699-25-70	699-32-62	64	699-8-17	699-9-E2	699-2-3
26	699-34-51	699-24-46	699-25-55	65	699-2-3	699-S19-11	699-S8-19
27	699-37-43	699-34-39A	299-E23-1	66	699-2-3	699-S19-11	699-S3-E12
28	699-34-51	699-28-40	699-24-46	67	699-9-E2	699-2-3	699-S3-E12
29	299-E23-1	299-E26-13	699-37-43	68	399-1-6	699-S3-E12	699-S19-11
30	699-37-43	299-E26-13	699-34-39A	69	699-9-E2	699-20-E12	699-S3-E12

Table 4-6. Well Triplets Used to Define Gradients

Triangle ID	Well 1	Well 2	Well 3	Triangle ID	Well 1	Well 2	Well 3
31	299-E23-1	699-28-40	699-34-39A	70	699-20-E12	699-9-E2	699-27-8
32	699-34-39A	299-E26-13	699-31-31	71	699-20-E12	699-40-1	699-27-8
33	699-24-33	699-34-39A	699-28-40	72	699-40-1	699-27-8	699-35-9
34	699-31-31	699-24-33	699-34-39A	73	699-40-1	699-42-12A	699-35-9
35	699-24-33	699-24-46	699-28-40	74	699-42-12A	699-35-9	699-41-23
36	699-24-46	699-25-55	699-19-43	75	699-42-12A	699-41-23	699-46-21B
37	699-25-70	699-25-55	699-19-43	76	699-46-21B	699-41-23	699-50-30
38	699-24-46	699-19-43	699-24-33	77	699-41-23	699-50-30	699-31-31
39	699-24-33	699-19-43	699-15-26	78	299-E23-1	299-E26-13	699-24-33

4.5.4.1 Implement CPGW Calibration

The P2R Model shares a portion of the model domain with the CPGW Version 8.4.5. Several features of the aquifer system included in the calibration of the CPGW Model Version 8.4.5 were implemented in the P2R Model at the onset of calibration. These include hydraulic properties, alterations to HSU delineations near 200-East Area, and recharge adjustments to B-Pond recharge that were developed as part of the model calibration that is documented in CP-47631, *Model Package Report: Central Plateau Groundwater Model, Version 8.4.5*. Details regarding these model features are found in Section 4.5 of CP-47631 and are inherited by the P2R Model. Further alterations to input parameters regarding these features completed as part of the model calibration process are documented in the following sections.

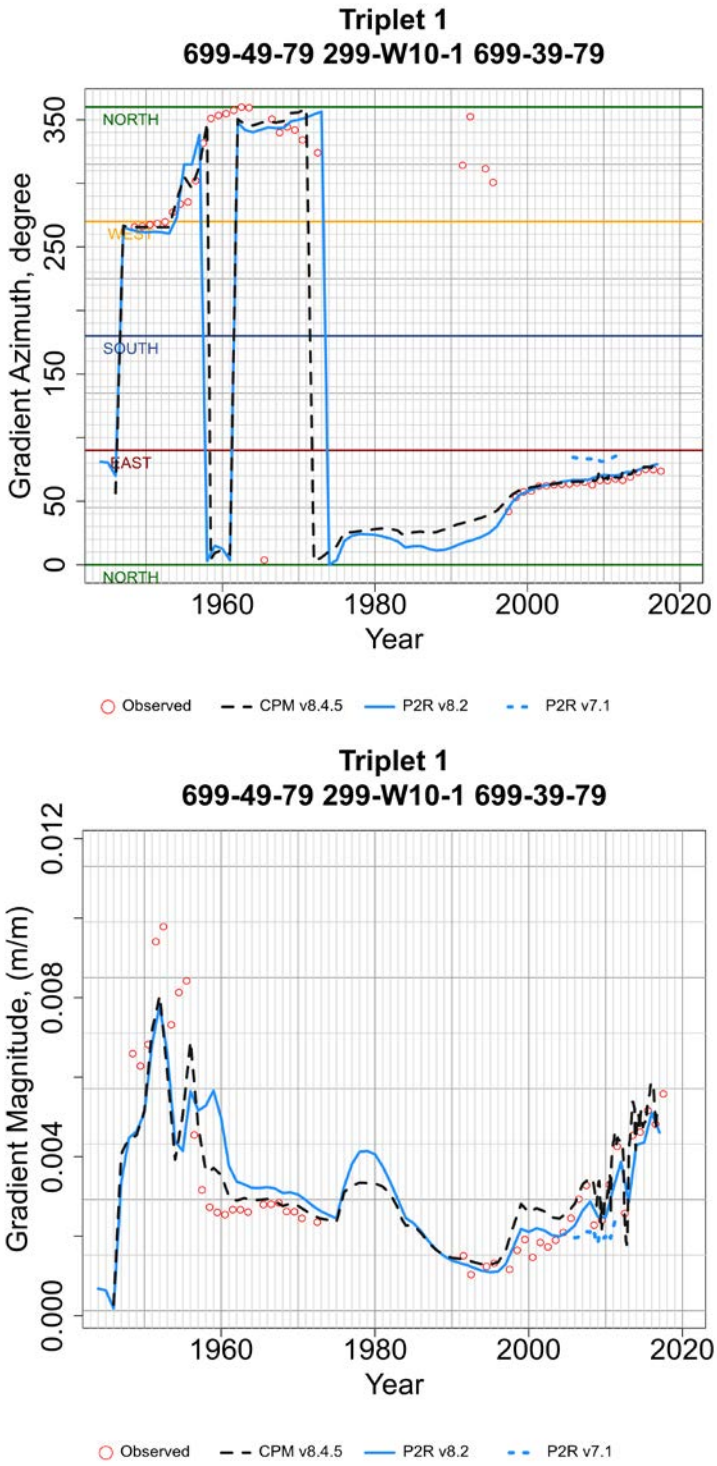

Figure 4-23. Gradient for Well Triplet 1 (699-28-40, 699-31-31, and 699-24-33)

4.5.4.2 Far-Field Calibration

The first step taken for model calibration was to calibrate the portion of the model that does not overlap the CPGW Model. Pilot point calibration of hydraulic conductivity was completed to develop input parameters in the far-field. Figure 4-24 shows the locations of the pilot points for the far-field. A set of

pilot points was included for the Hanford, Cold Creek, and Ringold Unit E HSUs. The Far-Field Ringold Unit A and Ringold Lower Mud were not calibrated using pilot point calibration. In these HSUs, the hydraulic conductivity remained constant. Initial values for the calibration were determined based on version 7.1 of the P2R model and allowed to vary from that state.

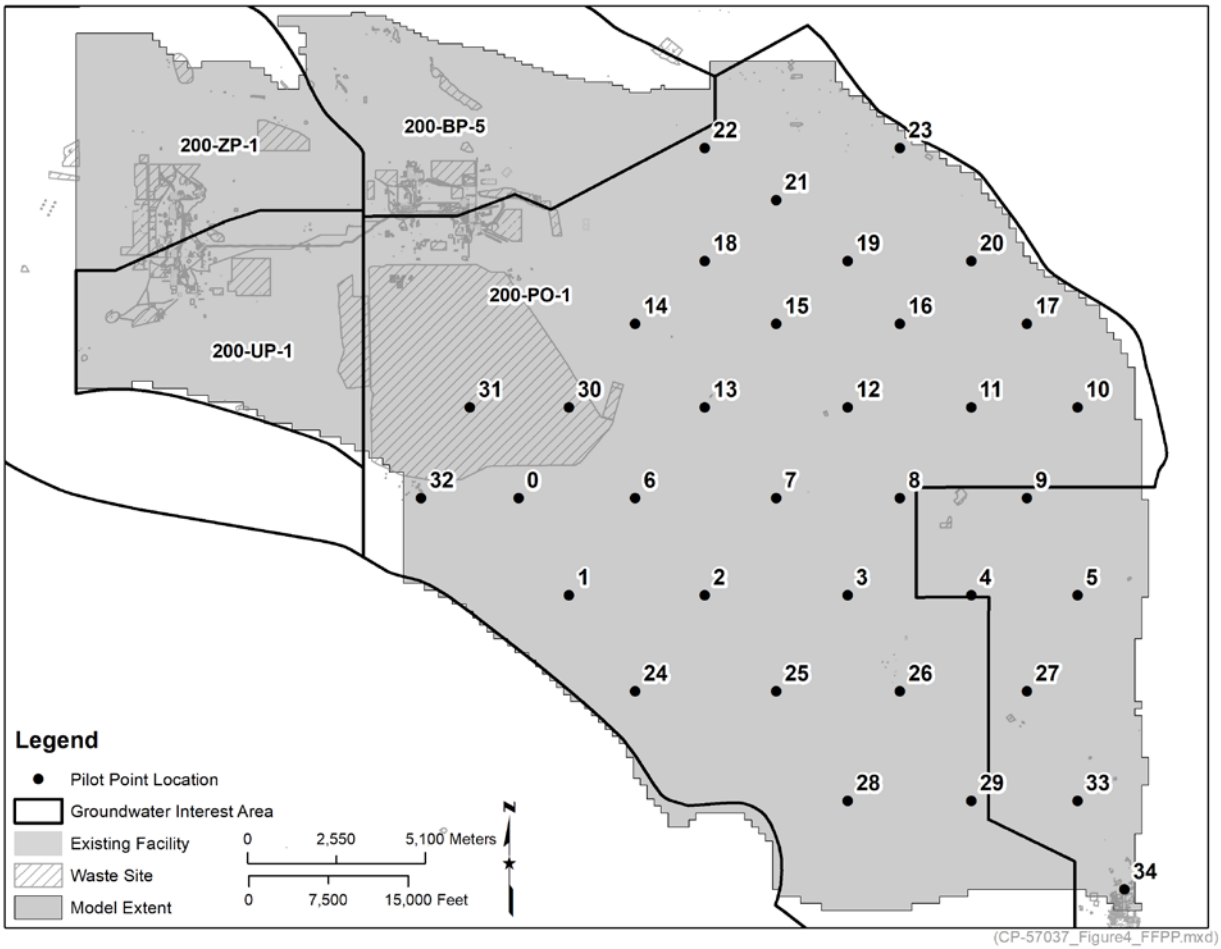

Figure 4-24. Locations of Pilot Points used to Interpolate Hydraulic Conductivity Values for the Far-Field Calibration of the P2R Model Version 8.2

4.5.4.3 200-West Area Calibration

After the initial completion of the pilot point calibration of the far-field portion of the model, the 200-West Area was also adjusted using pilot point calibration. Rather than interpolate the values of hydraulic conductivity for this portion of the model, the pilot points interpolated a multiplication factor used to adjust the previous calibrated conductivity field developed as part of the CPGW Model Version 8.4.5. Figure 4-25 shows the location of the pilot points used to adjust the calibration of hydraulic conductivity in this portion of the model. A unique set of multiplication pilot points was developed for layers 2 and 3, layers 4 and 5, and layer 7. The previously calibrated input parameters the CPGW Model Version 8.4.5 were maintained for layers 1 and 6.

An additional adjustment was made to the pilot points for assigned to the Cold Creek Unit as shown in Figure 4-24. Figure 4-26 shows how pilot points that were outside the extent of the Cold Creek Unit were either inactivated or moved to a portion of near 200-West. Since the pilot points shown in Figure 4-26 are

assigned only to the Cold Creek Unit inactivating pilot points 33 and 34 near 300-Area did not affect the calibration process. Moving pilot point locations outside of the Cold Creek Unit Extent in the far-field to the locations south of 200-West allowed for calibration of hydraulic conductivity values within this portion of the model. These pilot points continued to calibrate to hydraulic conductivity values, not multipliers as the pilot points shown in Figure 4-25. The multiplier values estimated for the pilot points shown in Figure 4-25 did not affect the hydraulic properties in the Cold Creek Unit sediments south of 200-West Area.

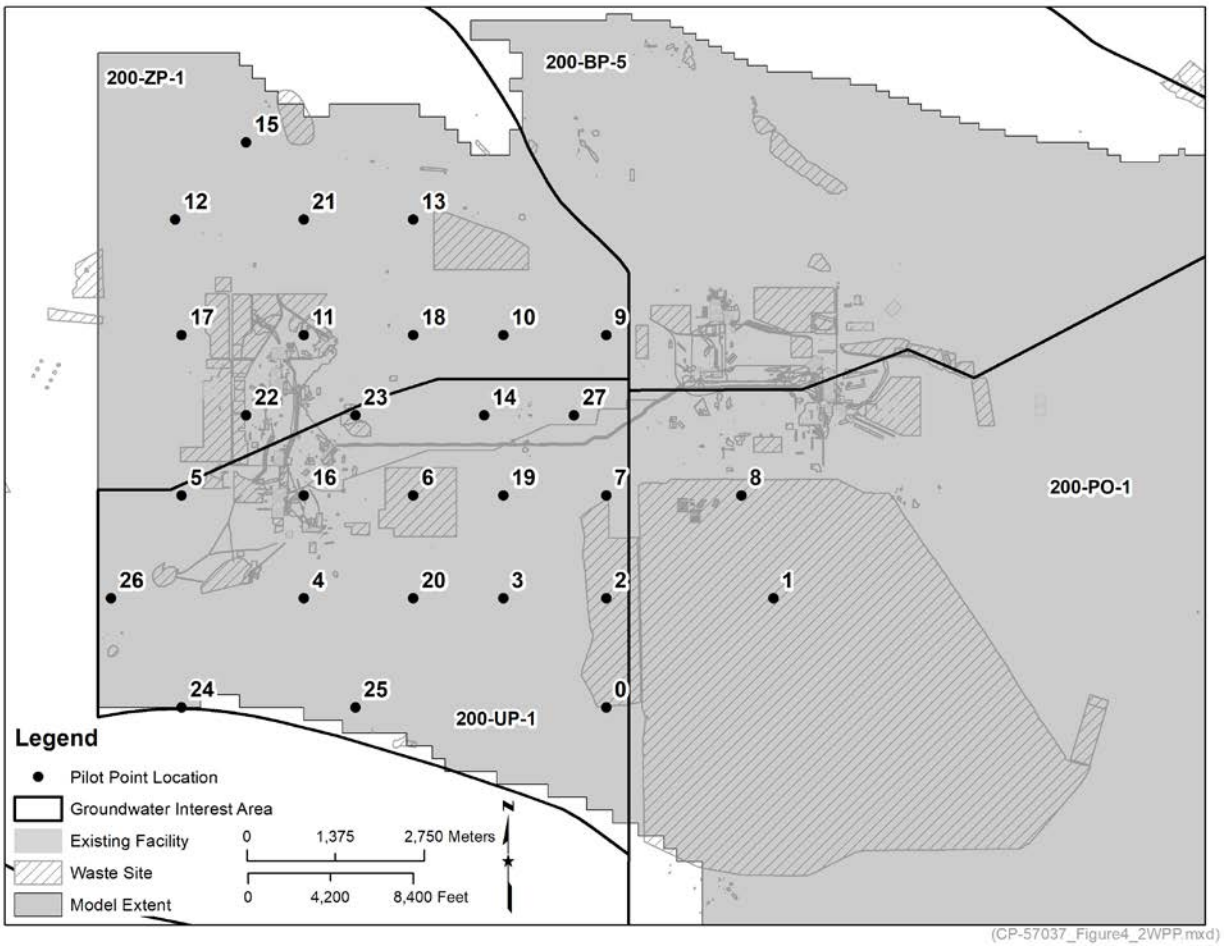

Figure 4-25. Locations of Pilot Points used to Interpolate Scaling Factors for the Hydraulic Conductivity Field near 200-West Area

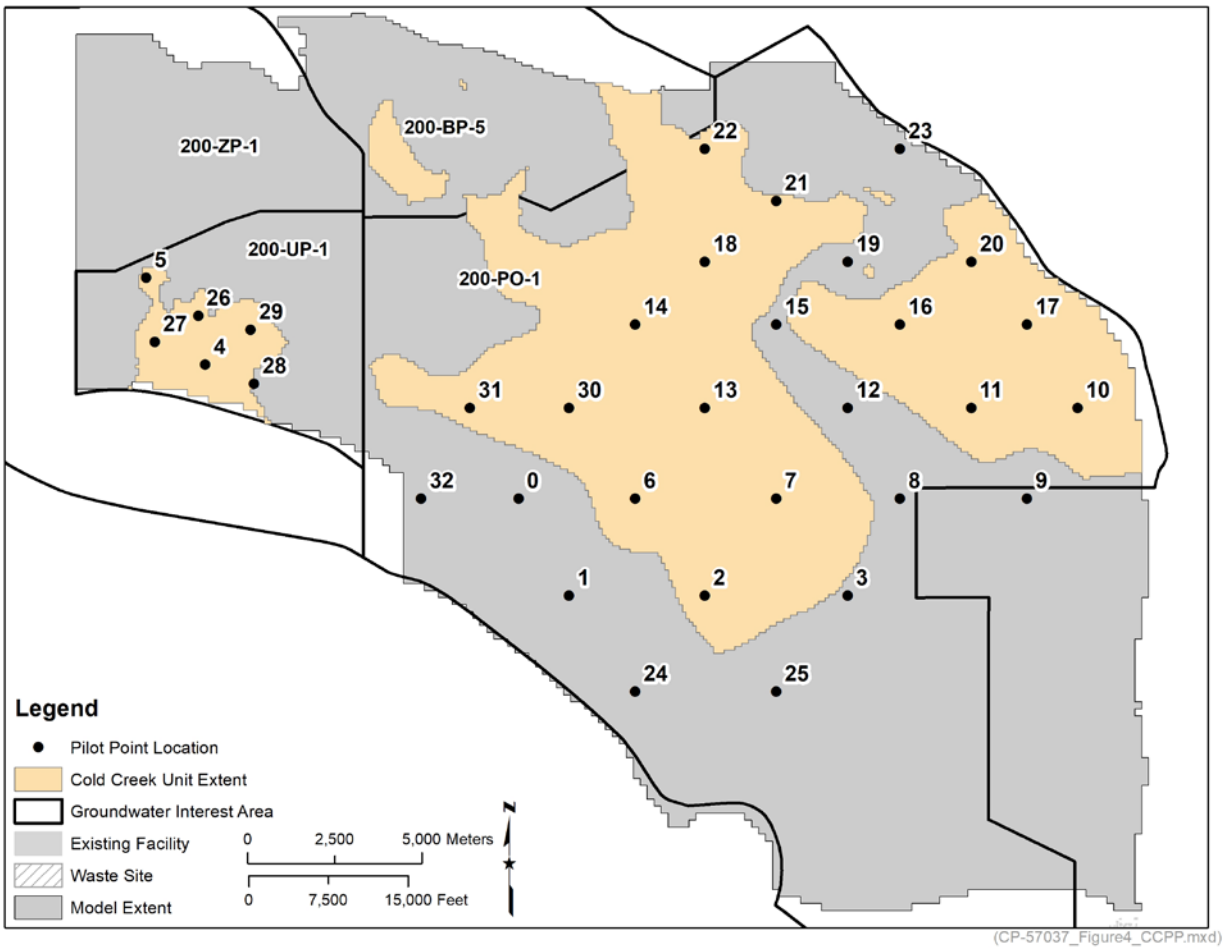

Figure 4-26. Alteration of the Pilot Point Locations used to Calibrate the Cold Creek Unit in both the Far-Field and 200-West Area

4.5.4.4 Recharge in 200-West

During operations in 200-West, large mounds of groundwater developed beneath 200-West Area. This phenomenon was discussed in Sections 3.2.1 and 3.2.2. The anthropogenic recharge applied to the model uses assumptions to assign the footprint of these discharges based on the geometry of the waste sites at the surface. The original geometry is taken from input in EMDT-BC-0002. The large effect of anthropogenic recharge in the southern portion of 200-West indicate the possibility that the effective footprint of large discharge sites in this portion of the model domain is larger than the ground surface expression of the discharge site. Given the uncertainty of the extent of the footprint where the large mounding was observed, the footprint of the recharge for the two largest discharge ponds, 216-S-16P and 216-U-10, in the southern portion of the 200-West Area was evaluated. Figure 4-27 shows the initial and final footprint used to assign anthropogenic recharge to the P2R Model Version 8.2 and the water table contours from 1965, when the water table mound was evident. The final footprint was developed using a circular footprint with the center of pond at ground surface as the center with a radius. Recharge was weighted more heavily toward the center of the final footprint as indicated in the figure. Figure 4-28 shows the hydrograph of 699-35-78A using both the initial (preliminary) and final footprint. The adjustment in footprint is within the bounds of the observed mounding and slightly improves the match between historic observed values and simulated results. No adjustment was made to the timing or total

volume of water that is released at the discharge site. The only parameter that was affected was the footprint where the water impacts the water table.

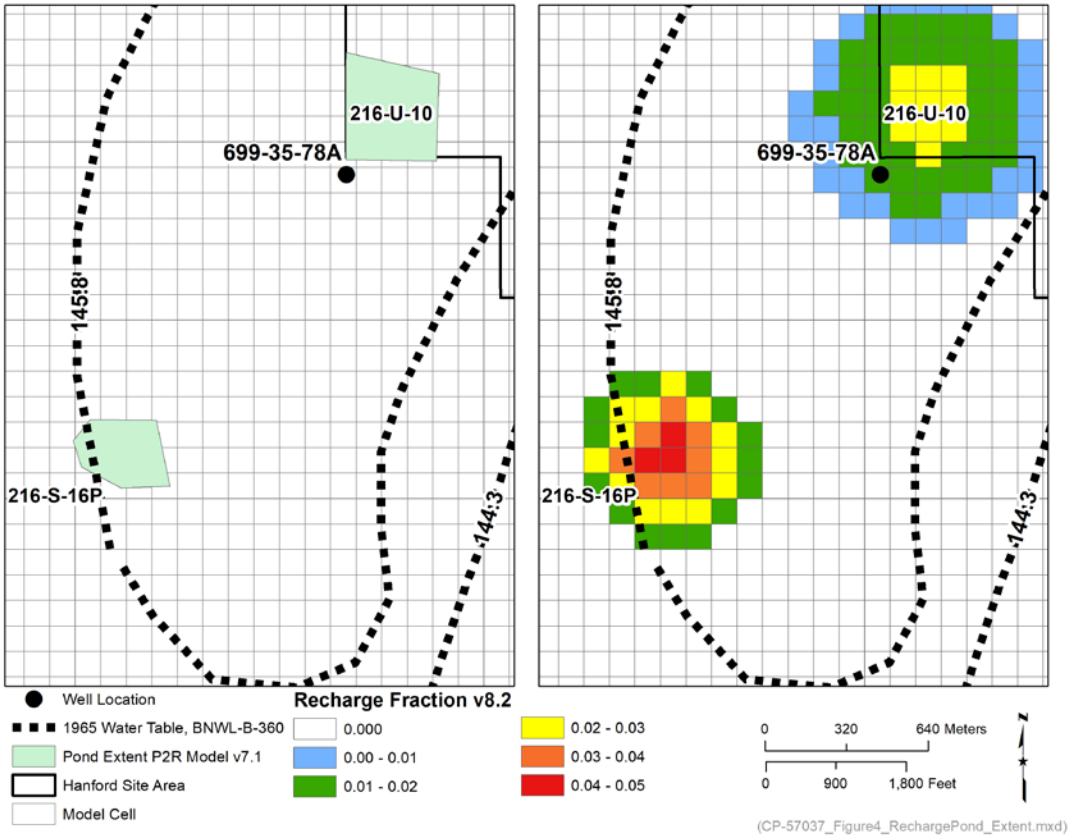

Figure 4-27. Adjustments of Recharge Extent made to Waste Sites 216-S-16P and 216-U-10 as part of the Calibration of P2R Model Version 8.2

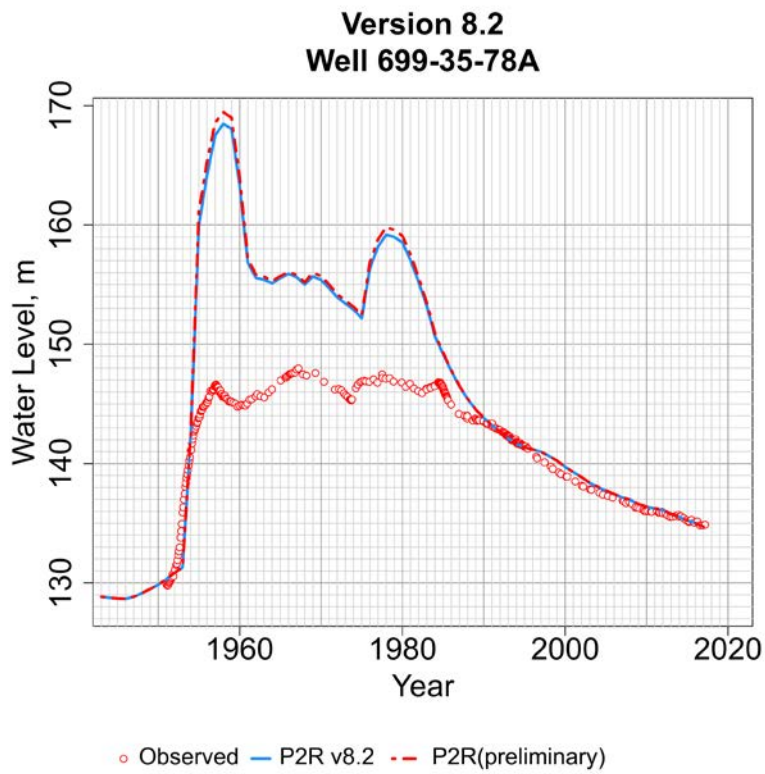

Figure 4-28. Hydrograph of Simulated and Observed Hydraulic Head Data for Well 699-35-78A Showing Results with and without the use of Adjusted Extents for the Recharge Footprint

4.5.4.5 High Conductivity Zone

The initial model grid was developed using the HSU boundaries presented in the HSGF as the boundaries of HSUs in the MODFLOW model grid. The same approach was used as part of the CPGW Model Version 8.4.5. Alterations to this approach were made in the CPGW Model Version 8.4.5 with regards to the Ringold Unit E near the southeastern portion of 200-East Area in order to increase the hydraulic conductivity in that region to reflect the high hydraulic conductivity channel. Therefore, similar adjustments to the Ringold Unit E zonation were made to the P2R Model Version 8.2 as part of implementing the CPGW Model calibration discussed in Section 4.5.4.1. Further adjustments to the extent of "channel" sediments were made in order to calibrate the P2R Model Version 8.2. These adjustments included: (1) adjusting the model grid to include a channel HSU and (2) using pilot point calibration to adjust the hydraulic conductivity values within the channel HSU. These adjustments are described in the following sections.

Implementing a Channel HSU

Two input sources were used to develop the extent of the Channel HSU. Figure 4-29 shows the extents of the tritium plume for calendar year 2000 (solid green), the extent of the high conductivity zone or channel used by DOE/EIS-0391 (blue-dashed line), and the extent used by the CPGW Model version 8.4.5 and consequently adopted in the P2R version 8.2 (solid orange). The figure also includes a new extent used in the P2R Model version 8.2 that is used in addition to the area previously included as part of CPGW version 8.4.5. The lateral extents of the additional channel area roughly mimics the flow direction of the historic tritium plume and the orientation of the high conductivity zone presented in DOE/EIS-0391. The location is west of the tritium plume assuming that the eastward groundwater flow gradient has shifted the

tritium plume to the east over the years. The lateral extent has less width than the extent indicated by DOE/EIS-0391. While it is possible that the channel sediments are as wide as estimated in DOE/EIS-0391, the width in the P2R Model Version 8.2 is only as wide as was needed to improve the model calibration. The vertical extent of the zone is equal to the extent proposed in DOE/EIS-0391, 115 m elevation. This model grid was altered so the channel zone exists only in the top two model layers. A cross-section showing the change made to the model grid is shown in Figure 4-30. Where model layer 2 to had an bottom elevation greater than 115 m, the bottom elevation of layer 2 was set at 115 m, and the lower layers were shifted down. Also, the grid cell HSU was assigned to the pilot point channel designation. In instances the original discretization, described in section 4.2.3, where the bottom of layer 2 was below 115 m, the HSU assignment was switched to the pilot point channel, no adjustments were made to the grid.

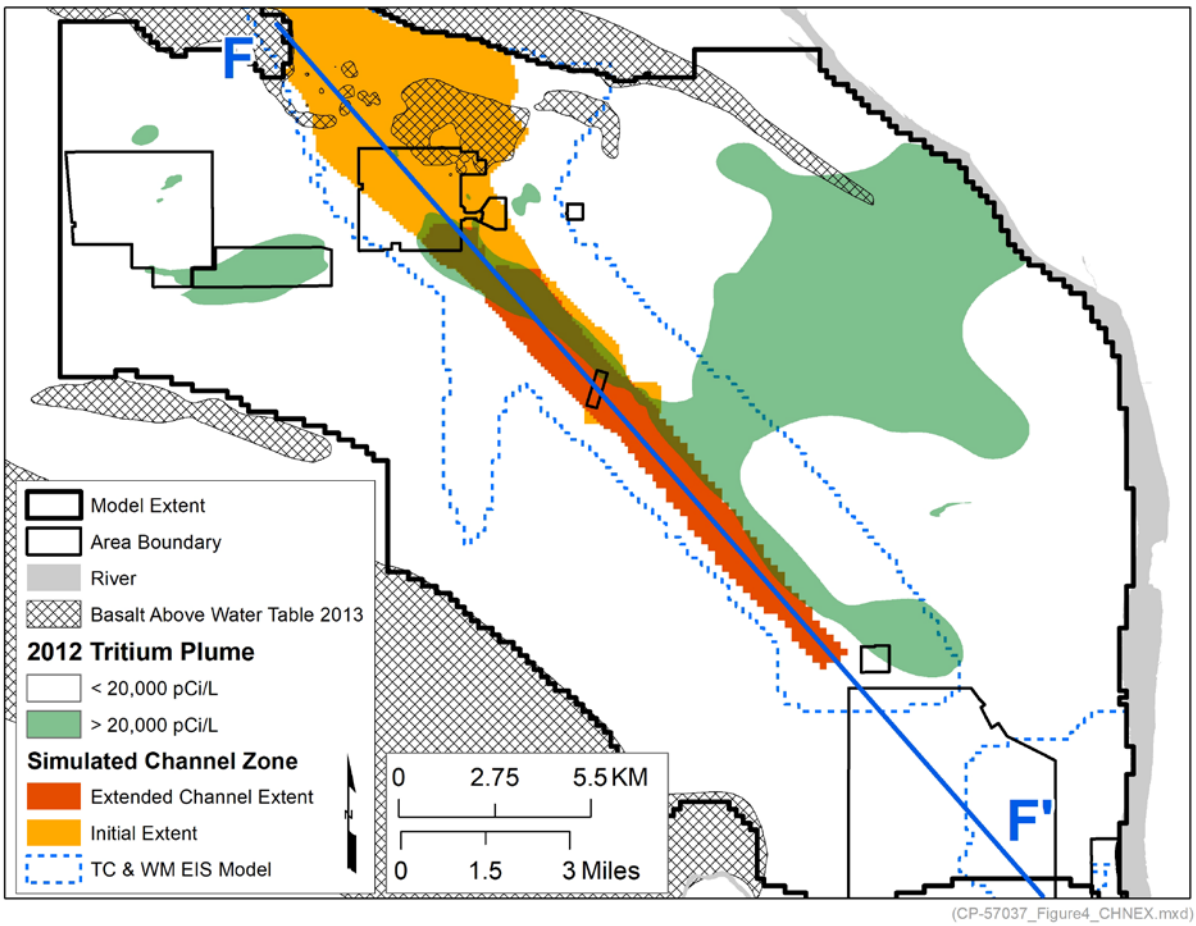

Figure 4-29. Extent of the HSU Zone Representing the High Conductivity Sediments within the P2R Model Domain

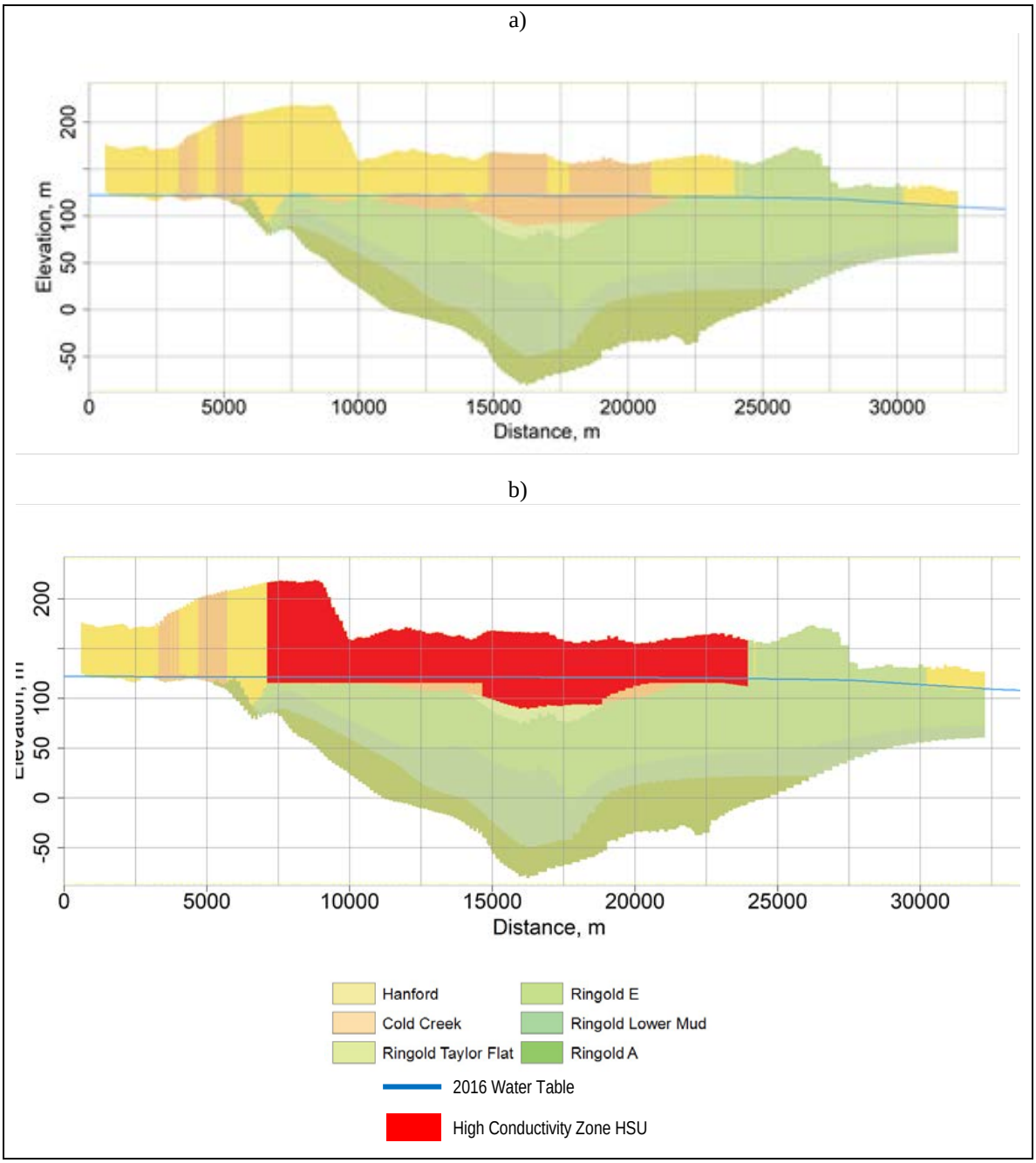

Figure 4-30. F-F' Cross-Section View of a) the Original Grid HSU Assignment and b) the Alteration Made to Simulate High Conductivity Zone with the P2R Model

Calibration of the Channel HSU

Addition of the channel zone south and east of 200-East Area required calibration of this portion of the model. Pilot points were used to estimate a spatially variable hydraulic head field within the channel zone. Figure 4-31 shows the locations of the pilot points used for this purpose. The calibrated values within channel HSU ranged from 1,002 to 21,514 m/d. The higher values were located in northeast section of the channel HSU closer to 200-East Area. Generally, the value for calibrated hydraulic conductivity trended downward as distance increased from 200-East Area.

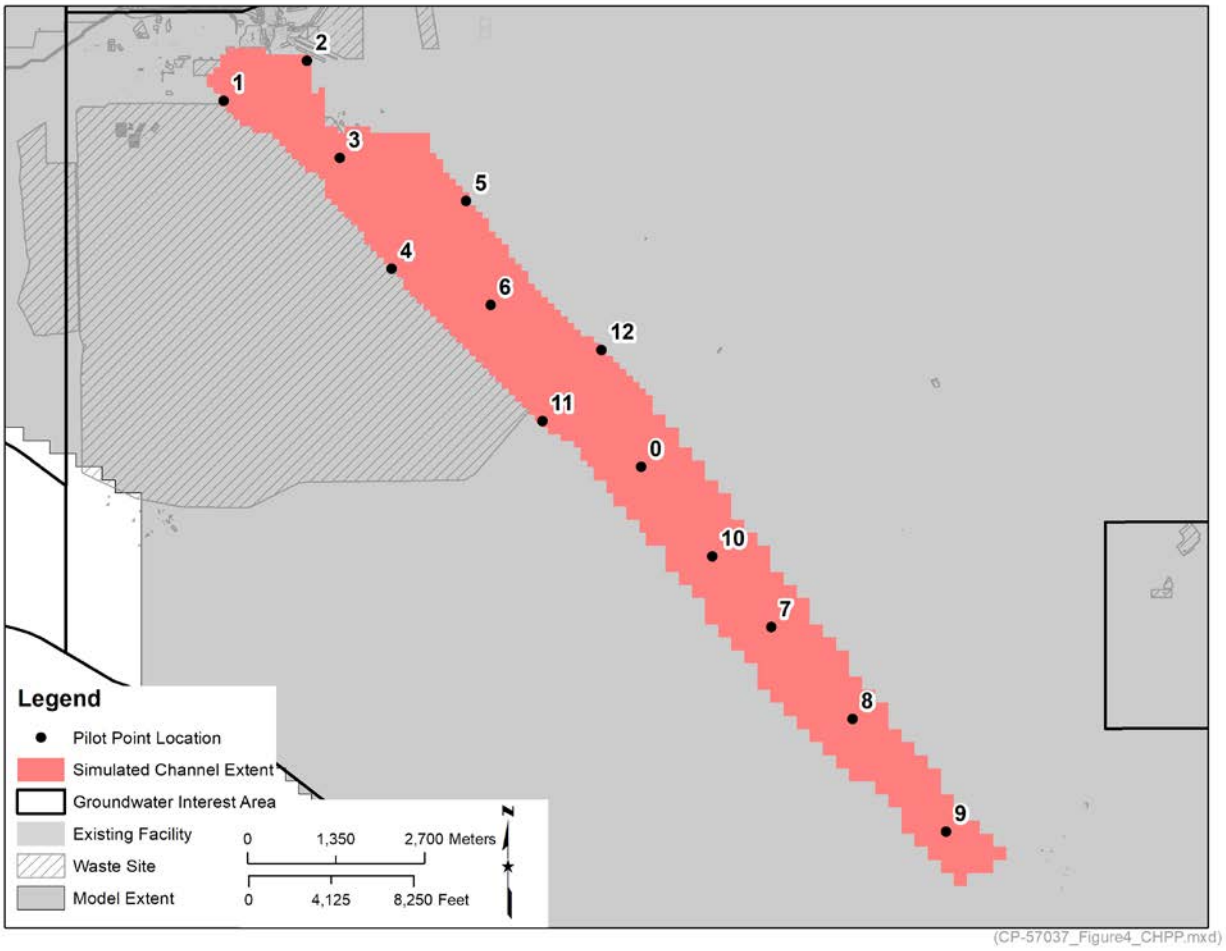

Figure 4-31. Locations of Pilot Points used to Interpolate Hydraulic Conductivity Values for the Channel HSU Zone of the P2R Model Version 8.2

4.5.4.6 Transport Calibration

An F&T simulation of tritium was completed to refine the calibration of P2R Model Version 8.2. The transport parameters used for this effort are discussed in Section 4.4.6. The simulation ran for the entire period of record of the model and, therefore, did not require an initial concentration estimate. All contaminant activity was added to the modeling as a activity flux from the vadose based on estimated rates of disposal during operations. The activity flux terms were obtained from F&T simulations presented in PNNL-14753.

Tritium Calibration Results

Figures 4-32 through 36 show the observed and simulated tritium concentrations for the years 1970, 1980, 1990, 2000, and 2010. The observed concentration contours were obtained from PNNL-14753 and *Hanford Site Groundwater Monitoring for 2010*, DOE/RL-2011-01. The simulated contours are derived from the calibrated P2R Model Version 8.2. The flow direction and velocities show reasonable agreement for the major tritium plumes. This is evident with respect to the location and concentration of the tritium plume movement toward the Columbia River (see Figures 4-33 and 34). The plume arrives at roughly 1970. The main plume in 200-West Area also shows a similar agreement in the flow direction of the tritium plume at the southern edge of the area. Conversely, there are several smaller plumes in the northern portions of both 200-West and 200-East that do not appear in the simulated contour plots. Also, the tritium plume at the southern edge of 200-West has a smaller lateral extent than the observed tritium plume. This could be due to uncertainty in the source term used as the input parameters in the source term. Differences in the concentrations and locations of plumes may be the result of inaccuracies in the inventory estimate used as input or uncertainty in the transport parameters. Overall, the model predictions do not demonstrate any characteristics that would preclude this model from use a F&T model for the objectives described in Section 1 and 2.

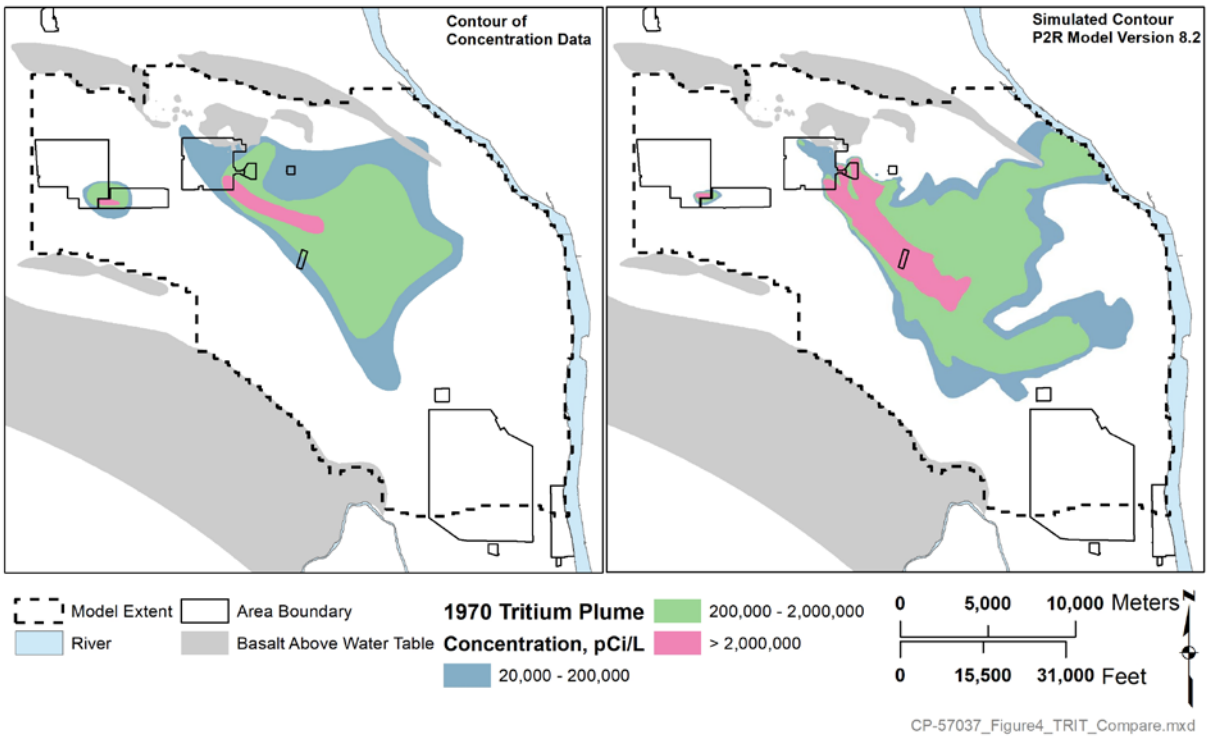

Figure 4-32. Comparison of Historic Contours Based on Field Data and Simulated Contours of Tritium Concentration from 1970

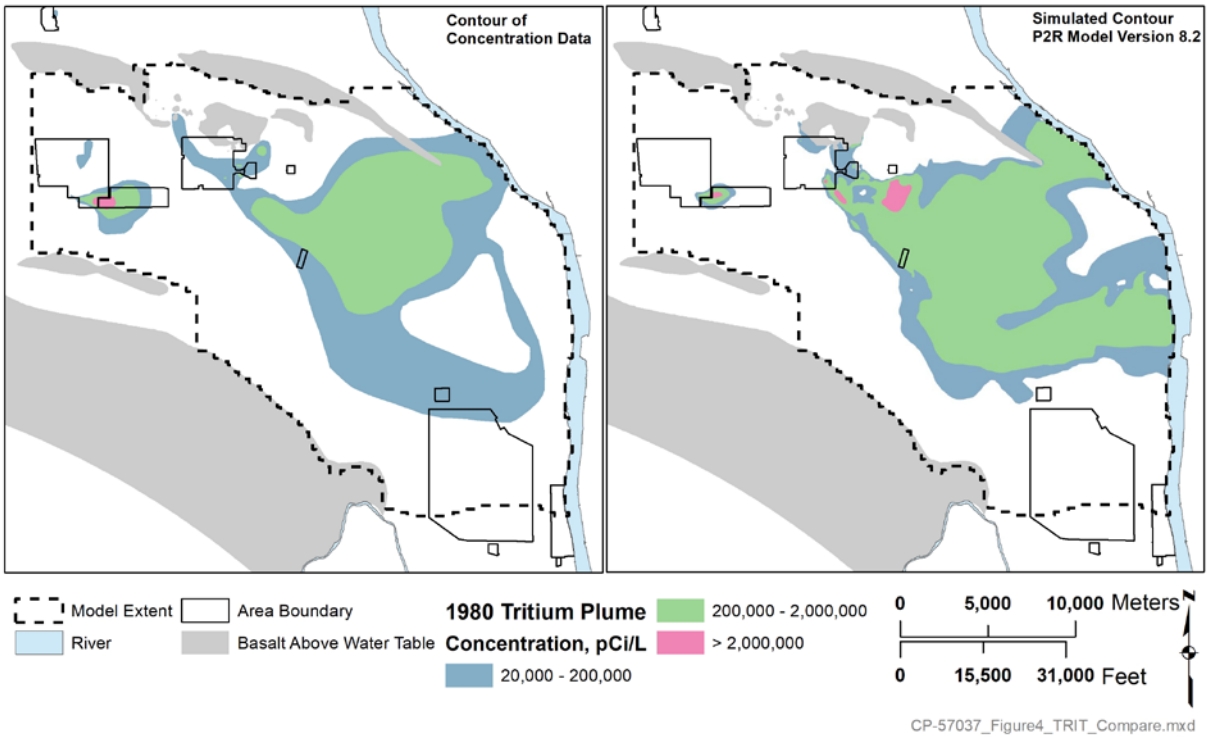

Figure 4-33. Comparison of Historic Contours Based on Field Data and Simulated Contours of Tritium Concentration from 1980

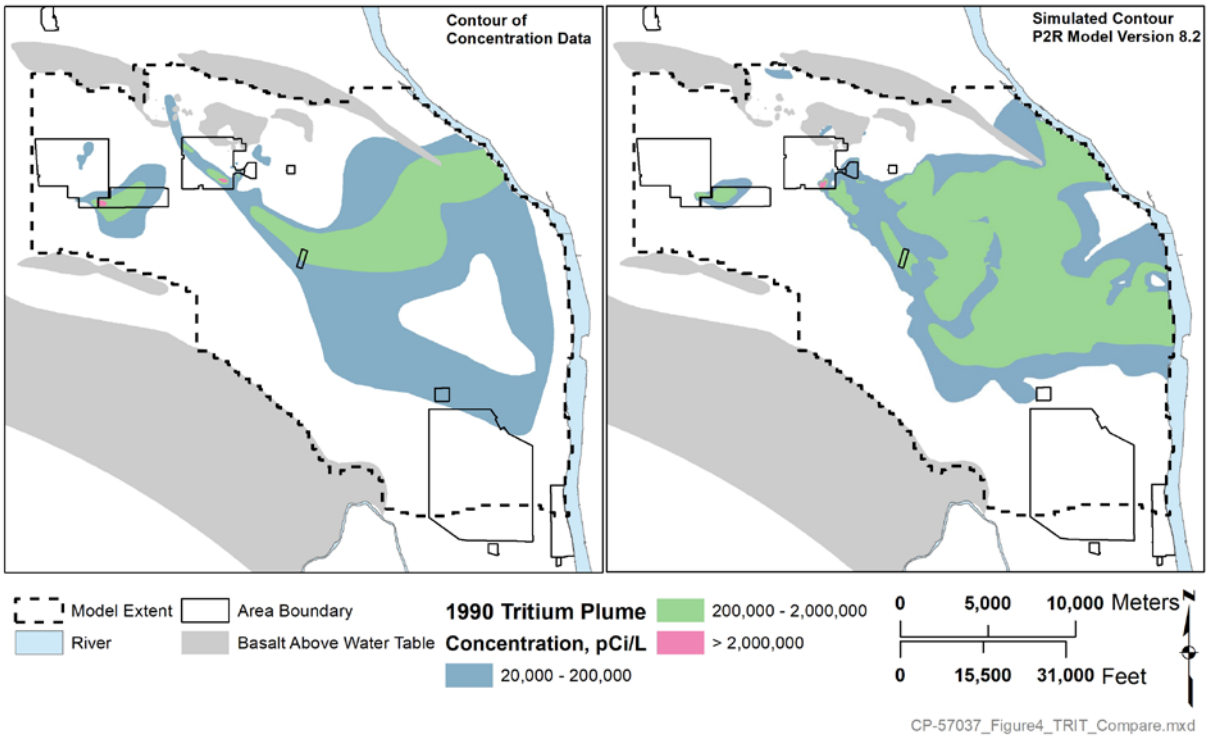

Figure 4-34. Comparison of Historic Contours based on Field Data and Simulated Contours of Tritium Concentration from 1990

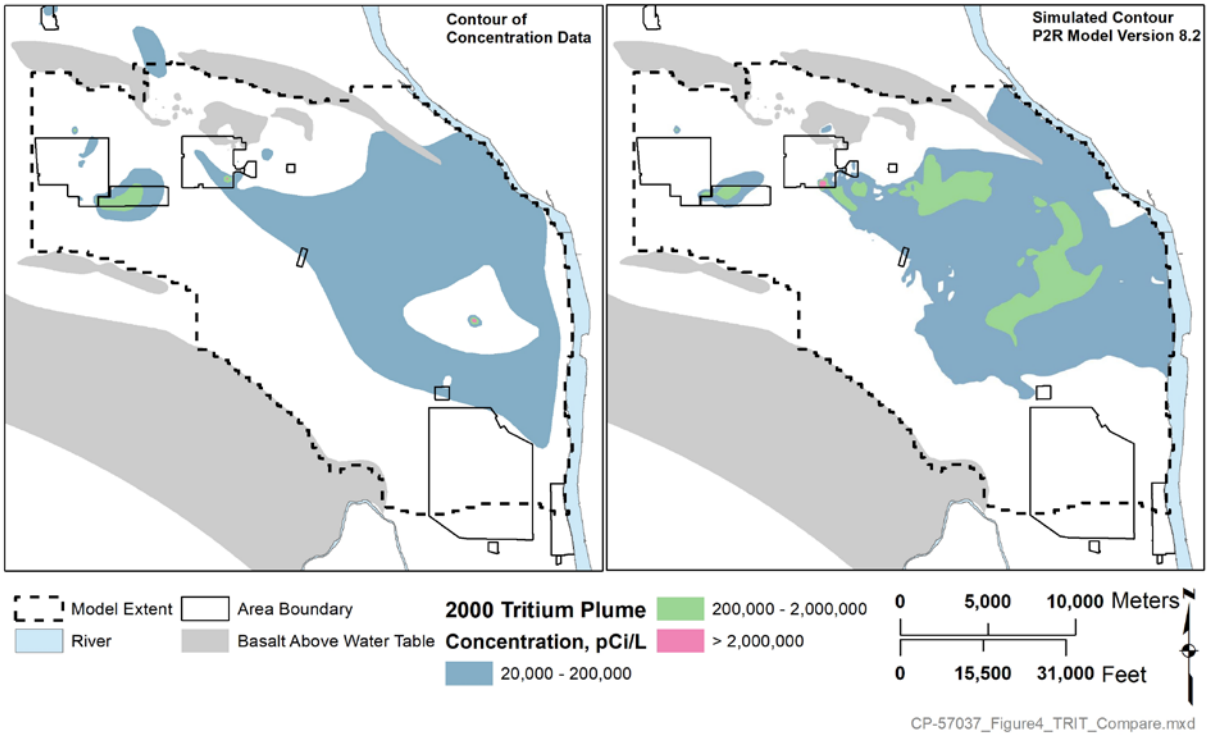

Figure 4-35. Comparison of Historic Contours based on Field Data and Simulated Contours of Tritium Concentration from 2000

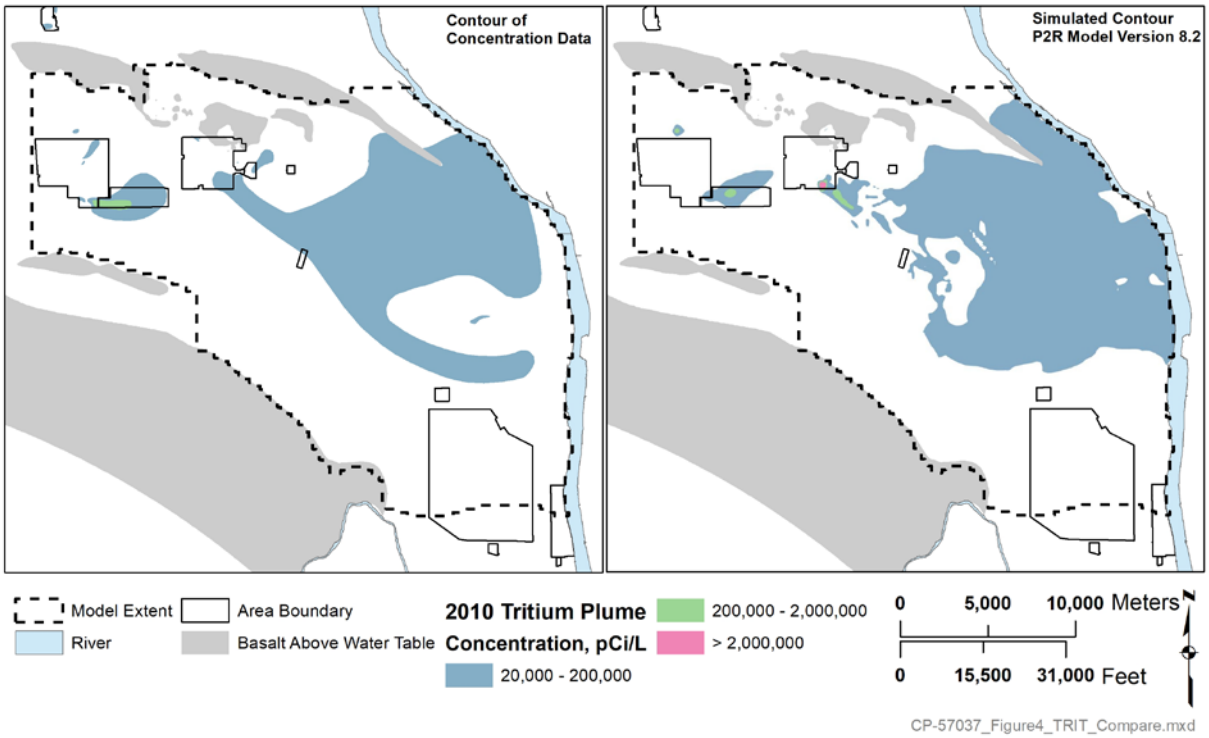

Figure 4-36. Comparison of Historic Contours based on Field Data and Simulated Contours of Tritium Concentration from 2010

4.5.4.7 Calibration Results

This section presents the results of the calibration process. This is split into a presentation of the calibrated parameters and the visual and statistical comparisons between observed and simulated data. Each of these is presented in the following sections.

Calibrated Input Parameters

Several input parameters were involved in the calibration process. These include hydraulic conductivity values, recharge extent, mountain front recharge flux, and river conductance. The calibration process did not alter the rates of the natural recharge presented in section 4.4.4. Table 4-7 provides a summary of the final calibration values for each of the input parameters included in the calibration process. Summary statistics for the hydraulic conductivity input parameters are included in Table 4-7. However, due to the variable nature of the parameter field figures 4-37 through 4-43 are included to illustrate the distribution of hydraulic conductivities for each HSU simulated within the model domain. The figures show the hydraulic conductivity distribution and includes the cumulative distribution function plotted for each HSU. Transmissivity plots for the P2R model during simulated years 1965 and 2016 are shown in Figures 4-44 and 4-45, respectively. In general, the total transmissivity value for the model is greater in 1965 than in 2016 due to an increased water table elevation. However, near the TEDF, east of 200-East, the simulated discharge shows a locally increased transmissivity due to an increase in the simulated saturated thickness in this region. Conversely, through Gable Gap in the middle of 200-East reductions in the transmissivity field are noticeable in pockets of what is has channel HSU sediments. These pockets of low transmissivity are areas where the basalt, north of 200-East, Ringold Unit A, middle of 200-East, are above the water table due to decrease in the saturated thickness from 1965 to 2016.

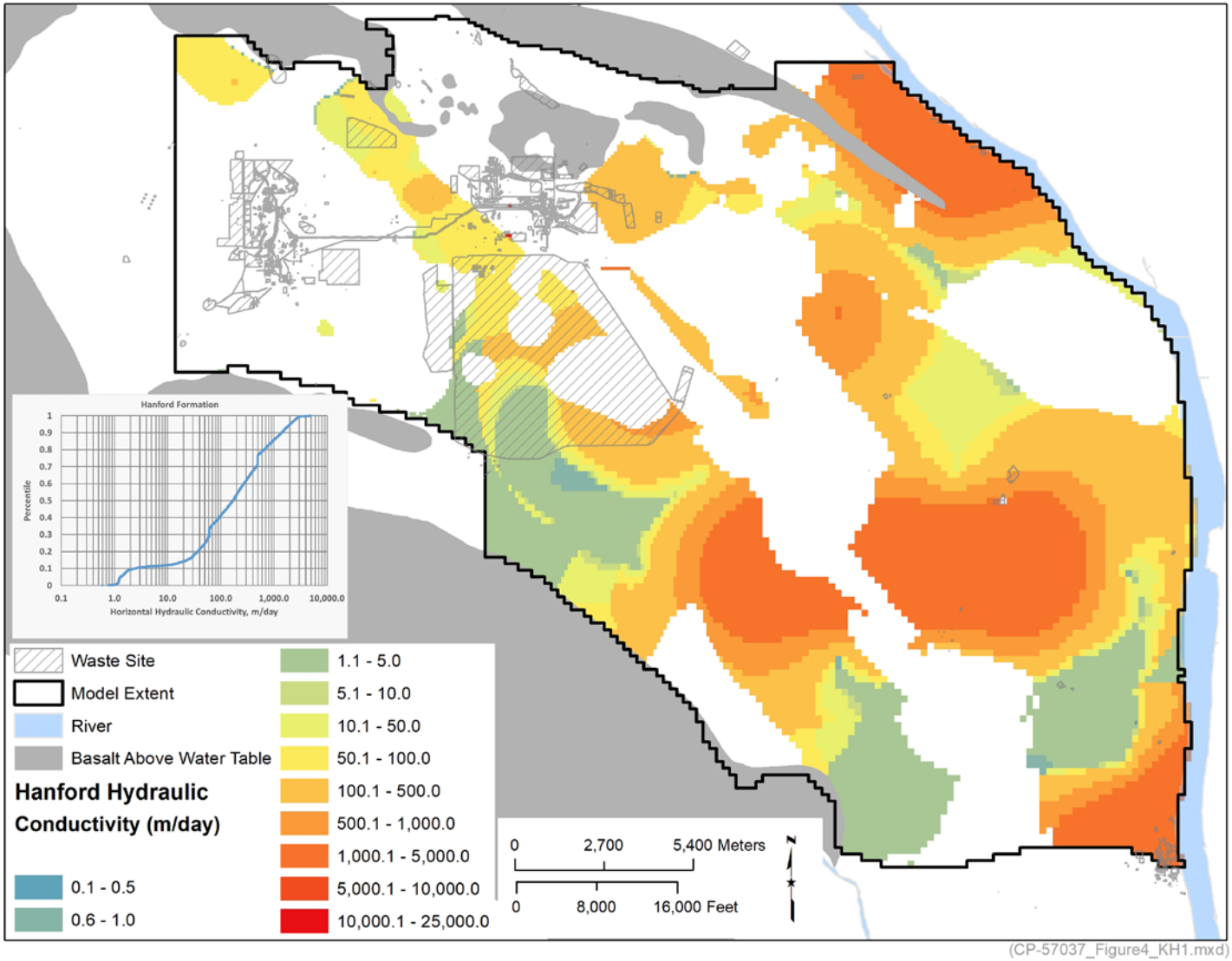

Figure 4-37. Simulated Hydraulic Conductivity Distribution for the Hanford Formation in the Calibrated P2R Model Version 8.2

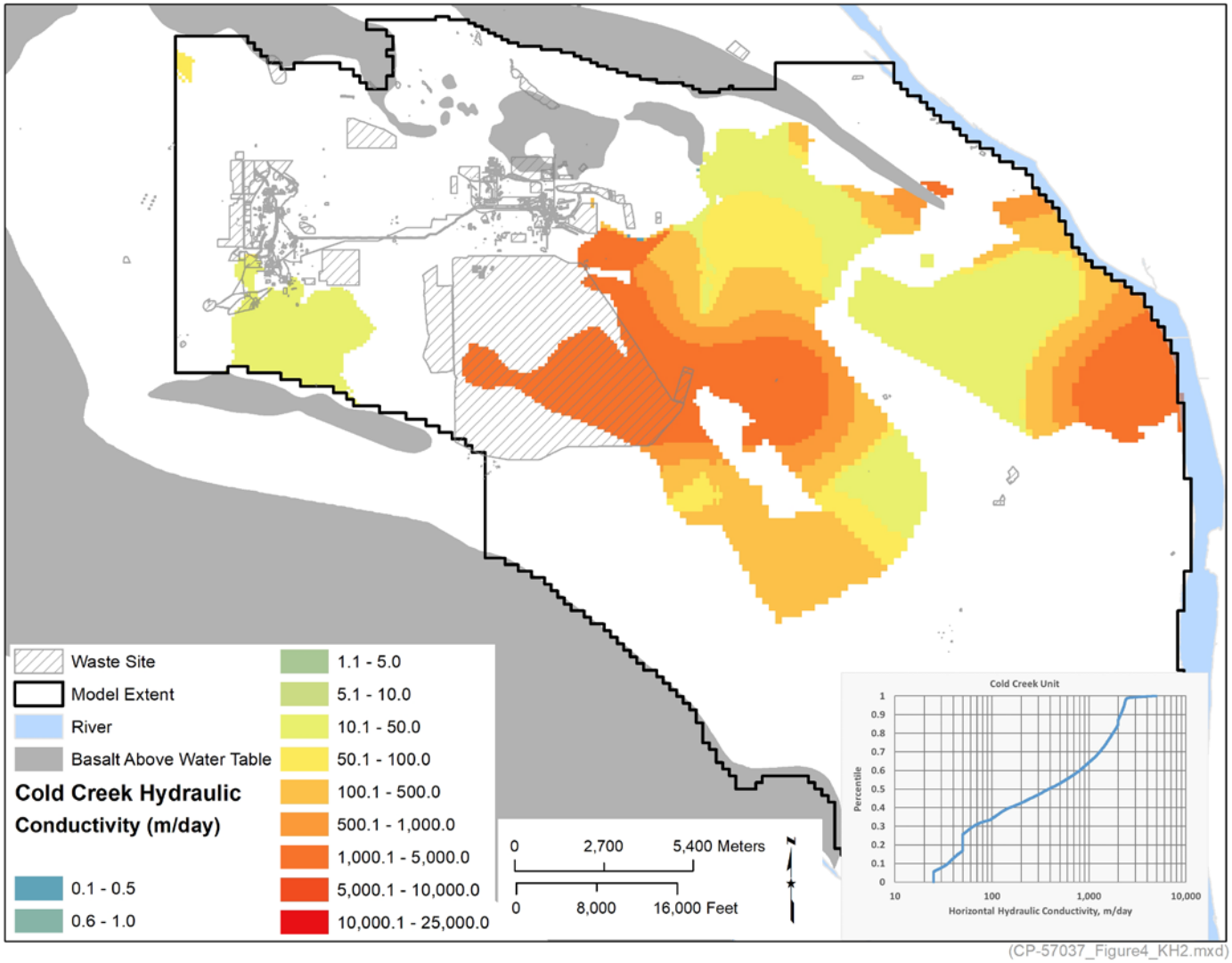

Figure 4-38. Simulated Hydraulic Conductivity Distribution for the Cold Creek Formation in the Calibrated P2R Model Version 8.2

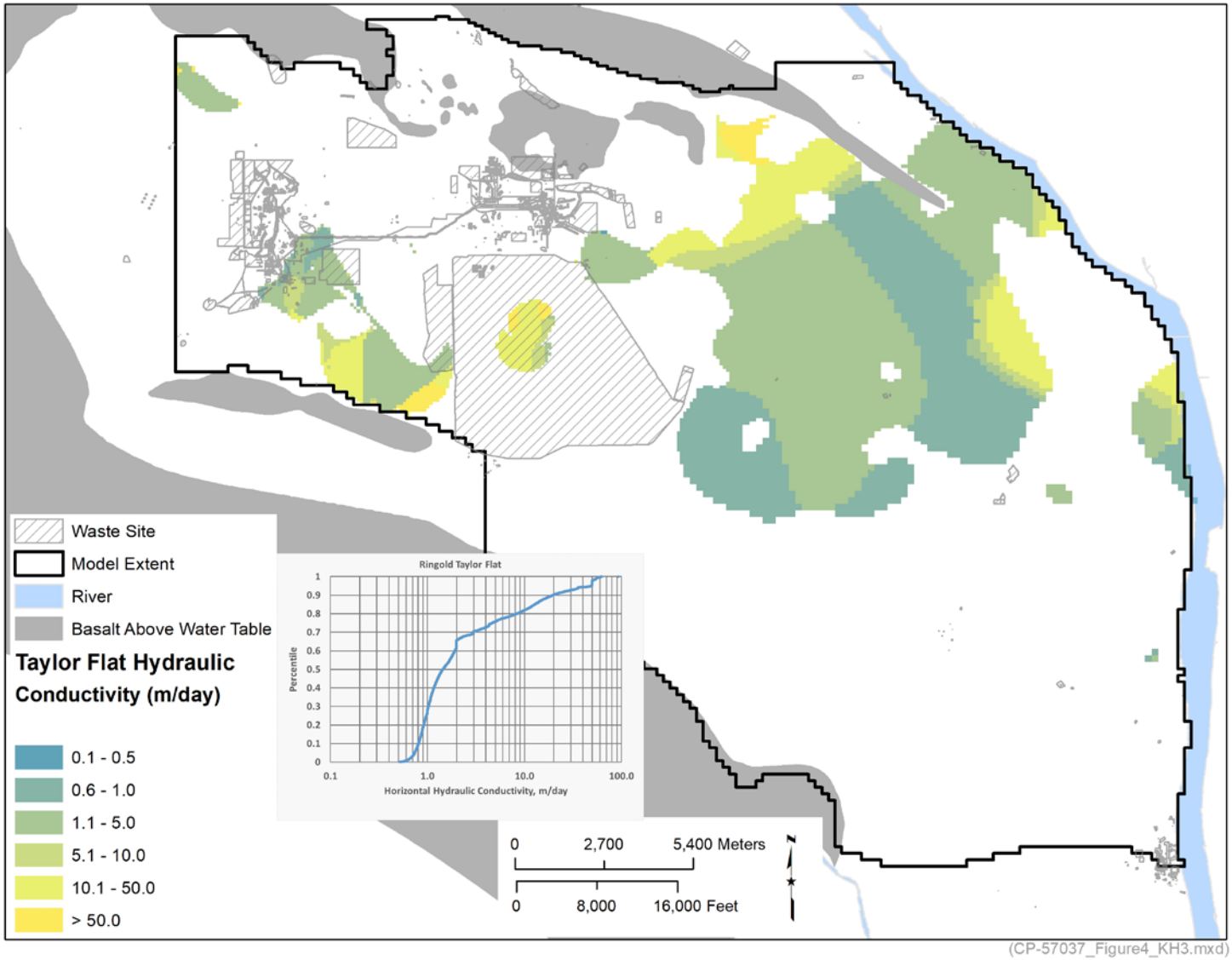

Figure 4-39. Simulated Hydraulic Conductivity Distribution for the Taylor Flat Unit of the Ringold Formation in the Calibrated P2R Model Version 8.2

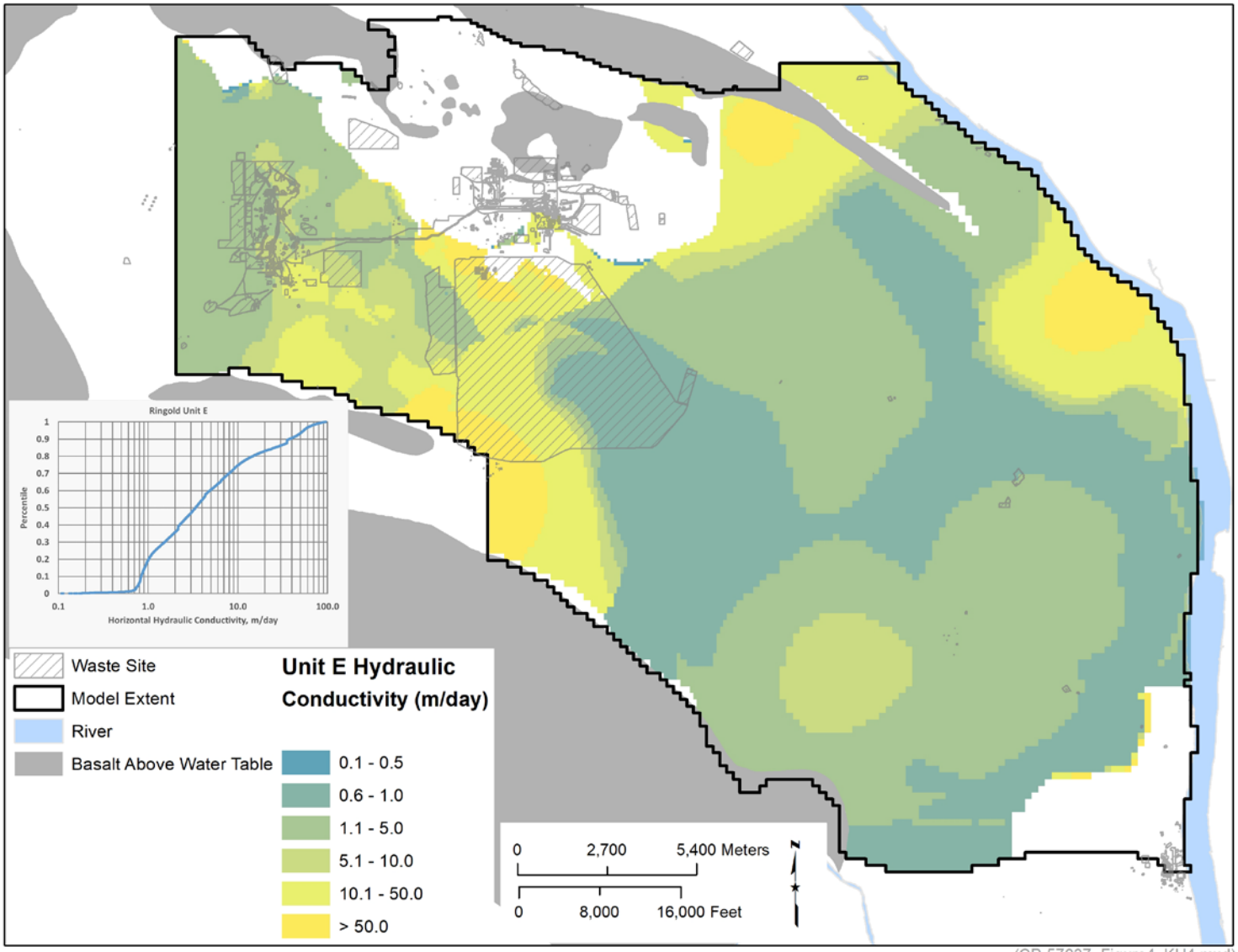

(CP-57037_Figure4_KH4.mxd)

Figure 4-40. Simulated Hydraulic Conductivity Distribution for the Unit E of the Ringold Formation in the Calibrated P2R Model Version 8.2

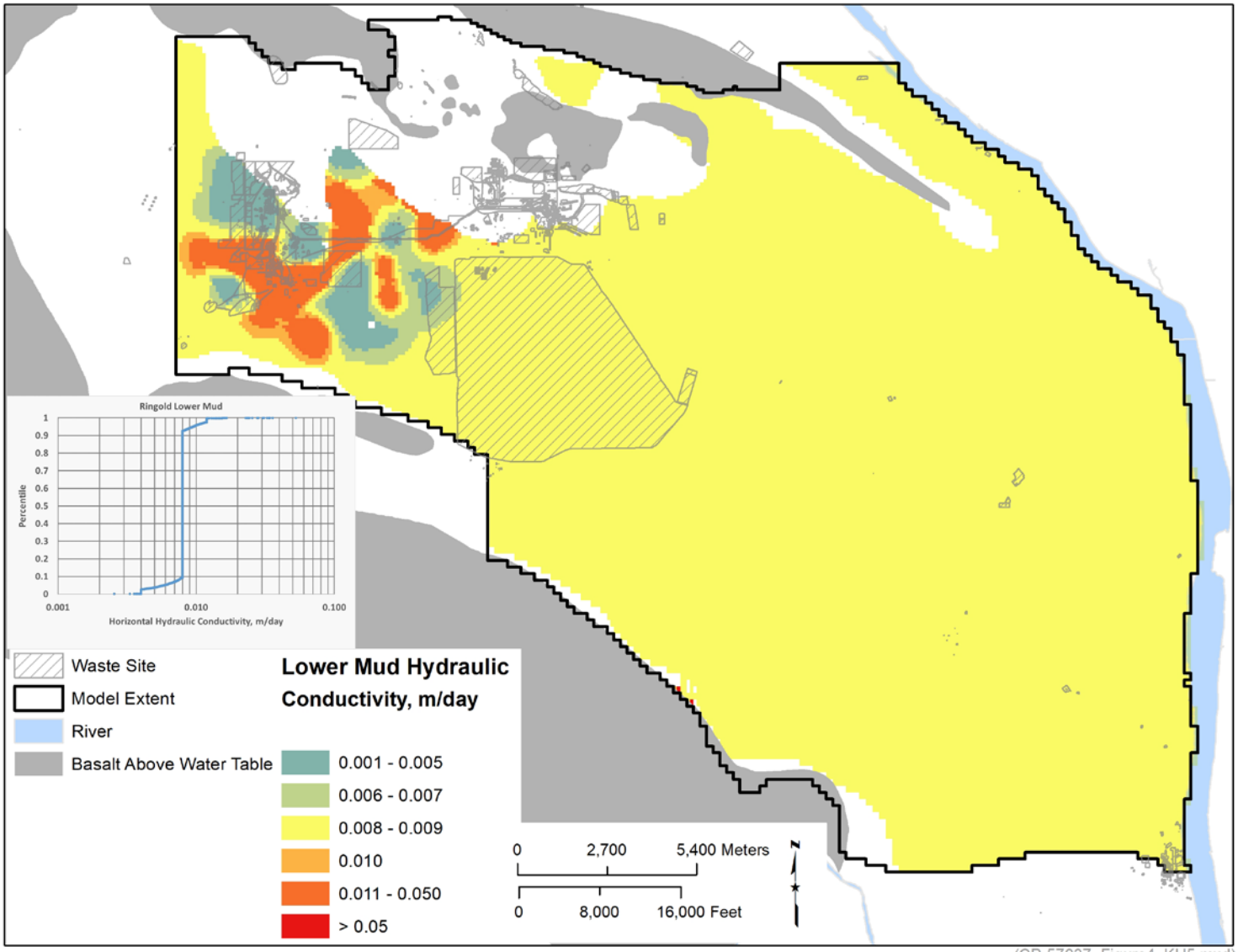

(CP-57037_Figure4_KH5.mxd)

Figure 4-41. Simulated Hydraulic Conductivity Distribution for the Lower Mud Unit of the Ringold Formation in the Calibrated P2R Model Version 8.2

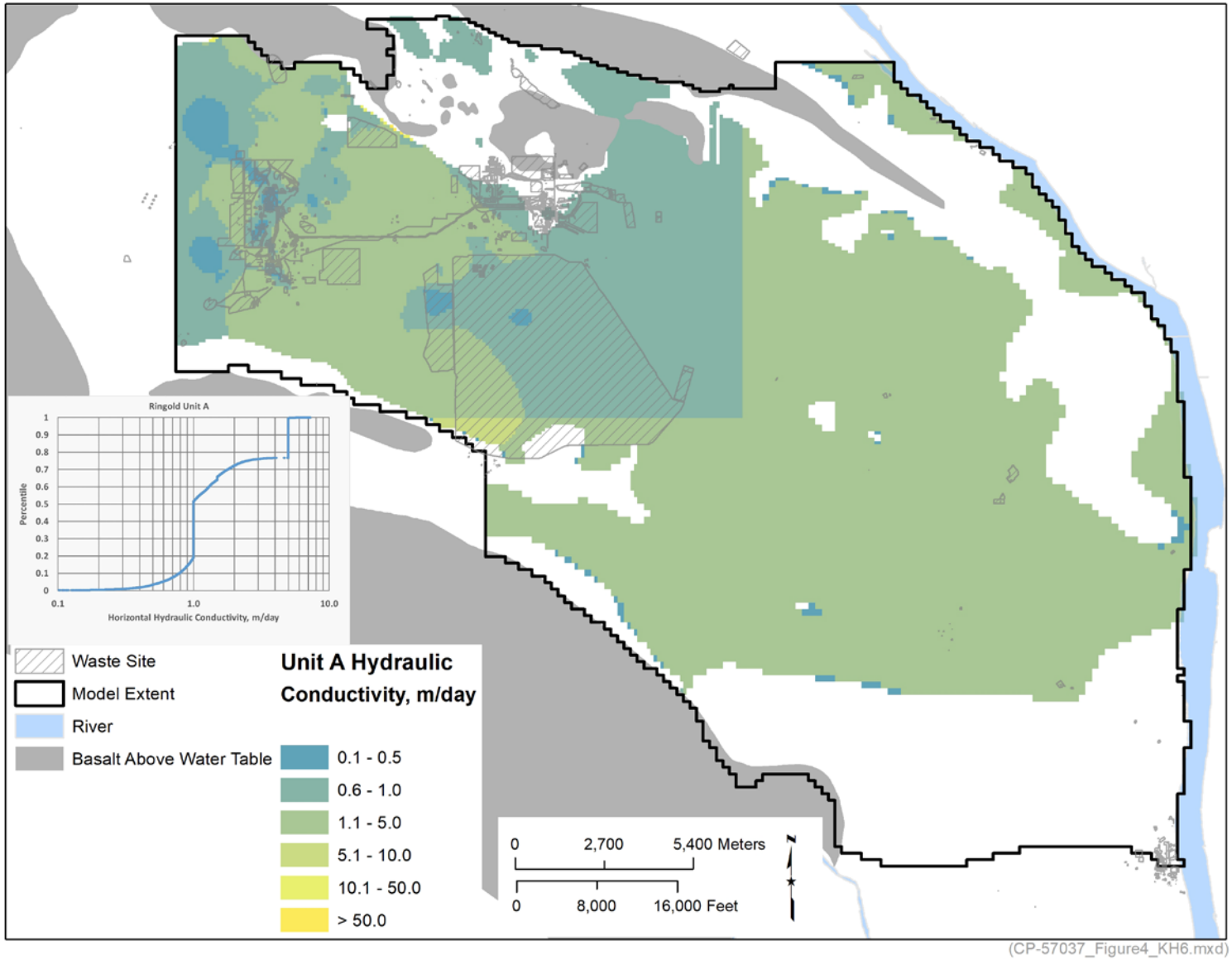

Figure 4-42. Simulated Hydraulic Conductivity Distribution for the Unit A of the Ringold Formation in the Calibrated P2R Model Version 8.2

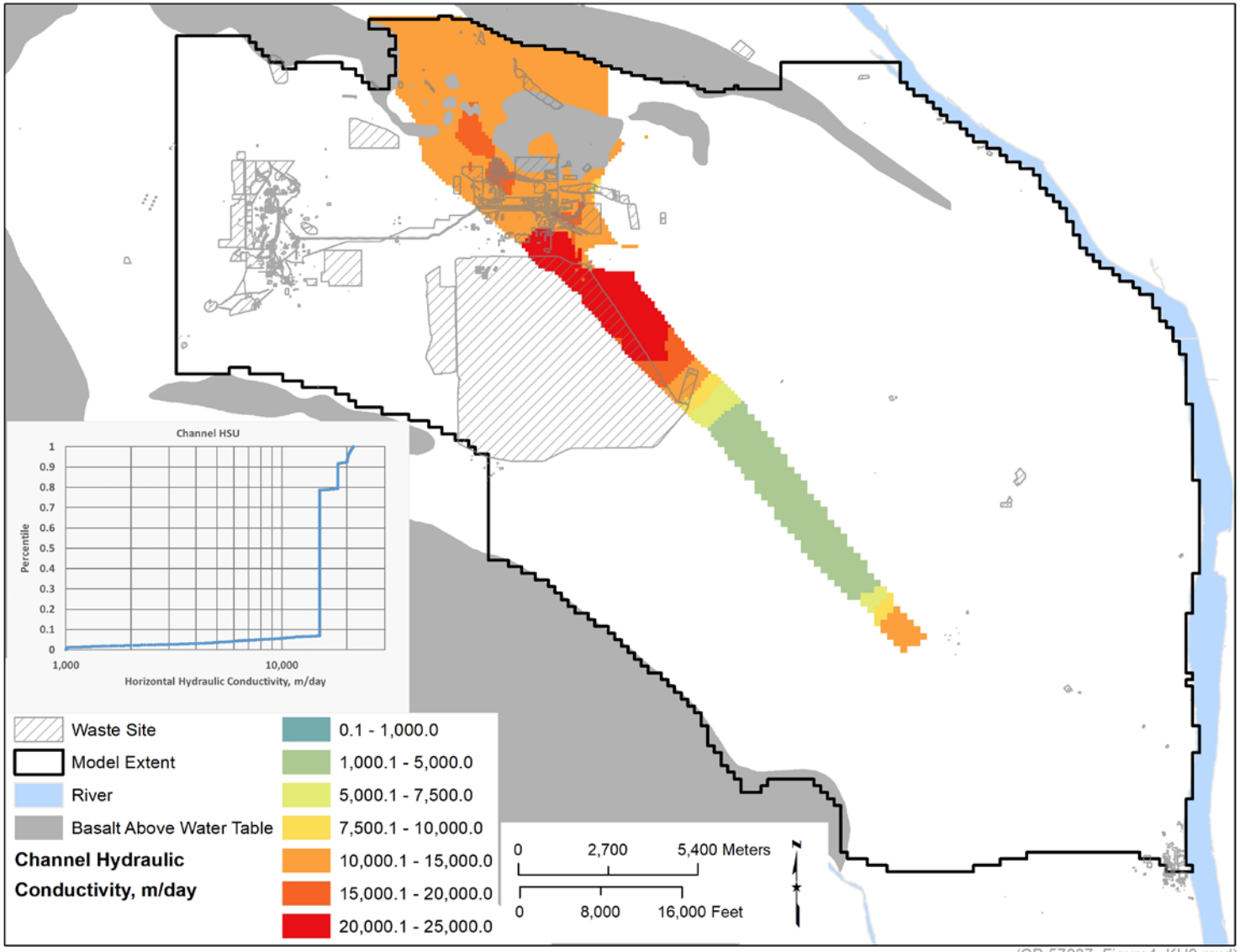

(CP-57037_Figure4_KH9.mxd)

Figure 4-43. Simulated Hydraulic Conductivity Distribution for the Channel HSU in the Calibrated P2R Model Version 8.2

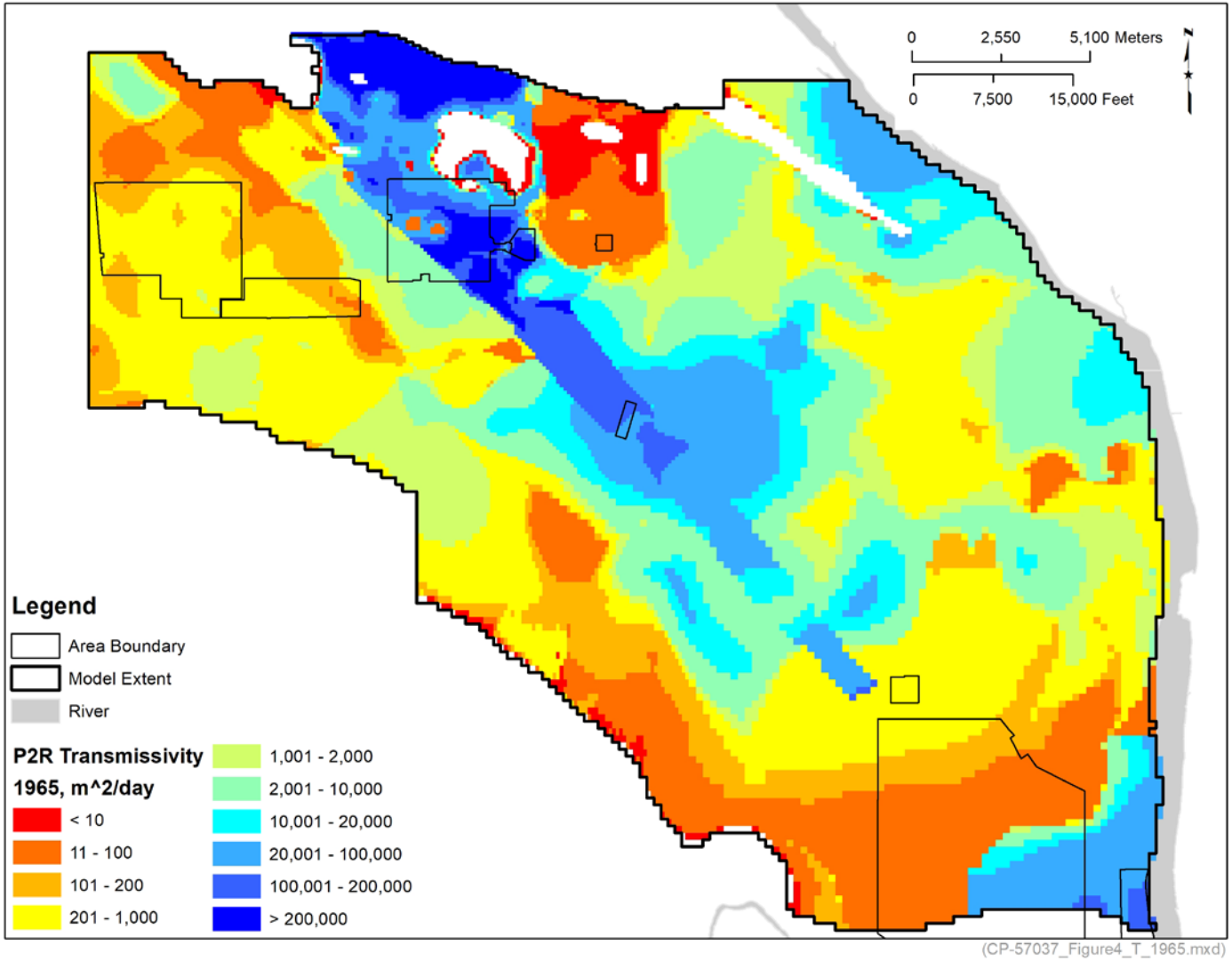

Figure 4-44. Simulated Total Transmissivity Distribution for Calendar Year 1965 in the Calibrated P2R Model Version 8.2

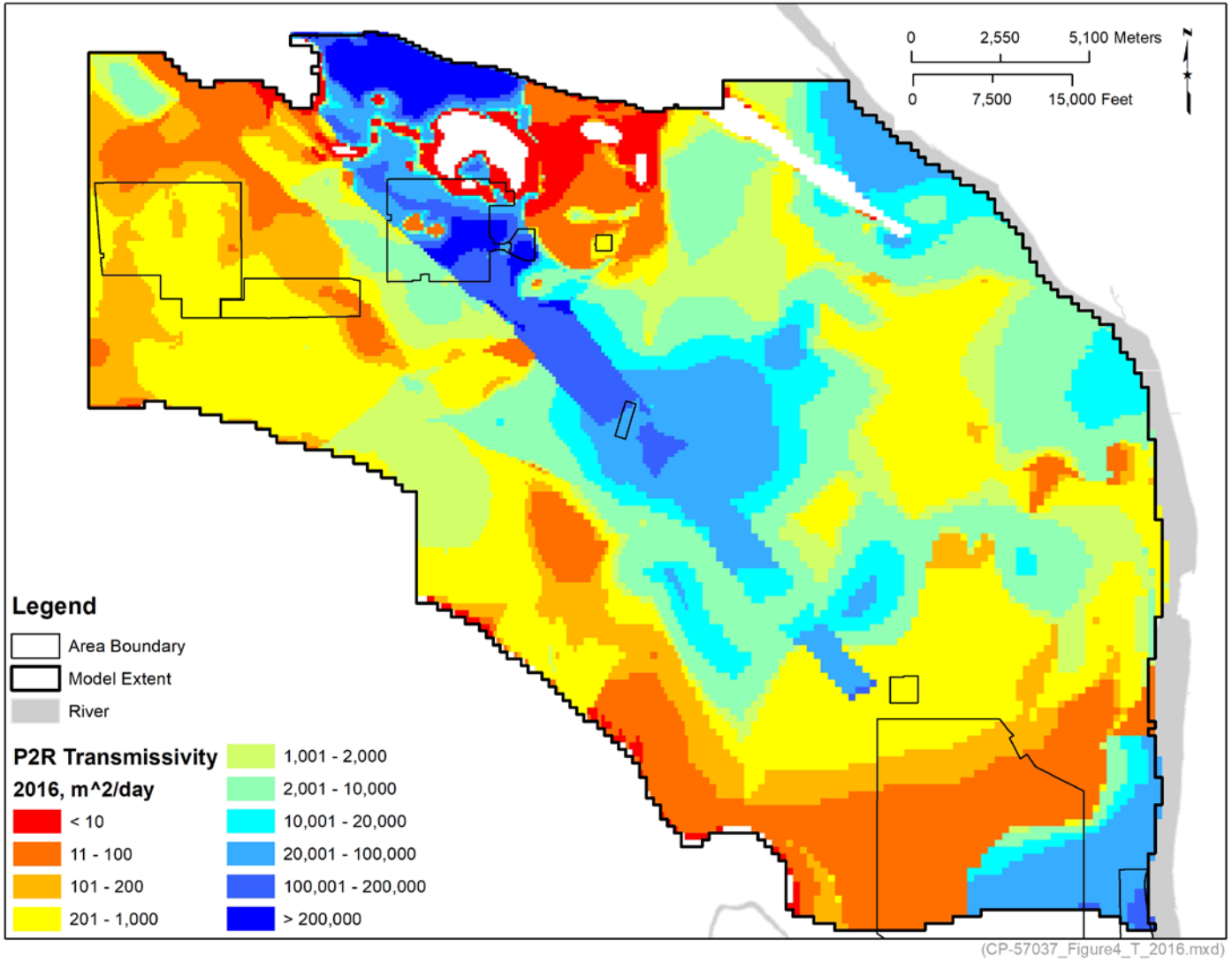

Figure 4-45. Simulated Total Transmissivity Distribution for Calendar Year 2016 in the Calibrated P2R Model Version 8.2

Table 4-7. Calibrated Model Input Parameter Summary for the P2R Model Version 8.2

Recharge Parameters						
Soil Type	**Units**	**Calibrated Value**				
Sandy Loam	mm/yr	2.6				
Silty Loam	mm/yr	3.4				
Sand	mm/yr	13.7				
Dune Sand	mm/yr	55.4				
Ponds	mm/yr	121				
Rattlesnake Mountain	mm/yr	197 (809 m^3/day total)				
Horizontal Hydraulic Conductivity (m/d)						
HSU	**Minimum**	**Maximum**	**Mean**	**50th Percentile**	**10th Percentile**	**90th Percentile**
Hanford Formation	0.6	4,959	454	172	3	1,406
Cold Creek Unit	1.0	4,959	807	389	35	2,132
Ringold Taylor Flat Unit	0.52	120	7	1.4	0.81	20
Ringold Unit E	0.11	96	11	3.4	0.84	37.8
Ringold Lower Mud	0.0026	0.053	0.008	0.008	0.008	0.008
Ringold Unit A	0.075	61.5	2	1.0	0.79	5
Channel HSU	1,002	21,514	15,216	15,000	15,000	18,200
River Conductance						
Columbia River	m^2/day	30.22				

Calibration Metrics

Simulated outputs for this model were compared to observed hydraulic head data, simulated results from the P2R Model Version 7.1 and simulated results from the CPGW Model version 8.4.5. The CPGW Model was included based on the shared model domain and the comparison only applies the portions of the model that overlap. Figures 4-46 through 4-72 provide hydrographs for the selected wells for comparison to those presented in Figure 4-20. The gradient azimuth and magnitude plots are shown in Figures 4-73 through 4-78 for the 6 selected triplets indicated including triplet 6, 15, 23, 40, 52, and 67.

A comparison of the average residuals plotted for each well location for the calibrated P2R Model Version 8.2 are provided in Figures 4-79 through 4-80. The former figure shows the average residuals for the entire model temporal domain the latter figure shows the average residuals from calendar year 2008 to 2016. This time range roughly coincides with the start of pump-and-treat practices in the 200-West Area. A map of average residuals for highlighting well locations in 200-West and 200-East Areas can be found in Figures 4-81 and 4-82, respectively. A plot of simulated heads versus observed heads is shown for the same time windows in Figures 4-83 and 4-84, respectively. The statistical goodness-of-fit metrics for the calibrated model are presented in this figure. Also, Table 4-8 provides the statistical metrics along with

those calculated for CPGW Model 8.4.5 and P2R Model version 7.1. The final calibrated model shows acceptable agreement between the simulated and observed data to fulfill the objectives. Not every hydrograph shows improvement of the goodness-of-fit to observed data over the previous version of the model or the CPGW Model. However, the calibration process brought the model as a whole to a relatively similar goodness-of-fit on par with the previous version of the model. The calibration also updated the model geology to the most current interpretation and included new data not previously considered through the calibration process to P2R Model development.

Table 4-8. Summary Statistics for Calibration of P2R Model Version 8.2

Statistic	Units	P2R Version 8.2	CPGW Version 8.4.5	P2R Version 7.1
RMS	m	1.47	1.39	0.8
Mean Error	m	0.07	0.27	0.2
Absolute Mean Error	m	0.73	0.82	0.5
Correlation Coefficient	--	0.99	0.99	Not Calculated

Contours comparing the simulated and observed water table for calendar years 1965 and 2016 were created to evaluate the final calibrated model. The two time periods reflect the water table when operations heavily influenced the groundwater flow at the site and from the current time period where operational influence has diminished. Figure 4-85 shows the comparison for 1965. Observed water levels are indicated in the figure by dashed line symbol and labeled with the elevation value. Simulated water table contours are shown using a color-flood approach where the elevation is shown by the color legend. Both sets of contours show the influence of operations at areas where mounds exist in the interior of the model. Figure 4-86 shows a similar figure for calendar year 2016. Simulated and observed water table contours show a reasonable match. There is a section of the model near basalt outcrops in 200-East where no observed contour plots were produced for the annual report. In this location the simulated water table is elevated due to simulated discharge from TEDF. In this area the model is functioning as expected. Figures 4-87 and 4-88 show the largest vertical difference in hydraulic head for calendar years 1965 and 2016. The figures indicate that there are notable differences in the hydraulic head vertically. The plots include the outlines of the extent for the Lower Mud and Unit A members of the Ringold Formation. The differences in head roughly coincide to a union of these extents. Downward gradients are most pronounced locations where active discharge is occurring. In those same locations, see the southern portion of 200-West, the downward gradients are less evident.

Figure 4-89 provides the volumetric budget portrayed as a time-series plot. For the purpose of groundwater simulations in MODFLOW, it is conventional to consider a positive value as water flowing into the aquifer and a negative value as water flowing out of the aquifer. Therefore, the positive recharge value indicates that water is added to the groundwater through recharge. Conversely, water exits the aquifer through the Columbia River, shown as a negative value. Comparison of the magnitudes illustrates that recharge to the aquifer and discharge to the Columbia River are the main factors in the water budget within the model domain. A second figure for volumetric budget, Figure 4-90, was created to compare the contribution to the volumetric budget of the smaller scale (< 10,000 m^3/day) components that cannot be evaluated on the large-scale figure. This figure illustrates that pre-operations at the Hanford site the 200-West boundary is a source of groundwater to the model but is overwhelmed during operational periods and then returns to a net contributor to the groundwater after approximately 1997. The Dry Creek boundary is shown to be a net contributor for the entire simulation. The volumes and timing of changes in

the volumetric budget show reasonable agreement with the with conceptual understanding presented in Section 3 of this document. One possible exception is simulated inflow at the Gable Gap from roughly 1957 through 1963. Based on disposal in 200-East it is presumed that flow would be moving out of the model domain during this time. However, it is possible that disposal of facilities to the north of the model domain may have affected the flow direction in this area. Historic water table maps shown in BNWL-B-360 for 1955 and 1960 indicate that it is possible that water flowed in this direction during that time. Thus, the behavior is not considered unreasonable.

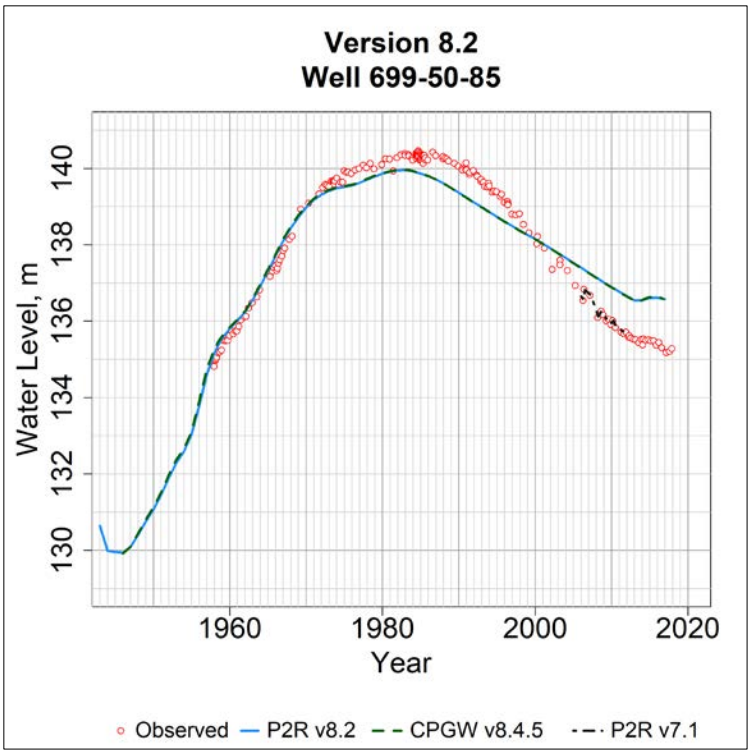

Figure 4-46. Comparison of Observed and Simulated Water Level for CPGW Model at Well 699-50-85

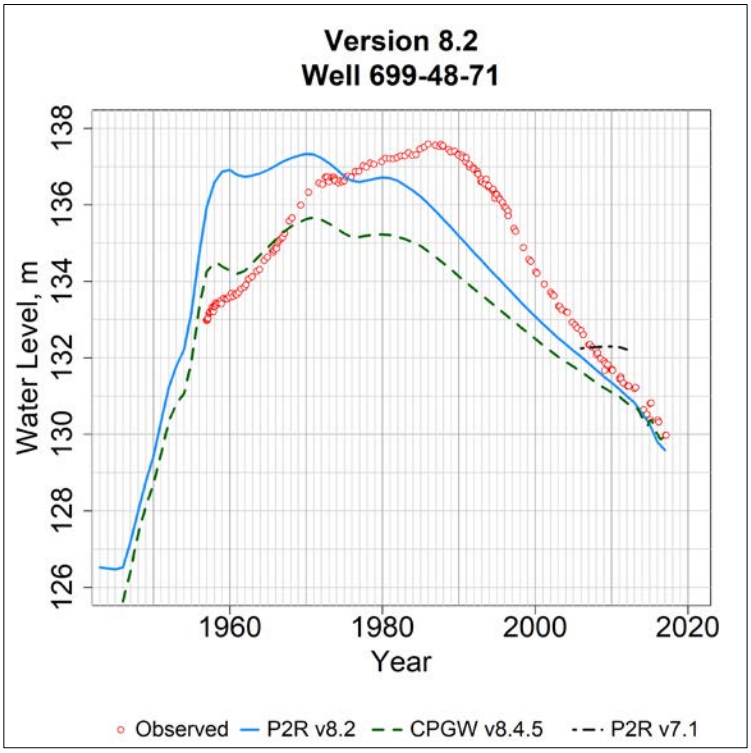

Figure 4-47. Comparison of Observed and Simulated Water Level for CPGW Model at Well 699-48-71

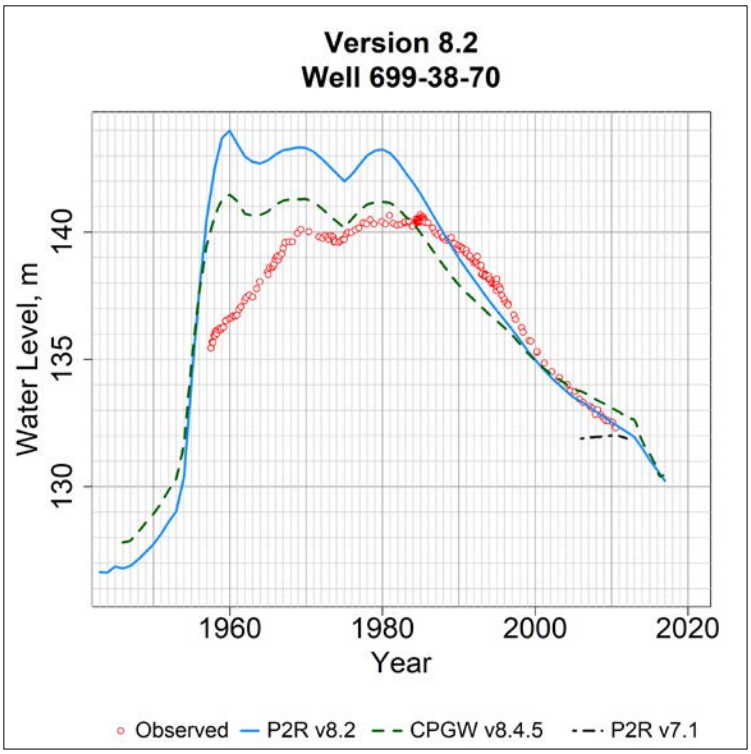

Figure 4-48. Comparison of Observed and Simulated Water Level for CPGW Model at Well 699-38-70

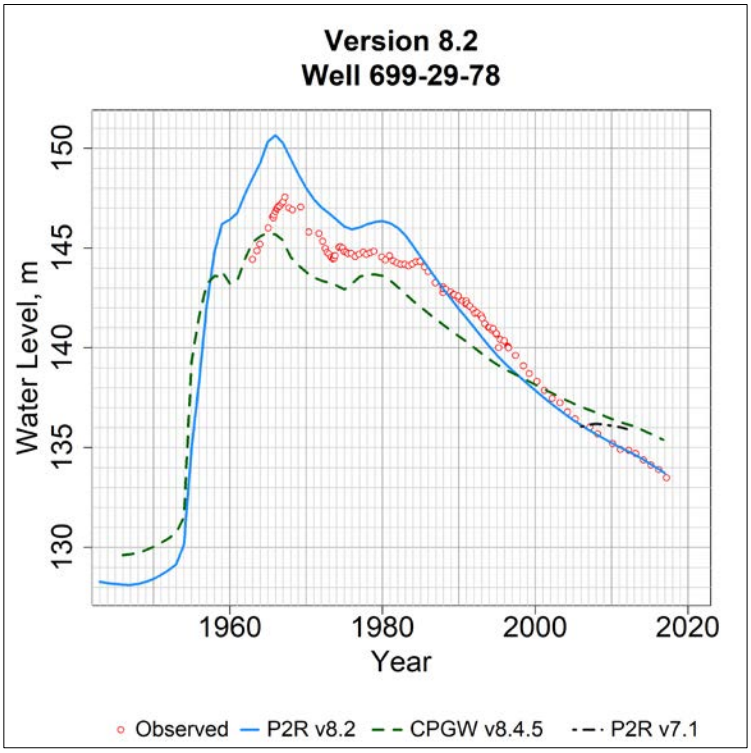

Figure 4-49. Comparison of Observed and Simulated Water Level for CPGW Model at Well 699-29-78

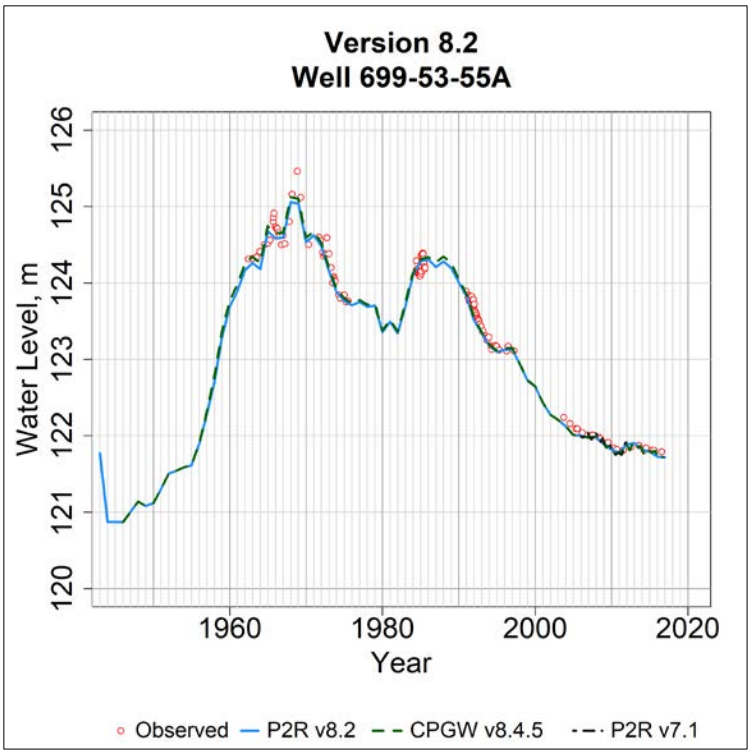

Figure 4-50. Comparison of Observed and Simulated Water Level for CPGW Model at Well 699-53-55A

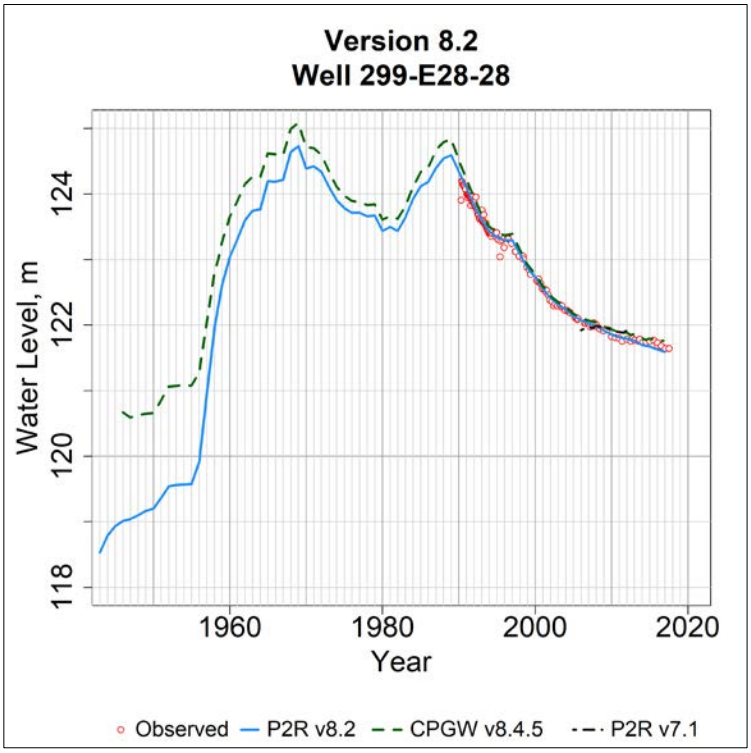

Figure 4-51. Comparison of Observed and Simulated Water Level for CPGW Model at Well 299-E28-28

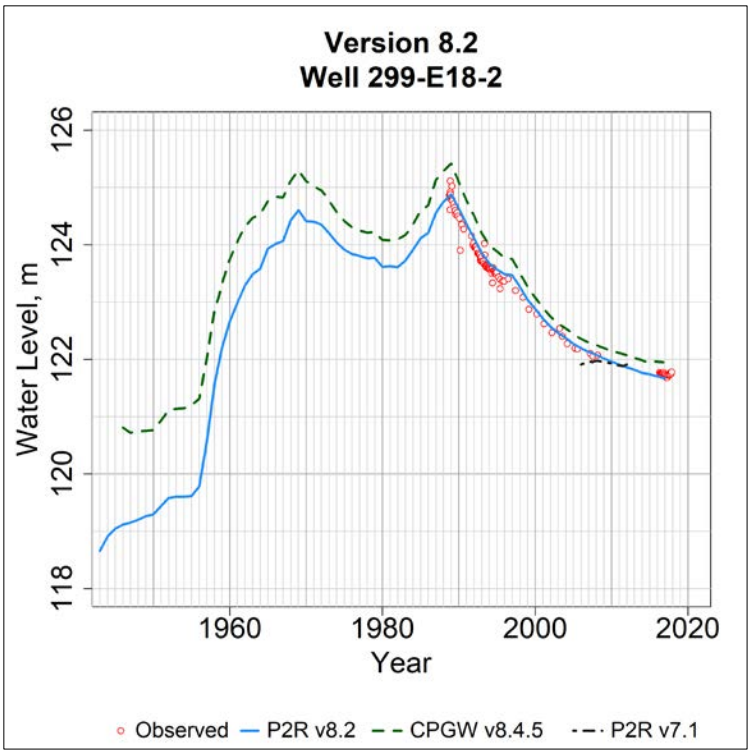

Figure 4-52. Comparison of Observed and Simulated Water Level for CPGW Model at Well 299-E18-2

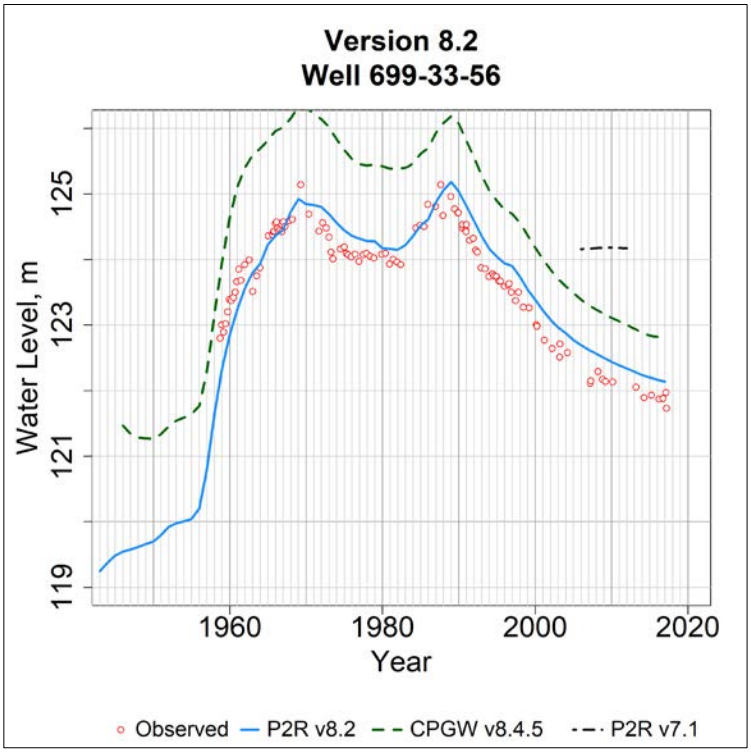

Figure 4-53. Comparison of Observed and Simulated Water Level for CPGW Model at Well 699-33-56

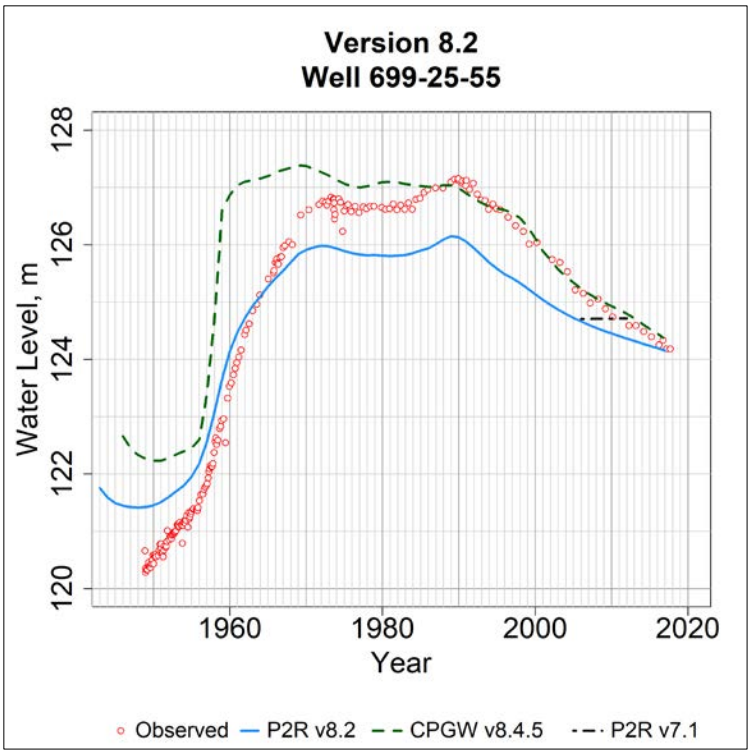

Figure 4-54. Comparison of Observed and Simulated Water Level for CPGW Model at Well 699-25-55

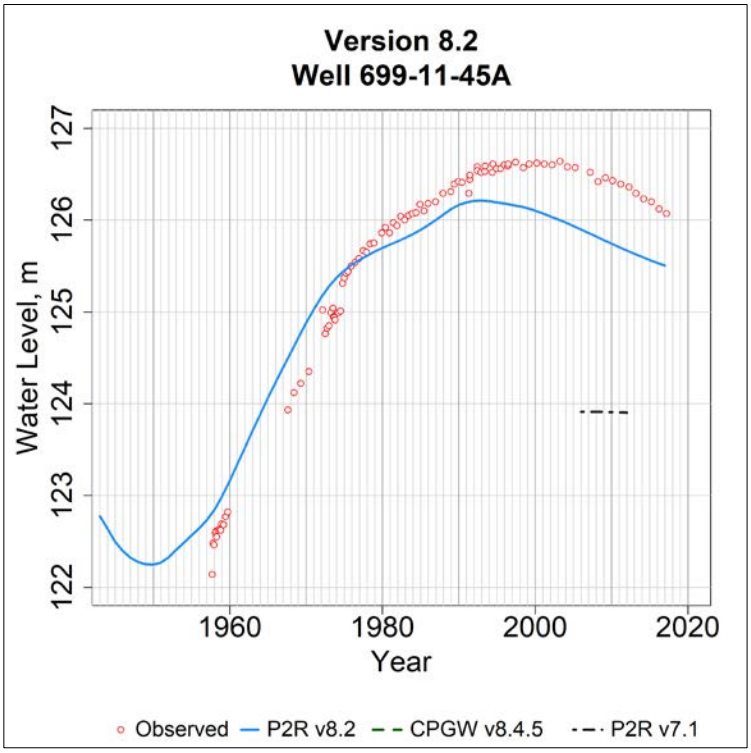

Figure 4-55. Comparison of Observed and Simulated Water Level for CPGW Model at Well 699-11-45A

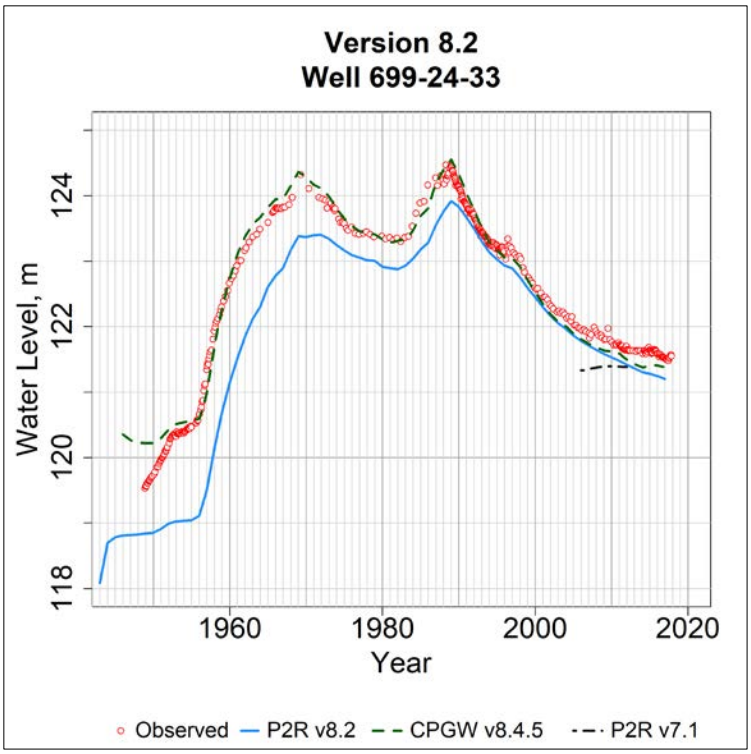

Figure 4-56. Comparison of Observed and Simulated Water Level for CPGW Model at Well 699-24-33

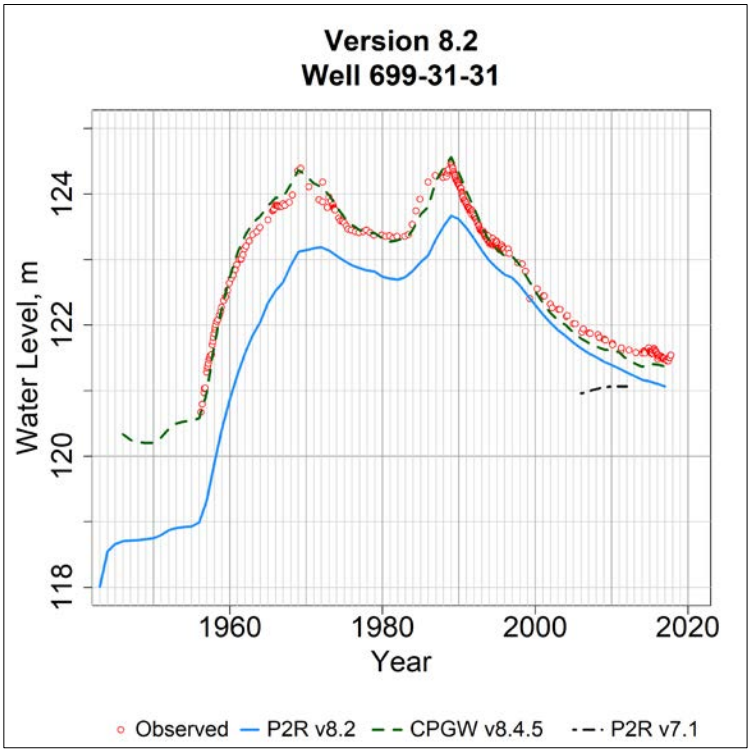

Figure 4-57. Comparison of Observed and Simulated Water Level for CPGW Model at Well 699-31-31

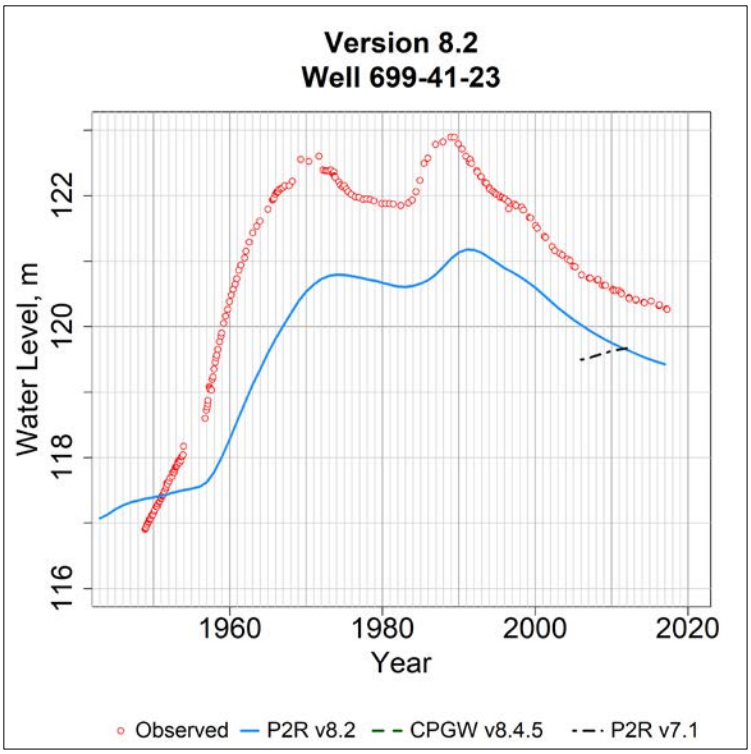

Figure 4-58. Comparison of Observed and Simulated Water Level for CPGW Model at Well 699-41-23

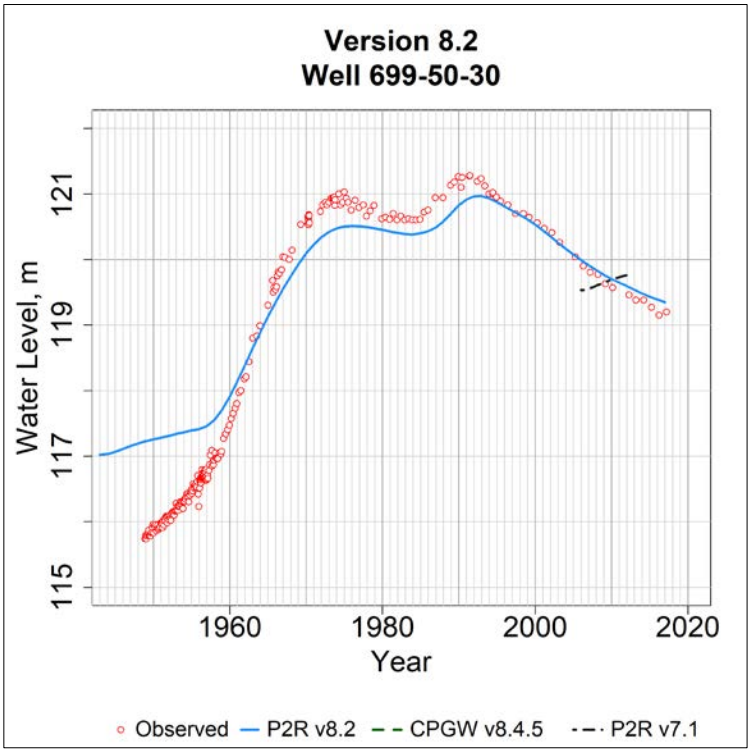

Figure 4-59. Comparison of Observed and Simulated Water Level for CPGW Model at Well 699-50-30

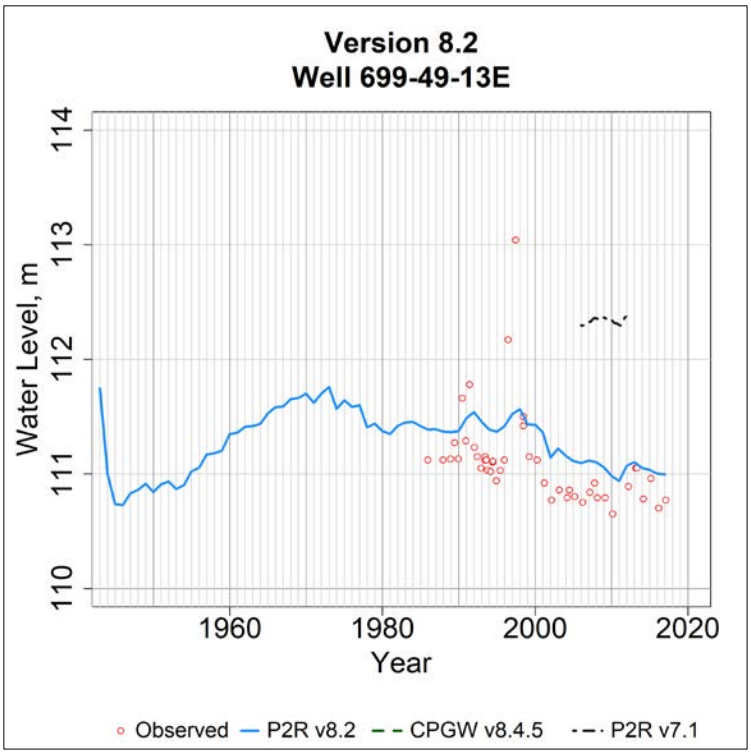

Figure 4-60. Comparison of Observed and Simulated Water Level for CPGW Model at Well 699-49-13E

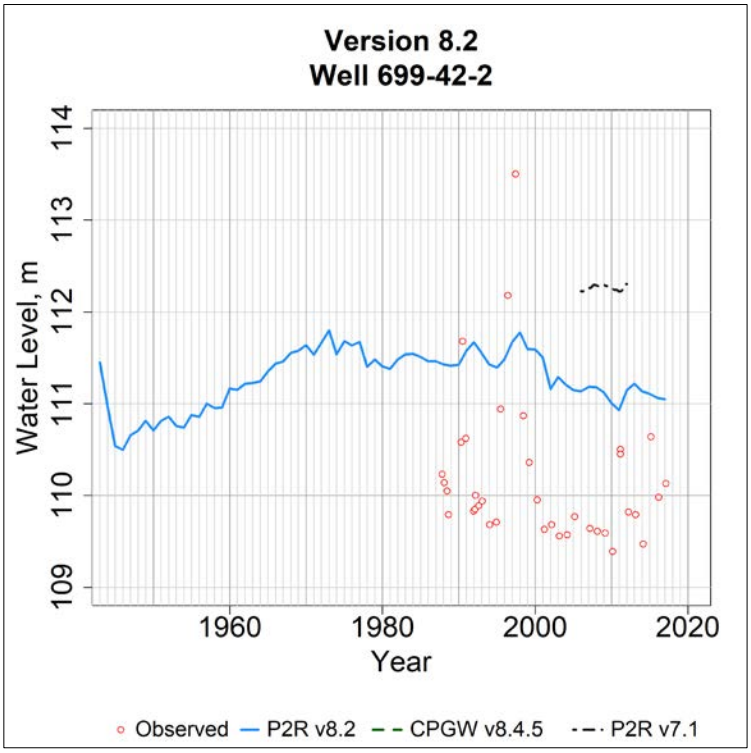

Figure 4-61. Comparison of Observed and Simulated Water Level for CPGW Model at Well 699-42-2

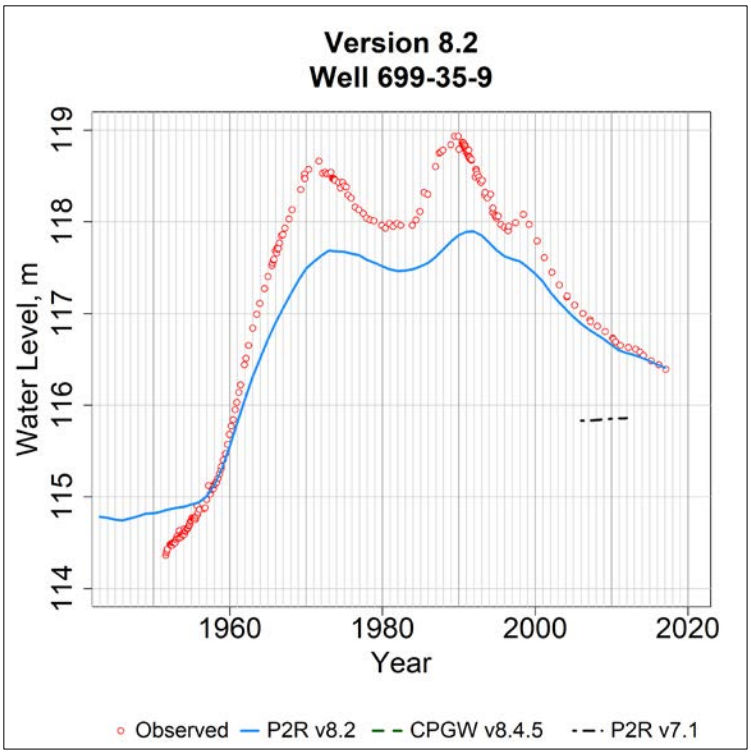

Figure 4-62. Comparison of Observed and Simulated Water Level for CPGW Model at Well 699-35-9

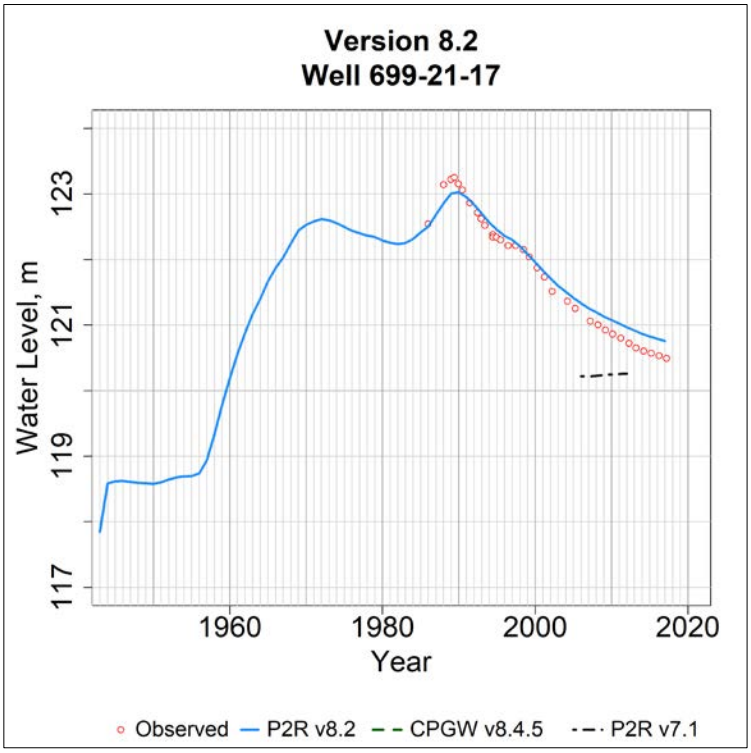

Figure 4-63. Comparison of Observed and Simulated Water Level for CPGW Model at Well 699-21-17

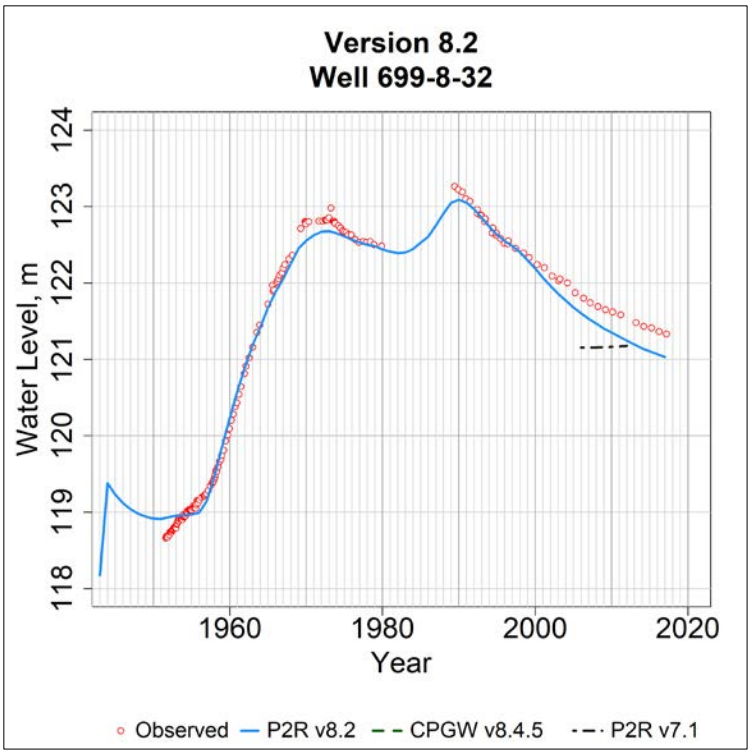

Figure 4-64. Comparison of Observed and Simulated Water Level for CPGW Model at Well 699-8-32

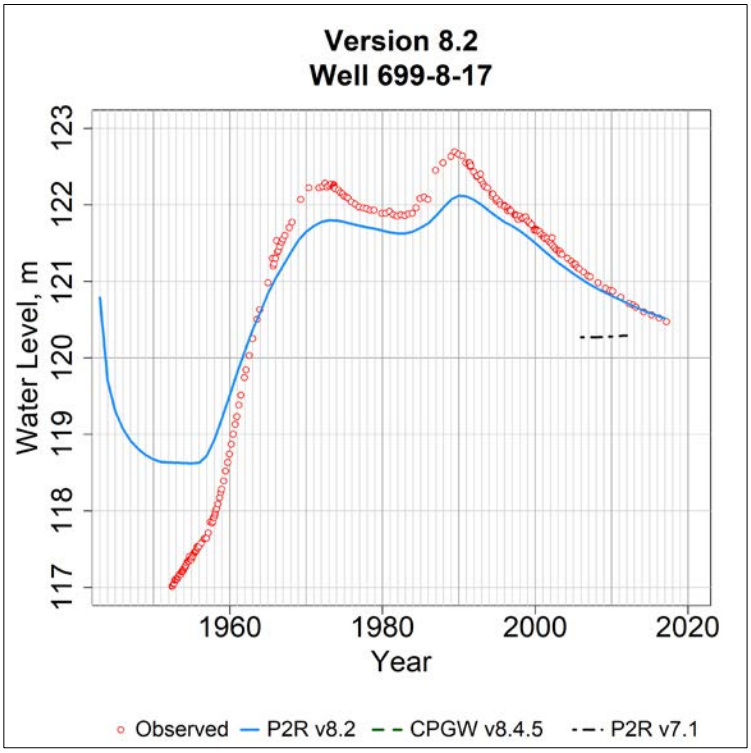

Figure 4-65. Comparison of Observed and Simulated Water Level for CPGW Model at Well 699-8-17

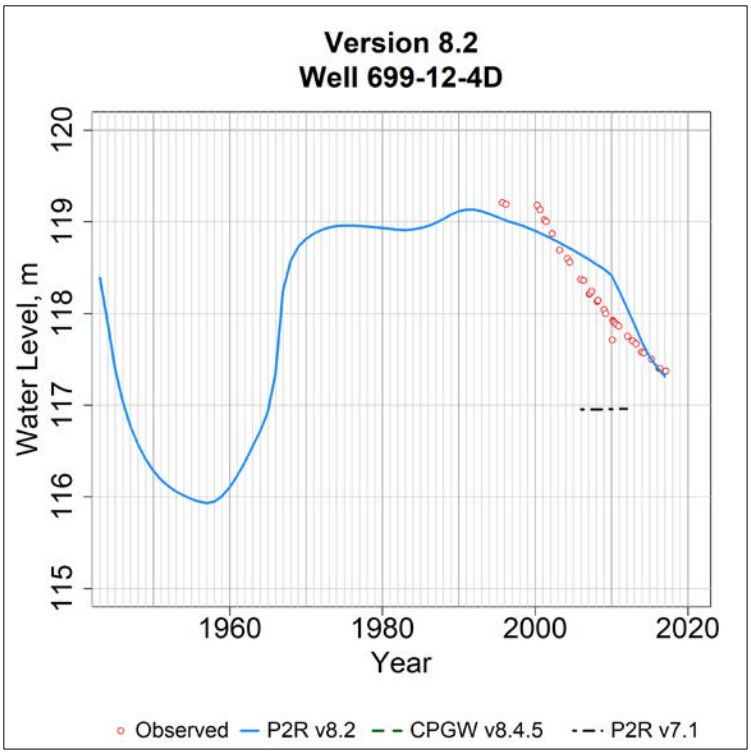

Figure 4-66. Comparison of Observed and Simulated Water Level for CPGW Model at Well 699-12-14D

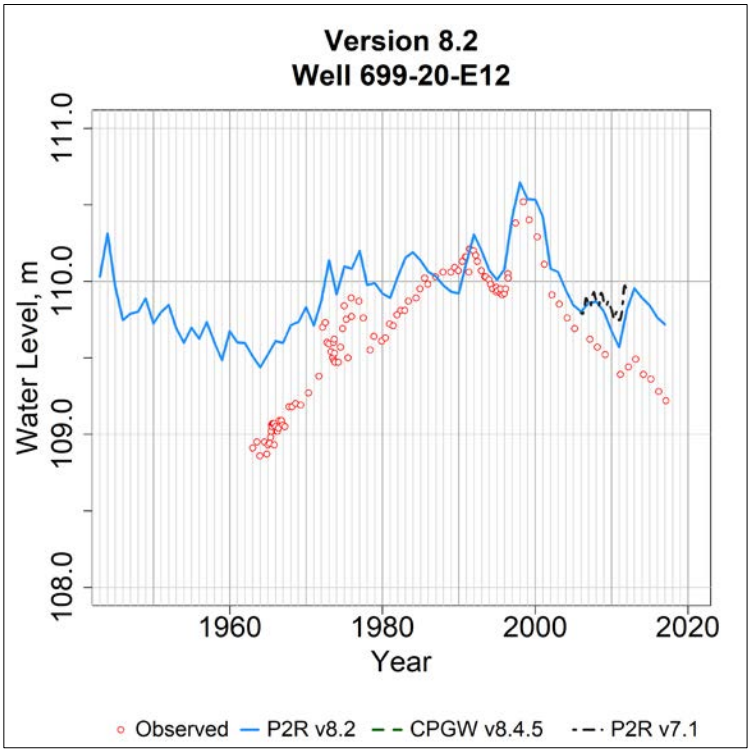

Figure 4-67. Comparison of Observed and Simulated Water Level for CPGW Model at Well 699-20-E12

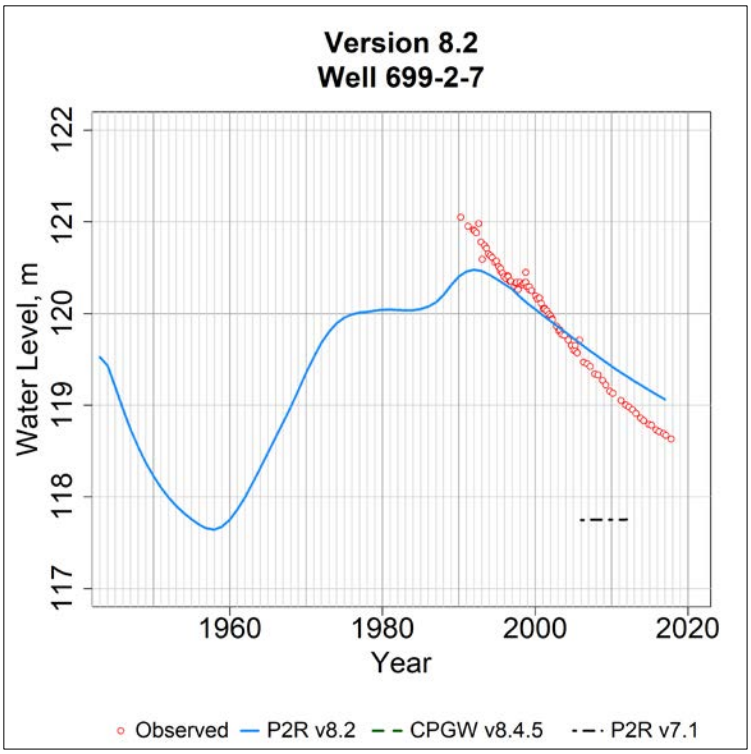

Figure 4-68. Comparison of Observed and Simulated Water Level for CPGW Model at Well 699-2-7

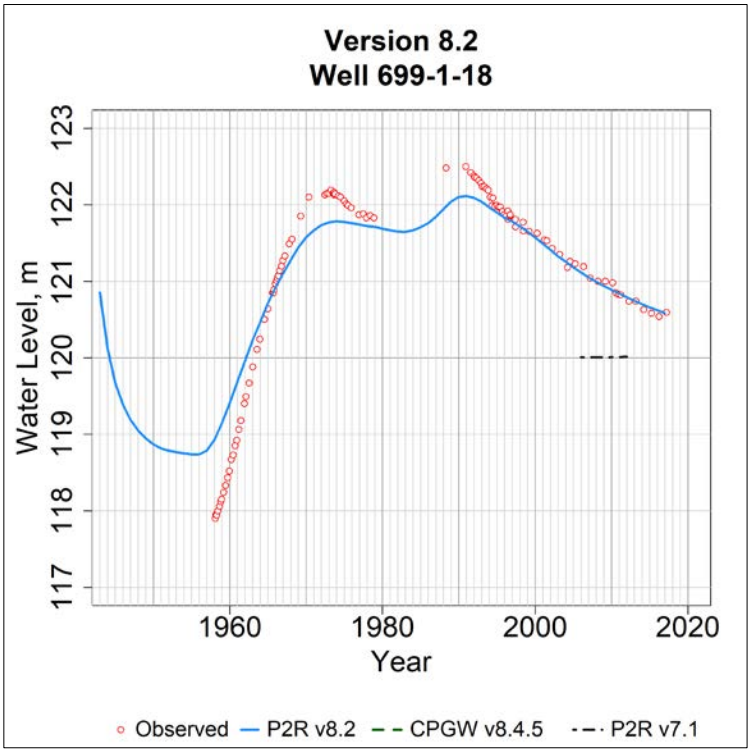

Figure 4-69. Comparison of Observed and Simulated Water Level for CPGW Model at Well 699-1-18

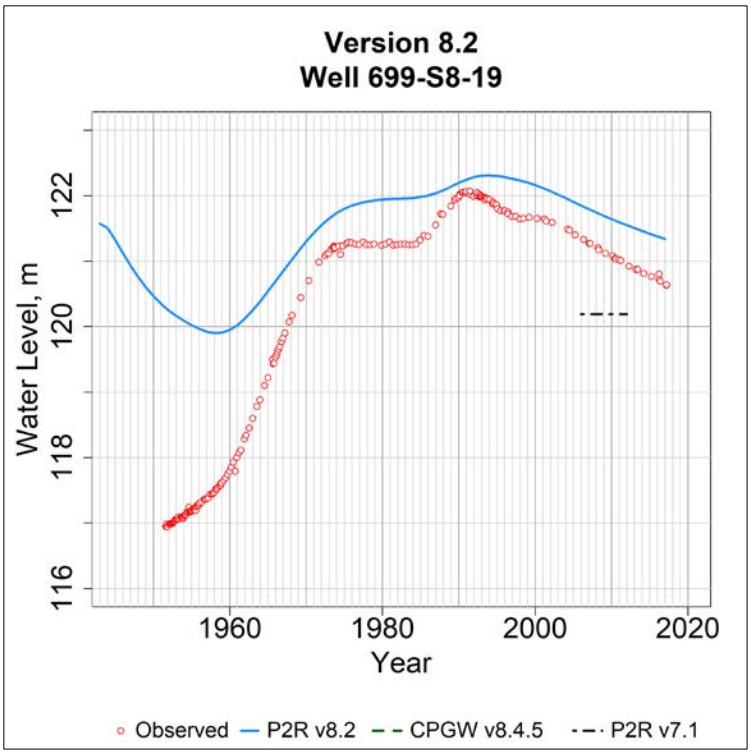

Figure 4-70. Comparison of Observed and Simulated Water Level for CPGW Model at Well 699-S8-19

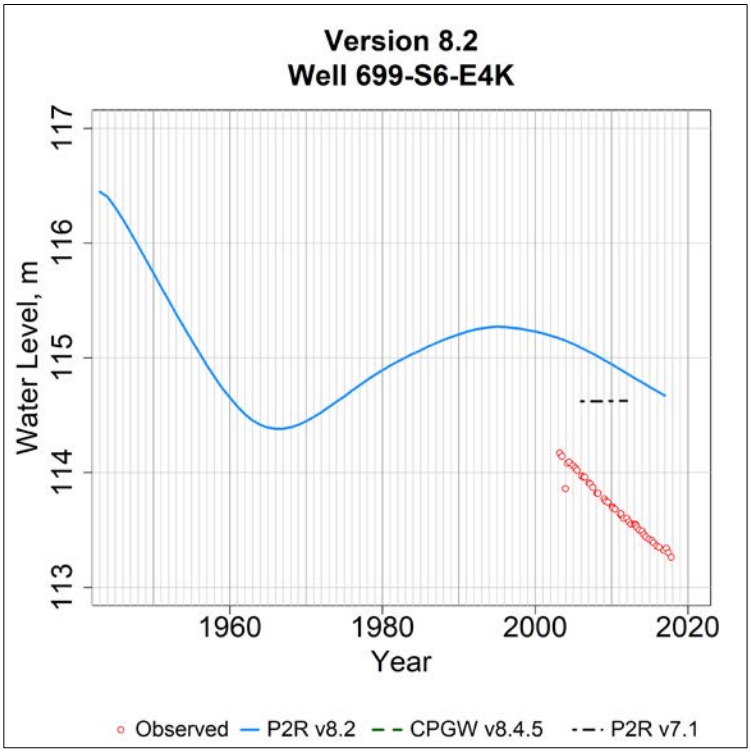

Figure 4-71. Comparison of Observed and Simulated Water Level for CPGW Model at Well 699-S6-45K

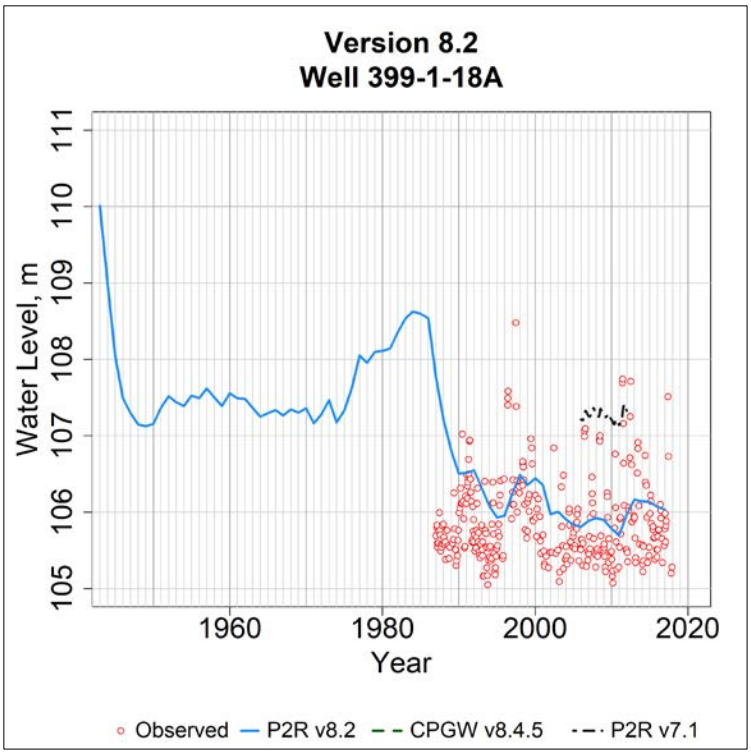

Figure 4-72. Comparison of Observed and Simulated Water Level for CPGW Model at Well 399-1-18A

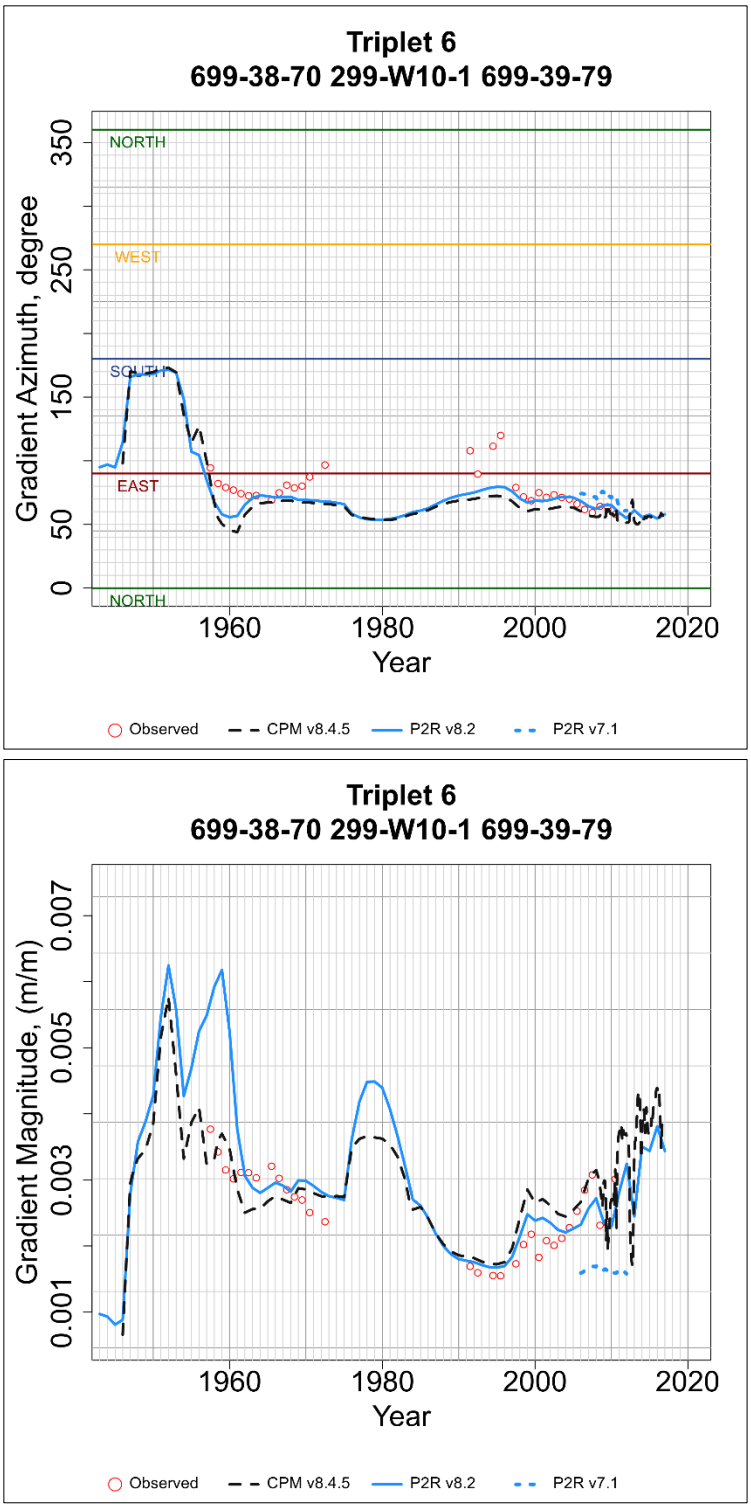

Figure 4-73. Comparison of Observed and Simulated Hydraulic Gradient Azimuth and Magnitude for Well Triplet 6

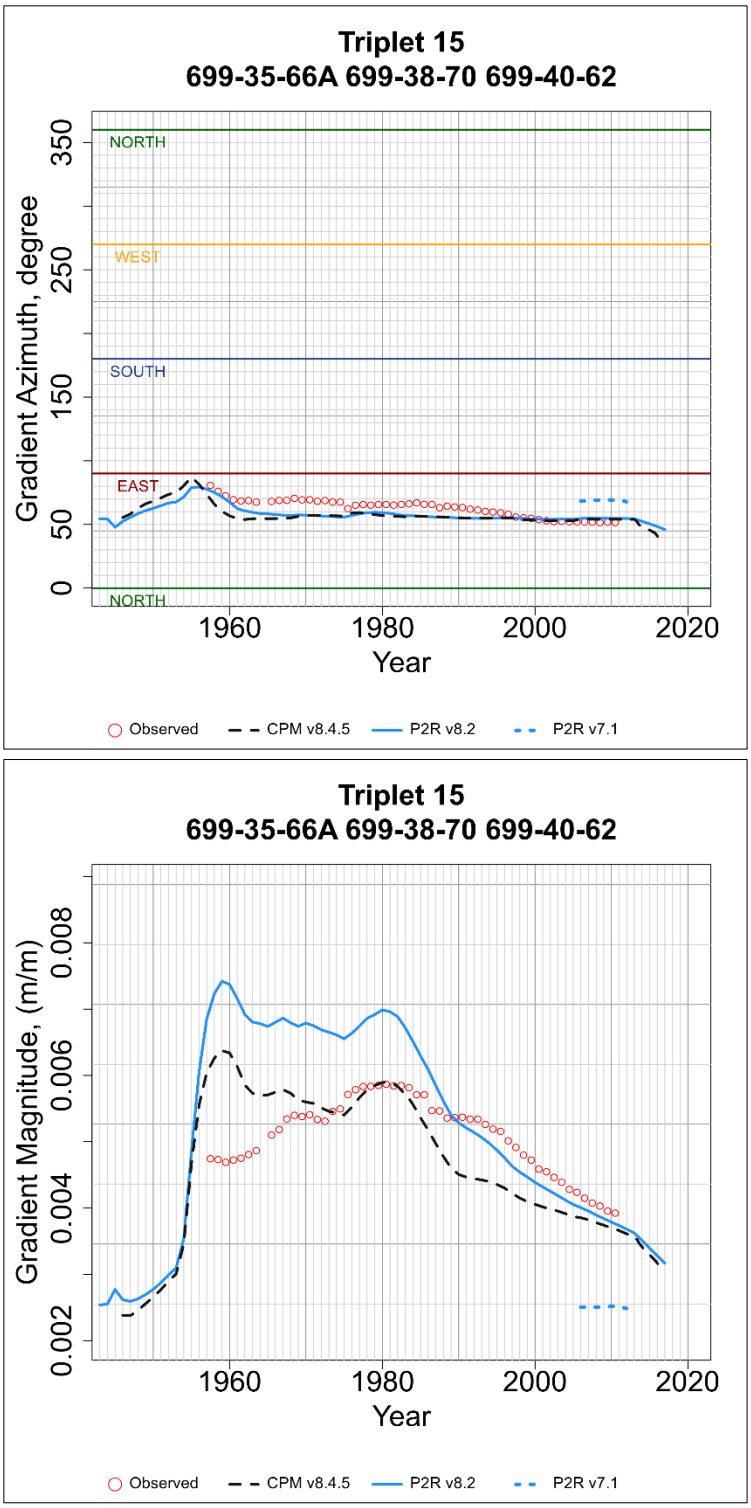

Figure 4-74. Comparison of Observed and Simulated Hydraulic Gradient Azimuth and Magnitude for Well Triplet 15

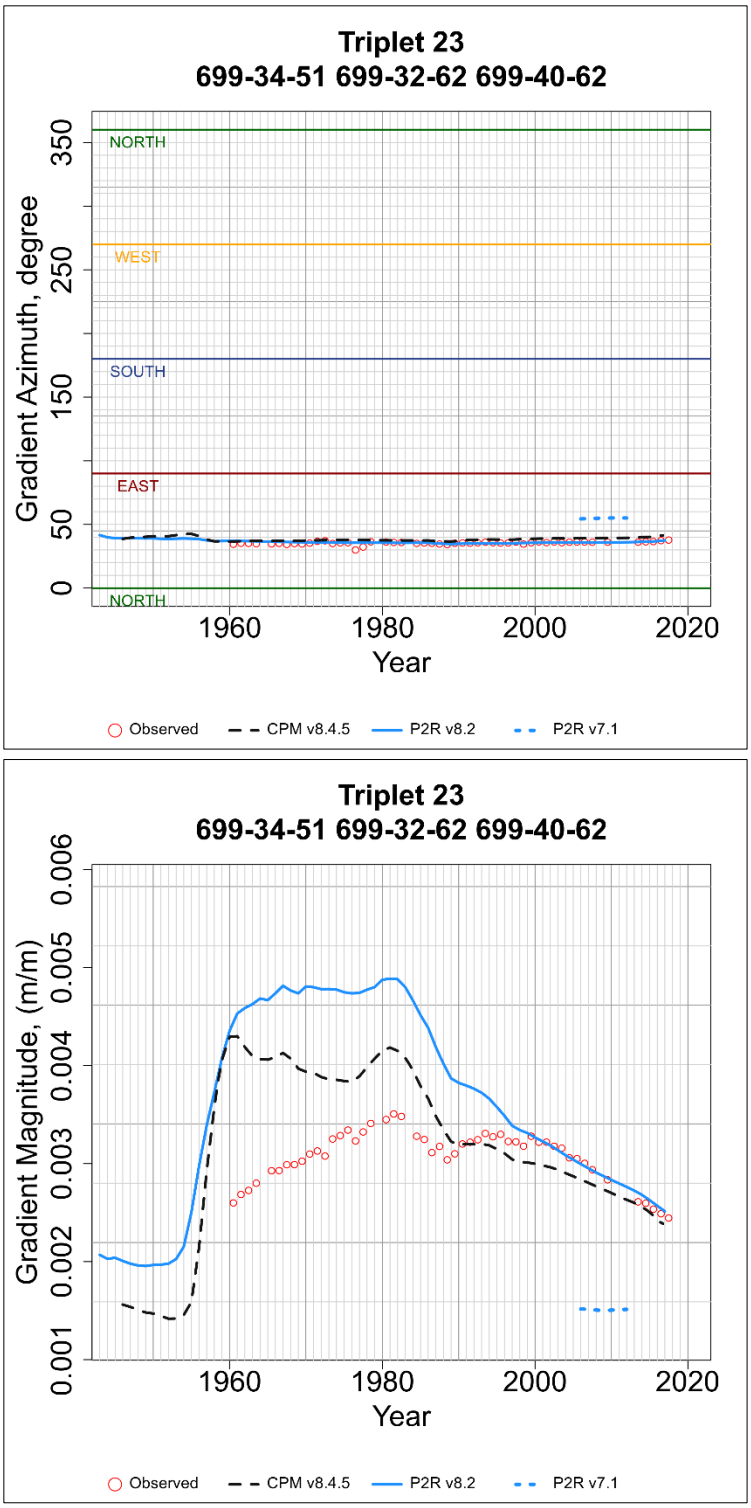

Figure 4-75. Comparison of Observed and Simulated Hydraulic Gradient Azimuth and Magnitude for Well Triplet 23

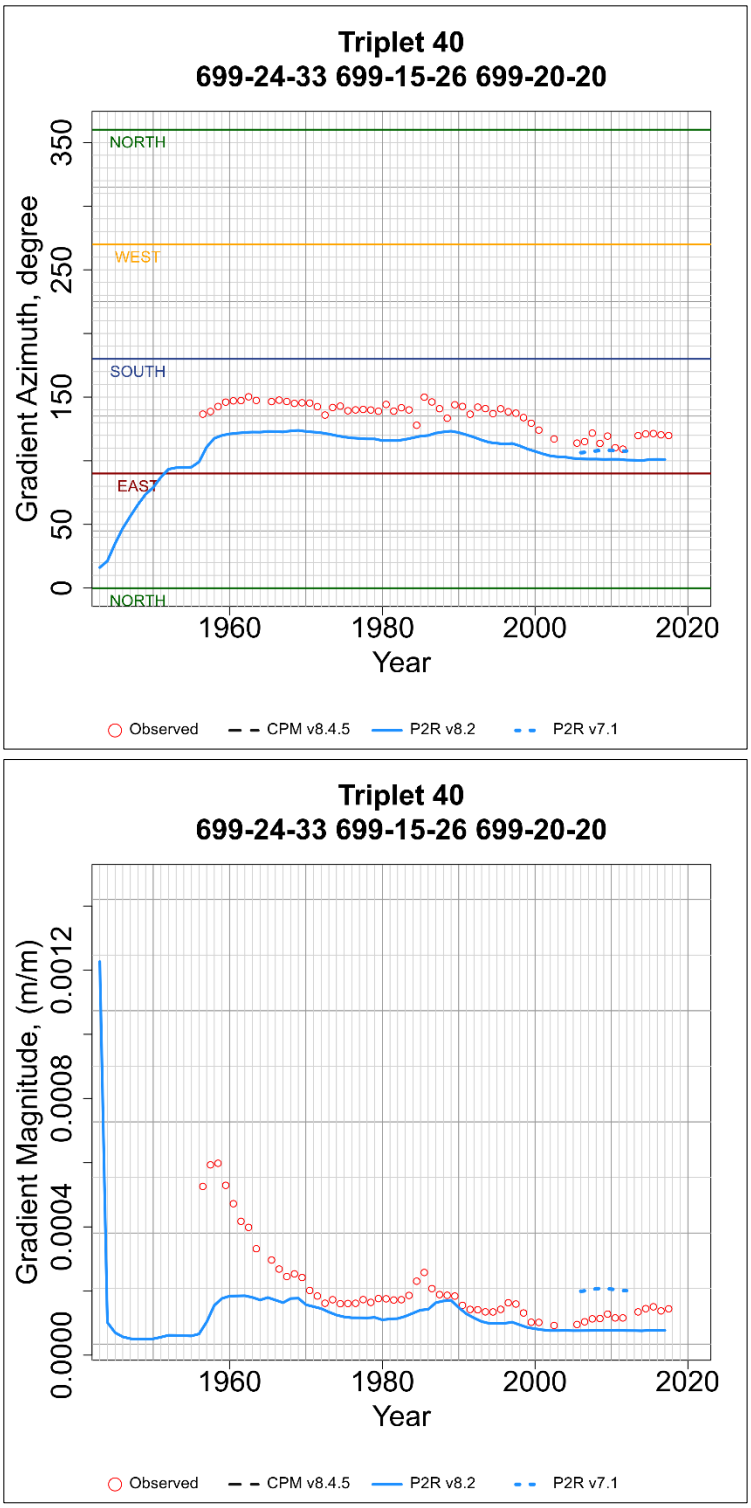

Figure 4-76. Comparison of Observed and Simulated Hydraulic Gradient Azimuth and Magnitude for Well Triplet 40

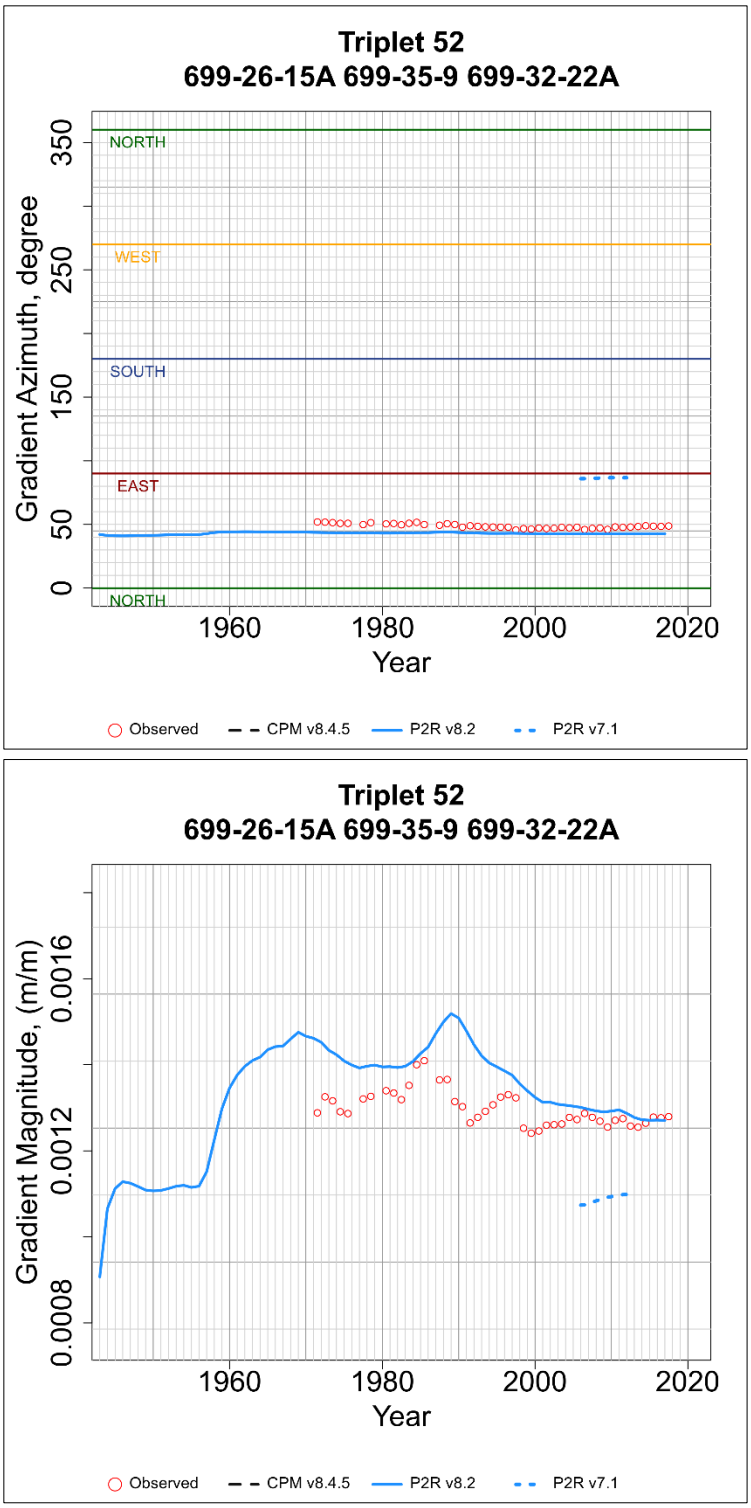

Figure 4-77. Comparison of Observed and Simulated Hydraulic Gradient Azimuth and Magnitude for Well Triplet 52

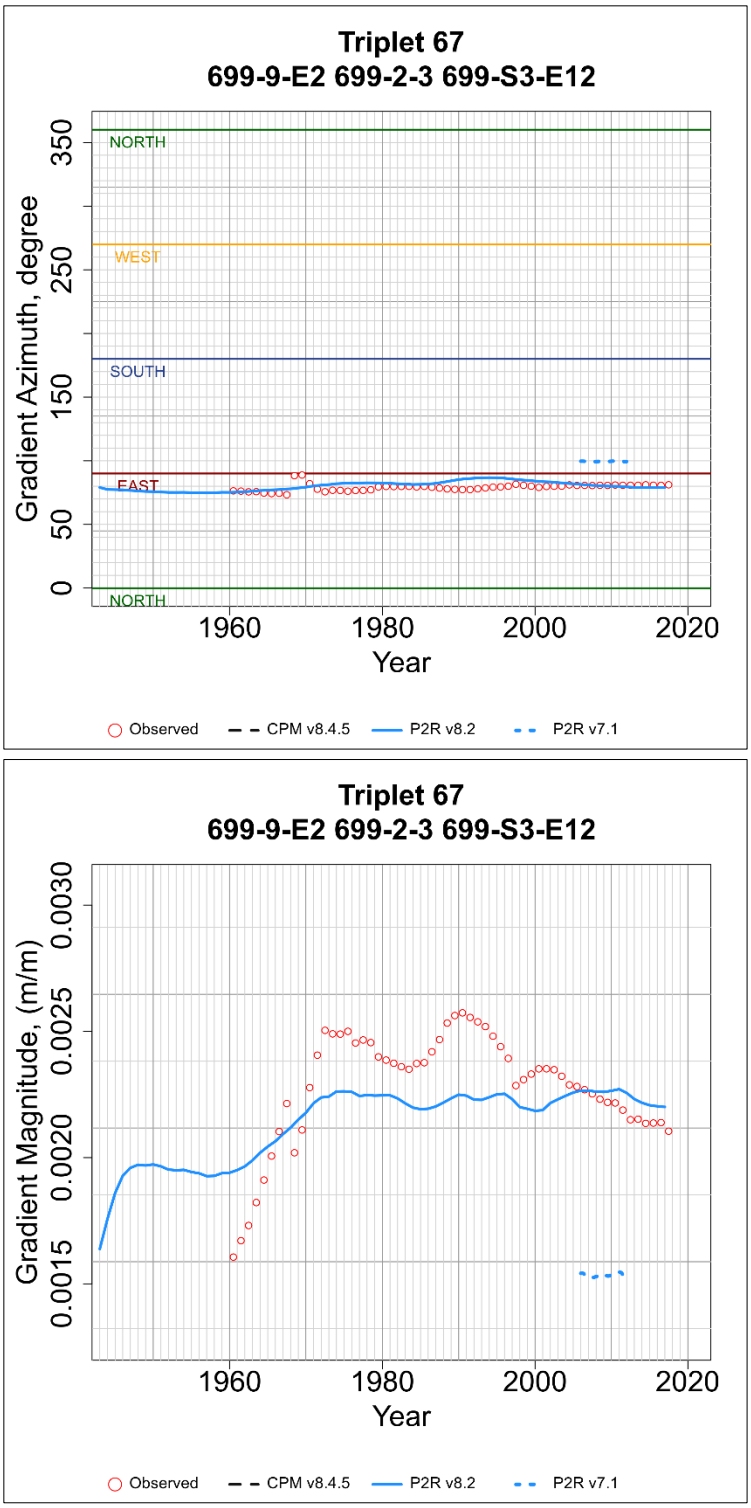

Figure 4-78. Comparison of Observed and Simulated Hydraulic Gradient Azimuth and Magnitude for Well Triplet 67

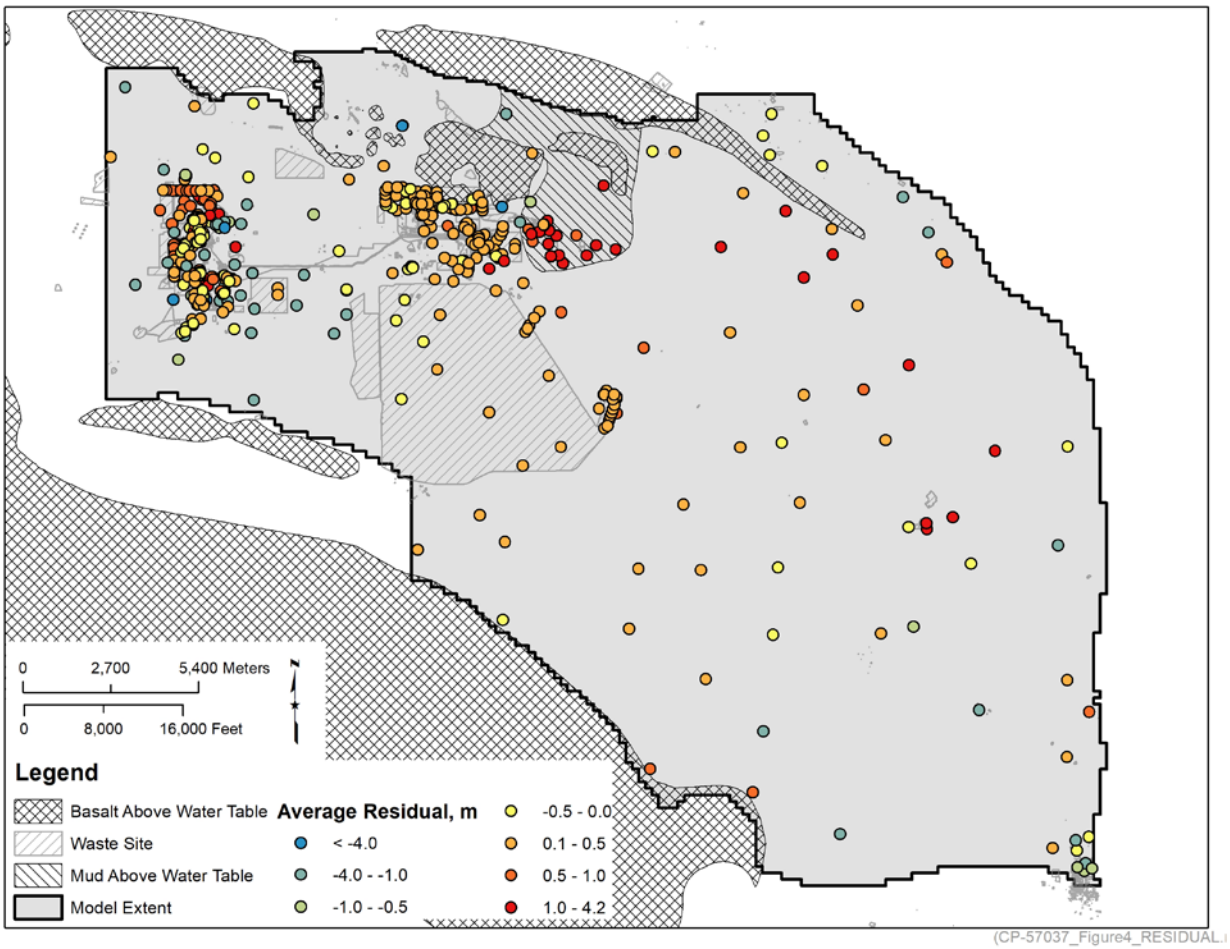

Figure 4-79. Average Residual for Final Calibrated P2R Model Version 8.2 for Model Years 1944 to 2016

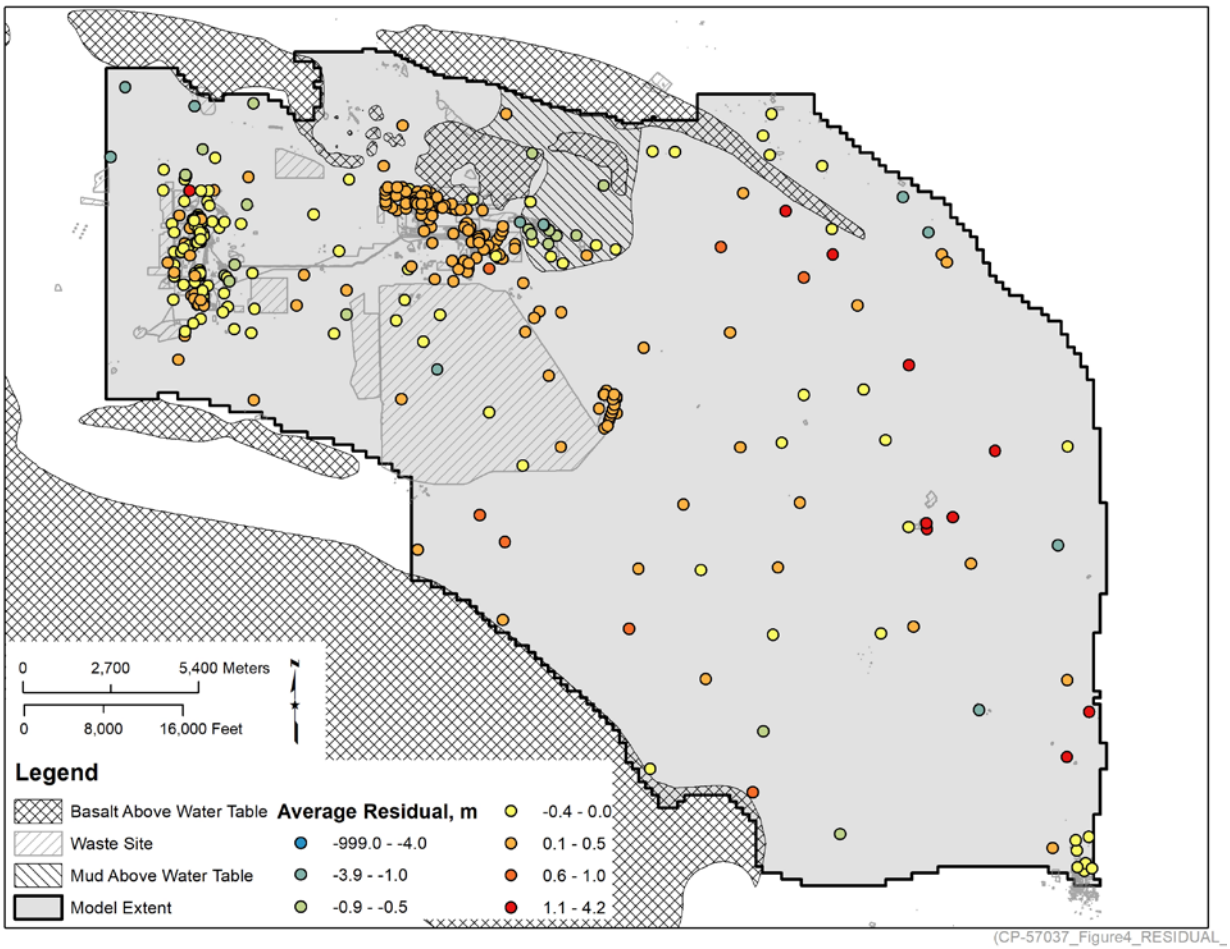

Figure 4-80. Average Residual for Final Calibrated P2R Model Version 8.2 for Model Years 2008 to 2016

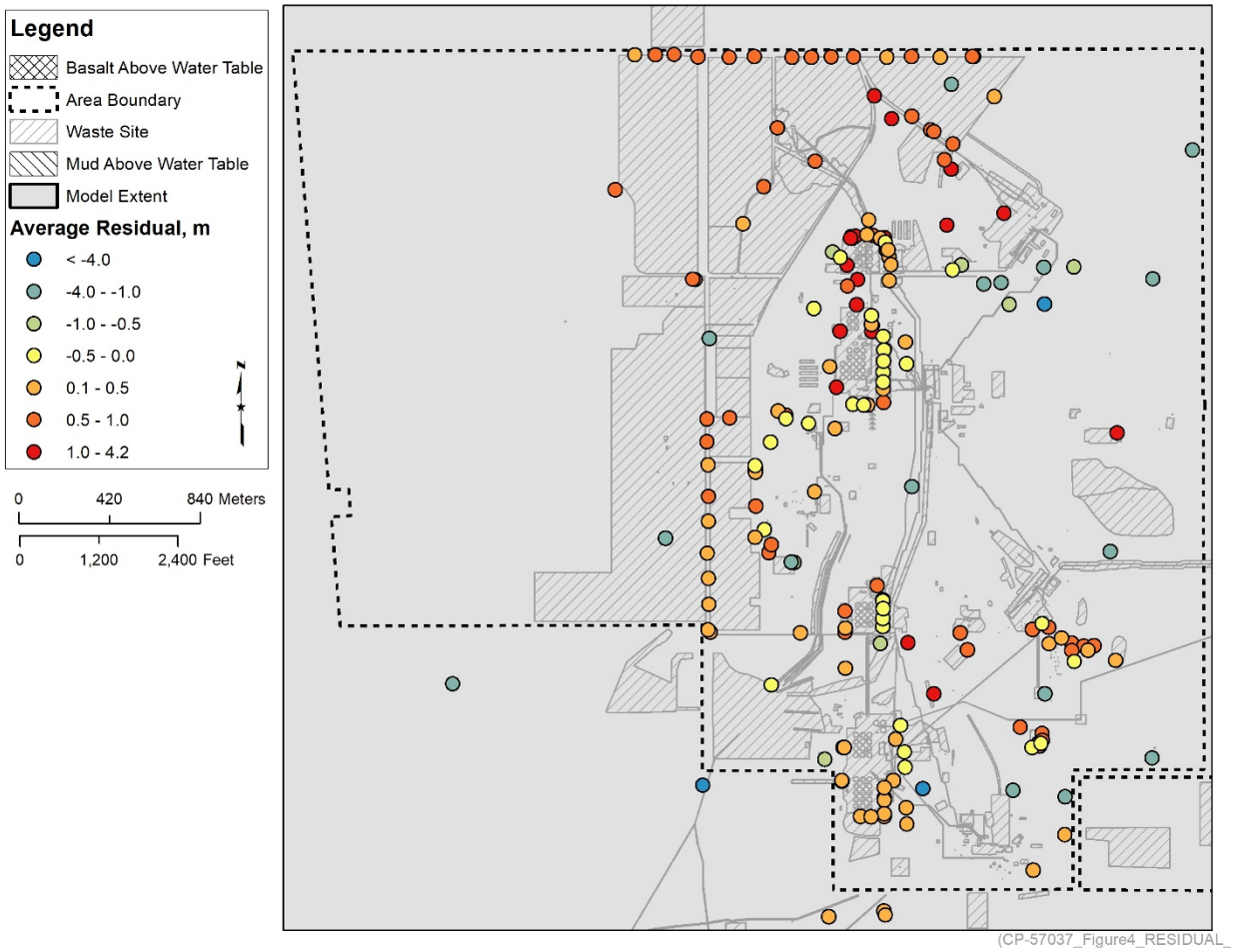

Figure 4-81. Average Residual for Wells near 200-West Area for Final Calibrated P2R Model Version 8.2 for Model Years 1944 to 2016

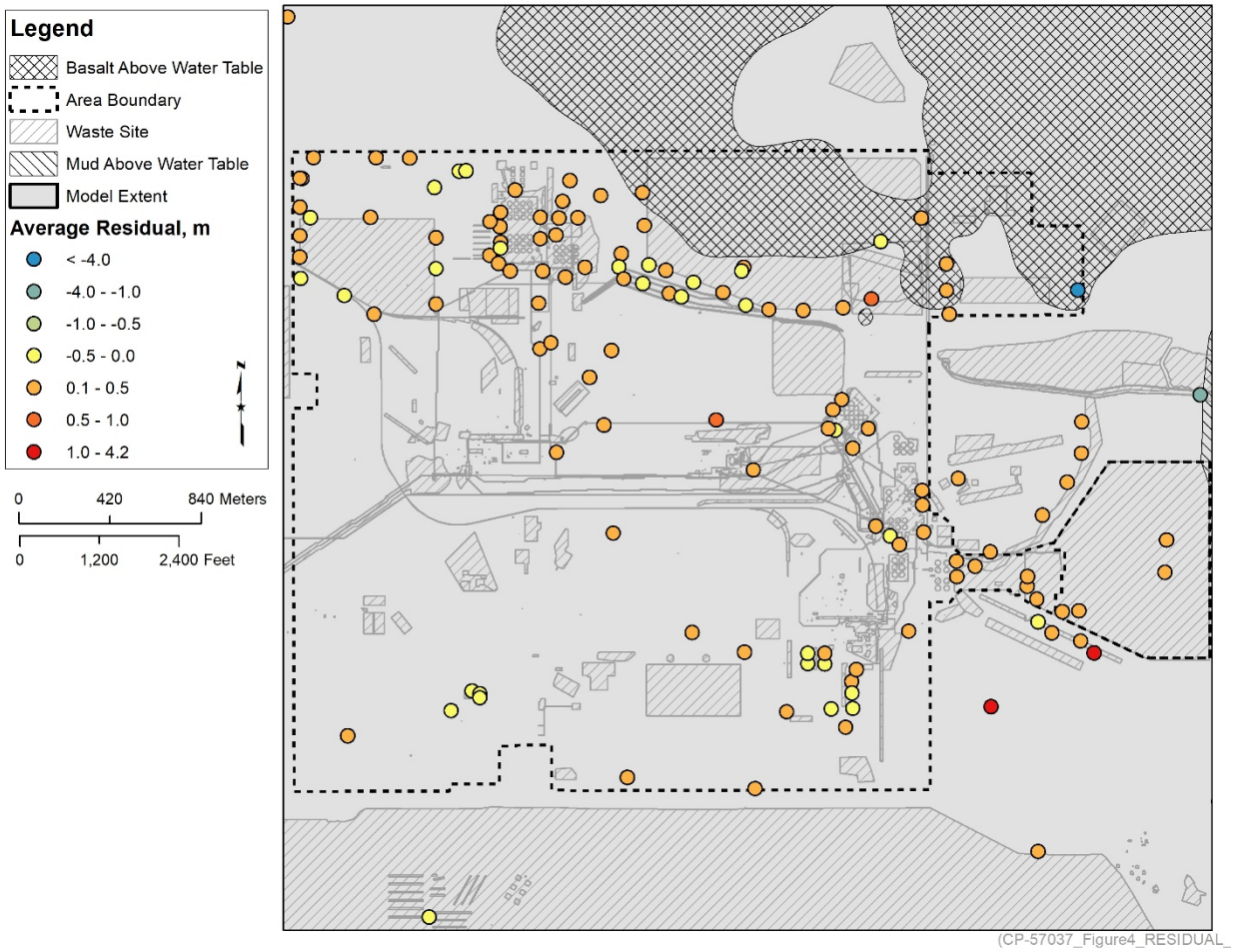

Figure 4-82. Average Residual for Wells near 200-East Area for Final Calibrated P2R Model Version 8.2 for Model Years 1944 to 2016

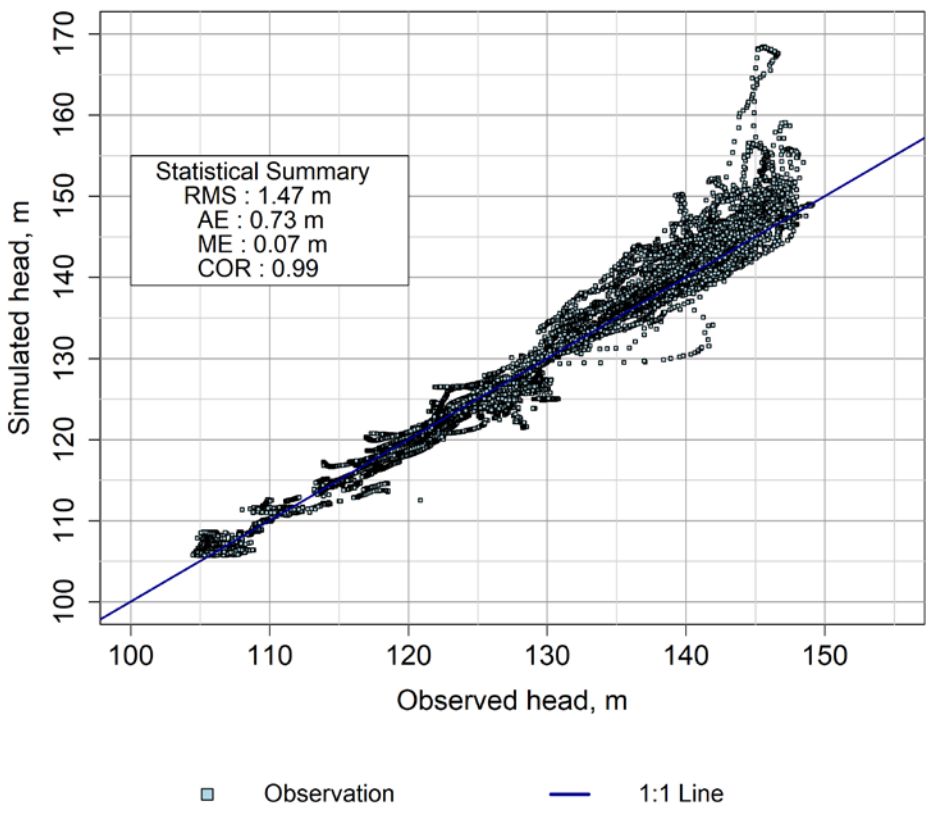

Figure 4-83. Plot of Simulated Heads vs Observed Heads for P2R Model Version 8.2 for Model Years 1944 to 2016

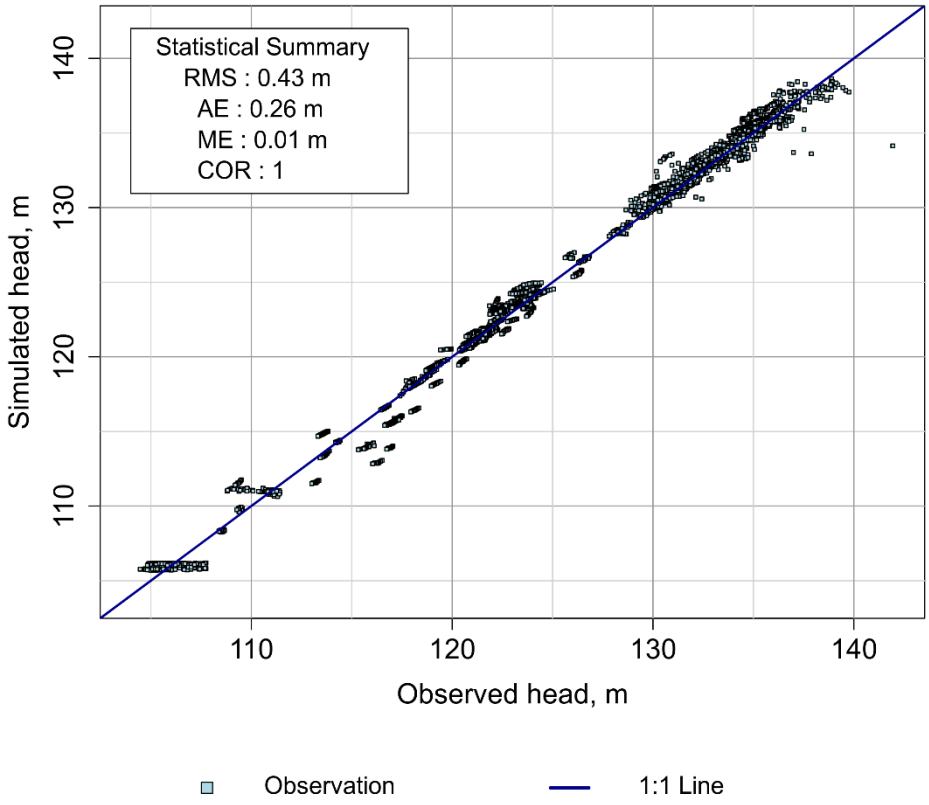

Figure 4-84. Plot of Simulated Heads vs Observed Heads for P2R Model Version 8.2 for Model Years 2008 to 2016

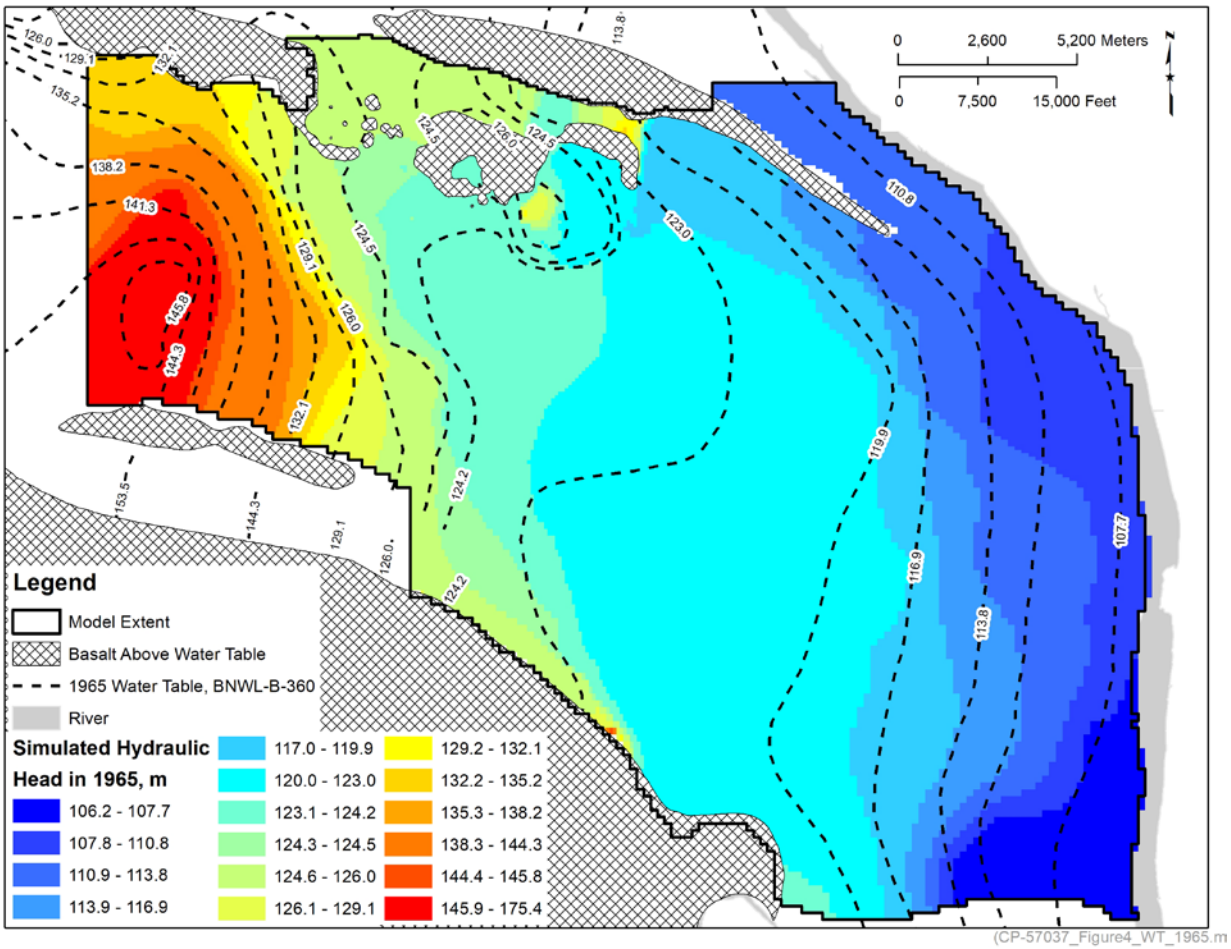

Figure 4-85. Comparison of Simulated and Observed Water Table Contours for Calendar Year 1965

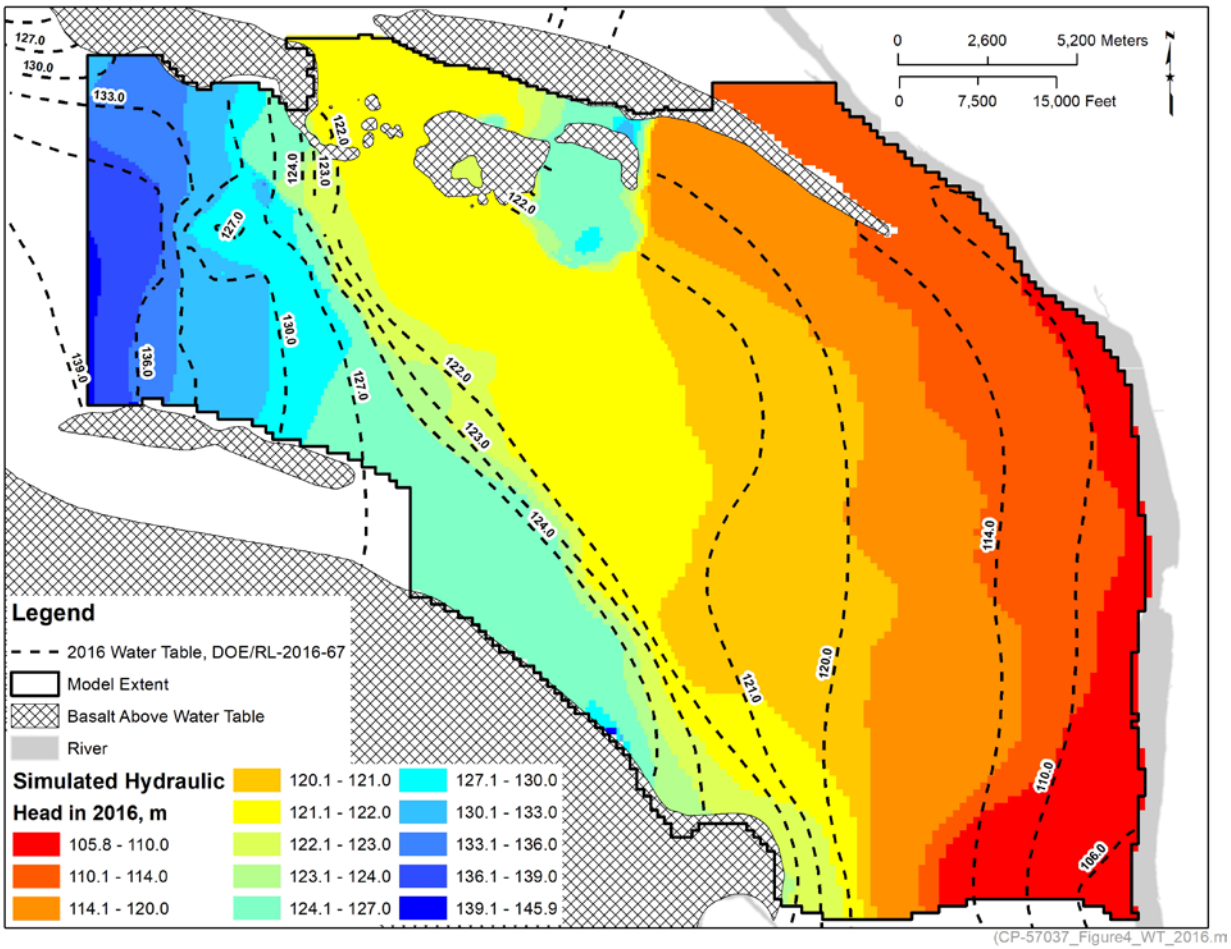

Figure 4-86. Comparison of Simulated and Observed Water Table Contours for Calendar Year 2016

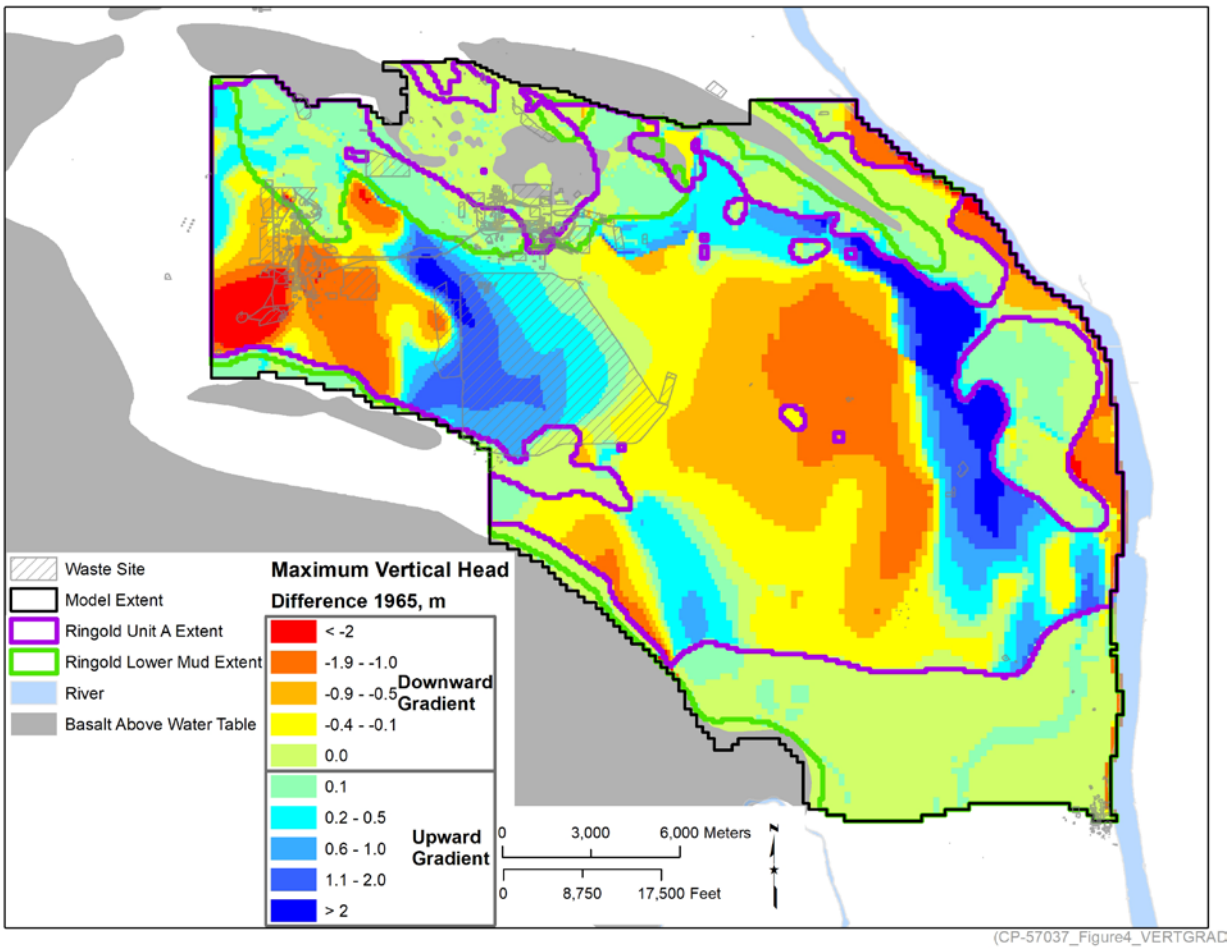

Figure 4-87. Vertical Difference between Simulated Hydraulic Head in the P2R Model Version 8.2 for Calendar Year 1965

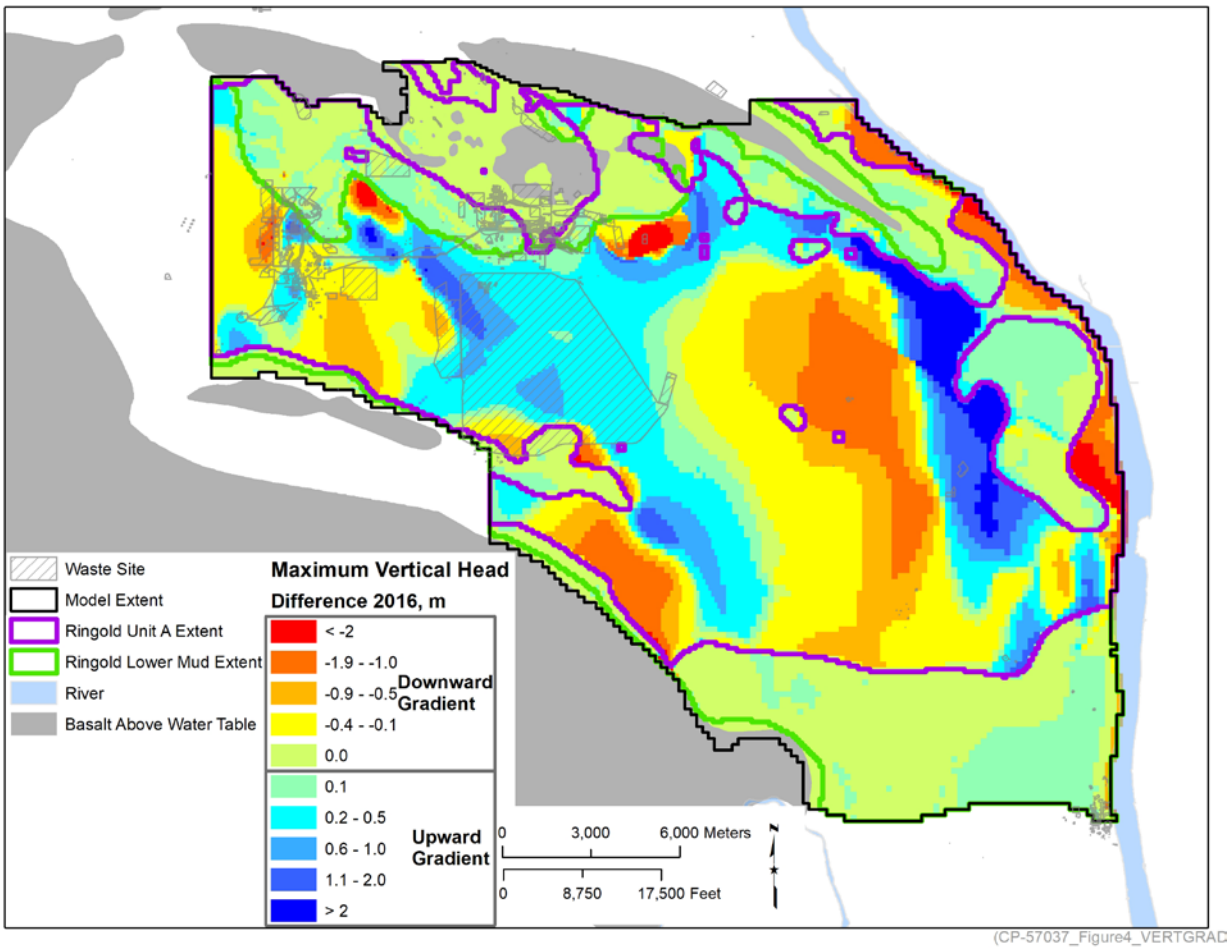

Figure 4-88. Vertical Difference between Simulated Hydraulic Head in the P2R Model Version 8.2 for Calendar Year 2016

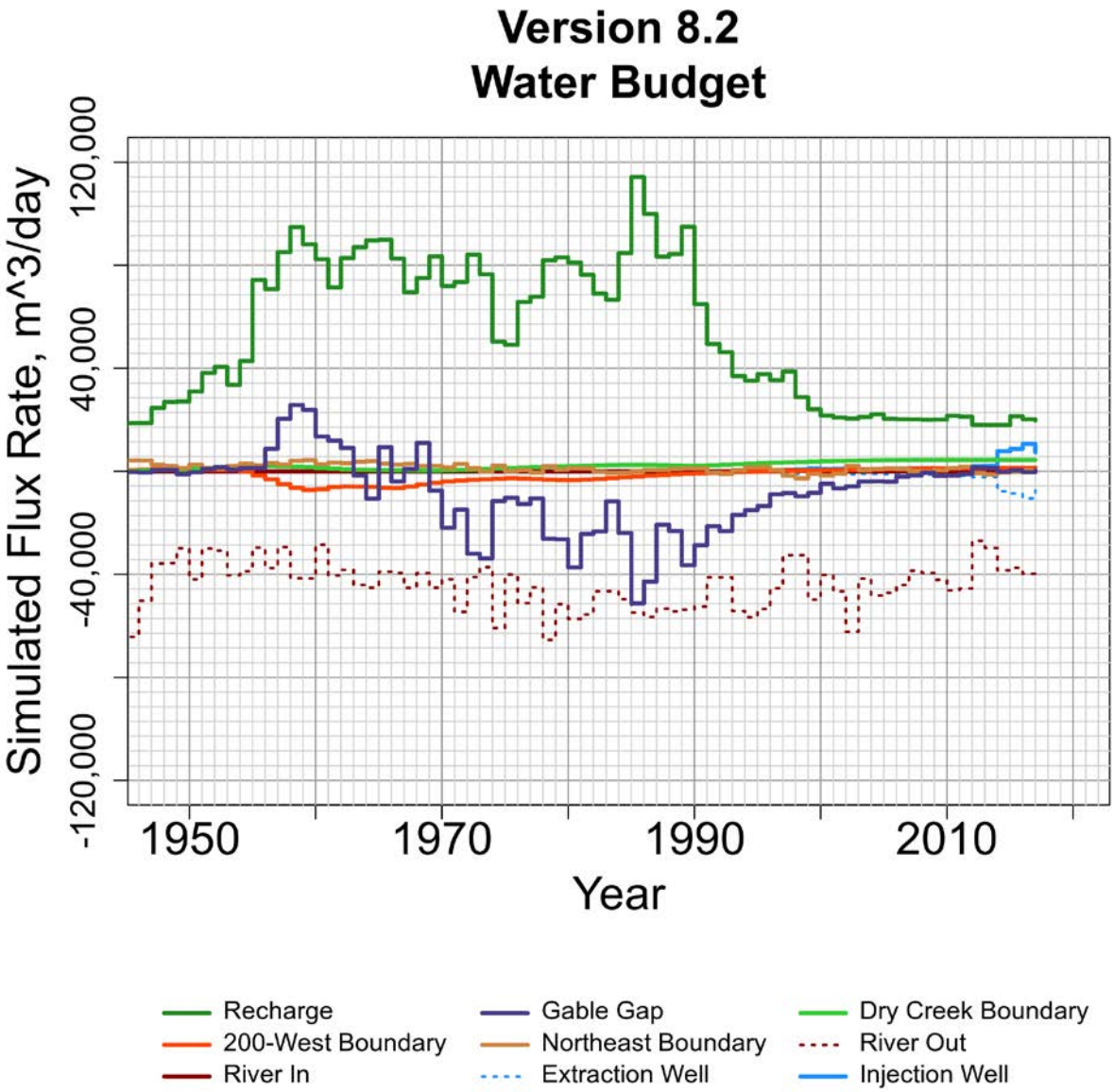

Figure 4-89. Volumetric Budget Time-Series Plot for the Calibrated P2R Model Version 8.2

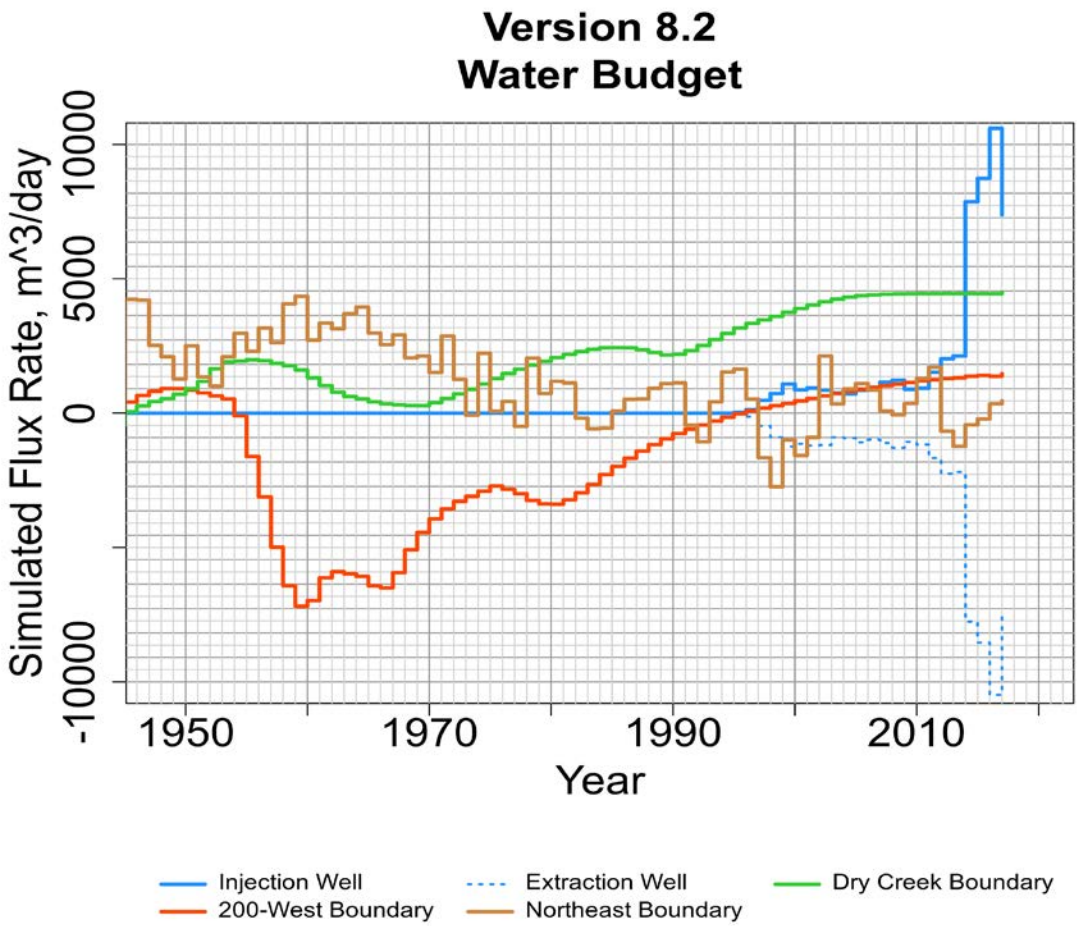

Figure 4-90. Volumetric Budget Time-Series Plot for Budget Components Less than 10,000 M^3/Day within the Calibrated P2R Model Version 8.2

This page intentionally left blank.

5 Model Sensitivity and Uncertainty Analyses

Sensitivity and uncertainty analyses are related aspects of model analysis that seek to identify the elements that have a significant effect on the outputs produced by the model and to determine how these outputs may vary as a result of changes in the model inputs. To the extent that an output of a model is sensitive to an element of the model for which there is imperfect knowledge (e.g., a parameter value, or a boundary condition), the outputs of the model are "uncertain" and, therefore, may not replicate observed conditions in all instances. Analysis sensitivities are useful in identifying this possibility. Sensitivity and/or uncertainty analyses can be performed in a variety of ways, from qualitative assessment of model outputs to formal quantitative analyses. This chapter discusses the quantitative sensitivity analysis and discusses parameter uncertainty in a qualitative fashion.

5.1 Sensitivity Analysis

PEST software was used to help calibrate the P2R Model. As part of the execution using PEST, the code calculates parameter sensitivities and correlation to help determine parameters that will increase the agreement between the model and observed data. Information gathered as part of the initial phases of the calibration was useful in quantifying the sensitivity of selected parameters with respect to the outputs. The hydraulic parameters include specific storage, horizontal hydraulic conductivity (K_h), and specific yield.

Parameter sensitivities and the correlation coefficient matrix were used to assess the calibration of the model. The parameters sensitivity indicates the parameters that are having the largest impact on the mismatch between field observed values and model output (Doherty, 2016). Additionally, the correlation coefficient matrix calculated by PEST provides an indication of the parameter uniqueness based on the specific observations included in the calibration process. Correlations between parameters above an absolute value 0.9 may indicate non-uniqueness of that parameter and will be identified and discussed in this section. Correlation coefficients at this level indicate the chance that the model is ill-posed to resolve an estimated value for that pair of parameters. However, it does not necessary mean that this value is inappropriate for use in the model. Two-hundred and seventeen parameters were used as part of the calibration process. The majority of these parameters were used to estimate a spatially varying hydraulic conductivity pattern for the model domain. A summary of the parameter sensitivities is provided in Tables 5-1 and 5-2 provide a summary of the correlation matrix. Due to the size of the full set of sensitivities and the correlation matrix, it is provided in spreadsheet format and archived with the model files in EMMA as discussed in Section 7.

In Table 5-1, the parameters are summarized by parameter category and ranked based from the most to least sensitive. A rank of 1 is the parameter that had the greatest effect on the match between field observations and model results. The recharge rate for the Rattlesnake Mountain was the most sensitive parameter by several orders of magnitude. This is due to the large footprint this parameter effects in the model (approximately 10 km of the western boundary is affected by this one parameter). None of the other parameters directly affect flux on as large of a scale. While the Columbia River conductance does apply to a larger length, the change in that parameter is dampened because it is dependent on the river stage which is fixed. Due to this order of magnitude difference the parameter estimation process was completed in two steps. First, the estimation process was carried out for recharge and then a separate step was completed for hydraulic conductivity. This was completed to reduce the ill-posedness of the PEST calibration process (Doherty, 2016). However, it is noted that the parameter had a large impact on solution. The radius of influence for recharge at two discharge ponds had the lowest sensitivity value. Rather than indicate that radius of influence does not impact the calibration, this may be that these recharge features had an impact in the early portion of the simulation when fewer observed values are

available. The average sensitivities of the remaining parameter groups that have to do with conductivity of soils are within a reasonable range of each other. The most sensitive response in the calibration parameters is due to changes in 200-West hydraulic conductivity field where the calibration targets are more densely located. The opposite is true for the far field hydraulic conductivity parameters that are located where the calibration targets are sparser.

Table 5-1. Summary Parameter Sensitivities Calculated by PEST

Parameter Type	Location	Parameter	Average Sensitivity	Range	Sensitivity Rank
			(dimensionless)		
Conductance	Columbia River	Conductance	1.19E-04	--	9
Recharge	200-West	216-S-11, 216-U-10	3.63E-06	5.31E-06	10
	Mountain Front	Rattlesnake Mountain	4.54433	--	1
Pilot Point Hydraulic Conductivity	Far Field	Channel	1.42E-02	1.54E-02	6
		Hanford formation	1.46E-02	1.53E-02	4
		Cold Creek Unit	1.41E-02	1.64E-02	7
		Ringold Taylor Flat and Unit E	1.45E-02	1.59E-02	5
	200-West	Model Layers 2 and 3	3.38E-02	1.37E-01	3
		Model Layers 4 and 5	3.72E-02	1.32E-01	2
		Model Layer 7	1.17E-02	1.32E-01	8

"--" denotes that only one parameter value was included for this parameter group. Thus no range was calculated.

The summary of the correlation coefficient matrix is shown in Figure 5-1 and in Table 5-2. The figure shows all values of the correlation coefficient matrix expressed as a cumulative distribution function. Two vertical dark green bars are shown in the figure to indicate parameter pairs that are outside the correlation coefficient bounds, 0.9, that indicate possible non-uniqueness. Table 5-2 provides a tabular summary of the cumulative distribution function. The 99th and 1st percentile are at values of 0.22 and -0.30, respectively. These illustrate that the majority of the correlation coefficients values fall well within acceptable bounds. Eight parameter pairs are outside the acceptable bounds of the analysis and indicate the possibility of an ill-posed non-unique solution. Each of these parameter pairs represents individual pilot point locations that are utilized to estimate the hydraulic conductivity field. The reason for the high correlation between these parameter pairs rises from the geometry used to define the location of the pilot points. This includes placement vertically and laterally. These pairs, listed in Table 5-3, are identified and discussed in the following subsections titled based on which type of geometric configuration is likely causing the high correlation.

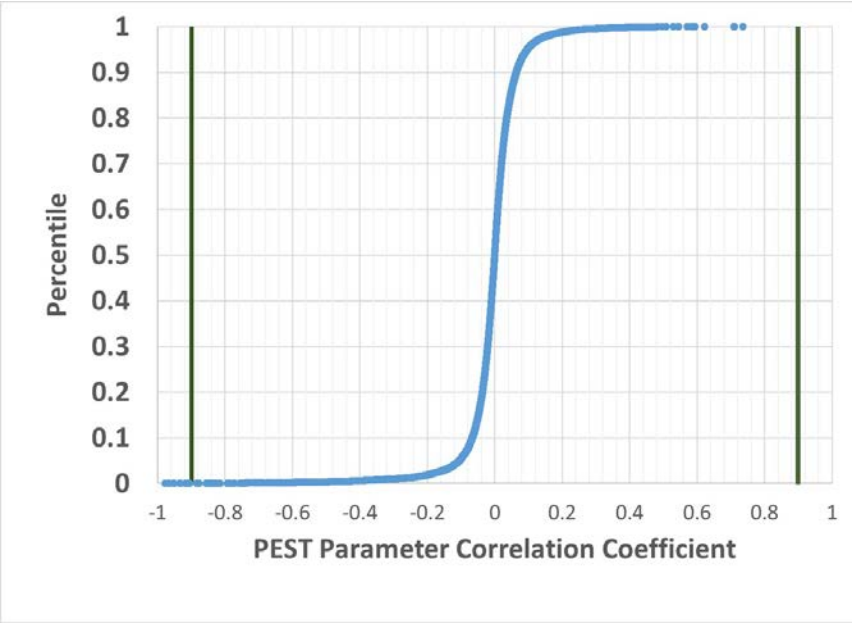

Figure 5-1. Cumulative Distribution Function showing a Summary of Values Produced in the Correlation Coefficient Matrix Produced by PEST for the Calibrated P2R Model Version 8.2

Table 5-2. Statistical Summary of Correlation Coefficient Cumulative Distribution Function

Parameter	Value
50th Percentile	-6.22E-04
99th Percentile	0.22
1st Percentile	-0.30
Maximum	0.81
Minimum	-1

Table 5-3. Correlation Coefficients for Parameter Pairs with values Exceeding the 0.9 Threshold

Spatial Configuration	Reference Figure	Area	Location ID	Correlation Coefficient
Vertical	Figure 4-24 and 26	Far Field	34	-0.98
			23	-0.95
	Figure 4-25	200-West	6	-0.95
			23	-0.93
			24	-0.92
			13	-0.91
Lateral	Figure 4-31	Channel HSU	4 and 5	-0.97
			7 and 10	-0.91

5.1.1 Vertical Placement

Six parameter pairs, used to estimate hydraulic conductivity within the calibrated model, resulted in correlation coefficients higher than the 0.9 threshold were likely caused by the spatial placement of the pilot points in the vertical direction. Table 5-3 lists the six parameter pairs, the figure that illustrates their general area in the model, the location ID, and the correlation coefficient of the pair. Only one location ID is listed for these parameter pairs because different values were used for different model layers within the model. For instance, Location 6 for 200-West Area had estimates for model layers 2 and 3 and model layers 4 and 5. The parameter pair is made up of these two estimates that were applied to different model layers. In all cases, the correlation coefficient is negative. This indicates that a change to one value in the parameter pair can be compensated for by a change to the other member of the pair. Given that all of these parameter pairs consist of locations that are exactly aligned vertically the high correlation is inferred to be because of geometric configuration rather than an error in the estimation process.

5.1.2 Lateral Placement

Two parameter pairs resulted in correlation coefficients outside the expected bounds. These pilot points represent the value of hydraulic conductivity in the simulated high conductivity channel. Figure 4-31 shows the locations of the pilot points. The location pairs in question are locations 4 and 5 and 7 and 10. The correlation coefficient for each pair was outside the bounds at values of -0.97 and -0.91, respectively. In both cases, the correlation was negative indicating a change in one value can be compensated by an opposite change in the other. Points 4 and 5 sit on either side of the simulated channel. Values for hydraulic conductivity within the channel were interpolated using a kriging algorithm that assumed no anisotropy. Thus, it is logical that changes in one parameter value could be compensated for by altering the other. Two other pairs of pilot points had a similar configuration with respect to the channel geometry. They were location pairs 1 and 2 and 11 and 12. These pairs had correlation coefficients of -0.63 and -0.65. Though these values are not outside the magnitude threshold, each have an elevated magnitude for correlation suggesting that the geometric configuration may cause this behavior.

The lateral configuration of 7 and 10 is slightly different from the configuration discussed above. As shown in figure 4-31 they are placed next to one another within the channel HSU zone. Based on the negative correlation and the proximity it is evident that raising one parameter value and lowering the other could compensate for simulation results. The high negative correlation between parameter pair 7 and 10 is interpreted as being due to the geometric configuration and not an error in the estimated value. For each of these parameter pairs the estimated value of hydraulic conductivity was similar. For pair location 4 and 5, the estimated values were 19,950 and 20,372 m/d, respectively. For pair locations 7 and 10, the estimated values were 1,013 and 1,000 m/d, respectively. Though it is possible that these values could compensate for a change in the other the PEST estimation process identified similar values as the best fit in each case.

5.2 Model Uncertainty

No attempt has been made to quantify uncertainty in the flow simulations formally beyond limited qualitative assessments performed throughout the model development process. As a result, the following qualitative discussion includes several sources of uncertainty and their implications to the objectives of the P2R Model.

5.2.1 Conceptual Model Uncertainty — Scale of Heterogeneity Represented by Hydrologic Stratigraphic Units

It is often argued that conceptual model uncertainty is the dominant form of uncertainty in a modeling exercise (Konikow, 1986, "Predictive Accuracy of a Ground-Water Model – Lessons from a Postaudit"; Konikow and Bredehoft, 1992, "Ground-water Models Cannot be Validated"; National Research Council, 2000, *Research Needs in Subsurface Science*; Oreskes and Belitz, 2001, "Philosophical Issues in Model Assessment"; and NUREG/CR-6805, *A Comprehensive Strategy of Hydrologic Modeling and Uncertainty Analysis for Nuclear Facilities and Sites*). This is likely also true for the P2R Model. An important source of conceptual uncertainty is the treatment of a geologically related HSU as a region of constant hydraulic properties, when it is acknowledged that a geologically contemporaneous HSU likely exhibits considerable intrinsic variability in its hydrologic (water-transmitting) characteristics. The fluvial environments that lead to deposition of most of the aquifer are associated with heterogeneous structures, especially for the Hanford formation and CCU. In version 8.2 of the P2R Model heterogeneous hydraulic conductivity values were utilized within HSU boundaries to mimic this aspect of the conceptual model. However, uncertainty with the boundaries between the HSUs is likely, given the scale of the estimate from the HSGF (ECF-HANFORD-13-0029).

Fluid flow and transport are sensitive to the interpretation of geology in the portion of the model near 200-East. This region is geologically complex and does not have a one-to-one correspondence between geologic formation and proper hydraulic representation. More variation may exist of hydraulic conductivity within the Hanford formation and the CCU than there is between representative values for these HSUs in this area. The interpreted distribution of hydrostratigraphy was influenced by historical contaminant plume interpretations that indicate the presence of a large conductive channel from just south of the 200-East Area to the extending to the southeast through NRDWL within the P2R Model domain. The hydraulic head data strongly correlate with this interpretation; however, limited geologic data are available from well log interpretations to corroborate this interpretation. The changes made to the structure of the model to approximate the high conductivity zone are discussed in Section 4.5.4.5.

While there is sufficient evidence to support a highly conductive channel, there is insufficient evidence to define its shape and size entirely. Examining historical plume movement helped to constrain the flow the geometry of the sediments that make up the high-conductivity channel. Because of the importance of the channel on water levels throughout the model domain, the inferred hydraulic conductivity for the channel region dominates the calibrated hydraulic conductivity value of the Hanford formation. The location and extent of an HSU is based on interpolation of sparse data. In areas where an HSU may have been eroded or is pinching out, not knowing the exact extent of the HSU can lead to uncertainty in flow and transport predictions.

5.2.2 Flow Estimates near Gable Gap

Three significant sources of uncertainty influence the flow near Gable Gap: the basalt ridge, inflow from the Cold and Dry Creek drainages into the western portion of the model, continued effects of operations at the site, and local variability in the hydraulic properties of the Hanford formation. These uncertainties in the P2R Model may effect whether future sources of contamination may flow north through the Gable Gap.

The first source of uncertainty is the influence of the elevation of the basalt saddle northwest of the 200-East Area (Section 3.2.5). Simulation results indicate that flow across the saddle is limited due to the basalt saddle, effectively closing the area to the north of the basalt saddle off from flow from the 200-West and 200-East Areas. Observations during the last several years (discussed in Section 3.4) suggest

that this may be the case. Uncertainty in the representation of flow across the basalt saddle may contribute to uncertain flow estimates in the northeast corner of the 200-East Area.

The second source of uncertainty is regarding how much flow is entering the model domain from the western streams, from surface infiltration, and through leakage upward from the basalt. Of these, flux from the western streams dominates, and has potential importance on the 200-West P&T systems that capture a portion of this inflow. Currently, the western boundary of the model is extracted from simulations of the CPGW Model version 8.4.5. The western stream influx in that model were determined from calibration of groundwater flow to data in 200-West Area.

The third source of uncertainty is non-equilibrium storage in the aquifer. The Central Plateau is currently not in equilibrium with respect to inflow and outflow. The Central Plateau unconfined aquifer still exhibits more outflow than inflow because of the remaining fraction of the tremendous buildup of stored water in the aquifer during the Hanford Site operational period. The aquifer is still attenuating this buildup, which ended after the termination of production activities at the Hanford Site in 1989. The calibration is such that uncertainty in these two influences do not lead to uncertainty in the current predictions of water levels but may affect flow rates. The uncertainty regarding future impacts of these factors may influence predictions of both head and flow rates.

5.2.3 CRBG Intercommunication

Section 4.2.3 indicates a basic assumption of the P2R Model is that the basalt underlying the unconsolidated suprabasalt aquifer can be treated as a no-flow barrier. This assumption is discussed in more detail in Section 3.2.4 where past studies regarding intercommunication between the suprabasalt aquifer and the upper aquifer of CRBG are discussed including *Transient Inverse Calibration of Site-Wide Groundwater Model to Hanford Operational Impacts from 1943 to 1996-Alternative Conceptual Model Considering Interaction with Uppermost Basalt Confined Aquifer*, PNNL-13623, PNNL-13641, PNNL-14398, and PNNL-14753. The discussion concluded that while this assumption does introduce some uncertainty into the model, it is not a significant source of uncertainty and is compensated by a relatively small increase in the simulated recharge rate. To evaluate the impact of this assumption on the P2R Model a sensitivity simulation including interaction with the basalt aquifer was completed. Previous studies indicated that the relative impact to the water budget was the basis for this assumption. The purpose of this study is to evaluate the conclusion that a no-flow boundary is sufficient using the assumptions presented in PNNL-13623 as an template for the evaluation. This section discusses the approach, parameterization, and results of the sensitivity run regarding basalt interaction.

5.2.3.1 Approach and Parameterization

The approach for simulating the intercommunication of the suprabasalt aquifer and the CRBG aquifer is similar to the approach that was adopted in the last attempt to simulate this phenomena detailed in PNNL-13623. The communication is conceptualized to occur through three main mechanisms for leakage. Including leakage through:

- an erosional window near Gable Gap,
- fractures in the dense interiors of the CRBG distributed throughout the confining layer,
- and the Yakima Ridge and Gable Mountain faults.

In PNNL-13623, intercommunication was simulated using head-dependent flux boundaries. In order to simulate this type of boundary condition, an estimate of both the hydraulic head and conductance term are needed. These values were taken from the calibrated site-wide model presented in PNNL-13623.

Conductance terms for the boundaries were determined using the calibrated vertical hydraulic conductivity value and the thickness map for the Elephant Mountain member (Figure 5-2). Model input files from PNNL-13623 simulations were used to extract the values containing hydraulic head data for the CRBG basalt aquifers. The thickness varies with space and the hydraulic head varies with both space and time. The general head boundary package was used to assign heads and conductance terms to the P2R Model cells. The following section describe the differences in how the separate mechanisms for intercommunication were implemented in the P2R Model.

Erosional Window

The erosional window near Gable Gap of the Elephant Mountain member of the CRBG is shown in Figure 5-2. Within the footprint of the erosional window, PNNL-13623 assumed the potentiometric surfaces for both the unconsolidated aquifer and basalt aquifer would be identical based on the lack of a low conductivity material separating the two aquifers. The same assumption was made for this exercise to remain consistent with the previous study. The amount of water intercommunicating between the two aquifers was simulated at the edge of the erosional window where a hydraulic gradient was estimated at the exposed face of the interbed aquifer. The conductivity at the nodes at the edge of the erosional window as assigned a vertical conductivity of 0.02 m/d (PNNL_13623).

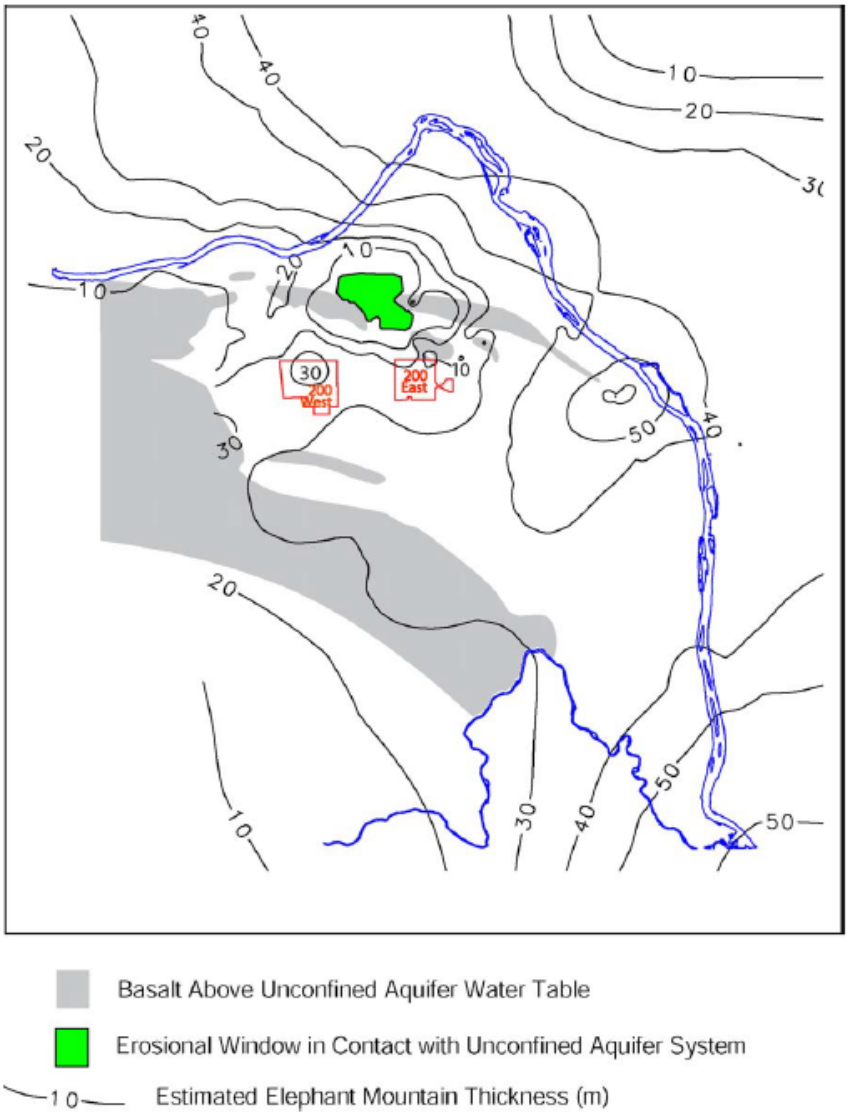

Source: PNNL-13623, *Transient Inverse Calibration of Site-Wide Groundwater Model to Hanford Operational Impacts from 1943 to 1996—Alternative Conceptual Model Considering Interaction with Uppermost Basalt Confined Aquifer*.

Figure 5-2. Estimate of the Thickness of the Elephant Mountain Basalt

Distributed Fracturing

The basalt underlying the majority of the Hanford Site and the P2R Model domain is the Elephant Mountain Member of the Saddle Mountain Basalt Formation. Intercommunication between the underlying basalt and the unconsolidated aquifer is indicated by data presented in PNNL-13623 and is assumed to travel through fractures in the dense interior of the Elephant Mountain Member. Flow between the two units, in this analysis, is simulated using head dependent leakage boundary. The vertical hydraulic conductivity, 1.4E-05 m/d, was taken from the final calibrated value documented in PNNL-14398, *Transient Inverse Calibration of the Site-Wide Groundwater Flow Model (ACM-2): FY 2003 Progress Report.*

Faults

Locations within the model that are influenced by the Yakima Ridge and Gable Mountain Faults are shown in Figure 3-12. Near these locations, the amount of intercommunication is likely to be increased because of the increased density of fracturing along the faults. The increased fracturing was simulated by using an increased vertical conductivity term near the fault. Similar to the approach outlined in PNNL-13623 a vertical hydraulic conductivity value of 0.05 m/d was assigned. The vertical hydraulic conductivity was area weighted to apply to only a 5 m wide portion of the numerical cell that was considered a part of the fault. The remainder of the cell was assumed the same conductivity term as the areally distributed leakage value of 1.4E-05 m/d.

5.2.3.2 Results

Three metrics were used to evaluate the relative impact of intercommunication with the basalt aquifer in the P2R Model. These metrics included, (1) comparison of the volumetric budget between the calibrated and alternative P2R Model simulations, (2) evaluation of the calibration statistics when intercommunication was simulated, and (3) assessment of the amount of activity that enters the basalt aquifer from the historic fate and transport tritium simulation. These metrics were chosen to evaluate if the effect of the basalt intercommunication is a dominant feature of the water and contaminant balance.

Volumetric Balance Comparison

The volumetric balance for the flow model was presented in Section 4.5 and shown in Figure 4-87. Figure 5-3 shows the same type of figure for sensitivity simulation. Figure 5-4 shows the volumetric fluxes for water budge components with magnitudes smaller than 10,000 m^3/day. Two time-series were added to show the volumetric flux of water moving into and out of the basalt. The total basalt flux was broken down into several components and illustrated in figure 5-5. The majority of the interaction occurs through the erosional window in the Elephant Mountain basalt. The figure indicates only small differences in the volumetric flux for each category of the total volumetric flux. Table 5-4 shows the maximum simulated percent change within a year of simulation for each of the volumetric budget elements included in the calibrated P2R Model version 8.2. Most illustrate a minimal amount of change to the water budget. The water flux through the Gable Gap boundary showed the highest percent change toward the end of the simulation time frame. The relatively large change reflects simulated inflow from the CRBG aquifer to the suprabasalt aquifer through the erosional window. While the percent value is higher than the others, total flow is not a large portion of the water budget. The maximum change occurs when the total flow is at its smallest value. Thus, the large percentage difference is the product of a small change to a small number. The contribution of the erosional window to the aquifer during the early 1980s is not consistent with the conceptual model that when operations were disposing waste at a high level the mounds would have caused water to flow into the erosional window. This could be due to inaccurate representation of the heads in the data set used to define the hydraulic head in the Elephant Mountain interflow bed. Overall, the small percentage of change to the volumetric water balance indicates that the boundary condition, based on the parameterization found in PNNL-13623, does not produce a large impact on the simulation results.

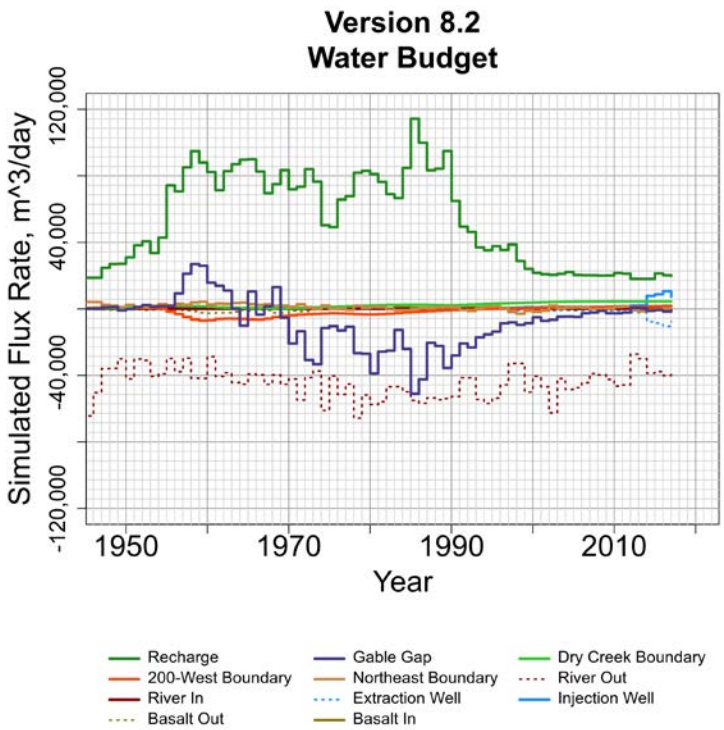

Figure 5-3. Volumetric Water Budget of the P2R Model CRBG Sensitivity Simulation Including the Volumes Over Time that Enter and Exit the CRBG

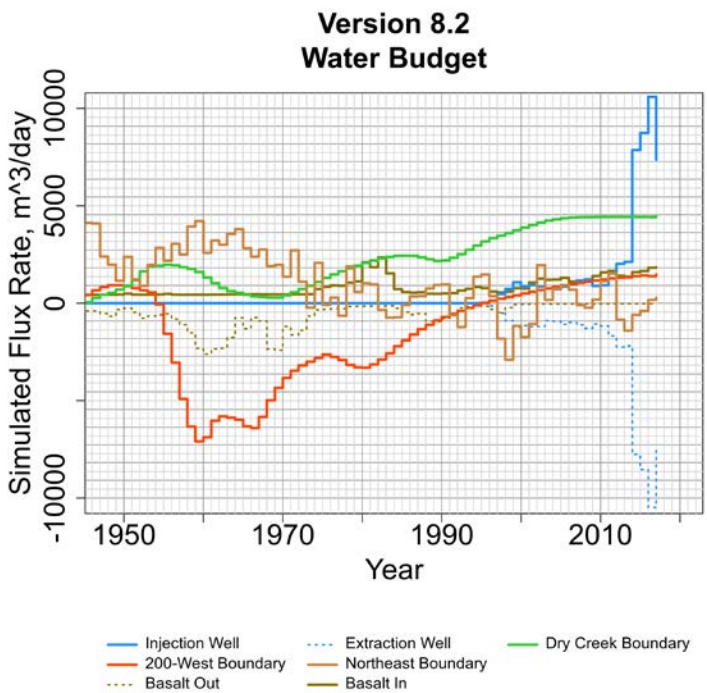

Figure 5-4. Volumetric Water Budget for Components Smaller than 10,000 m^3/day of the P2R Model CRBG Sensitivity Simulation Including the Volumes over Time that Enter and Exit the CRBG

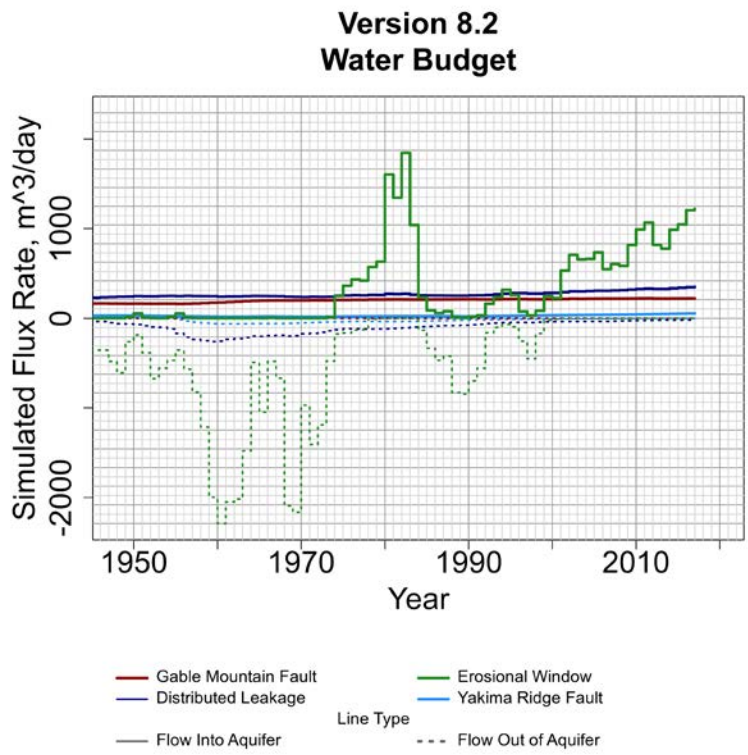

Figure 5-5. Volumetric Water Budget for Components Related to Basalt Intercommunication of the P2R Model CRBG Sensitivity Simulation

Table 5-4. Percent Change Comparison of Volumetric Budget Elements between the Calibrated P2R Model and the CRBG Sensitivity Simulation

Volumetric Budget Element	Max Percent Change (%)	Simulation Year Maximum Occurred
River Inflow	0.1	2012
River Outflow	0.8	2012
Recharge	0.3	1985
Western Boundary	0.2	1975
Dry Creek Boundary	0.0	2013
Northeast Boundary	0.6	2009
Gable Gap	3.7	2016

Calibration Statistics

Table 5-5 shows the summary statistics regarding hydraulic head for both simulations. Extra precision was included in Table 5-5 to illustrate the small impact the CRBG sensitivity analysis had on the simulated hydraulic head field. Four filters were applied to the calculation of the summary statistics. These were: (1) all available data, (2) all data after 2007, (3) wells near the erosional window, and (4)

data since 2007 for wells near the erosional window. The filters were selected to evaluate the effect of the CRBG sensitivity on the calibration during later time periods and the how the calibration was effected near the erosional window where the volumetric budget indicated the largest impact occurred. Figure 5-6 shows the wells that were closest to the erosional window used for this analysis. The maximum effect, 0.013 m, was observed in the bias statistic for the all available data. The small magnitude indicates the CRBG intercommunication, as parameterized in this model, does not alter the model calibration.

Table 5-5. Comparison of Summary Statistics between the Calibrated P2R Model and the CRBG Sensitivity Simulation

Simulation	Data Filter	Time Frame	RMS	Bias	Mean	Corr
Calibrated Model	All Data	1944 through 2016	1.478	0.077	0.731	0.988
		2008 through 2016	0.434	0.013	0.256	0.998
	Near Erosional Window	1944 through 2016	0.551	-0.023	0.231	0.859
		2008 through 2016	0.094	0.061	0.066	0.745
CRBG Sensitivity	All Data	1944 through 2016	1.474	0.090	0.733	0.988
		2008 through 2016	0.431	0.013	0.252	0.998
	Near Erosional Window	1944 through 2016	0.551	-0.024	0.230	0.858
		2008 through 2016	0.091	0.056	0.062	0.744
Difference	All Data	1944 through 2016	0.004	0.013	0.002	0.000
		2008 through 2016	0.003	0.000	0.004	0.000
	Near Erosional Window	1944 through 2016	0.000	0.002	0.001	0.000
		2008 through 2016	0.003	0.004	0.004	0.002

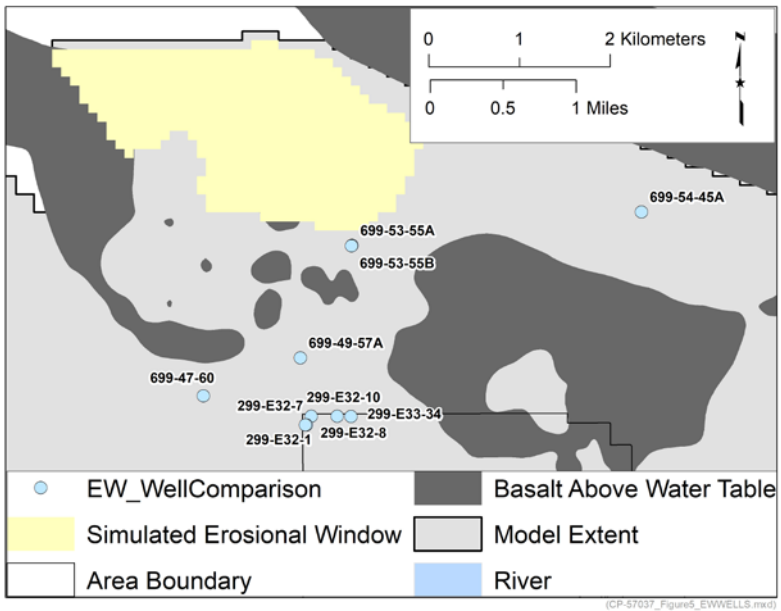

Figure 5-6. Location of Wells used to compare Calibration Statistics near the CRBG Erosional Window in the Gable Gap Region of the P2R Model

Tritium Activity

The same fate and transport simulation carried out as part of the model calibration process for the P2R Model version 8.2 was executed for the CRBG sensitivity simulation results. Simulated tritium concentration and activity were tabulated over time to evaluate differences between the simulation with and without CRBG intercommunication. Table 5-6 shows the activity flux through the different boundaries of the model for both simulations. The simulation results indicated relatively small amounts tritium activity entered the CRBG through the erosional window and the distributed fractures of the Elephant Mountain Formation dense interior. The result to the other boundaries that are common among the two models indicates a relatively small impact on the overall results.

Table 5-6. Comparison of Tritium Activity for Model Boundaries for the Calibrated Model and the CRBG Sensitivity Simulation

Location	CRBG Sensitivity		Calibrated Model	
	Total Activity (Ci)	Percent of Total Discharged (%)	Total Activity (Ci)	Percent of Total Discharged (%)
Distributed Fractures	0.2	0.00003	--	--
Erosional Window	18	0.003	--	--
Western Boundary	0.00	0.0	7.3E-06	0.00
Gable Gap	1,793	0.28	1,823	0.28
Northeast Boundary	69	0.01	521	0.01
Total simulated tritium activity (Ci) discharged to the aquifer				649,805

Figure 5-7 shows the time-series plot for peak simulated tritium concentration passing through several boundaries of the model. The chart is annotated to indicate what general discharge location within the P2R Model causes the simulated peak concentration. Simulated concentrations above the cleanup level exit the model domain and enter the CRBG within the erosional window and through the distributed fractures of the Elephant Mountain Formation dense interior. Radionuclide presence in the upper interbed was noted in RHO-ST-38, *Geohydrology of the Rattlesnake Ridge Interbed in the Gable Mountain Pond Area.* So, simulated intercommunication is not unexpected. The trend in the concentration of the entering the CRBG through distributed fractures near SALDS indicates the possibility of tritium entering the aquifer above cleanup levels at the end of the simulation in 2016. This could reflect conditions near SALDS or be due to inaccuracies in the model conceptualization of aquifer interaction at this location. Site-specific analysis is required to determine which is correct.

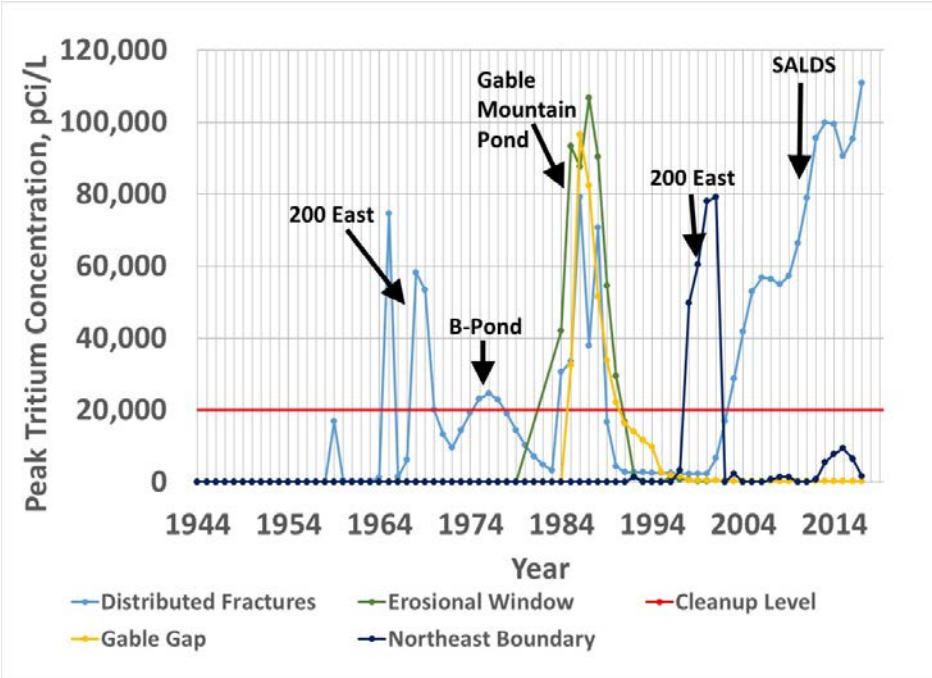

Figure 5-7. Peak Simulated Tritium Concentration in the P2R Model that Exits the Specified Head Model Boundaries

Conclusion

Based on the three metrics that were evaluated the assumption made of the CRBG basalt surface acting as a no flow barrier does not appear to change the representativeness of the P2R Model version 8.2. Simulations including the head dependent flux boundaries to represent the CRBG did not have a large effect on the volumetric and activity balance or the match between simulated and observed hydraulic head. Fate and transport simulations indicated flux entering the CRBG with simulated concentrations above the cleanup level for tritium near the SALDS facility. The amount of activity that this accounted for was a small fraction of a percent of the total activity budget for the simulation. Site-specific analysis of tritium and head data near SALDS would help indicate if this is just due to inaccuracy of how the boundary condition was defined for the CRBG sensitivity simulation or reflects actual conditions near SALDS. Overall, the assumption of the CRBG simulated as a no-flow boundary is not invalidated due to the relatively small impact of the head dependent boundary condition in the CRBG sensitivity simulation.

6 Model Limitations

The P2R Model is limited in intent and purpose to the simulation of saturated flow in the unconsolidated aquifer above the underlying basalts. As a result, the model is suitable for calculating water levels, hydraulic gradients, and groundwater flow directions and rates throughout the Central Plateau and toward the Columbia River. Predictions made using the P2R Model will be most reliable in those areas with a high density of water-level data that were incorporated in the model calibration, and for those areas where model outputs correspond closely with the measured data. Conversely, model predictions will be less reliable in those areas where limited water-level data are available, as well as in those areas where model predictions do not closely correspond to measured data. It is expected that the results of groundwater flow simulations completed using the P2R Model will be used to evaluate the F&T of contaminants using advection-only (particle tracking) and advective/dispersive/reactive transport, as embodied in the MT3DMS simulation code. For all of these intended applications of the P2R Model, the following limitations apply:

- The flow model is regional in nature. Hydraulic property variation is generally recognized at the scale of HSUs (kilometers to tens of kilometers horizontally). At the scale of the HSUs down to the model grid scale (100 m [328.1 ft] to 200 m [656.2 ft]).
- The model grid represents the aquifer with cells of dimension 100 m by 100 m (328.1 ft by 328.1 ft) up to 200 m by 200 m (656.2 ft by 656.2 ft). It is expected that the model is most suitable for making predictions of heads, hydraulic gradients, and groundwater flow rates over areas that comprise many model cells, and that predictions of these quantities on scales smaller than 100 m (328.1 ft) are not reliable except in circumstances of uniform hydraulic gradients.
- The model grid dimensions near the Columbia River have either 100 m by 200 m (328.1 ft by 656.2 ft) or 200 m by 200 m (656.2 ft by 656.2 ft) dimensionality. This cell size along with the annual temporal discretization is likely not sufficient to analyze local scale phenomena such as bank storage effects at the river. Spatial and temporal refinement should be undertaken for detailed analysis near the Columbia River.
- The western boundary of the groundwater flow domain for the P2R Model version 8.2 is the edge of 200-West Area. The boundary condition for this location is extracted from simulations results of the CPGW Model version 8.4.5. Significant changes to injection and extraction rates within 200-West could affect the reasonableness of the extracted values. When significant changes are made to rates, the boundary condition should be extracted from an executed simulation of the CPGW Model version 8.4.5 to create a reasonable boundary condition.
- Fluid flow and transport in the vadose zone above the aquifer are not explicitly simulated.
- The application of recharge derived from deep percolation of precipitation at the land surface implicitly represents the effects of vadose zone migration and storage. The rates used represent a best-practice combination of empirical data and model simulations of vadose zone migration characteristics at the Hanford Site to arrive at a fractional rate of meteoric water that constitutes natural recharge to the unconfined aquifer. However, the impact local scale effects of land-use change and timing on natural recharge should be considered when utilizing this model for analysis.
- This version of the P2R model includes an assumed representation of the Hanford channel extent that has in part been modified from the Hanford South Framework Model. The extent of the simulated channel in this version of the model is inferred based on the water table map, historic plume extent, and hydrographs of wells near the channel. Alternative interpretations of the Hanford channel extent

have been made in other products, including the TC&WM EIS, that could, if implemented, impact the groundwater flow regime in the 200 East Area and downgradient of the 200 East Area. The potential impacts of this uncertainty should be considered in any use of this model in those areas of the Central Plateau.

- Attenuation of facility discharges to the ground surface, cribs, trenches, shallow wells, ponds, ditches, and other infiltration areas is indirectly accounted for using STOMP simulations of the discharge sites following the methodology of EMDT-BC-0002. The predicted attenuation (delay of recharge arrival and reduction in peak volume) of discharge to the surface at the water table is included as data input for the P2R Model. This methodology does provide an improvement compared to ignoring the presence of the considerable vadose zone when incorporating artificial discharges, but it currently has several limitations:
  - The vadose zone for each liquid discharge site is simulated as a quasi-two-dimensional cross-section model using local hydraulic stratigraphy, scaling the horizontal dimension to achieve unit gradient conditions in the lowest conductivity layer during the highest artificial discharge period. Some calibration was applied for certain sites where more detailed three-dimensional modeling studies were available.
  - This approach achieves rapid simulation times and a generally representative treatment of vadose zone attenuation of liquid discharges, but it is not entirely adequate where water perching occurs on fine-grained layers and with subsequent lateral redistribution of moisture in the vadose zone.
  - Perching is believed to have been a significant vadose zone process in the 200-West Area (200-ZP-1 and 200-UP-1 OUs) and is suspected to be the reason for the inability of the calibration to date to match measured water levels in these locations. This should be considered in applying the model to historic transport analsyis.
  - Contribution to anthropogenic recharge at the ERDF facility reported in EMDT-BC-0002 appears to be relatively high with respect to the facilities expected function. While this may be due to the large size of the facility it is noted this value may impact calibration of hydraulic properties in this region of the model. This feature should be considered when evaluating the use of this model in that region.
  - Uncertainty in the discharge volume or its temporal distribution of the arrival at the water table may result in uncertainty in the calibrated hydraulic properties. Consideration of this uncertainty should be made when applying hydraulic property values to other analyses.
  - Application of the model to specific locations should evaluate the input data used for both natural and anthropogenic recharge to evaluate the applicability of these rates for their individual objectives.
- Fluid flow through the basalt bedrock is assumed negligible and, as a result, is not explicitly simulated except for limited sensitivity calculations. If sources and/or sinks of water are associated with the basalt bedrock, then the model is limited with respect to the exclusion of this FEPs item (Section 3.2.4).
- The basalt saddle north of 200-East is based on uppermost basalt surface defined in the HSGF. Uncertainty associated with this surface could affect the flow of groundwater through this region. Analysis of model results near this portion of the model should consider the effects of the basalt saddle on flow direction and magnitude.

- Application of the model where vertical gradients appear to be significant should consider the models ability to reproduce this phenomena on the scale of the application. Model parameter assignment on the HSU scale may not capture some vertical gradient behavior observed locally. The sensitivity of the value used for vertical anisotropy of hydraulic conductivity was not included in the sensitivity analysis and may impact results.
- Considerable areas remain with limited well control in the Central Plateau. Consequently, the assignment of HSUs is subject to continued refinement as additional information becomes available for these areas.
- The southern boundary condition was established using the water table contours published in DOE/RL-2011-01, *Hanford Site Groundwater Monitoring for 2011*, to represent the flow perpendicular to the observed water table. Comparison to the updated contours found in DOE/RL-2016-67, *Hanford Site Groundwater Monitoring Report for 2016*, indicated no adjustments were needed to the southern boundary based on water table contours.
    - This boundary runs through the middle of the 300 Area at the Hanford Site. While the boundary is appropriate for simulating groundwater flow on the Central Plateau and in the Far Field, the P2R Model should not be used for estimating conditions on a local scale within the 300 Area of the Hanford Site.

This page intentionally left blank

7 Model Configuration Management

The model described in this model package report is uniquely designated as the "Plateau to River Groundwater Transport Model" and in abbreviation form as the "P2R Model".

Version control for this model will conform to the following version numbering convention:

- P2R Model Version #.# (or #.#.#)
    - The first version index will match the CHPRC-approved build number of MODFLOW and Related Codes in which the model is implemented.
    - The second version index will denote sequential versions of the model grid (the use of "grid" here refers to both the grid structure and parameter values).
    - The optional third index is reserved to denote 'variant' versions. A variant version here is defined as a unique model configuration in which key hydraulic or structural parameters have been changed for specific purposes without recalibration of the model.

For example, P2R Model Version 7.1 would refer to the Plateau-to-River Groundwater Transport Model, implemented in MODFLOW-2000-MST CHPRC Build 7 using grid version 1. Similarly, P2R Model Version 7.2.1 would refer to (as an example) the Plateau to River Groundwater Transport Model, implemented in MODFLOW-2000-MST CHPRC Build 7 using grid version 2, and a variant treatment of (for example) the structure of the basalt top in the Gable Gap area.

Note that individual simulations (or applications) are separately configuration controlled following the guidance provided in Appendix G of CHPRC-00189. Simple changes in model stresses (e.g., pump-and-treat system injection and extraction rates) do not constitute a variant because these will not impact model calibration; these are properly the subject of an ECF and model files for those will be archived in the EMMA application bin by ECF number.

As required by Appendix G of CHPRC-00189, all inputs and outputs for the development of this model will be committed to EMMA to maintain and preserve this configuration-managed basis of this model. Basis information (that information collected to form the basis for model input parameterization; e.g., historical pump-and-treat rates) is also stored in the EMMA for traceability purposes.

The software used to implement the version of the model documented in this model package report, CHPRC Build 8 of MODFLOW-2000, is configuration-managed as discussed in Section 4.1. Configuration-managed software is obtained from the Hanford Site MKS Integrity™ configuration management system as required by CHPRC-00258.

7.1 Model Version History

The P2R Model is not a single-use tool, but rather represents the product of ongoing development and continued improvement of modeling work at the Hanford Site. Figure 7-1 shows a timeline for the development of the model. Each of the versions shown in the figure is discussed below including a brief overview of the major changes that highlight the differences between current and previous versions of the model.

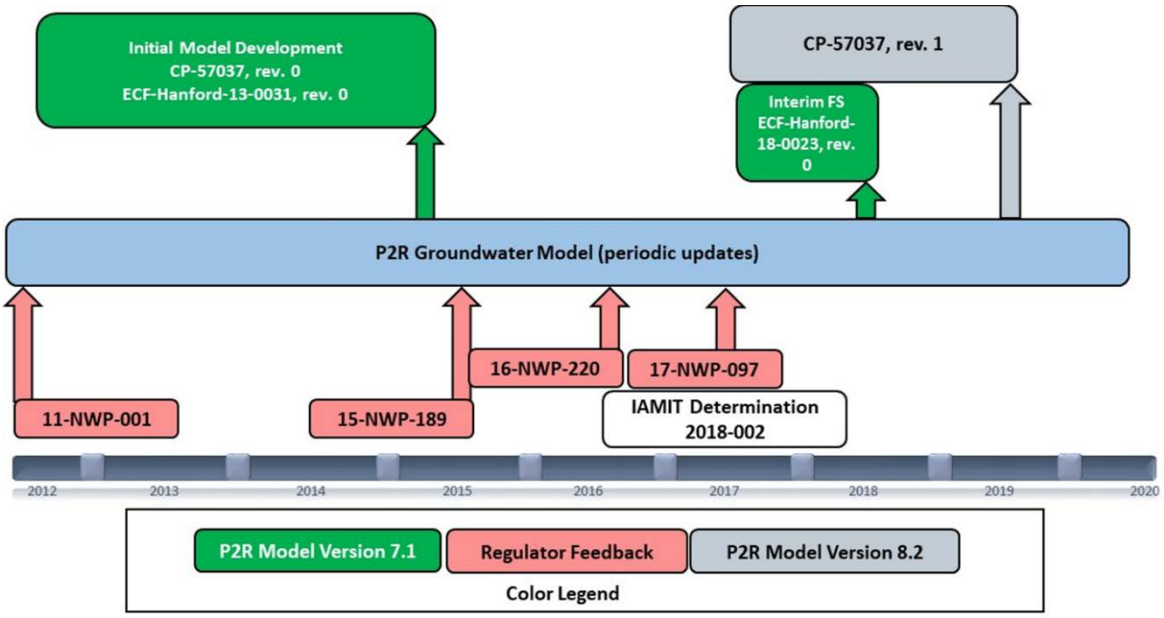

Figure 7-1. Timeline Illustrating the Development and Version History of the P2R Model

7.1.1 Version 7.1

The P2R Model was developed in response to comments received as part of 11-NWP-001, *Department of Ecology Comments on the Remedial Investigation Report for the 200-PO-1 Groundwater Operable Unit, DOE/RL-2009-83, Draft A*. Initially, the CPGW version 3.3 was utilized to develop fate and transport estimates for the RI. However, the comments encouraged the eastern boundary of the model be adjusted to extend the entire distance to the Columbia River. Development of the initial model used similar methods as those used to develop the CPGW Model version 3.3 but with an extended model extent. This resulted in the development of version 7.1 of the model. Lateral model discretization was selected to be consistent the TC & WM EIS groundwater model (DOE/EIS-0391, 2012) where the extents overlapped. Updated geologic information and a calibration period of 2006 to 2012 was used to adjust hydraulic properties for the various HSUs in the model domain to better match hydraulic head data.

7.1.2 Version 8.2

Version 8.2 of the P2R Model is documented in this revision of the report. It differs from the previous version due to a new grid structure, a longer calibration period, and spatially varying hydraulic properties. The new grid structure is based on an algorithm that improved the match between the HSGF and the MODLFOW grid (Section 4.2.3). The calibration period was extended to represent conditions from 1944 through 2016 to evaluate the performance of the model against the historical hydraulic head data (Section 4.5.1). The methodologies for developing boundary conditions and their values is similar to the previous version (Section 4.4). Contaminant fate and transport was used as a qualitative calibration tool with the newer version of the model (Section 4.5.4.6). Finally, the use of PEST and pilot points for varying hydraulic conductivity within HSUs was applied to the model (Section 4.5).

7.2 Model Application History

Table 7-1 lists application environmental calculations and other documents that have utilized the P2R Model.

Table 7-1. Applications of the P2R Model

Model Version	Year	Application
Version 7.1.1	2013	ECF-HANFORD-13-0031, Rev. 0, *Fate and Transport Modeling for Baseline Conditions for Remedial Investigation/Feasibility Studies of the 200-BP-5 and 200-PO-1 Groundwater Operable Units*
	2015	ECF-200BP5-15-0009, Rev. 0, *Evaluation of Plume Capture and Hydraulic Performance for B-Complex Vicinity Submodel for 200-BP-5 and 200-PO-1 Operable Units Feasibility Study Evaluation of Remedial Alternatives*
	2016	CHPRC-02868-VA, Rev. 0, Foundation for BP-5 Modeling Approach
	2016	CHPRC-02869-VA, Rev. 1, Modeling Workshop: Objectives, Inputs, Calibration, and Documentation
	2016	ECF-200BP5-16-0145, Rev. 0, Particle Tracking and Transport Modeling in Support of Removal Action Memorandum
	2018	ECF-HANFORD-18-0023, Rev. 0, *Evaluation of Contaminant Transport for the 200-BP-5 and 200-PO-1 Operable Units Feasibility Study Evaluation of Remedial Alternatives*

Note: This table lists notable applications of the Plateau to River Groundwater Model identified by version applied, but not every application of this model is necessary listed.

This page intentionally left blank.

8 Model Enhancement Recommendations

The P2R Model has been used almost continuously since its inception to support multiple *Resource Conservation and Recovery Act of 1976* and *Comprehensive Environmental Response, Compensation, and Liability Act of 1980* needs. The model is subject to review to identify previously unidentified limitations and opportunities for improvement. Recommendations for future development of the P2R Model are under evaluation as part of a larger strategy for Hanford Site model maintenance. As these limitations, opportunities, and recommendations are identified, they are documented as enhancement recommendations in this section of the report. Many of the key limitations and opportunities are identified during the model development and calibration process. In some cases, these opportunities may not be addressed in the current version of the model. In those cases, recommendations are made in this section in order to provide input to the future development of the model. This section discusses several enhancements that can be evaluated to further enhance the P2R Model.

8.1 Channel Delineation

Section 4.5.4.5 discusses the calibration of the hydraulic properties in the aquifer to represent the high conductivity area within the central portion of the P2R Model domain. Figure 4-31 shows the extent of a zone that represents the area used to represent this conductivity zone. While this feature of the model is a critical feature in improving the model calibration, there is some uncertainty to the lateral bounds of the high conductivity zone. Similar to the approach in the P2R Model, both the CPGW Model and the TC & WM EIS Model delineate a zone that represents the high conductivity sediments in the aquifer. However, each arrived at a different extent for the channel. Given that this is feature is key in understanding any threat of contamination moving off the Central Plateau, more data would be beneficial in order to reduce uncertainty in its lateral and vertical extent and the variability of hydraulic properties. Beneficial data would include pumping tests within separate HSUs including flow meter analysis at several wells and tracer studies to indicate flow directions and timing. Analysis of currently available data with regard to geophysics and historic hydraulic head data could aid in identifying wells that behave consistent with channel influence. One analysis of the data includes altering the model calibration method for the P2R model that removes the explicit zonation within the model grid for the high conductivity region. Pilot point methods used in the current P2R Model calibration can be adjusted to use available hydraulic head information to estimate the extent of the channel rather than defining the zone beforehand.

8.2 Grid Structure Alterations

Changes to the grid structure could be made in order to accommodate two developments to the model. First, the western boundary can be extended to basalt outcrops to the west. Second, the vertical discretization could be altered in order to remove abrupt changes to the model layers. These alteration are discussed below.

8.2.1 Western Boundary

The western edge of the P2R Model, shown in Figure 8-CPGW is positioned at the western boundary of the 200-West Groundwater Interest Areas. This includes the extent of all of the plumes delineated in DOE/RL-2016-67 and lines up with well 699-50-85, which was used to establish a specified head boundary condition in version 7.1 of the P2R model. Currently, the specified head boundary condition for this edge of the P2R model is extracted from the calibrated CPGW Model version 8.4.5. The CPGW Model is used because its western boundary extends to the outcropping basalt in the west and provides a reasonable match to the historic trends in this area. Extending the western boundary of the P2R Model to match the western boundary of the CPGW Model would eliminate the need to use either the CPGW

Model or the historic well data at 699-50-85 for establishing the boundary condition of the model. The proposed union of the model domains is illustrated in Figure 8-1.

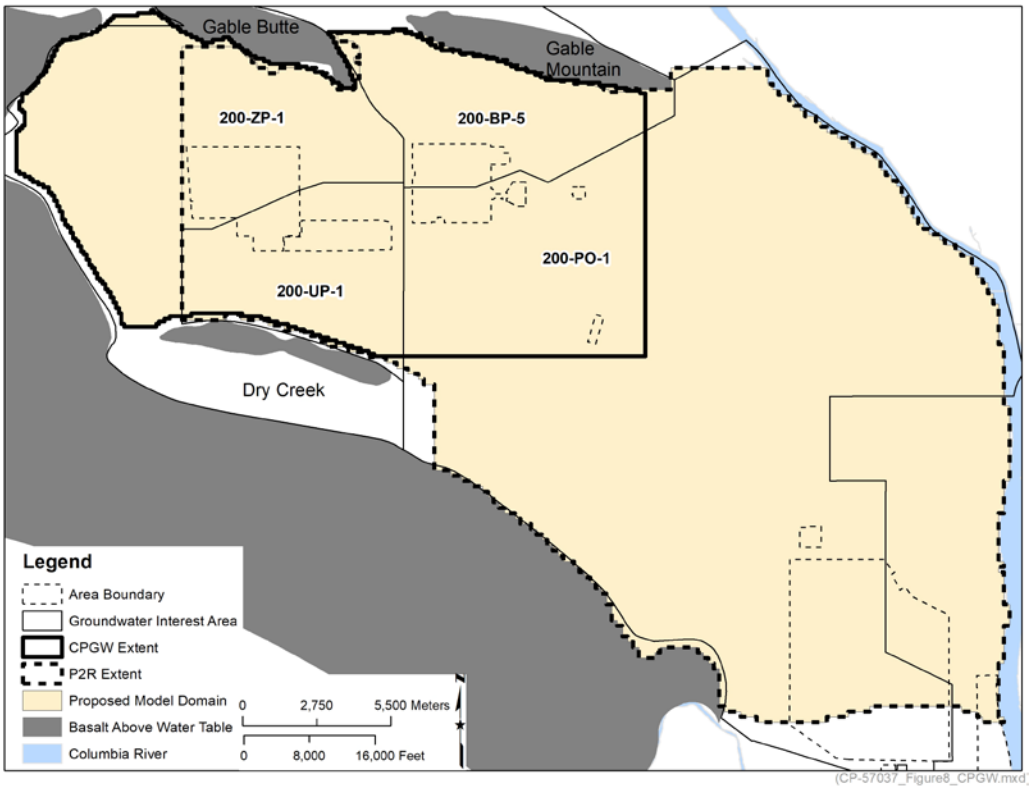

Figure 8-1. Current Lateral Extent of the P2R and CPGW models and the Proposed Extended Extent of an Update to the P2R Model

8.2.2 Model Layering

The model layering algorithm, discussed section 4.2.3, was updated to increase the match between the model HSU assignments and the HSU definition in the HSGF. This goal was accomplished as part of the current model update. Exceptions were made in the case of the high conductivity zone where model cells assigned to the Hanford Formation, Cold Creek Unit, and Ringold E, were combined into an HSU not defined by the HSGF. As discussed in section 8.1, this delineation is made with the acknowledgement that the actual extent of this high conductivity zone boundary is uncertain. An alteration to the model layering algorithm could include the improvements gained in the assignment of hydraulic properties using the HSGF as the guide and not introduce explicit changes to the grid structure where boundaries are less certain. A hybrid approach to the boundary matching algorithm documented in Jones et. al., 2002 and the method discussed in Anderman and Hill (2000) could be used to capture the major changes in hydraulic conductivity and allow for less explicit model structure where the extent of the HSU is less certain and properties are more similar between HSUs.

8.3 Null Space Monte Carlo

Section 5.2 discusses model uncertainty in a qualitative fashion and acknowledges that a quantitative assessment of uncertainty has not been undertaken with the P2R Model. Applying the null-space Monte Carlo approach for quantifying parameter uncertainty, documented in Doherty, 2016, is proposed to enhance the understanding of model uncertainty in hydraulic properties assigned to the P2R Model. The

null-space Monte Carlo approach includes creating a set of calibrated models that indicate the variability in the hydraulic properties that is capable of matching historically observed data with similar statistical precision and accuracy. Thus, the uncertainty in the hydraulic properties can be evaluated to inform further data collection and analysis that might be beneficial to constraining the uncertainty in future development of the P2R Model.

8.4 Recharge

Uncertainty in the estimates used for recharge are called out in Section 6.0 of this document. Current estimates used and documented in Section 3.0 are considered adequate for the objectives of the P2R Model version 8.2 calibration. Still, enhancements to both the volumes of discharge and the area of impact the discharge applies to may provide more certainty in the models ability to simulate observed phenomena. This section discusses two enhancements that may enhance the models capability as a predictive tool. They are adjustments to the discharge rates and temporal distribution at the water table and evaluation of the impact footprint caused by waste discharge.

8.4.1 Recharge Rates

Update of the currently available estimate of anthropogenic recharge dataset could provide a more robust handling of anthropogenic and natural recharge at the site. Currently, EMDT-BC-0002 is used as the estimate of anthropogenic recharge. This estimate is based on two-dimensional models that may not reflect the nature of movement in the vadose zone in three-dimensions. Further, updated estimates of geology in the vadose zone could help delineate the effects perching of discharge water could have in altering both the time of arrival and the spatial extent for groundwater flux reaching the water table. Use of updated models and geology could also indicate the effect changes to surface features plays in altering meteoric recharge. This application should also consider sources of recharge that are not due to discharge of waste, but might be enhanced by anthropogenic effects such as storm sewers, transportation infrastructure, etc.

8.4.2 Recharge Footprint

The effect of the area used to disperse recharge for two major discharge locations in 200-West Area was discussed in Section 4.5.4.4. The two locations were selected because of the significant impact they had on the simulated water table near 200-West Area. However, the uncertainty in location that discharge ultimately impacts groundwater applies to all discharge locations at the site. Currently, the shape of the waste site is provided as part of EMDT-BC-0002. These boundaries may not reflect the footprint of the saturated zone that is impacted by this infiltration. In the absence of three dimensional vadose zone simulation analysis discussed in the previous section, discharge site impact extents could be interrogated as part of the model calibration to better understand the possible area of impact. A similar approach to what was employed in this version of the P2R Model for discharge ponds 216-S-16P and 216-U-10 could be employed to evaluate the area of impact other significant discharge locations. This evaluation would depend on hydraulic head data as an indicator of whether the extent is reasonable. The evaluation would remain uncertain as to the cause of the impact extent. Thus, three-dimensional simulation is the preferred approach.

8.5 Cold Creek Irrigation

As shown in Figure 8-1, the proposed extent of the a revised P2R Model would extend to the west where flux input from Cold Creek watershed would be used as an input to the model. The estimates for inflow from the Cold Creek watershed ranges over about an order of magnitude. Previous work on both Greater Cold Creek (GCC) watershed modeling in PNNL-14717, *Natural Recharge to the Unconfined Aquifer*

System on the Hanford Site from the Greater Cold Creek Watershed: Progress Report 2004, indicates the need for evaluating impacts of irrigated agriculture on shallow aquifer recharge, as these can have an impact on boundary water flow assumed by groundwater models at the Hanford Site. Thus, in addition to the estimated uncertainty, the conceptualization of this boundary may also be uncertain, and inflow solely from natural recharge may not be an accurate representation of the total recharge.

A combination of satellite imagery and metered well data from the Washington State Department of Ecology's Geographic Water Information System may aid in producing a more accurate estimate. Satellite imagery is available from the U.S. Geological Survey Landsat and the U.S Department of Agriculture National Agriculture Imagery Program imagery. Data have been available since 1984 in the GCC watershed area. Using these types of data, the normalized difference vegetation index (NDVI) can be estimated. NDVI contrasts the chlorophyll pigment absorption in the red band and the high reflectivity of plant materials in the near-infrared band to evaluate the relative growth of biomass along the season. Figure 8-2 provides an example of this type of analysis for the GCC.

Existing water meter records for irrigation are limited. Therefore, applied water irrigation amounts can be derived using literature values based on crop types, which are derived from crop surveys and U.S. Department of Agriculture data. Permitted amounts in the water rights for irrigation provide an upper limit on the amount of water used for irrigation. This upper limit could be used as a constraint on the model related to shallow aquifer recharge in the GCC watershed.

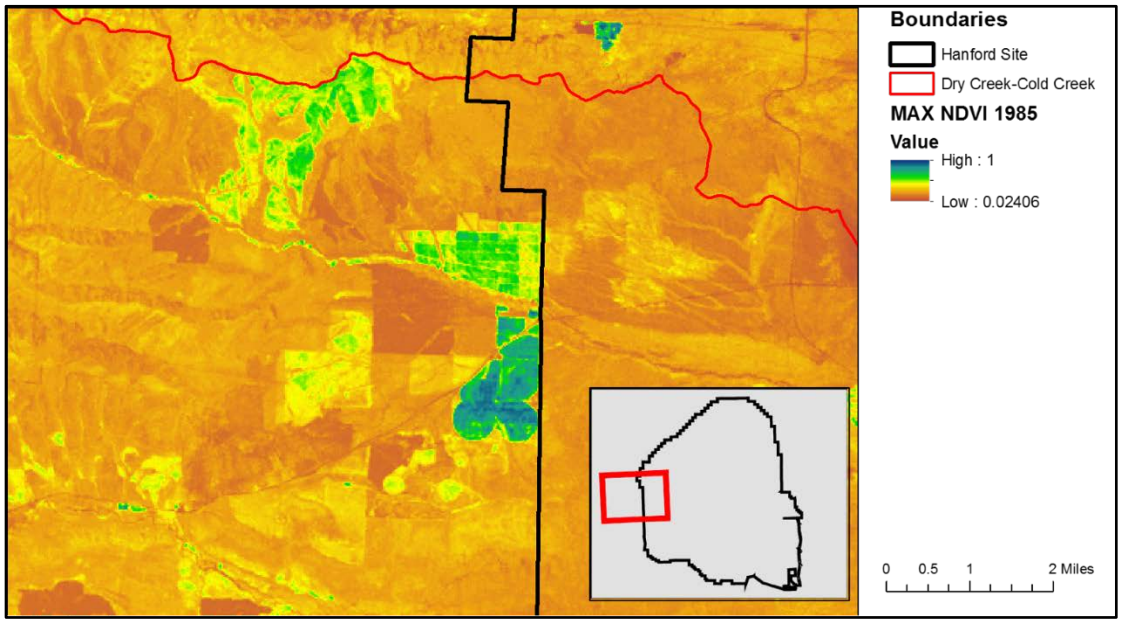

Figure 8-2. Annual Maximum NDVI for CY 1985 at Cold Creek (Hanford Site West Boundary)

9 References

11-NWP-001, *Department of Ecology Comments on the Remedial Investigation Report for the 200-PO-1 Groundwater Operable Unit, DOE/RL-2009-83, Draft A*, State of Washington Department of Ecology, Richland, Washington, Available at: https://pdw.hanford.gov/arpir/index.cfm/docDetail?accession=1103020149

Anderman, E.R., and Hill, M.C., 2000, *MODFLOW-2000, the U.S. Geological Survey Modular Ground-Water Model – Documentation of the Hydrogeologic-Unit Flow (HUF) Package*, USGS Open-File Report 00-342, Denver, Colorado. Available at: https://pubs.er.usgs.gov/publication/ofr00342

BHI-00184, 1995, *Miocene- to Pliocene-Aged Suprabasalt Sediments of the Hanford Site, South-Central Washington*, Rev. 00, Bechtel Hanford, Inc., Richland, Washington. Available at: http://pdw.hanford.gov/arpir/pdf.cfm?accession=0083482H.

BHI-01573, 2001, *The Groundwater/Vadose Zone Integration Project: The Application of Features, Events, and Process Methodology at the Hanford Site*, Rev. 0, Bechtel Hanford, Inc., Richland, Washington.

BNWL-243, 1966, *Soil Survey Hanford Project in Benton County Washington*, Battelle Pacific Northwest Laboratory, Richland, Washington. Available at: http://pdw.hanford.gov/arpir/index.cfm/viewDoc?accession=D196018787.

BNWL-B-360, 1975, *Selected Water Table Contour Maps and Well Hydrographs for the Hanford Reservation 1944-1973*, Battelle Pacific Northwest Laboratory, Richland, Washington. Available at: https://doi.org/10.2172/4285961

CHPRC-00189, 2014, *CH2M Hill Plateau Remediation Company Environmental Quality Assurance Program Plan*, Rev. 12, CH2M HILL Plateau Remediation Company, Richland, Washington. Available at: http://pdw.hanford.gov/arpir/index.cfm/viewDoc?accession=0071641H.

CHPRC-00257, 2010, *MODFLOW and Related Codes Functional Requirements Document*, Rev. 1, CH2M HILL Plateau Remediation Company, Richland, Washington.

CHPRC-00258, 2015, *MODFLOW and Related Codes Software Management Plan*, Rev. 4, CH2M HILL Plateau Remediation Company, Richland, Washington.

CHPRC-00259, 2014, *MODFLOW and Related Codes Software Test Plan*, Rev. 3, CH2M HILL Plateau Remediation Company, Richland, Washington.

CHPRC-00260, 2015, *MODFLOW and Related Codes Requirements Traceability Matrix*, Rev. 8, CH2M HILL Plateau Remediation Company, Richland, Washington.

CHPRC-00261, 2015, *MODFLOW and Related Codes Acceptance Test Report*, CHPRC Build 8, Rev. 8, CH2M HILL Plateau Remediation Company, Richland, Washington.

CHPRC-02868-VA, 2015, *Foundation for BP-5 Modeling Approach*, Rev. 0, CH2M HILL Plateau Remediation Company, Richland, Washington.

CHPRC-02869-VA, 2015, *Modeling Workshop: Objectives, Inputs, Calibration, and Documentation*, Rev. 1, CH2M HILL Plateau Remediation Company, Richland, Washington.

CP-47631, 2013, Model Package Report: Central Plateau Groundwater Model Version 3.4, Rev. 1, CH2M HILL Plateau Remediation Company, Richland, Washington. Available at: https://pdw.hanford.gov/arpir/index.cfm/viewDoc?accession=0077215H

CP-47631, 2018, Model Package Report: Central Plateau Groundwater Model, Version 8.4.5, Rev. 4, CH2M HILL Plateau Remediation Company, Richland, Washington. Available at: https://pdw.hanford.gov/arpir/index.cfm/viewDoc?accession=0066449H

DOE/EIS-0391, 2012, *Final Tank Closure and Waste Management Environmental Impact Statement for the Hanford Site, Richland, Washington (TC & WM EIS)*, U.S. Department of Energy, Office of River Protection, Richland, Washington. Available at: http://energy.gov/nepa/downloads/eis-0391-final-environmental-impact-statement.

DOE/RL-2002-39, 2002, *Standardized Stratigraphic Nomenclature for Post-Ringold-Formation Sediments Within the Central Pasco Basin*, Rev. 0, U.S. Department of Energy, Richland Operations Office, Richland, Washington. Available at: http://pdw.hanford.gov/arpir/index.cfm/viewDoc?accession=0081471H.

DOE/RL-2007-28, 2008, *Feasibility Study Report for the 200-ZP-1 Groundwater Operable Unit*, Rev. 0, U.S. Department of Energy, Richland Operations Office, Richland, Washington. Available at: http://pdw.hanford.gov/arpir/index.cfm/viewDoc?accession=0808050315. http://pdw.hanford.gov/arpir/index.cfm/viewDoc?accession=00098828.

DOE/RL-2008-56, 2012, *200-West Area Pre-Conceptual Design for Final Extraction/Injection Well Network: Modeling Analyses*, Rev. 0, U.S. Department of Energy, Richland Operations Office, Richland, Washington. Available at: http://pdw.hanford.gov/arpir/index.cfm/viewDoc?accession=0081011H.

DOE/RL-2008-66, 2009, *Hanford Site Groundwater Monitoring for Fiscal Year 2008*, Rev. 0, U.S. Department of Energy, Richland Operations Office, Richland, Washington. Available at: http://pdw.hanford.gov/arpir/index.cfm/viewDoc?accession=0905131281. http://pdw.hanford.gov/arpir/index.cfm/viewDoc?accession=0905131282.

DOE/RL-2008-78, 2009, *200-West Area 200-ZP-1 Pump-and-Treat Remedial Design/Remedial Action Work Plan*, Rev. 0 REISSUE, U.S. Department of Energy, Richland Operations Office, Richland, Washington. Available at: http://pdw.hanford.gov/arpir/index.cfm/viewDoc?accession=0084101.

DOE/RL-2009-38, 2009, *Description of Modeling Analyses in Support of the 200-ZP-1 Remedial Design/Remedial Action Work Plan*, Rev. 0, U.S. Department of Energy, Richland Operations Office, Richland, Washington. Available at: http://pdw.hanford.gov/arpir/index.cfm/viewDoc?accession=0095363.

DOE/RL-2009-85, 2012, *Remedial Investigation Report for the 200-PO-1 Groundwater Operable Unit*, Rev. 1, U.S. Department of Energy, Richland Operations Office, Richland, Washington. Available at: https://pdw.hanford.gov/arpir/index.cfm/viewDoc?accession=0091415

DOE/RL-2011-01, *Hanford Site Groundwater Monitoring for 2011*, Rev. 0, U.S. Department of Energy, Richland Operations Office, Richland, Washington. Available at: https://pdw.hanford.gov/arpir/index.cfm/viewDoc?accession=0093693

DOE/RL-2015-75, 2016, *Aquifer Treatability Test Report for the 200-BP-5 Groundwater Operable Unit*, Rev. 0, U.S. Department of Energy, Richland Operations Office, Richland, Washington. Available at: http://pdw.hanford.gov/arpir/index.cfm/viewDoc?accession=0074649H.

DOE/RL-2016-09, 2016, *Hanford Site Groundwater Monitoring Report for 2015*, Rev. 0, U.S. Department of Energy, Richland Operations Office, Richland, Washington. Available at: http://pdw.hanford.gov/arpir/index.cfm/viewDoc?accession=0075314H.

DOE/RL-2016-67, *Hanford Site Groundwater Monitoring Report for 2016*, Rev. 0, U.S. Department of Energy, Richland Operations Office, Richland, Washington. Available at: https://pdw.hanford.gov/arpir/index.cfm/viewDoc?accession=0068229H

Doherty, John, 2016, *PEST Model-Independent Parameter Estimation User Manual: 6th Edition*, Watermark Numerical Computing, Brisbane, Australia. Available at: http://www.pesthomepage.org/files/pestman.pdf.

ECF-200BP5-15-0009, 2017,*Evaluation of Plume Capture and Hydraulic Performance for B-Complex Vicinity Submodel for 200-BP-5 and 200-PO-1 Operable Units Feasibility Study Evaluation of Remedial Alternatives*, Rev. 0, CH2M HILL Plateau Remediation Company, Richland, Washington. Available at: https://pdw.hanford.gov/arpir/index.cfm/viewDoc?accession=0067510H

ECF-200E-16-0093, 2016, *Preparation of 200-East Area Water Table Maps for Calendar Year 2015*, Rev. 0, CH2M HILL Plateau Remediation Company, Richland, Washington. Available at: http://pdw.hanford.gov/arpir/index.cfm/viewDoc?accession=0072754H.

ECF-200BP5-16-0145, 2018, *Particle Tracking and Transport Modeling in Support of Removal Action Memorandum*, Rev. 0, CH2M HILL Plateau Remediation Company, Richland, Washington. Available at: https://pdw.hanford.gov/arpir/index.cfm/viewDoc?accession=0066643H

ECF-200ZP1-16-0076, 2016, *Description of Groundwater Calculations and Assessments for the Calendar Year 2015 (CY 2015) 200 Areas Pump and Treat Report*, Rev. 0, CH2M HILL Plateau Remediation Company, Richland, Washington. Available at: http://pdw.hanford.gov/arpir/index.cfm/viewDoc?accession=0074966H.

ECF-HANFORD-13-0029, 2017, *Development of the Hanford South Geologic Framework Model, Hanford Site, Washington – Fiscal Year 2016 Update*, Rev. 5, CH2M HILL Plateau Remediation Company, Richland, Washington. Available at: http://pdw.hanford.gov/arpir/index.cfm/viewDoc?accession=0072357H.

ECF-HANFORD-13-0031, 2015, *Fate and Transport Modeling for Baseline Conditions for Remedial Investigation/Feasibility Studies of the 200-BP-5 and 200-PO-1 Groundwater Operable Units*, Rev. 0, CH2M HILL Plateau Remediation Company, Richland, Washington. Available at: https://pdw.hanford.gov/arpir/index.cfm/viewDoc?accession=0080142H

ECF-HANFORD-18-0023, 2018, *Evaluation of Contaminant Transport for the 200-BP-5 and 200-PO-1 Operable Units Feasibility Study Evaluation of Remedial Alternatives*, Rev. 0, CH2M HILL Plateau Remediation Company, Richland, Washington. Available at: https://pdw.hanford.gov/arpir/index.cfm/viewDoc?accession=0064587H

EPA 402-R-99-001, 1999, Cancer Risk Coefficients for Environmental Exposure to Radionuclides, Federal Guidance Report No. 13, Office of Radiation and Indoor Air, U.S. Environmental Protection Agency, Washington, D.C. Available at: https://www.epa.gov/sites/production/files/2015-05/documents/402-r-99-001.pdf.

Fecht, K.R., S.P. Reidel, and A.M. Tallman, 1987, "Paleodrainage of the Columbia River on the Columbia Plateau of Washington State - A Summary," in *Selected Papers on the Geology of Washington*, Bulletin 77:219-248, Washington Department of Natural Resources, Olympia, Washington.

Gee, G.W., M.J. Fayer, M.L. Rockhold, and M.D. Campbell, 1992, "Variations in Recharge at the Hanford Site," *Northwest Science* 66:237-250. Available at: https://research.wsulibs.wsu.edu:8443/xmlui/bitstream/handle/2376/1618/v66?sequence=1.

Jones, N.L., T.J. Budge, A.M. Lemon, and A.K. Zundel, 2002, "Generating MODFLOW Grids from Boundary Representation Solid Models," *Ground Water*, 40(2):194-200.

Klein, 2006, "MEMO: Contract No. DE-AC06-96RL13200 – Hanford Groundwater Modeling Integration" (memorandum to R.G. Gallagher from K.A. Klein), U.S. Department of Energy, Richland Operations Office, Richland, Washington.

Konikow, Leonard F., 1986, "Predictive Accuracy of a Ground-Water Model – Lessons from a Postaudit," *Groundwater* 24(2):173-185.

Konikow, Leonard F. and John D. Bredehoeft, 1992, "Ground-water Models Cannot be Validated," *Advances in Water Resources* 15:75-83. Available at: https://hydro.geo.ua.edu/gw_modeling/Konilow1992.pdf.

Last, G.V., V.J. Rohay, F.J. Schelling, A.L. Bunn, M.A. Delamare, R.L. Dirkes, R.D. Hildebrand, J.G. Morse, B.A. Napier, R.G. Riley, L. Soler, and P.D. Thorne, 2004, "A Comprehensive and Systematic Approach to Developing and Documenting Conceptual Models of Contaminant Release and Migration at the Hanford Site," *Journal of Stochastic Environmental Research and Risk Assessment* 18(2):109-116.

National Research Council, 2000, *Research Needs in Subsurface Science*, National Academy Press, Washington, D.C.

NUREG/CR-6805, 2003, *A Comprehensive Strategy of Hydrogeologic Modeling and Uncertainty Analysis for Nuclear Facilities and Sites*, Office of Nuclear Regulatory Research, U.S. Nuclear Regulatory Commission, Washington, D.C. Available at: https://www.nrc.gov/docs/ML0324/ML032470827.pdf.

O'Conner, Jim E. and John E. Costa, 2004, *The World's Largest Floods, Past and Present – Their Causes and Magnitudes*, U.S. Geological Survey, Washington, D.C. Available at: http://pubs.usgs.gov/circ/2004/circ1254/pdf/circ1254.pdf.

Oreskes, Naomi and Kenneth Belitz, 2001, "Philosophical Issues in Model Assessment," in *Model Validation: Perspectives in Hydrological Science*, Anderson and Bates (eds.), pp. 23-41, John Wily & Sons, Ltd. Available at: http://history.ucsd.edu/_files/faculty/oreskes-naomi/PhilIssuesModelAssessOreskes.pdf.

PNL-6403, 1987, *Recharge at the Hanford Site: Status Report*, Pacific Northwest Laboratory, Richland, Washington. Available at: http://pdw.hanford.gov/arpir/index.cfm/viewDoc?accession=D196008009.

PNL-10285, 1995, *Estimated Recharge Rates at the Hanford Site*, Pacific Northwest Laboratory, Richland, Washington. Available at: https://www.osti.gov/scitech/servlets/purl/10122247.

PNL-10886, 1995, *Development of a Three-Dimensional Ground-Water Model of the Hanford Site Unconfined Aquifer System: FY 1995 Status Report*, Pacific Northwest Laboratory, Richland, Washington. Available at: https://www.osti.gov/scitech/servlets/purl/195772.

PNNL-11216, 1997, *STOMP Subsurface Transport Over Multiple Phases: Application Guide*, Pacific Northwest National Laboratory, Richland, Washington. Available at: https://www.osti.gov/scitech/servlets/purl/553735.

PNNL-12261, 2000, *Revised Hydrogeology for the Suprabasalt Aquifer System, 200-East Area and Vicinity, Hanford Site, Washington*, Pacific Northwest National Laboratory, Richland, Washington. Available at: http://pdw.hanford.gov/arpir/index.cfm/viewDoc?accession=0906180659.

PNNL-13623, 2001, *Transient Inverse Calibration of Site-Wide Groundwater Model to Hanford Operational Impacts from 1943 to 1996—Alternative Conceptual Model Considering Interaction with Uppermost Basalt Confined Aquifer*, Pacific Northwest National Laboratory, Richland, Washington. Available at: http://www.pnl.gov/main/publications/external/technical_reports/pnnl-13623.pdf.

PNNL-13641, 2001, *Uncertainty Analysis Framework – Hanford Site-Wide Groundwater Flow and Transport Model*, Pacific Northwest National Laboratory, Richland, Washington. Available at: http://www.pnl.gov/main/publications/external/technical_reports/pnnl-13641.pdf.

PNNL-13858, 2002, *Revised Hydrogeology for the Suprabasalt Aquifer System, 200-West Area and Vicinity, Hanford Site, Washington*, Pacific Northwest National Laboratory, Richland, Washington. Available at: http://www.pnl.gov/main/publications/external/technical_reports/PNNL-13858.pdf.

PNNL-14058, 2002, *Prototype Database and User's Guide of Saturated Zone Hydraulic Properties for the Hanford Site*, Pacific Northwest National Laboratory, Richland, Washington. Available at: http://www.pnl.gov/main/publications/external/technical_reports/PNNL-14058.pdf.

PNNL-14070, 2002, *Groundwater Monitoring Plan for the 216-S-10 Pond and Ditch*, Pacific Northwest National Laboratory, Richland, Washington. Available at: https://www.pnnl.gov/main/publications/external/technical_reports/PNNL-14070.pdf

PNNL-14398, 2003, *Transient Inverse Calibration of the Site-Wide Groundwater Flow Model (ACM-2): FY 2003 Progress Report*, Pacific Northwest National Laboratory, Richland, Washington. Available at: http://www.pnl.gov/main/publications/external/technical_reports/PNNL-14398.pdf.

PNNL-14717, 2004, *Natural Recharge to the Unconfined Aquifer System on the Hanford Site from the Greater Cold Creek Watershed: Progress Report 2004*, Pacific Northwest National Laboratory, Richland, Washington. Available at: http://www.pnl.gov/main/publications/external/technical_reports/PNNL-14717.pdf

PNNL-14753, 2006, *Groundwater Data Package for Hanford Assessments*, Rev. 1, Pacific Northwest National Laboratory, Richland, Washington. Available at: http://pdw.hanford.gov/arpir/index.cfm/viewDoc?accession=0912020007. http://pdw.hanford.gov/arpir/index.cfm/viewDoc?accession=0912020126.

PNNL-14898, *Results of Groundwater Modeling for Tritium Tracking at the Hanford Site 200 Area State-Approved Land Disposal Site – 2004*, Pacific Northwest Laboratory, Richland, Washington. Available at: http://www.pnl.gov/main/publications/external/technical_reports/PNNL-14898.pdf

PNNL-15837, 2007, *Data Package for Past and Current Groundwater Flow and Contamination Beneath Single-Shell Tank Waste Management Areas*, Pacific Northwest National Laboratory, Richland, Washington. Available at: http://pdw.hanford.gov/arpir/index.cfm/viewDoc?accession=0911240061.

PNNL-17841, 2008, *Compendium of Data for the Hanford Site (Fiscal Years 2004 to 2008) Applicable to Estimation of Recharge Rates*, Pacific Northwest National Laboratory, Richland, Washington. Available at: http://www.pnl.gov/main/publications/external/technical_reports/PNNL-17841.pdf.

PNNL-17913, 2009, *Hydrogeology of the Hanford Site Central Plateau – A Status Report for the 200-West Area*, Rev. 1, Pacific Northwest National Laboratory, Richland, Washington. Available at: http://www.pnl.gov/main/publications/external/technical_reports/PNNL-17913rev1.pdf.

PNNL-18564, 2009, *Selection and Traceability of Parameters to Support Hanford-Specific RESRAD Analyses: Fiscal Year 2008 Status Report*, Pacific Northwest National Laboratory, Richland, Washington. Available at: http://www.pnl.gov/main/publications/external/technical_reports/PNNL-18564.pdf.

PNNL-18732, 2009, *Field Test Report: Preliminary Aquifer Test Characterization Results for Well 299-W15-225: Supporting Phase I of the 200-ZP-1 Groundwater Operable Unit Remedial Design*, Pacific Northwest National Laboratory, Richland, Washington. Availabe at: http://www.pnl.gov/main/publications/external/technical_reports/PNNL-18732.pdf.

PNNL-19702, 2010, *Hydrogeologic Model for the Gable Gap Area, Hanford Site*, Pacific Northwest National Laboratory, Richland, Washington. Available at: www.pnl.gov/main/publications/external/technical_reports/PNNL-19702.pdf.

RHO-ST-38, 1982, *Geohydrology of the Rattlesnake Ridge Interbed in the Gable Mountain Pond Area*, Rockwell International, Richland, Washington, Available at: https://pdw.hanford.gov/arpir/index.cfm/viewDoc?accession=0081058H

Schulze-Makuch, D., 2005, "Longitudinal Dispersivity Data and Implication for Scaling Behavior", *Ground Water* 43(3):443-456.

SGW-42604, 2009, *Results of Tritium Tracking and Groundwater Monitoring at the Hanford Site 200 Area State-Approved Land Disposal Site, Fiscal Year 2009*, Rev. 0, CH2M HILL Plateau Remediation Company, Richland, Washington.

SGW-48478, 2012, *Interpretation and Integration of Seismic Data in the Gable Gap*, Rev. 1, CH2M HILL Plateau Remediation Company, Richland, Washington.

SGW-62323,2018, *Central Plateau Groundwater Tracer Study Phase I Report*, Rev. 0, CH2M HILL Plateau Remediation Company, Richland, Washington. Available at: https://pdw.hanford.gov/arpir/index.cfm/viewDoc?accession=0064369H

USGS, 2000, *MODFLOW-2000, the U.S. Geological Survey Modular Ground-water Model – User Guide to Modularization Concepts and the Ground-Water Flow Process*, USGS Open File Report 00-92, U.S. Geological Survey, Denver, Colorado. Available at: http://water.usgs.gov/nrp/gwsoftware/modflow2000/ofr00-92.pdf.

WHC-EP-0698, 1994, *Groundwater Impact Assessment Report for the 216-U-14 Ditch*, Rev. 0, Westinghouse Hanford Company, Richland, Washington. Available at: http://pdw.hanford.gov/arpir/index.cfm/viewDoc?accession=D196093455.

WHC-SA-0699-FP, 1990, *Effects of Varying Recharge on Radionuclide Flux Rates to the Water Table at the Low-Level Solid Waste Burial Site*, Washington Hanford Company, Richland, Washington. Available at: http://pdw.hanford.gov/arpir/index.cfm/viewDoc?accession=D196000242 .

Zheng, Chunmiao and Patrick P. Wang, 1999, *MT3DMS: A Modular Three-Dimensional Multispecies Transport Model for Simulation of Advection, Dispersion, and Chemical Reactions of Contaminants in Groundwater Systems; Documentation and User's Guide*, Contract Report SERDP-99-1, U.S. Army Engineer Research and Development Center, U.S. Army Corps of Engineers, Vicksburg, Mississippi. Available at: Available at: http://www.dtic.mil/cgi-bin/GetTRDoc?Location=U2&doc=GetTRDoc.pdf&AD=ADA373474.

This page intentionally left blank.

Attachment A

Software Installation and Checkout Forms for Approved Software Installations

CHPRC SOFTWARE INSTALLATION AND CHECKOUT FORM

Software Owner Instructions:
Complete Fields 1-13, then run test cases in Field 14. Compare test case results listed in Field 15 to corresponding Test Report outputs. If results are the same, sign and date Field 19. If not, resolve differences and repeat above steps.

Software Subject Matter Expert Instructions:
Assign test personnel. Approve the installation of the code by signing and dating Field 21, then maintain form as part of the software support documentation.

GENERAL INFORMATION:

1. Software Name: MODFLOW and Related Codes Software Version No.: Bld 8

EXECUTABLE INFORMATION:

2. Executable Name (include path):

Following executable files in directory: (All Machines)

MD5 Signature (unique ID)	Executable File Name	
919F74196F5FB5BF0364FC373011B507	mf2k-chprc08dpl.exe	MODFLOW-2000 double precision
EAF037703ADD2C62CDD9CBC47468D2F6	mf2k-chprc08spl.exe	MODFLOW-2000 single precision
4E7F29DD5496D2CBA7144ADACB13DAAD	mf2k-mst-chprc08dpv.exe	MODFLOW-2000-MST double prec
CEB80288C616E0552E4CE5A2D4719387	mf2k-mst-chprc08spv.exe	MODFLOW-2000-MST single prec
ECA9828530B68D2D7C34078C019D5D0C	mt3d-chprc08dpl.exe	MT3DMS double precision
0920CC235862665D9400A3FC80F682DD	mt3d-chprc08spl.exe	MT3DMS single precision
5C61432D2C898E83DDFE242C52A755AB	mt3d-mst-chprc08dpv.exe	MT3DMS-MST double precision
68F89DAF2E6913D2578DE53CBD34FBA0	mt3d-mst-chprc08spv.exe	MT3DMS-MST single precision

3. Executable Size (bytes): MD5 signatures listed above uniquely identify executable files

COMPILATION INFORMATION:

4. Hardware System (i.e., property number or ID):

Vendor Provided (SSP&A)

5. Operating System (include version number):

Vendor Provided (SSP&A)

INSTALLATION AND CHECKOUT INFORMATION:

6. Hardware System (i.e., property number or ID):

VEJOVIS CLUSTER (CHPRC),DELL OPTIPLEX 9020, (WF33435, WF33438, WF33436, WF33441, WF33440, WF33437, WF33442, WF33442, WF33439)

7. Operating System (include version number):

WF33435, Windows 10 Enterprise Build 1709, Build 16299.547
All others - Windows 7 Professional Service Pack 1

8. Open Problem Report? ◉ No ○ Yes PR/CR No.

TEST CASE INFORMATION:

9. Directory/Path:

(All Machines) C:\

10. Procedure(s):

CHPRC-00259 Rev 3, MODFLOW and Related Codes Software Test Plan

11. Libraries:

N/A (static linking)

12. Input Files:

MF-ITC-1 and MT-ITC-1 inputs

Page 1 of 2 A-6005-149 (REV 0)

CHPRC SOFTWARE INSTALLATION AND CHECKOUT FORM (continued)

1. Software Name: MODFLOW and Related Codes Software Version No.: Bld 8

13. Output Files:

MF-ITC-1 and MT-ITC-1 outputs

14. Test Cases:

MF-ITC-1 (both standard and MST versions of MODFLOW)- run for single & double precision
MT-ITC-1 - run for single and double precision

15. Test Case Results:

All tests returned identical results to the documented test cases.

16. Test Performed By: Trevor Budge

17. Test Results: (●) Satisfactory, Accepted for Use ( ) Unsatisfactory

18. Disposition (include HISI update):

Added to HISI Entries 2157 and 2158.

Prepared By:

19.	WE Nichols	7-26-2018
Software Owner (Signature)	Print	Date

20. Test Personnel:

	Trevor Budge	8-6-18
Sign	Print	Date
Sign	Print	Date
Sign	Print	Date

Approved By:

21.	N/R (CHPRC-00258 Rev 3)	
Software SME (Signature)	Print	Date

A-6005-149 (REV 0)

Attachment B

List of Observation Wells Used in the Calibration Process

Table B-1. Well names for wells included in the P2R Model version 8.2 calibration					
299-E13-10	299-E25-42	299-E32-1	299-E34-10	299-W11-24	299-W15-22
299-E16-1	299-E25-43	299-E32-10	299-E34-11	299-W11-27	299-W15-23
299-E17-14	299-E25-44	299-E32-2	299-E34-12	299-W11-3	299-W15-24
299-E17-15	299-E25-45	299-E32-3	299-E34-2	299-W11-30	299-W15-25
299-E17-16	299-E25-46	299-E32-4	299-E34-7	299-W11-31	299-W15-30
299-E17-17	299-E25-47	299-E32-5	299-E34-8	299-W11-39	299-W15-31A
299-E17-18	299-E25-48	299-E32-6	299-E34-9	299-W11-4	299-W15-4
299-E17-19	299-E25-93	299-E32-7	299-E35-1	299-W11-40	299-W15-40
299-E17-20	299-E26-1	299-E32-8	299-E35-2	299-W11-41	299-W15-41
299-E17-21	299-E26-10	299-E33-14	299-W10-1	299-W11-42	299-W15-42
299-E17-22	299-E26-11	299-E33-15	299-W10-10	299-W11-5	299-W15-7
299-E17-23	299-E26-12	299-E33-16	299-W10-11	299-W11-6	299-W15-763
299-E17-3	299-E26-13	299-E33-17	299-W10-12	299-W11-7	299-W18-10
299-E18-1	299-E26-9	299-E33-18	299-W10-13	299-W11-8	299-W18-15
299-E18-2	299-E27-1	299-E33-21	299-W10-14	299-W11-9	299-W18-2
299-E18-3	299-E27-10	299-E33-25	299-W10-15	299-W12-1	299-W18-21
299-E18-4	299-E27-11	299-E33-26	299-W10-16	299-W14-10	299-W18-22
299-E19-1	299-E27-12	299-E33-28	299-W10-17	299-W14-12	299-W18-23
299-E23-1	299-E27-13	299-E33-29	299-W10-18	299-W14-13	299-W18-24
299-E24-16	299-E27-14	299-E33-30	299-W10-19	299-W14-14	299-W18-25
299-E24-17	299-E27-15	299-E33-31	299-W10-20	299-W14-15	299-W18-26
299-E24-18	299-E27-16	299-E33-32	299-W10-21	299-W14-16	299-W18-27
299-E24-19	299-E27-17	299-E33-33	299-W10-22	299-W14-17	299-W18-28
299-E24-20	299-E27-18	299-E33-334	299-W10-23	299-W14-18	299-W18-30
299-E24-7	299-E27-19	299-E33-335	299-W10-24	299-W14-19	299-W18-31
299-E25-10	299-E27-21	299-E33-337	299-W10-26	299-W14-5	299-W18-32
299-E25-21	299-E27-4	299-E33-338	299-W10-27	299-W14-6	299-W18-33
299-E25-22	299-E27-5	299-E33-339	299-W10-28	299-W14-9	299-W18-4
299-E25-23	299-E27-8	299-E33-34	299-W10-3	299-W15-1	299-W18-40
299-E25-24	299-E27-9	299-E33-35	299-W10-4	299-W15-10	299-W18-5
299-E25-25	299-E28-1	299-E33-36	299-W10-5	299-W15-11	299-W18-9
299-E25-31	299-E28-10	299-E33-37	299-W10-8	299-W15-12	299-W19-1
299-E25-33	299-E28-2	299-E33-38	299-W10-9	299-W15-13	299-W19-13
299-E25-34	299-E28-26	299-E33-39	299-W11-1	299-W15-15	299-W19-15
299-E25-35	299-E28-27	299-E33-41	299-W11-10	299-W15-16	299-W19-19
299-E25-36	299-E28-28	299-E33-42	299-W11-12	299-W15-17	299-W19-2
299-E25-37	299-E28-4	299-E33-43	299-W11-14	299-W15-18	299-W19-23
299-E25-39	299-E28-5	299-E33-44	299-W11-18	299-W15-19	299-W19-24
299-E25-40	299-E28-6	299-E33-8	299-W11-19	299-W15-2	299-W19-25
299-E25-41	299-E28-8	299-E34-1	299-W11-23	299-W15-20	299-W19-26

Table B-1. Well names for wells included in the P2R Model version 8.2 calibration (cont'd)					
299-W19-27	299-W22-85	299-W9-1	699-25-55	699-37-68	699-47-35A
299-W19-28	299-W22-9	399-1-10A	699-25-70	699-37-82A	699-47-60
299-W19-29	299-W23-13	399-1-11	699-26-15A	699-38-15	699-48-18
299-W19-30	299-W23-14	399-1-14A	699-26-33	699-38-65	699-48-71
299-W19-31	299-W23-15	399-1-18A	699-26-34A	699-38-70	699-48-77A
299-W19-32	299-W23-20	399-1-6	699-26-34B	699-39-0	699-48-77C
299-W19-36	299-W23-21	699-10-54A	699-26-35A	699-39-39	699-48-77D
299-W19-37	299-W23-4	699-10-E12Q	699-26-35C	699-39-79	699-49-13E
299-W19-4	299-W23-8	699-11-45A	699-2-7	699-40-1	699-49-57A
299-W19-40	299-W26-10	699-1-18	699-27-8	699-40-12C	699-49-79
299-W19-41	299-W26-12	699-12-2C	699-28-40	699-40-33A	699-50-28B
299-W19-42	299-W26-13	699-12-4D	699-28-52A	699-40-36	699-50-30
299-W19-44	299-W26-14	699-13-0A	699-29-4	699-40-39	699-50-42
299-W19-45	299-W26-6	699-13-2D	699-29-78	699-40-40A	699-50-74
299-W19-46	299-W26-7	699-14-47	699-31-31	699-40-40B	699-50-85
299-W19-6	299-W26-8	699-15-15A	699-31-53B	699-40-62	699-51-75
299-W21-1	299-W27-2	699-15-26	699-32-22A	699-41-23	699-52-19
299-W22-20	299-W6-1	699-19-43	699-32-42	699-41-35	699-53-55A
299-W22-22	299-W6-10	699-20-20	699-32-43	699-41-40	699-54-18B
299-W22-23	299-W6-11	699-20-39	699-32-62	699-41-42	699-54-45A
299-W22-39	299-W6-12	699-20-E12	699-32-70B	699-42-12A	699-55-70
299-W22-4	299-W6-2	699-20-E5A	699-32-72B	699-42-2	699-55-76
299-W22-40	299-W6-3	699-21-17	699-32-77	699-42-37	699-57-83A
299-W22-41	299-W6-4	699-21-6	699-33-42	699-42-39A	699-8-17
299-W22-42	299-W6-6	699-22-35	699-33-56	699-42-39B	699-8-25
299-W22-43	299-W6-7	699-2-3	699-34-39A	699-42-40A	699-8-32
299-W22-44	299-W6-8	699-23-34A	699-34-41B	699-42-40B	699-9-E2
299-W22-45	299-W6-9	699-23-34B	699-34-42	699-42-41	699-S11-E12A
299-W22-46	299-W7-1	699-2-33A	699-3-45	699-42-42A	699-S12-29
299-W22-48	299-W7-10	699-24-33	699-34-51	699-42-42B	699-S14-20A
299-W22-49	299-W7-11	699-24-34A	699-34-61	699-43-40	699-S19-11
299-W22-50	299-W7-12	699-24-34B	699-35-66A	699-43-41E	699-S19-E13
299-W22-7	299-W7-2	699-24-34C	699-35-70	699-43-41F	699-S19-E14
299-W22-79	299-W7-4	699-24-35	699-35-78A	699-43-41G	699-S20-E10
299-W22-8	299-W7-5	699-24-46	699-35-9	699-43-44	699-S3-25
299-W22-80	299-W7-6	699-25-33A	699-36-46S	699-44-16	699-S3-E12
299-W22-81	299-W7-7	699-25-34A	699-36-61A	699-44-64	699-S6-E14A
299-W22-82	299-W7-8	699-25-34B	699-36-61B	699-45-42	699-S6-E4K
299-W22-83	299-W7-9	699-25-34C	699-36-67	699-46-21B	699-S8-19
299-W22-84	299-W8-1	699-25-34D	699-37-43	699-46-4	

Attachment C

Hydraulic Gradient Plots for Observed Data and Simulated Results

Figure C-1. Observed and simulated hydraulic gradient azimuth and magnitude for well triplet 1..... 5
Figure C-2. Observed and simulated hydraulic gradient azimuth and magnitude for well triplet 2..... 6
Figure C-3. Observed and simulated hydraulic gradient azimuth and magnitude for well triplet 3..... 7
Figure C-4. Observed and simulated hydraulic gradient azimuth and magnitude for well triplet 4..... 8
Figure C-5. Observed and simulated hydraulic gradient azimuth and magnitude for well triplet 5..... 9
Figure C-6. Observed and simulated hydraulic gradient azimuth and magnitude for well triplet 6..... 10
Figure C-7. Observed and simulated hydraulic gradient azimuth and magnitude for well triplet 7..... 11
Figure C-8. Observed and simulated hydraulic gradient azimuth and magnitude for well triplet 8..... 12
Figure C-9. Observed and simulated hydraulic gradient azimuth and magnitude for well triplet 9..... 13
Figure C-10. Observed and simulated hydraulic gradient azimuth and magnitude for well triplet 10..... 14
Figure C-11. Observed and simulated hydraulic gradient azimuth and magnitude for well triplet 11..... 15
Figure C-12. Observed and simulated hydraulic gradient azimuth and magnitude for well triplet 12..... 16
Figure C-13. Observed and simulated hydraulic gradient azimuth and magnitude for well triplet 13..... 17
Figure C-14. Observed and simulated hydraulic gradient azimuth and magnitude for well triplet 14..... 18
Figure C-15. Observed and simulated hydraulic gradient azimuth and magnitude for well triplet 15..... 19
Figure C-16. Observed and simulated hydraulic gradient azimuth and magnitude for well triplet 16..... 20
Figure C-17. Observed and simulated hydraulic gradient azimuth and magnitude for well triplet 17..... 21
Figure C-18. Observed and simulated hydraulic gradient azimuth and magnitude for well triplet 18..... 22
Figure C-19. Observed and simulated hydraulic gradient azimuth and magnitude for well triplet 19..... 23
Figure C-20. Observed and simulated hydraulic gradient azimuth and magnitude for well triplet 20..... 24
Figure C-21. Observed and simulated hydraulic gradient azimuth and magnitude for well triplet 21..... 25
Figure C-22. Observed and simulated hydraulic gradient azimuth and magnitude for well triplet 22..... 26
Figure C-23. Observed and simulated hydraulic gradient azimuth and magnitude for well triplet 23..... 27
Figure C-24. Observed and simulated hydraulic gradient azimuth and magnitude for well triplet 24..... 28
Figure C-25. Observed and simulated hydraulic gradient azimuth and magnitude for well triplet 25..... 29
Figure C-26. Observed and simulated hydraulic gradient azimuth and magnitude for well triplet 26..... 30
Figure C-27. Observed and simulated hydraulic gradient azimuth and magnitude for well triplet 27..... 31
Figure C-28. Observed and simulated hydraulic gradient azimuth and magnitude for well triplet 28..... 32
Figure C-29. Observed and simulated hydraulic gradient azimuth and magnitude for well triplet 29..... 33
Figure C-30. Observed and simulated hydraulic gradient azimuth and magnitude for well triplet 30..... 34
Figure C-31. Observed and simulated hydraulic gradient azimuth and magnitude for well triplet 31..... 35
Figure C-32. Observed and simulated hydraulic gradient azimuth and magnitude for well triplet 32..... 36
Figure C-33. Observed and simulated hydraulic gradient azimuth and magnitude for well triplet 33..... 37
Figure C-34. Observed and simulated hydraulic gradient azimuth and magnitude for well triplet 34..... 38
Figure C-35. Observed and simulated hydraulic gradient azimuth and magnitude for well triplet 35..... 39
Figure C-36. Observed and simulated hydraulic gradient azimuth and magnitude for well triplet 36..... 40
Figure C-37. Observed and simulated hydraulic gradient azimuth and magnitude for well triplet 37..... 41

Figure C-38. Observed and simulated hydraulic gradient azimuth and magnitude for well triplet 38..... 42
Figure C-39. Observed and simulated hydraulic gradient azimuth and magnitude for well triplet 39..... 43
Figure C-40. Observed and simulated hydraulic gradient azimuth and magnitude for well triplet 40..... 44
Figure C-41. Observed and simulated hydraulic gradient azimuth and magnitude for well triplet 41..... 45
Figure C-42. Observed and simulated hydraulic gradient azimuth and magnitude for well triplet 42..... 46
Figure C-43. Observed and simulated hydraulic gradient azimuth and magnitude for well triplet 43..... 47
Figure C-44. Observed and simulated hydraulic gradient azimuth and magnitude for well triplet 44..... 48
Figure C-45. Observed and simulated hydraulic gradient azimuth and magnitude for well triplet 45..... 49
Figure C-46. Observed and simulated hydraulic gradient azimuth and magnitude for well triplet 46..... 50
Figure C-47. Observed and simulated hydraulic gradient azimuth and magnitude for well triplet 47..... 51
Figure C-48. Observed and simulated hydraulic gradient azimuth and magnitude for well triplet 48..... 52
Figure C-49. Observed and simulated hydraulic gradient azimuth and magnitude for well triplet 49..... 53
Figure C-50. Observed and simulated hydraulic gradient azimuth and magnitude for well triplet 50..... 54
Figure C-51. Observed and simulated hydraulic gradient azimuth and magnitude for well triplet 51..... 55
Figure C-52. Observed and simulated hydraulic gradient azimuth and magnitude for well triplet 52..... 56
Figure C-53. Observed and simulated hydraulic gradient azimuth and magnitude for well triplet 53..... 57
Figure C-54. Observed and simulated hydraulic gradient azimuth and magnitude for well triplet 54..... 58
Figure C-55. Observed and simulated hydraulic gradient azimuth and magnitude for well triplet 55..... 59
Figure C-56. Observed and simulated hydraulic gradient azimuth and magnitude for well triplet 56..... 60
Figure C-57. Observed and simulated hydraulic gradient azimuth and magnitude for well triplet 57..... 61
Figure C-58. Observed and simulated hydraulic gradient azimuth and magnitude for well triplet 58..... 62
Figure C-59. Observed and simulated hydraulic gradient azimuth and magnitude for well triplet 59..... 63
Figure C-60. Observed and simulated hydraulic gradient azimuth and magnitude for well triplet 60..... 64
Figure C-61. Observed and simulated hydraulic gradient azimuth and magnitude for well triplet 61..... 65
Figure C-62. Observed and simulated hydraulic gradient azimuth and magnitude for well triplet 62..... 66
Figure C-63. Observed and simulated hydraulic gradient azimuth and magnitude for well triplet 63..... 67
Figure C-64. Observed and simulated hydraulic gradient azimuth and magnitude for well triplet 64..... 68
Figure C-65. Observed and simulated hydraulic gradient azimuth and magnitude for well triplet 65..... 69
Figure C-66. Observed and simulated hydraulic gradient azimuth and magnitude for well triplet 66..... 70
Figure C-67. Observed and simulated hydraulic gradient azimuth and magnitude for well triplet 67..... 71
Figure C-68. Observed and simulated hydraulic gradient azimuth and magnitude for well triplet 68..... 72
Figure C-69. Observed and simulated hydraulic gradient azimuth and magnitude for well triplet 69..... 73
Figure C-70. Observed and simulated hydraulic gradient azimuth and magnitude for well triplet 70..... 74
Figure C-71. Observed and simulated hydraulic gradient azimuth and magnitude for well triplet 71..... 75
Figure C-72. Observed and simulated hydraulic gradient azimuth and magnitude for well triplet 72..... 76
Figure C-73. Observed and simulated hydraulic gradient azimuth and magnitude for well triplet 73..... 77
Figure C-74. Observed and simulated hydraulic gradient azimuth and magnitude for well triplet 74..... 78
Figure C-75. Observed and simulated hydraulic gradient azimuth and magnitude for well triplet 75..... 79
Figure C-76. Observed and simulated hydraulic gradient azimuth and magnitude for well triplet 76..... 80

Figure C-77. Observed and simulated hydraulic gradient azimuth and magnitude for well triplet 77..... 81
Figure C-78. Observed and simulated hydraulic gradient azimuth and magnitude for well triplet 78..... 82
Figure C-79. Observed and simulated hydraulic gradient azimuth and magnitude for well triplet 79..... 83

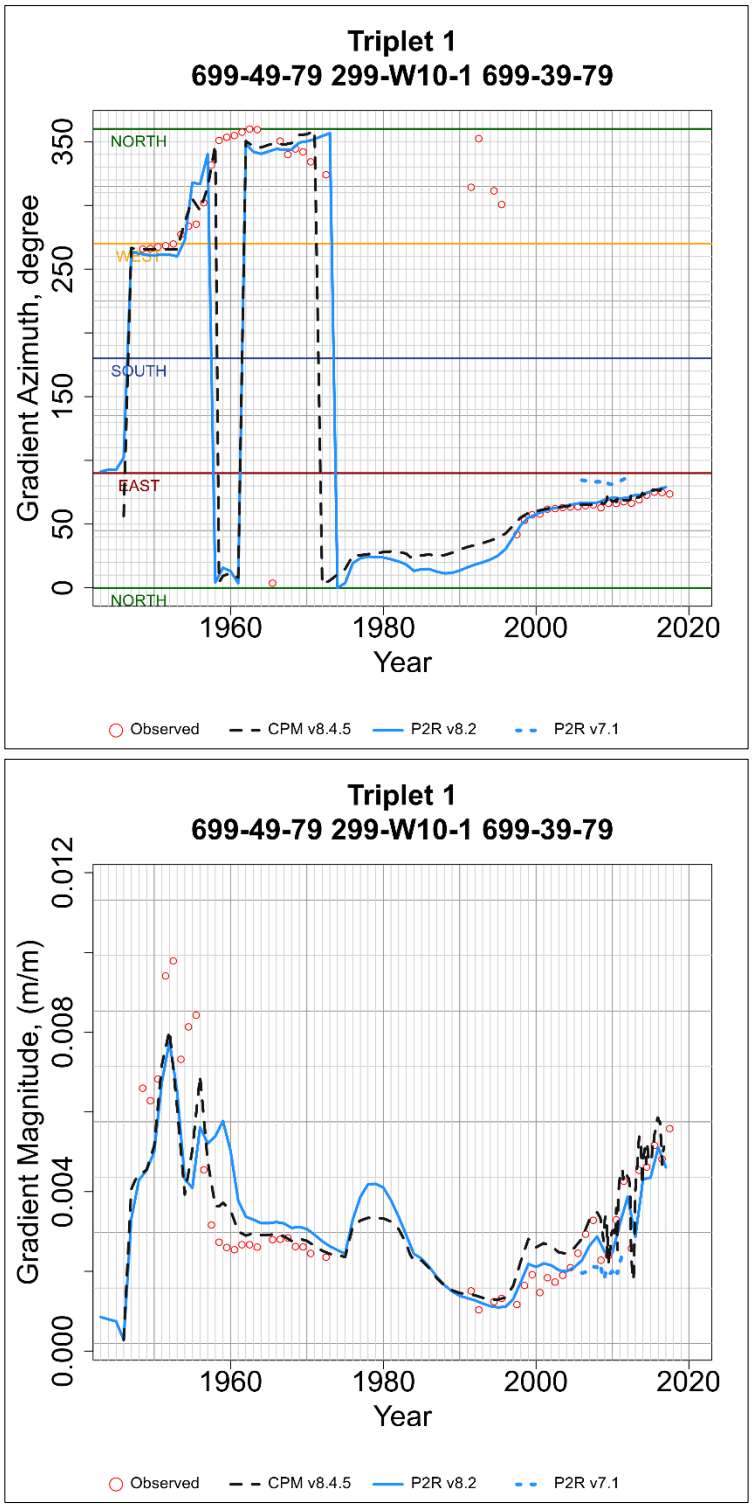

Figure C-1. Observed and simulated hydraulic gradient azimuth and magnitude for well triplet 1.

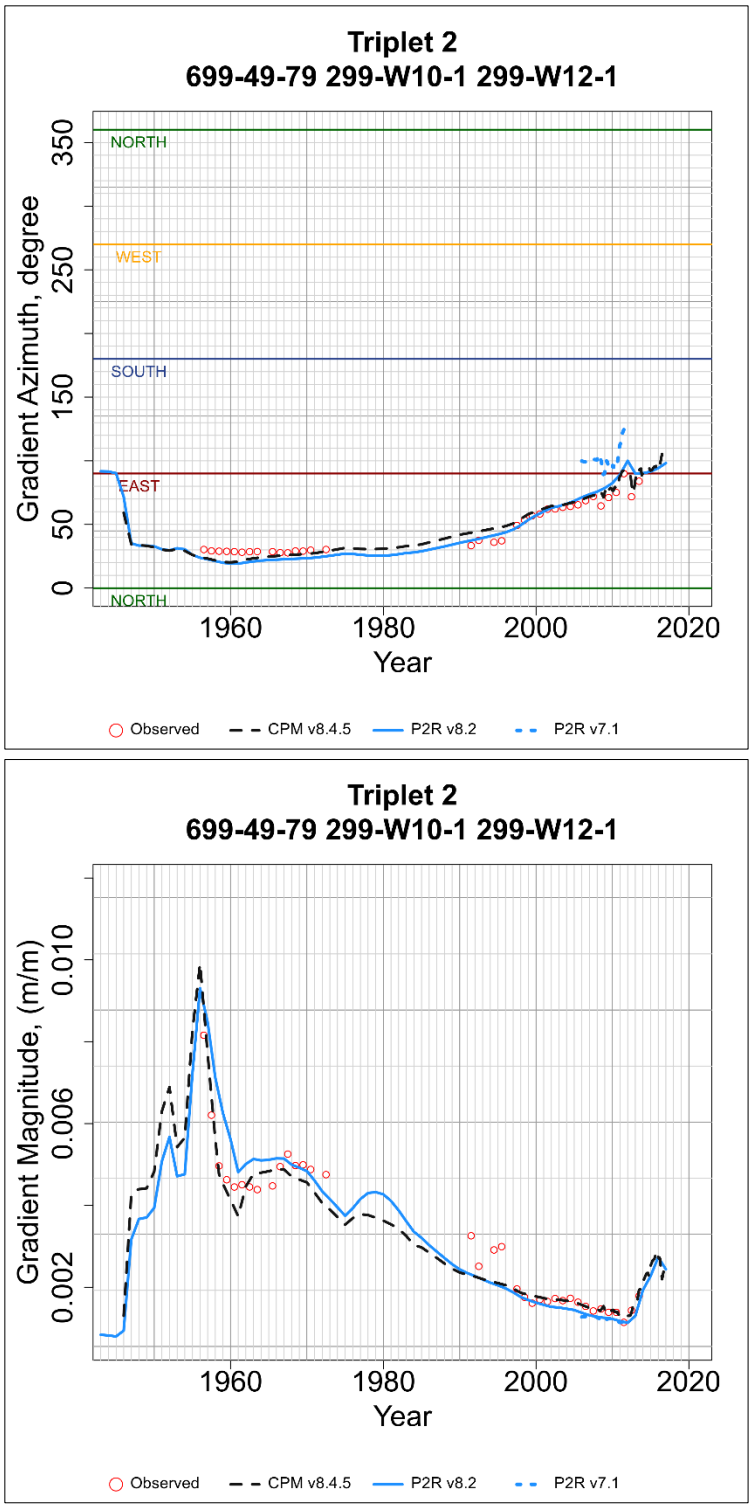

Figure C-2. Observed and simulated hydraulic gradient azimuth and magnitude for well triplet 2.

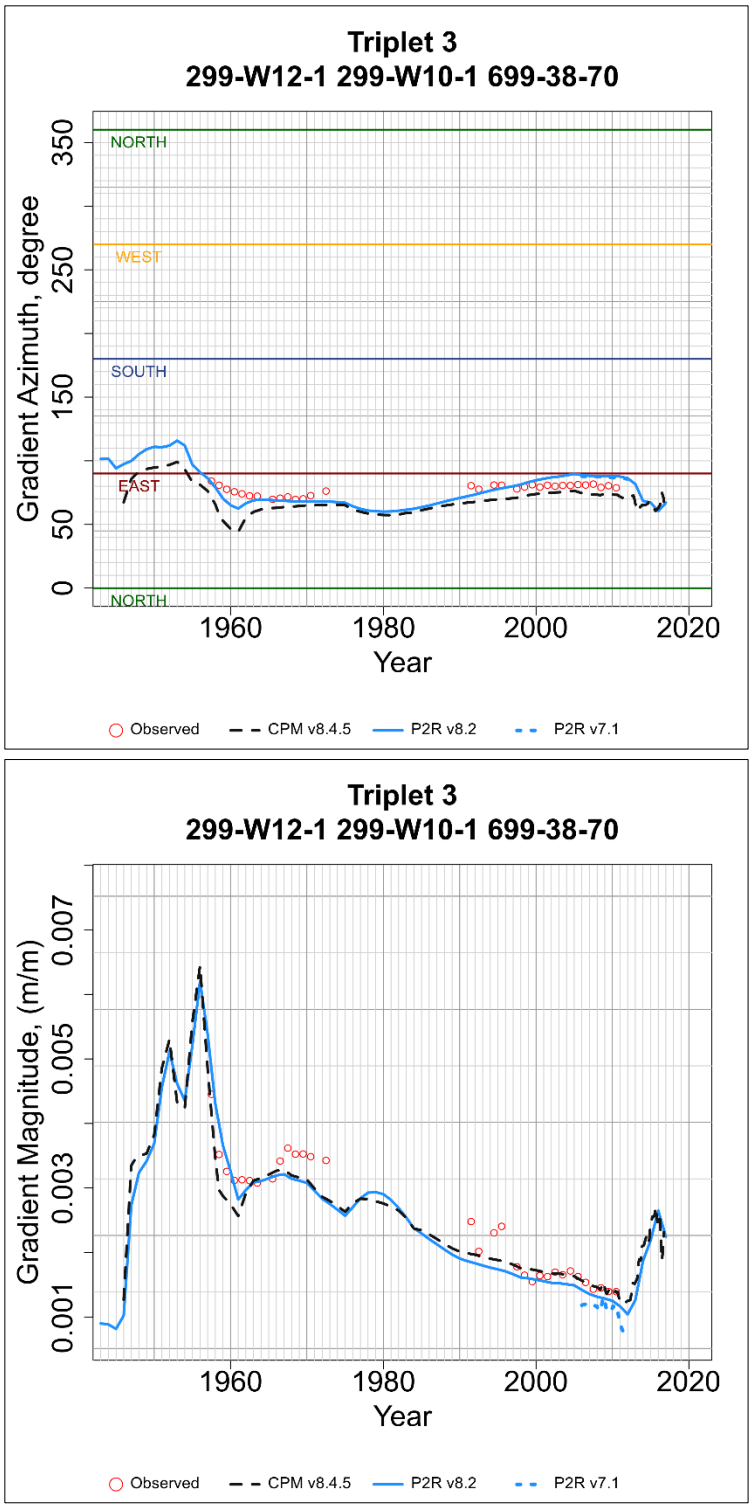

Figure C-3. Observed and simulated hydraulic gradient azimuth and magnitude for well triplet 3.

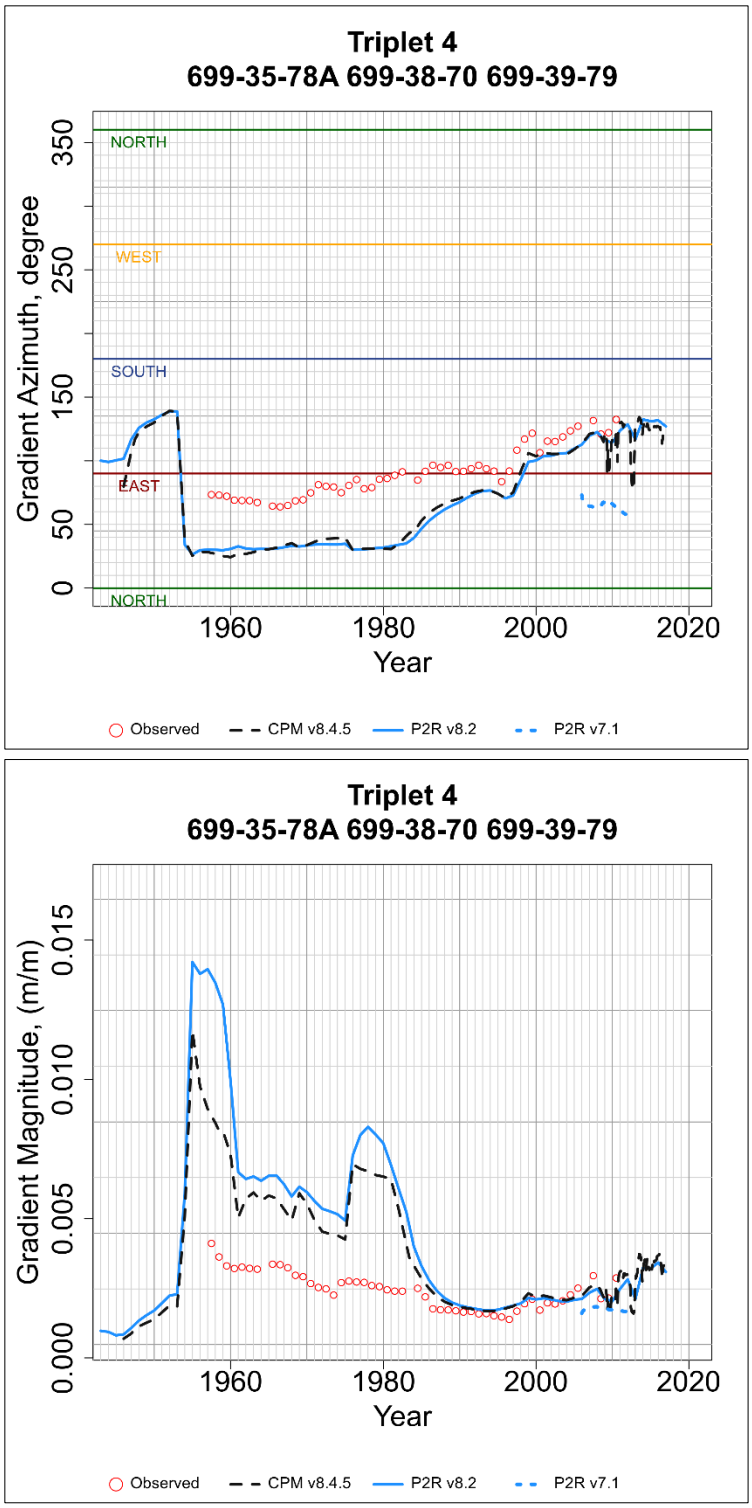

Figure C-4. Observed and simulated hydraulic gradient azimuth and magnitude for well triplet 4.

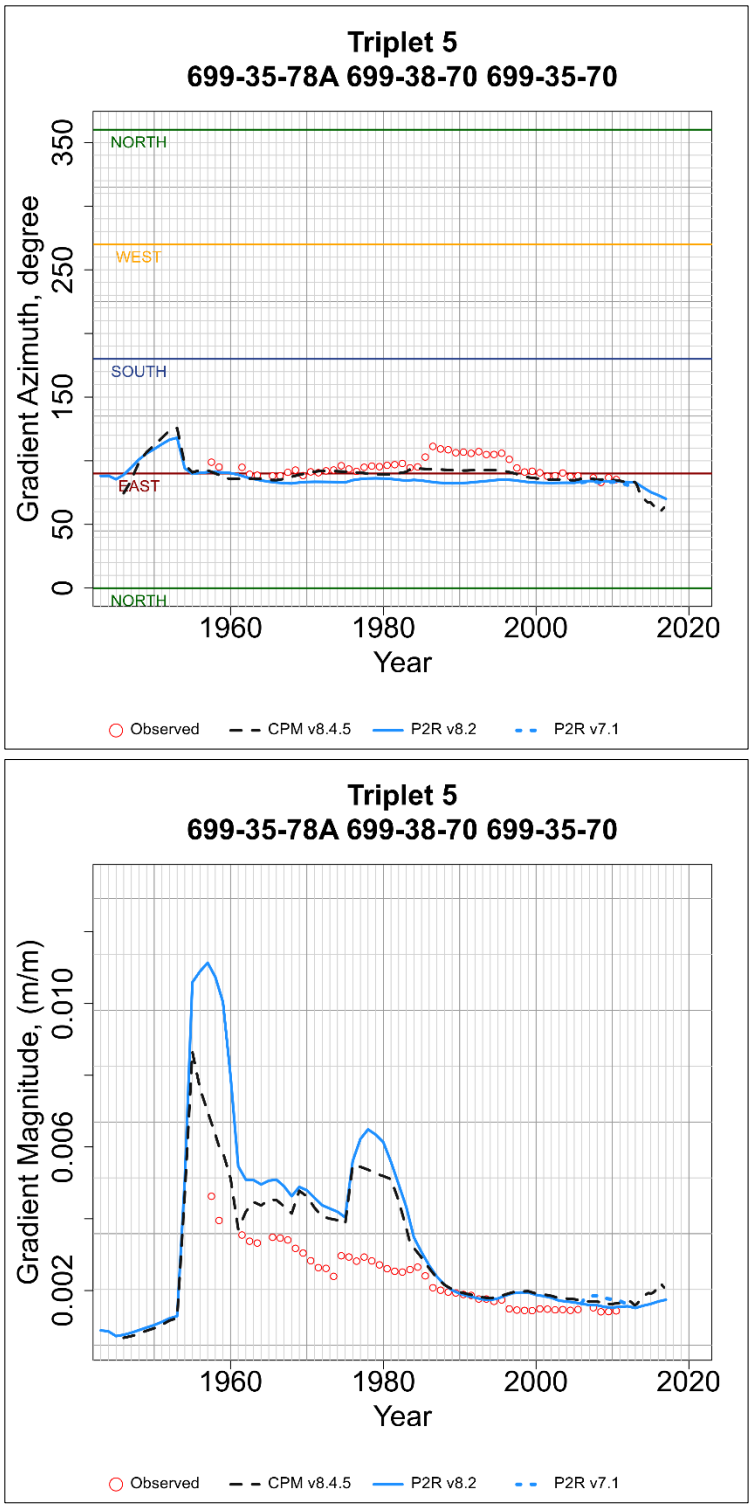

Figure C-5. Observed and simulated hydraulic gradient azimuth and magnitude for well triplet 5.

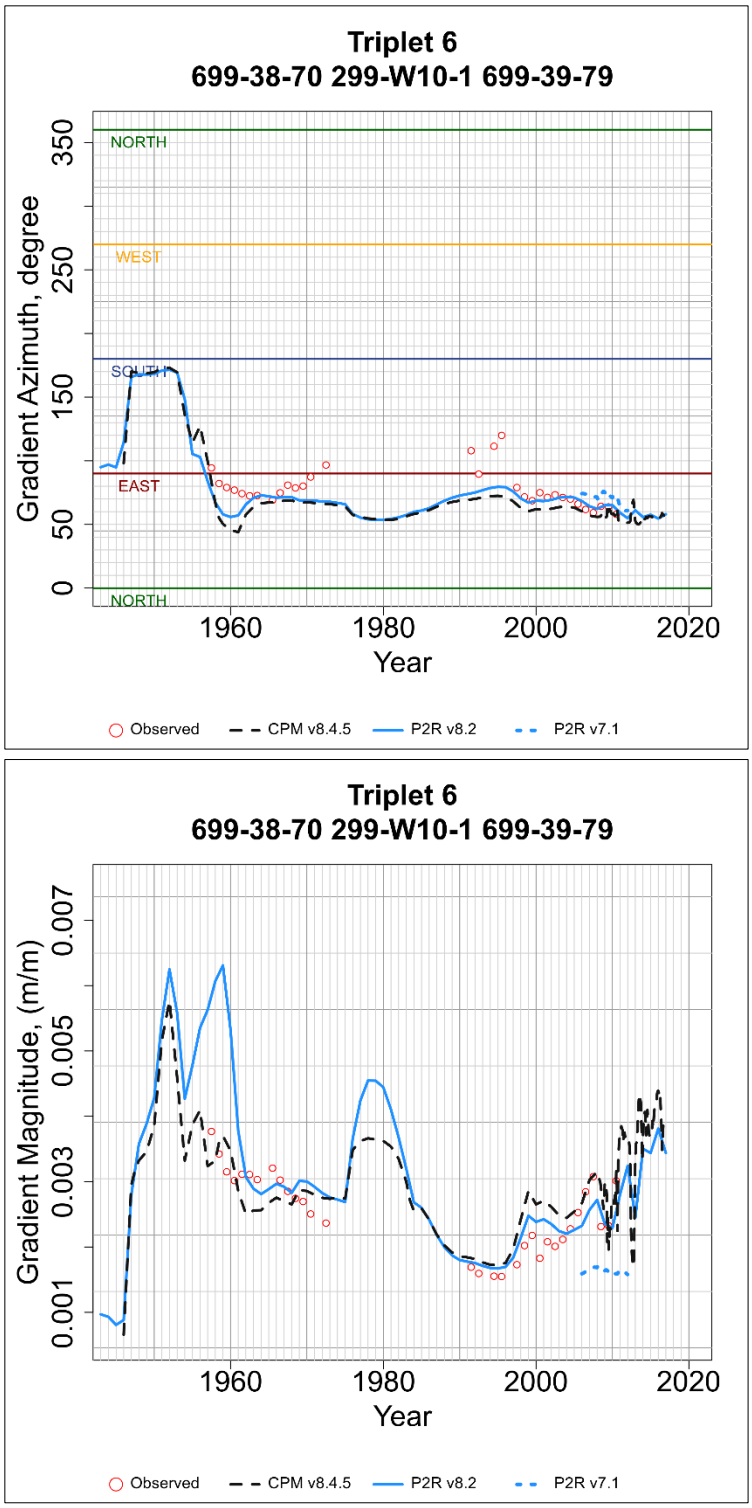

Figure C-6. Observed and simulated hydraulic gradient azimuth and magnitude for well triplet 6.

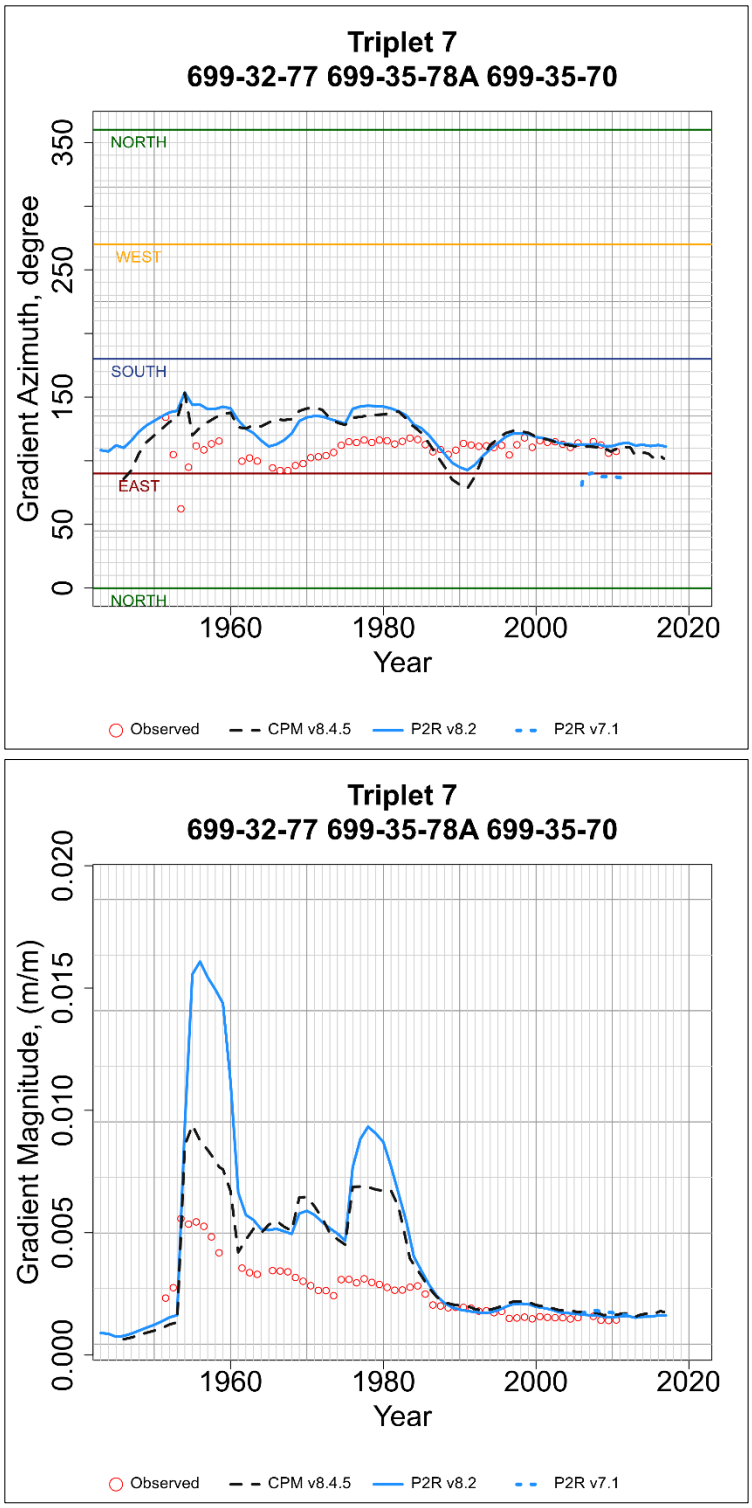

Figure C-7. Observed and simulated hydraulic gradient azimuth and magnitude for well triplet 7.

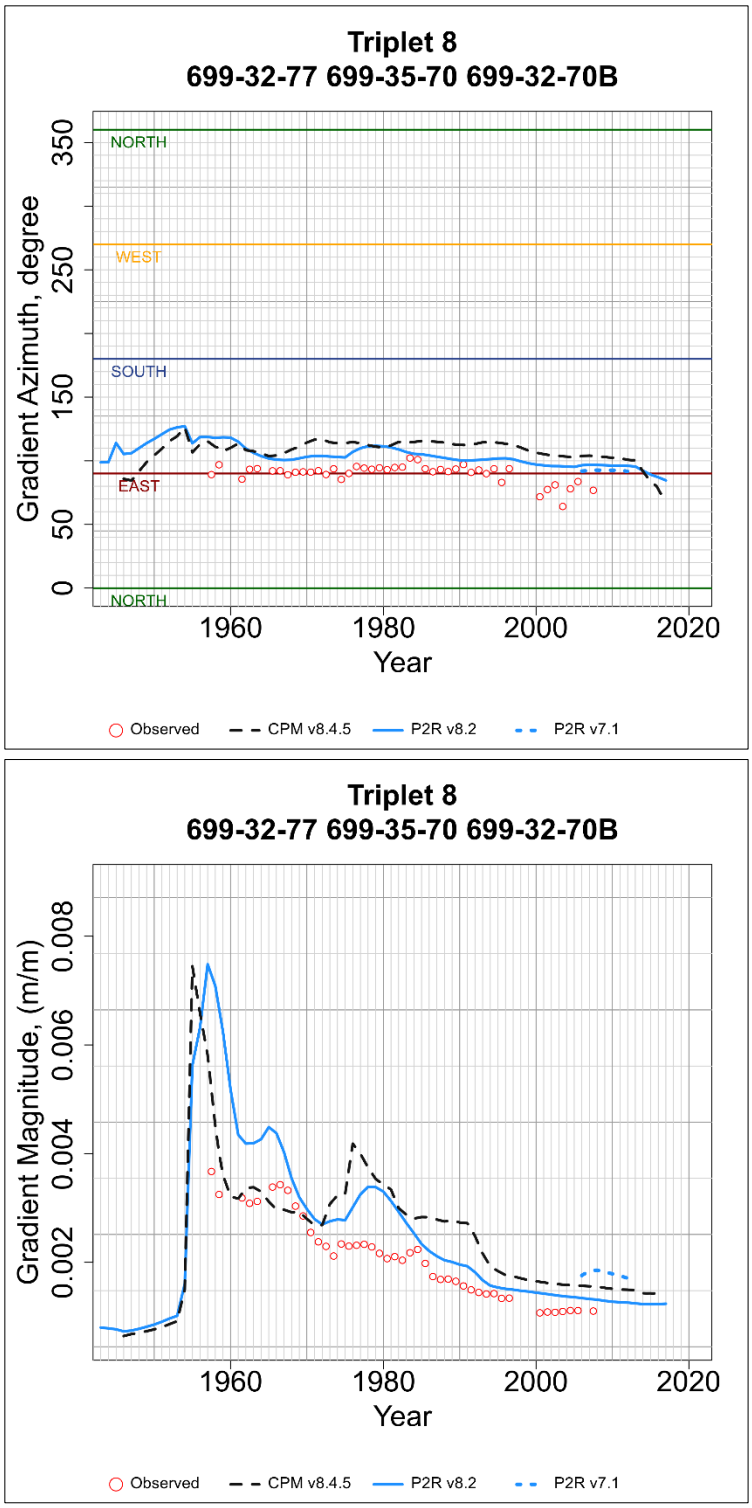

Figure C-8. Observed and simulated hydraulic gradient azimuth and magnitude for well triplet 8.

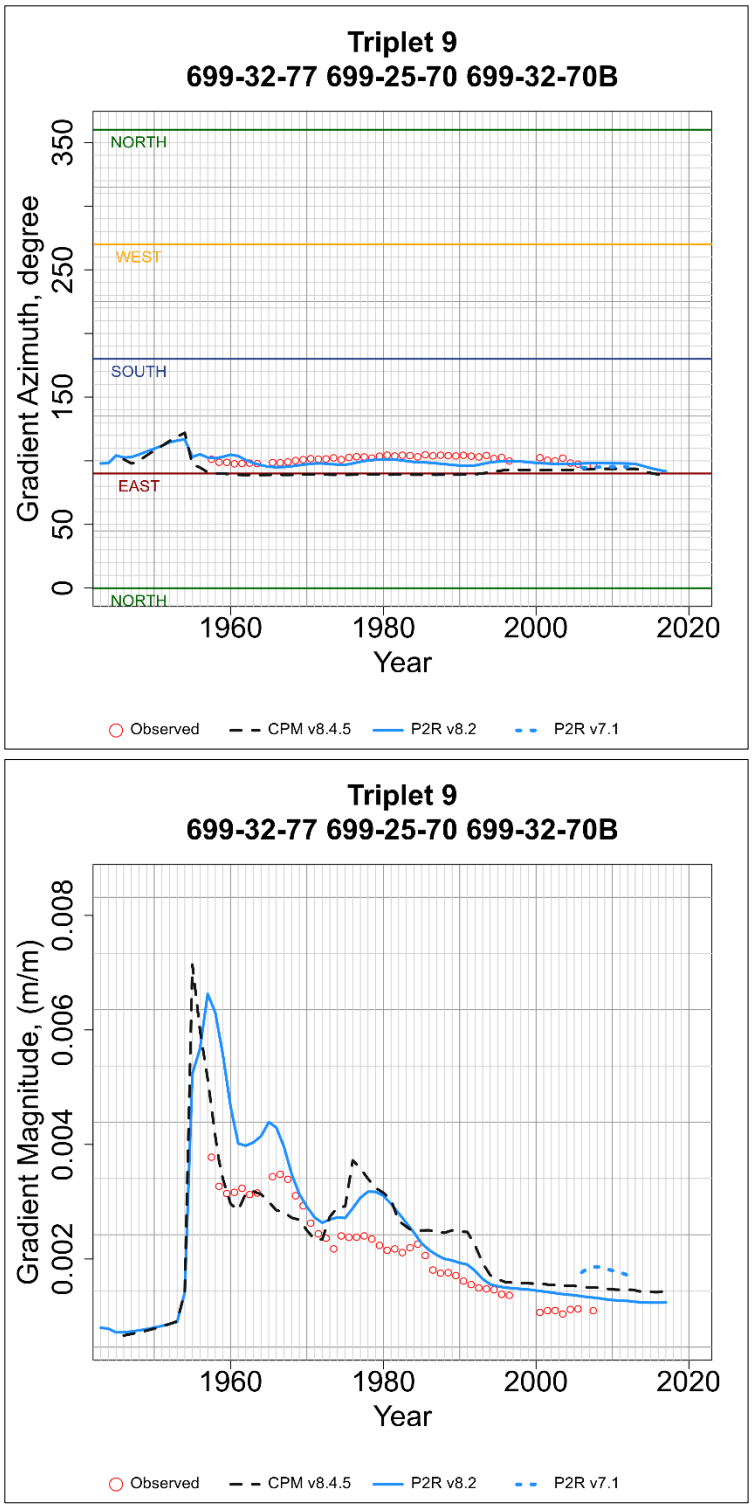

Figure C-9. Observed and simulated hydraulic gradient azimuth and magnitude for well triplet 9.

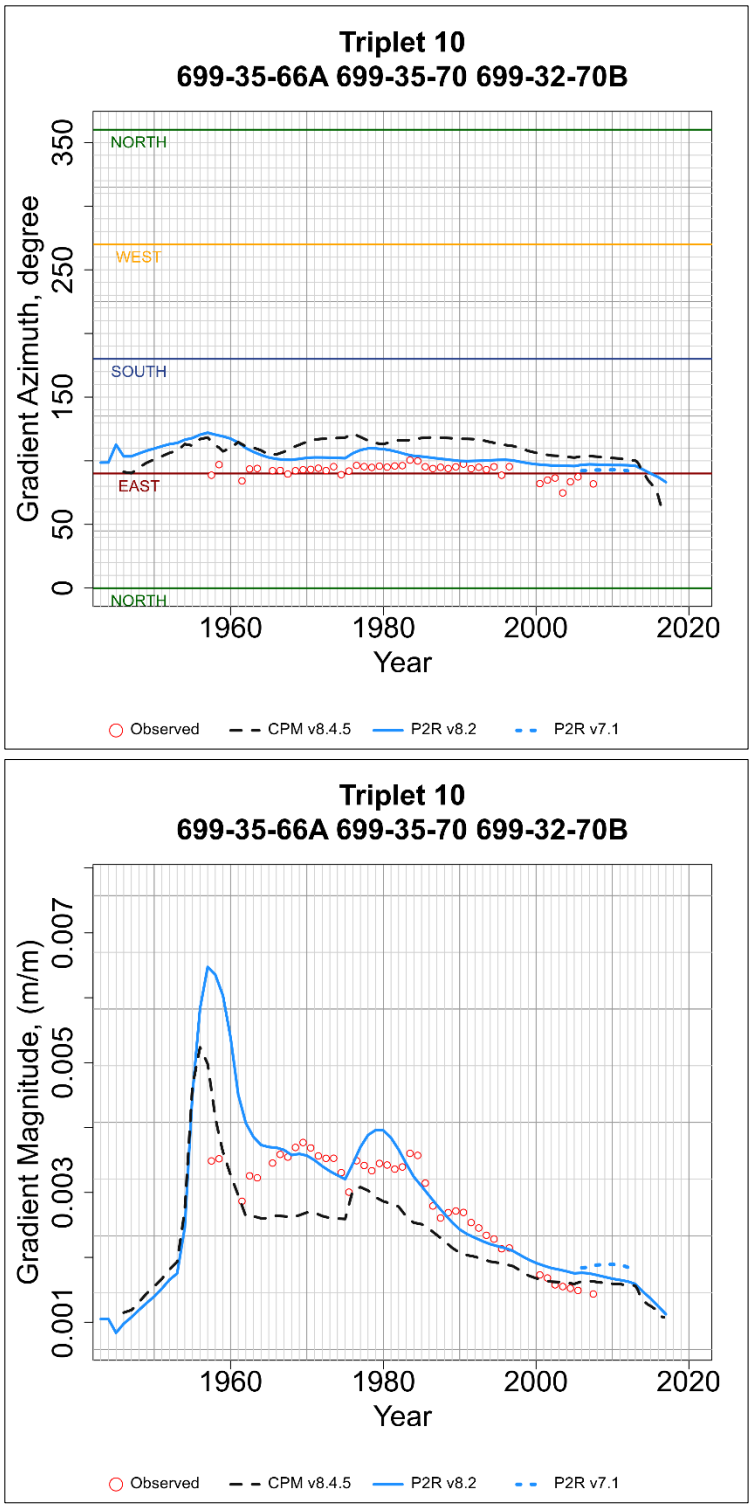

Figure C-10. Observed and simulated hydraulic gradient azimuth and magnitude for well triplet 10.

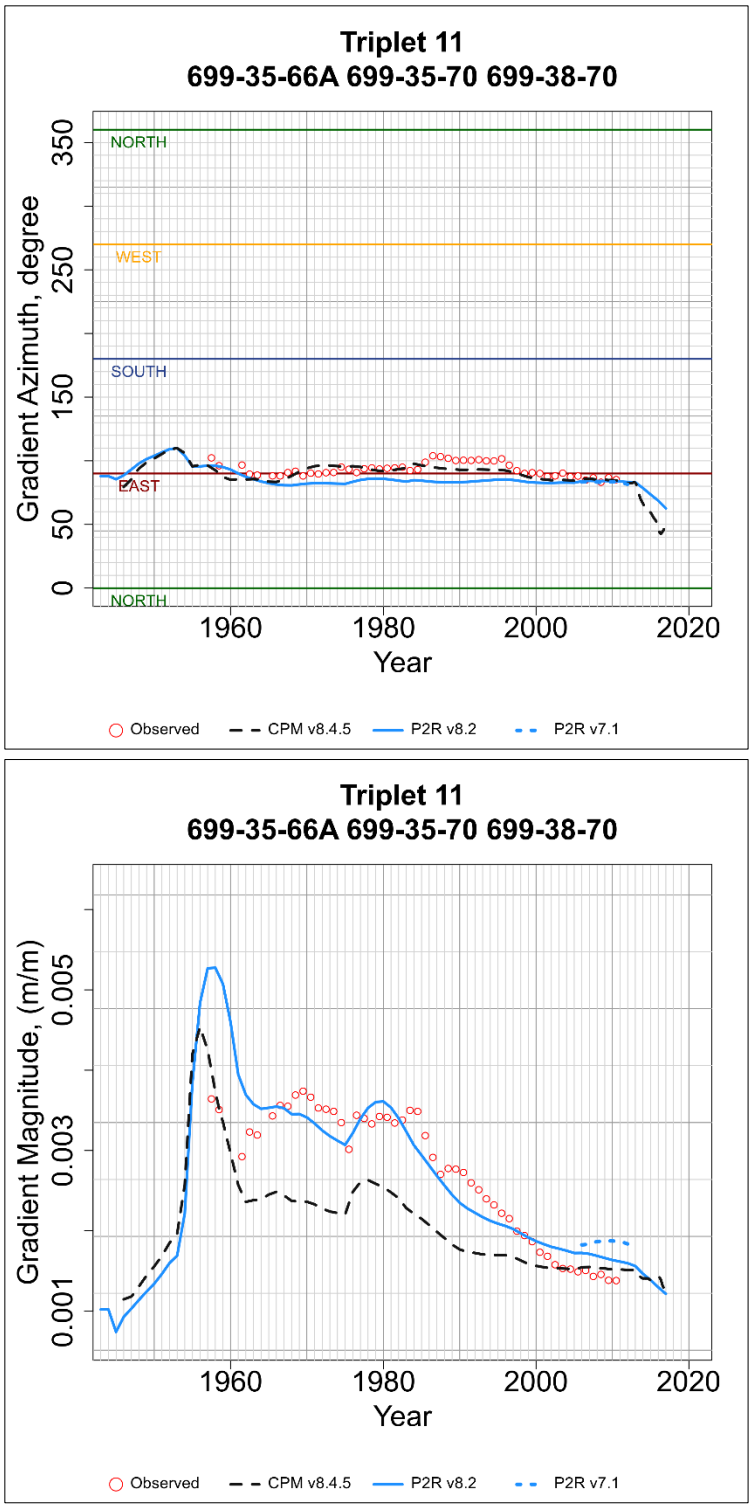

Figure C-11. Observed and simulated hydraulic gradient azimuth and magnitude for well triplet 11.

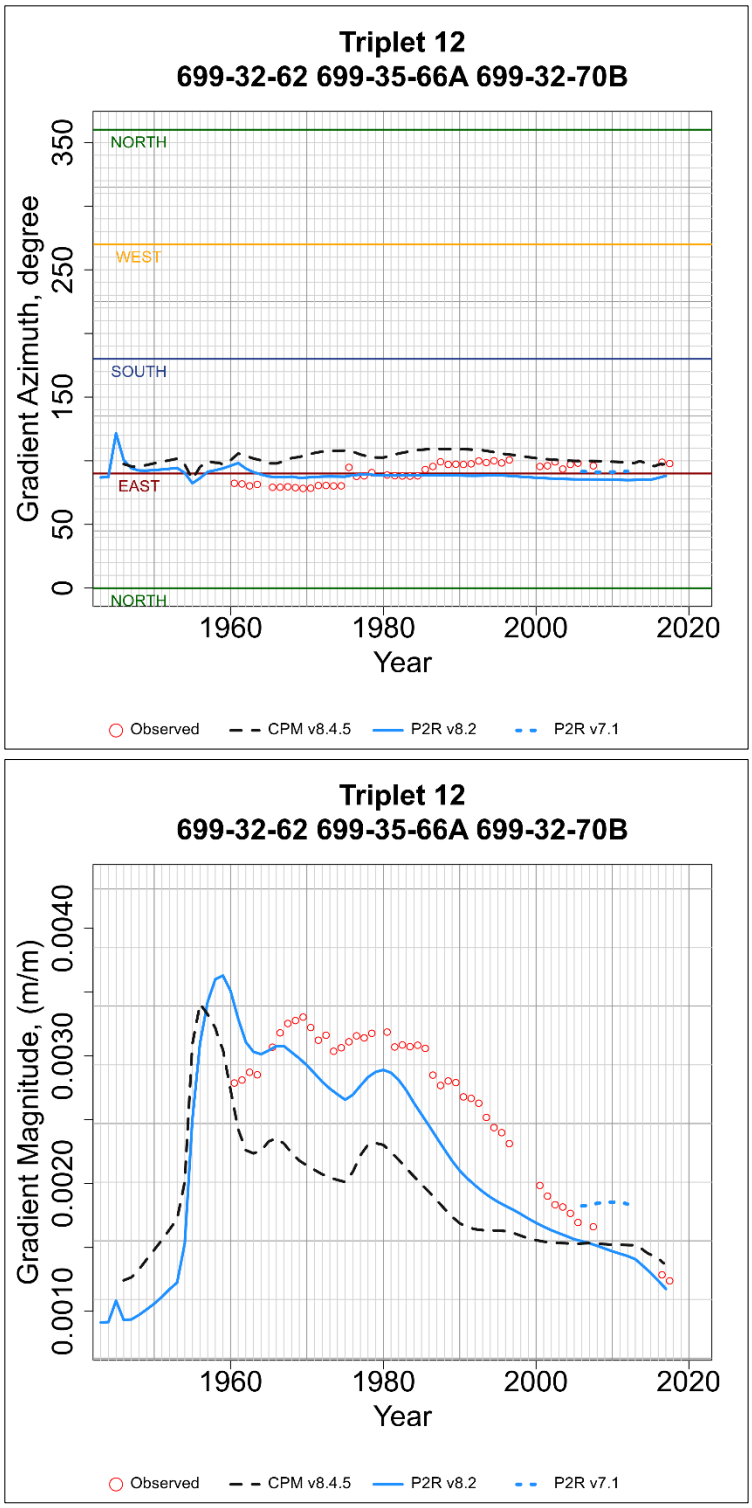

Figure C-12. Observed and simulated hydraulic gradient azimuth and magnitude for well triplet 12.

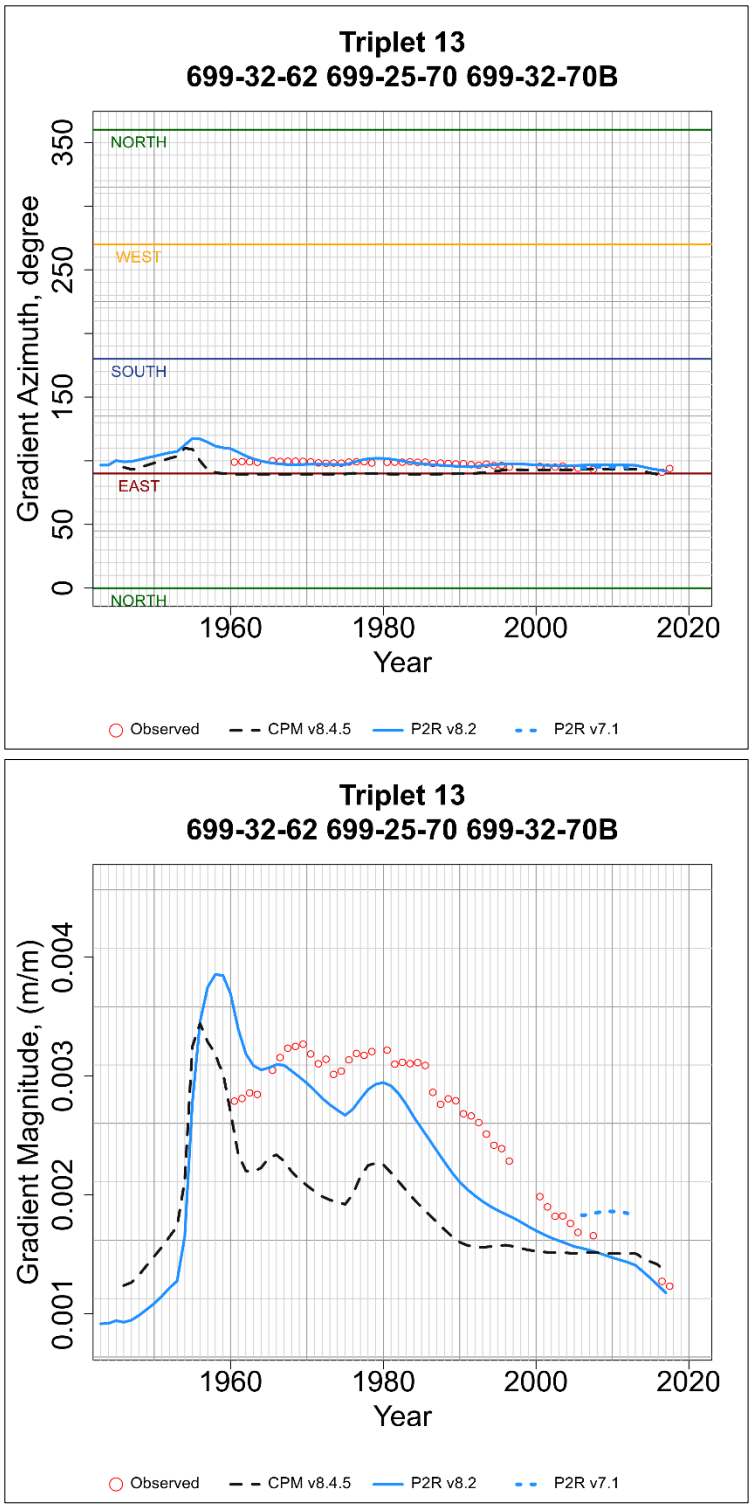

Figure C-13. Observed and simulated hydraulic gradient azimuth and magnitude for well triplet 13.

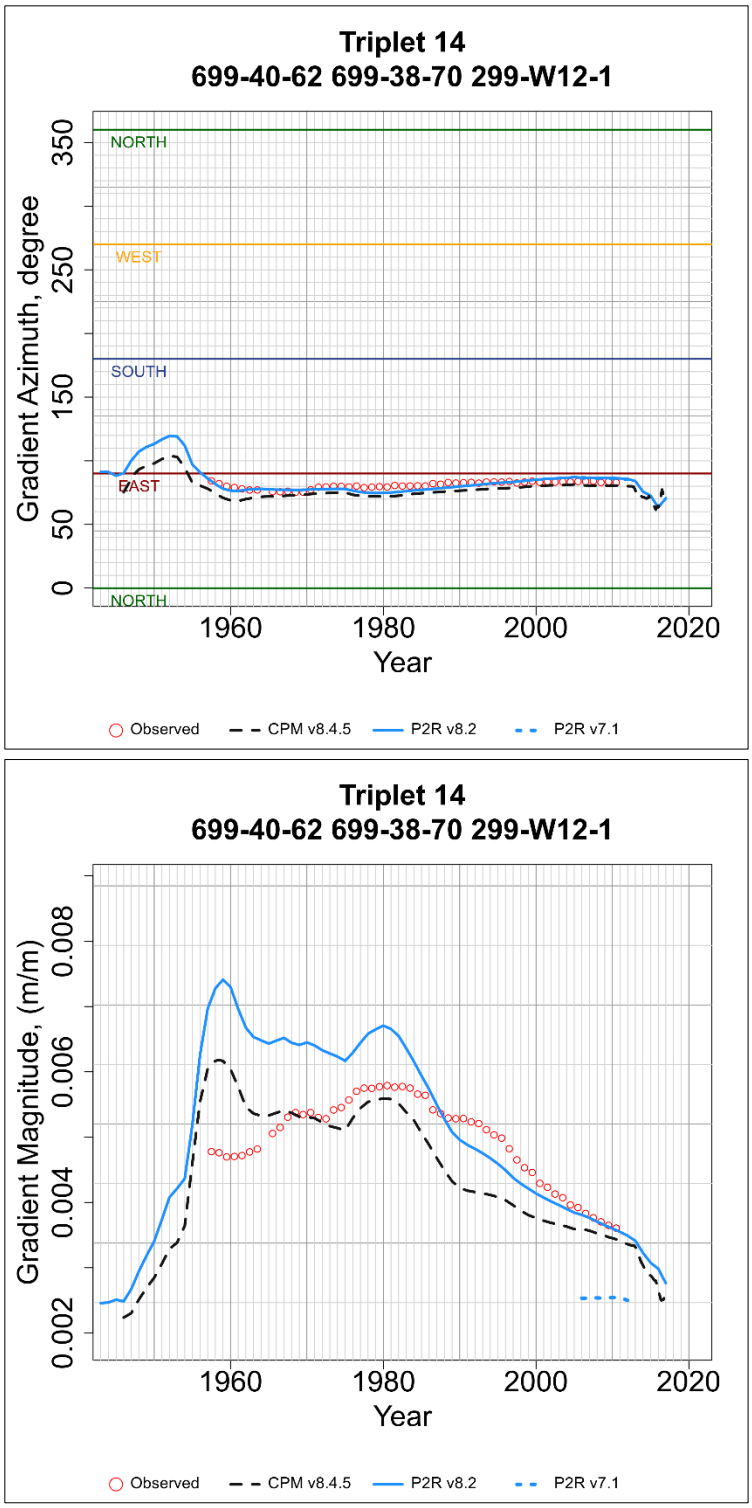

Figure C-14. Observed and simulated hydraulic gradient azimuth and magnitude for well triplet 14.

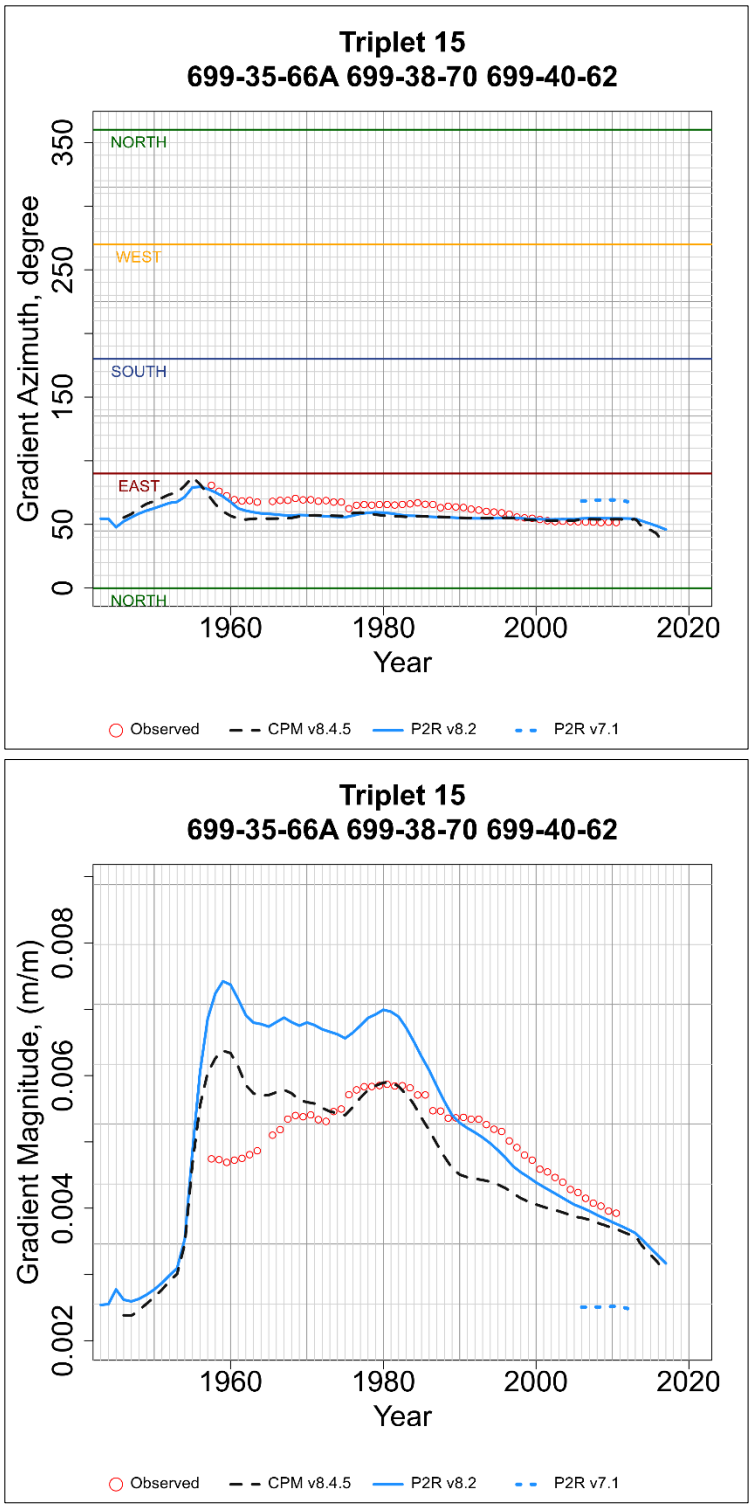

Figure C-15. Observed and simulated hydraulic gradient azimuth and magnitude for well triplet 15.

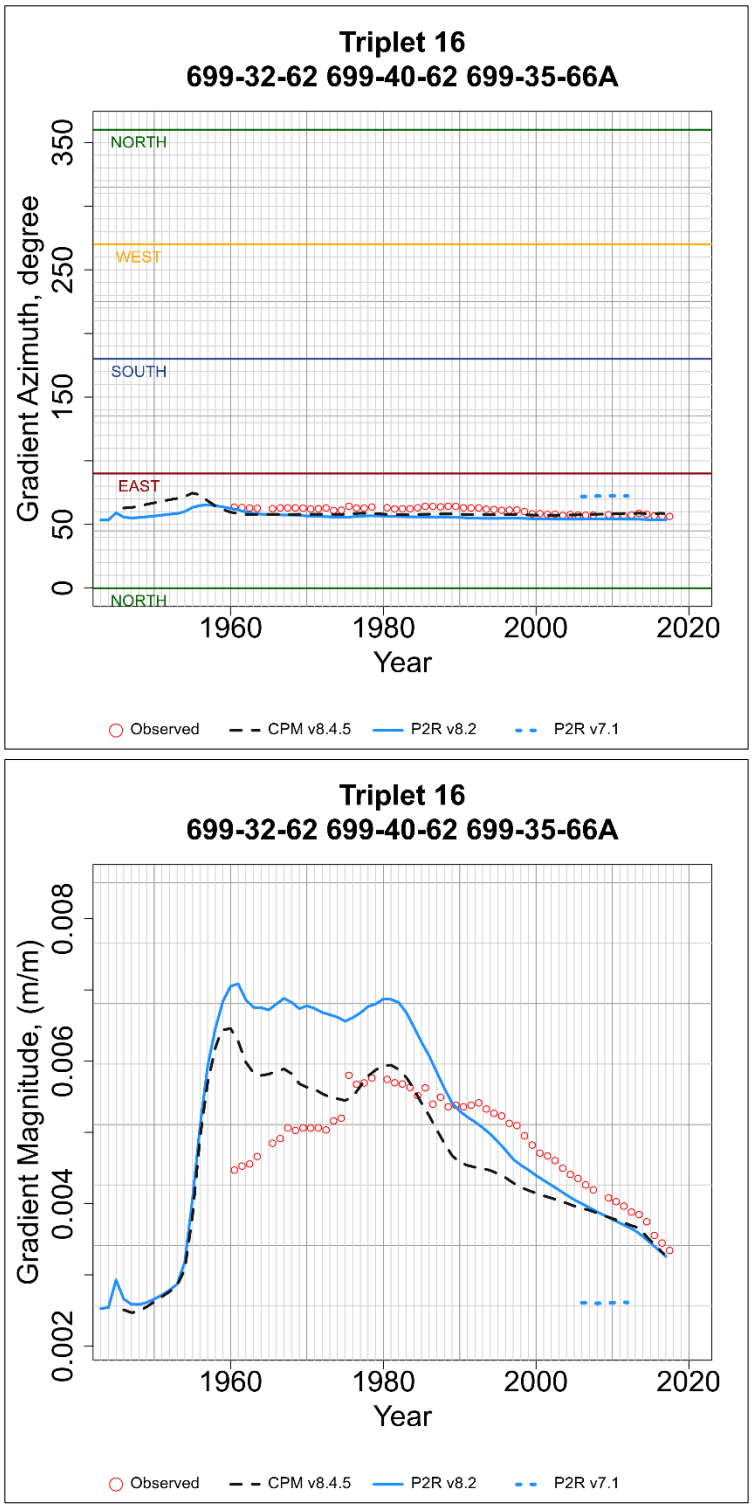

Figure C-16. Observed and simulated hydraulic gradient azimuth and magnitude for well triplet 16.

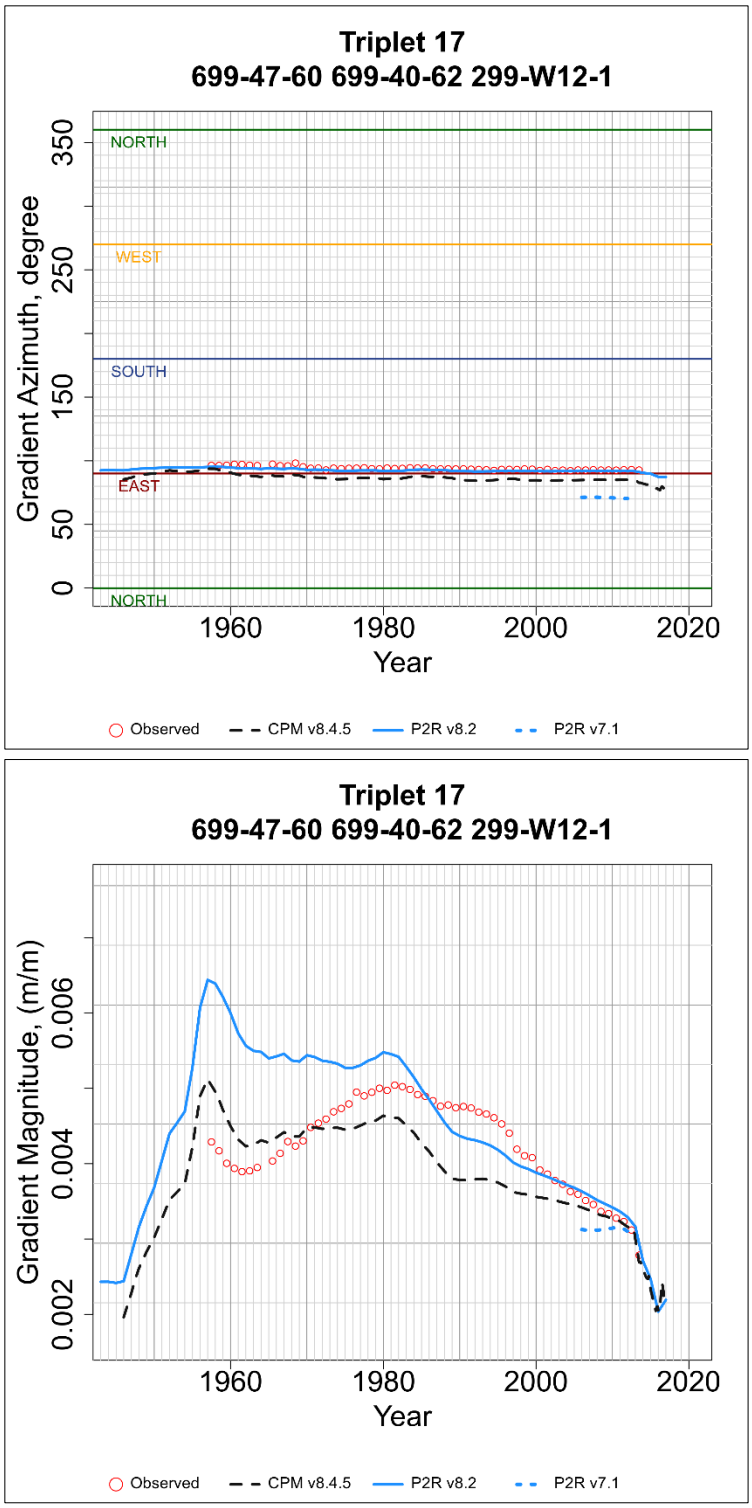

Figure C-17. Observed and simulated hydraulic gradient azimuth and magnitude for well triplet 17.

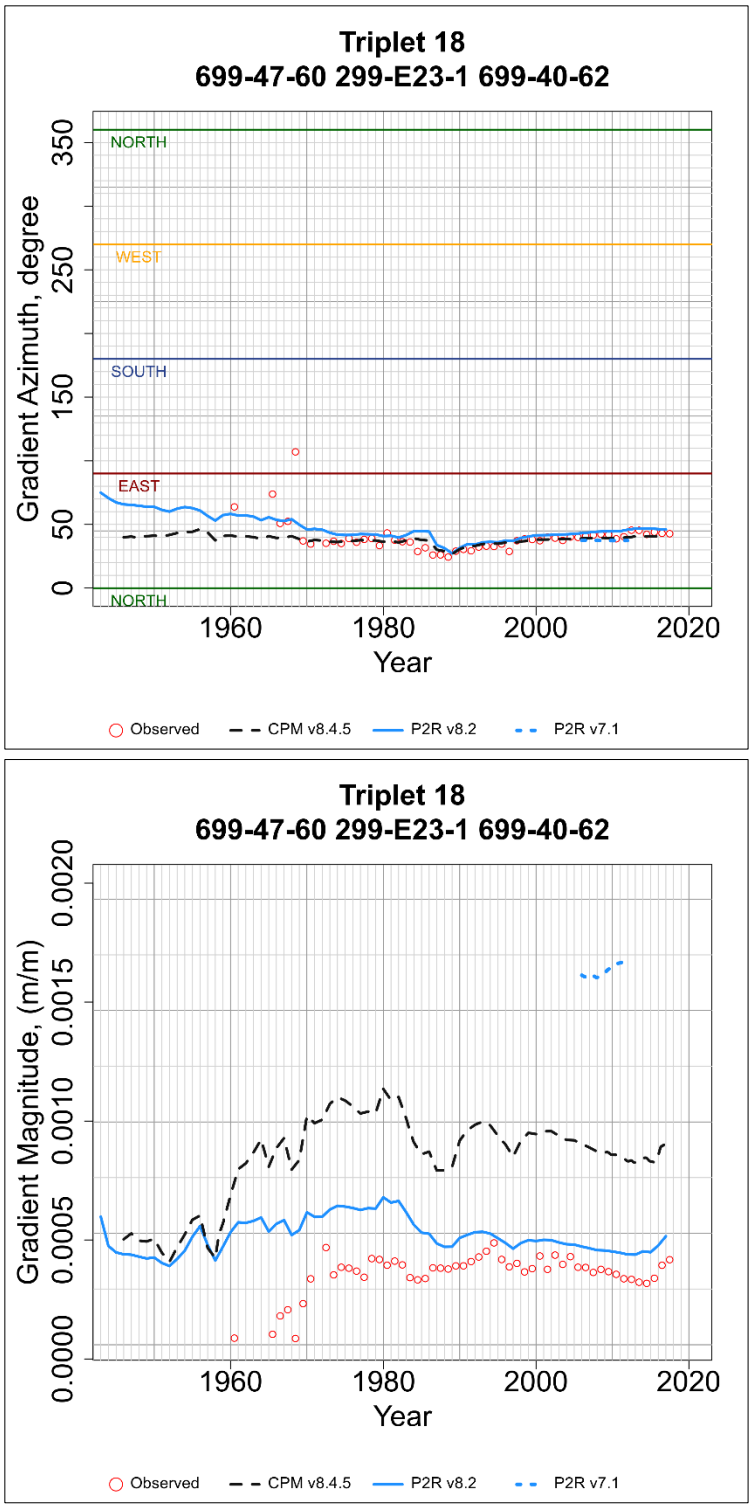

Figure C-18. Observed and simulated hydraulic gradient azimuth and magnitude for well triplet 18.

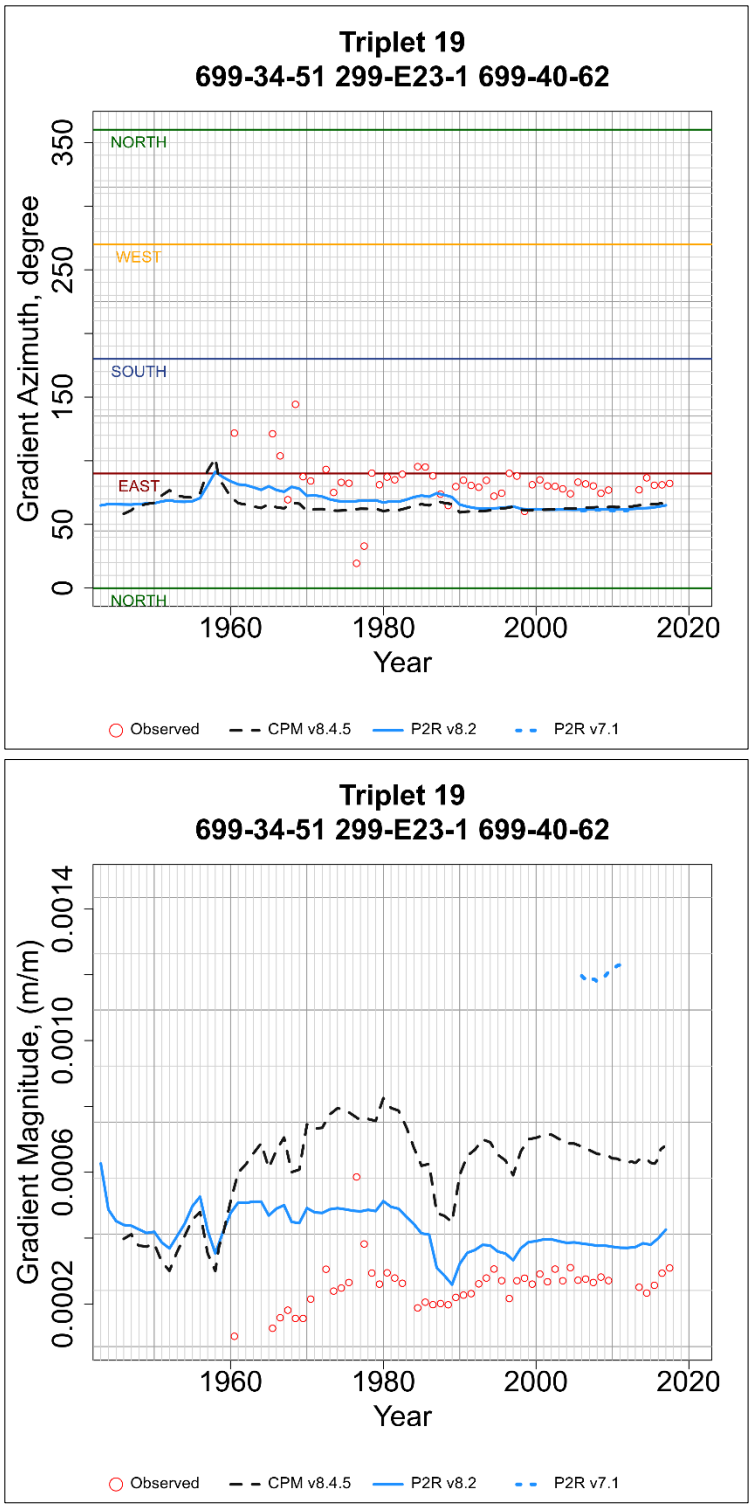

Figure C-19. Observed and simulated hydraulic gradient azimuth and magnitude for well triplet 19.

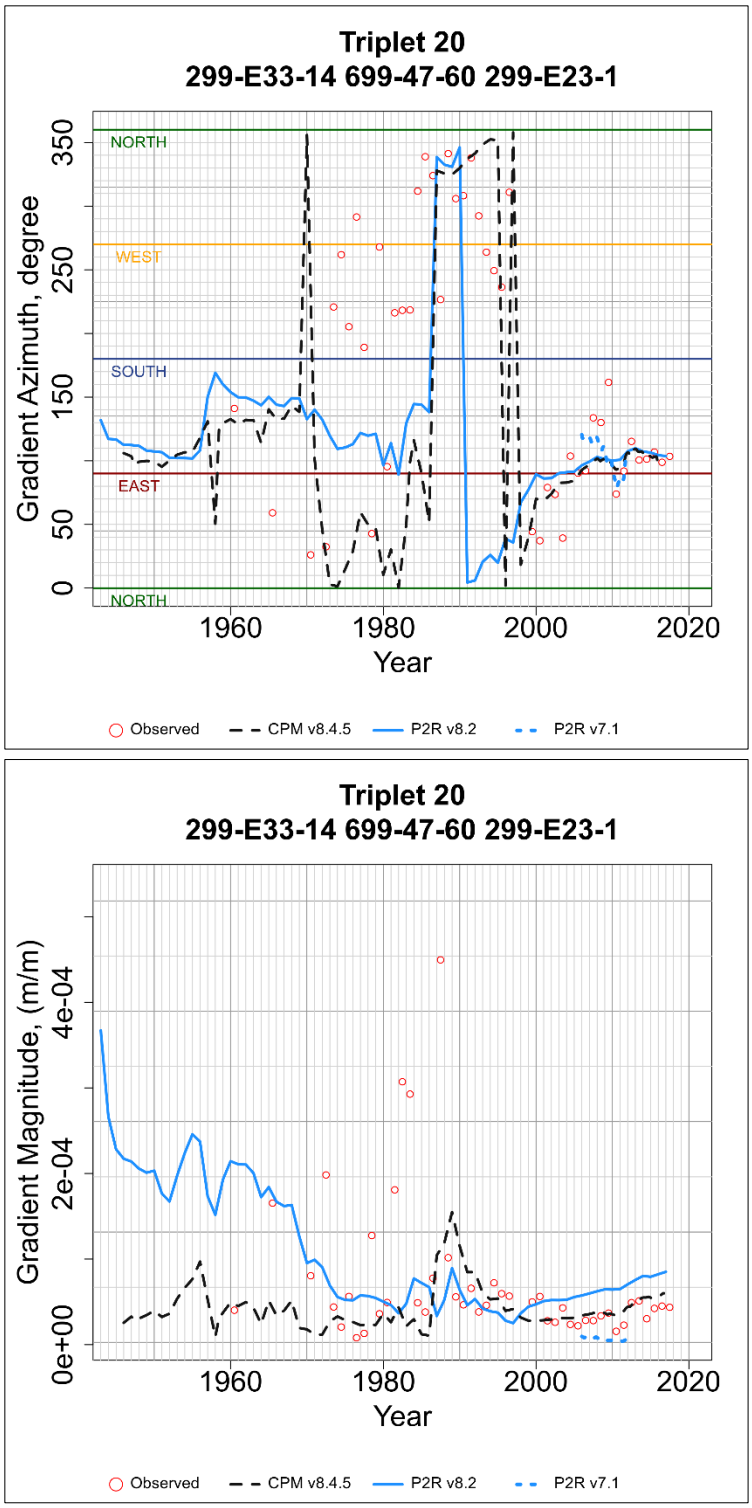

Figure C-20. Observed and simulated hydraulic gradient azimuth and magnitude for well triplet 20.

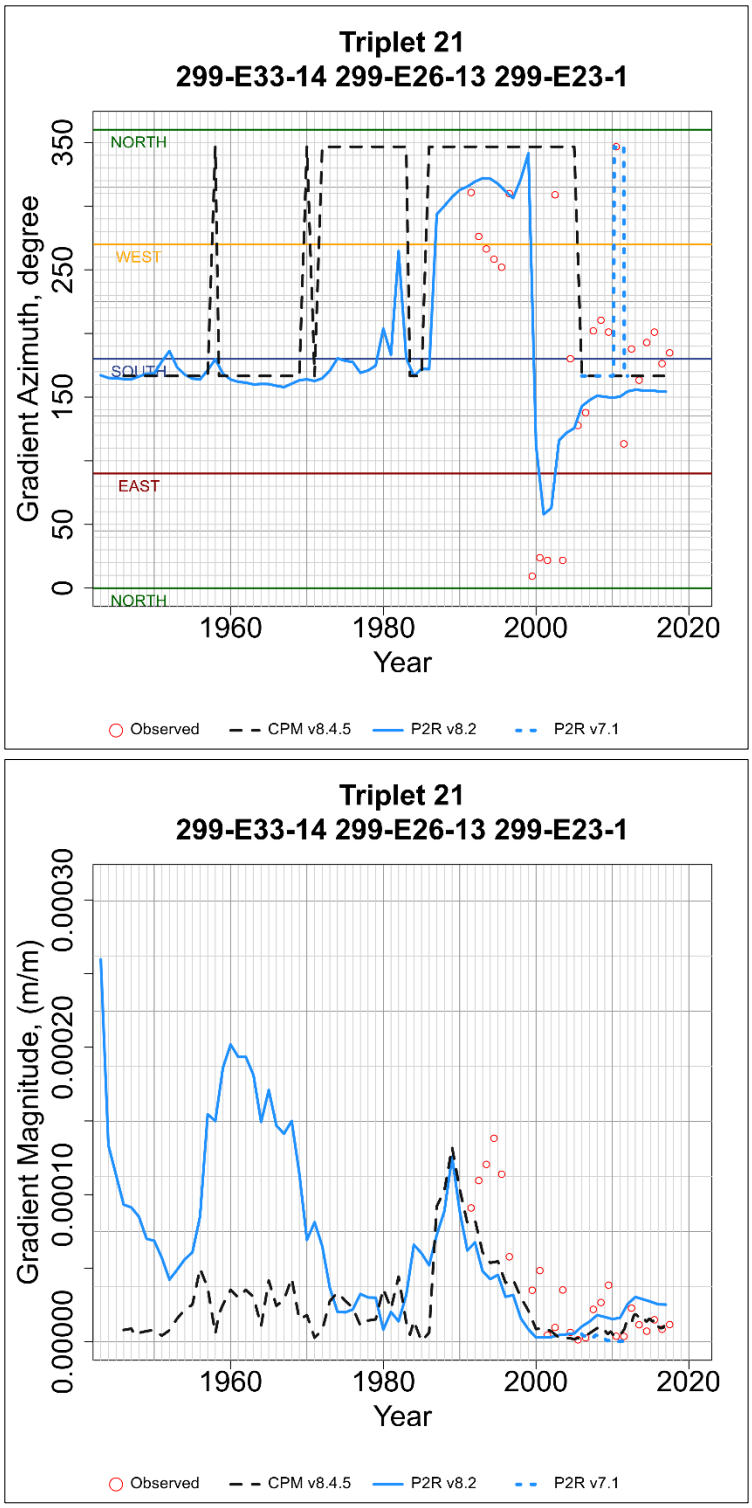

Figure C-21. Observed and simulated hydraulic gradient azimuth and magnitude for well triplet 21.

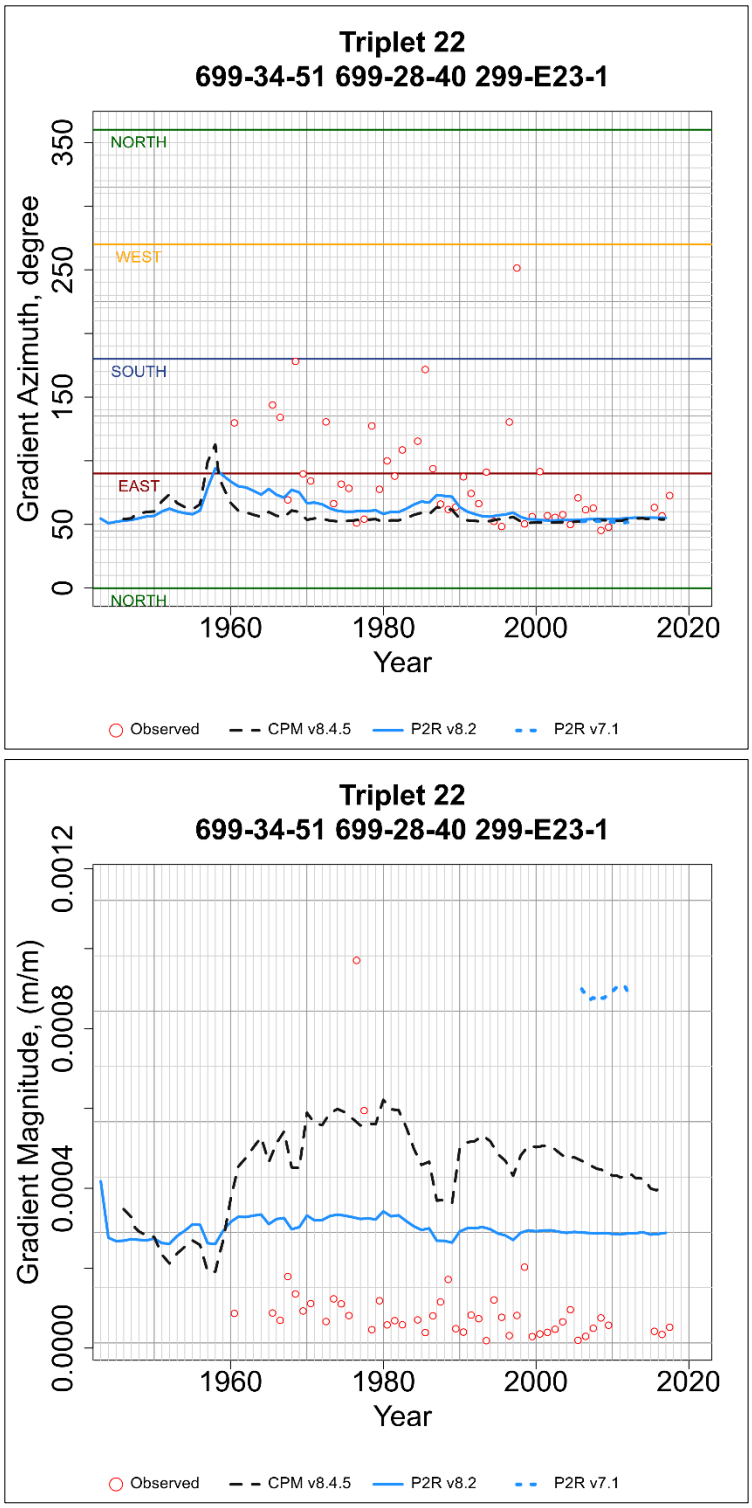

Figure C-22. Observed and simulated hydraulic gradient azimuth and magnitude for well triplet 22.

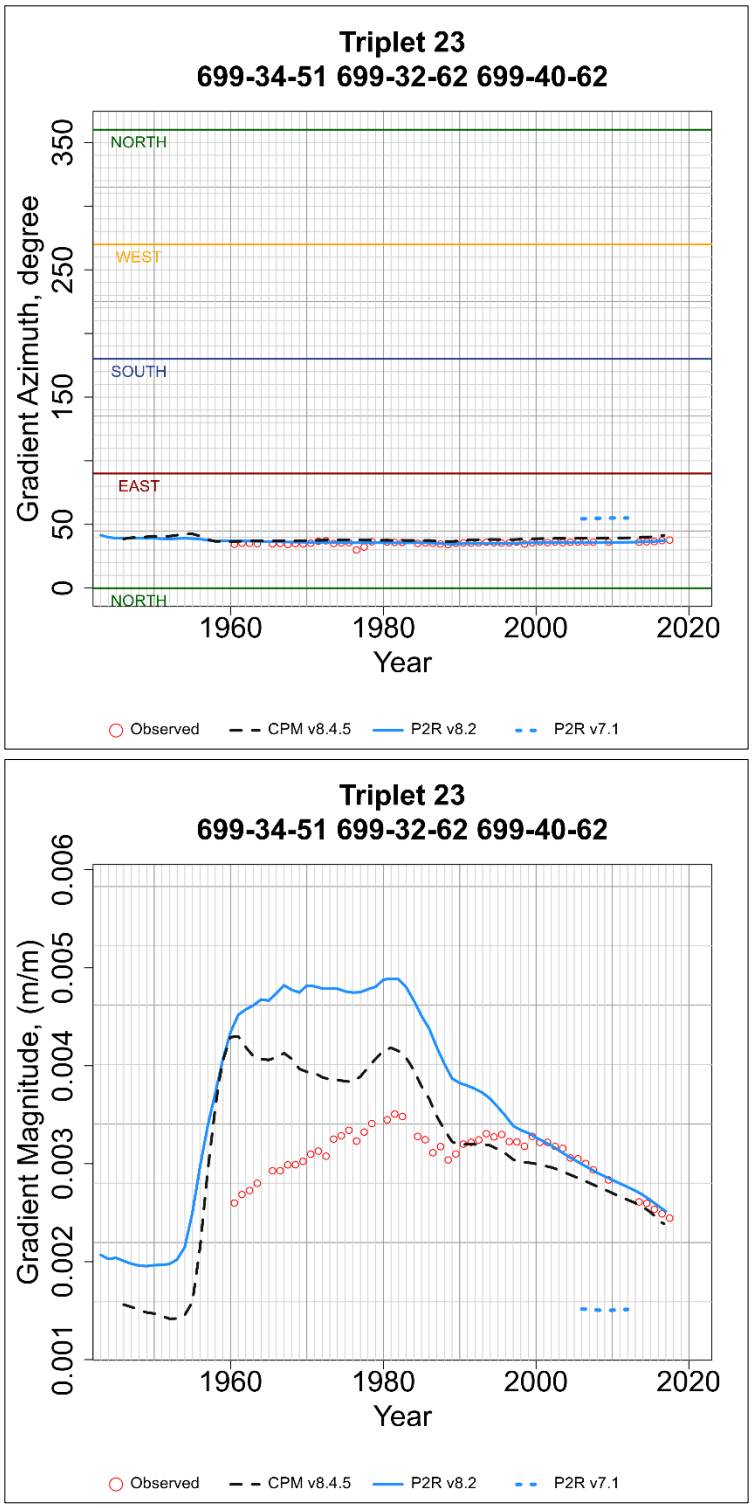

Figure C-23. Observed and simulated hydraulic gradient azimuth and magnitude for well triplet 23.

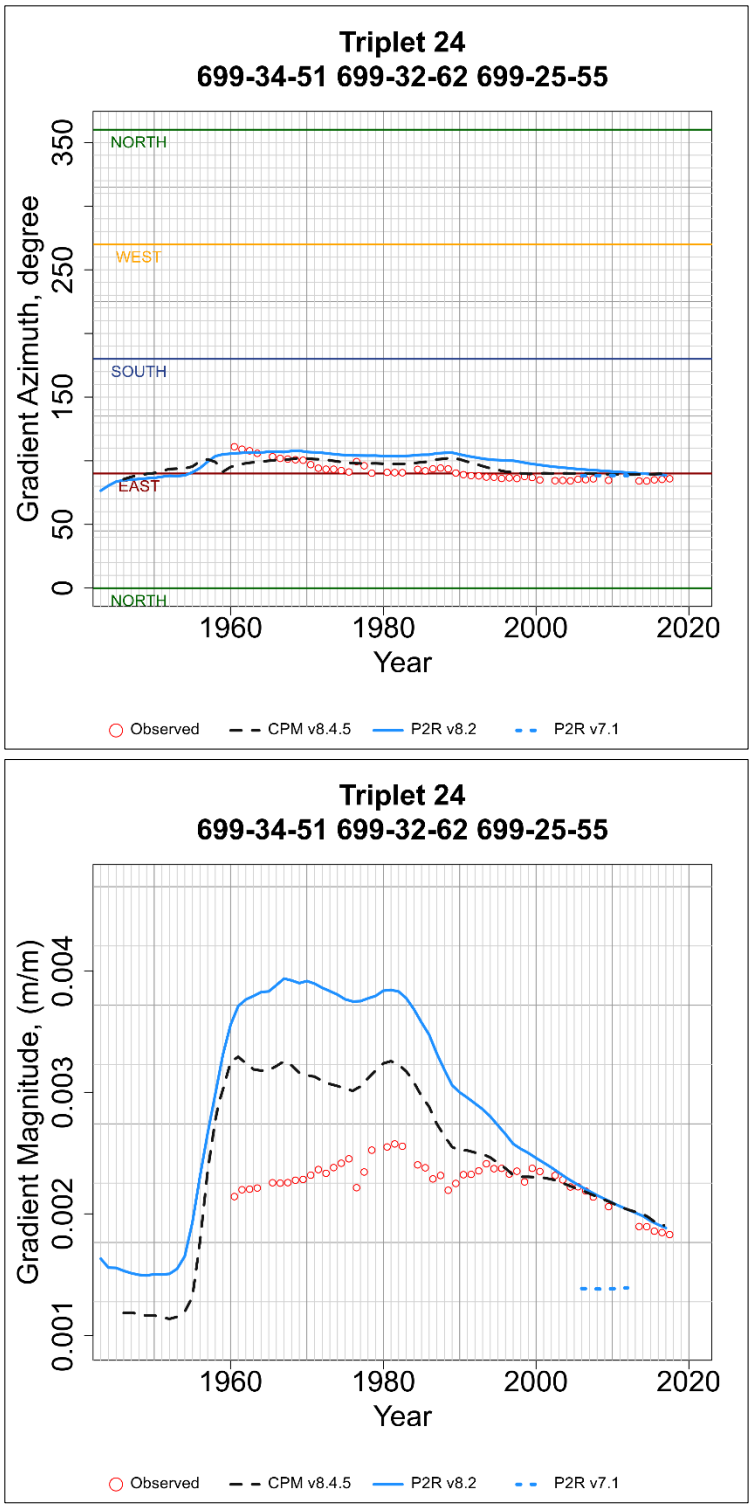

Figure C-24. Observed and simulated hydraulic gradient azimuth and magnitude for well triplet 24.

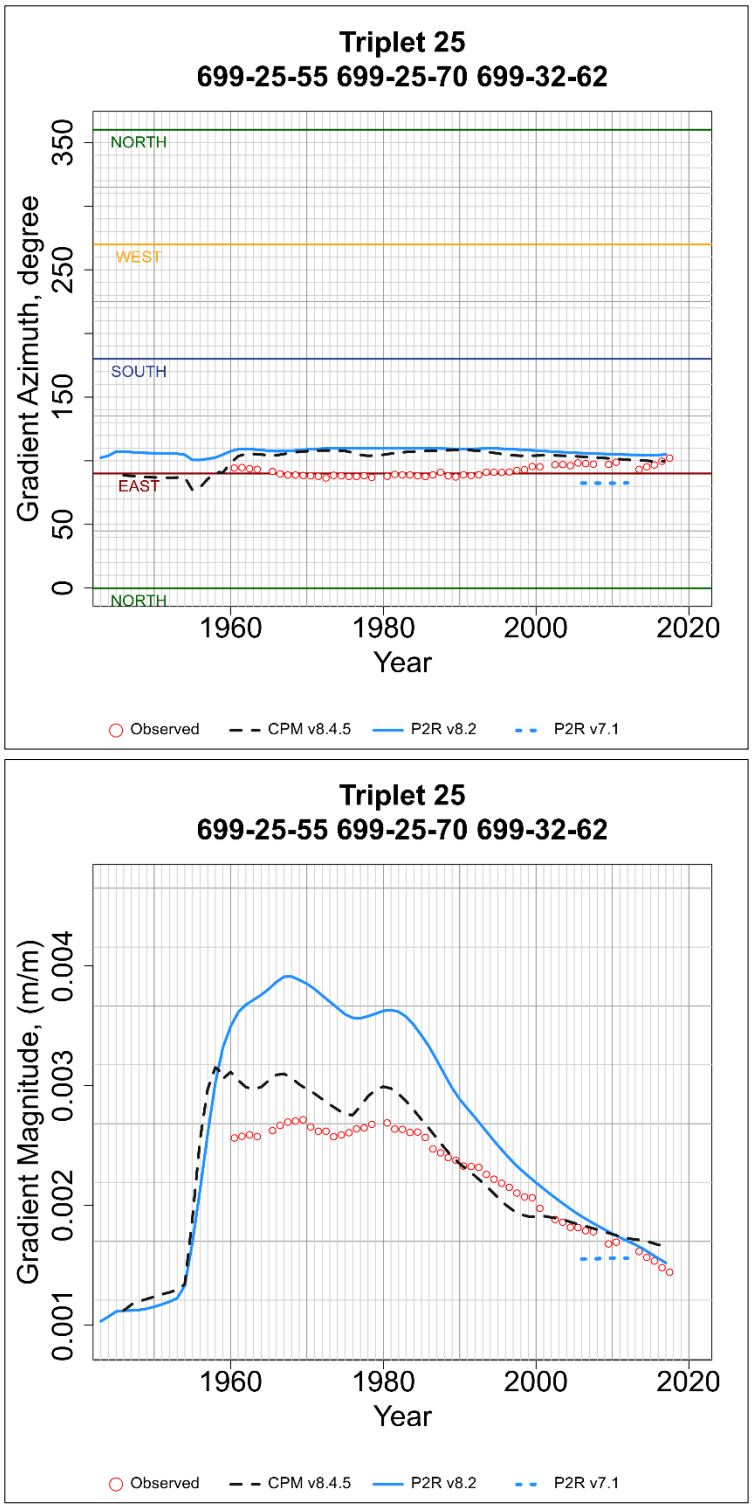

Figure C-25. Observed and simulated hydraulic gradient azimuth and magnitude for well triplet 25.

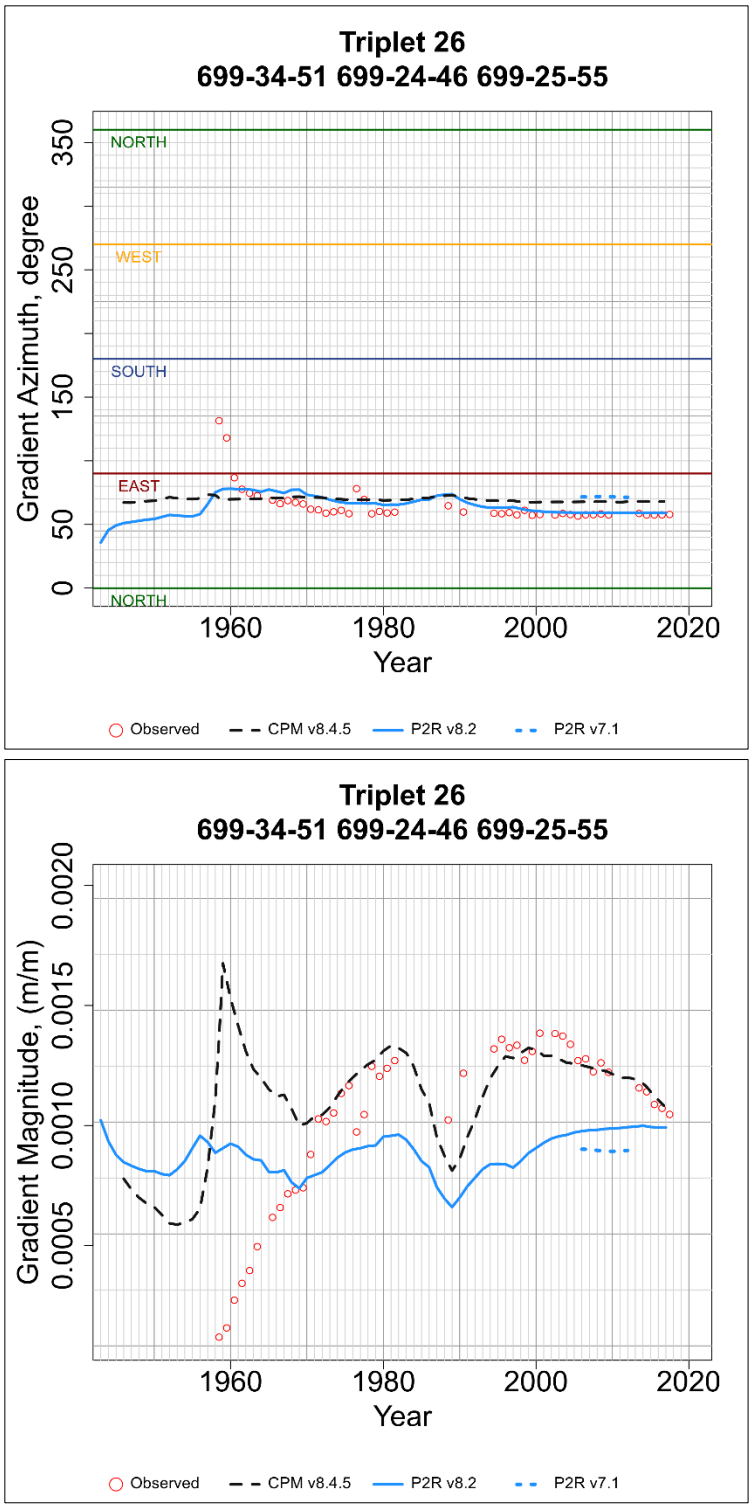

Figure C-26. Observed and simulated hydraulic gradient azimuth and magnitude for well triplet 26.

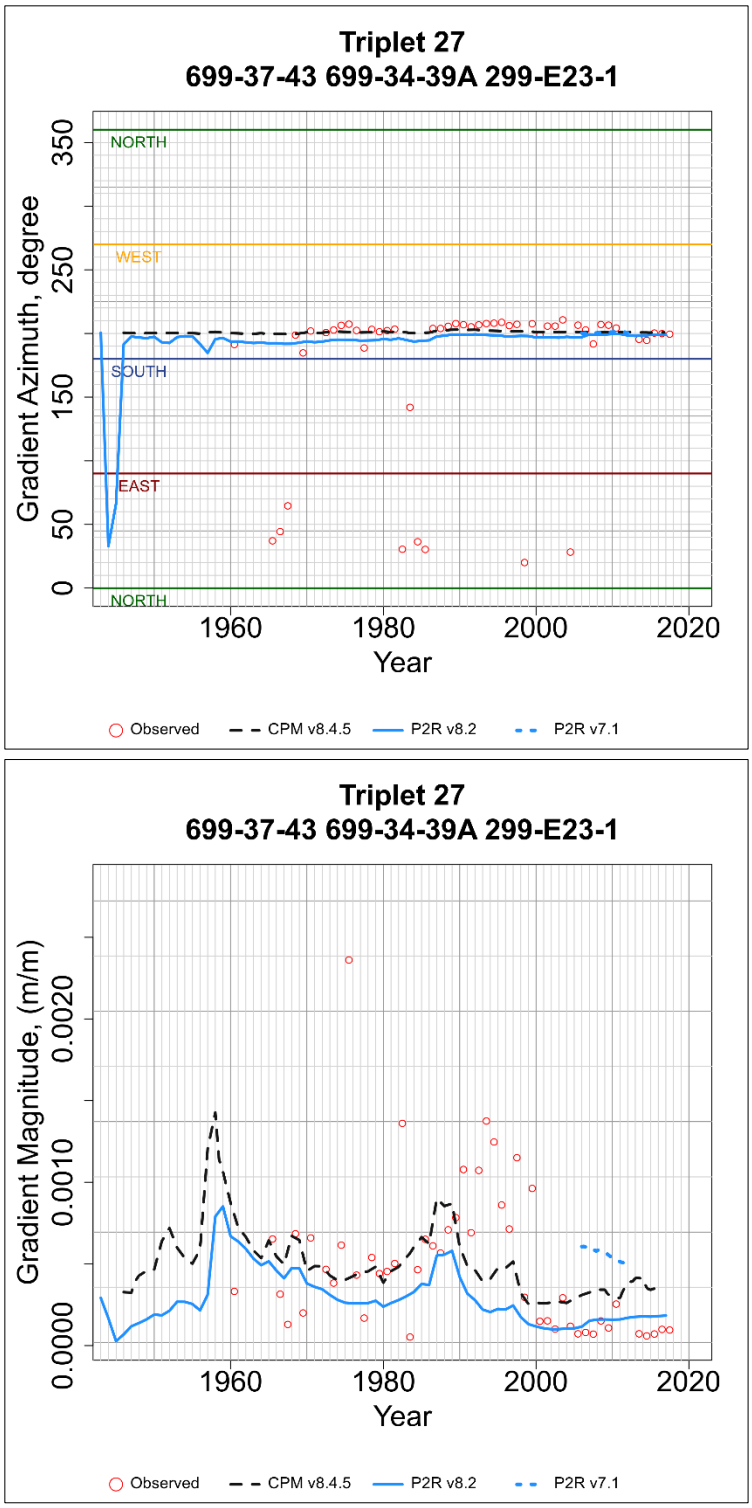

Figure C-27. Observed and simulated hydraulic gradient azimuth and magnitude for well triplet 27.

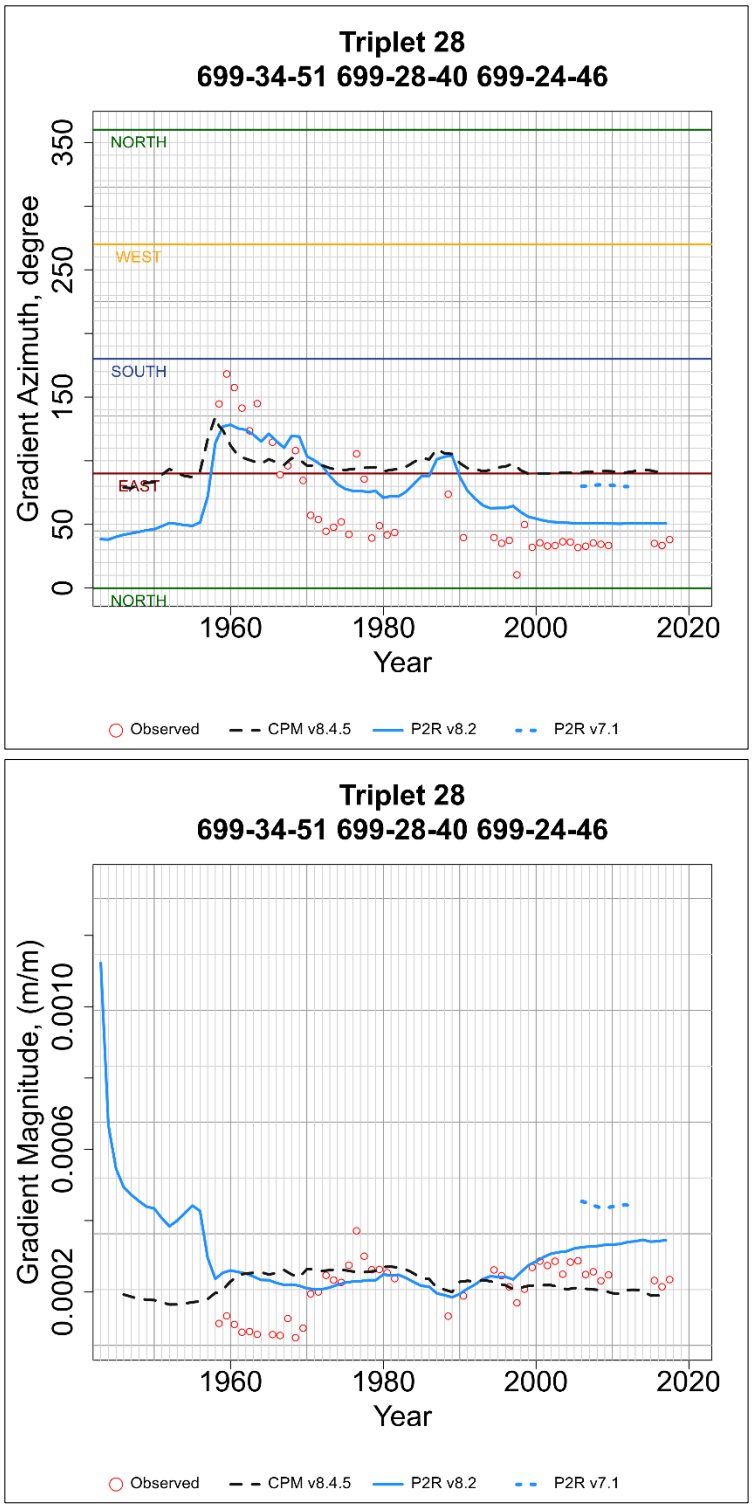

Figure C-28. Observed and simulated hydraulic gradient azimuth and magnitude for well triplet 28.

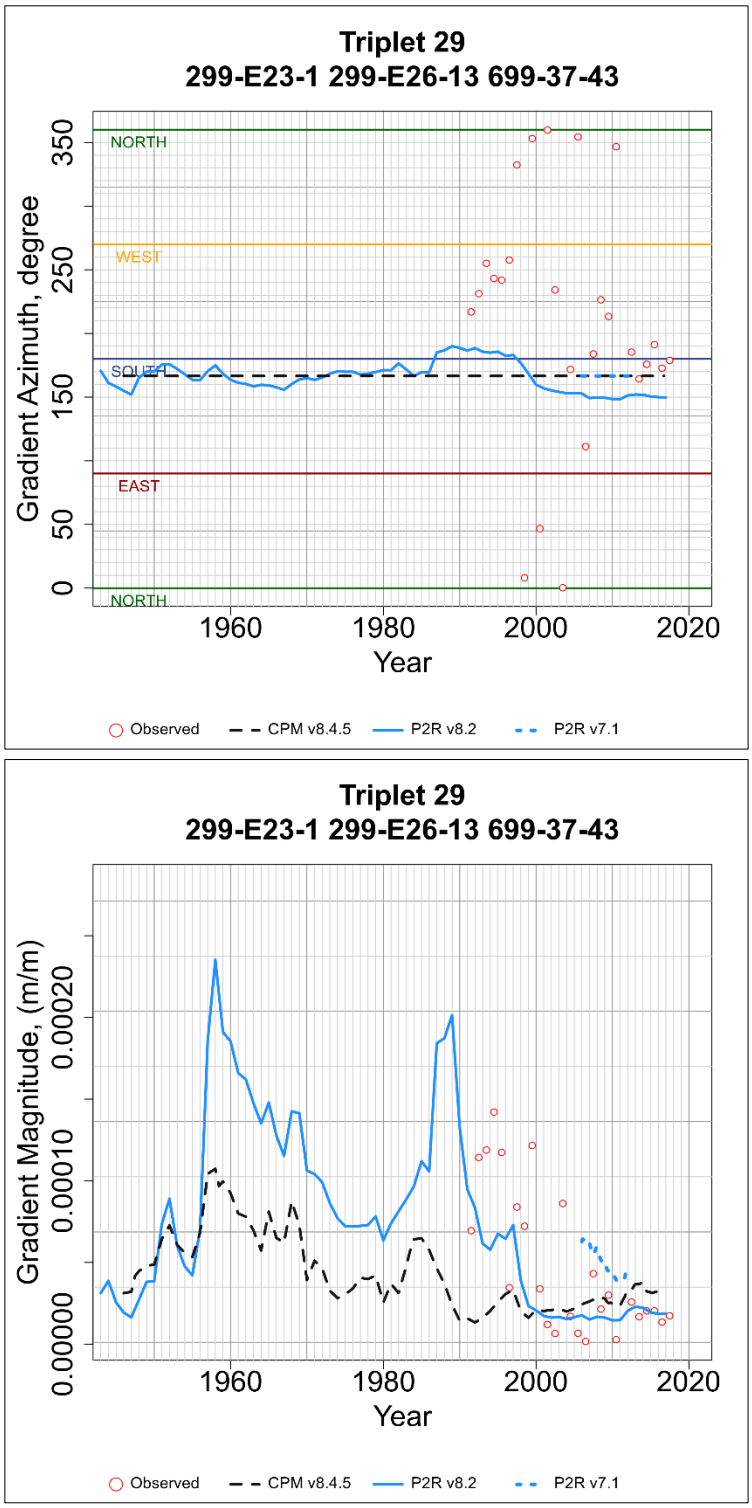

Figure C-29. Observed and simulated hydraulic gradient azimuth and magnitude for well triplet 29.

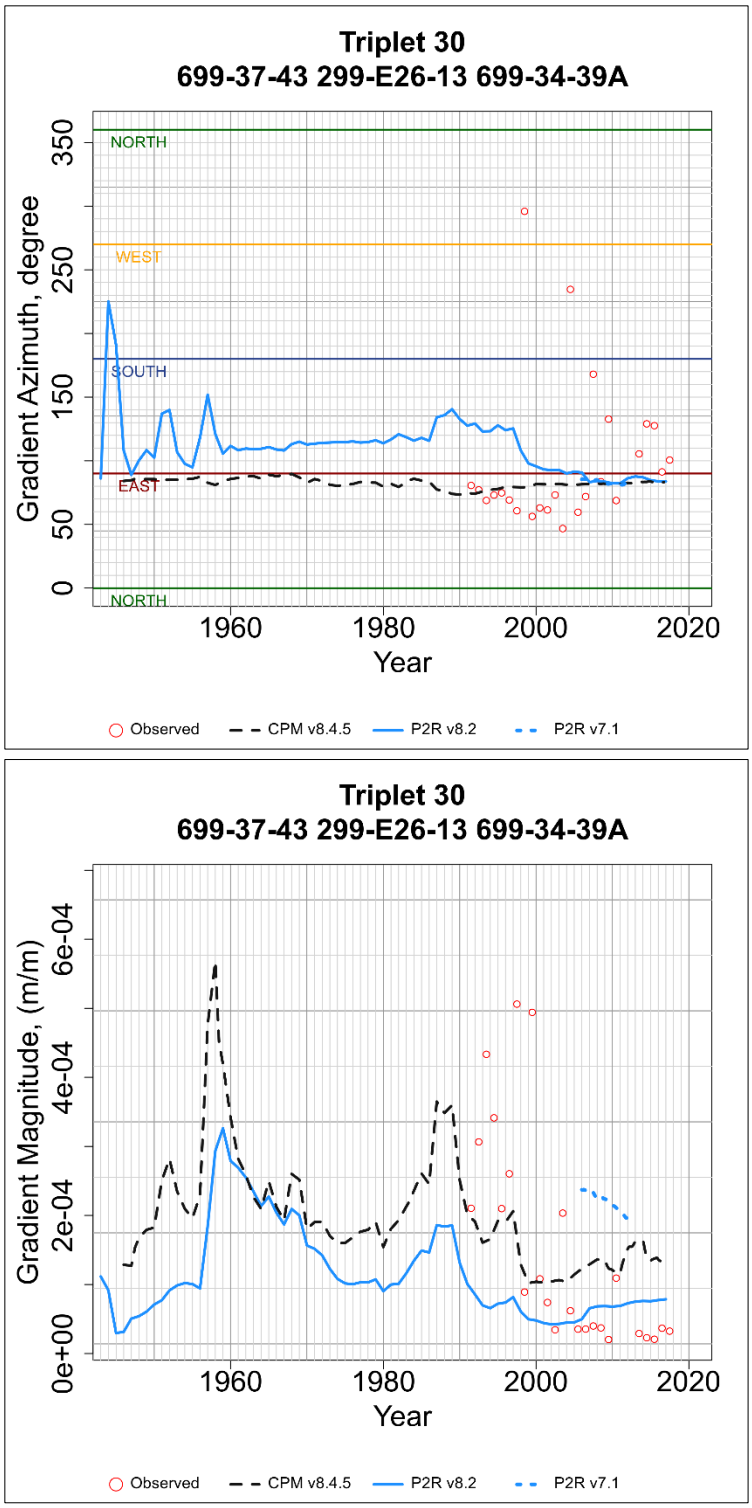

Figure C-30. Observed and simulated hydraulic gradient azimuth and magnitude for well triplet 30.

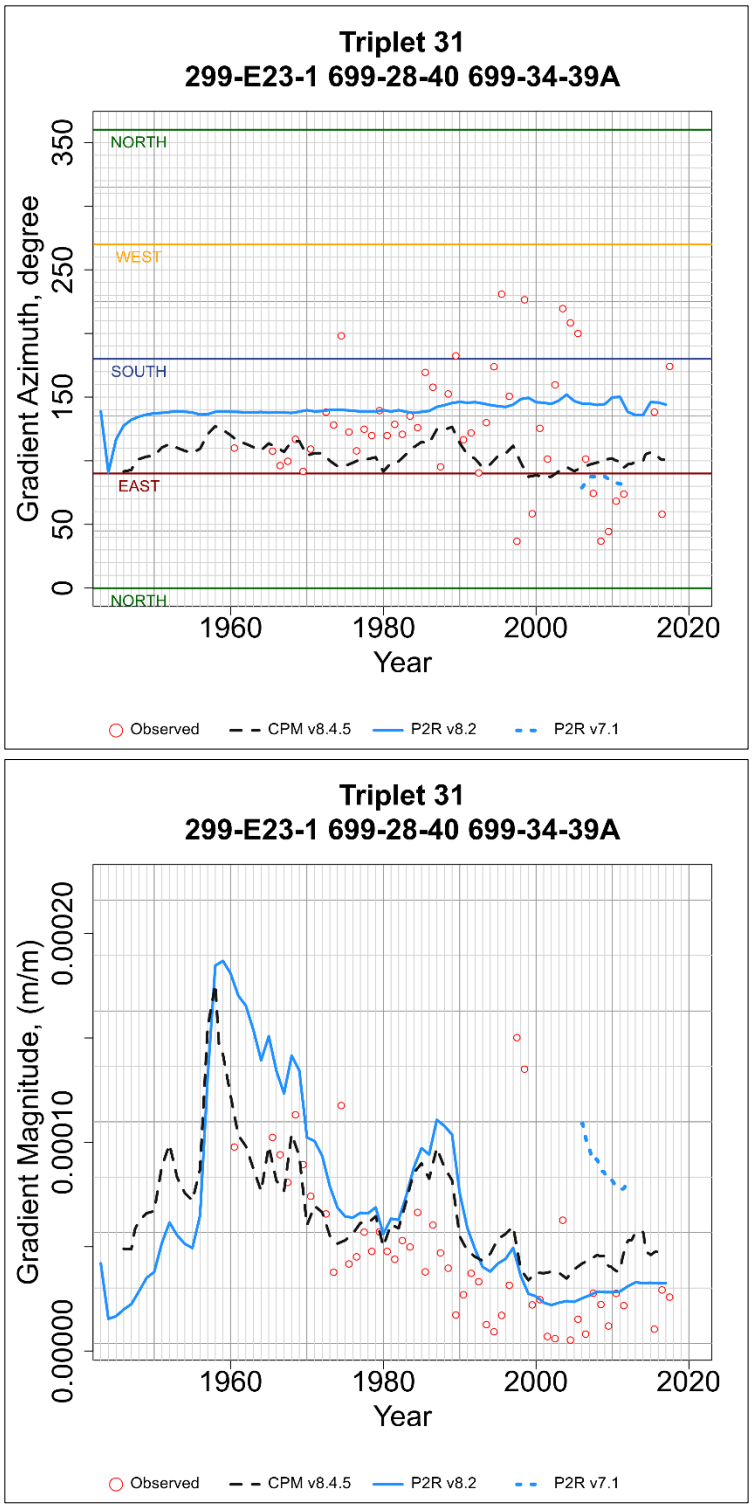

Figure C-31. Observed and simulated hydraulic gradient azimuth and magnitude for well triplet 31.

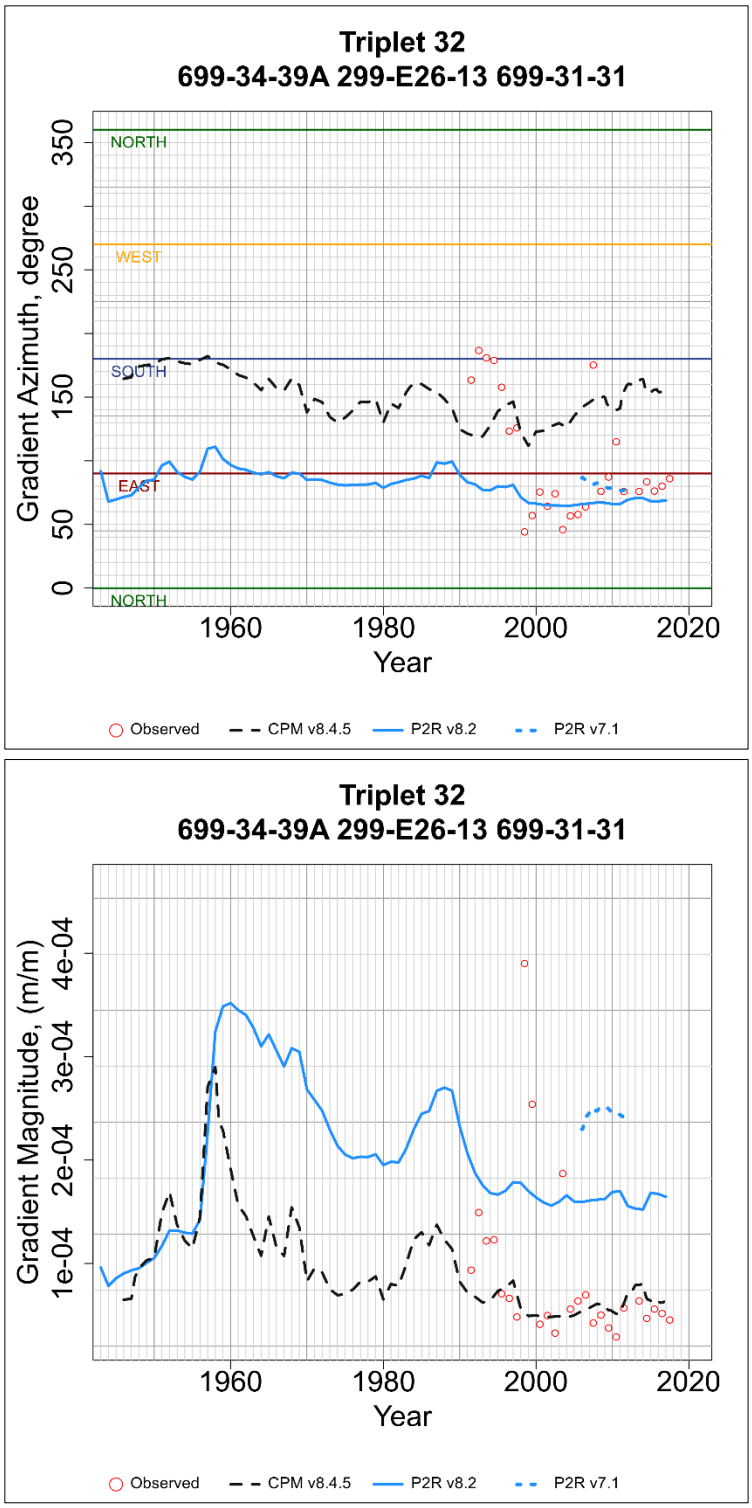

Figure C-32. Observed and simulated hydraulic gradient azimuth and magnitude for well triplet 32.

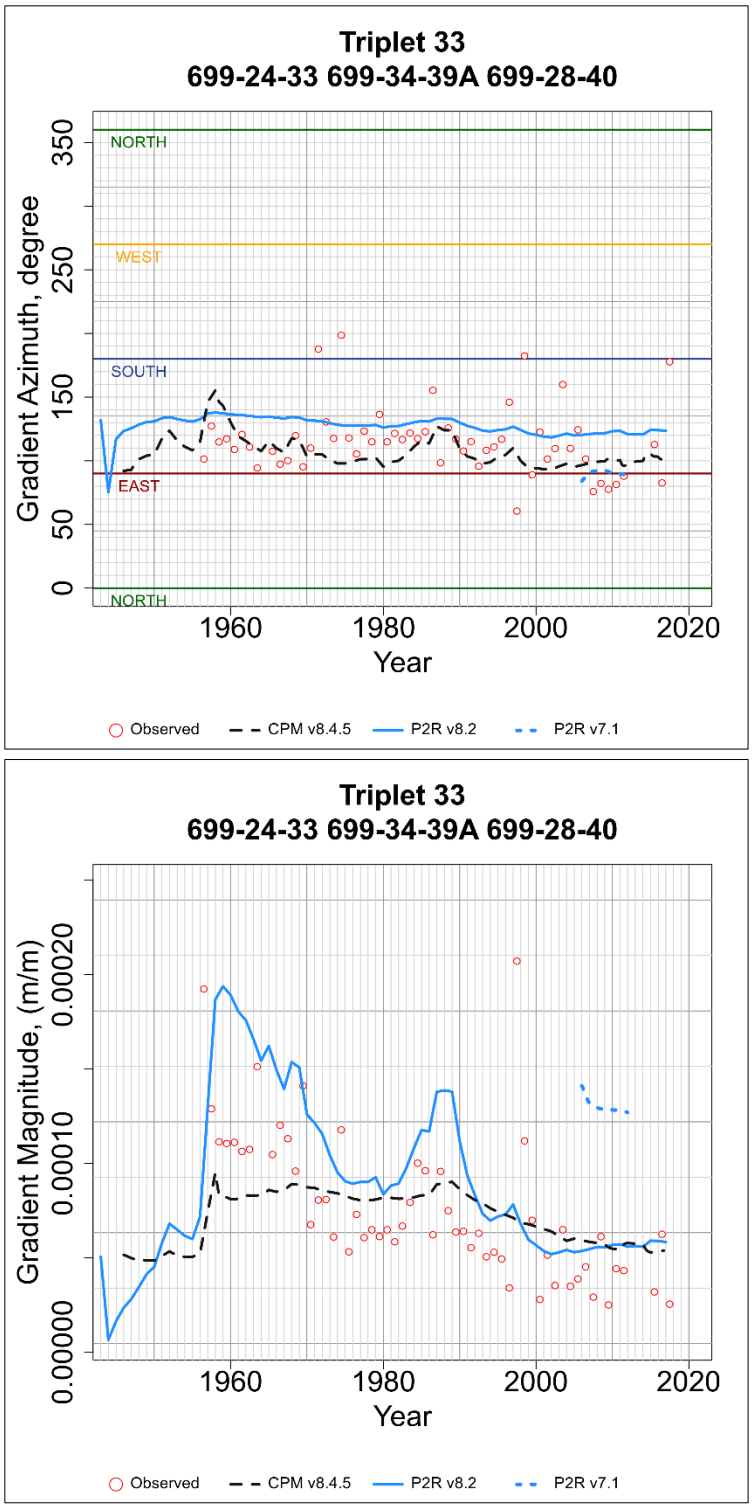

Figure C-33. Observed and simulated hydraulic gradient azimuth and magnitude for well triplet 33.

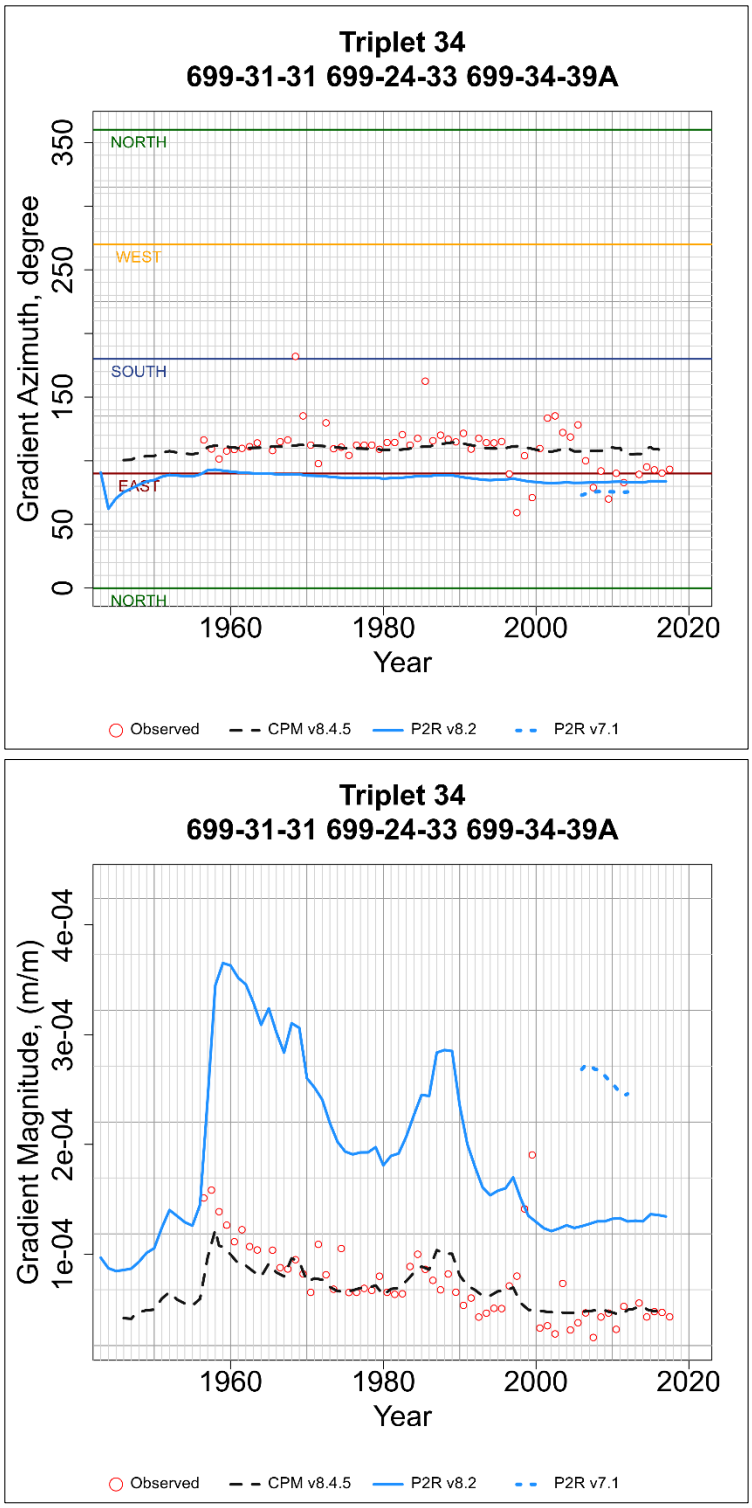

Figure C-34. Observed and simulated hydraulic gradient azimuth and magnitude for well triplet 34.

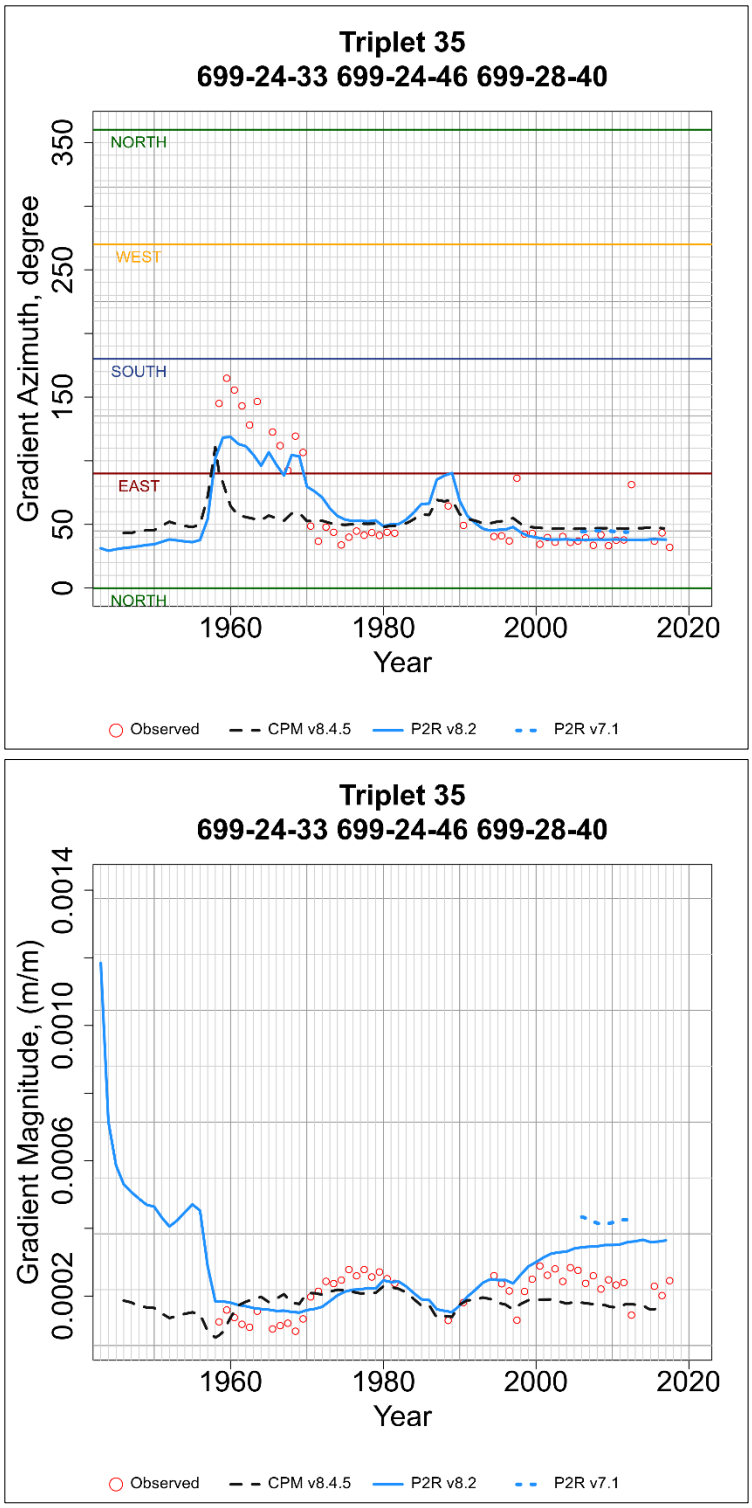

Figure C-35. Observed and simulated hydraulic gradient azimuth and magnitude for well triplet 35.

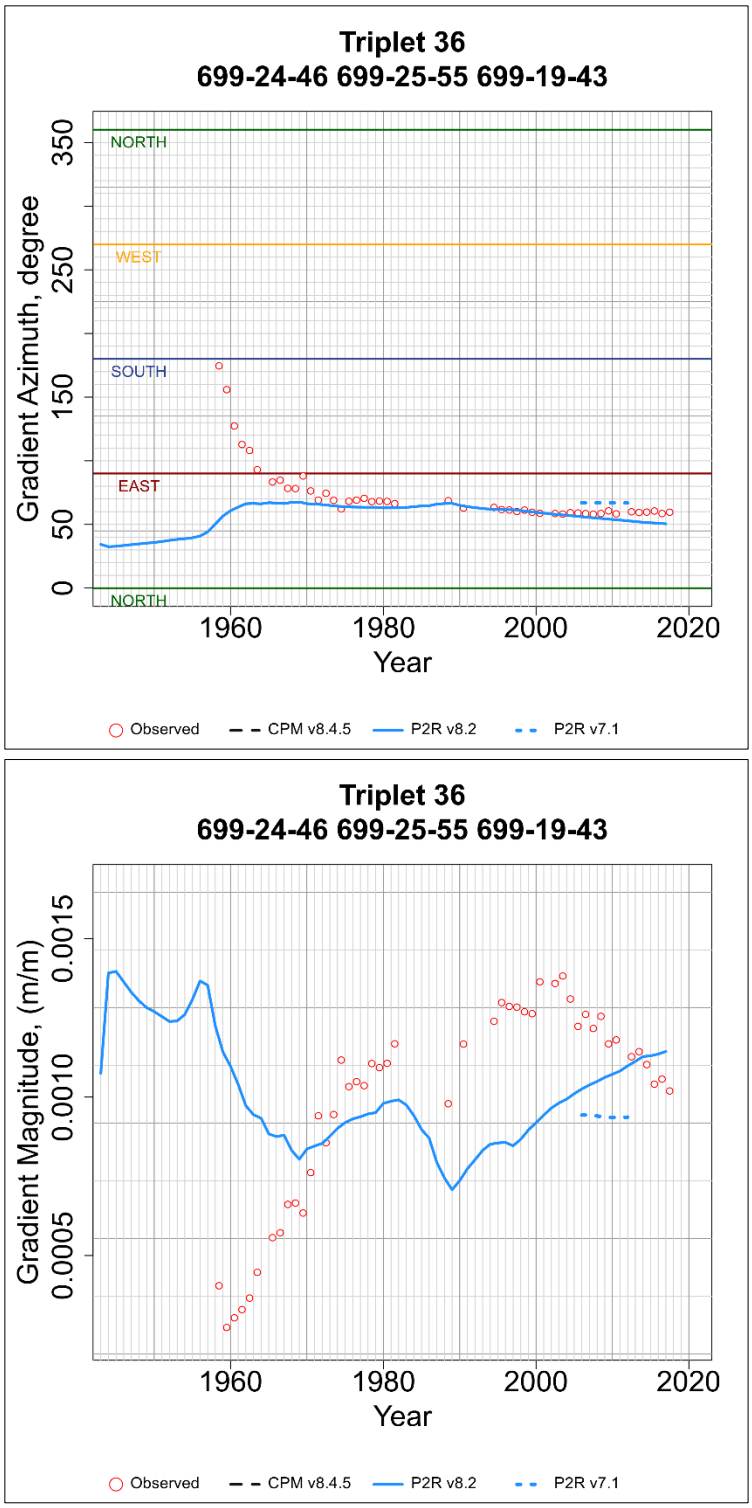

Figure C-36. Observed and simulated hydraulic gradient azimuth and magnitude for well triplet 36.

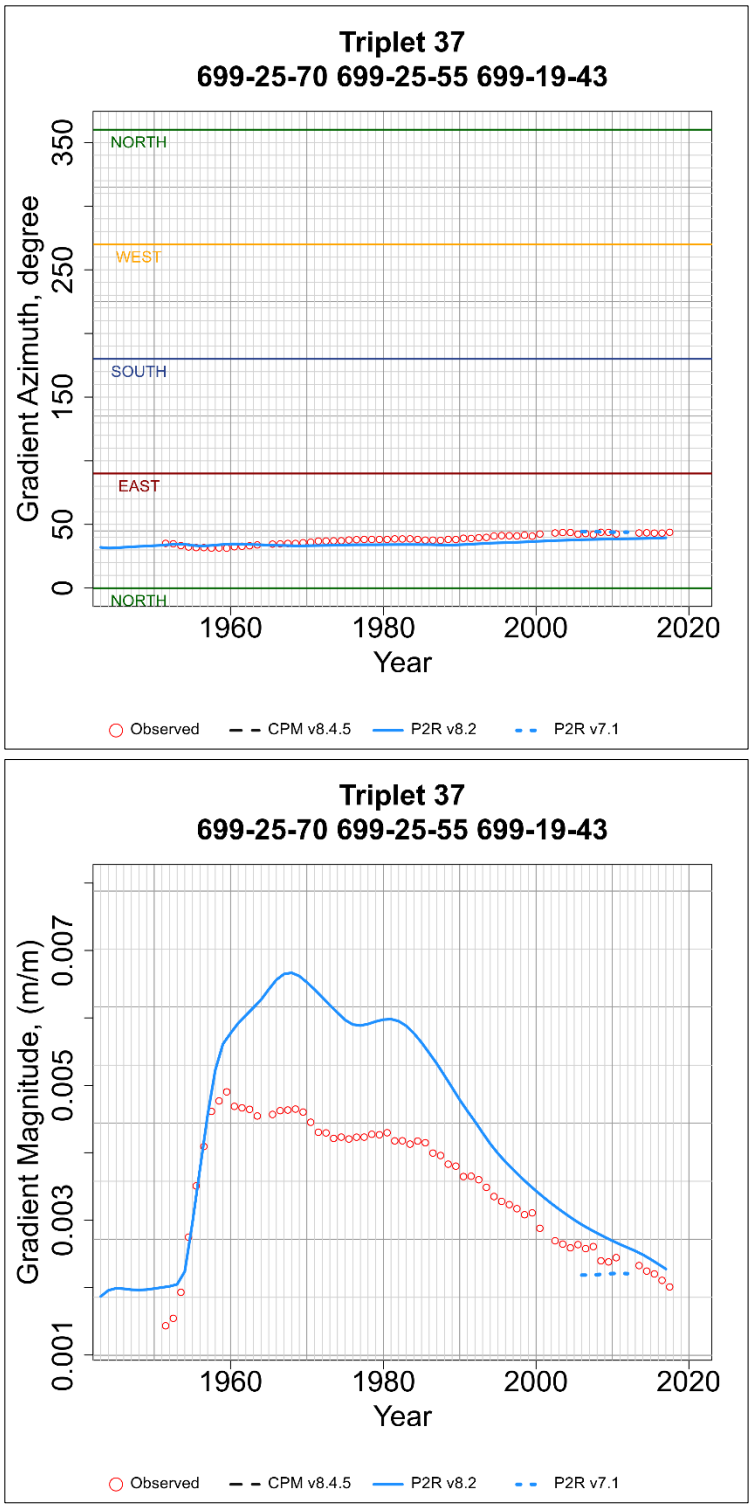

Figure C-37. Observed and simulated hydraulic gradient azimuth and magnitude for well triplet 37.

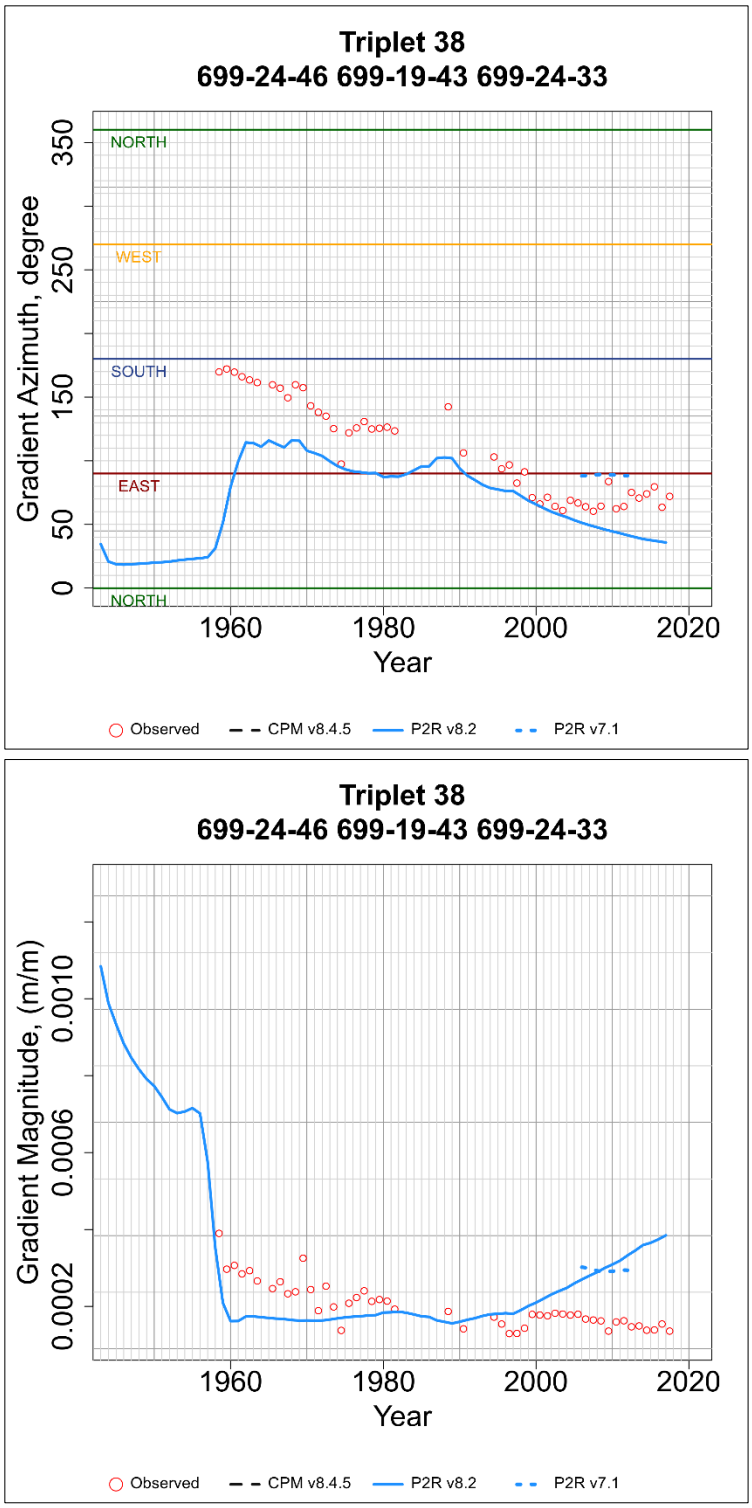

Figure C-38. Observed and simulated hydraulic gradient azimuth and magnitude for well triplet 38.

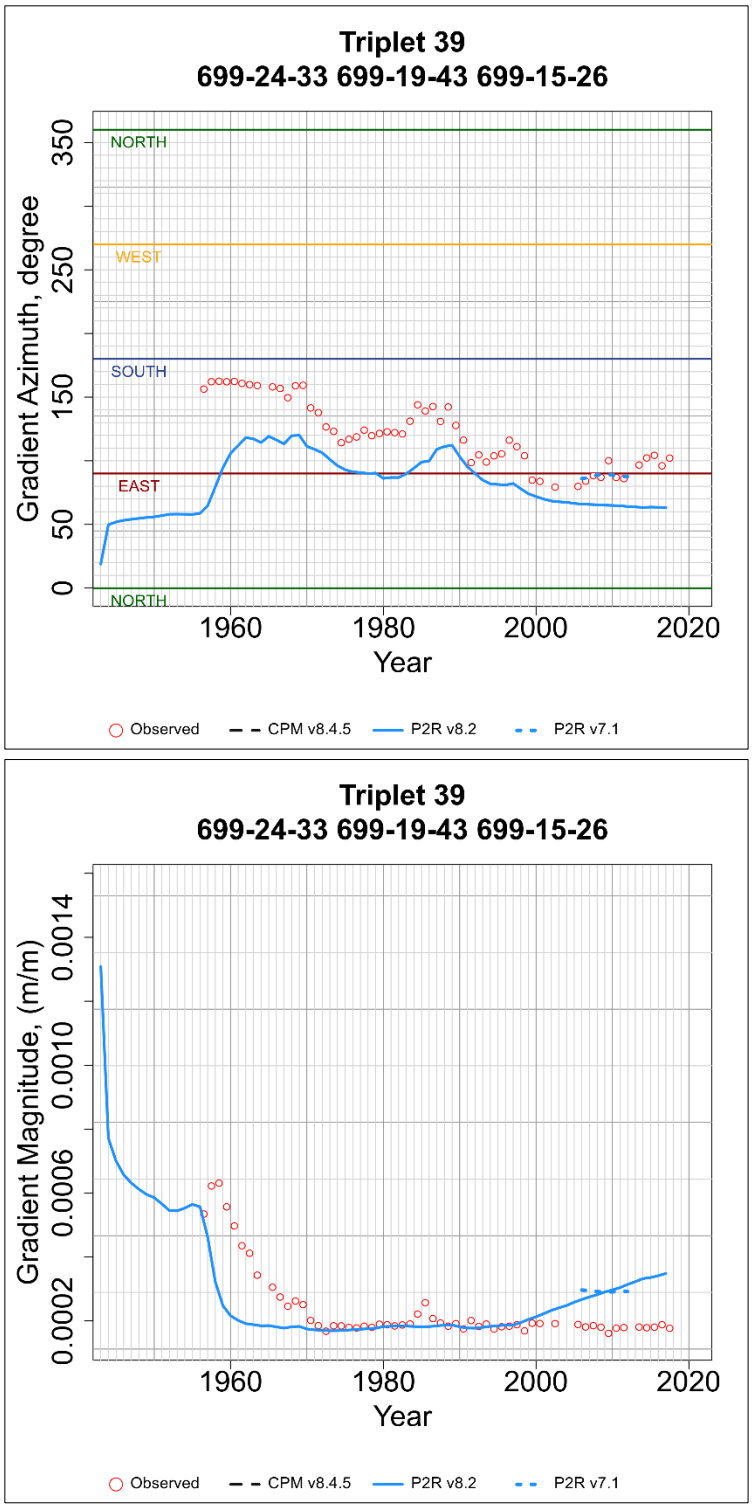

Figure C-39. Observed and simulated hydraulic gradient azimuth and magnitude for well triplet 39.

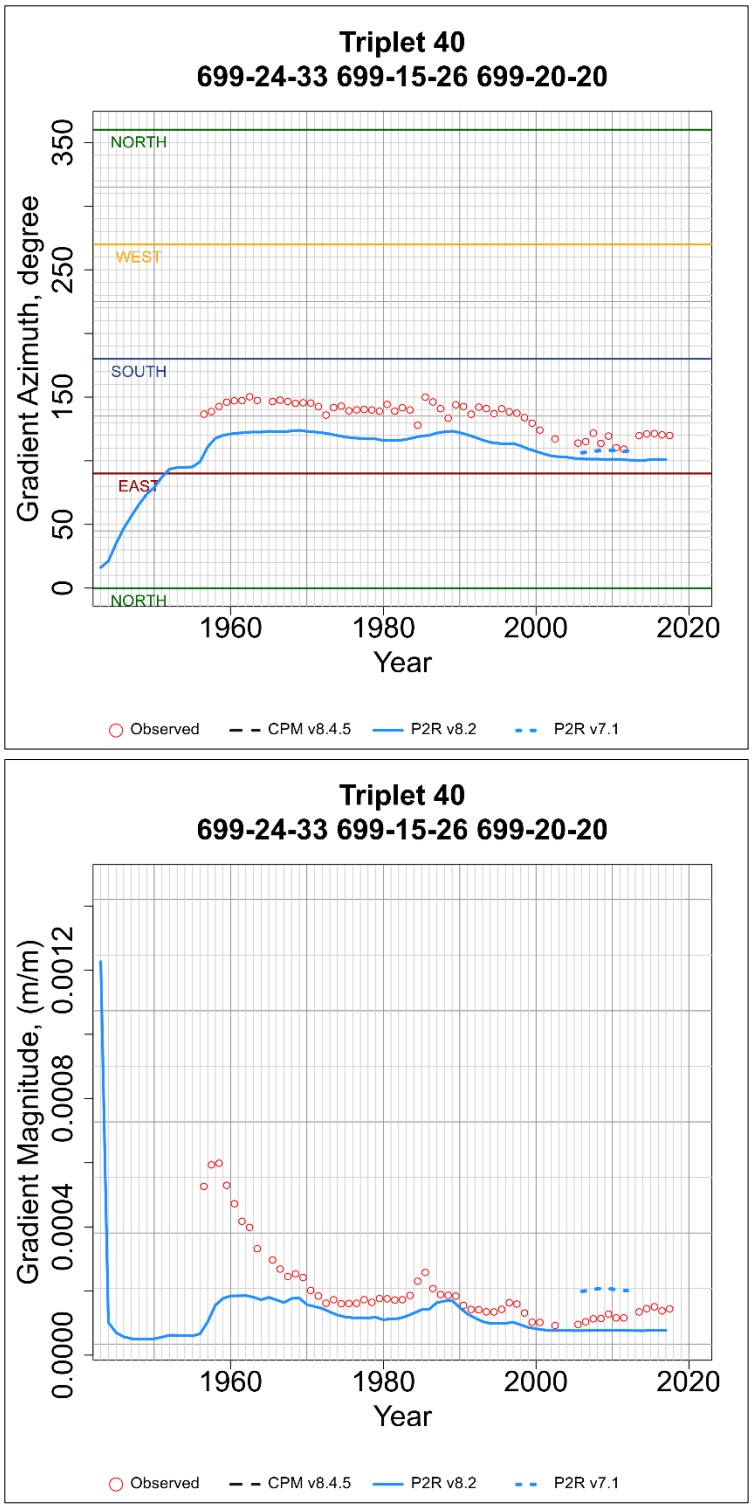

Figure C-40. Observed and simulated hydraulic gradient azimuth and magnitude for well triplet 40.

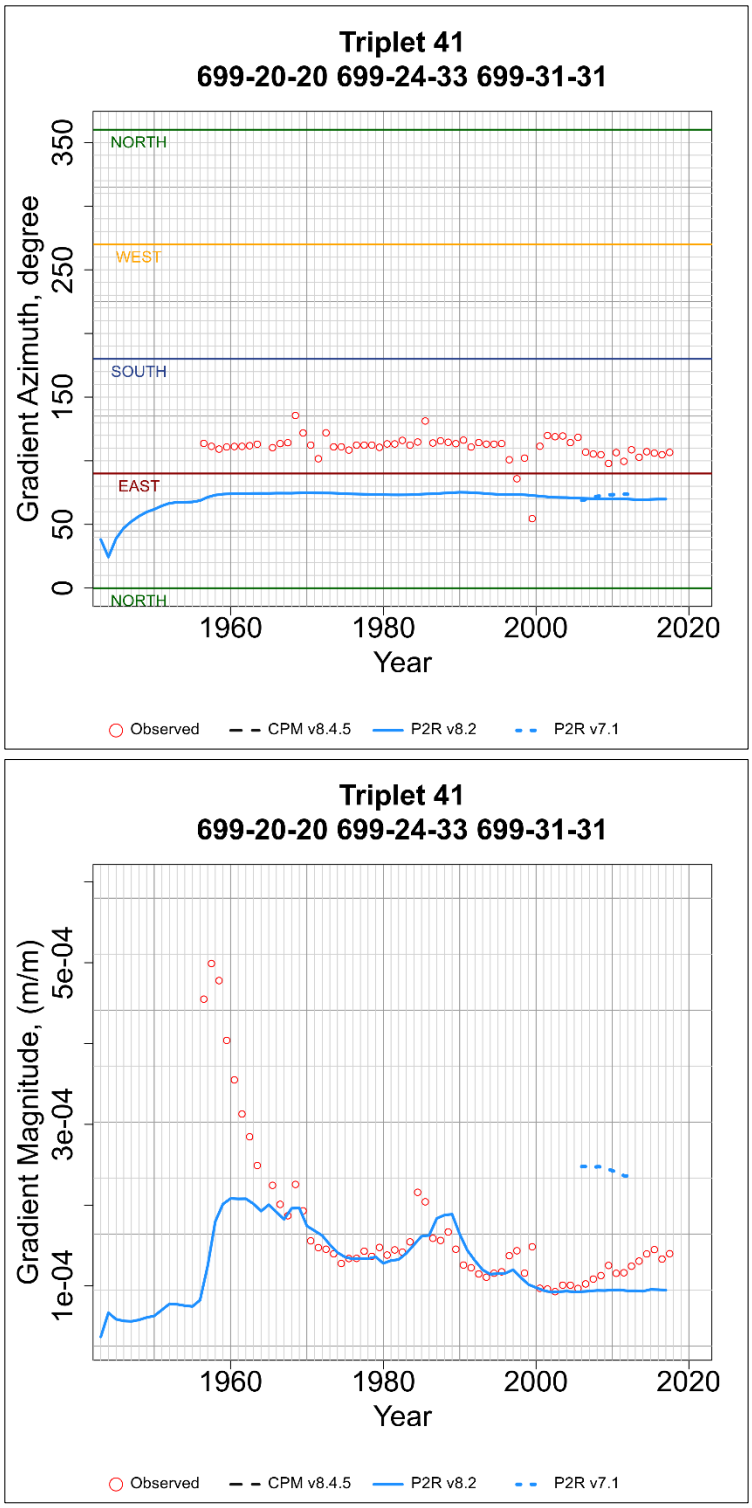

Figure C-41. Observed and simulated hydraulic gradient azimuth and magnitude for well triplet 41.

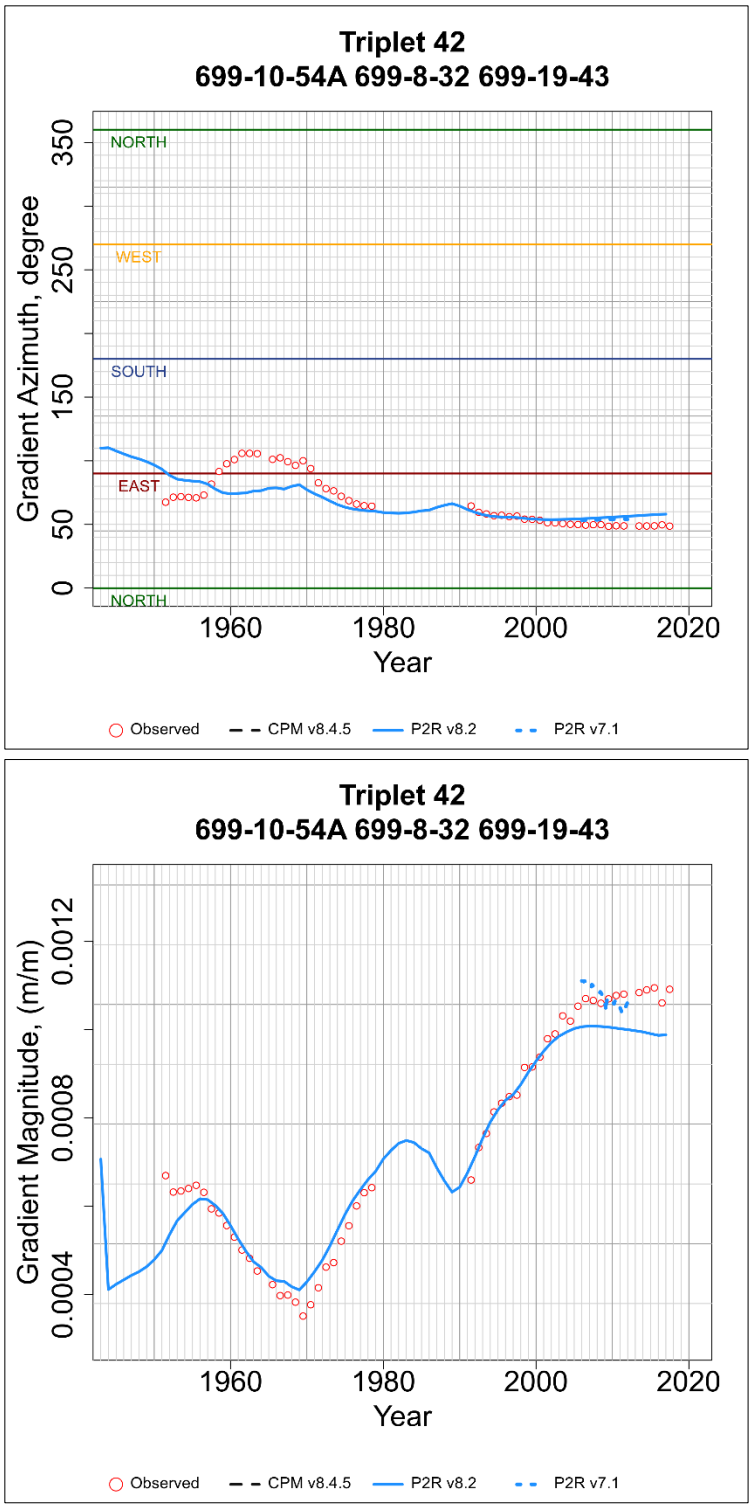

Figure C-42. Observed and simulated hydraulic gradient azimuth and magnitude for well triplet 42.

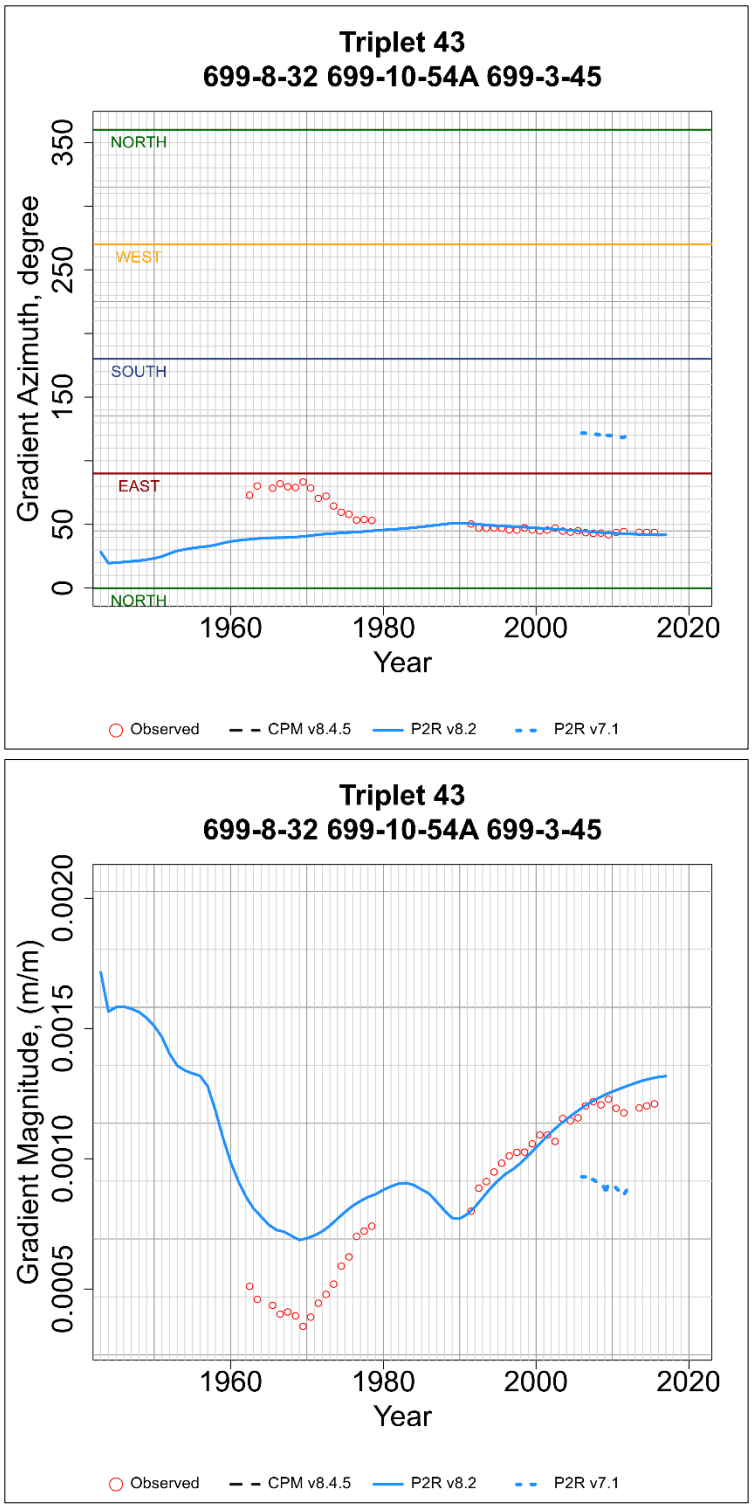

Figure C-43. Observed and simulated hydraulic gradient azimuth and magnitude for well triplet 43.

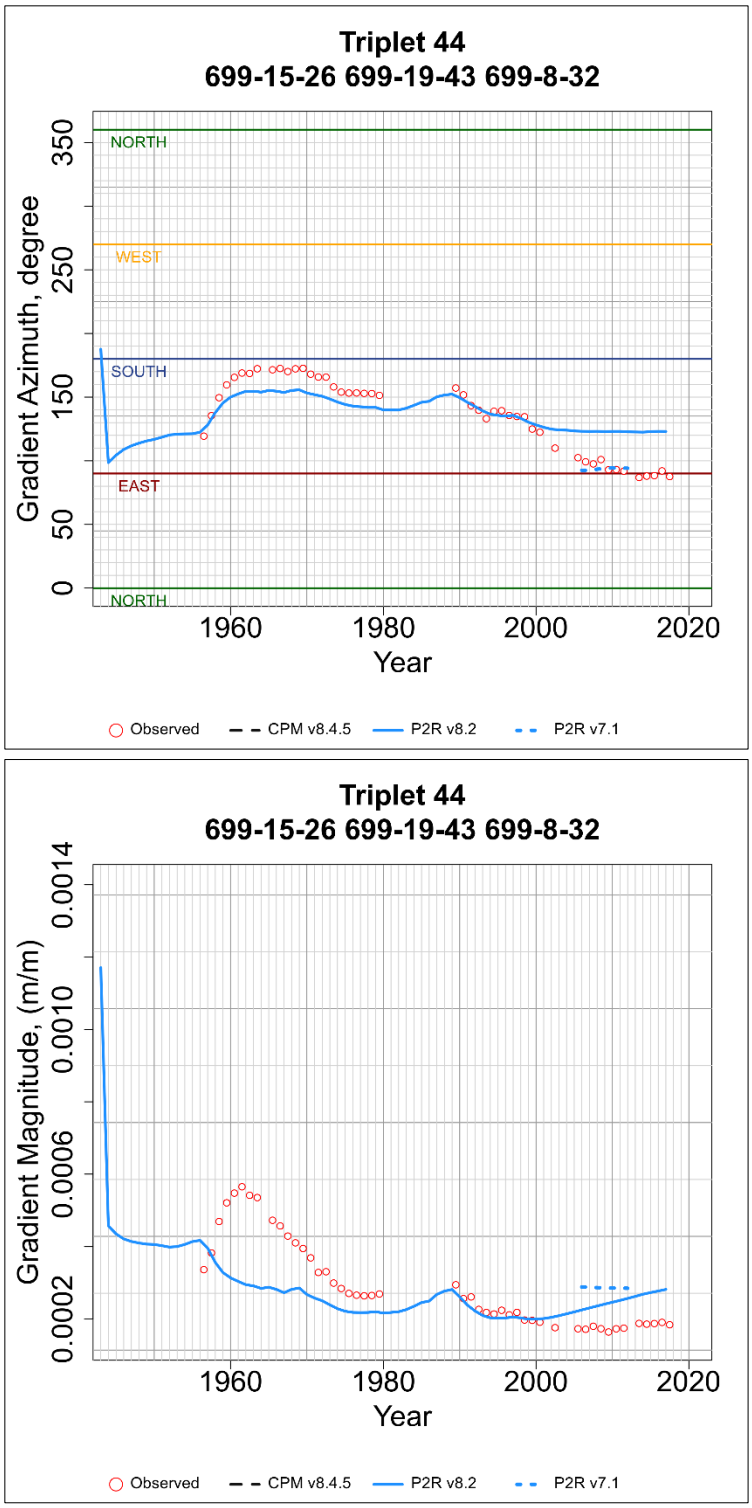

Figure C-44. Observed and simulated hydraulic gradient azimuth and magnitude for well triplet 44.

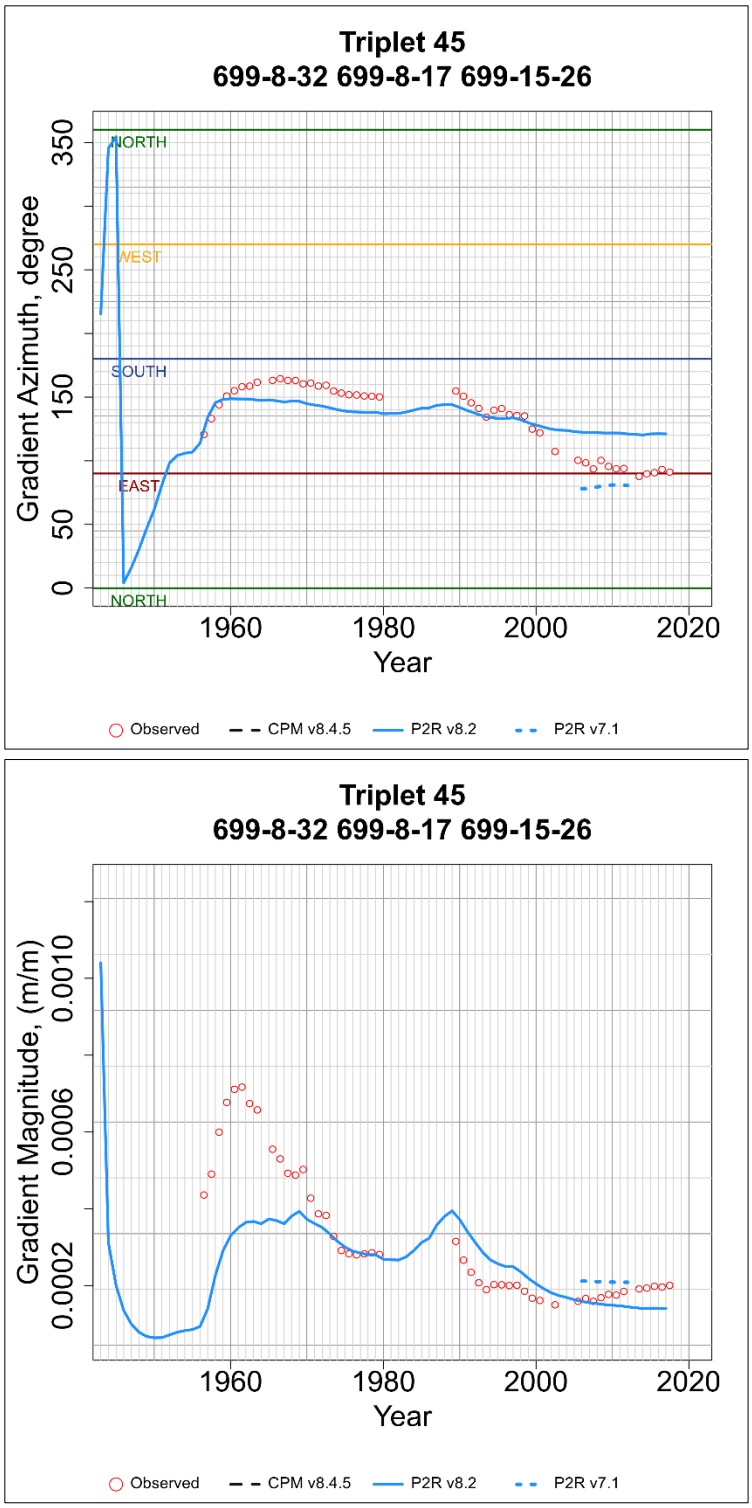

Figure C-45. Observed and simulated hydraulic gradient azimuth and magnitude for well triplet 45.

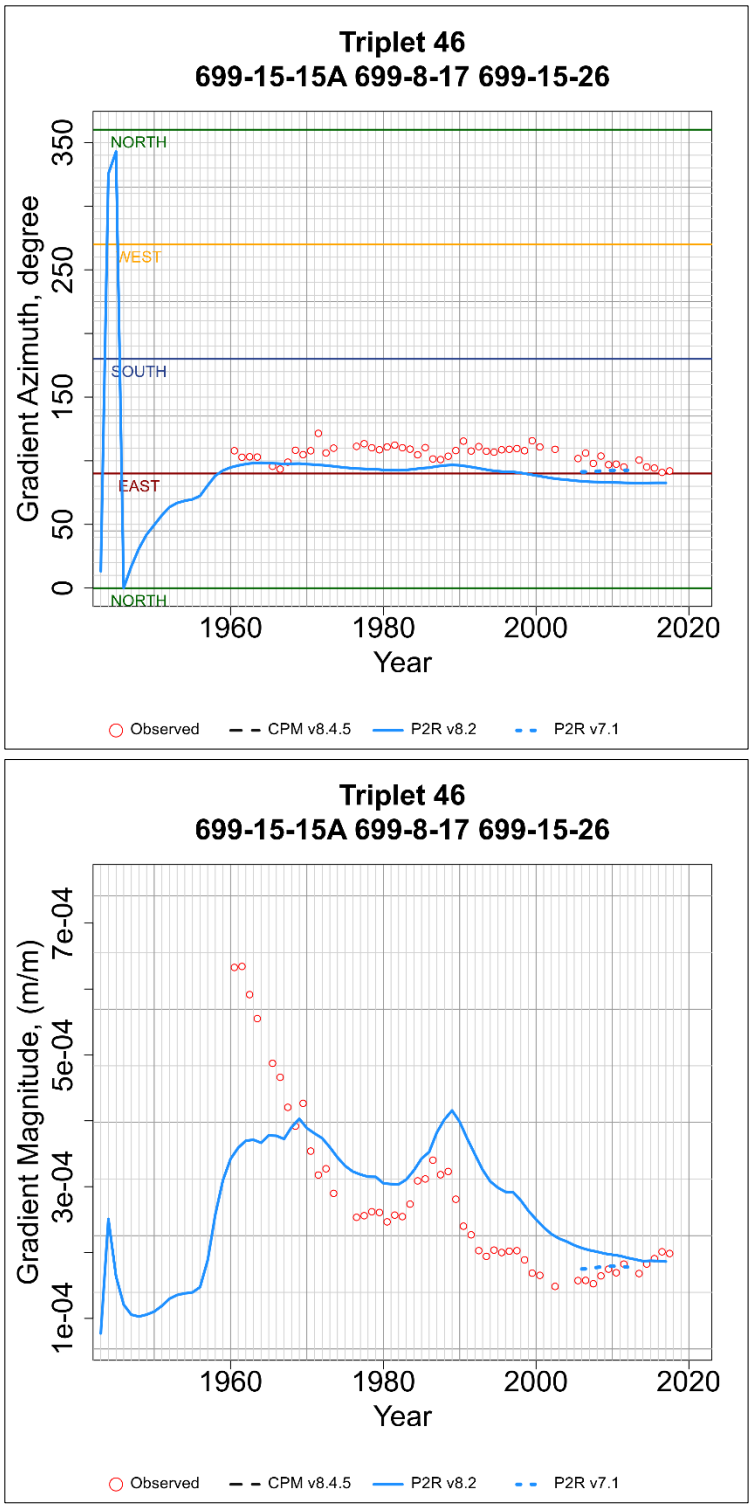

Figure C-46. Observed and simulated hydraulic gradient azimuth and magnitude for well triplet 46.

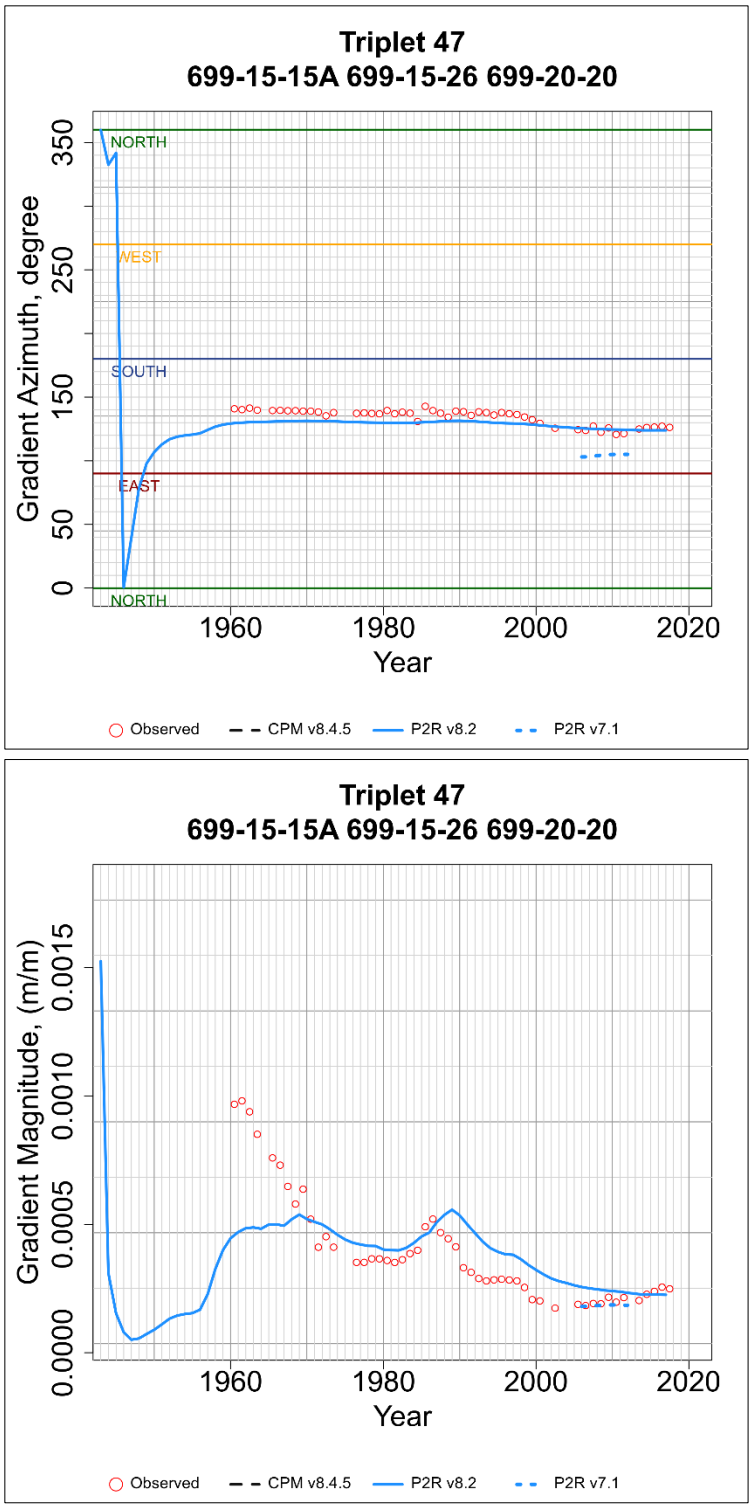

Figure C-47. Observed and simulated hydraulic gradient azimuth and magnitude for well triplet 47.

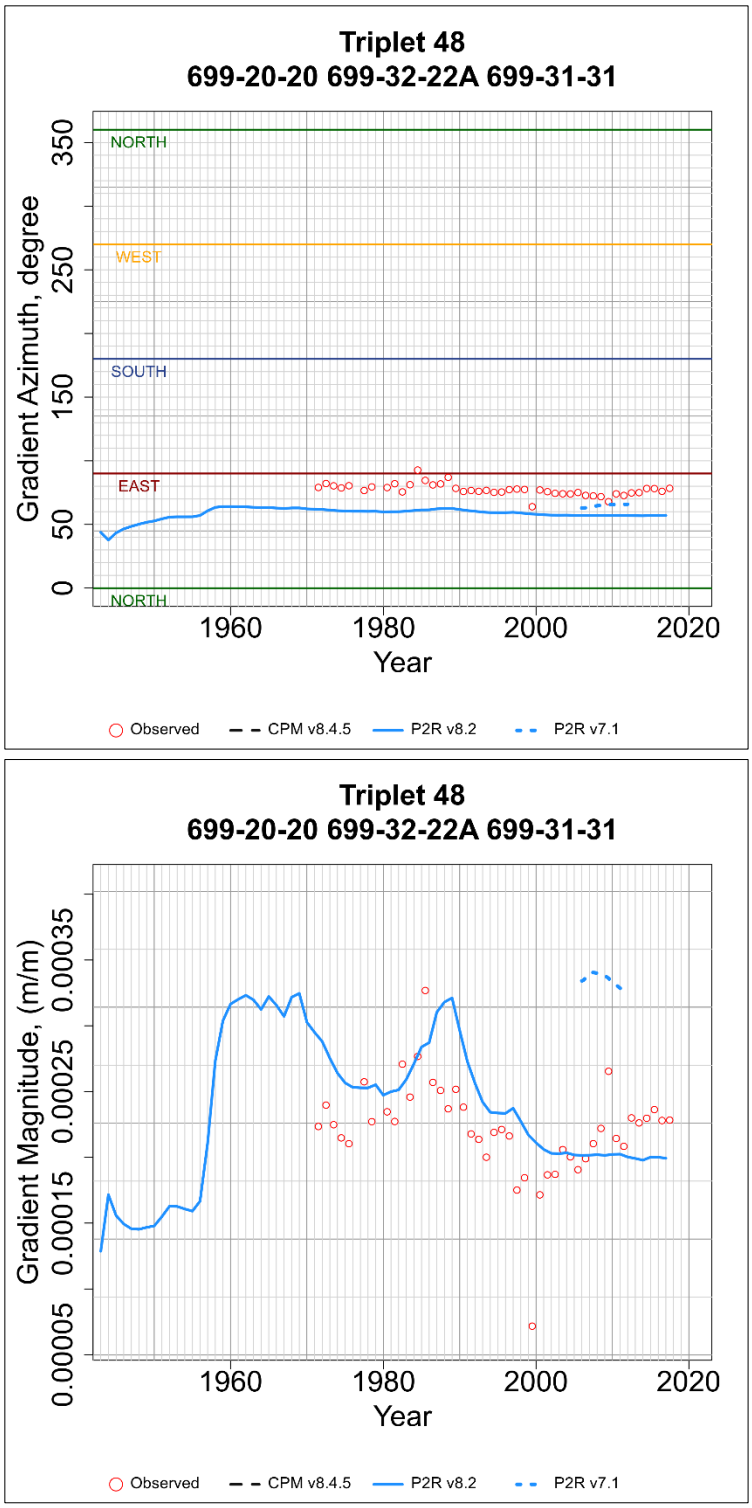

Figure C-48. Observed and simulated hydraulic gradient azimuth and magnitude for well triplet 48.

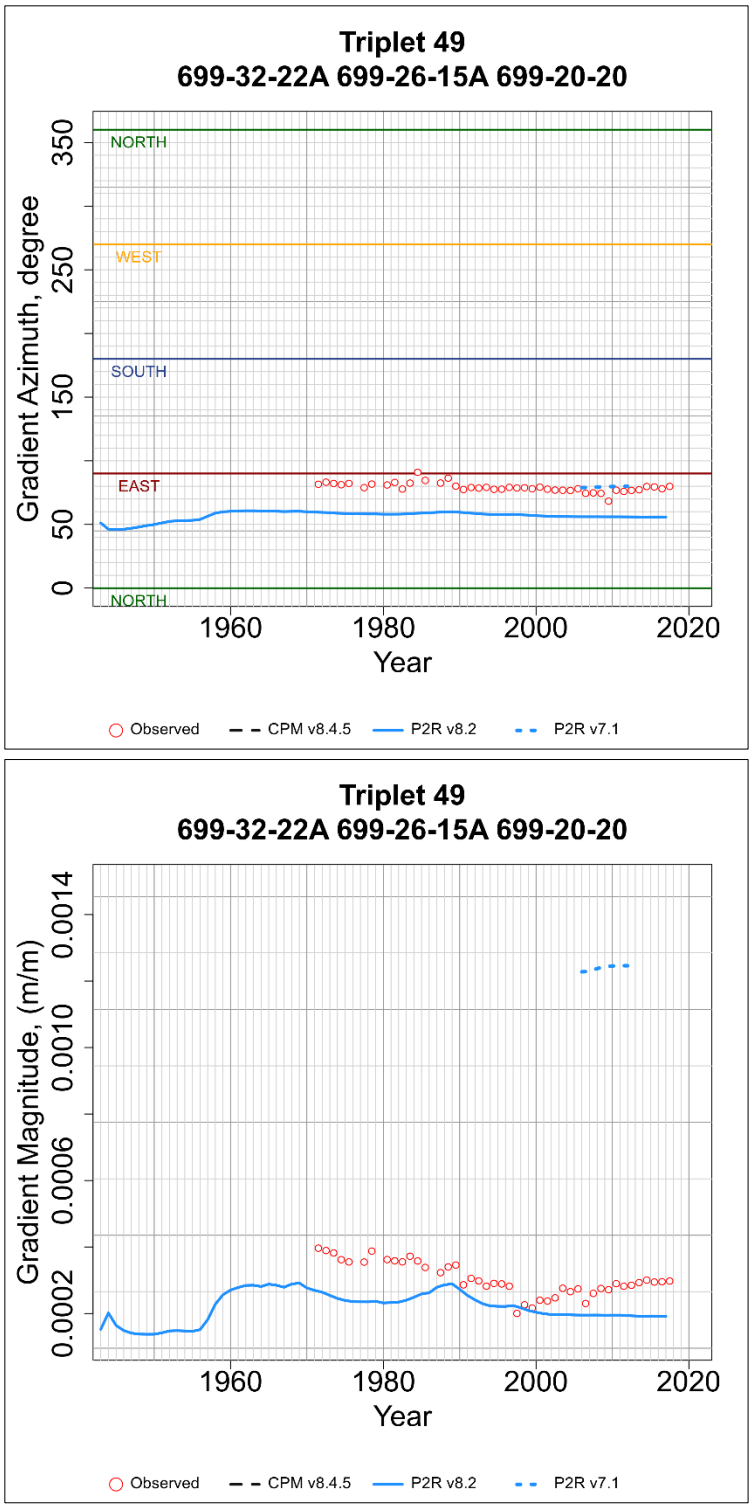

Figure C-49. Observed and simulated hydraulic gradient azimuth and magnitude for well triplet 49.

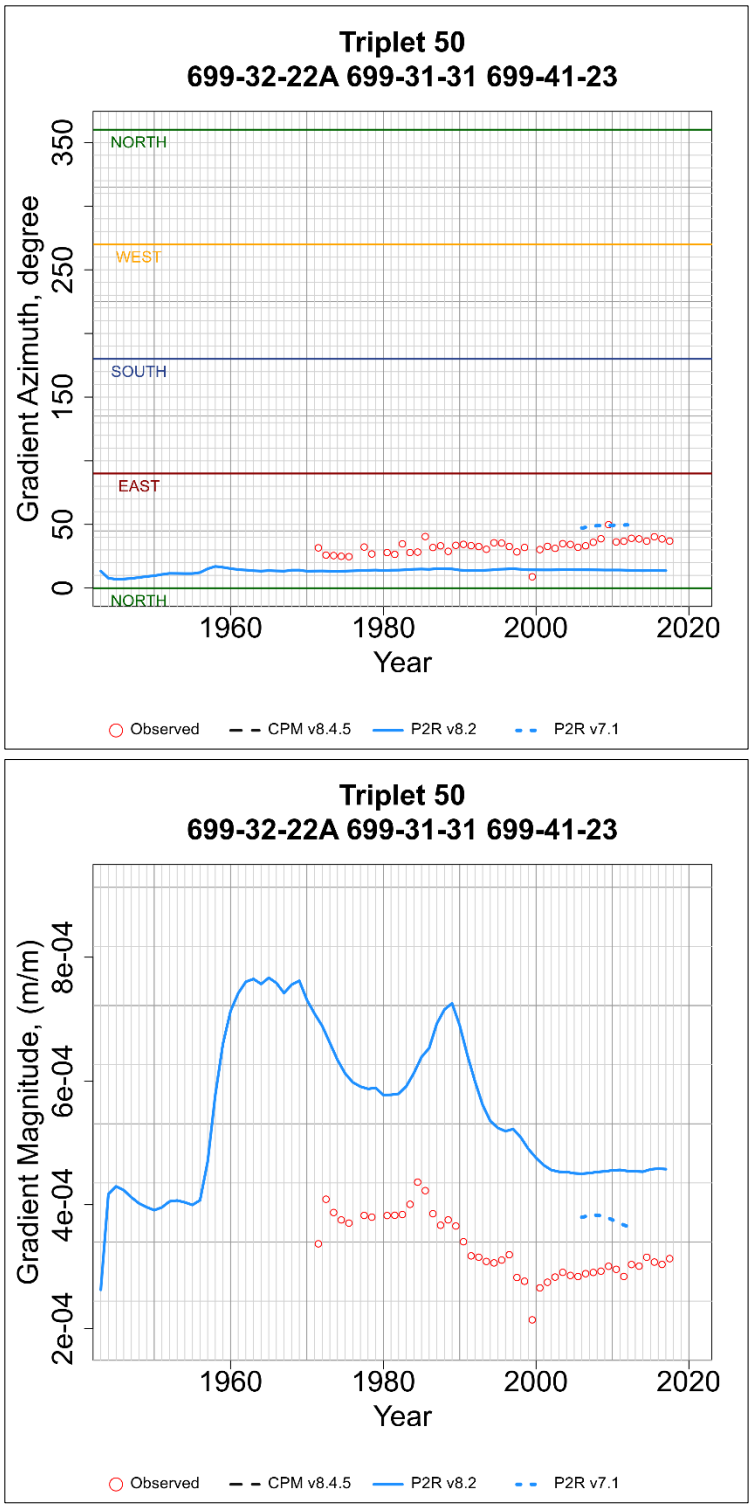

Figure C-50. Observed and simulated hydraulic gradient azimuth and magnitude for well triplet 50.

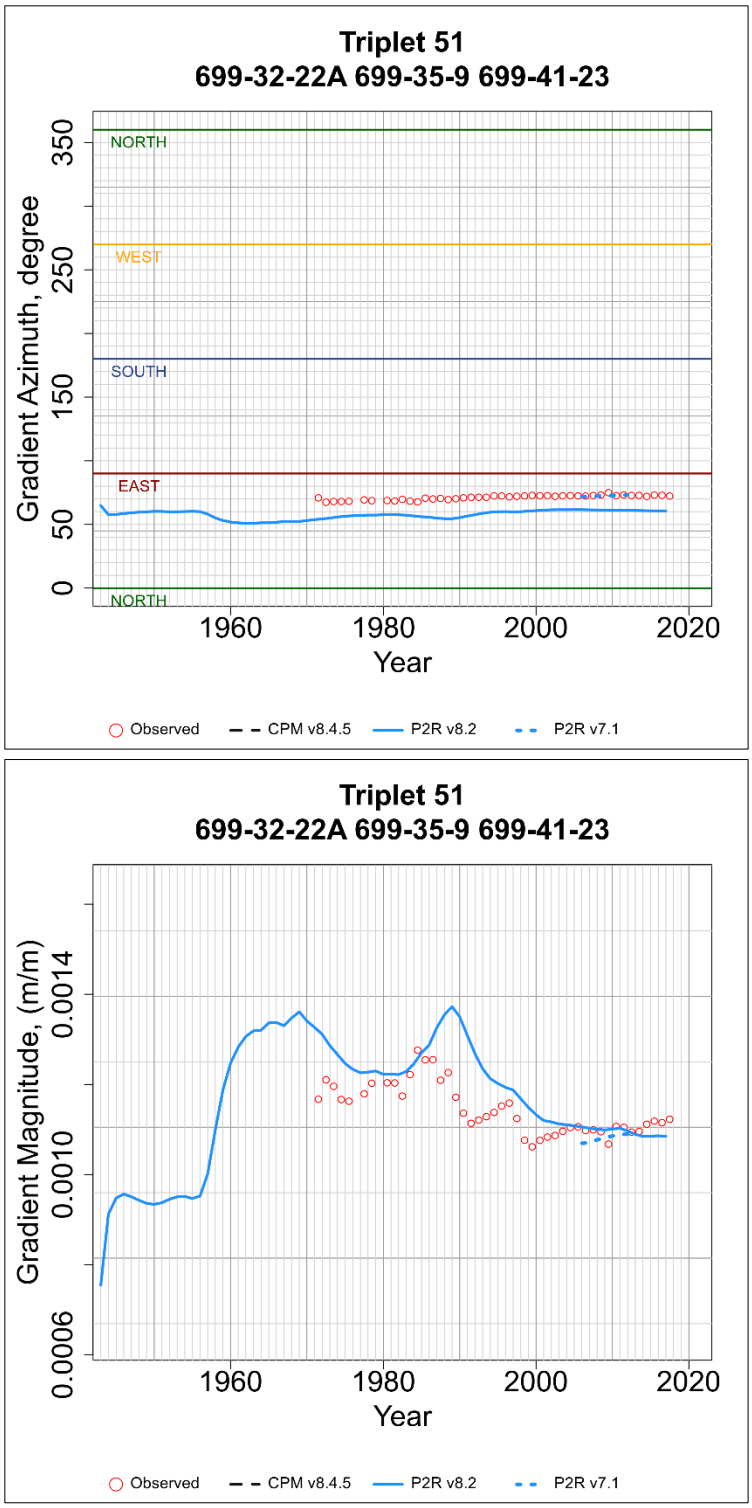

Figure C-51. Observed and simulated hydraulic gradient azimuth and magnitude for well triplet 51.

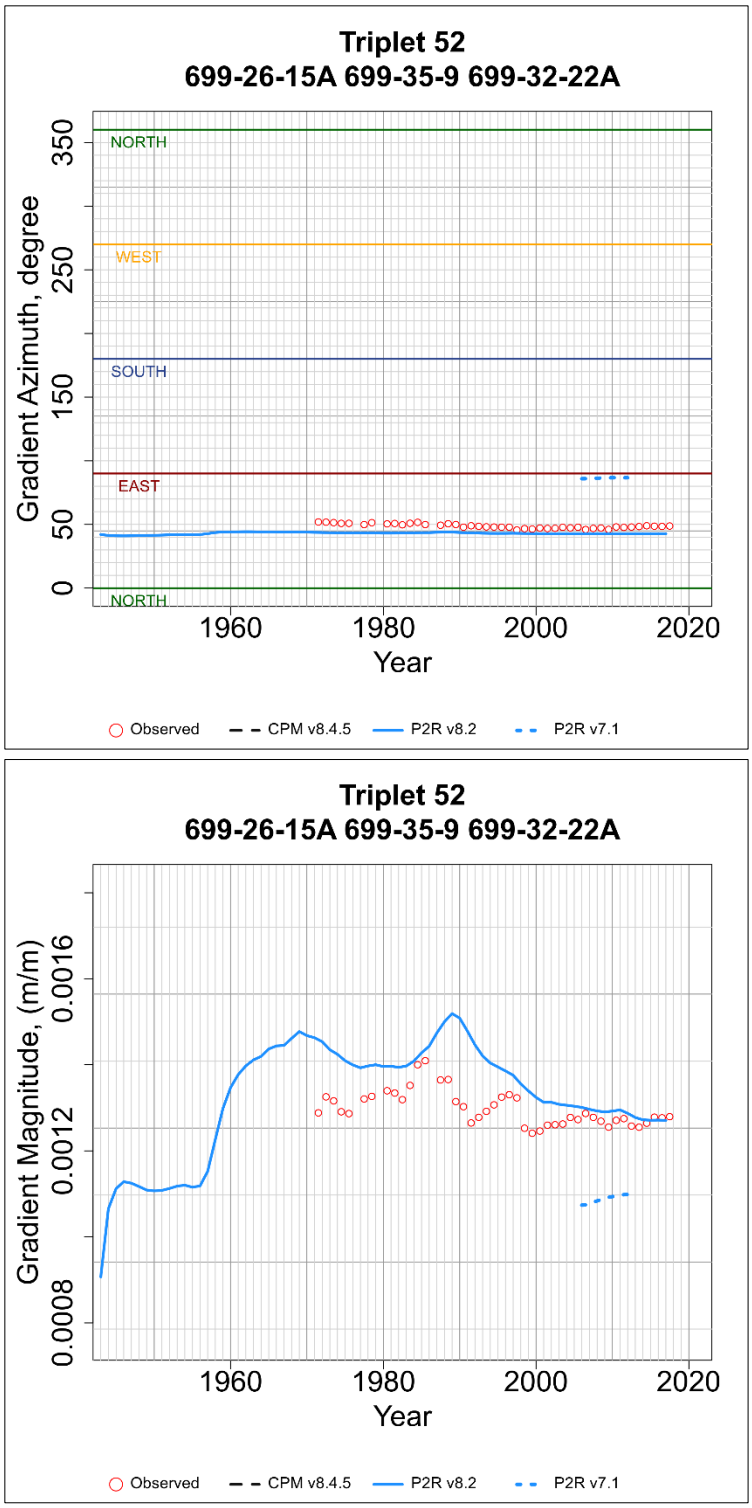

Figure C-52. Observed and simulated hydraulic gradient azimuth and magnitude for well triplet 52.

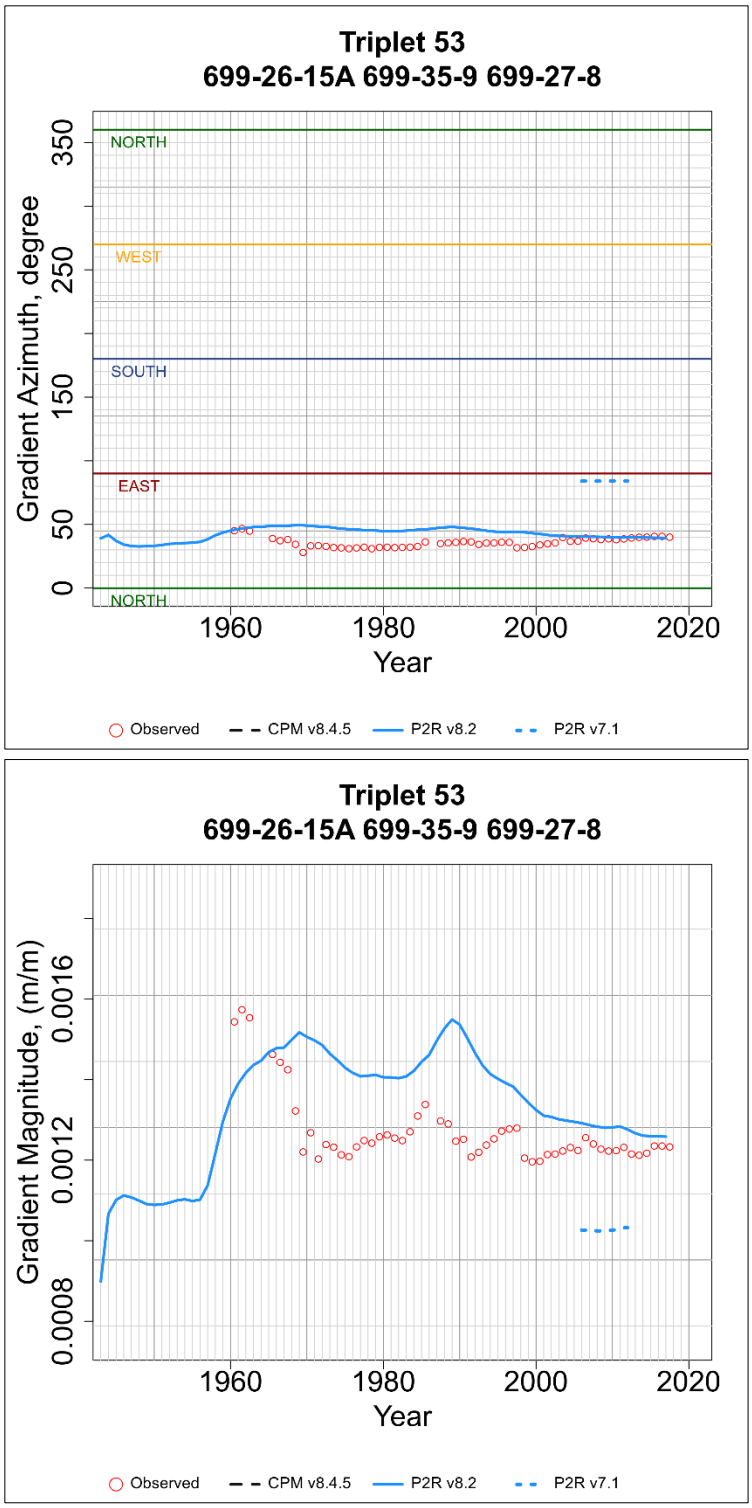

Figure C-53. Observed and simulated hydraulic gradient azimuth and magnitude for well triplet 53.

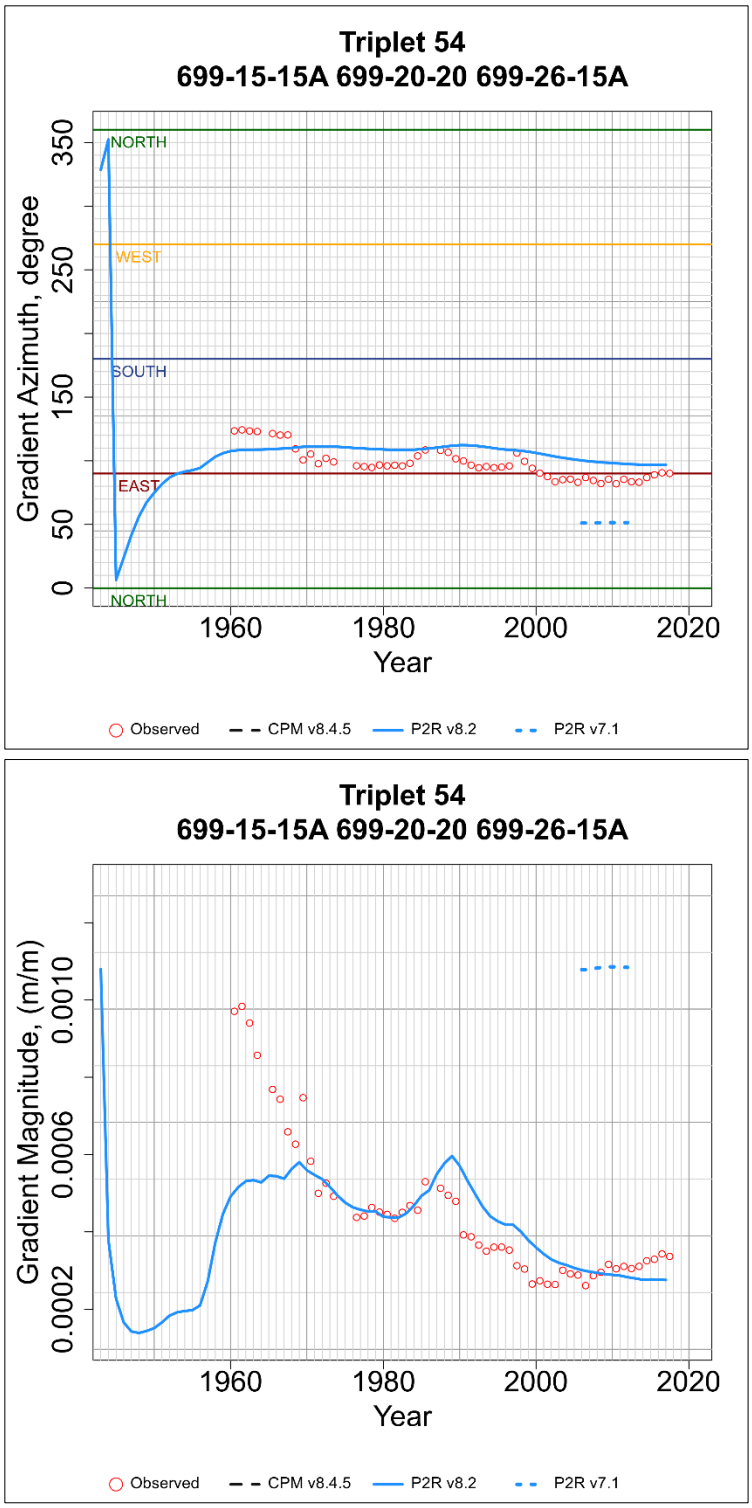

Figure C-54. Observed and simulated hydraulic gradient azimuth and magnitude for well triplet 54.

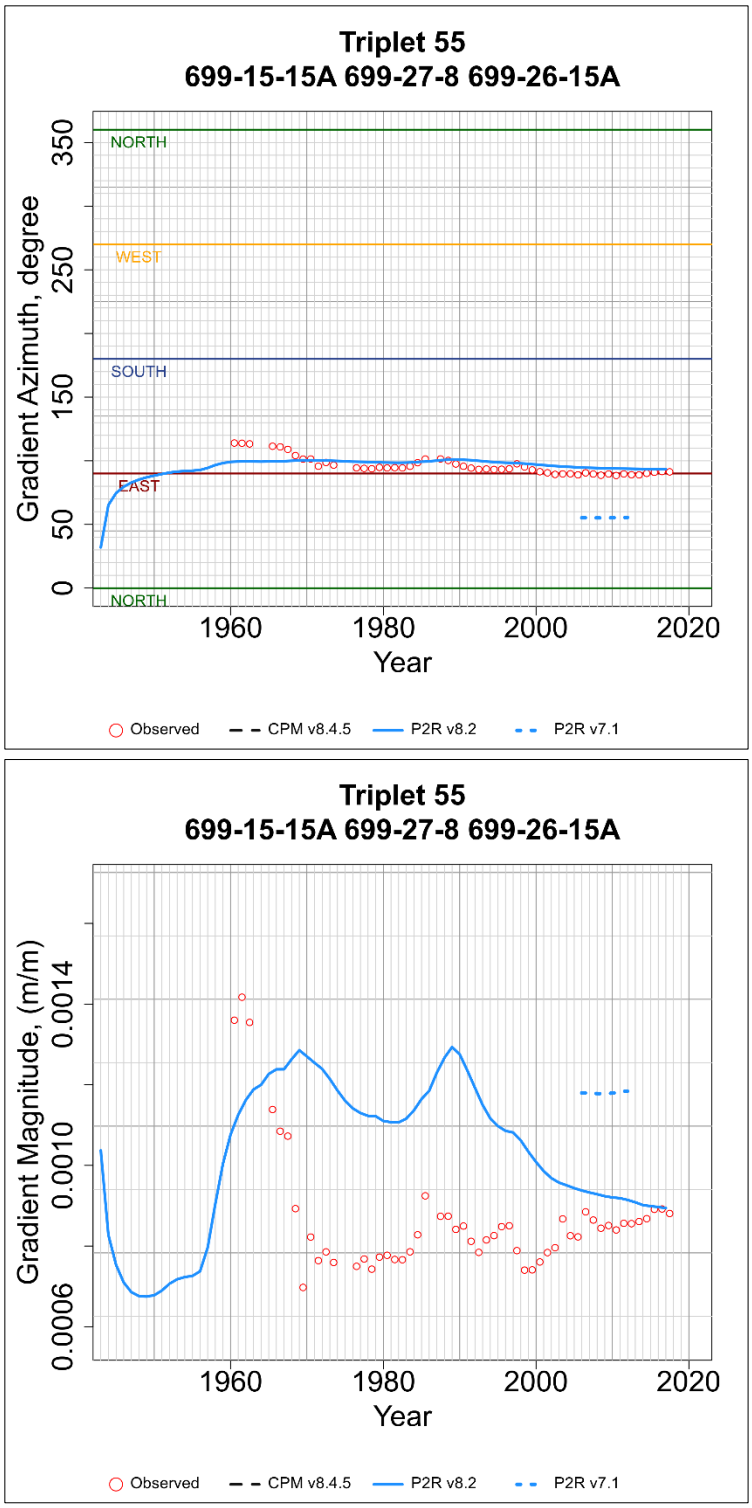

Figure C-55. Observed and simulated hydraulic gradient azimuth and magnitude for well triplet 55.

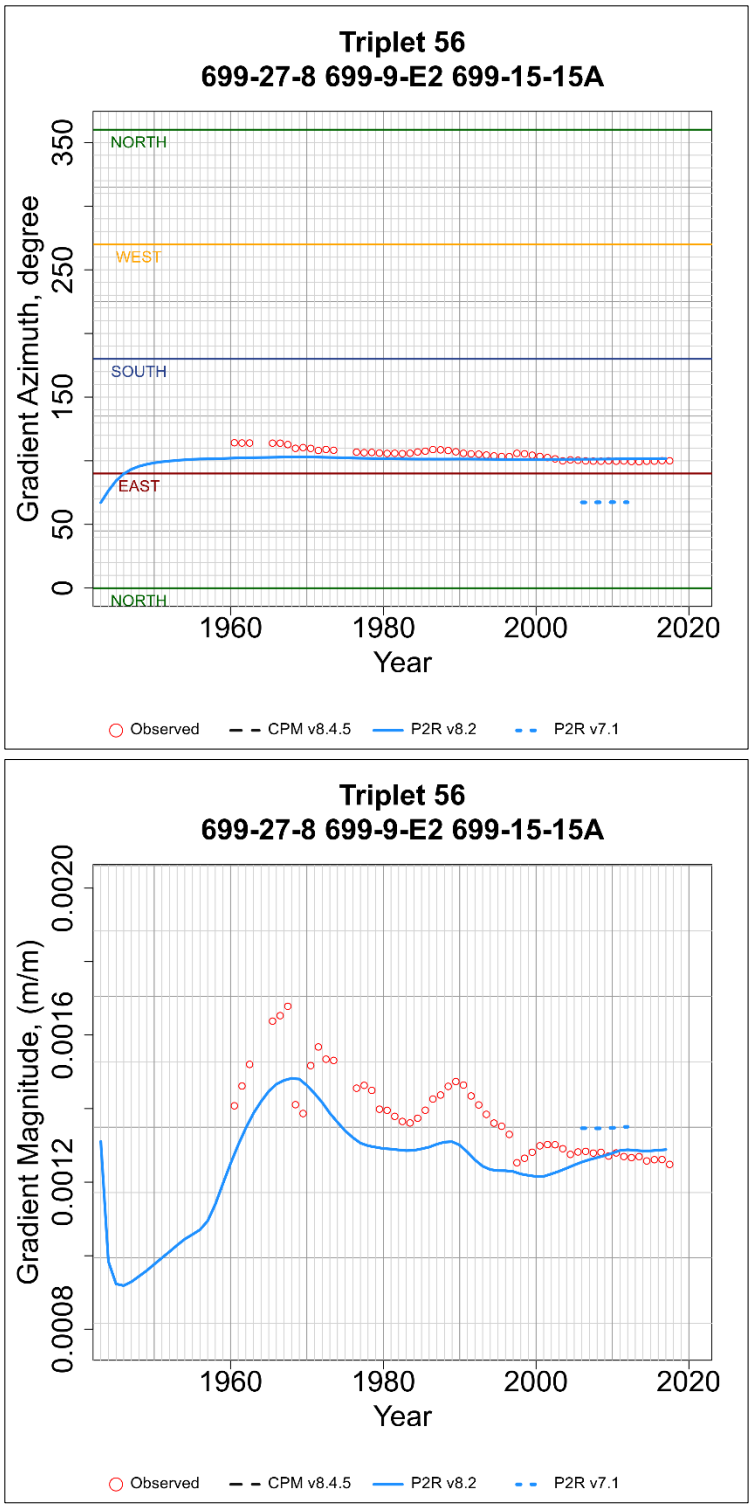

Figure C-56. Observed and simulated hydraulic gradient azimuth and magnitude for well triplet 56.

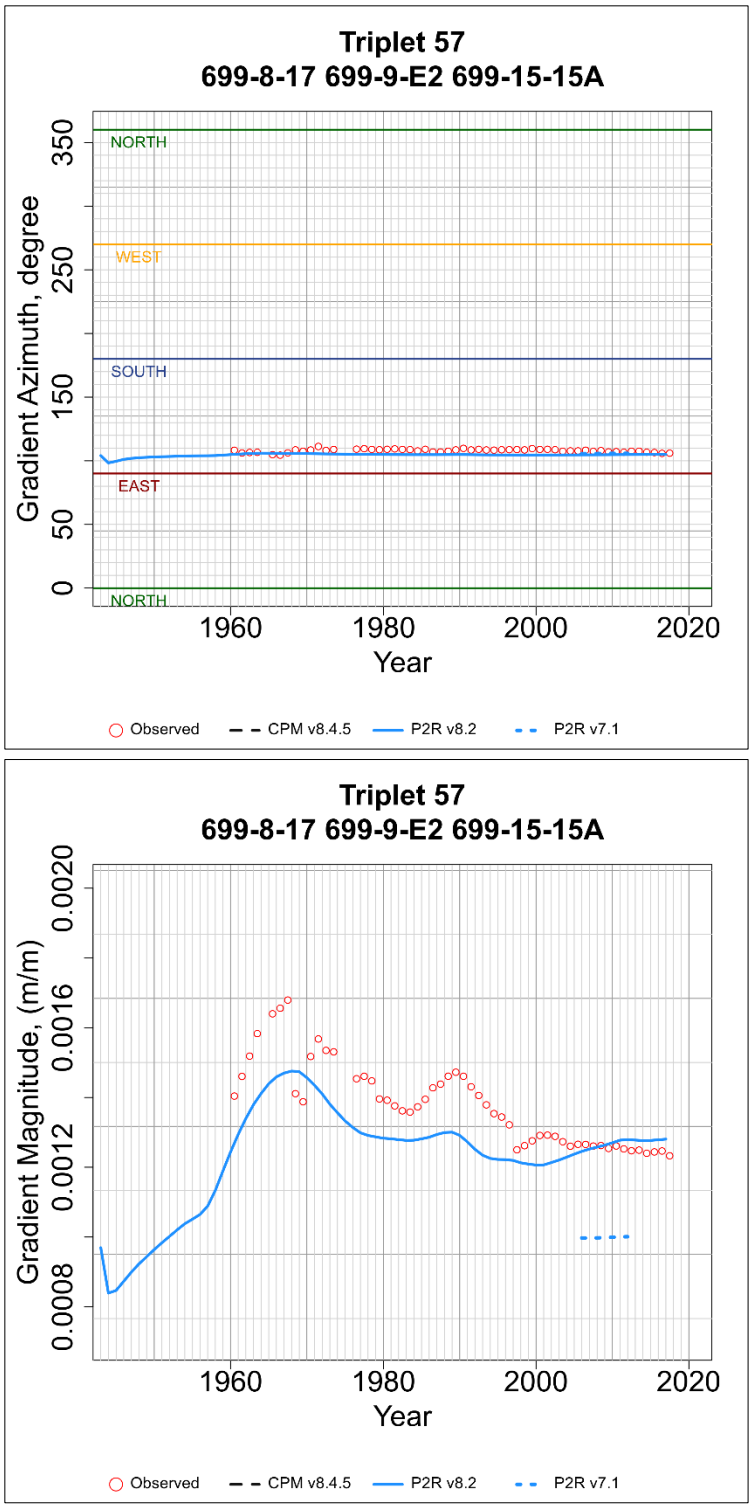

Figure C-57. Observed and simulated hydraulic gradient azimuth and magnitude for well triplet 57.

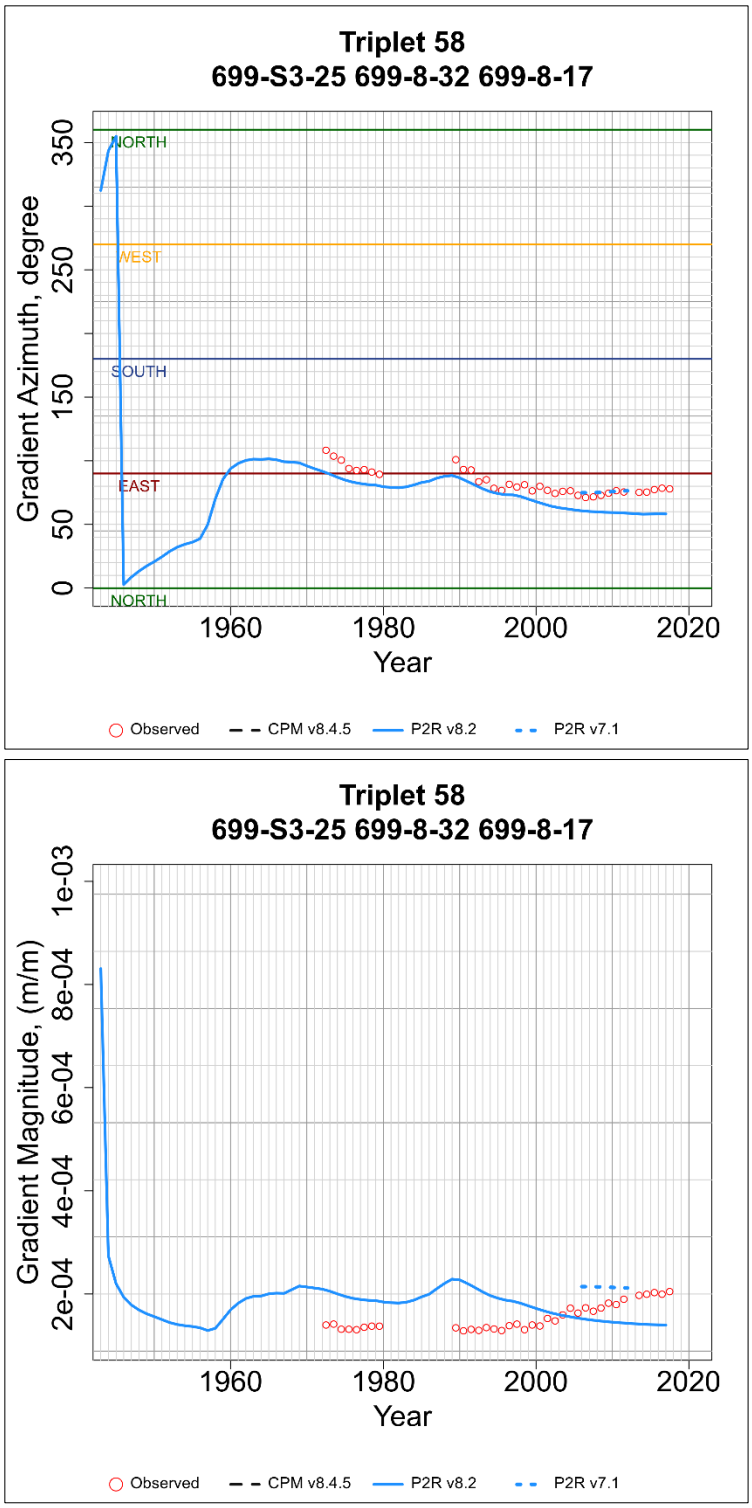

Figure C-58. Observed and simulated hydraulic gradient azimuth and magnitude for well triplet 58.

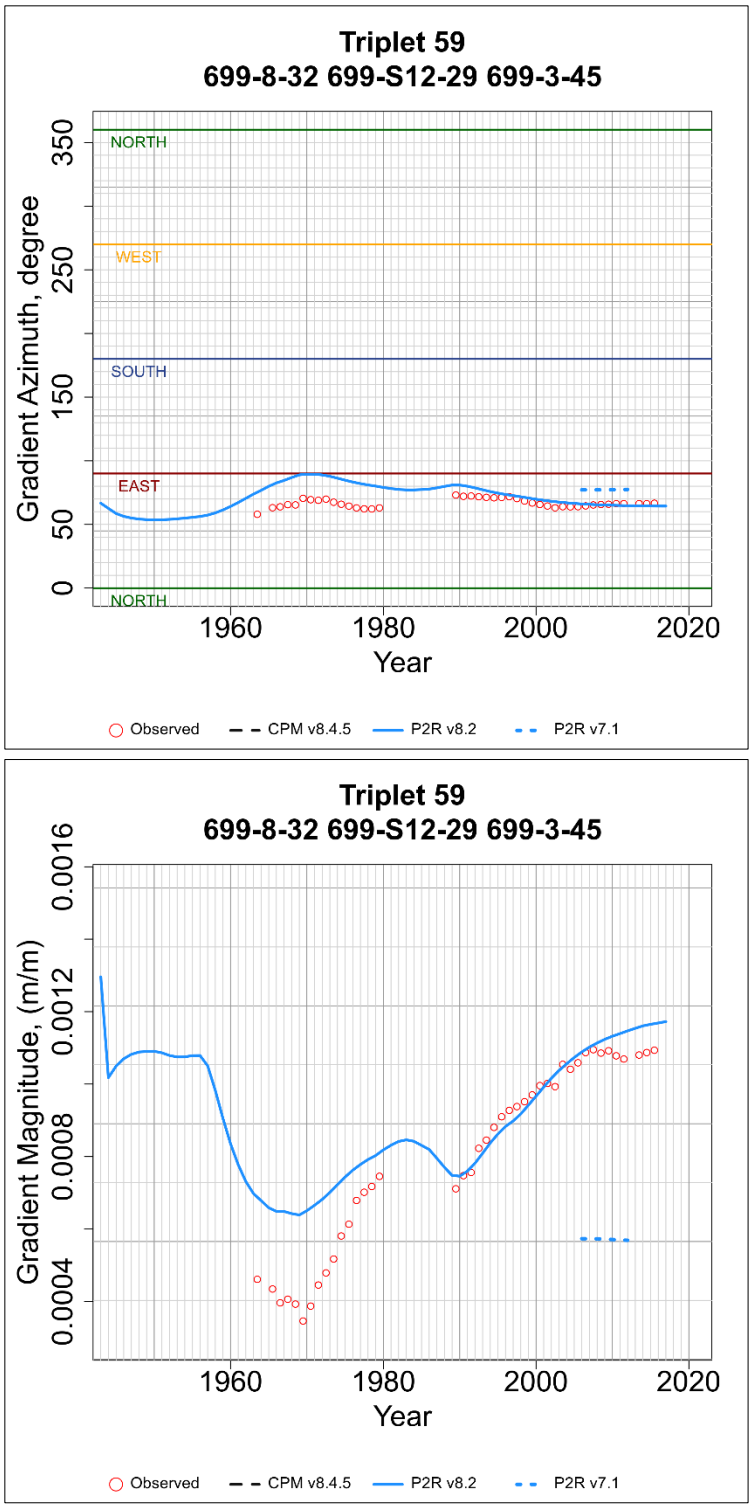

Figure C-59. Observed and simulated hydraulic gradient azimuth and magnitude for well triplet 59.

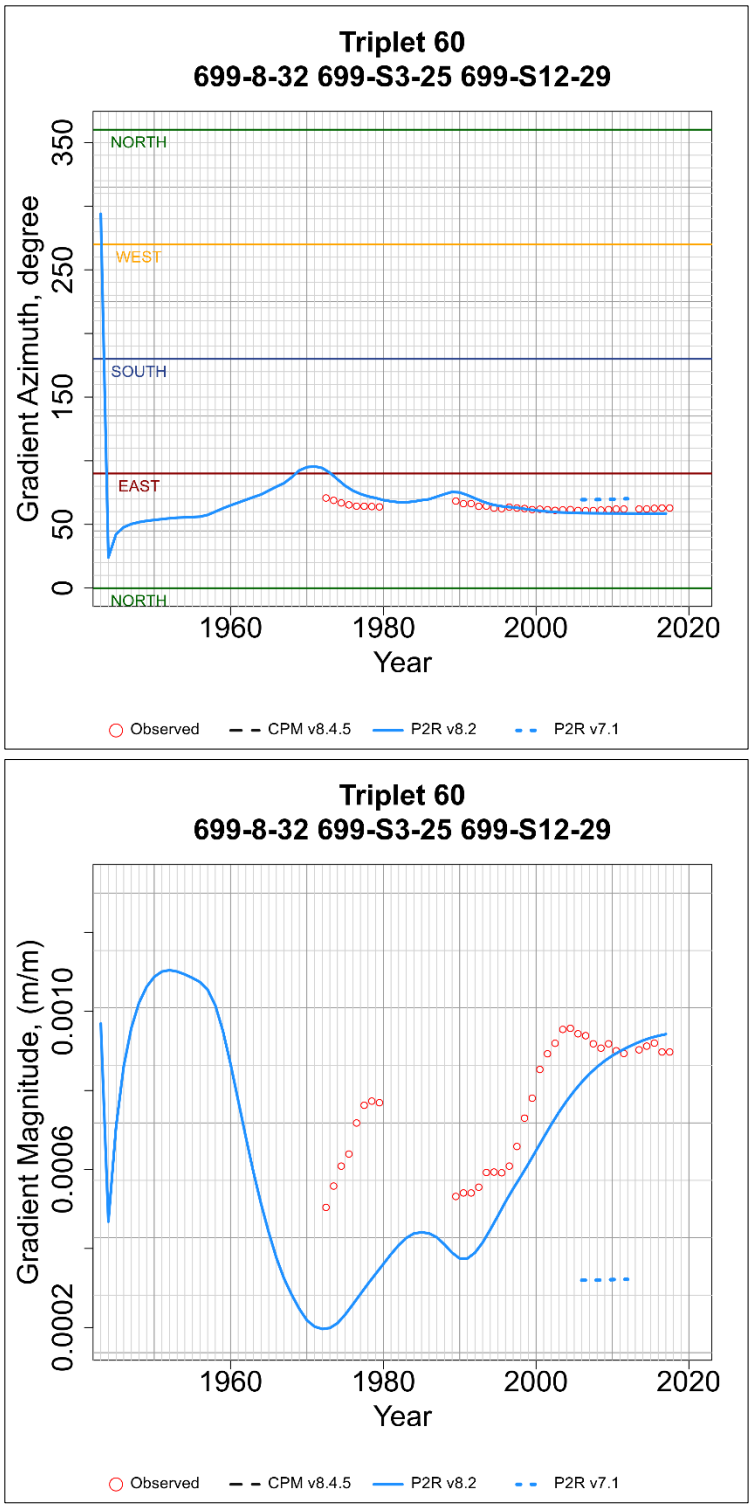

Figure C-60. Observed and simulated hydraulic gradient azimuth and magnitude for well triplet 60.

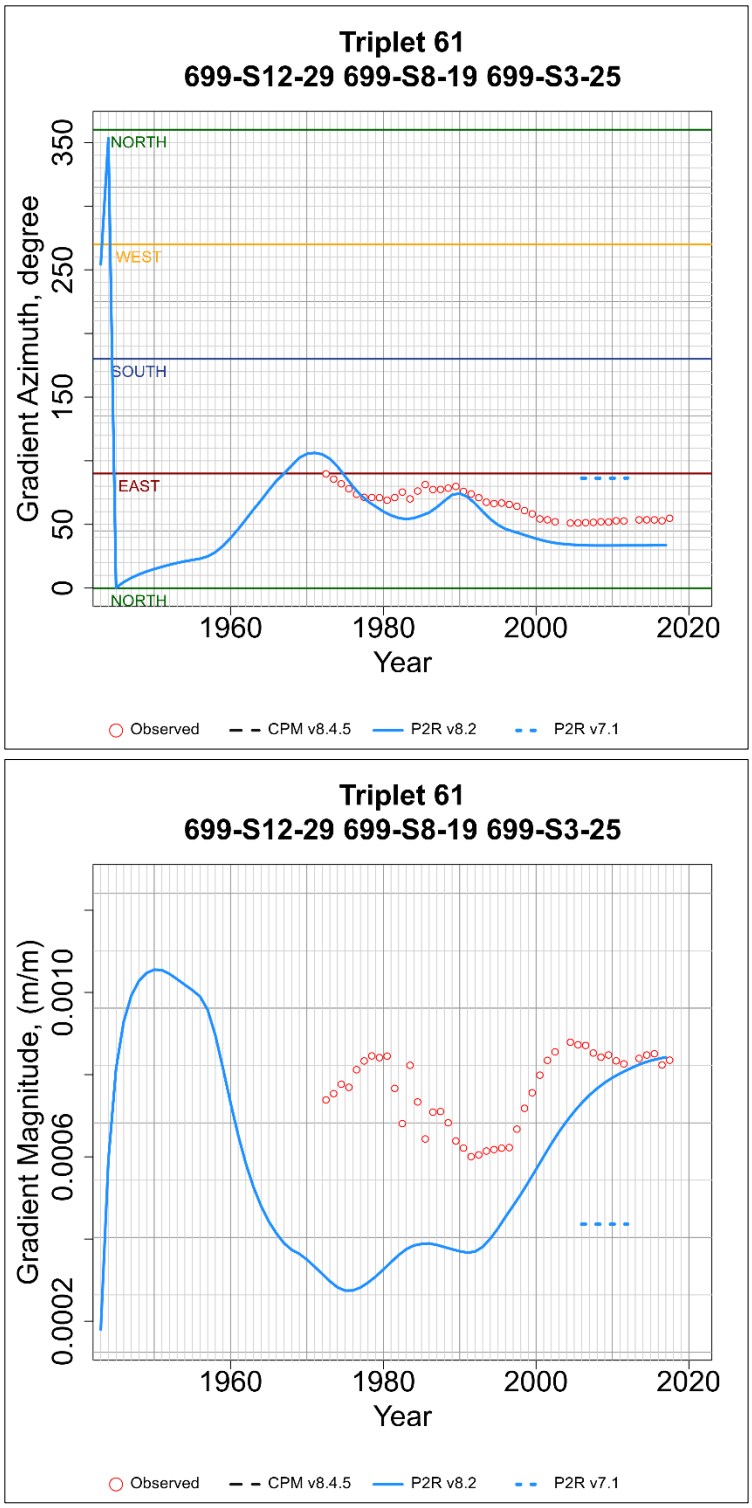

Figure C-61. Observed and simulated hydraulic gradient azimuth and magnitude for well triplet 61.

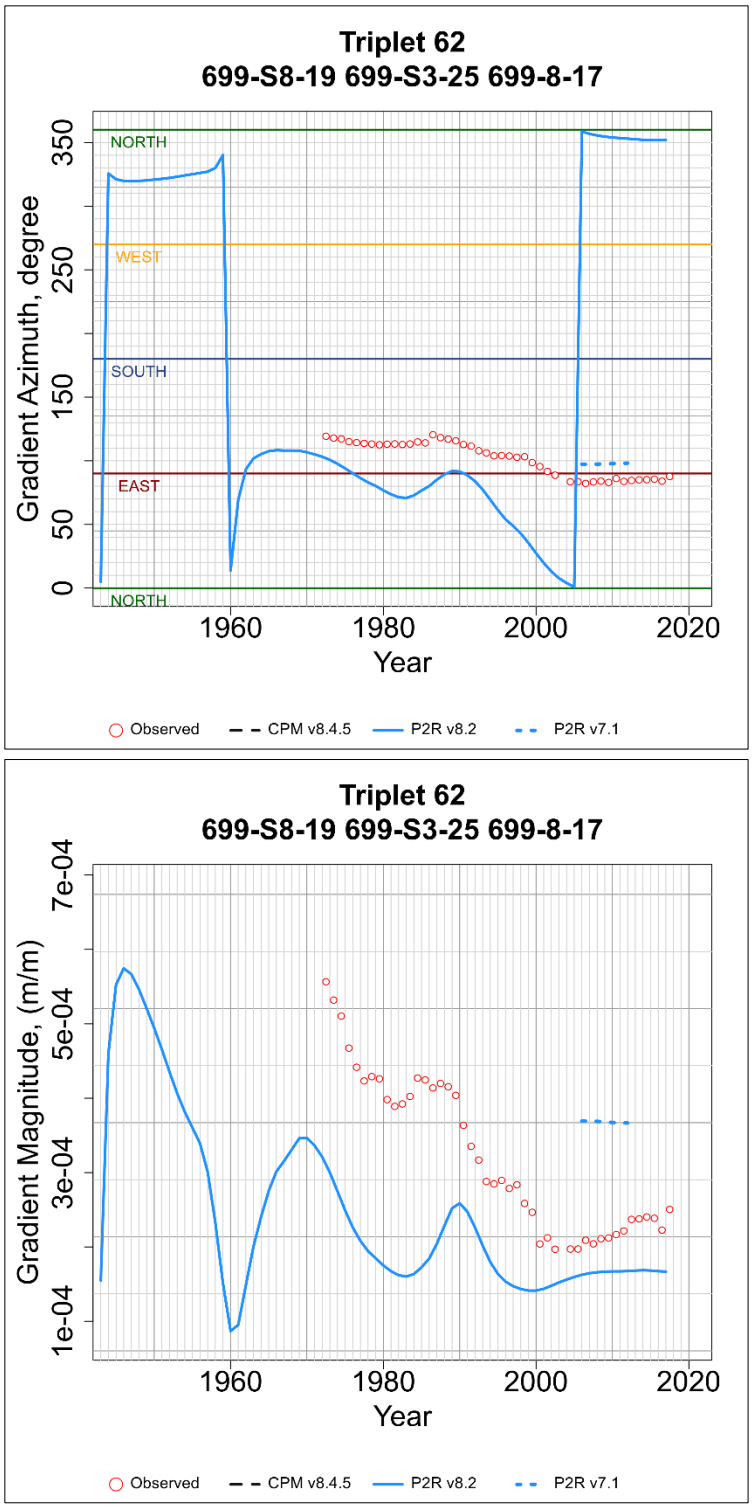

Figure C-62. Observed and simulated hydraulic gradient azimuth and magnitude for well triplet 62.

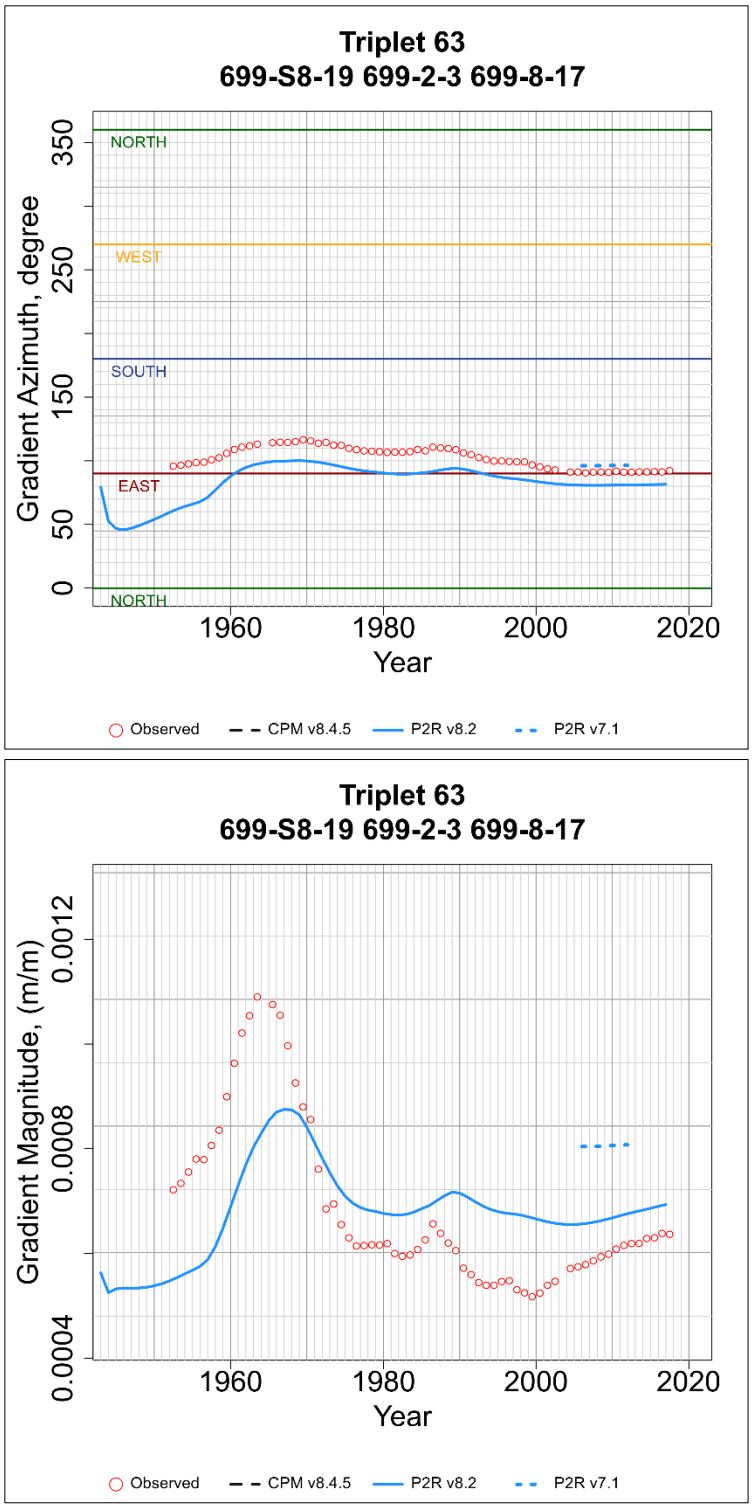

Figure C-63. Observed and simulated hydraulic gradient azimuth and magnitude for well triplet 63.

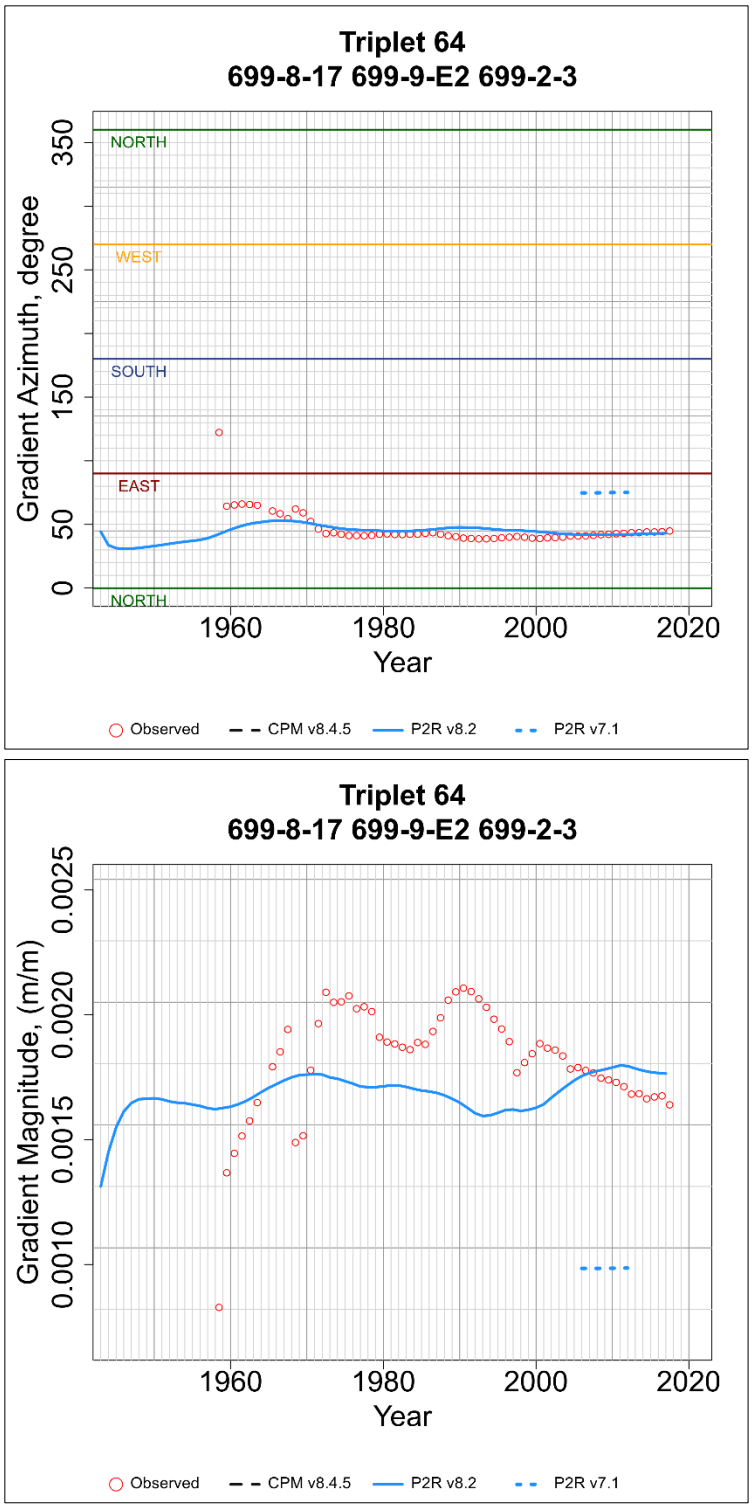

Figure C-64. Observed and simulated hydraulic gradient azimuth and magnitude for well triplet 64.

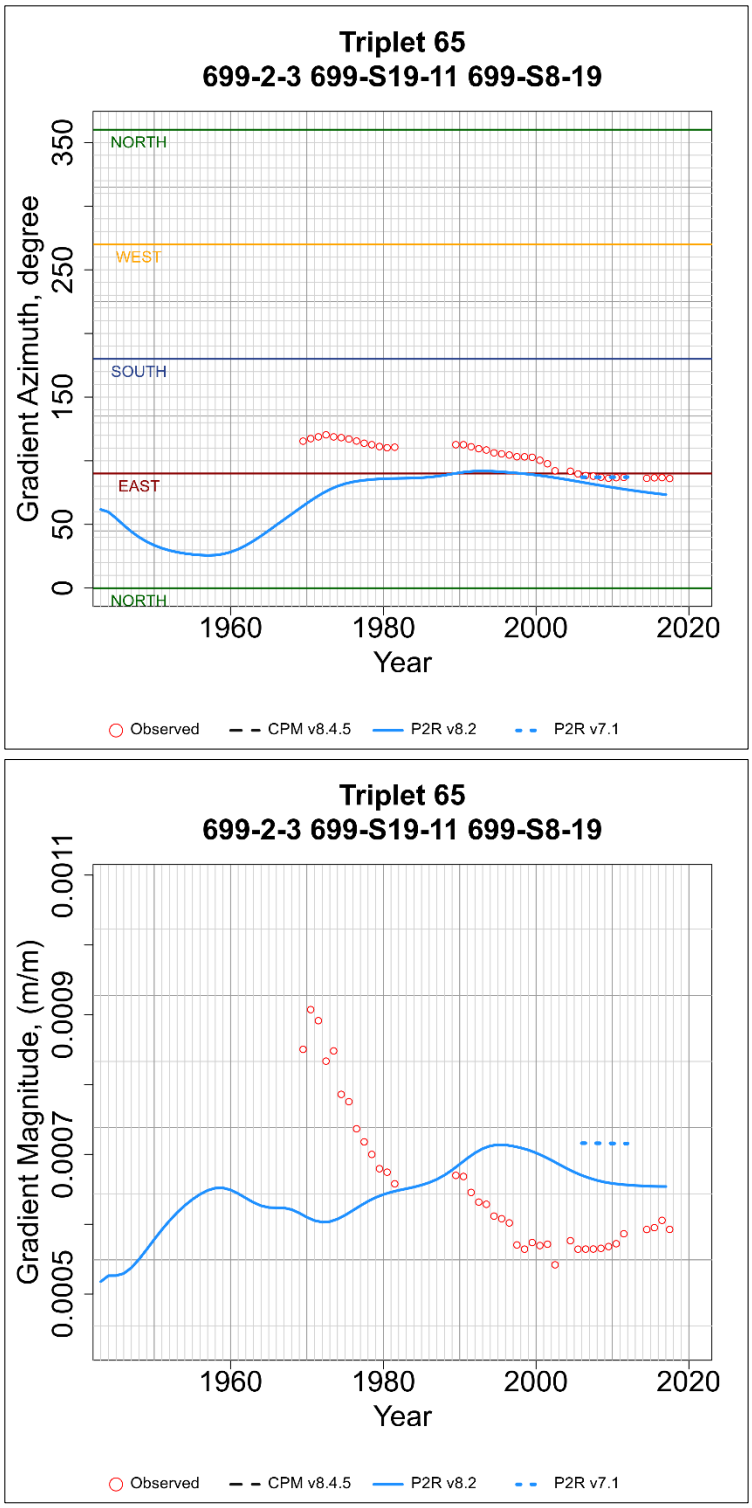

Figure C-65. Observed and simulated hydraulic gradient azimuth and magnitude for well triplet 65.

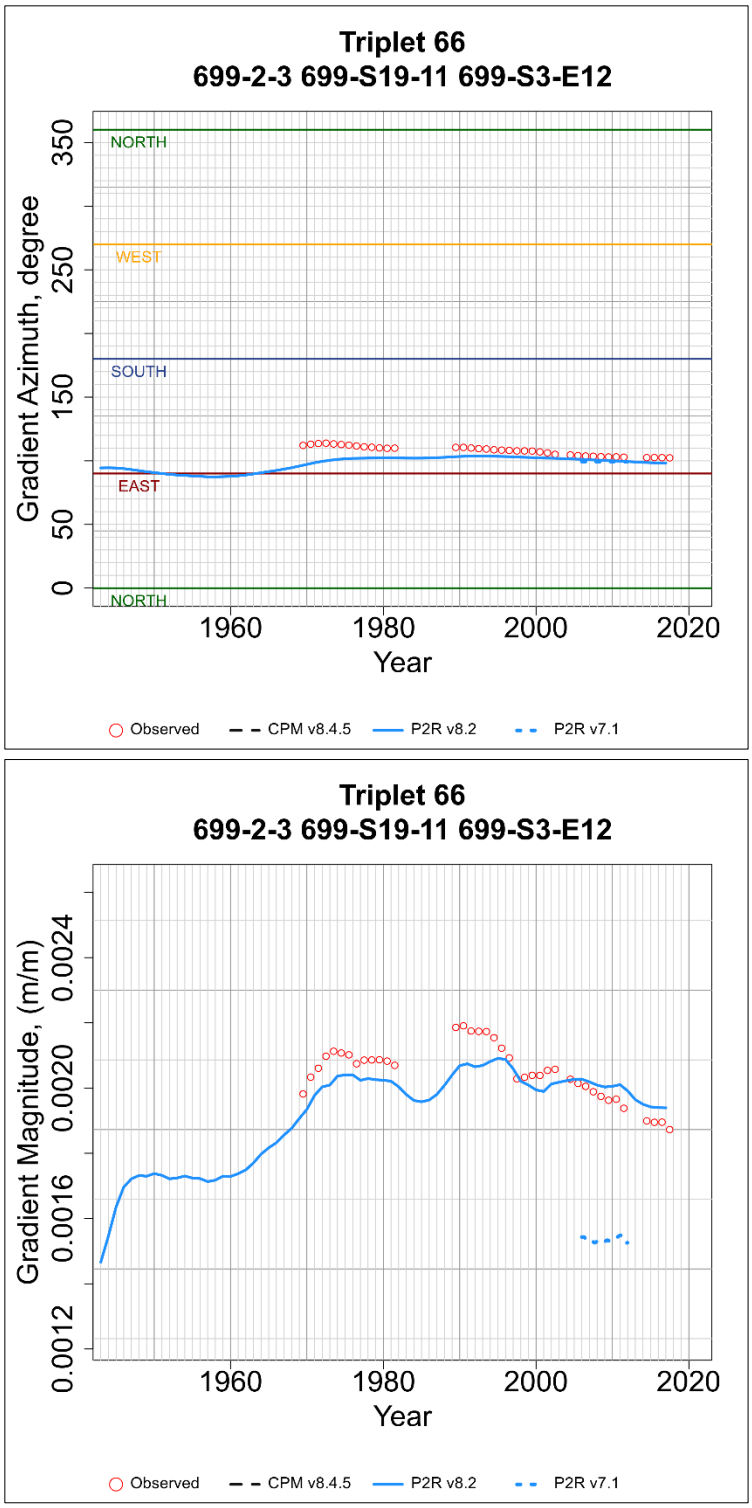

Figure C-66. Observed and simulated hydraulic gradient azimuth and magnitude for well triplet 66.

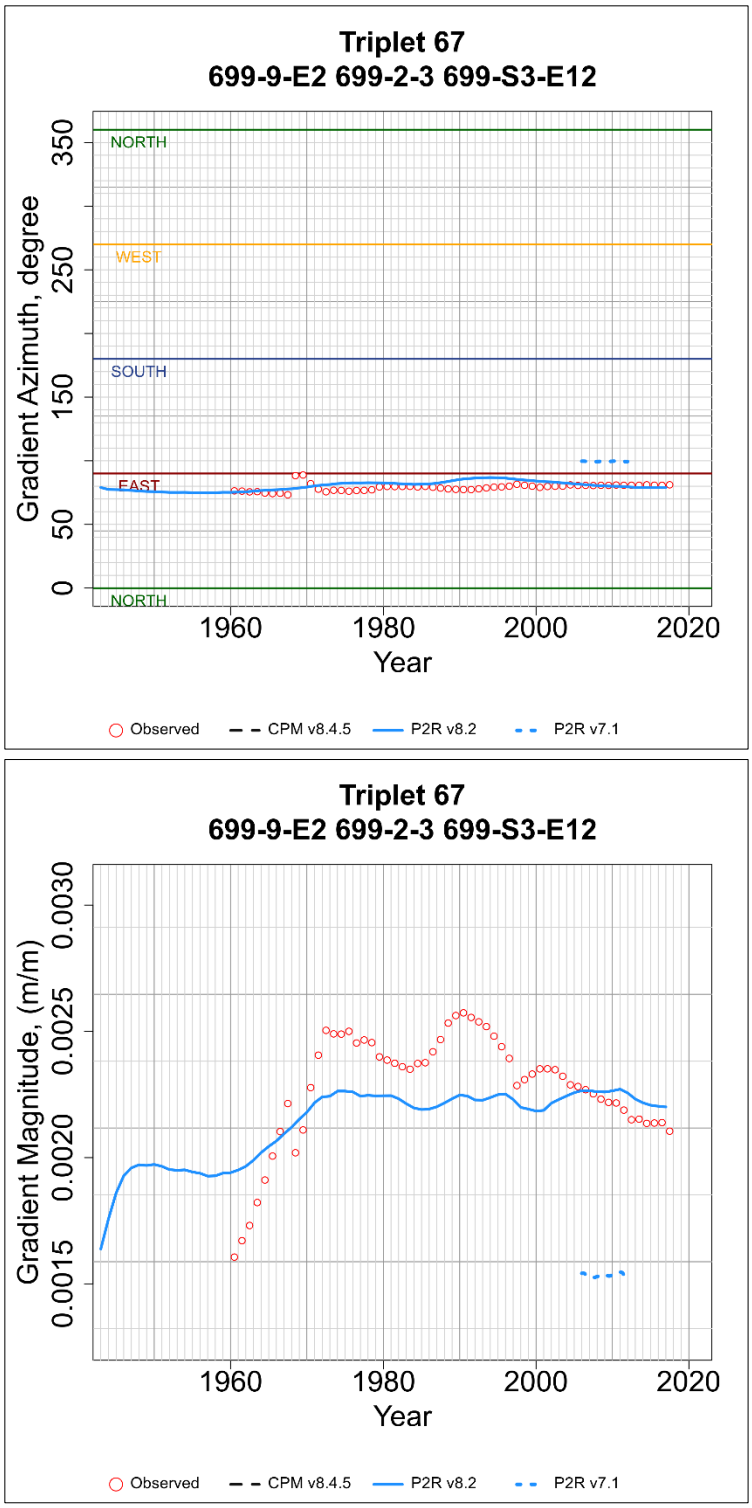

Figure C-67. Observed and simulated hydraulic gradient azimuth and magnitude for well triplet 67.

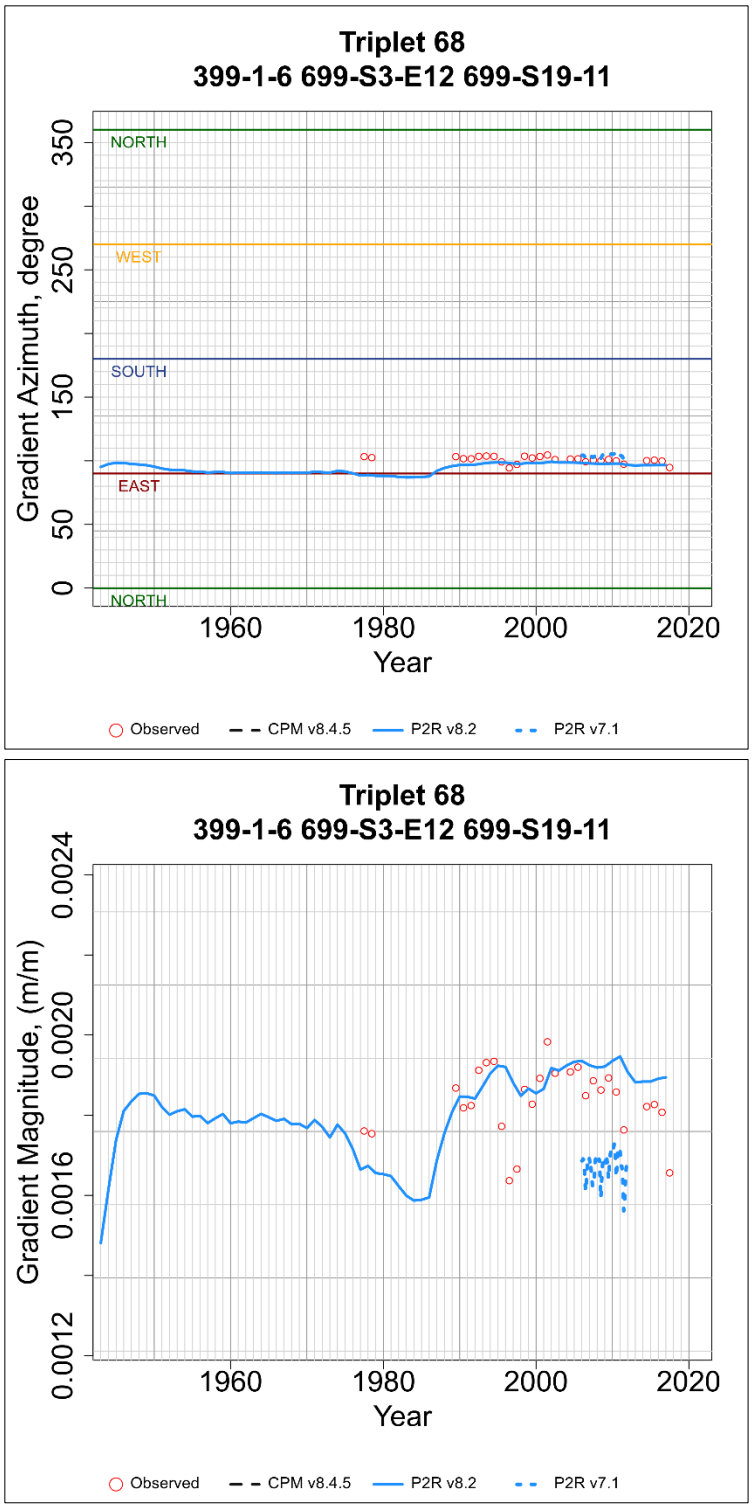

Figure C-68. Observed and simulated hydraulic gradient azimuth and magnitude for well triplet 68.

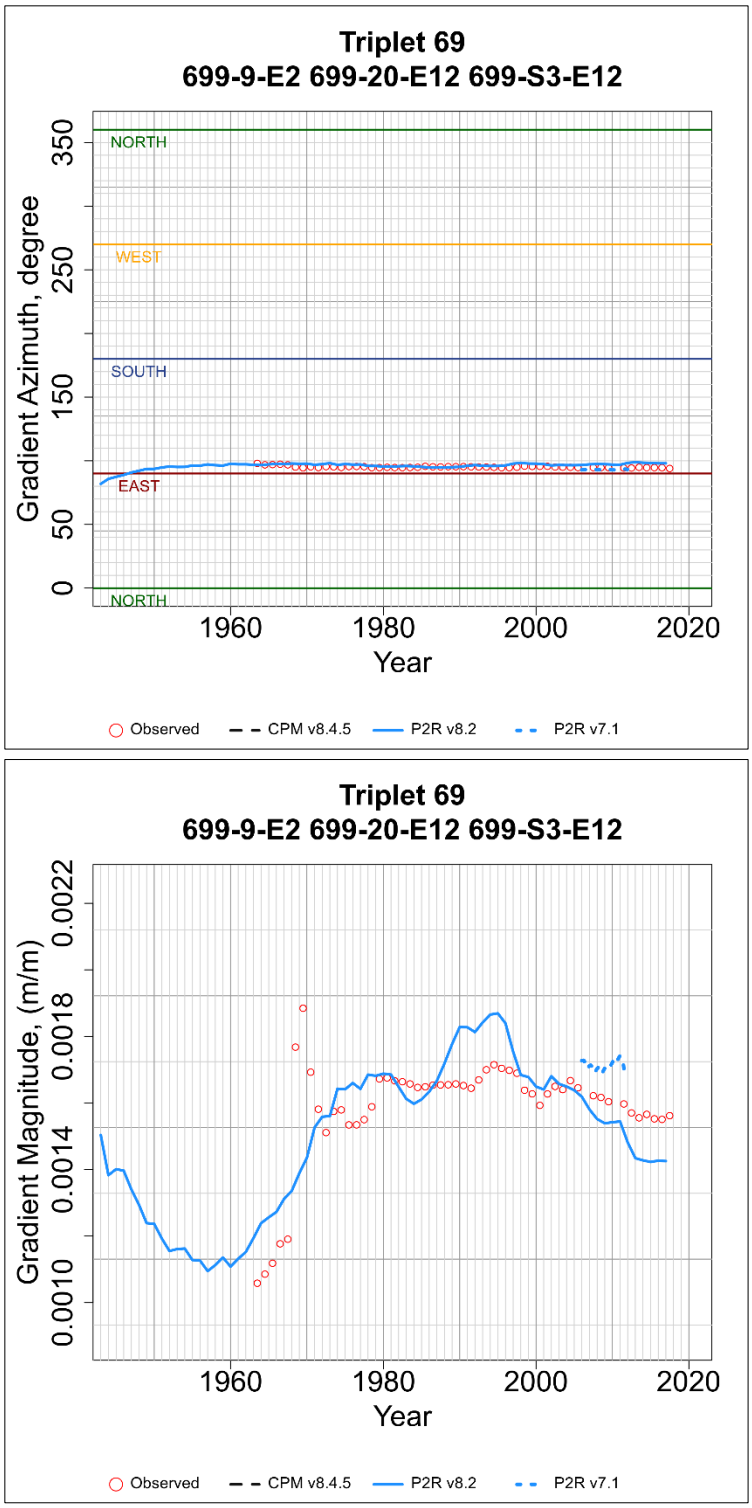

Figure C-69. Observed and simulated hydraulic gradient azimuth and magnitude for well triplet 69.

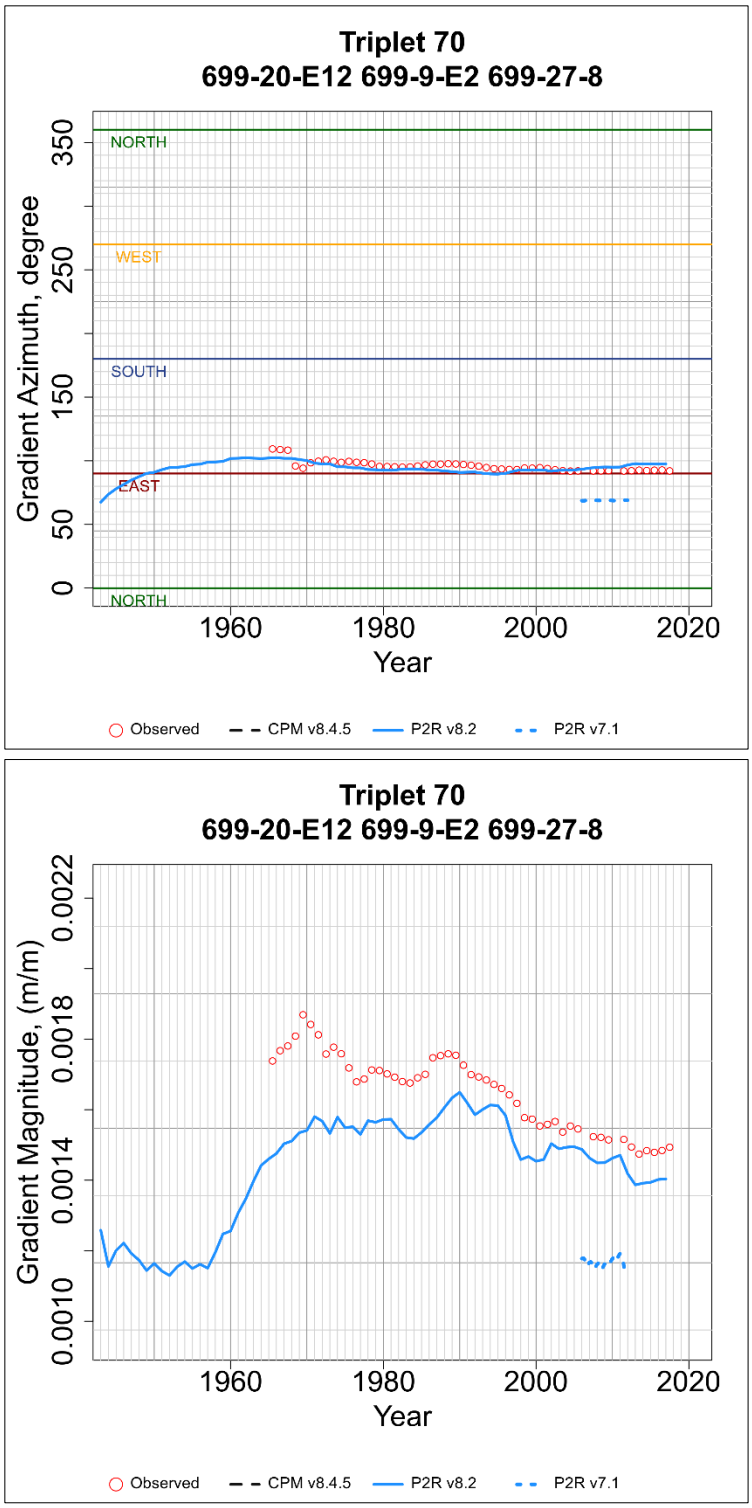

Figure C-70. Observed and simulated hydraulic gradient azimuth and magnitude for well triplet 70.

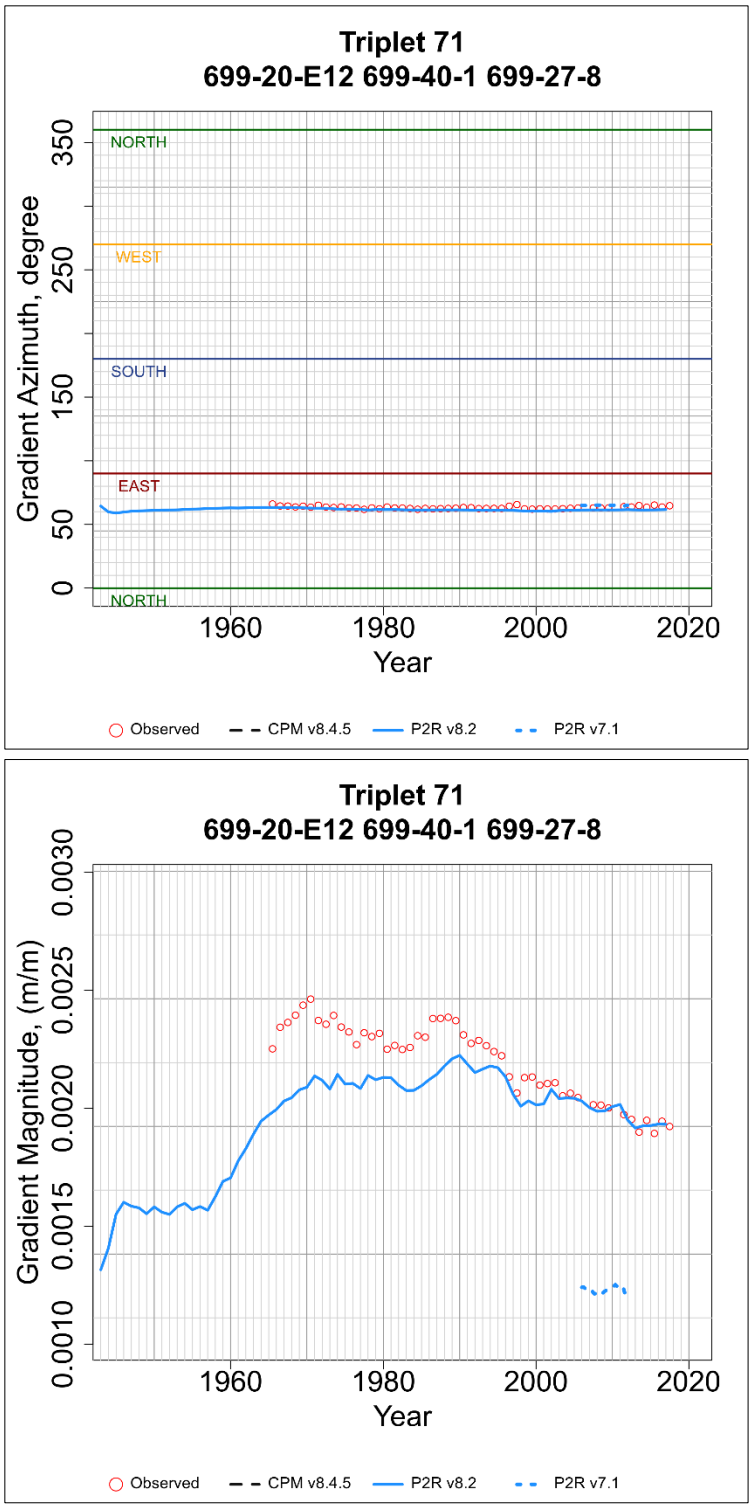

Figure C-71. Observed and simulated hydraulic gradient azimuth and magnitude for well triplet 71.

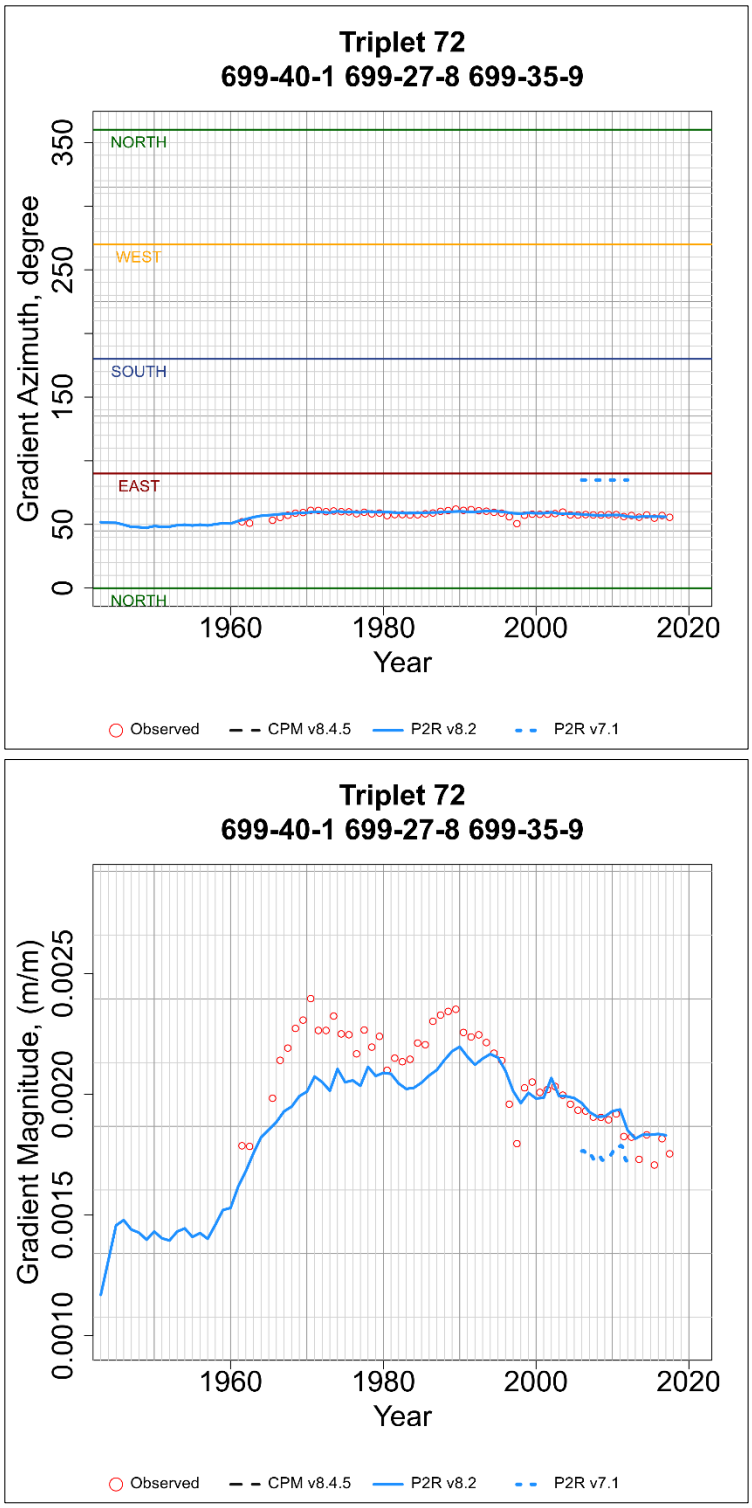

Figure C-72. Observed and simulated hydraulic gradient azimuth and magnitude for well triplet 72.

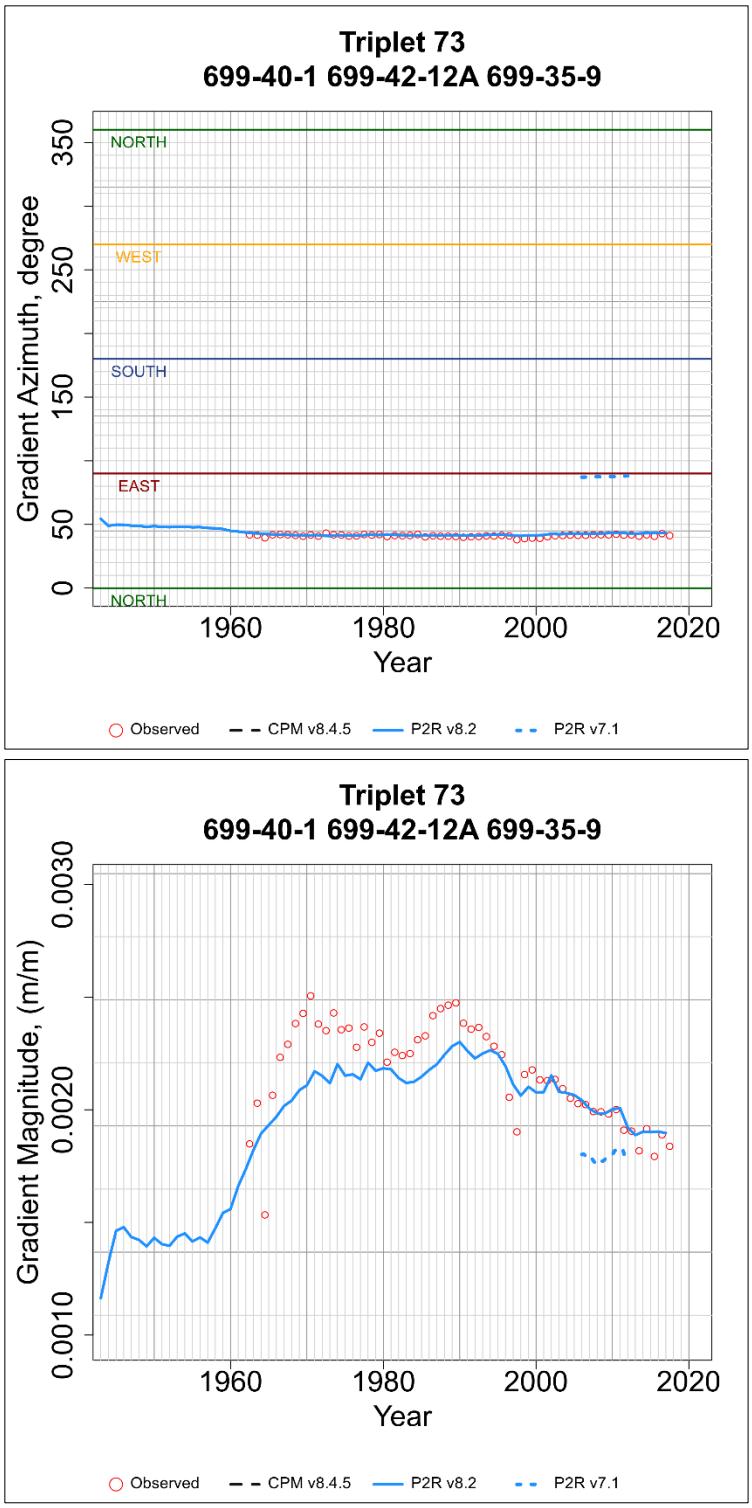

Figure C-73. Observed and simulated hydraulic gradient azimuth and magnitude for well triplet 73.

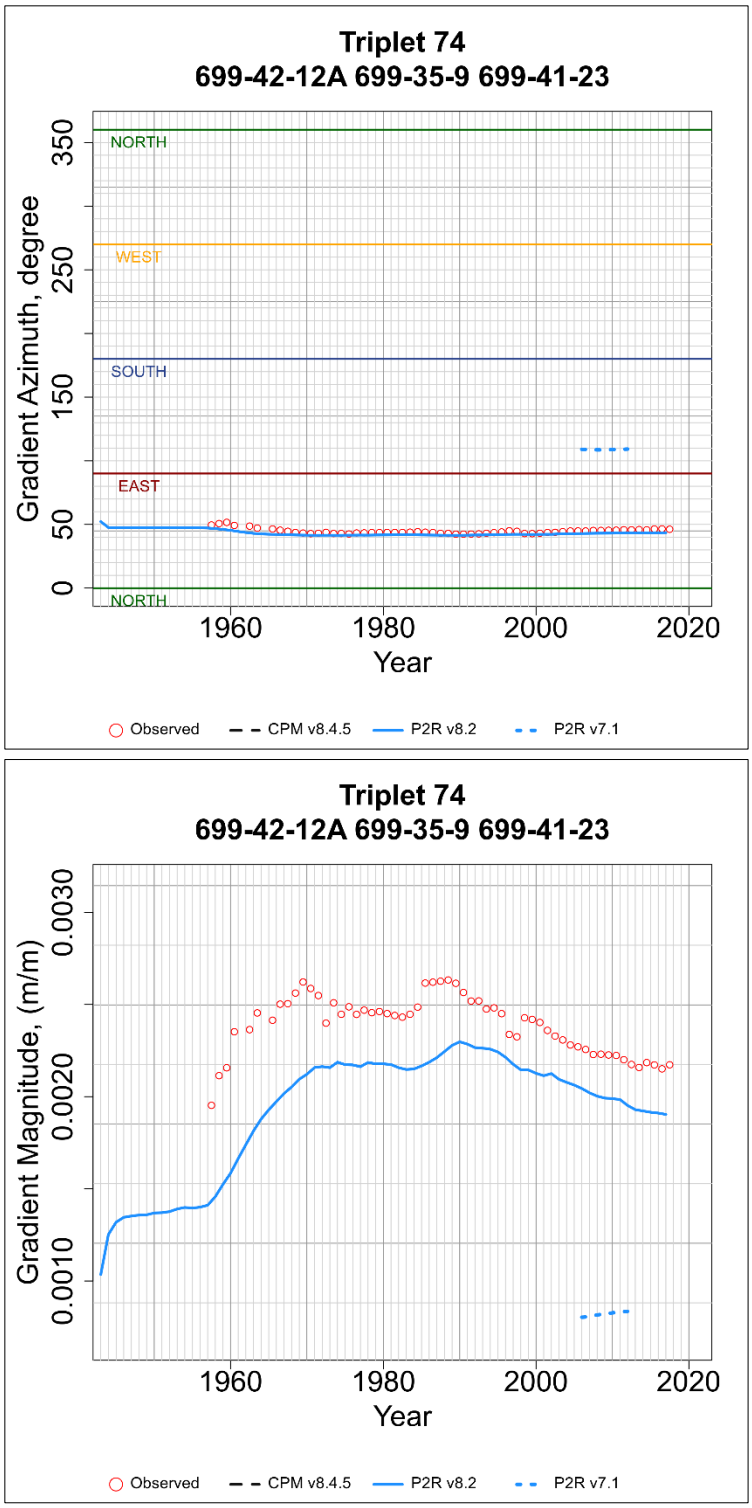

Figure C-74. Observed and simulated hydraulic gradient azimuth and magnitude for well triplet 74.

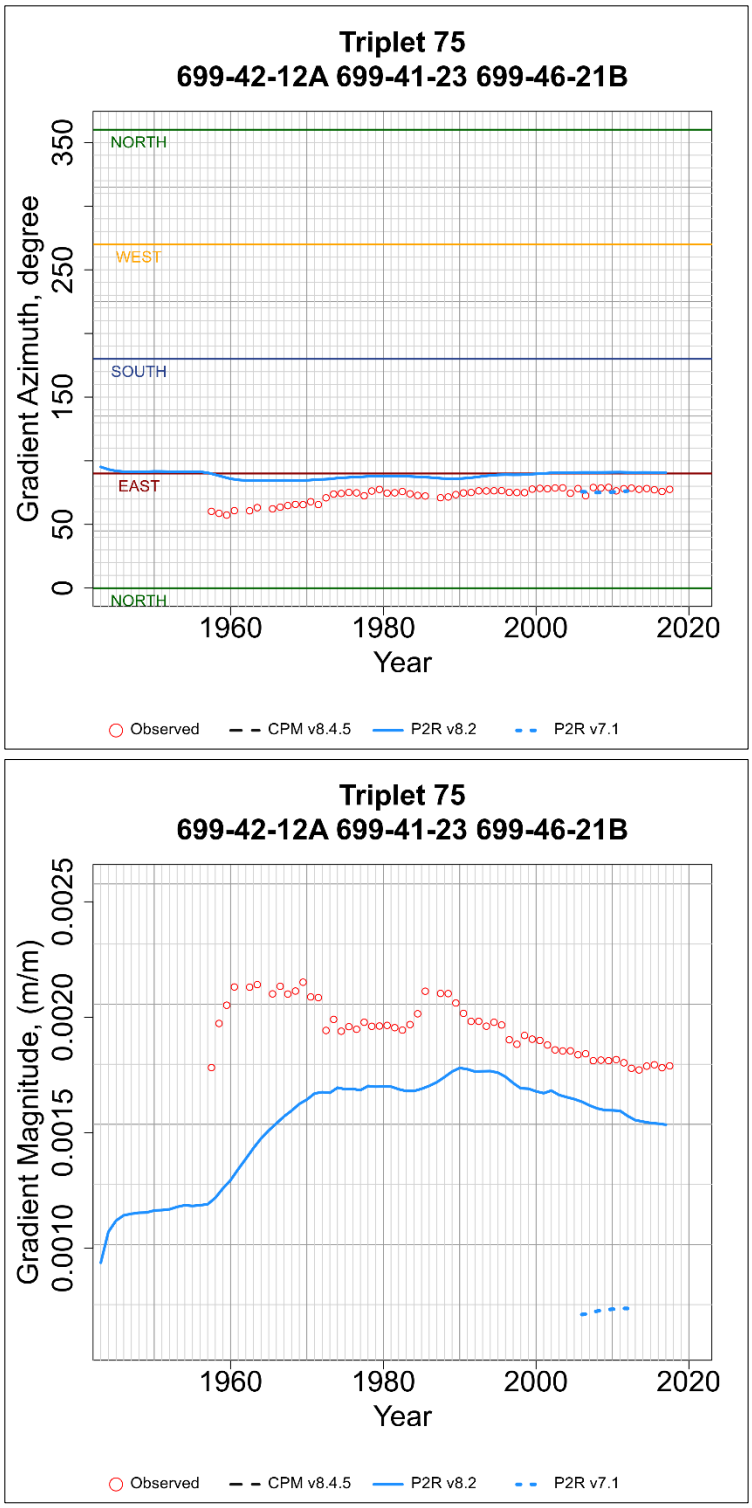

Figure C-75. Observed and simulated hydraulic gradient azimuth and magnitude for well triplet 75.

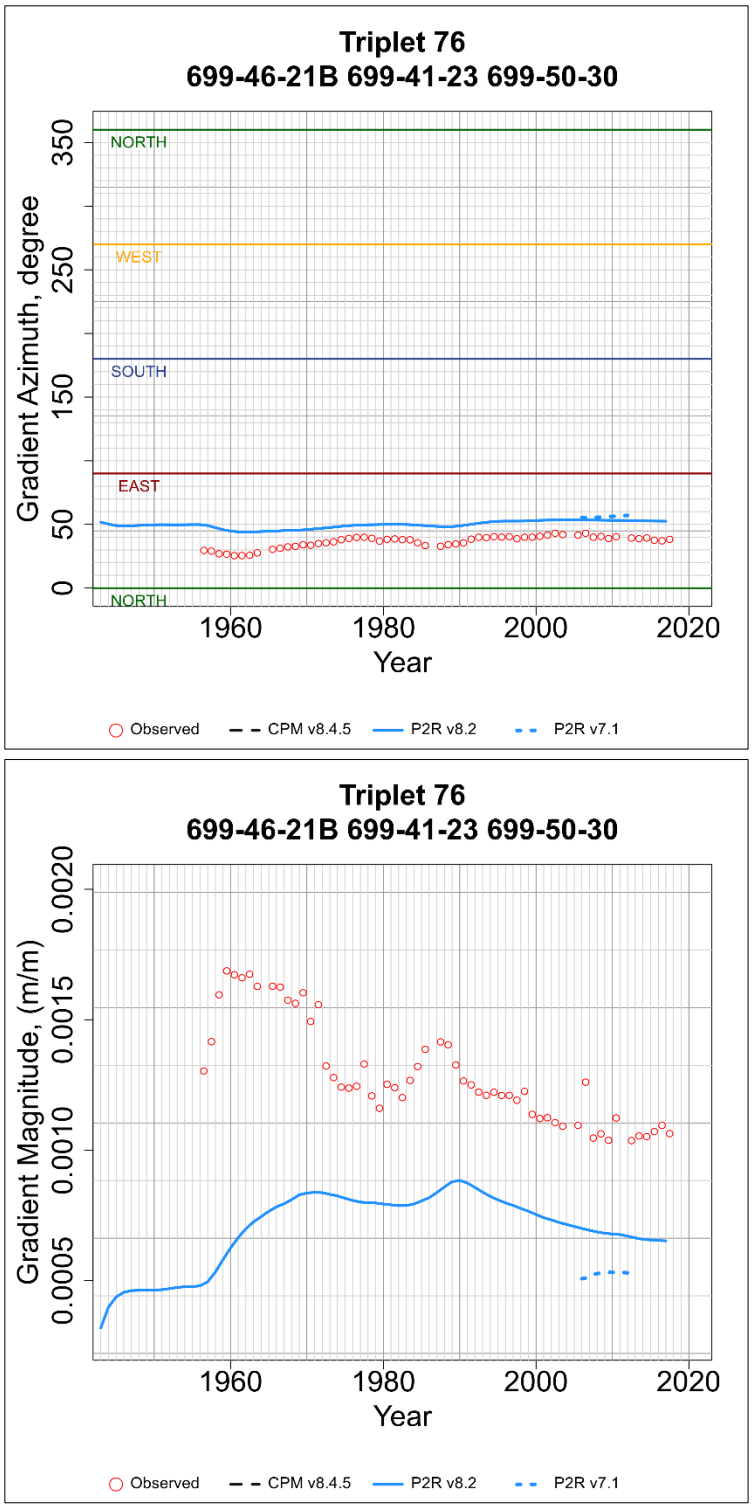

Figure C-76. Observed and simulated hydraulic gradient azimuth and magnitude for well triplet 76.

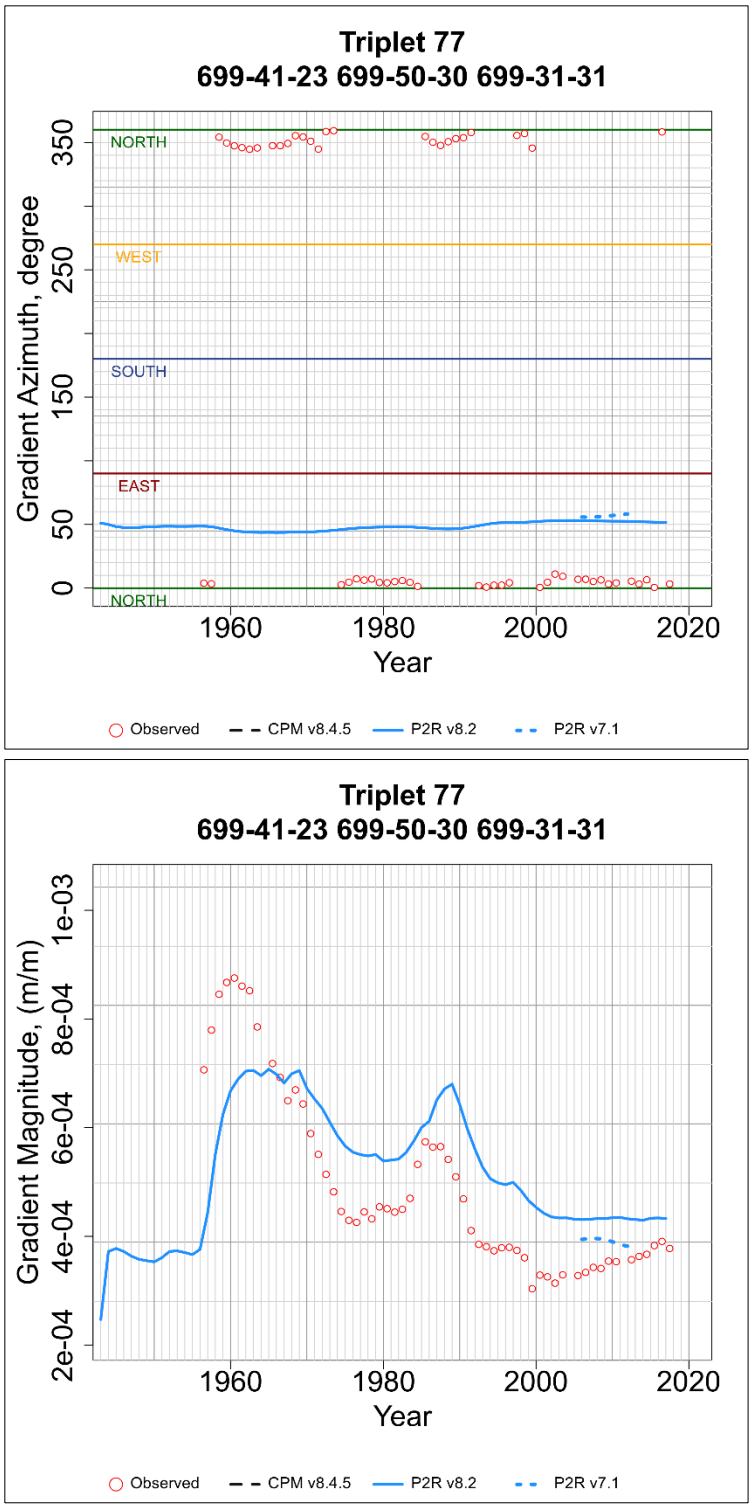

Figure C-77. Observed and simulated hydraulic gradient azimuth and magnitude for well triplet 77.

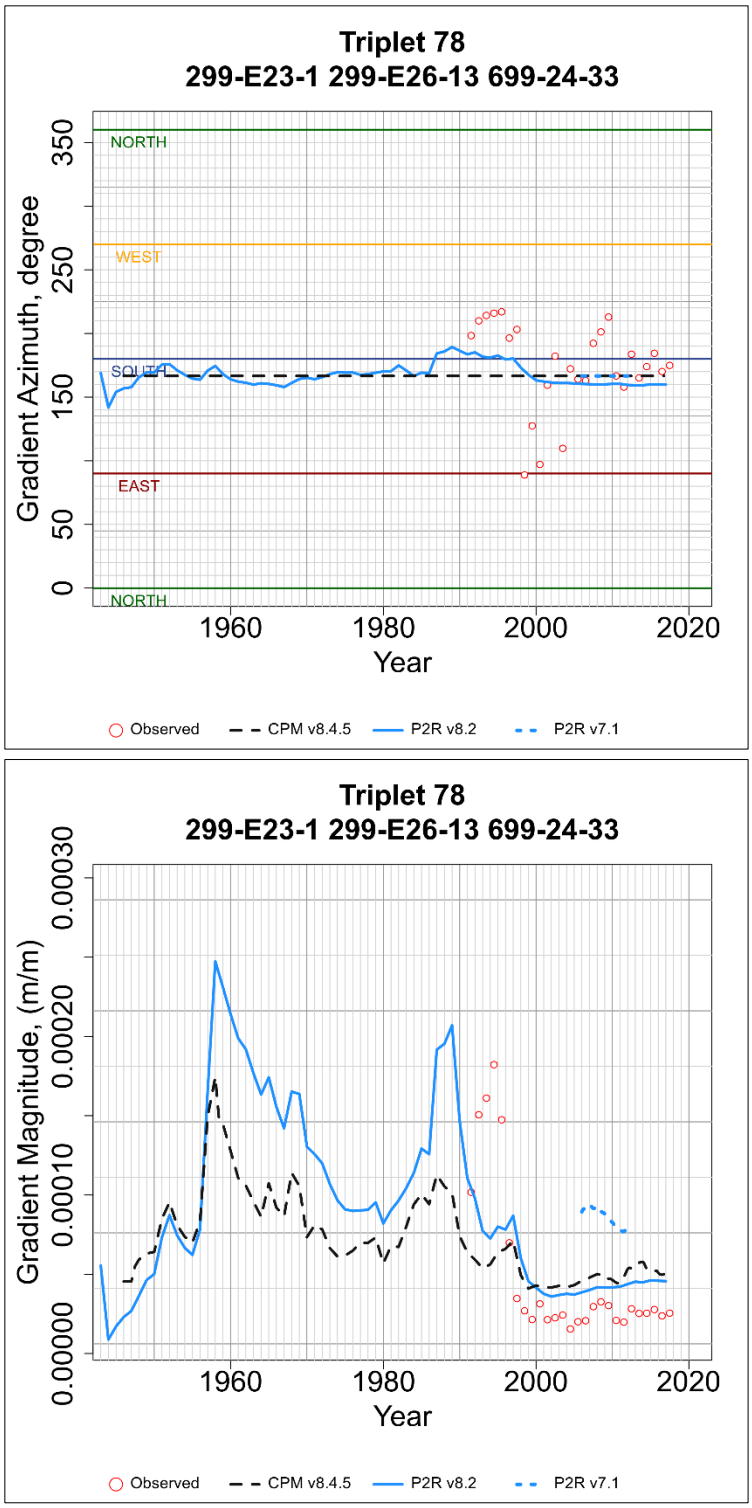

Figure C-78. Observed and simulated hydraulic gradient azimuth and magnitude for well triplet 78.

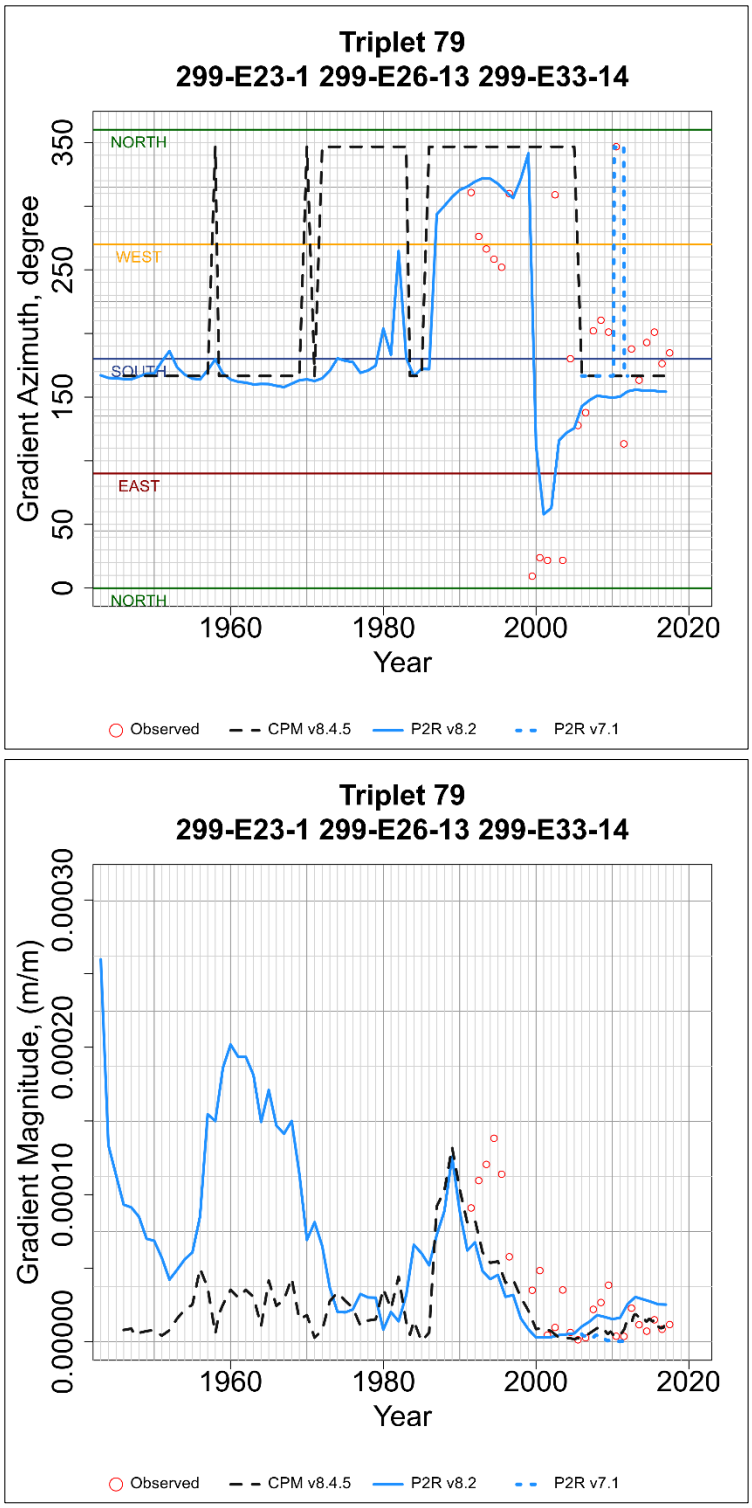

Figure C-79. Observed and simulated hydraulic gradient azimuth and magnitude for well triplet 79.

Attachment D

Hydrographs for Observed Data and Simulated Results at Observation Wells

Figure D-1. Observed and simulated water level in the P2R Model at well 299-E13-10.png. 15
Figure D-2. Observed and simulated water level in the P2R Model at well 299-E16-1.png. 15
Figure D-3. Observed and simulated water level in the P2R Model at well 299-E17-14.png. 16
Figure D-4. Observed and simulated water level in the P2R Model at well 299-E17-15.png. 16
Figure D-5. Observed and simulated water level in the P2R Model at well 299-E17-16.png. 17
Figure D-6. Observed and simulated water level in the P2R Model at well 299-E17-17.png. 17
Figure D-7. Observed and simulated water level in the P2R Model at well 299-E17-18.png. 18
Figure D-8. Observed and simulated water level in the P2R Model at well 299-E17-19.png. 18
Figure D-9. Observed and simulated water level in the P2R Model at well 299-E17-20.png. 19
Figure D-10. Observed and simulated water level in the P2R Model at well 299-E17-21.png. 19
Figure D-11. Observed and simulated water level in the P2R Model at well 299-E17-22.png. 20
Figure D-12. Observed and simulated water level in the P2R Model at well 299-E17-23.png. 20
Figure D-13. Observed and simulated water level in the P2R Model at well 299-E17-3.png. 21
Figure D-14. Observed and simulated water level in the P2R Model at well 299-E18-1.png. 21
Figure D-15. Observed and simulated water level in the P2R Model at well 299-E18-2.png. 22
Figure D-16. Observed and simulated water level in the P2R Model at well 299-E18-3.png. 22
Figure D-17. Observed and simulated water level in the P2R Model at well 299-E18-4.png. 23
Figure D-18. Observed and simulated water level in the P2R Model at well 299-E19-1.png. 23
Figure D-19. Observed and simulated water level in the P2R Model at well 299-E23-1.png. 24
Figure D-20. Observed and simulated water level in the P2R Model at well 299-E24-16.png. 24
Figure D-21. Observed and simulated water level in the P2R Model at well 299-E24-17.png. 25
Figure D-22. Observed and simulated water level in the P2R Model at well 299-E24-18.png. 25
Figure D-23. Observed and simulated water level in the P2R Model at well 299-E24-19.png. 26
Figure D-24. Observed and simulated water level in the P2R Model at well 299-E24-20.png. 26
Figure D-25. Observed and simulated water level in the P2R Model at well 299-E24-7.png. 27
Figure D-26. Observed and simulated water level in the P2R Model at well 299-E25-10.png. 27
Figure D-27. Observed and simulated water level in the P2R Model at well 299-E25-21.png. 28
Figure D-28. Observed and simulated water level in the P2R Model at well 299-E25-22.png. 28
Figure D-29. Observed and simulated water level in the P2R Model at well 299-E25-23.png. 29
Figure D-30. Observed and simulated water level in the P2R Model at well 299-E25-24.png. 29
Figure D-31. Observed and simulated water level in the P2R Model at well 299-E25-25.png. 30
Figure D-32. Observed and simulated water level in the P2R Model at well 299-E25-31.png. 30
Figure D-33. Observed and simulated water level in the P2R Model at well 299-E25-33.png. 31
Figure D-34. Observed and simulated water level in the P2R Model at well 299-E25-34.png. 31
Figure D-35. Observed and simulated water level in the P2R Model at well 299-E25-35.png. 32
Figure D-36. Observed and simulated water level in the P2R Model at well 299-E25-36.png. 32
Figure D-37. Observed and simulated water level in the P2R Model at well 299-E25-37.png. 33
Figure D-38. Observed and simulated water level in the P2R Model at well 299-E25-39.png. 33
Figure D-39. Observed and simulated water level in the P2R Model at well 299-E25-40.png. 34

Figure D-40. Observed and simulated water level in the P2R Model at well 299-E25-41.png. 34
Figure D-41. Observed and simulated water level in the P2R Model at well 299-E25-42.png. 35
Figure D-42. Observed and simulated water level in the P2R Model at well 299-E25-43.png. 35
Figure D-43. Observed and simulated water level in the P2R Model at well 299-E25-44.png. 36
Figure D-44. Observed and simulated water level in the P2R Model at well 299-E25-45.png. 36
Figure D-45. Observed and simulated water level in the P2R Model at well 299-E25-46.png. 37
Figure D-46. Observed and simulated water level in the P2R Model at well 299-E25-47.png. 37
Figure D-47. Observed and simulated water level in the P2R Model at well 299-E25-48.png. 38
Figure D-48. Observed and simulated water level in the P2R Model at well 299-E25-93.png. 38
Figure D-49. Observed and simulated water level in the P2R Model at well 299-E26-1.png. 39
Figure D-50. Observed and simulated water level in the P2R Model at well 299-E26-10.png. 39
Figure D-51. Observed and simulated water level in the P2R Model at well 299-E26-12.png. 40
Figure D-52. Observed and simulated water level in the P2R Model at well 299-E26-13.png. 40
Figure D-53. Observed and simulated water level in the P2R Model at well 299-E26-9.png. 41
Figure D-54. Observed and simulated water level in the P2R Model at well 299-E27-1.png. 41
Figure D-55. Observed and simulated water level in the P2R Model at well 299-E27-10.png. 42
Figure D-56. Observed and simulated water level in the P2R Model at well 299-E27-11.png. 42
Figure D-57. Observed and simulated water level in the P2R Model at well 299-E27-12.png. 43
Figure D-58. Observed and simulated water level in the P2R Model at well 299-E27-13.png. 43
Figure D-59. Observed and simulated water level in the P2R Model at well 299-E27-14.png. 44
Figure D-60. Observed and simulated water level in the P2R Model at well 299-E27-15.png. 44
Figure D-61. Observed and simulated water level in the P2R Model at well 299-E27-16.png. 45
Figure D-62. Observed and simulated water level in the P2R Model at well 299-E27-17.png. 45
Figure D-63. Observed and simulated water level in the P2R Model at well 299-E27-18.png. 46
Figure D-64. Observed and simulated water level in the P2R Model at well 299-E27-19.png. 46
Figure D-65. Observed and simulated water level in the P2R Model at well 299-E27-21.png. 47
Figure D-66. Observed and simulated water level in the P2R Model at well 299-E27-4.png. 47
Figure D-67. Observed and simulated water level in the P2R Model at well 299-E27-5.png. 48
Figure D-68. Observed and simulated water level in the P2R Model at well 299-E27-8.png. 48
Figure D-69. Observed and simulated water level in the P2R Model at well 299-E27-9.png. 49
Figure D-70. Observed and simulated water level in the P2R Model at well 299-E28-1.png. 49
Figure D-71. Observed and simulated water level in the P2R Model at well 299-E28-10.png. 50
Figure D-72. Observed and simulated water level in the P2R Model at well 299-E28-2.png. 50
Figure D-73. Observed and simulated water level in the P2R Model at well 299-E28-26.png. 51
Figure D-74. Observed and simulated water level in the P2R Model at well 299-E28-27.png. 51
Figure D-75. Observed and simulated water level in the P2R Model at well 299-E28-28.png. 52
Figure D-76. Observed and simulated water level in the P2R Model at well 299-E28-4.png. 52
Figure D-77. Observed and simulated water level in the P2R Model at well 299-E28-5.png. 53
Figure D-78. Observed and simulated water level in the P2R Model at well 299-E28-6.png. 53

Figure D-79. Observed and simulated water level in the P2R Model at well 299-E28-8.png. 54
Figure D-80. Observed and simulated water level in the P2R Model at well 299-E32-1.png. 54
Figure D-81. Observed and simulated water level in the P2R Model at well 299-E32-10.png. 55
Figure D-82. Observed and simulated water level in the P2R Model at well 299-E32-2.png. 55
Figure D-83. Observed and simulated water level in the P2R Model at well 299-E32-3.png. 56
Figure D-84. Observed and simulated water level in the P2R Model at well 299-E32-4.png. 56
Figure D-85. Observed and simulated water level in the P2R Model at well 299-E32-5.png. 57
Figure D-86. Observed and simulated water level in the P2R Model at well 299-E32-6.png. 57
Figure D-87. Observed and simulated water level in the P2R Model at well 299-E32-7.png. 58
Figure D-88. Observed and simulated water level in the P2R Model at well 299-E32-8.png. 58
Figure D-89. Observed and simulated water level in the P2R Model at well 299-E33-14.png. 59
Figure D-90. Observed and simulated water level in the P2R Model at well 299-E33-15.png. 59
Figure D-91. Observed and simulated water level in the P2R Model at well 299-E33-16.png. 60
Figure D-92. Observed and simulated water level in the P2R Model at well 299-E33-17.png. 60
Figure D-93. Observed and simulated water level in the P2R Model at well 299-E33-18.png. 61
Figure D-94. Observed and simulated water level in the P2R Model at well 299-E33-21.png. 61
Figure D-95. Observed and simulated water level in the P2R Model at well 299-E33-25.png. 62
Figure D-96. Observed and simulated water level in the P2R Model at well 299-E33-26.png. 62
Figure D-97. Observed and simulated water level in the P2R Model at well 299-E33-28.png. 63
Figure D-98. Observed and simulated water level in the P2R Model at well 299-E33-29.png. 63
Figure D-99. Observed and simulated water level in the P2R Model at well 299-E33-30.png. 64
Figure D-100. Observed and simulated water level in the P2R Model at well 299-E33-31.png. 64
Figure D-101. Observed and simulated water level in the P2R Model at well 299-E33-32.png. 65
Figure D-102. Observed and simulated water level in the P2R Model at well 299-E33-33.png. 65
Figure D-103. Observed and simulated water level in the P2R Model at well 299-E33-334.png. 66
Figure D-104. Observed and simulated water level in the P2R Model at well 299-E33-335.png. 66
Figure D-105. Observed and simulated water level in the P2R Model at well 299-E33-337.png. 67
Figure D-106. Observed and simulated water level in the P2R Model at well 299-E33-338.png. 67
Figure D-107. Observed and simulated water level in the P2R Model at well 299-E33-339.png. 68
Figure D-108. Observed and simulated water level in the P2R Model at well 299-E33-34.png. 68
Figure D-109. Observed and simulated water level in the P2R Model at well 299-E33-35.png. 69
Figure D-110. Observed and simulated water level in the P2R Model at well 299-E33-36.png. 69
Figure D-111. Observed and simulated water level in the P2R Model at well 299-E33-37.png. 70
Figure D-112. Observed and simulated water level in the P2R Model at well 299-E33-38.png. 70
Figure D-113. Observed and simulated water level in the P2R Model at well 299-E33-39.png. 71
Figure D-114. Observed and simulated water level in the P2R Model at well 299-E33-41.png. 71
Figure D-115. Observed and simulated water level in the P2R Model at well 299-E33-42.png. 72
Figure D-116. Observed and simulated water level in the P2R Model at well 299-E33-43.png. 72
Figure D-117. Observed and simulated water level in the P2R Model at well 299-E33-44.png. 73

Figure D-118. Observed and simulated water level in the P2R Model at well 299-E33-8.png. 73
Figure D-119. Observed and simulated water level in the P2R Model at well 299-E34-1.png. 74
Figure D-120. Observed and simulated water level in the P2R Model at well 299-E34-10.png. 74
Figure D-121. Observed and simulated water level in the P2R Model at well 299-E34-11.png. 75
Figure D-122. Observed and simulated water level in the P2R Model at well 299-E34-12.png. 75
Figure D-123. Observed and simulated water level in the P2R Model at well 299-E34-2.png. 76
Figure D-124. Observed and simulated water level in the P2R Model at well 299-E34-7.png. 76
Figure D-125. Observed and simulated water level in the P2R Model at well 299-E34-8.png. 77
Figure D-126. Observed and simulated water level in the P2R Model at well 299-E34-9.png. 77
Figure D-127. Observed and simulated water level in the P2R Model at well 299-E35-1.png. 78
Figure D-128. Observed and simulated water level in the P2R Model at well 299-E35-2.png. 78
Figure D-129. Observed and simulated water level in the P2R Model at well 299-W10-1.png. 79
Figure D-130. Observed and simulated water level in the P2R Model at well 299-W10-10.png. 79
Figure D-131. Observed and simulated water level in the P2R Model at well 299-W10-11.png. 80
Figure D-132. Observed and simulated water level in the P2R Model at well 299-W10-12.png. 80
Figure D-133. Observed and simulated water level in the P2R Model at well 299-W10-13.png. 81
Figure D-134. Observed and simulated water level in the P2R Model at well 299-W10-14.png. 81
Figure D-135. Observed and simulated water level in the P2R Model at well 299-W10-15.png. 82
Figure D-136. Observed and simulated water level in the P2R Model at well 299-W10-16.png. 82
Figure D-137. Observed and simulated water level in the P2R Model at well 299-W10-17.png. 83
Figure D-138. Observed and simulated water level in the P2R Model at well 299-W10-18.png. 83
Figure D-139. Observed and simulated water level in the P2R Model at well 299-W10-19.png. 84
Figure D-140. Observed and simulated water level in the P2R Model at well 299-W10-20.png. 84
Figure D-141. Observed and simulated water level in the P2R Model at well 299-W10-21.png. 85
Figure D-142. Observed and simulated water level in the P2R Model at well 299-W10-22.png. 85
Figure D-143. Observed and simulated water level in the P2R Model at well 299-W10-23.png. 86
Figure D-144. Observed and simulated water level in the P2R Model at well 299-W10-24.png. 86
Figure D-145. Observed and simulated water level in the P2R Model at well 299-W10-26.png. 87
Figure D-146. Observed and simulated water level in the P2R Model at well 299-W10-27.png. 87
Figure D-147. Observed and simulated water level in the P2R Model at well 299-W10-28.png. 88
Figure D-148. Observed and simulated water level in the P2R Model at well 299-W10-3.png. 88
Figure D-149. Observed and simulated water level in the P2R Model at well 299-W10-4.png. 89
Figure D-150. Observed and simulated water level in the P2R Model at well 299-W10-5.png. 89
Figure D-151. Observed and simulated water level in the P2R Model at well 299-W10-8.png. 90
Figure D-152. Observed and simulated water level in the P2R Model at well 299-W10-9.png. 90
Figure D-153. Observed and simulated water level in the P2R Model at well 299-W11-1.png. 91
Figure D-154. Observed and simulated water level in the P2R Model at well 299-W11-10.png. 91
Figure D-155. Observed and simulated water level in the P2R Model at well 299-W11-12.png. 92
Figure D-156. Observed and simulated water level in the P2R Model at well 299-W11-14.png. 92

Figure D-157. Observed and simulated water level in the P2R Model at well 299-W11-18.png. 93
Figure D-158. Observed and simulated water level in the P2R Model at well 299-W11-19.png. 93
Figure D-159. Observed and simulated water level in the P2R Model at well 299-W11-23.png. 94
Figure D-160. Observed and simulated water level in the P2R Model at well 299-W11-24.png. 94
Figure D-161. Observed and simulated water level in the P2R Model at well 299-W11-27.png. 95
Figure D-162. Observed and simulated water level in the P2R Model at well 299-W11-3.png. 95
Figure D-163. Observed and simulated water level in the P2R Model at well 299-W11-30.png. 96
Figure D-164. Observed and simulated water level in the P2R Model at well 299-W11-31.png. 96
Figure D-165. Observed and simulated water level in the P2R Model at well 299-W11-39.png. 97
Figure D-166. Observed and simulated water level in the P2R Model at well 299-W11-4.png. 97
Figure D-167. Observed and simulated water level in the P2R Model at well 299-W11-40.png. 98
Figure D-168. Observed and simulated water level in the P2R Model at well 299-W11-41.png. 98
Figure D-169. Observed and simulated water level in the P2R Model at well 299-W11-42.png. 99
Figure D-170. Observed and simulated water level in the P2R Model at well 299-W11-5.png. 99
Figure D-171. Observed and simulated water level in the P2R Model at well 299-W11-6.png. 100
Figure D-172. Observed and simulated water level in the P2R Model at well 299-W11-7.png. 100
Figure D-173. Observed and simulated water level in the P2R Model at well 299-W11-8.png. 101
Figure D-174. Observed and simulated water level in the P2R Model at well 299-W11-9.png. 101
Figure D-175. Observed and simulated water level in the P2R Model at well 299-W12-1.png. 102
Figure D-176. Observed and simulated water level in the P2R Model at well 299-W14-10.png. 102
Figure D-177. Observed and simulated water level in the P2R Model at well 299-W14-12.png. 103
Figure D-178. Observed and simulated water level in the P2R Model at well 299-W14-13.png. 103
Figure D-179. Observed and simulated water level in the P2R Model at well 299-W14-14.png. 104
Figure D-180. Observed and simulated water level in the P2R Model at well 299-W14-15.png. 104
Figure D-181. Observed and simulated water level in the P2R Model at well 299-W14-16.png. 105
Figure D-182. Observed and simulated water level in the P2R Model at well 299-W14-17.png. 105
Figure D-183. Observed and simulated water level in the P2R Model at well 299-W14-18.png. 106
Figure D-184. Observed and simulated water level in the P2R Model at well 299-W14-19.png. 106
Figure D-185. Observed and simulated water level in the P2R Model at well 299-W14-5.png. 107
Figure D-186. Observed and simulated water level in the P2R Model at well 299-W14-6.png. 107
Figure D-187. Observed and simulated water level in the P2R Model at well 299-W14-9.png. 108
Figure D-188. Observed and simulated water level in the P2R Model at well 299-W15-1.png. 108
Figure D-189. Observed and simulated water level in the P2R Model at well 299-W15-10.png. 109
Figure D-190. Observed and simulated water level in the P2R Model at well 299-W15-11.png. 109
Figure D-191. Observed and simulated water level in the P2R Model at well 299-W15-12.png. 110
Figure D-192. Observed and simulated water level in the P2R Model at well 299-W15-13.png. 110
Figure D-193. Observed and simulated water level in the P2R Model at well 299-W15-15.png. 111
Figure D-194. Observed and simulated water level in the P2R Model at well 299-W15-16.png. 111
Figure D-195. Observed and simulated water level in the P2R Model at well 299-W15-17.png. 112

Figure D-196. Observed and simulated water level in the P2R Model at well 299-W15-18.png. 112
Figure D-197. Observed and simulated water level in the P2R Model at well 299-W15-19.png. 113
Figure D-198. Observed and simulated water level in the P2R Model at well 299-W15-2.png. 113
Figure D-199. Observed and simulated water level in the P2R Model at well 299-W15-20.png. 114
Figure D-200. Observed and simulated water level in the P2R Model at well 299-W15-22.png. 114
Figure D-201. Observed and simulated water level in the P2R Model at well 299-W15-23.png. 115
Figure D-202. Observed and simulated water level in the P2R Model at well 299-W15-24.png. 115
Figure D-203. Observed and simulated water level in the P2R Model at well 299-W15-25.png. 116
Figure D-204. Observed and simulated water level in the P2R Model at well 299-W15-30.png. 116
Figure D-205. Observed and simulated water level in the P2R Model at well 299-W15-31A.png. 117
Figure D-206. Observed and simulated water level in the P2R Model at well 299-W15-4.png. 117
Figure D-207. Observed and simulated water level in the P2R Model at well 299-W15-40.png. 118
Figure D-208. Observed and simulated water level in the P2R Model at well 299-W15-41.png. 118
Figure D-209. Observed and simulated water level in the P2R Model at well 299-W15-42.png. 119
Figure D-210. Observed and simulated water level in the P2R Model at well 299-W15-7.png. 119
Figure D-211. Observed and simulated water level in the P2R Model at well 299-W15-763.png. 120
Figure D-212. Observed and simulated water level in the P2R Model at well 299-W18-10.png. 120
Figure D-213. Observed and simulated water level in the P2R Model at well 299-W18-15.png. 121
Figure D-214. Observed and simulated water level in the P2R Model at well 299-W18-2.png. 121
Figure D-215. Observed and simulated water level in the P2R Model at well 299-W18-21.png. 122
Figure D-216. Observed and simulated water level in the P2R Model at well 299-W18-22.png. 122
Figure D-217. Observed and simulated water level in the P2R Model at well 299-W18-23.png. 123
Figure D-218. Observed and simulated water level in the P2R Model at well 299-W18-24.png. 123
Figure D-219. Observed and simulated water level in the P2R Model at well 299-W18-25.png. 124
Figure D-220. Observed and simulated water level in the P2R Model at well 299-W18-26.png. 124
Figure D-221. Observed and simulated water level in the P2R Model at well 299-W18-27.png. 125
Figure D-222. Observed and simulated water level in the P2R Model at well 299-W18-28.png. 125
Figure D-223. Observed and simulated water level in the P2R Model at well 299-W18-30.png. 126
Figure D-224. Observed and simulated water level in the P2R Model at well 299-W18-31.png. 126
Figure D-225. Observed and simulated water level in the P2R Model at well 299-W18-32.png. 127
Figure D-226. Observed and simulated water level in the P2R Model at well 299-W18-33.png. 127
Figure D-227. Observed and simulated water level in the P2R Model at well 299-W18-4.png. 128
Figure D-228. Observed and simulated water level in the P2R Model at well 299-W18-40.png. 128
Figure D-229. Observed and simulated water level in the P2R Model at well 299-W18-5.png. 129
Figure D-230. Observed and simulated water level in the P2R Model at well 299-W18-9.png. 129
Figure D-231. Observed and simulated water level in the P2R Model at well 299-W19-1.png. 130
Figure D-232. Observed and simulated water level in the P2R Model at well 299-W19-13.png. 130
Figure D-233. Observed and simulated water level in the P2R Model at well 299-W19-15.png. 131
Figure D-234. Observed and simulated water level in the P2R Model at well 299-W19-19.png. 131

Figure D-235. Observed and simulated water level in the P2R Model at well 299-W19-2.png. 132
Figure D-236. Observed and simulated water level in the P2R Model at well 299-W19-23.png. 132
Figure D-237. Observed and simulated water level in the P2R Model at well 299-W19-24.png. 133
Figure D-238. Observed and simulated water level in the P2R Model at well 299-W19-25.png. 133
Figure D-239. Observed and simulated water level in the P2R Model at well 299-W19-26.png. 134
Figure D-240. Observed and simulated water level in the P2R Model at well 299-W19-27.png. 134
Figure D-241. Observed and simulated water level in the P2R Model at well 299-W19-28.png. 135
Figure D-242. Observed and simulated water level in the P2R Model at well 299-W19-29.png. 135
Figure D-243. Observed and simulated water level in the P2R Model at well 299-W19-30.png. 136
Figure D-244. Observed and simulated water level in the P2R Model at well 299-W19-31.png. 136
Figure D-245. Observed and simulated water level in the P2R Model at well 299-W19-32.png. 137
Figure D-246. Observed and simulated water level in the P2R Model at well 299-W19-36.png. 137
Figure D-247. Observed and simulated water level in the P2R Model at well 299-W19-37.png. 138
Figure D-248. Observed and simulated water level in the P2R Model at well 299-W19-4.png. 138
Figure D-249. Observed and simulated water level in the P2R Model at well 299-W19-40.png. 139
Figure D-250. Observed and simulated water level in the P2R Model at well 299-W19-41.png. 139
Figure D-251. Observed and simulated water level in the P2R Model at well 299-W19-42.png. 140
Figure D-252. Observed and simulated water level in the P2R Model at well 299-W19-44.png. 140
Figure D-253. Observed and simulated water level in the P2R Model at well 299-W19-45.png. 141
Figure D-254. Observed and simulated water level in the P2R Model at well 299-W19-46.png. 141
Figure D-255. Observed and simulated water level in the P2R Model at well 299-W19-6.png. 142
Figure D-256. Observed and simulated water level in the P2R Model at well 299-W21-1.png. 142
Figure D-257. Observed and simulated water level in the P2R Model at well 299-W22-20.png. 143
Figure D-258. Observed and simulated water level in the P2R Model at well 299-W22-22.png. 143
Figure D-259. Observed and simulated water level in the P2R Model at well 299-W22-23.png. 144
Figure D-260. Observed and simulated water level in the P2R Model at well 299-W22-39.png. 144
Figure D-261. Observed and simulated water level in the P2R Model at well 299-W22-4.png. 145
Figure D-262. Observed and simulated water level in the P2R Model at well 299-W22-40.png. 145
Figure D-263. Observed and simulated water level in the P2R Model at well 299-W22-41.png. 146
Figure D-264. Observed and simulated water level in the P2R Model at well 299-W22-42.png. 146
Figure D-265. Observed and simulated water level in the P2R Model at well 299-W22-43.png. 147
Figure D-266. Observed and simulated water level in the P2R Model at well 299-W22-44.png. 147
Figure D-267. Observed and simulated water level in the P2R Model at well 299-W22-45.png. 148
Figure D-268. Observed and simulated water level in the P2R Model at well 299-W22-46.png. 148
Figure D-269. Observed and simulated water level in the P2R Model at well 299-W22-48.png. 149
Figure D-270. Observed and simulated water level in the P2R Model at well 299-W22-49.png. 149
Figure D-271. Observed and simulated water level in the P2R Model at well 299-W22-50.png. 150
Figure D-272. Observed and simulated water level in the P2R Model at well 299-W22-7.png. 150
Figure D-273. Observed and simulated water level in the P2R Model at well 299-W22-79.png. 151

Figure D-274. Observed and simulated water level in the P2R Model at well 299-W22-8.png. 151
Figure D-275. Observed and simulated water level in the P2R Model at well 299-W22-80.png. 152
Figure D-276. Observed and simulated water level in the P2R Model at well 299-W22-81.png. 152
Figure D-277. Observed and simulated water level in the P2R Model at well 299-W22-82.png. 153
Figure D-278. Observed and simulated water level in the P2R Model at well 299-W22-83.png. 153
Figure D-279. Observed and simulated water level in the P2R Model at well 299-W22-84.png. 154
Figure D-280. Observed and simulated water level in the P2R Model at well 299-W22-85.png. 154
Figure D-281. Observed and simulated water level in the P2R Model at well 299-W22-9.png. 155
Figure D-282. Observed and simulated water level in the P2R Model at well 299-W23-13.png. 155
Figure D-283. Observed and simulated water level in the P2R Model at well 299-W23-14.png. 156
Figure D-284. Observed and simulated water level in the P2R Model at well 299-W23-15.png. 156
Figure D-285. Observed and simulated water level in the P2R Model at well 299-W23-20.png. 157
Figure D-286. Observed and simulated water level in the P2R Model at well 299-W23-21.png. 157
Figure D-287. Observed and simulated water level in the P2R Model at well 299-W23-4.png. 158
Figure D-288. Observed and simulated water level in the P2R Model at well 299-W23-8.png. 158
Figure D-289. Observed and simulated water level in the P2R Model at well 299-W26-10.png. 159
Figure D-290. Observed and simulated water level in the P2R Model at well 299-W26-12.png. 159
Figure D-291. Observed and simulated water level in the P2R Model at well 299-W26-13.png. 160
Figure D-292. Observed and simulated water level in the P2R Model at well 299-W26-14.png. 160
Figure D-293. Observed and simulated water level in the P2R Model at well 299-W26-6.png. 161
Figure D-294. Observed and simulated water level in the P2R Model at well 299-W26-7.png. 161
Figure D-295. Observed and simulated water level in the P2R Model at well 299-W26-8.png. 162
Figure D-296. Observed and simulated water level in the P2R Model at well 299-W27-2.png. 162
Figure D-297. Observed and simulated water level in the P2R Model at well 299-W6-1.png. 163
Figure D-298. Observed and simulated water level in the P2R Model at well 299-W6-10.png. 163
Figure D-299. Observed and simulated water level in the P2R Model at well 299-W6-11.png. 164
Figure D-300. Observed and simulated water level in the P2R Model at well 299-W6-12.png. 164
Figure D-301. Observed and simulated water level in the P2R Model at well 299-W6-2.png. 165
Figure D-302. Observed and simulated water level in the P2R Model at well 299-W6-3.png. 165
Figure D-303. Observed and simulated water level in the P2R Model at well 299-W6-4.png. 166
Figure D-304. Observed and simulated water level in the P2R Model at well 299-W6-6.png. 166
Figure D-305. Observed and simulated water level in the P2R Model at well 299-W6-7.png. 167
Figure D-306. Observed and simulated water level in the P2R Model at well 299-W6-8.png. 167
Figure D-307. Observed and simulated water level in the P2R Model at well 299-W6-9.png. 168
Figure D-308. Observed and simulated water level in the P2R Model at well 299-W7-1.png. 168
Figure D-309. Observed and simulated water level in the P2R Model at well 299-W7-10.png. 169
Figure D-310. Observed and simulated water level in the P2R Model at well 299-W7-11.png. 169
Figure D-311. Observed and simulated water level in the P2R Model at well 299-W7-12.png. 170
Figure D-312. Observed and simulated water level in the P2R Model at well 299-W7-2.png. 170

Figure D-313. Observed and simulated water level in the P2R Model at well 299-W7-4.png. 171
Figure D-314. Observed and simulated water level in the P2R Model at well 299-W7-5.png. 171
Figure D-315. Observed and simulated water level in the P2R Model at well 299-W7-6.png. 172
Figure D-316. Observed and simulated water level in the P2R Model at well 299-W7-7.png. 172
Figure D-317. Observed and simulated water level in the P2R Model at well 299-W7-8.png. 173
Figure D-318. Observed and simulated water level in the P2R Model at well 299-W7-9.png. 173
Figure D-319. Observed and simulated water level in the P2R Model at well 299-W8-1.png. 174
Figure D-320. Observed and simulated water level in the P2R Model at well 299-W9-1.png. 174
Figure D-321. Observed and simulated water level in the P2R Model at well 399-1-10A.png. 175
Figure D-322. Observed and simulated water level in the P2R Model at well 399-1-11.png. 175
Figure D-323. Observed and simulated water level in the P2R Model at well 399-1-14A.png. 176
Figure D-324. Observed and simulated water level in the P2R Model at well 399-1-18A.png. 176
Figure D-325. Observed and simulated water level in the P2R Model at well 399-1-6.png. 177
Figure D-326. Observed and simulated water level in the P2R Model at well 699-10-54A.png. 177
Figure D-327. Observed and simulated water level in the P2R Model at well 699-10-E12Q.png..... 178
Figure D-328. Observed and simulated water level in the P2R Model at well 699-11-45A.png. 178
Figure D-329. Observed and simulated water level in the P2R Model at well 699-1-18.png. 179
Figure D-330. Observed and simulated water level in the P2R Model at well 699-12-2C.png. 179
Figure D-331. Observed and simulated water level in the P2R Model at well 699-12-4D.png. 180
Figure D-332. Observed and simulated water level in the P2R Model at well 699-13-0A.png. 180
Figure D-333. Observed and simulated water level in the P2R Model at well 699-13-2D.png. 181
Figure D-334. Observed and simulated water level in the P2R Model at well 699-14-47.png. 181
Figure D-335. Observed and simulated water level in the P2R Model at well 699-15-15A.png. 182
Figure D-336. Observed and simulated water level in the P2R Model at well 699-15-26.png. 182
Figure D-337. Observed and simulated water level in the P2R Model at well 699-19-43.png. 183
Figure D-338. Observed and simulated water level in the P2R Model at well 699-20-20.png. 183
Figure D-339. Observed and simulated water level in the P2R Model at well 699-20-39.png. 184
Figure D-340. Observed and simulated water level in the P2R Model at well 699-20-E12.png. 184
Figure D-341. Observed and simulated water level in the P2R Model at well 699-20-E5A.png..... 185
Figure D-342. Observed and simulated water level in the P2R Model at well 699-21-17.png. 185
Figure D-343. Observed and simulated water level in the P2R Model at well 699-21-6.png. 186
Figure D-344. Observed and simulated water level in the P2R Model at well 699-22-35.png. 186
Figure D-345. Observed and simulated water level in the P2R Model at well 699-2-3.png. 187
Figure D-346. Observed and simulated water level in the P2R Model at well 699-23-34A.png. 187
Figure D-347. Observed and simulated water level in the P2R Model at well 699-23-34B.png. 188
Figure D-348. Observed and simulated water level in the P2R Model at well 699-2-33A.png. 188
Figure D-349. Observed and simulated water level in the P2R Model at well 699-24-33.png. 189
Figure D-350. Observed and simulated water level in the P2R Model at well 699-24-34A.png. 189
Figure D-351. Observed and simulated water level in the P2R Model at well 699-24-34B.png. 190

Figure D-352. Observed and simulated water level in the P2R Model at well 699-24-34C.png. 190
Figure D-353. Observed and simulated water level in the P2R Model at well 699-24-35.png. 191
Figure D-354. Observed and simulated water level in the P2R Model at well 699-24-46.png. 191
Figure D-355. Observed and simulated water level in the P2R Model at well 699-25-33A.png. 192
Figure D-356. Observed and simulated water level in the P2R Model at well 699-25-34A.png. 192
Figure D-357. Observed and simulated water level in the P2R Model at well 699-25-34B.png. 193
Figure D-358. Observed and simulated water level in the P2R Model at well 699-25-34C.png. 193
Figure D-359. Observed and simulated water level in the P2R Model at well 699-25-34D.png. 194
Figure D-360. Observed and simulated water level in the P2R Model at well 699-25-55.png. 194
Figure D-361. Observed and simulated water level in the P2R Model at well 699-25-70.png. 195
Figure D-362. Observed and simulated water level in the P2R Model at well 699-26-15A.png. 195
Figure D-363. Observed and simulated water level in the P2R Model at well 699-26-33.png. 196
Figure D-364. Observed and simulated water level in the P2R Model at well 699-26-34A.png. 196
Figure D-365. Observed and simulated water level in the P2R Model at well 699-26-34B.png. 197
Figure D-366. Observed and simulated water level in the P2R Model at well 699-26-35A.png. 197
Figure D-367. Observed and simulated water level in the P2R Model at well 699-26-35C.png. 198
Figure D-368. Observed and simulated water level in the P2R Model at well 699-2-7.png. 198
Figure D-369. Observed and simulated water level in the P2R Model at well 699-27-8.png. 199
Figure D-370. Observed and simulated water level in the P2R Model at well 699-28-40.png. 199
Figure D-371. Observed and simulated water level in the P2R Model at well 699-28-52A.png. 200
Figure D-372. Observed and simulated water level in the P2R Model at well 699-29-4.png. 200
Figure D-373. Observed and simulated water level in the P2R Model at well 699-29-78.png. 201
Figure D-374. Observed and simulated water level in the P2R Model at well 699-31-31.png. 201
Figure D-375. Observed and simulated water level in the P2R Model at well 699-31-53B.png. 202
Figure D-376. Observed and simulated water level in the P2R Model at well 699-32-22A.png. 202
Figure D-377. Observed and simulated water level in the P2R Model at well 699-32-42.png. 203
Figure D-378. Observed and simulated water level in the P2R Model at well 699-32-43.png. 203
Figure D-379. Observed and simulated water level in the P2R Model at well 699-32-62.png. 204
Figure D-380. Observed and simulated water level in the P2R Model at well 699-32-70B.png. 204
Figure D-381. Observed and simulated water level in the P2R Model at well 699-32-72B.png. 205
Figure D-382. Observed and simulated water level in the P2R Model at well 699-32-77.png. 205
Figure D-383. Observed and simulated water level in the P2R Model at well 699-33-42.png. 206
Figure D-384. Observed and simulated water level in the P2R Model at well 699-33-56.png. 206
Figure D-385. Observed and simulated water level in the P2R Model at well 699-34-39A.png. 207
Figure D-386. Observed and simulated water level in the P2R Model at well 699-34-41B.png. 207
Figure D-387. Observed and simulated water level in the P2R Model at well 699-34-42.png. 208
Figure D-388. Observed and simulated water level in the P2R Model at well 699-3-45.png. 208
Figure D-389. Observed and simulated water level in the P2R Model at well 699-34-51.png. 209
Figure D-390. Observed and simulated water level in the P2R Model at well 699-34-61.png. 209

Figure D-391. Observed and simulated water level in the P2R Model at well 699-35-66A.png. 210
Figure D-392. Observed and simulated water level in the P2R Model at well 699-35-70.png. 210
Figure D-393. Observed and simulated water level in the P2R Model at well 699-35-78A.png. 211
Figure D-394. Observed and simulated water level in the P2R Model at well 699-35-9.png. 211
Figure D-395. Observed and simulated water level in the P2R Model at well 699-36-46S.png. 212
Figure D-396. Observed and simulated water level in the P2R Model at well 699-36-61A.png. 212
Figure D-397. Observed and simulated water level in the P2R Model at well 699-36-61B.png. 213
Figure D-398. Observed and simulated water level in the P2R Model at well 699-36-67.png. 213
Figure D-399. Observed and simulated water level in the P2R Model at well 699-37-43.png. 214
Figure D-400. Observed and simulated water level in the P2R Model at well 699-37-68.png. 214
Figure D-401. Observed and simulated water level in the P2R Model at well 699-37-82A.png. 215
Figure D-402. Observed and simulated water level in the P2R Model at well 699-38-15.png. 215
Figure D-403. Observed and simulated water level in the P2R Model at well 699-38-65.png. 216
Figure D-404. Observed and simulated water level in the P2R Model at well 699-38-70.png. 216
Figure D-405. Observed and simulated water level in the P2R Model at well 699-39-0.png. 217
Figure D-406. Observed and simulated water level in the P2R Model at well 699-39-39.png. 217
Figure D-407. Observed and simulated water level in the P2R Model at well 699-39-79.png. 218
Figure D-408. Observed and simulated water level in the P2R Model at well 699-40-1.png. 218
Figure D-409. Observed and simulated water level in the P2R Model at well 699-40-12C.png. 219
Figure D-410. Observed and simulated water level in the P2R Model at well 699-40-33A.png. 219
Figure D-411. Observed and simulated water level in the P2R Model at well 699-40-36.png. 220
Figure D-412. Observed and simulated water level in the P2R Model at well 699-40-39.png. 220
Figure D-413. Observed and simulated water level in the P2R Model at well 699-40-40A.png. 221
Figure D-414. Observed and simulated water level in the P2R Model at well 699-40-40B.png. 221
Figure D-415. Observed and simulated water level in the P2R Model at well 699-40-62.png. 222
Figure D-416. Observed and simulated water level in the P2R Model at well 699-41-23.png. 222
Figure D-417. Observed and simulated water level in the P2R Model at well 699-41-35.png. 223
Figure D-418. Observed and simulated water level in the P2R Model at well 699-41-40.png. 223
Figure D-419. Observed and simulated water level in the P2R Model at well 699-41-42.png. 224
Figure D-420. Observed and simulated water level in the P2R Model at well 699-42-12A.png. 224
Figure D-421. Observed and simulated water level in the P2R Model at well 699-42-2.png. 225
Figure D-422. Observed and simulated water level in the P2R Model at well 699-42-37.png. 225
Figure D-423. Observed and simulated water level in the P2R Model at well 699-42-39A.png. 226
Figure D-424. Observed and simulated water level in the P2R Model at well 699-42-39B.png. 226
Figure D-425. Observed and simulated water level in the P2R Model at well 699-42-40A.png. 227
Figure D-426. Observed and simulated water level in the P2R Model at well 699-42-40B.png. 227
Figure D-427. Observed and simulated water level in the P2R Model at well 699-42-41.png. 228
Figure D-428. Observed and simulated water level in the P2R Model at well 699-42-42A.png. 228
Figure D-429. Observed and simulated water level in the P2R Model at well 699-42-42B.png. 229

Figure D-430. Observed and simulated water level in the P2R Model at well 699-43-40.png. 229
Figure D-431. Observed and simulated water level in the P2R Model at well 699-43-41E.png. 230
Figure D-432. Observed and simulated water level in the P2R Model at well 699-43-41F.png. 230
Figure D-433. Observed and simulated water level in the P2R Model at well 699-43-41G.png. 231
Figure D-434. Observed and simulated water level in the P2R Model at well 699-43-44.png. 231
Figure D-435. Observed and simulated water level in the P2R Model at well 699-44-16.png. 232
Figure D-436. Observed and simulated water level in the P2R Model at well 699-44-64.png. 232
Figure D-437. Observed and simulated water level in the P2R Model at well 699-45-42.png. 233
Figure D-438. Observed and simulated water level in the P2R Model at well 699-46-21B.png. 233
Figure D-439. Observed and simulated water level in the P2R Model at well 699-46-4.png. 234
Figure D-440. Observed and simulated water level in the P2R Model at well 699-47-35A.png. 234
Figure D-441. Observed and simulated water level in the P2R Model at well 699-47-60.png. 235
Figure D-442. Observed and simulated water level in the P2R Model at well 699-48-18.png. 235
Figure D-443. Observed and simulated water level in the P2R Model at well 699-48-71.png. 236
Figure D-444. Observed and simulated water level in the P2R Model at well 699-48-77A.png. 236
Figure D-445. Observed and simulated water level in the P2R Model at well 699-48-77C.png. 237
Figure D-446. Observed and simulated water level in the P2R Model at well 699-48-77D.png. 237
Figure D-447. Observed and simulated water level in the P2R Model at well 699-49-13E.png. 238
Figure D-448. Observed and simulated water level in the P2R Model at well 699-49-57A.png. 238
Figure D-449. Observed and simulated water level in the P2R Model at well 699-49-79.png. 239
Figure D-450. Observed and simulated water level in the P2R Model at well 699-50-28B.png. 239
Figure D-451. Observed and simulated water level in the P2R Model at well 699-50-30.png. 240
Figure D-452. Observed and simulated water level in the P2R Model at well 699-50-42.png. 240
Figure D-453. Observed and simulated water level in the P2R Model at well 699-50-74.png. 241
Figure D-454. Observed and simulated water level in the P2R Model at well 699-50-85.png. 241
Figure D-455. Observed and simulated water level in the P2R Model at well 699-51-75.png. 242
Figure D-456. Observed and simulated water level in the P2R Model at well 699-52-19.png. 242
Figure D-457. Observed and simulated water level in the P2R Model at well 699-53-55A.png. 243
Figure D-458. Observed and simulated water level in the P2R Model at well 699-54-18B.png. 243
Figure D-459. Observed and simulated water level in the P2R Model at well 699-54-45A.png. 244
Figure D-460. Observed and simulated water level in the P2R Model at well 699-55-70.png. 244
Figure D-461. Observed and simulated water level in the P2R Model at well 699-55-76.png. 245
Figure D-462. Observed and simulated water level in the P2R Model at well 699-57-83A.png. 245
Figure D-463. Observed and simulated water level in the P2R Model at well 699-8-17.png. 246
Figure D-464. Observed and simulated water level in the P2R Model at well 699-8-25.png. 246
Figure D-465. Observed and simulated water level in the P2R Model at well 699-8-32.png. 247
Figure D-466. Observed and simulated water level in the P2R Model at well 699-9-E2.png. 247
Figure D-467. Observed and simulated water level in the P2R Model at well 699-S11-E12A.png. 248
Figure D-468. Observed and simulated water level in the P2R Model at well 699-S12-29.png. 248

Figure D-469. Observed and simulated water level in the P2R Model at well 699-S14-20A.png. 249
Figure D-470. Observed and simulated water level in the P2R Model at well 699-S19-11.png. 249
Figure D-471. Observed and simulated water level in the P2R Model at well 699-S19-E13.png. 250
Figure D-472. Observed and simulated water level in the P2R Model at well 699-S19-E14.png. 250
Figure D-473. Observed and simulated water level in the P2R Model at well 699-S20-E10.png. 251
Figure D-474. Observed and simulated water level in the P2R Model at well 699-S3-25.png. 251
Figure D-475. Observed and simulated water level in the P2R Model at well 699-S3-E12.png. 252
Figure D-476. Observed and simulated water level in the P2R Model at well 699-S6-E14A.png. 252
Figure D-477. Observed and simulated water level in the P2R Model at well 699-S6-E4K.png. 253
Figure D-478. Observed and simulated water level in the P2R Model at well 699-S8-19.png. 253

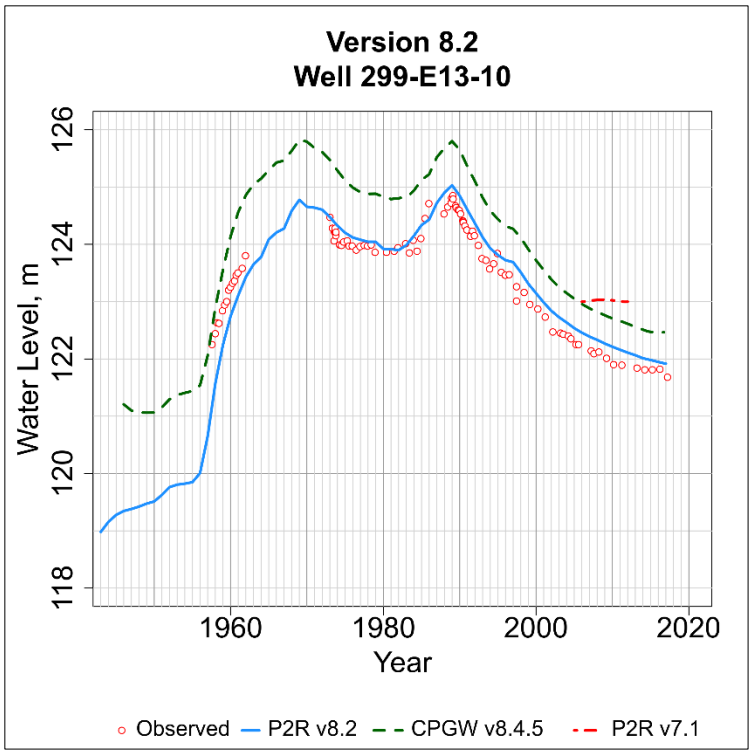

Figure D-1. Observed and simulated water level in the P2R Model at well 299-E13-10.png.

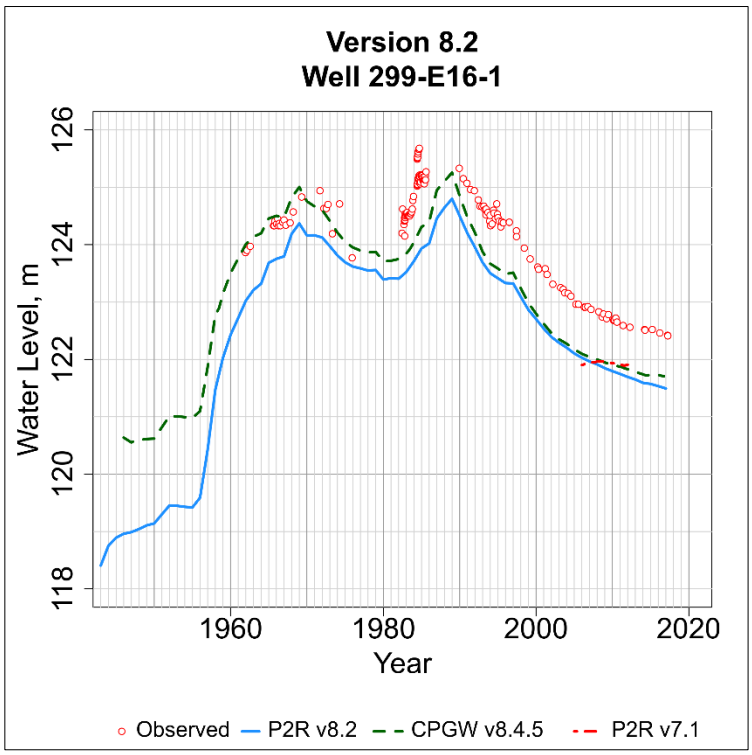

Figure D-2. Observed and simulated water level in the P2R Model at well 299-E16-1.png.

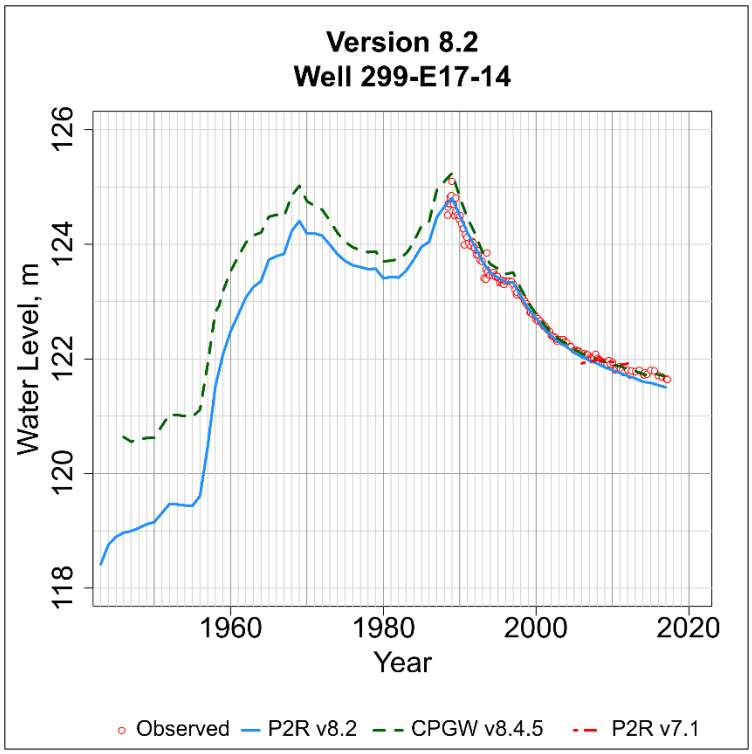

Figure D-3. Observed and simulated water level in the P2R Model at well 299-E17-14.png.

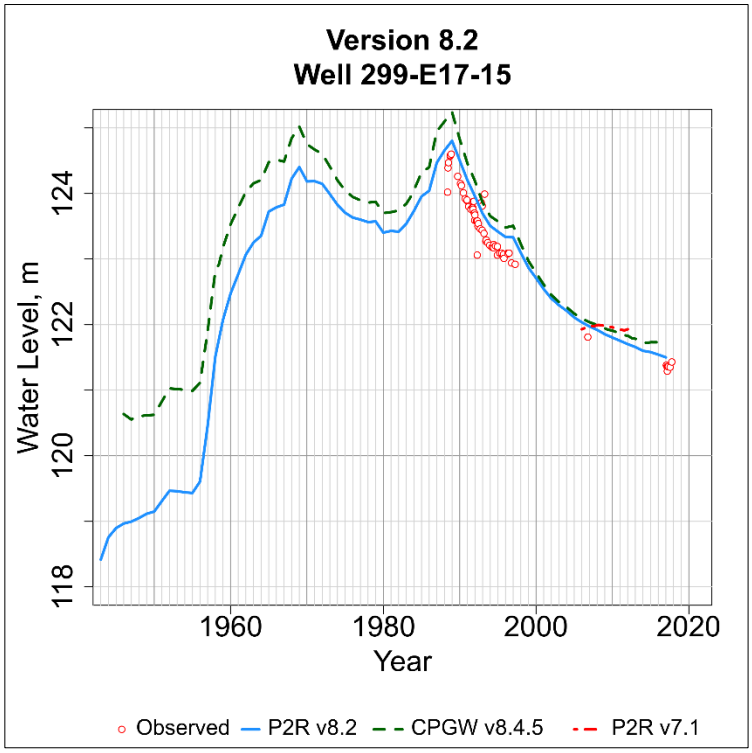

Figure D-4. Observed and simulated water level in the P2R Model at well 299-E17-15.png.

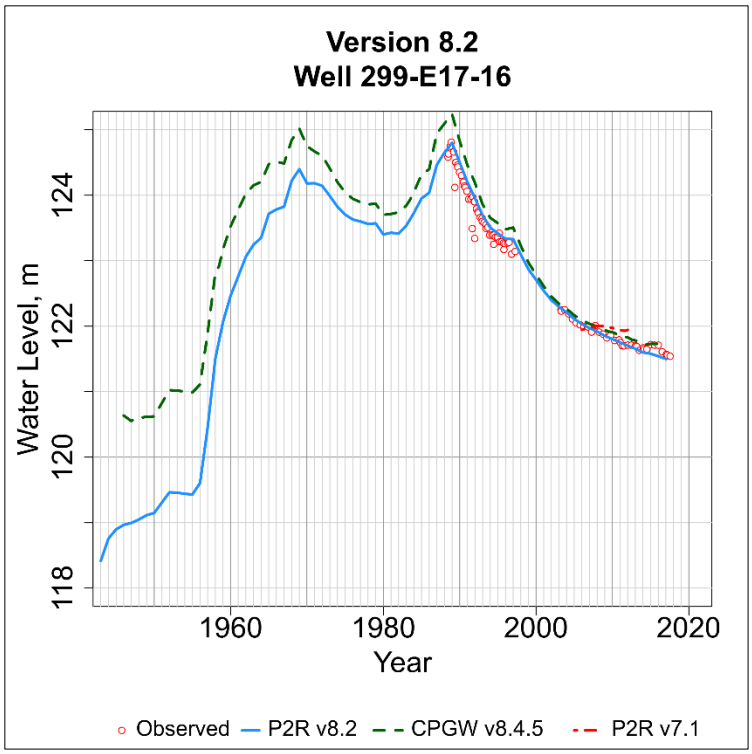

Figure D-5. Observed and simulated water level in the P2R Model at well 299-E17-16.png.

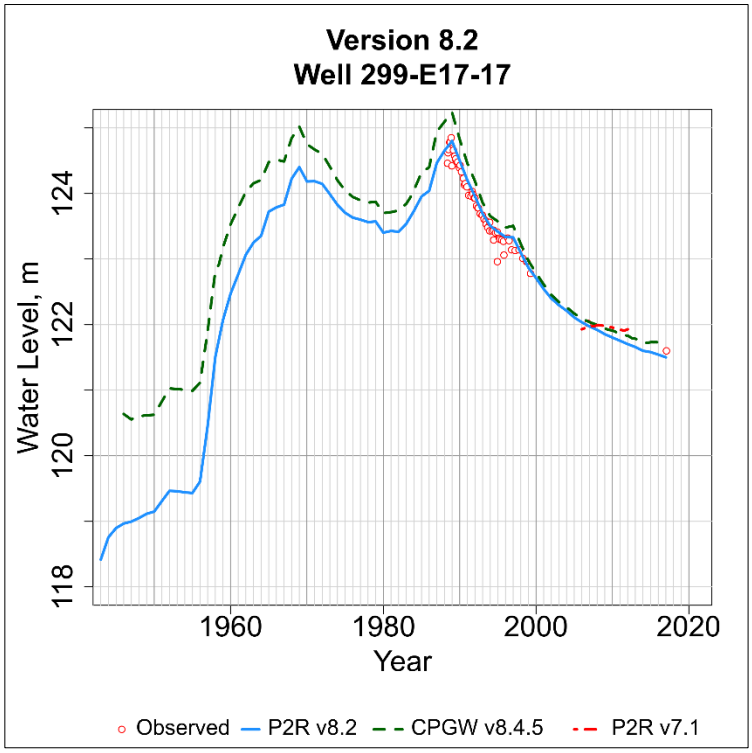

Figure D-6. Observed and simulated water level in the P2R Model at well 299-E17-17.png.

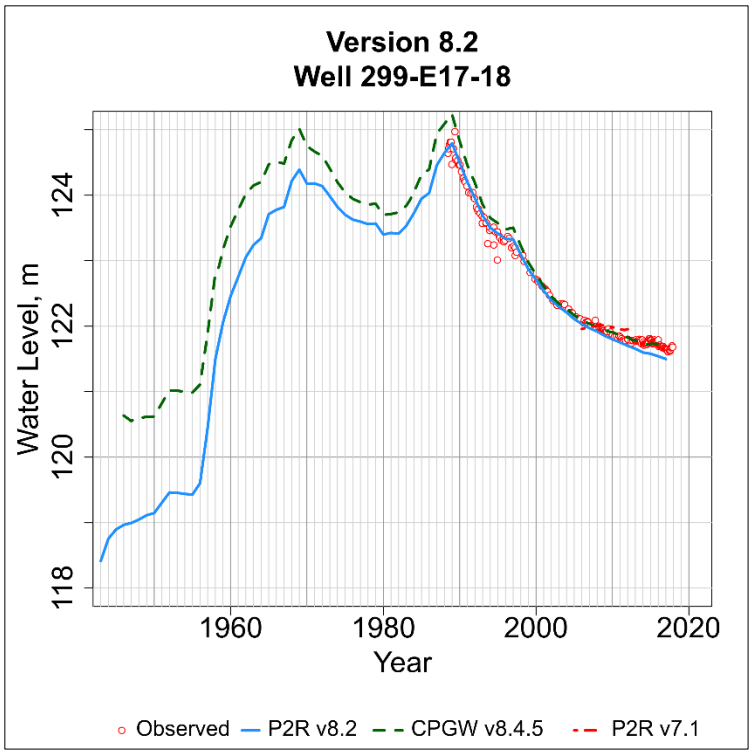

Figure D-7. Observed and simulated water level in the P2R Model at well 299-E17-18.png.

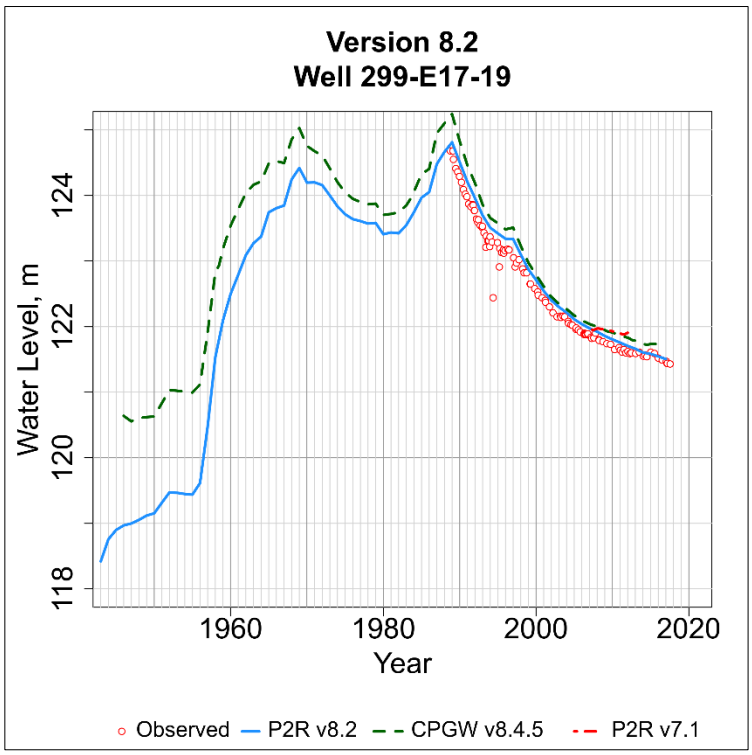

Figure D-8. Observed and simulated water level in the P2R Model at well 299-E17-19.png.

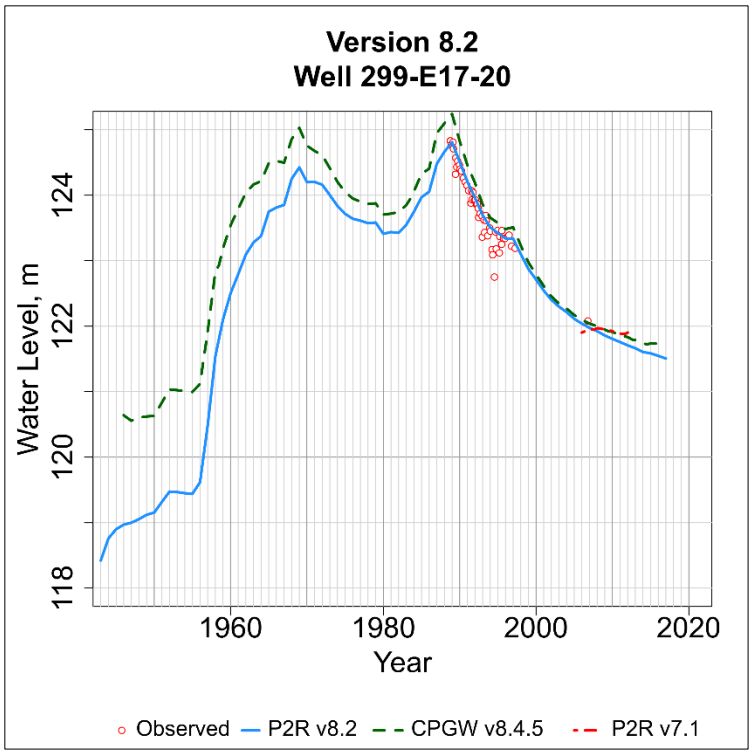

Figure D-9. Observed and simulated water level in the P2R Model at well 299-E17-20.png.

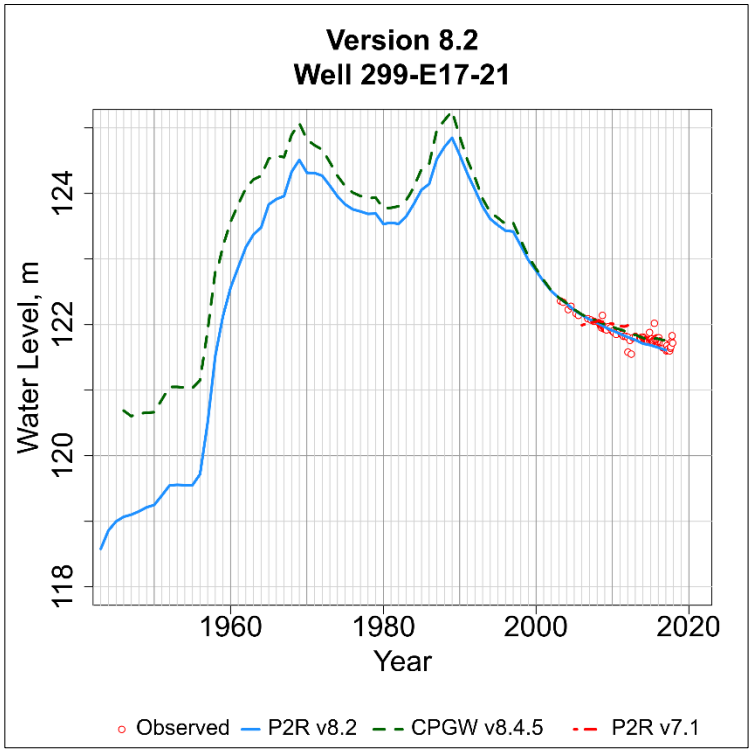

Figure D-10. Observed and simulated water level in the P2R Model at well 299-E17-21.png.

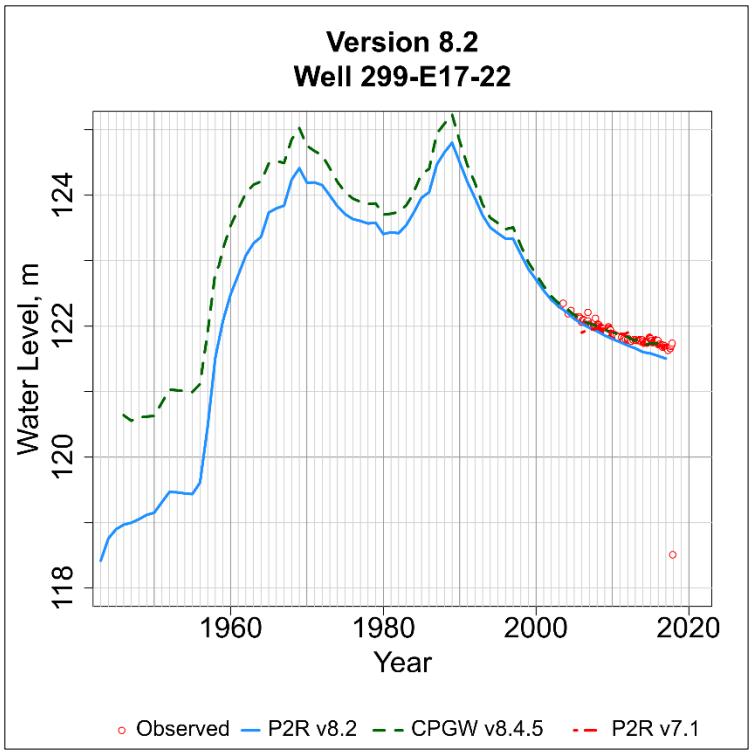

Figure D-11. Observed and simulated water level in the P2R Model at well 299-E17-22.png.

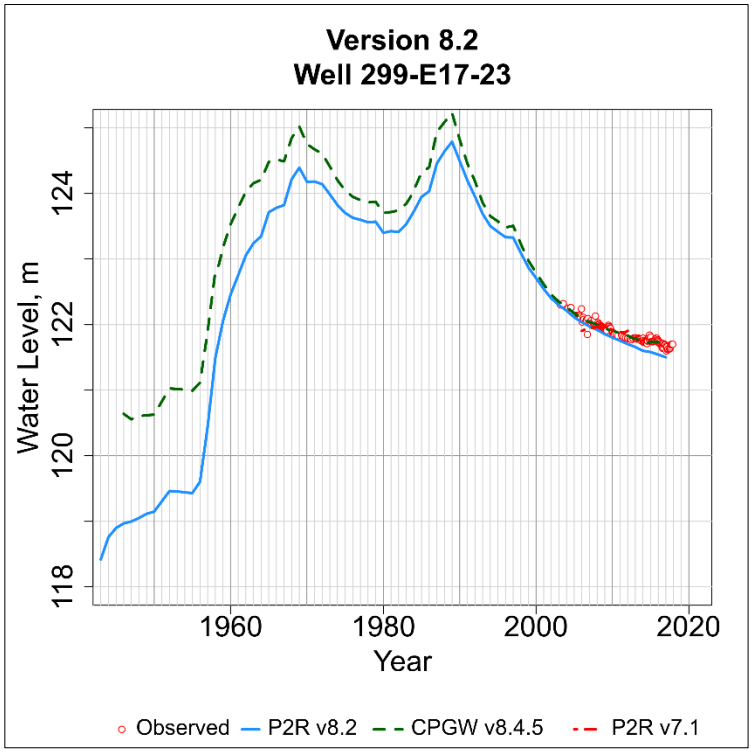

Figure D-12. Observed and simulated water level in the P2R Model at well 299-E17-23.png.

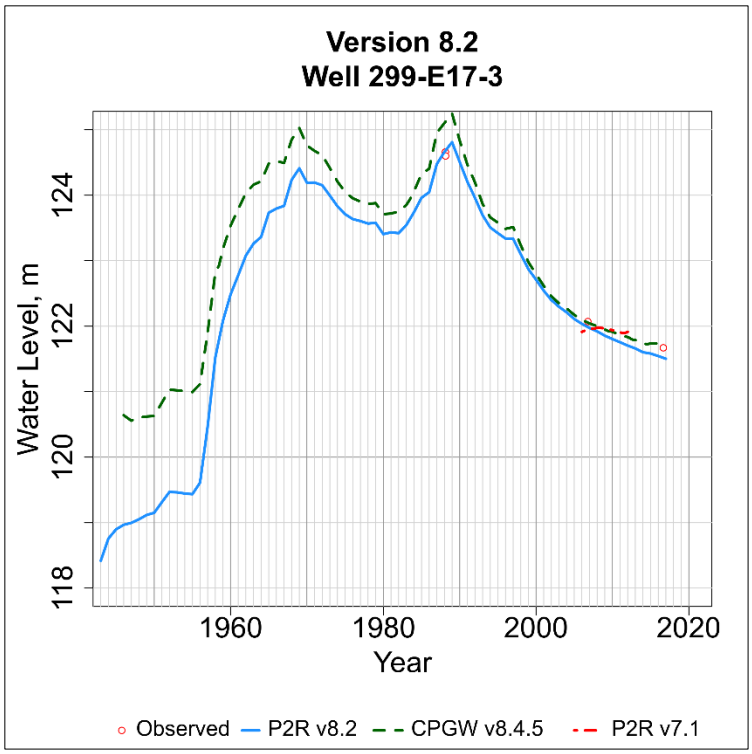

Figure D-13. Observed and simulated water level in the P2R Model at well 299-E17-3.png.

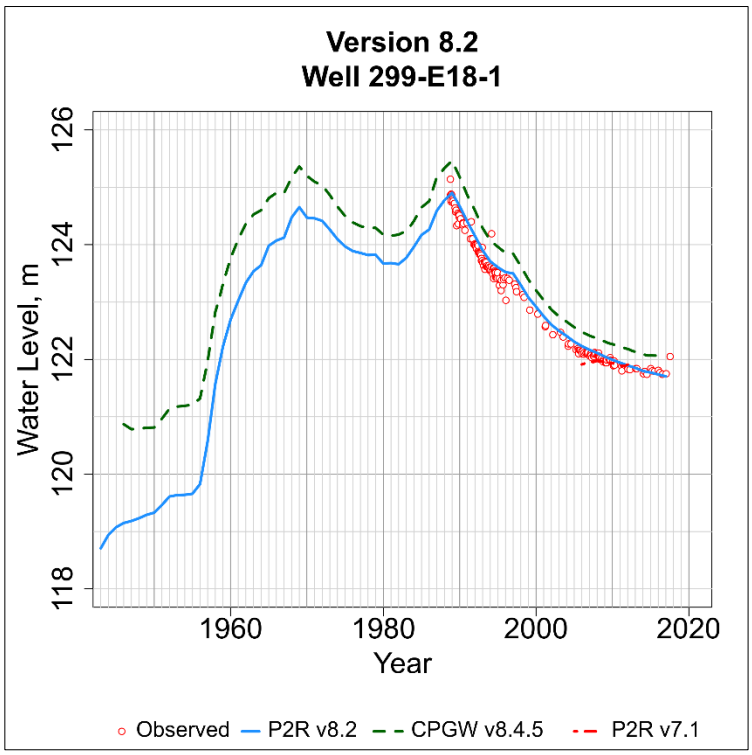

Figure D-14. Observed and simulated water level in the P2R Model at well 299-E18-1.png.

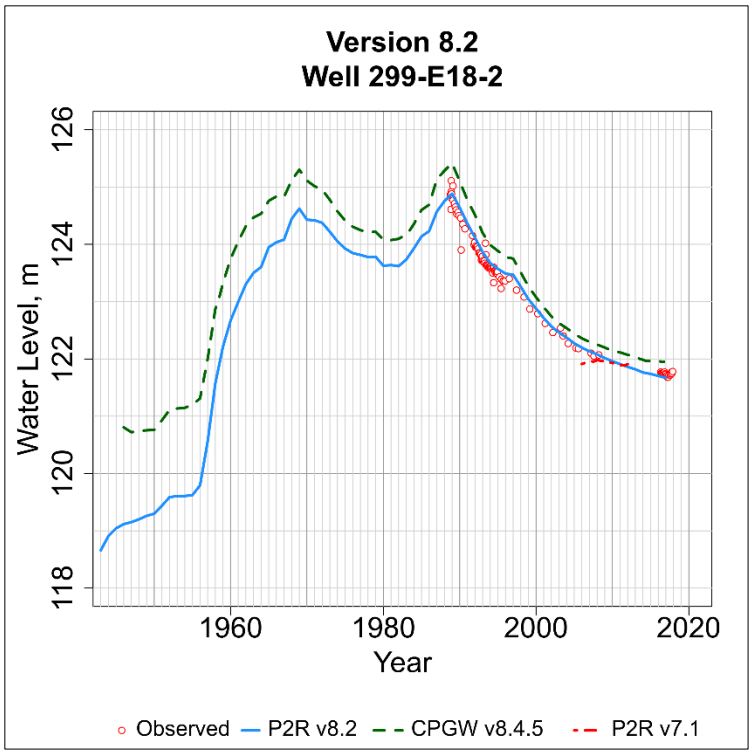

Figure D-15. Observed and simulated water level in the P2R Model at well 299-E18-2.png.

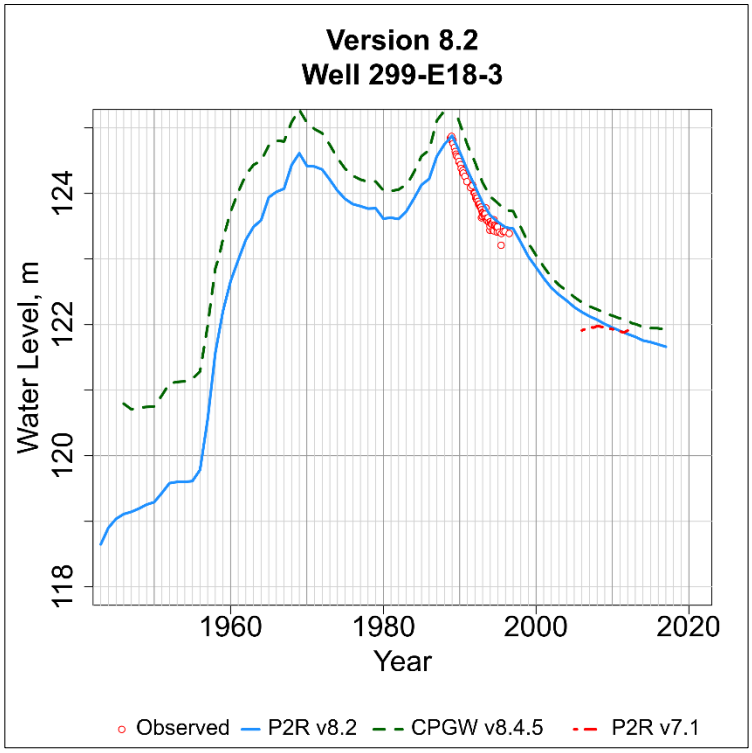

Figure D-16. Observed and simulated water level in the P2R Model at well 299-E18-3.png.

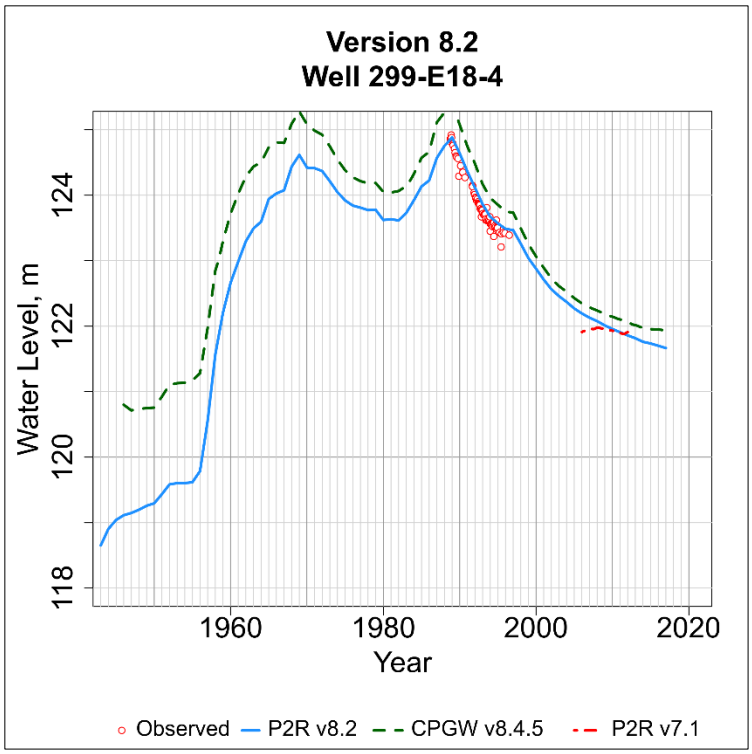

Figure D-17. Observed and simulated water level in the P2R Model at well 299-E18-4.png.

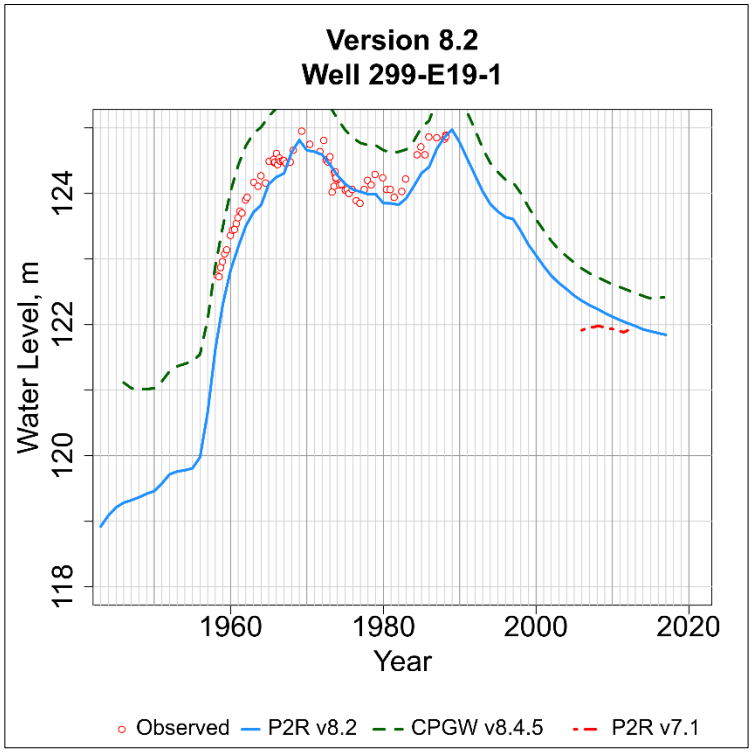

Figure D-18. Observed and simulated water level in the P2R Model at well 299-E19-1.png.

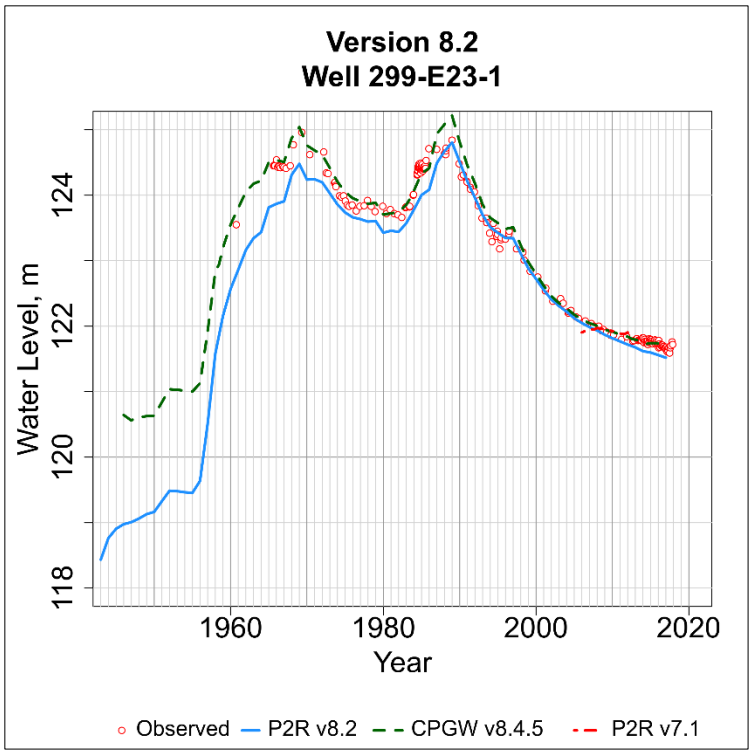

Figure D-19. Observed and simulated water level in the P2R Model at well 299-E23-1.png.

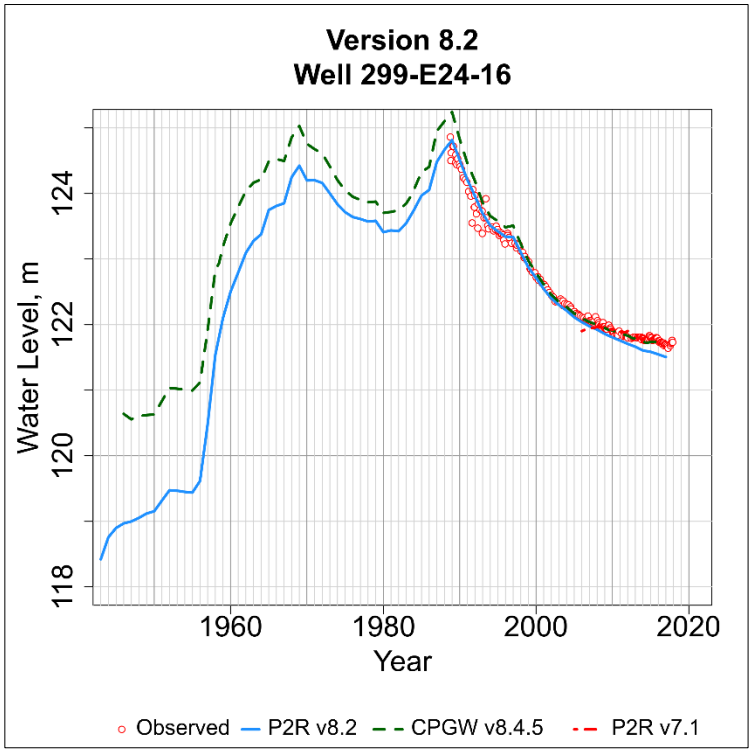

Figure D-20. Observed and simulated water level in the P2R Model at well 299-E24-16.png.

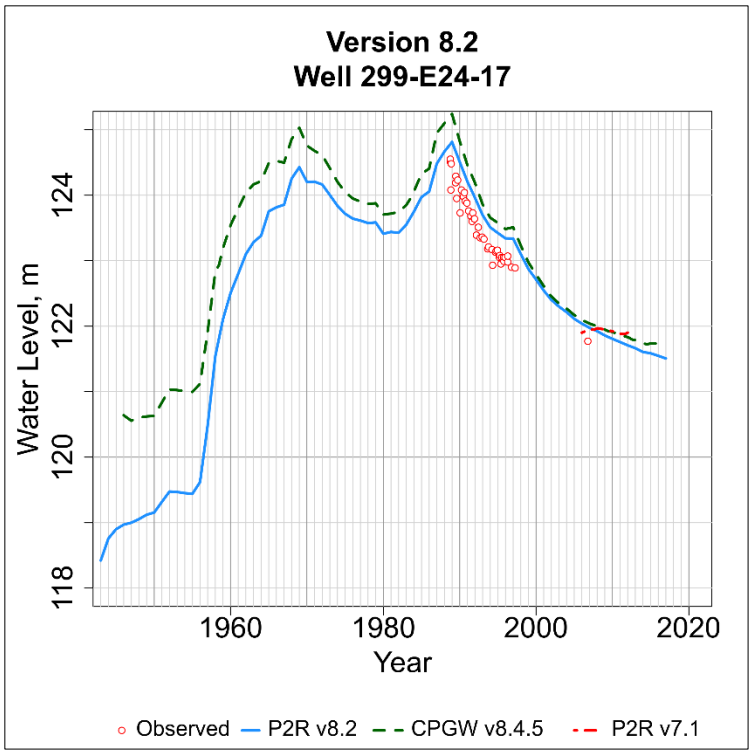

Figure D-21. Observed and simulated water level in the P2R Model at well 299-E24-17.png.

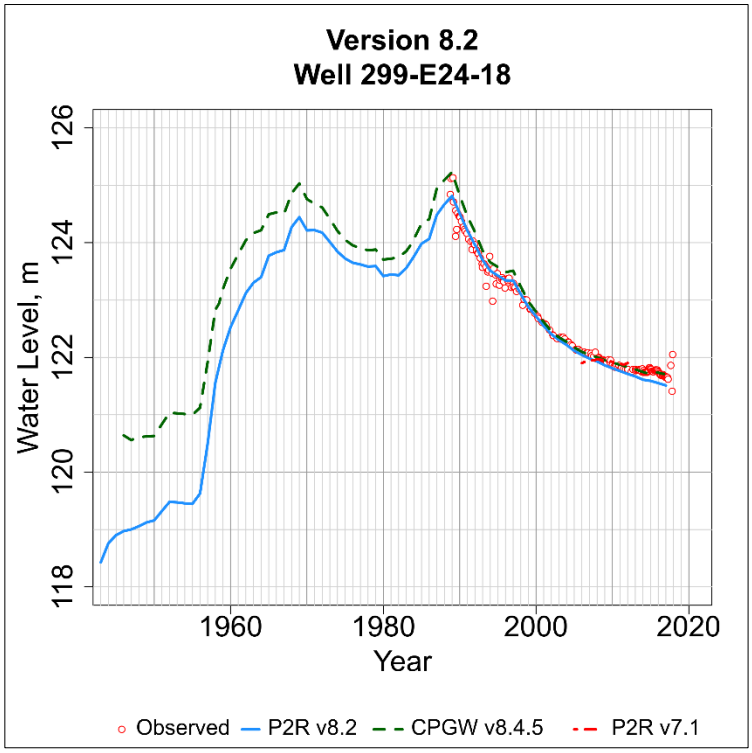

Figure D-22. Observed and simulated water level in the P2R Model at well 299-E24-18.png.

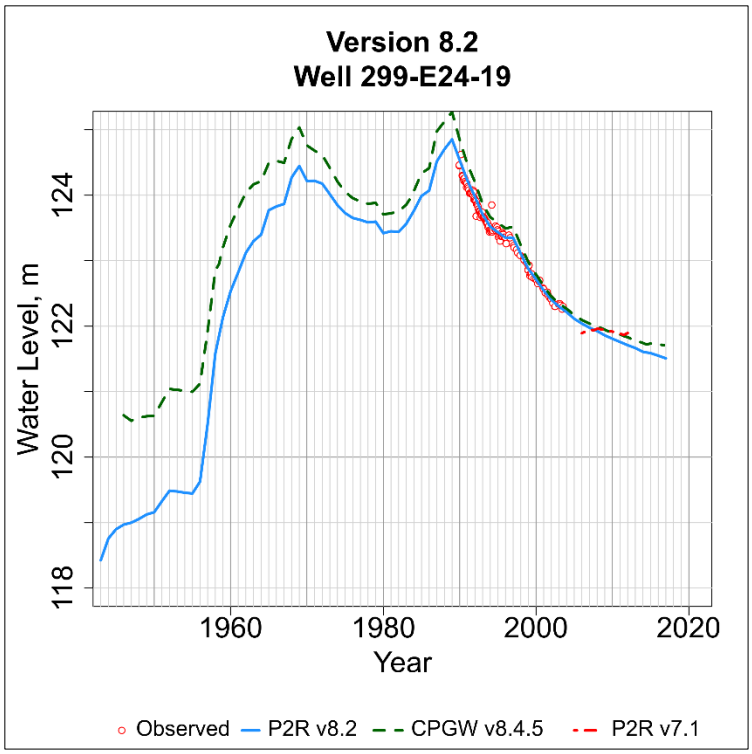

Figure D-23. Observed and simulated water level in the P2R Model at well 299-E24-19.png.

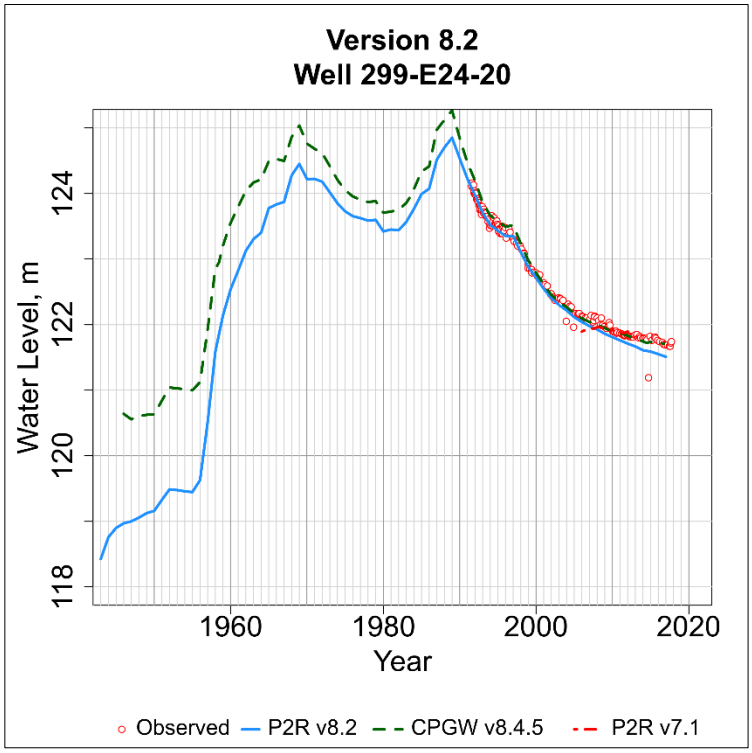

Figure D-24. Observed and simulated water level in the P2R Model at well 299-E24-20.png.

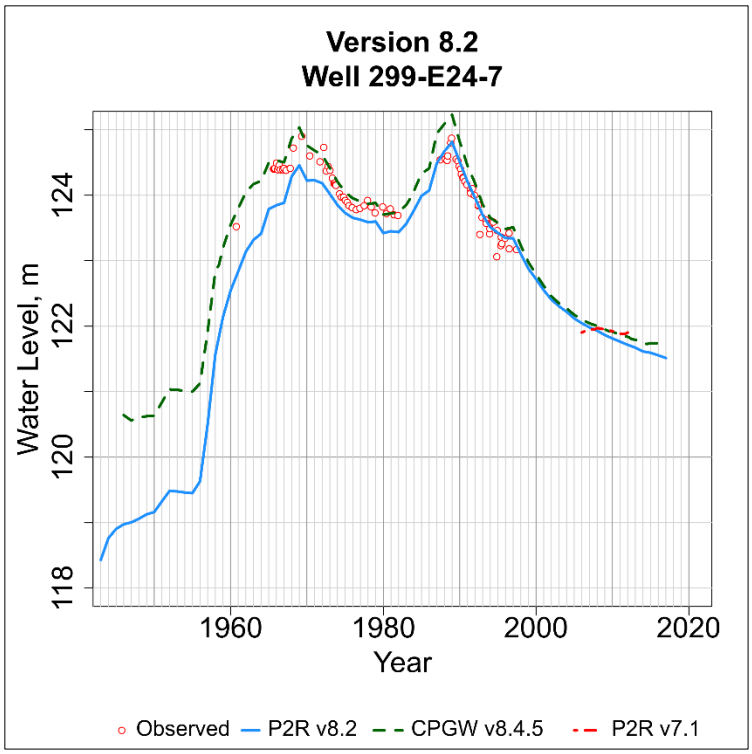

Figure D-25. Observed and simulated water level in the P2R Model at well 299-E24-7.png.

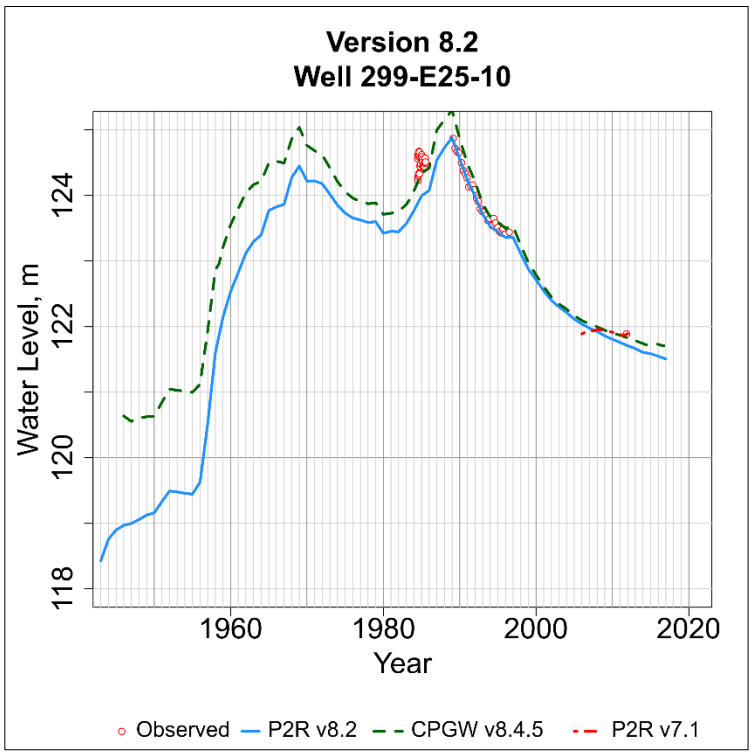

Figure D-26. Observed and simulated water level in the P2R Model at well 299-E25-10.png.

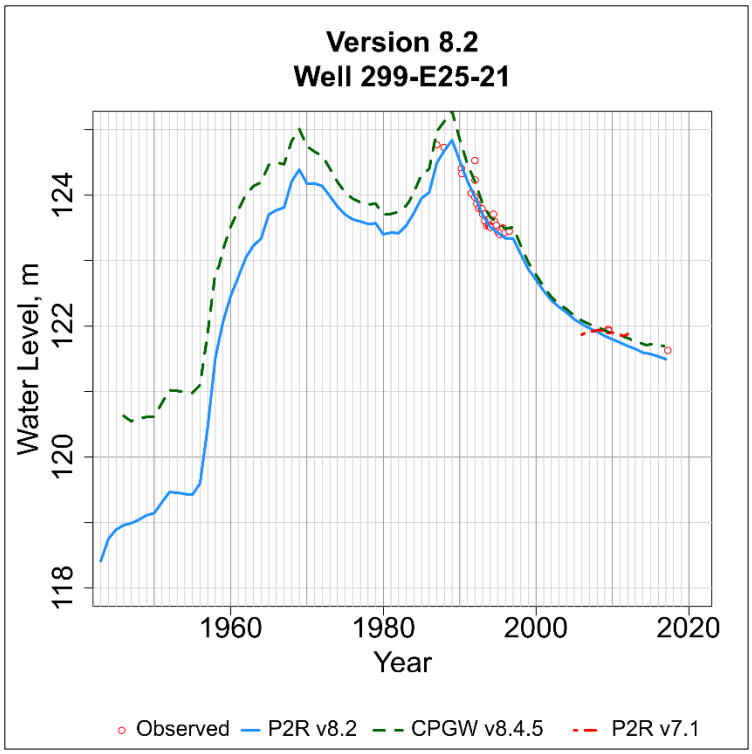

Figure D-27. Observed and simulated water level in the P2R Model at well 299-E25-21.png.

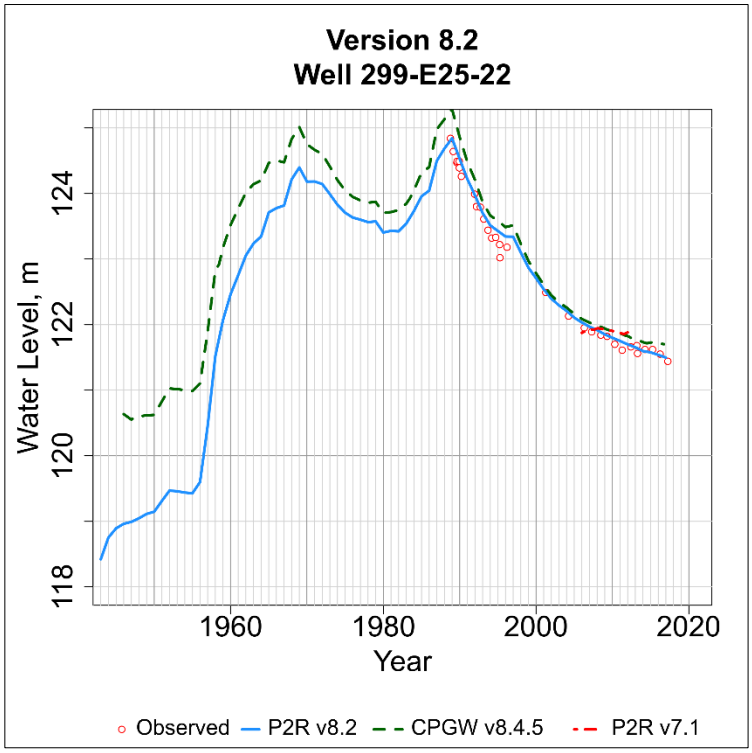

Figure D-28. Observed and simulated water level in the P2R Model at well 299-E25-22.png.

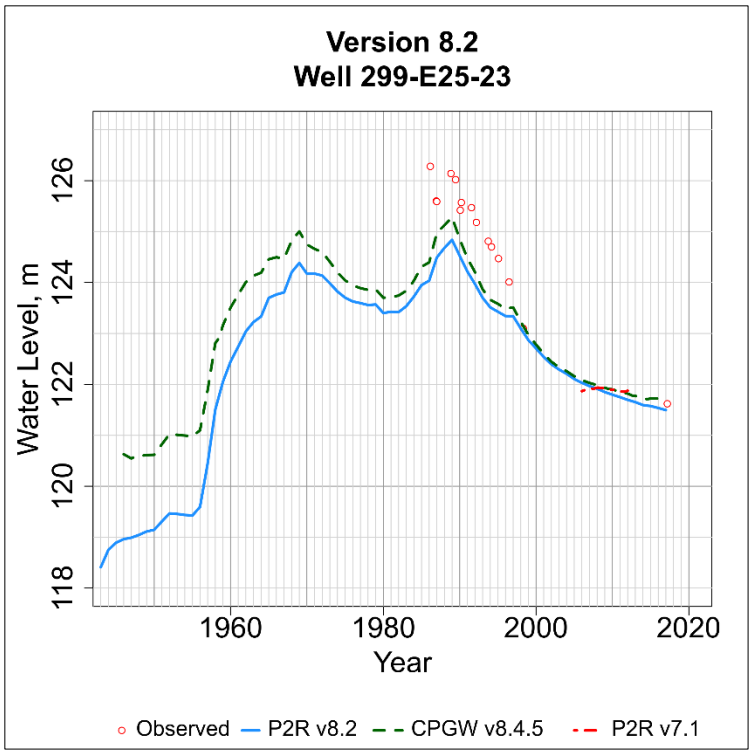

Figure D-29. Observed and simulated water level in the P2R Model at well 299-E25-23.png.

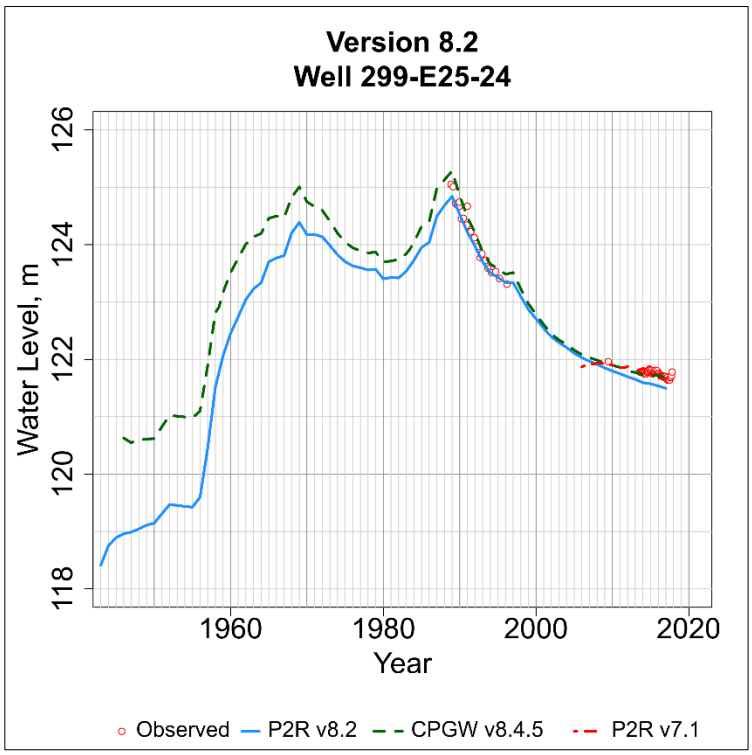

Figure D-30. Observed and simulated water level in the P2R Model at well 299-E25-24.png.

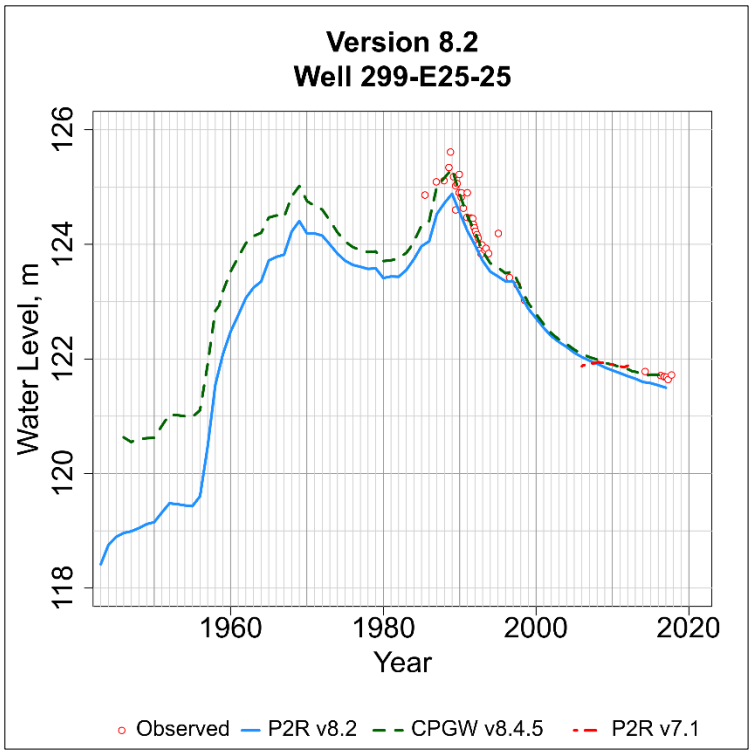

Figure D-31. Observed and simulated water level in the P2R Model at well 299-E25-25.png.

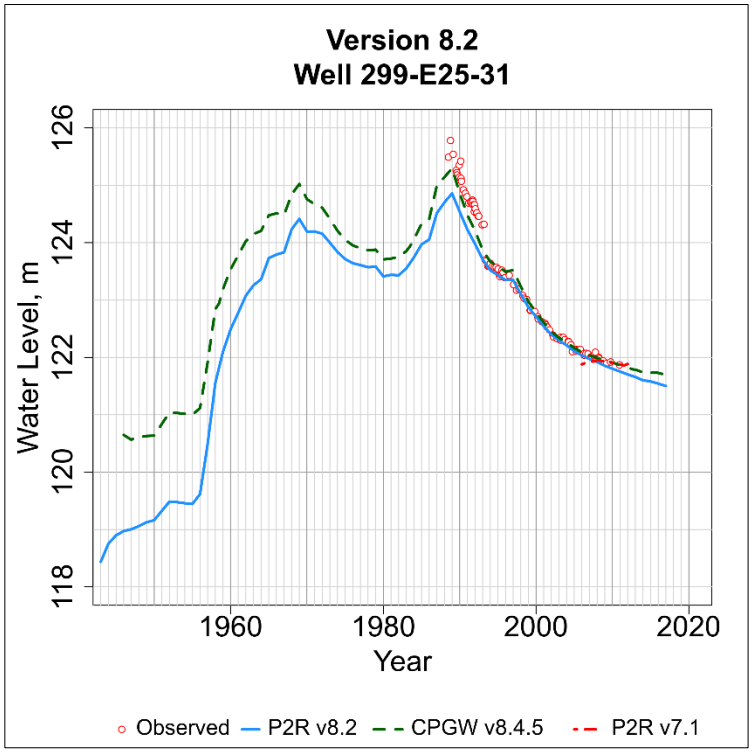

Figure D-32. Observed and simulated water level in the P2R Model at well 299-E25-31.png.

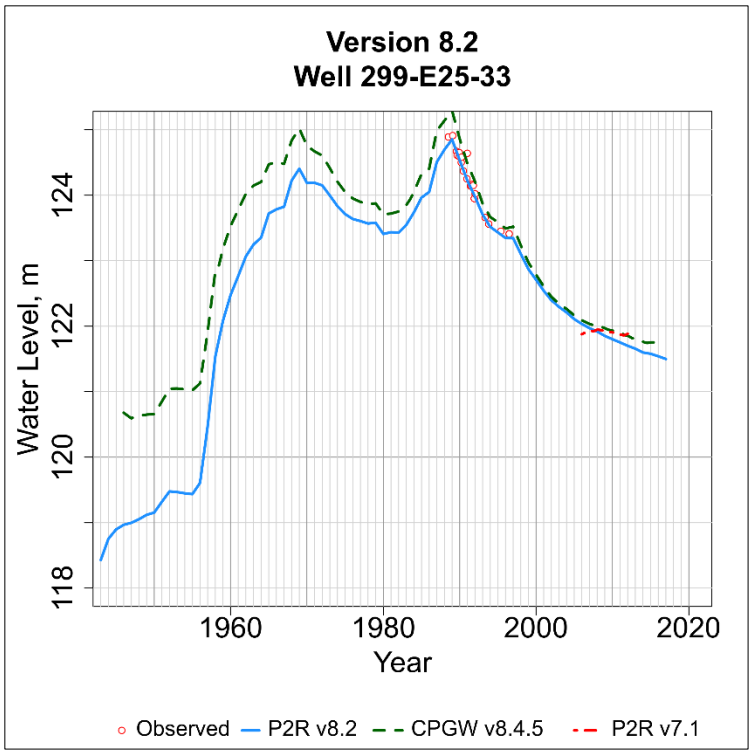

Figure D-33. Observed and simulated water level in the P2R Model at well 299-E25-33.png.

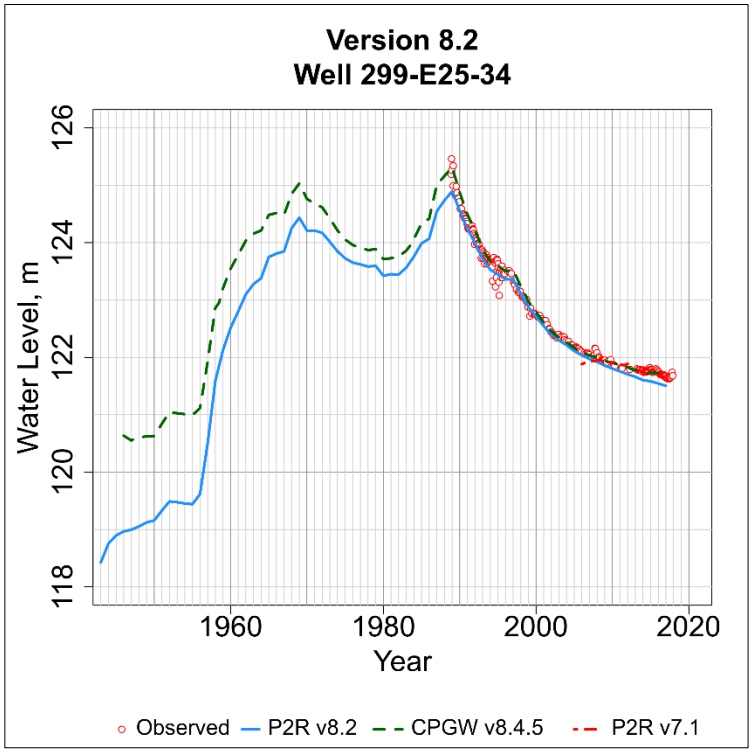

Figure D-34. Observed and simulated water level in the P2R Model at well 299-E25-34.png.

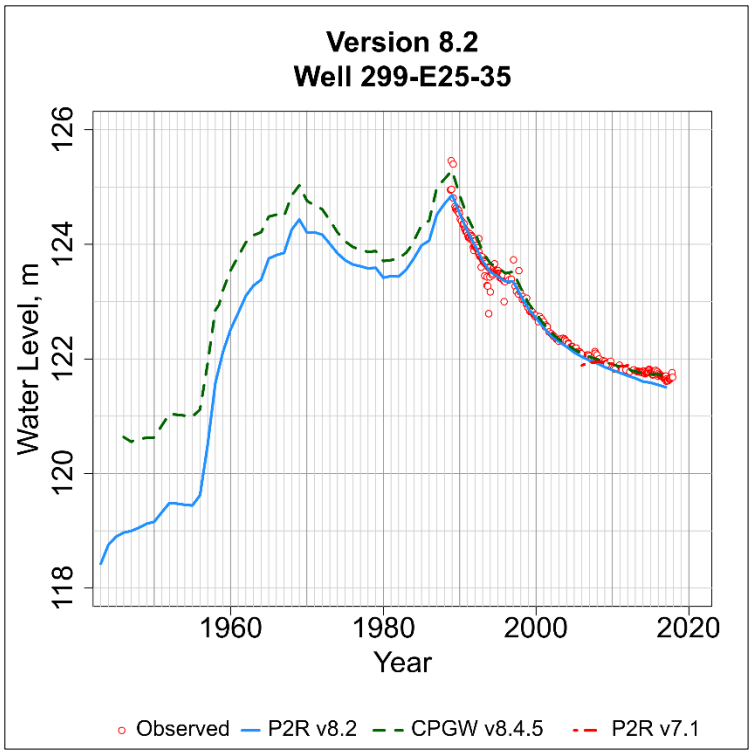

Figure D-35. Observed and simulated water level in the P2R Model at well 299-E25-35.png.

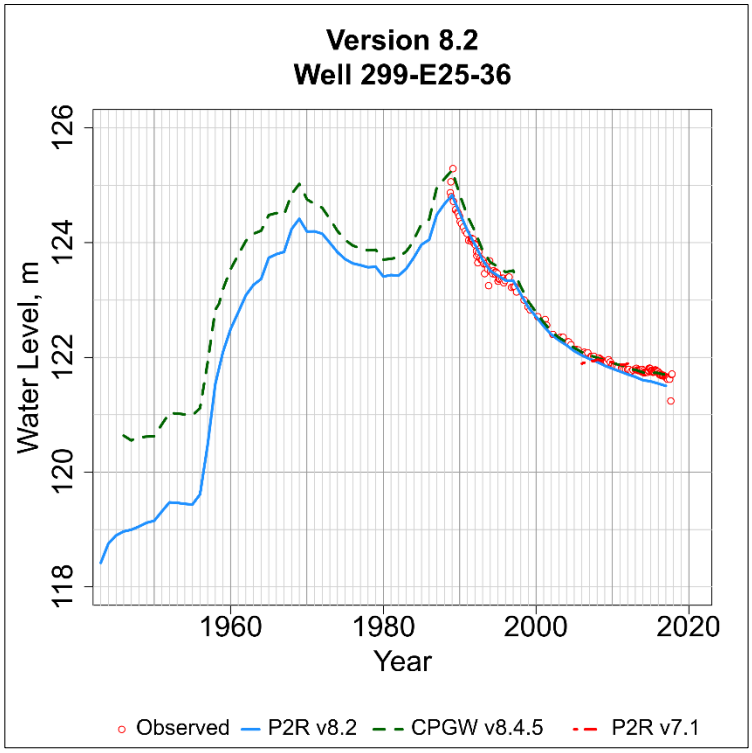

Figure D-36. Observed and simulated water level in the P2R Model at well 299-E25-36.png.

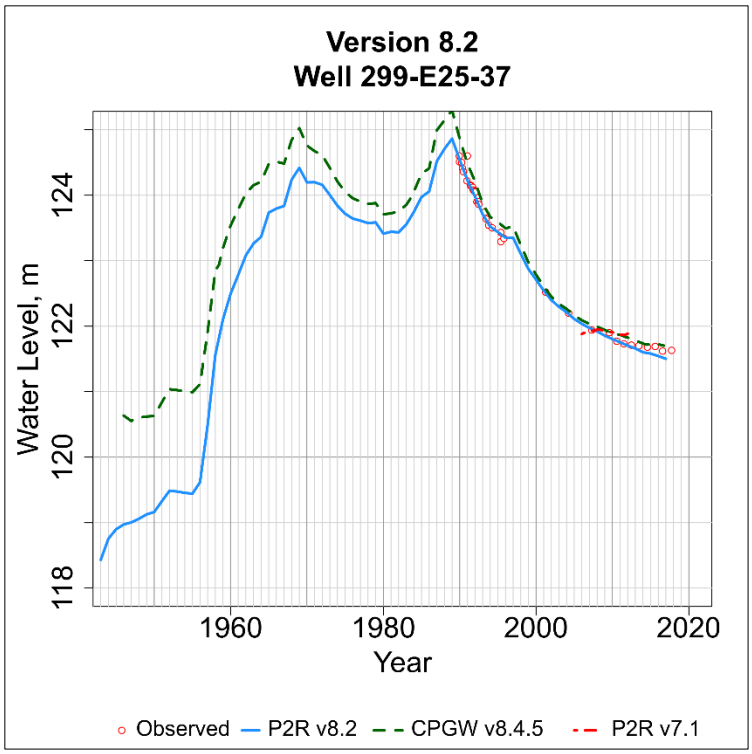

Figure D-37. Observed and simulated water level in the P2R Model at well 299-E25-37.png.

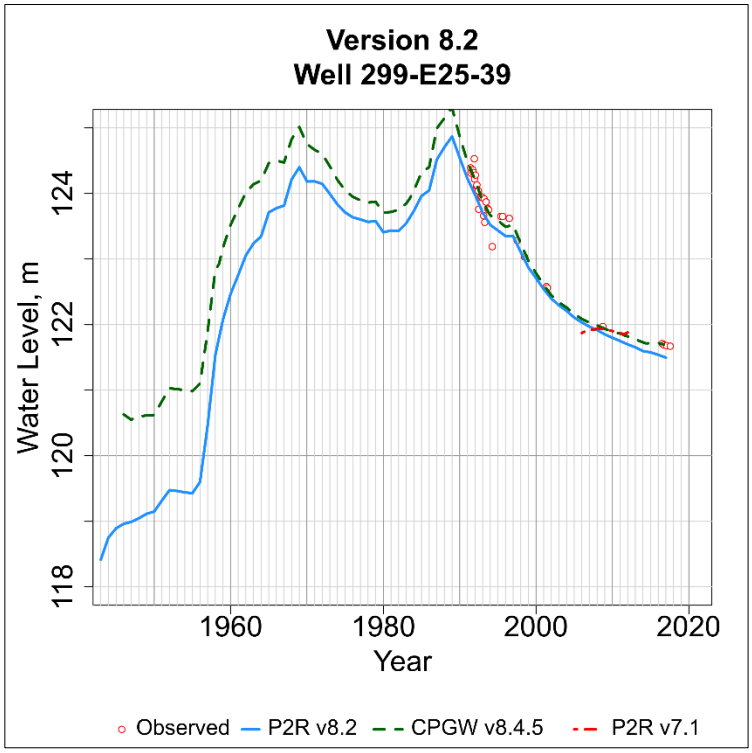

Figure D-38. Observed and simulated water level in the P2R Model at well 299-E25-39.png.

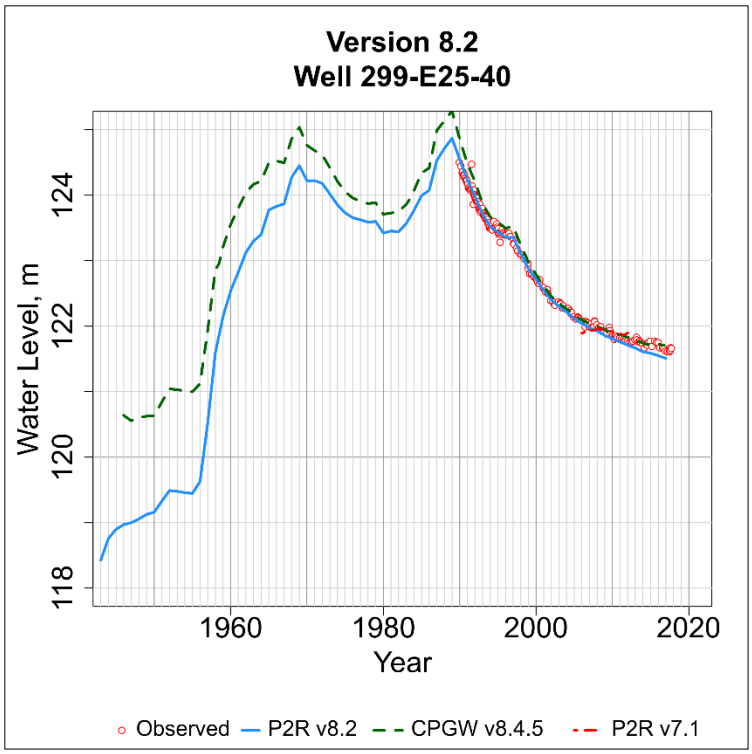

Figure D-39. Observed and simulated water level in the P2R Model at well 299-E25-40.png.

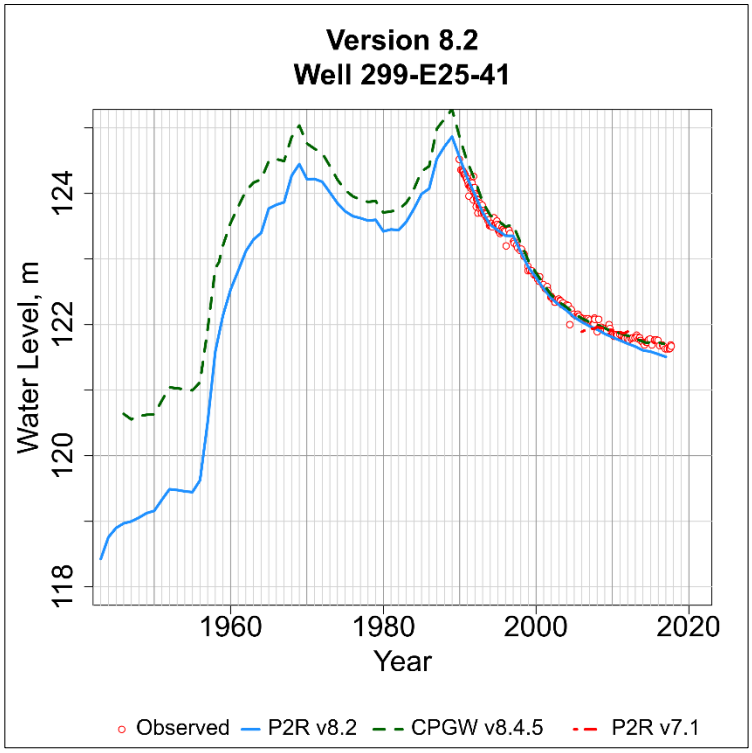

Figure D-40. Observed and simulated water level in the P2R Model at well 299-E25-41.png.

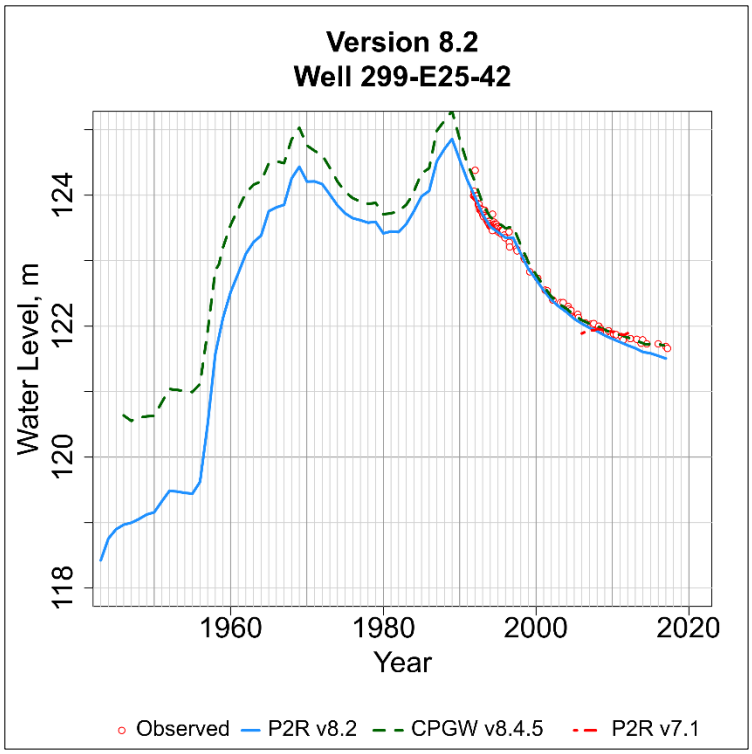

Figure D-41. Observed and simulated water level in the P2R Model at well 299-E25-42.png.

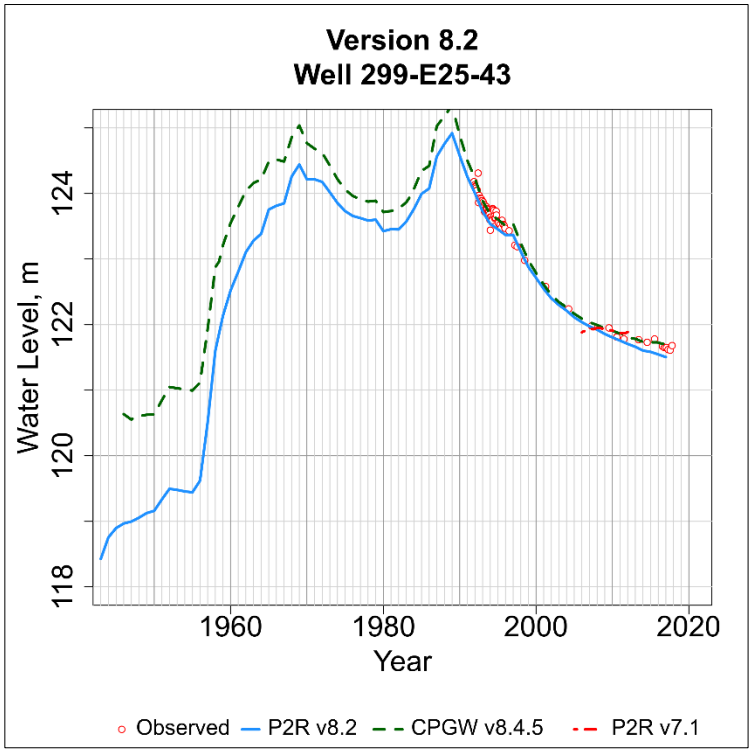

Figure D-42. Observed and simulated water level in the P2R Model at well 299-E25-43.png.

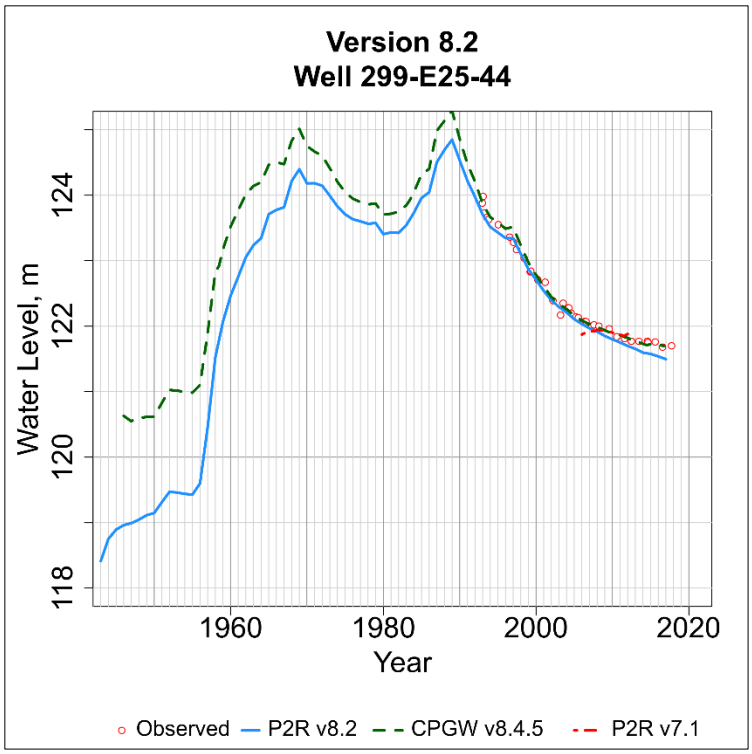

Figure D-43. Observed and simulated water level in the P2R Model at well 299-E25-44.png.

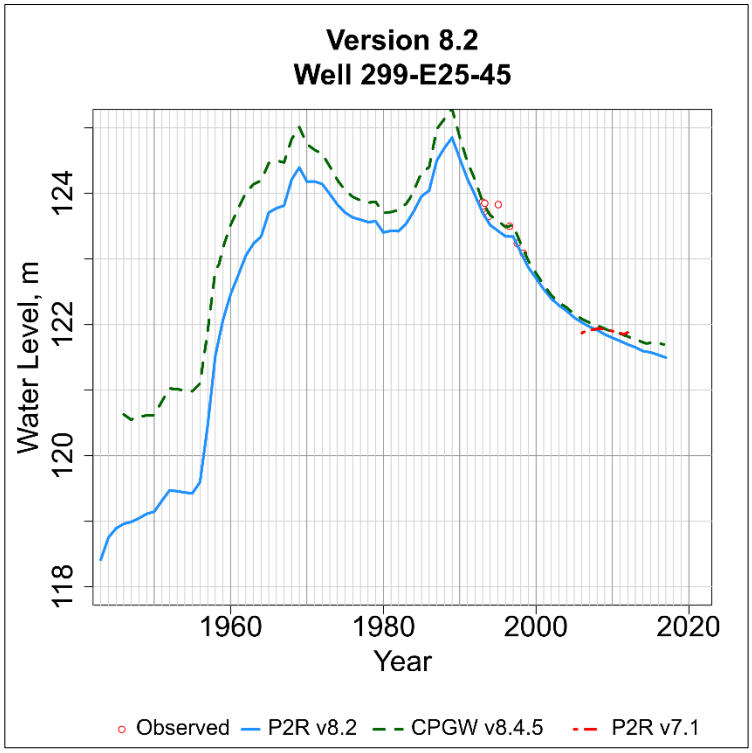

Figure D-44. Observed and simulated water level in the P2R Model at well 299-E25-45.png.

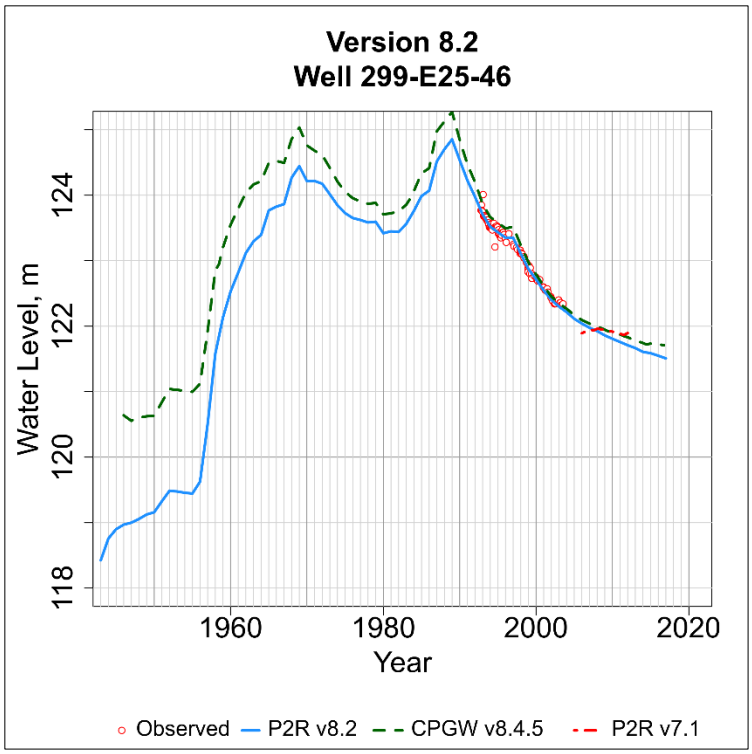

Figure D-45. Observed and simulated water level in the P2R Model at well 299-E25-46.png.

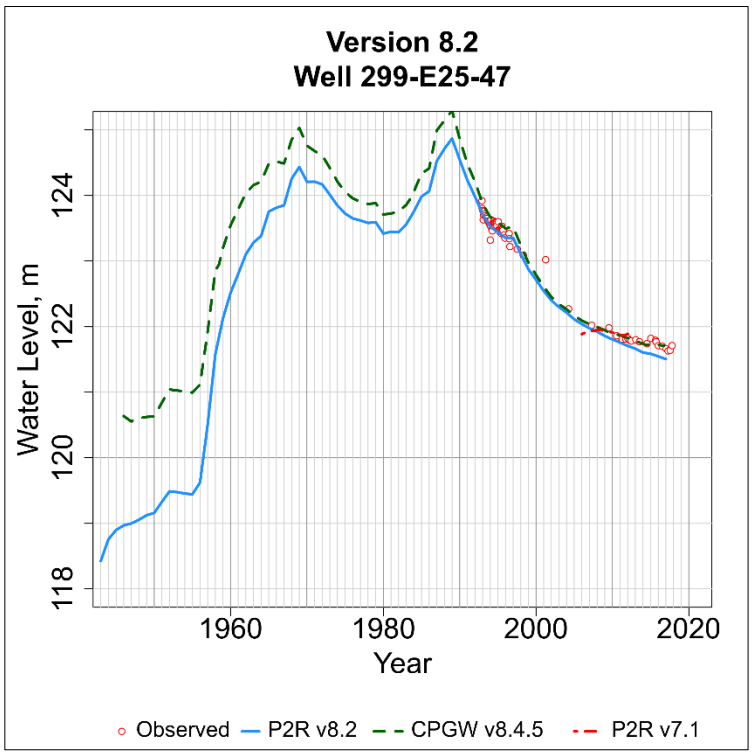

Figure D-46. Observed and simulated water level in the P2R Model at well 299-E25-47.png.

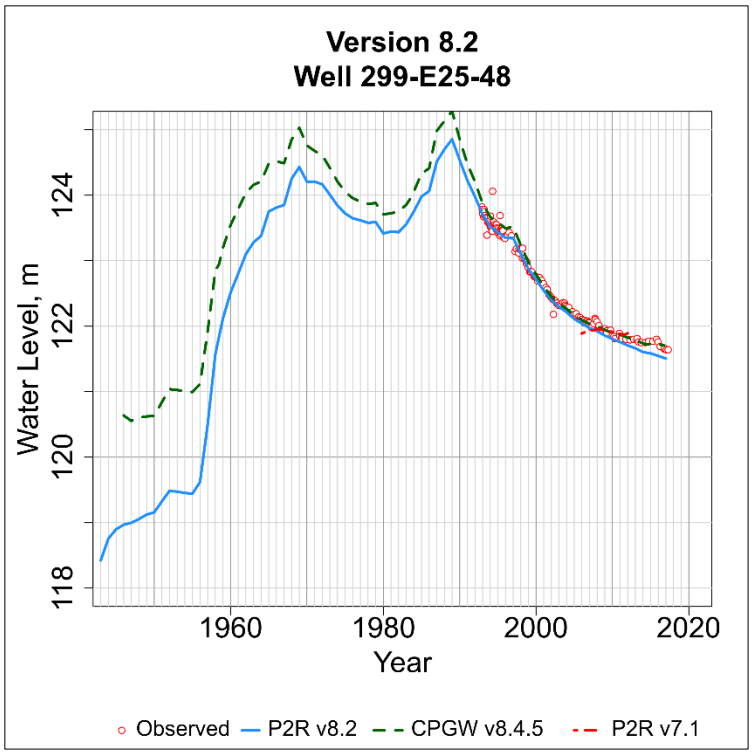

Figure D-47. Observed and simulated water level in the P2R Model at well 299-E25-48.png.

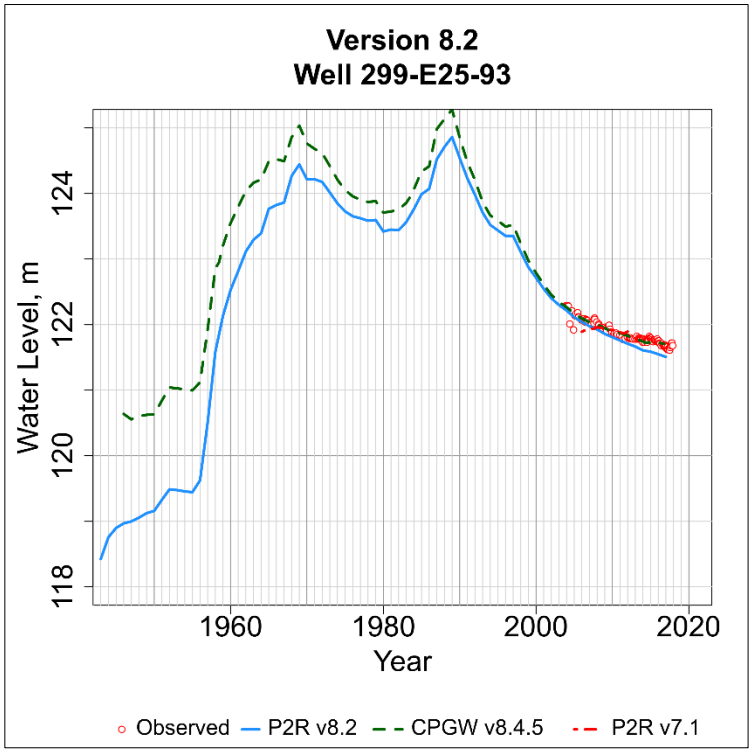

Figure D-48. Observed and simulated water level in the P2R Model at well 299-E25-93.png.

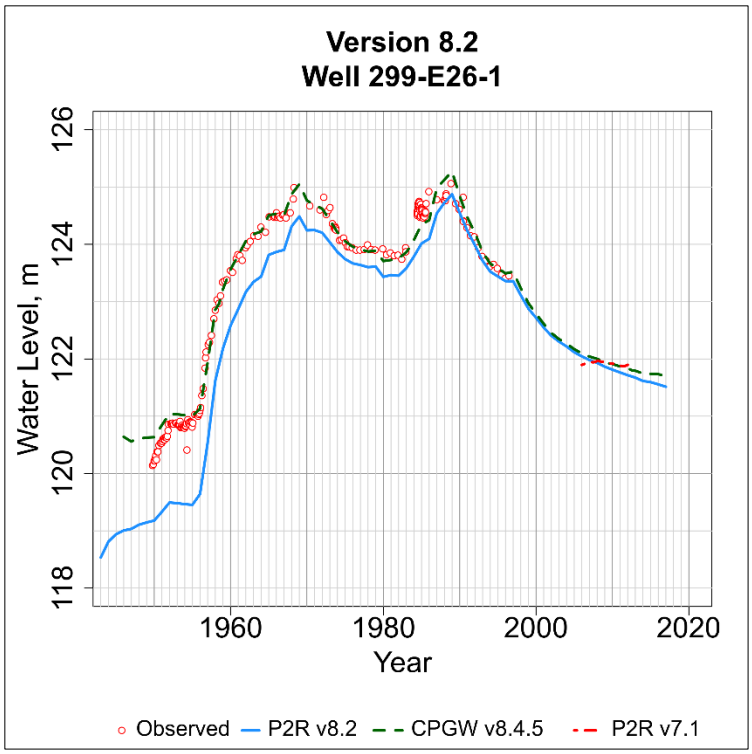

Figure D-49. Observed and simulated water level in the P2R Model at well 299-E26-1.png.

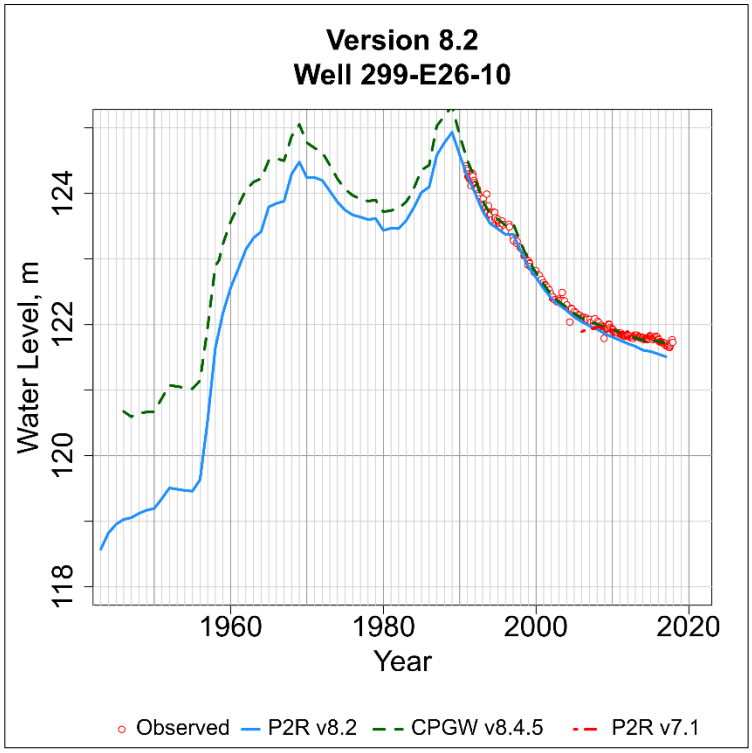

Figure D-50. Observed and simulated water level in the P2R Model at well 299-E26-10.png.

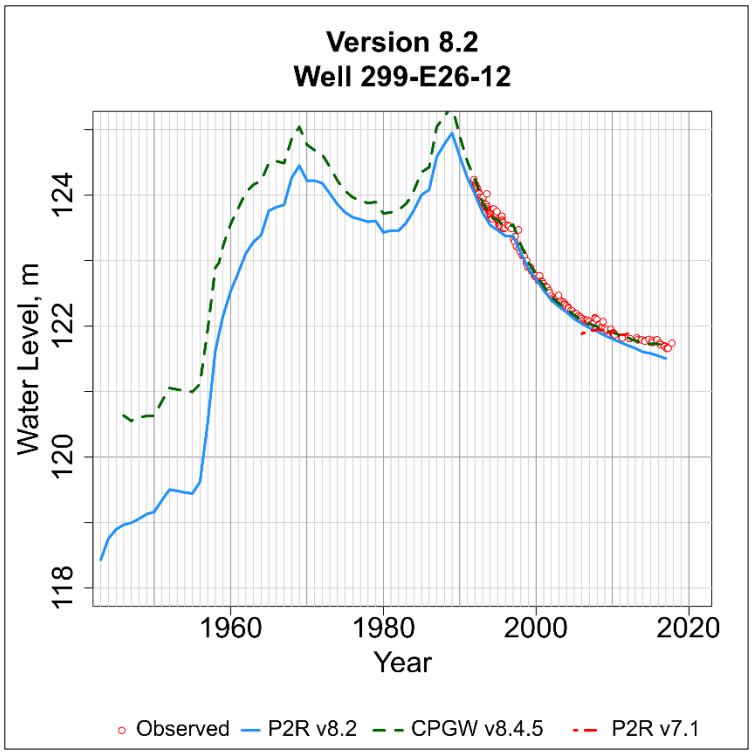

Figure D-51. Observed and simulated water level in the P2R Model at well 299-E26-12.png.

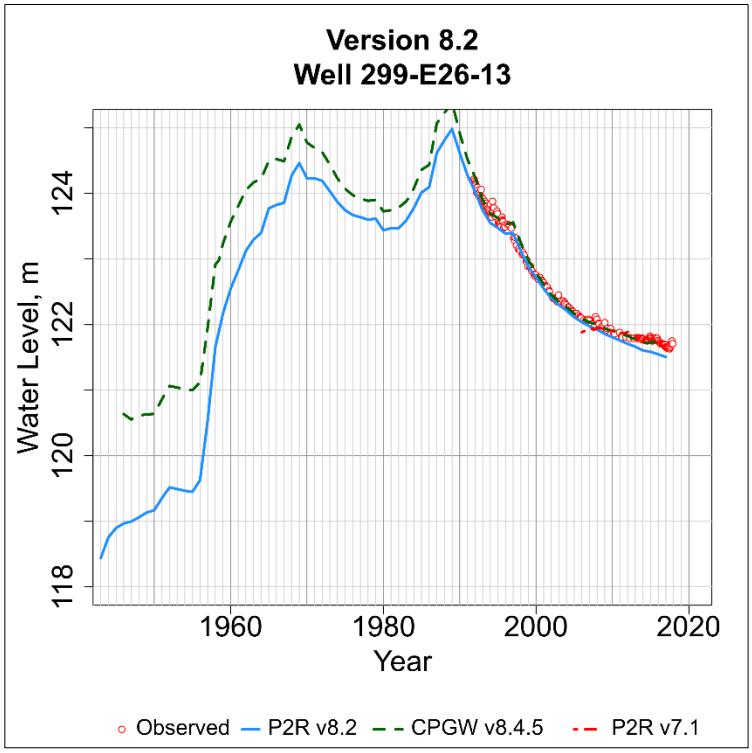

Figure D-52. Observed and simulated water level in the P2R Model at well 299-E26-13.png.

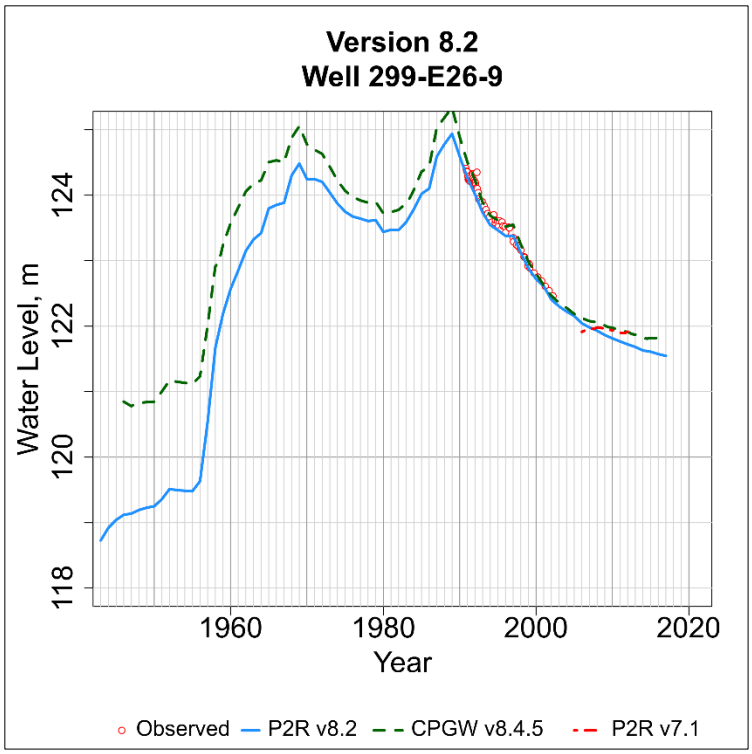

Figure D-53. Observed and simulated water level in the P2R Model at well 299-E26-9.png.

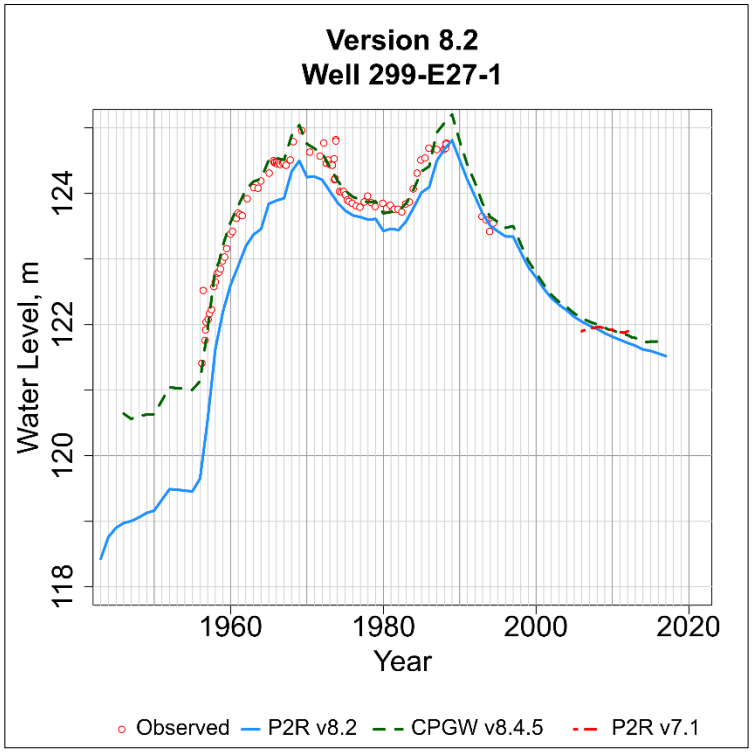

Figure D-54. Observed and simulated water level in the P2R Model at well 299-E27-1.png.

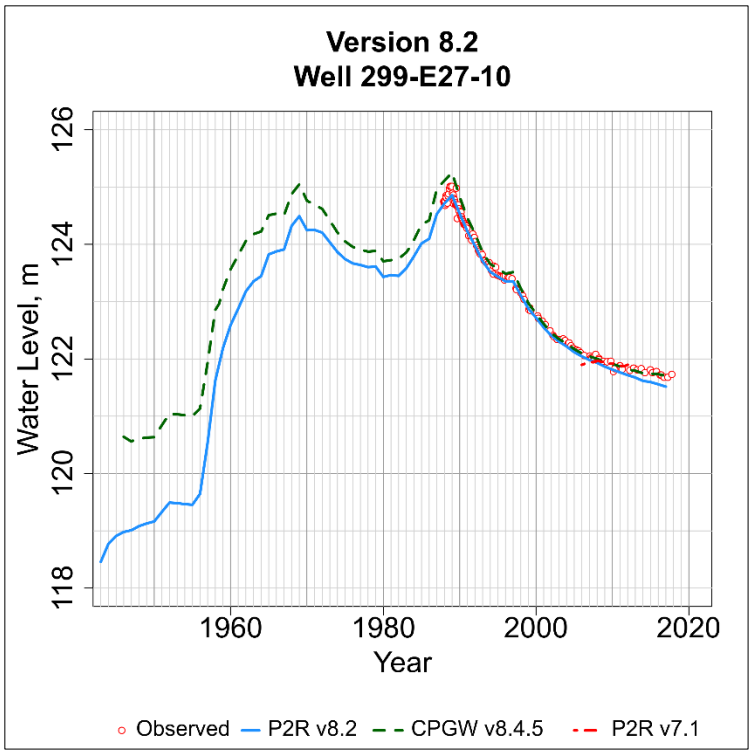

Figure D-55. Observed and simulated water level in the P2R Model at well 299-E27-10.png.

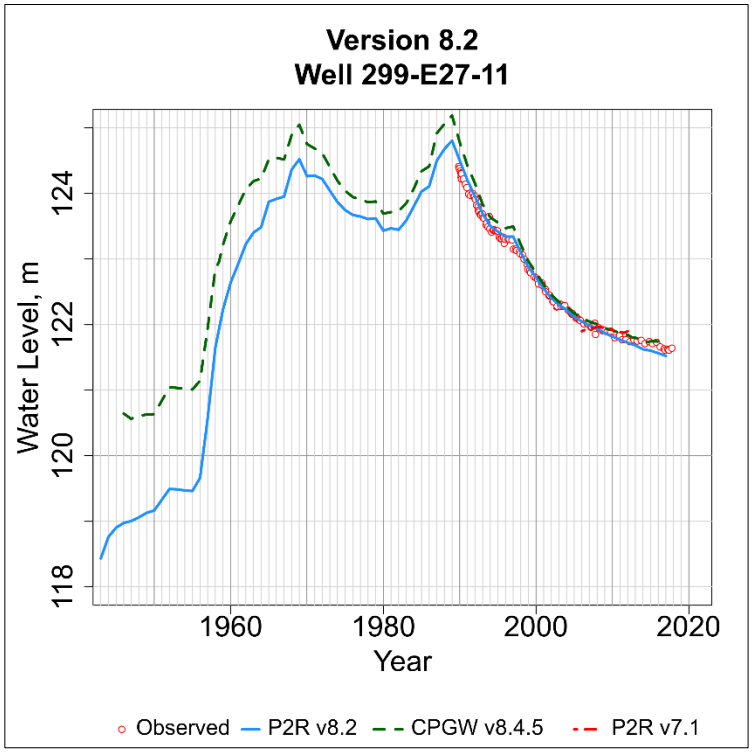

Figure D-56. Observed and simulated water level in the P2R Model at well 299-E27-11.png.

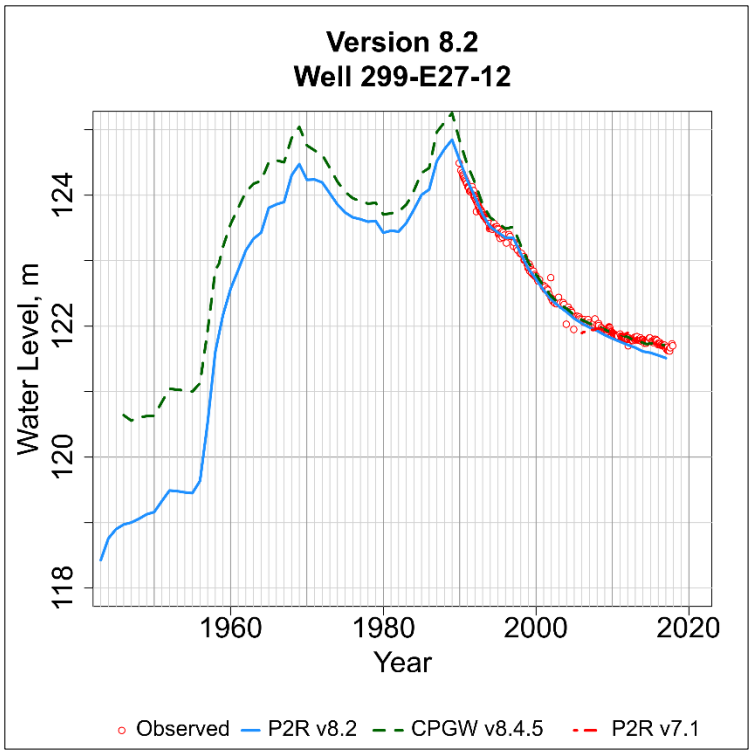

Figure D-57. Observed and simulated water level in the P2R Model at well 299-E27-12.png.

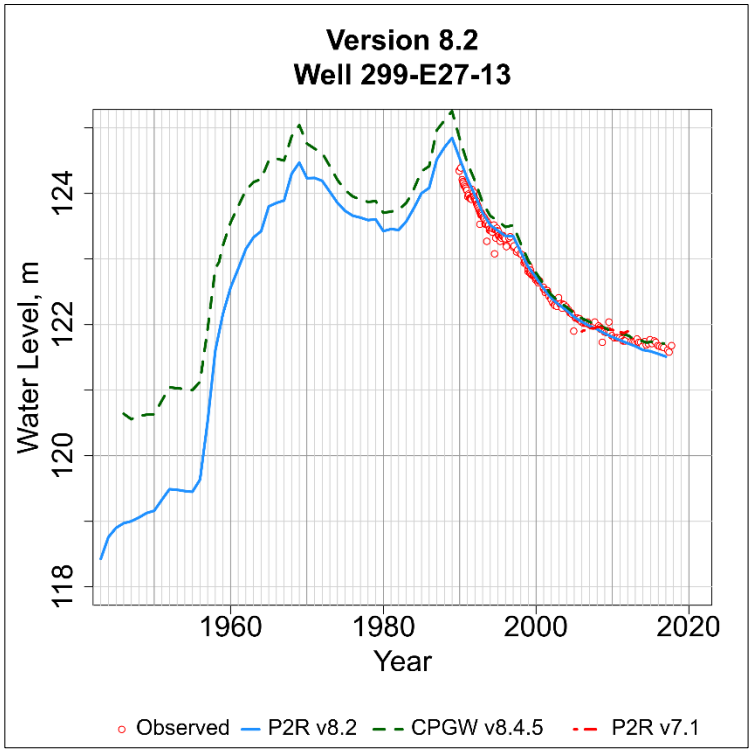

Figure D-58. Observed and simulated water level in the P2R Model at well 299-E27-13.png.

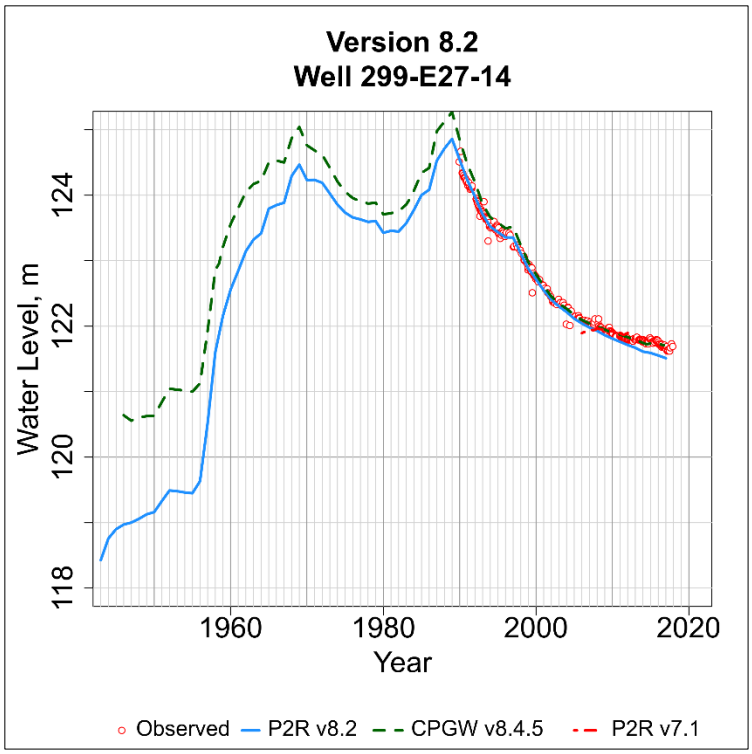

Figure D-59. Observed and simulated water level in the P2R Model at well 299-E27-14.png.

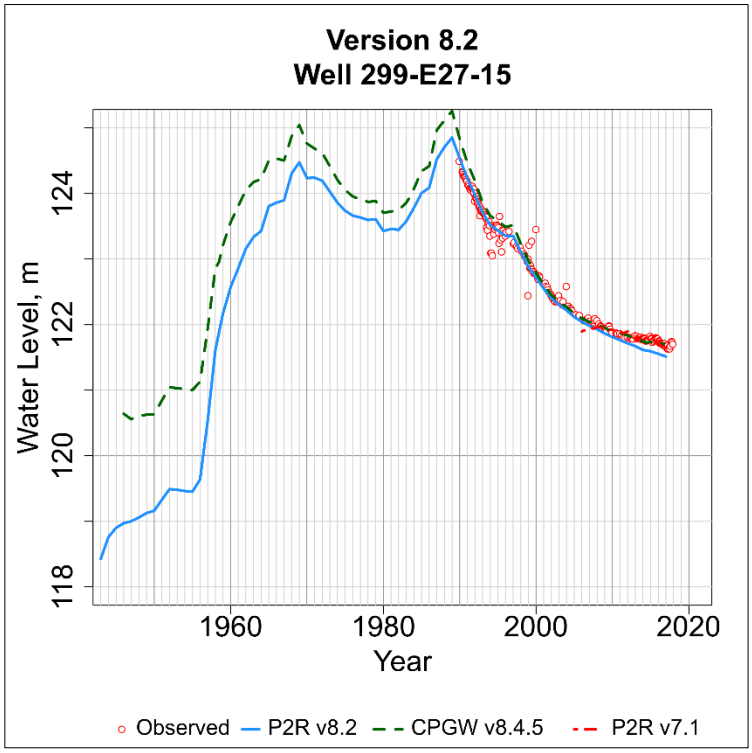

Figure D-60. Observed and simulated water level in the P2R Model at well 299-E27-15.png.

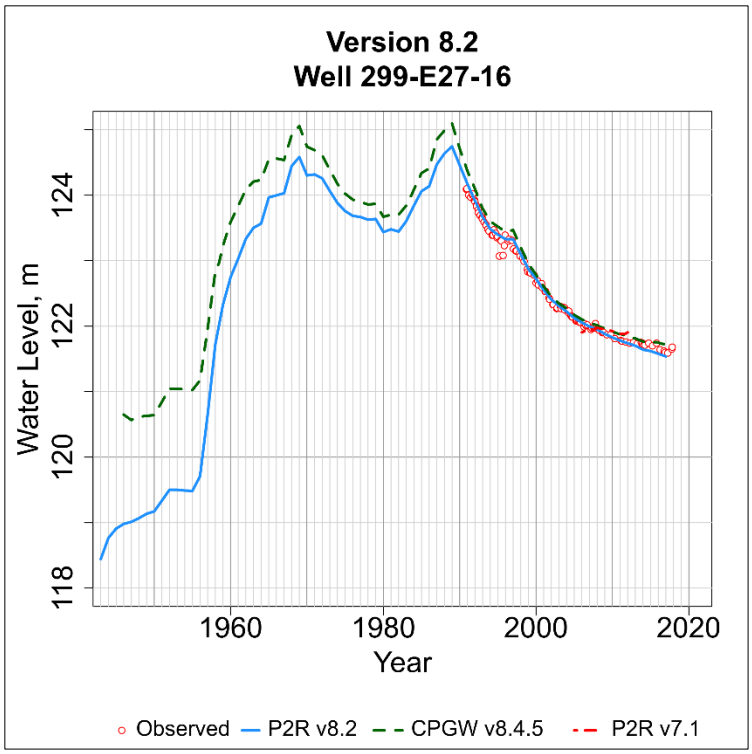

Figure D-61. Observed and simulated water level in the P2R Model at well 299-E27-16.png.

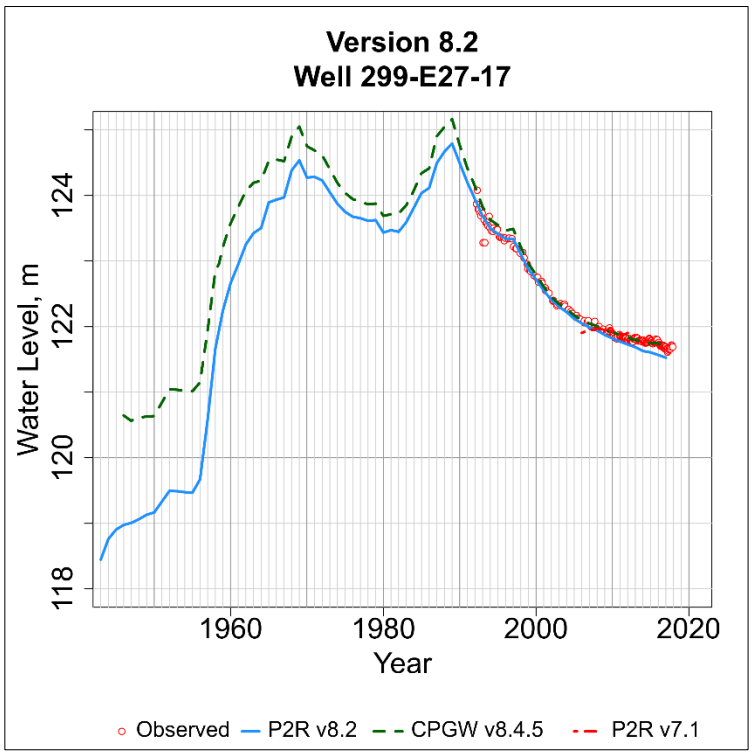

Figure D-62. Observed and simulated water level in the P2R Model at well 299-E27-17.png.

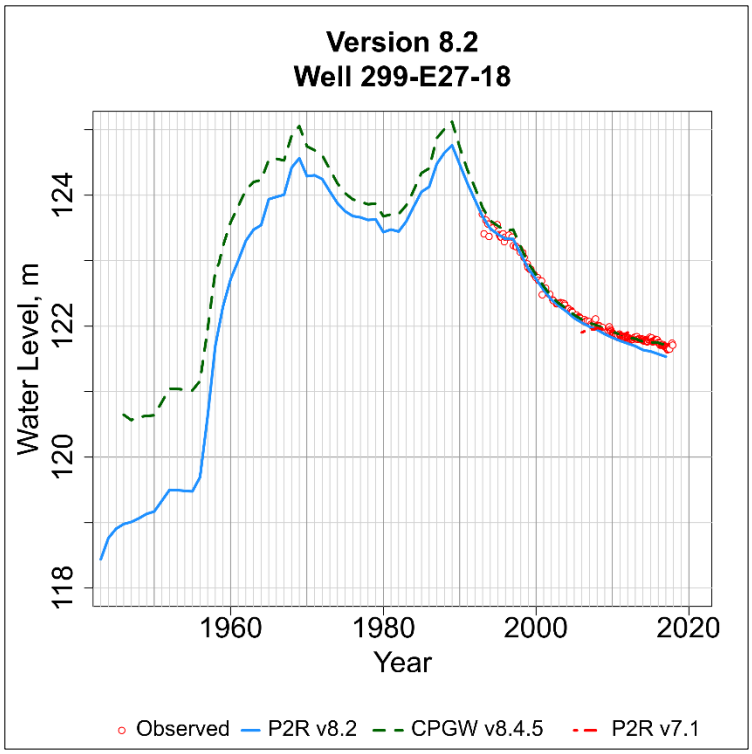

Figure D-63. Observed and simulated water level in the P2R Model at well 299-E27-18.png.

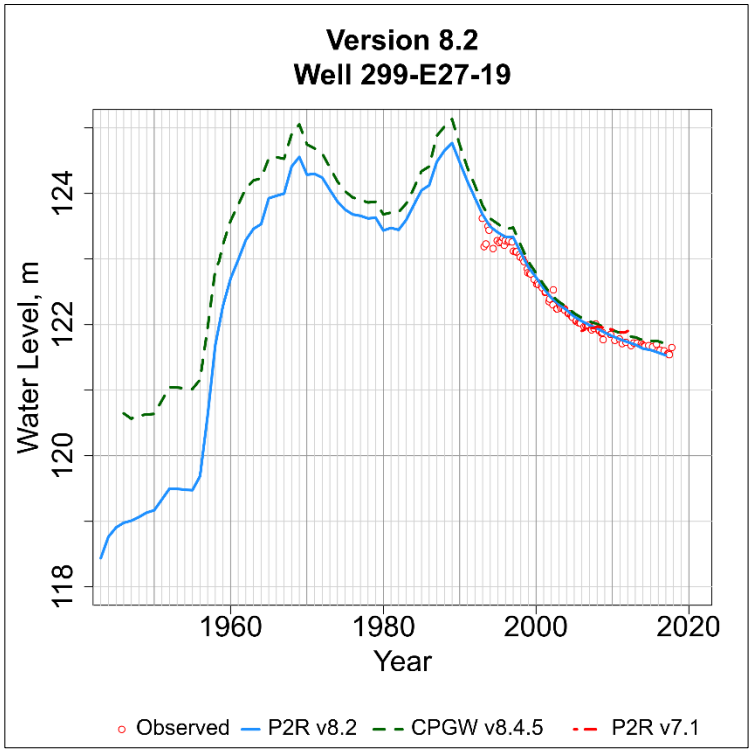

Figure D-64. Observed and simulated water level in the P2R Model at well 299-E27-19.png.

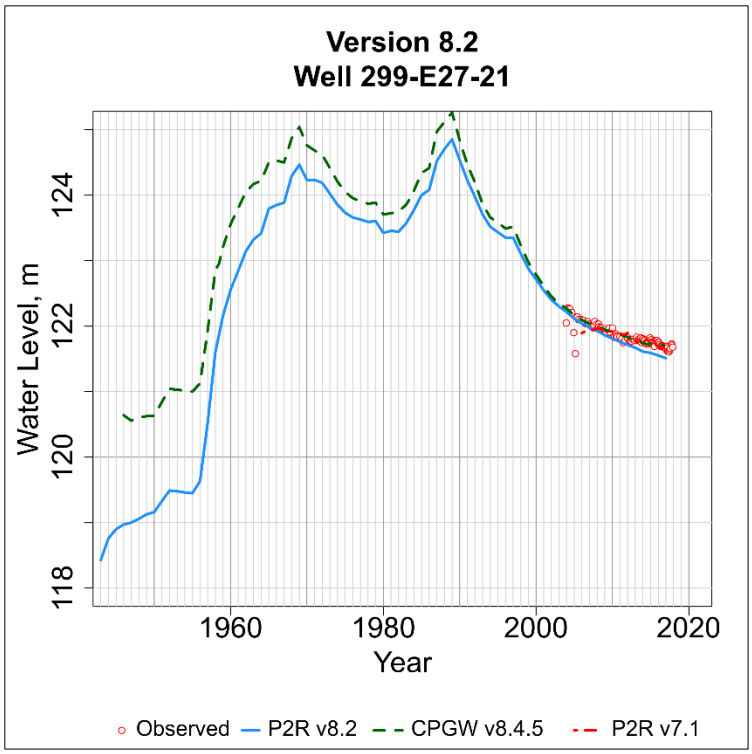

Figure D-65. Observed and simulated water level in the P2R Model at well 299-E27-21.png.

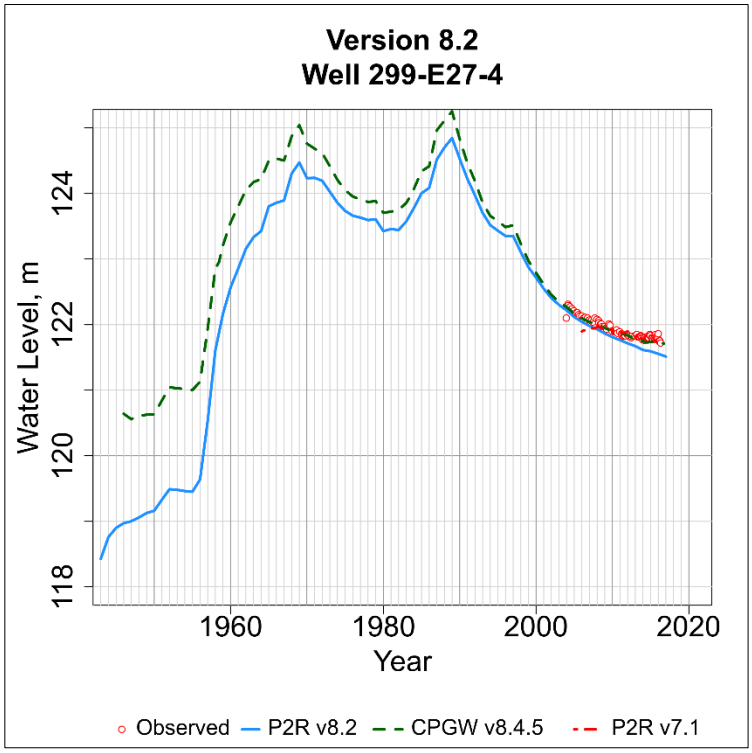

Figure D-66. Observed and simulated water level in the P2R Model at well 299-E27-4.png.

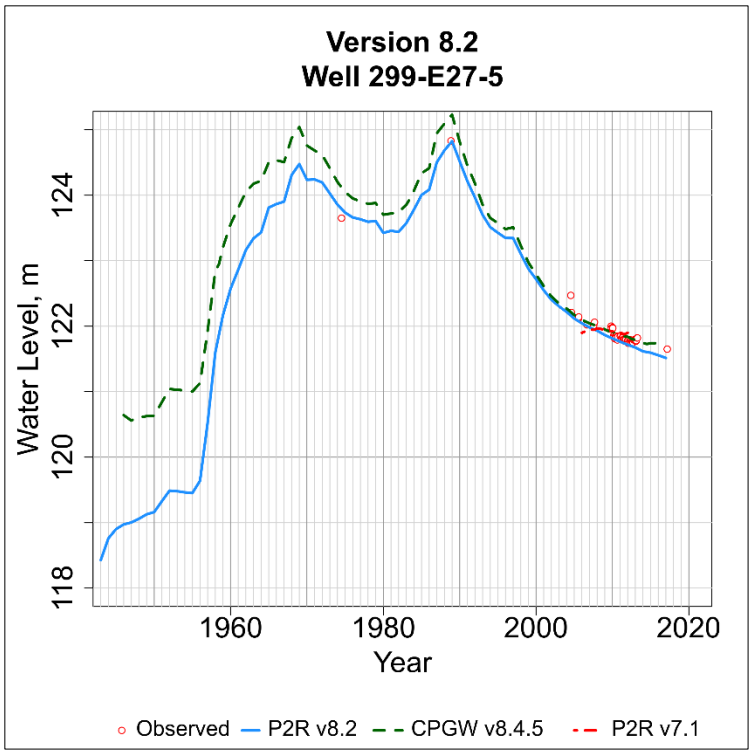

Figure D-67. Observed and simulated water level in the P2R Model at well 299-E27-5.png.

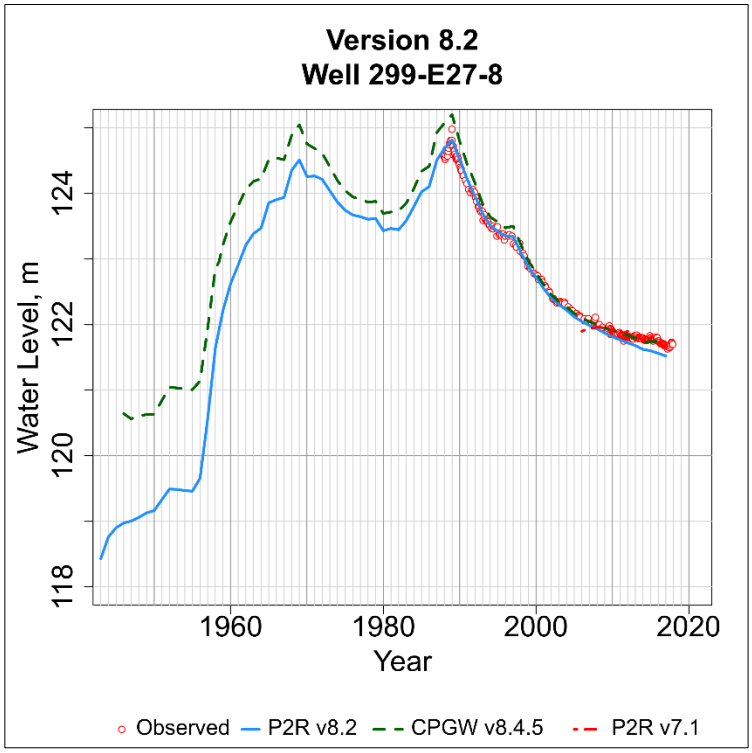

Figure D-68. Observed and simulated water level in the P2R Model at well 299-E27-8.png.

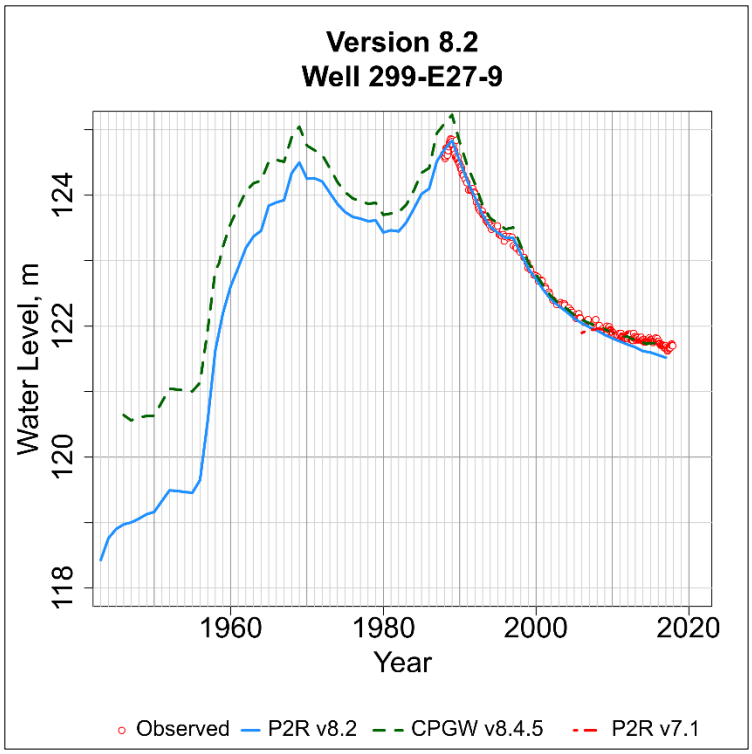

Figure D-69. Observed and simulated water level in the P2R Model at well 299-E27-9.png.

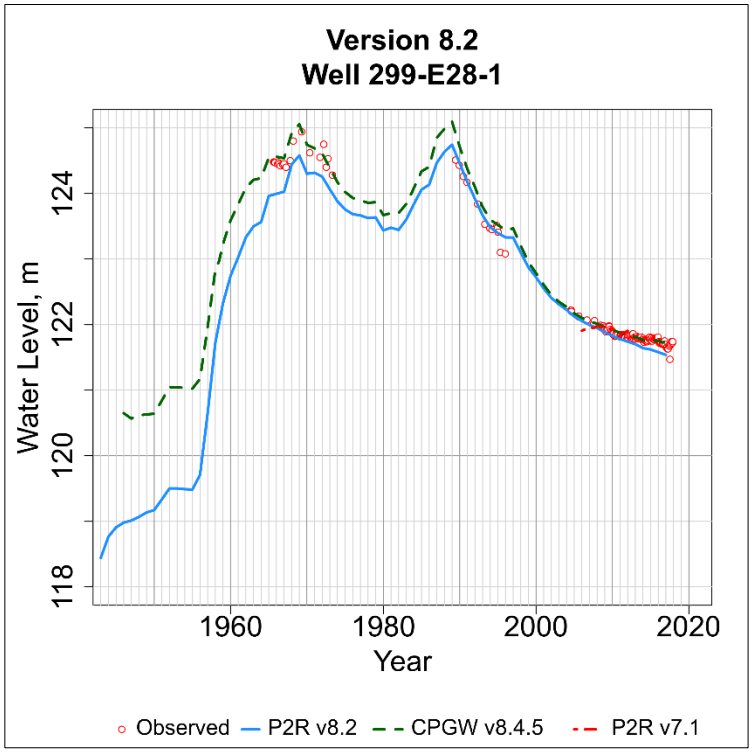

Figure D-70. Observed and simulated water level in the P2R Model at well 299-E28-1.png.

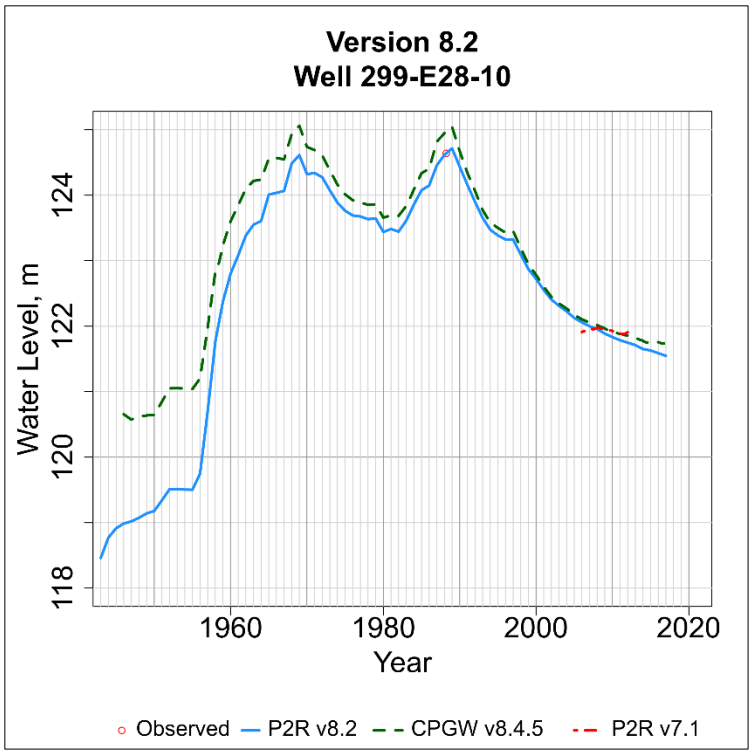

Figure D-71. Observed and simulated water level in the P2R Model at well 299-E28-10.png.

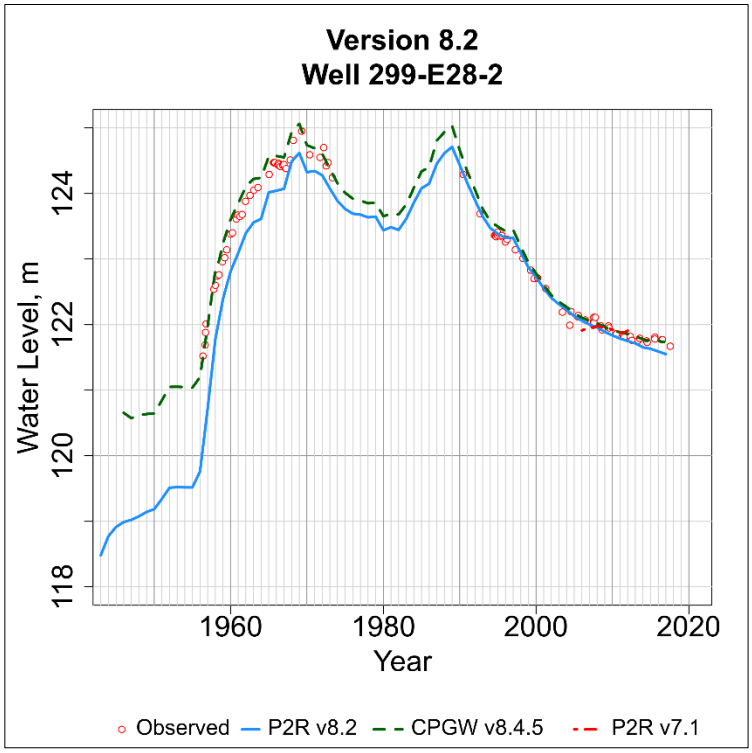

Figure D-72. Observed and simulated water level in the P2R Model at well 299-E28-2.png.

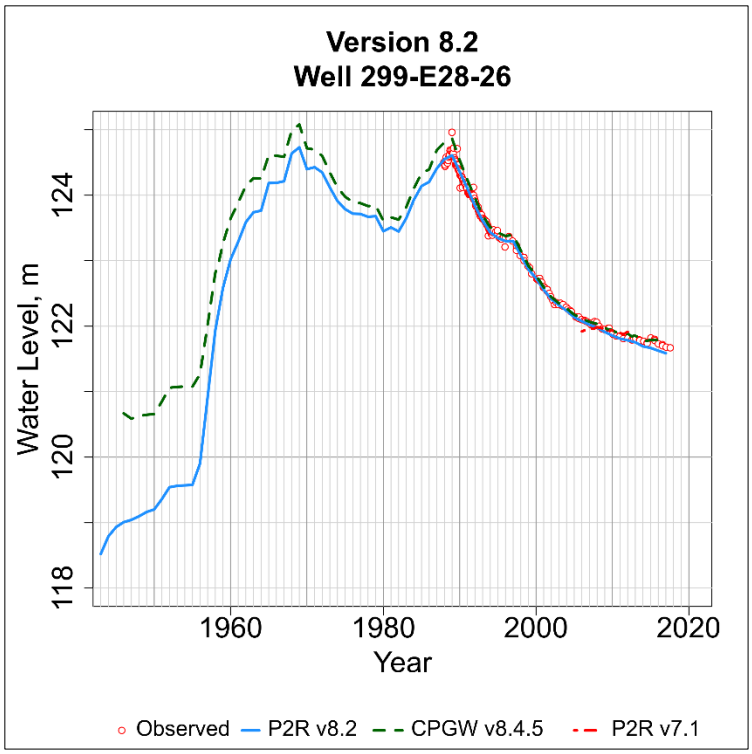

Figure D-73. Observed and simulated water level in the P2R Model at well 299-E28-26.png.

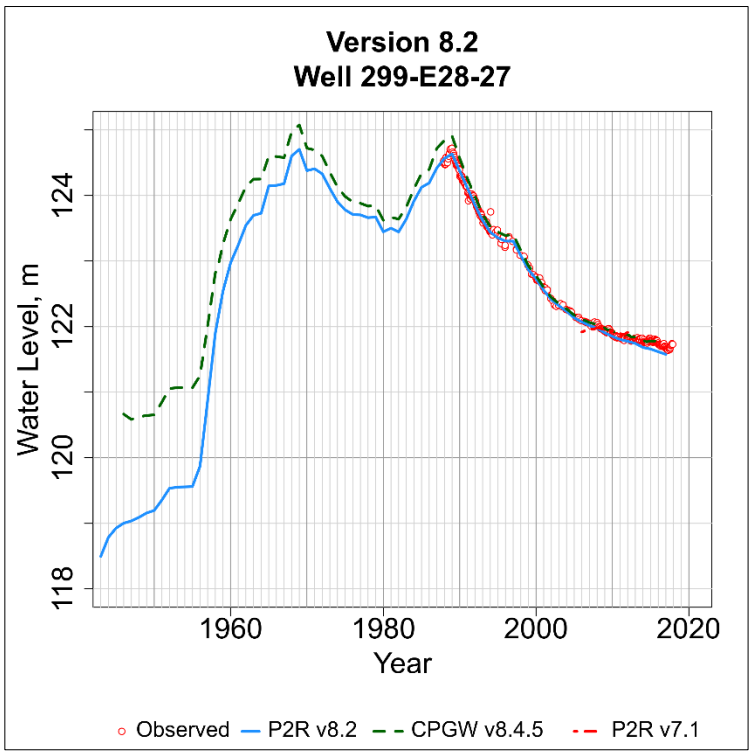

Figure D-74. Observed and simulated water level in the P2R Model at well 299-E28-27.png.

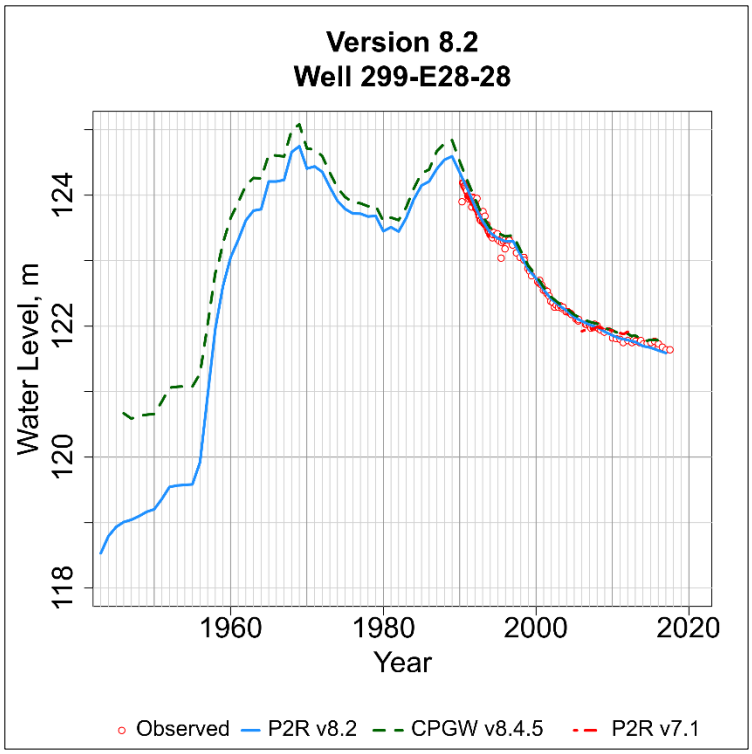

Figure D-75. Observed and simulated water level in the P2R Model at well 299-E28-28.png.

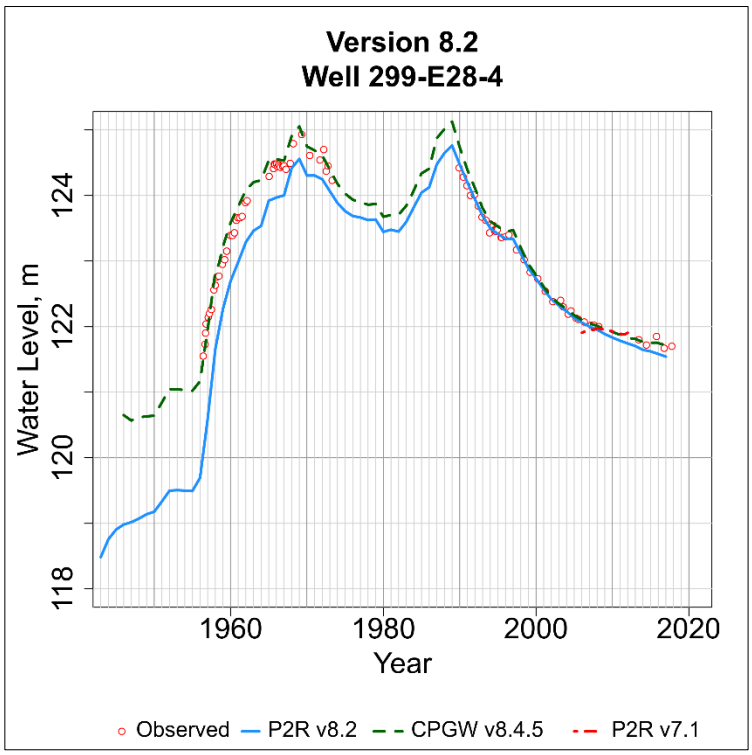

Figure D-76. Observed and simulated water level in the P2R Model at well 299-E28-4.png.

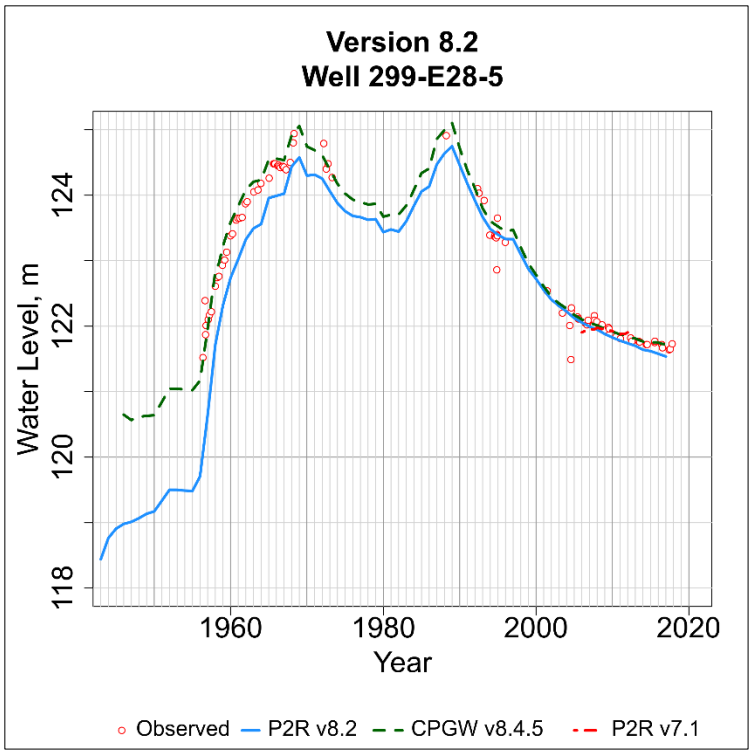

Figure D-77. Observed and simulated water level in the P2R Model at well 299-E28-5.png.

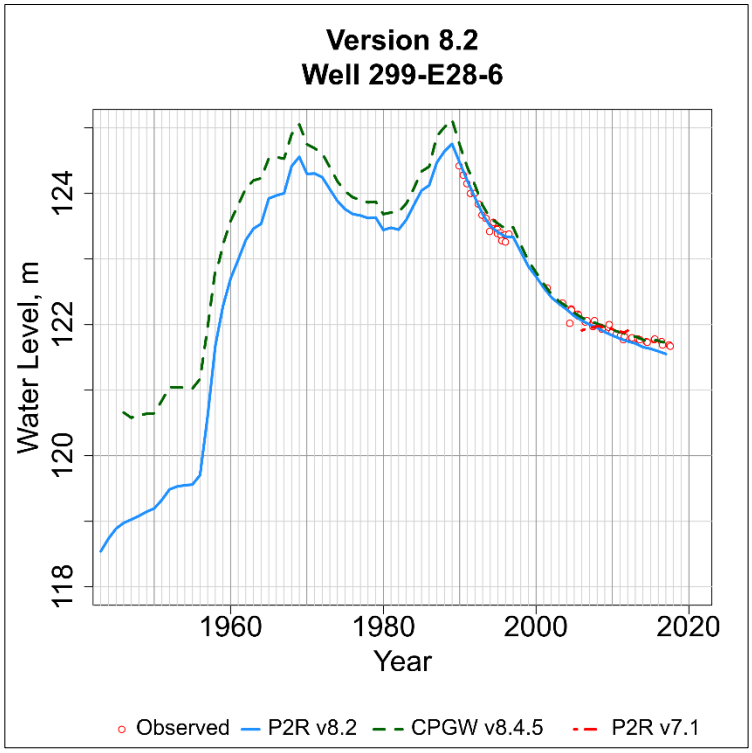

Figure D-78. Observed and simulated water level in the P2R Model at well 299-E28-6.png.

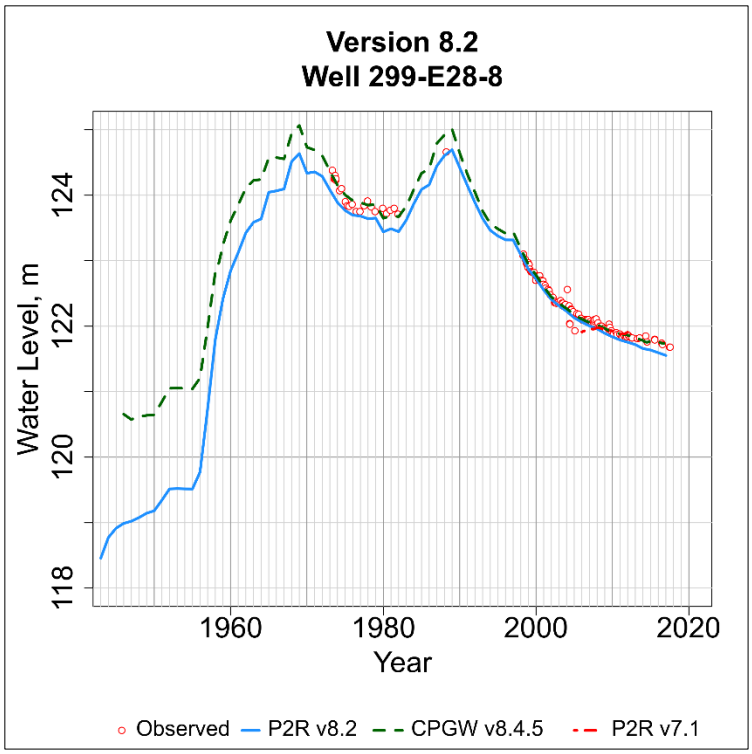

Figure D-79. Observed and simulated water level in the P2R Model at well 299-E28-8.png.

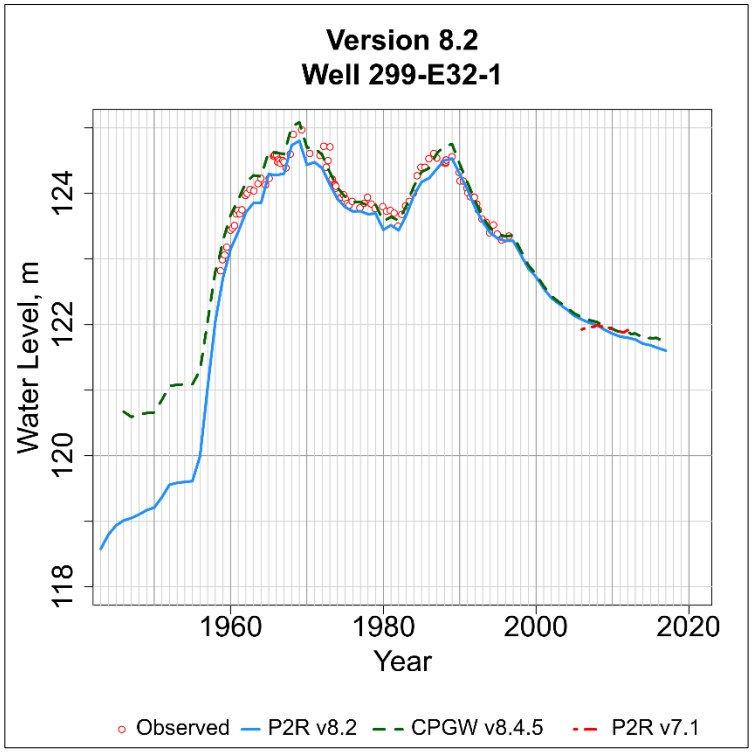

Figure D-80. Observed and simulated water level in the P2R Model at well 299-E32-1.png.

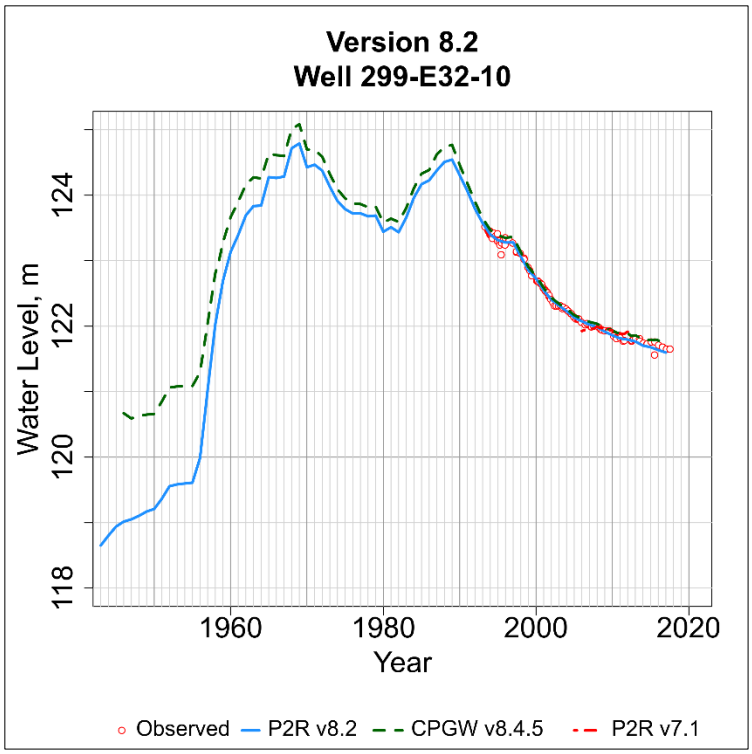

Figure D-81. Observed and simulated water level in the P2R Model at well 299-E32-10.png.

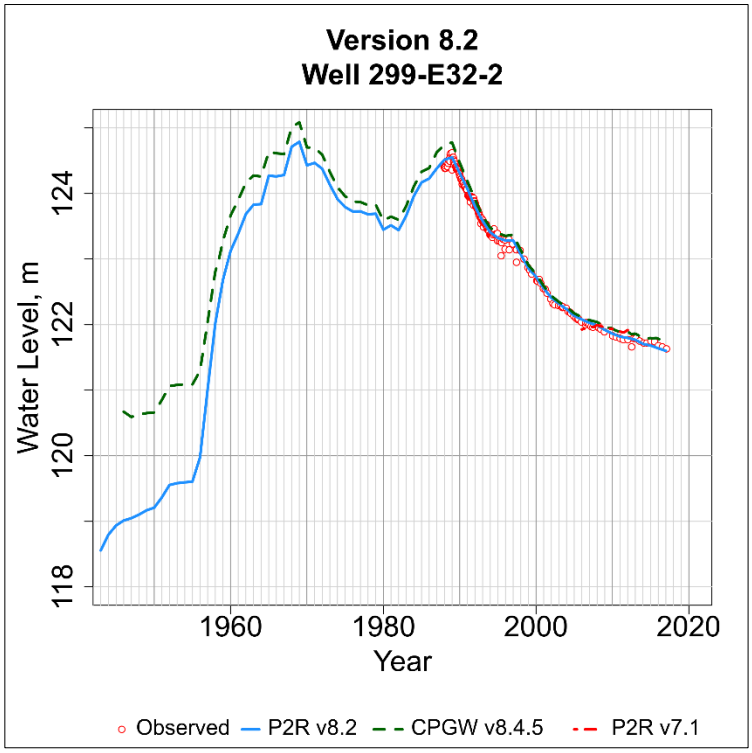

Figure D-82. Observed and simulated water level in the P2R Model at well 299-E32-2.png.

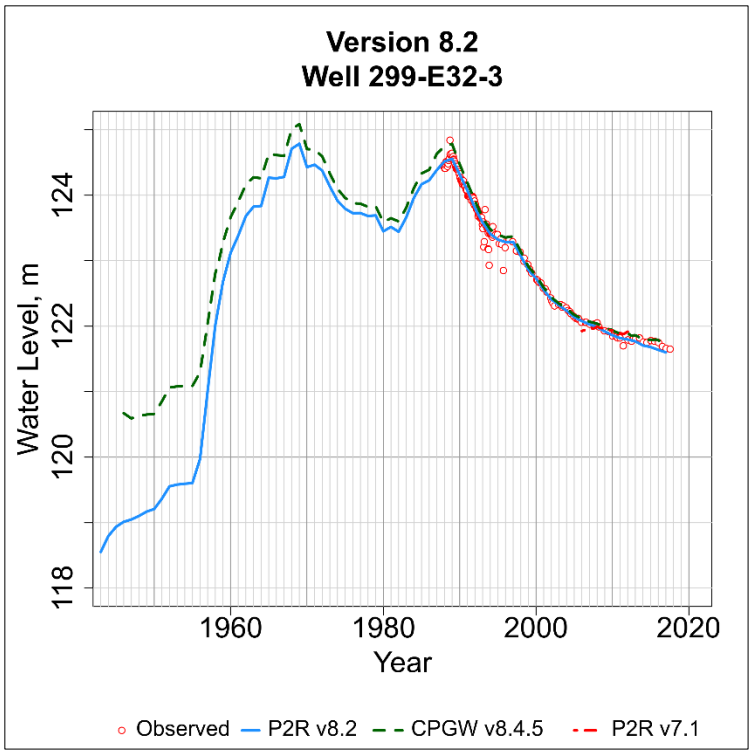

Figure D-83. Observed and simulated water level in the P2R Model at well 299-E32-3.png.

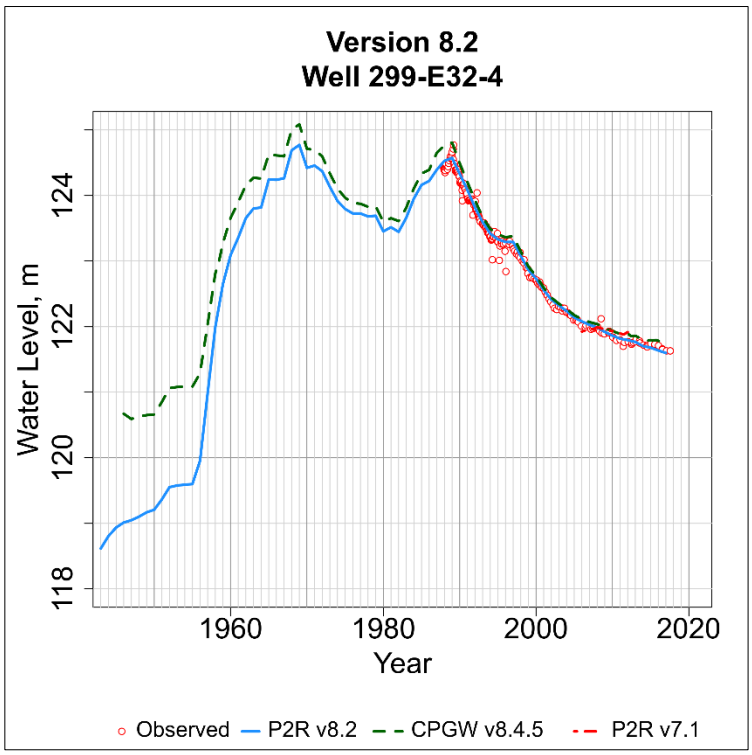

Figure D-84. Observed and simulated water level in the P2R Model at well 299-E32-4.png.

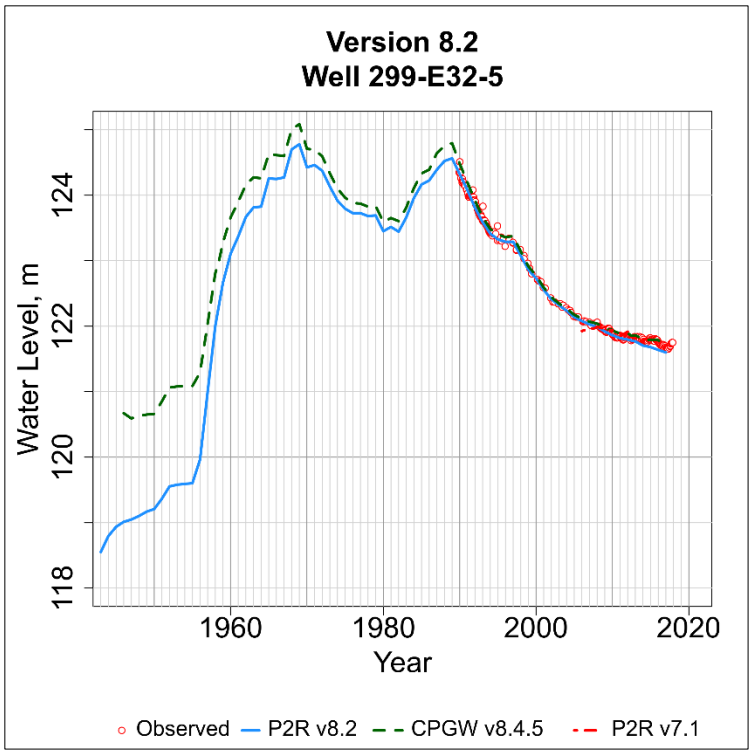

Figure D-85. Observed and simulated water level in the P2R Model at well 299-E32-5.png.

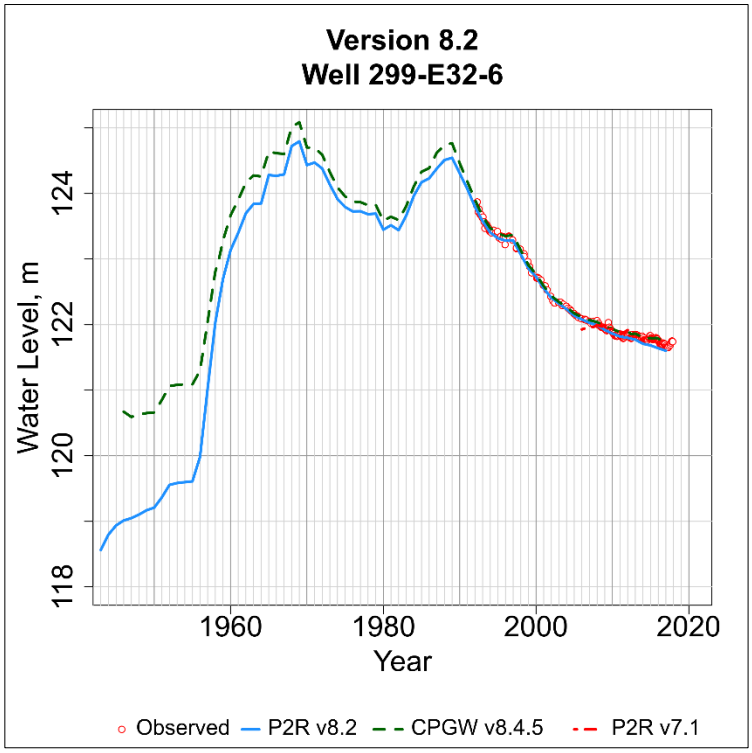

Figure D-86. Observed and simulated water level in the P2R Model at well 299-E32-6.png.

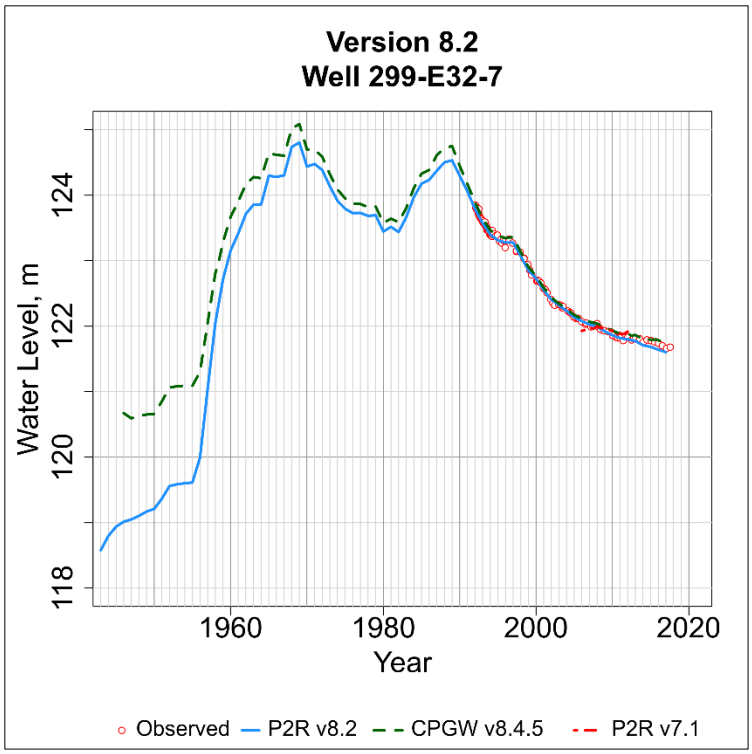

Figure D-87. Observed and simulated water level in the P2R Model at well 299-E32-7.png.

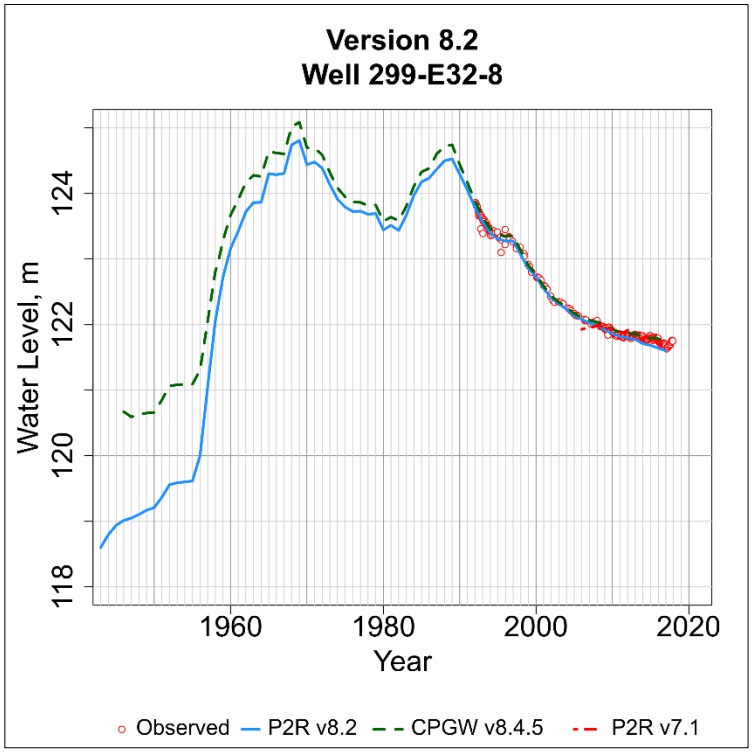

Figure D-88. Observed and simulated water level in the P2R Model at well 299-E32-8.png.

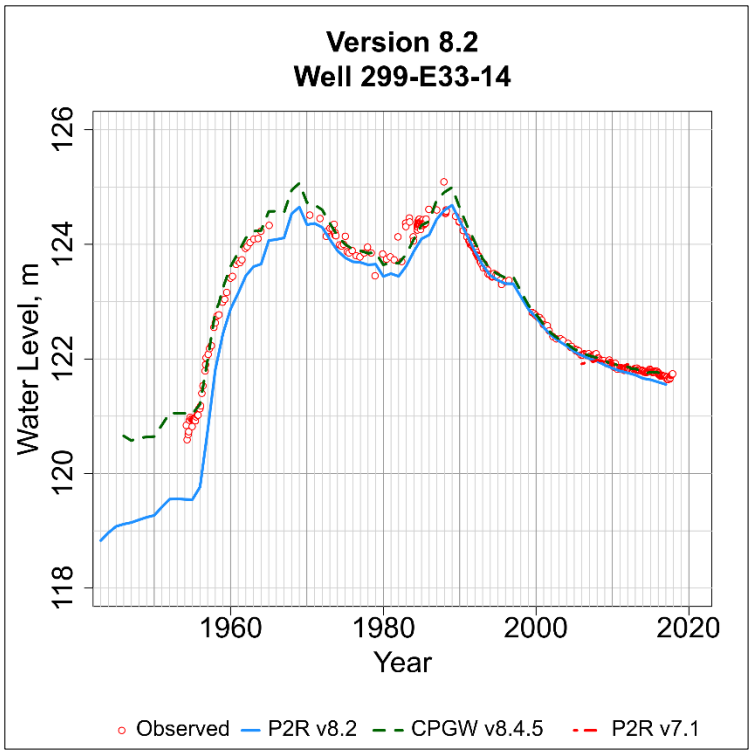

Figure D-89. Observed and simulated water level in the P2R Model at well 299-E33-14.png.

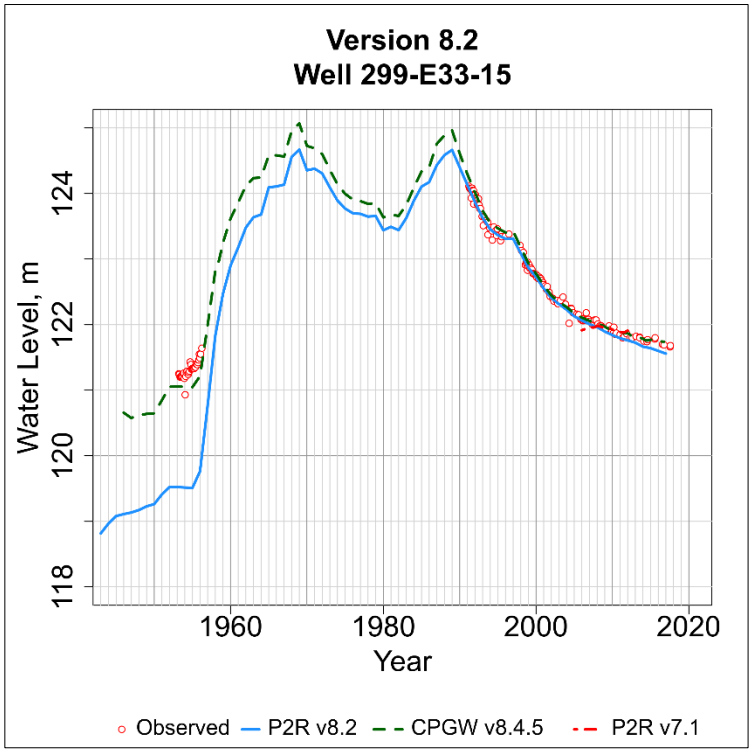

Figure D-90. Observed and simulated water level in the P2R Model at well 299-E33-15.png.

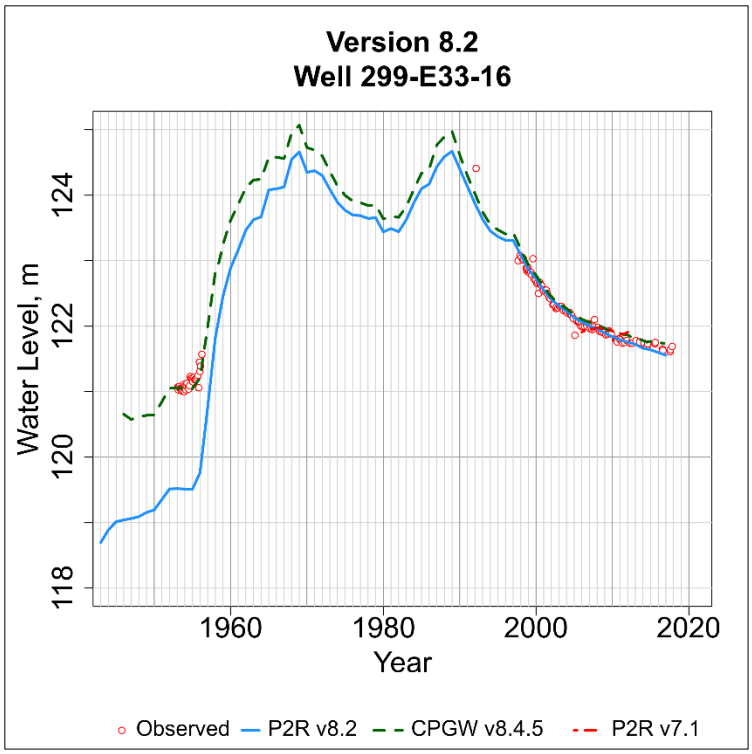

Figure D-91. Observed and simulated water level in the P2R Model at well 299-E33-16.png.

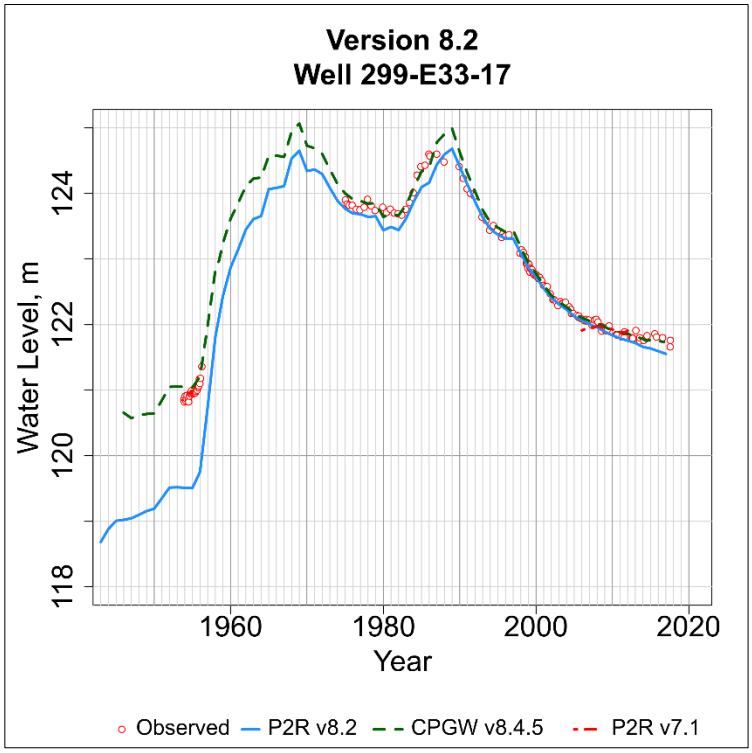

Figure D-92. Observed and simulated water level in the P2R Model at well 299-E33-17.png.

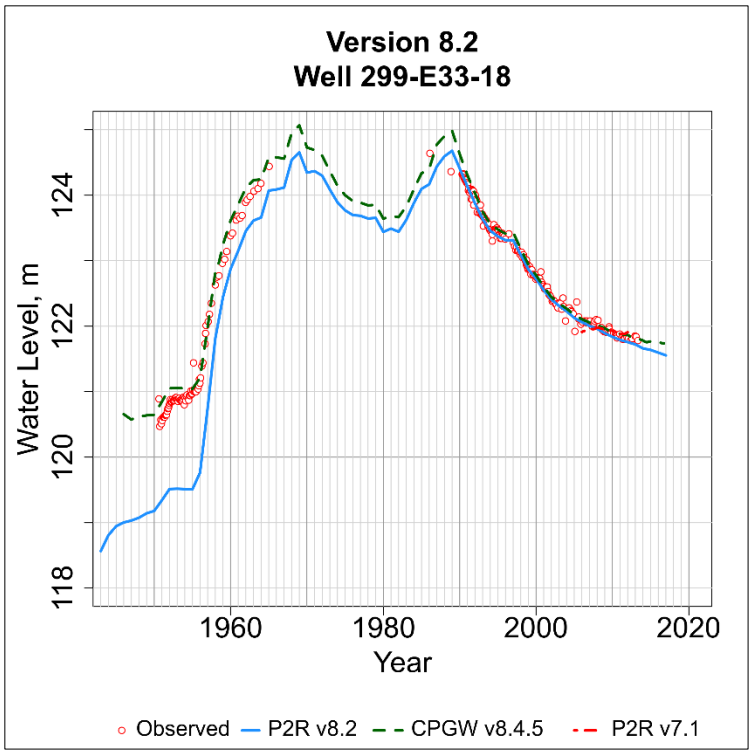

Figure D-93. Observed and simulated water level in the P2R Model at well 299-E33-18.png.

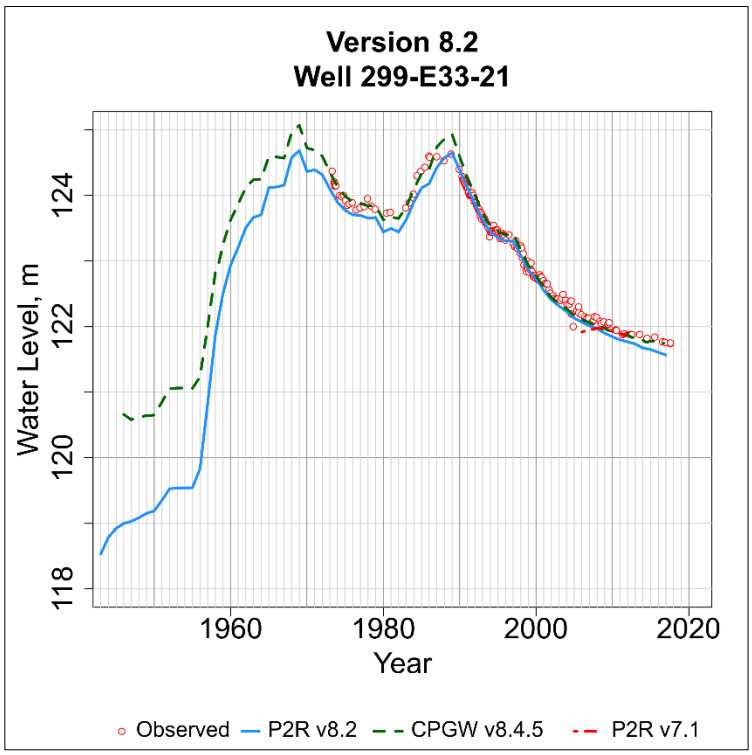

Figure D-94. Observed and simulated water level in the P2R Model at well 299-E33-21.png.

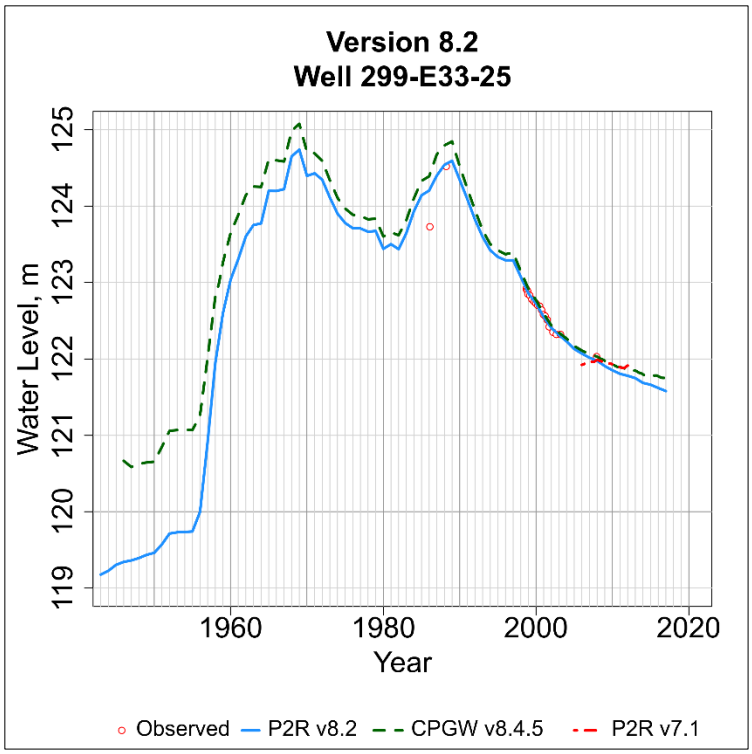

Figure D-95. Observed and simulated water level in the P2R Model at well 299-E33-25.png.

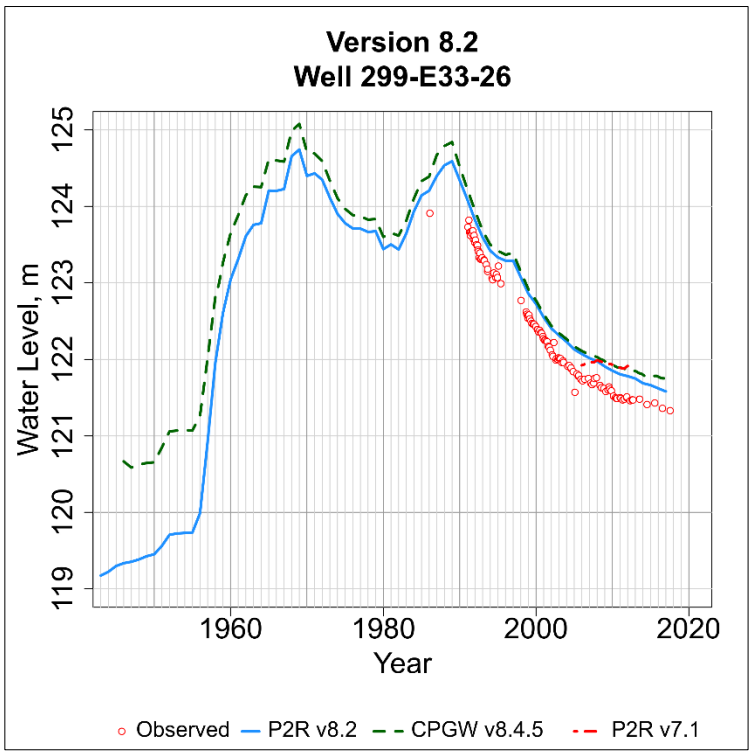

Figure D-96. Observed and simulated water level in the P2R Model at well 299-E33-26.png.

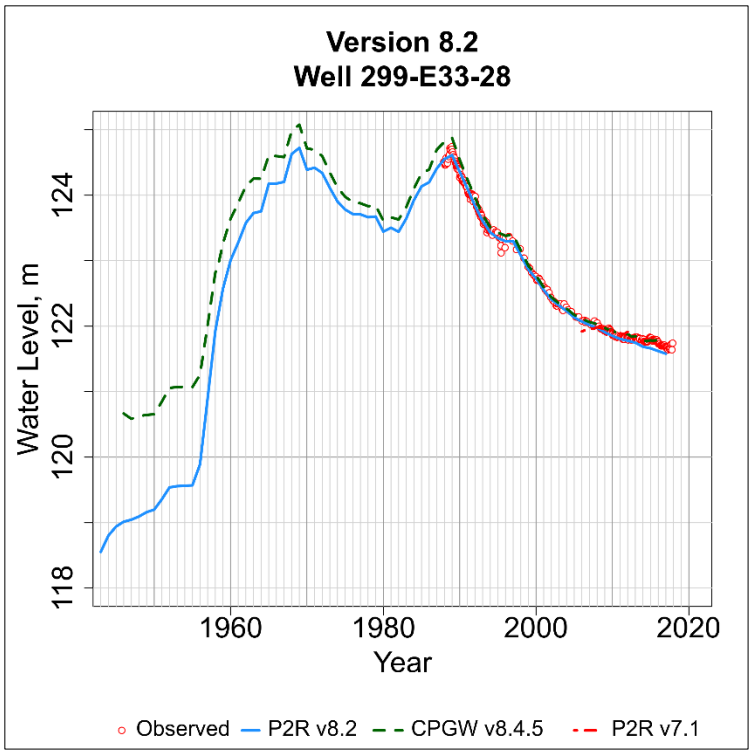

Figure D-97. Observed and simulated water level in the P2R Model at well 299-E33-28.png.

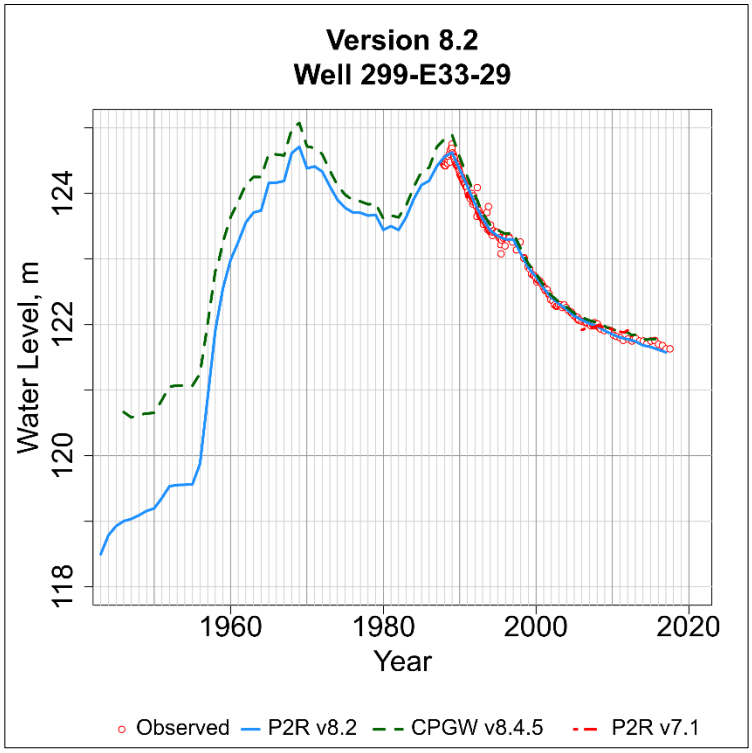

Figure D-98. Observed and simulated water level in the P2R Model at well 299-E33-29.png.

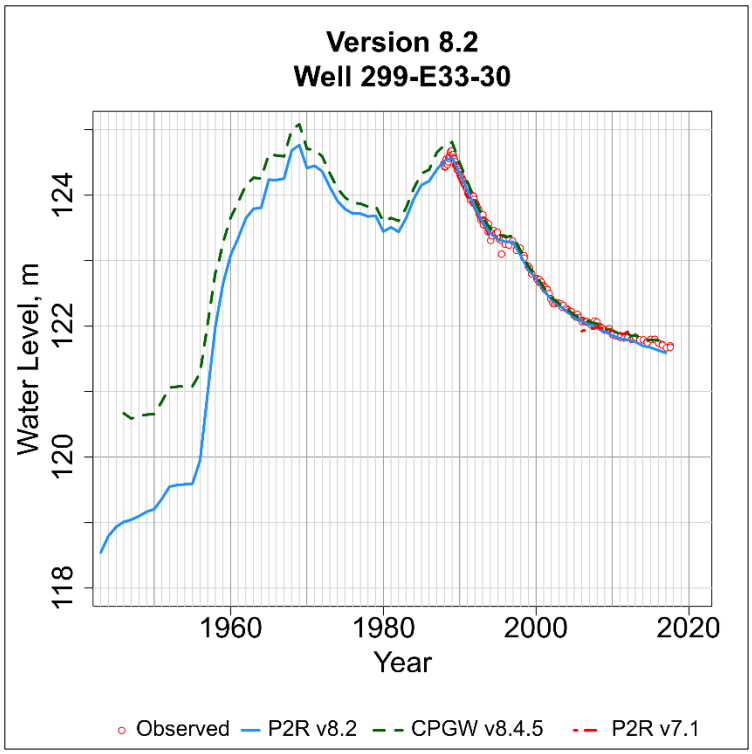

Figure D-99. Observed and simulated water level in the P2R Model at well 299-E33-30.png.

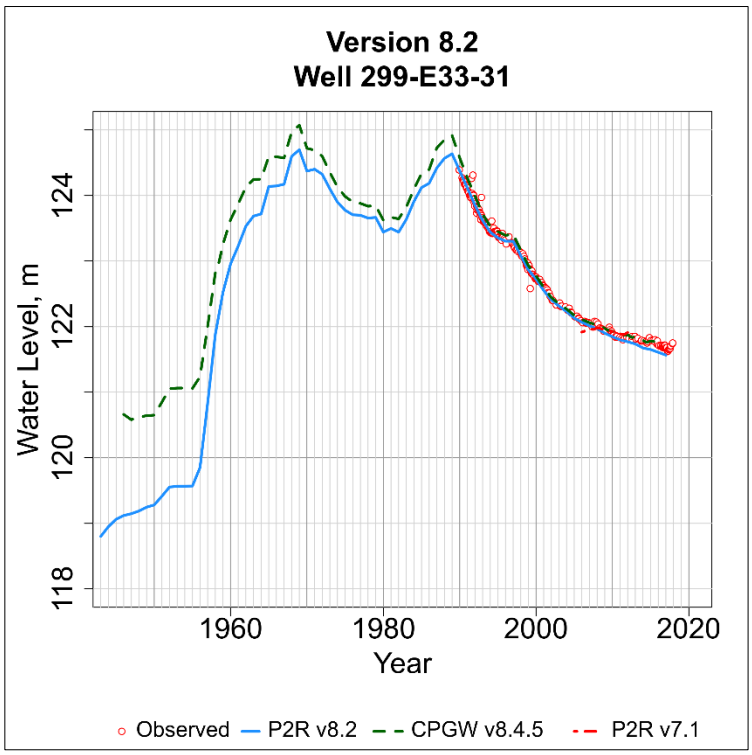

Figure D-100. Observed and simulated water level in the P2R Model at well 299-E33-31.png.

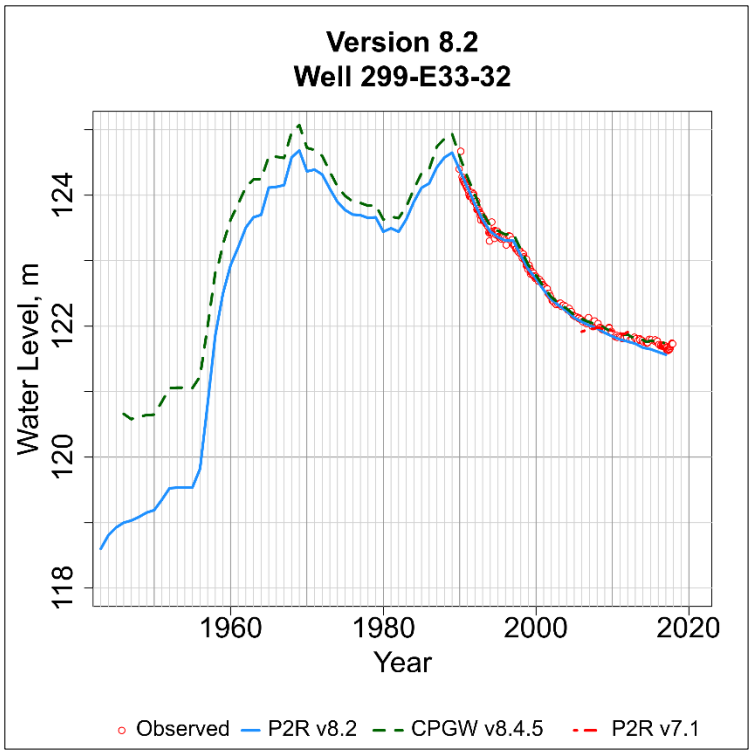

Figure D-101. Observed and simulated water level in the P2R Model at well 299-E33-32.png.

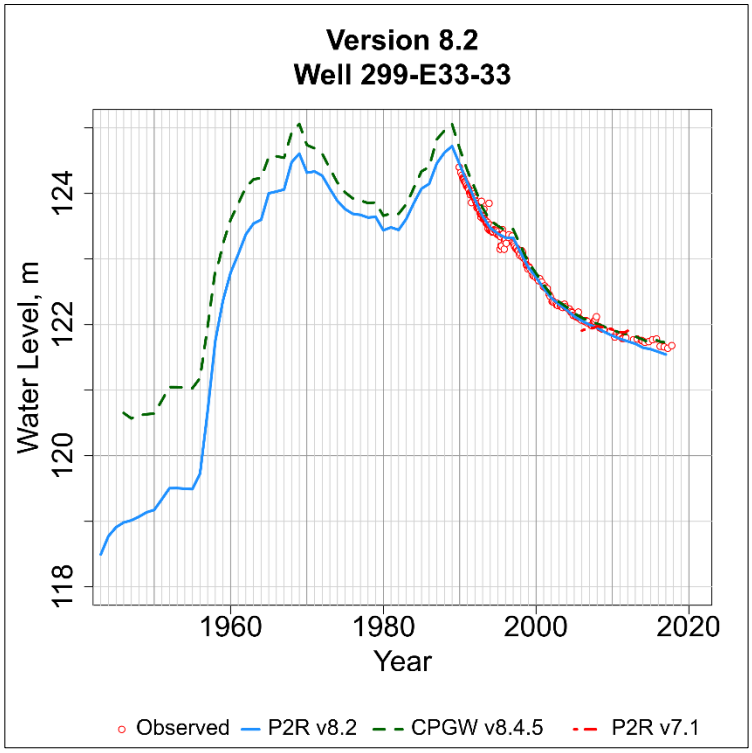

Figure D-102. Observed and simulated water level in the P2R Model at well 299-E33-33.png.

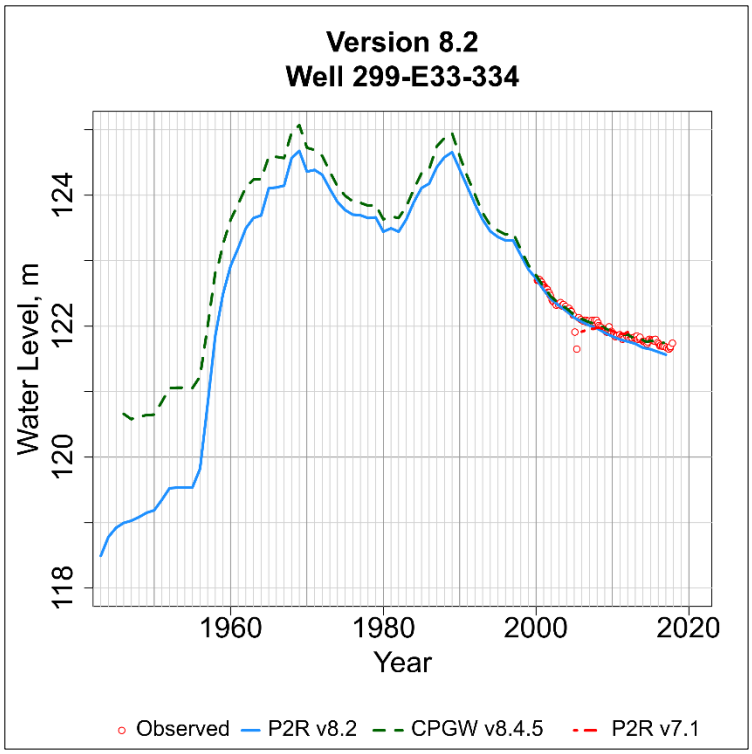

Figure D-103. Observed and simulated water level in the P2R Model at well 299-E33-334.png.

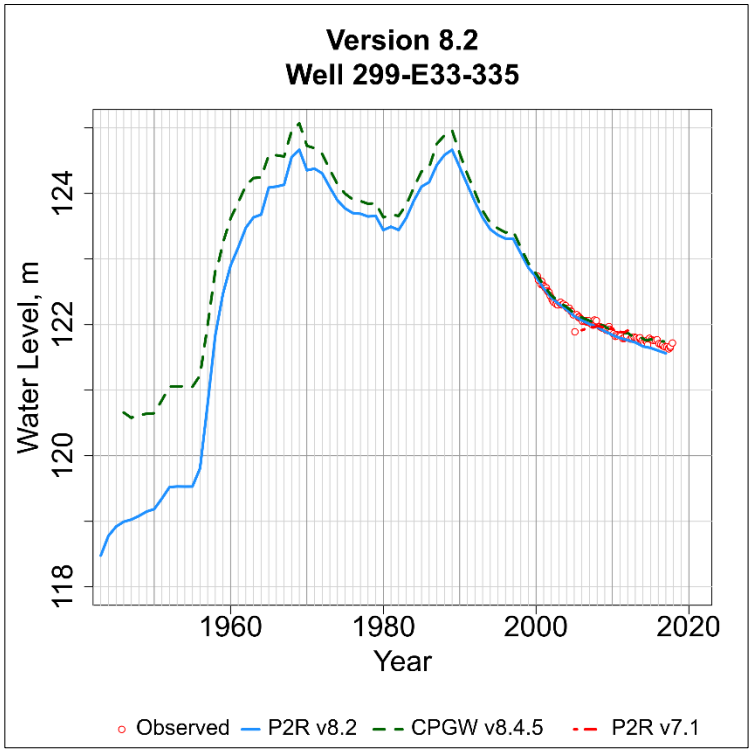

Figure D-104. Observed and simulated water level in the P2R Model at well 299-E33-335.png.

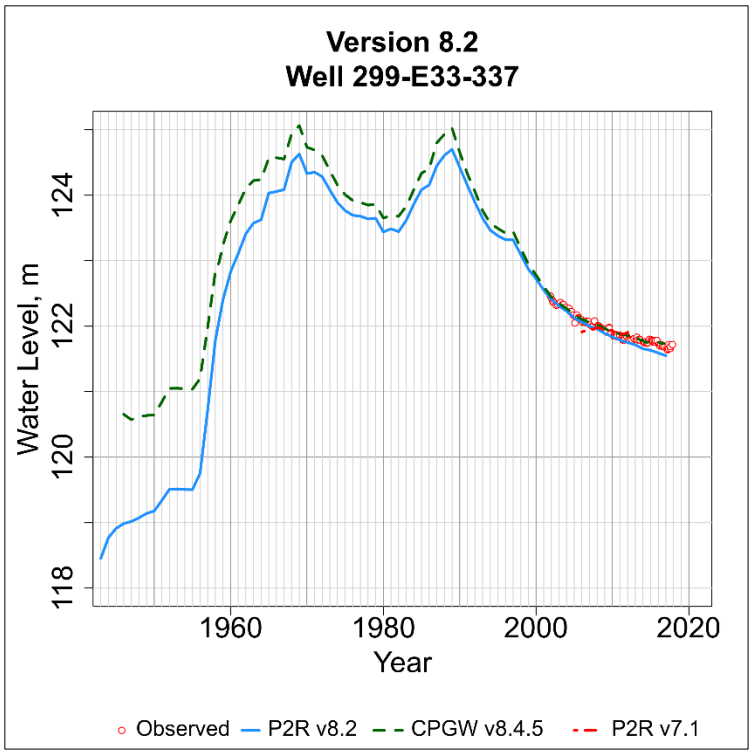

Figure D-105. Observed and simulated water level in the P2R Model at well 299-E33-337.png.

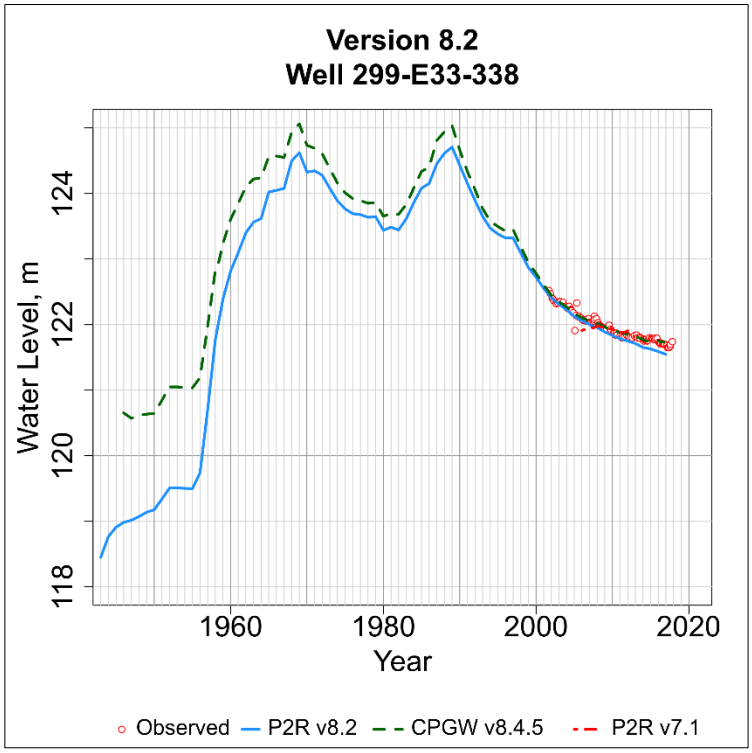

Figure D-106. Observed and simulated water level in the P2R Model at well 299-E33-338.png.

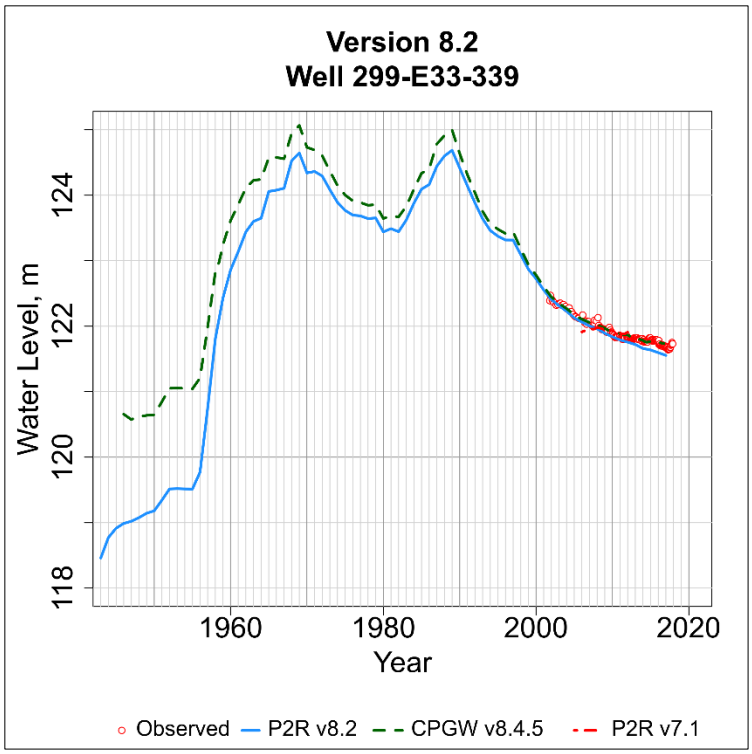

Figure D-107. Observed and simulated water level in the P2R Model at well 299-E33-339.png.

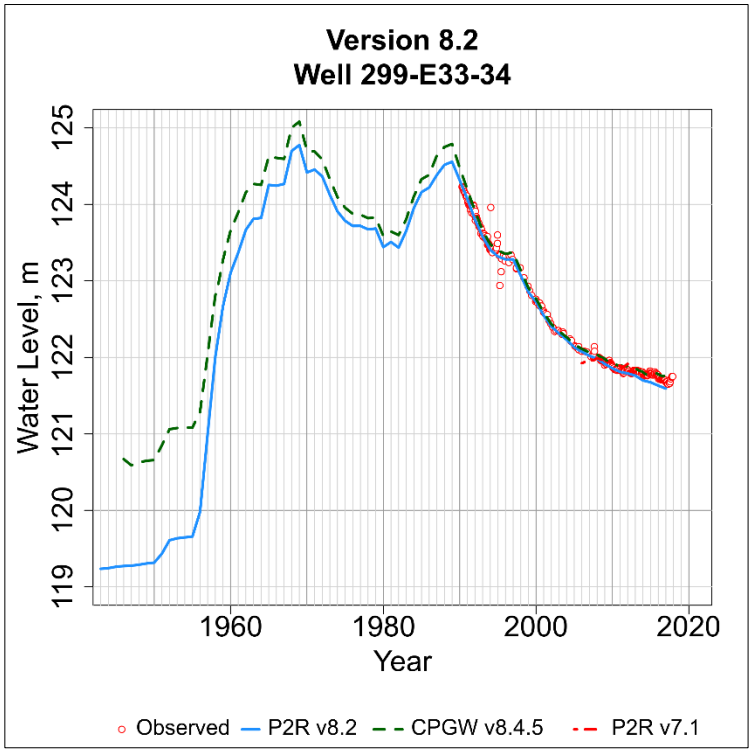

Figure D-108. Observed and simulated water level in the P2R Model at well 299-E33-34.png.

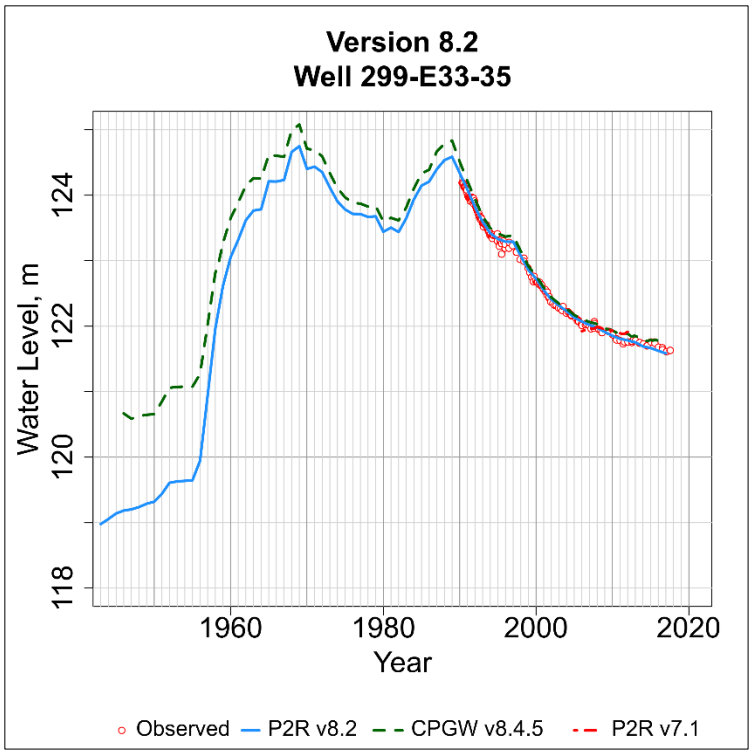

Figure D-109. Observed and simulated water level in the P2R Model at well 299-E33-35.png.

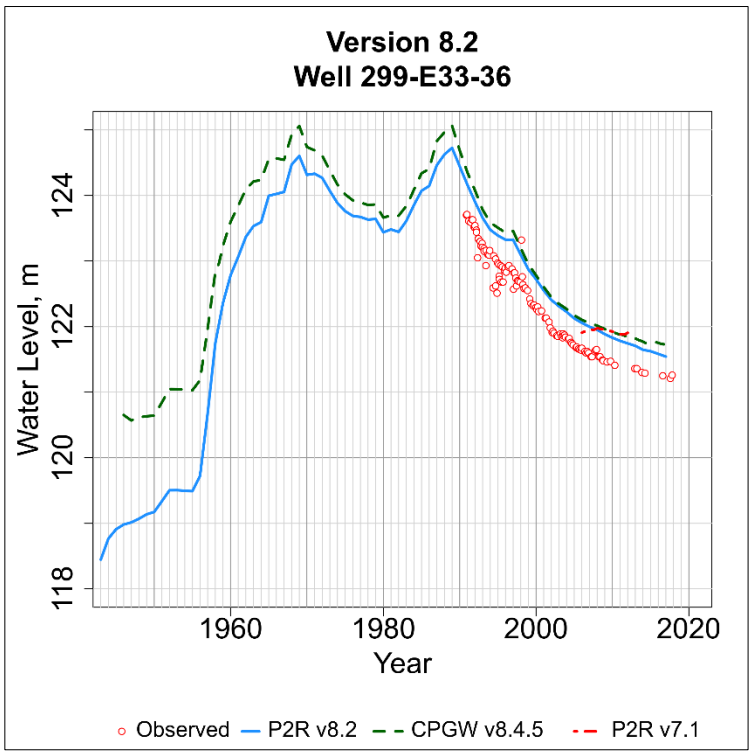

Figure D-110. Observed and simulated water level in the P2R Model at well 299-E33-36.png.

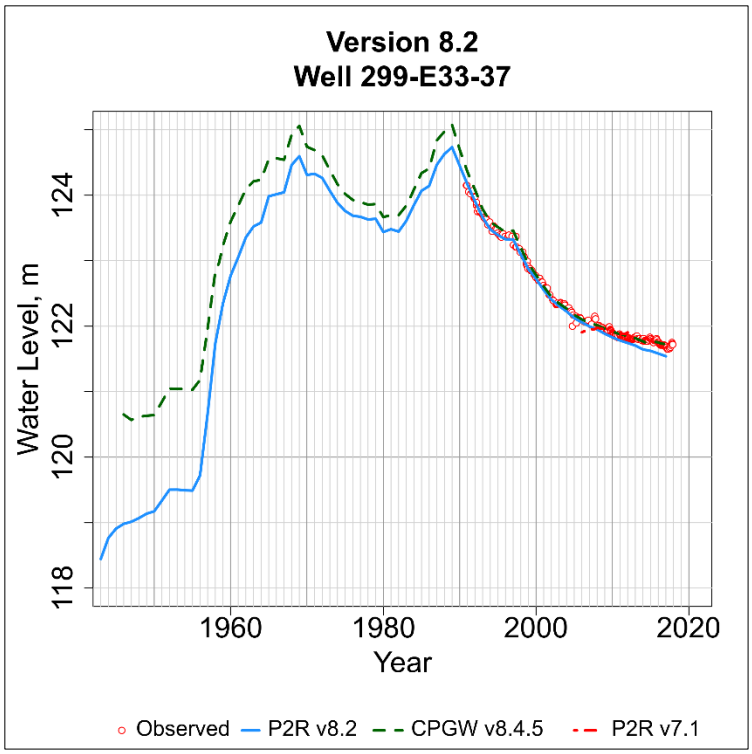

Figure D-111. Observed and simulated water level in the P2R Model at well 299-E33-37.png.

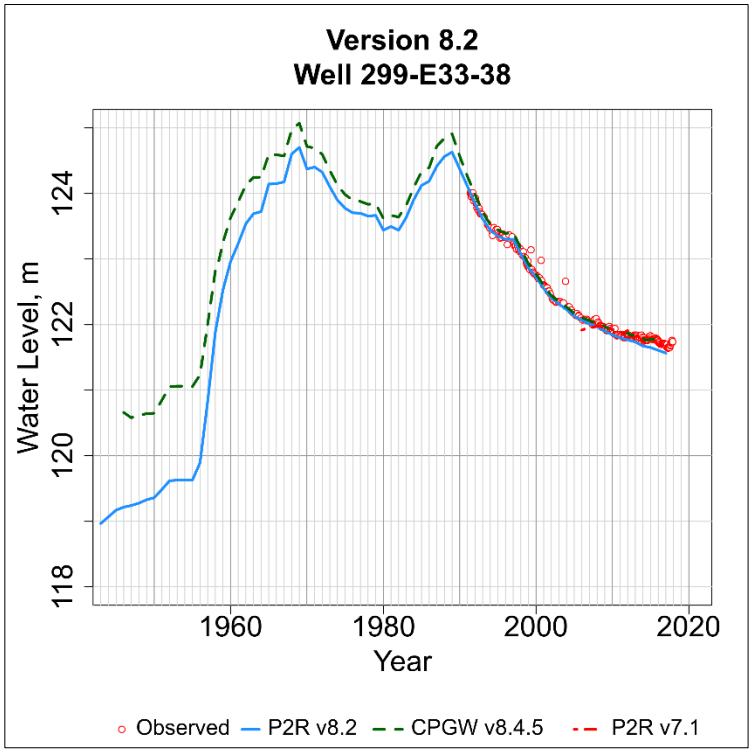

Figure D-112. Observed and simulated water level in the P2R Model at well 299-E33-38.png.

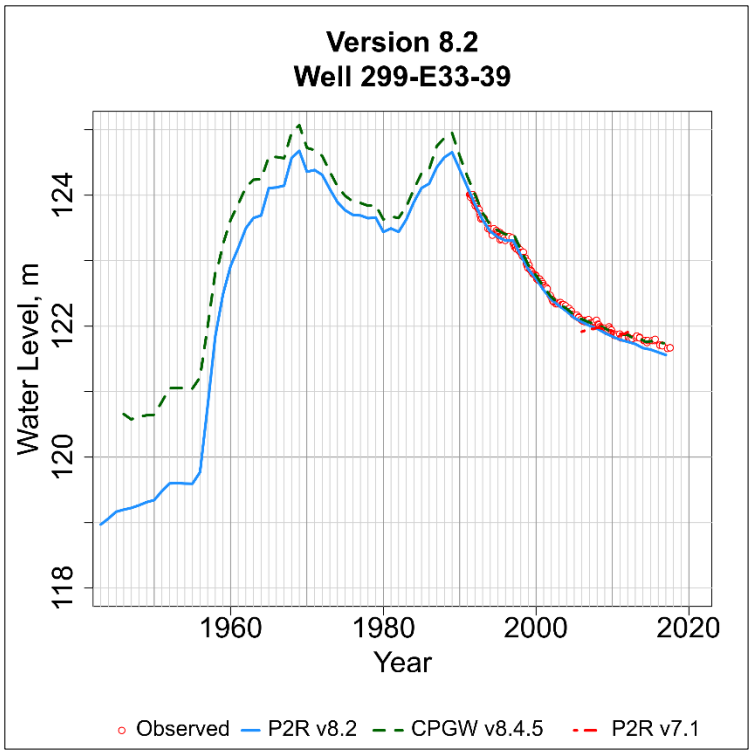

Figure D-113. Observed and simulated water level in the P2R Model at well 299-E33-39.png.

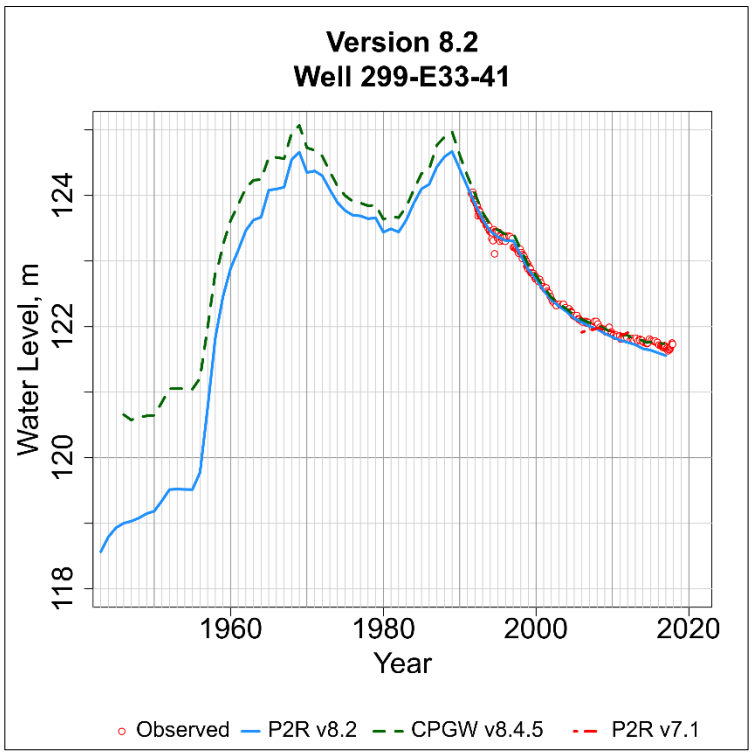

Figure D-114. Observed and simulated water level in the P2R Model at well 299-E33-41.png.

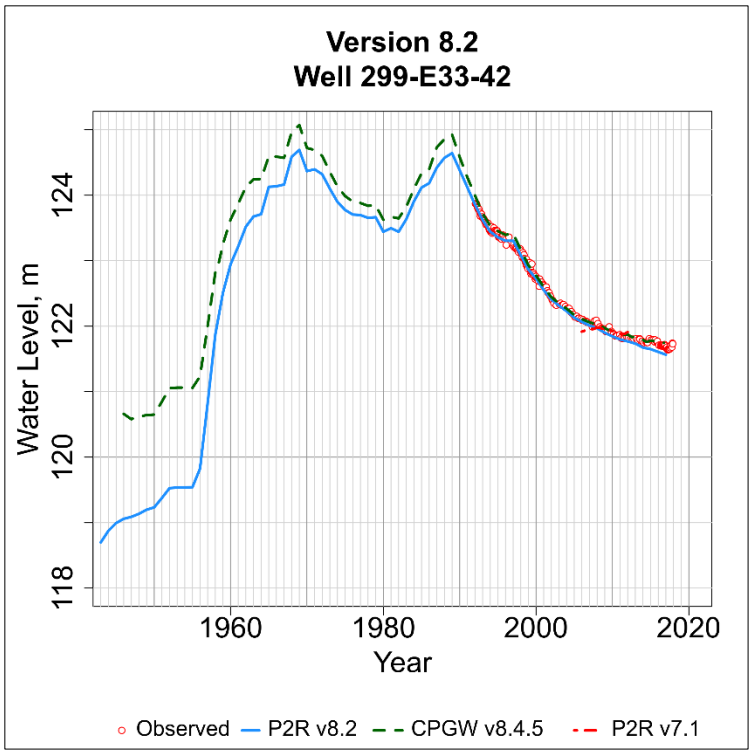

Figure D-115. Observed and simulated water level in the P2R Model at well 299-E33-42.png.

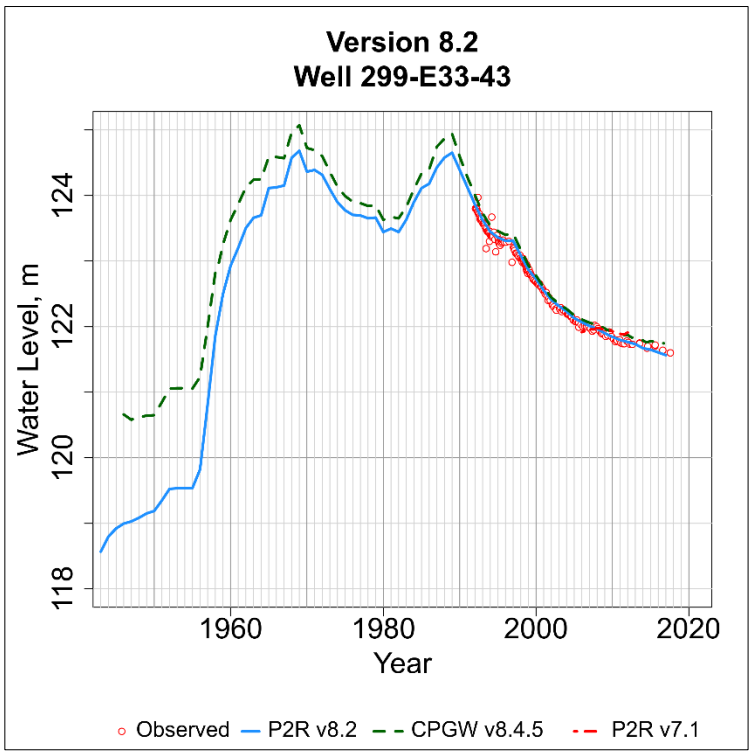

Figure D-116. Observed and simulated water level in the P2R Model at well 299-E33-43.png.

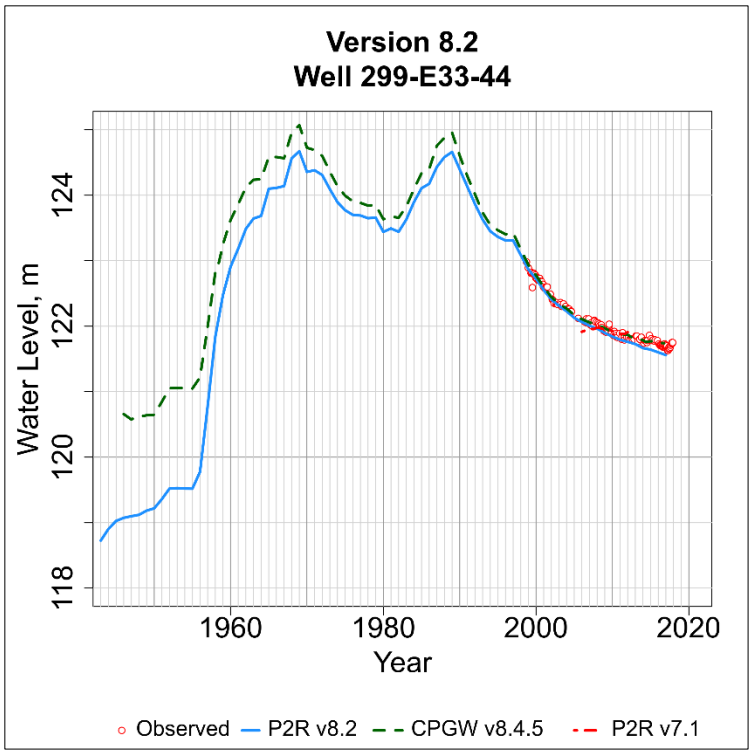

Figure D-117. Observed and simulated water level in the P2R Model at well 299-E33-44.png.

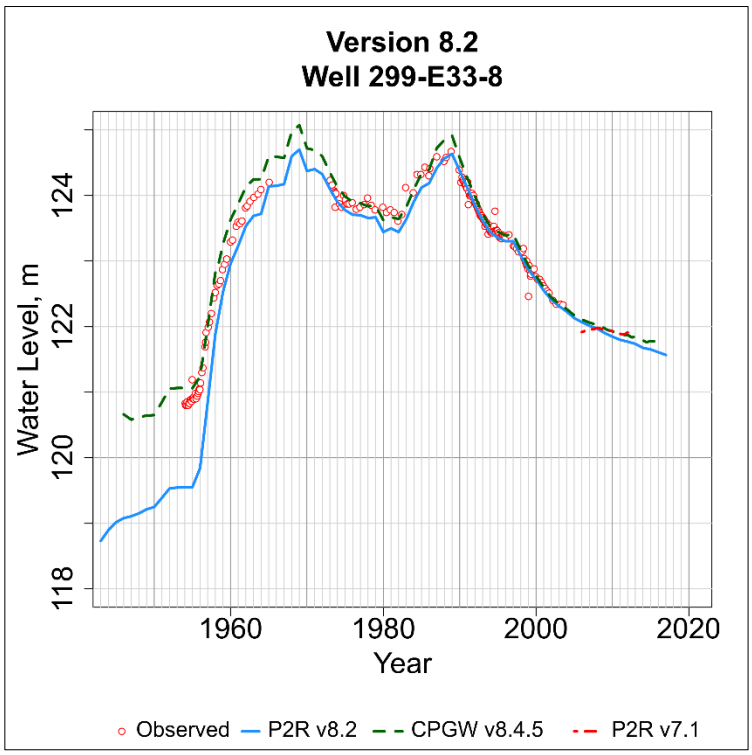

Figure D-118. Observed and simulated water level in the P2R Model at well 299-E33-8.png.

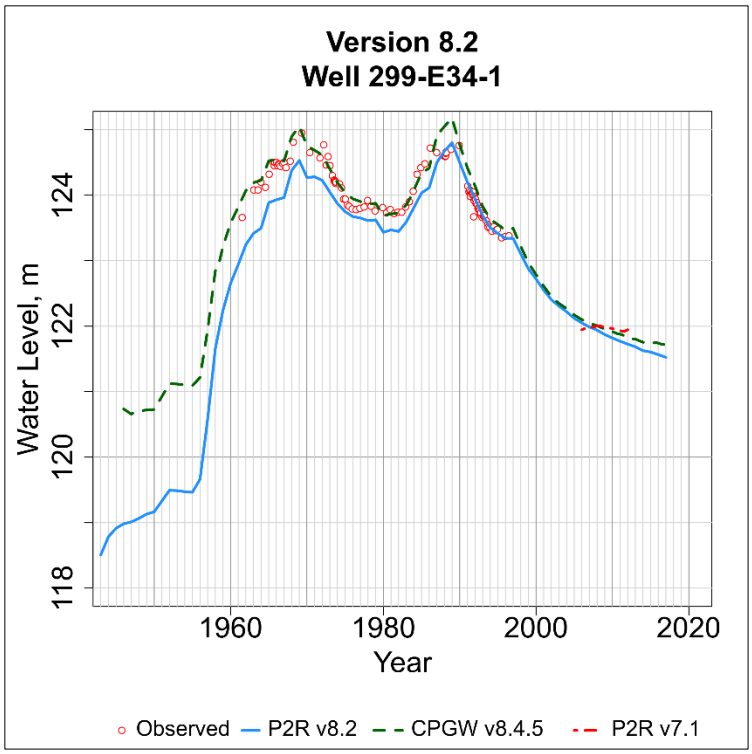

Figure D-119. Observed and simulated water level in the P2R Model at well 299-E34-1.png.

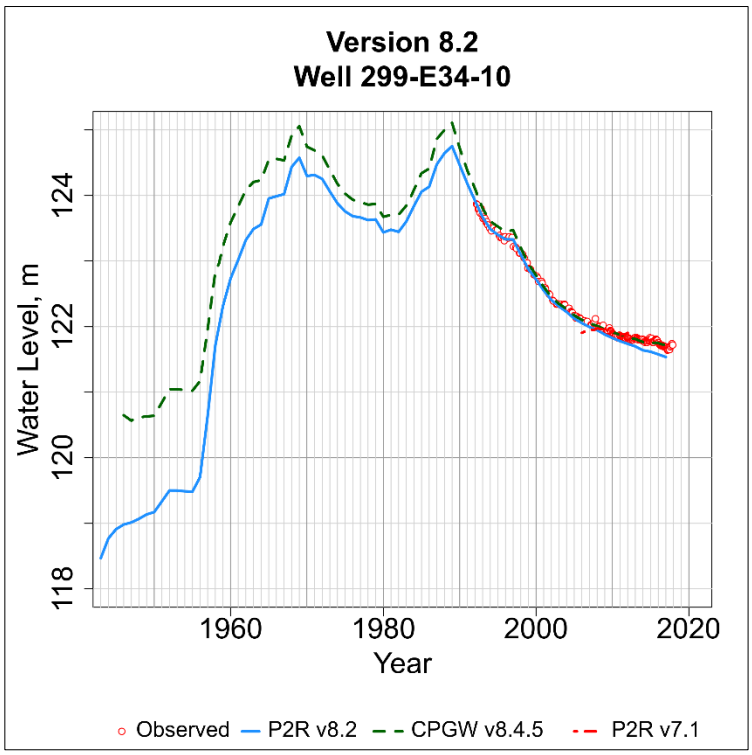

Figure D-120. Observed and simulated water level in the P2R Model at well 299-E34-10.png.

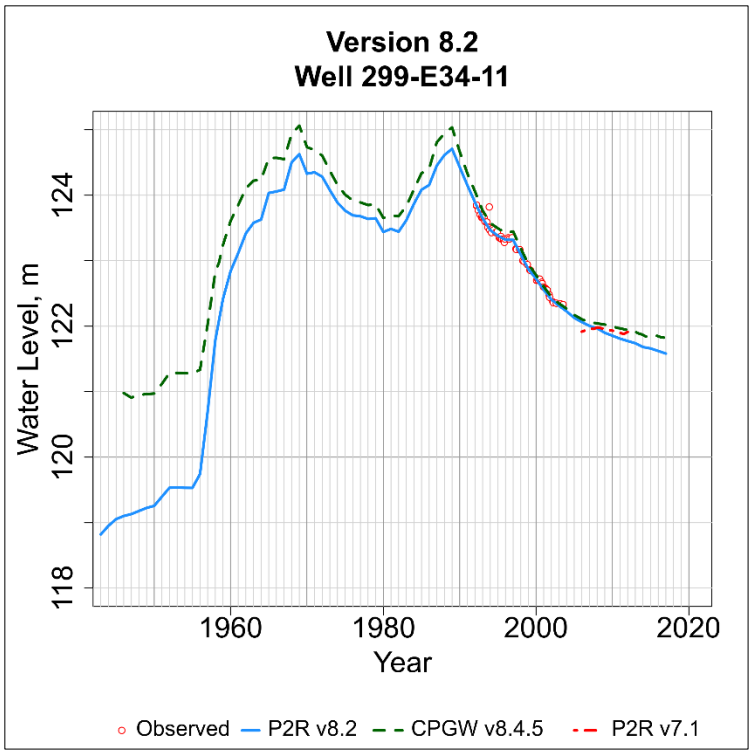

Figure D-121. Observed and simulated water level in the P2R Model at well 299-E34-11.png.

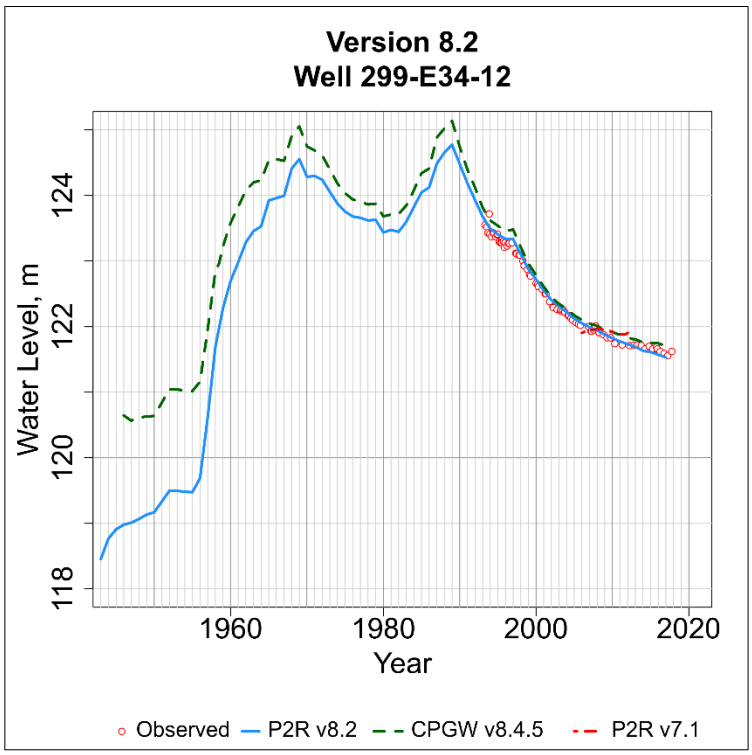

Figure D-122. Observed and simulated water level in the P2R Model at well 299-E34-12.png.

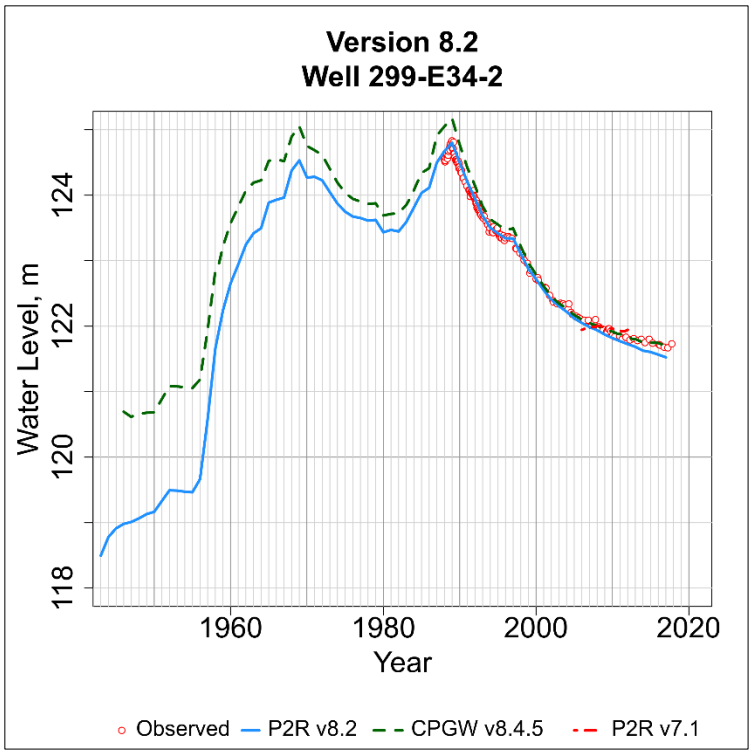

Figure D-123. Observed and simulated water level in the P2R Model at well 299-E34-2.png.

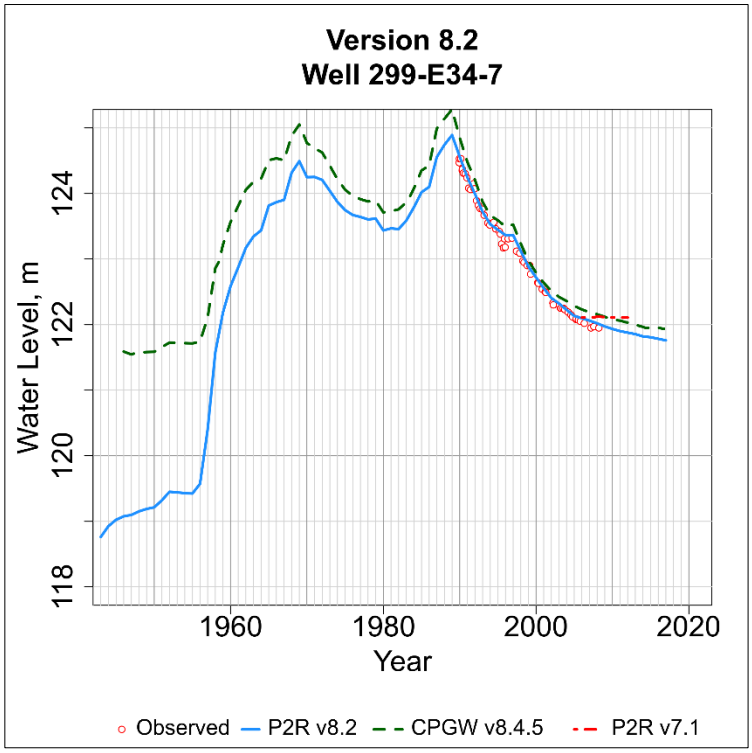

Figure D-124. Observed and simulated water level in the P2R Model at well 299-E34-7.png.

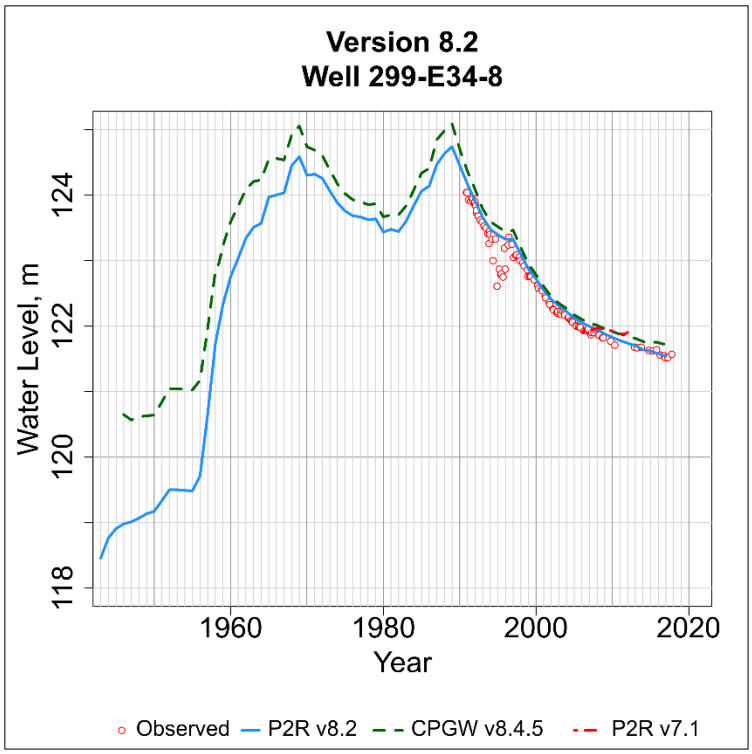

Figure D-125. Observed and simulated water level in the P2R Model at well 299-E34-8.png.

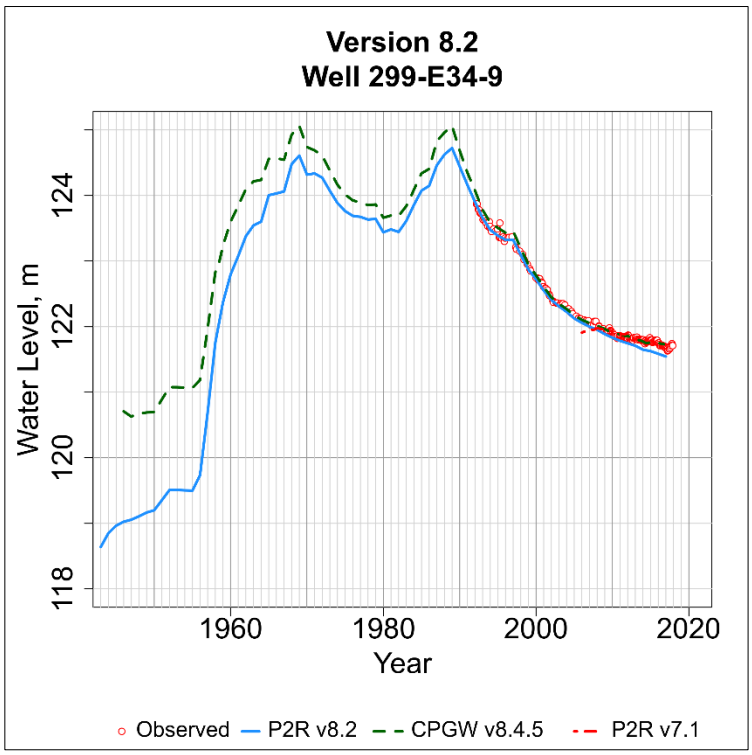

Figure D-126. Observed and simulated water level in the P2R Model at well 299-E34-9.png.

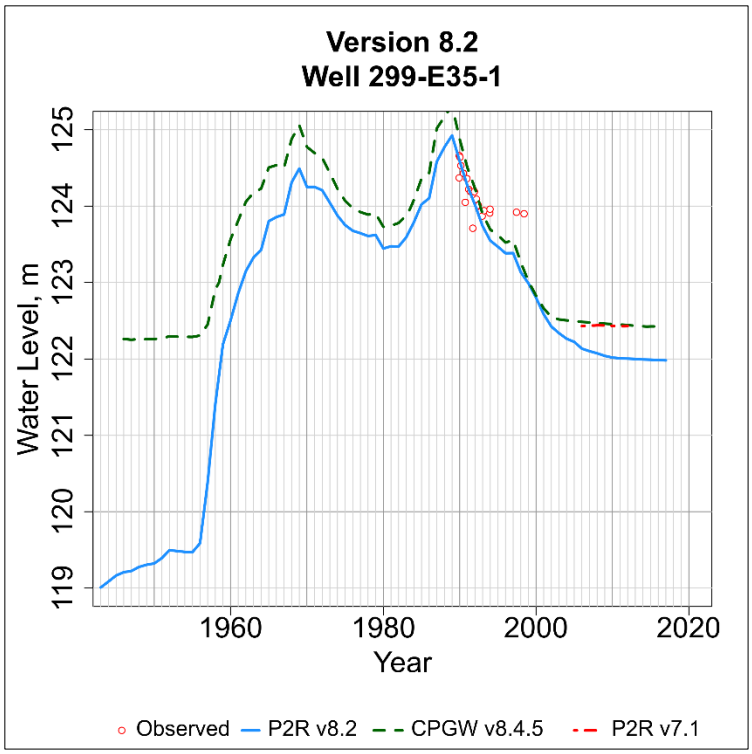

Figure D-127. Observed and simulated water level in the P2R Model at well 299-E35-1.png.

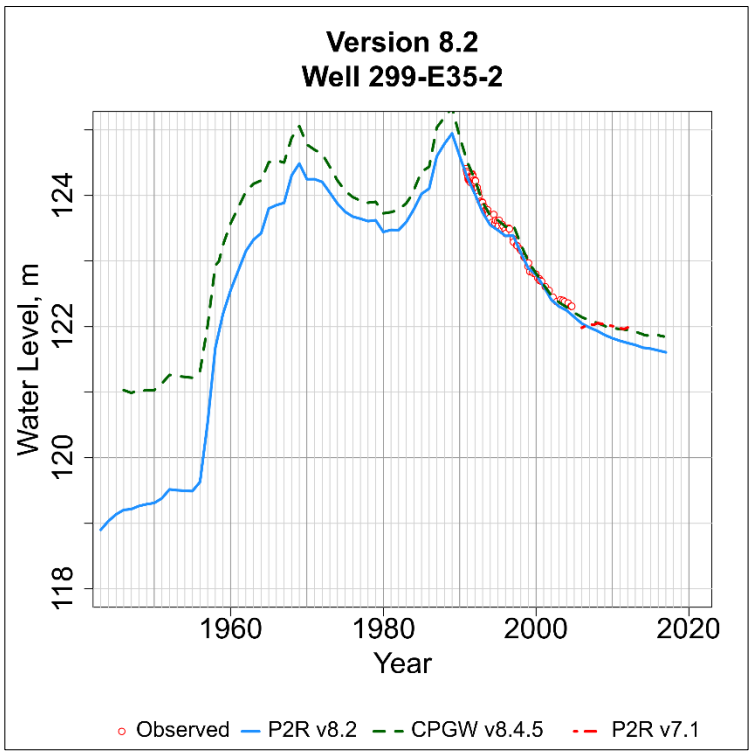

Figure D-128. Observed and simulated water level in the P2R Model at well 299-E35-2.png.

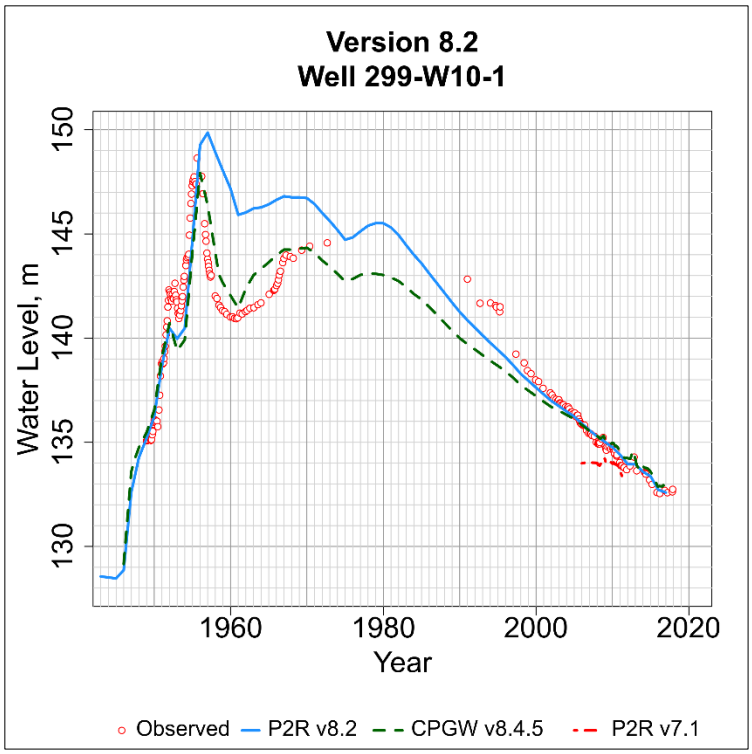

Figure D-129. Observed and simulated water level in the P2R Model at well 299-W10-1.png.

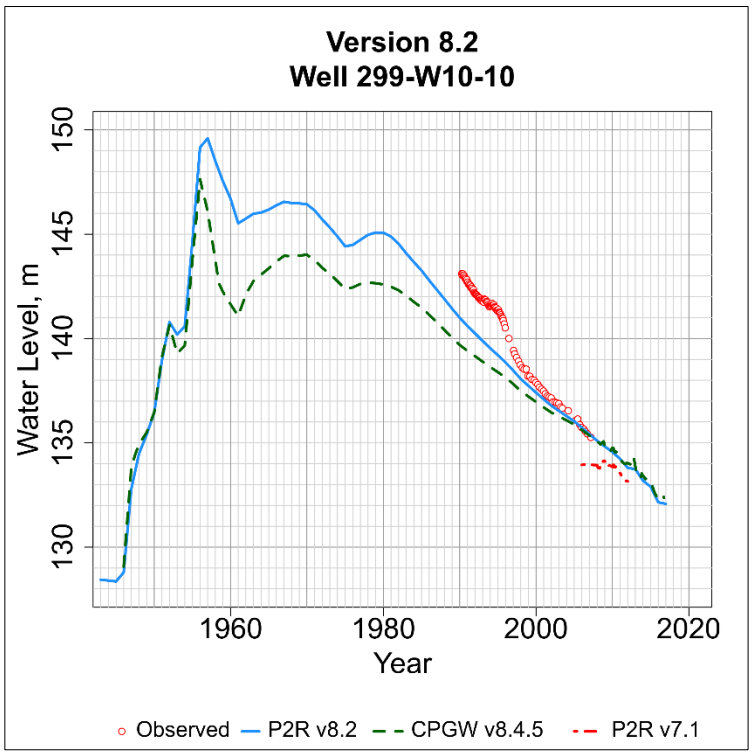

Figure D-130. Observed and simulated water level in the P2R Model at well 299-W10-10.png.

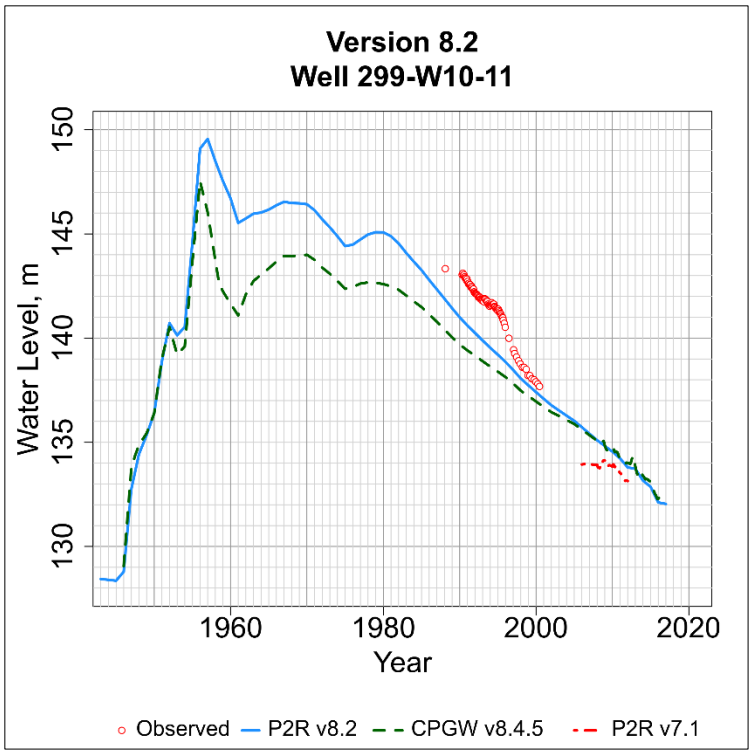

Figure D-131. Observed and simulated water level in the P2R Model at well 299-W10-11.png.

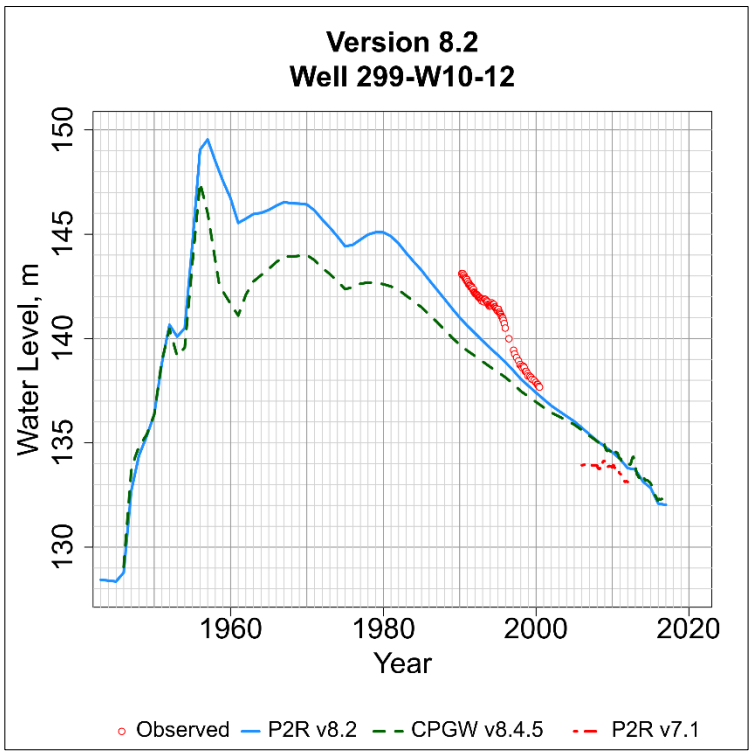

Figure D-132. Observed and simulated water level in the P2R Model at well 299-W10-12.png.

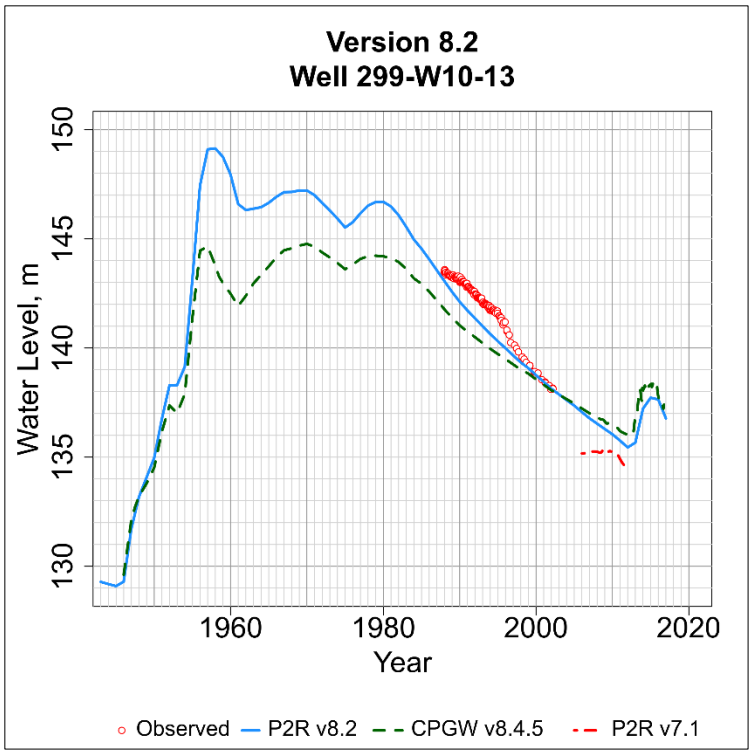

Figure D-133. Observed and simulated water level in the P2R Model at well 299-W10-13.png.

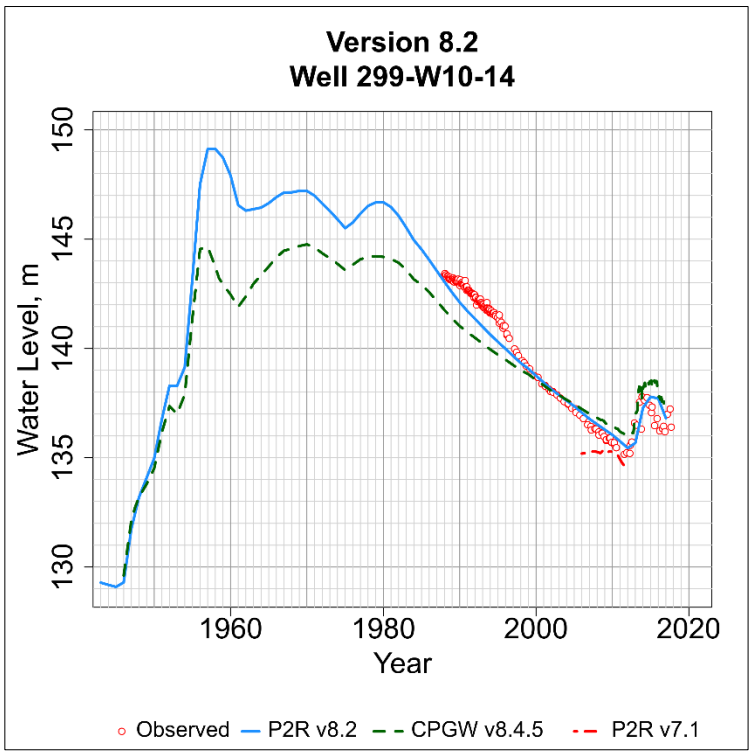

Figure D-134. Observed and simulated water level in the P2R Model at well 299-W10-14.png.

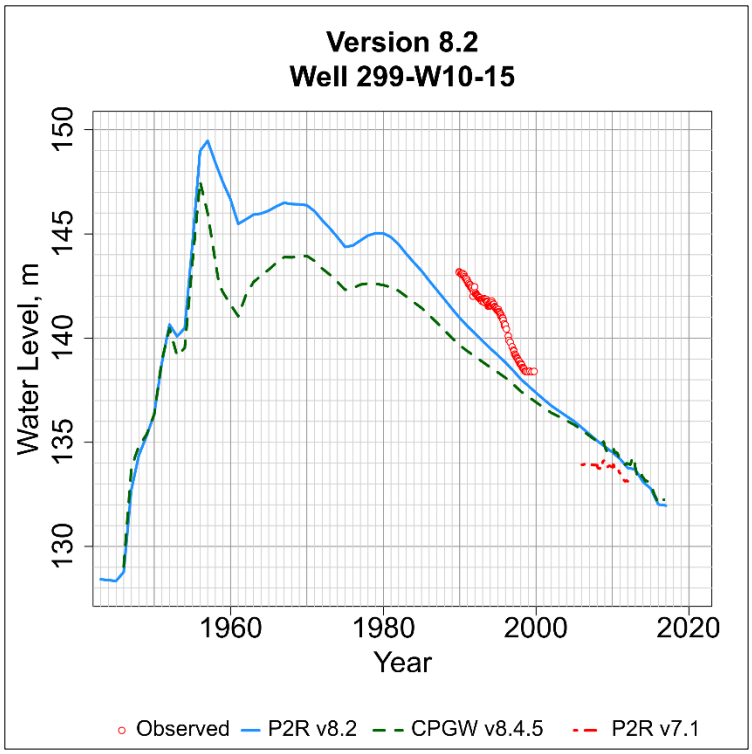

Figure D-135. Observed and simulated water level in the P2R Model at well 299-W10-15.png.

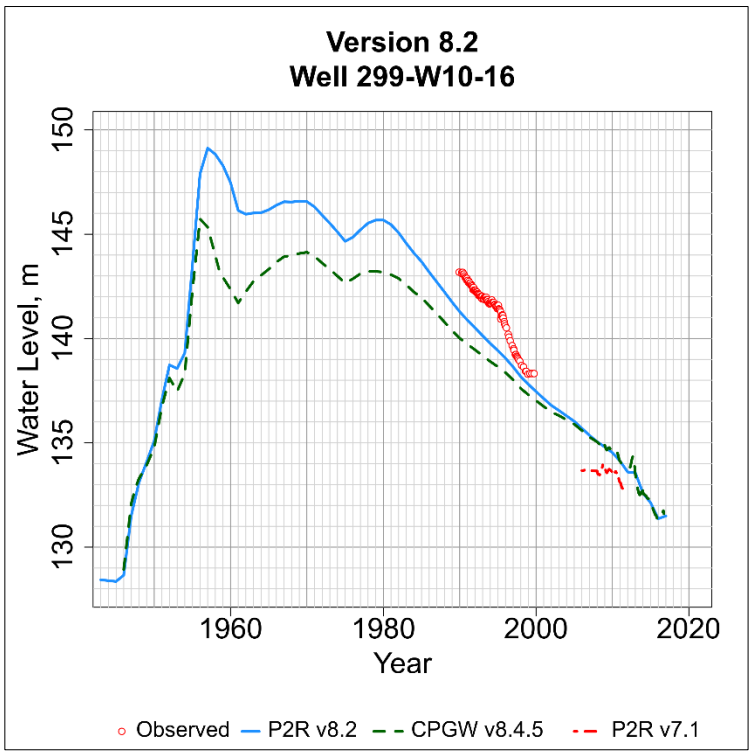

Figure D-136. Observed and simulated water level in the P2R Model at well 299-W10-16.png.

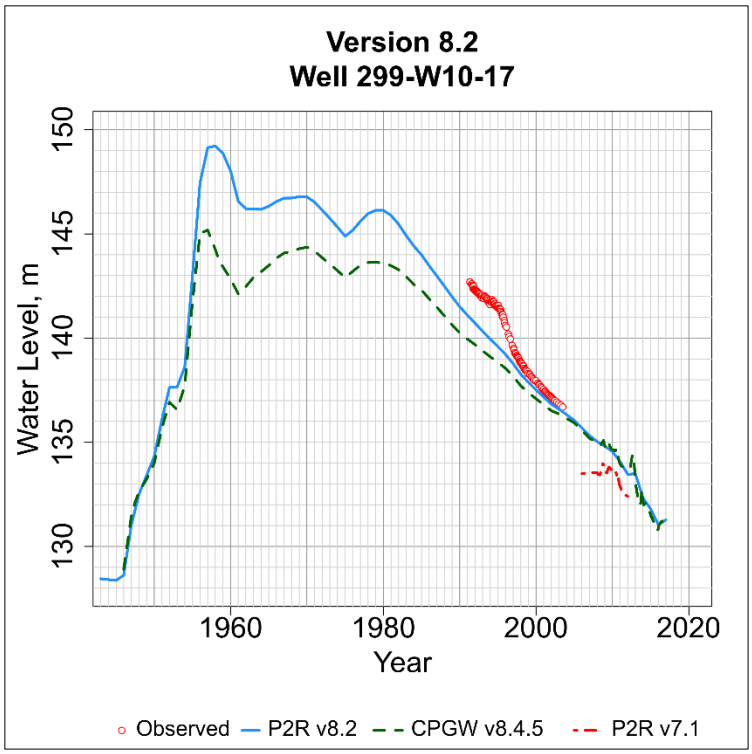

Figure D-137. Observed and simulated water level in the P2R Model at well 299-W10-17.png.

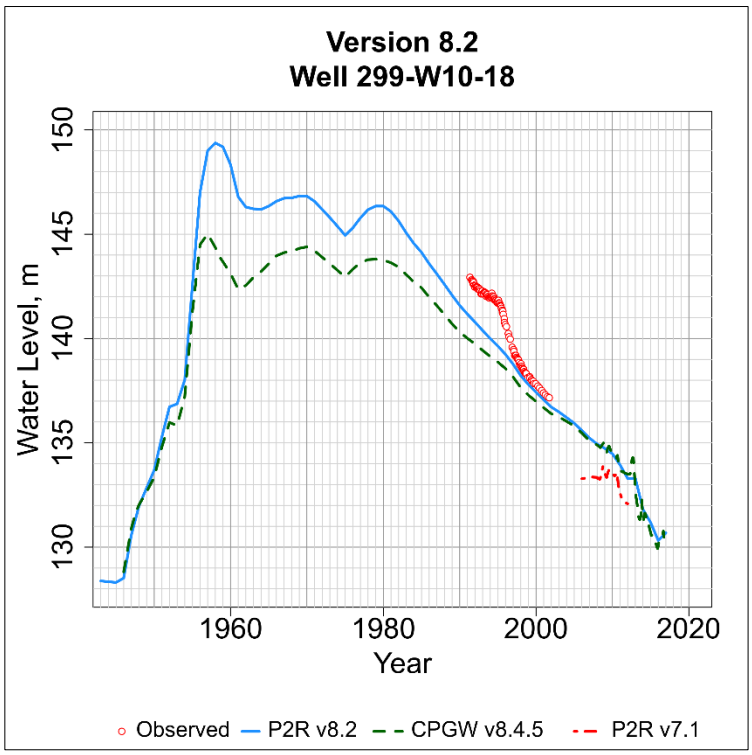

Figure D-138. Observed and simulated water level in the P2R Model at well 299-W10-18.png.

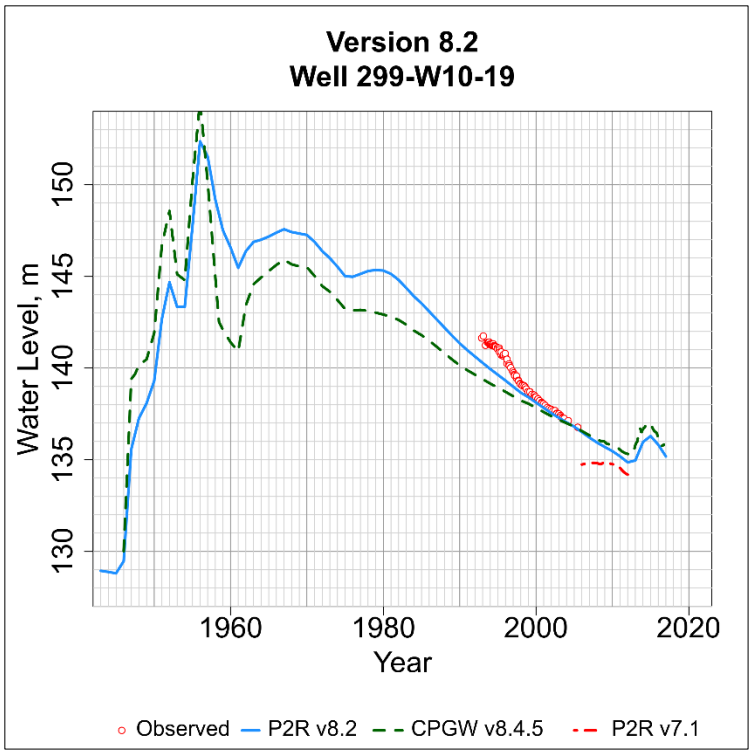

Figure D-139. Observed and simulated water level in the P2R Model at well 299-W10-19.png.

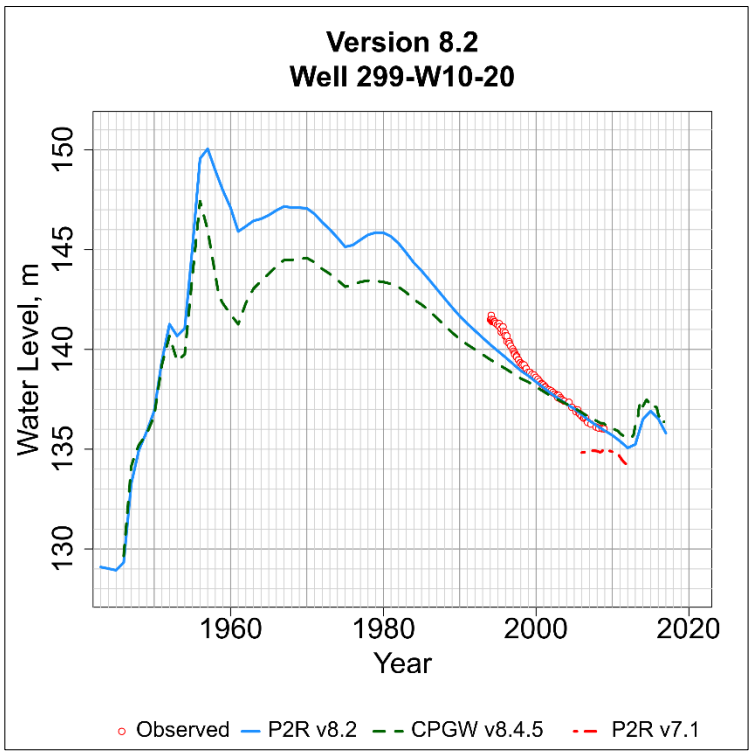

Figure D-140. Observed and simulated water level in the P2R Model at well 299-W10-20.png.

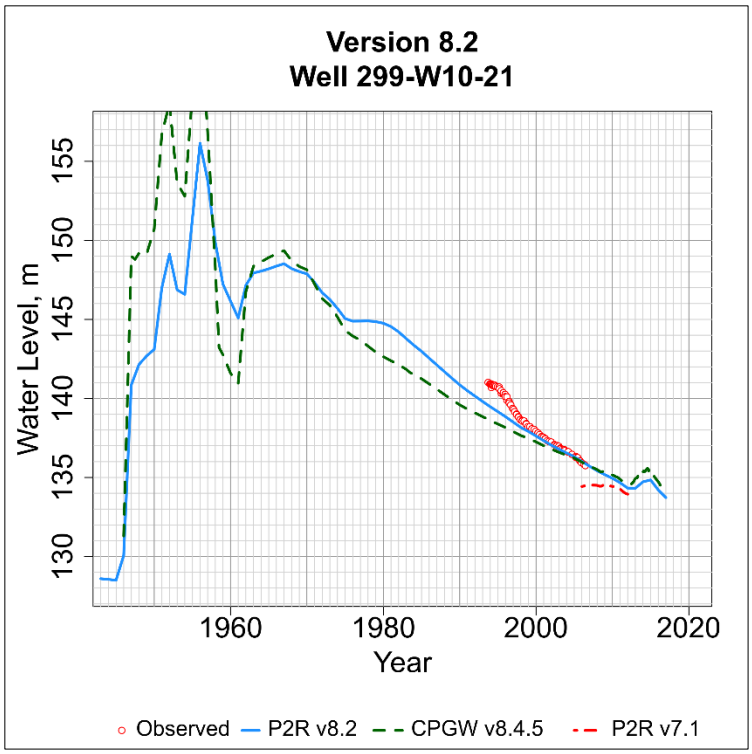

Figure D-141. Observed and simulated water level in the P2R Model at well 299-W10-21.png.

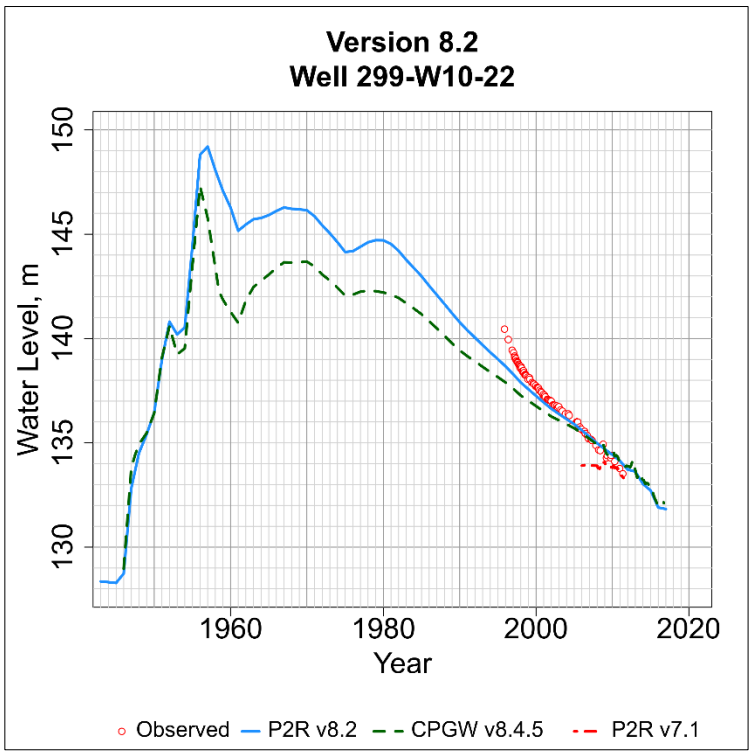

Figure D-142. Observed and simulated water level in the P2R Model at well 299-W10-22.png.

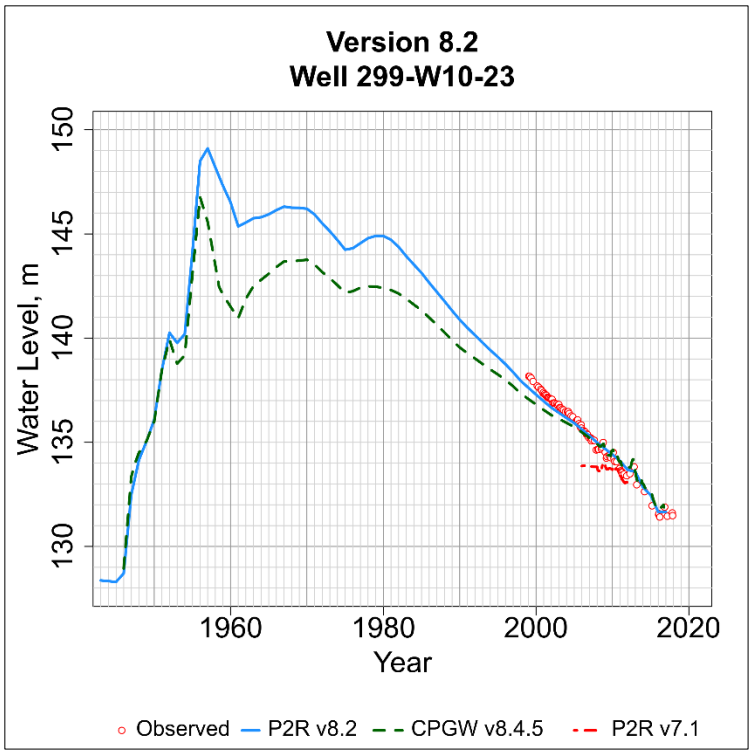

Figure D-143. Observed and simulated water level in the P2R Model at well 299-W10-23.png.

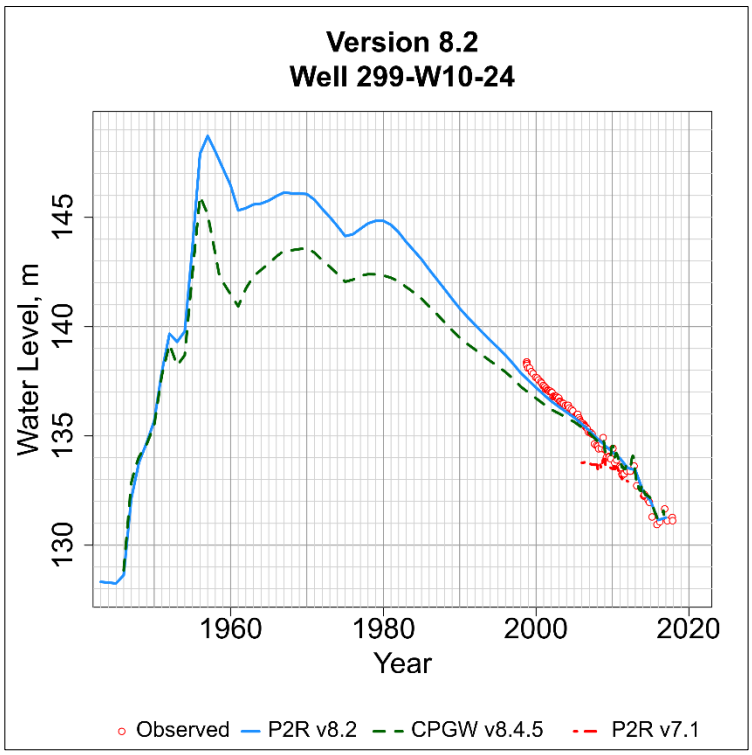

Figure D-144. Observed and simulated water level in the P2R Model at well 299-W10-24.png.

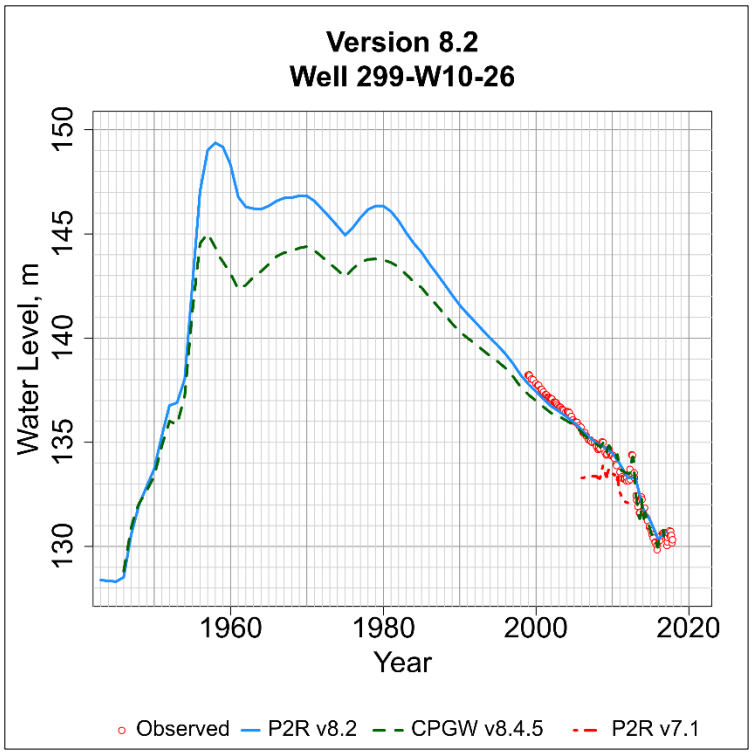

Figure D-145. Observed and simulated water level in the P2R Model at well 299-W10-26.png.

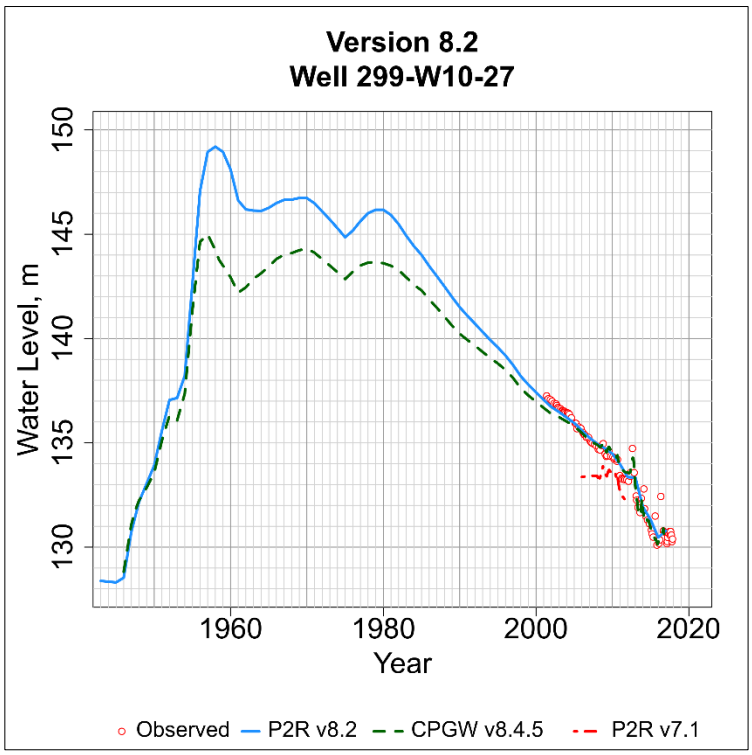

Figure D-146. Observed and simulated water level in the P2R Model at well 299-W10-27.png.

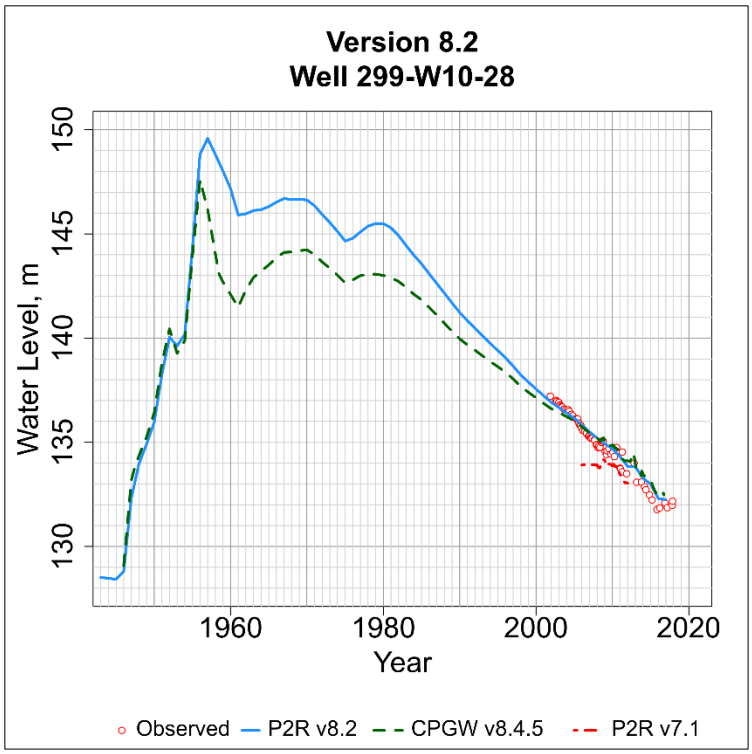

Figure D-147. Observed and simulated water level in the P2R Model at well 299-W10-28.png.

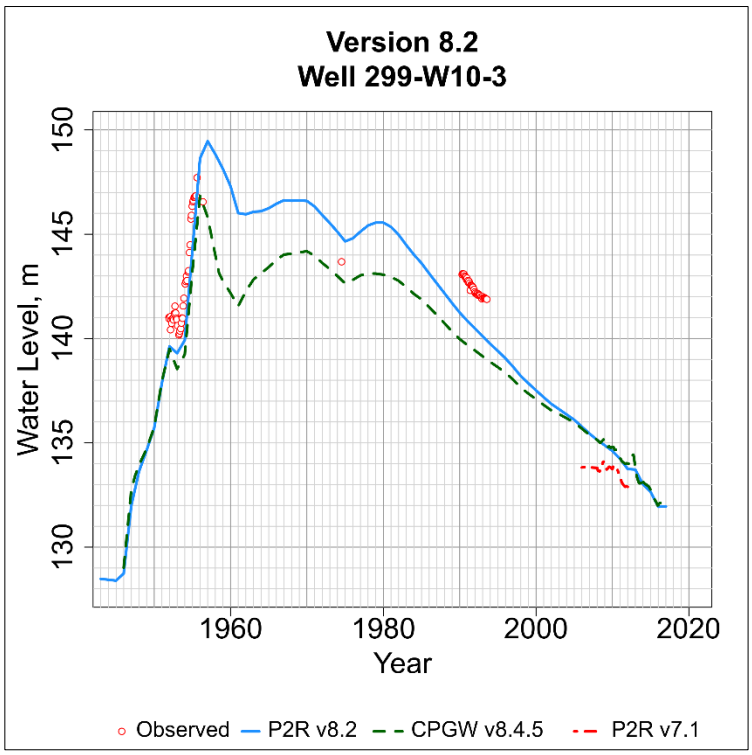

Figure D-148. Observed and simulated water level in the P2R Model at well 299-W10-3.png.

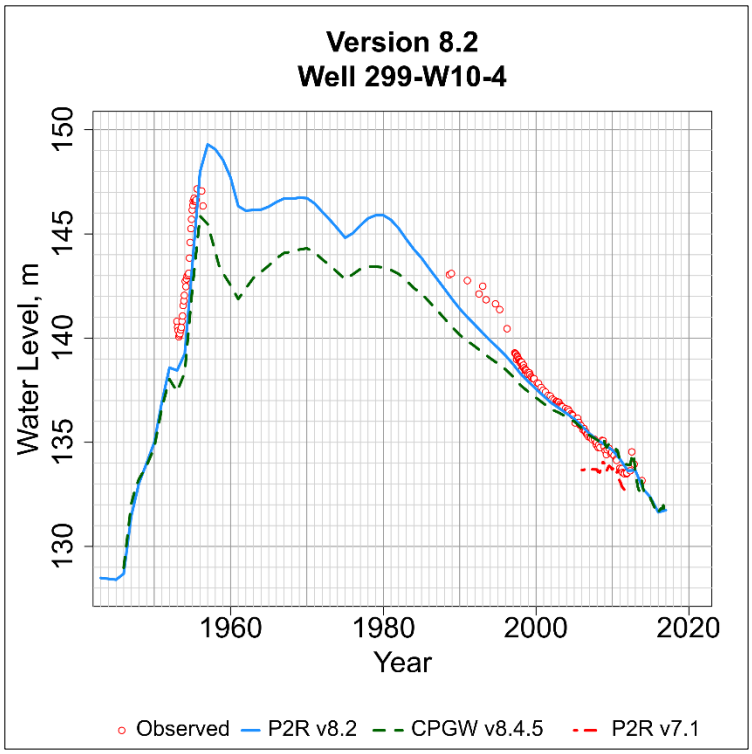

Figure D-149. Observed and simulated water level in the P2R Model at well 299-W10-4.png.

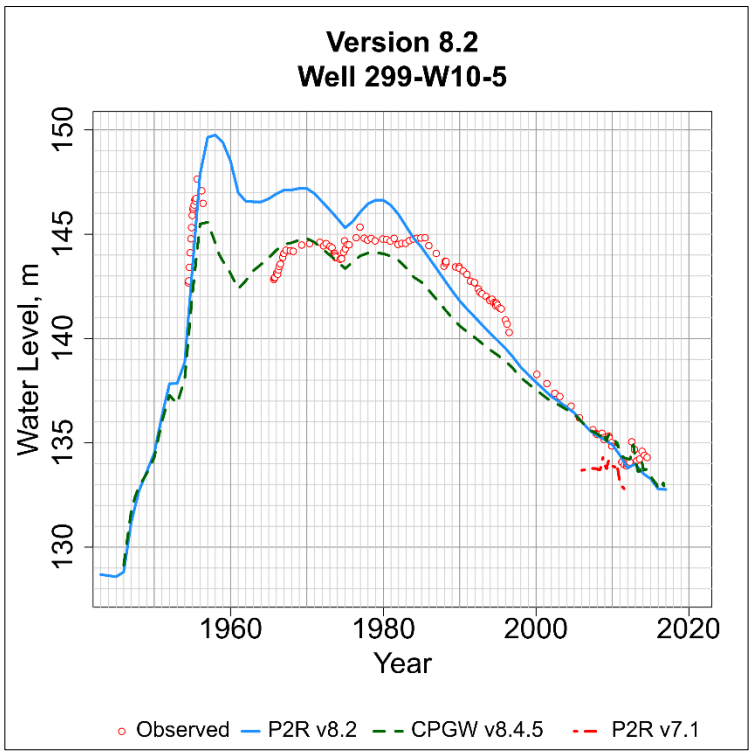

Figure D-150. Observed and simulated water level in the P2R Model at well 299-W10-5.png.

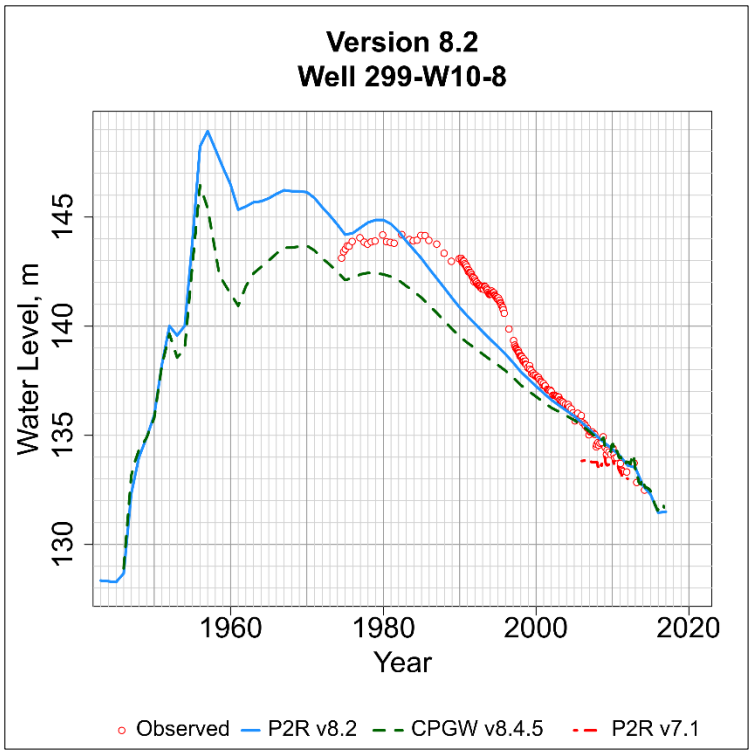

Figure D-151. Observed and simulated water level in the P2R Model at well 299-W10-8.png.

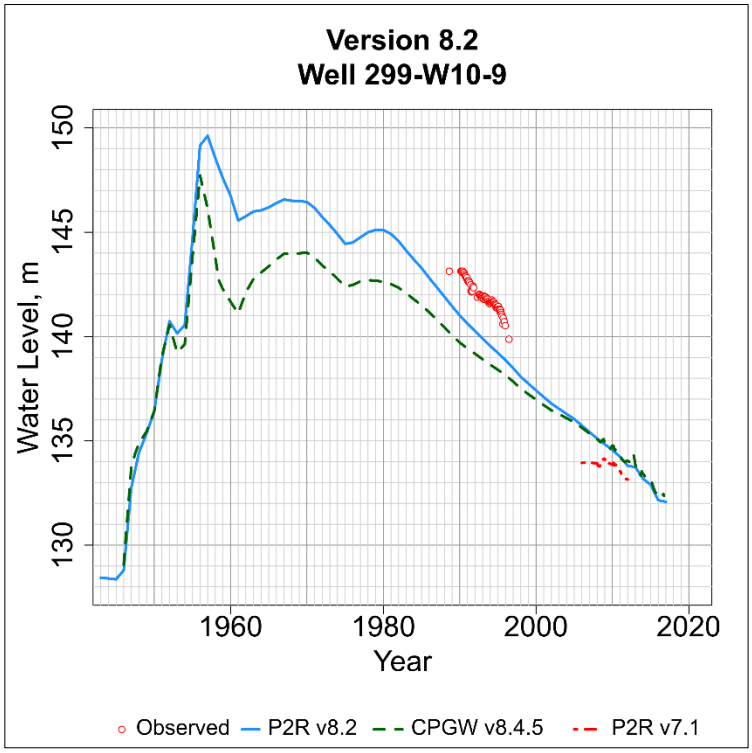

Figure D-152. Observed and simulated water level in the P2R Model at well 299-W10-9.png.

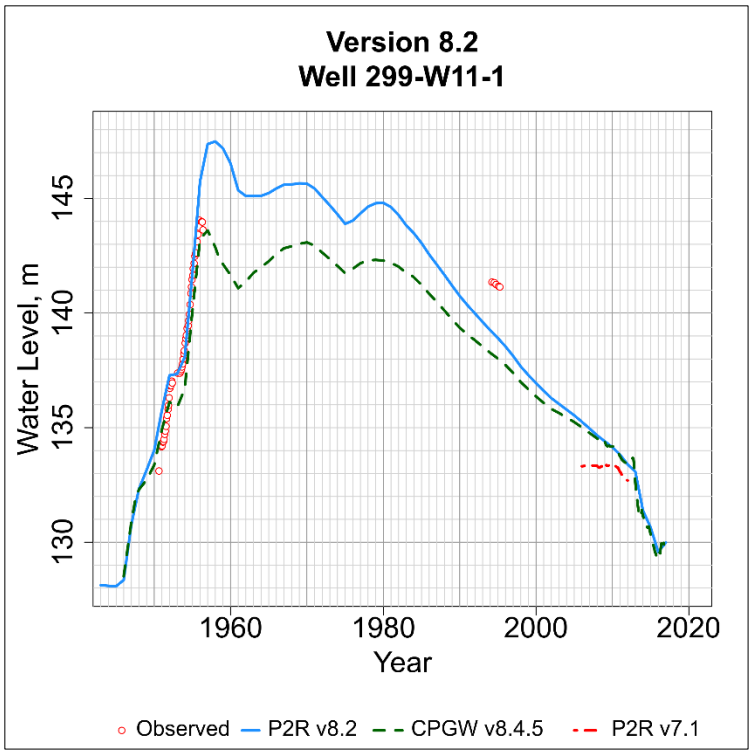

Figure D-153. Observed and simulated water level in the P2R Model at well 299-W11-1.png.

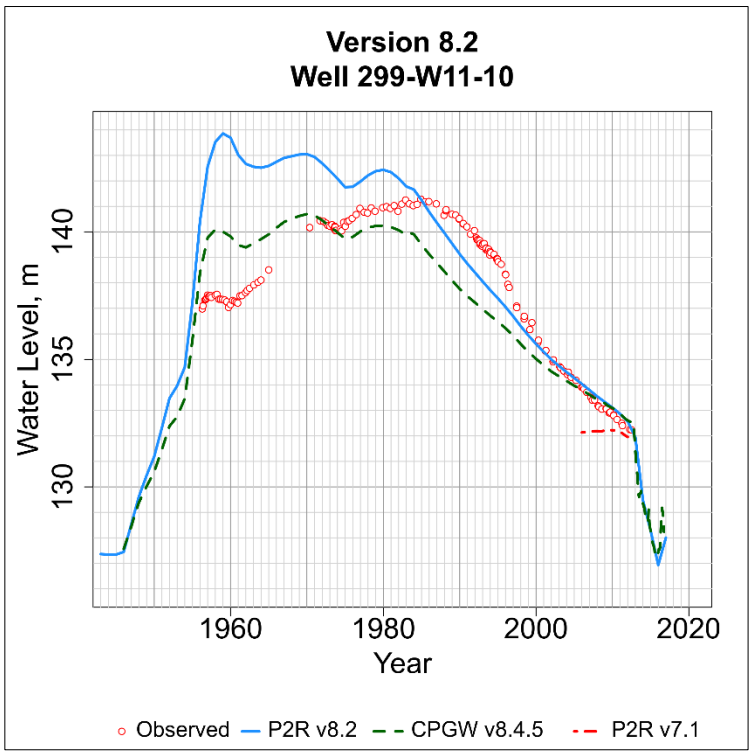

Figure D-154. Observed and simulated water level in the P2R Model at well 299-W11-10.png.

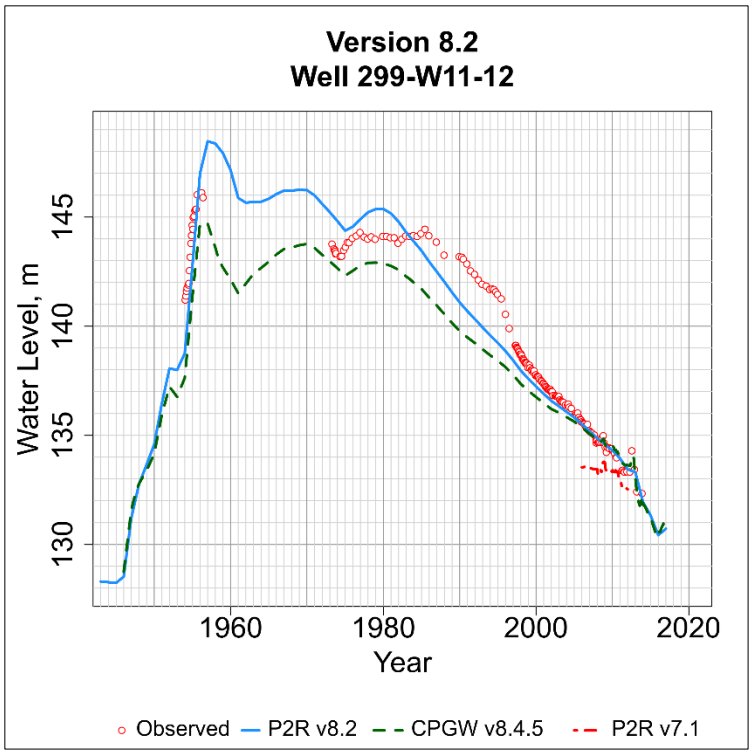

Figure D-155. Observed and simulated water level in the P2R Model at well 299-W11-12.png.

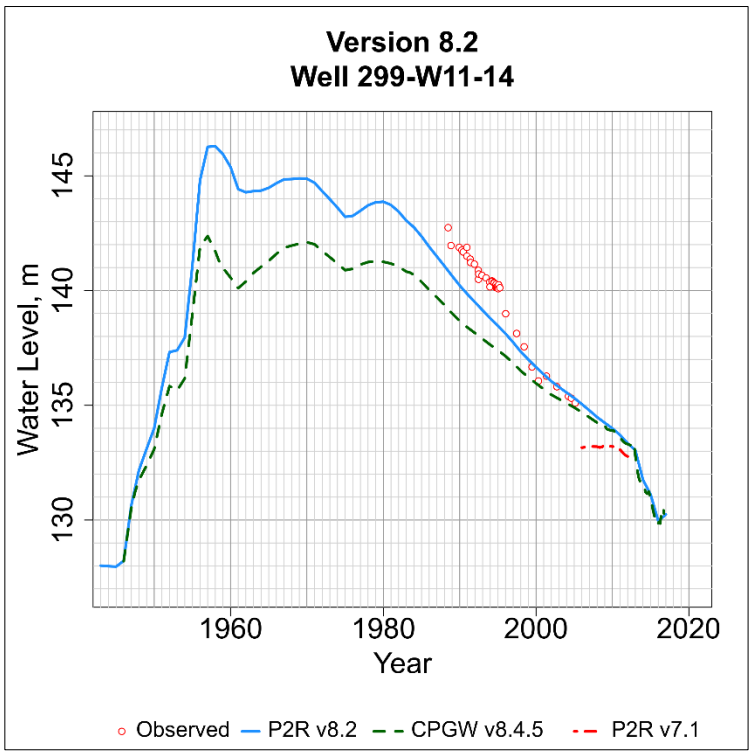

Figure D-156. Observed and simulated water level in the P2R Model at well 299-W11-14.png.

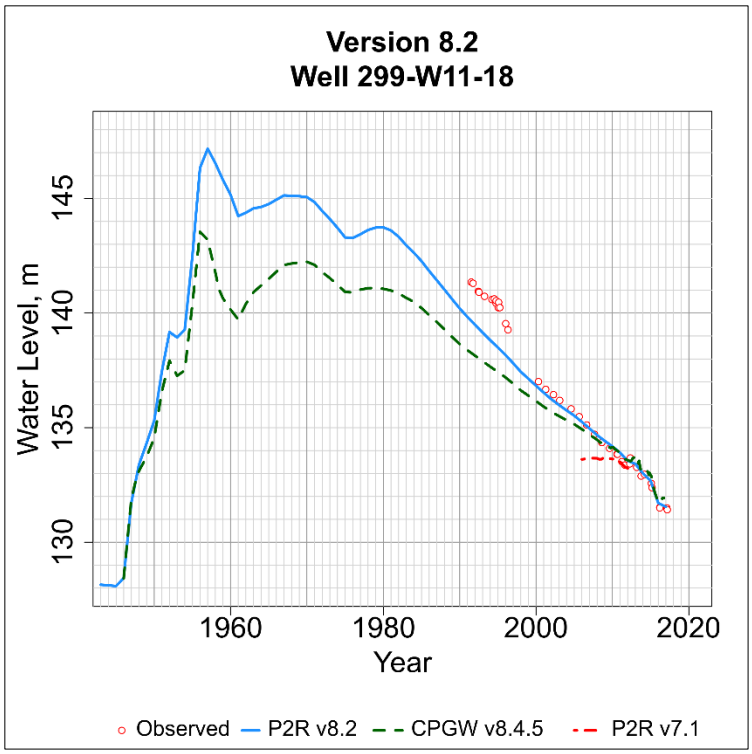

Figure D-157. Observed and simulated water level in the P2R Model at well 299-W11-18.png.

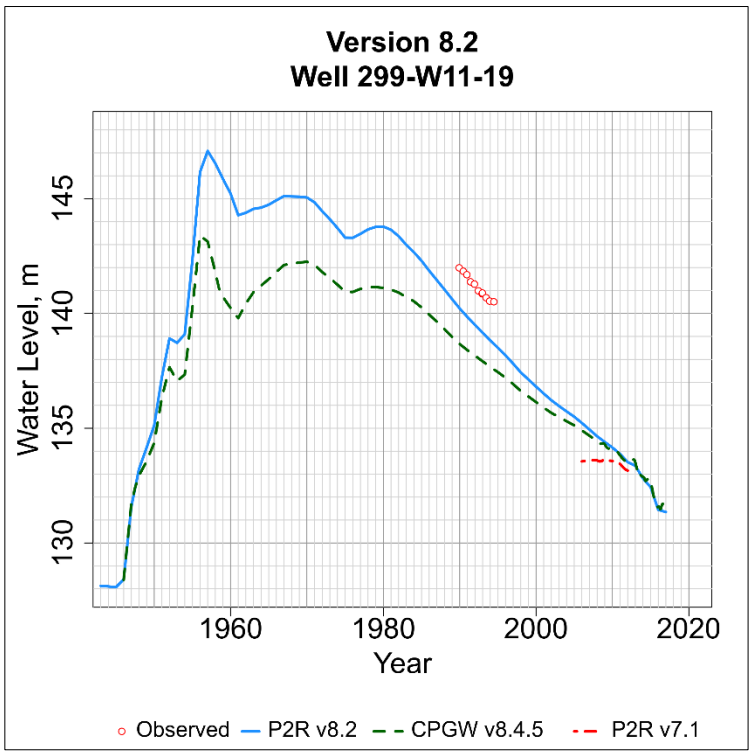

Figure D-158. Observed and simulated water level in the P2R Model at well 299-W11-19.png.

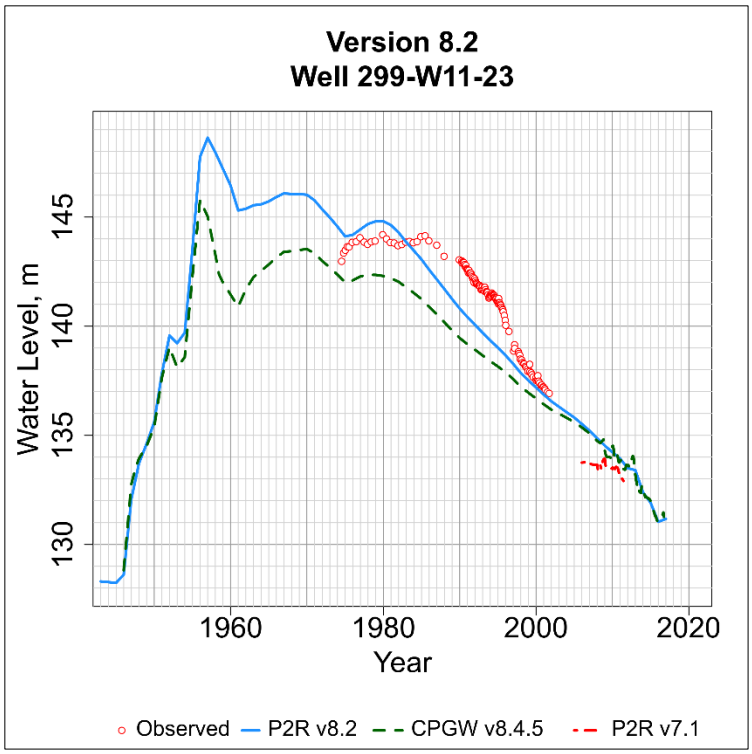

Figure D-159. Observed and simulated water level in the P2R Model at well 299-W11-23.png.

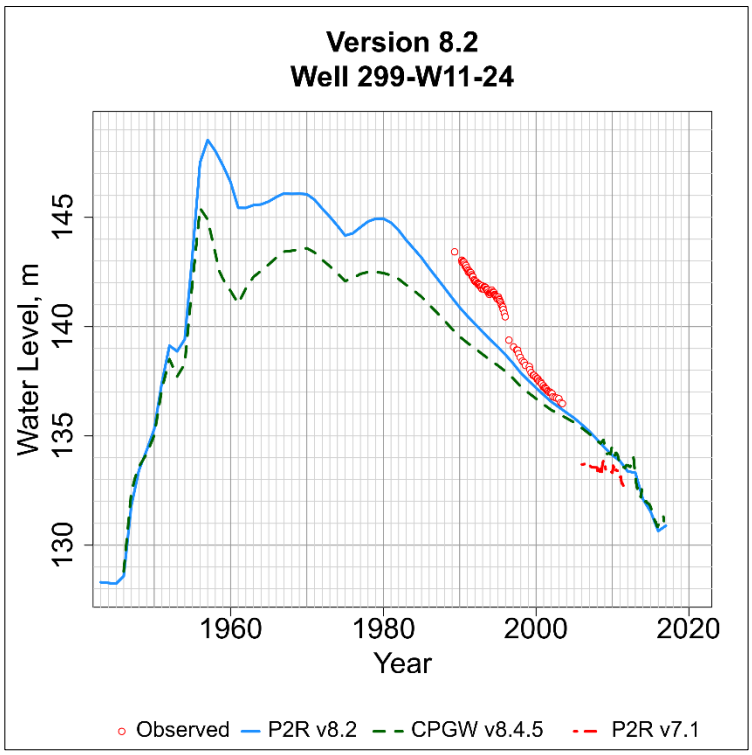

Figure D-160. Observed and simulated water level in the P2R Model at well 299-W11-24.png.

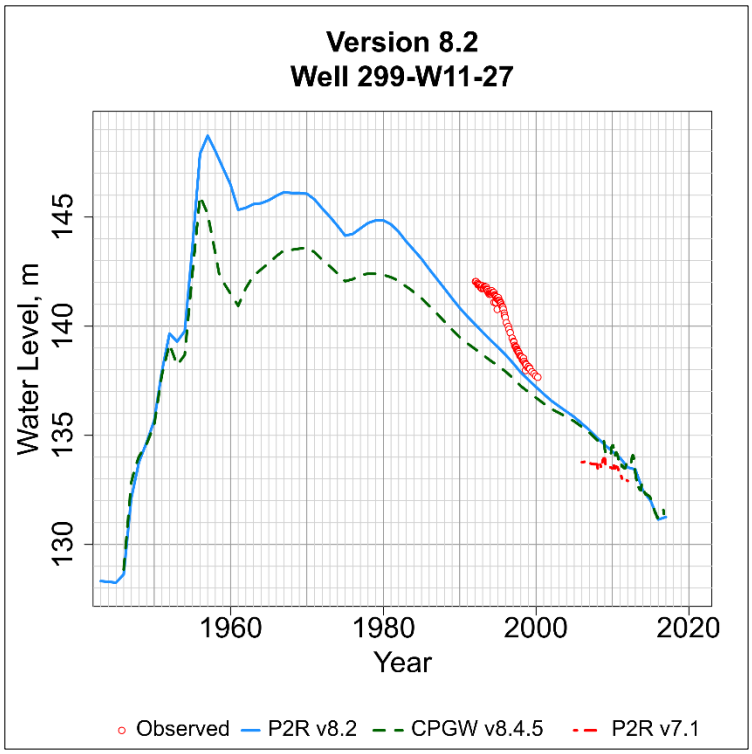

Figure D-161. Observed and simulated water level in the P2R Model at well 299-W11-27.png.

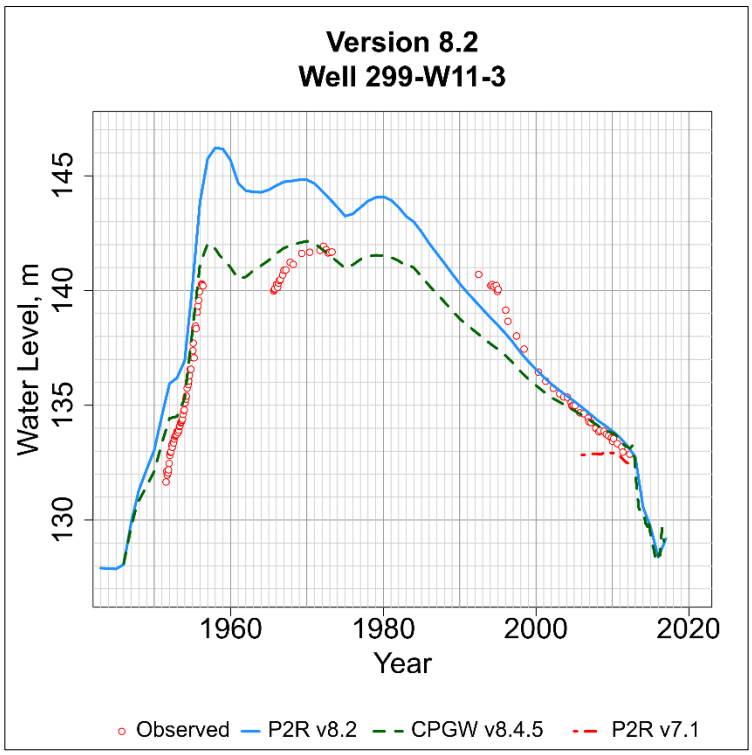

Figure D-162. Observed and simulated water level in the P2R Model at well 299-W11-3.png.

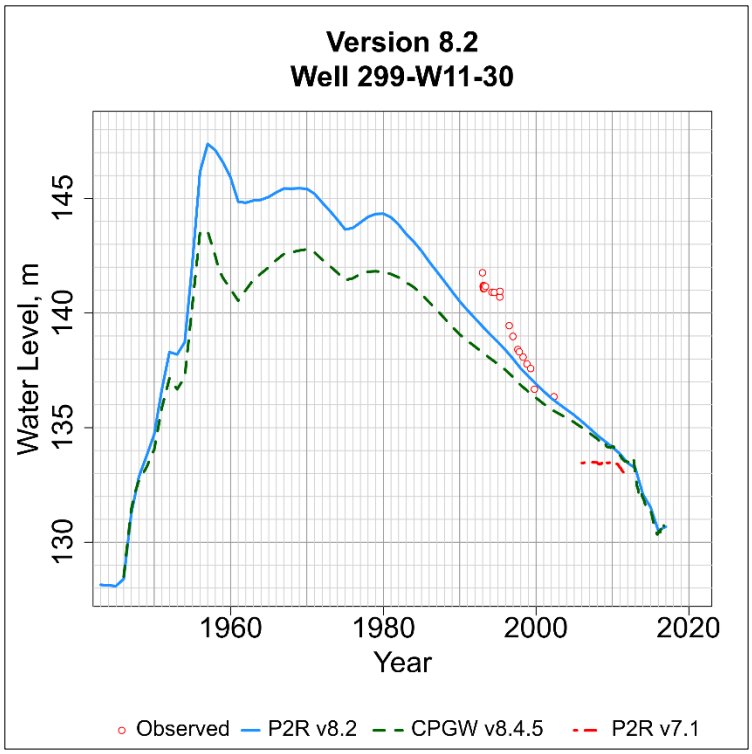

Figure D-163. Observed and simulated water level in the P2R Model at well 299-W11-30.png.

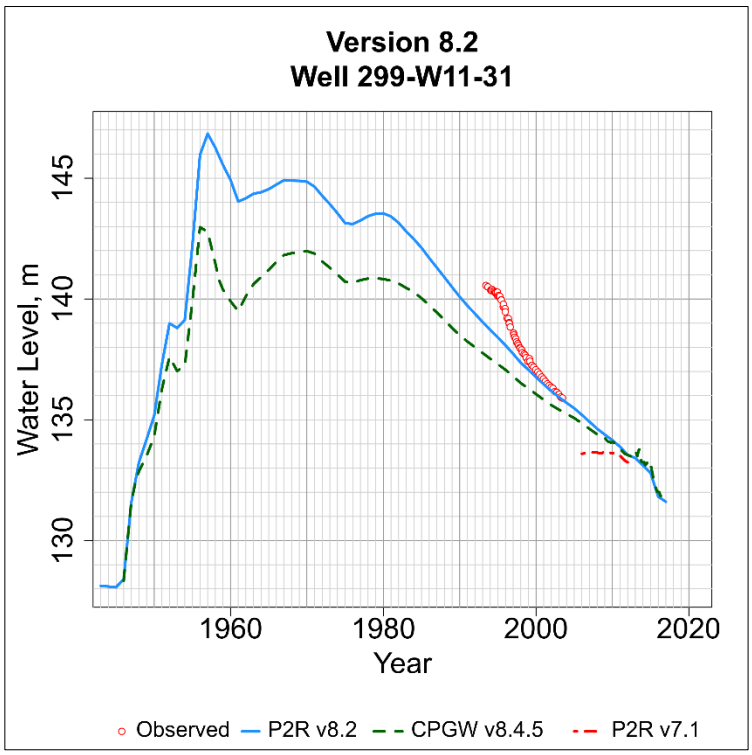

Figure D-164. Observed and simulated water level in the P2R Model at well 299-W11-31.png.

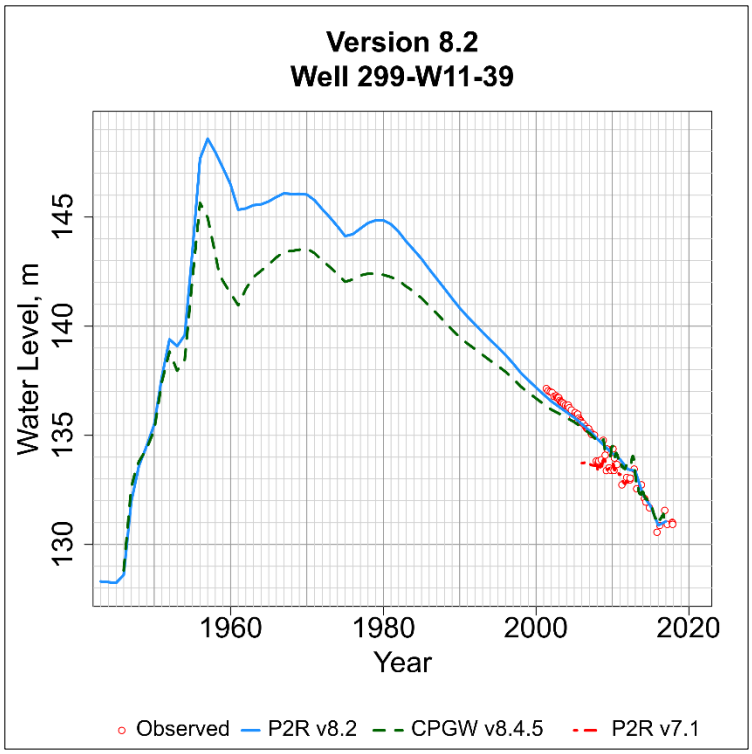

Figure D-165. Observed and simulated water level in the P2R Model at well 299-W11-39.png.

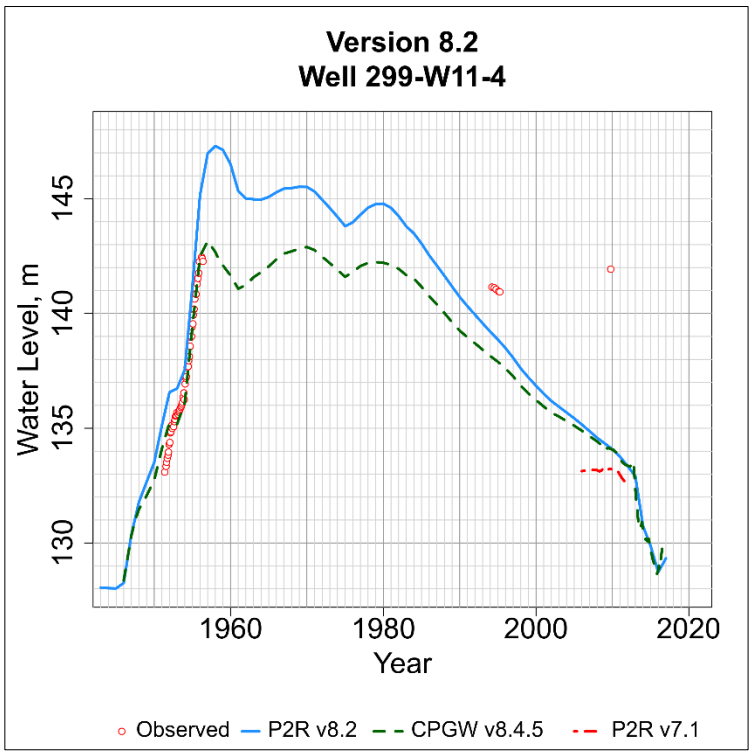

Figure D-166. Observed and simulated water level in the P2R Model at well 299-W11-4.png.

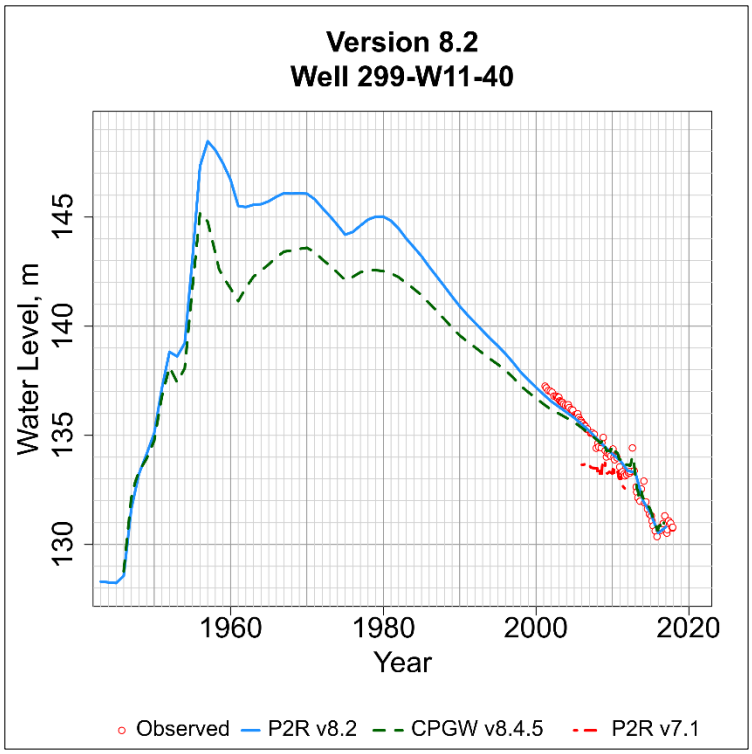

Figure D-167. Observed and simulated water level in the P2R Model at well 299-W11-40.png.

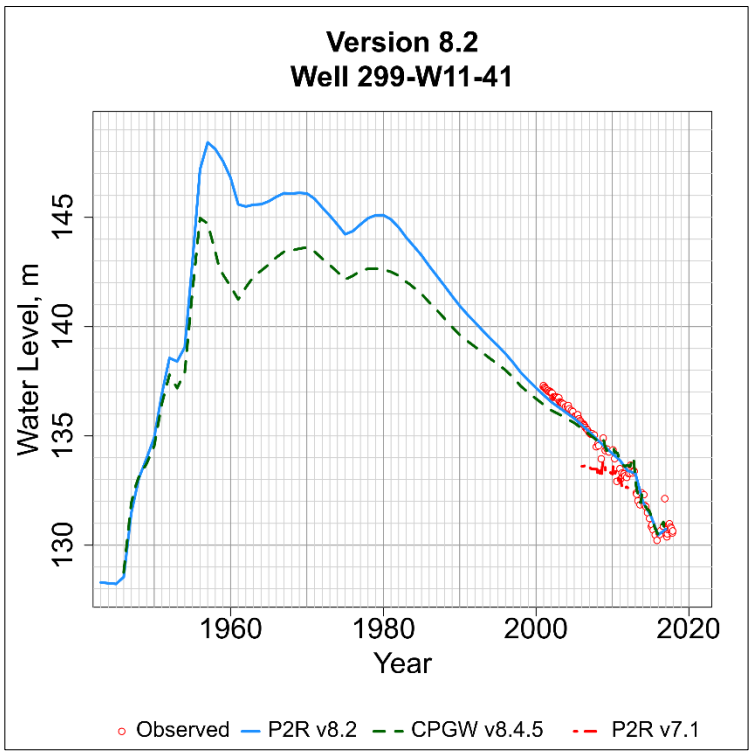

Figure D-168. Observed and simulated water level in the P2R Model at well 299-W11-41.png.

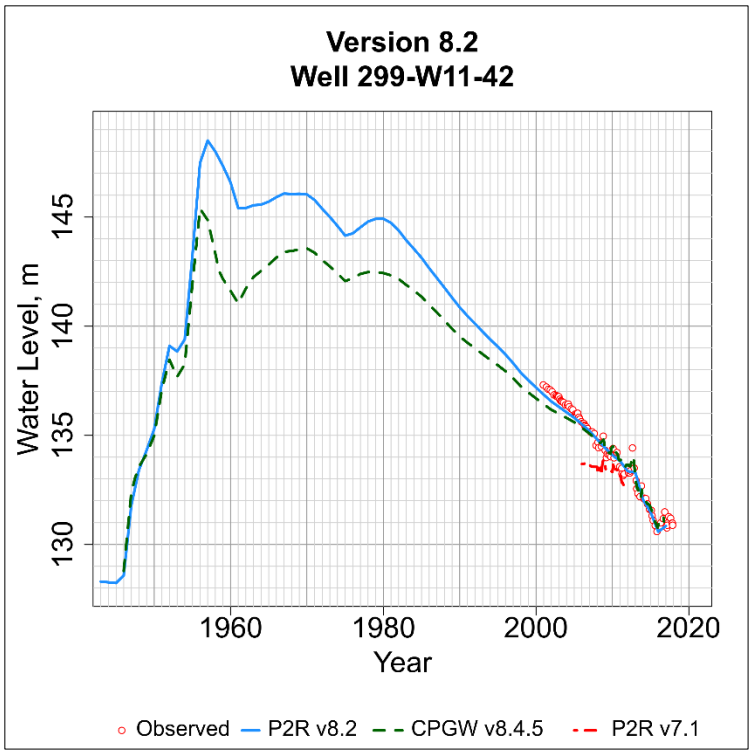

Figure D-169. Observed and simulated water level in the P2R Model at well 299-W11-42.png.

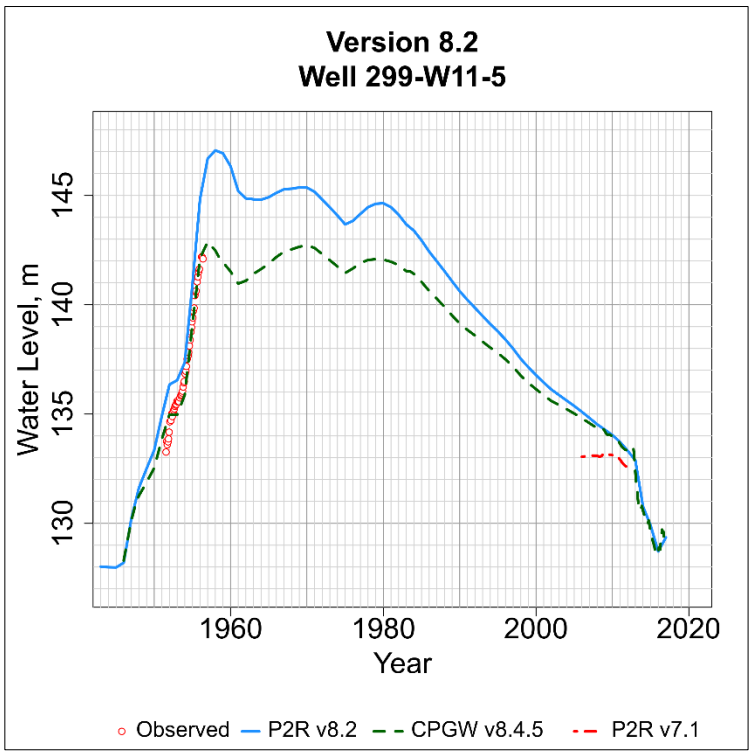

Figure D-170. Observed and simulated water level in the P2R Model at well 299-W11-5.png.

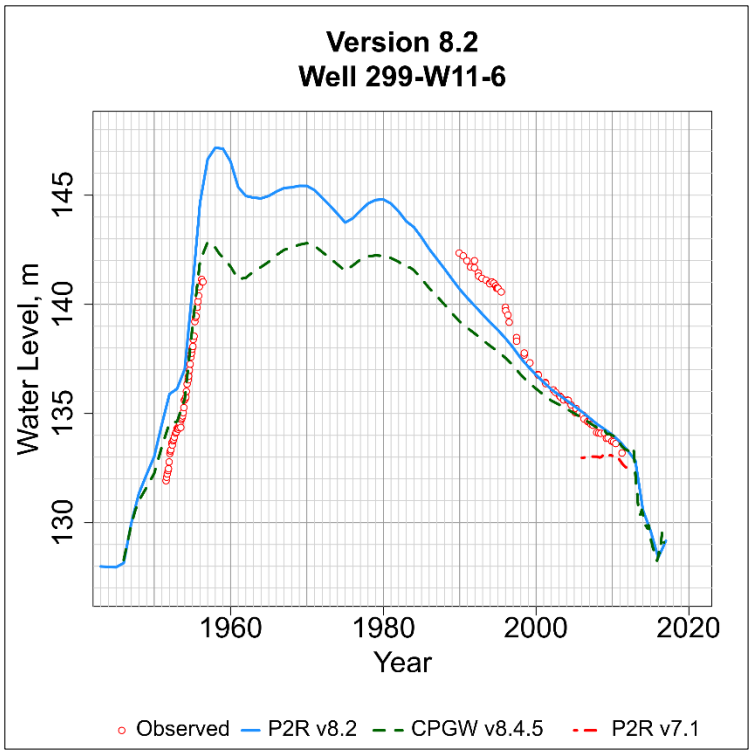

Figure D-171. Observed and simulated water level in the P2R Model at well 299-W11-6.png.

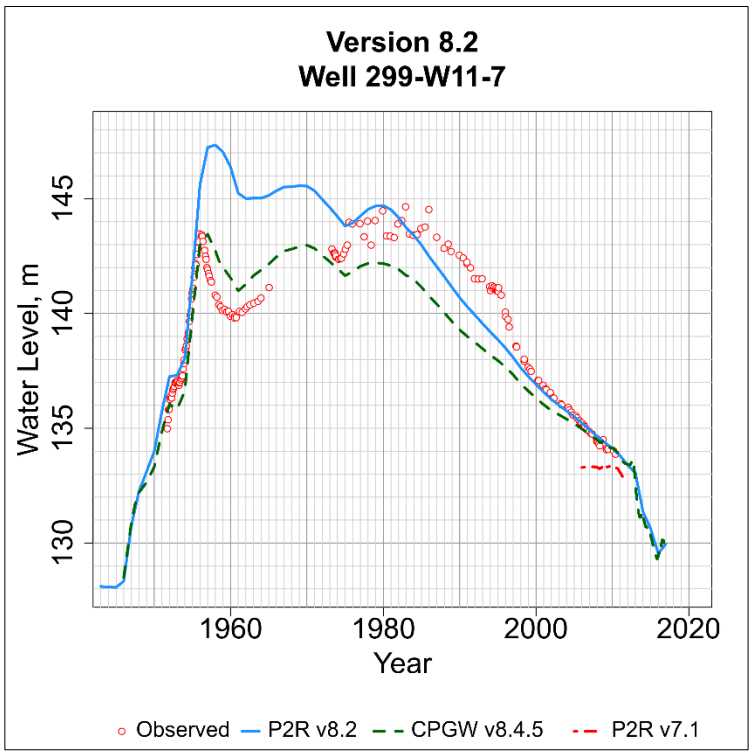

Figure D-172. Observed and simulated water level in the P2R Model at well 299-W11-7.png.

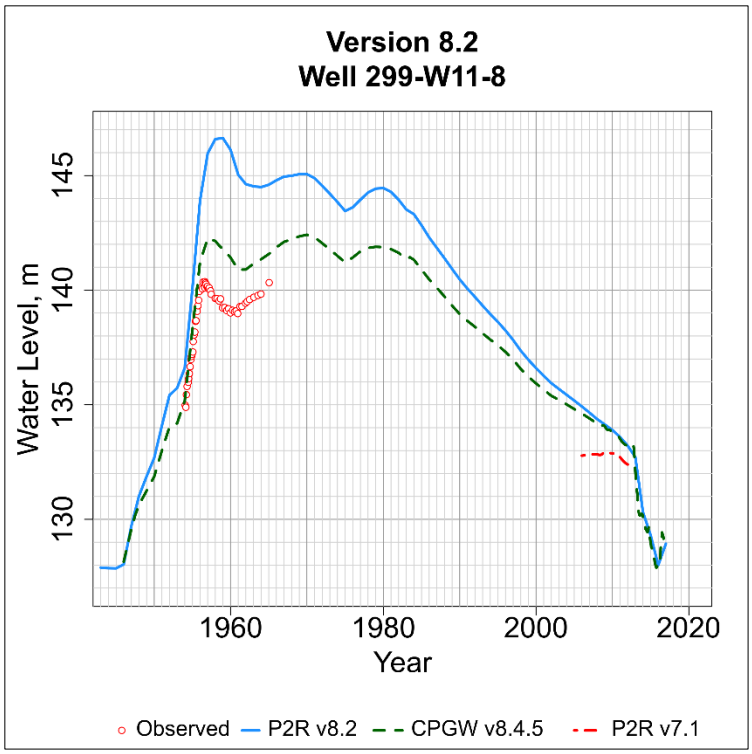

Figure D-173. Observed and simulated water level in the P2R Model at well 299-W11-8.png.

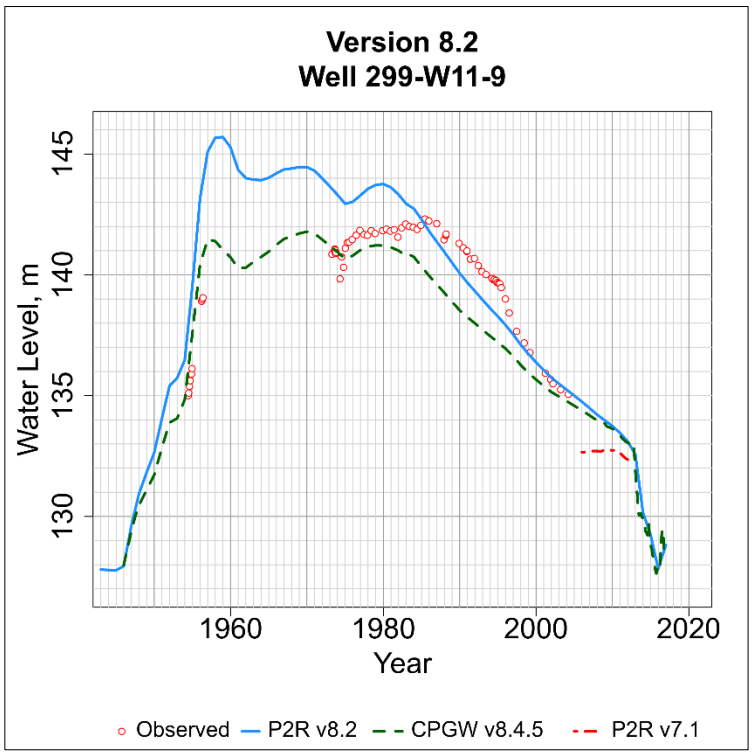

Figure D-174. Observed and simulated water level in the P2R Model at well 299-W11-9.png.

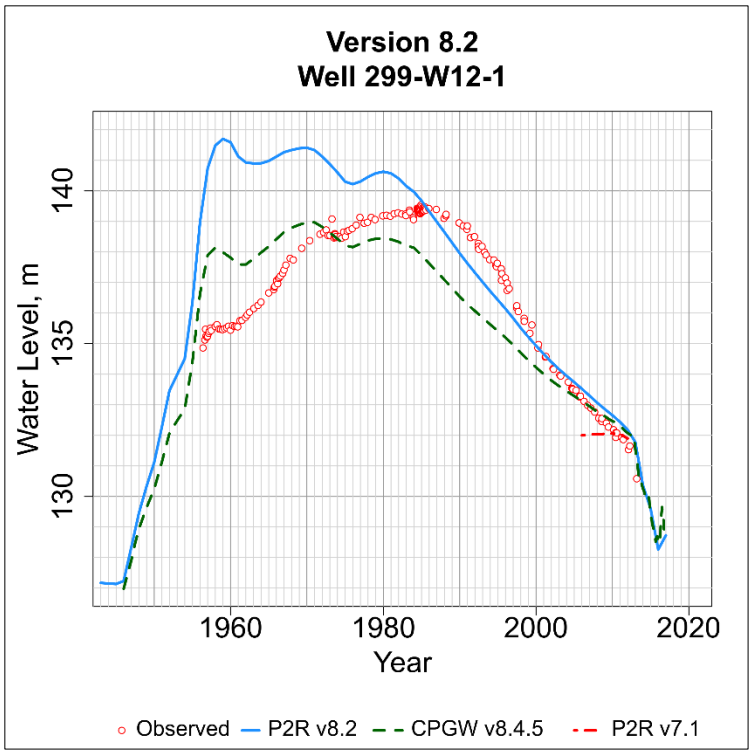

Figure D-175. Observed and simulated water level in the P2R Model at well 299-W12-1.png.

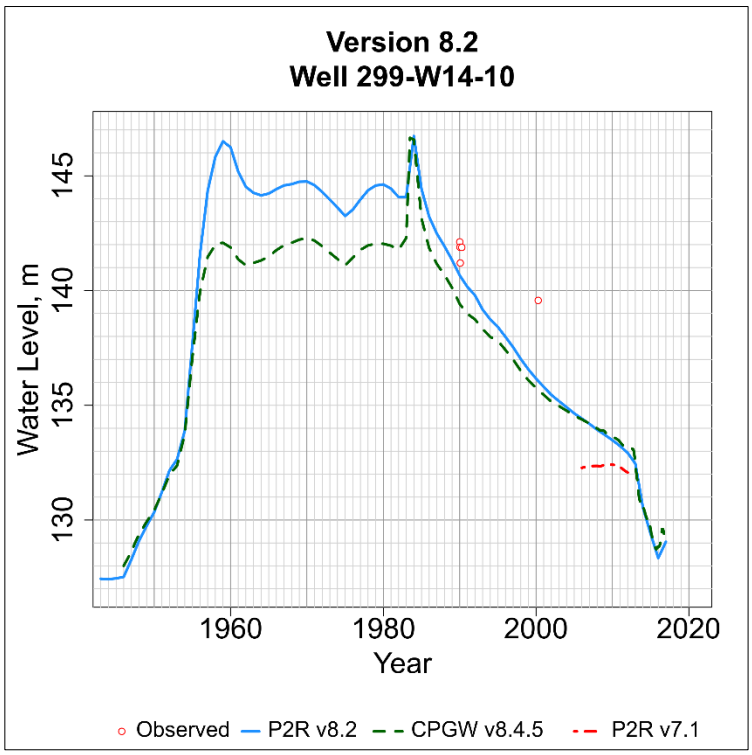

Figure D-176. Observed and simulated water level in the P2R Model at well 299-W14-10.png.

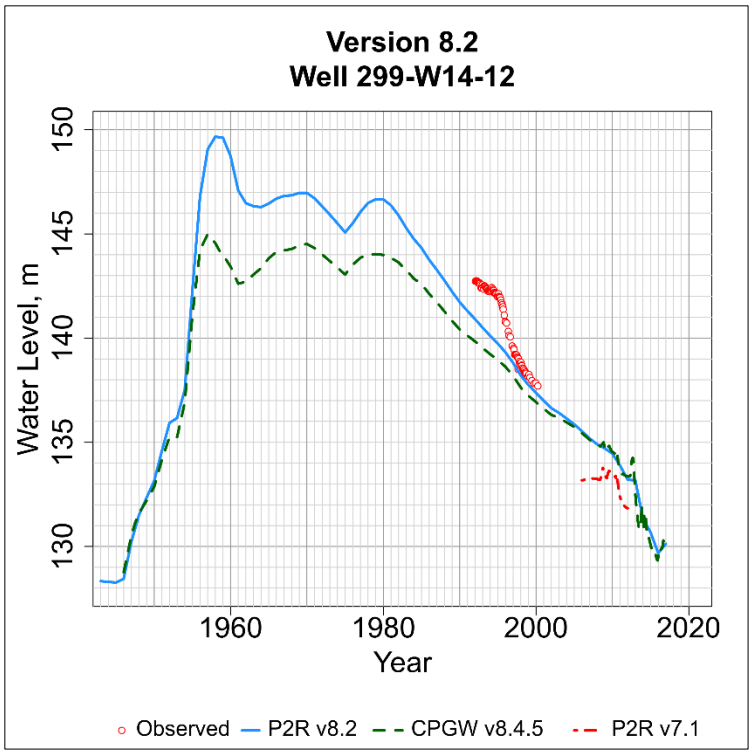

Figure D-177. Observed and simulated water level in the P2R Model at well 299-W14-12.png.

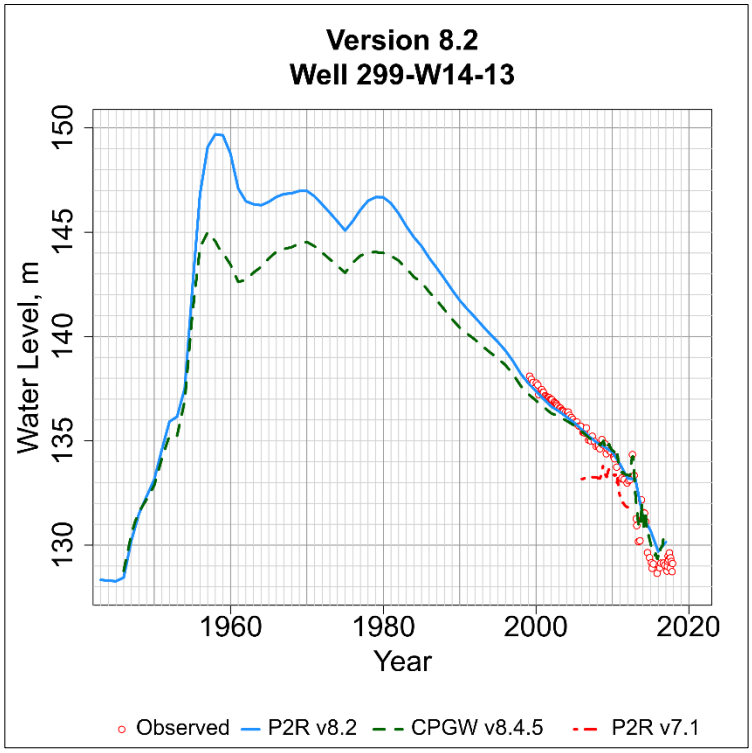

Figure D-178. Observed and simulated water level in the P2R Model at well 299-W14-13.png.

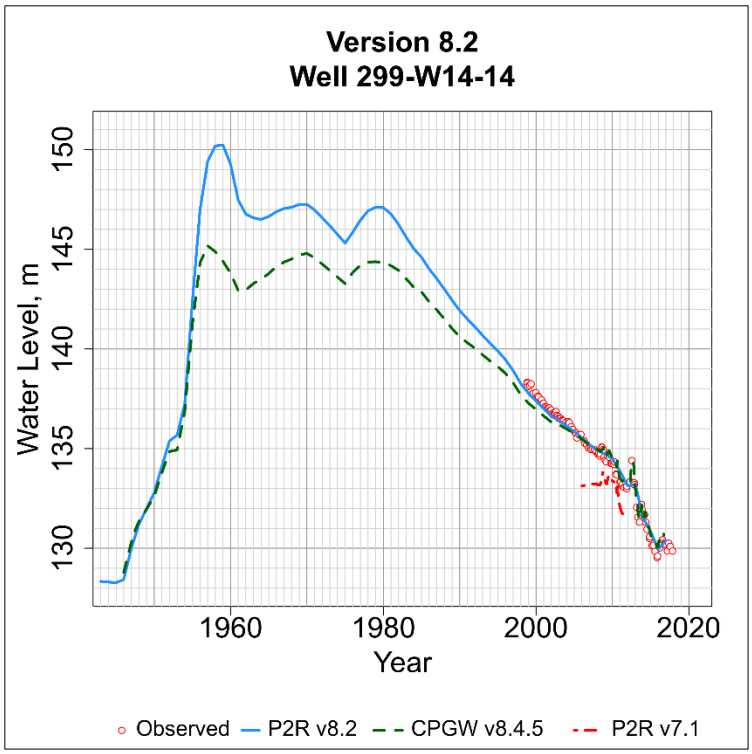

Figure D-179. Observed and simulated water level in the P2R Model at well 299-W14-14.png.

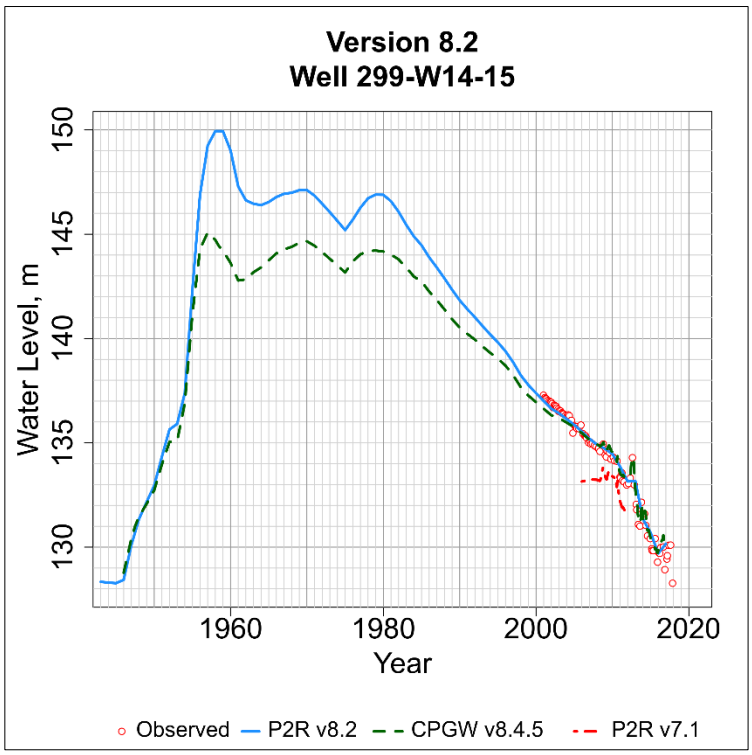

Figure D-180. Observed and simulated water level in the P2R Model at well 299-W14-15.png.

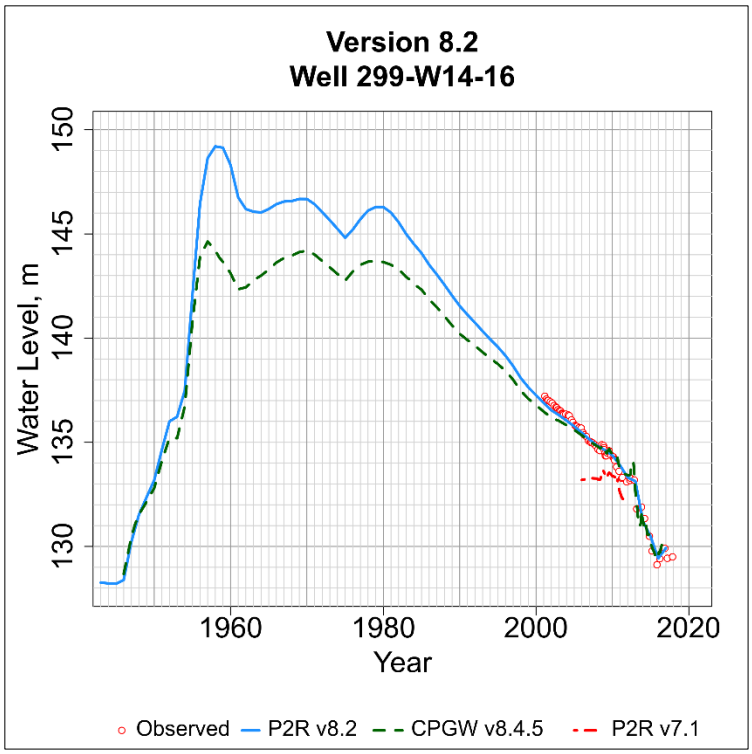

Figure D-181. Observed and simulated water level in the P2R Model at well 299-W14-16.png.

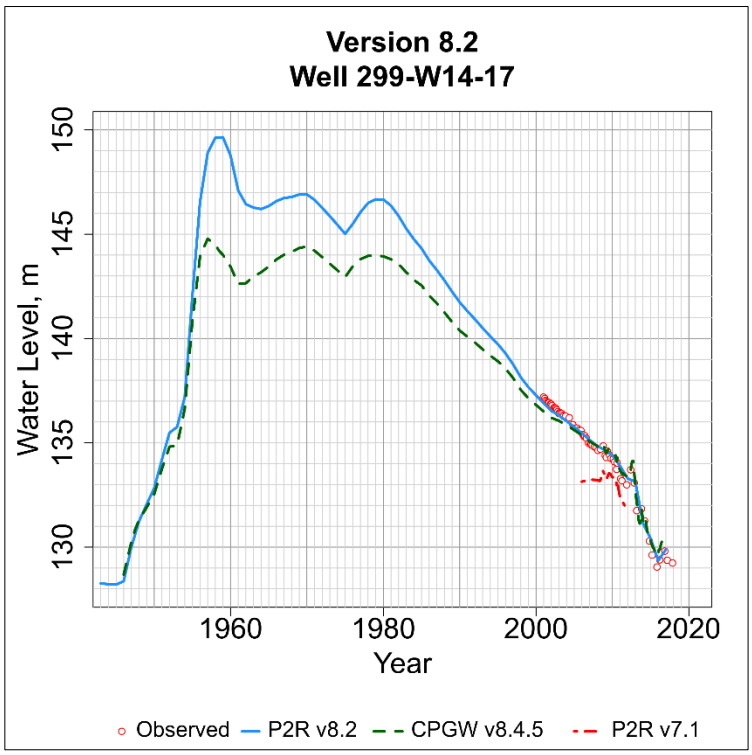

Figure D-182. Observed and simulated water level in the P2R Model at well 299-W14-17.png.

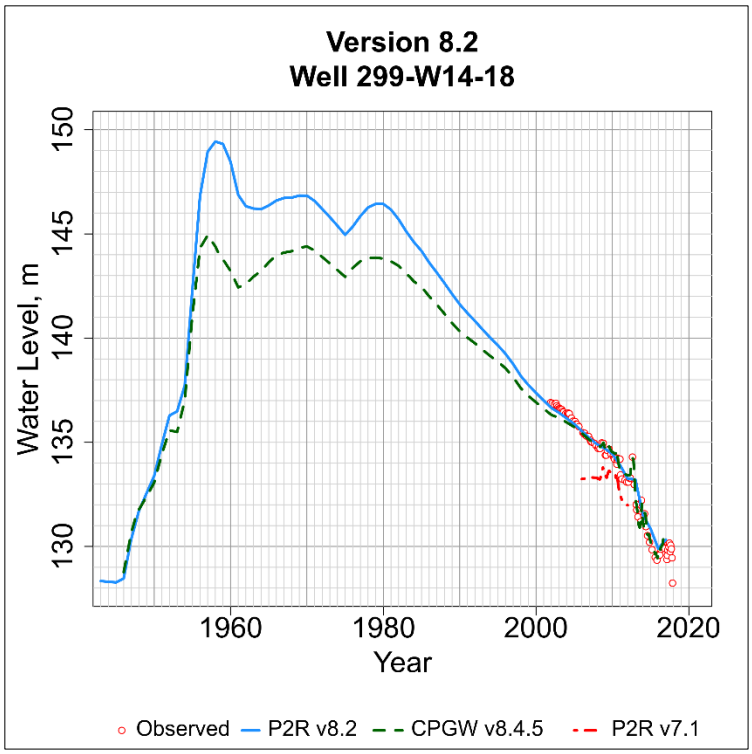

Figure D-183. Observed and simulated water level in the P2R Model at well 299-W14-18.png.

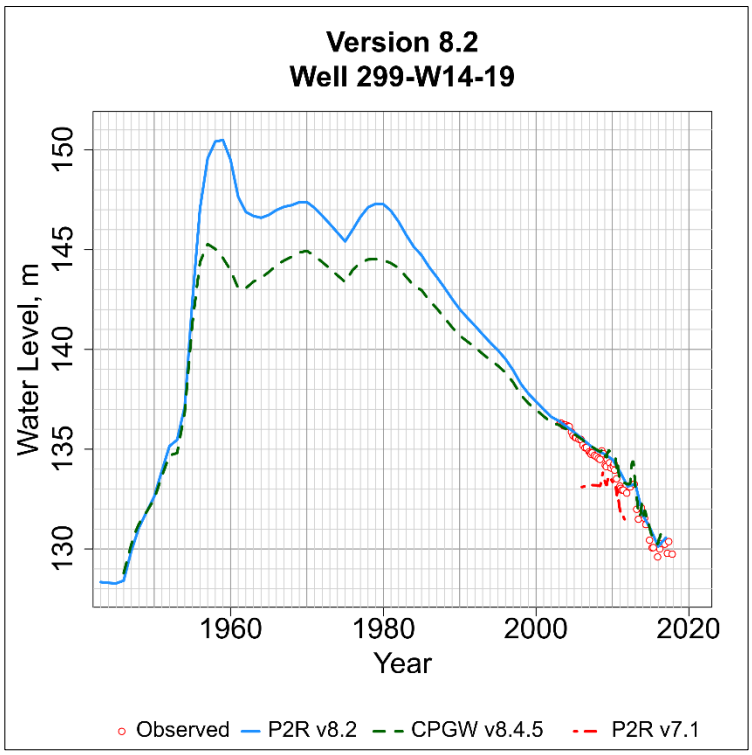

Figure D-184. Observed and simulated water level in the P2R Model at well 299-W14-19.png.

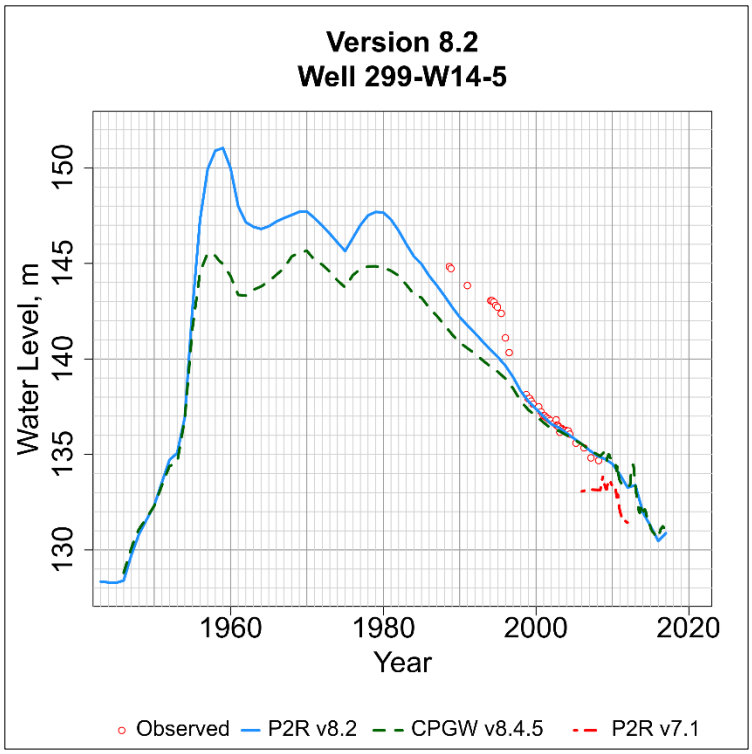

Figure D-185. Observed and simulated water level in the P2R Model at well 299-W14-5.png.

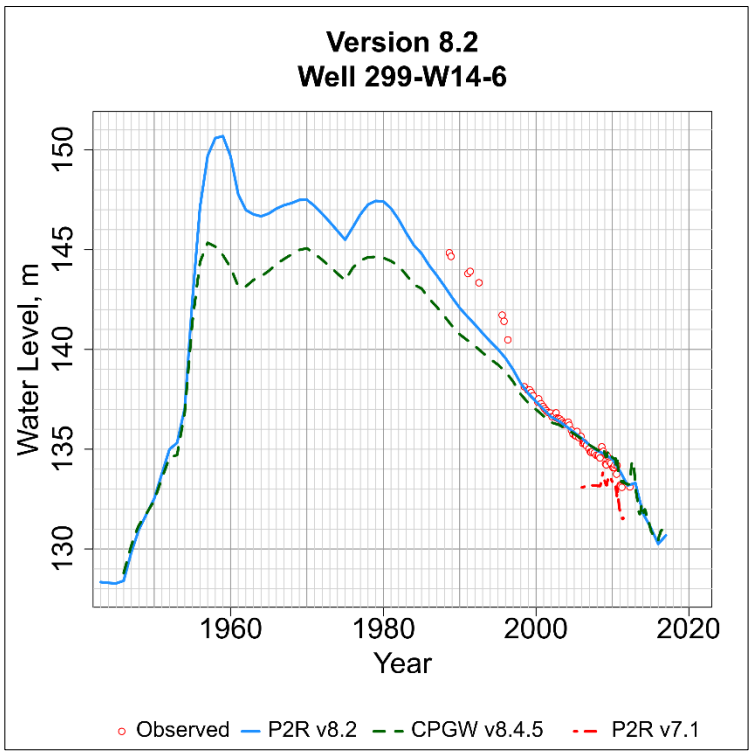

Figure D-186. Observed and simulated water level in the P2R Model at well 299-W14-6.png.

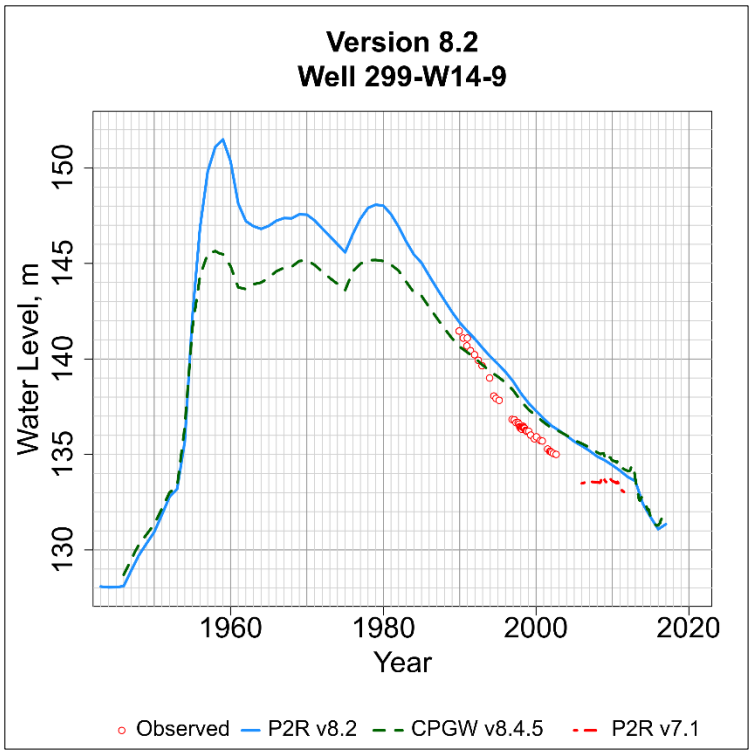

Figure D-187. Observed and simulated water level in the P2R Model at well 299-W14-9.png.

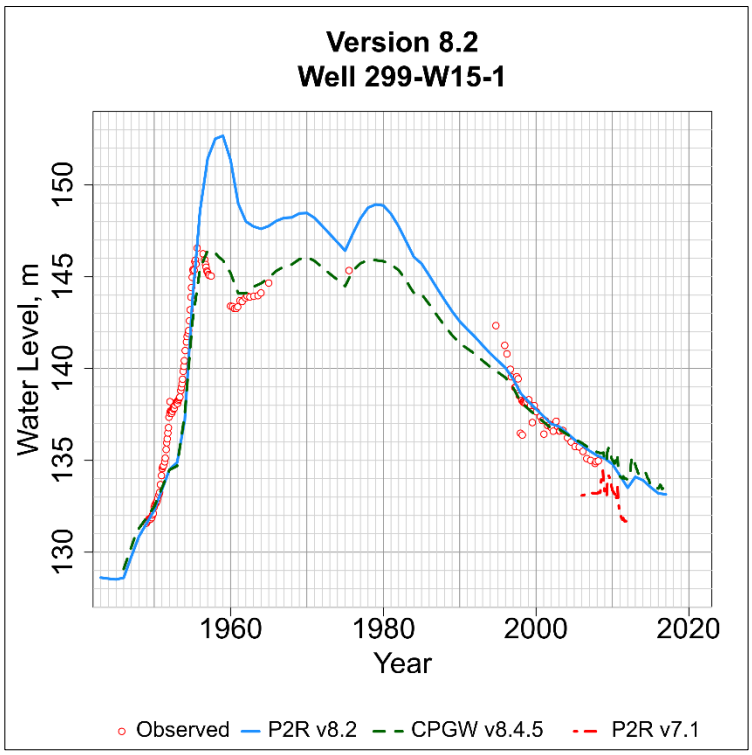

Figure D-188. Observed and simulated water level in the P2R Model at well 299-W15-1.png.

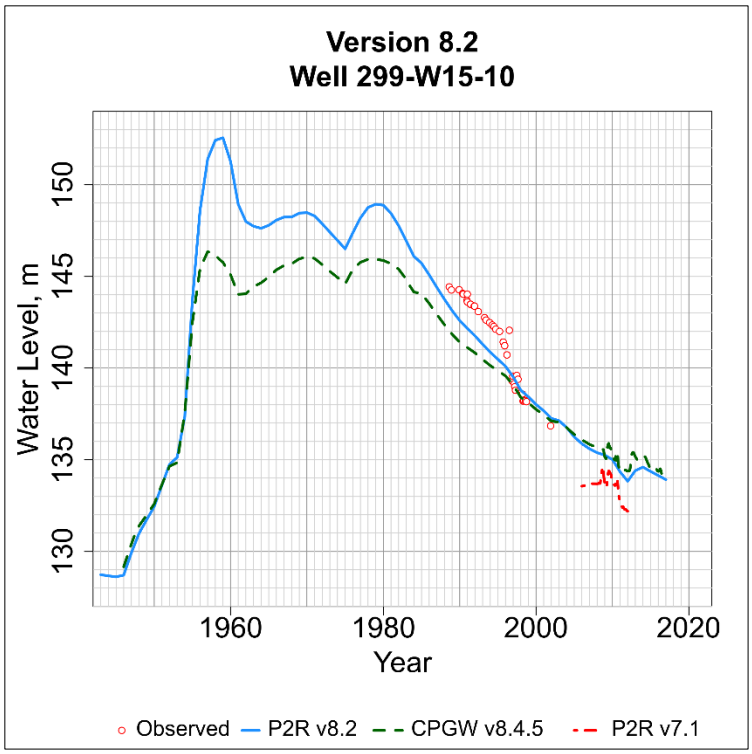

Figure D-189. Observed and simulated water level in the P2R Model at well 299-W15-10.png.

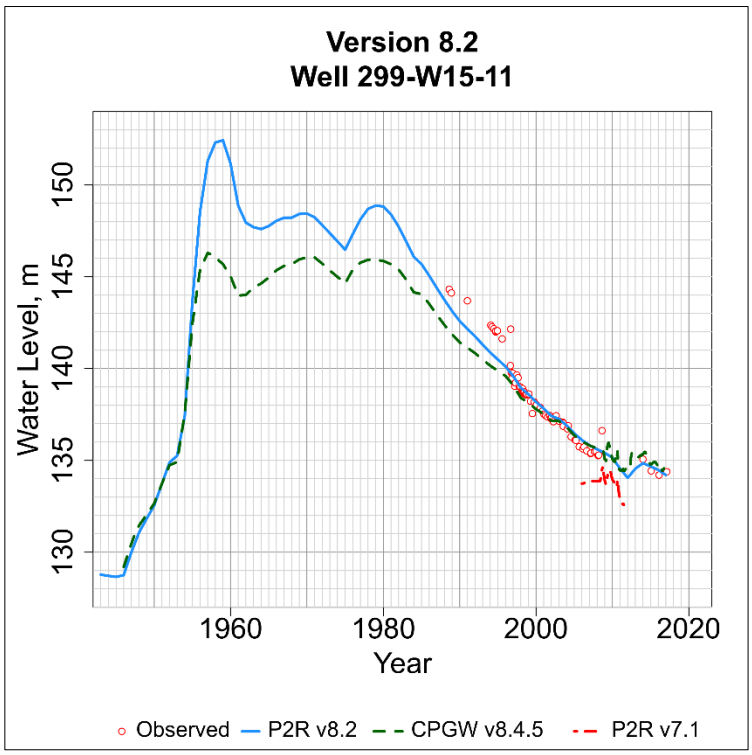

Figure D-190. Observed and simulated water level in the P2R Model at well 299-W15-11.png.

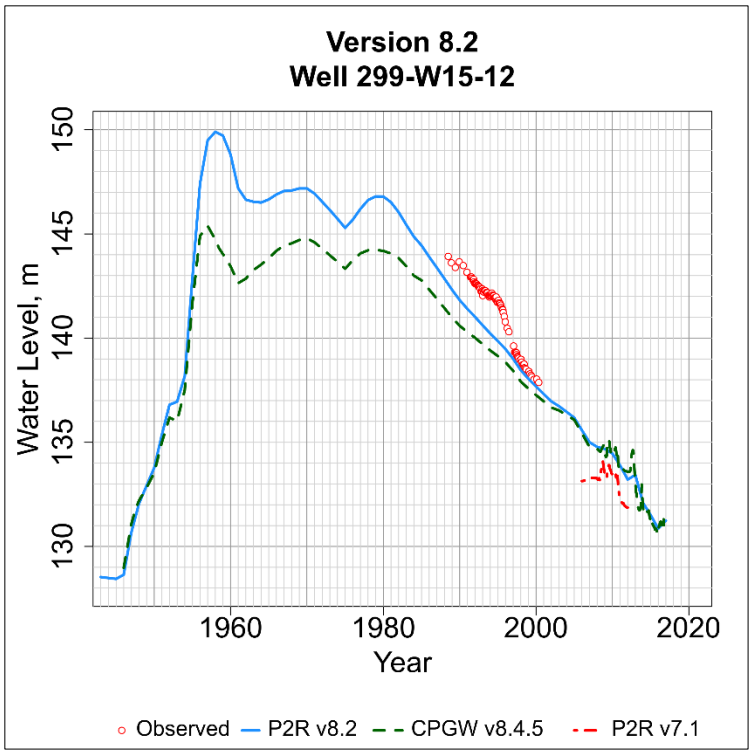

Figure D-191. Observed and simulated water level in the P2R Model at well 299-W15-12.png.

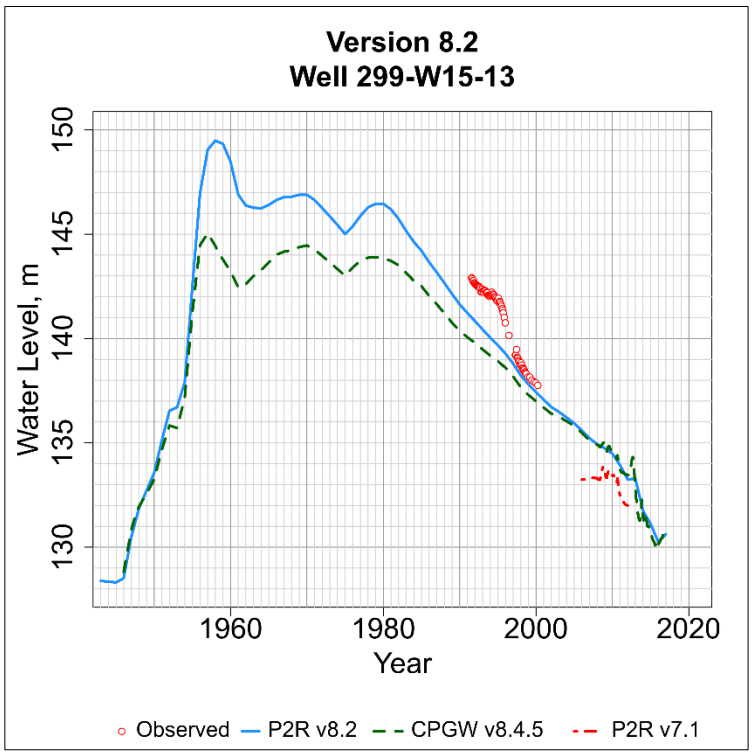

Figure D-192. Observed and simulated water level in the P2R Model at well 299-W15-13.png.

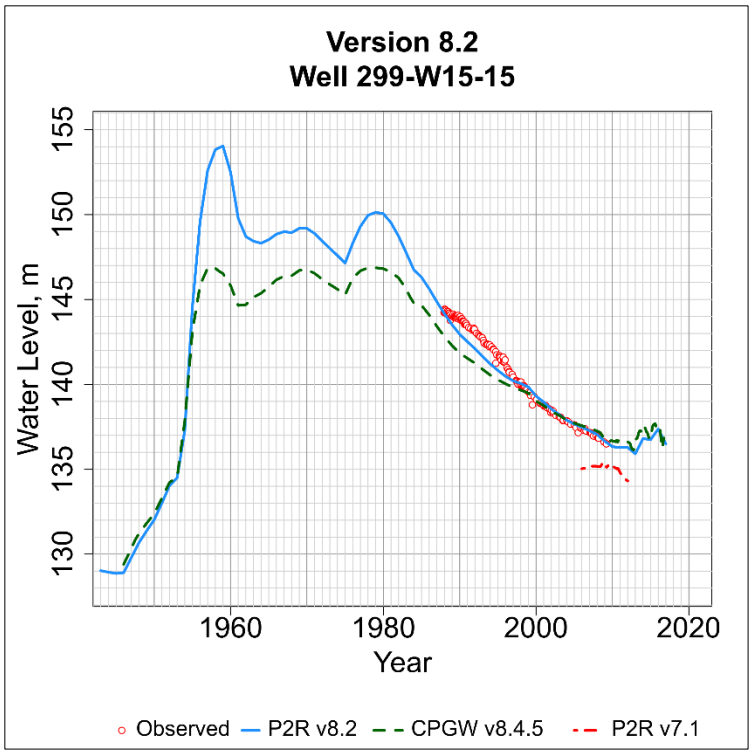

Figure D-193. Observed and simulated water level in the P2R Model at well 299-W15-15.png.

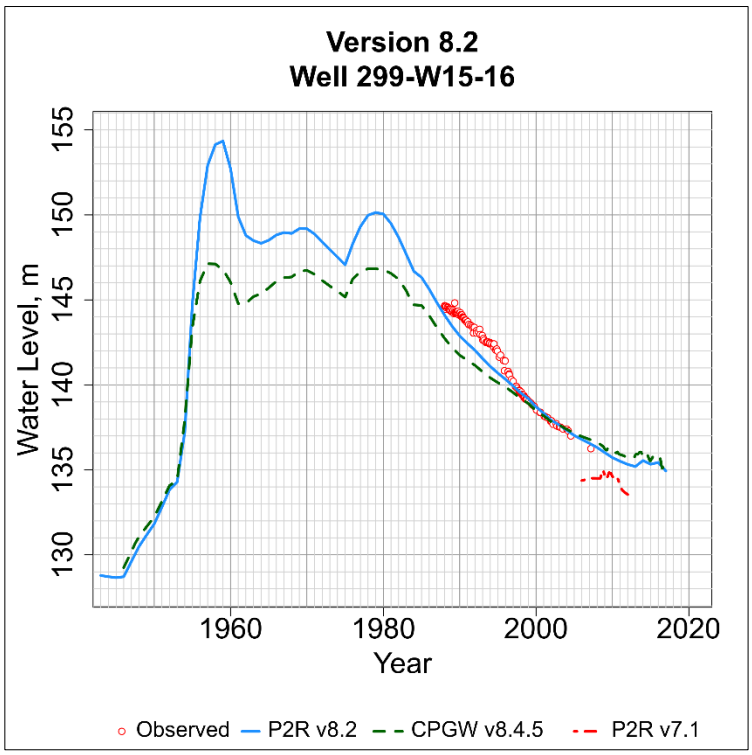

Figure D-194. Observed and simulated water level in the P2R Model at well 299-W15-16.png.

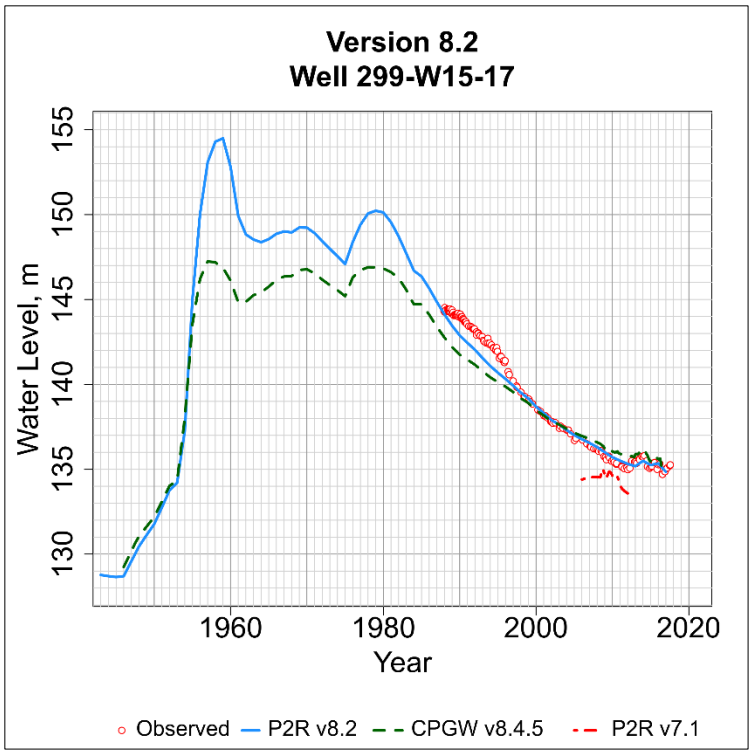

Figure D-195. Observed and simulated water level in the P2R Model at well 299-W15-17.png.

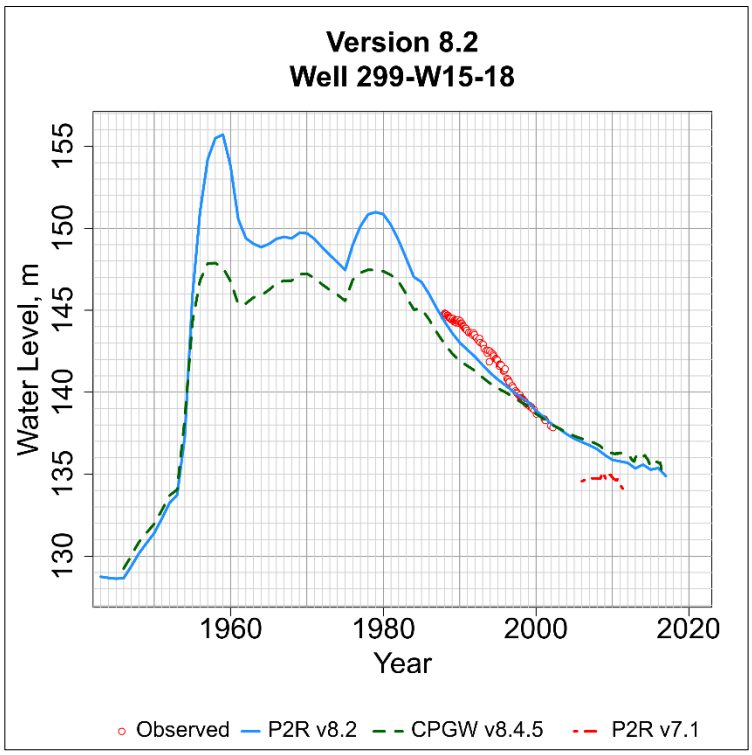

Figure D-196. Observed and simulated water level in the P2R Model at well 299-W15-18.png.

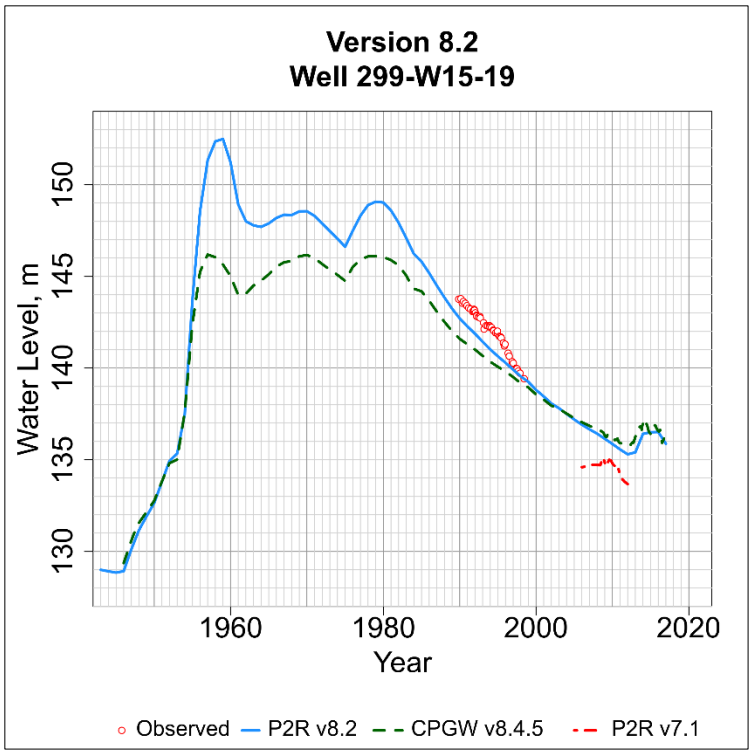

Figure D-197. Observed and simulated water level in the P2R Model at well 299-W15-19.png.

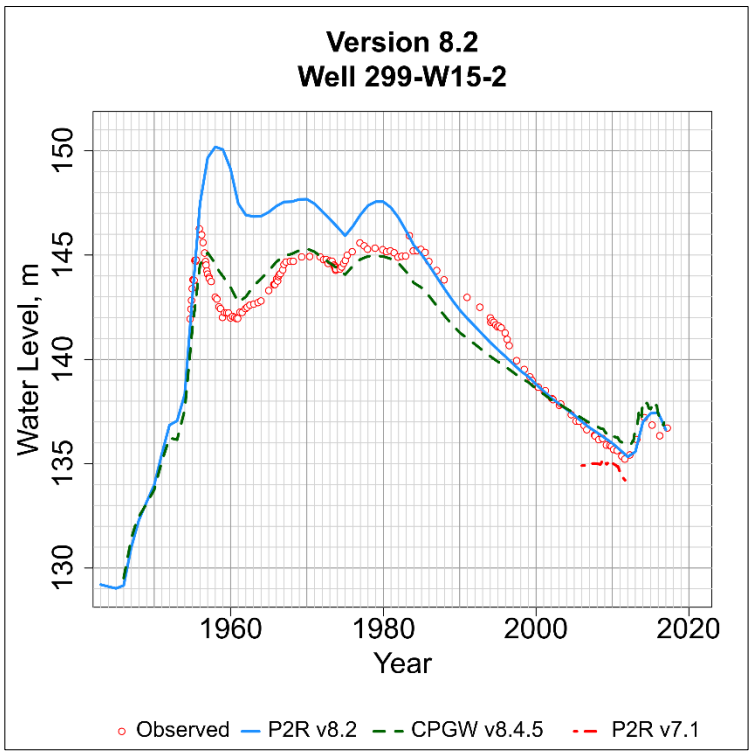

Figure D-198. Observed and simulated water level in the P2R Model at well 299-W15-2.png.

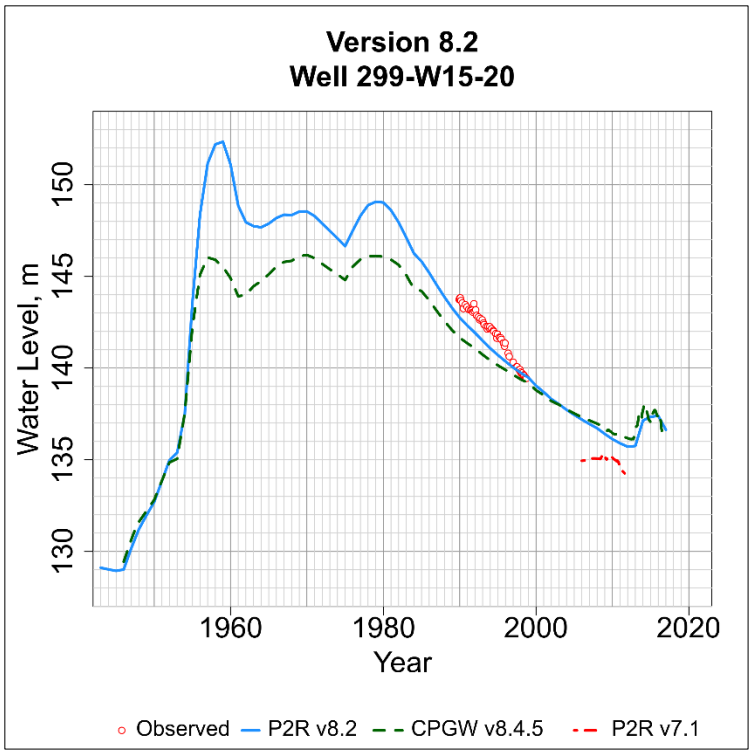

Figure D-199. Observed and simulated water level in the P2R Model at well 299-W15-20.png.

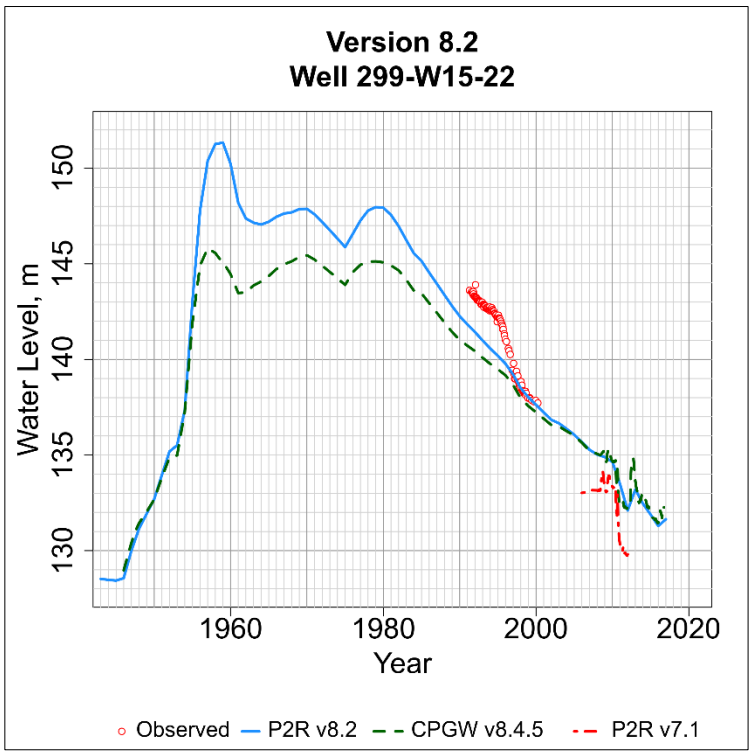

Figure D-200. Observed and simulated water level in the P2R Model at well 299-W15-22.png.

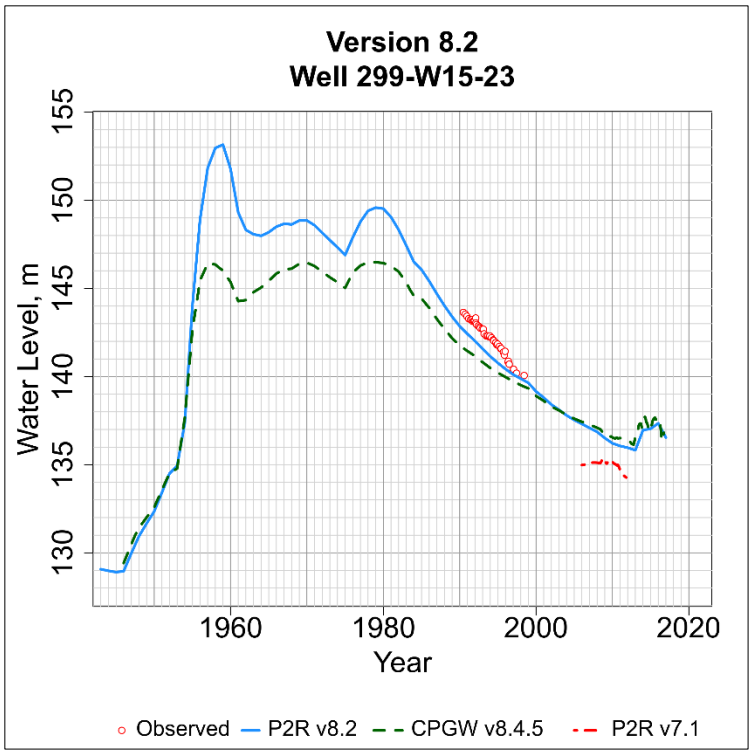

Figure D-201. Observed and simulated water level in the P2R Model at well 299-W15-23.png.

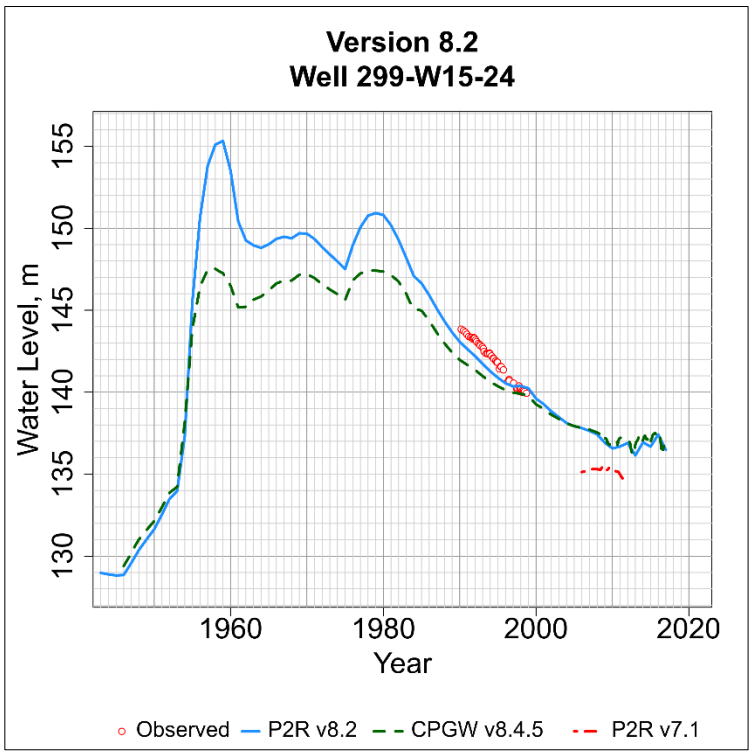

Figure D-202. Observed and simulated water level in the P2R Model at well 299-W15-24.png.

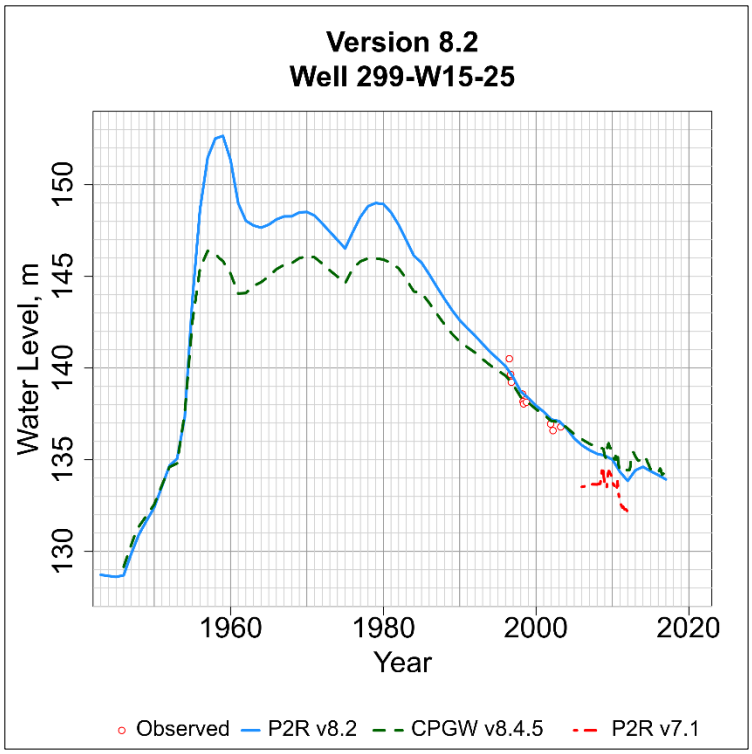

Figure D-203. Observed and simulated water level in the P2R Model at well 299-W15-25.png.

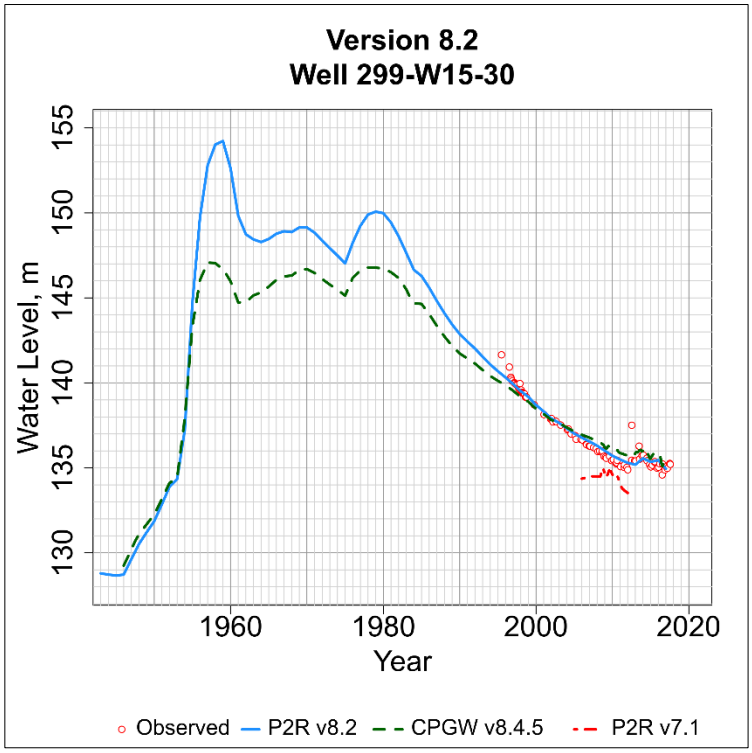

Figure D-204. Observed and simulated water level in the P2R Model at well 299-W15-30.png.

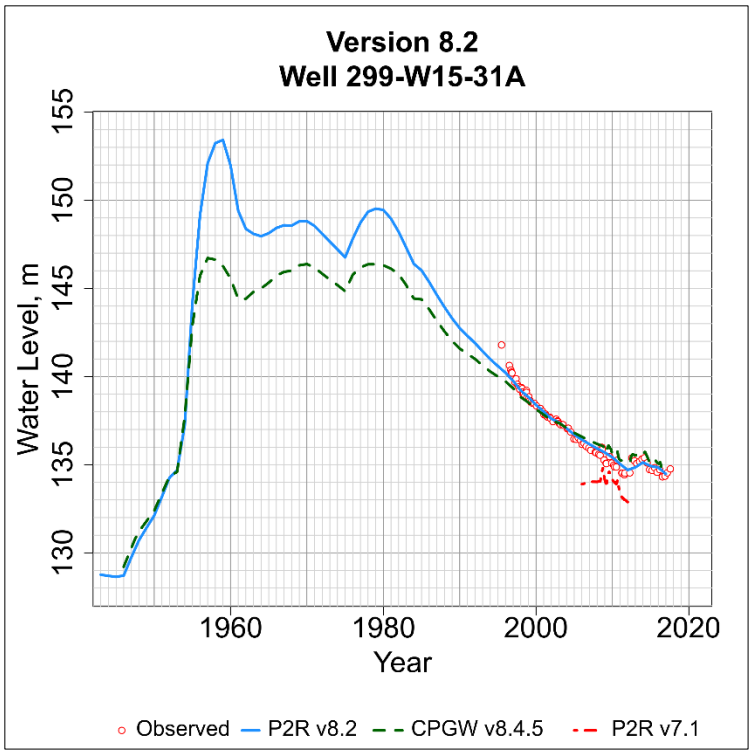

Figure D-205. Observed and simulated water level in the P2R Model at well 299-W15-31A.png.

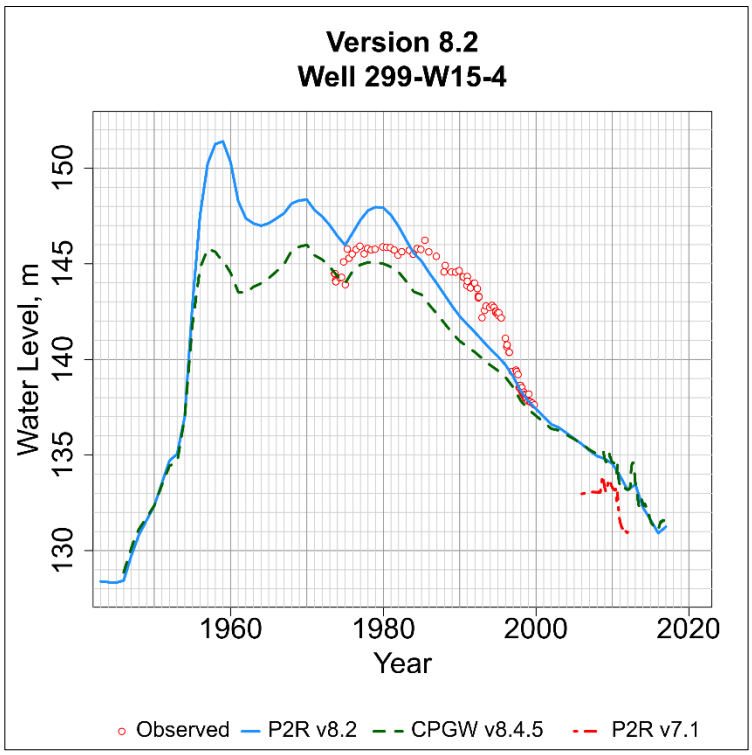

Figure D-206. Observed and simulated water level in the P2R Model at well 299-W15-4.png.

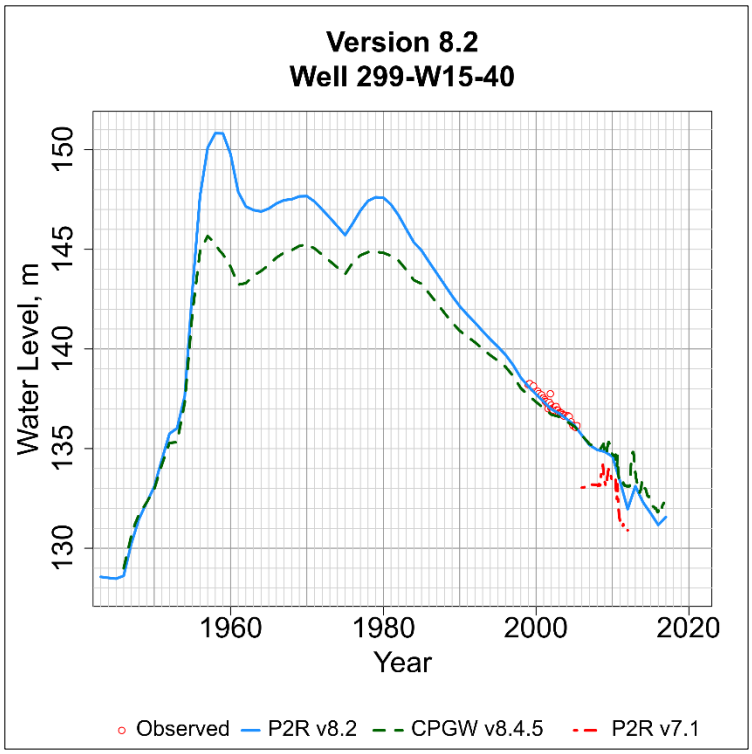

Figure D-207. Observed and simulated water level in the P2R Model at well 299-W15-40.png.

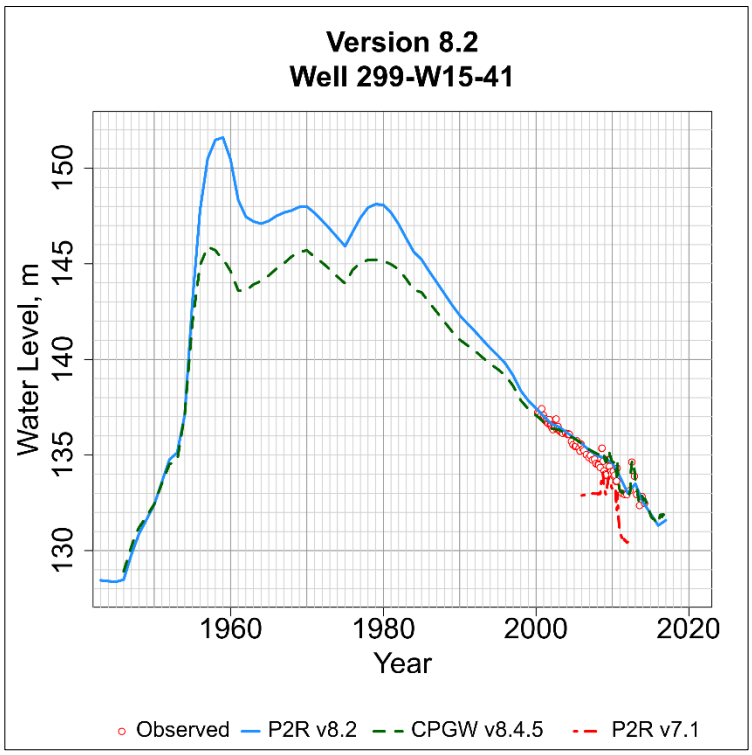

Figure D-208. Observed and simulated water level in the P2R Model at well 299-W15-41.png.

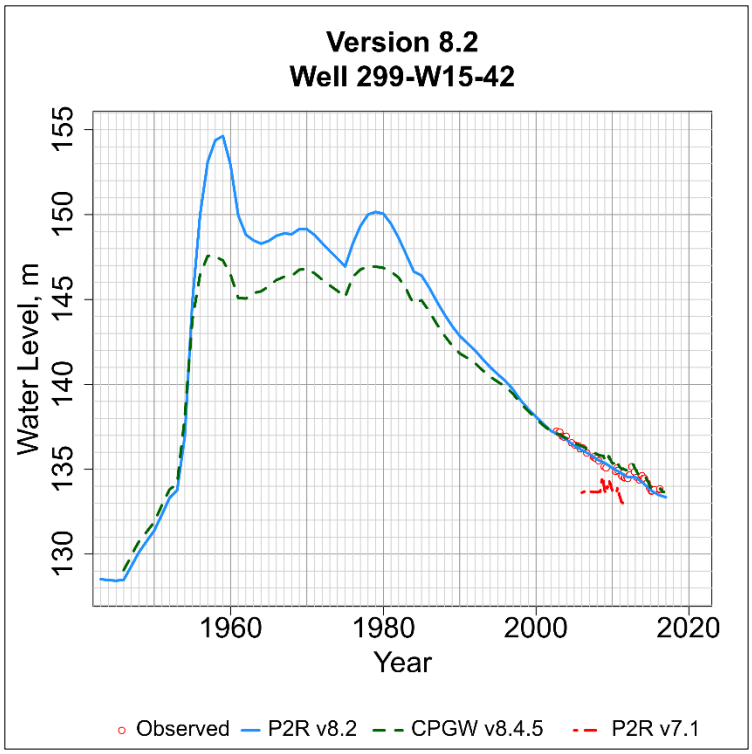

Figure D-209. Observed and simulated water level in the P2R Model at well 299-W15-42.png.

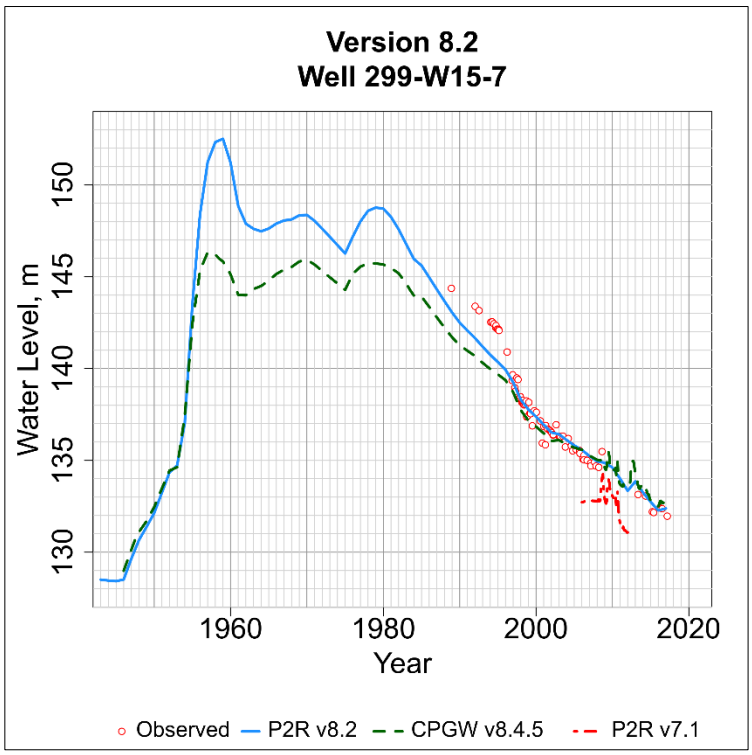

Figure D-210. Observed and simulated water level in the P2R Model at well 299-W15-7.png.

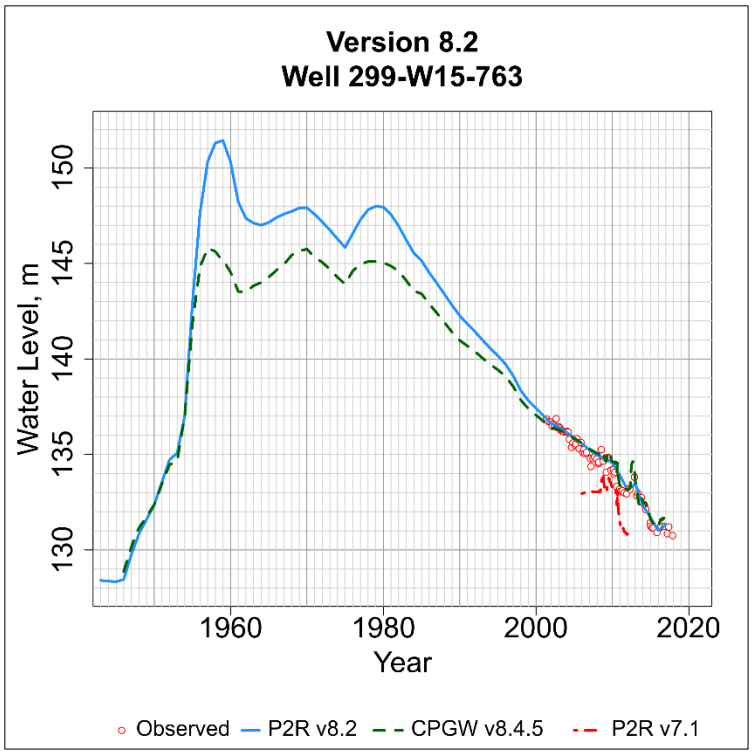

Figure D-211. Observed and simulated water level in the P2R Model at well 299-W15-763.png.

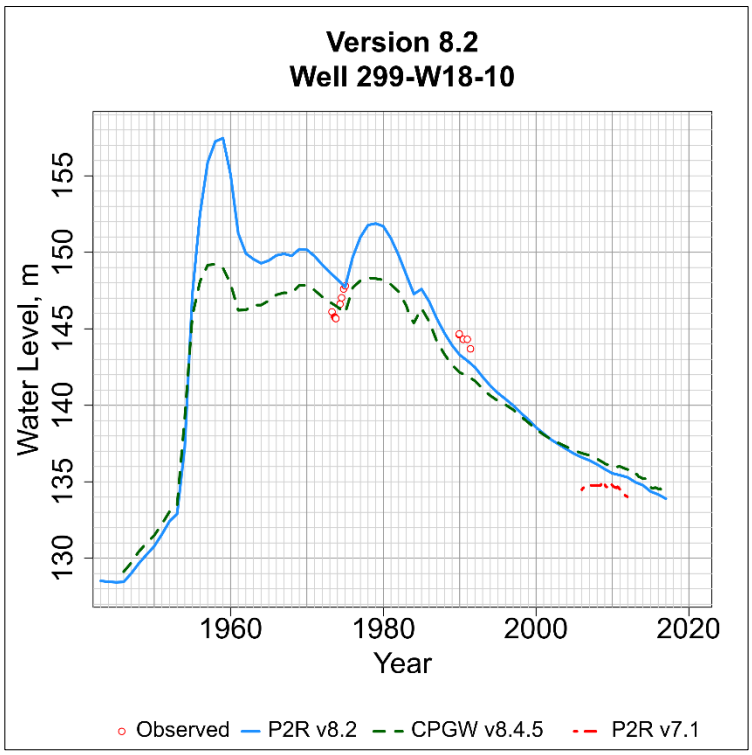

Figure D-212. Observed and simulated water level in the P2R Model at well 299-W18-10.png.

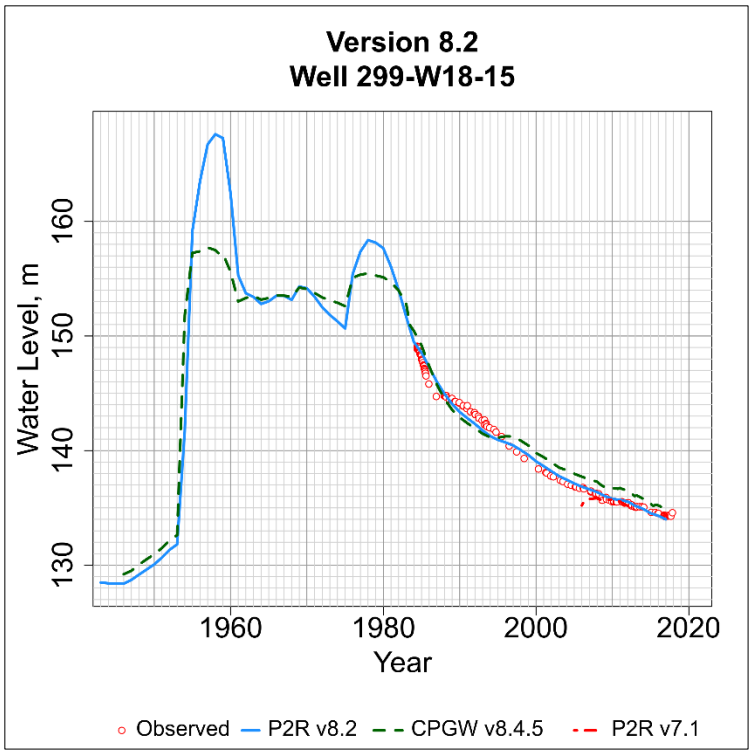

Figure D-213. Observed and simulated water level in the P2R Model at well 299-W18-15.png.

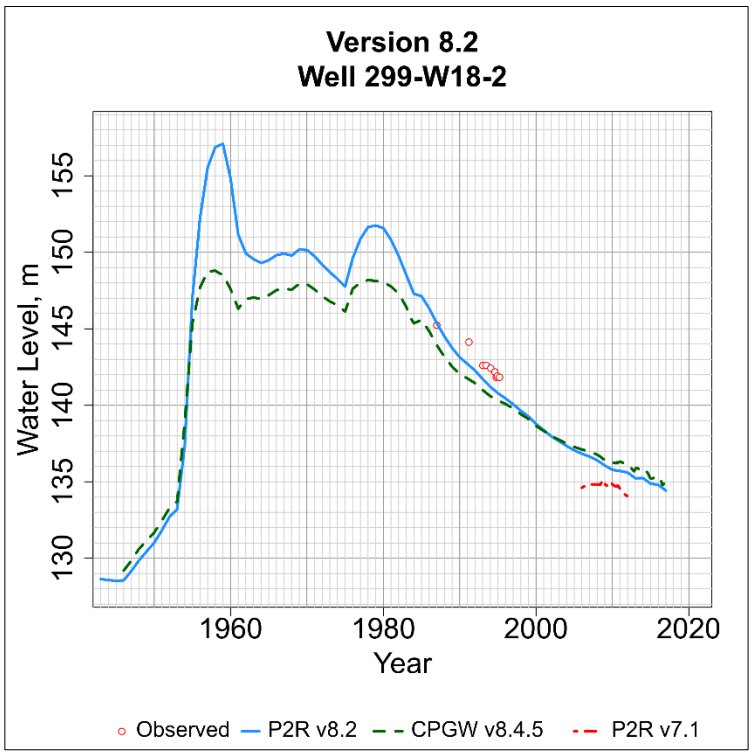

Figure D-214. Observed and simulated water level in the P2R Model at well 299-W18-2.png.

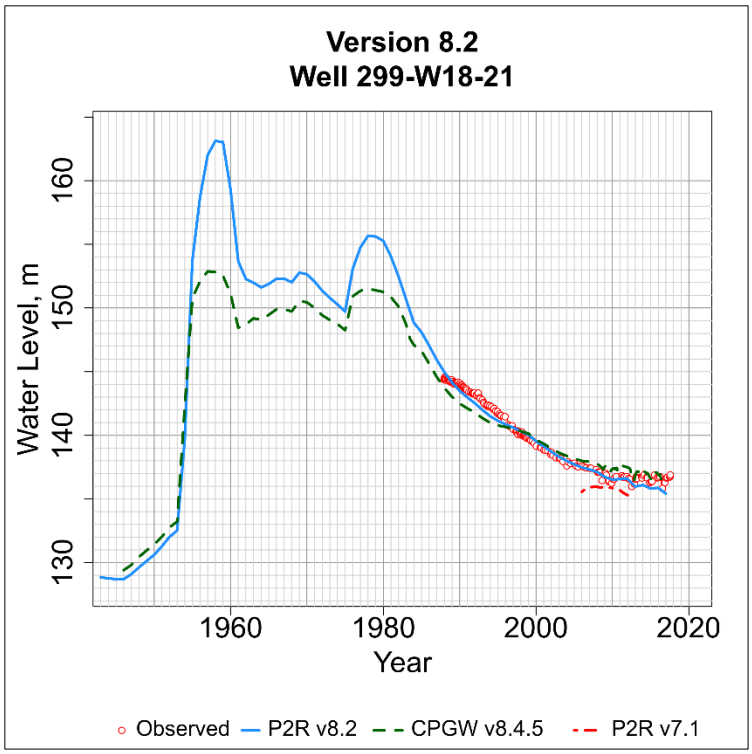

Figure D-215. Observed and simulated water level in the P2R Model at well 299-W18-21.png.

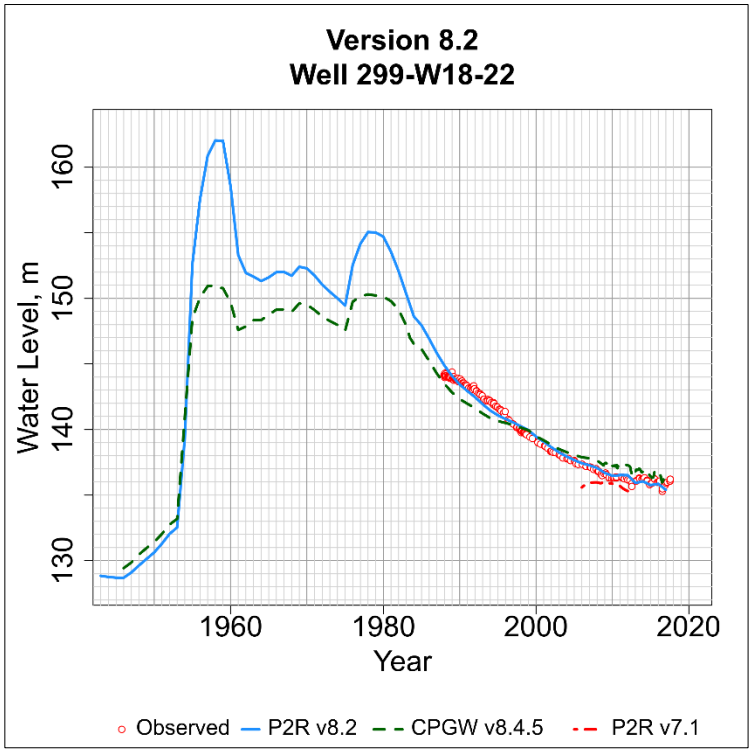

Figure D-216. Observed and simulated water level in the P2R Model at well 299-W18-22.png.

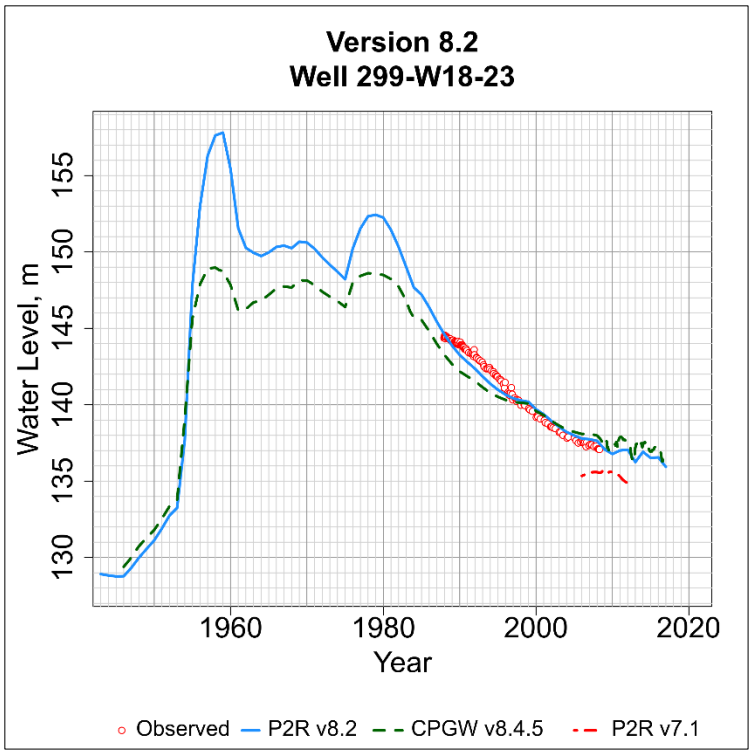

Figure D-217. Observed and simulated water level in the P2R Model at well 299-W18-23.png.

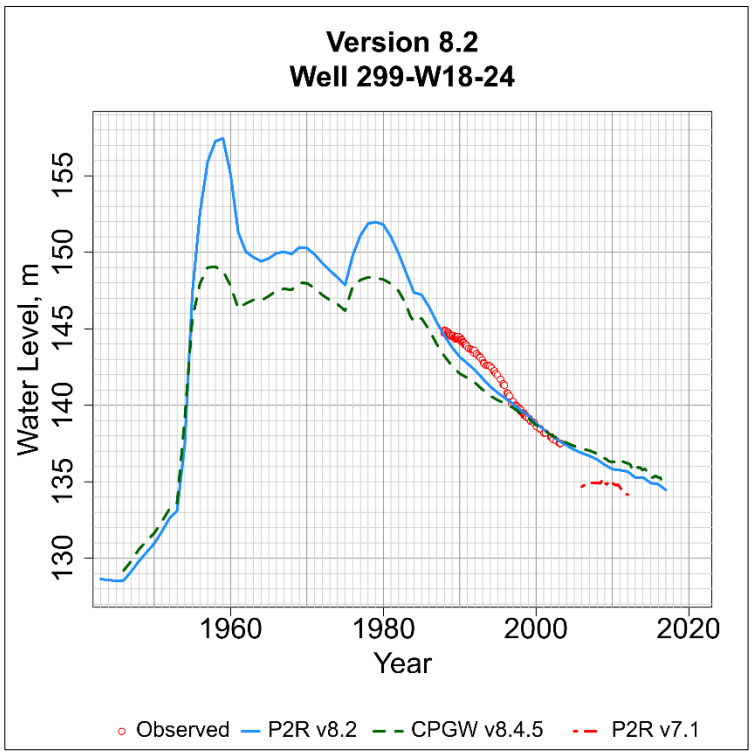

Figure D-218. Observed and simulated water level in the P2R Model at well 299-W18-24.png.

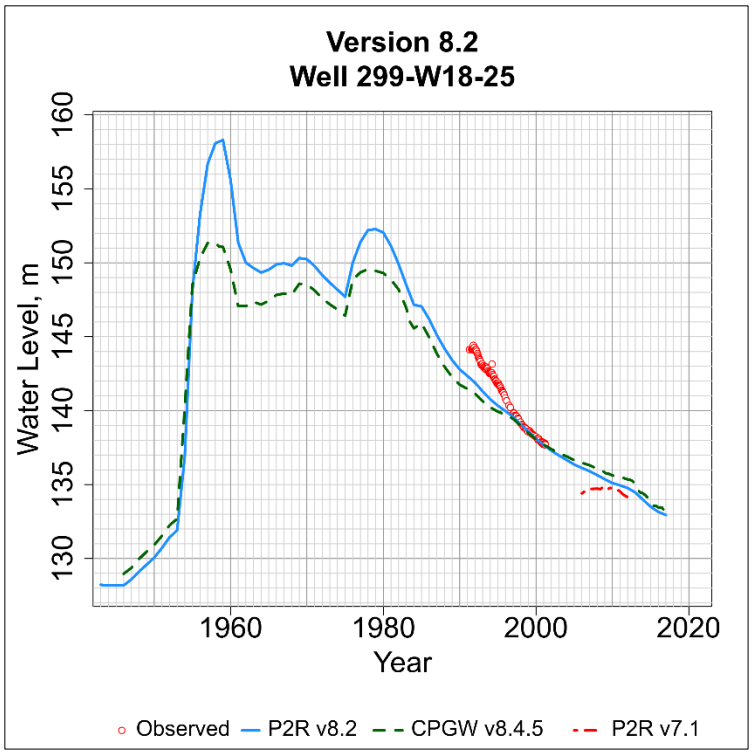

Figure D-219. Observed and simulated water level in the P2R Model at well 299-W18-25.png.

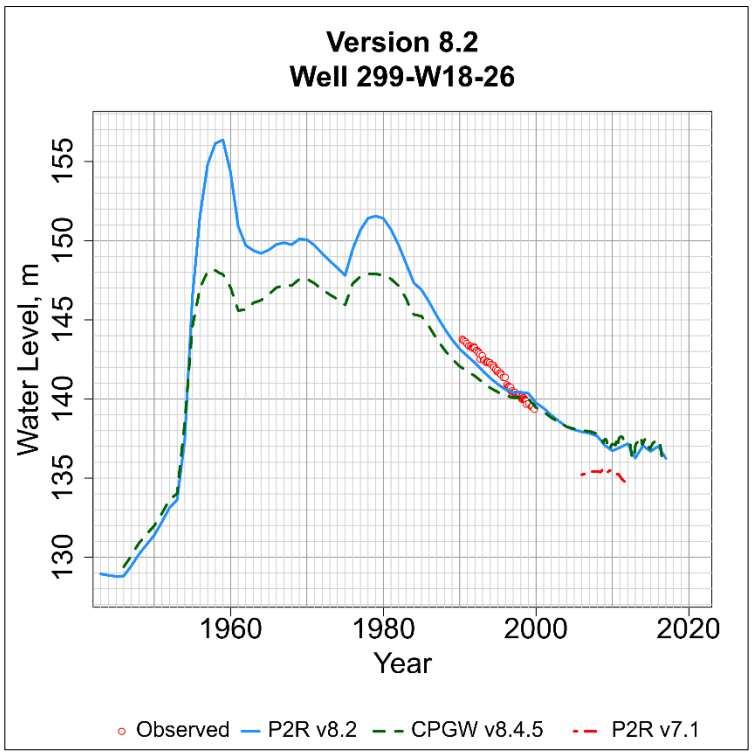

Figure D-220. Observed and simulated water level in the P2R Model at well 299-W18-26.png.

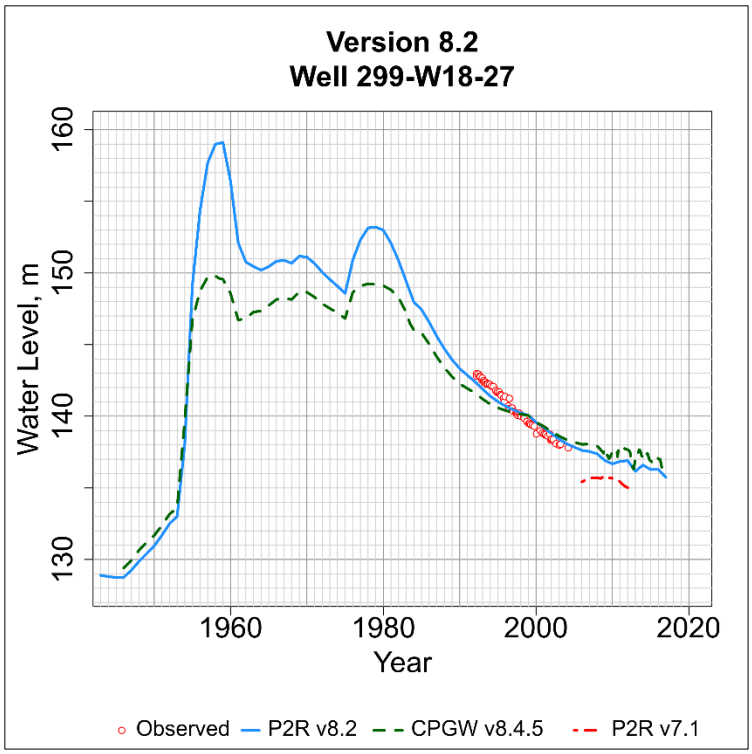

Figure D-221. Observed and simulated water level in the P2R Model at well 299-W18-27.png.

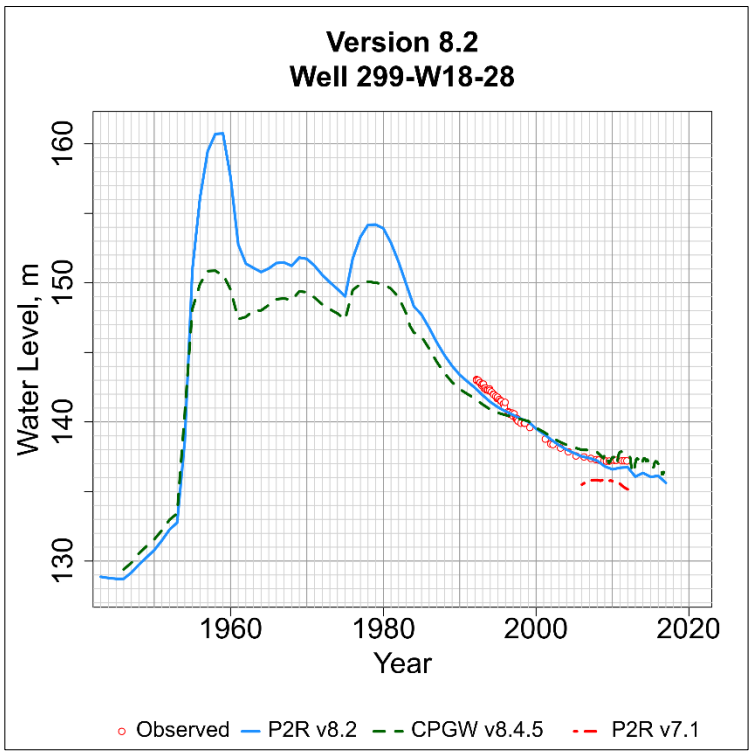

Figure D-222. Observed and simulated water level in the P2R Model at well 299-W18-28.png.

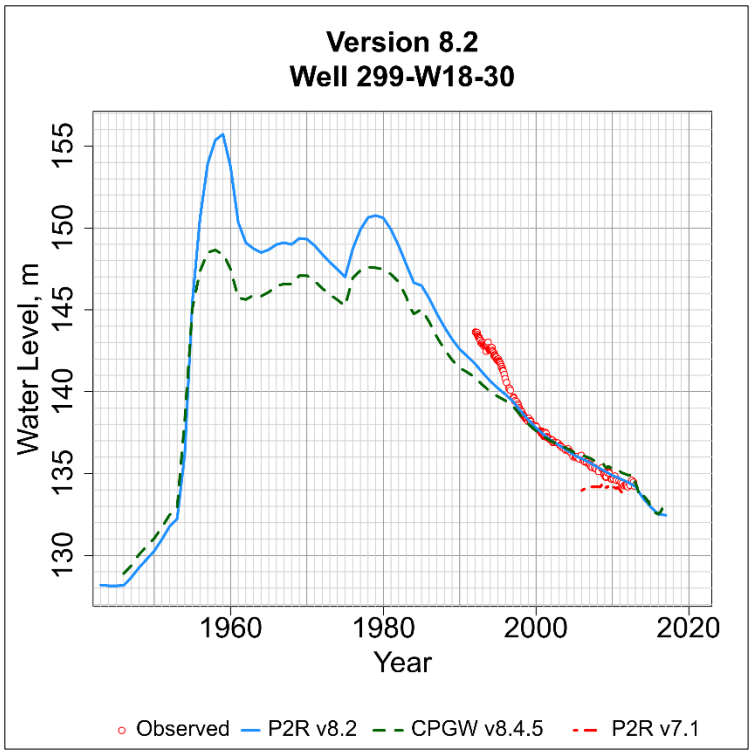

Figure D-223. Observed and simulated water level in the P2R Model at well 299-W18-30.png.

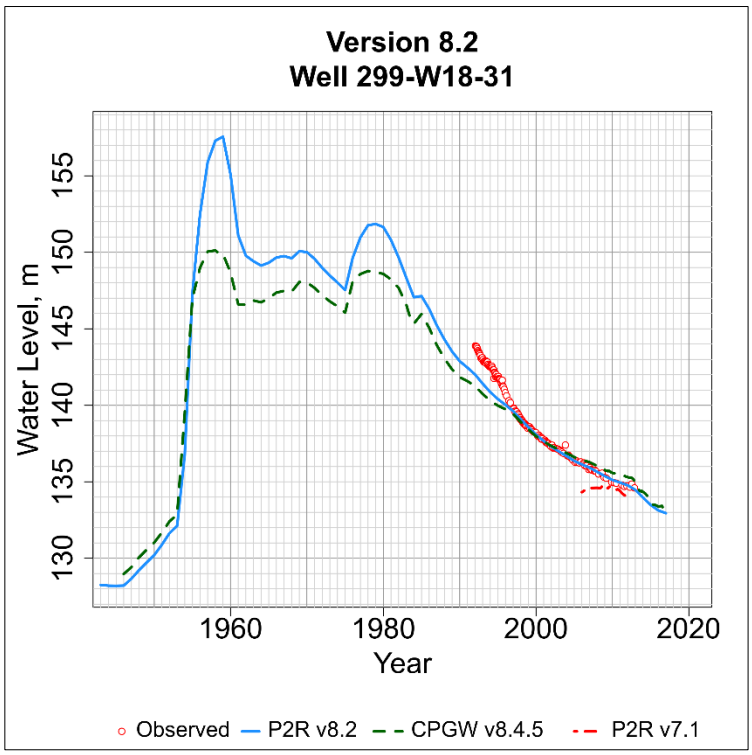

Figure D-224. Observed and simulated water level in the P2R Model at well 299-W18-31.png.

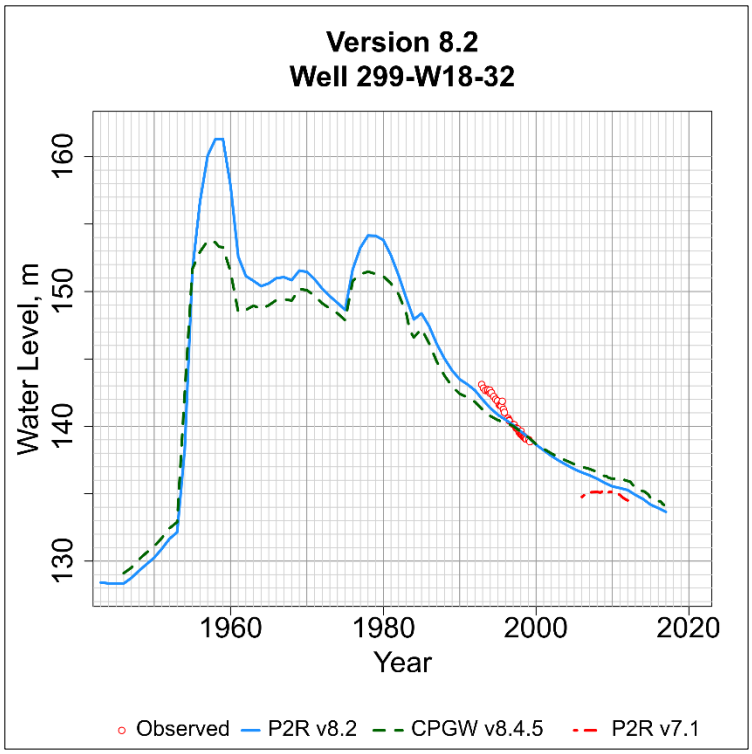

Figure D-225. Observed and simulated water level in the P2R Model at well 299-W18-32.png.

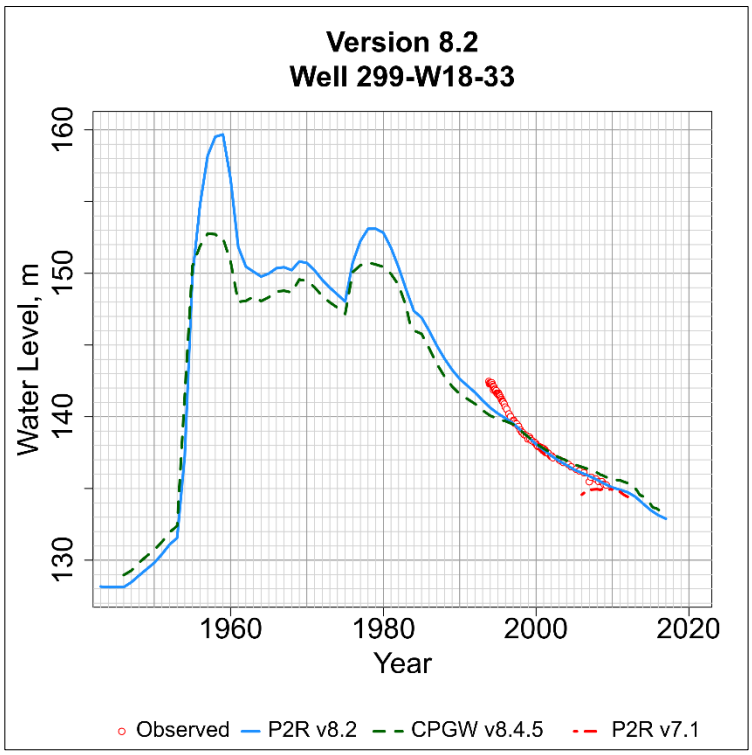

Figure D-226. Observed and simulated water level in the P2R Model at well 299-W18-33.png.

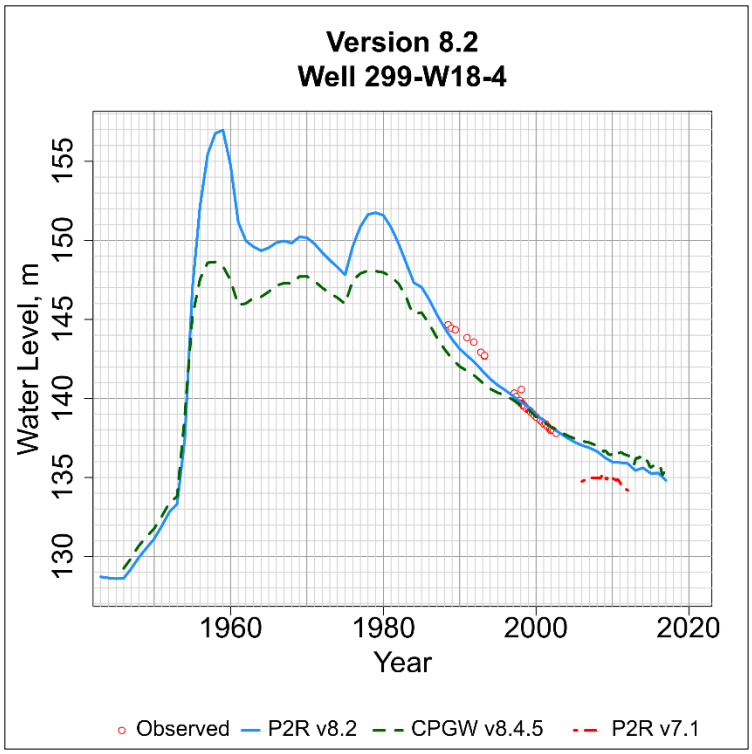

Figure D-227. Observed and simulated water level in the P2R Model at well 299-W18-4.png.

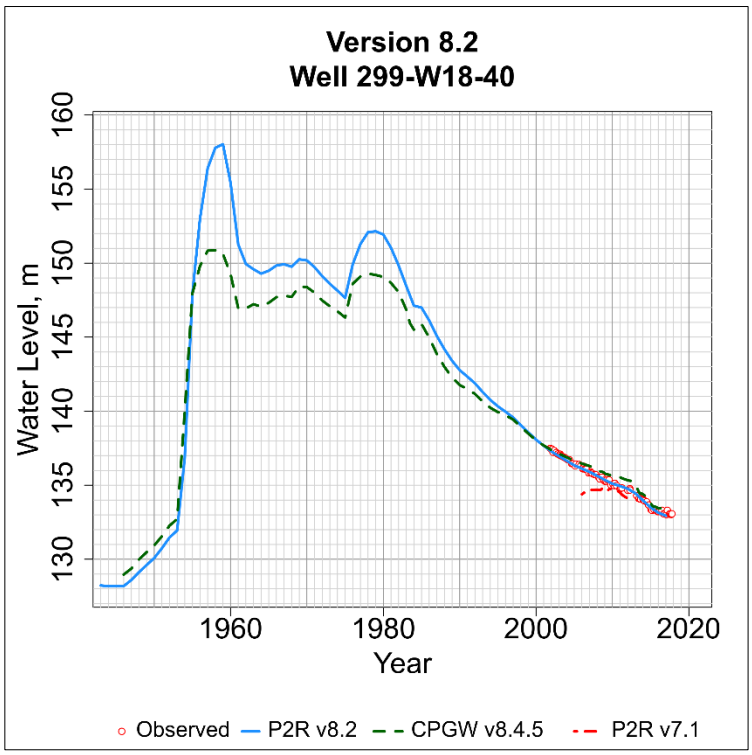

Figure D-228. Observed and simulated water level in the P2R Model at well 299-W18-40.png.

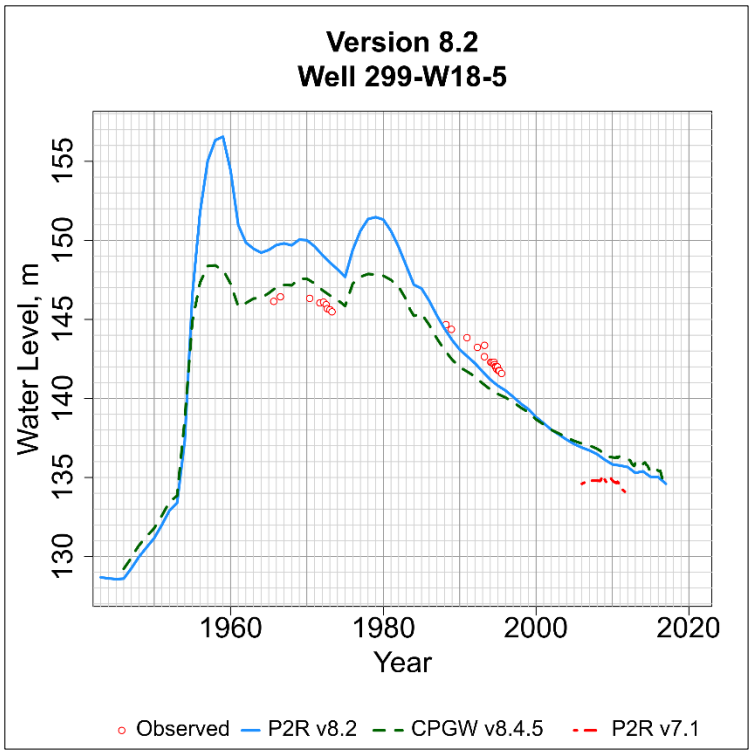

Figure D-229. Observed and simulated water level in the P2R Model at well 299-W18-5.png.

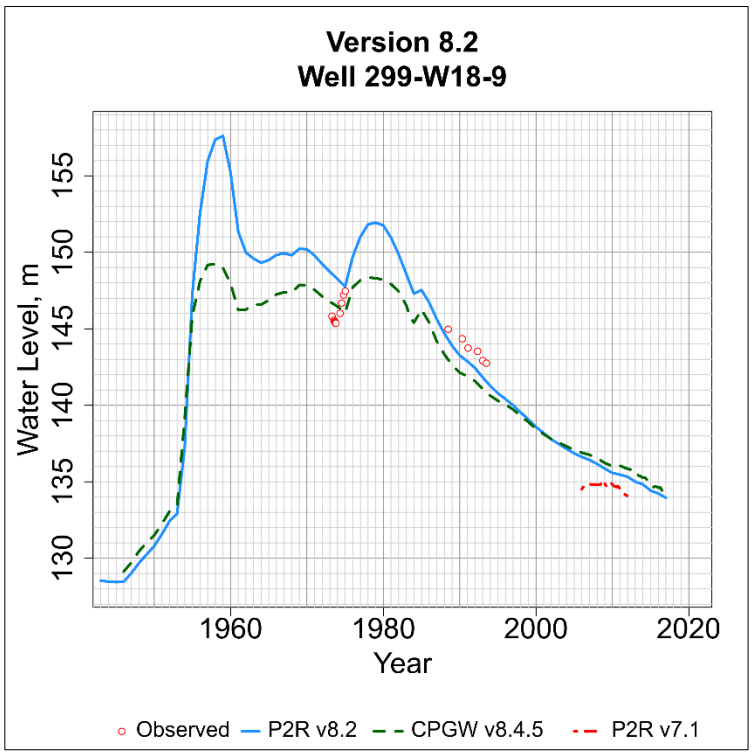

Figure D-230. Observed and simulated water level in the P2R Model at well 299-W18-9.png.

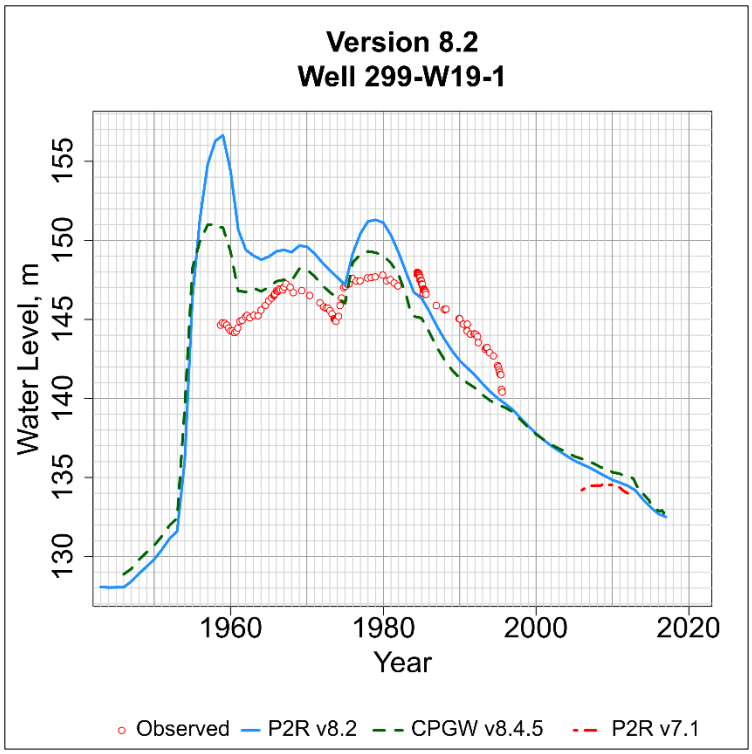

Figure D-231. Observed and simulated water level in the P2R Model at well 299-W19-1.png.

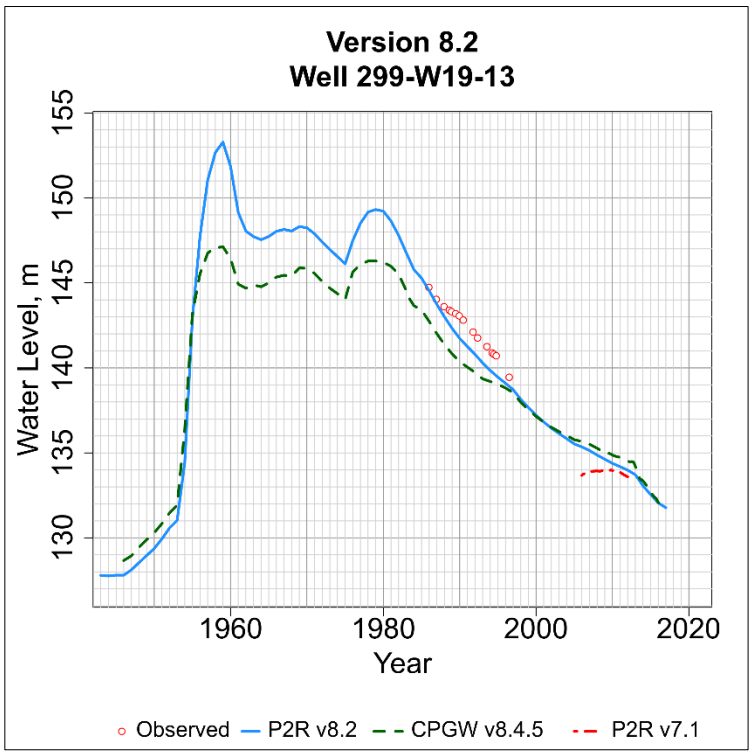

Figure D-232. Observed and simulated water level in the P2R Model at well 299-W19-13.png.

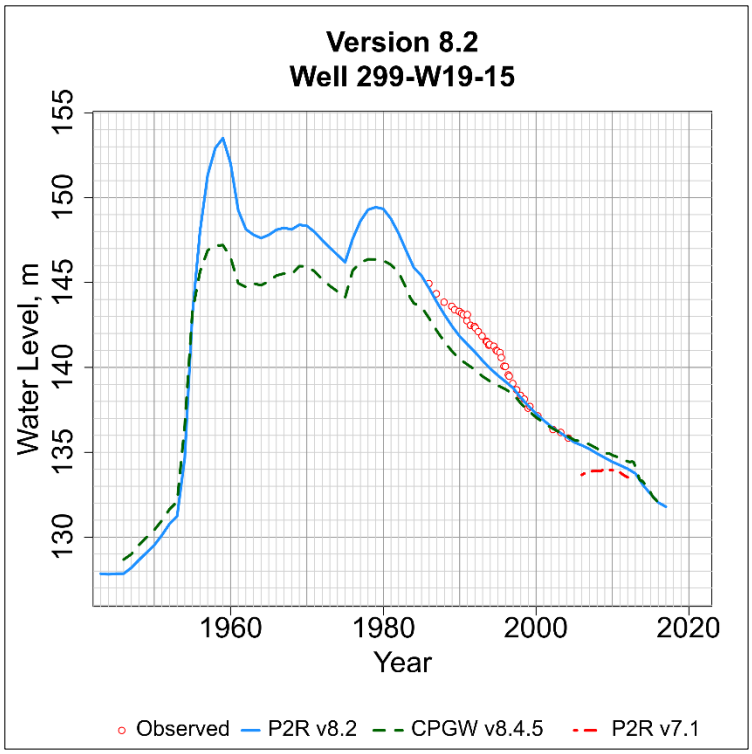

Figure D-233. Observed and simulated water level in the P2R Model at well 299-W19-15.png.

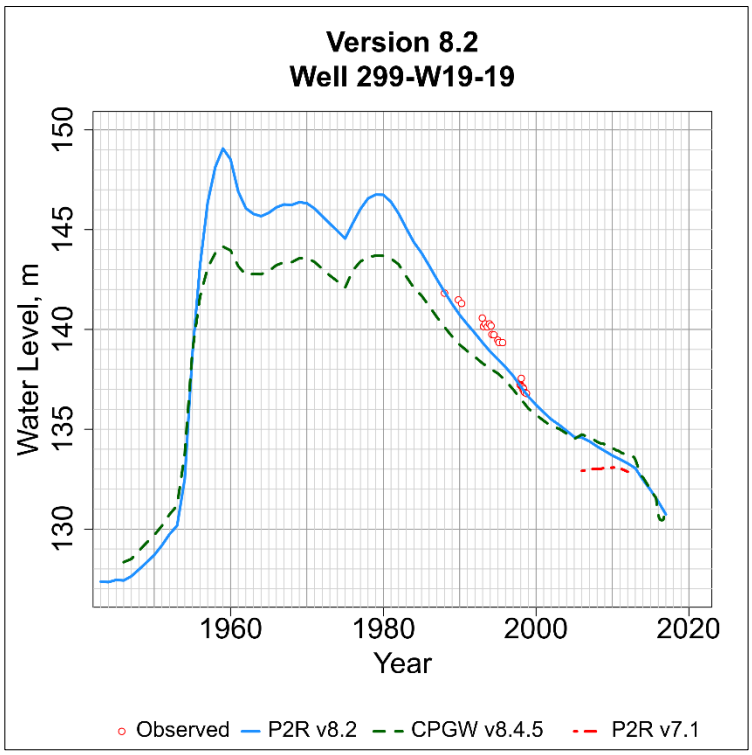

Figure D-234. Observed and simulated water level in the P2R Model at well 299-W19-19.png.

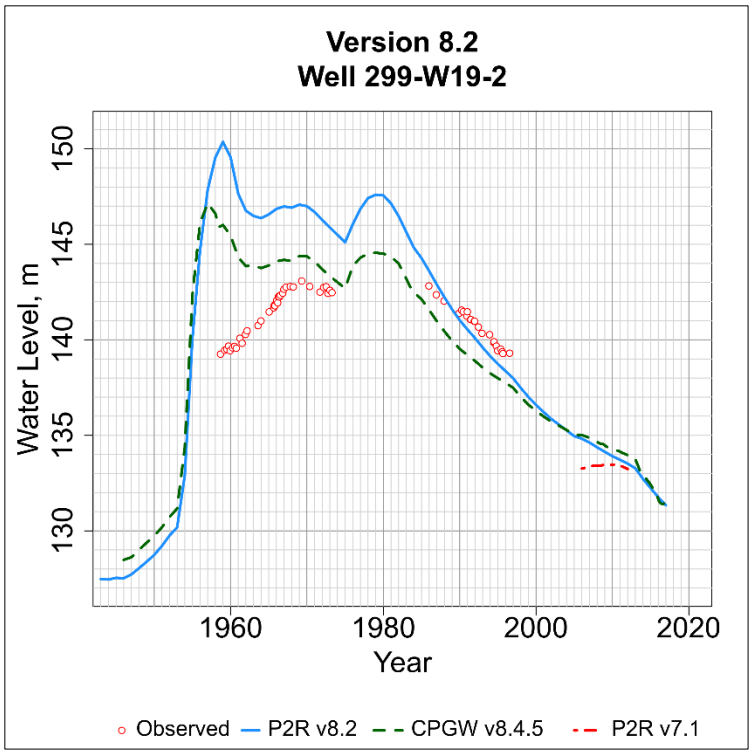

Figure D-235. Observed and simulated water level in the P2R Model at well 299-W19-2.png.

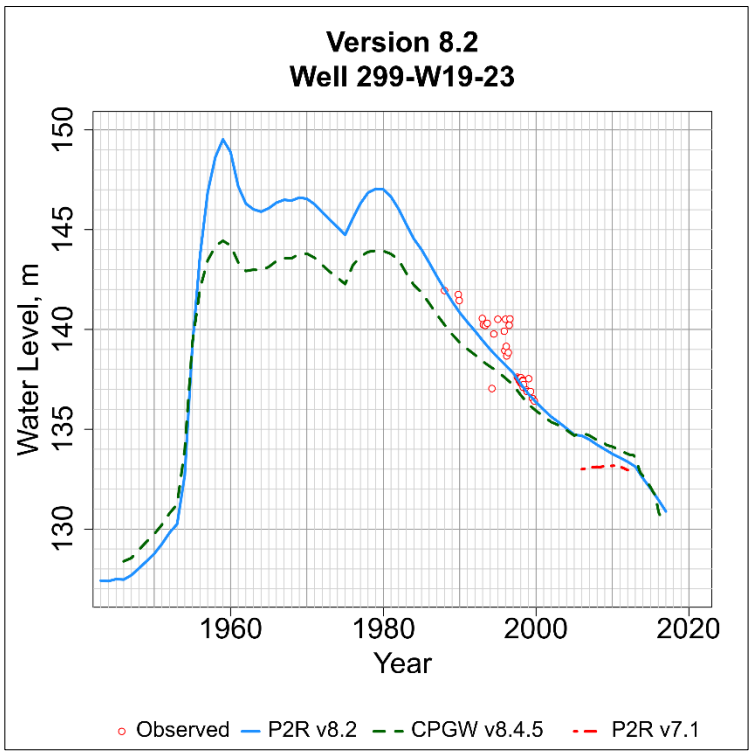

Figure D-236. Observed and simulated water level in the P2R Model at well 299-W19-23.png.

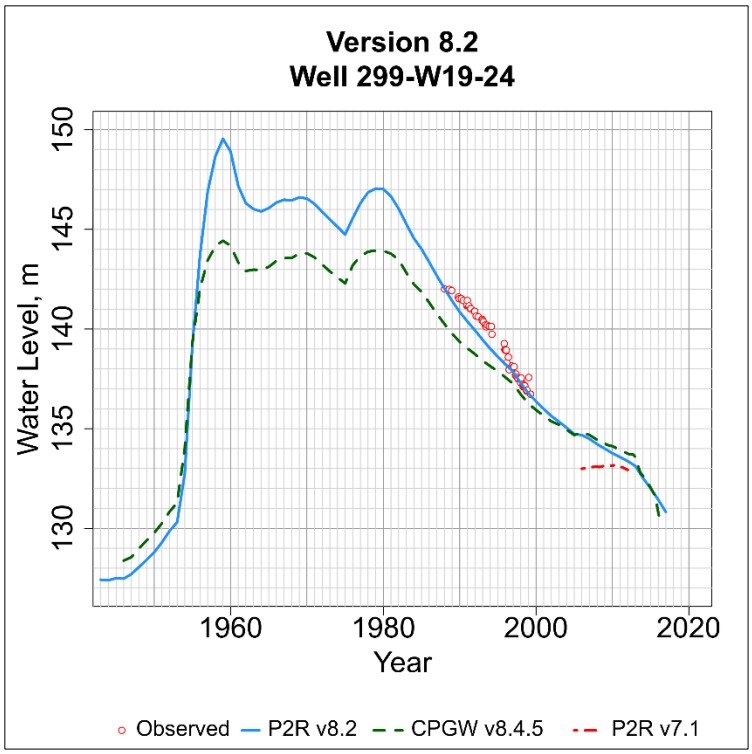

Figure D-237. Observed and simulated water level in the P2R Model at well 299-W19-24.png.

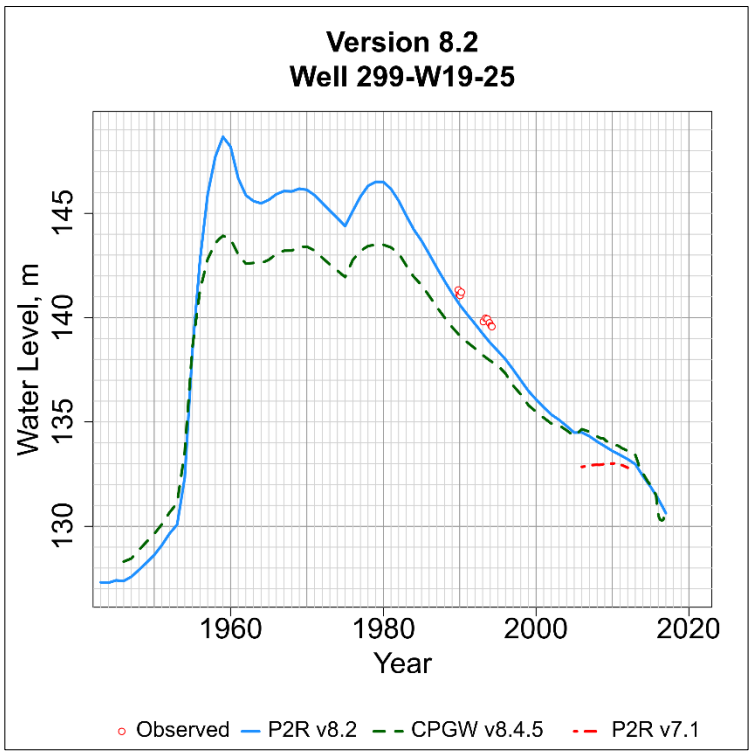

Figure D-238. Observed and simulated water level in the P2R Model at well 299-W19-25.png.

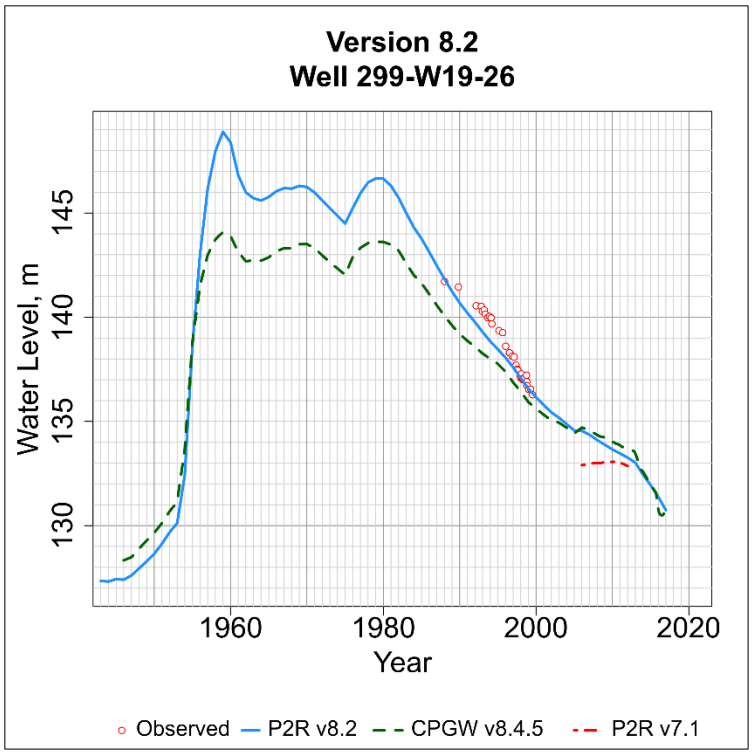

Figure D-239. Observed and simulated water level in the P2R Model at well 299-W19-26.png.

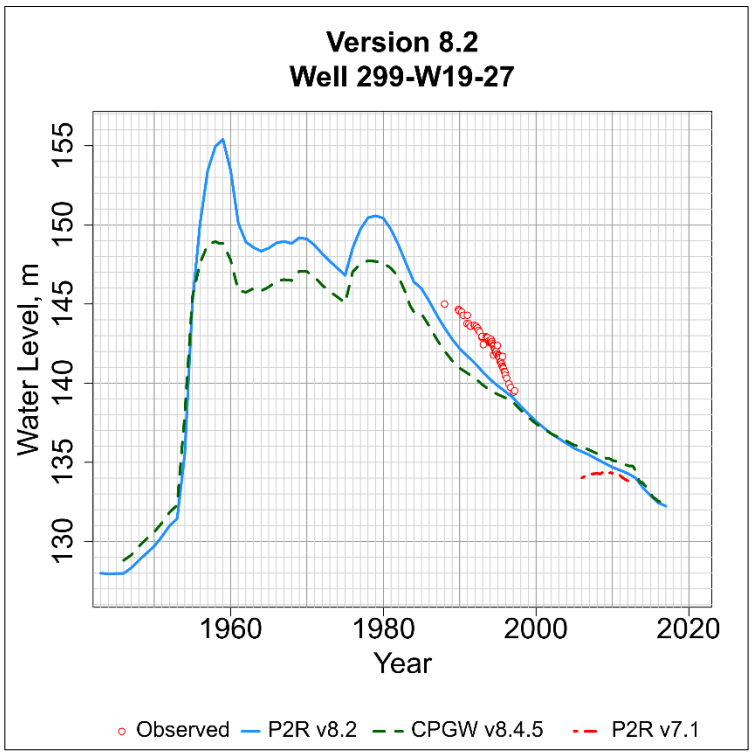

Figure D-240. Observed and simulated water level in the P2R Model at well 299-W19-27.png.

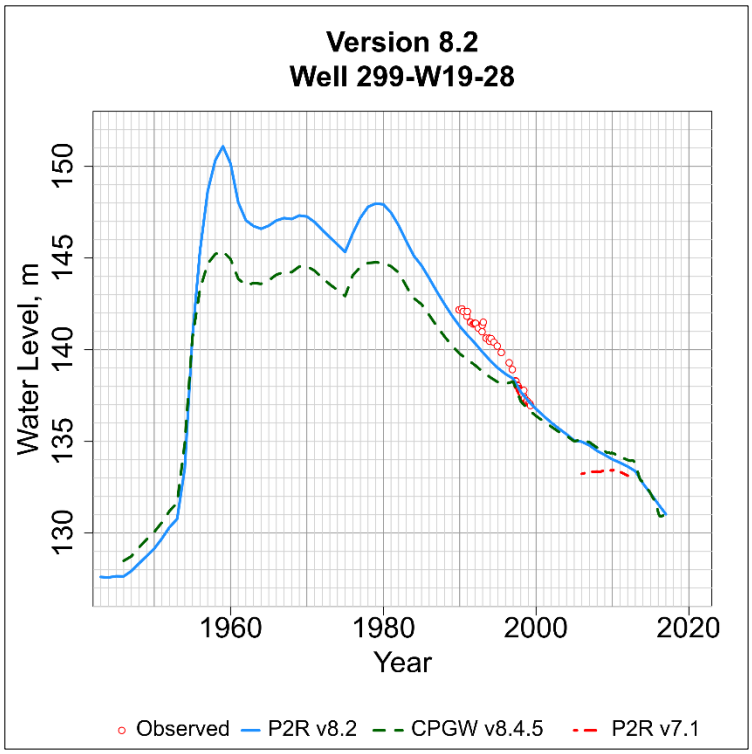

Figure D-241. Observed and simulated water level in the P2R Model at well 299-W19-28.png.

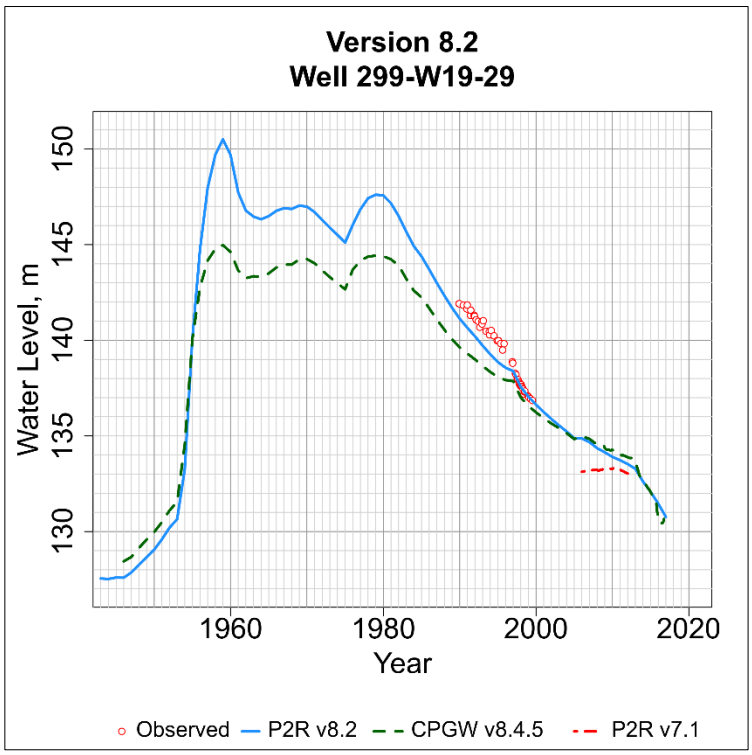

Figure D-242. Observed and simulated water level in the P2R Model at well 299-W19-29.png.

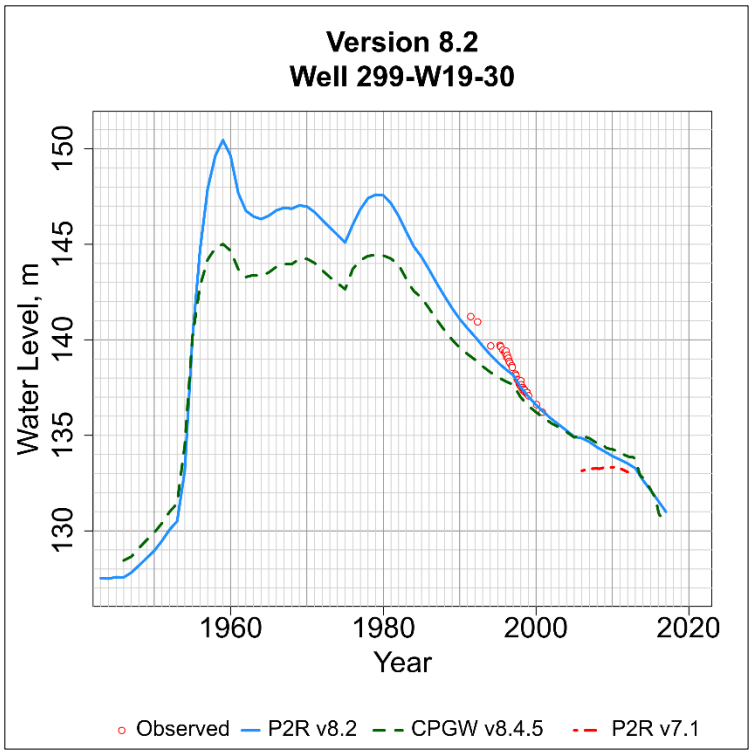

Figure D-243. Observed and simulated water level in the P2R Model at well 299-W19-30.png.

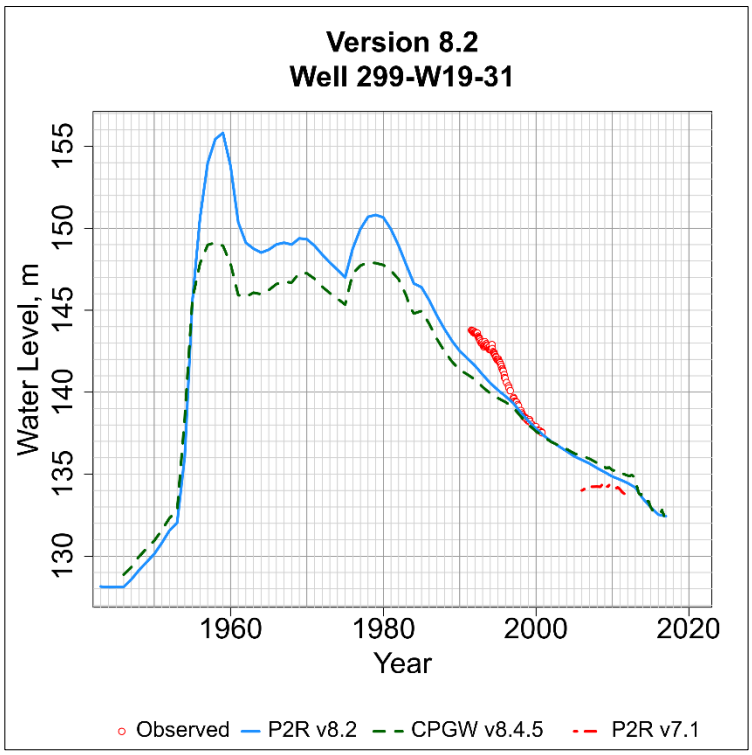

Figure D-244. Observed and simulated water level in the P2R Model at well 299-W19-31.png.

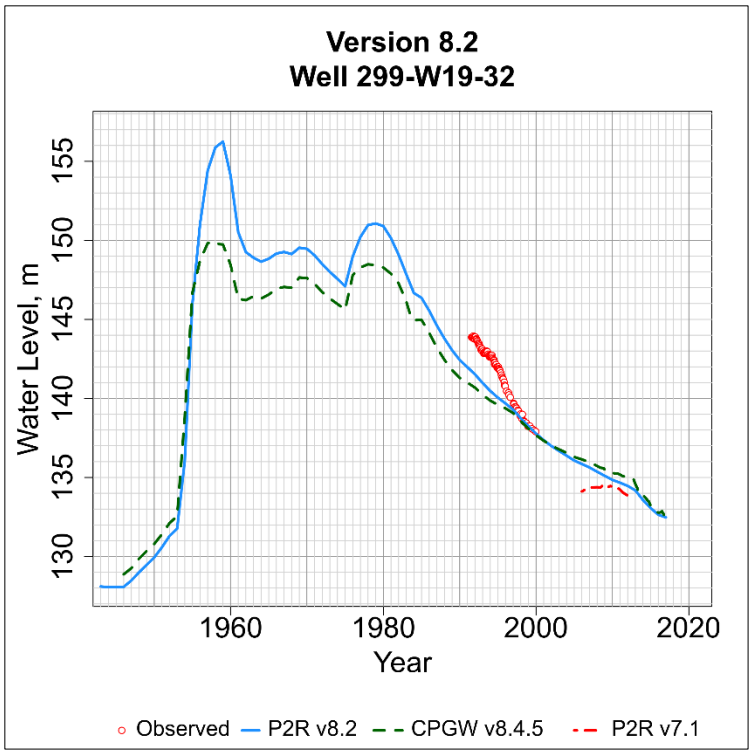

Figure D-245. Observed and simulated water level in the P2R Model at well 299-W19-32.png.

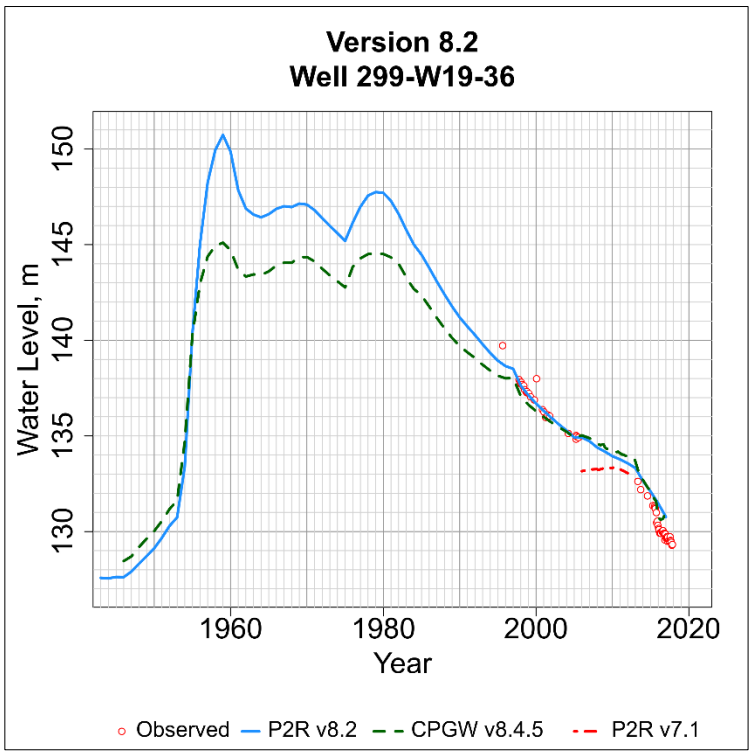

Figure D-246. Observed and simulated water level in the P2R Model at well 299-W19-36.png.

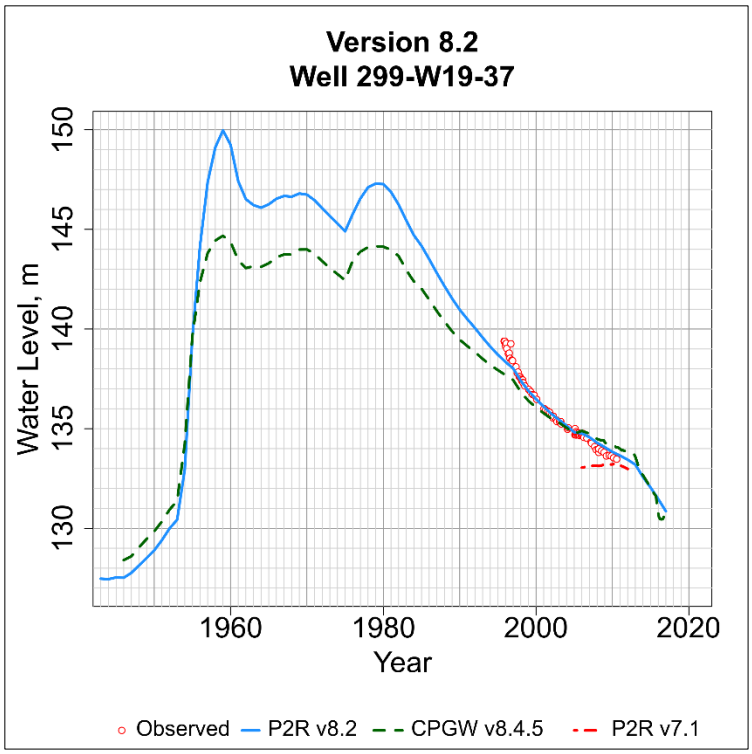

Figure D-247. Observed and simulated water level in the P2R Model at well 299-W19-37.png.

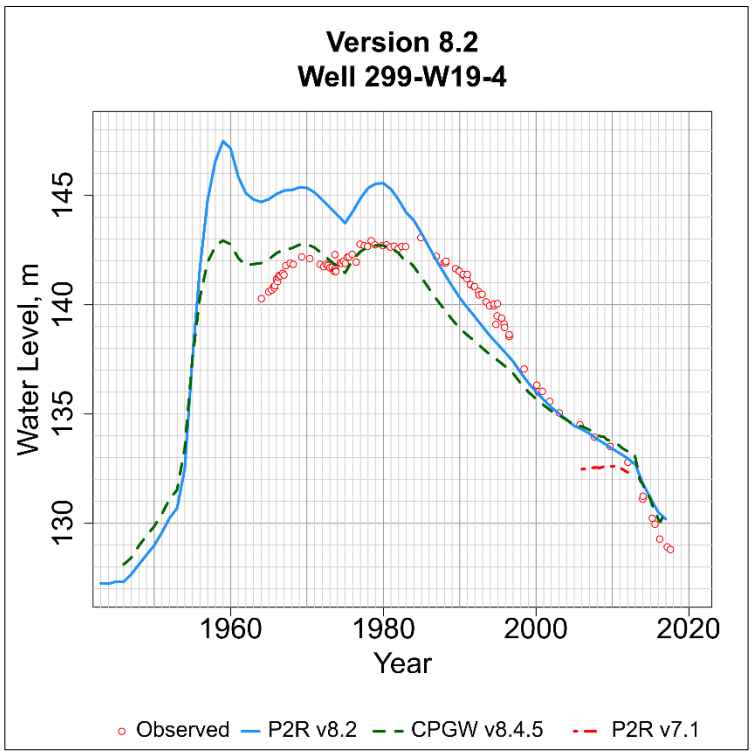

Figure D-248. Observed and simulated water level in the P2R Model at well 299-W19-4.png.

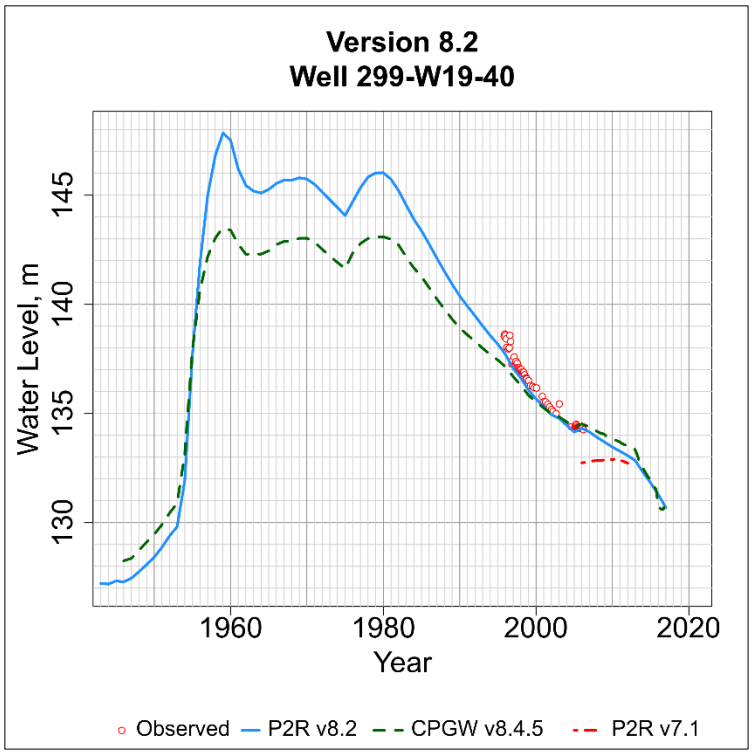

Figure D-249. Observed and simulated water level in the P2R Model at well 299-W19-40.png.

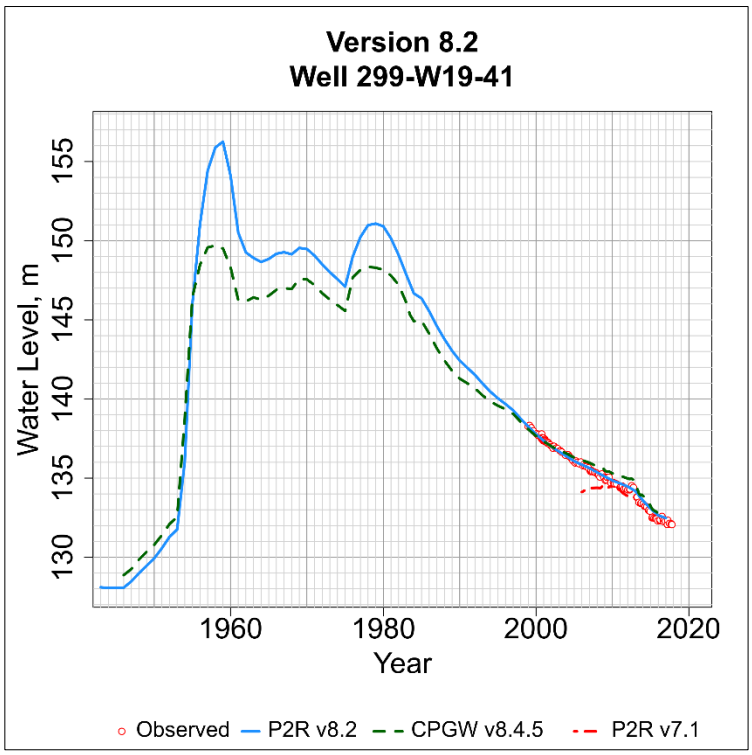

Figure D-250. Observed and simulated water level in the P2R Model at well 299-W19-41.png.

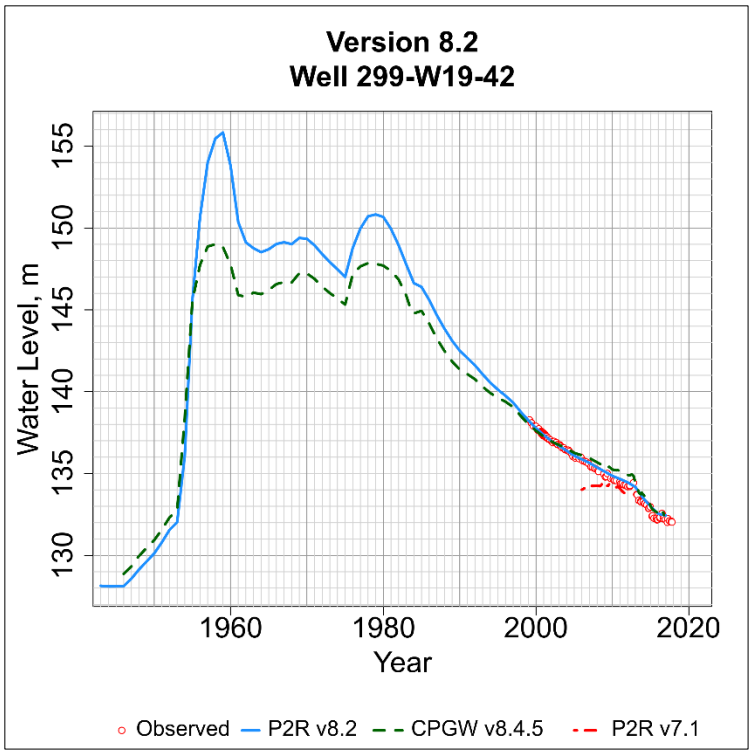

Figure D-251. Observed and simulated water level in the P2R Model at well 299-W19-42.png.

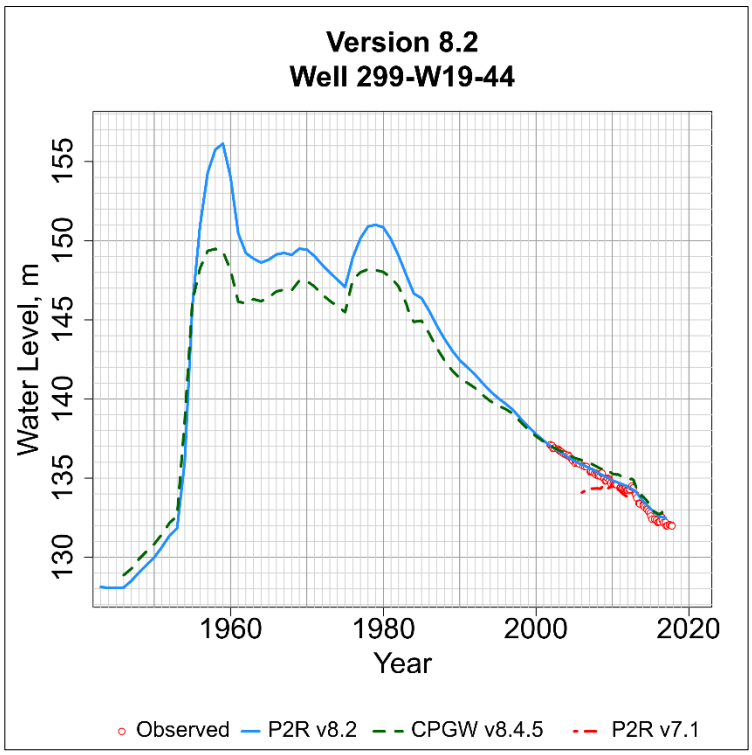

Figure D-252. Observed and simulated water level in the P2R Model at well 299-W19-44.png.

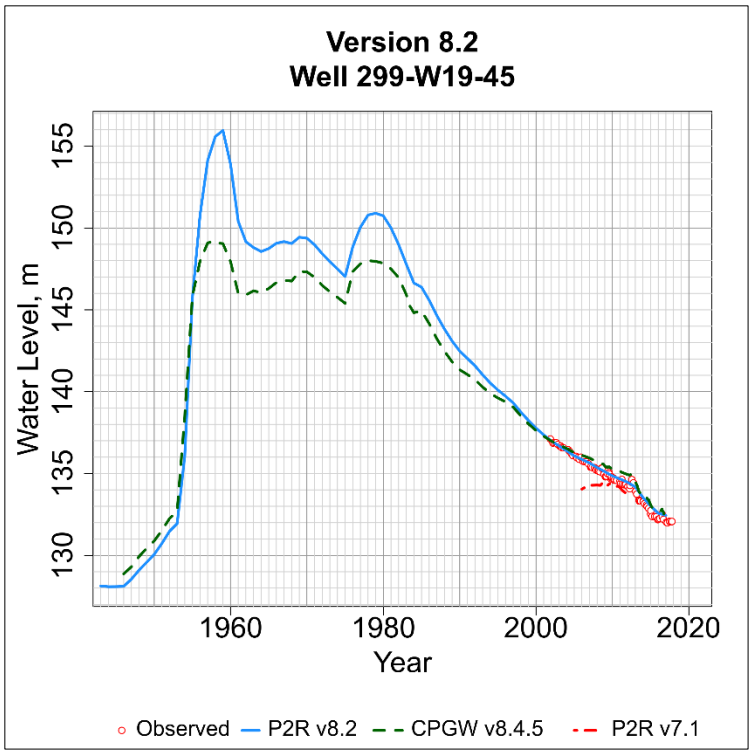

Figure D-253. Observed and simulated water level in the P2R Model at well 299-W19-45.png.

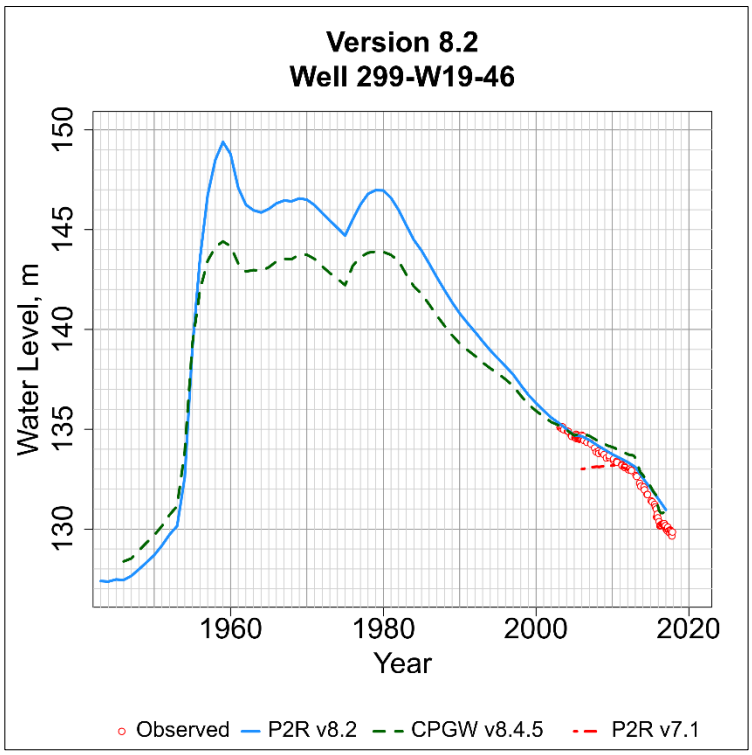

Figure D-254. Observed and simulated water level in the P2R Model at well 299-W19-46.png.

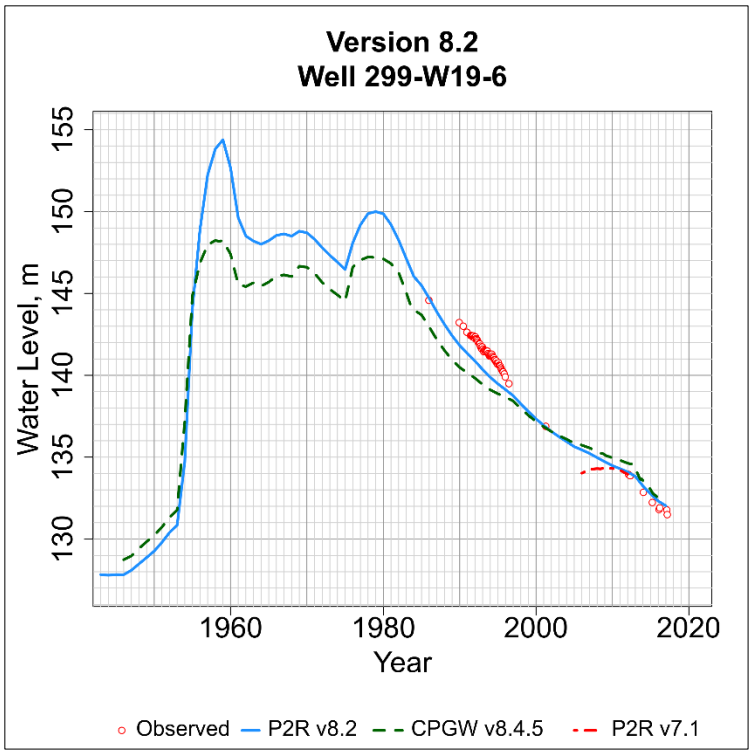

Figure D-255. Observed and simulated water level in the P2R Model at well 299-W19-6.png.

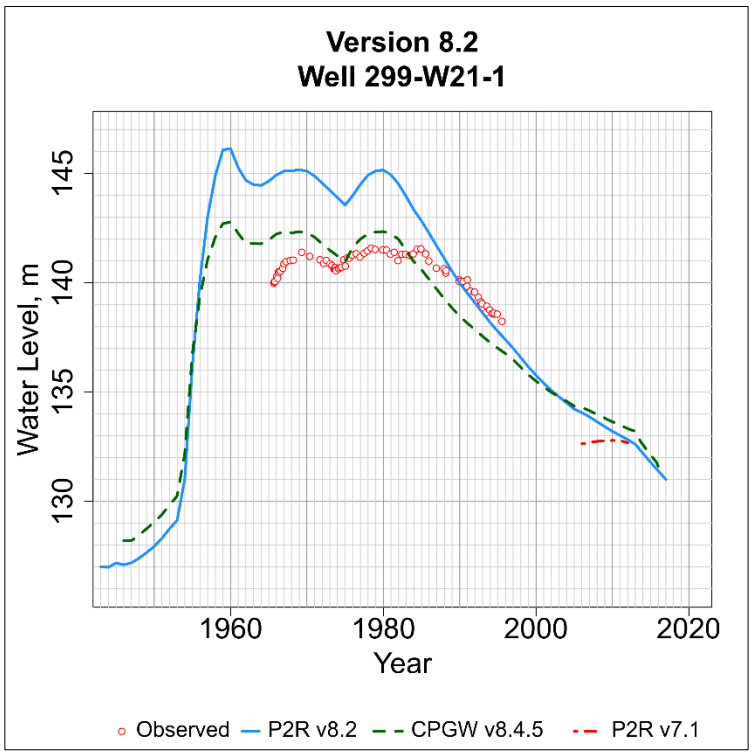

Figure D-256. Observed and simulated water level in the P2R Model at well 299-W21-1.png.

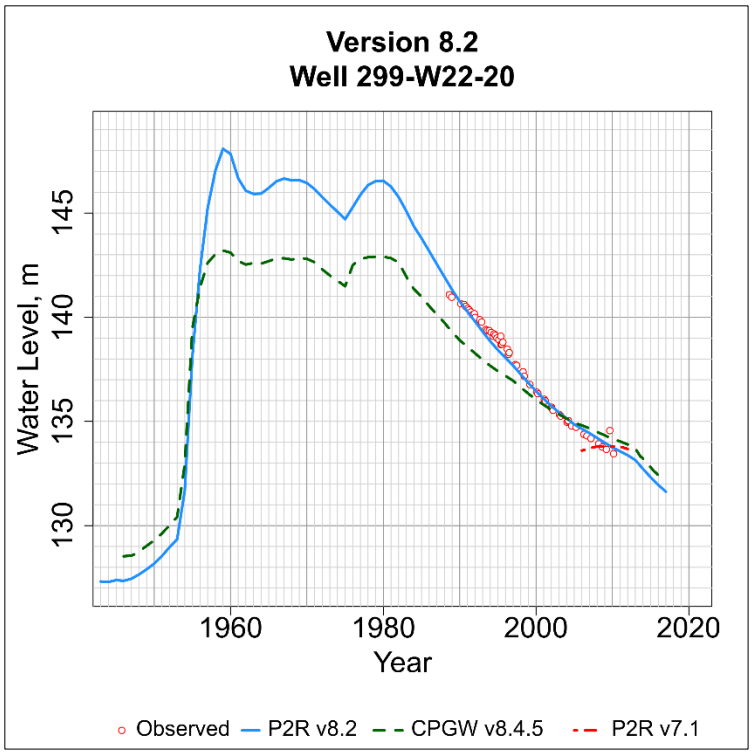

Figure D-257. Observed and simulated water level in the P2R Model at well 299-W22-20.png.

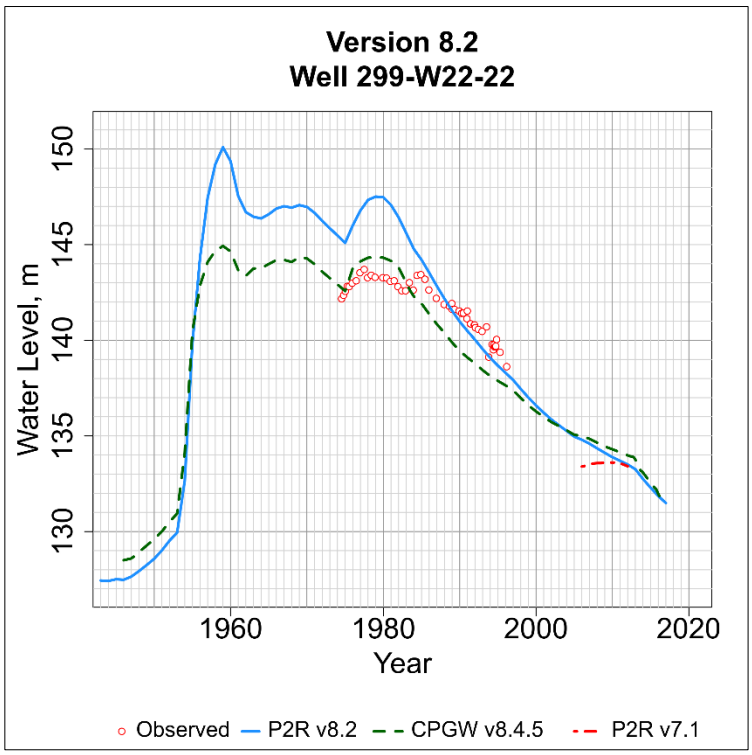

Figure D-258. Observed and simulated water level in the P2R Model at well 299-W22-22.png.

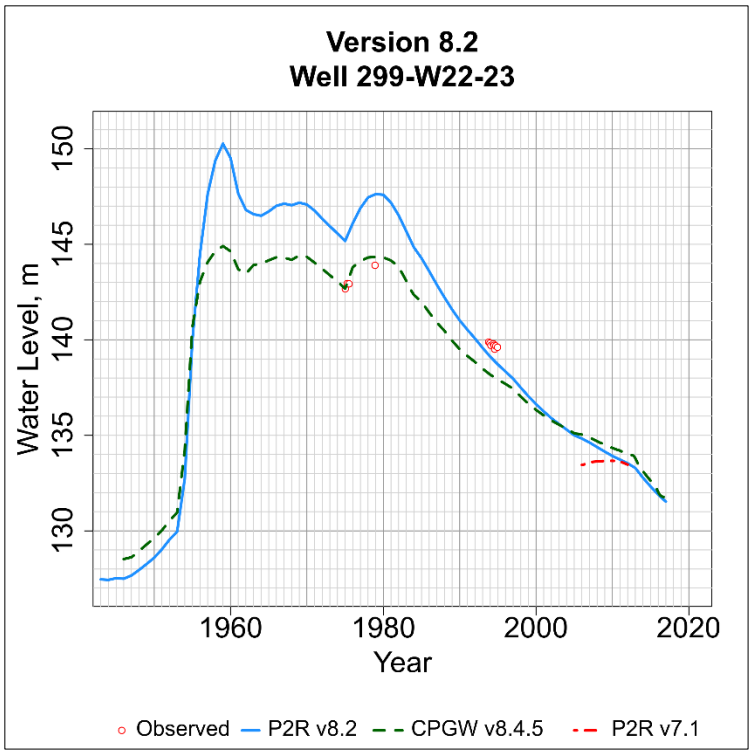

Figure D-259. Observed and simulated water level in the P2R Model at well 299-W22-23.png.

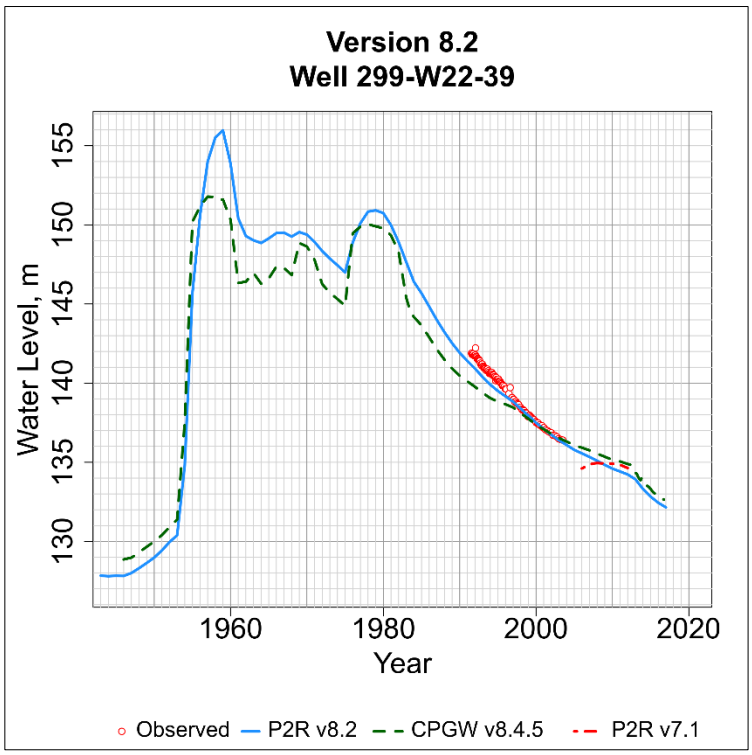

Figure D-260. Observed and simulated water level in the P2R Model at well 299-W22-39.png.

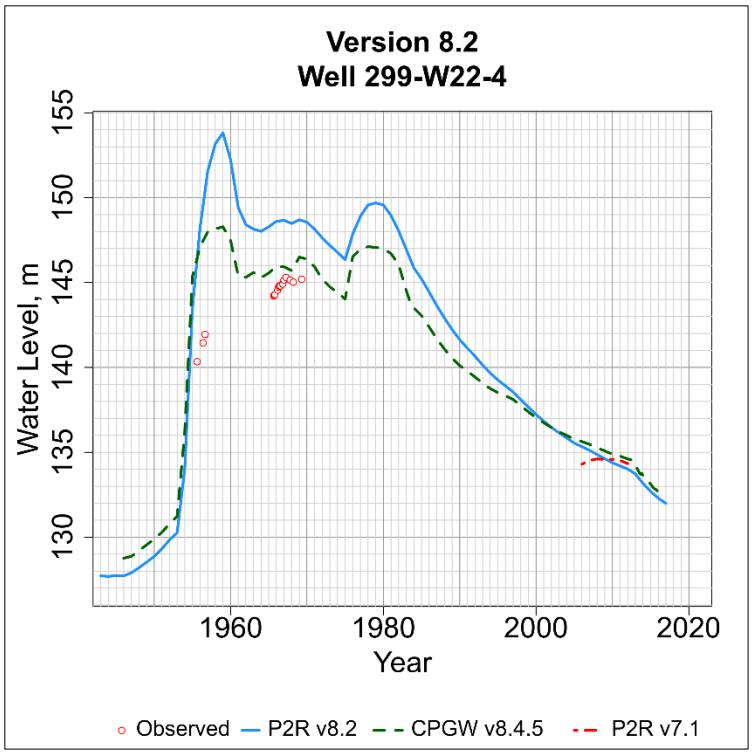

Figure D-261. Observed and simulated water level in the P2R Model at well 299-W22-4.png.

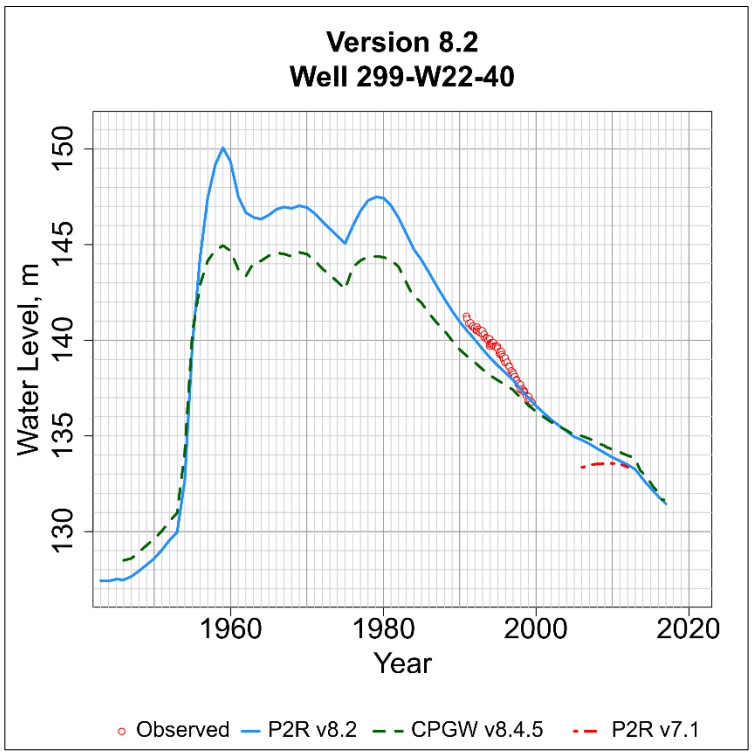

Figure D-262. Observed and simulated water level in the P2R Model at well 299-W22-40.png.

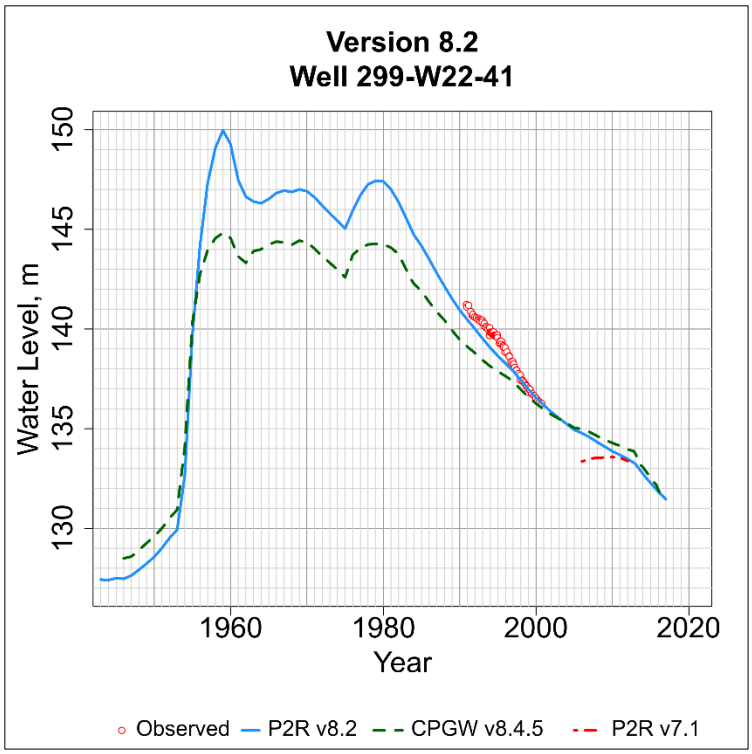

Figure D-263. Observed and simulated water level in the P2R Model at well 299-W22-41.png.

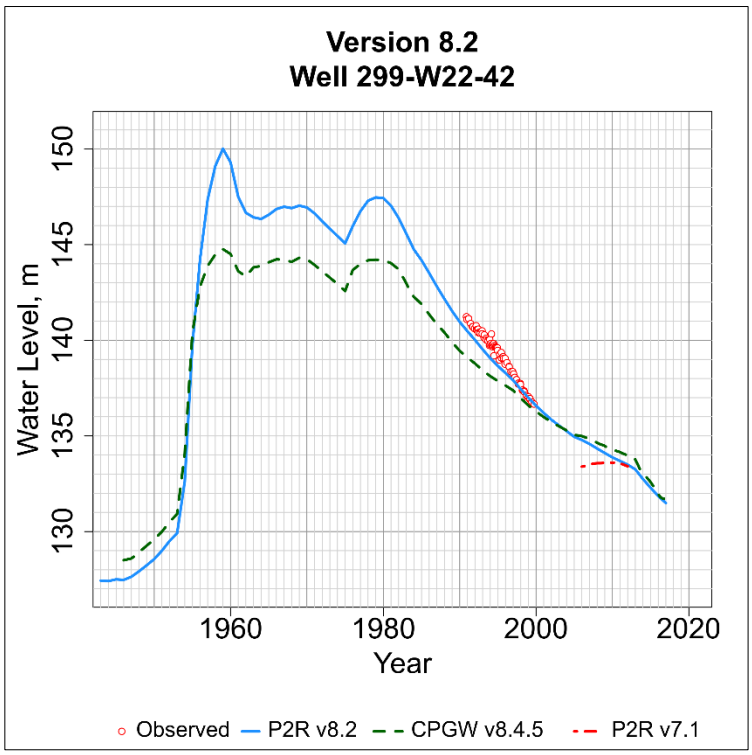

Figure D-264. Observed and simulated water level in the P2R Model at well 299-W22-42.png.

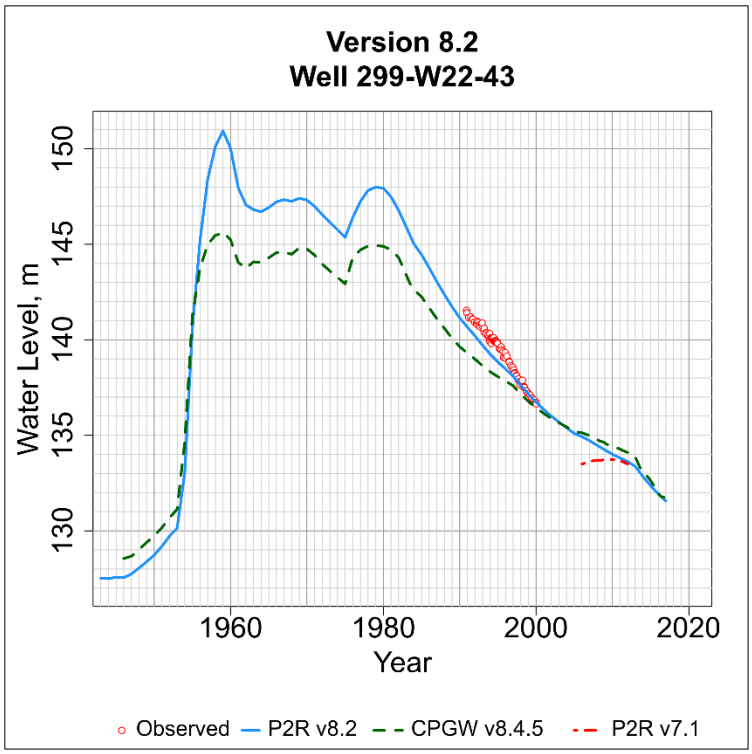

Figure D-265. Observed and simulated water level in the P2R Model at well 299-W22-43.png.

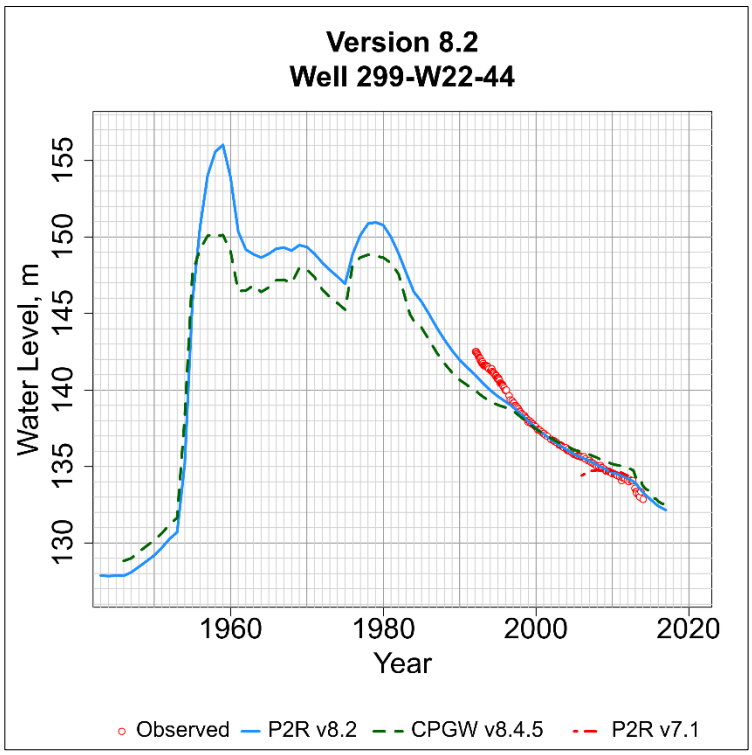

Figure D-266. Observed and simulated water level in the P2R Model at well 299-W22-44.png.

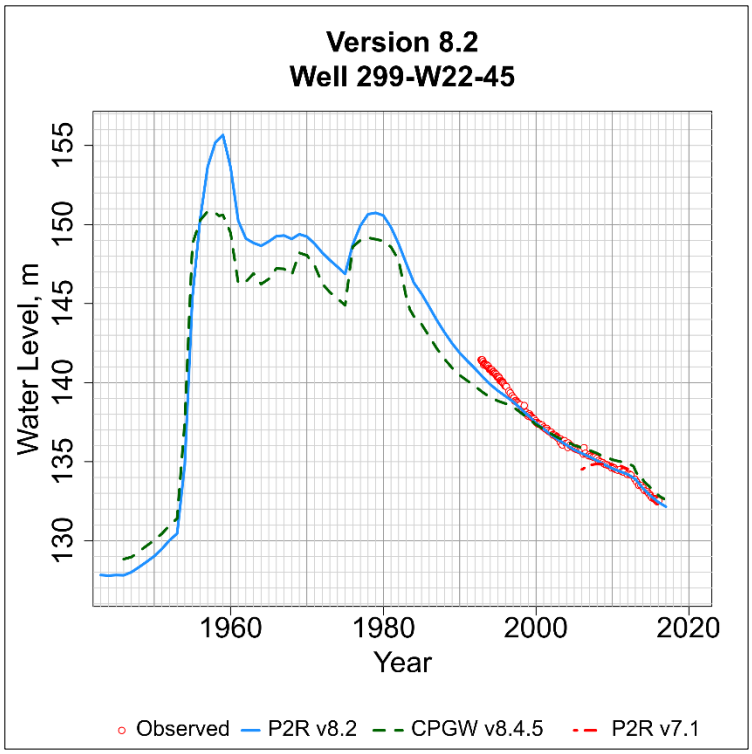

Figure D-267. Observed and simulated water level in the P2R Model at well 299-W22-45.png.

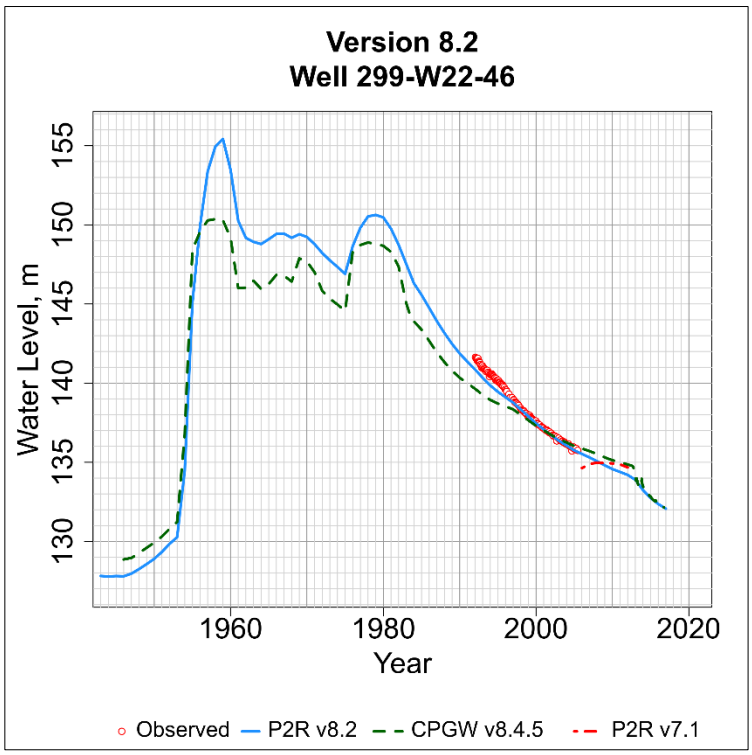

Figure D-268. Observed and simulated water level in the P2R Model at well 299-W22-46.png.

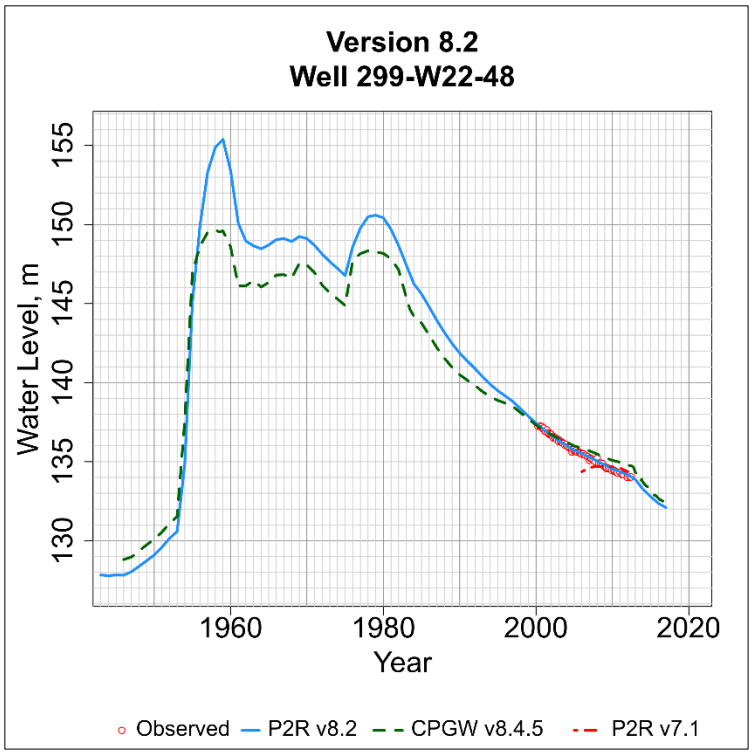

Figure D-269. Observed and simulated water level in the P2R Model at well 299-W22-48.png.

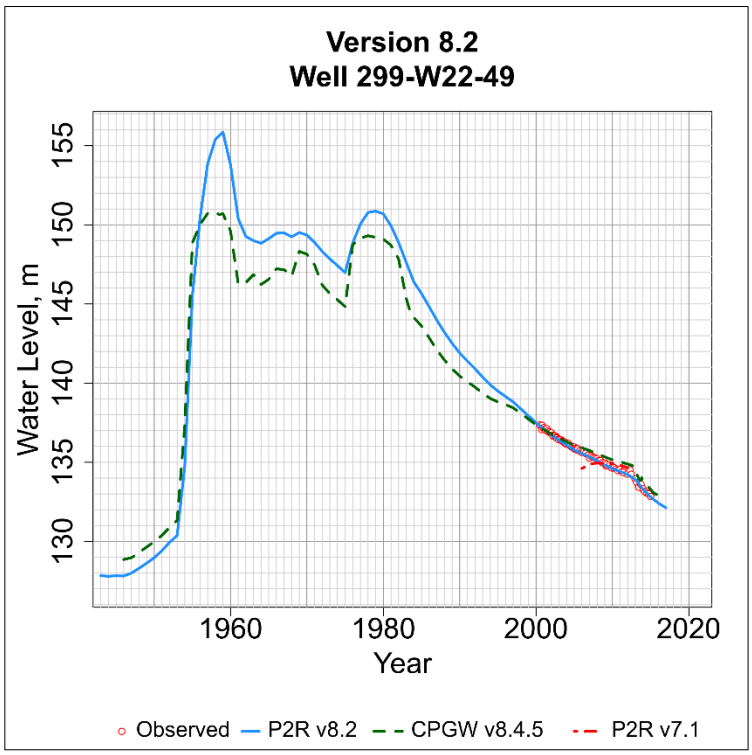

Figure D-270. Observed and simulated water level in the P2R Model at well 299-W22-49.png.

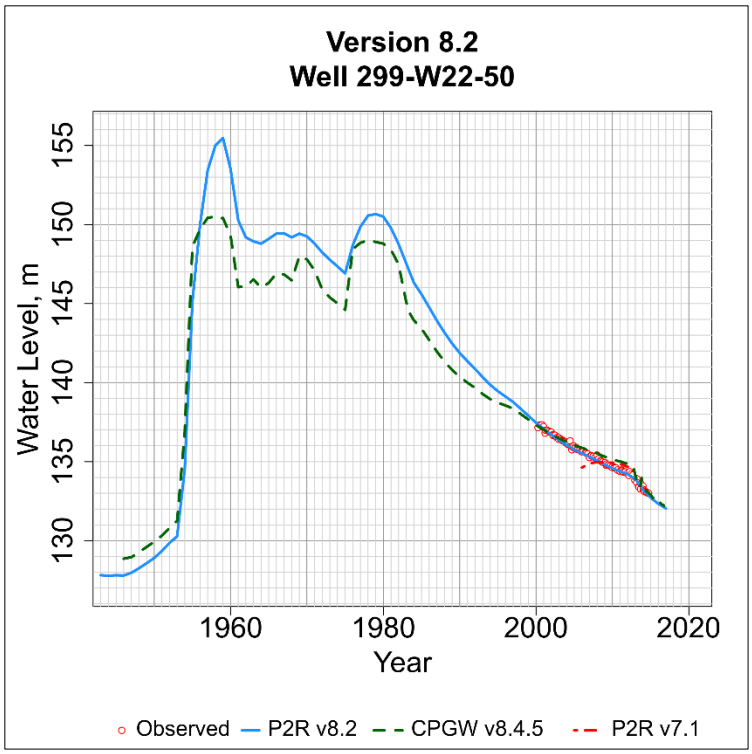

Figure D-271. Observed and simulated water level in the P2R Model at well 299-W22-50.png.

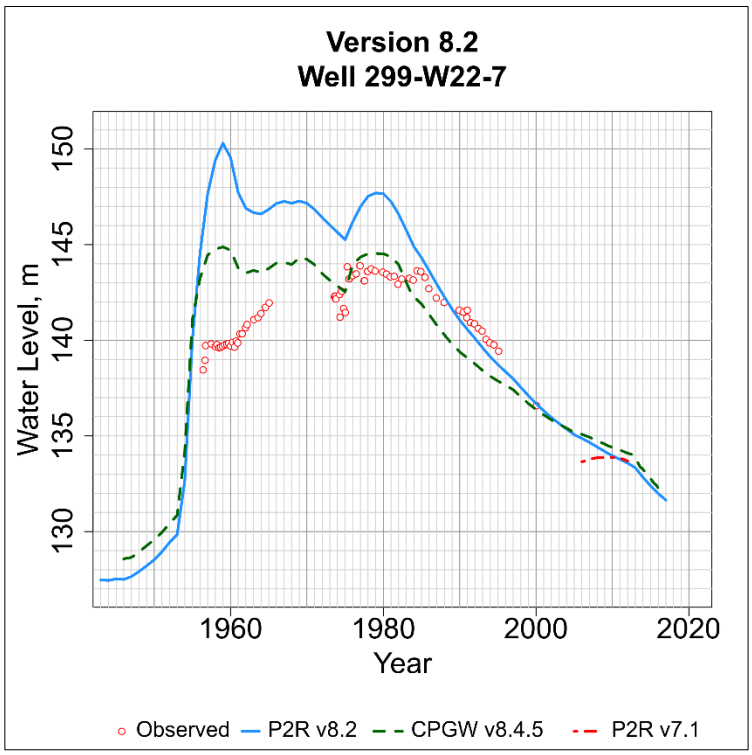

Figure D-272. Observed and simulated water level in the P2R Model at well 299-W22-7.png.

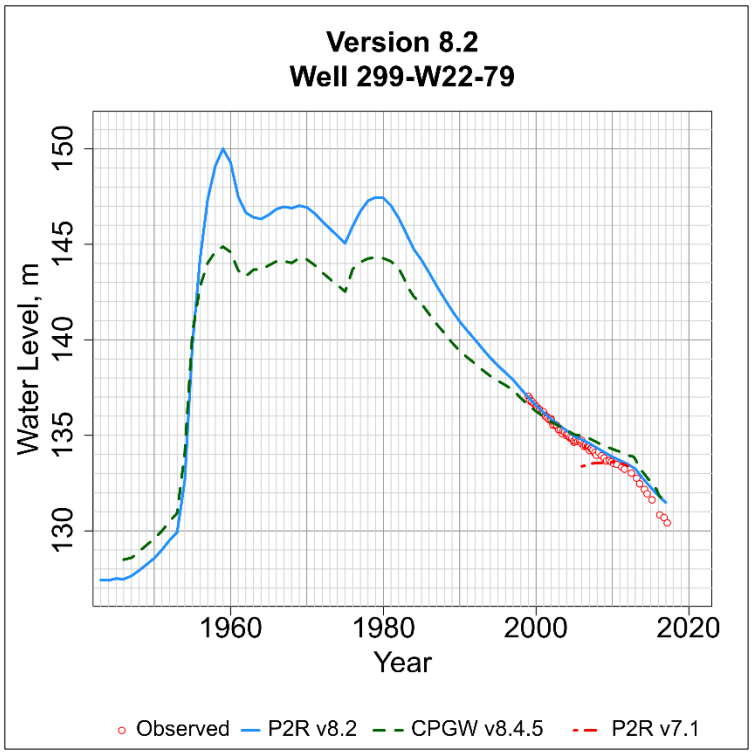

Figure D-273. Observed and simulated water level in the P2R Model at well 299-W22-79.png.

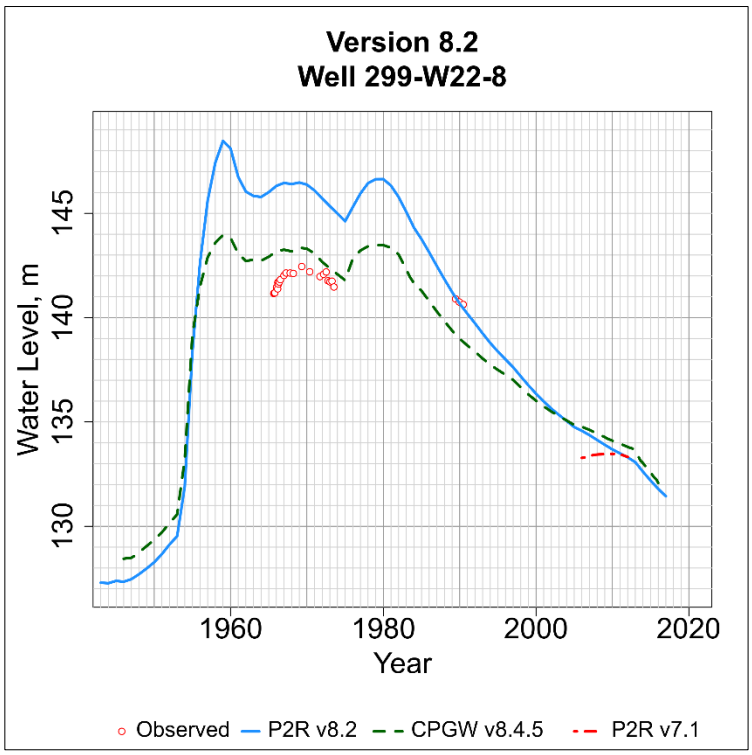

Figure D-274. Observed and simulated water level in the P2R Model at well 299-W22-8.png.

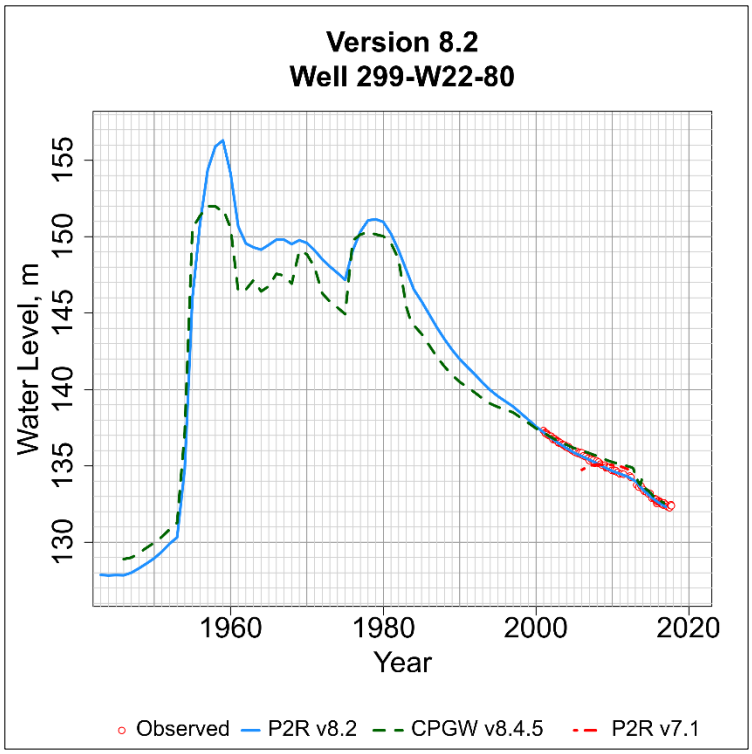

Figure D-275. Observed and simulated water level in the P2R Model at well 299-W22-80.png.

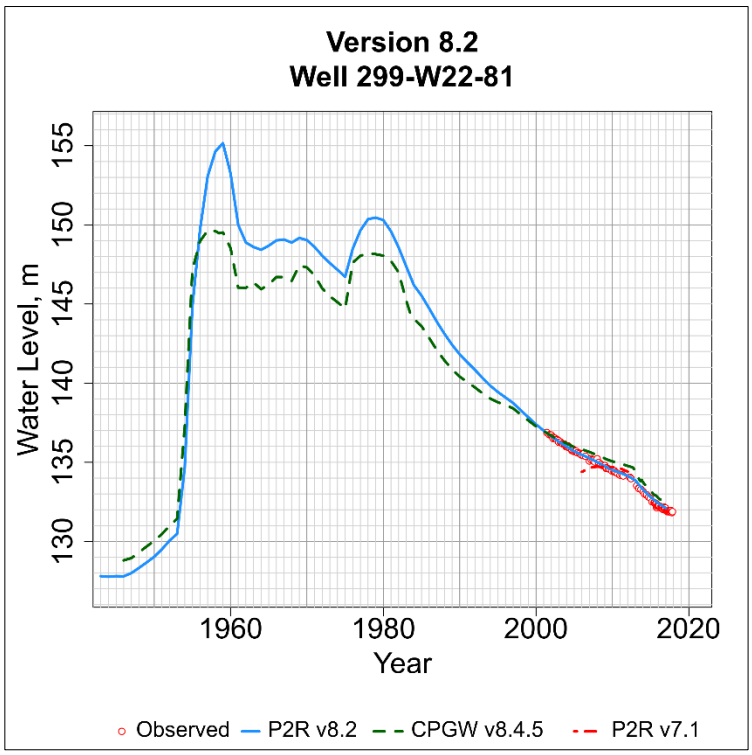

Figure D-276. Observed and simulated water level in the P2R Model at well 299-W22-81.png.

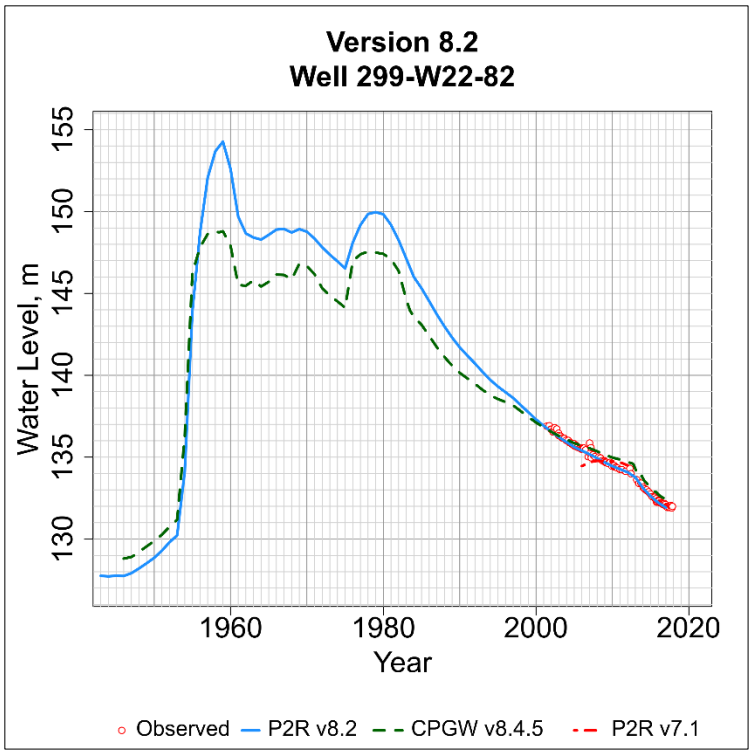

Figure D-277. Observed and simulated water level in the P2R Model at well 299-W22-82.png.

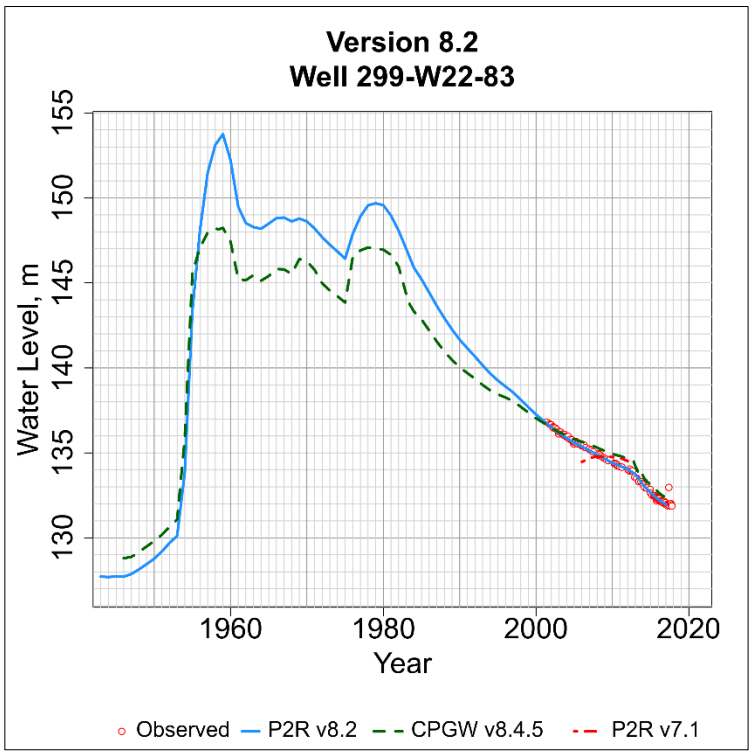

Figure D-278. Observed and simulated water level in the P2R Model at well 299-W22-83.png.

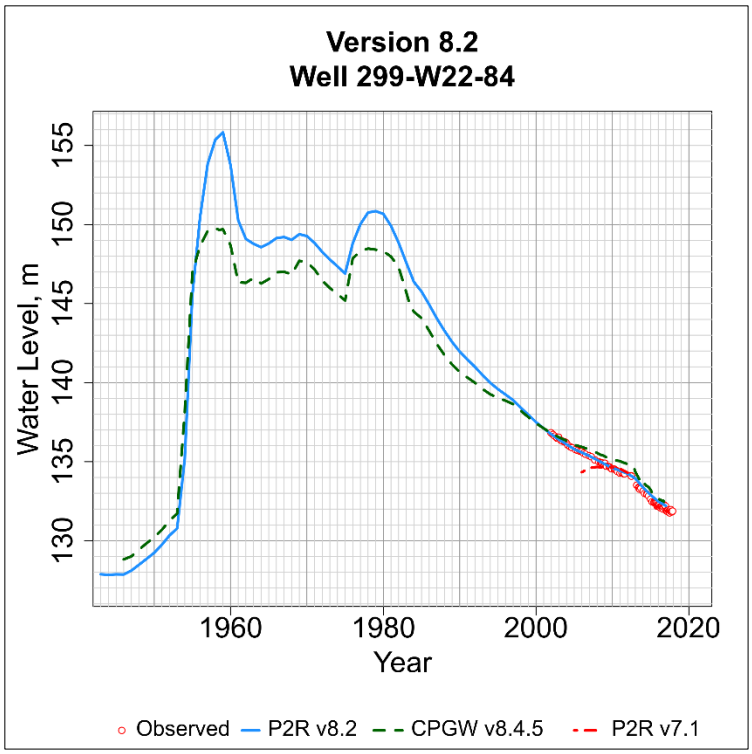

Figure D-279. Observed and simulated water level in the P2R Model at well 299-W22-84.png.

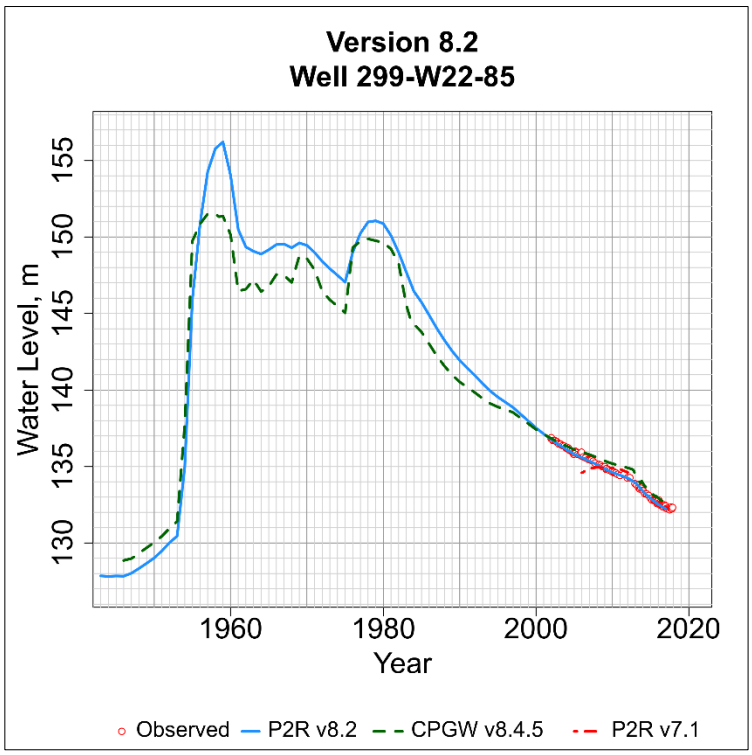

Figure D-280. Observed and simulated water level in the P2R Model at well 299-W22-85.png.

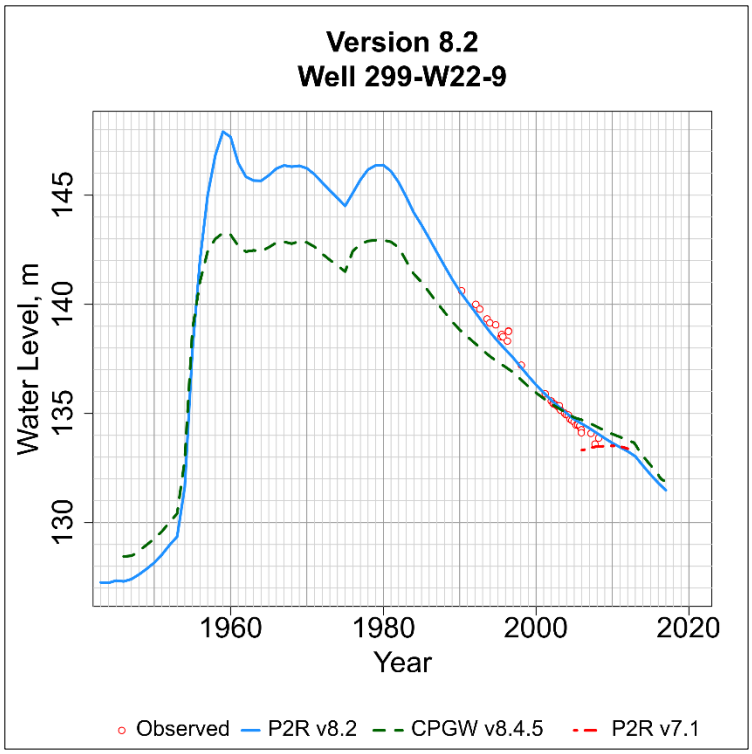

Figure D-281. Observed and simulated water level in the P2R Model at well 299-W22-9.png.

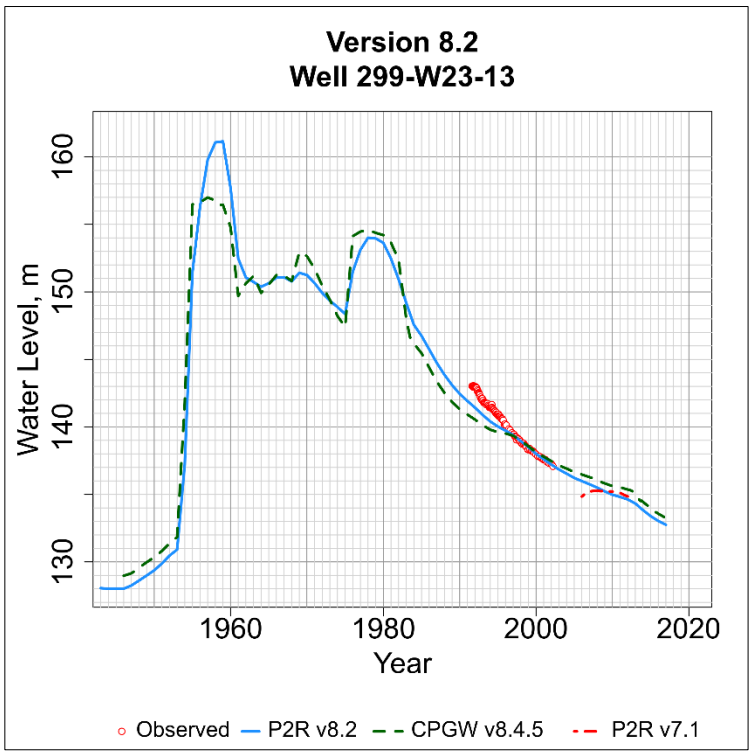

Figure D-282. Observed and simulated water level in the P2R Model at well 299-W23-13.png.

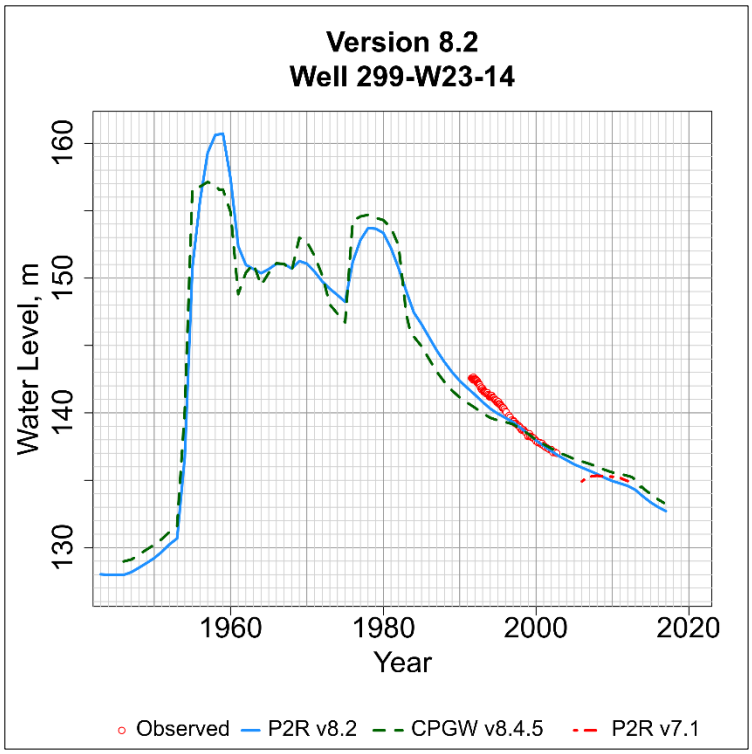

Figure D-283. Observed and simulated water level in the P2R Model at well 299-W23-14.png.

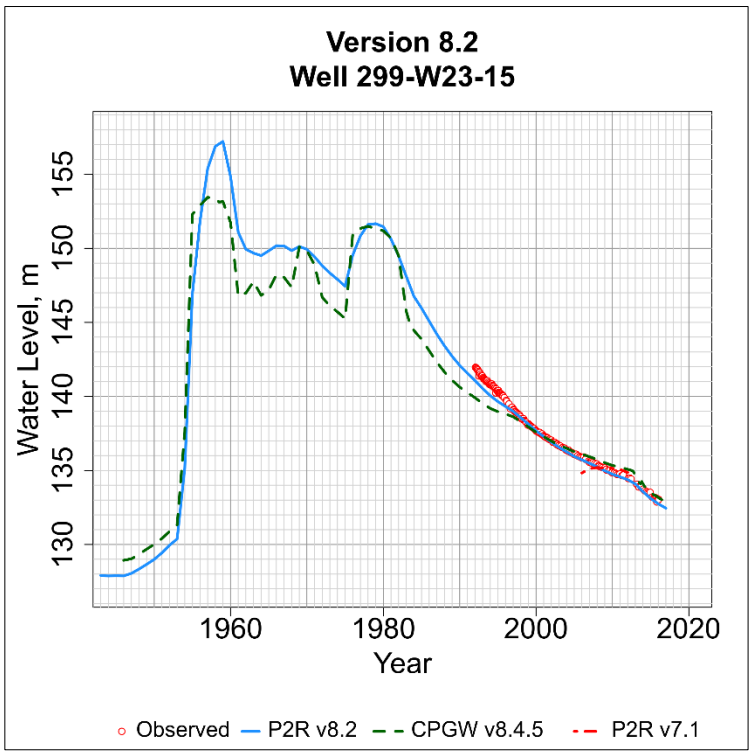

Figure D-284. Observed and simulated water level in the P2R Model at well 299-W23-15.png.

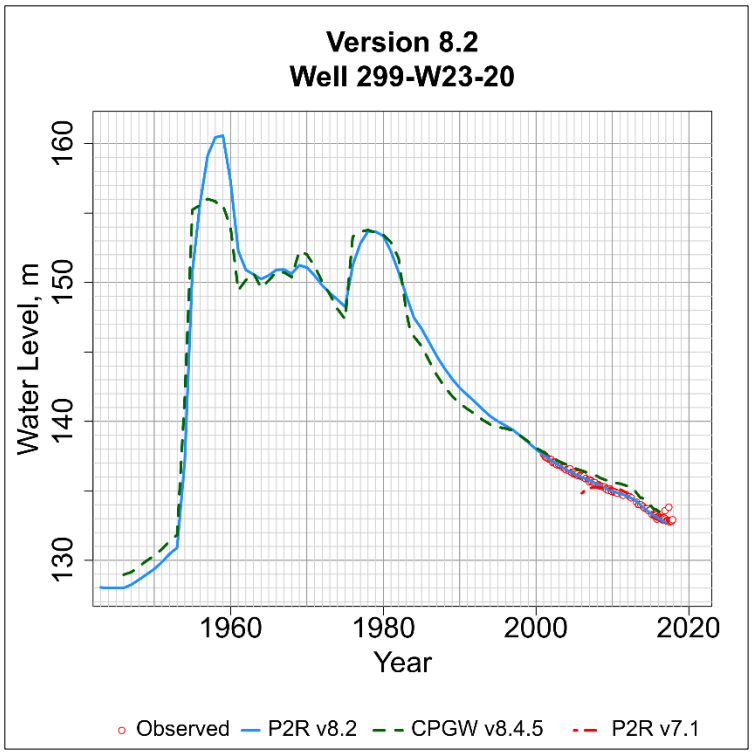

Figure D-285. Observed and simulated water level in the P2R Model at well 299-W23-20.png.

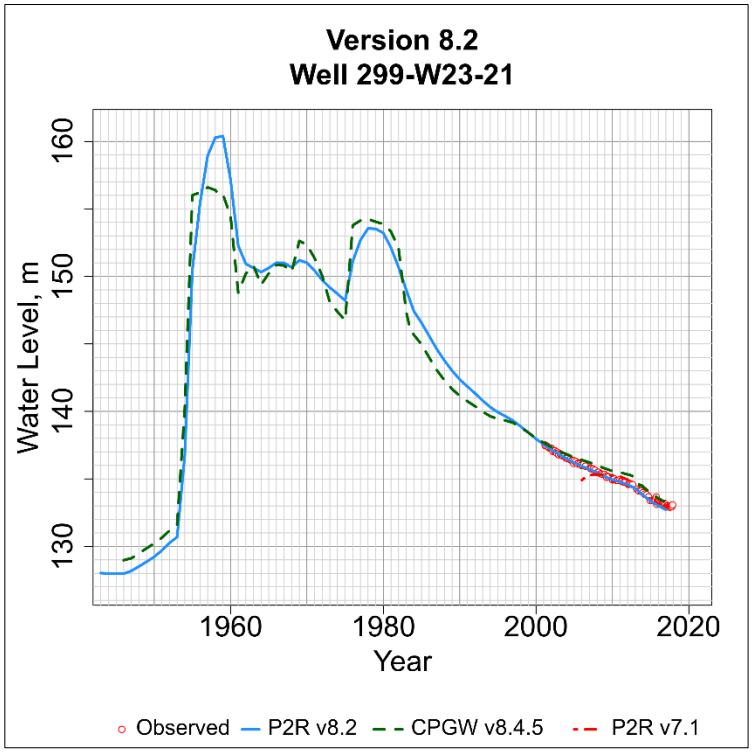

Figure D-286. Observed and simulated water level in the P2R Model at well 299-W23-21.png.

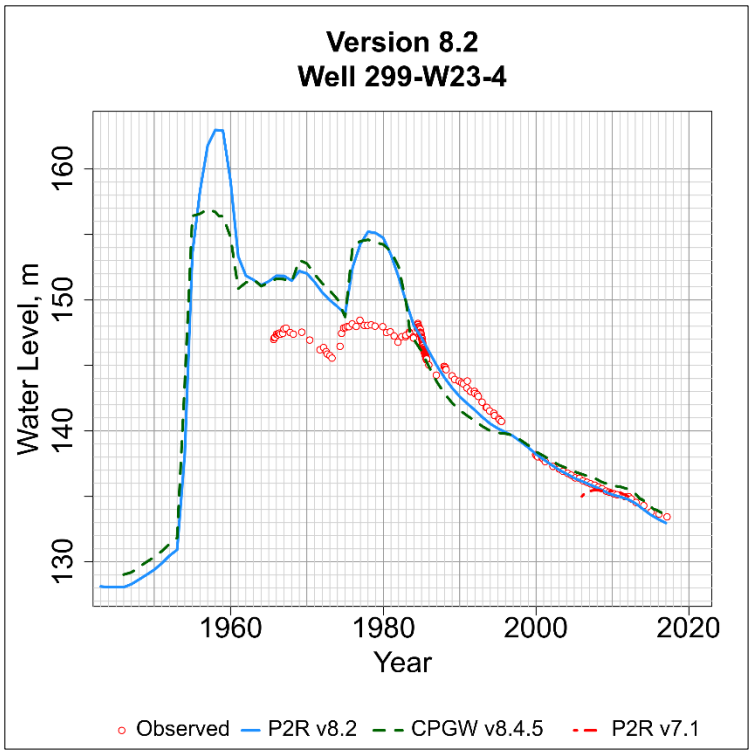

Figure D-287. Observed and simulated water level in the P2R Model at well 299-W23-4.png.

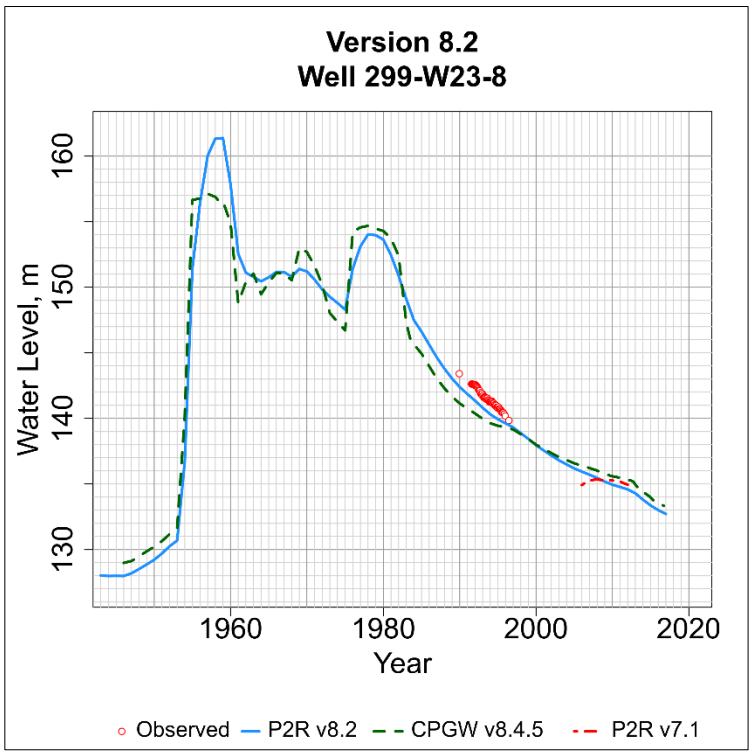

Figure D-288. Observed and simulated water level in the P2R Model at well 299-W23-8.png.

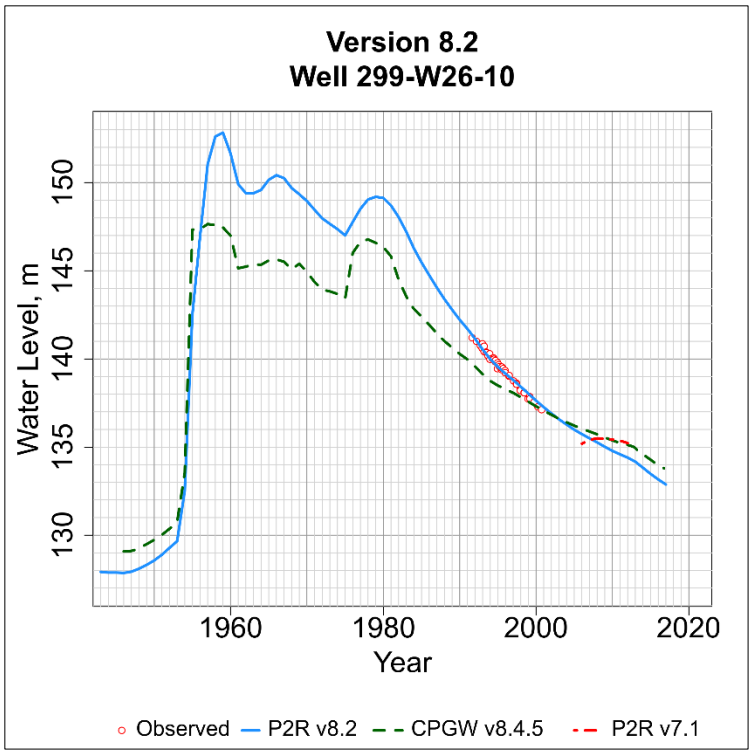

Figure D-289. Observed and simulated water level in the P2R Model at well 299-W26-10.png.

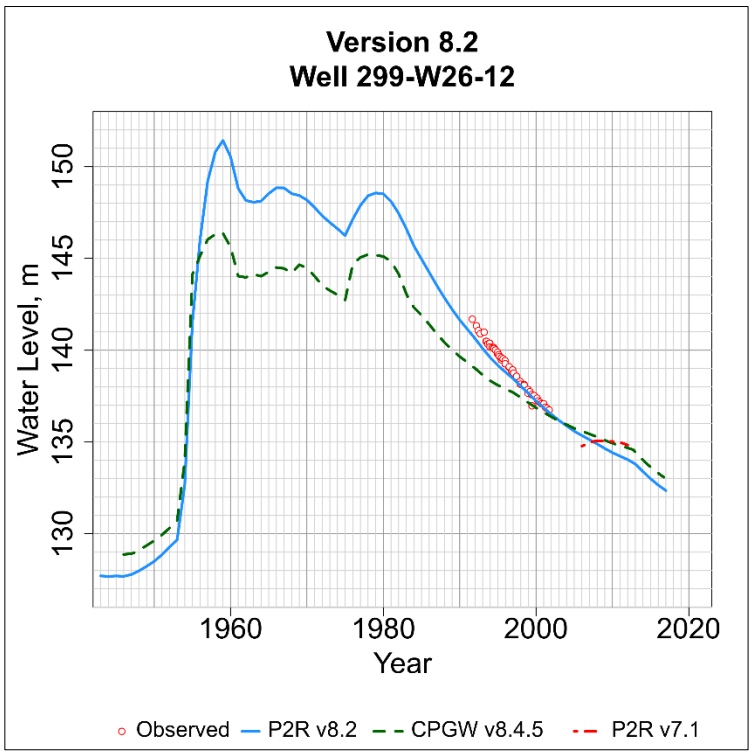

Figure D-290. Observed and simulated water level in the P2R Model at well 299-W26-12.png.

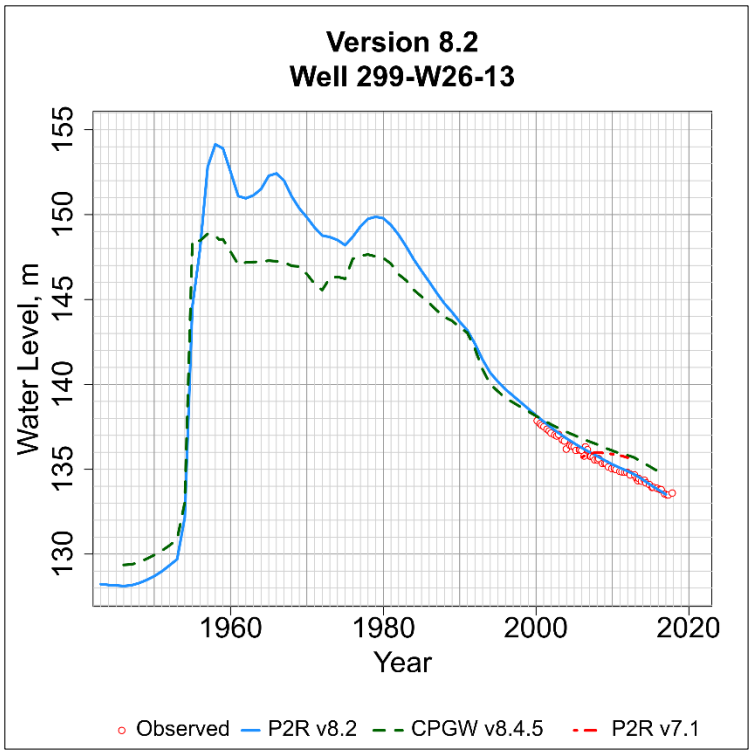

Figure D-291. Observed and simulated water level in the P2R Model at well 299-W26-13.png.

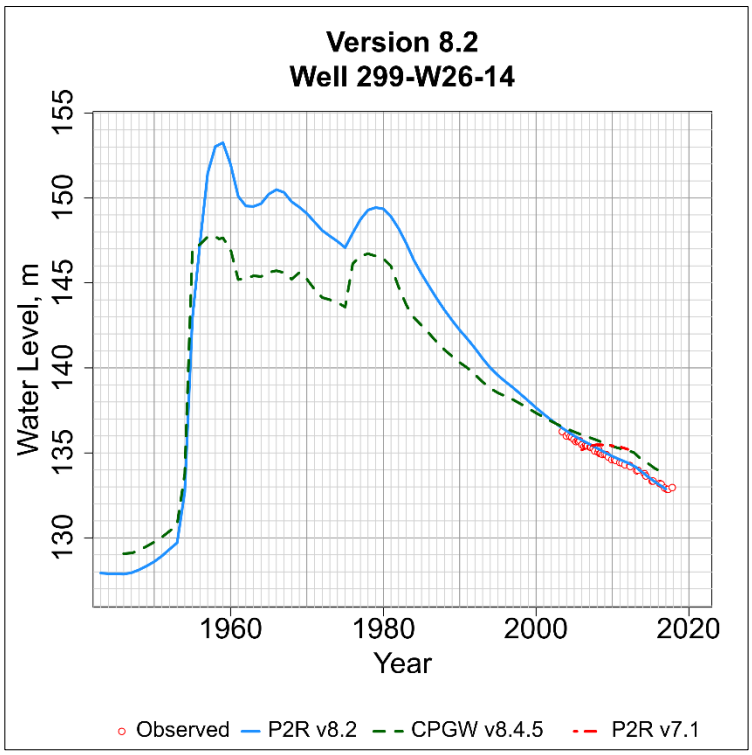

Figure D-292. Observed and simulated water level in the P2R Model at well 299-W26-14.png.

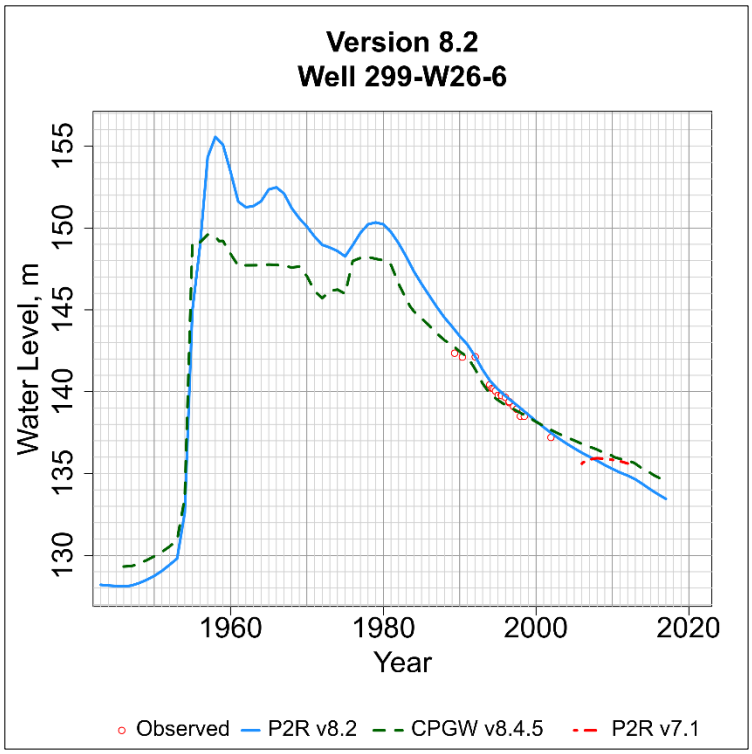

Figure D-293. Observed and simulated water level in the P2R Model at well 299-W26-6.png.

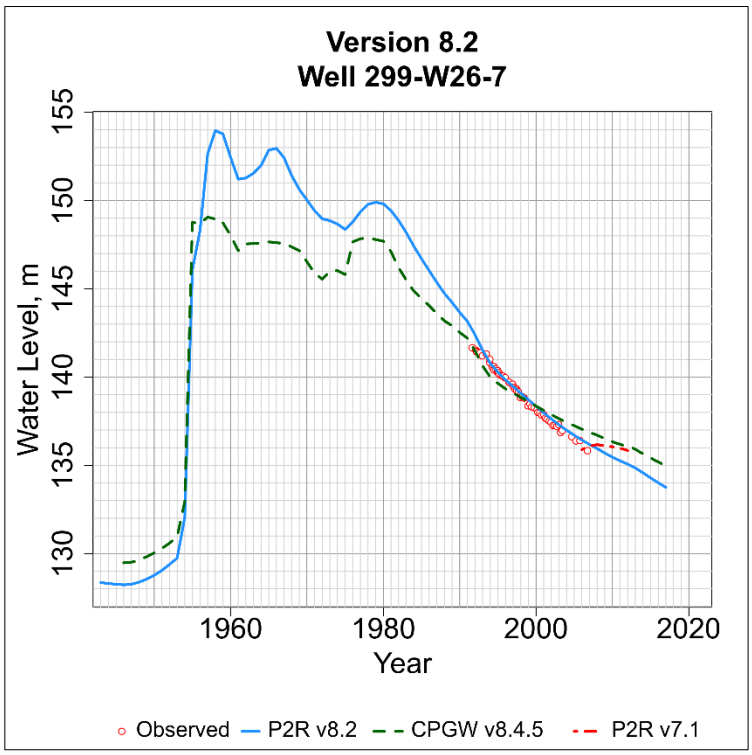

Figure D-294. Observed and simulated water level in the P2R Model at well 299-W26-7.png.

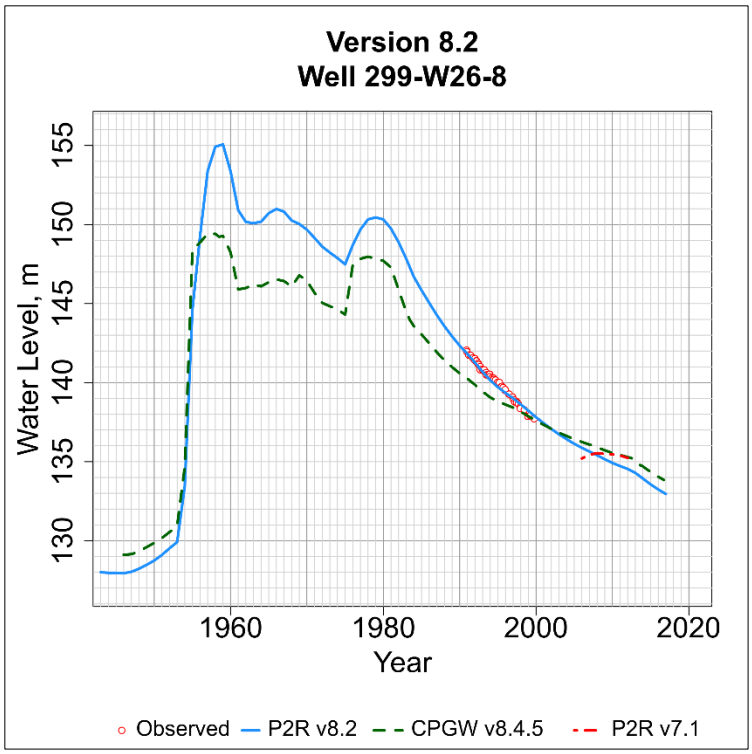

Figure D-295. Observed and simulated water level in the P2R Model at well 299-W26-8.png.

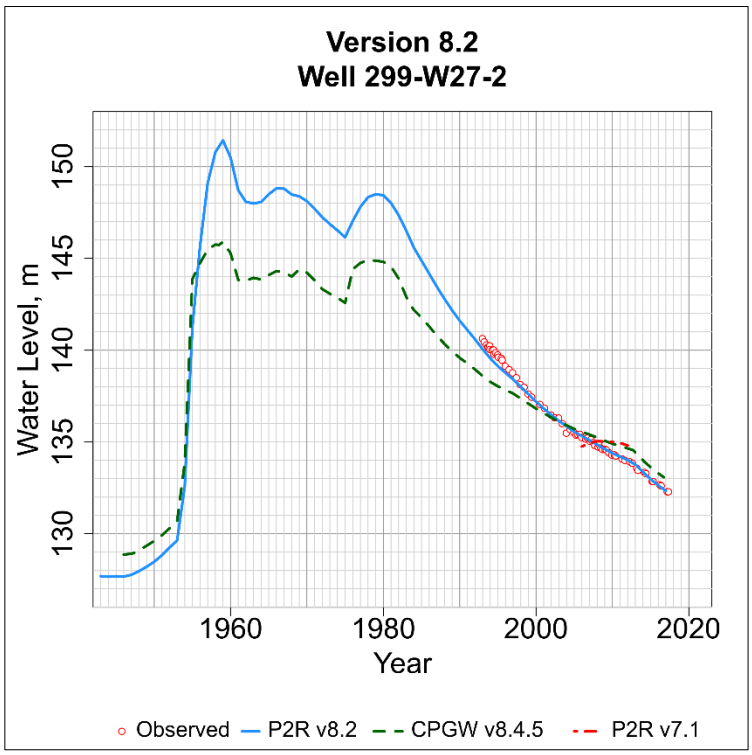

Figure D-296. Observed and simulated water level in the P2R Model at well 299-W27-2.png.

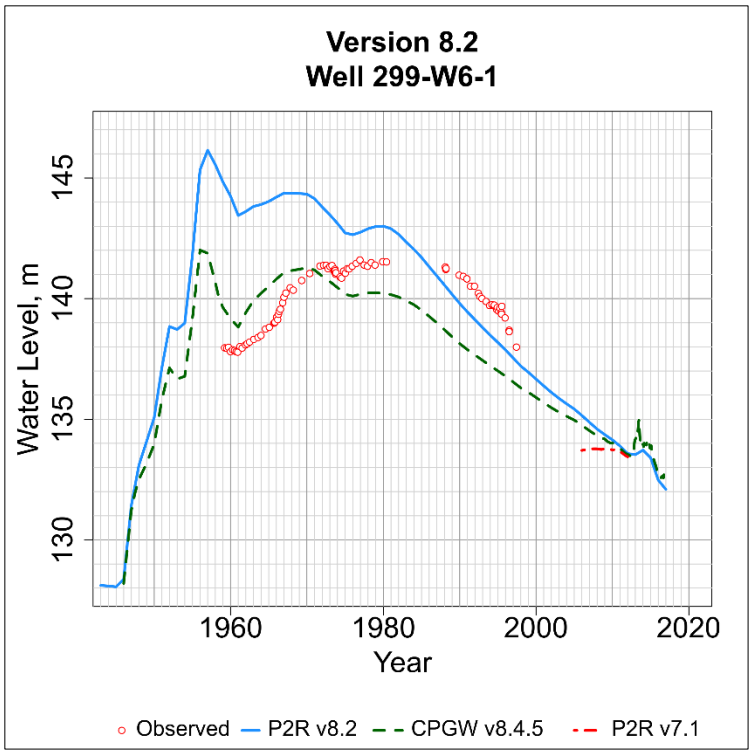

Figure D-297. Observed and simulated water level in the P2R Model at well 299-W6-1.png.

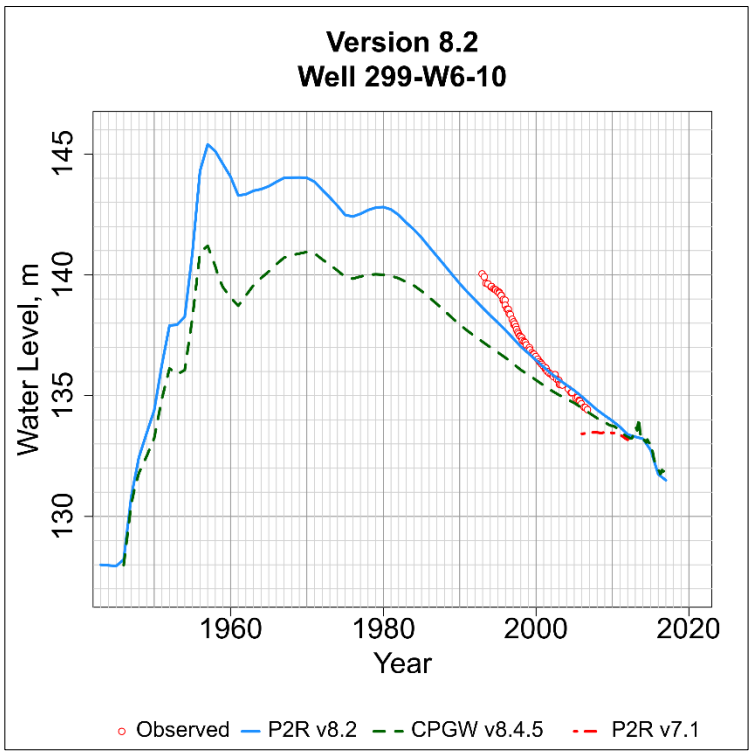

Figure D-298. Observed and simulated water level in the P2R Model at well 299-W6-10.png.

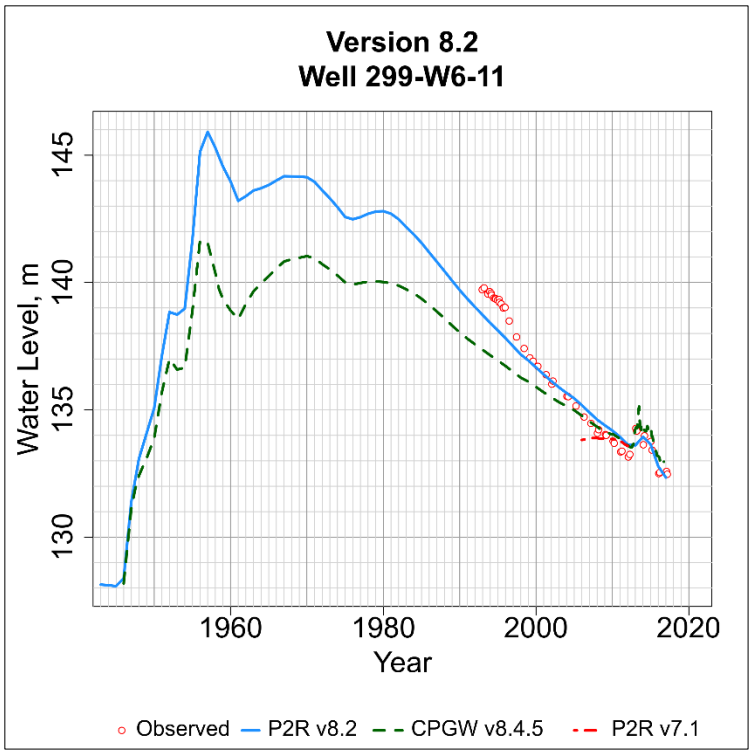

Figure D-299. Observed and simulated water level in the P2R Model at well 299-W6-11.png.

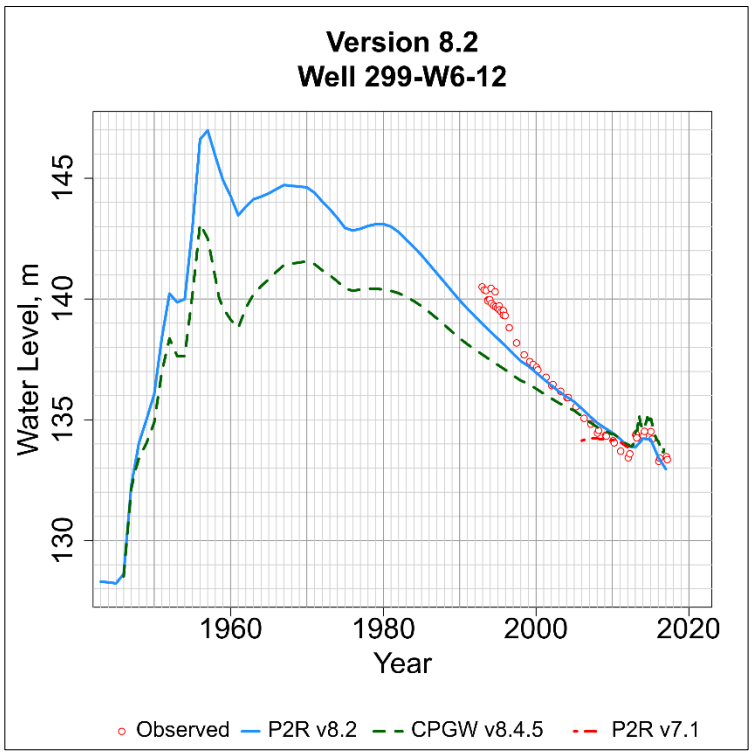

Figure D-300. Observed and simulated water level in the P2R Model at well 299-W6-12.png.

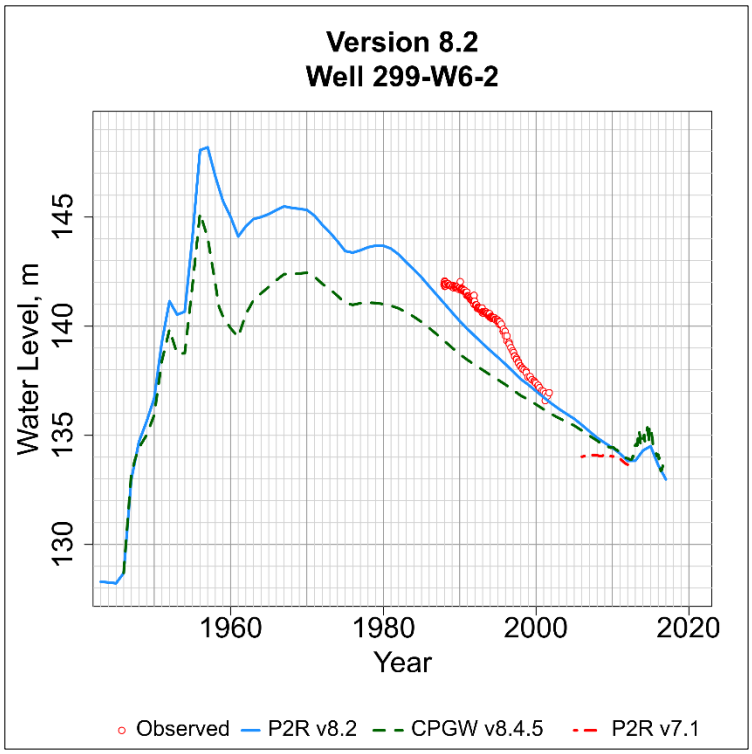

Figure D-301. Observed and simulated water level in the P2R Model at well 299-W6-2.png.

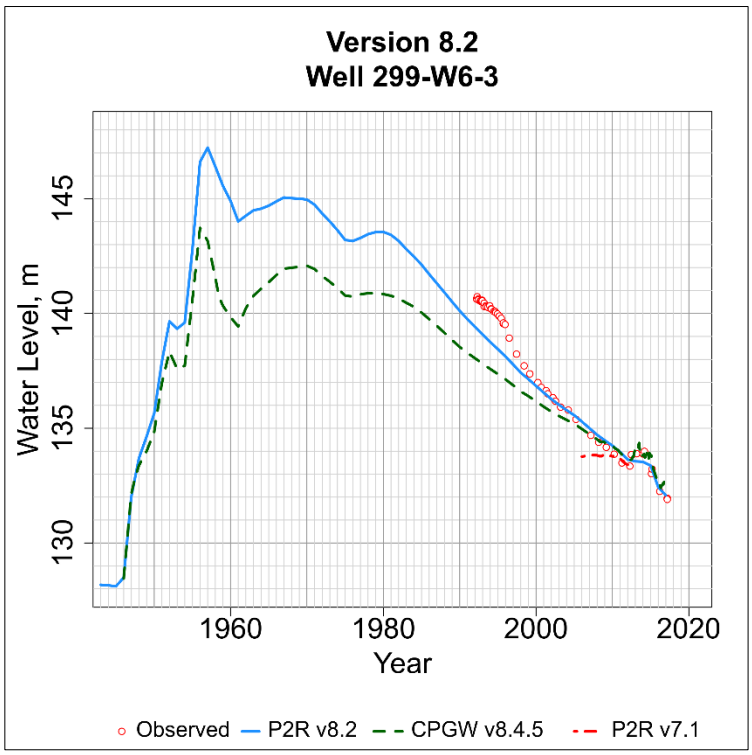

Figure D-302. Observed and simulated water level in the P2R Model at well 299-W6-3.png.

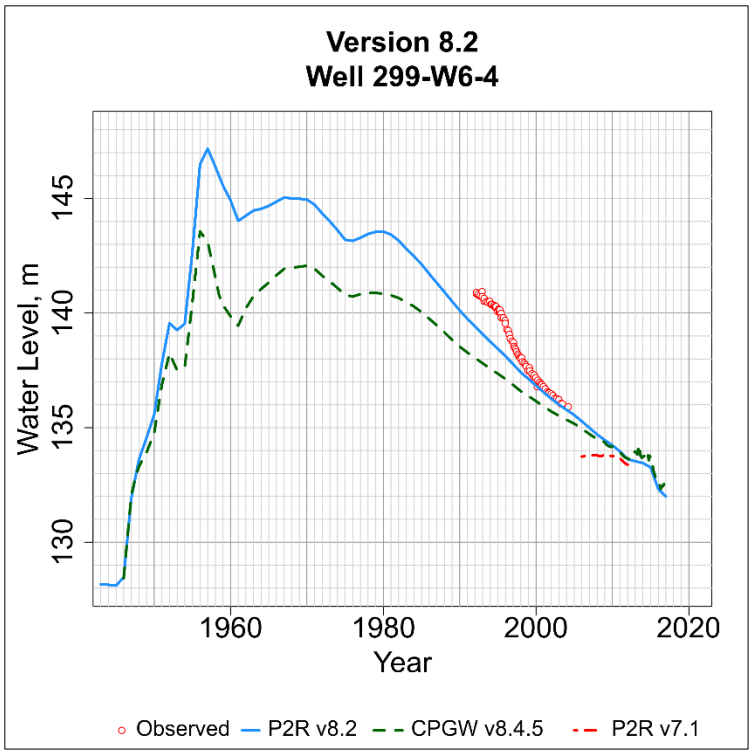

Figure D-303. Observed and simulated water level in the P2R Model at well 299-W6-4.png.

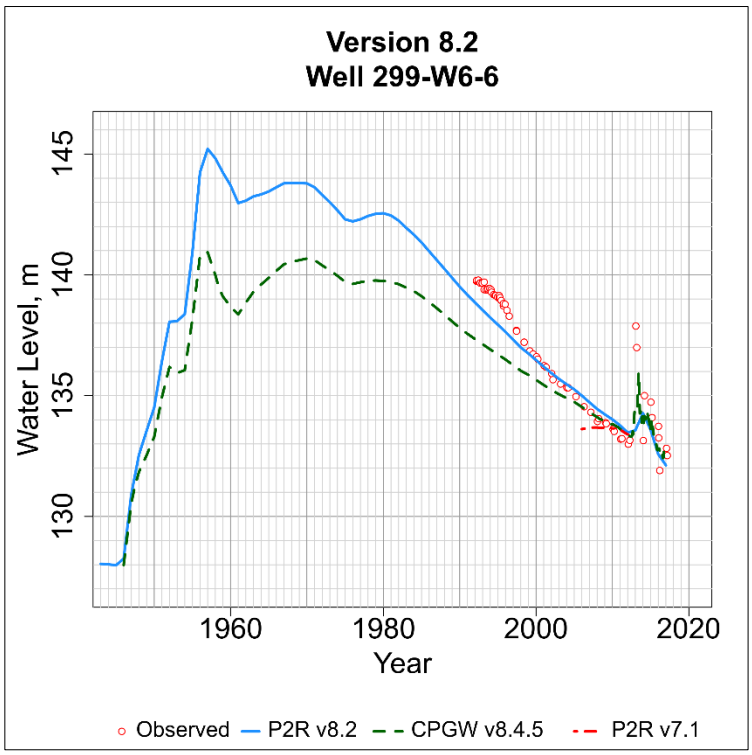

Figure D-304. Observed and simulated water level in the P2R Model at well 299-W6-6.png.

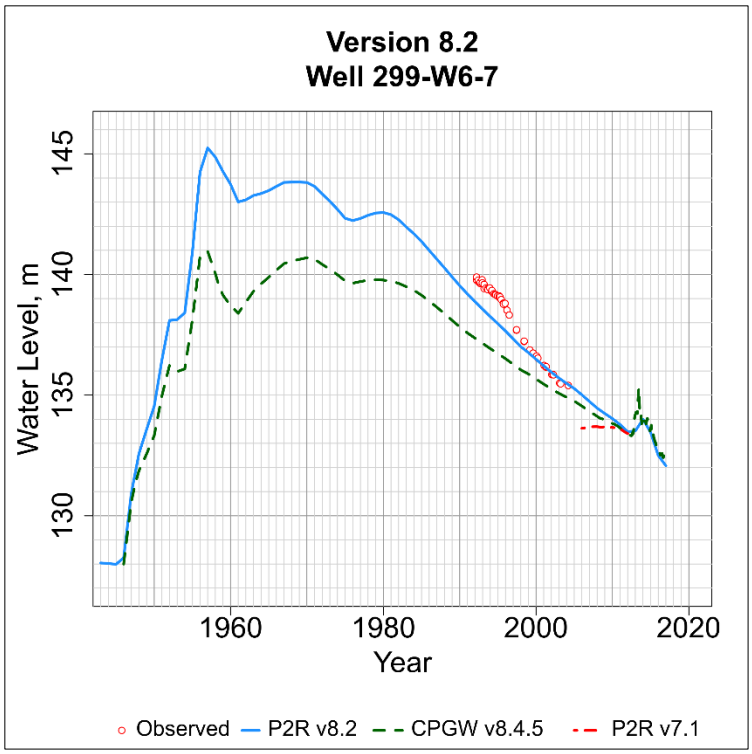

Figure D-305. Observed and simulated water level in the P2R Model at well 299-W6-7.png.

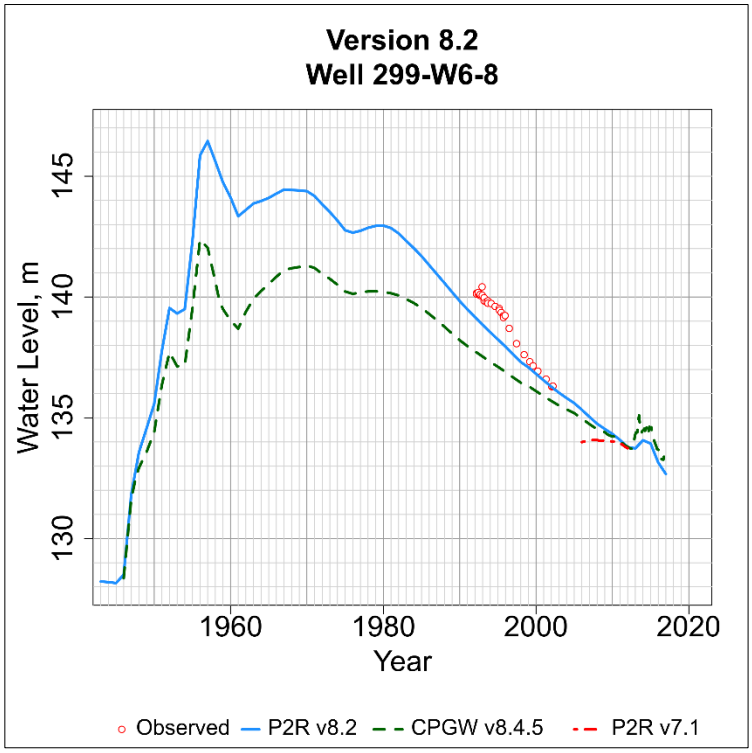

Figure D-306. Observed and simulated water level in the P2R Model at well 299-W6-8.png.

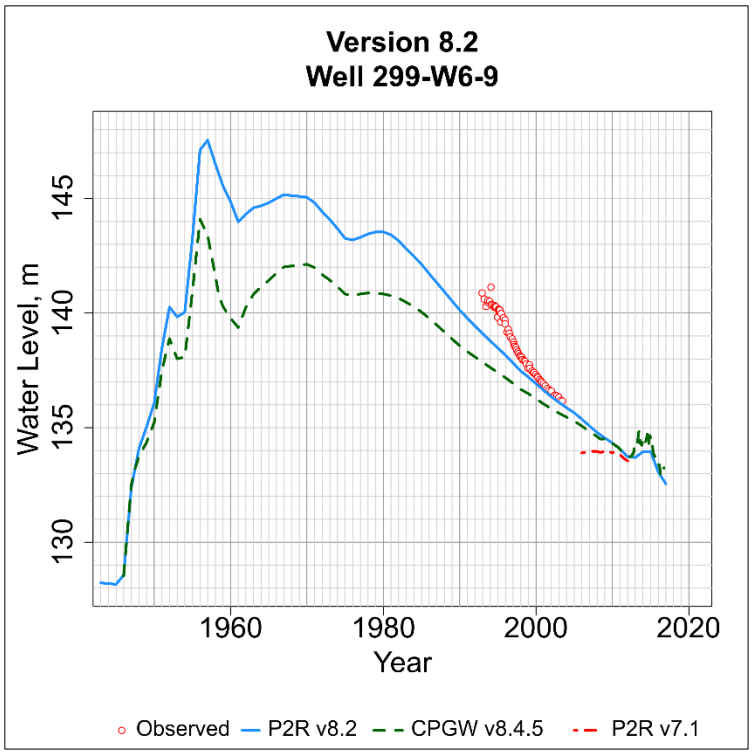

Figure D-307. Observed and simulated water level in the P2R Model at well 299-W6-9.png.

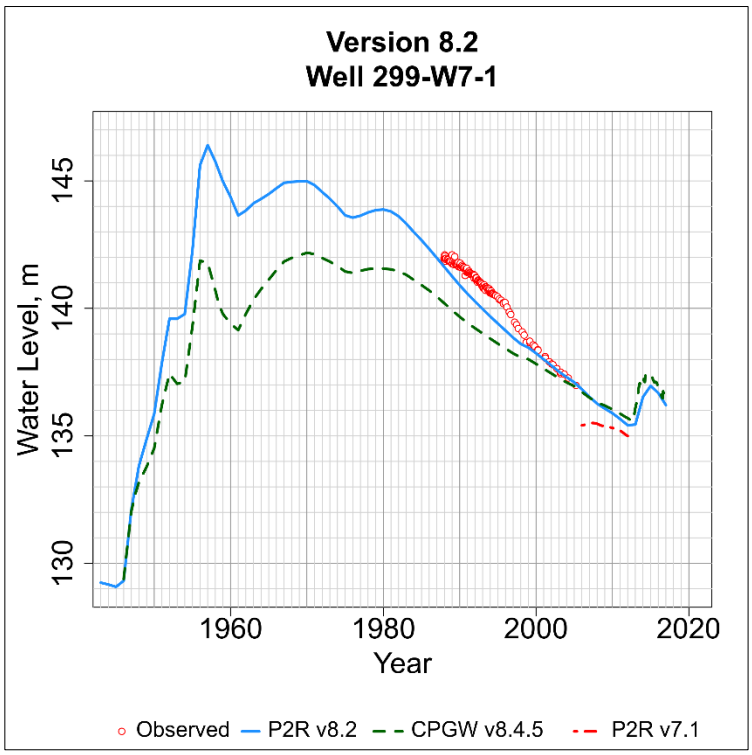

Figure D-308. Observed and simulated water level in the P2R Model at well 299-W7-1.png.

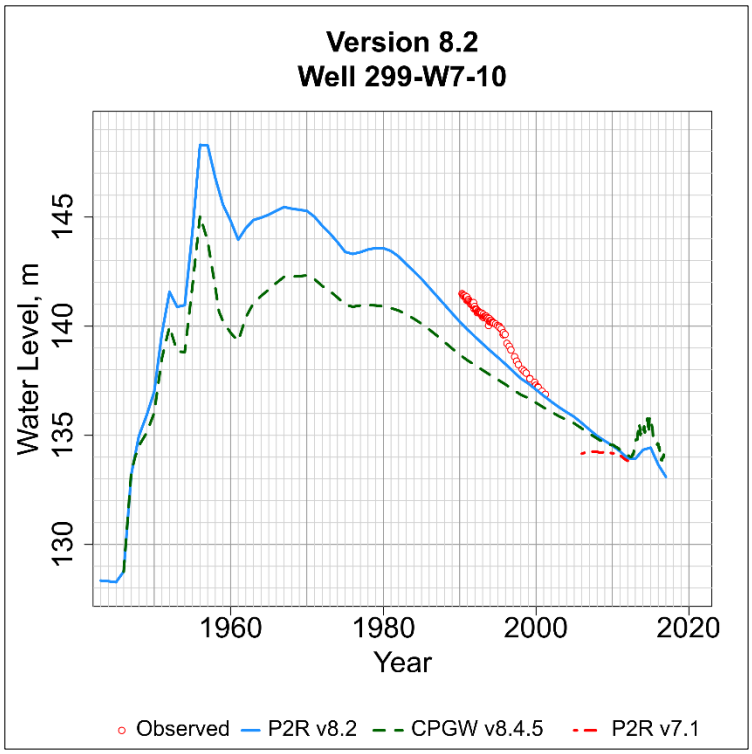

Figure D-309. Observed and simulated water level in the P2R Model at well 299-W7-10.png.

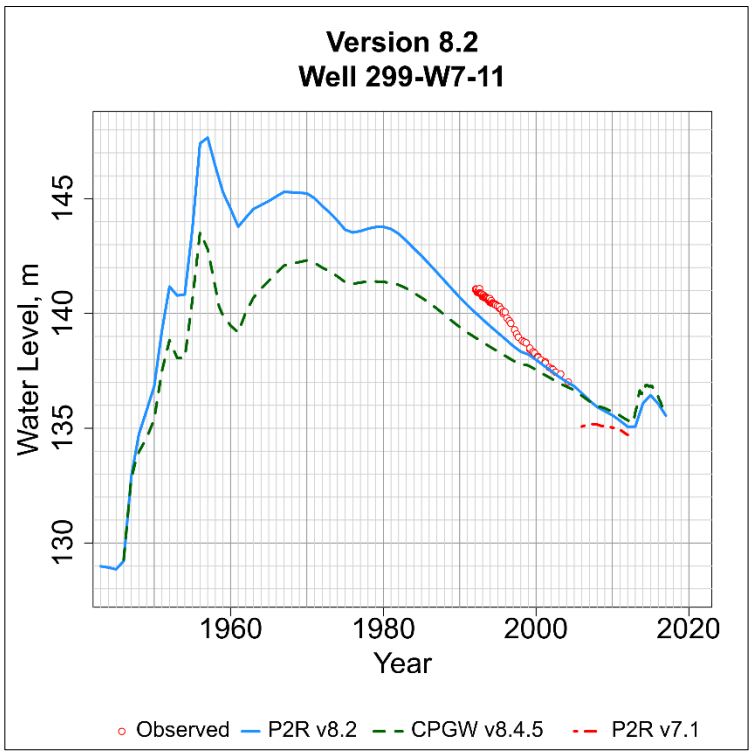

Figure D-310. Observed and simulated water level in the P2R Model at well 299-W7-11.png.

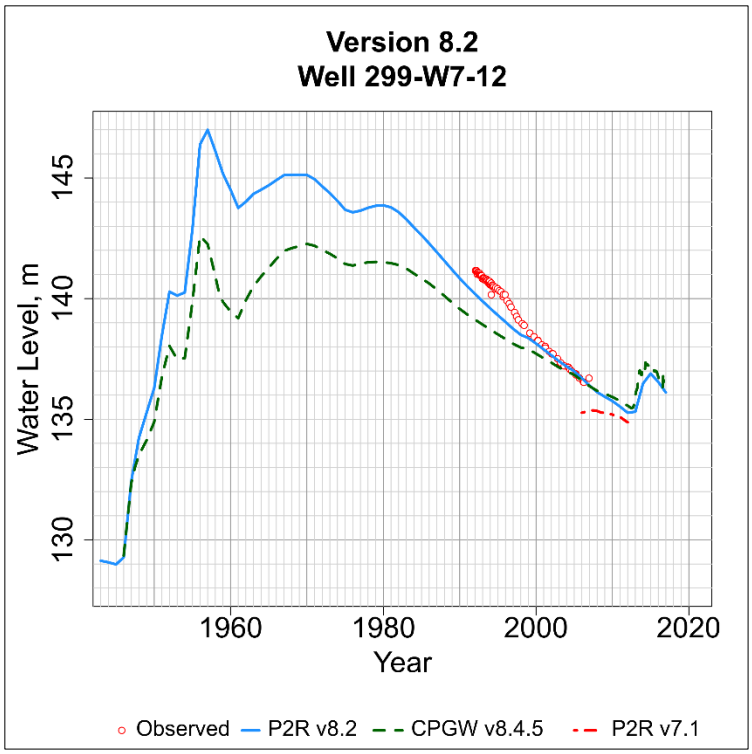

Figure D-311. Observed and simulated water level in the P2R Model at well 299-W7-12.png.

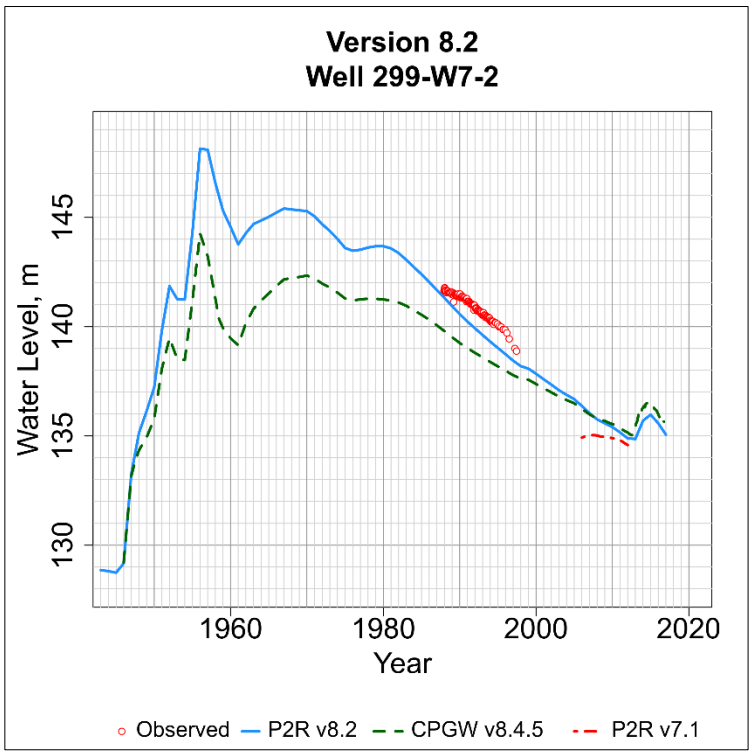

Figure D-312. Observed and simulated water level in the P2R Model at well 299-W7-2.png.

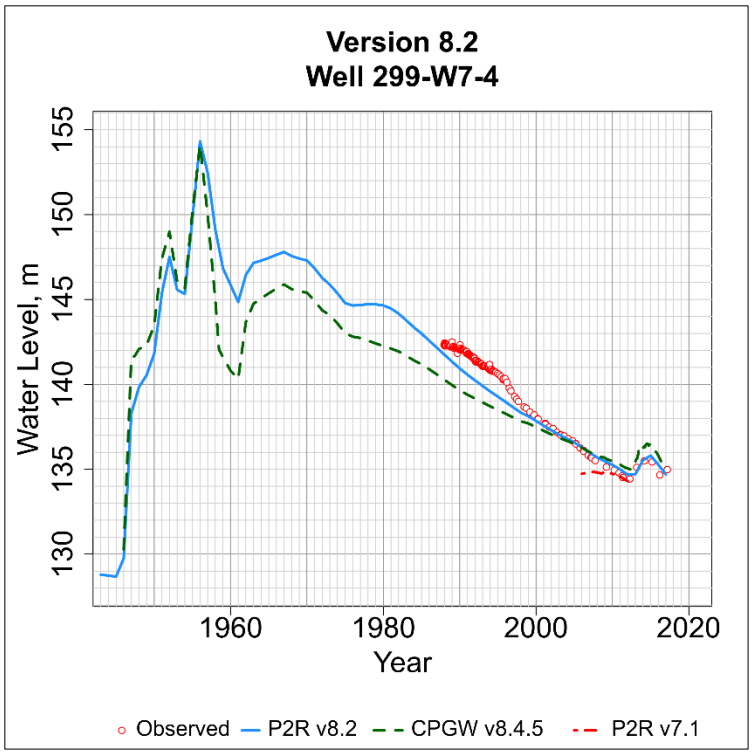

Figure D-313. Observed and simulated water level in the P2R Model at well 299-W7-4.png.

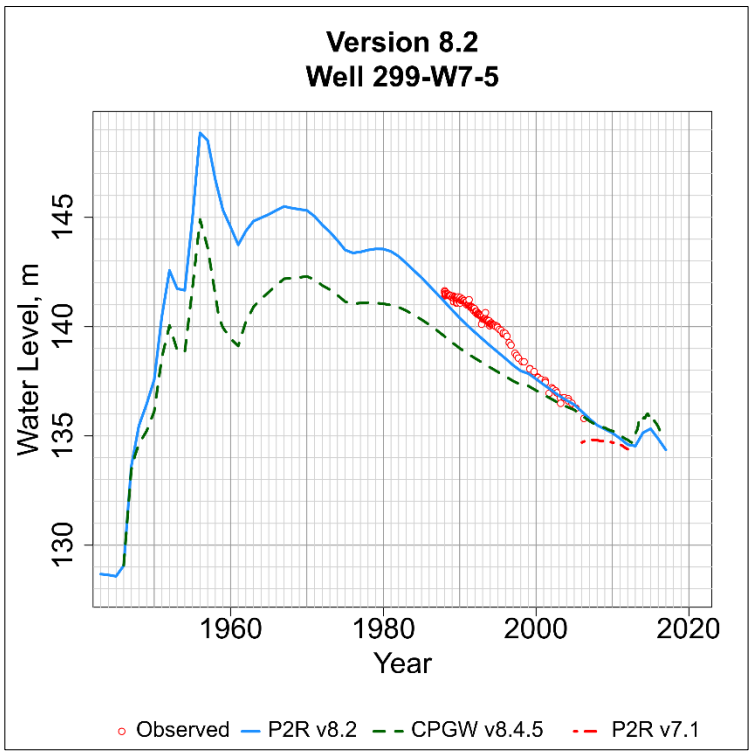

Figure D-314. Observed and simulated water level in the P2R Model at well 299-W7-5.png.

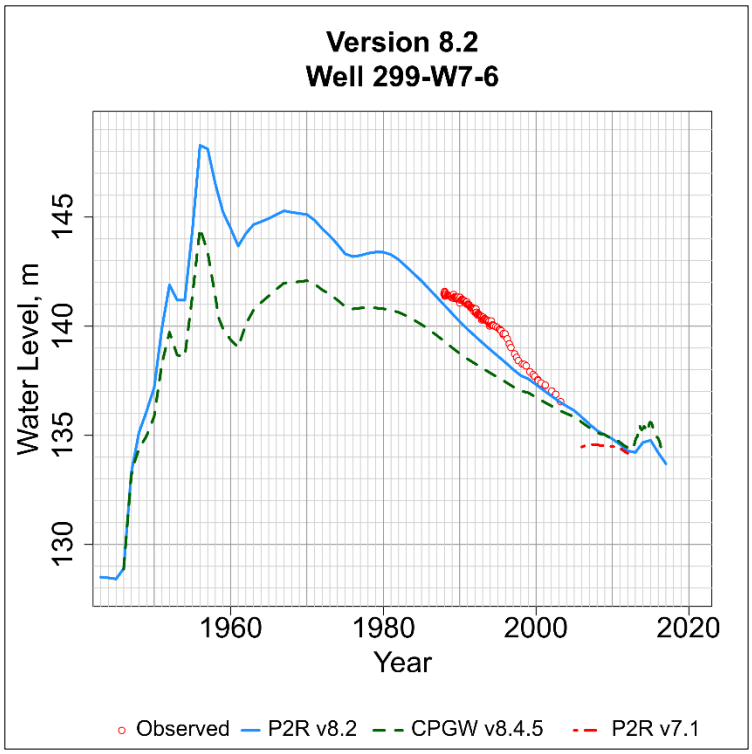

Figure D-315. Observed and simulated water level in the P2R Model at well 299-W7-6.png.

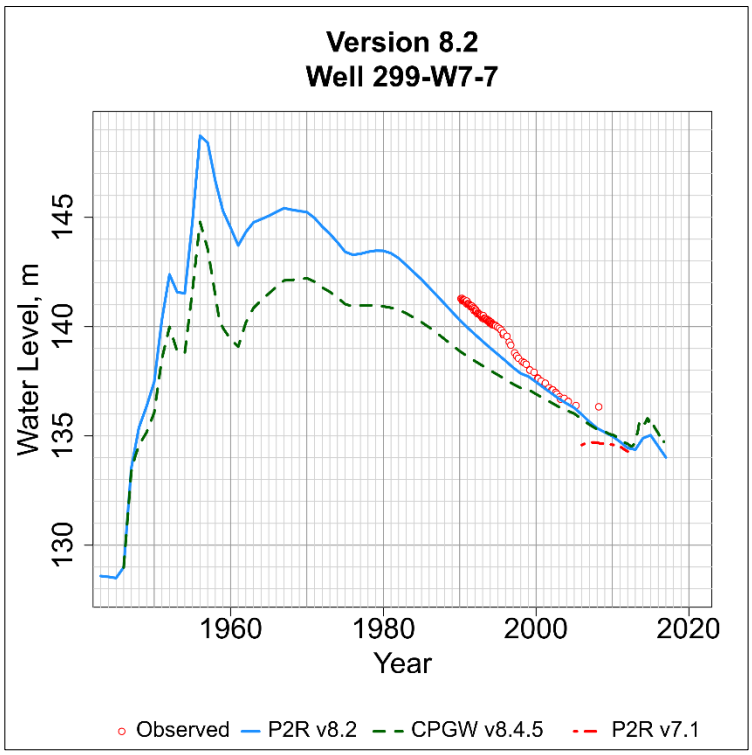

Figure D-316. Observed and simulated water level in the P2R Model at well 299-W7-7.png.

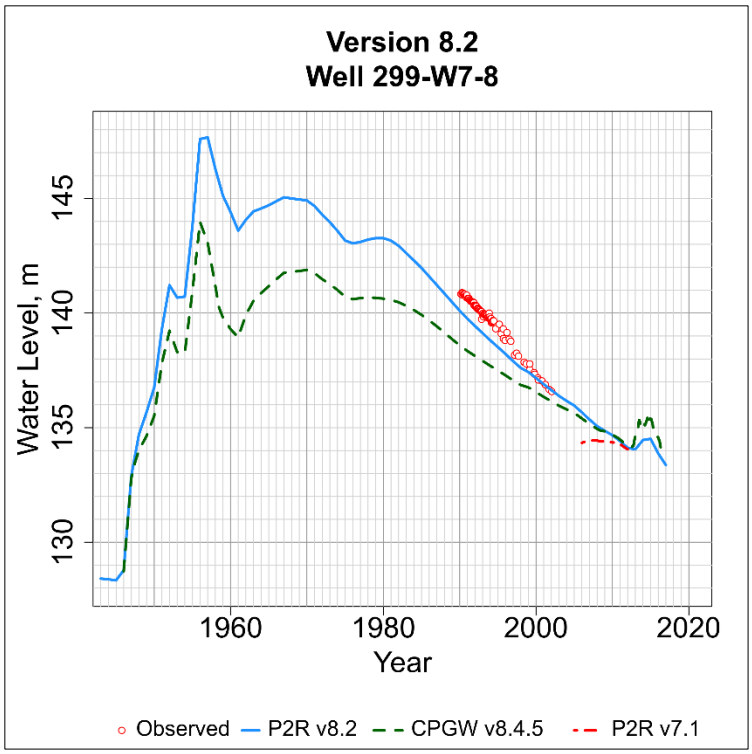

Figure D-317. Observed and simulated water level in the P2R Model at well 299-W7-8.png.

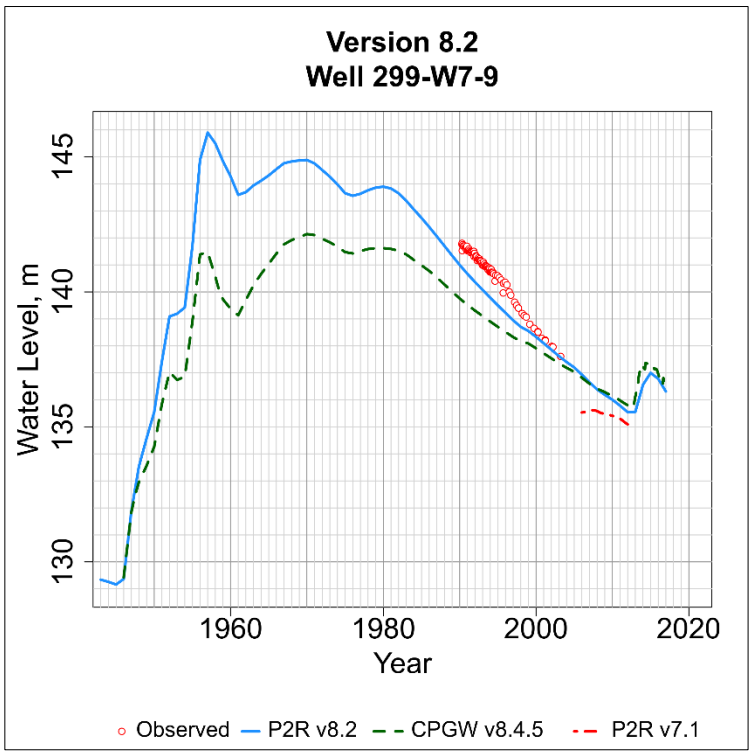

Figure D-318. Observed and simulated water level in the P2R Model at well 299-W7-9.png.

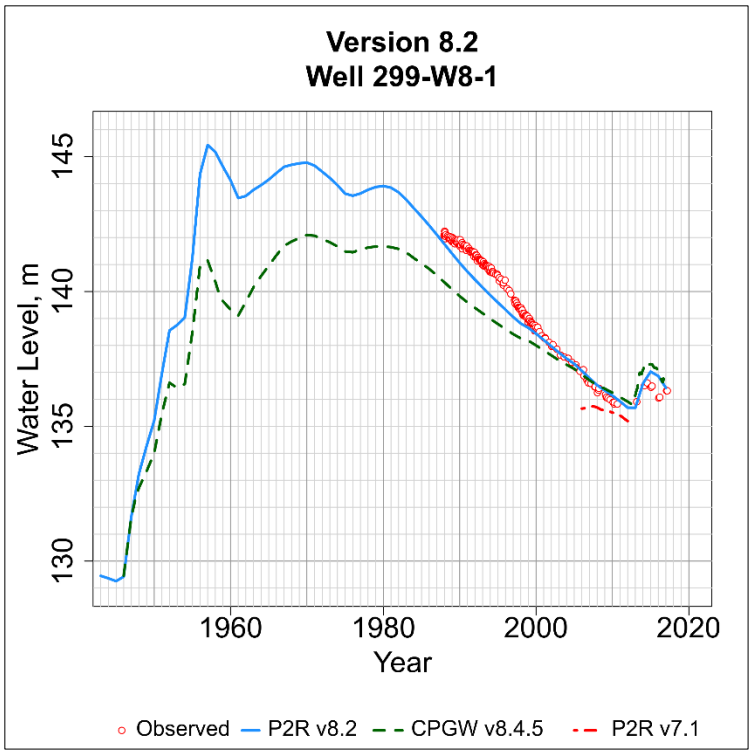

Figure D-319. Observed and simulated water level in the P2R Model at well 299-W8-1.png.

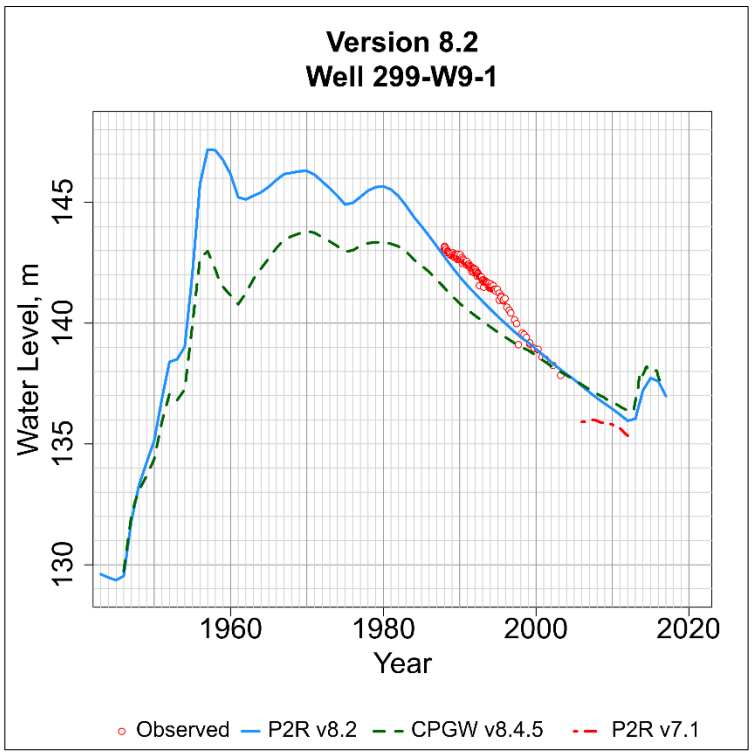

Figure D-320. Observed and simulated water level in the P2R Model at well 299-W9-1.png.

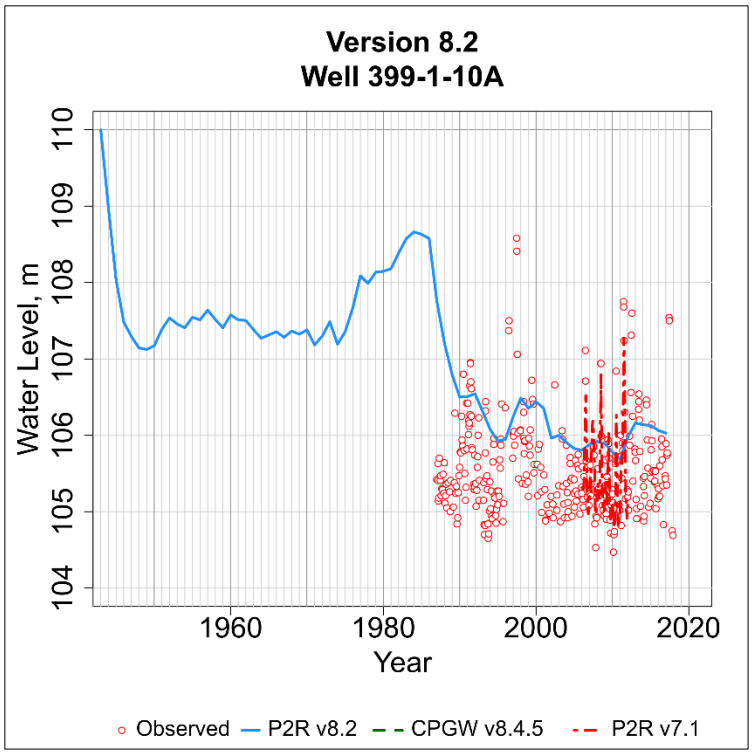

Figure D-321. Observed and simulated water level in the P2R Model at well 399-1-10A.png.

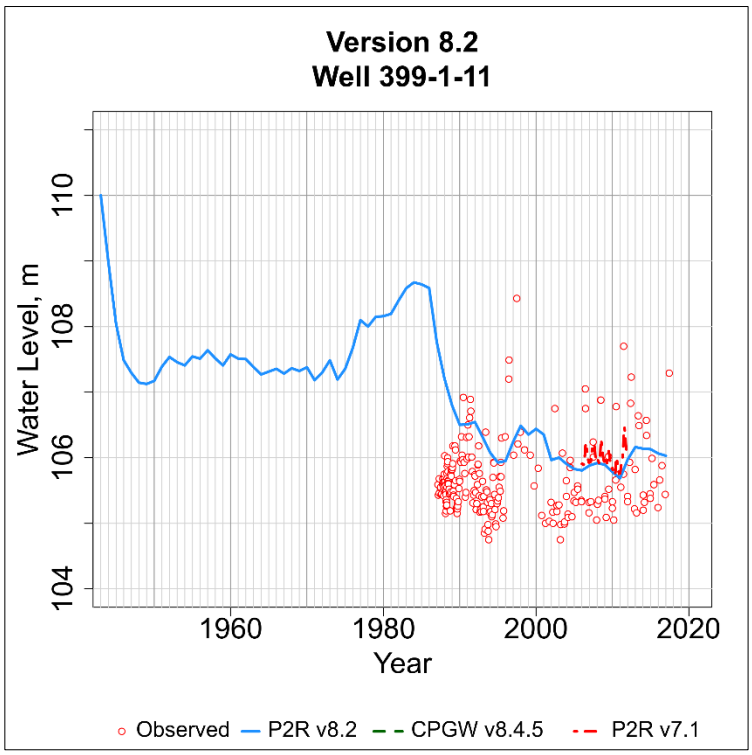

Figure D-322. Observed and simulated water level in the P2R Model at well 399-1-11.png.

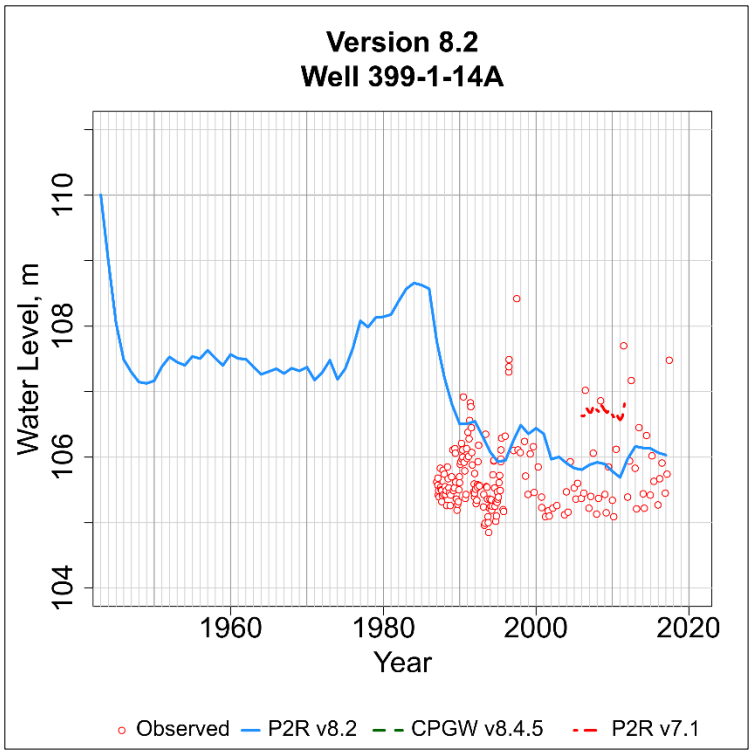

Figure D-323. Observed and simulated water level in the P2R Model at well 399-1-14A.png.

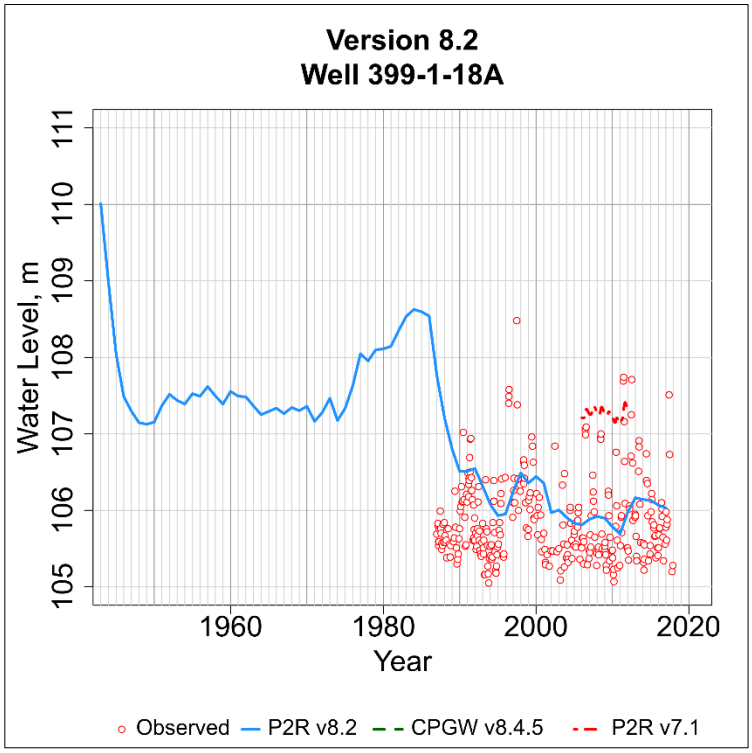

Figure D-324. Observed and simulated water level in the P2R Model at well 399-1-18A.png.

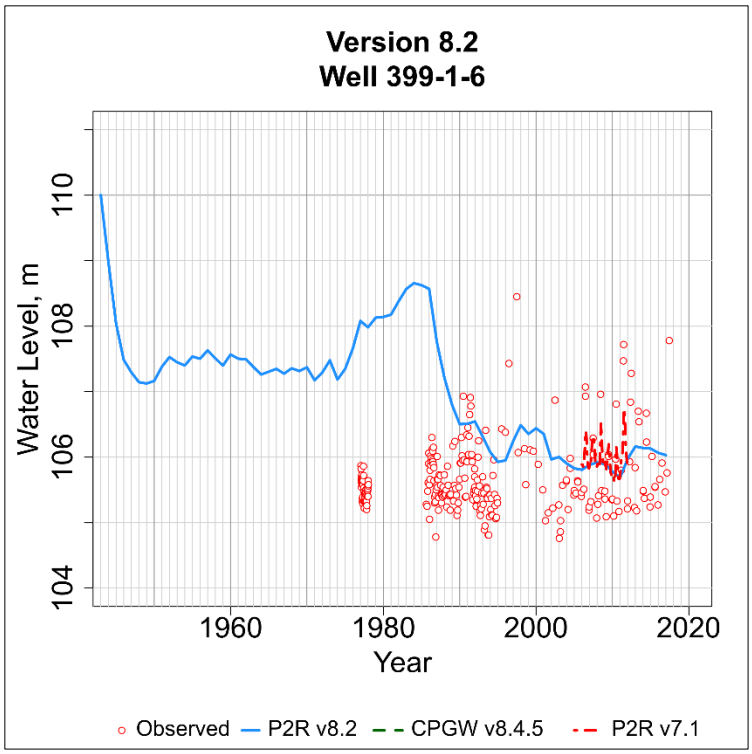

Figure D-325. Observed and simulated water level in the P2R Model at well 399-1-6.png.

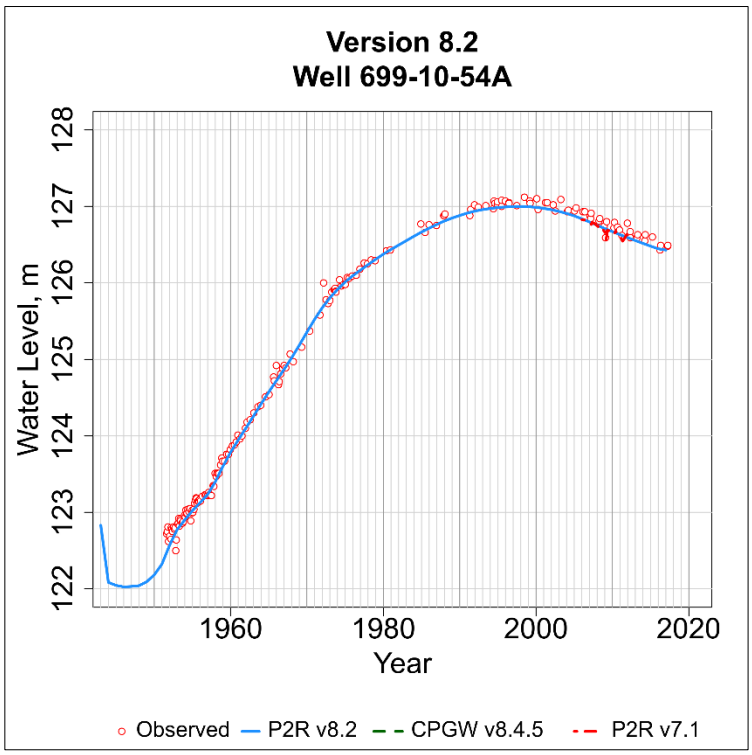

Figure D-326. Observed and simulated water level in the P2R Model at well 699-10-54A.png.

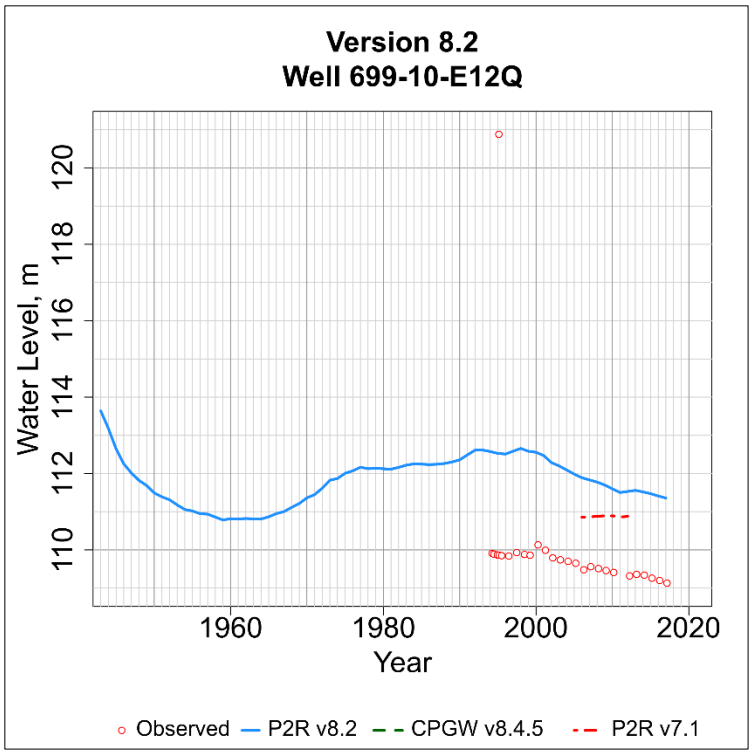

Figure D-327. Observed and simulated water level in the P2R Model at well 699-10-E12Q.png.

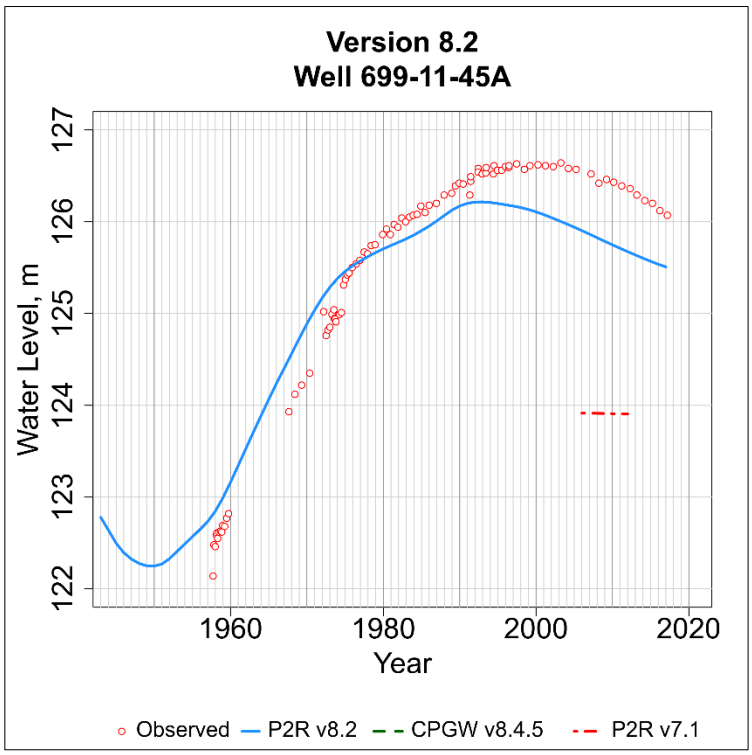

Figure D-328. Observed and simulated water level in the P2R Model at well 699-11-45A.png.

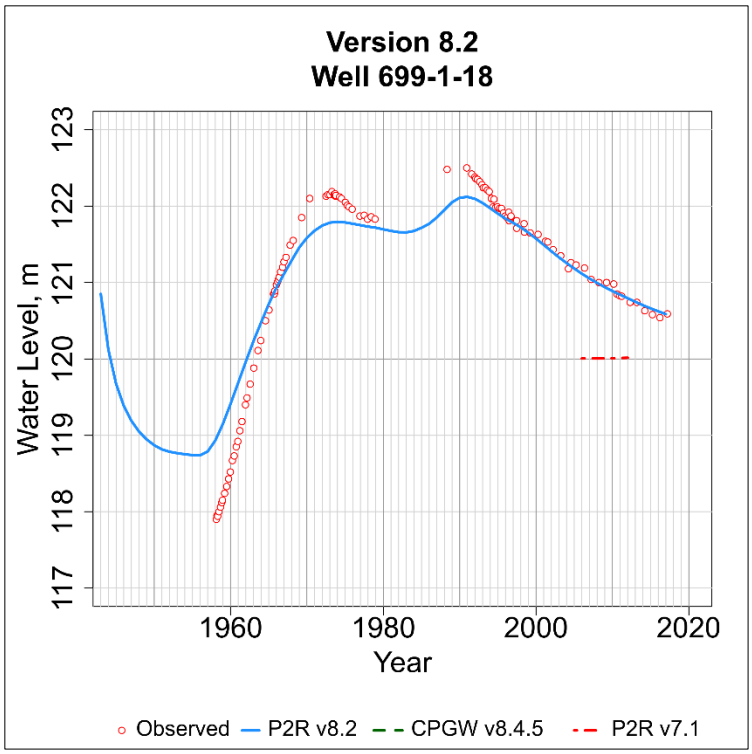

Figure D-329. Observed and simulated water level in the P2R Model at well 699-1-18.png.

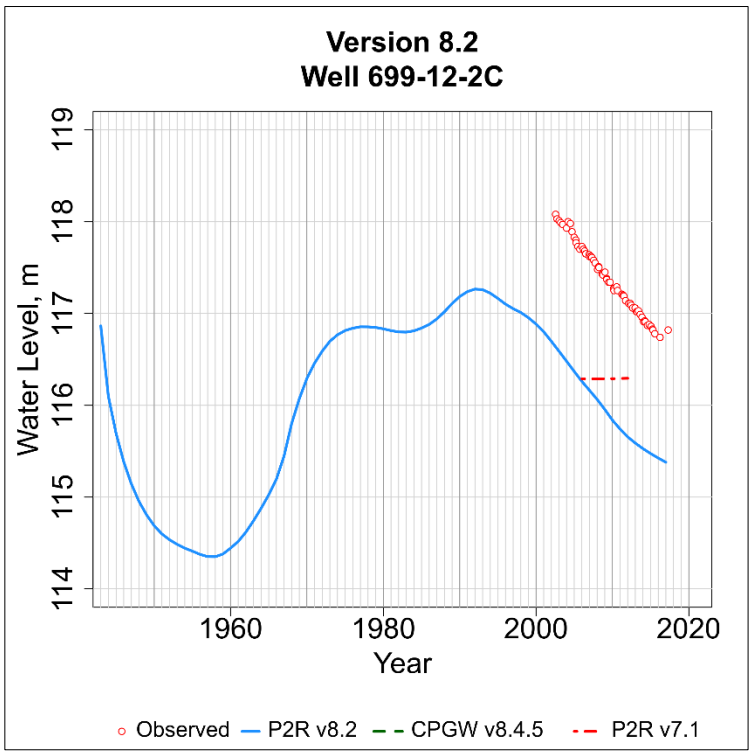

Figure D-330. Observed and simulated water level in the P2R Model at well 699-12-2C.png.

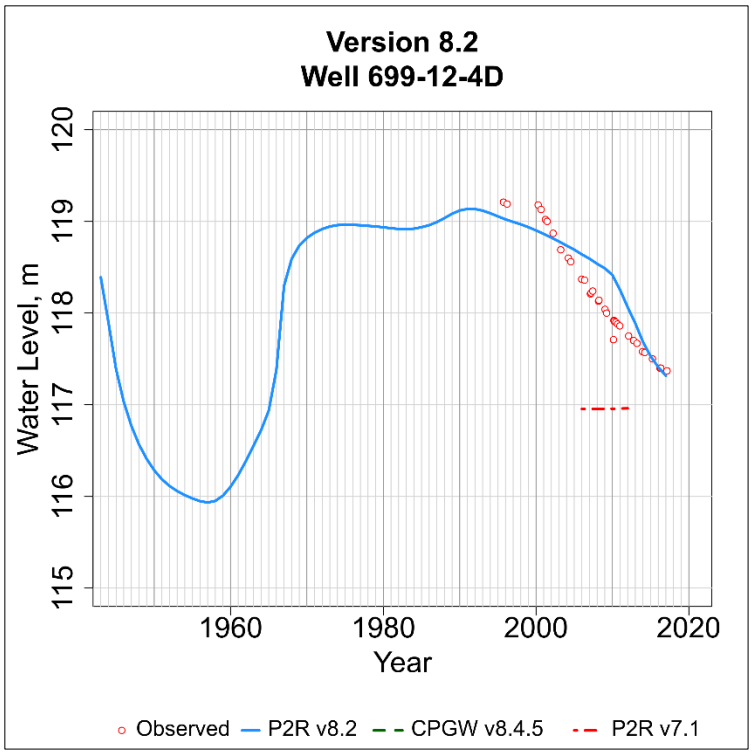

Figure D-331. Observed and simulated water level in the P2R Model at well 699-12-4D.png.

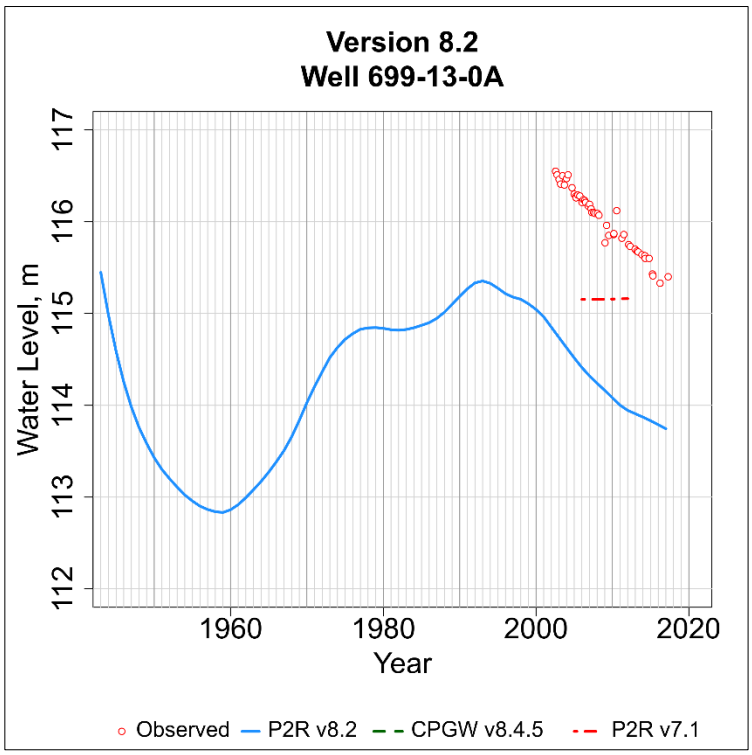

Figure D-332. Observed and simulated water level in the P2R Model at well 699-13-0A.png.

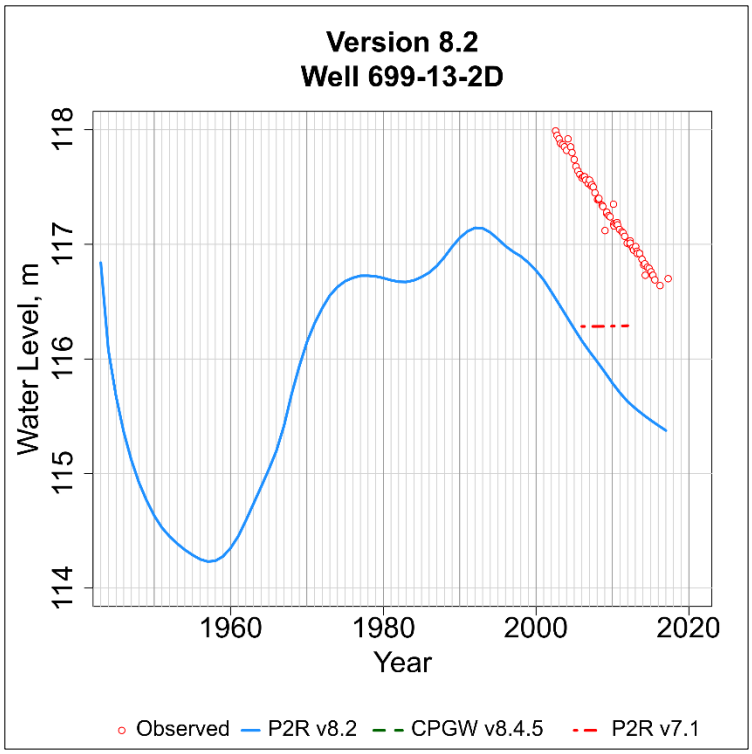

Figure D-333. Observed and simulated water level in the P2R Model at well 699-13-2D.png.

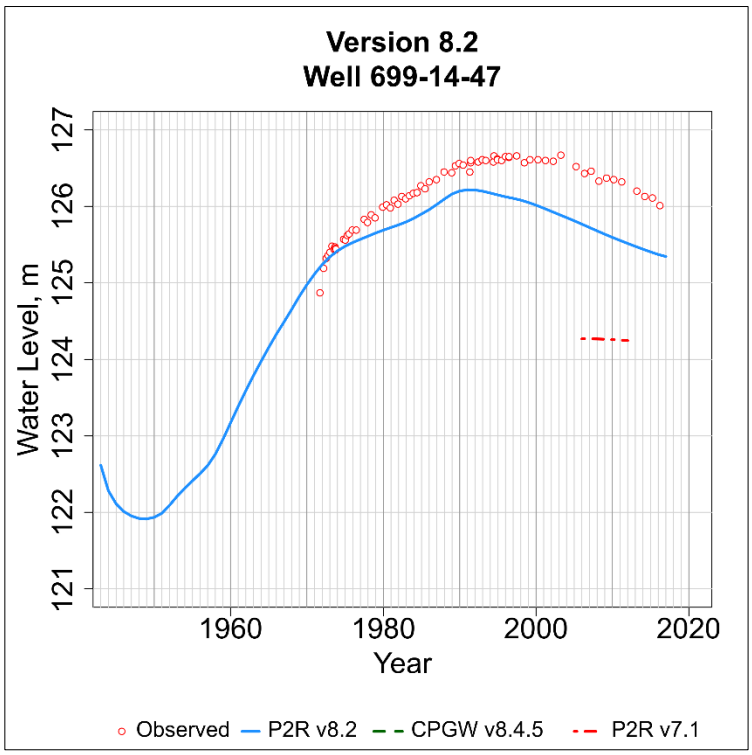

Figure D-334. Observed and simulated water level in the P2R Model at well 699-14-47.png.

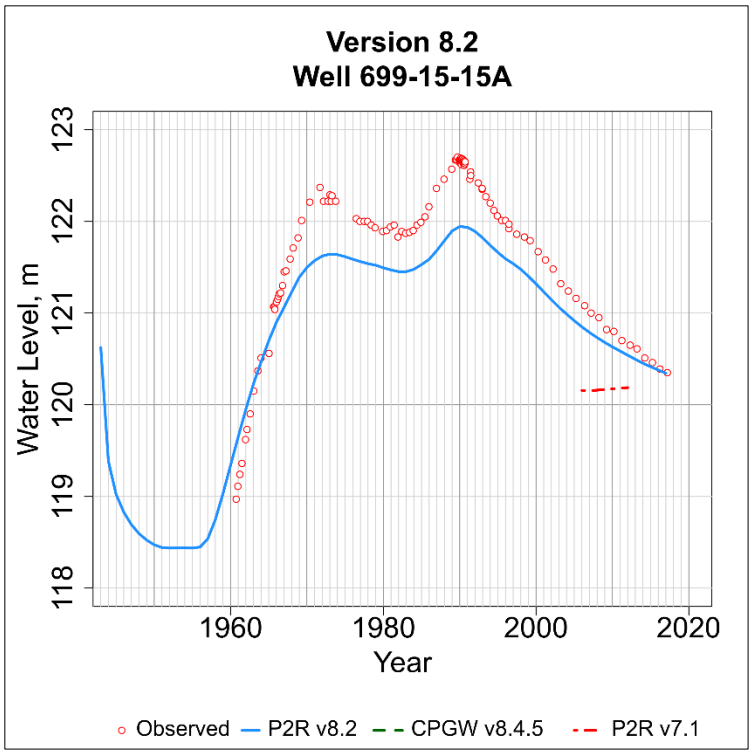

Figure D-335. Observed and simulated water level in the P2R Model at well 699-15-15A.png.

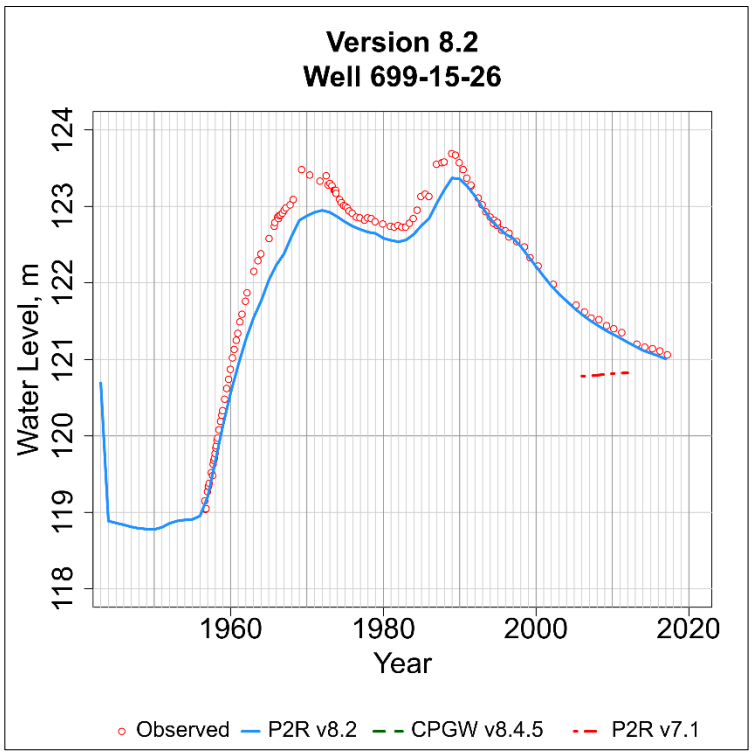

Figure D-336. Observed and simulated water level in the P2R Model at well 699-15-26.png.

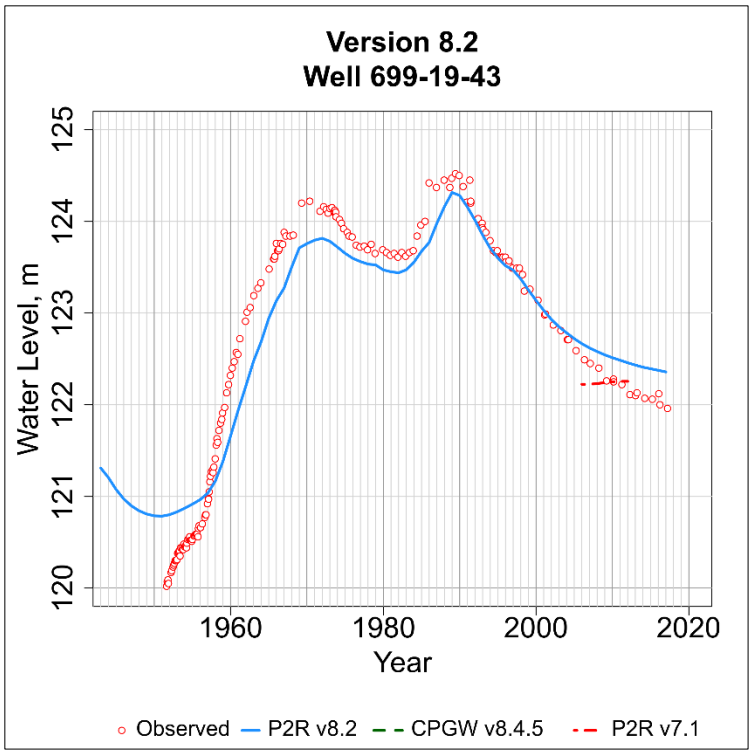

Figure D-337. Observed and simulated water level in the P2R Model at well 699-19-43.png.

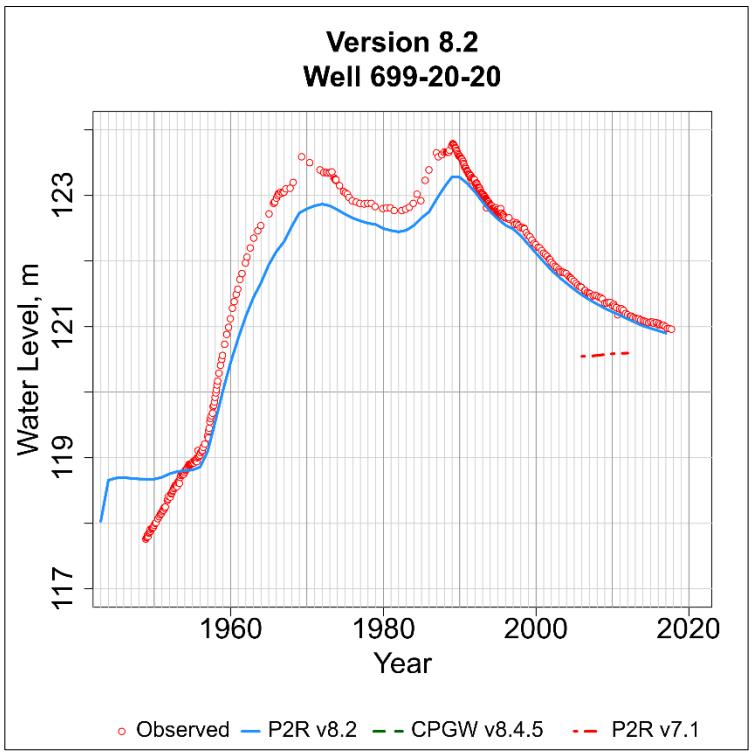

Figure D-338. Observed and simulated water level in the P2R Model at well 699-20-20.png.

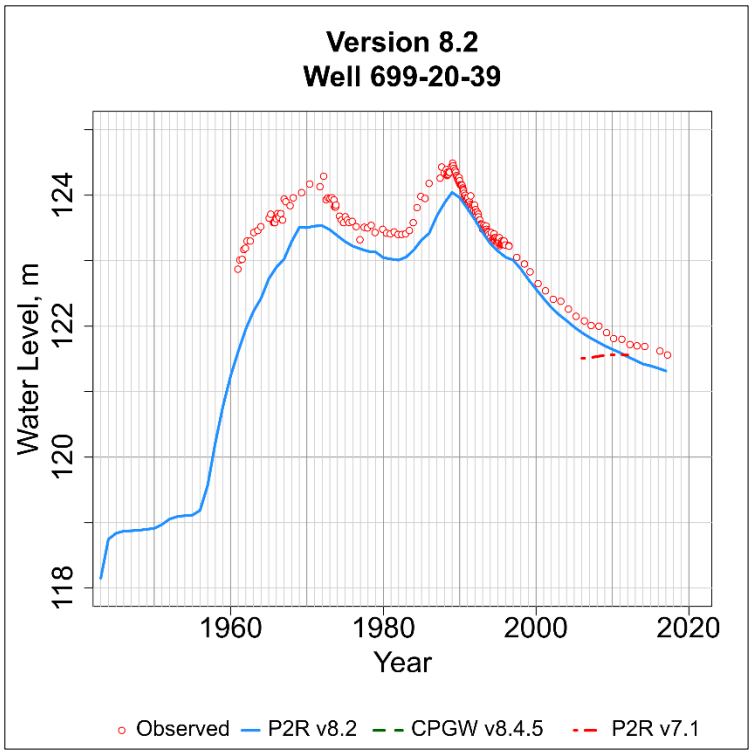

Figure D-339. Observed and simulated water level in the P2R Model at well 699-20-39.png.

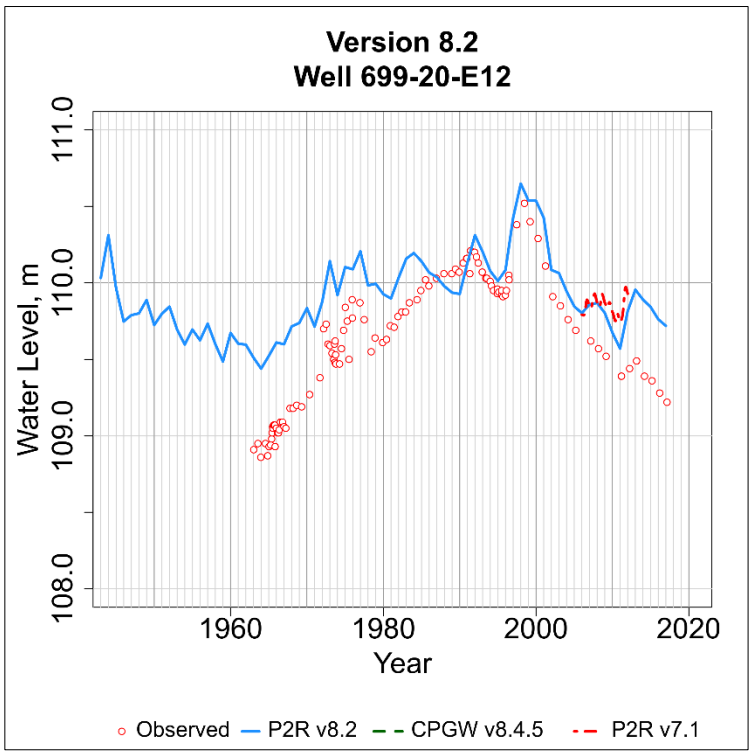

Figure D-340. Observed and simulated water level in the P2R Model at well 699-20-E12.png.

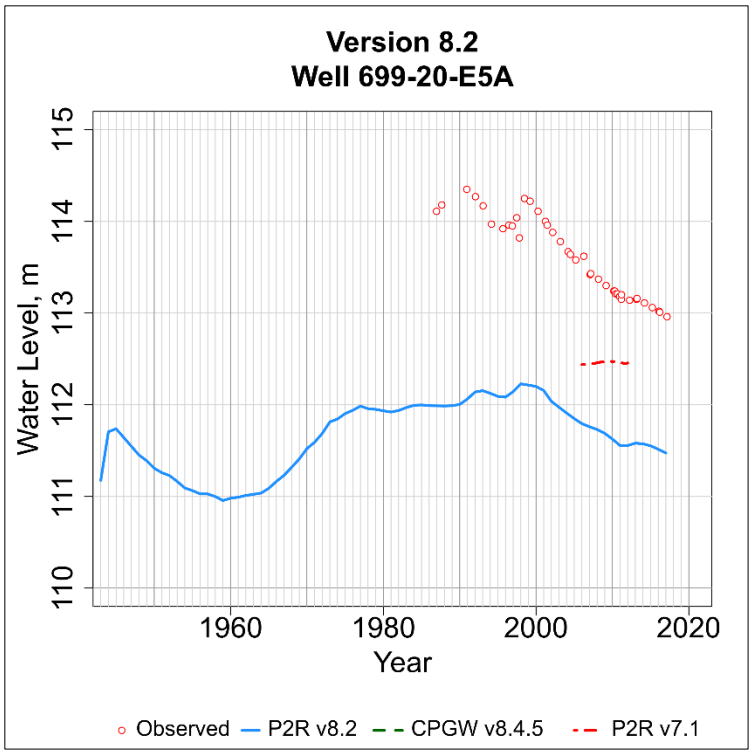

Figure D-341. Observed and simulated water level in the P2R Model at well 699-20-E5A.png.

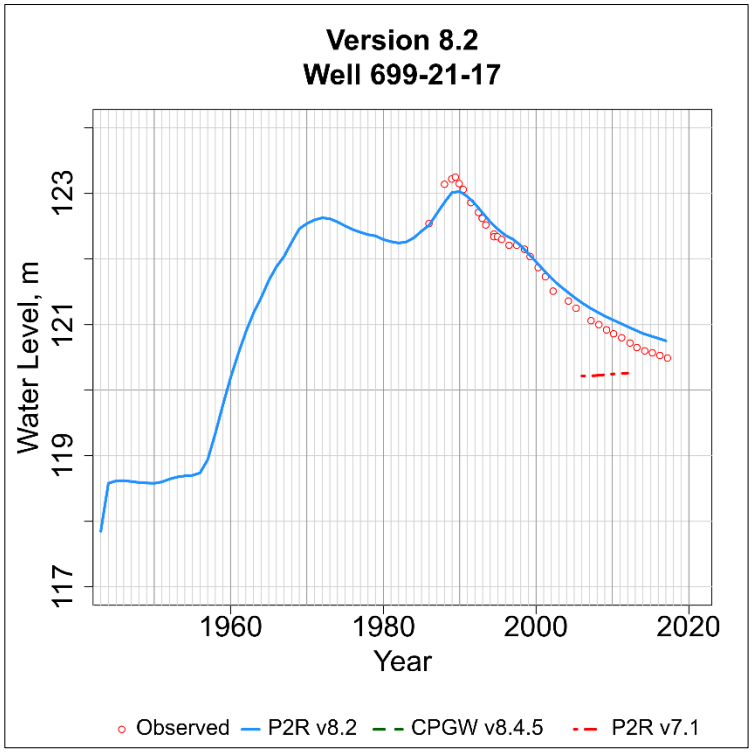

Figure D-342. Observed and simulated water level in the P2R Model at well 699-21-17.png.

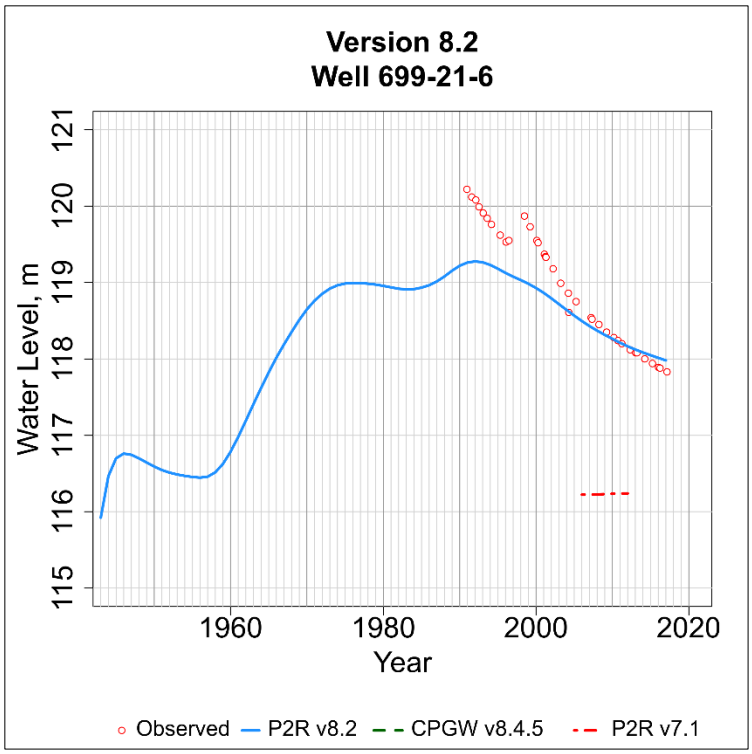

Figure D-343. Observed and simulated water level in the P2R Model at well 699-21-6.png.

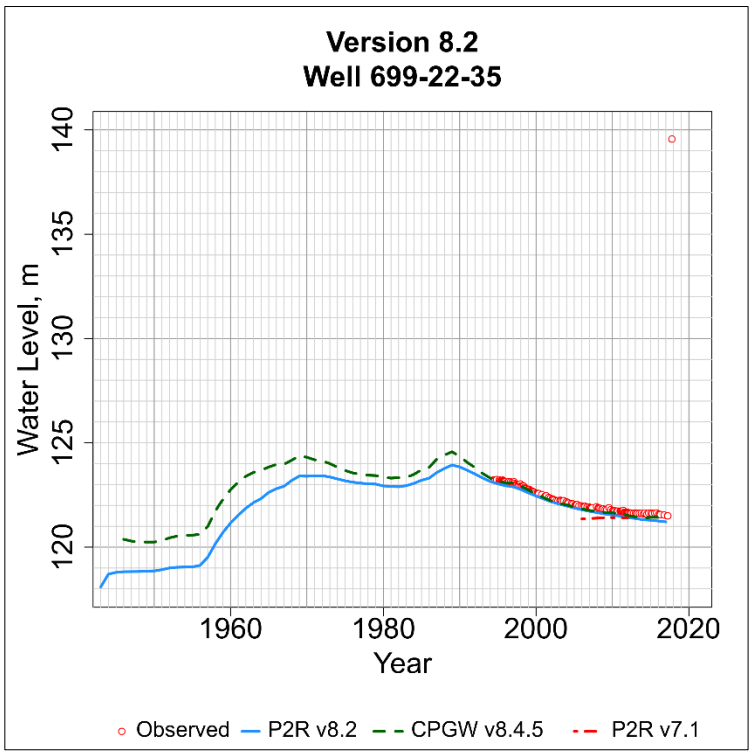

Figure D-344. Observed and simulated water level in the P2R Model at well 699-22-35.png.

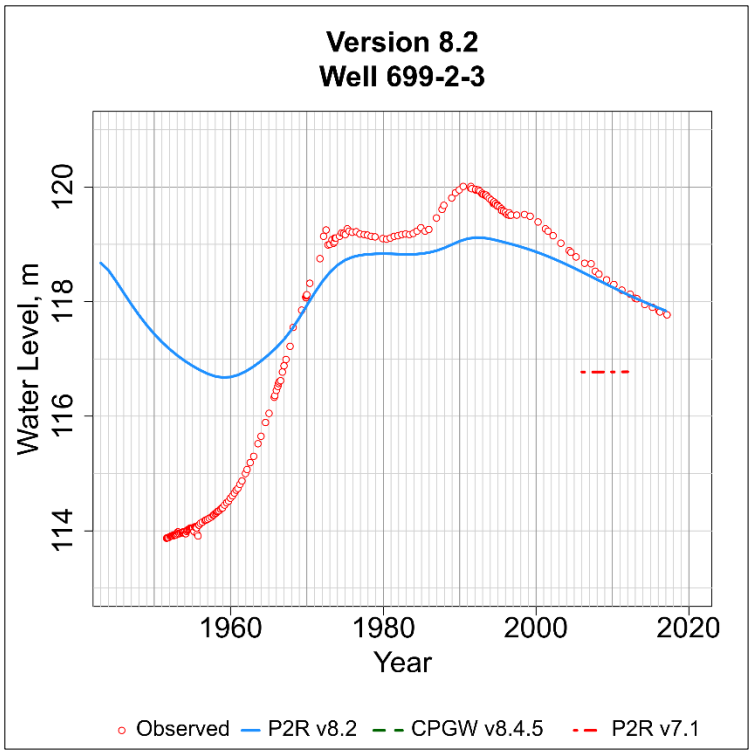

Figure D-345. Observed and simulated water level in the P2R Model at well 699-2-3.png.

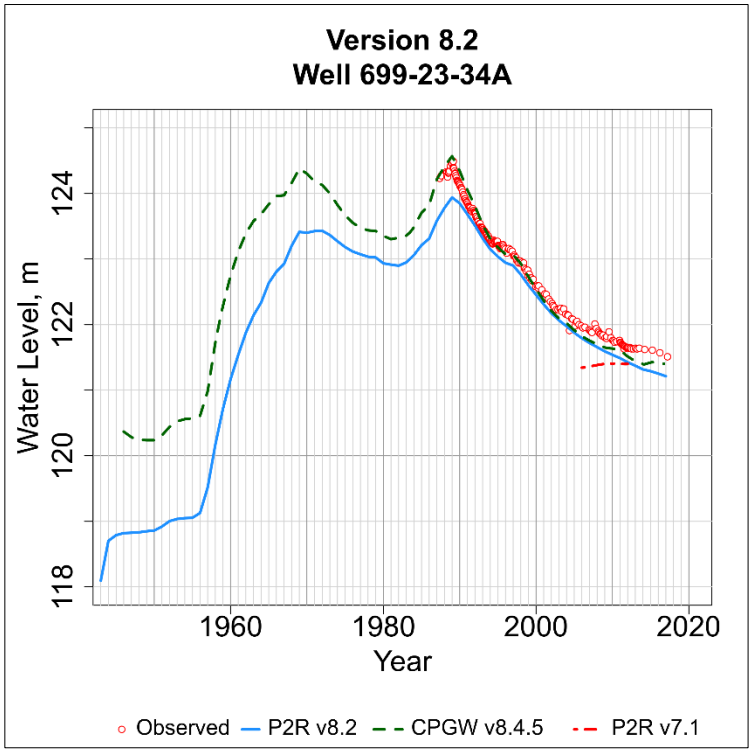

Figure D-346. Observed and simulated water level in the P2R Model at well 699-23-34A.png.

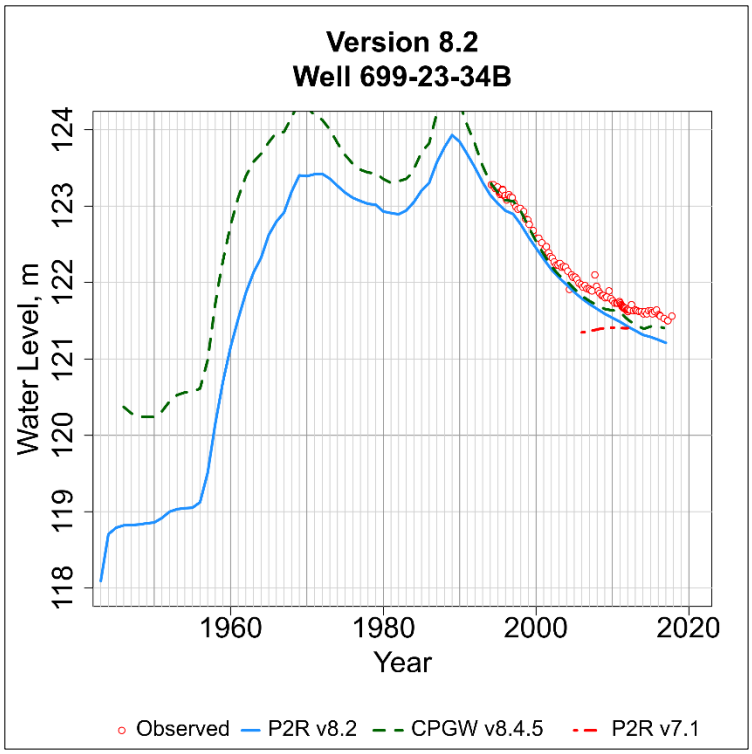

Figure D-347. Observed and simulated water level in the P2R Model at well 699-23-34B.png.

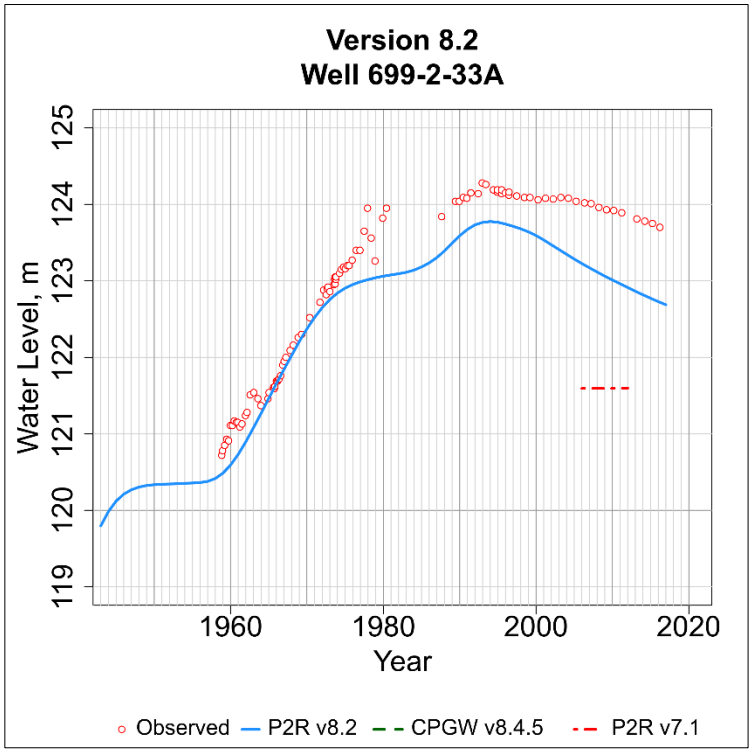

Figure D-348. Observed and simulated water level in the P2R Model at well 699-2-33A.png.

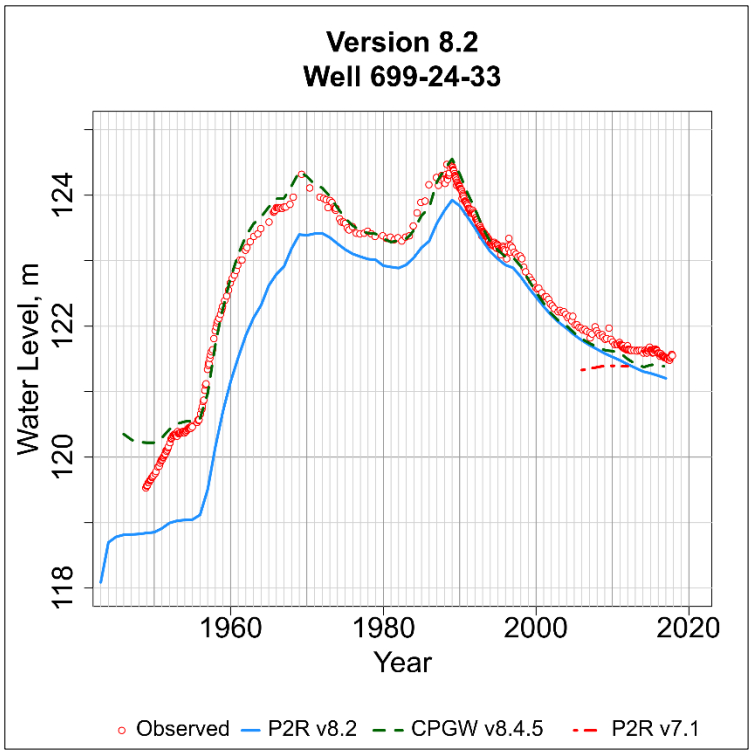

Figure D-349. Observed and simulated water level in the P2R Model at well 699-24-33.png.

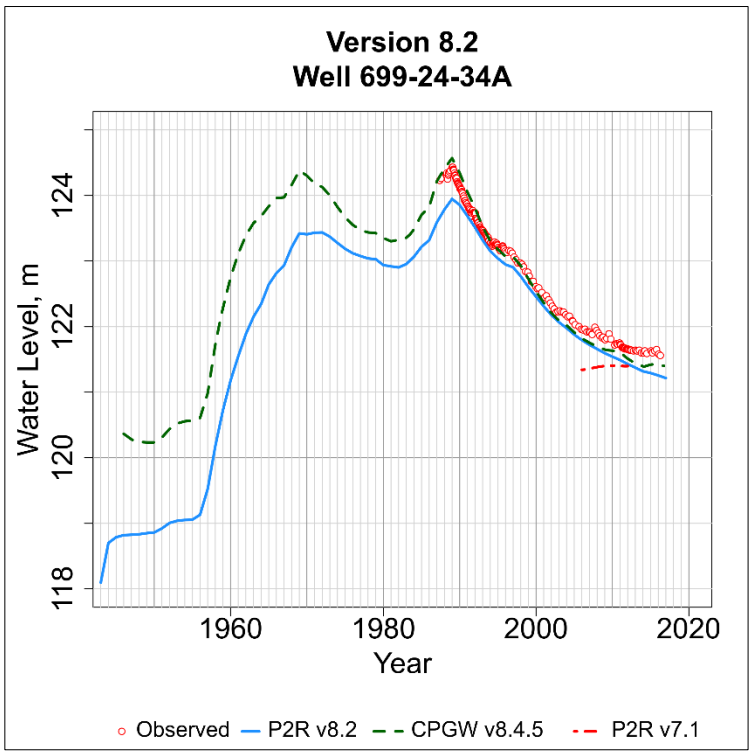

Figure D-350. Observed and simulated water level in the P2R Model at well 699-24-34A.png.

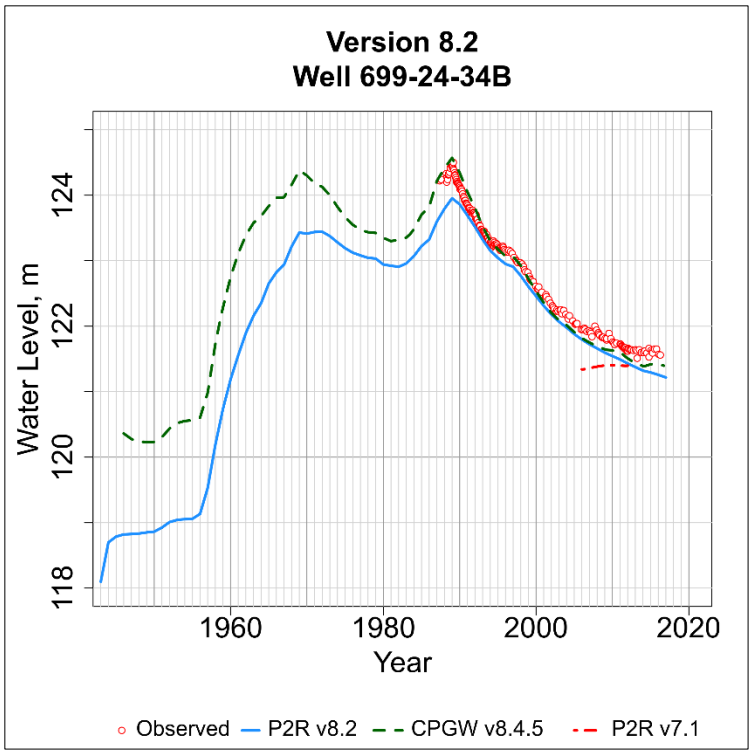

Figure D-351. Observed and simulated water level in the P2R Model at well 699-24-34B.png.

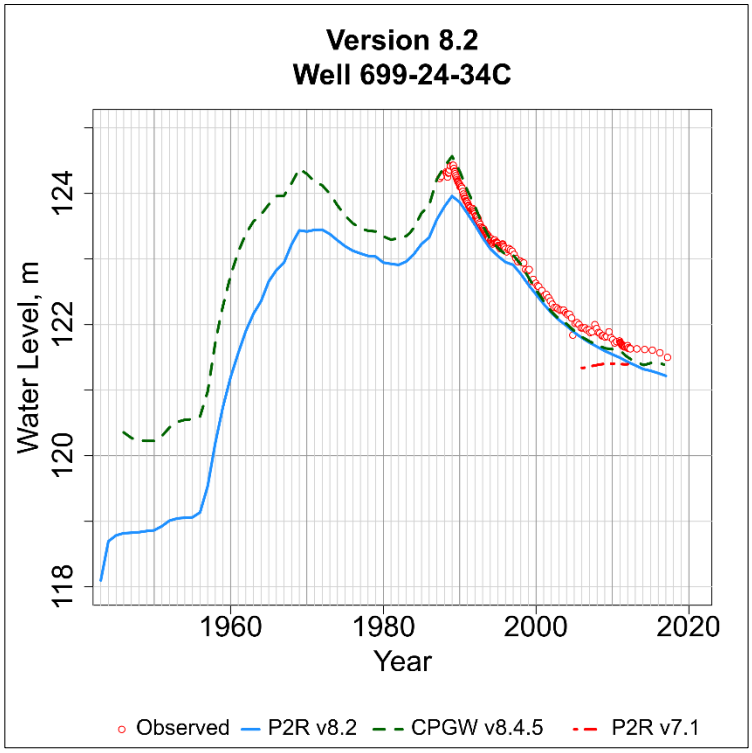

Figure D-352. Observed and simulated water level in the P2R Model at well 699-24-34C.png.

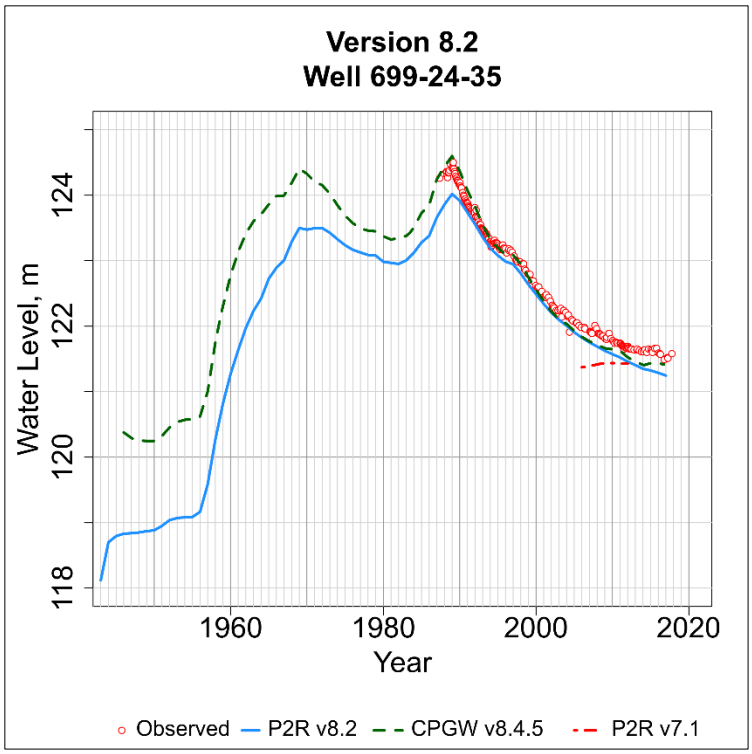

Figure D-353. Observed and simulated water level in the P2R Model at well 699-24-35.png.

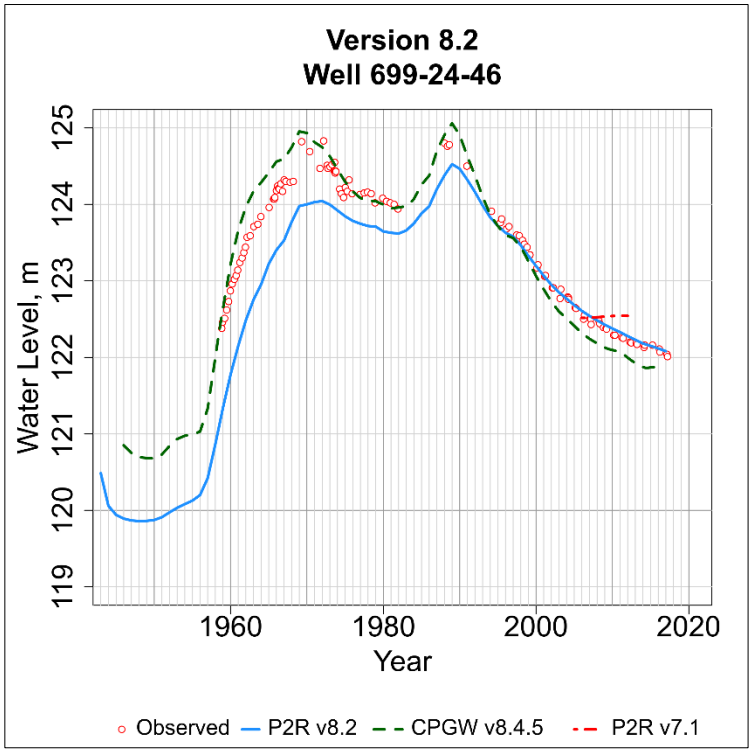

Figure D-354. Observed and simulated water level in the P2R Model at well 699-24-46.png.

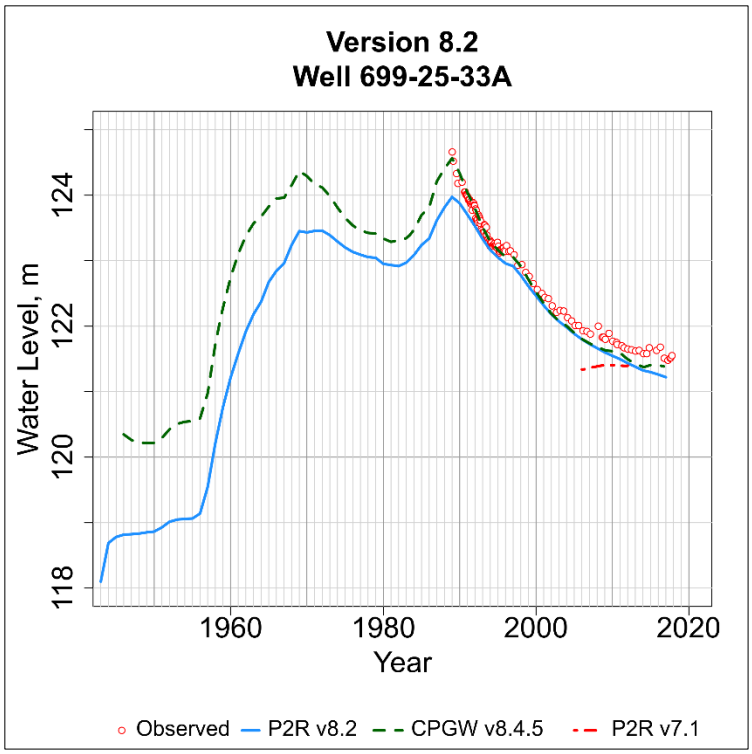

Figure D-355. Observed and simulated water level in the P2R Model at well 699-25-33A.png.

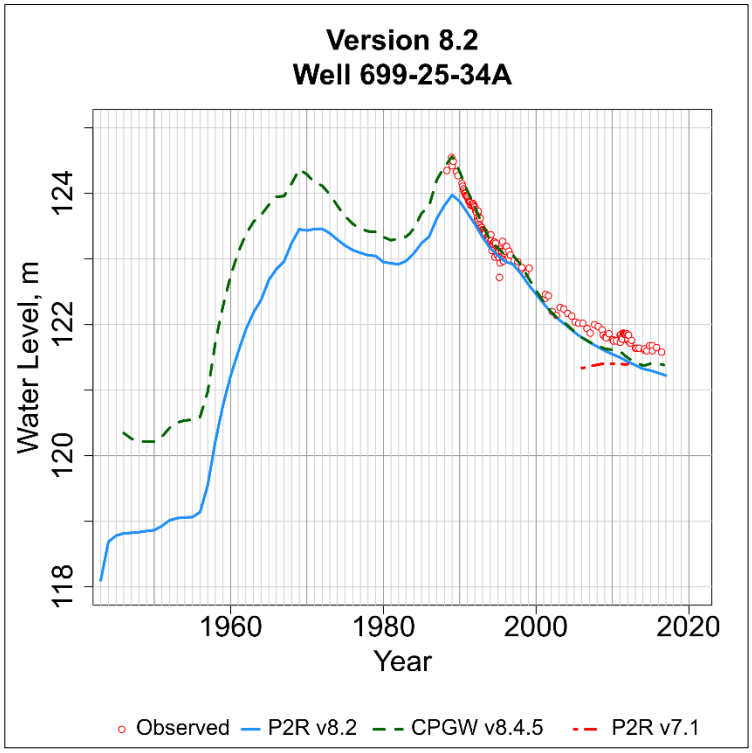

Figure D-356. Observed and simulated water level in the P2R Model at well 699-25-34A.png.

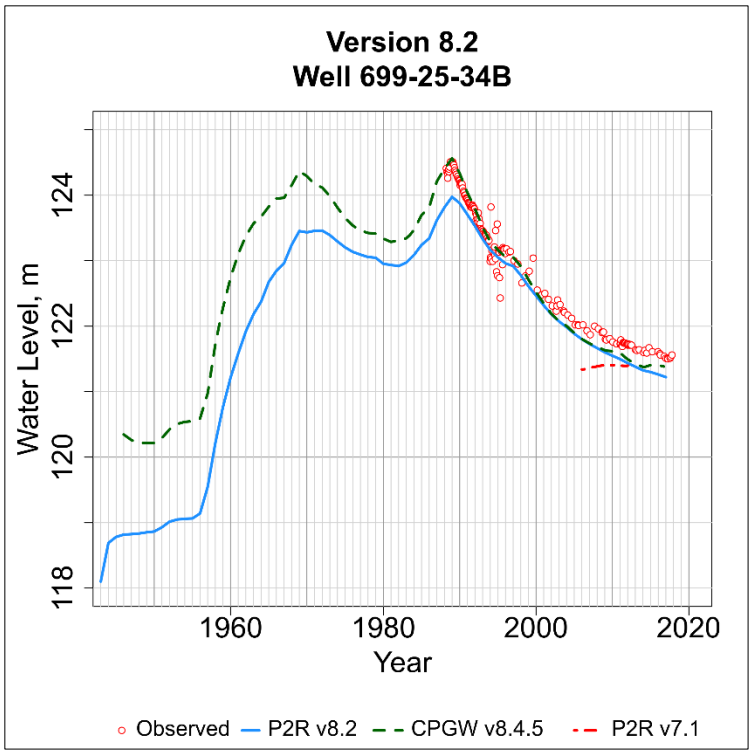

Figure D-357. Observed and simulated water level in the P2R Model at well 699-25-34B.png.

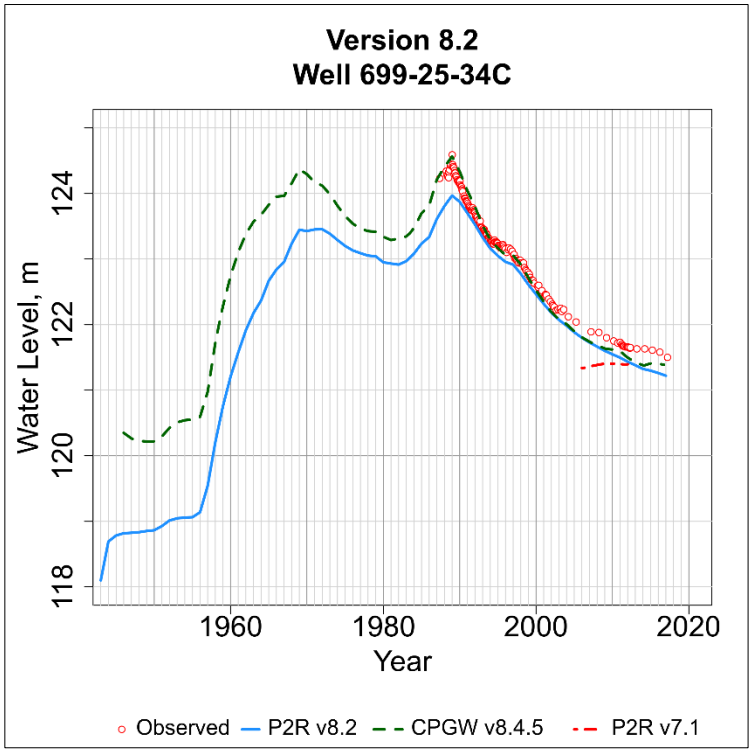

Figure D-358. Observed and simulated water level in the P2R Model at well 699-25-34C.png.

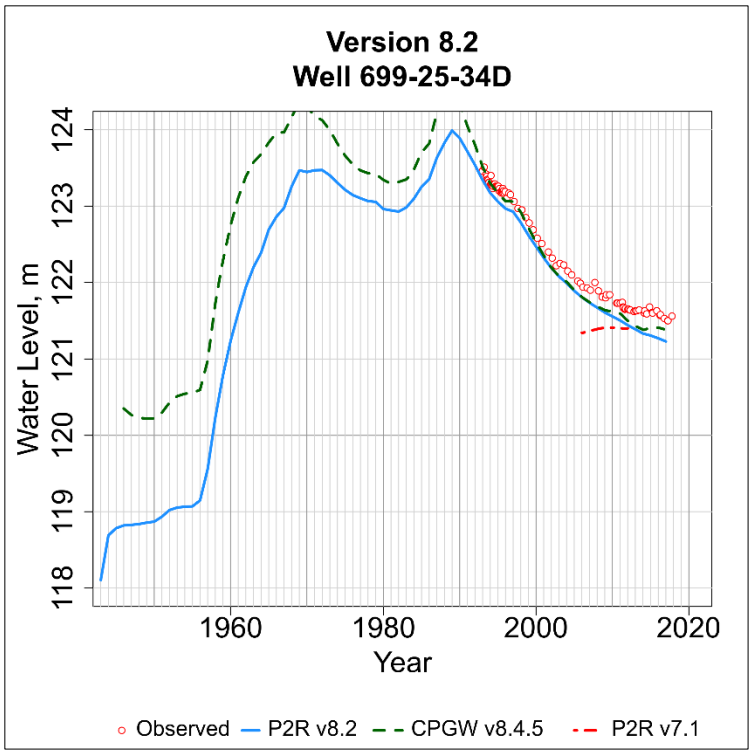

Figure D-359. Observed and simulated water level in the P2R Model at well 699-25-34D.png.

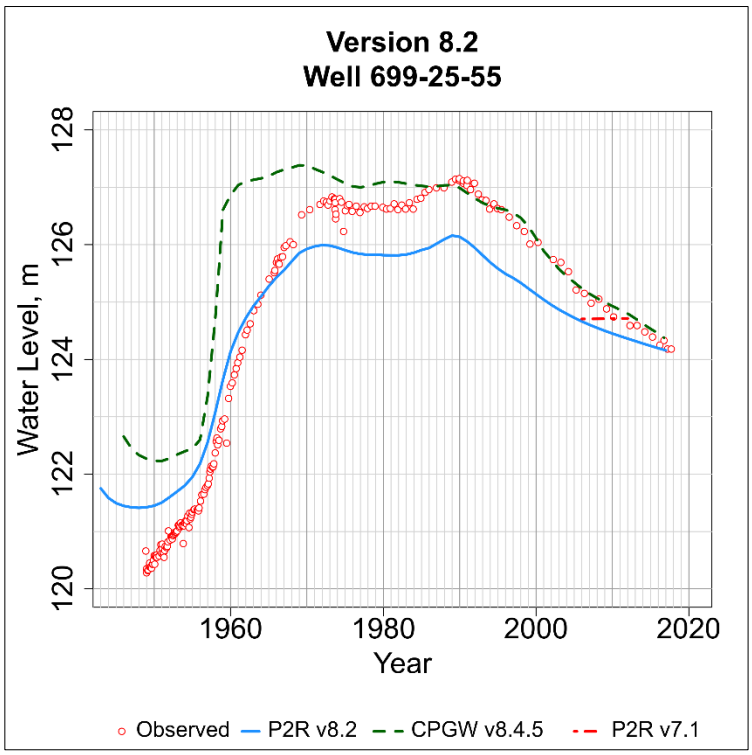

Figure D-360. Observed and simulated water level in the P2R Model at well 699-25-55.png.

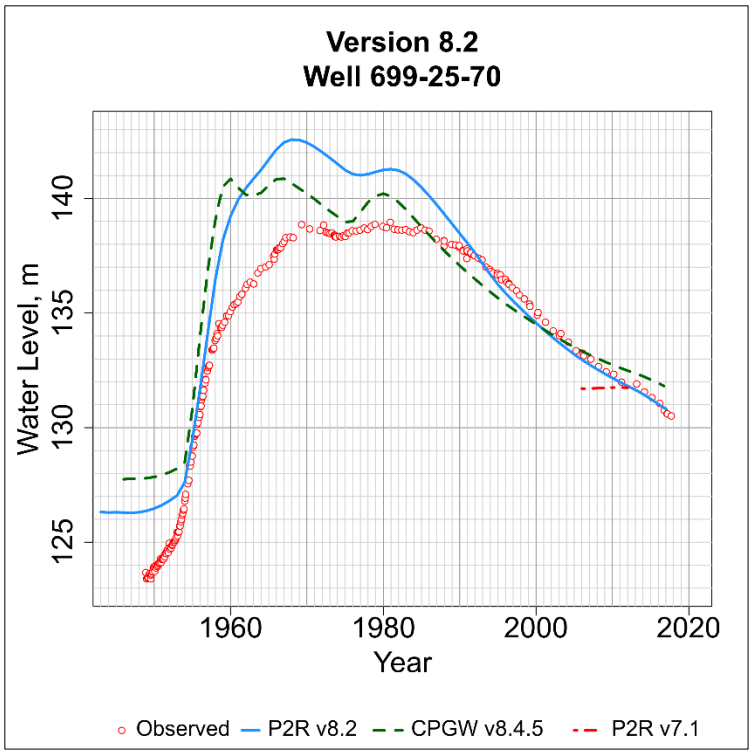

Figure D-361. Observed and simulated water level in the P2R Model at well 699-25-70.png.

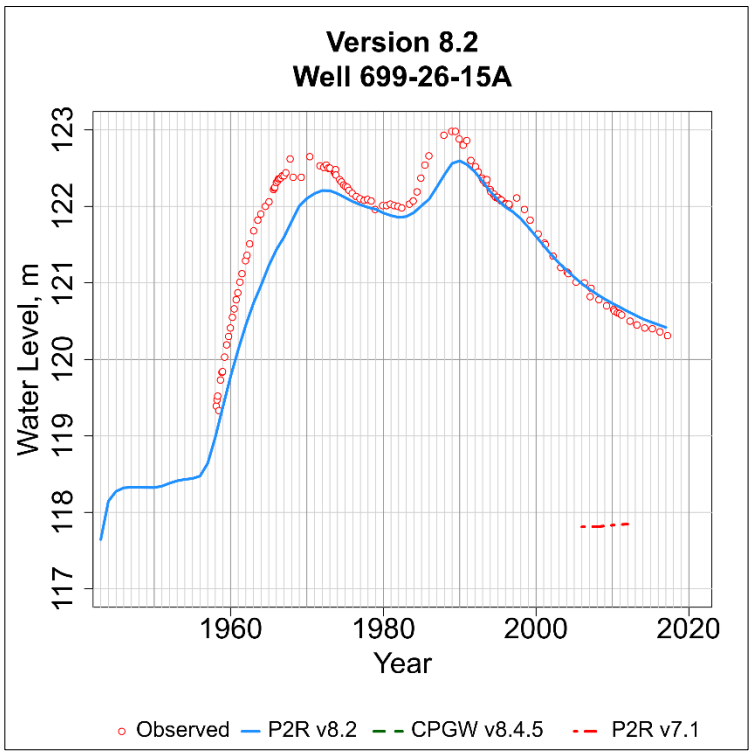

Figure D-362. Observed and simulated water level in the P2R Model at well 699-26-15A.png.

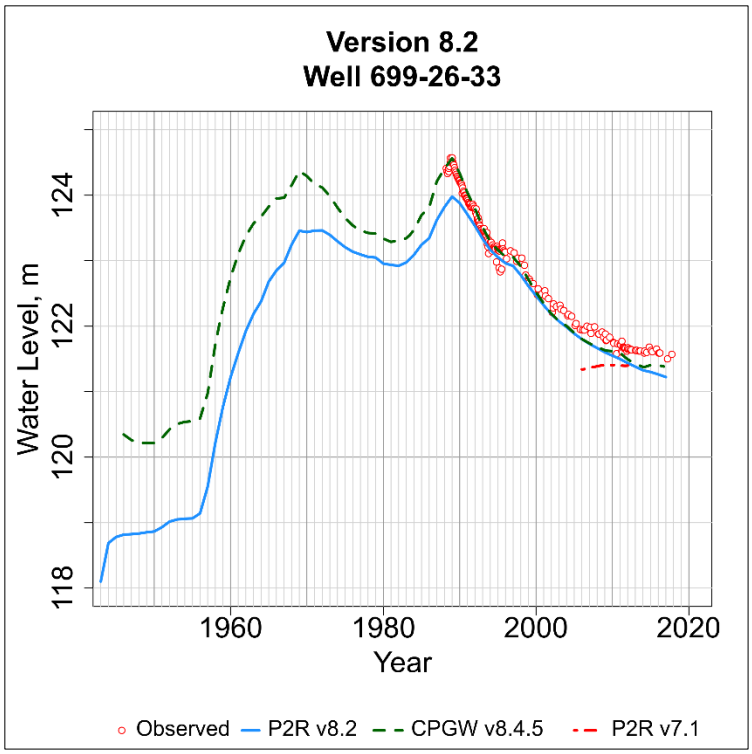

Figure D-363. Observed and simulated water level in the P2R Model at well 699-26-33.png.

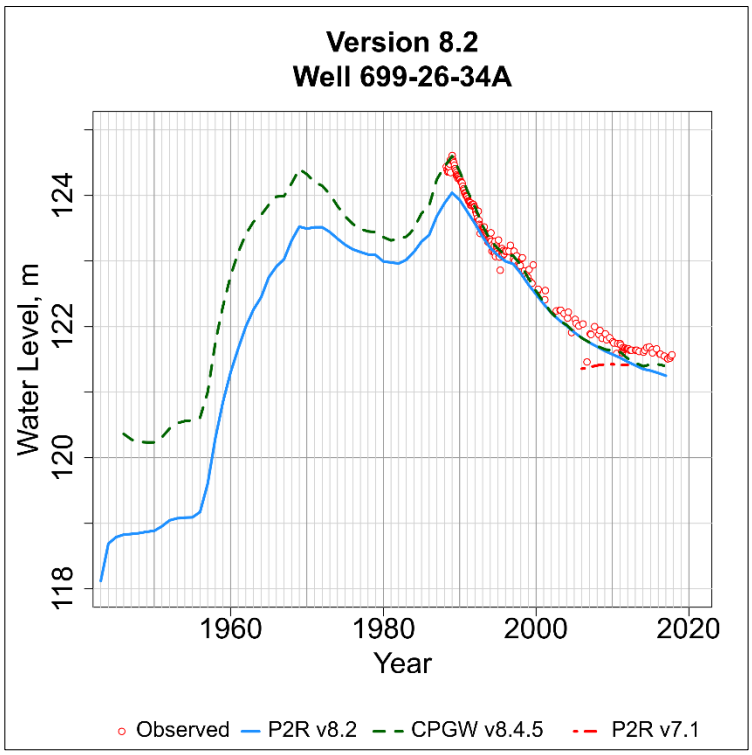

Figure D-364. Observed and simulated water level in the P2R Model at well 699-26-34A.png.

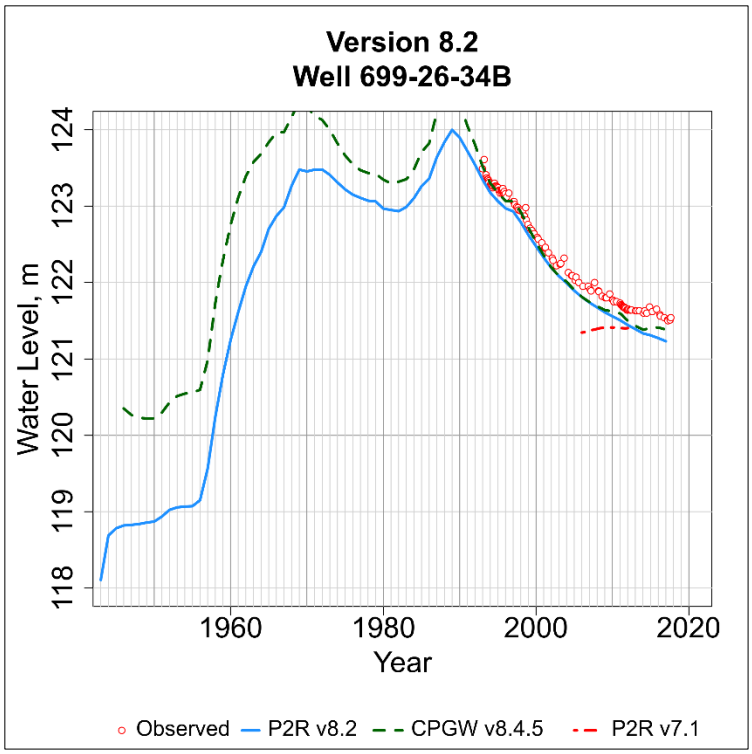

Figure D-365. Observed and simulated water level in the P2R Model at well 699-26-34B.png.

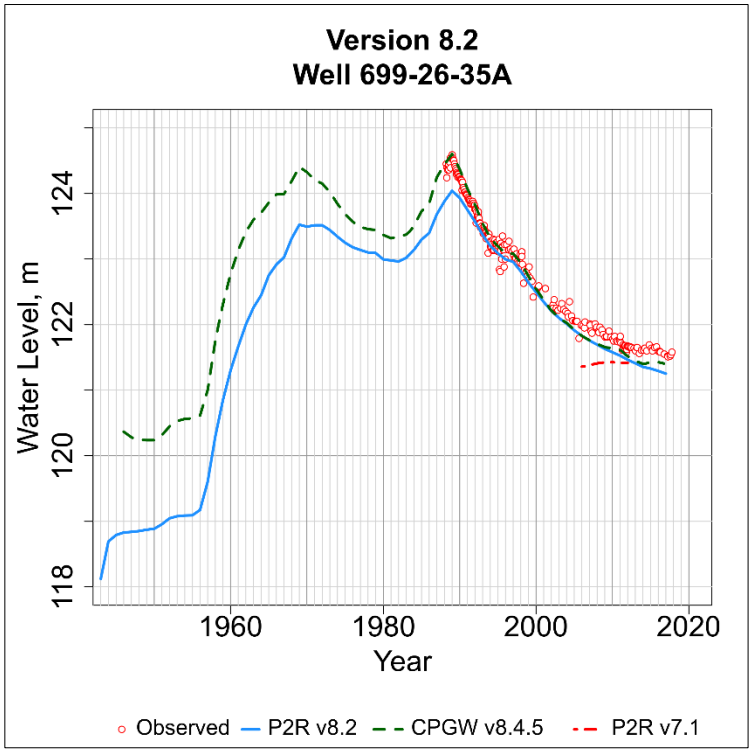

Figure D-366. Observed and simulated water level in the P2R Model at well 699-26-35A.png.

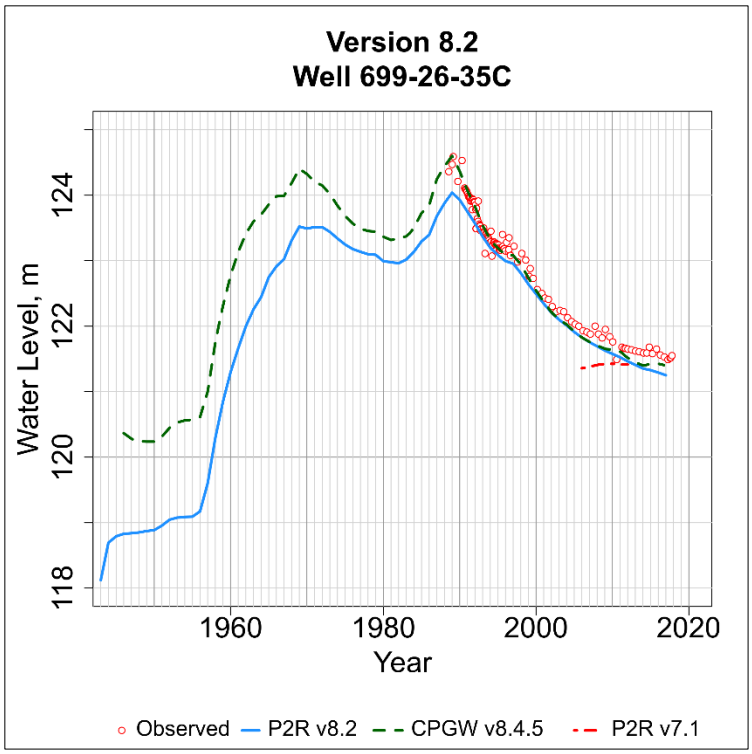

Figure D-367. Observed and simulated water level in the P2R Model at well 699-26-35C.png.

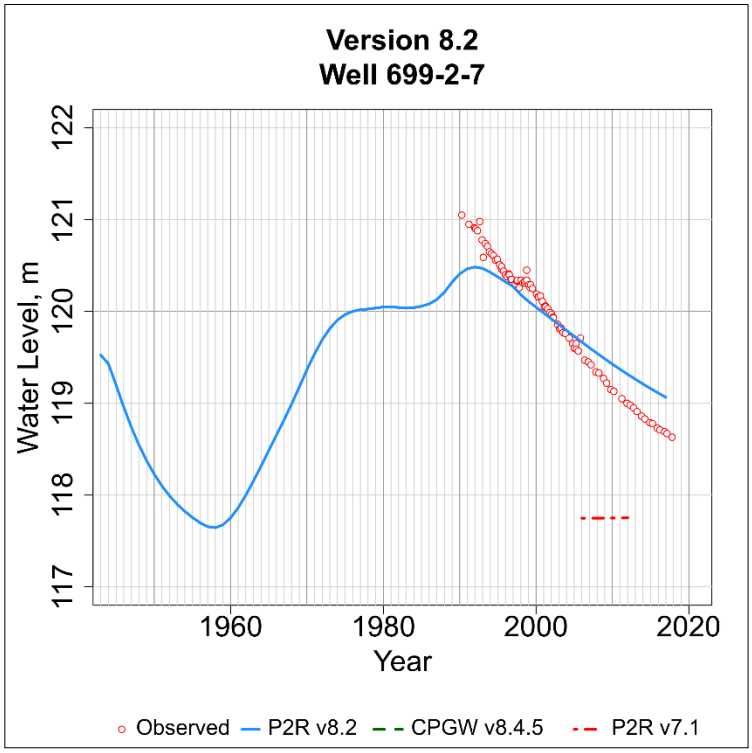

Figure D-368. Observed and simulated water level in the P2R Model at well 699-2-7.png.

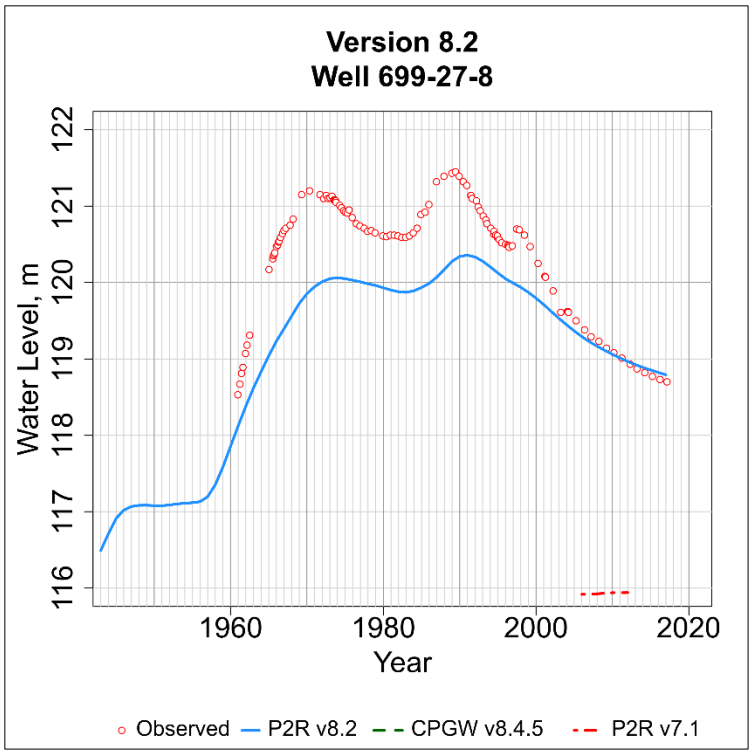

Figure D-369. Observed and simulated water level in the P2R Model at well 699-27-8.png.

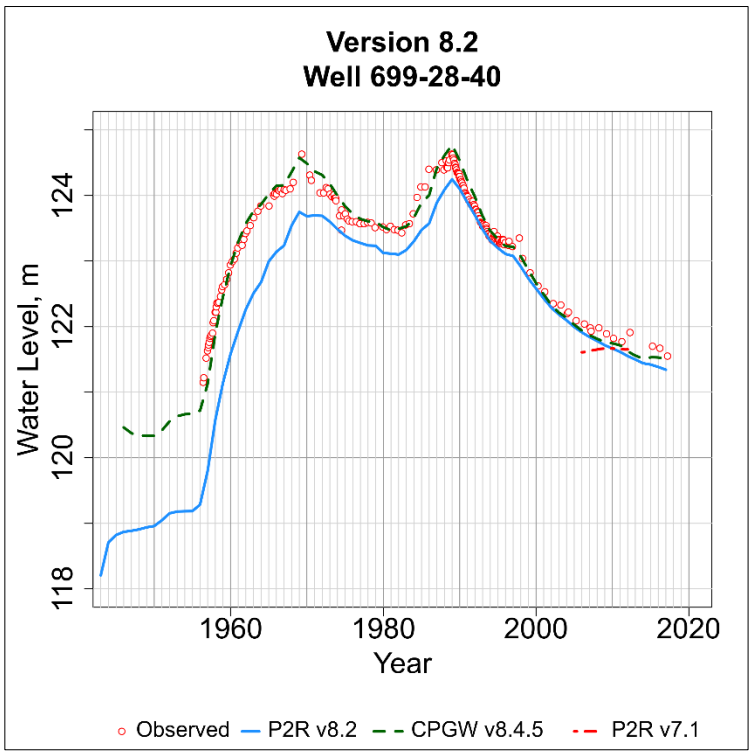

Figure D-370. Observed and simulated water level in the P2R Model at well 699-28-40.png.

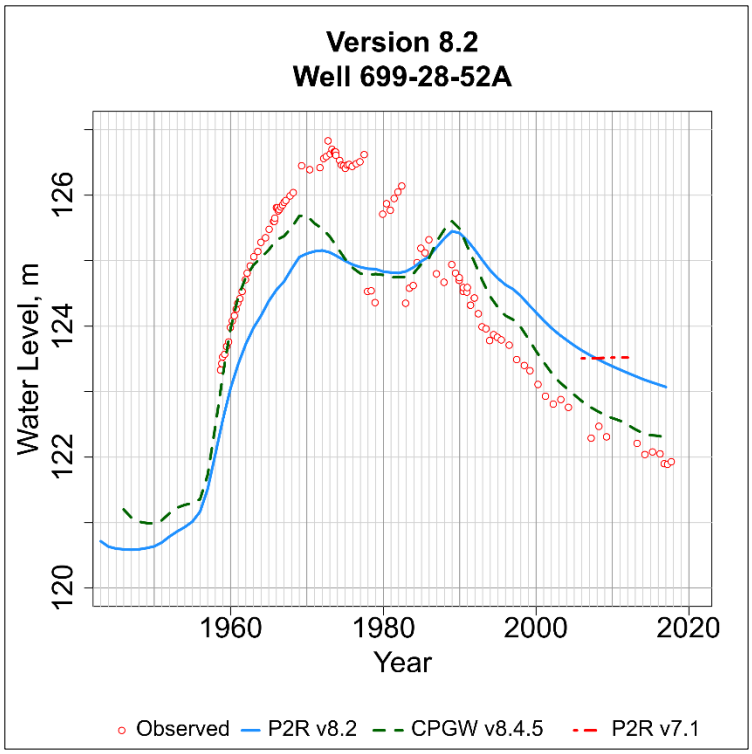

Figure D-371. Observed and simulated water level in the P2R Model at well 699-28-52A.png.

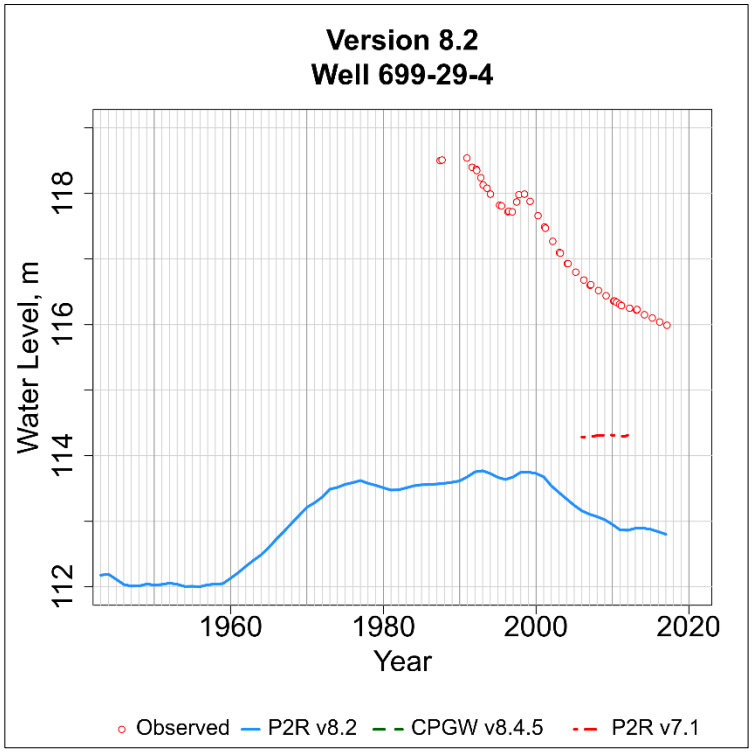

Figure D-372. Observed and simulated water level in the P2R Model at well 699-29-4.png.

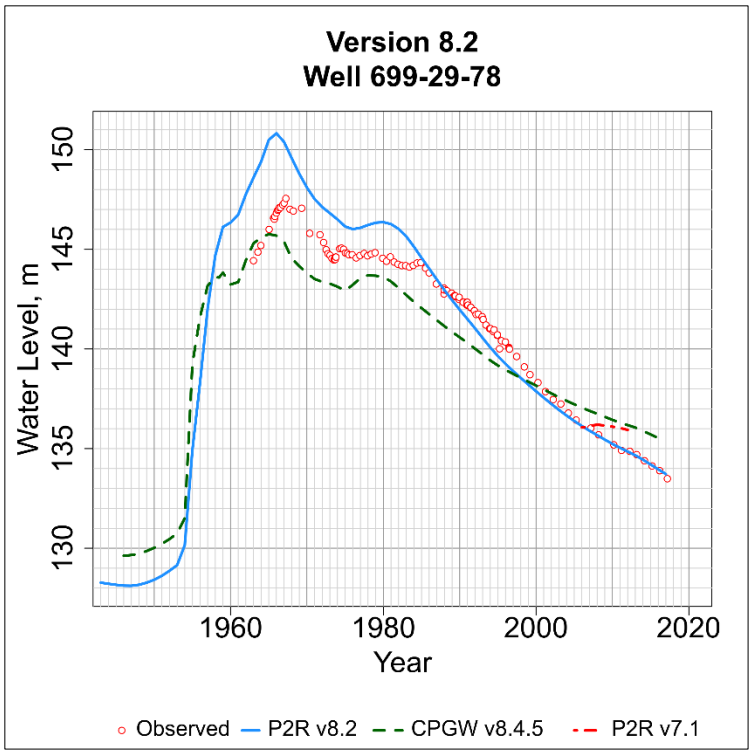

Figure D-373. Observed and simulated water level in the P2R Model at well 699-29-78.png.

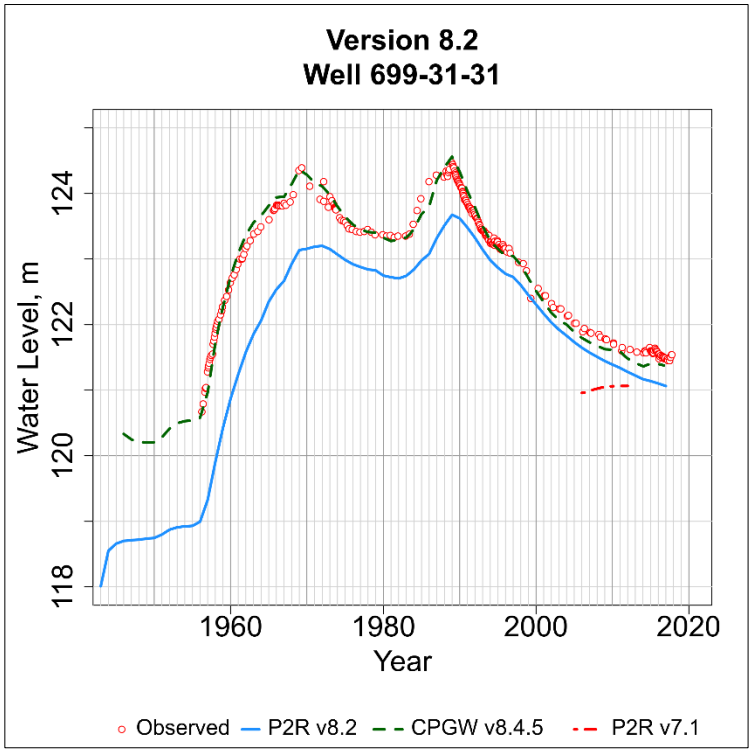

Figure D-374. Observed and simulated water level in the P2R Model at well 699-31-31.png.

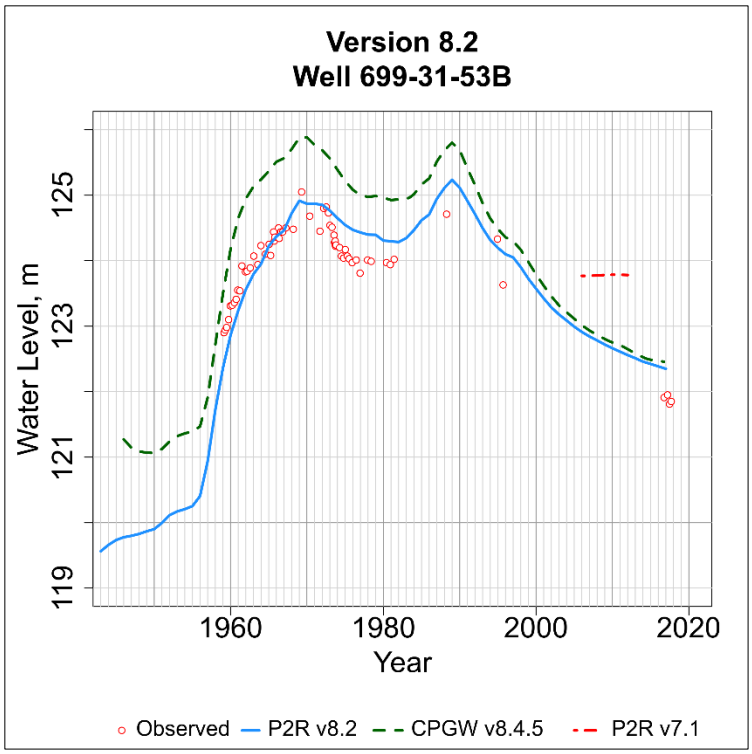

Figure D-375. Observed and simulated water level in the P2R Model at well 699-31-53B.png.

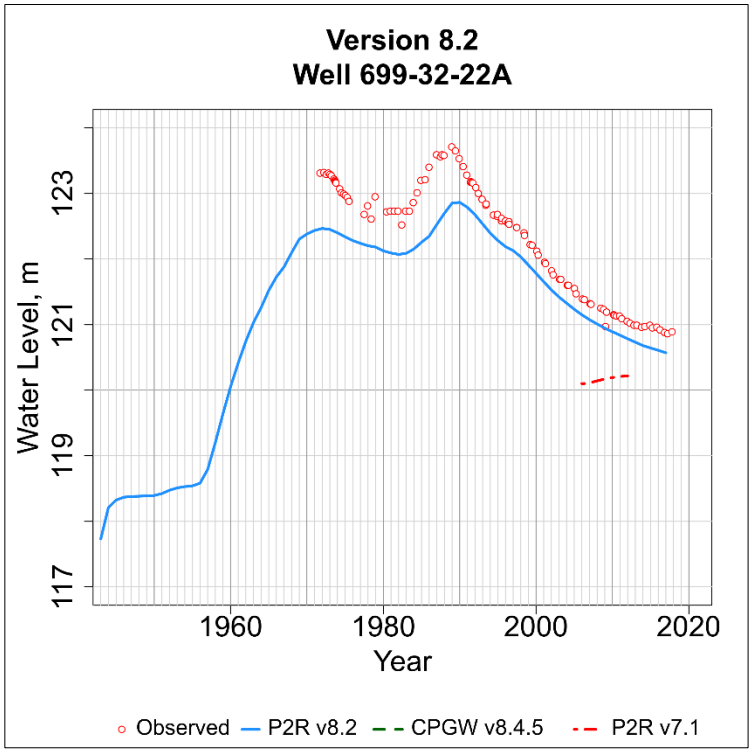

Figure D-376. Observed and simulated water level in the P2R Model at well 699-32-22A.png.

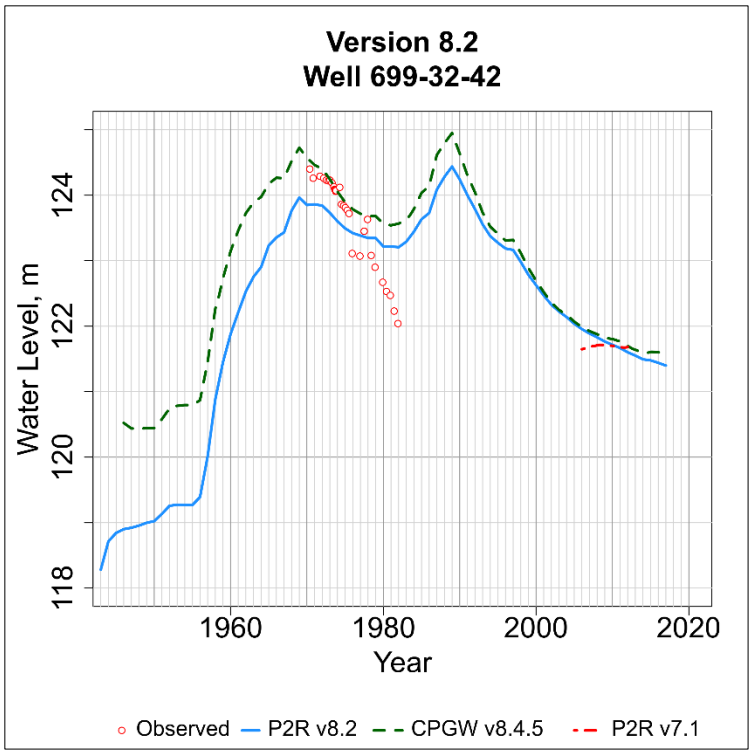

Figure D-377. Observed and simulated water level in the P2R Model at well 699-32-42.png.

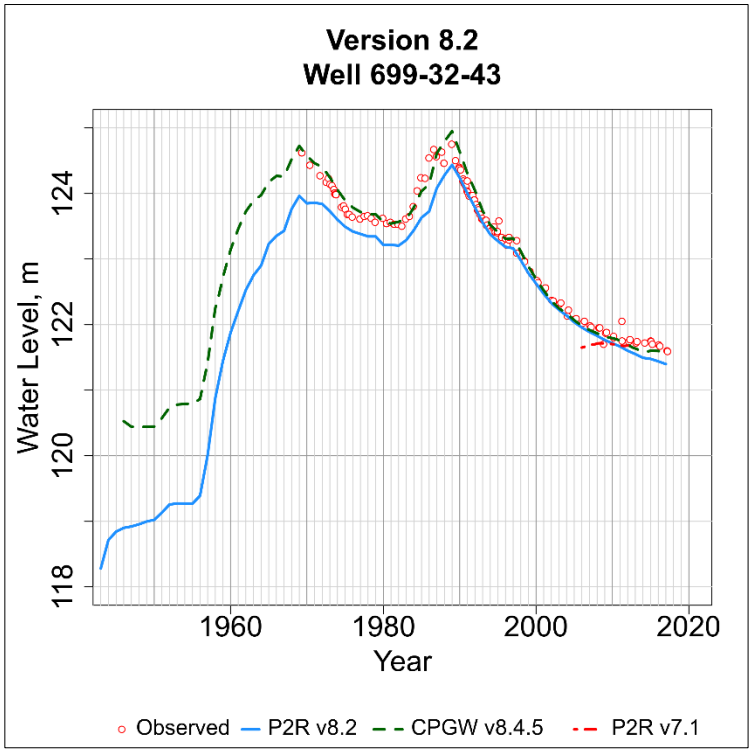

Figure D-378. Observed and simulated water level in the P2R Model at well 699-32-43.png.

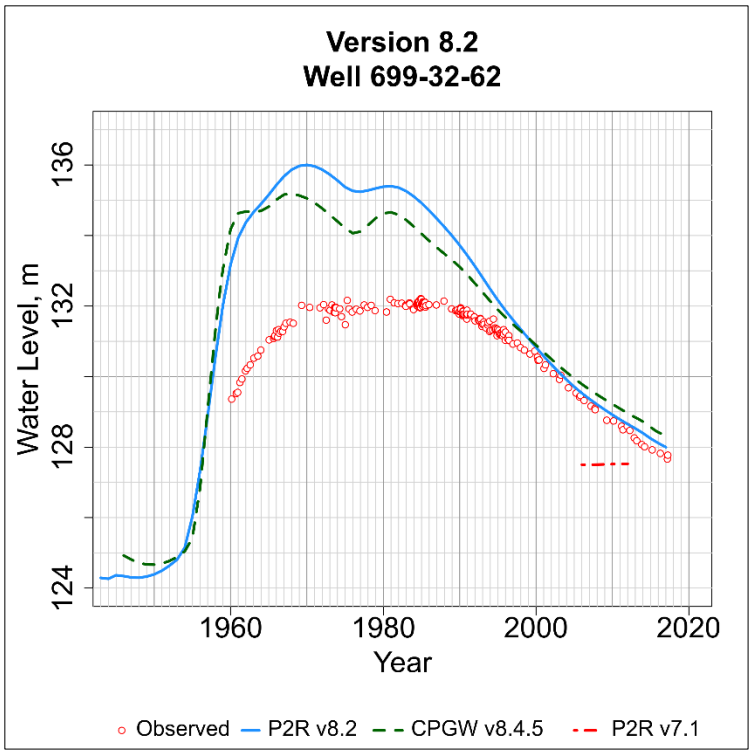

Figure D-379. Observed and simulated water level in the P2R Model at well 699-32-62.png.

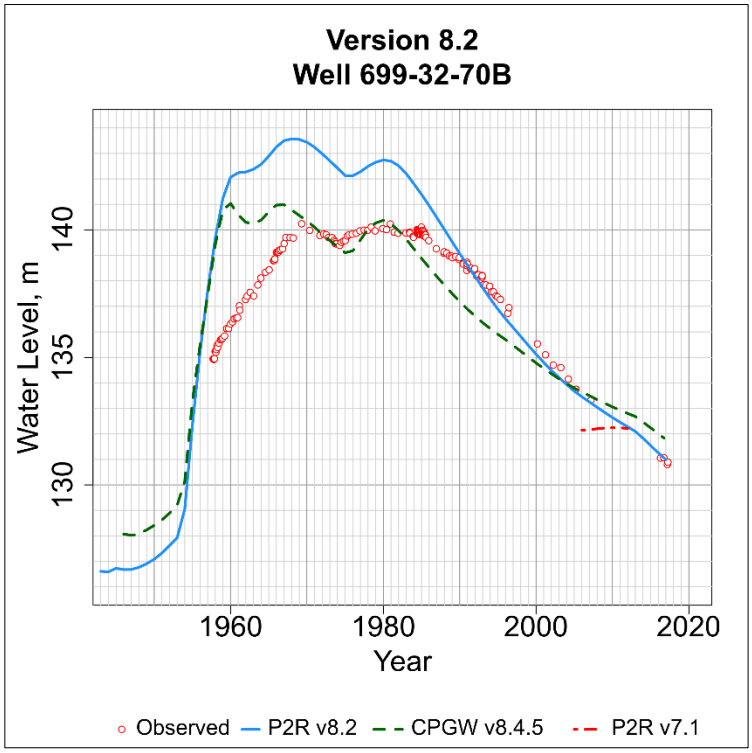

Figure D-380. Observed and simulated water level in the P2R Model at well 699-32-70B.png.

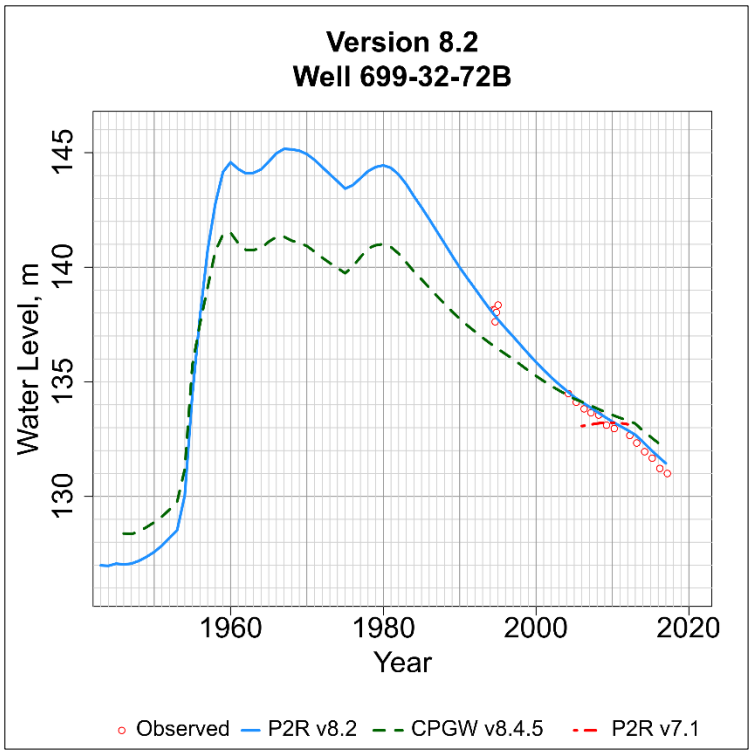

Figure D-381. Observed and simulated water level in the P2R Model at well 699-32-72B.png.

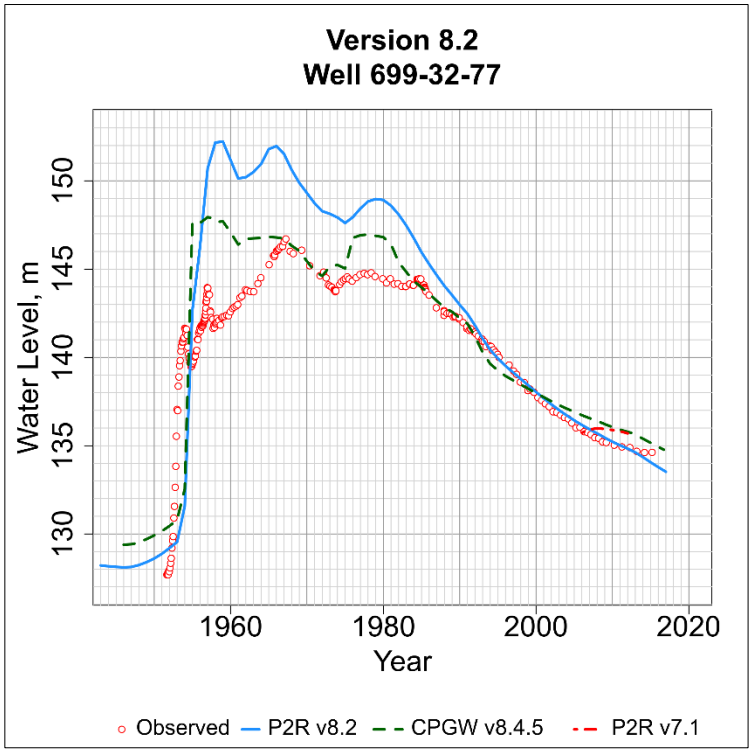

Figure D-382. Observed and simulated water level in the P2R Model at well 699-32-77.png.

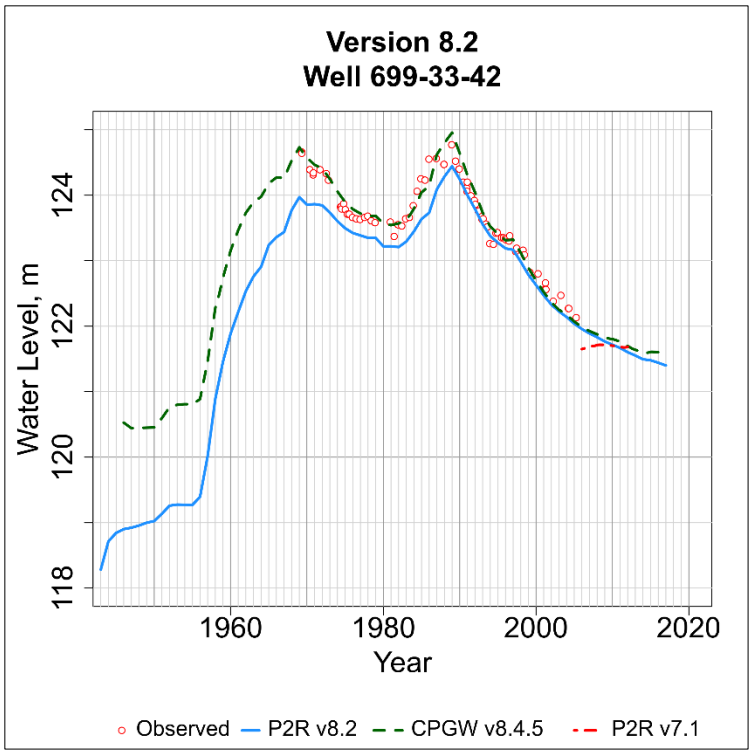

Figure D-383. Observed and simulated water level in the P2R Model at well 699-33-42.png.

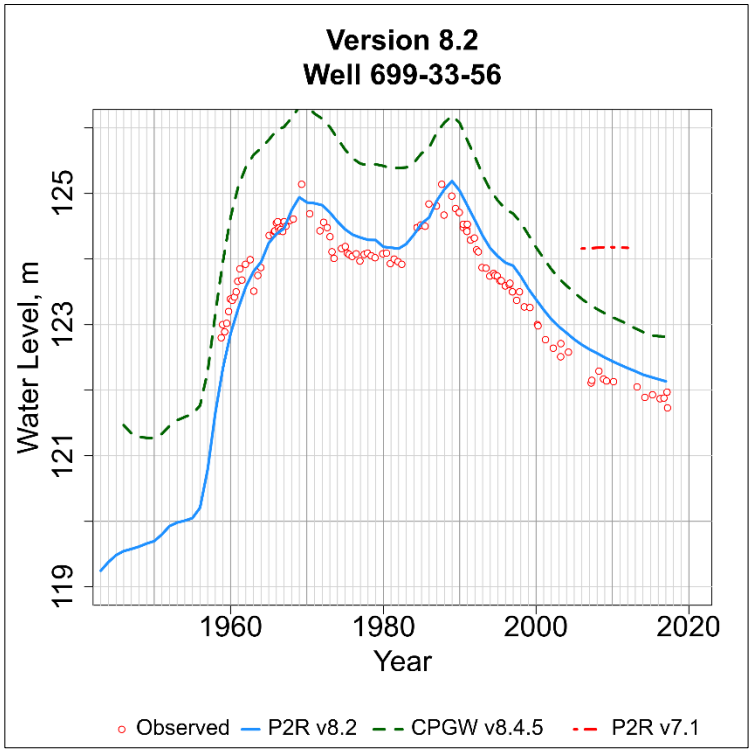

Figure D-384. Observed and simulated water level in the P2R Model at well 699-33-56.png.

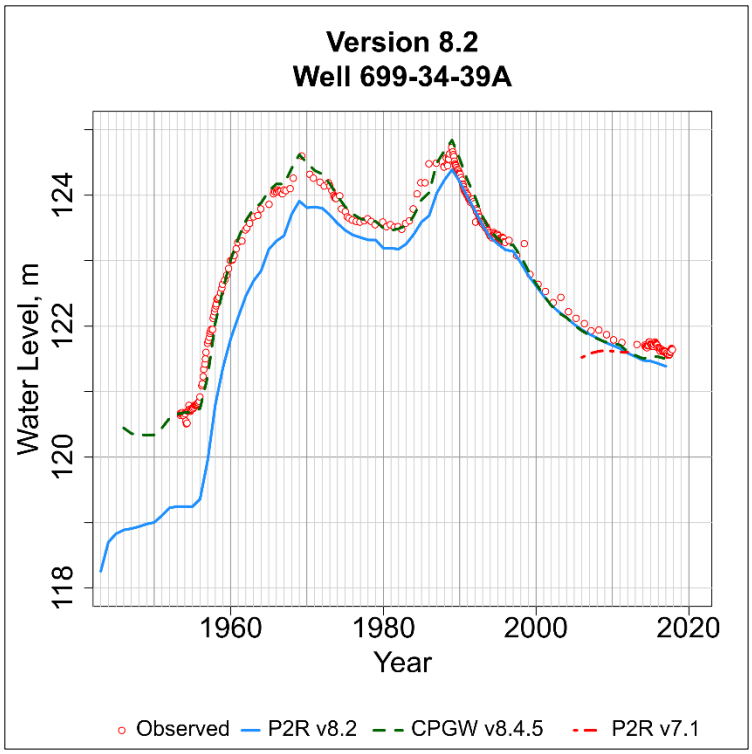

Figure D-385. Observed and simulated water level in the P2R Model at well 699-34-39A.png.

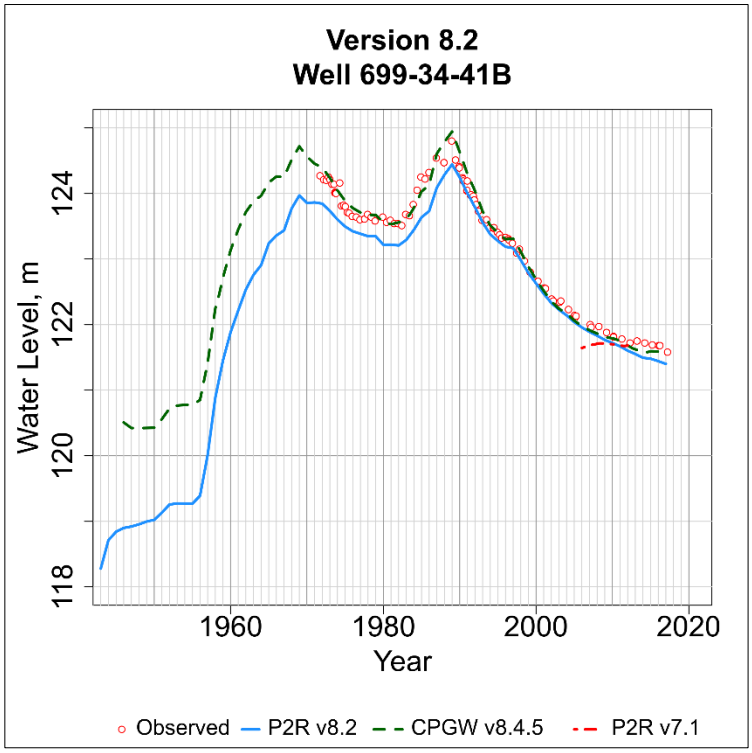

Figure D-386. Observed and simulated water level in the P2R Model at well 699-34-41B.png.

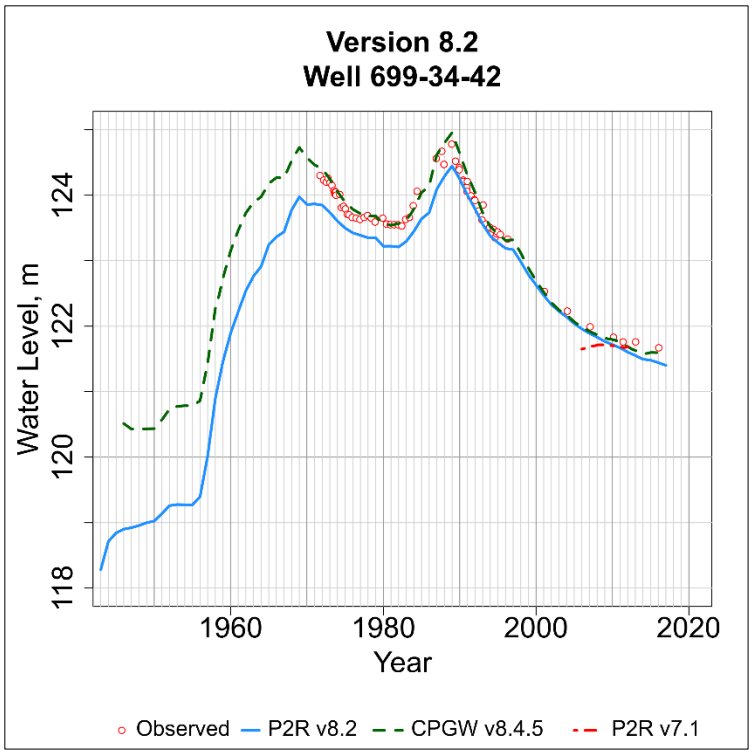

Figure D-387. Observed and simulated water level in the P2R Model at well 699-34-42.png.

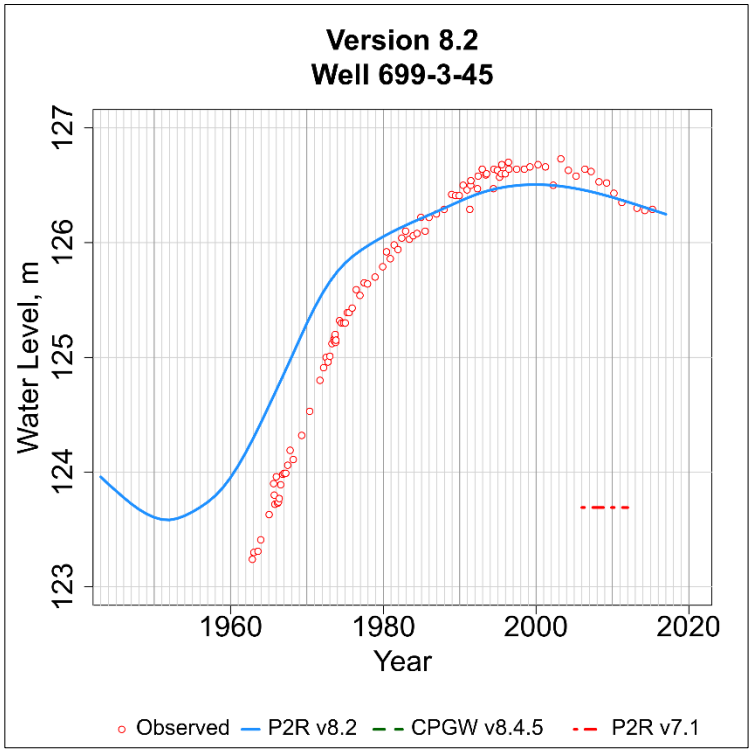

Figure D-388. Observed and simulated water level in the P2R Model at well 699-3-45.png.

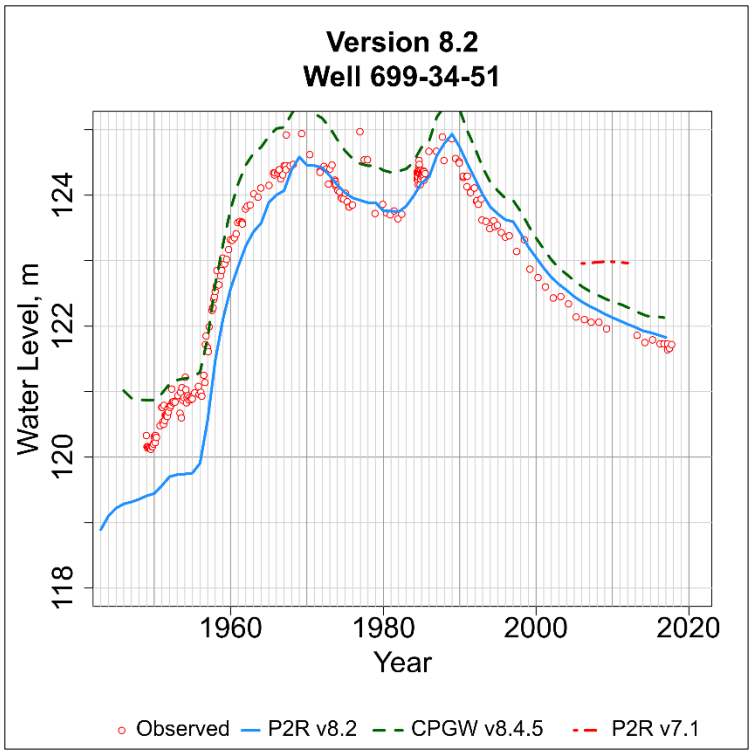

Figure D-389. Observed and simulated water level in the P2R Model at well 699-34-51.png.

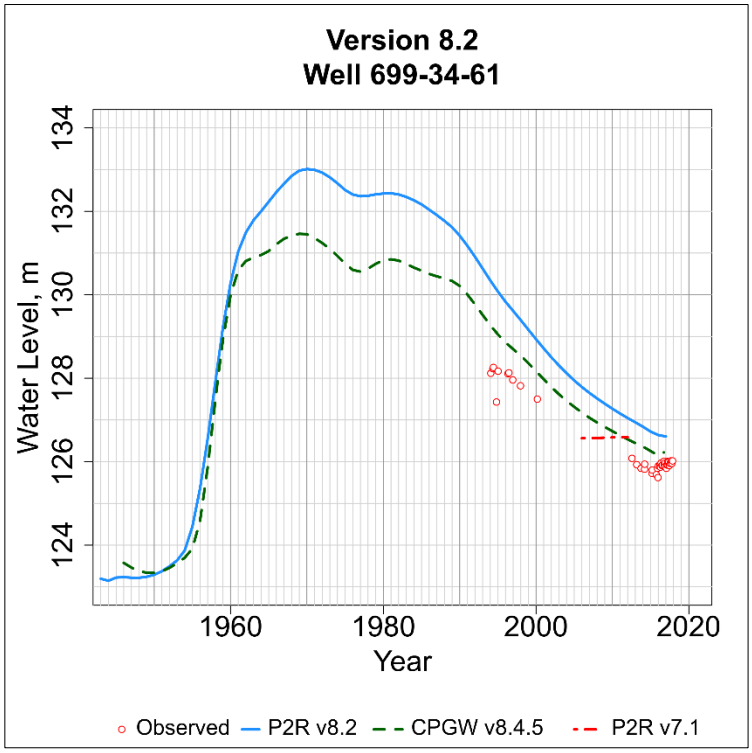

Figure D-390. Observed and simulated water level in the P2R Model at well 699-34-61.png.

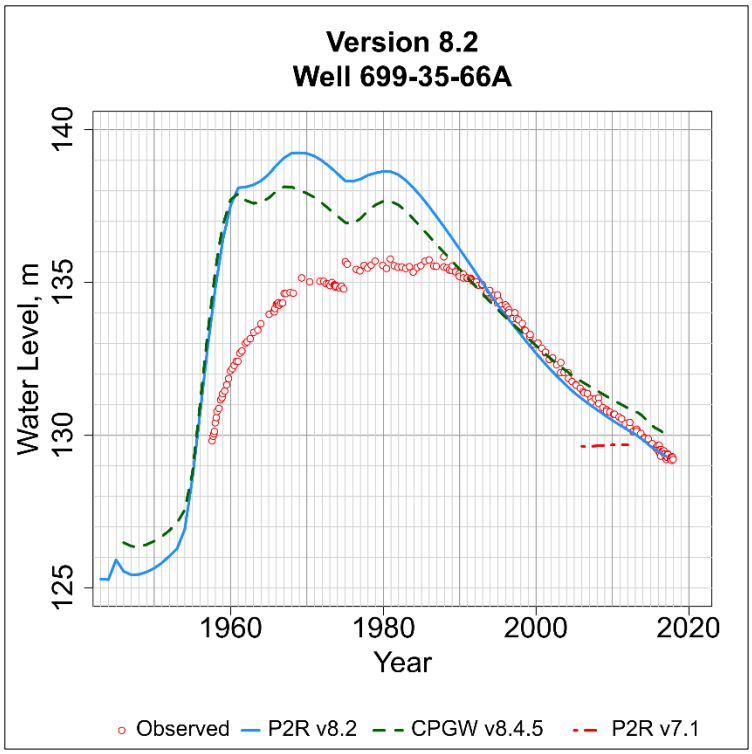

Figure D-391. Observed and simulated water level in the P2R Model at well 699-35-66A.png.

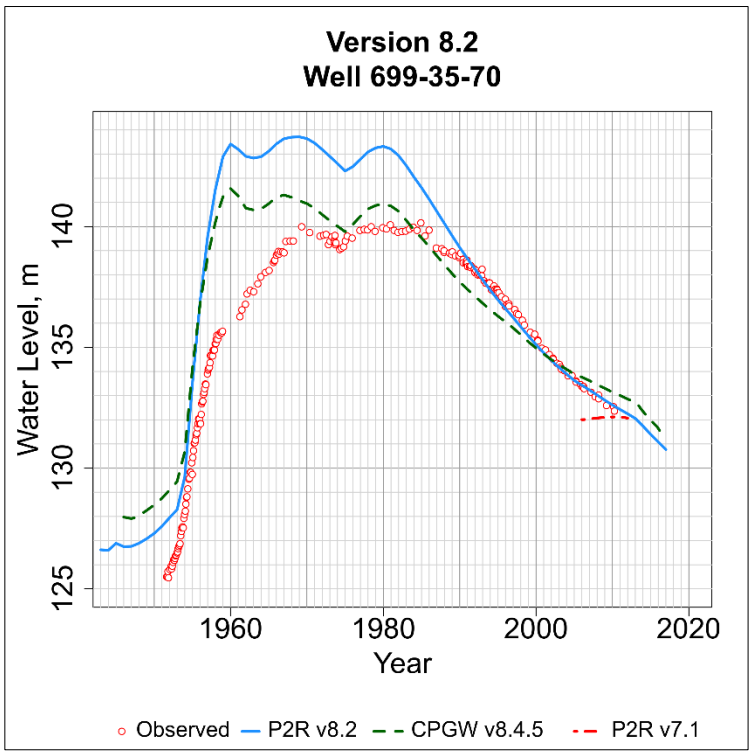

Figure D-392. Observed and simulated water level in the P2R Model at well 699-35-70.png.

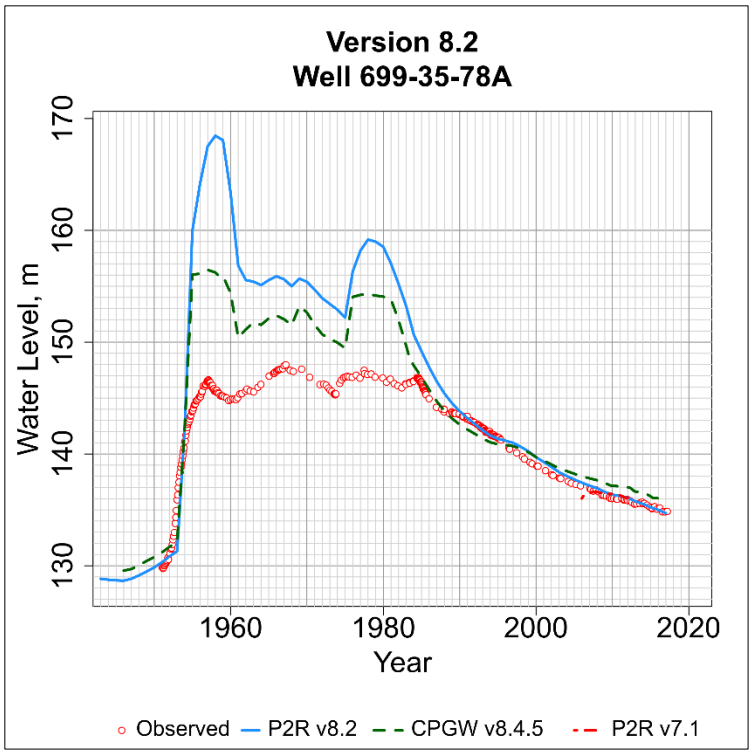

Figure D-393. Observed and simulated water level in the P2R Model at well 699-35-78A.png.

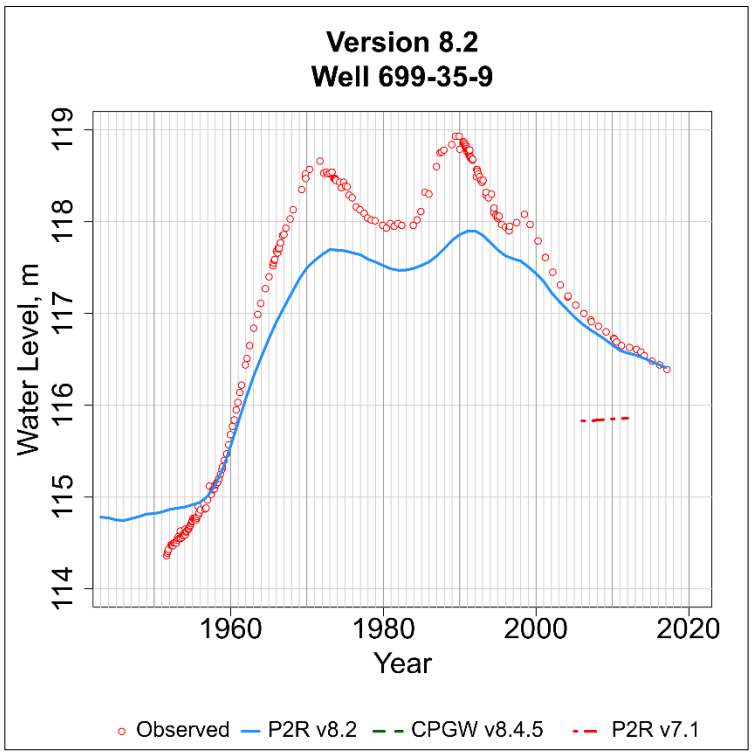

Figure D-394. Observed and simulated water level in the P2R Model at well 699-35-9.png.

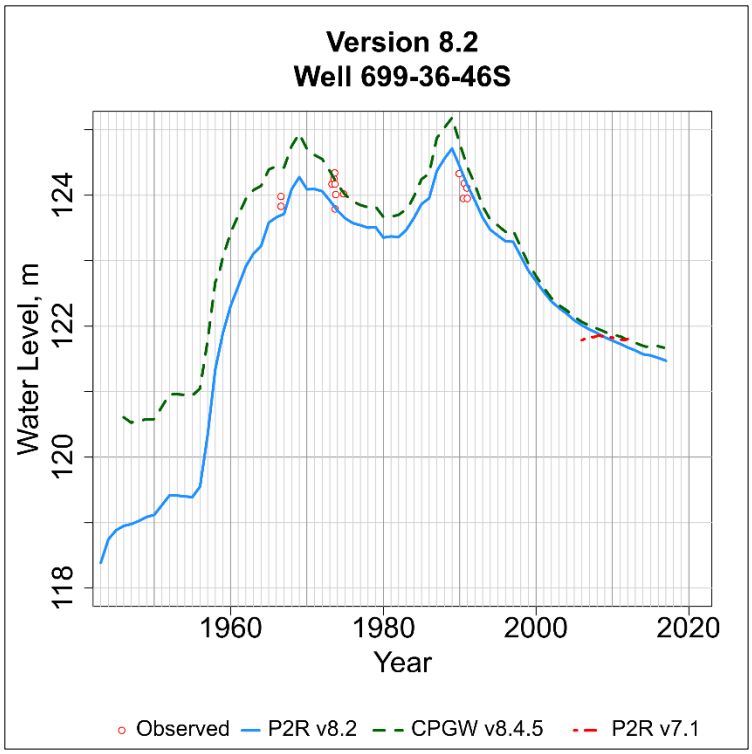

Figure D-395. Observed and simulated water level in the P2R Model at well 699-36-46S.png.

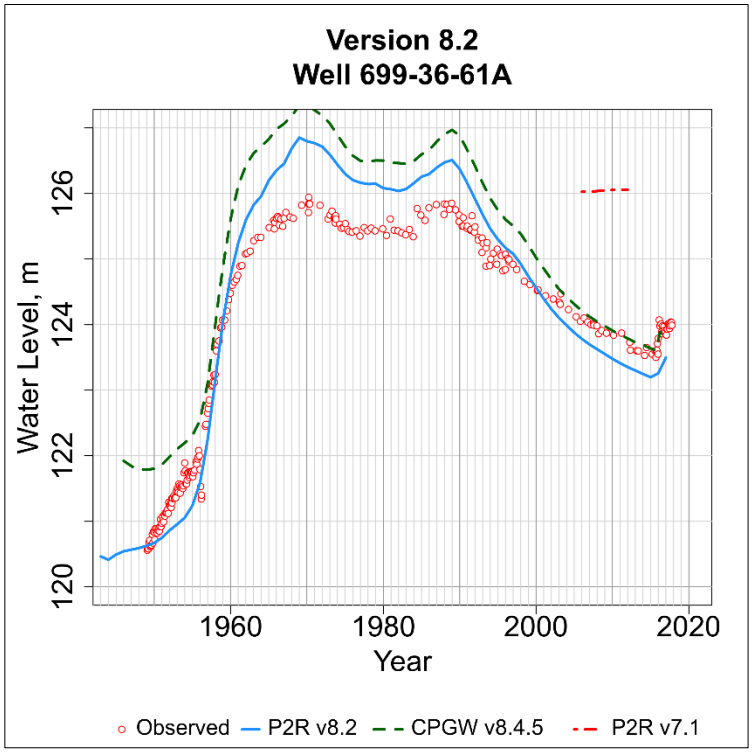

Figure D-396. Observed and simulated water level in the P2R Model at well 699-36-61A.png.

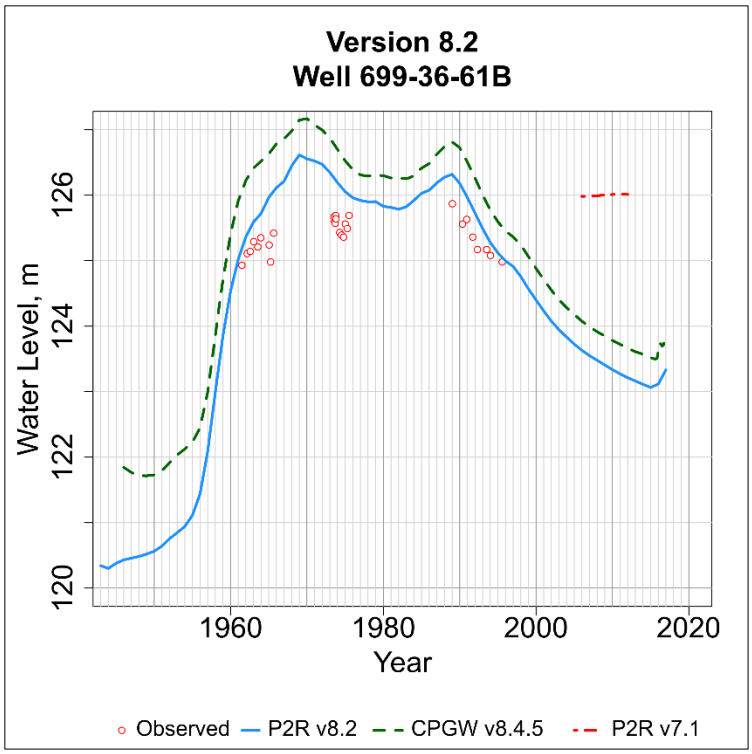

Figure D-397. Observed and simulated water level in the P2R Model at well 699-36-61B.png.

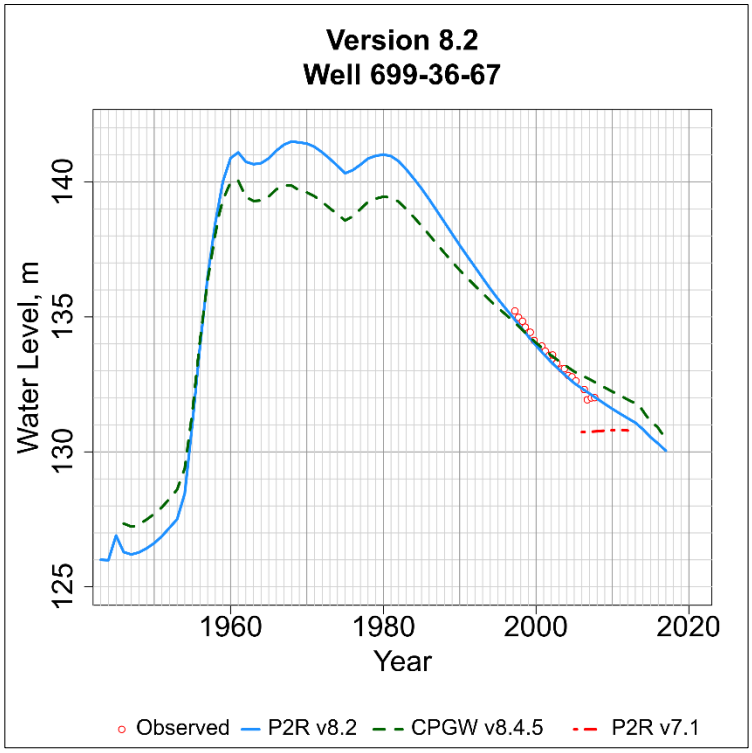

Figure D-398. Observed and simulated water level in the P2R Model at well 699-36-67.png.

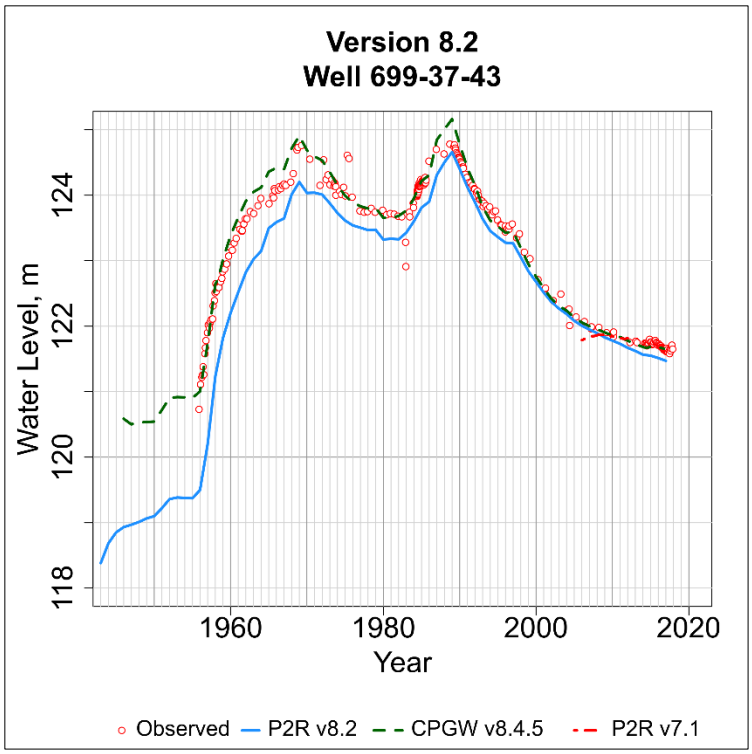

Figure D-399. Observed and simulated water level in the P2R Model at well 699-37-43.png.

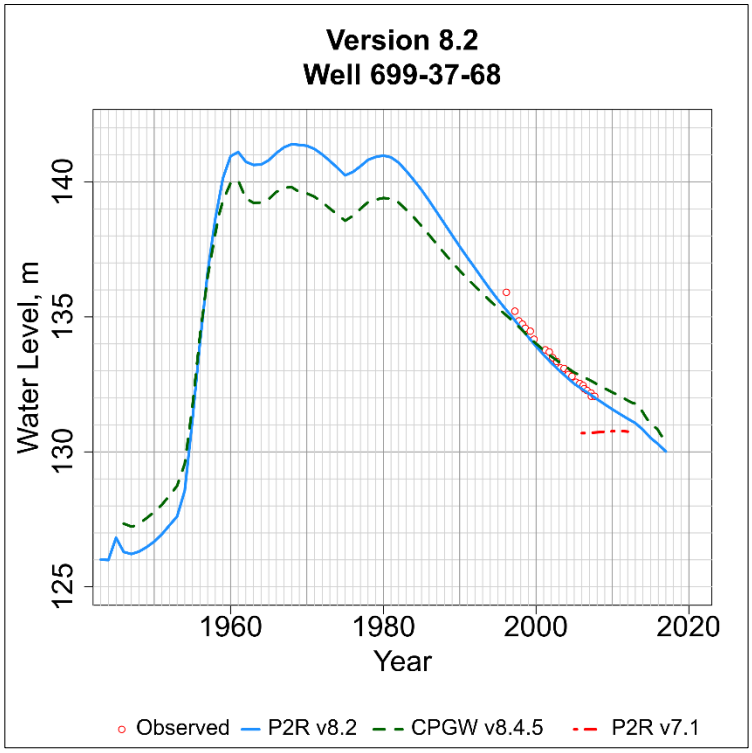

Figure D-400. Observed and simulated water level in the P2R Model at well 699-37-68.png.

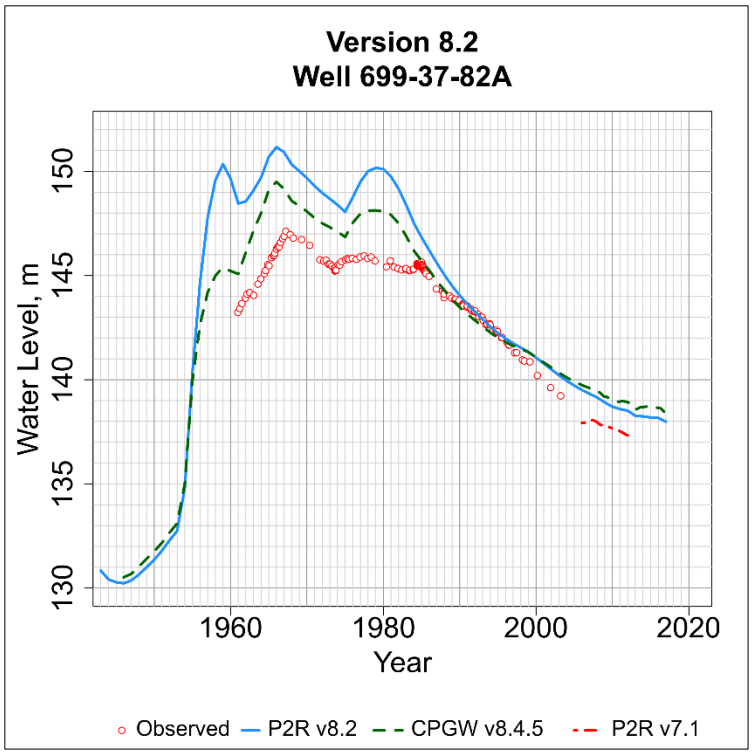

Figure D-401. Observed and simulated water level in the P2R Model at well 699-37-82A.png.

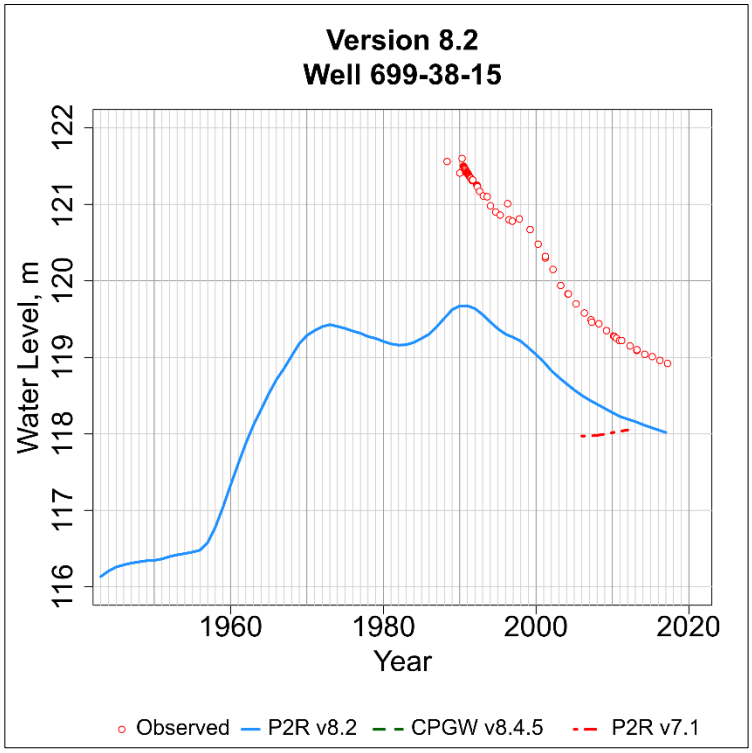

Figure D-402. Observed and simulated water level in the P2R Model at well 699-38-15.png.

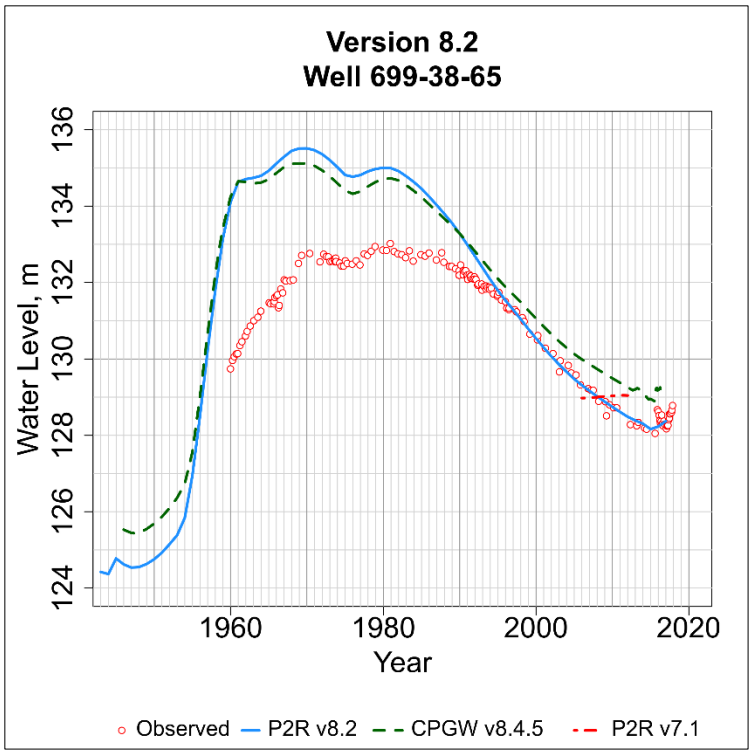

Figure D-403. Observed and simulated water level in the P2R Model at well 699-38-65.png.

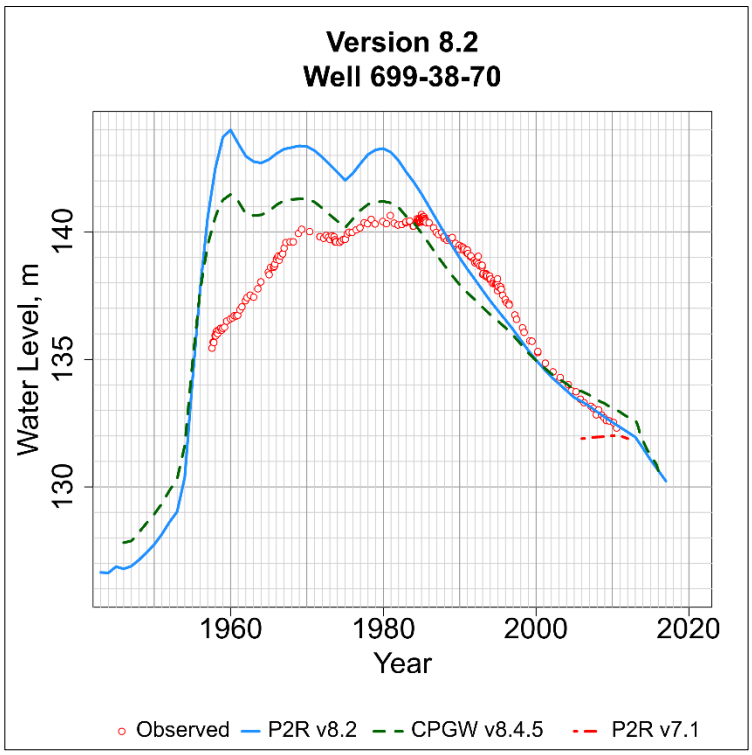

Figure D-404. Observed and simulated water level in the P2R Model at well 699-38-70.png.

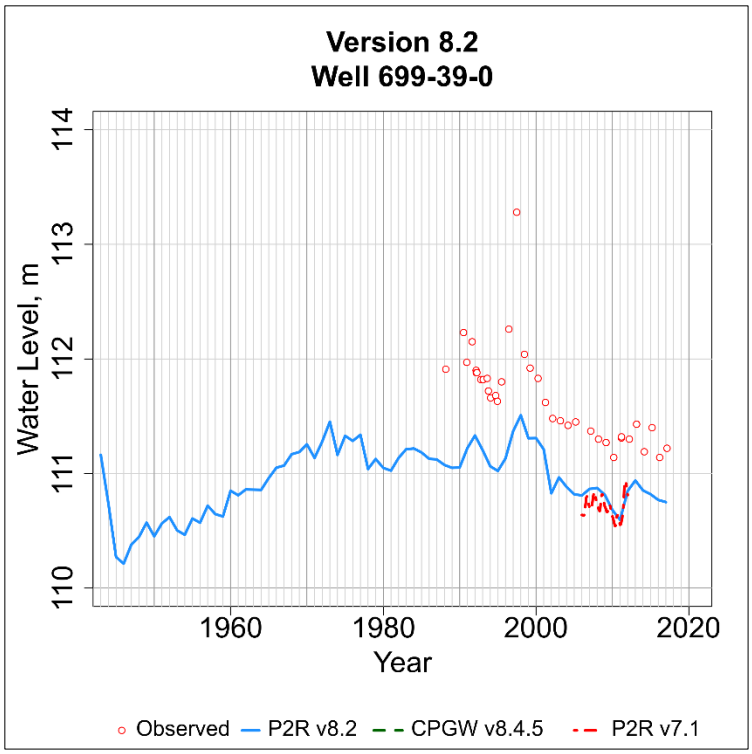

Figure D-405. Observed and simulated water level in the P2R Model at well 699-39-0.png.

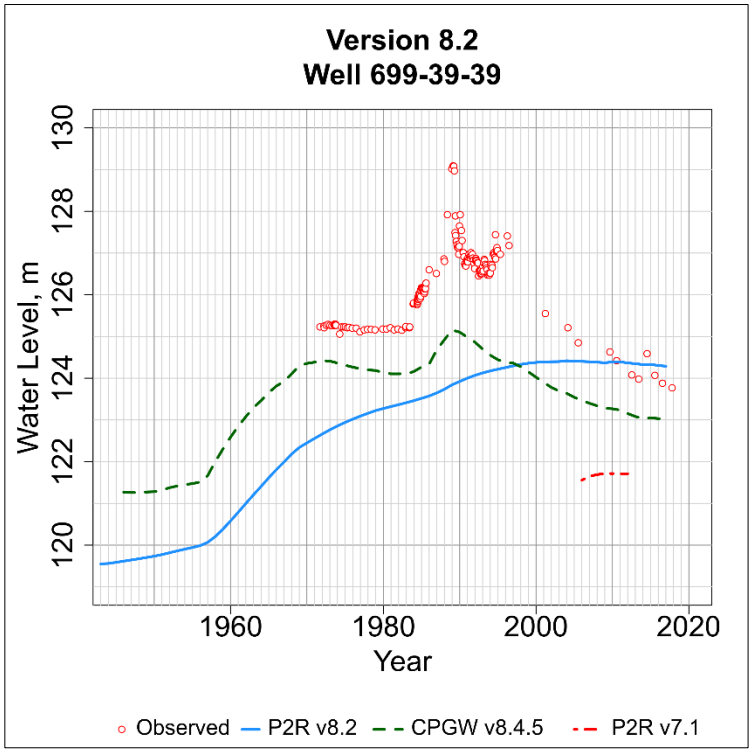

Figure D-406. Observed and simulated water level in the P2R Model at well 699-39-39.png.

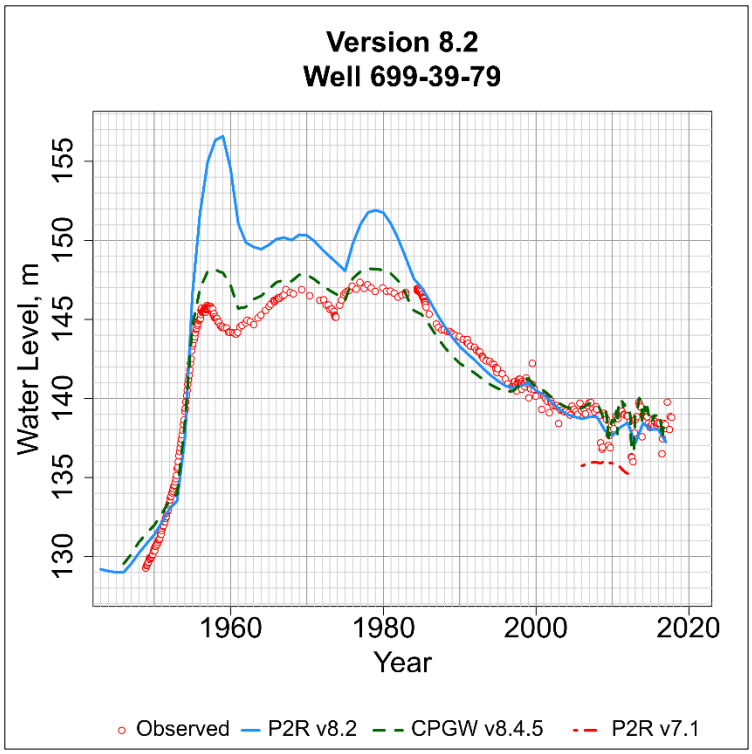

Figure D-407. Observed and simulated water level in the P2R Model at well 699-39-79.png.

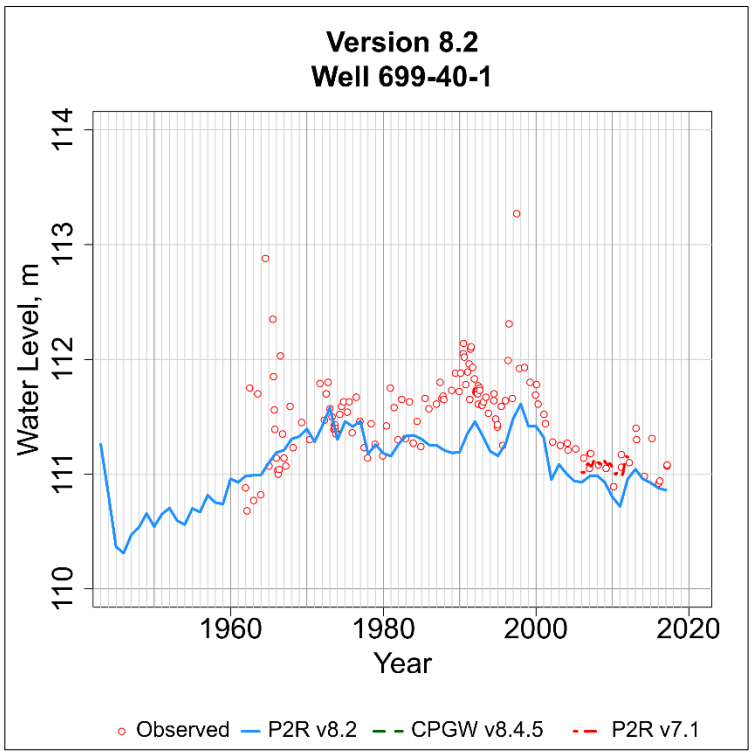

Figure D-408. Observed and simulated water level in the P2R Model at well 699-40-1.png.

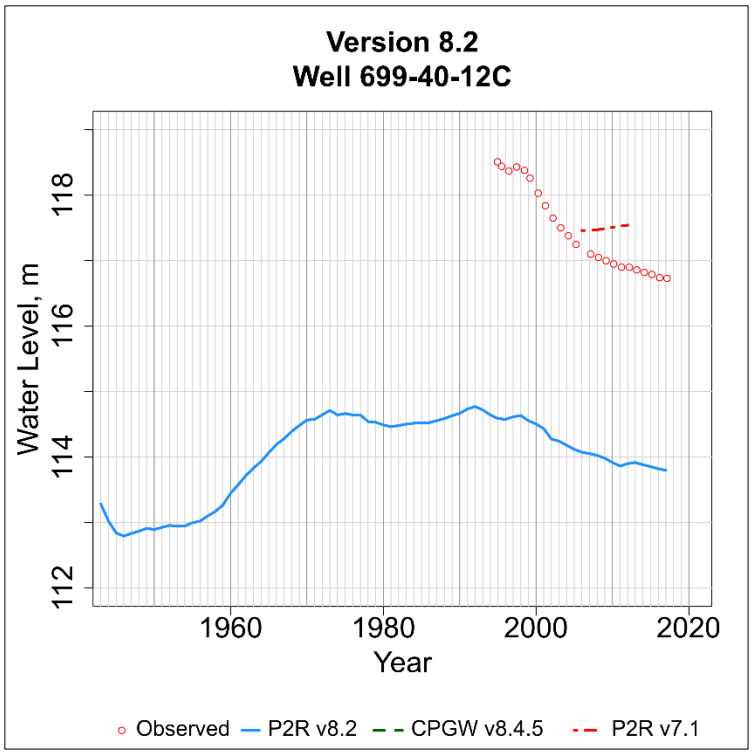

Figure D-409. Observed and simulated water level in the P2R Model at well 699-40-12C.png.

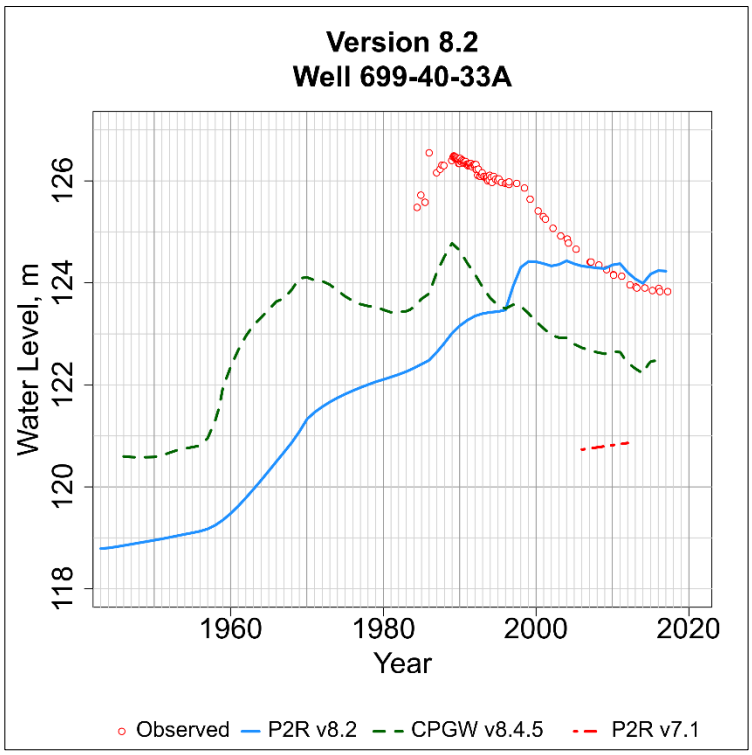

Figure D-410. Observed and simulated water level in the P2R Model at well 699-40-33A.png.

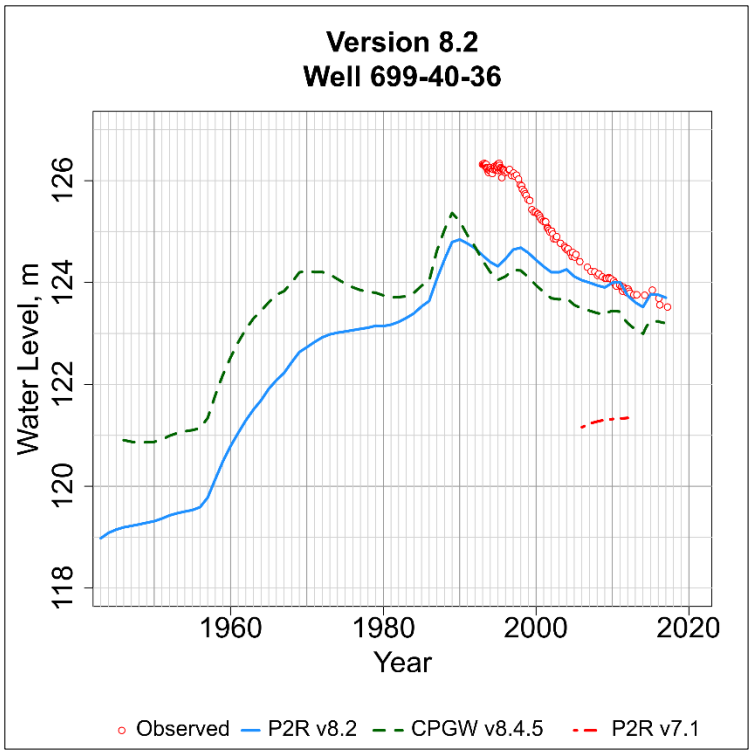

Figure D-411. Observed and simulated water level in the P2R Model at well 699-40-36.png.

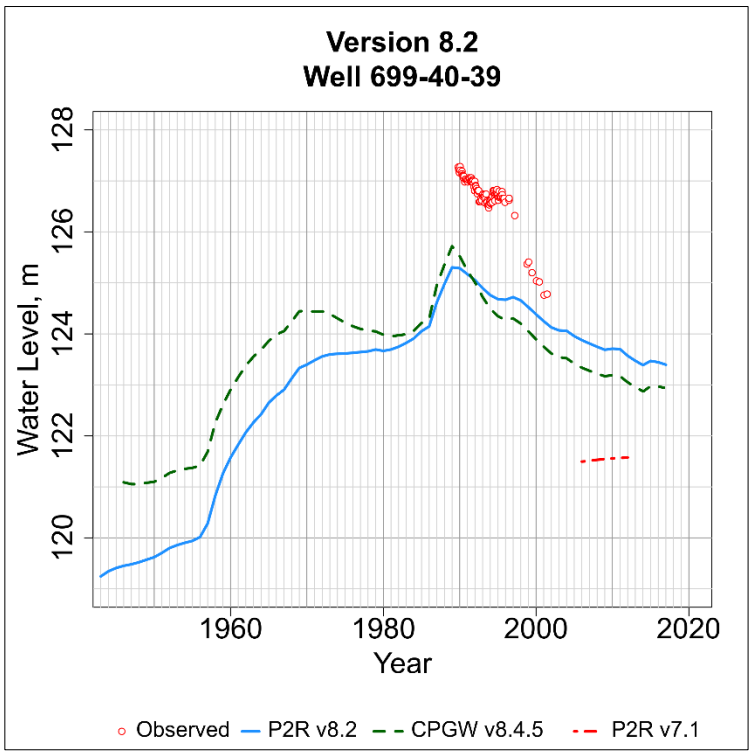

Figure D-412. Observed and simulated water level in the P2R Model at well 699-40-39.png.

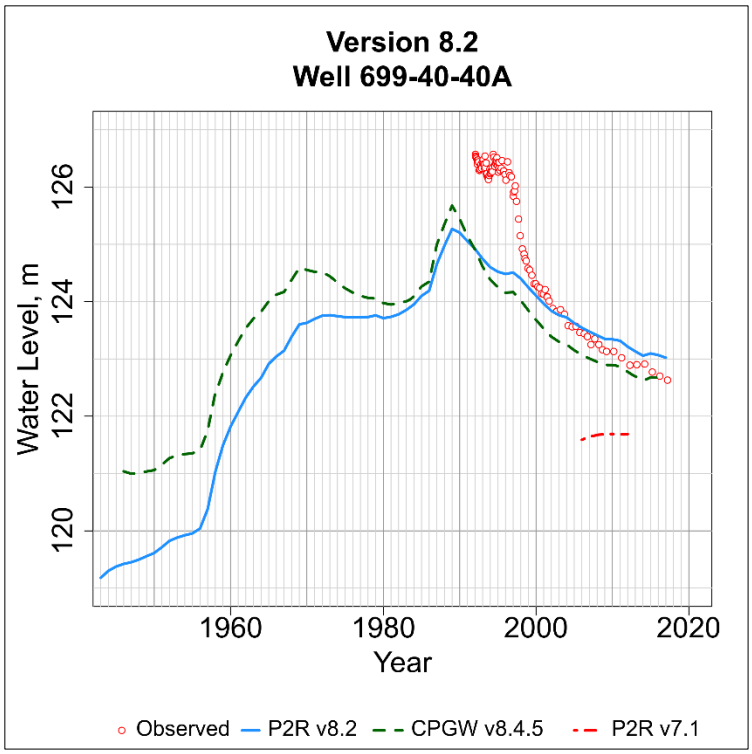

Figure D-413. Observed and simulated water level in the P2R Model at well 699-40-40A.png.

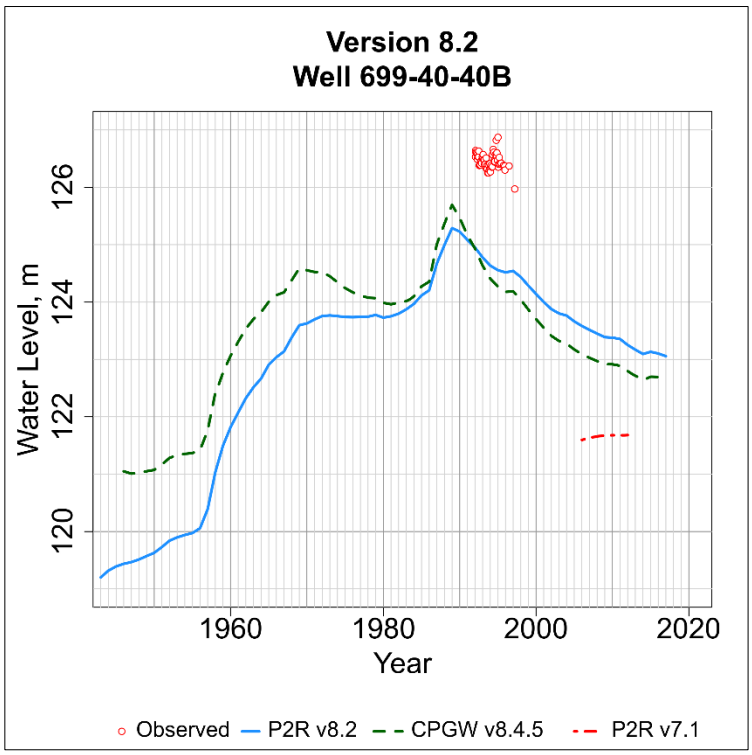

Figure D-414. Observed and simulated water level in the P2R Model at well 699-40-40B.png.

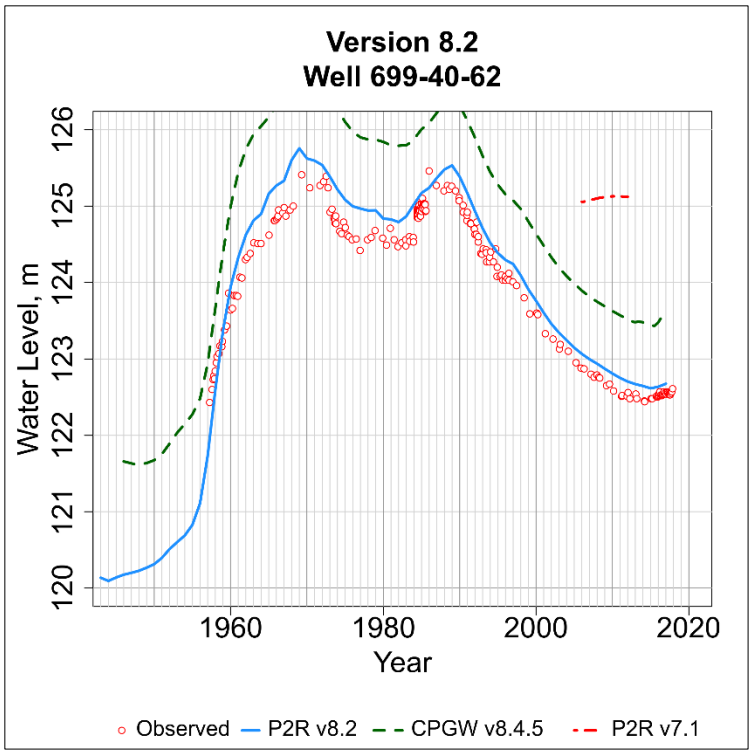

Figure D-415. Observed and simulated water level in the P2R Model at well 699-40-62.png.

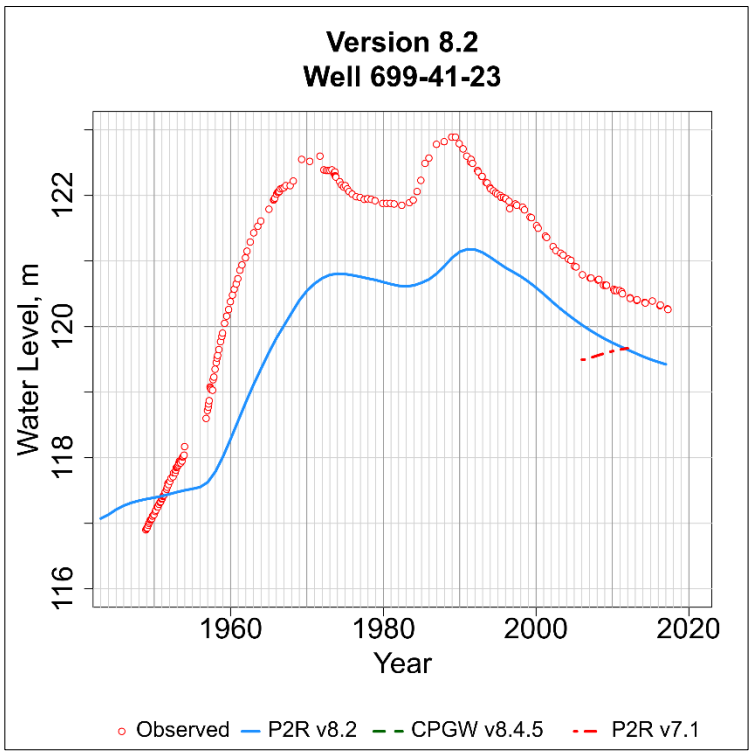

Figure D-416. Observed and simulated water level in the P2R Model at well 699-41-23.png.

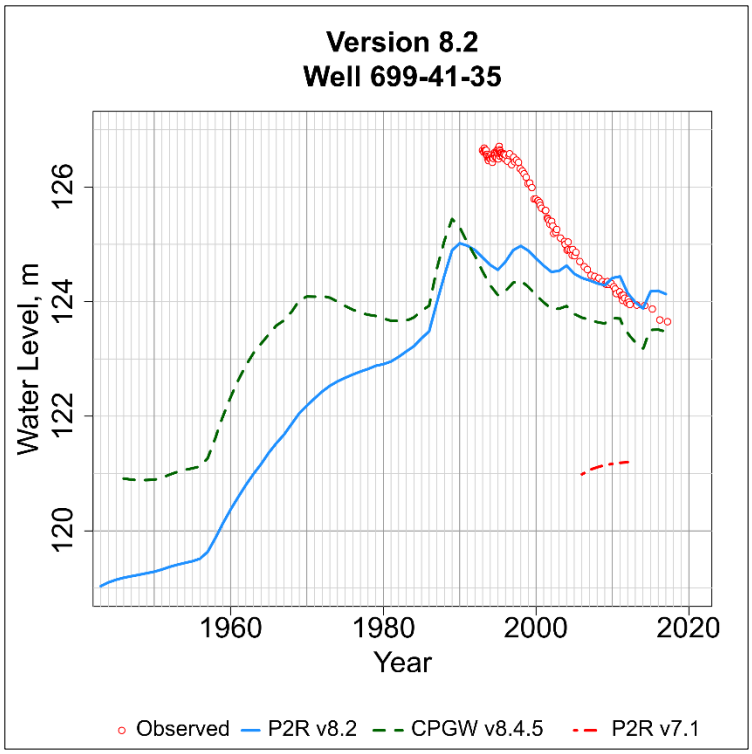

Figure D-417. Observed and simulated water level in the P2R Model at well 699-41-35.png.

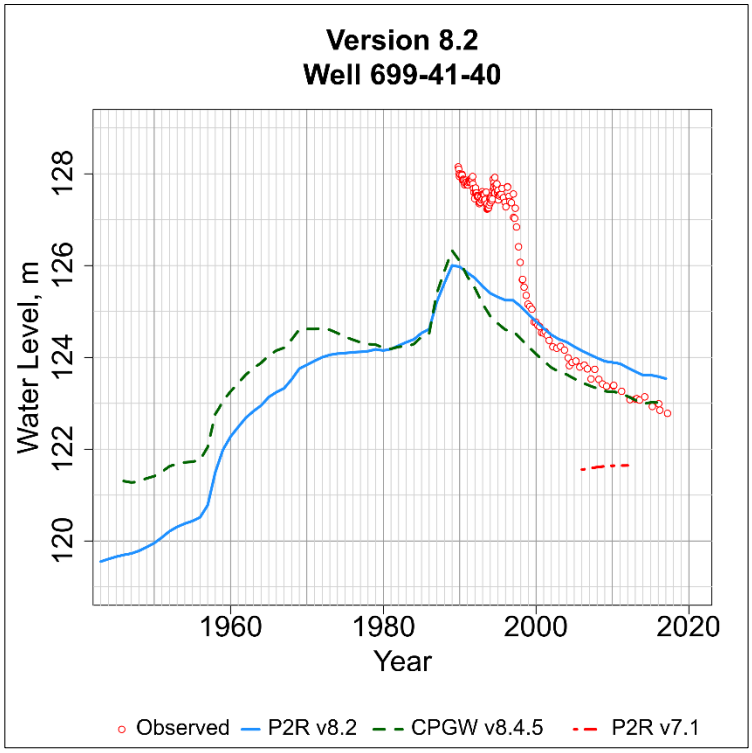

Figure D-418. Observed and simulated water level in the P2R Model at well 699-41-40.png.

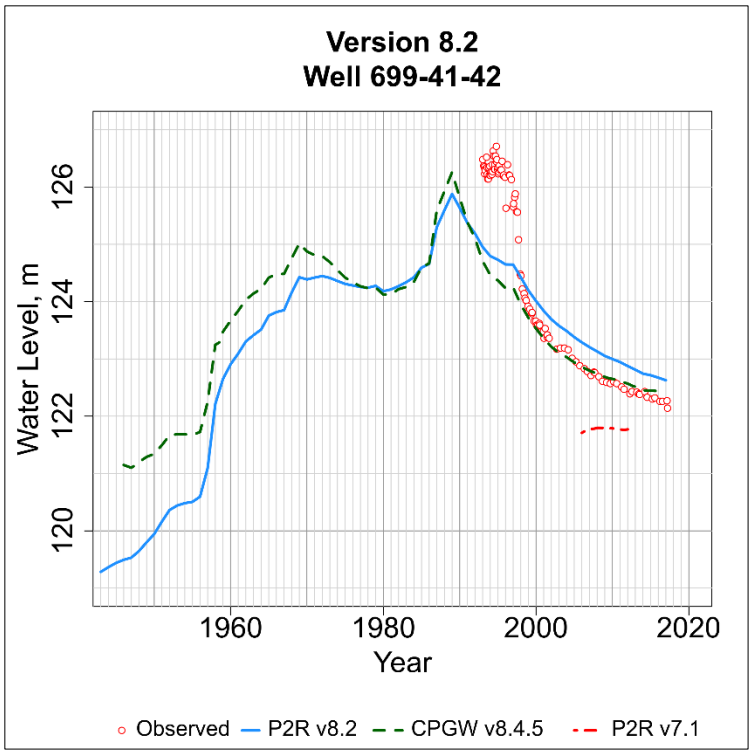

Figure D-419. Observed and simulated water level in the P2R Model at well 699-41-42.png.

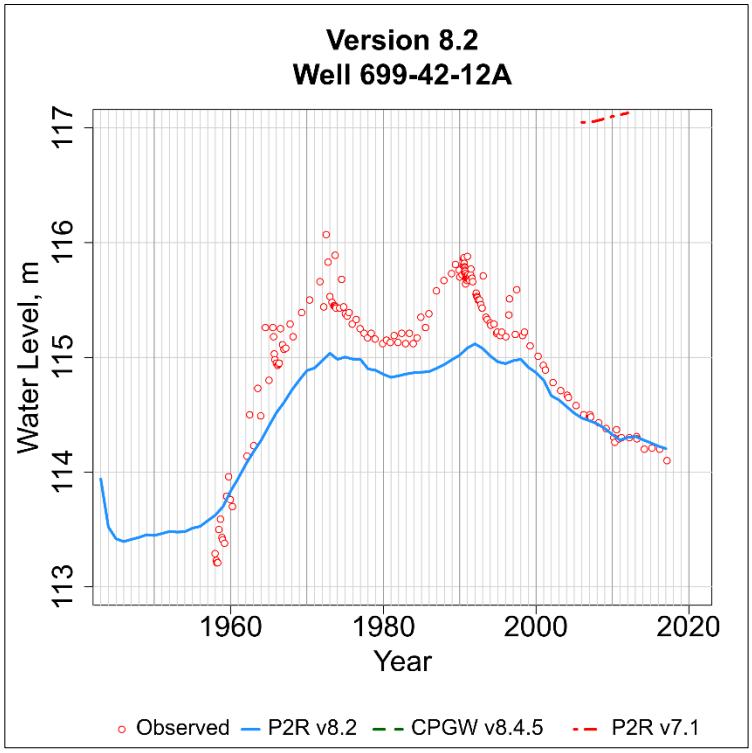

Figure D-420. Observed and simulated water level in the P2R Model at well 699-42-12A.png.

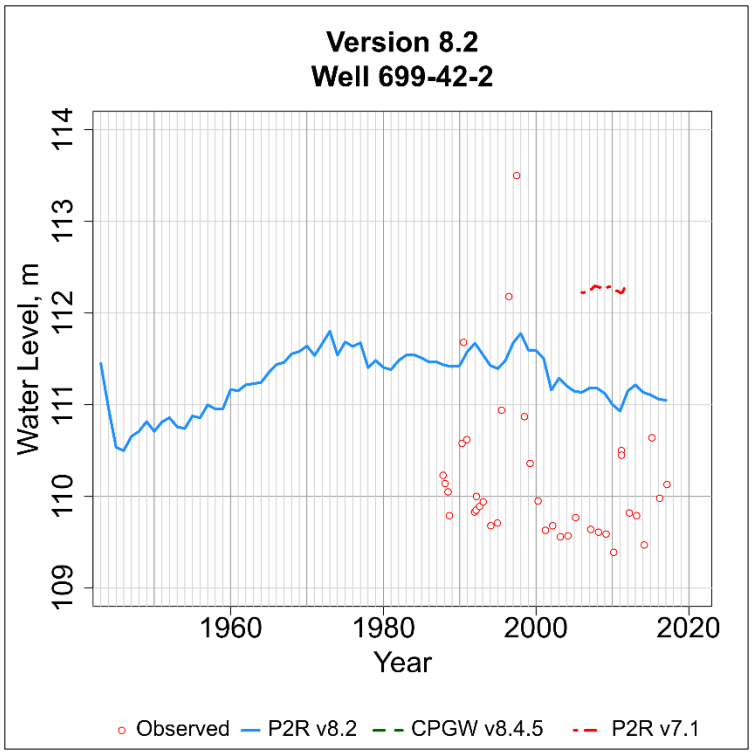

Figure D-421. Observed and simulated water level in the P2R Model at well 699-42-2.png.

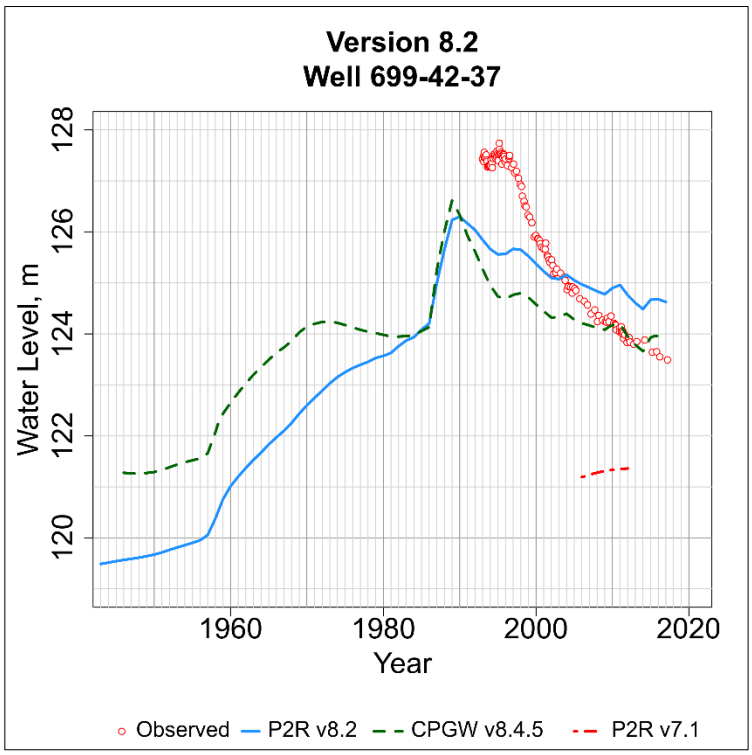

Figure D-422. Observed and simulated water level in the P2R Model at well 699-42-37.png.

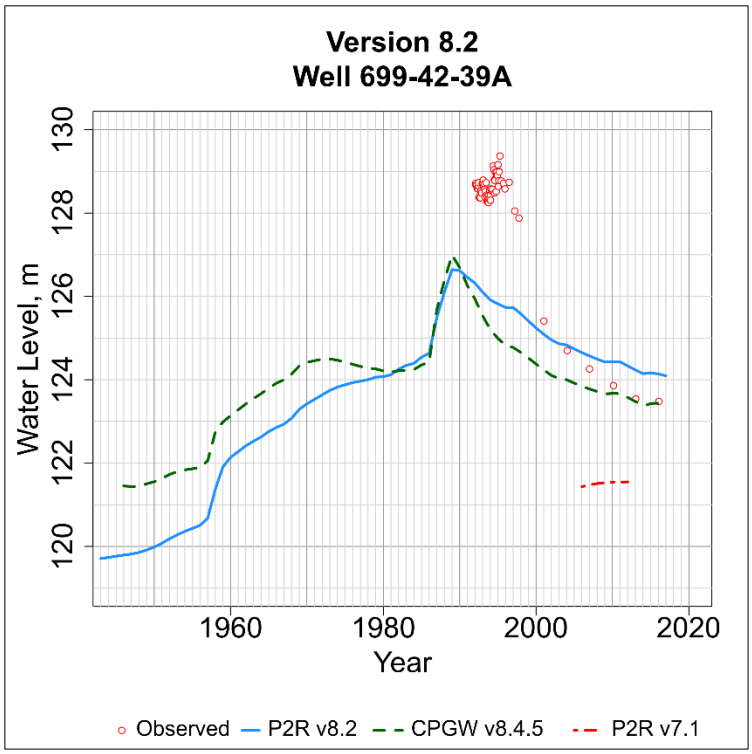

Figure D-423. Observed and simulated water level in the P2R Model at well 699-42-39A.png.

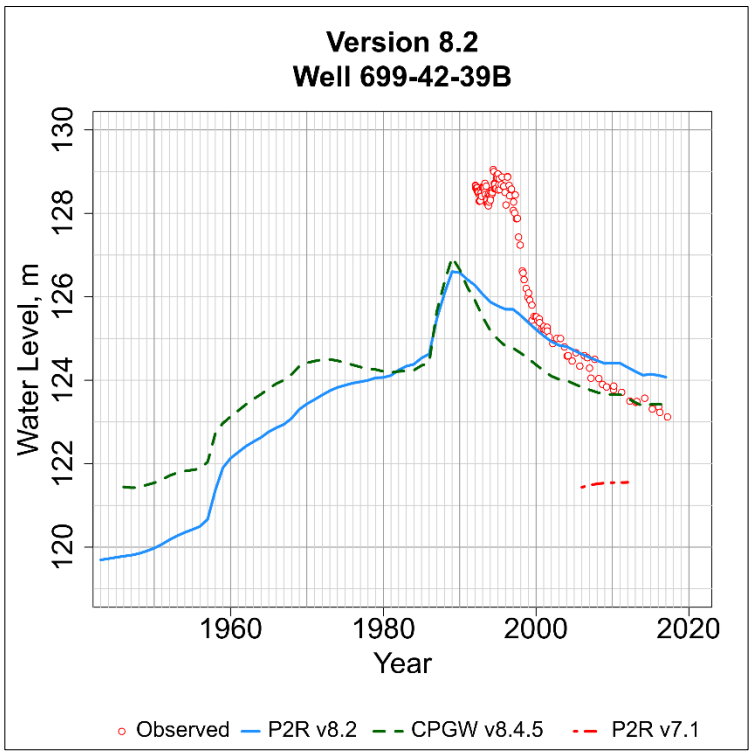

Figure D-424. Observed and simulated water level in the P2R Model at well 699-42-39B.png.

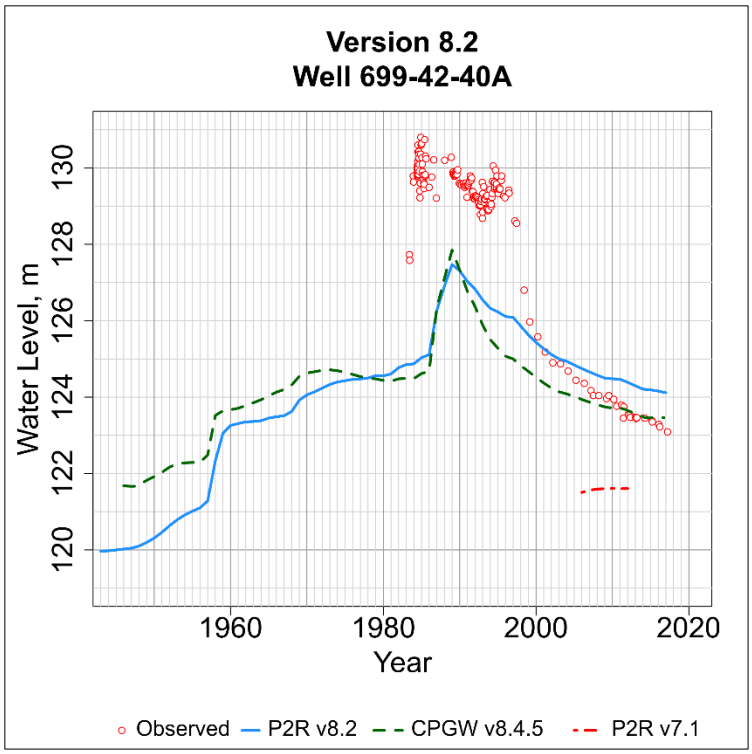

Figure D-425. Observed and simulated water level in the P2R Model at well 699-42-40A.png.

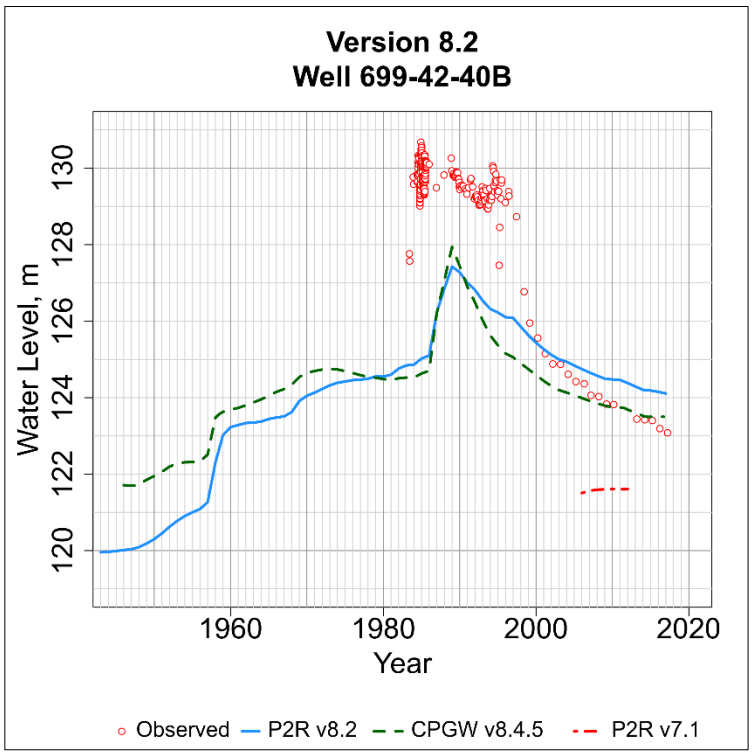

Figure D-426. Observed and simulated water level in the P2R Model at well 699-42-40B.png.

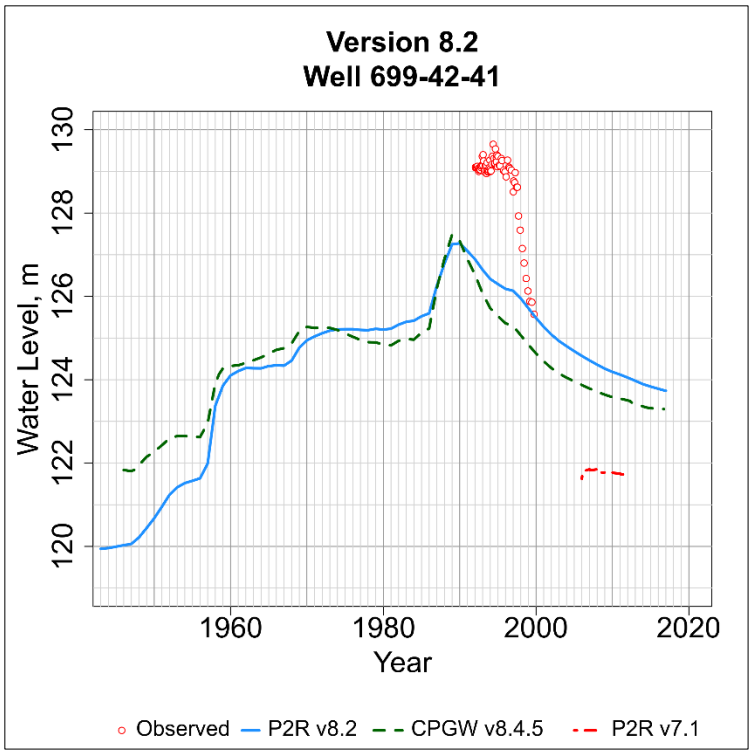

Figure D-427. Observed and simulated water level in the P2R Model at well 699-42-41.png.

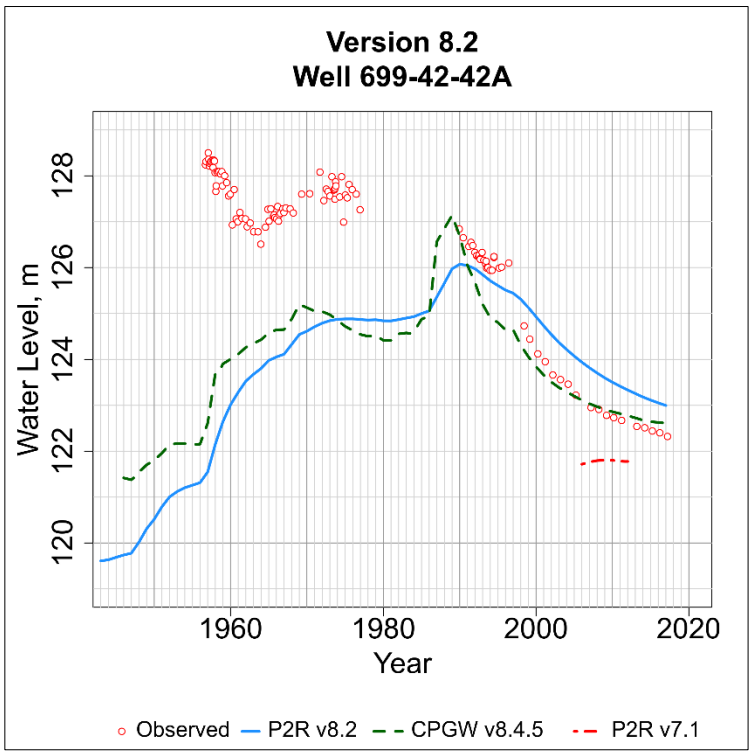

Figure D-428. Observed and simulated water level in the P2R Model at well 699-42-42A.png.

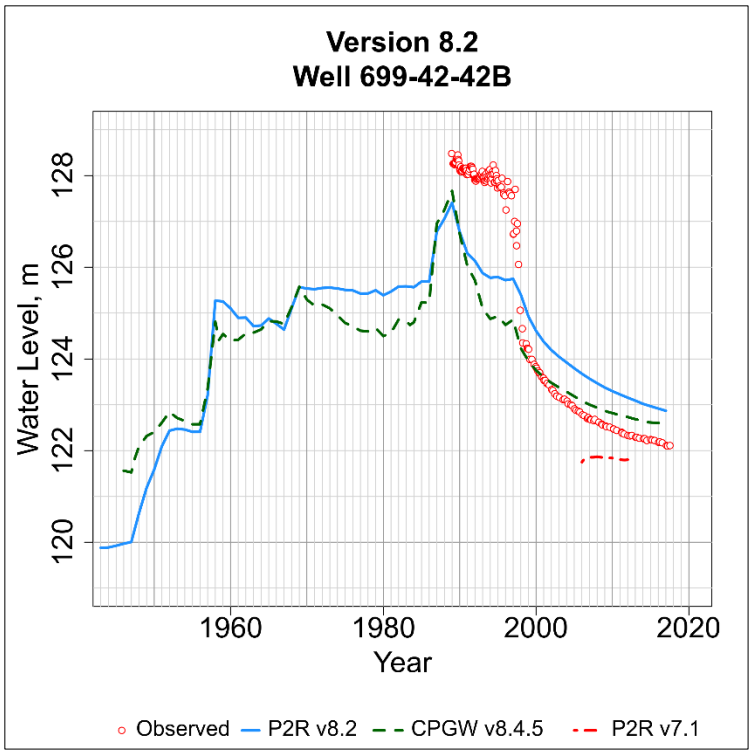

Figure D-429. Observed and simulated water level in the P2R Model at well 699-42-42B.png.

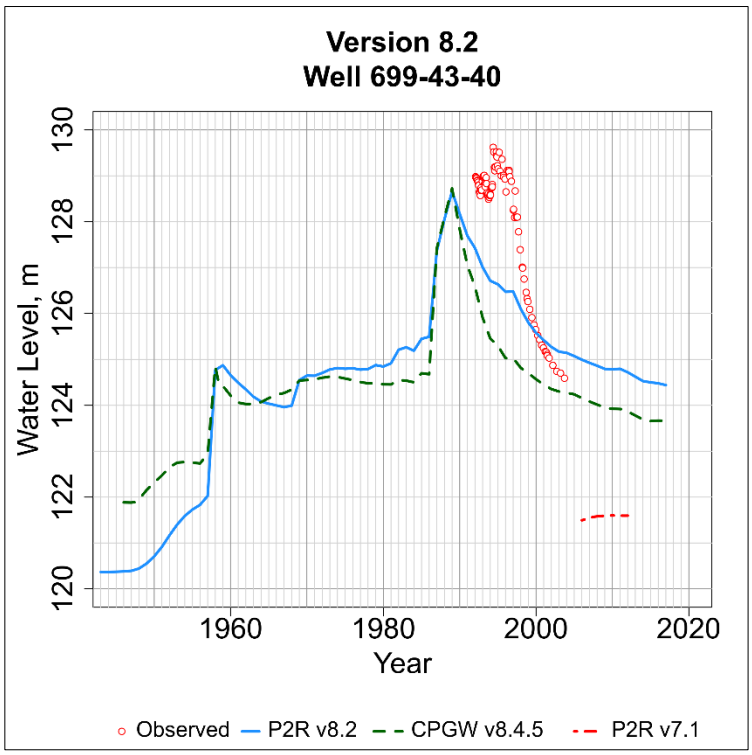

Figure D-430. Observed and simulated water level in the P2R Model at well 699-43-40.png.

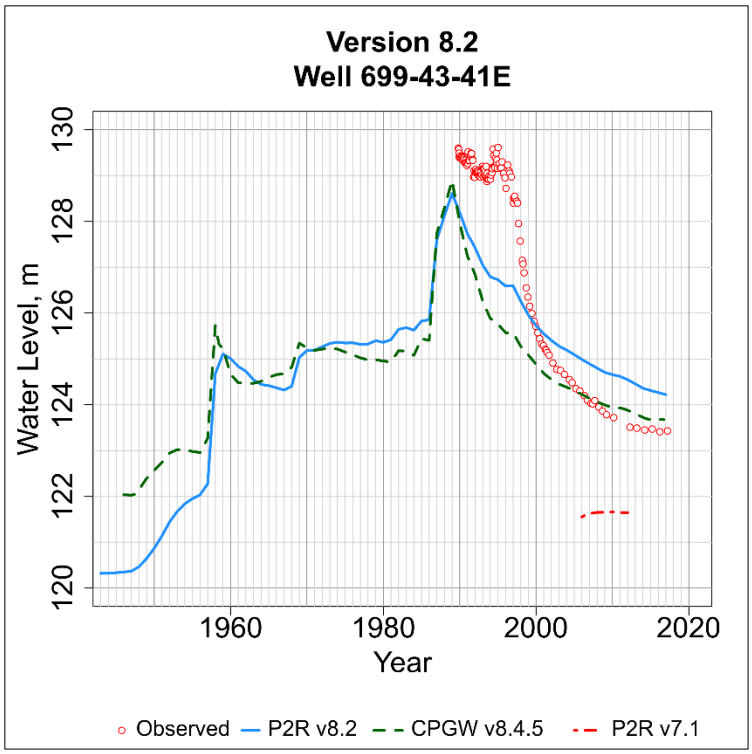

Figure D-431. Observed and simulated water level in the P2R Model at well 699-43-41E.png.

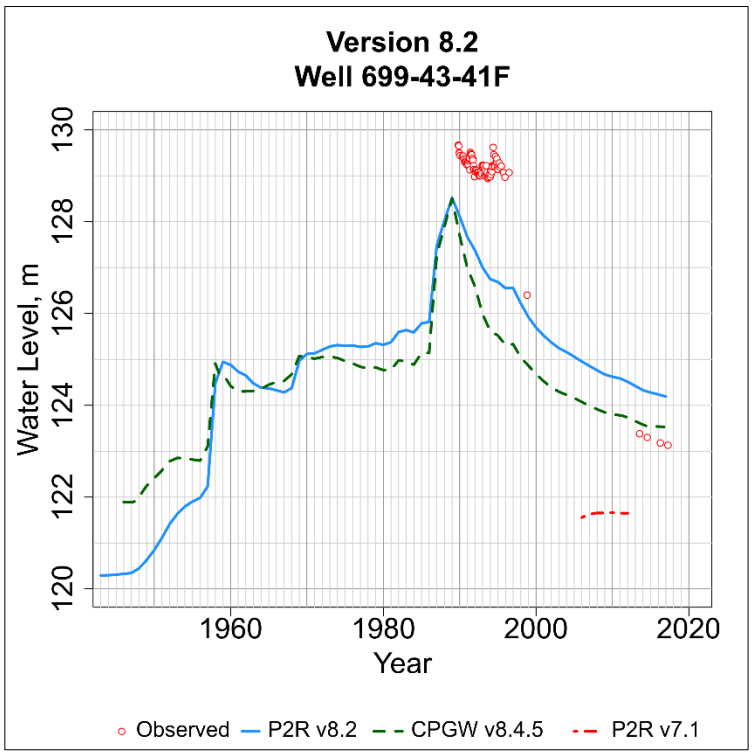

Figure D-432. Observed and simulated water level in the P2R Model at well 699-43-41F.png.

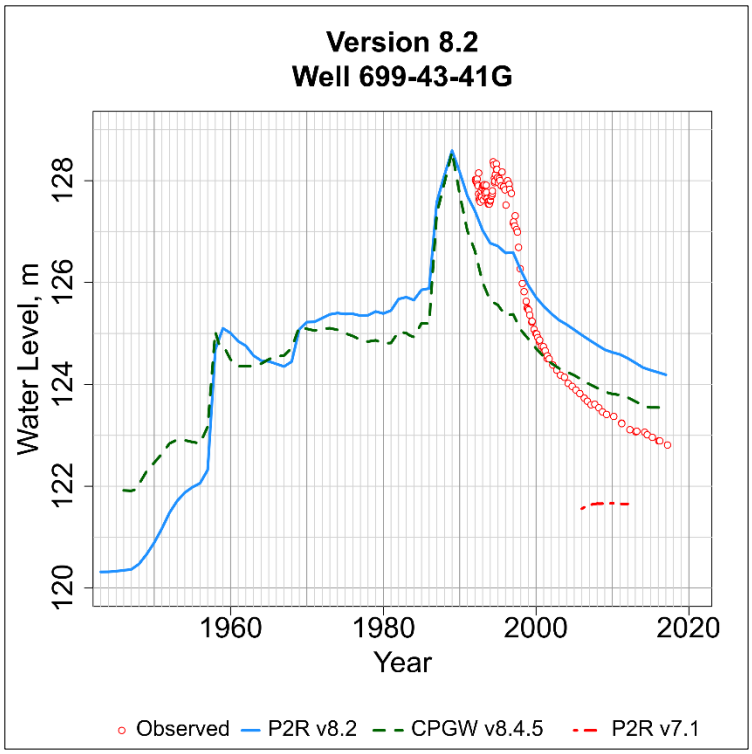

Figure D-433. Observed and simulated water level in the P2R Model at well 699-43-41G.png.

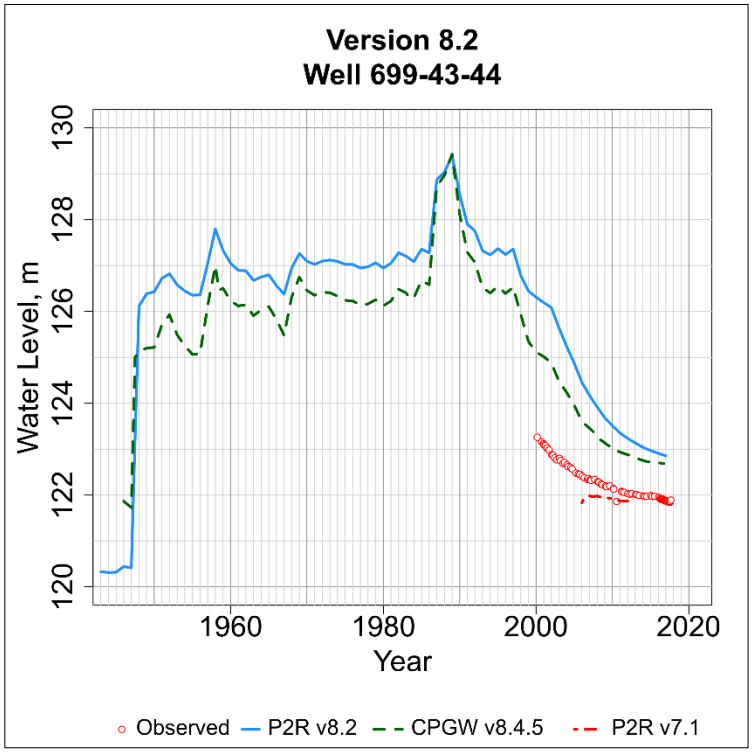

Figure D-434. Observed and simulated water level in the P2R Model at well 699-43-44.png.

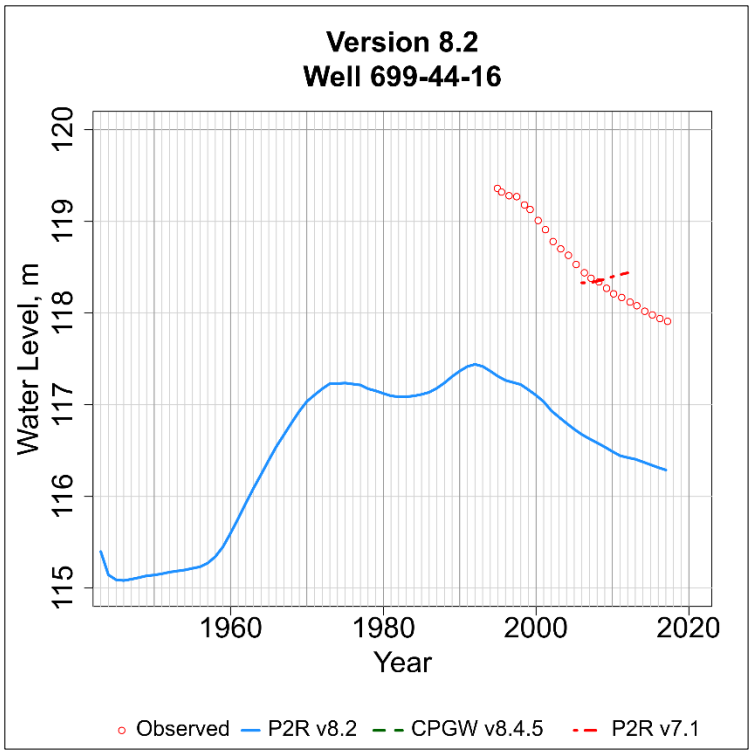

Figure D-435. Observed and simulated water level in the P2R Model at well 699-44-16.png.

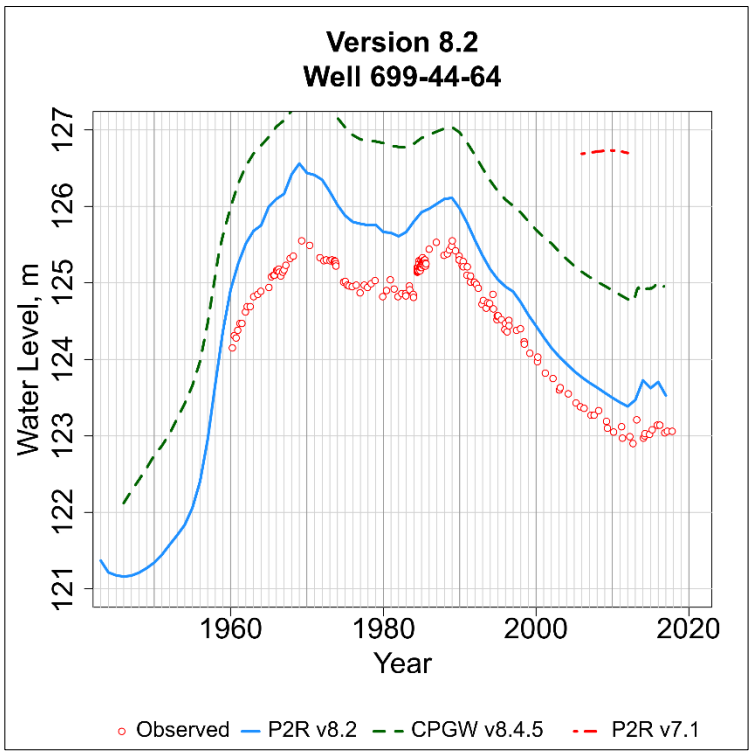

Figure D-436. Observed and simulated water level in the P2R Model at well 699-44-64.png.

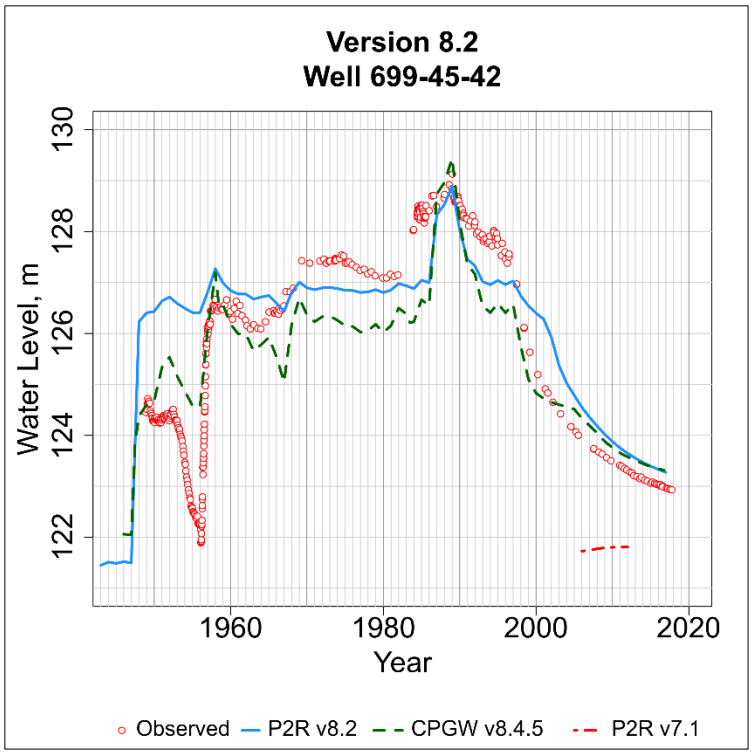

Figure D-437. Observed and simulated water level in the P2R Model at well 699-45-42.png.

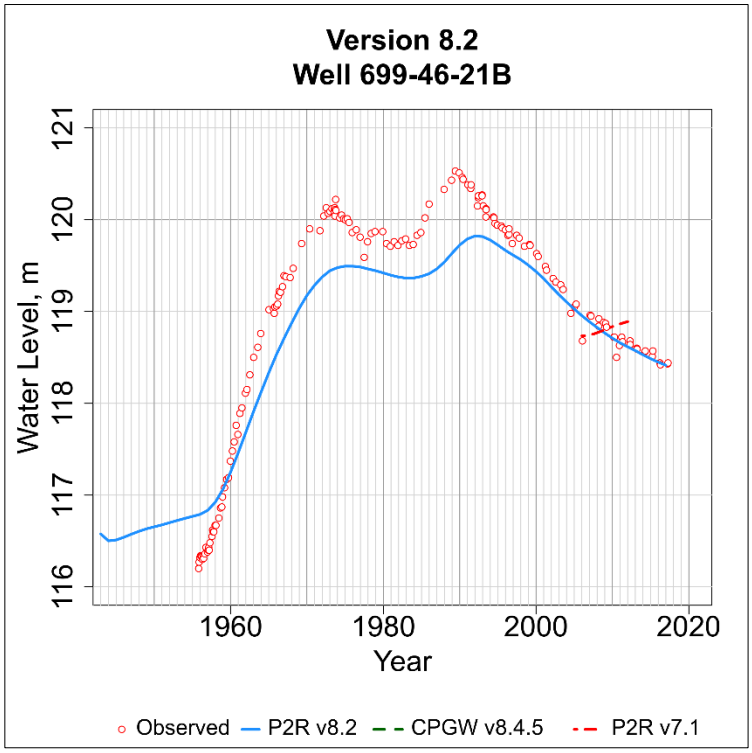

Figure D-438. Observed and simulated water level in the P2R Model at well 699-46-21B.png.

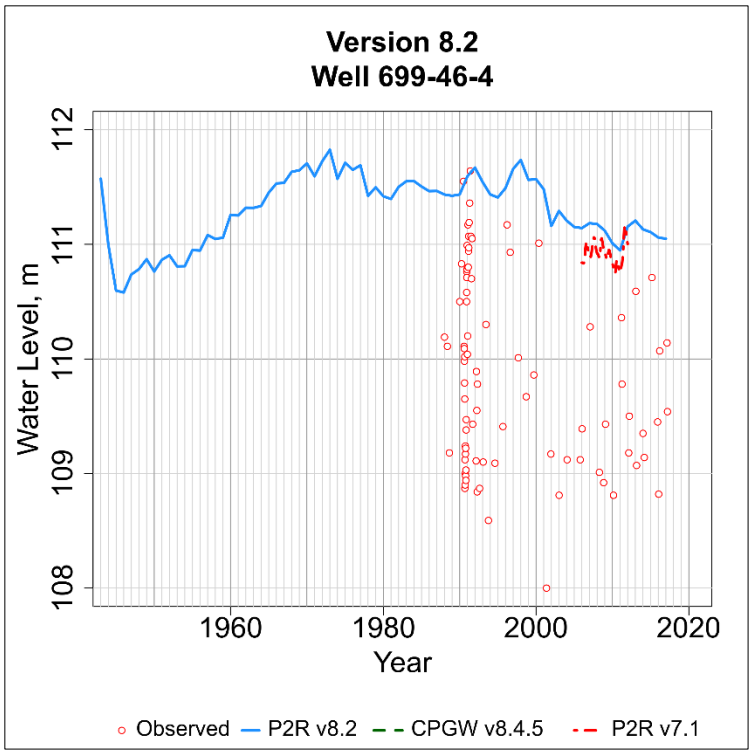

Figure D-439. Observed and simulated water level in the P2R Model at well 699-46-4.png.

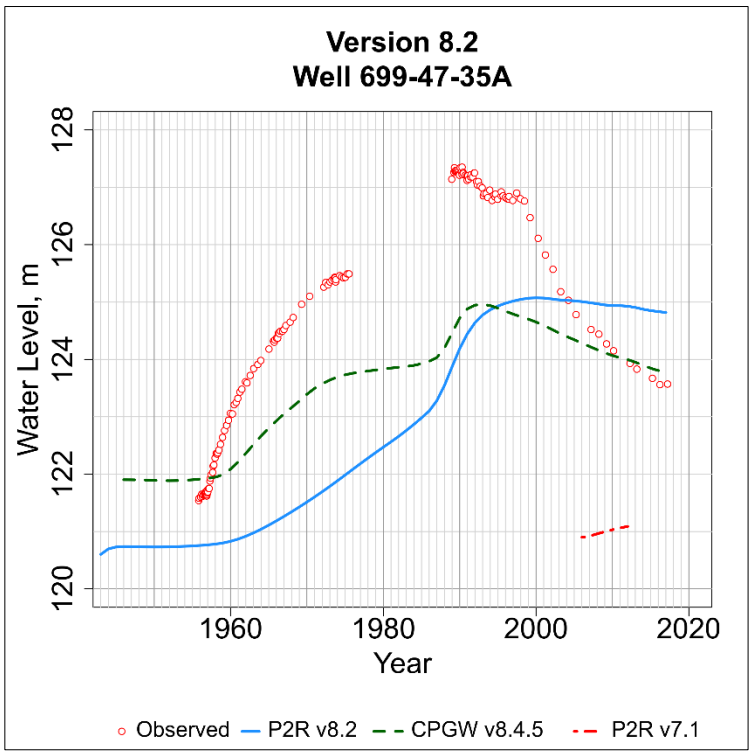

Figure D-440. Observed and simulated water level in the P2R Model at well 699-47-35A.png.

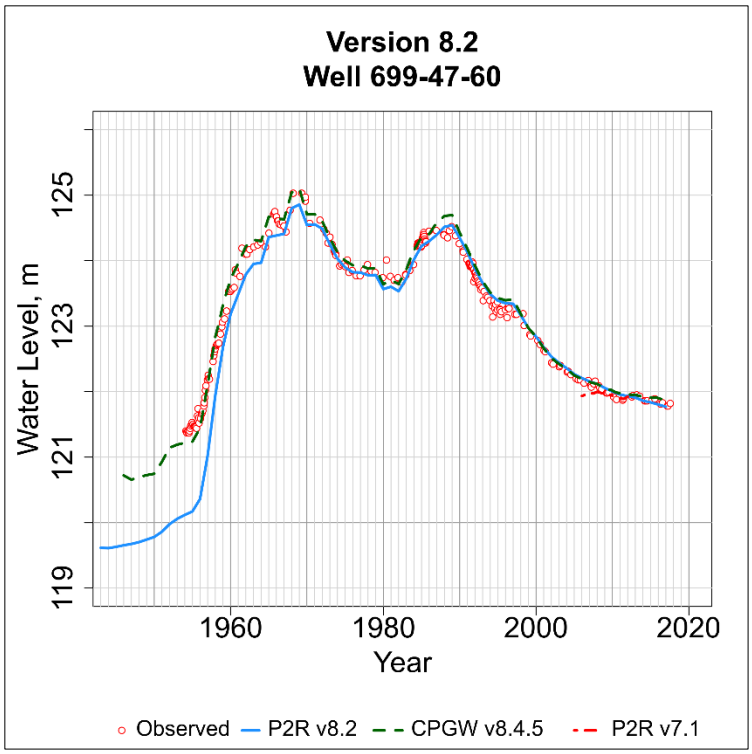

Figure D-441. Observed and simulated water level in the P2R Model at well 699-47-60.png.

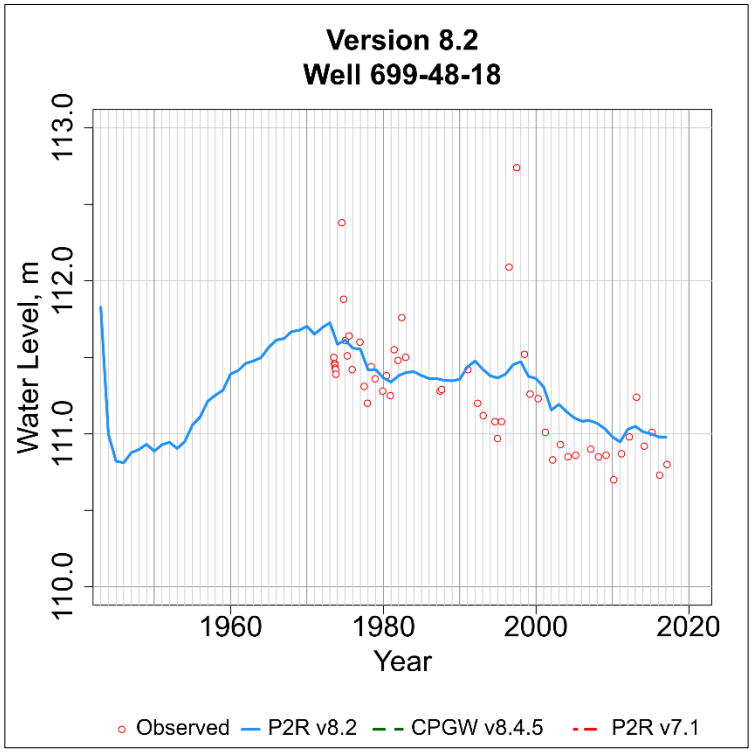

Figure D-442. Observed and simulated water level in the P2R Model at well 699-48-18.png.

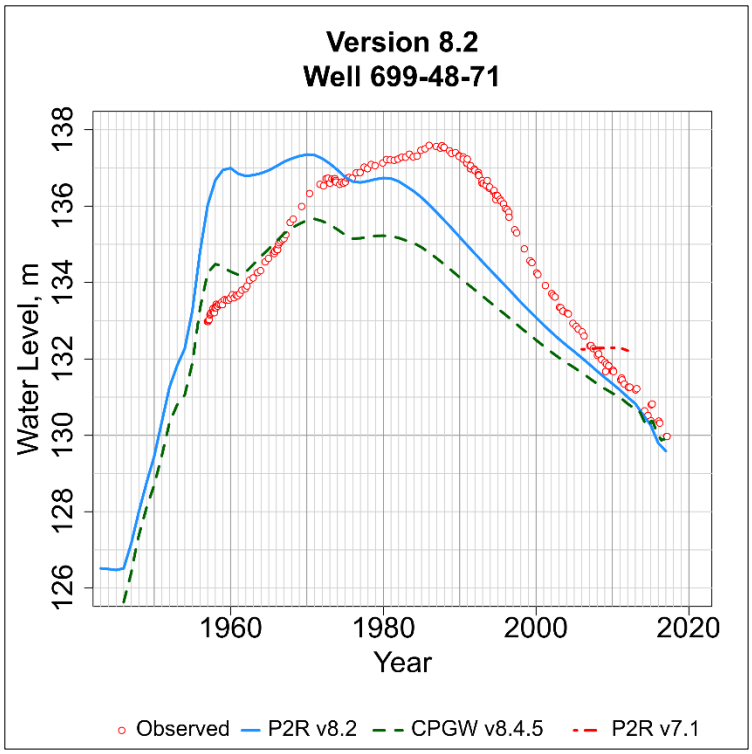

Figure D-443. Observed and simulated water level in the P2R Model at well 699-48-71.png.

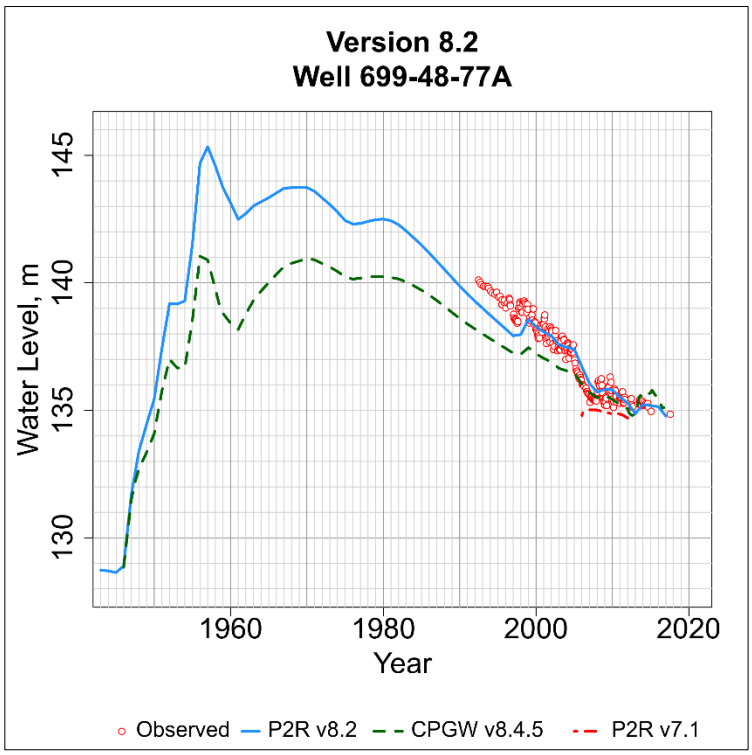

Figure D-444. Observed and simulated water level in the P2R Model at well 699-48-77A.png.

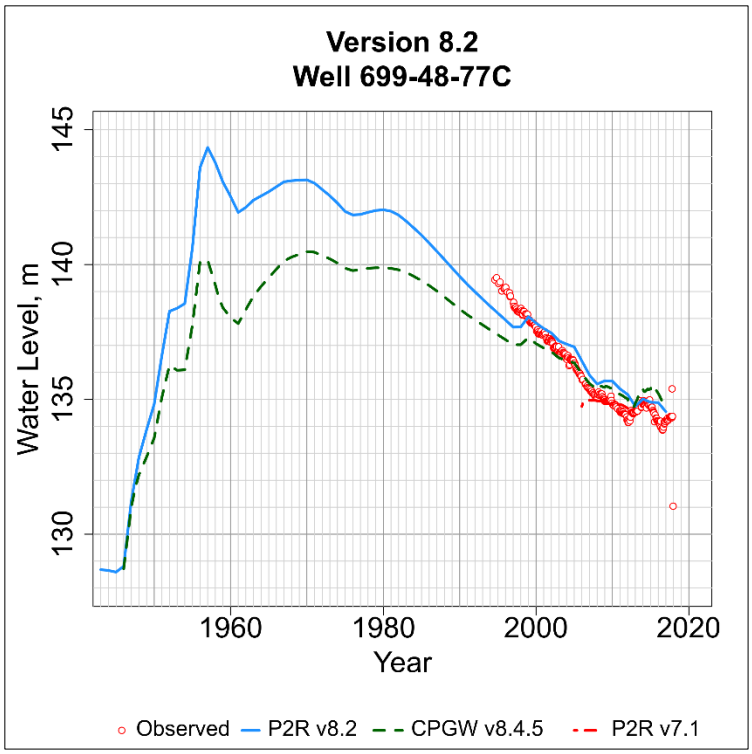

Figure D-445. Observed and simulated water level in the P2R Model at well 699-48-77C.png.

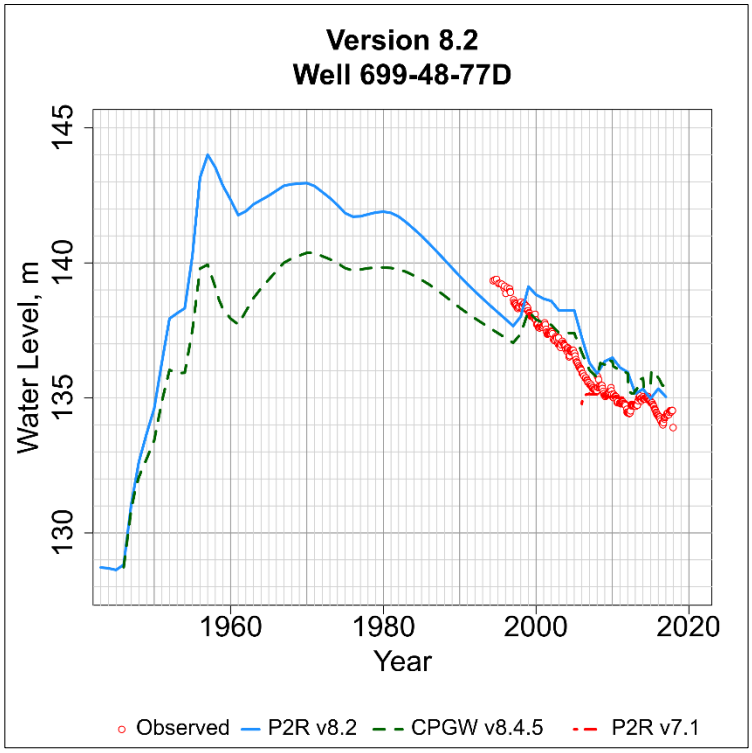

Figure D-446. Observed and simulated water level in the P2R Model at well 699-48-77D.png.

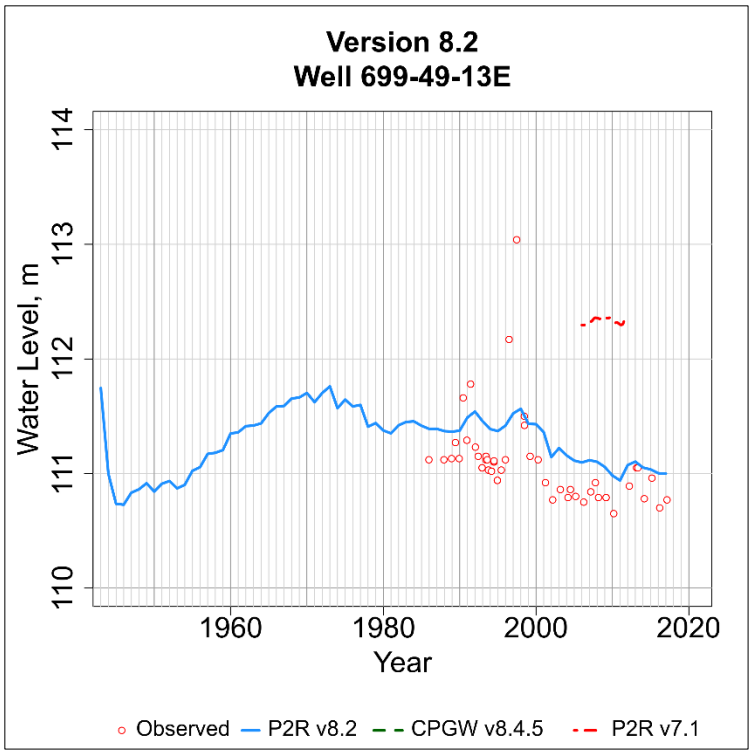

Figure D-447. Observed and simulated water level in the P2R Model at well 699-49-13E.png.

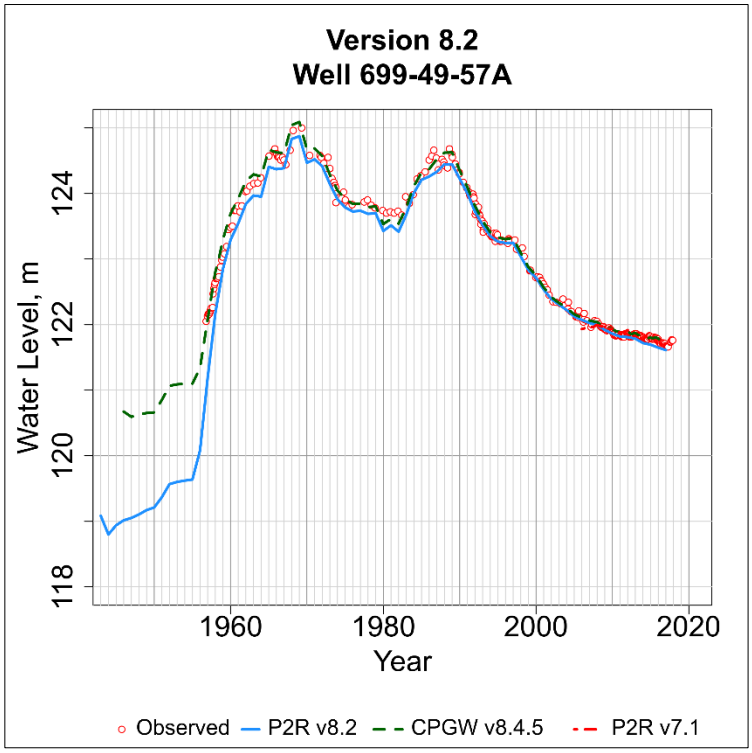

Figure D-448. Observed and simulated water level in the P2R Model at well 699-49-57A.png.

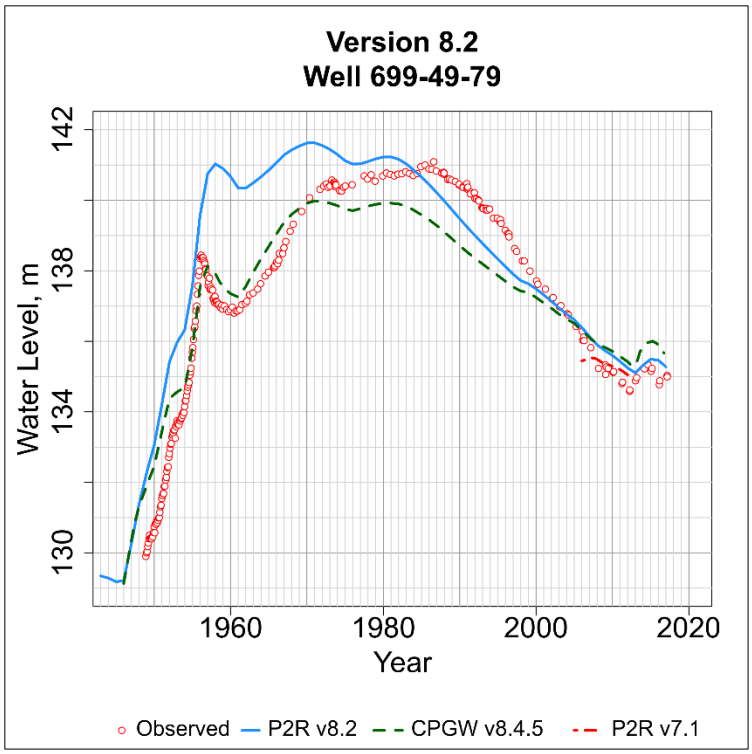

Figure D-449. Observed and simulated water level in the P2R Model at well 699-49-79.png.

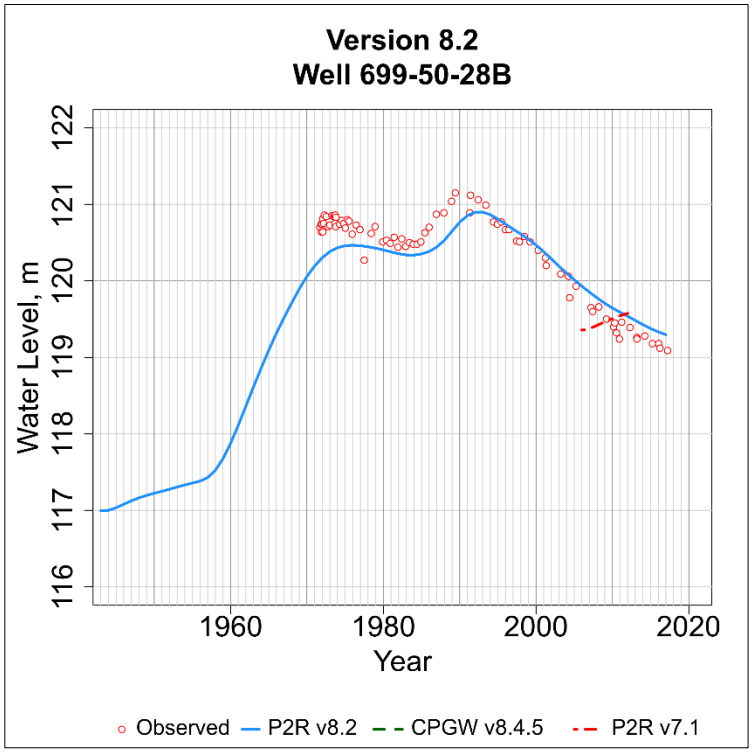

Figure D-450. Observed and simulated water level in the P2R Model at well 699-50-28B.png.

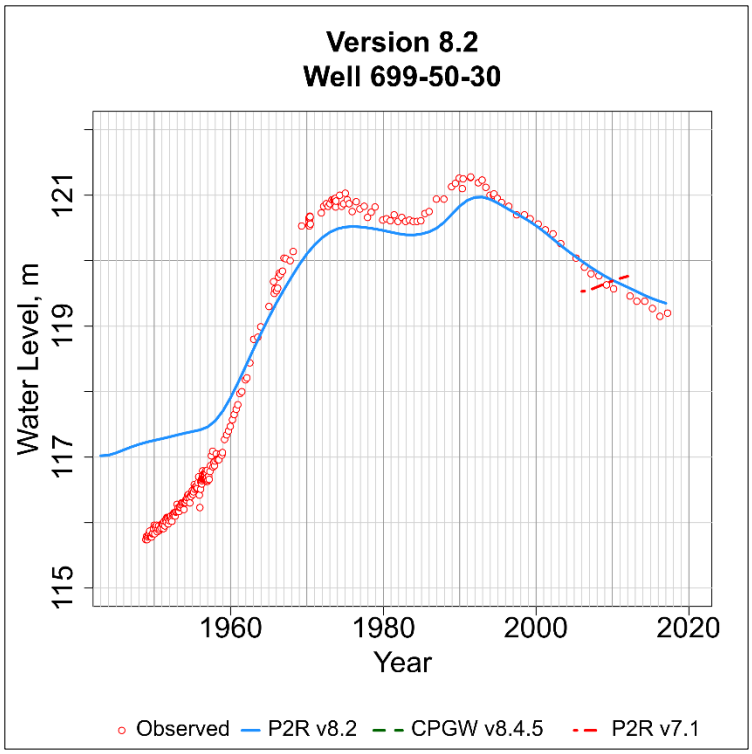

Figure D-451. Observed and simulated water level in the P2R Model at well 699-50-30.png.

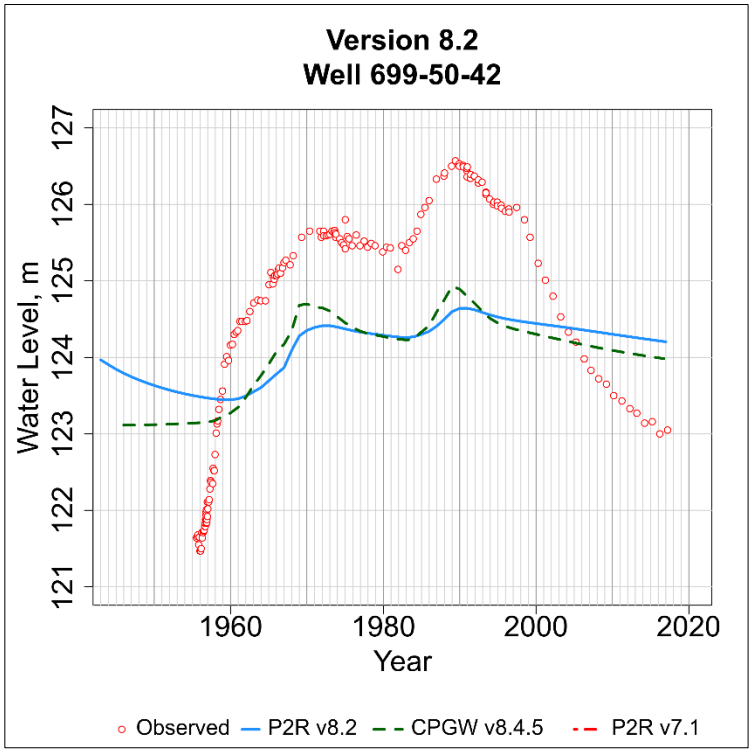

Figure D-452. Observed and simulated water level in the P2R Model at well 699-50-42.png.

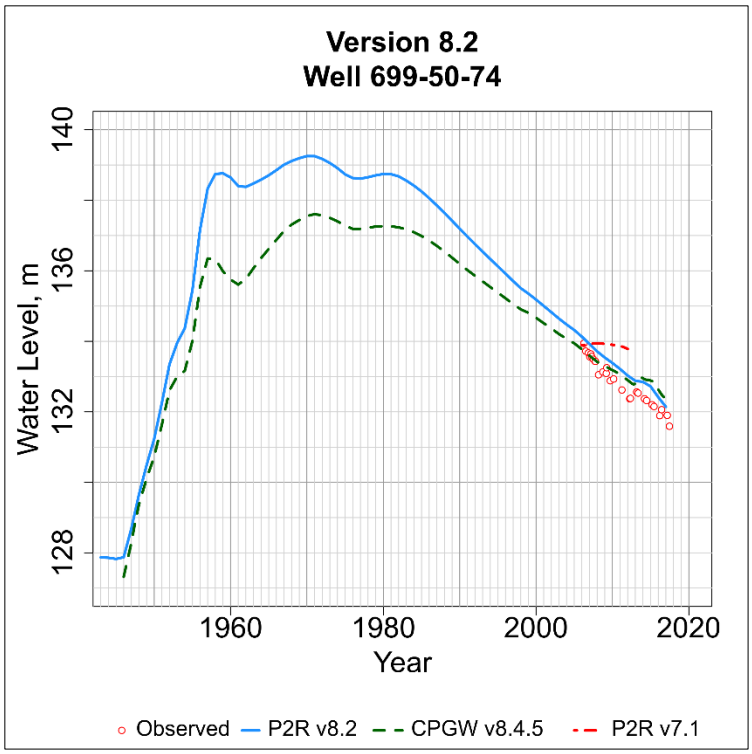

Figure D-453. Observed and simulated water level in the P2R Model at well 699-50-74.png.

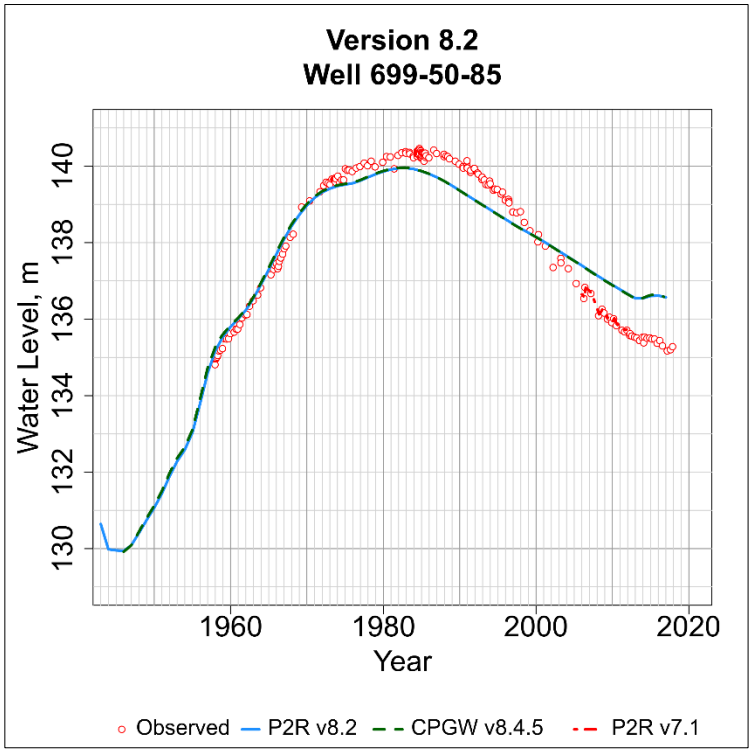

Figure D-454. Observed and simulated water level in the P2R Model at well 699-50-85.png.

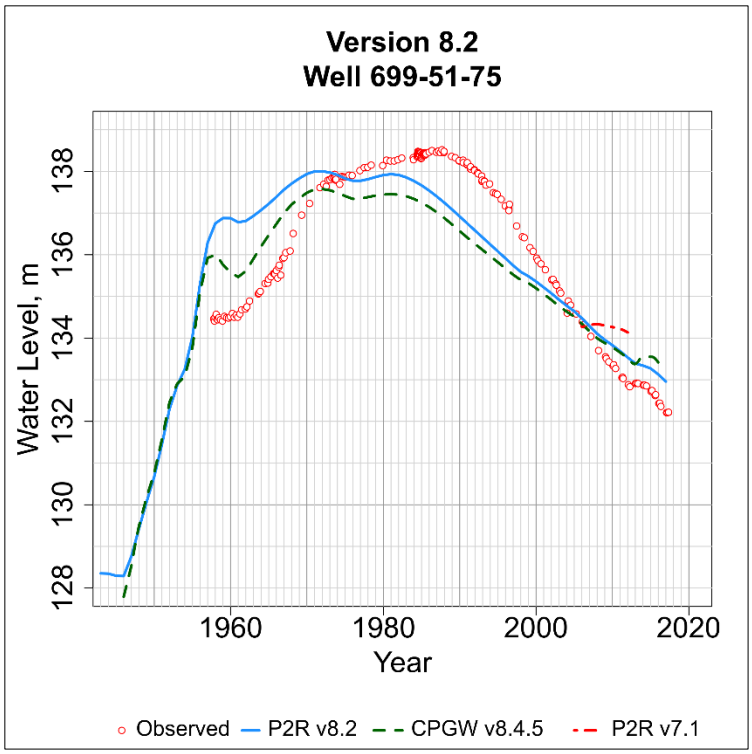

Figure D-455. Observed and simulated water level in the P2R Model at well 699-51-75.png.

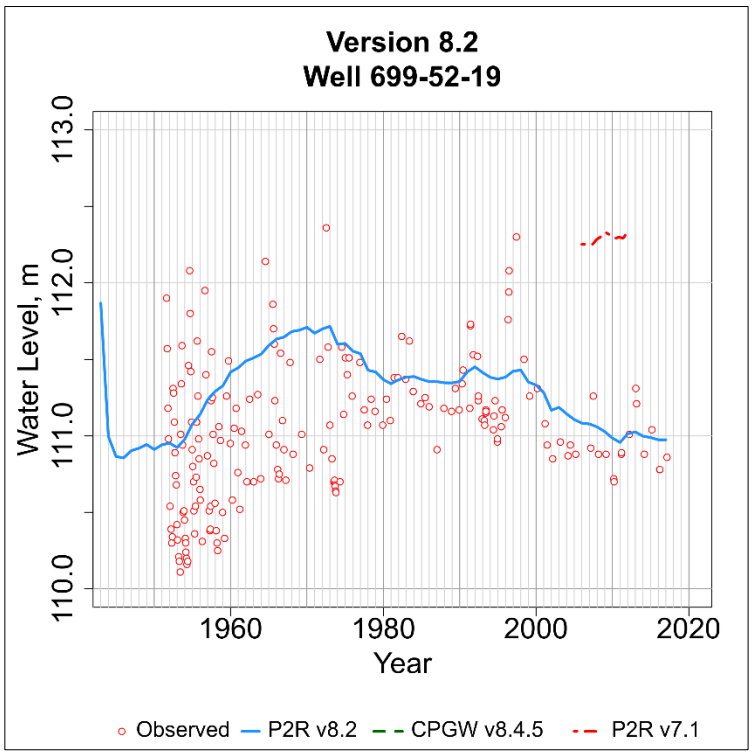

Figure D-456. Observed and simulated water level in the P2R Model at well 699-52-19.png.

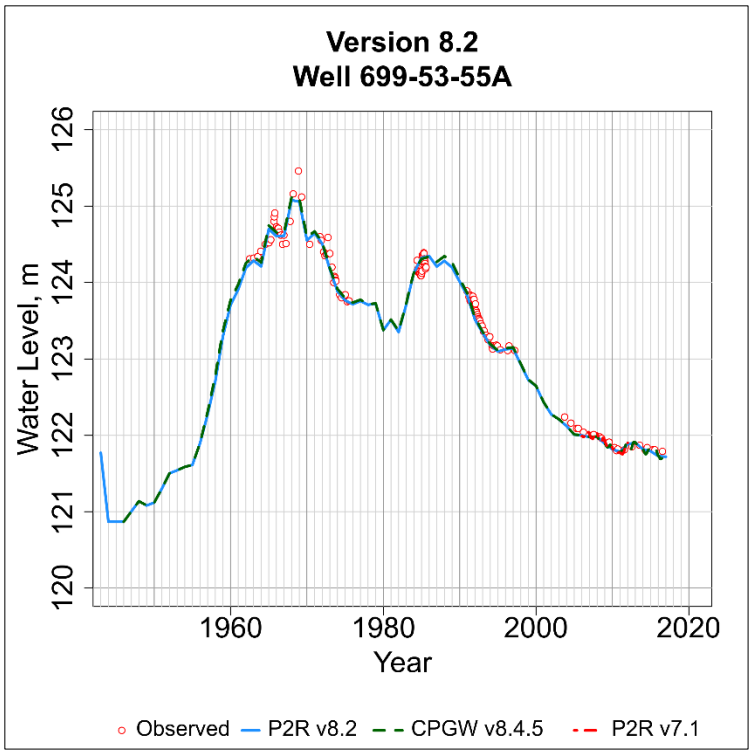

Figure D-457. Observed and simulated water level in the P2R Model at well 699-53-55A.png.

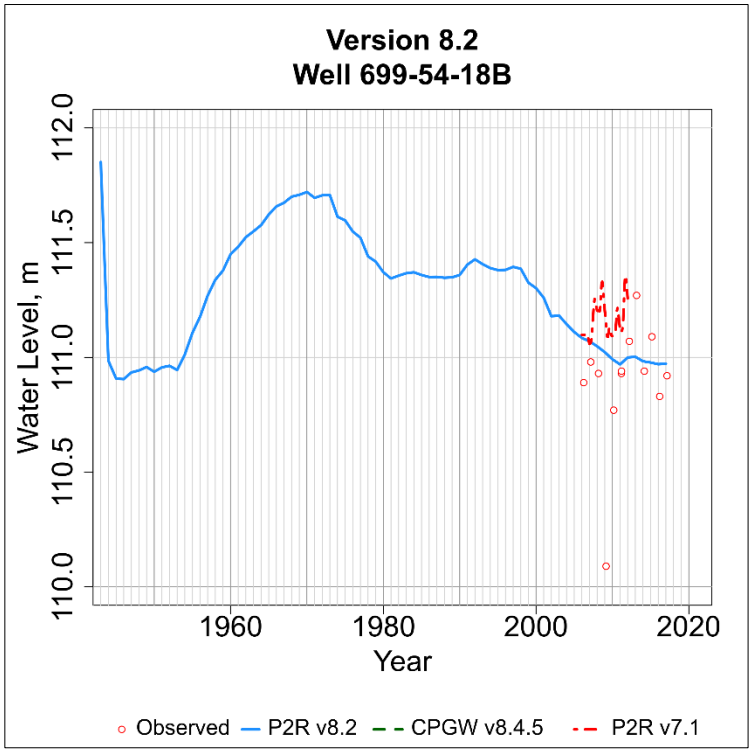

Figure D-458. Observed and simulated water level in the P2R Model at well 699-54-18B.png.

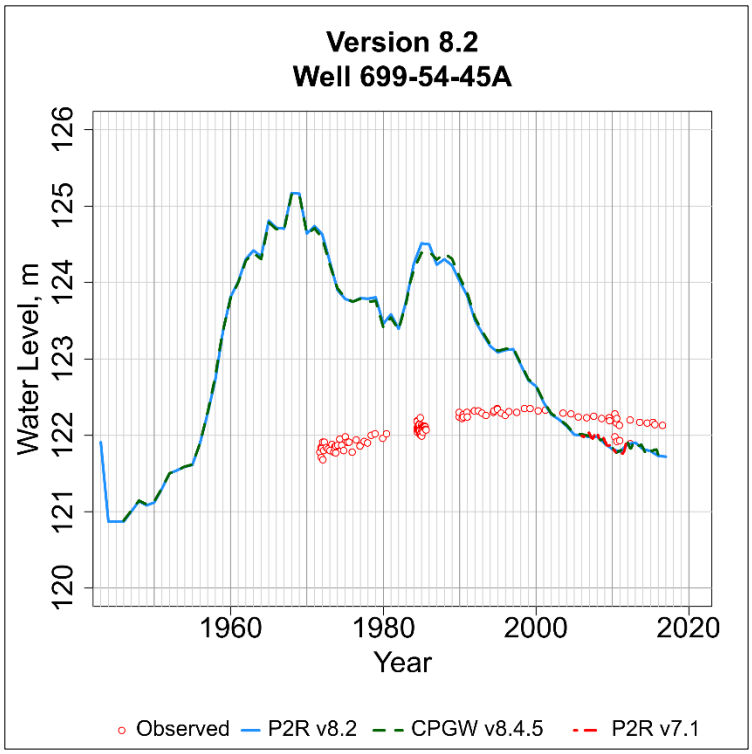

Figure D-459. Observed and simulated water level in the P2R Model at well 699-54-45A.png.

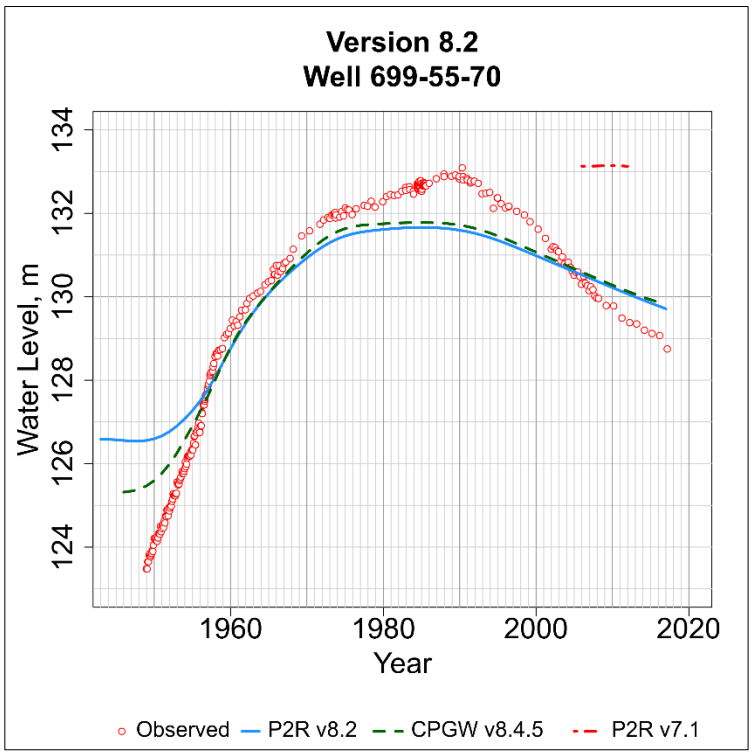

Figure D-460. Observed and simulated water level in the P2R Model at well 699-55-70.png.

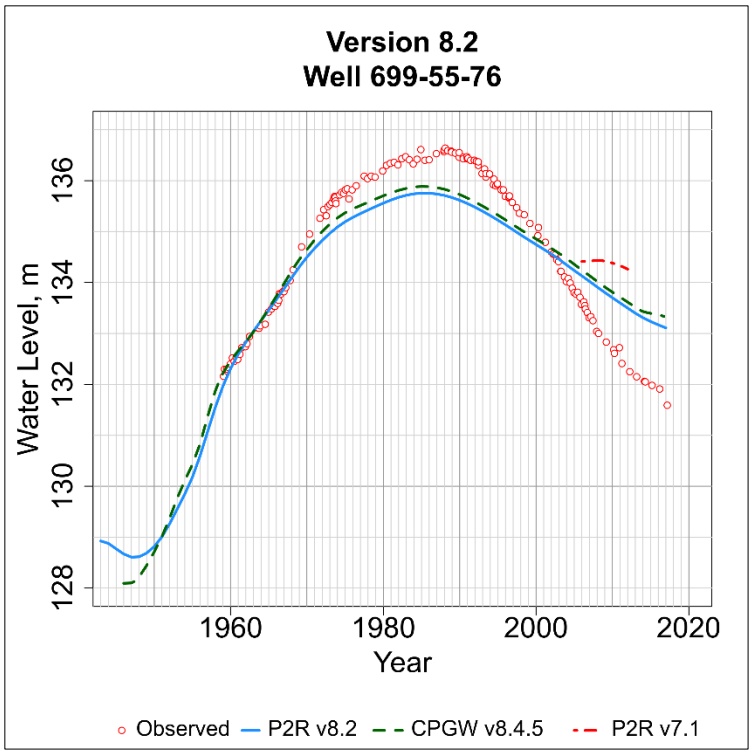

Figure D-461. Observed and simulated water level in the P2R Model at well 699-55-76.png.

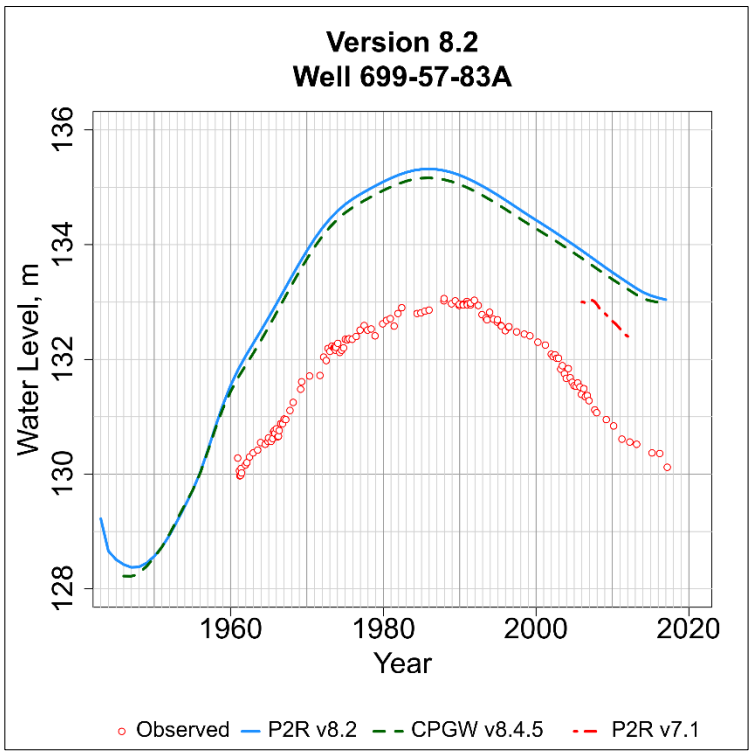

Figure D-462. Observed and simulated water level in the P2R Model at well 699-57-83A.png.

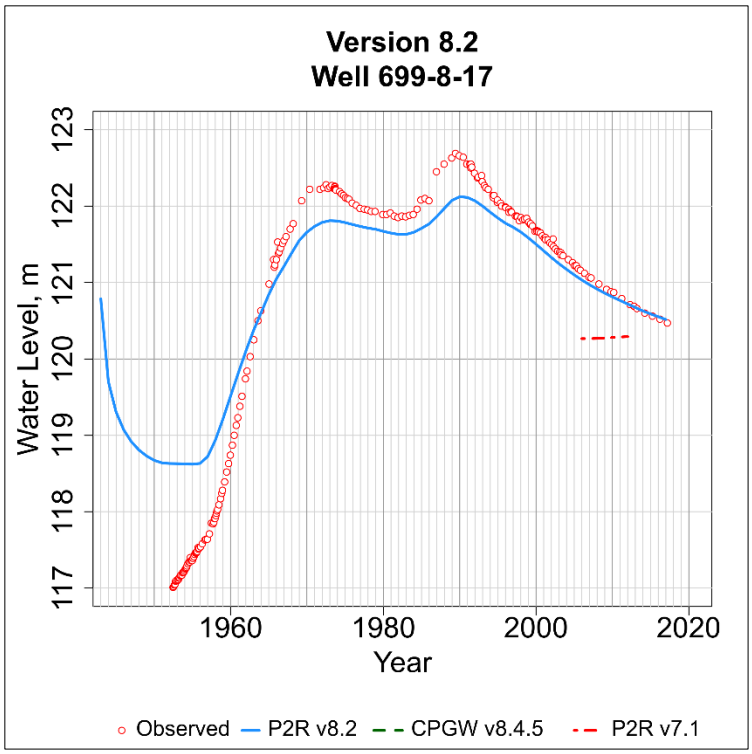

Figure D-463. Observed and simulated water level in the P2R Model at well 699-8-17.png.

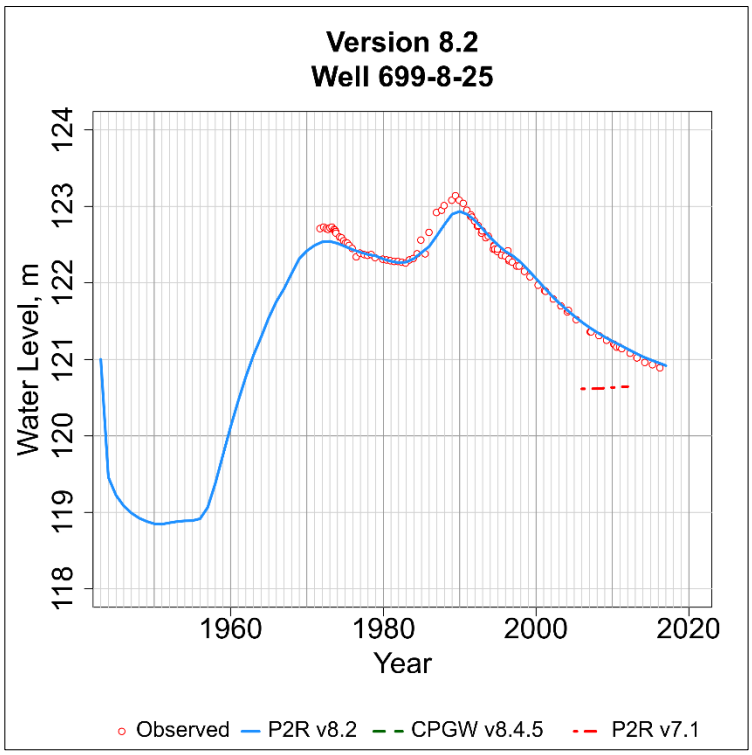

Figure D-464. Observed and simulated water level in the P2R Model at well 699-8-25.png.

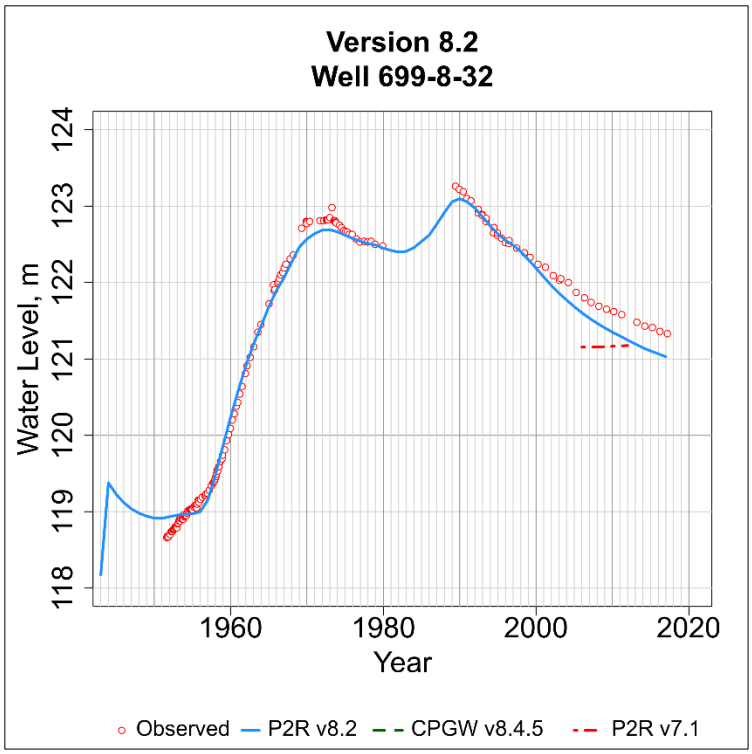

Figure D-465. Observed and simulated water level in the P2R Model at well 699-8-32.png.

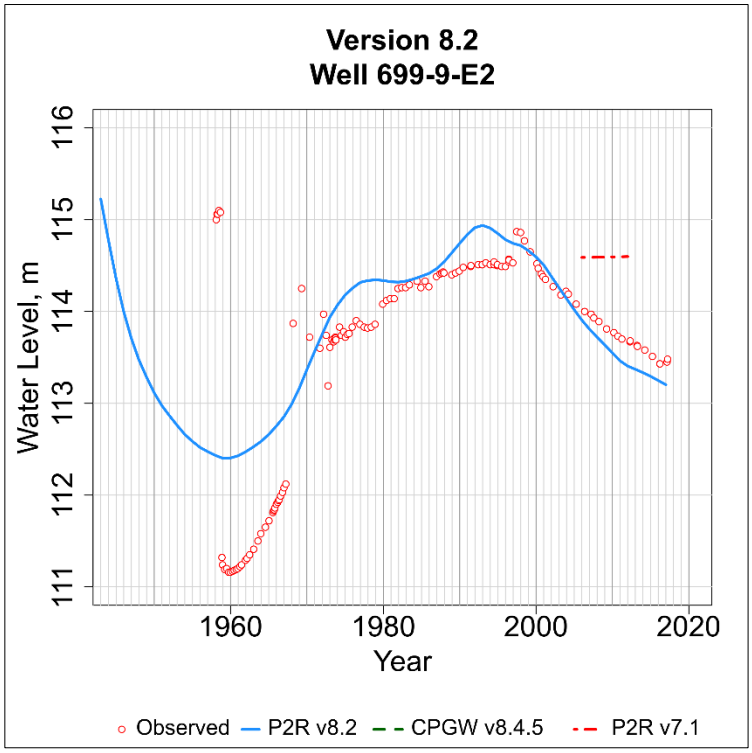

Figure D-466. Observed and simulated water level in the P2R Model at well 699-9-E2.png.

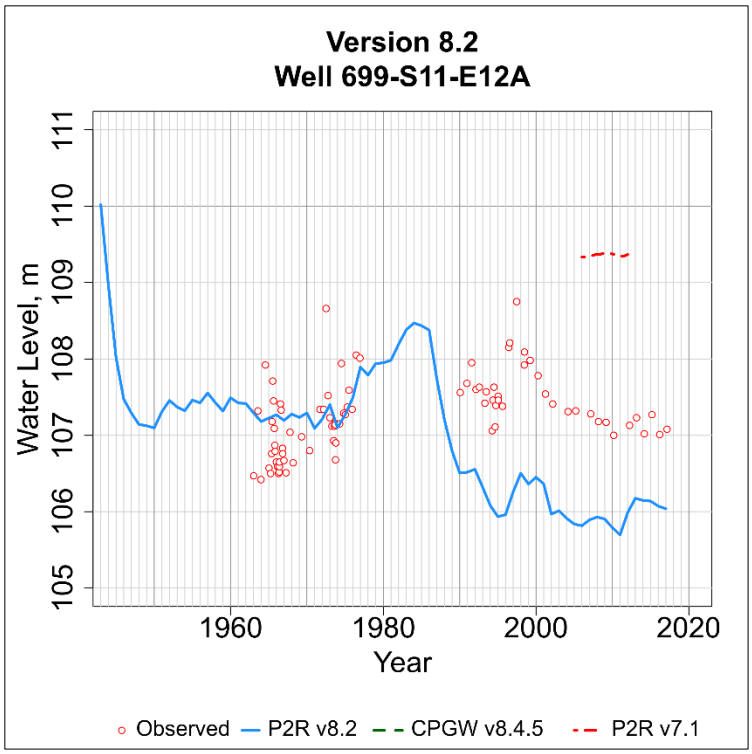

Figure D-467. Observed and simulated water level in the P2R Model at well 699-S11-E12A.png.

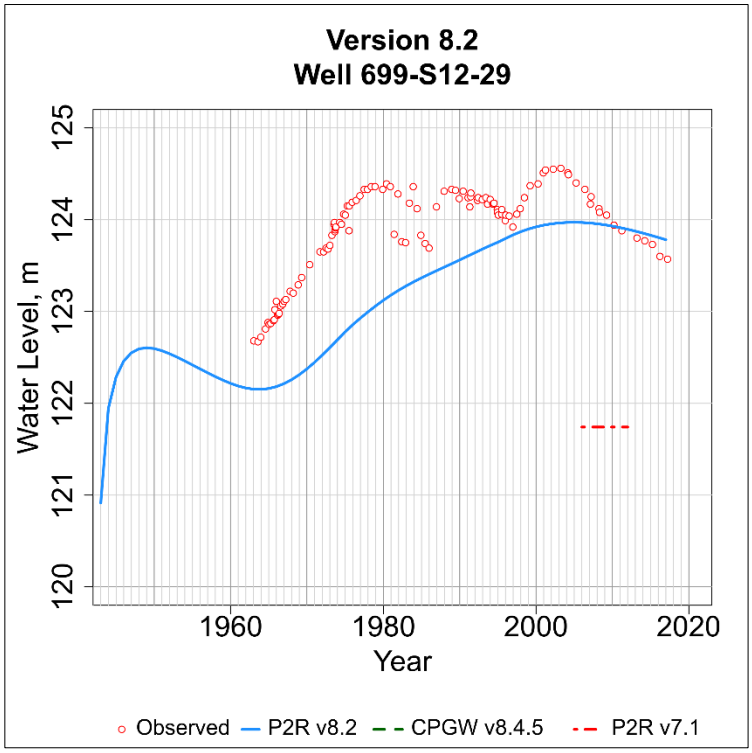

Figure D-468. Observed and simulated water level in the P2R Model at well 699-S12-29.png.

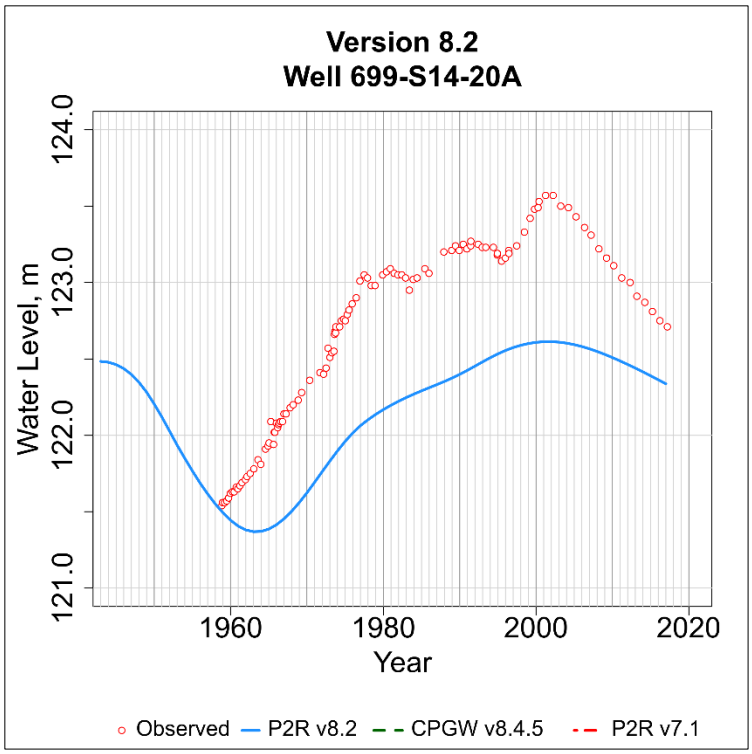

Figure D-469. Observed and simulated water level in the P2R Model at well 699-S14-20A.png.

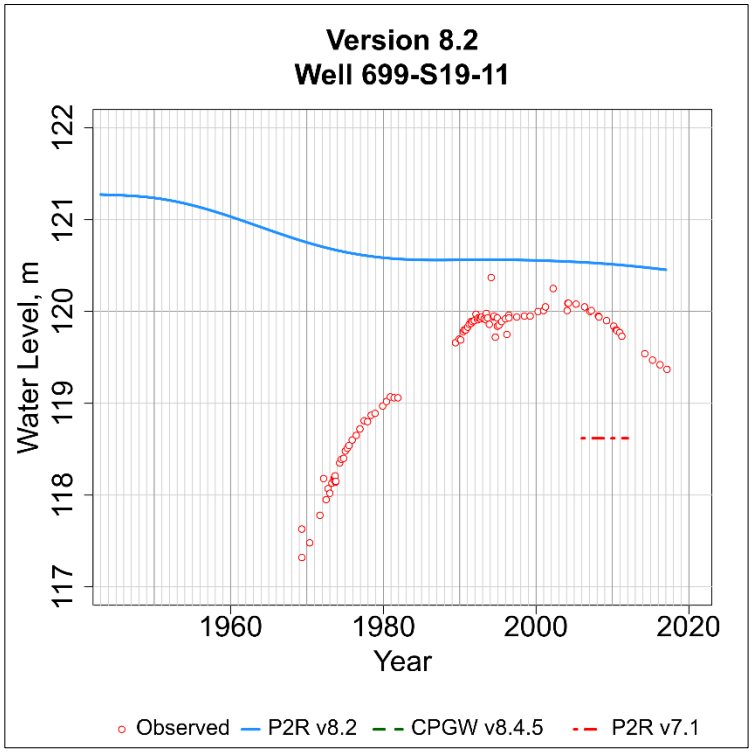

Figure D-470. Observed and simulated water level in the P2R Model at well 699-S19-11.png.

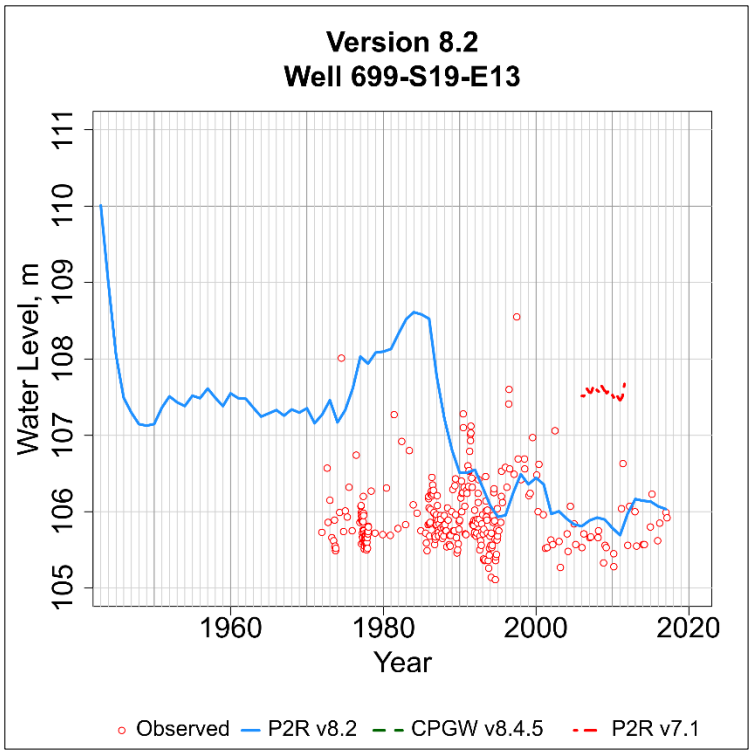

Figure D-471. Observed and simulated water level in the P2R Model at well 699-S19-E13.png.

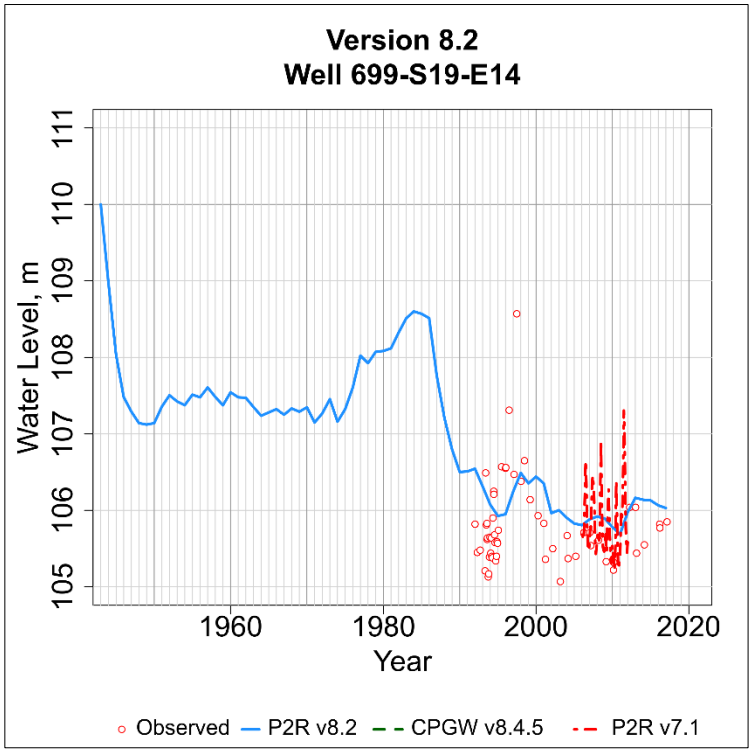

Figure D-472. Observed and simulated water level in the P2R Model at well 699-S19-E14.png.

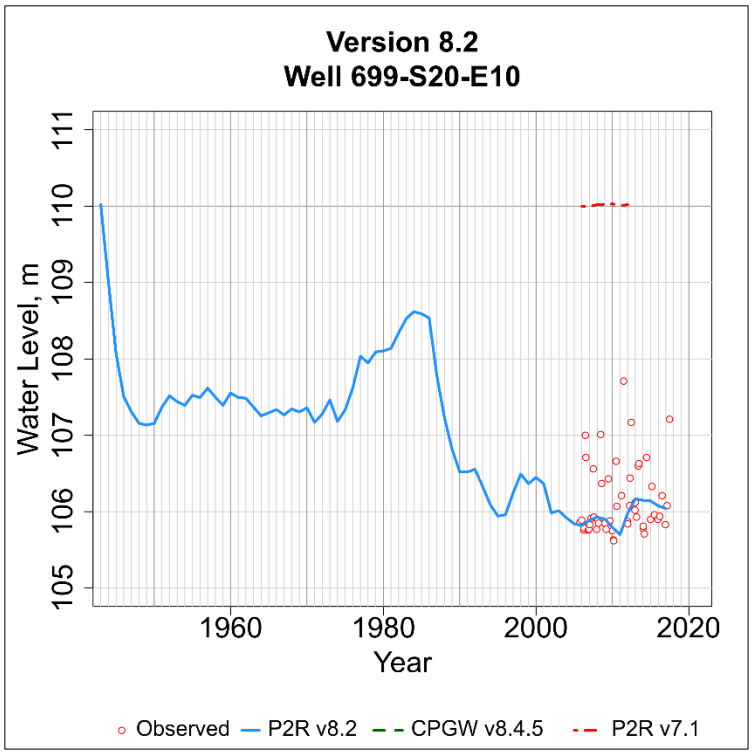

Figure D-473. Observed and simulated water level in the P2R Model at well 699-S20-E10.png.

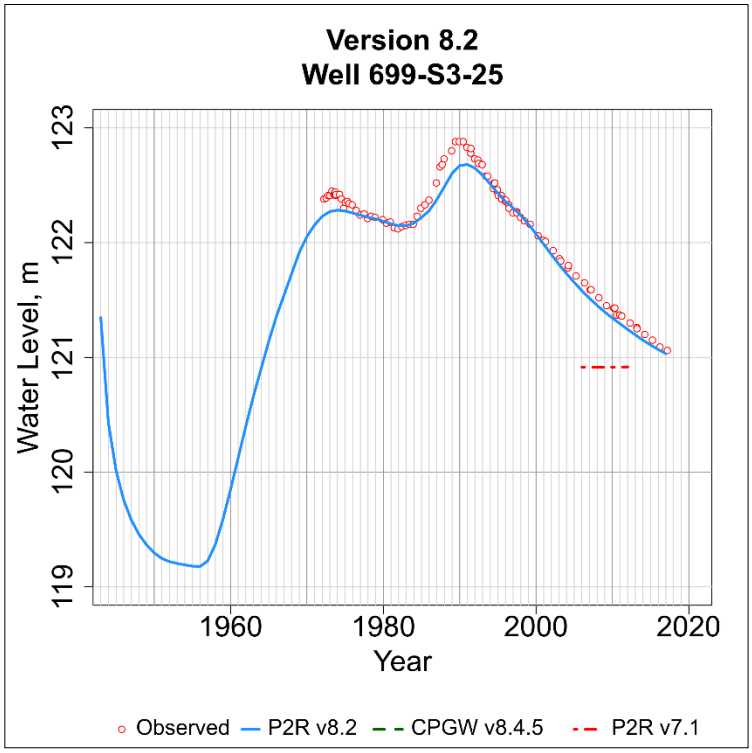

Figure D-474. Observed and simulated water level in the P2R Model at well 699-S3-25.png.

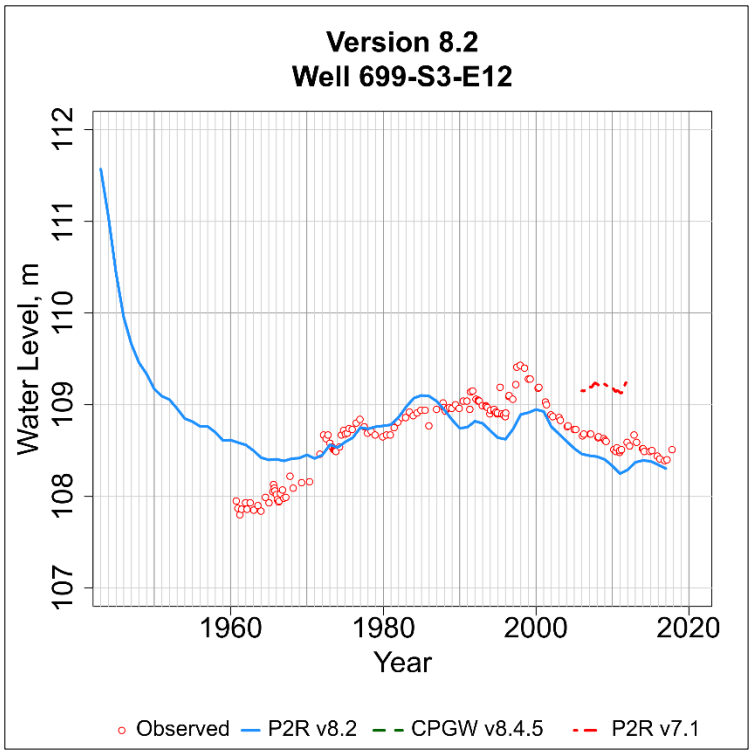

Figure D-475. Observed and simulated water level in the P2R Model at well 699-S3-E12.png.

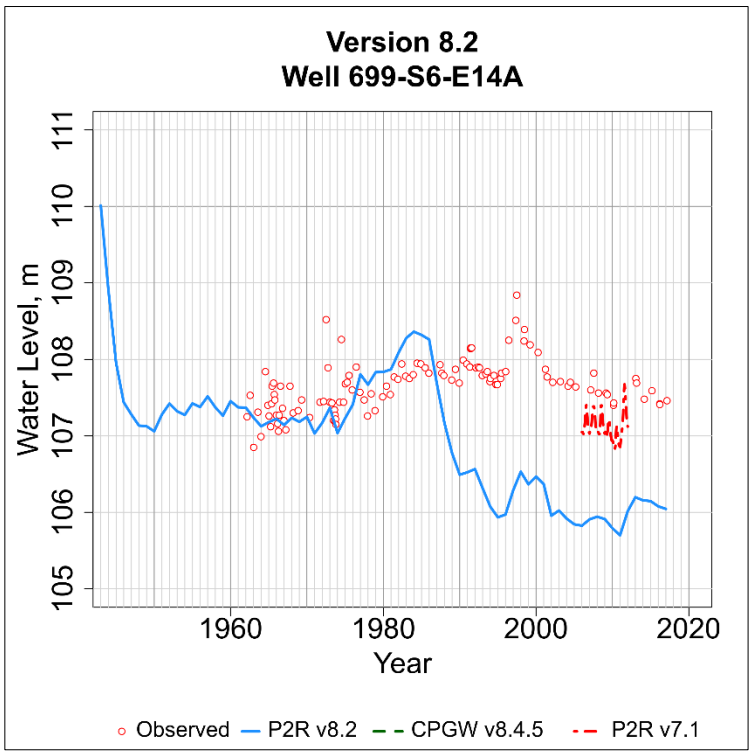

Figure D-476. Observed and simulated water level in the P2R Model at well 699-S6-E14A.png.

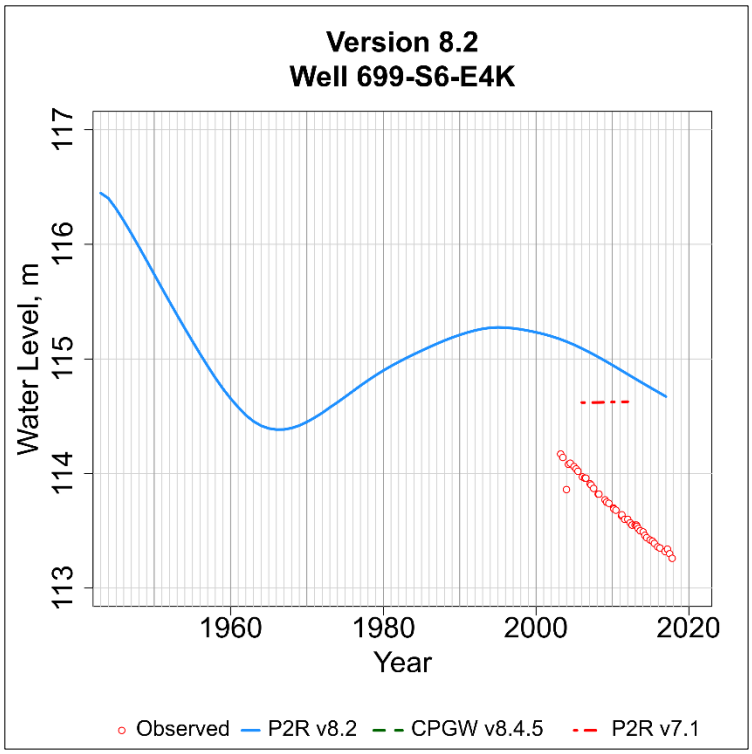

Figure D-477. Observed and simulated water level in the P2R Model at well 699-S6-E4K.png.

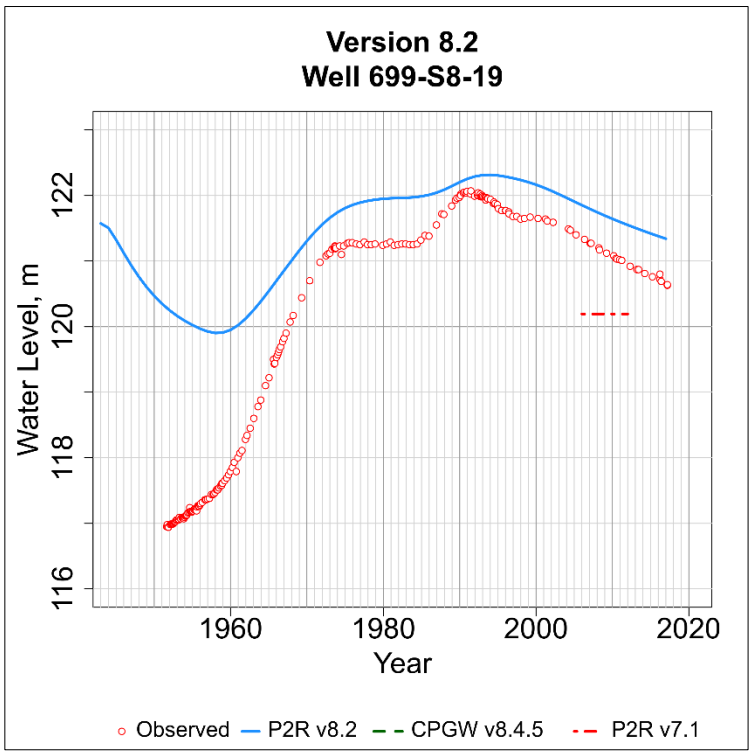

Figure D-478. Observed and simulated water level in the P2R Model at well 699-S8-19.png.

Appendix E

Copy of EMDT-BC-0002 Rev. 1

Electronic Model Data Transmittal: Vadose Zone Attenuated Recharge from Inflow-04 Assessment

Environmental Modeling Data Transmittal Cover Page

No.: EMDT-BC-0002 **Revision No.:** 1

[Request EMDT number from Modeling Team Leader]

Title: Vadose Zone Attenuated Recharge from Inflow-04 Assessment **Date:** 01/07/2019

1. Data Description

Provide the description of data set or data type.

Vadose zone attenuation of artificial recharge (originating from liquid discharges to ground) has been noted to be important to improvement of calibration for groundwater models in the Hanford setting. This data transmittal is to furnish the results of the SAC Rev. 1 Inflow-04 Assessment that was devoted to calculating vadose-zone attenuated artificial recharge for 1062 sites from 1994 through 2400 to support the calibration of the Central Plateau Groundwater Model Version 3. It is noted that future versions of this model should be provided with artificial recharge values generated from a new vadose zone attenuation assessment (tentatively named "Inflow-05") that includes updated discharge data for TEDF, SALDS, and any other sites for the years 2005 to 2009 and updated future year projections.

The summary graphic of summed total recharge by calendar year for the 1944 to 2000 period is provided here

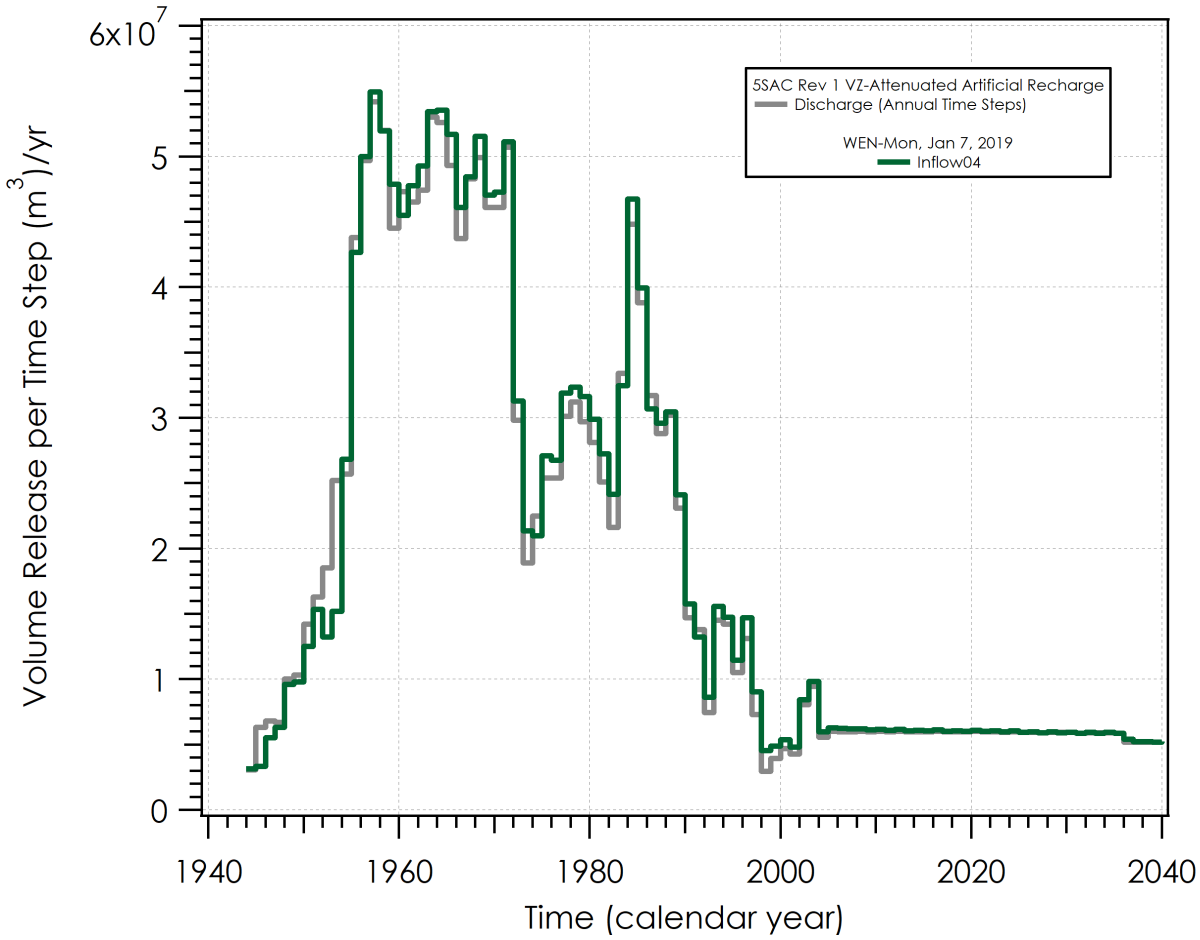

Environmental Modeling Data Transmittal Cover Page

No.: EMDT-BC-0002 **Revision No.:** 1

[Request EMDT number from Modeling Team Leader]

Title: Vadose Zone Attenuated Recharge from Inflow-04 Assessment **Date:** 01/07/2019

2. Data Intended Use

Identify the data's intended use. Describe the rationale for its selection and how the data will be incorporated into a model, report, or database. Include discussion of the extent to which the data demonstrate the properties of interest.

This data set represents a calculated vadose zone attenuated flux rate to the top of the Hanford Site suprabasalt aquifer over time based on vadose zone simulation of hundreds of recorded effluent discharges during and following the Hanford Site production period (1944 to 1989), intended for use as a boundary condition input for groundwater flow models.

3. Data Sources

List databases, documents, etc. – provide sufficient detail to enable data to be located by independent reviewer

Liquid discharge data were collected and configuration managed by the Characterization of Systems Project to support the System Assessment Capability (SAC). One of the functions of the SAC software framework was to provide a means to efficiently model vadose zone flow and transport at hundreds of individual sites and pass contaminant releases to a groundwater model (Nichols et al. 2005, "Vadose Zone Modeling of Dispersed Waste Sites in the Framework of an Integrated Stochastic Environmental Transport and Impacts Assessment Code for the Hanford Site" in *Stochastic Environmental Research and Risk Assessment* 19:24-32). A corollary benefit was that the framework proved very amenable to modeling attenuation of artificial discharges in the vadose zone; accounting for this attenuation was identified as the most significant factor considered for improvement of a site-wide groundwater model calibration (PNNL-14398**,** *Transient Inverse Calibration of the Site-Wide Groundwater Flow Model (ACM-2): FY03 Progress Report*. Vadose zone attenuated fluxes were included in the 2006 Groundwater Data Package for Hanford Assessments (PNNL-14753 Rev 1, *Groundwater Data Package for Hanford Assessments*) and the technique for calculating artificial recharge was later improved upon (Nichols et al. 2007, "Vadose Zone-Attenuated Artificial Recharge for Input to a Ground Water Model" in *Groundwater* 45(4):491-498). The latest calculation available, using the technique described in Nichols et al. 2007, is found in the "Inflow-04" Assessment performed with SAC Rev. 1. This data transmittal provides calendar year values of artificial recharge for 1062 vadose zone sites from the Inflow-04 Assessment.

The Inflow-04 Assessment itself is documented in an Assessment Report, which is provided with this data transmittal. The primary data feed is a .CSV (comma separated variable) format file titled "Inflow-04_artificial-recharge.csv". The first four lines are header information, followed by data lines containing year, site ID, and artificial recharge values. The format is very much similar to that found in the 2006 Groundwater Data Package PNNL-14753 Rev 1.

Revision 1 of this EMDT changes no data, but does annualize fluxes to full calendar years (these data were previously presented in six-month time steps that were used in the earlier PNNL Sitewide Groundwater Model).

Environmental Modeling Data Transmittal Cover Page

No.: EMDT-BC-0002 **Revision No.:** 1

[Request EMDT number from Modeling Team Leader]

Title: Vadose Zone Attenuated Recharge from Inflow-04 Assessment **Date:** 01/07/2019

4. Impact of Use or Nonuse of Data

Describe the importance of the data to the model, report, and/or conclusions which they support. Identify the value added and discuss the impacts of not using the data.

This data set represents the only calculation or estimate of vadose zone attenuated effluent flux to the suprabasalt aquifer available at the scale of the Hanford Site or at the scale of the entire Central Plateau. All other modeling efforts that account for effluent discharge to groundwater have neglected the attenuation effects of the vadose zone. The importance of vadose zone attenuation in improving groundwater model calibration and predictive capability were established in PNNL-14398.

5. Prior Uses

Identify the data's prior uses. Describe whether the data have been used in similar applications by the scientific or regulatory community. Include the associated verification processes and prior reviews and review results.

This data has been applied in the following models:

- Hanford Site Groundwater Model (PNNL-14398, *Transient Inverse Calibration of the Site-Wide Groundwater Flow Model (ACM-2): FY03 Progress Report*; PNNL-16425, *Transient Inverse Calibration of Facies-Based Hanford Site-Wide Groundwater Flow and Transport Model Using Tritium and Hydraulic Head Data (ACM-3)*; PNNL-14753 Rev 1, *Groundwater Data Package for Hanford Assessments*).
- Central Plateau Groundwater Model (CP-47631 Rev. 4, *Model Package Report: Central Plateau*
- *Groundwater Model, Version 8.4.5*)
- Plateau-to-River Model (CP-57037 Rev. 0, *Model Package Report: Plateau to River Groundwater Transport Model Version 7.1*)

Environmental Modeling Data Transmittal Cover Page

No.: EMDT-BC-0002 **Revision No.:** 1

[Request EMDT number from Modeling Team Leader]

Title: Vadose Zone Attenuated Recharge from Inflow-04 Assessment **Date:** 01/07/2019

6. Data Acquisition Method(s)

Describe the data acquisition method and associated QA/QC, considering the following:

a. Qualifications of personnel or organizations generating the data;
b. Technical adequacy of equipment and procedures used;
c. Environmental and programmatic conditions if germane to the data quality;
d. The extent to which acquisition processes reflect modeling requirements;
e. The quality and reliability of the measurement control program;
f. The degree to which independent audits of the process were conducted;
g. Extent and reliability of the associated documentation.

The VZGRAB data extraction utility was used to extract data from both the “natural recharge only” set of vadose zone simulations for all years and vadose zone sites and the “total recharge” (natural and artificial) set of vadose zone simulations for all years and vadose zone sites. The keyword files used for VZGRAB is included in this transmittal (vzgrab.key). It was run against the ESD keyword files for the Inflow-04 assessment.

Following the differencing technique (Nichols et al. 2007), the extracted fluxes were differenced using a short utility code written for this purpose to support this data transmittal. The source code for this utility, “artdis.f90”, is included in this transmittal. It’s only function is to read the natural and total recharge files produced using VZGRAB, difference the recharge, and write a third file to contain the (net) artificial recharge values. This is considered a simple, single-use utility code that should be reviewed as part of reviewing this data transmittal.

For databases, identify query language used to obtain data from database (SQL, etc.), briefly describe the query description and attach copy

Not applicable.

Environmental Modeling Data Transmittal Cover Page

No.: EMDT-BC-0002 **Revision No.:** 1

[Request EMDT number from Modeling Team Leader]

Title: Vadose Zone Attenuated Recharge from Inflow-04 Assessment **Date:** 01/07/2019

7. Corroborating Data

Identify and discuss any corroborating datasets. Provide any documentation that confirms the corroborating data substantiate existing parameter values, distributions, or data quality.

The Inflow-04 results are an improvement on prior simulations (Inflow-01, Inflow-02, Inflow-03) including results reported in PNNL-14753 Rev 1. The results of Inflow-02, Inflow-03, and Inflow-04 are shown in the figure below for total flux to demonstrate the comparability (the differences represent improvement in the computational methodology, as discussed in Nichols et al. 2007). Note, this figure represents the fluxes before annualizing (i.e., in original six-month time steps).

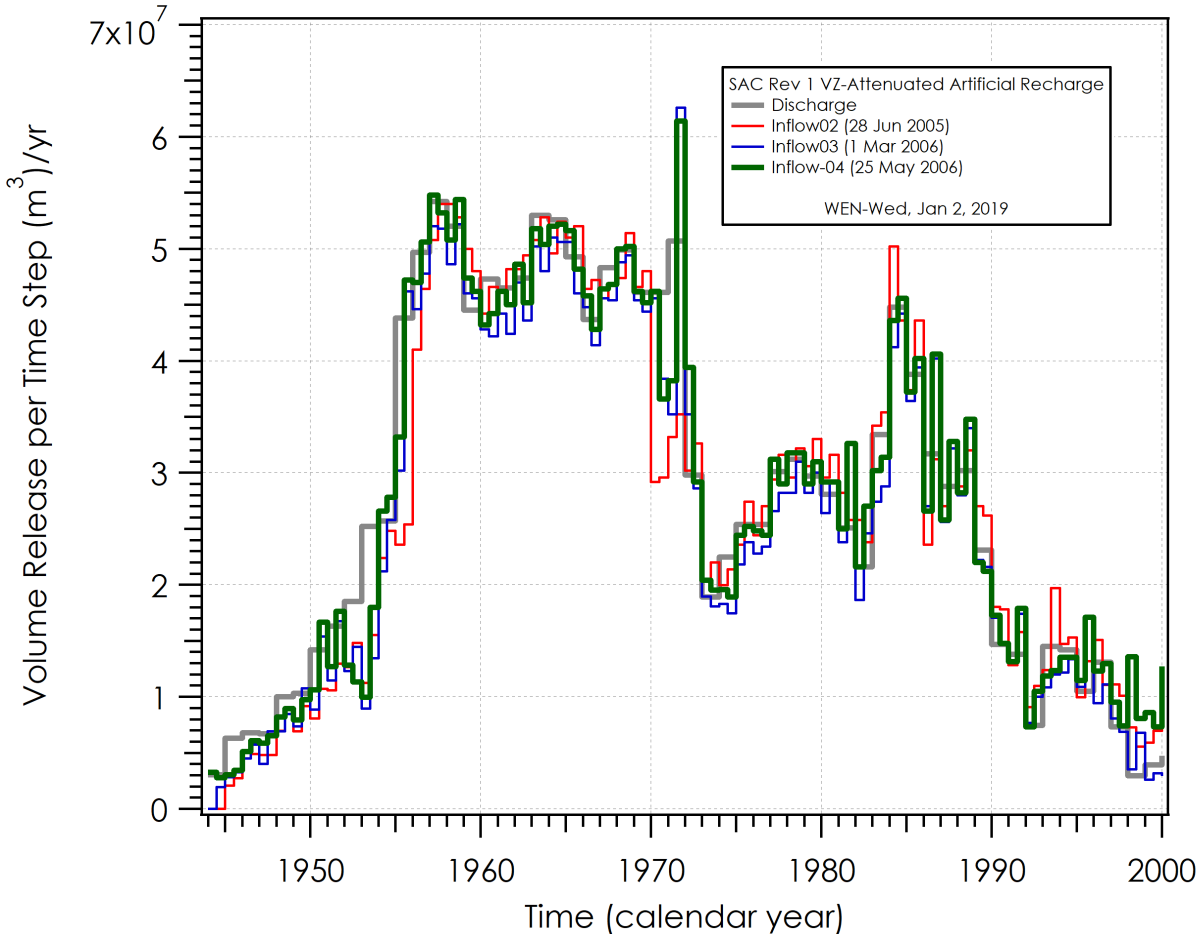

CH2MHILL Plateau Remediation Company

Environmental Modeling Data Transmittal Cover Page

No.: EMDT-BC-0002 **Revision No.:** 1

[Request EMDT number from Modeling Team Leader]

Title: Vadose Zone Attenuated Recharge from Inflow-04 Assessment **Date:** 01/07/2019

8. Data Quality Considerations

Discuss data quality considerations not identified in other sections. Include discussion of data quality indicators (i.e., accuracy, precision, representativeness, completeness, and comparability).

The Inflow-04 assessment was completed under QA requirements in place at the time of the run at Pacific Northwest National Laboratory as documented in "Application Log for Assessment Inflow-04" dated August 3, 2006. The log details the full computational process applied to produce the vadose zone attenuated effluent fluxes to groundwater. This log is included in this electronic model Data transmittal.

9. Assumptions and Limitations on Data Use

Document known uncertainties, assumptions, constraints or limits on data.

The effluent discharges accounted for in the Inflow-04 run are based on all recorded effluent discharges available at the time of the simulation (2005 through 2014) with projected discharges for TEDF and SALDS through end of expected life of those facilities. However, there are other anthropogenic liquid discharge sources not accounted for in this simulation. For example, dust suppression water, purge testing, water supply line leaks, and other unmetered discharges are not accounted for in this estimate. Further work is required to account for (estimate) these sources. A new Inflow-## style simulation would need to be performed with qualified software when the simulation capability is available to accomplish what is provided in the Inflow-04 simulation with additional liquid sources.

Data Configuration Item Submittal:

Data Provider Submittal

William E. Nichols / Modeling Team Leader
NAME/POSITION

SIGNATURE

1 MAY 2019
DATE

Data Configuration Item Review and Verification:

10. Verification Process

Describe steps taken to verify that these data are appropriate for intended use, noting any limitations

Reviewed, and requested time step revisions. Accepted.

CH2MHILL

Environmental Modeling Data Transmittal Cover Page

No.: EMDT-BC-0002 **Revision No.:** 1

[Request EMDT number from Modeling Team Leader]

Title: Vadose Zone Attenuated Recharge from Inflow-04 Assessment **Date:** 01/07/2019

11. Summary of Data Review

The review shall ensure that the report meets the listed criteria. Consideration includes ensuring that the data collection method employed was appropriate for the type of data being considered and confidence in the data acquisition and subsequent processing methodology is warranted.

Is documentation technically adequate, complete, and correct?	[✓] Yes	[ ] No
Are uncertainties and limitations on appropriate use of data discussed?	[✓] Yes	[ ] No
Are the assumptions, constraints, bounds, or limits on the data identified?	[✓] Yes	[ ] No

Data Reviewer Approval *Approval of Data Configuration Item*

TREVOR BUDGE SENIOR HYDROGEOLOGIST

NAME/POSITION

SIGNATURE

5-1-2019

DATE

Appendix F

Copy of EMDT-DE-0006 Rev. 1

Electronic Model Data Transmittal: Half Lives for Typical Hanford Site Radioactive Contaminants

Environmental Modeling Data Transmittal Cover Page

No.: EMDT-DE-0006 **Revision No.:** 1

[Request EMDT number from Modeling Team Leader]

Title: Half-lives for Typical Hanford Site Radioactive Contaminants. **Date:** 18-May-2015

1. Data Description

Provide the description of data set or data type.

Radioactive half-lives for reported radionuclides at Hanford site.

2. Data Intended Use

Identify the data's intended use. Describe the rationale for its selection and how the data will be incorporated into a model, report, or database. Include discussion of the extent to which the data demonstrate the properties of interest.

Numerical simulation of contaminant transport and fate

3. Data Sources

List databases, documents, etc. – provide sufficient detail to enable data to be located by independent reviewer

ICRP, 2008, Nuclear Decay Data for Dosimetric Calculations, International Commission on Radiological Protection (ICRP), Publication 107, Vol 38-3, ISBN 978-0-7020-3475-6.

4. Impact of Use or Nonuse of Data

Describe the importance of the data to the model, report, and/or conclusions which they support. Identify the value added and discuss the impacts of not using the data.

The half-life data are required to be consistent with PA studies and the model implementations in GoldSim and STOMP

5. Prior Uses

Identify the data's prior uses. Describe whether the data have been used in similar applications by the scientific or regulatory community. Include the associated verification processes and prior reviews and review results.

The ICRP Publication 107 data is used by the U.S. EPA calculation tool for radiation dose and risk.

CH2MHILL Plateau Remediation Company

Environmental Modeling Data Transmittal Cover Page

No.: EMDT-DE-0006 **Revision No.:** 1

[Request EMDT number from Modeling Team Leader]

Title: Half-lives for Typical Hanford Site Radioactive Contaminants. **Date:** 18-May-2015

6. Data Acquisition Method(s)

Describe the data acquisition method and associated QA/QC, considering the following:

a. *Qualifications of personnel or organizations generating the data;*
b. *Technical adequacy of equipment and procedures used;*
c. *Environmental and programmatic conditions if germane to the data quality;*
d. *The extent to which acquisition processes reflect modeling requirements;*
e. *The quality and reliability of the measurement control program;*
f. *The degree to which independent audits of the process were conducted;*
g. *Extent and reliability of the associated documentation.*

In addition to the listing tables in the ICRP publication 107 (ICRP, 2008), ICRP provides a database for electronic access. The database contains information on the half-lives, decay chains, yields and energies of radiations emitted in nuclear transformations of 1252 radionuclide isotopes of 97 elements. The database can be accessed by a user-defined software such as the Windows-based application provided by ICRP.

For databases, identify query language used to obtain data from database (SQL, etc.), briefly describe the query description and attach copy

The nuclear decay data are embodied in five formatted (hence can be viewed with an ASCII editor) direct-access files. Find a copy of text files and inquiry software: (P107JAICRP_38_3_Nuclear_Decay_Data_suppl_data.zip)

7. Corroborating Data

Identify and discuss any corroborating datasets. Provide any documentation that confirms the corroborating data substantiate existing parameter values, distributions, or data quality.

The ICRP half-lives were compared with three other sources that were listed in the rev 0 of this document. The best match to ICRP-P107 was source 2: DOE-STD-1196-2011, DOE Standard, Derived Concentration Technical Standard (April 2011). Differences were compared to four significant digits, while some half-lives were reported to only two significant digits.

8. Data Quality Considerations

Discuss data quality considerations not identified in other sections. Include discussion of data quality indicators (i.e., accuracy, precision, representativeness, completeness, and comparability).

For the radionuclides reported at the Hanford site, the ICRP half-life parameters match very closely the U.S. DOE standard DOE-STD-1196-2011, which is implemented in the U.S. EPA decay calculation tools. Additionally, the ICRP library is implemented in the GoldSim software that is approved for Hanford Site and used for PA's system models.

The %relative difference between the ICRP-P107 and the DOE-STD-1196-2011 data is less than 0.36% for all Hanford site radionuclides isotopes.

CH2MHILL Plateau Remediation Company

Environmental Modeling Data Transmittal Cover Page

No.: EMDT-DE-0006 **Revision No.:** 1

[Request EMDT number from Modeling Team Leader]

Title: Half-lives for Typical Hanford Site Radioactive Contaminants. **Date:** 18-May-2015

9. Assumptions and Limitations on Data Use

Document known uncertainties, assumptions, constraints or limits on data.

The ICRP–P107 provides a reliable information on physical characteristics of a radionuclide (half-life, modes of decay, energies, intensities of the emitted radiations, etc.) that is the starting point in assessing the radiological significance of a radionuclide's presence in the workplace or in the environment. Uncertainties of these information would result from different limitation in accounting for the fraction of the available decay energy given to radiations of discrete energy (alpha particles, gamma rays, conversion electrons, Auger elections, and characteristic x rays) as well as the continuous energy spectra of beta particles. Accounting for such details requires very specific expertise and is a laborious task that is not needed for the subject calculation. The ICRP reported half-lifes provide adequate accuracy for the forward and backward decay calculations needed to accompany transport and fate studies of radionuclides in the environment and the associated risk.

Data Configuration Item Submittal:

Data Provider Submittal

Usama Zaher/ Environmental Engineer – Process Modeling Specialist
NAME/POSITION

Usama
SIGNATURE

6/12/2017
DATE

Data Configuration Item Review and Verification:

10. Verification Process

Describe steps taken to verify that these data are appropriate for intended use, noting any limitations

Implementation in 1st and 2nd order decay calculations in spread sheet. Initial and decayed state estimations was verified in both forward and backward (regrow) decay. The forward decay was also compared with the integration solution in GoldSim. Secular equilibrium is considered for the 2nd order calculations with rapidly decaying daughters relative to parents.

11. Summary of Data Review

The review shall ensure that the report meets the listed criteria. Consideration includes ensuring that the data collection method employed was appropriate for the type of data being considered and confidence in the data acquisition and subsequent processing methodology is warranted.

Is documentation technically adequate, complete, and correct?	[X] Yes	[ ] No
Are uncertainties and limitations on appropriate use of data discussed?	[X] Yes	[ ] No
Are the assumptions, constraints, bounds, or limits on the data identified?	[X] Yes	[ ] No

Data Reviewer Approval	*Approval of Data Configuration Item*
	M Lord / Senior Hydrogeologist (Signature by WE Nichols with attached email authorization from M Lord) NAME/POSITION
	SIGNATURE — DATE: 12 JUN 2017

signature authorization

Michael Lord

Mon 6/12/2017 4:03 PM

To:Will Nichols <wnichols@intera.com>;

I give Will Nichols authorization to sign for me the Environmental Modeling Data Transmittal Cover Page (EMDT) document in file EMDT-DE-00060rev1.docx. I have inspected the data for the radioactive half-lives for reported radionuclides at the Hanford site. My suggested edits to the data and the EMDT document were implemented and with this authorization I am signing my approval of the data configuration item.

Michael Lord

Appendix G

Copy of EMDT-HP-0010 Rev. 0

Electronic Model Data Transmittal: Hydraulic and Transport Properties for Site-Wide Models

CH2MHILL
Plateau Remediation Company

Environmental Modeling Data Transmittal Cover Page

No.: EMDT-HP-0010 **Revision No.:** 0

[Request EMDT number from Will Nichols]

Title: Hydraulic and Transport Parameters for Site-wide Models **Date:** 27 Feb 2014

Data Sources

List databases, documents, etc. – provide sufficient detail to enable data to be located by independent reviewer

Bouwer and Rice, 1976, "A Slug Test for Determining Hydraulic Conductivity of Unconfined Aquifers with Completely or Partially Penetrating Wells."

CCN 024566, "Field Summary Report 100-H Area Well Production Testing."

Cooper and Jacob, 1946, "A Generalized Graphical Method for Evaluating Formation Constants and Summarizing Well Field History."

DOE/RL-93-43, Limited Field Investigation Report for the 100-HR-3 Operable Unit.

DOE/RL-93-79, Limited Field Investigation Report for the 100-KR-4 Operable Unit.

ECF-100BC5-11-0145, Analysis of Slug Test Data at the 100-BC-5 Operable Unit.

ECF-100FR3-11-0146, Analysis of Slug Test Data at the 100-FR-3 Operable Unit.

ECF-100HR3-12-0011, Analysis of Slug Testing Data at the 100-HR-3 Operable Unit.

ECF-100KR4-12-0010, Analysis of Slug Test Data at the 100-KR-4 OU.

ECF-100NR2-12-0031, Analysis of Data Collected from Slug Tests Conducted in Remedial Investigation Boreholes within the 100-NR-2 Groundwater Operable Unit.

ECF-HANFORD-11-0149, Aquifer Test Analyses for Wells 199-B2-15 and 199-F5-53.

PNL-10886, Development of a Three-Dimensional Ground-Water Model of the Hanford Site Unconfined Aquifer System: FY 1995 Status Report.

PNL-6471, Interim Characterization Report for the Area Surrounding the 183-H Basins.

PNL-6728, Geohydrologic Characterization of the Area Surrounding the 183-H Solar Evaporation Basins.

PNL-8337, Summary and Evaluation of Available Hydraulic Property Data for the Hanford Site Unconfined Aquifer System.

PNL-10886, Development of a Three-Dimensional Ground-Water Model of the Hanford Site Unconfined Aquifer System: FY 1995 Status Report.

PNNL-13349, 100-D Area in Situ Redox Treatability Test for Chromate-Contaminated Groundwater.

PNNL-16894, Investigation of the Strontium-90 Contaminant Plume Along the Shoreline of the Columbia River at the 10-N Area of the Hanford Site.

SGW-38757, Investigation of Hexavalent Chromium Source in the Southwest 100-D Area.

Theis, 1935, "The Relation Between the Lowering of the Piezometric Surface and the Rate and Duration of Discharge of a Well Using Ground-Water Storage."

WHC-SD-EN-DP-090, Borehole Data Package for the 100-K Area Ground Water Wells, CY 1994.

WHC-SD-EN-TI-221, Geology of the 100-FR-3 Operable Unit, Hanford Site, South-Central Washington.

Note: ISOAQX and WTAQ3 are automated computer programs for analyzing aquifer drawdown data. ISOAQX is described in "A Reassessment of Ground Water Flow Conditions and Specific Yield at Borden and Cape Cod" (Grimestad, 2002). WTAQ3 is described in "Flow to a Well of Finite Diameter in a Homogeneous, Anisotropic Water-Table Aquifer" (Moench, 1997).

Data Query Tools

For databases, identify query language used to obtain data from database (SQL, etc.), briefly describe the query description and attach copy

N/A

Data Package Review & Approval:

Data Provider

R Khaleel / Senior Hydrogeologist (INTERA)

NAME/POSITION

SIGNATURE

4/11/16

DATE

CH2MHILL
Plateau Remediation Company

Environmental Modeling Data Transmittal Cover Page

No.: EMDT-HP-0010 **Revision No.:** 0

[Request EMDT number from Will Nichols]

Title: Hydraulic and Transport Parameters for Site-wide Models **Date:** 27 Feb 2014

Data Reviewer

Describe steps taken to verify that the data are appropriate for intended use (note limitations):

Reviewed data description and incorporated into a draft of a model package report that is under development. Parameters and referenced sources of information are appropriate for the intended use to support development of a site-wide model.

WE Nichols / Modeling Team Leader (CHRPC)

NAME/POSITION

SIGNATURE

11 APR 2016

DATE

CH2MHILL
Plateau Remediation Company

Environmental Modeling Data Transmittal Cover Page

No.: EMDT-HP-0010 **Revision No.:** 0

[Request EMDT number from Will Nichols]

Title: Hydraulic and Transport Parameters for Site-wide Models **Date:** 27 Feb 2014

Data Description

Central Plateau Hydraulic Parameters

File: **CENTRAL PLATEAU Database_hyd_prop_Sept_2010.xls**

A PNNL database has been developed to provide an accessible repository for saturated media hydraulic properties; it is based on results and supporting data from aquifer tests conducted at the Hanford Site over the past 50 years (Thorne 2008; Thorne and Newcomer 2003). The database includes results from in-situ aquifer tests including pumping tests, slug tests, injection tests, and tracer tests. It does not include hydraulic properties determined from laboratory analysis of discrete samples (e.g., permeameter testing). Selection of hydraulic properties included in the database was based on requirements of the numerical and analytical models. These parameters include the following:

- Transmissivity (T)
- Storativity (S)
- Aquifer thickness (b)
- Hydraulic conductivity (K)
- Storage coefficient (S_s)
- Specific yield (S_y)
- Vertical anisotropy (K_v/K_h)
- Effective porosity (n_e)

The preceding parameters are calculated from measured aquifer response data combined with information on well and aquifer conditions and often based on assumptions about the aquifer flow system. None of these parameters can generally be determined from a single aquifer test analysis. Sometimes, one or more of these parameters must be assumed in order to calculate others. Therefore, each of these fields has a corresponding field to indicate whether the parameter was determined from the analysis, calculated from another parameter, or assumed. Additional fields in the database tables contain information on test analysis methods, well configuration, aquifer conditions, and test conditions. The reliability of hydraulic property estimates from aquifer tests varies widely depending on the appropriateness of applied analysis methods, the amount and duration of applied stress, the well/aquifer configuration, and the quality of data collected. Therefore, a reliability flag field has been created for each of the analysis parameters. This flag will indicate that the reliability of the calculated hydraulic properties is either: R= reliable, Q=questionable or U= unknown. A comment field also exists for each test analysis to document the basis for the reliability flag.

Site-specific data on storage properties are limited; however, some data are available for the Hanford and Ringold units based on field tests conducted in the 200 Areas. According to PNL-10886, *Development of a Three-Dimensional Ground-Water Model of the Hanford Site Unconfined Aquifer System: FY 1995 Status Report*, and PNL-8337, *Summary and Evaluation of Available Hydraulic Property Data for the Hanford Site Unconfined Aquifer System*, specific yield for the Hanford formation is estimated to range from about 0.1 to 0.3 and is expected to be higher for coarse, well-sorted gravel than for poorly sorted mixtures of sand and gravel. From previous work (PNL-10886; PNL-8337), specific yields of the poorly sorted sediments of the Ringold Formation are estimated to range from 0.05 to 0.2.

CH2MHILL
Plateau Remediation Company

Environmental Modeling Data Transmittal Cover Page

No.: EMDT-HP-0010 **Revision No.:** 0

[Request EMDT number from Will Nichols]

Title: Hydraulic and Transport Parameters for Site-wide Models **Date:** 27 Feb 2014

River Corridor Hydraulic Parameters

File: **100 Area Storage_parameters.xlsx**

The saturated conductivities for the 100 Areas are based on field data (i.e., pumping and slug testing). If available, the analysis msethod used for the field data is noted. In addition to values based on slug and pumping tests, a few conductivity estimates exist for laboratory-scale permeameter tests, which are not included, but can be retrieved from the Hanford Environmental Information System (HEIS) database.

The hydraulic conductivities are grouped by the geologic unit (Hanford/Ringold). For multiple entries of saturated hydraulic conductivity for the same location, an average conductivity value should be used. The user is cautioned regarding the presence of outliers; such outliers should be apparent whenever the overall statistics for each geologic unit are tabulated. For information regarding the test (screen) interval, the original sources should be consulted. Included are hydraulic conductivity estimates for a few "699-" series wells, which are located in between the 100-D and 100-H Areas.

The 100 Area hydraulic conductivity of the Hanford formation ranged from 27 to 118 m/day. Hydraulic conductivity of Ringold Formation unit E is somewhat lower, and ranged from 12 to 38 m/day. Slug tests and a pumping test in wells screened in a water-bearing zone of the RUM reflect very low hydraulic conductivity ranging from 0.1 to 1.6 m/day.

A series of slug injection and withdrawal tests were performed in in 2010 and 2011 in 100-HR-3 Area and other OU's in 100 Area as part of RI/FS activities. See, for example, ECF-100HR3-12-0011, *Analysis of Slug Testing Data at the 100-HR-3 Operable Unit*, for more information about the calculations of saturated conductivities for the new wells (including specific well capacity estimates)

Appendix H

Copy of EMDT-ST-0004 Rev. 0

Electronic Model Data Transmittal: Historical Pumping Rates 200 West Area

Environmental Modeling Data Transmittal Cover Page

No.: EMDT-ST-0004 **Revision No.:** 0

Electronic Modeling Data Transmittal – Boundary Condition (Historical Pumping Rates) – 0001

Title: *Historical Pumping Rates 200 West Area* **Date:** 16-Jan-2014

Data Description

The data package described in this document contains historical pumping rates compiled for use as input data for creating inputs to the Central Plateau (CP) groundwater model Multi-Aquifer Well (MNW2) Package, and includes historical daily pumping rates based on reported daily pumping rates/volumes and estimated daily pumping rates for other periods (as calculated from reported annual pumping volumes). The total period of the data covered by this submittal comprises January 1994 through December 2012. This data package includes pumping rates for the 200-ZP-1, 200-UP-1 and T-Tank operable units (OUs). The data were gathered and compiled into a Microsoft Excel file named "200WestHystoricalPumpingSummary3.xlsm", which is included as an electronic submittal with this electronic modeling data transmittal.

Data Sources

The data used to compile this transmittal come from various sources, including:

- E-Mails received by SSPA personnel
- Annual Summary Reports for the 200-ZP-1 and 200-UP-1 OU's.

The complete list of source files used to create this data submittal set is identified in the worksheet "DataSources" in the file "200WestHystoricalPumpingSummary3.xlsm". This worksheet also lists a series of Excel files generated by SSPA personal to process the original data (representing a variety of schedules and integration time-lengths) into daily pumping rates and to QC/QA the source files to the extent possible. Data compiled in these various Excel files were imported into the worksheets "HistoricalPumping_PhaseI&II" and "ZP_PT_PhaseIII_2012", in the file "200WestHystoricalPumpingSummary3.xlsm". To help record and visually depict the data sources used throughout the calculation, the worksheet cells are color-coded based on their source document.

The original source files are located in the folder "SourceFiles" within the electronic submittal; intermediate files used to process the source data are located in the folder "SSPAProducedFiles" within the electronic submittal; and the various Annual Report files are stored in the folder "200Area Annual Reports" within the electronic submittal.

CH2MHILL Plateau Remediation Company

Environmental Modeling Data Transmittal Cover Page

No.: EMDT-ST-0004 **Revision No.:** 0

Electronic Modeling Data Transmittal – Boundary Condition (Historical Pumping Rates) – 0001

Title: *Historical Pumping Rates 200 West Area* **Date:** 16-Jan-2014

Color	File modified by SSPA	Original Files	Comment
	Calculated from Cumulative Treated volumes from Annual Reports		
	PumpingPrior2006.xlsx	ZP-1 Recovery Well Rates 1997-2006 (Doughty).xls	Vista. Received by SSPA 11/30/2006
		Zp1_Injection_historic_from_VISTA.xls	
	UP1 Pump Rates_MK.xls	UP1 Pump Rates.xls	From: Kelty, George [mailto:George_Kelty@RL.gov] Sent: Monday, January 26, 2009 2:15 PM To: 'Matt Tonkin'
	ETF_TOTALIZER_CY2010_011311_2_forDB.xlsx	ETF_TOTALIZER_CY2010_011311_2.xlsx	email from Gene Freeman to Rachel 1/18/2011. File sent by Gene was called "ETF_TOTALIZER_CY2010_011311.xlsx". Added "2_forDB". (The "2" is because this is a revised version of a file he sent the day before).
	ZP-1 History_MK.xlsx	ZP-1 History.xlsx	email from Garry Scheidegger to Rachel 4/4/2011
	ZP2011_2012Combined_MK.xlsx	ZP1_Totals_Oct Nov & to Dec 27 2011.xlsx	sent by email from Sally Simmonds to Rachel 2/8/2012
		ZP1_Totals_2012.csv	sent by email from Frederick Biebesheimer to Matt 6/13/2012.
		ZP-1_(Injection_Jan-Sep_2011)_ttbl_Daily_Volume_Report.csv	sent by email from Art Lee to Matt 1/18/2012
		ZP-1_(Extraction_Jan-Sep_2011)_ttbl_Daily_Volume_Report.csv	sent by email from Art Lee to Matt 1/18/2012

Figure 1. Color-coding used to identify source documents

In the case that daily pumping rates were unavailable or incomplete, quarterly treated volumes as reported in the Annual Summary Reports were used as a basis for deriving approximate rates. These calculations are compiled in the worksheets "ZP-1Cumulative", "UP-1_Cumulative" and "T-Tank_Cumulative" in the file "200WestHystoricalPumpingSummary3.xlsm". To calculate individual pumping rates from quarterly cumulative values, well rates are prorated on the basis of their reported annual average pumping rates.

For example: the 200-ZP-1 Treatment system for the period from August to December of 1996 reported a total of 20,556,824 gallons of treated water, and it is also reported that there were three active extraction wells: 299-W15-33, 299-W15-34 and 299-W15-35 with average flow rates of 29, 39 and 81 gallons per minute (GPM), respectively. These average flow rates were used to calculate how much of the water was pumped by each individual well by calculating a fraction for each well and multiplying this by the total reported volume. These calculated prorated volumes are then used to calculate average daily pumping rates over the year.

The worksheet "ModelRates(GPM)" contains the final pumping rates used as inputs to generate an MNW2 package input file for the Central Plateau (CP) model. The rates tabulated in this worksheet are

averaged on either a monthly or a yearly basis depending on the length of the corresponding model stress period. The averaging is performed within a pivot table in the worksheet "AverageGPM": the Visual Basic (VB) macro "UpdateRates" is then used to populate the averaged values to appropriate columns in the worksheet "ModelRates(GPM)".

To QA/QC the compiled pumping rates, calculated cumulative extraction and injection volumes were compared to the 200-ZP-1 reported cumulative treated volumes over time. This analysis discovered periods during which there were significant discrepancies between the extracted and reported cumulative volumes. While calculated injection volumes show only small discrepancies compared to the reported values, calculated extraction volumes appear to be systematically lower than the reported values for the period from 1998 to 2001 in particular. This discrepancy was also noted in the Fiscal Year 1998 Annual Report where it was stated:

> *"It should be noted that there was a discrepancy between the total flow rate calculated using the flow meters for each extraction well and the other flow monitoring locations (Figure 3-2). It was determined that the flow totalizer at the TSL02 location (just prior to transport to the air stripper) provides the most accurate total flow rate. Since July, this monitoring location has been used to monitor the combined flow rates. Because of this discrepancy, the average flow rate reported for the fiscal year is probably about 10% below the actual flow rate."*

CH2MHILL Plateau Remediation Company

Environmental Modeling Data Transmittal Cover Page

No.: EMDT-ST-0004 **Revision No.:** 0

Electronic Modeling Data Transmittal – Boundary Condition (Historical Pumping Rates) – 0001

Title: *Historical Pumping Rates 200 West Area* **Date:** 16-Jan-2014

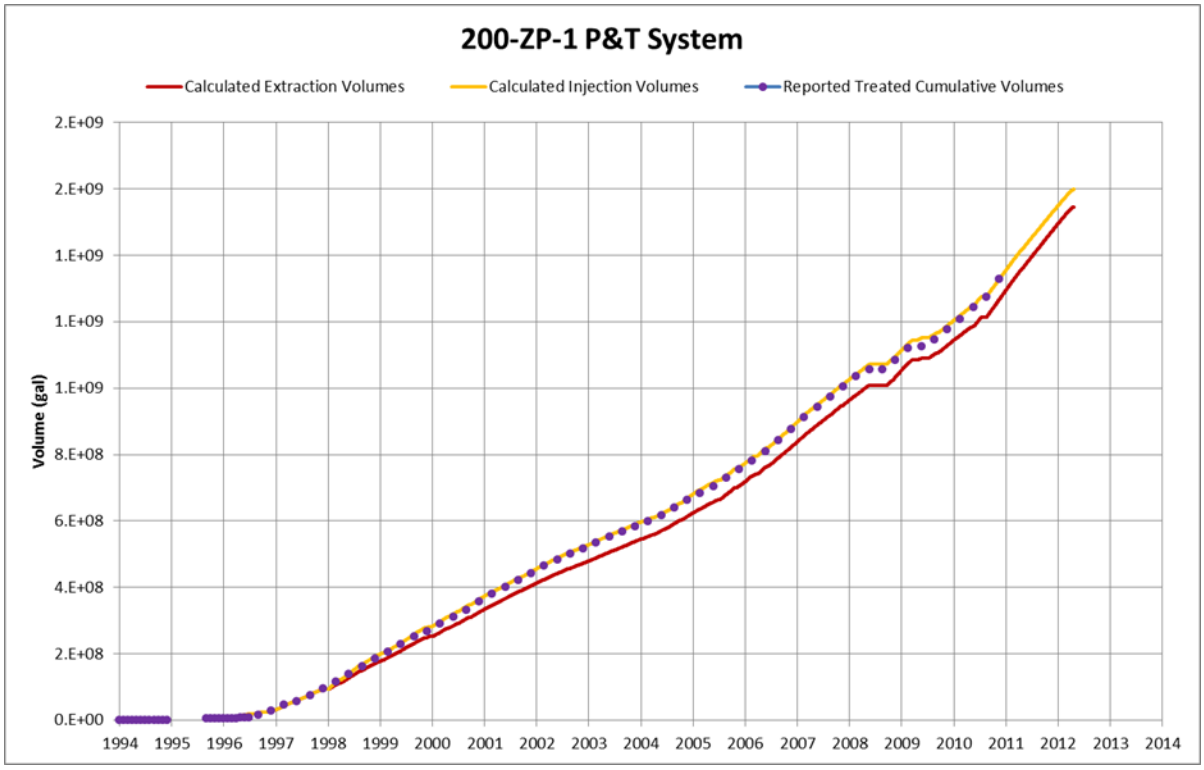

Figure 2. 200-ZP-1 Treatment plant cumulative reported and calculated volumes

Although no reports after 1998 Annual Report mention problems with measured extraction rates, from the plot presented above in figure 2 it is evident that this problem continued for several years. To correct for this imbalance, extraction rates were multiplied by the reported estimated correction factor (i.e., scaled by a factor of 1.10) for the period from January 1998 through December 2001, which resulted better correspondence and a net flow balance within about 5% of the total flows. Nonetheless, the average yearly extraction volumes still fell systematically bellow the reported volumes. It was determined through trial-and-error that a correction factor of 1.15 resulted in very good correspondence between the calculated volumes determined from the estimated rates versus the reported volumes. Given the strength of this correspondence, a correction factor of 1.15 was used for the final data submittal.

CH2MHILL Plateau Remediation Company

Environmental Modeling Data Transmittal Cover Page

No.: EMDT-ST-0004 **Revision No.:** 0

Electronic Modeling Data Transmittal – Boundary Condition (Historical Pumping Rates) – 0001

Title: *Historical Pumping Rates 200 West Area* **Date:** 16-Jan-2014

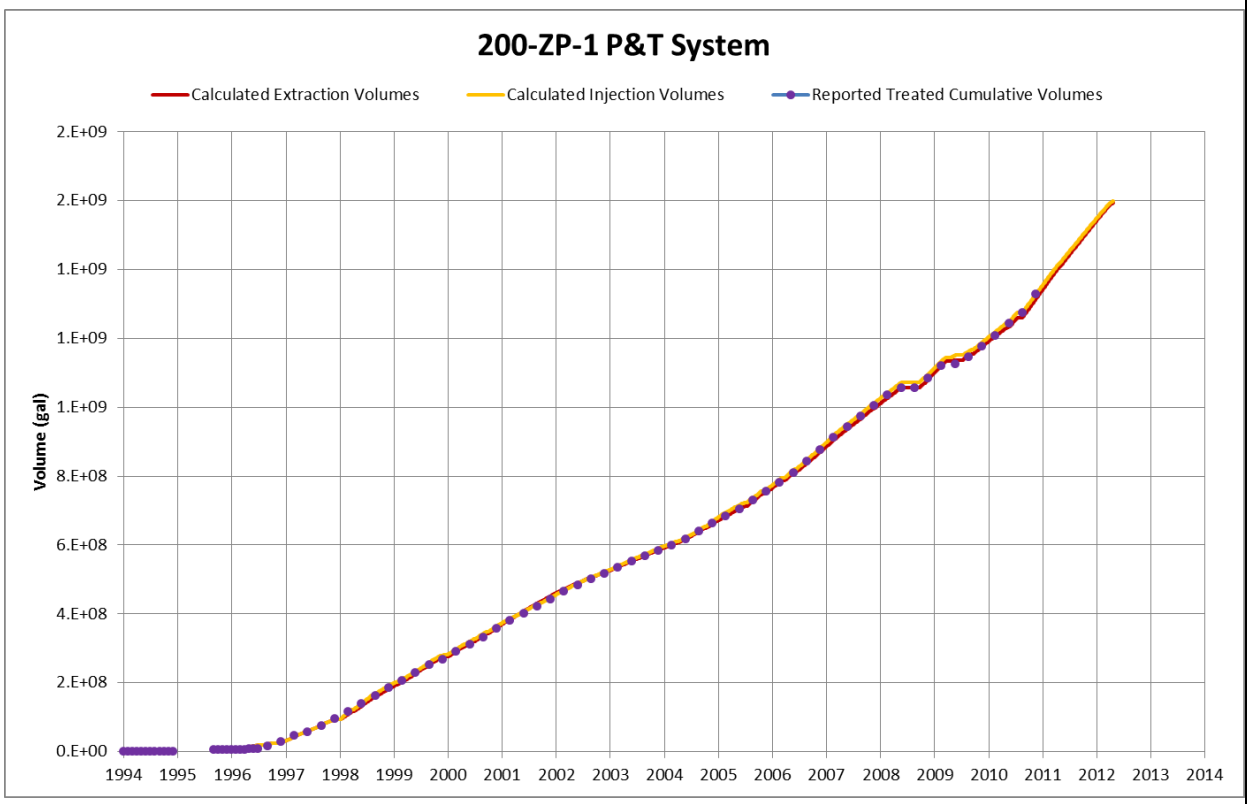

Figure 3. 200-ZP-1 Treatment plant cumulative reported and calculated volumes after the correction of 15%.

The groundwater pump-and-treat (P&) system at the 200-UP-1 OU began operation in 1994 as a pilot scale treatability test and ended in March 2011. Reported and calculated cumulative volumes for this OU (Figure 4) show fairly good correspondence without any need to apply a correction factor to achieve a satisfactory water balance.

Environmental Modeling Data Transmittal Cover Page

No.: EMDT-ST-0004 **Revision No.:** 0

Electronic Modeling Data Transmittal – Boundary Condition (Historical Pumping Rates) – 0001

Title: *Historical Pumping Rates 200 West Area* **Date:** 16-Jan-2014

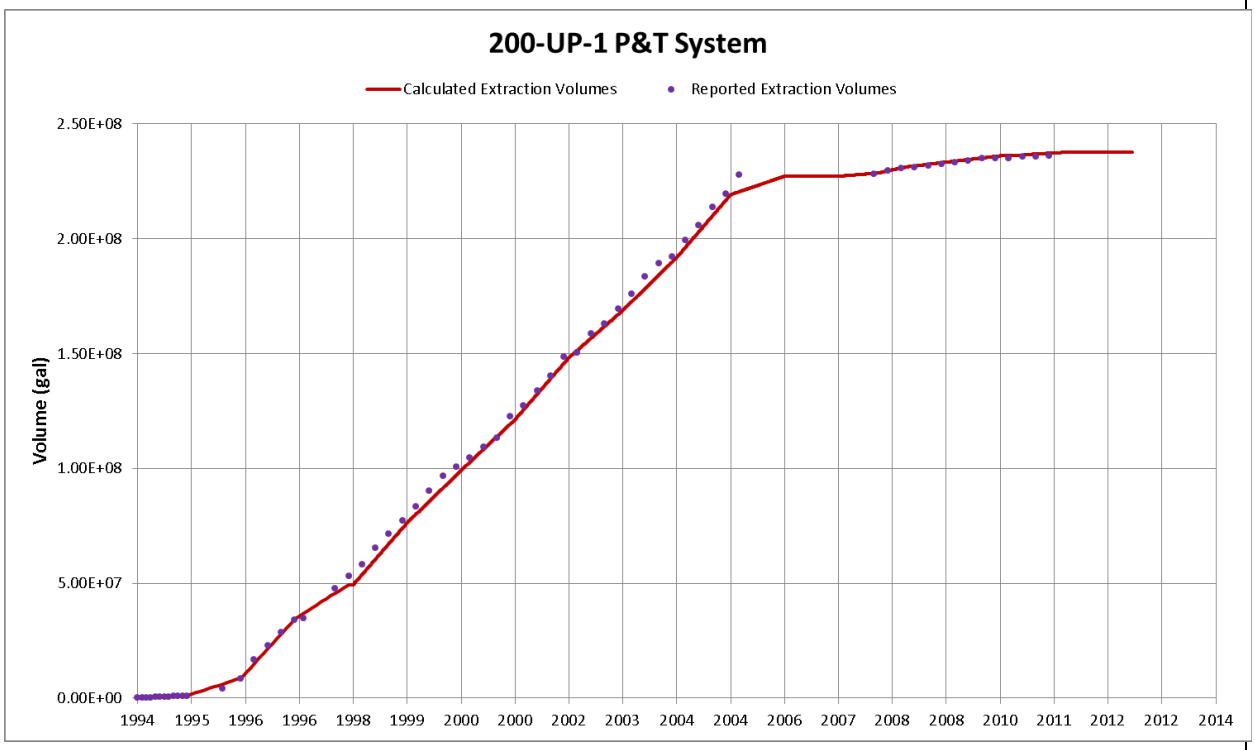

Figure 4. Correspondence of reported and calculated cumulative extraction volumes for 200-UP-1.

CH2MHILL Plateau Remediation Company

Environmental Modeling Data Transmittal Cover Page

No.: EMDT-ST-0004 **Revision No.:** 0

Electronic Modeling Data Transmittal – Boundary Condition (Historical Pumping Rates) – 0001

Title: *Historical Pumping Rates 200 West Area* **Date:** 16-Jan-2014

List of Annual Reports used to compile this data set:

DOE/RL-95-02, Rev. 0 Treatability Test Report for the 200-U P-1 Operable Unit - Hanford Site, 1995.

DOE/RL-95-02, Rev. 0, 200-ZP-1 Operable Unit Treatability Test Report, 1995.

BHI-00952-01,Rev. 0, 200-ZP-1 Phase II - Interim Remedial Measure, Quarterly Report, August - October 1996

DOE-RL, 1996, 200-ZP-1 IRM Phase II and III Remedial Design Report, DOE/RL-96-07, Rev. 1, U.S. Department of Energy, Richland Operations Office, Richland, Washington.

DOE/RL-98-38, Fiscal Year 1997 Annual Report for the 100-NR-2, 200-UP-1, and 200-ZP-1 Pump-and-Treat Operations and Operable Units

DOE/RL-99-02, Fiscal Year 1998 Annual Summary Report for the 200-UP-1, 200-ZP-1, and 100-NR-2 Pump-and-Treat Operations and Operable Units

DOE/RL-99-79, Fiscal Year 1999 Annual Summary Report for the 200-UP-1, 200-ZP-1, and 100-NR-2 Pump-and-Treat Operations and Operable Units

DOE/RL-2000-71, Fiscal Year 2000 Annual Summary Report for the 200-UP-1 and 200-ZP-1 Pump-and-Treat Operations

DOE/RL-2001-53, Fiscal Year 2001 Annual Summary Report for the 200-UP-1 and 200-ZP-1 Pump-and-Treat Operations

DOE/RL-2002-67, Fiscal Year 2002 Annual Summary Report for 200-UP-1 and 200-ZP-1 Pump-and-Treat Operations.

DOE/RL-2003-58, Fiscal Year 2003 Annual Summary Report for 200-UP-1 and 200-ZP-1.

WMP-26558, Revision 0, 200-UP-1 and 200-ZP-1Pump-and-Treat Semi-Annual Technical Memorandum, FY2005P ump-and-Treat Operations

DOE/RL-2004-72, Fiscal Year 2004 Annual Summary Report for 200-UP-1 and 200-ZP-1 Pump-and-

CH2MHILL Plateau Remediation Company

Environmental Modeling Data Transmittal Cover Page

No.: EMDT-ST-0004 **Revision No.:** 0

Electronic Modeling Data Transmittal – Boundary Condition (Historical Pumping Rates) – 0001

Title: *Historical Pumping Rates 200 West Area* **Date:** 16-Jan-2014

Treat Operations

DOE/RL-2005-91, Fiscal Year 2005 Annual Summary Report for 200-UP-1 and 200-ZP-1 Pump-and-Treat Operations

DOE/RL-2006-73, Fiscal Year 2006 Annual Summary Report for 200-UP-1 and 200-ZP-1 Pump-and-Treat Operations

WMP-30847, 200-UP-1 Operable Unit Rebound Study Report, 2006

DOE/RL-2008-02, 200-UP-1 and 200-ZP-1 Operable Units Pump and Treat Annual Report for FY07

DOE/RL-2008-77, 200-UP-1 and 200-ZP-1 Operable Units Pump-and-Treat System Annual Report for Fiscal Year 2008

DOE/RL-2010-11, Hanford Site Groundwater Monitoring and Performance Report for 2009: Volumes 1&2

DOE/RL-2011-26, Calendar Year 2010 Annual Summary Report for the 200-ZP-1 and 200-UP-1 Operable Unit Pump-and-Treat Operations

DOE/RL-20 12-03, Revision 0, Calendar Year 2011 Annual Summary Report for the 200-Z P-1 and 200-UP-I Operable Unit Pump-and-Treat Operations.

DOE/RL-2011-26, Calendar Year 2010 Annual Summary Report for the 200-ZP-1 and 200-UP-1 Operable Unit Pump-and-Treat Operations

Data Query Tools

N/A

Data Package Review & Approval:

Data Provider

Matt Tonkin / Senior Hydrogeologist (SSP&A)

NAME/POSITION

1/16/2014

SIGNATURE DATE

Data Reviewer

Describe steps taken to verify that the data are appropriate for intended use (note limitations):

Followed 12 pumping rates from final spreadsheet back to original sources so than each SSPA modified sheet was tested and all source data sheets were involved.

Examined data flow for 1998-2001 injection rate correction.

Tom Clemo / Senior Hydrogeologist (INTERA)

NAME/POSITION

20-Jan-2014

CH2MHILL
Plateau Remediation Company

Environmental Modeling Data Transmittal Cover Page

No.: EMDT-ST-0004 **Revision No.:** 0

Electronic Modeling Data Transmittal – Boundary Condition (Historical Pumping Rates) – 0001

Title: *Historical Pumping Rates 200 West Area* **Date:** 16-Jan-2014

Tom Clem

SIGNATURE DATE